PROCEEDINGS OF THE 27TH ANNUAL MEETING OF THE AMERICAN SOCIETY OF BIOMECHANICS

Editors:

Rodger Kram, Ph.D.
Associate Professor, Department of Integrative Physiology
University of Colorado, Boulder

Gary Heise, Ph.D.
Professor, School of Kinesiology and Physical Education
University of Northern Colorado

Vijay K. Goel, Ph.D.
Professor and Chair, Department of Bioengineering
College of Engineering
The University of Toledo

Danny M. Pincivero, Ph.D.
Assistant Professor, Department of Kinesiology
College of Health and Human Services
The University of Toledo

CD-ROM Produced by X-CD Technologies

EFFECT OF AGE ON DETECTING A LOSS OF BALANCE IN A SEATED WHOLE-BODY BALANCING TASK

Alaa A. Ahmed[1], M.S. and James Ashton-Miller[1,2], PhD.

Biomechanics Research Laboratory
Departments of [1]Biomedical and [2]Mechanical Engineering
University of Michigan, Ann Arbor, MI, U.S.A.[aaahmed@umich.edu]

INTRODUCTION

Falls in the elderly are associated with considerable morbidity and mortality. All unintentional falls are attributable to a 'loss of balance' (LOB). However, a precise definition of a LOB is lacking. It has earlier been proposed that a LOB is required for the central nervous system to trigger a compensatory response to prevent the ensuing fall (Ahmed, 2002). The LOB is posited as a *loss of effective control*, detectable, both internally and externally, as a control error signal anomaly (CEA).

A model-reference adaptive controller and failure-detection algorithm were used to represent central nervous system decision-making based on input and output signals obtained during a challenging whole-body planar balancing task. Control error was defined as the residual generated when the actual system output is compared to the predicted output of a simple model of the system. A CEA is hypothesized to occur when the error exceeds a threshold three standard deviations (3Σ) beyond the mean baseline signal. The quality of the signals involved is inherently dependent on the accuracy of the afferent signals which is known to decline with the neuropathic changes associated with aging. This deterioration could result in an inability to detect a CEA and respond appropriately.

Our goal was to (a) detect CEA in both healthy young (YA) and older (OA) subjects performing a challenging seated balancing task, and (b) compare the performance of the 3Σ detection algorithm in predicting any impending compensatory response. We tested the null hypothesis (H1) that there would be no age effect on the successful detection of CEA using a 3Σ threshold criterion on the controller error signal. The secondary (null) hypothesis (H2) was tested that age would not affect the performance of the 3Σ threshold in predicting the occurrence of any compensatory reaction by 100 ms.

METHODS

Twenty YA (10 females) and 20 OA (10 females) volunteers were tested (ages were 18-25 and 65-80 years, respectively). Seated subjects were asked to balance a custom high-backed chair for as long as possible over its rear legs, P (Fig. 1). Each performed five trials with eyes open. The ground reaction force under the dominant foot, which constituted the sole input to the system, was measured using a two-axis load cell. The position of three LEDs on the head and two on the chair were tracked using an Optotrak 3020 system. The error signal formed from the difference between the expected system output due to the given force input and the actual output, chair acceleration was calculated. CEA was defined to have occurred once the error signal crossed a

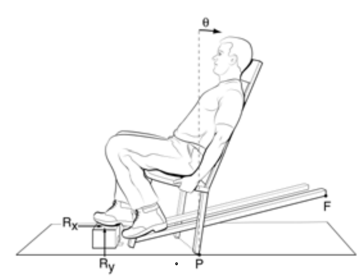

Figure 1: Experimental Setup

threshold level set at three standard deviations (3Σ) above the mean value in a 2-second-wide moving window, **b**, which lagged the current time instant, **t**, by 100 msec (Fig 2: The threshold calculation begins at '**Start**', initially using data in **a** as baseline data. Points 'F' on the chair must strike the ground within **c**, a two-second post-CEA interval.) The occurrence of a natural righting response, a large acceleration of the head in flexion (relative to the chair), was defined as a compensatory response, and evidence of CEA perception. Reaction time (RT) was defined as the latency of this response and could occur no earlier than 100 ms after CEA.

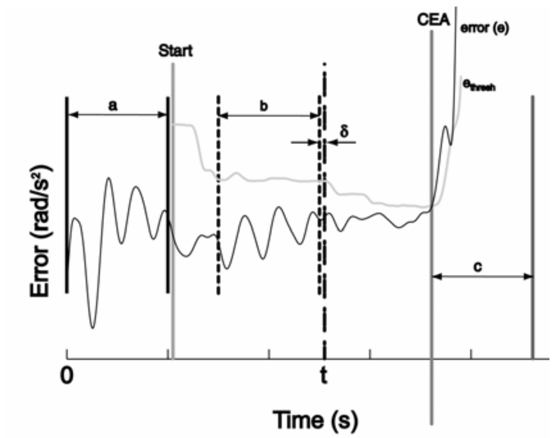

Figure 2: Sample time history of the control error signal (black) along with the moving threshold (gray) from one trial

RESULTS

The primary hypothesis (H1) was supported in that the 3Σ algorithm successfully detected CEA in 91.6% of the 99 YA trials and in 91.9% of the 95 OA trials (no significant age difference: χ^2: p>0.995). The secondary hypothesis was rejected in that a compensatory reaction was successfully predicted using the 3Σ algorithm in 92.7% of the 82 YA trials with reactions, and in 67.5% of 80 OA trials with reactions (age effect significant: χ^2: p<0.005). Applying a lower threshold (2Σ) to the H2 trials in which 3Σ was unsuccessful did successfully predict reactions in a further 2% of YA trials and 10% of OA trials. However, a sensitivity analysis in both YA and OA demonstrated that the optimal threshold level was 3Σ; lower levels resulted in more false positives, while higher levels resulted in delayed CEA detection times (Fig. 3).

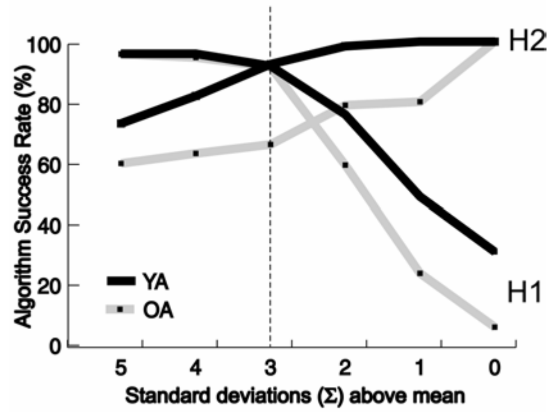

Figure 3: Sensitivity analysis results

DISCUSSION

The results suggest that a CEA is detectable by an external observer in both YA and OA. There are, however, age-related changes in a healthy subject's ability to internally detect a CEA. The 3Σ threshold did not predict a reaction in OA as accurately as in YA. Two OA in particular seemed to respond to a lower threshold, or perhaps another signal due to decreased sensor accuracy (manifested as a lower error threshold for CEA detection in OA), and/or a more conservative strategy. CEA detection provides a novel approach to understanding and quantifying the effect of aging on postural control.

REFERENCES

Ahmed, A.A., Ashton-Miller, J.A..(2002) WCB & Gait & Posture, *accepted*.

ACKNOWLEDGEMENTS

PHS Grants AG 08808, 10542 & 00116

FORCE DEPENDENT VARIABILITY IN THE INTERPOLATED TWITCH TORQUE

M.A.E. Oskouei, B.C.F. van Mazijk, M.H.C. Schuiling, and W. Herzog

Human Performance Laboratory, University of Calgary, Calgary, Alberta, T2N 1N4, Canada
E-mail: oskouei@kin.ucalgary.ca

INTRODUCTION

The interpolated twitch technique is frequently used to study the degree of motor unit activation during voluntary effort (Belanger and McComas, 1981). During contraction, an electrical stimulus (typically a single or doublet twitch) is superimposed to a muscle or its nerve, and the evoked interpolated twitch torque (ITT) is measured (Belanger and McComas, 1981; Suter and Herzog, 2001). The ITT is a measure of the amount of motor units that are not, or not maximally, recruited during voluntary contraction. Therefore, the ITT is an indication of the level of completeness of muscle activation. This technique is one of the preferred methods to determine activation deficit (AD) in normal, athletic, and patient populations. One of the limitations of the superimposed twitch technique is its variability for given contractile conditions. The general objective of this research was to determine the force dependent source for this great variability in ITT values for repeat measurements.

METHODS

Sixteen healthy subjects (age 27 ± 6 years; height 173 ± 10 cm; mass 72 ± 19 kg) participated in a sub-maximal protocol involving efforts of 50% of maximal voluntary contractions (MVC). Twelve healthy subjects (age 30 years ± 7; height 178cm ± 10; mass 73.kg ± 11) participated in a protocol involving 100% MVC. Three test protocols involving knee extensor contractions on a dynamometer (Biodex) comprised the main test. Subjects were strapped to the dynamometer chair for isometric knee extensor strength assessment at 90 degrees of knee flexion. During the test contractions, the knee extensor muscles were electrically activated via percutaneous stimulation of the femoral nerve, using supra-maximal doublet twitches.

Protocol 1: Subjects were asked to perform a 50% of MVC for 8s. Once the steady-state target force was reached (50% MVC), subjects were given four superimposed doublet stimulations, at 1s, 3s, 5s, and 7s.

Protocol 2: Subjects increased force until 40% of MVC was reached, held this force for 2 s, then steadily increased to 60% of MVC, and held that force for another 2 s. A doublet twitch was superimposed at the instant when the subjects crossed the 50% of MVC value. A second test was performed that was identical to the first one, except that subjects started at 60% of MVC and decreased force to 40% of MVC. Non-parametric, repeat measures statistics were used to determine differences between the ITTs obtained from protocol 1 and those obtained from protocol 2.

Protocol 3: Subjects performed ten MVC knee extensions for 5s with a two-minute (minimum) interval between contractions. Four seconds after reaching a steady-state force, a doublet twitch stimulus was superimposed onto the fully contracted muscle. Linear regression was used to test for statistical trends between activation deficit and knee extensor force.

RESULTS AND DISCUSSION

The mean superimposed twitch forces determined at 1s, 3s, 5s, and 7s of the 50% of MVC target force were the same. The superimposed twitch torques obtained from 50% of MVC, showed statistically significant, negative correlation with the actual force (the force obtained at the instant of twitch application). We determined not only the 50% of MVC target force, but also the actual force at twitch application. Therefore, when plotting the ITT relative to the actual force magnitude, rather than the target 50% of MVC, variations in the ITT were greatly reduced (Figure 1).

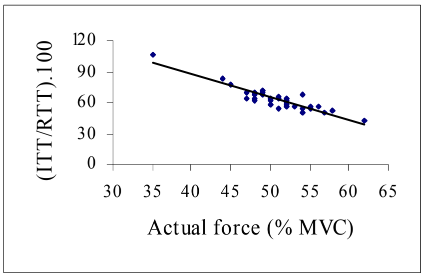

Figure 1: ITT normalized to resting twitch torques (RTT) as a function of the actual force at twitch application (representative data for one subject).

Similarly, the ITT and the corresponding activation deficit determined for the maximal efforts, varied greatly. When expressing the ITT relative to the actual force values, rather than the target 100% MVC, the variations in ITT were not reduced substantially (Figure 2).
In protocol 2, when accounting for the electromechanical delay, the ITTs were

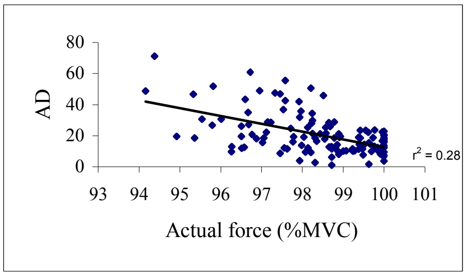

Figure 2: Activation deficit (AD) as a function of the percentage of MVC for twelve subjects and ten 10 trials each.

the same for all conditions.
These results suggest that small variations in the actual force from the target force explain a great part of the variations in ITT for sub-maximal but not for maximal or near maximal effort contractions. For near maximal effort contractions, great variations in the superimposed twitch force persist without a ready explanation.

SUMMARY

We concluded from these results that ITTs are very sensitive to small changes in voluntary forces at sub-maximal effort contractions. If variations in voluntary forces are not accounted for, there is great variability in both the ITTs and the activation deficit values. If these variations in voluntary forces are properly accounted for, the variations in activation deficit are greatly reduced. For maximal effort contractions, the ITT still varied greatly.

REFERENCES

Belanger AY, and McComas AJ. (1981). *J Appl Physiol* **51**(5): 1131-1135.
Merton PA. (1954). *J Physiol* **123**: 553-564.
Suter E, and Herzog W. (2001). *J Appl Physiol* **90**: 1036-1040.

LOWER EXTREMITY STRENGTH PLAYS ONLY A SMALL ROLE IN DETERMINING THE MAXIMUM RECOVERABLE LEAN ANGLE IN OLDER ADULTS

Tammy M. Owings[1], Michael J. Pavol[2], and Mark D. Grabiner[1,3]

[1]Department of Biomedical Engineering, The Cleveland Clinic Foundation
[2]Department of Exercise Science and Sport, Oregon State University
[3]School of Kinesiology, University of Illinois at Chicago
Email: grabiner@uic.edu

INTRODUCTION

The susceptibility of older adults to falling has been associated with diminished ability to perform stepping responses following large postural perturbations. When released from a forward-leaning position and instructed to restore stability using a single step, healthy older adults have a significantly smaller maximum recoverable lean angle than young subjects (Thelen et al., 1997). Further, compared to older men, older women have significantly smaller maximum recoverable lean angles (Wojcik et al., 1999). These age- and gender-related findings were attributed to the maximum speeds attained by the lower extremities during the step.

It is reasonable to expect that lower extremity muscle strength and power contribute to the lower extremity speed during this task, and, therefore, maximum recoverable lean angle. Thus, the purpose of this study was to determine the extent to which lower extremity strength and power contribute to the maximum recoverable lean angle in older adults.

METHODS

The maximum recoverable lean angle was determined for 56 older women and men (>65 years). Subjects, protected from falls to the ground by a safety harness system, were released without warning from a statically unstable forward lean by means of a remotely controlled electromagnetic support system. Upon release, the subjects were instructed to take a single step to regain their balance. Subjects performed two consecutive trials at each of 5, 10, 15, and 20 degrees of forward lean unless two failed recoveries occurred at a given angle of lean. A recovery was classified as a failure if, following the initial step, the arms came unfolded, the stepping foot moved entirely from the position at which it was initially placed after the recovery, the entire non-stepping foot moved, or the body was completely supported by the dynamic ropes.

Maximum recoverable lean angle was determined as the included sagittal plane angle between the vertical and the axis from the ankle joint to the center of mass of the body.

Maximum isometric strength was measured for the ankle, knee and hip (Pavol et al., 2002).

The initial statistical approach consisted of a discriminant analysis performed on a subset of the subjects. Subjects were separated into one of two groups based on whether the maximum recoverable lean angle placed the subject in either the lowest or highest quartiles of the sample. The maximum isometric moment values for which the between group differences were significant were entered into a discriminant analysis to determine the extent to which the variable set could correctly classify these subjects. Lastly, a stepwise regression procedure was conducted to predict maximum recoverable lean angle using the variables included in the discriminant analysis procedure. The stepwise regression was conducted using all of the subjects in the sample (n=56).

RESULTS

The difference between the maximum recoverable lean angle of those subjects who fell at or below the 25th percentile was 11±2degrees (n=14) and those subjects at or above the 75th percentile was 20±3 degrees (n=14) was significant ($p<0.001$). Notably, and in contrast to the findings of Wojcik et al. (1999) the gender-based differences were not significant ($p=0.635$)

Only maximum isometric hip extension moment failed to achieve a significant difference between the subjects in the lowest and highest quartiles of maximum recoverable lean angle ($p=0.095$). The stepwise discriminant analysis to classify subjects into the lowest and highest quartile of maximum recoverable lean angle reduced the remaining variable set to maximum isometric plantarflexion moment (Wilk's lambda=0.738, p =0.005)). The discriminant function correctly classified 68 percent of the subjects.

The stepwise regression procedure conducted to predict maximum recoverable lean angle as a function of maximum isometric plantarflexion moment and applied to the entire sample of older adults was significant ($p<0.001$) and accounted for 16 percent (adjusted) of the shared variation.

DISCUSSION

Generally, lower extremity strength appears to be an important determinant of maximum recoverable lean angle of healthy older women and men. The particular measure of strength identified as the key determinant was surprising. In light of previous research using this protocol that has indicated the importance of lower extremity speed to performance of this task (Thelen et al., 1997; Wojcik et al., 1999; Wocjik et al., 2001), the hip extensor muscles and, possibly the knee extensor muscles were expected to emerge as important contributors to performance.

The fact that 84 percent of the variance was not accounted for suggests key contributions to performance of other, non-strength related variables. One such variable for a lower extremity, time critical task is lower extremity coordination (Tomioka et al., 2001).

REFERENCES

Thelen et al (9197). *J Gerontol*, 52A:M8-M13.

Wojcik et al. (1999). *J Gerontol,* 54A:M44-M50.

Pavol et al. (2002) *J Amer Geriatrics* Soc, 50:256-262.

Wojcik et al. (2001) *J Biomechanics* 34:64-73.

Tomioka et al. (2001) *J Appl Biomech*, 17:181-187.

ACKNOWLEDGEMENTS

Supported by NIH RO1AG10557 (awarded to MDG)

EFFECT OF A COGNITIVE TASK ON LATERAL BALANCE AND GAIT PARAMETERS DURING WALKING

Christine Y. Wong[1], Daniel P. Ferris[2], and Arthur D. Kuo[3]

[1]Dept. of Biomedical Engineering, [2]Dept. of Kinesiology, [3]Dept. of Mechanical Engineering, University of Michigan, Ann Arbor. Email contact: chriswon@umich.edu

INTRODUCTION

Human walking appears to be passively unstable in the lateral direction, requiring active feedback control for stability (Kuo, 1999). One mechanism for stabilizing balance is lateral foot placement, indicated by the amount of step width variability during walking (Bauby & Kuo, 2000). A way to reduce the instability, and therefore the amount of control needed, is to take wider steps (Kuo, 1999), which decreases the amount of lateral foot placement needed to maintain balance, but increases the metabolic cost of walking (Donelan et al., 2001). Humans typically prefer relatively narrow steps (about 0.12 m) that are less costly, but which require more control of lateral foot placement for stability. We hypothesize that the amount of control required could be reduced by taking wider steps.

One way to test this hypothesis is to apply a cognitive load to subjects as they walk. Walking is a cognitively demanding task (Ebersach et al., 1995). The increased cognitive load of a secondary task could potentially be met by decreasing the effort placed in control of balance, i.e. by taking wider and more stable steps. Indeed, secondary tasks appear to affect step width and step width variability in the elderly (Grabiner et al., 2001).

This study seeks to test how a concurrent cognitive task affects lateral balance during walking, in terms of step width and step width variability. We tested whether humans used this tradeoff in response to a cognitive load. We expected that a cognitive task would help to reveal the presence of a negative correlation between step width and step width variability.

METHODS

We measured the gait of human subjects under three conditions of cognitive distraction: *Reaction Time* (RT) required each subject to press a button in response to a series of randomly spaced audio tones; *1-Back* (1B) required the subject to listen to a random series of 2 differently-pitched tones and to indicate whether the current tone was the same or different from the tone 2 before by pressing buttons carried in the left and right hands. In both tasks, the subject was asked to respond as quickly and as accurately as possible. The final task condition was a control (C), in which the subject pressed the buttons randomly. Each task was performed under 2 different gait conditions: walking on a treadmill at a pace of 1.2 m/s, and a control where subjects performed the secondary task while seated.

Testing was performed on 10 young healthy adults (4 females, 6 males). Step width and length were recorded from reflective markers placed on the subject's heels. Two force plates located under the treadmill measured each subject's ground reaction forces and moments. We calculated the changes in step width and step length due to distraction tasks, as well as changes in reaction times due to walking.

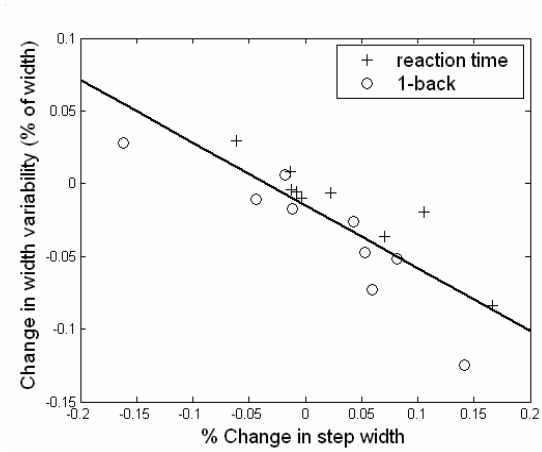

Fig. 1 Changes in step width (horizontal axis) and step width variability (vertical axis) have a high correlation ($r = -0.846$, $p < 0.0001$). Data points indicate change in gait parameters relative to each subject's normal gait when walking without a concurrent cognitive task.

RESULTS AND DISCUSSION

We found that subjects did exhibit a trade-off between step width and step width variability. When performing a concurrent cognitive task, subjects tended to increase their step width by varying amounts, with step width variability decreasing accordingly (Fig. 1). The correlation between step width and step width variability was found to be quite strong ($r = -0.846$, $p < 0.0001$) while that of step length and step length variability is not significant ($r = -0.105$, $p = 0.68$). An implication of this finding is that humans may exploit the tradeoff between step width and stability in response to stabilization or cognitive demands.

Subjects seems to compensate for a greater cognitive load by selecting a step width that reduces the demands of stabilization but increases the metabolic cost. Wider steps make walking more laterally stable, but there also appears to be a metabolic cost with wide steps, increasing approximately with the square of step width (Donelan et al., 2001). Humans normally select the step width that minimizes metabolic cost.

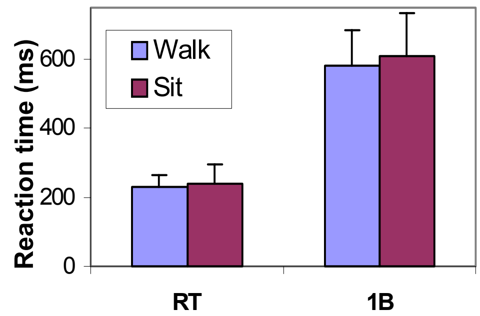

Fig. 2 Average response times (ms) to reaction time (RT) and 1-back tasks while walking and sitting.

There was no significant difference in reaction times between sitting and walking conditions ($p = 0.51$ for RT, $p = 0.15$ for 1B). Previous studies on elderly subjects have shown significantly increased response time for a secondary task while walking (Lajoie, 1993; Woollacott et al., 2002). The subjects in this study were all young healthy adults whereas the previous studies focused on elderly subjects. If younger subjects have more variable mental arousal (Stankard, 1990), or have a much higher capacity for multiple cognitive demands, they might be less affected by the combination of walking and a secondary task than the elderly.

REFERENCES

Ebersbach G, Dimitrijevic MR, Poewe W. (1995) *Percept Mot Skills*, **81**, 107-13.
Grabiner PC, Biswas ST, Grabiner MD. (2001) *Arch Phys Med Rehab*, **82**, 31-35.
Bauby CE, Kuo AD. (2000) *J Biomech*, **33**,1433-40.
Donelan JM, Kram R, Kuo AD. (2001) *Proc R Soc Lond*, **268**, 1985-92.
Woollacott M, Shumway-Cook A. (2002) *Gait & Pos*, **16**, 1-14.
Stankard W. (1990) *Percept Mot Skills*, **71**, 935-46.

ACKNOWLEDGEMENTS

C.Y.W. was supported by a UM fellowship.

MODELING OF POSTURAL SWAY ON CARPETS THROUGH FRACTIONAL BROWNIAN MOTION

Jianhua Wu[1], Ning Pan[1] and Keith R.Williams[2]
[1]Division of Textiles and Clothing, Department of Biological and Agricultural Engineering,
[2]Exercise Biology Program, University of California, Davis, CA 95616

Email: wjhwu@ucdavis.edu

INTRODUCTION

Carpets are widely applied in senior nursing homes to provide better comfort. However, inappropriate carpets tend to induce unstable posture and even potential falls. To better understand carpet performance, postural stability is usually examined by the center-of-pressure (COP). Recently fractional Brownian motion has been employed to investigate the dynamic COP characteristics (Collins and De Luca, 1993). Though this model has been applied to study the COP under various visual or postural conditions, little has been undertaken to investigate the floor effects. The goal of this study was to investigate the validity of fractional Brownian motion in modeling the COP along the antero-posterior direction for various carpets and also to explore the underlying neuromuscular mechanism.

METHODS

Subjects. Two male and four female healthy students participated this study. The mean age was 22.1 (range 20–28 years), mean weight 58.9 kg (range 45.2–66.9 kg), and mean height 166.7 cm (range 155–175 cm).

Apparatus. Five floors were tested including four carpets (denoted as A to D) and the hard floor denoted as F (a Kistler® 9281B force platform). The compressive moduli of carpets A to D were 16.2, 29.7, 43.5 and 71.9 N/mm, respectively. Two visual conditions were examined with (1) eyes-open (EO) and (2) eyes-closed (EC).

Experimental procedure. Each participant performed 10 trials on each floor under both visual conditions. The COP was collected for 15 seconds at 100 Hz. Enough time was provided between trials to eliminate fatigue. The order of the floors was randomized.

Fractional Brownian motion. $\left\langle \Delta x^2 \right\rangle \sim \Delta t^{2H}$ (Feder, 1988), where Δt is the time interval, $<\Delta x^2>$ is the mean square displacement, and H is the scaling exponent with any number between 0 and 1. If $H > 0.5$, an increased past COP implies generally an increasing future COP - persistence. A higher H leads to a more unstable posture. If $H < 0.5$, the COP yields antipersistence. A lower H leads to a more stable posture on a carpet.

Data analysis. The double logarithmic plot of $<\Delta x^2>$ versus Δt (Figure 1) was used to calculate H. Transition time T was found by Rougier's algorithm (1999), where the pure walk denotes the totally stochastic process with $H = 0.5$. Hs and H_l denote H in the region before T (short-term) and after T (long-term). A within-subject ANOVA and post-hoc Tukey's test were used to analyze averaged T and H among the floors. A correlation analysis was performed between floor modulus and T or H.

RESULTS AND DISCUSSION

The ANOVA reveals the significant difference among the floors with $F(1,20) = 8.03$, $p < 0.01$ under EO and $F(1,20) = 3.69$,

$p < 0.05$ under EC, in terms of T (Table 1). Carpet A generated a significantly shorter T under both visual conditions. Also in Figure 2, Hs was greater than 0.5 (persistence) and H_l was less than 0.5 (antipersistence). Only H_l was significant among the floors with $F(1,20) = 3.44$, $p < 0.05$ under EO and $F(1,20) = 3.50$, $p < 0.05$ under EC. Carpet A yielded the significantly lower H_l under EO and higher H_l under EC. Correlation coefficients were 0.88 under EO and –0.99 under EC between H_l and floor modulus.

The timing of T indicates how soon the posture will transfer from persistence to antipersistence, i.e. from an unstable to a stable posture. Carpet A is then expected to provide a better stability in terms of T due to the shorter period of an unstable stance, potentially reducing the possibility of falls. In terms of H_l in Figure 2, carpet A provides a more stable posture under EO and a less stable posture under EC. It can be postulated that under EO a firm floor yields a higher foot pressure, which leads a person to sway more to relieve the stress in muscles and joints. However, under EC a person may rely heavily on the somatosensory inputs. The fewer and conflicting somatosensory inputs generated by a compliant floor may impede the postural control and lead to a more uncontrollable sway in quiet standing.

SUMMARY

A compliant carpet gives a faster transition from an unstable to a stable posture, and also provides a more stable posture under EO and a less stable posture under EC.

REFERENCES

Collins, J.J., De Luca, C.J. (1993). *Experimental Brain Research*, **95**, 308-318.

Feder, J. (1988). *Fractals*. Plenum Press.

Rougier, P. (1999). *Archives of Physiology and Biochemistry*, **107**, 35-42.

ACKNOWLEDGEMENT

We thank the Wool Research Organization of New Zealand for partial financial support.

Table 1: The mean and SD of T (sec)

	A	B	C	D	F
EO	0.58	0.66	0.67	0.71	0.78
	(0.11)	(0.15)	(0.15)	(0.09)	(0.17)
EC	0.66	0.73	0.90	0.70	0.79
	(0.26)	(0.17)	(0.25)	(0.15)	(0.08)

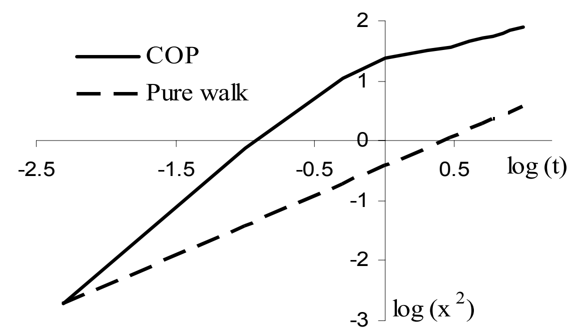

Figure 1: The double logarithmic plot

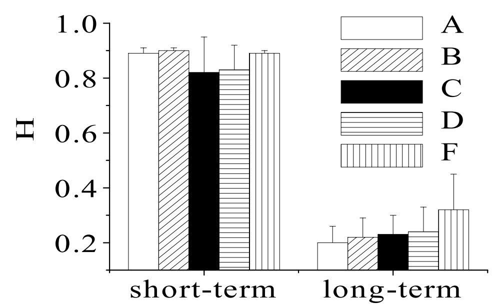

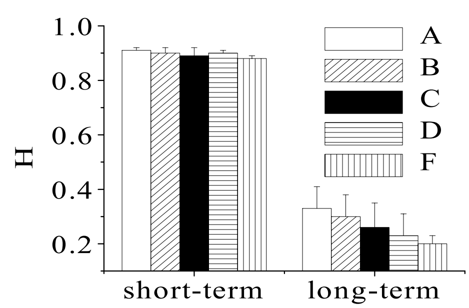

Figure 2: H under EO (top) and EC (bottom)

IS TRIP RECOVERY CAPABILITY ASYMMETRICAL?

Emily Lloyd and Michael L. Madigan

Musculoskeletal Biomechanics Laboratory, Virginia Tech, Blacksburg, VA, USA
E-mail: mlm@vt.edu   Web: www.esm.vt.edu/~mmadigan/msbiolab/

INTRODUCTION

Tripping causes up to 53% of falls in the elderly population (Blake et al. 1988). As such, a growing number of researchers are studying trips in the laboratory. Studying trips in the laboratory frequently requires the investigator to specify which foot will be tripped (Pavol et al. 2001) or which foot will be used for trip recovery (Thelen et al. 1997). Previous trip studies have selected the dominant lower limb (LL) for these functions presumably by default due to the lack of data to do otherwise. Significant asymmetries between dominant and non-dominant LL kinematics and kinetics have been documented during able-bodied gait (Sadeghi et al. 2000). If similar asymmetries exist during trip recovery, this information would be useful in the design of future trip studies. The purpose of this study was to investigate if the ability to recover from a trip differs when using the dominant or non-dominant LL for balance recovery.

METHODS

A total of twenty male subjects participated, including 10 young (19-23 years, mean 20.6 years) and 10 older (65-83 years, mean 74 years) adults. The tripping protocol was adapted from Thelen et al. (1997). Subjects were released from a forward-leaning posture and asked to recover their balance using a single step of the LL specified by the investigator. Upon successful balance recovery, the lean angle was increased and the process repeated until balance could not be recovered with a single step. The maximum lean angle from which subjects could recover their balance with a single step was used to quantify balance recovery capability. Subjects performed the protocol twice, once stepping with the dominant LL and once stepping with the non-dominant LL, to determine if balance recovery capability was asymmetrical. LL order was randomized. Lean angle was quantified by measuring the tension in a cable used to hold the subjects in the forward-leaning posture. This tension was measured as percent body weight (BW). The initial lean angle was 12% BW and increments were 4% BW. Subjects were given two attempts at each lean angle with failure criteria described elsewhere (Wojcik et al. 1999).

In the initial forward-lean posture, subjects stood with each foot on a separate force platform, and stepped onto a third force platform. Kinematic and force platform data were collected during the trip recoveries. The independent measure was LL used for trip recovery (dominant or non-dominant). The dependent measures were maximum lean angle and five kinematic parameters including: reaction time (time from release to the minimum reaction force from the LL tested), step time (time from foot lift-off to landing with the tested LL), total balance recovery time (time from release to landing with tested LL), step length (length of step in percent body height), and step velocity (velocity of step in body height per second).

The Wilcoxon-Ranked-Signs Test was used to test for differences in the dependent measures between dominant and non-dominant LL.

RESULTS AND DISCUSSION

Results indicated no difference in balance recovery capability between dominant and non-dominant LL ($p>0.05$, Figure 1). Kinematic data showed a shorter total time ($p<0.05$) and larger step velocity ($p<0.05$) with the dominant LL. No other kinematic variables were significant. Kinematic data indicate that a different strategy may be used for the dominant and non-dominant LL despite the fact that no significant difference in trip recovery capability was found. Future work investigating differences in dominant and non-dominant LL kinetics during trip recovery may help determine if different strategies were used between LL.

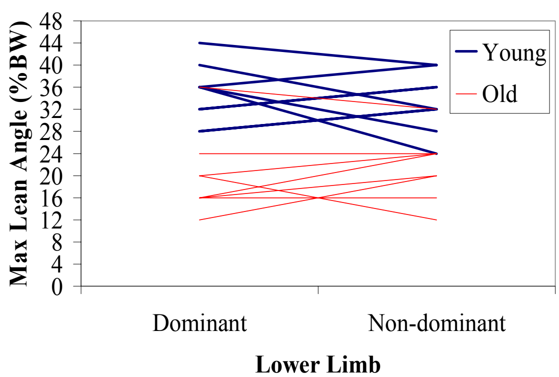

Figure 1: Maximum lean angles for dominant and non-dominant lower limbs.

SUMMARY

Although most subjects did exhibit an asymmetry in balance recovery capability (Figure 1), no recognizable trend was found in the populations sampled. These data do not provide evidence to recommend the specific use of the dominant or non-dominant LL in future trip recovery studies.

REFERENCES

Blake, A.J. et al. (1988). *Age Ageing*, **17**, 365-372

Pavol, M.J. et al. (2001). *J. Gerontol Med Sci.*, **56A**, M428-M437

Sadeghi, H. et al. (2000). *Gait and Posture*, **12**, 34-45.

Thelen, D.G. et al. (1997). *J. Gerontol Med Sci.*, **52A**, M8-M13.

Wojcik, L.A. et al. (1999). *J. Gerontol Med Sci.*, **54A**, M44-M50

ACKNOWLEDGEMENTS

We would like to acknowledge lab assistance from Matthew Runion as well as graduate research assistantship funding from Virginia Tech's Department of Engineering Science and Mechanics for summer 2002.

SLIP ANTICIPATION EFFECTS ON HIP/KNEE KINEMATICS
PART II: GAIT ON GLYCEROL CONTAMINATED FLOORS

April J. Chambers (ajcst49@pitt.edu), Kathleen Bieryla and Rakié Cham
Human Movement and Balance Laboratory, University of Pittsburgh, Pittsburgh, PA, USA

INTRODUCTION

A significant number of accidental injuries and deaths are attributed to slips and falls. The US National Health Interview questionnaire of 1997 showed that 64% of falls at work resulted from slipping, tripping or stumbling (Cham R., 2001). Causes of slips involve complex interactions of environmental and human factors (Redfern M.S., 2001). In order to better understand the impact of body reactions on the outcomes of a slip, i.e. recovery or fall, this paper will focus on the human factors, in particular, the knee and hip kinematics. Previous studies have shown knee flexion reactions recorded about 200 ms into stance were generated in the slipping leg as an attempt to recover balance during slips (Cham R., 2001). The goal of this study is to investigate the impact of proactive strategies, i.e. gait adaptations at heel contact (HC) with the slippery surfaces, on the slip severity. The impact of hip and knee kinematics on slip distance was compared between unexpected and anticipated slips.

METHODS

Equipment: Subjects walked naturally across a vinyl tile walkway instrumented with 2 Bertec force plates (FP), each foot contacted one FP. The contaminant (glycerol solution) was applied on the left FP, the slipping foot was the stance leg and the right foot was the trailing leg (no glycerol was applied on the right FP). Subjects wore a safety harness to prevent injury. Ground reaction forces were recorded at 600 Hz. Whole body motion (8 Vicon 612 motion capture cameras) was recorded at 120 Hz. Markers on the shank, thigh and pelvis were used to derive 3D kinematics of the knee and hip. (Fig 1)

Protocol: Five healthy subjects, aged 35 years or less, were screened for neurological, vestibular and orthopedic abnormalities prior to their recruitment. Subjects were told that the initial trials were dry. Without the subject's knowledge, a glycerol solution was applied to the left FP prior to the 3rd trial, 'unexpected' slippery condition. The subject was then informed that all of the following trials might be slippery. After 5 dry trials, the glycerol solution was applied to the left FP, the 'alert' slippery condition. After 5 more dry trials, the glycerol solution was applied one final time with the subjects' knowledge, the 'no-doubt condition'.

Data processing and analysis: A biomechanical rigid body model (left/right shank, left/right thigh and pelvis) was built to derive the 3D kinematics of the knee and hip (Fig 1). Flexion angles of the knee were derived by considering the rotation of the shank's local frame with respect to the thigh's local z-axis. Similarly, the hip angle was derived from the rotation of the thigh's local frame with respect to the pelvis' local sagittal axis. The knee and hip angles, measured during standing anatomical position, were subtracted from the absolute measurements during gait trials. Within-subjects repeated measures ANOVA were conducted on the slip distance to investigate the impact of knee/hip angles, evaluated at

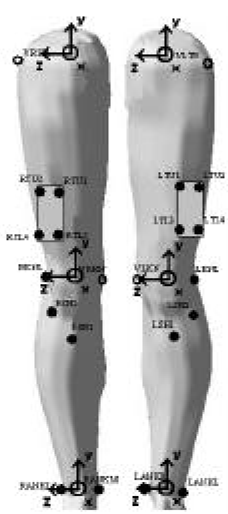

Fig 1: Biomechanical model of lower body used to derive 3D kinematics of hip/knee.

the time of left heel contact, on slip severity. HC time was determined using FP data.

RESULTS AND DISCUSSION

At HC time, increased hip extension and knee flexion were recorded (Fig 2 and 3). Fig 2 also shows that, later in stance, knee flexion is used as a recovery strategy (Cham R., 2001).

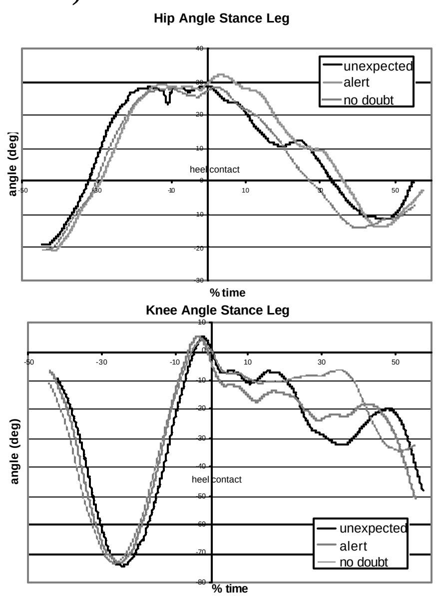

Fig 2: Typical profiles of left knee and hip angles during each slip condition. HC occurs at zero % time. Positive corresponds to extension while negative is flexion.

Right hip/knee angles at left HC showed no statistically significant impact ($p > 0.1$) on the slip distances. The relationships between slip distance and both the left hip/knee angle were statistically significant ($p < 0.05$). At HC, left hip extension and knee flexion increased significantly when subjects anticipated slippery conditions (Fig 3).

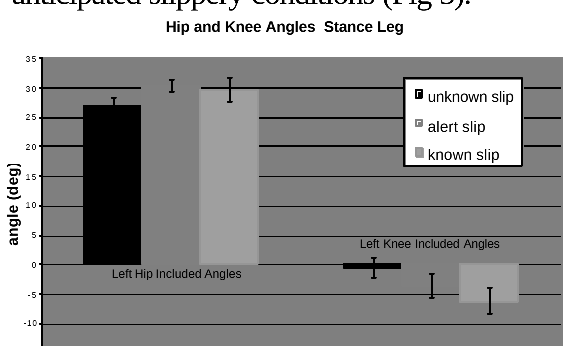

Fig 3:Angle at HC for the left hip/knee for each slippery condition. Error bars are standard errors.

Gait adaptations due to slippery surfaces anticipation in fewer falls and smaller slip distances (Table 1).

Subject number	Slip Anticipation Condition	Slip Distance (mm)	Outcome
1	Unexpected	76.37	Recovery
2	Unexpected	129.042	Fall
3	Unexpected	34.52	Recovery
4	Unexpected	351.44	Fall
5	Unexpected	151.33	Fall
1	Alert	47.42	Recovery
2	Alert	178.97	Fall
3	Alert	43.78	Recovery
4	Alert	73.93	Recovery
5	Alert	34.63	Recovery
1	No-doubt	23.75	Recovery
2	No-doubt	113.14	Recovery
3	No-doubt	41.89	Recovery
4	No-doubt	-16.29	No Slip
5	No-doubt	1.91	No Slip

Table 1: Raw slip distances and slip outcomes.

DISCUSSION

At HC, anticipation conditions showed a significant increase in hip extension and knee flexion. These gait adaptations, were associated with an improved chance of completing a successful recovery after the slip. It is believed that an increase in hip extension and knee flexion recorded at HC during the anticipation conditions “improved balance”. This anticipatory strategy resulted in reduced slip distances and less falls. Other gait adaptations, changes in foot-floor angles, exist and are beyond the scope of this paper. Those results are reported in another ASB submission (Margerum S., 2003).

REFERENCES

Cham, R. & Redfern, M.S. (2001). *J Biomech*, 34, 1439-1445.

Redfern, M.S. et al (2001). *Ergonomics*, 44(13), 1038-1166.

Margerum S. et al. (2003) *submitted to American Society of Biomechanics*.

ACKNOWLEDGEMENTS

Funding source: NIOSH R03 OH007533

Neurological screening: Dr. Joseph Furman.

EFFECTS OF AGE AND PHYSICAL ACTIVITY LEVEL ON BERG BALANCE SCORE IN ELDERLY THAI WOMEN

Wipawan Chewwasung, Vimonwan Hiengkaew and Roongtiwa Vachalathiti

Faculty of Physical Therapy and Applied Movement Science, Mahidol University, Thailand
E-mail: roongti@usc.edu

INTRODUCTION

Ability to control posture is important to maintain safety during functional activity of daily living. Reduction in balance has been related with high incidence of fall in elderly (Liechtenstein et al, 1988; Lord et al, 1994). Decreased physical activity has also been related with increased incidence of fall in elderly (Gill et al., 1995). In addition, evidence exists for age-related changes in postural control, which lead to balance impairment and fall (Liechtenstein et al, 1988; Lord et al, 1994; Tinetti et al, 1995). However, active elderly may be able to decrease the fall risk by maintaining balance through physical activity. Therefore, the purpose of this study was to determine the effects of age and physical activity level on the postural balance performance by using the Berg balance test (Berg, 1989) in elderly Thai female subjects.

METHODS

Thai female subjects aged 60 years and over were recruited in this study. One hundred and nineteen elderly female subjects participated in this study. All subjects gave their consent and the Ethical Committee on Research Involving Human Subject, Faculty of Medicine Siriraj Hospital, Bangkok, Thailand approved the study.

Subjects were categorized into one of the following six groups based on age (WHO: Young and Older elderly) and physical activity levels (High, Moderate, and Low).

The young elderly group aged from 60-74 years, while the older elderly group aged from 75-89 years. The selected four physical activities; going outdoors, exercises, activity of daily living and other activities, were used as criteria of physical activity levels (Jitapunkul et al., 1998). The high activity group was able to do all four activities, while the moderate and low groups were able to do any three and two of the four activities, respectively.

The Berg balance test was used to evaluate the postural balance performance of each subject. In addition, a questionnaire was also used to obtain information regarding history of fall and physical environment.

Non-parametric, two-way ANOVA was used to compare the effect of age and physical activity level on Berg balance score. Significant level was accepted at $p < 0.05$.

RESULTS AND DISCUSSION

Ability to maintain balance was found to be more influenced by physical activity level as compared to age. When compared within age group, physical activity level was shown to effect Berg balance score (BSS). The high physical activity group demonstrated a significant higher BBS than the low physical activity group (Table 1). These results suggest that active elderly persons would be able to maintain the ability to control both static and dynamic balance regardless of their age.

In the low and moderate activity level groups, the effect of age on BBS was accentuated. Significantly lower BBS was observed in older elderly groups as compared to the younger elderly groups (Figure 1). In addition, the lowest BBS of 41.5 was found in older elderly with low activity level. These results indicated that elderly persons with low physical activity level would be more susceptible to fall as compared to elderly persons with higher physical activity levels. Furthermore, these results also supported that higher activity level will enable the elderly persons to maintain their balance performance.

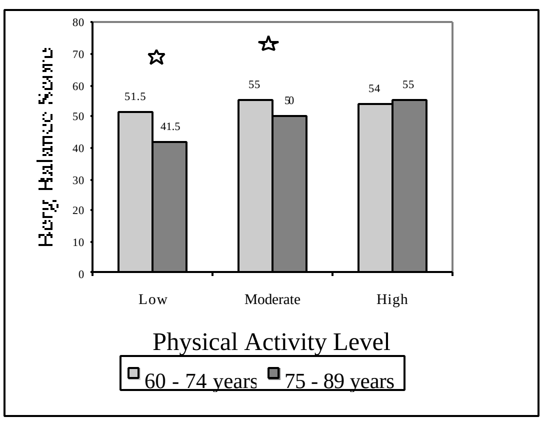

Figure 1: Comparison of Berg balance score between two age groups at low, moderate and high physical activity levels (*p<0.05).

CONCLUSION

Physical activity such as going outdoors, sports and daily exercise, and activity of daily living, is shown to influence both static and dynamic balance performance in elderly persons as indicated by the BBS. Elderly persons with high physical activity are able to maintain their balance. Whereas, the elderly persons with low physical activity are at a greater risk of fall due to decreased control of balance.

REFERENCES

Berg, K.O. (1989). *Physither Can*, **41**, 240-6.

Gill, T.M. et al. (1995). *J. Am Geriatr Soc*, **43**, 603-9.

Jitapunkul, S. et al. (1998). *J. Med Assoc Thai*, **81**, 233-42.

Liechtenstein, M.J. et al. (1988). *J. AM Geriatr Soc*, **36**, 996-1002.

Lord, S.R. et al. (1994). *J. AM Geriatr Soc*, **42**, 1110-7.

Tinetti, M.E. et al. (1995). *J. Am Geriatr Soc*, **43**, 1214-21.

Table 1: Median (Q1, Q3) of Berg balance score of six groups of subjects

Group	Median (Q1,Q3)	p-value
60-74 years High (n=22)	54.0 (51.0,56.0)	$p = 0.025$ *
Moderate (n=25)	55.0 (51.0,56.0)	
Low (n=20)	51.5 (46.25,55.0)	
75-89 years High (n=12)	55.0 (50.75,56.0)	$p = 0.001$ *
Moderate (n=20)	50.0 (45.25,53.0)	
Low (n=20)	41.5 (37.5,50.75)	

* = Statistically significant difference at p-value< 0.05

A PASSIVE DYNAMIC WALKING MODEL THAT WALKS ON LEVEL GROUND

Mario W. Gomes[1] Andy L. Ruina[2]

Department of Theoretical and Applied Mechanics
The Human Power, Biomechanics, and Robotics Laboratory
Cornell University, Ithaca, NY, USA
http://www.tam.cornell.edu/ ruina/hplab
[1]mwg1@cornell.edu [2]ruina@cornell.edu

INTRODUCTION

Previous walking models based on passive elements with no control (so called passive-dynamic models) consume gravitational energy as they walk downhill. This gravitational energy may be thought of as a primitive proxy for simple muscular activation. These models may be relevant to human walking because they manage to mimic aspects of human gait while also using little energy. Assuming that evolution favors energetic efficiency, it is natural to wonder how energetically efficient a walking mechanism can be. Previous passive-dynamic walkers have previously been shown to be (theoretically) capable of a perfectly efficient gait (zero specific cost of transport) in the limit of infinitely slow walking. Here we show a new passive-dynamic walking model that is capable of walking at finite speed on level ground. That is, it consumes no energy to walk. This is achieved by finding a mechanism that has only zero-velocity collisions with the ground. The mechanism we have found does use elastic springs, a model component not used in many previous passive-dynamic simulations.

METHODS

The model we examine consists of three rigid bodies coupled to each other by pin joints and torsional springs and is depicted in Figure 1. These represent two legs and a torso. As for the previous simpler 2D kneeless theoretical passive-dynamic models, we assume that the swing foot is able to pass by the stance foot without scuffing the ground. We restrict ourselves to searching for motions where only one foot is in contact with the ground at any moment (double support only lasts for an instant).
There is no external energy put into the system and the only way mechanical energy can leave the system is from a collision between the swing foot and the ground. Since we are looking for perfectly energy efficient motions, we need to look for motions with no non-zero-speed collisions. We must find periodic motions where the swing foot has dissipation free collisions with the ground (collides with the ground at a relative velocity of zero).
We set up the differential equations for the model shown in Figure 1. The search for periodic dissipation free solutions is a root finding problem that we solve by a mixture of heuristic and formal numerical

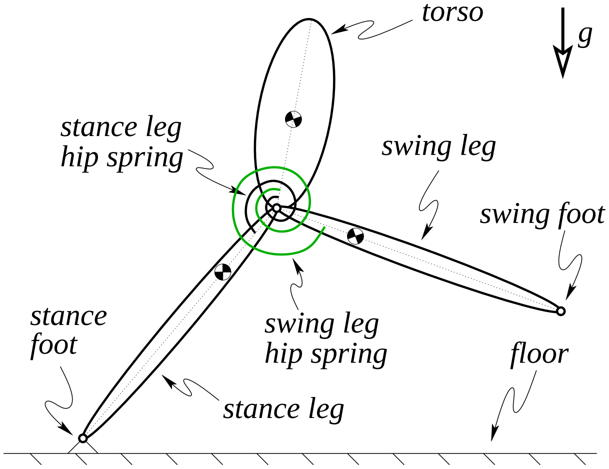

Figure 1: A 3link walker, which is capable of collisionless walking motions

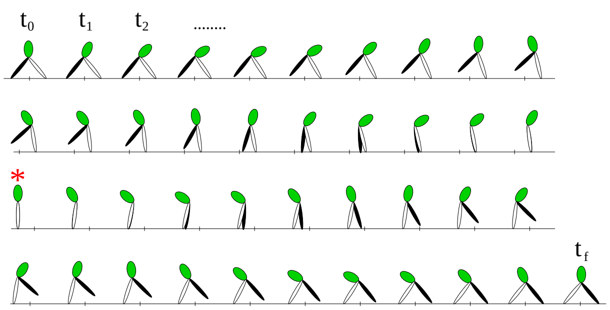

Figure 2: A collisionless walking motion of the 3 link model

methods where both the initial conditions and the system parameters can be varied.

RESULTS

For this model, we were able to find many such solutions. Typically we could find one such solution for each appropriate combination of parameters.

These collisionless walking motions are somewhat reminiscent of cartoon characters exaggerated walking motions when trying to sneak up on something without making a noise.

SUMMARY

Perfectly energy efficient walking with a non-zero step length is possible with a rigid body model. The addition of an upper body coupled with springs allows these collisionless motions to progress forward without dissipation. This mechanism for the avoidance of collisions when walking might be seen when attempting to walk very quietly or on thin ice and may provide some intuitive guidance about mechanisms that the human design and coordination strategies might use.

REFERENCES

Chatterjee, A., Garcia, M. (2000), Dynamics and Stability of Systems, v15, No 2, 139-157.

Chatterjee, A., Reddy, C., Ruina, A. (2002), International Journal of Robotics Research, v21, No 7, 621-634.

ACKNOWLEDGEMENTS

This work was partially funded by an NSF biomechanics grant and NSF IGERT program. We thank Anindya Chatterjee for his inspirational ideas concerning these collisionless motions.

THE STABILITY OF THE LYAPUNOV EXPONENT AT DIFFERENT SAMPLING FREQUENCIES DURING TREADMILL WALKING

Scott M. Keenan[1], Nick Stergiou[1], Max J. Kurz[1], Jack Heidel[2] and Daniel Blanke[1]

[1]HPER Biomechanics Lab, University of Nebraska at Omaha, Omaha, NE, USA
[2]Department of Mathematics, University of Nebraska at Omaha, Omaha, NE, USA
Email: nstergiou@mail.unomaha.edu Web: www.unocoe.unomaha.edu/hper.htm

INTRODUCTION

Human locomotion has been shown to vary from one stride to the next. The examination of this variability has been recently conducted with tools from nonlinear dynamics, such as the Lyapunov Exponent (LyE; Dingwell et al., 2000; Buzzi et al., 2003). The LyE allows biomechanists to examine variations during locomotion that were once believed to be just noise. The LyE is a measure of the rate at which nearby trajectories from a time series in phase space diverge (Sprott and Rowlands, 1992). It is a measure of the stability of a dynamical system and its dependence on initial conditions. However, its usage with time series of biomechanical data implies that we know how many strides (footfalls) and data points we should collect. This information is currently unknown. Recently, Keenan and Stergiou (2002) analyzed time series collected at 180 Hz from a tibia located accelerometer during walking on a treadmill. They found that after thirty footfalls (FF), and approximately 6,000 data points, the LyE is a statistically stable nonlinear tool. Thus, they suggested that these numbers are the minimum criteria of a data collection for an accurate assessment of the LyE during treadmill walking. However, they also suggested that their study should be replicated with different sampling frequencies to investigate the interplay between number of data points and the number of FF. Thus, the purpose of this study is to examine the stability of the LyE at different sampling frequencies during treadmill walking.

METHODS

Twenty subjects with no known pathologies were asked to walk on a treadmill at a self-selected pace while accelerometer data were collected at 180 Hz for 80 continuous FF. The accelerometer (PCB Piezotronics) was attached at the subjects' distal anteromedial aspect of the right tibia. The time series were reconstructed at 120 and 60 Hz using Shannon's sampling theorem (Hamill et al., 1997). This algorithm reconstructs points based on frequencies present in the original signal. The time series from the 60 and 120 Hz sampling frequencies were then separated and analyzed using the number of FF. The first analysis consisted of the initial five FF (Keenan and Stergiou, 2002). Then, five FF were added to each subsequent analysis, until 80 FF were included. The LyE was calculated for each one of the analyses groups using the Chaos Data Analyzer (Sprott & Rowlands, 1992). All LyE calculations were performed using five embedded dimensions. The embedded dimension was calculated from a Global False Nearest Neighbor analysis (Abarbanel, 1996). Mean group values for LyE from each sampling frequency were analyzed using a repeated measures ANOVA ($p<0.05$) with a Tukey test as post-hoc.

RESULTS AND DISCUSSION

The ANOVA results indicated significant differences between the mean group values. The post-hoc analysis for the frequency of 60 Hz revealed numerous statistical differences between the small groups of FF (5, 10, 15, 20, and 25) and the large ones. However, no differences between groups were found from the 30 FF and beyond. For the 120 Hz, the post-hoc analysis indicated similar results with the exception that no differences between groups were found from the 50 FF and beyond. It is important to notice here that for the 60 Hz, 30 FF correspond to approximately 2000 data points. For the 120 Hz, 50 FF correspond to approximately 5000 data points. In the table below we can see that no matter the sampling frequency, as the data points increase, the LyE values become statistically similar. However, what was very interesting is the fact that the number of data points, where the LyE values stabilized statistically, was different between frequencies. Actually, they increased from 2000 to 6000 as the sampling frequency increased. There was more similarity regarding the number of FF, since for both 60 and 180 Hz, the absolute minimum was 30 FF.

SUMMARY

The time series collected from a tibia located accelerometer were used to evaluate the stability of the LyE at different frequencies during treadmill walking. Our study attempted to find out the minimum numbers of data points and cycles of movement that we need to establish a stable and accurate LyE. Our results indicated that regardless the sampling frequency, a larger number of data points is better for LyE calculations. However, regarding the actual cycles of movement, it seems that somewhere between 30 and 50 cycles are needed for an accurate assessment of the LyE during treadmill walking. Lastly, we still feel that we have generated even more questions, regarding the validity of our results for over ground walking and other types of cyclic movements. In addition, it will be interesting to examine the repeatability of our findings with actual data from the different frequencies and not from reconstructed.

REFERENCES

Abarbanel, H.D.I. (1996). *Analysis of Observed Chaotic Data*, Springer-Verlag.

Buzzi, U.H. et al. (2003). *Clin Biomech*, in press.

Hamill, J. et al. (1997). *J Appl Biomech*, **13**,226-238.

Dingwell, J.B. et al. (2000). *J Biomech*, **33**, 1269-1277.

Keenan, S.M., Stergiou, N. (2002). *Proc World Congress Biomech*.

Sprott, J., Rowlands, G. (1992). *Chaos Data Analyzer*. American Physics Institute.

Table 1: LyE group means based on footfalls. 180 Hz data are from Keenan & Stergiou (2002).

		5 FF	**10 FF**	**15 FF**	**20 FF**	**25 FF**	**30 FF**	**35 FF**	**40 FF**
WALK – LyE	**60Hz**	0.091	0.162	0.147	0.137	0.146	0.152	0.149	0.159
	120Hz	0.155	0.174	0.181	0.188	0.196	0.195	0.196	0.201
	180Hz	0.131	0.144	0.155	0.158	0.160	0.157	0.161	0.163
		45 FF	**50 FF**	**55 FF**	**60 FF**	**65 FF**	**70 FF**	**75 FF**	**80 FF**
WALK – LyE	**60Hz**	0.159	0.162	0.163	0.165	0.164	0.164	0.165	0.167
	120Hz	0.206	0.208	0.213	0.217	0.217	0.217	0.221	0.223
	180Hz	0.166	0.170	0.170	0.170	0.171	0.172	0.174	0.170

CONTROL OF BODY SEGMENT ORIENTATION RELATIVE TO THE REACTION FORCE MAINTAINS LOWER EXTREMITY LOAD DISTRIBUTION

W. Mathiyakom,[1] J. L. McNitt-Gray,[1,2,3] and Henryk Flashner[1,3,4]
Departments of [1]Kinesiology, [2]Biomedical Engineering, [3]Integrative and Evolutionary Biology and [4]Aerospace and Mechanical Engineering
University of Southern California, Los Angeles, CA, USA
mcnitt@usc.edu

INTRODUCTION

Identification of control strategies implemented during impulse generation under diverse conditions reveals how constraints imposed by task objectives influences motor behavior and distribution of mechanical load within the musculoskeletal system. Impulse applied to the ground is result of coordinated activation of muscles that accelerate and perform mechanical work on the segments. For example, during tasks requiring the generation of vertical impulse (e.g. maximum vertical jump), orientation of the segments during impulse generation influences the proportion of segment energy contributing to the task objective (Bobbert and van Soest, 2001). However, during tasks requiring the generation of angular impulse, the reaction force must pass a distance from to the total body center of mass (TBCM) such that a net angular impulse in the desired direction is generated during contact with the ground.

In this study, we hypothesized that the distribution of net joint moments across lower extremity joints would differ between related tasks requiring generation of horizontal reaction forces in opposite directions. To test hypothesis we compared ankle, knee, and hip net joint moments (NJM) generated during the take-off phase of back (translate and rotate backward) and reverse (translate forward, rotate backward) somersaults. We expected that the distribution of the mechanical demand imposed on the lower extremity joints would be dependent on the orientation of the reaction force in global space.

METHODS

Skilled athletes (n=6) performed a series of back and reverse somersaults from a force plate onto a foam pit in accordance with the Institutional Review Board. Reaction forces were recorded using a force plate (600 Hz, Kistler, 0.4 x 0.6m force plate). Sagittal plane kinematics were recorded simultaneously using digital video camera (60Hz, AG455, Panasonic). Each coordinate of the body landmarks (de Leva, 1996) were digitized, filtered using a fourth order Butterworth Filter (Saito & Yokoi, 1982) with cut-off frequencies determined using a method based on Jackson (1979). Kinematic and reaction force data were synchronized at the time of last foot contact with the force plate. Joint kinetics were determined using Newtonian mechanics.

RESULTS AND DISCUSSION

No significant differences in ankle, knee, and hip NJMs during the push phase were observed between tasks (Figure 1). These results support the hypothesis the mechanical demand imposed on the ankle, knee, and hip is dependent on the orientation of the reaction force relative to foot, shank, and thigh segments.

As in horizontal jumping (Ridderikhoff et al., 1999), performers positioned their total TBCM relative to the feet in the direction of desired horizontal impulse (Back: backward; Reverse: forward). The need to strategically position the TBCM relative to the feet contributed to between task differences in segment orientation in global space. To achieve between task differences in the direction of horizontal impulse generation, between task differences in resultant force orientation were also observed between tasks. As a result, no significant differences in the relative angle between the segments and reaction force and net joint forces were observed between tasks.

Individuals participating in this study may have found that generation of impulse using the same set of NJMs advantageous from both a physiological and control perspective. Generation of near maximum levels of impulse requires that muscles contributing to the NJMs generate force at advantageous lengths and rates (Herzog et al., 1991).

SUMMARY

Identification of control strategies implemented under diverse conditions reveals how constraints imposed by task objectives influences motor behavior and mechanical load distribution within the musculoskeletal system. In this study, we hypothesized that the distribution of NJMs across lower extremity joints would differ between related tasks requiring generation of horizontal reaction forces in opposite directions. Despite the between-task differences in linear impulse generation, no differences in NJMs were observed. Generation of impulse using the same set of NJMs may prove to be advantageous from both a physiological and control perspective.

REFERENCES

Bobbert, M.F., van Soest, A.J. (2001). *Exerc Sports Sci Rev*, **23**, 95-102.

de Leva, P. (1996). *J Biomech.* **29**, 1223-1230.

Herzog, W. et al. (1991). *Med Sci Sports Exerc*. **23**, 1289-1296.

Jackson, K. M. (1979). *IEEE Trans Biomed Eng.* 26:122-124.

Ridderikhoff, A. et al. (1999). *Med Sci Sports Exerc*, **31**, 1196-1204.

Saito, S., and T. Yokio. (1982). *T. Bull of Health and Sport Science, University of Tsukuba*. 201-206.

ACKNOWLEDGEMENTS Intel, USOC NGBs

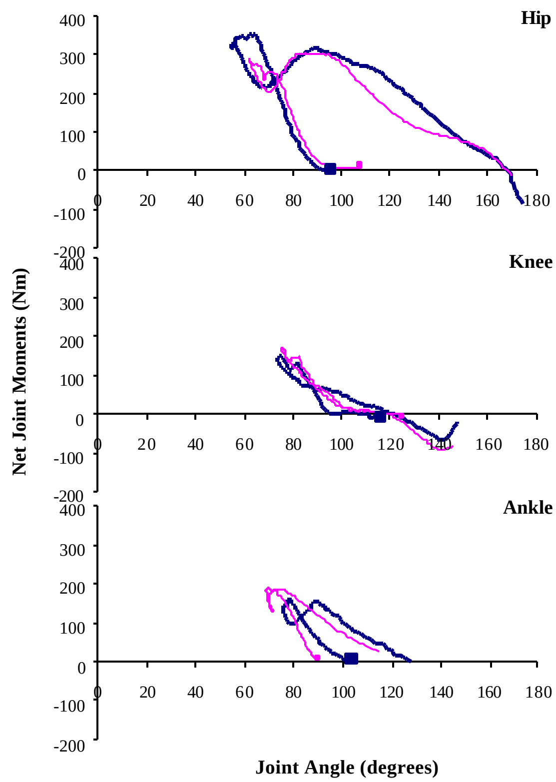

Figure 1. NJMs at the hip, knee and ankle joint during the back (thick line) and reverse saltos (thin line) of an exemplar subject. Note between-task similarities in NJM magnitude and joint range of motion where the NJMs were generated.

CONTROLLING BIFURCATIONS AND CHAOTIC GAIT WITH HIP JOINT ACTUATIONS IN A SIMPLE WALKING MODEL

Max J. Kurz[1], Nicholas Stergiou[1] and Terry Foster[2]
[1]HPER Biomechanics Laboratory, University of Nebraska at Omaha, Omaha, NE
[2] College of Engineering and Technology, University of Nebraska at Omaha, Omaha, NE
E-mail: mkurz@mail.unomaha.edu Web: http://www.unocoe.unomaha.edu/hper.htm

INTRODUCTION

Current investigations have indicated that human walking has a chaotic structure (Buzzi *et al.*, 2003). In addition, Garcia *et al.* (1998) developed a passive dynamic walking model that exhibits period doublings that appear to lead to chaos (Garcia *et al.*, 1998). Recently, we have replicated Garcia *et al.*'s work and have confirmed the presence of chaos through a rigorous exploration of the Lyapunov Exponents (LyE) of the model's gait (Kurz and Stergiou, 2003). In this present investigation we added a torsional hip spring actuator to the model that provided a burst of energy to the swing leg during gait. Our inspiration for adding a hip joint actuator was based on previous investigations that have indicated that parametric forcing could be used to control bifurcations in a pendular apparatus (Starrett & Tagg, 1995). We speculated that hip joint actuation may provide similar forcing that would allow for the control of chaotic gait in the model. Thus, the purpose of this investigation was to explore the effect of hip joint actuation on the control of the dynamics of the model.

METHODS

The passive dynamic gait model consists of two rigid legs connected by a frictionless hinge at the hip (Figure 1). We supplied actuation of the hip joint using a torsional spring. Energy was supplied to the model via a sloped walking surface. Two coupled second-order differential equations were used to define the behavior of the legs. The equations of motion were simplified by

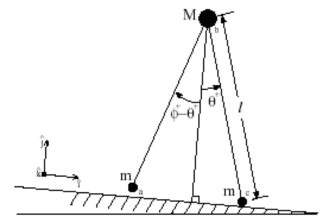

Figure 1: Chaotic passive dynamic walking model (Garcia *et al.*, 1998).

assuming that the mass of the model was concentrated at the hip.

$$\ddot{\theta}(t) - \sin(\theta(t) - \gamma) = 0$$

$$\ddot{\theta}(t) - \ddot{\phi}(t) + \dot{\theta}(t)^2 \sin\phi(t) - \cos(\theta(t) - \gamma)\sin\phi = k\phi(t)$$

where θ is the stance leg angle, ϕ is the swing leg angle, k is the normalized torsional spring constant, and γ is the ramp angle. Simulating the model consisted of integrating the equations of motion and applying a transition rule at heel-contact. Similar to Garcia *et al.* (1998), we modeled heel-contact as instantaneous and perfectly inelastic.

The model was simulated for 5000 steps at each ramp angle with no hip joint actuation ($k=0\ s^{-2}$). The first 500 steps of the simulation were discarded. Poincaré sections were used to confirm the order of the gait simulations (Figure 2). The Poincaré section was composed of the angular displacement vs. the angular velocity for the initial conditions of the stance leg for each step in the simulated gait. An increased number of orderly points in the section indicated higher order gaits. LyE were calculated from the data used to create the Poincaré sections to confirm the presence of chaos. A positive LyE value indicated a chaotic gait pattern.

Once all period-n gaits were identified, we systematically increased hip joint actuation at each of the period-n gaits. The effect of hip joint actuation was determined through inspection of the Poincaré sections.

RESULTS AND DISCUSSION

With no added hip joint actuation, the model had a cascade of bifurcations that lead to a chaotic gait pattern as γ was increased (i.e. period-one, period-two, period-four, etc.). A chaotic gait pattern was present for slopes of 0.01839 rad < γ < 0.019 rad (LyE range = +0.002 to +0.158). Our simulations also indicated that hip joint actuation was a mechanism to control the cascade of bifurcations that lead to chaos in our walking model. As the hip joint actuation was increased, the order of the period-n gait at γ was decreased. For example, a period-8 gait was reduced in order to a period-4 gait to period-2 gait to period-1 gait as the hip joint actuation was systematically increased (Figure 2). Our simulations suggest that altered hip joint actuation may be related to modifications in the chaotic structure of gait patterns previously seen in pathological populations (Buzzi *et al.*, 2003).

Adjustments in hip joint actuation appeared to be most beneficial in regions where the model was not previously able to walk. Without the addition of hip joint actuation (k=0 s^{-2}) the model would fall down at ramp angles larger than 0.019 rad. However, the addition of hip joint actuation allowed the model to walk with a chaotic gait at ramp angles that were previously considered unstable. Buzzi *et al.* (2003) suggested that a chaotic gait is more stable due to greater flexibility in the gait pattern. We suggest that modifications in hip joint actuation may be a mechanism to help the gait pattern remain in the chaotic basin of attraction where the neuromuscular system can take advantage of such flexibility.

SUMMARY

Simulations of the walking model indicate that hip joint actuation is a mechanism to control the structure and stability of chaotic gait. These simulations provided a novel mechanical approach to explain how the biological system functions to control chaotic gait.

ACKNOWLEDGEMENT

This investigation was funded in part by the UNO Rhoden Biological Research Fellowship granted to Max J. Kurz.

REFERENCES

Buzzi U.H. *et al.* (2003). *Clin. Biomech.*, in press.

Garcia M. *et al.* (1998). A*SME J. Biomech. Eng.* **120(2)**:281-8.

Kurz M.J., Stergiou, N. (2003). *Proc. of NASPSPA,* Savanna, GA.

Starrett, J., Tagg R. (1995). *Phys. Rev. Let.* **74(11)**:1974-1977.

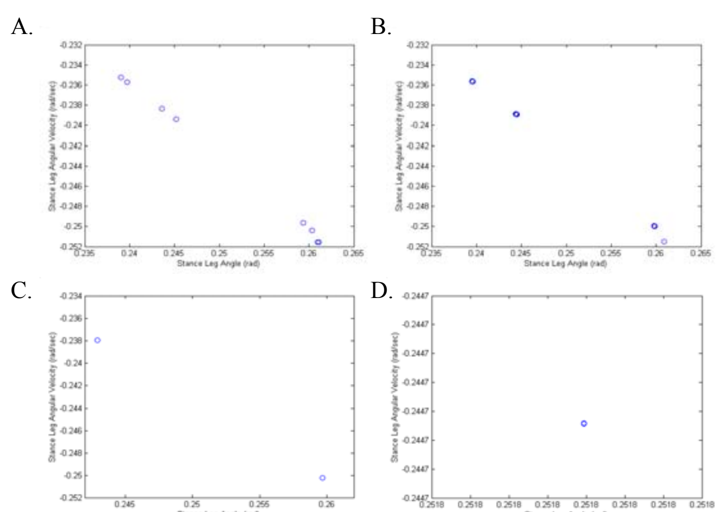

Figure 2: Poincaré sections for the model while walking at γ = 0.01823 rad and k=0 s^{-2} (A), k=0.001 s^{-2} (B), k=0.01 s^{-2} (C), k=0.06 s^{-2} (D).

A MODEL FOR THE GENERATION OF SYNTHETIC SURFACE EMG SIGNALS

David A. Gabriel

Biomechanics Laboratory, Brock University, St. Catharines, ON, Canada L2S 3A1
E-mail: dgabriel@arnie.pec.brocku.ca

INTRODUCTION

A volume conduction model for generating surface electromyographic (SEMG) signals was developed. The model will be used to validate interference pattern (IP) analysis as a method for studying motor unit (MU) firing patterns. The advantage of this approach is that it allows an *a priori* knowledge of the MU firing patterns that generated the SEMG signal.

METHODS

Model Description: The model was based on volume conducted current (Plonsey, 1974). The potential at a point in the field due to impulses propagated along the muscle fiber of unlimited length is given by equation 1, where V is a Gaussian function for the intracellular potential, x is the coordinate for length of the muscle fiber, r is the distance from the point electrode in the conducting medium to the element of the fiber dx.

$$\Phi(P) = -\frac{1}{4\pi}\int_{-\infty}^{+\infty}\frac{\partial^2 V}{\partial x^2}\frac{1}{r}\,dx \qquad \text{eq. 1}$$

The analytic solution (eq. 2) describes the motor unit action potential ($MUAP$) as a function of time (t).

$$MUAP(t) = ne^{-\frac{t^2}{B^2}}\left[A_1\left(\frac{2}{B^2}t^2 - 1\right) - A_2 t\right] \qquad \text{eq. 2}$$

Values of the coefficients (n, A_1, A_2, and B) were selected to shape the MUAP according to the standard triphasic waveform outline by DeLuca (1975) and depicted in Figure 1.

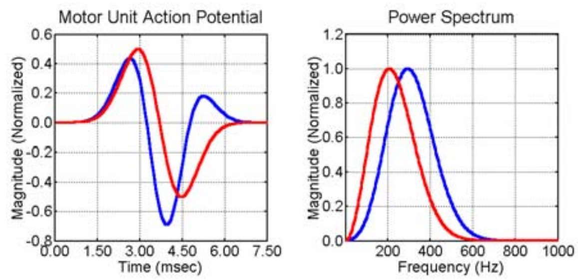

Figure 1: Simulated biphasic (red) and triphasic (blue) motor unit action potentials.

The standard MUAPs were shaped to match empirical observations for the biceps brachii. Amplitude (412 ± 79 µV to 972 ± 117 µV) and firing frequency (17.8 ± 5.5 Hz to 24 ± 4.1 Hz) were taken from Moritani and Muro (1987). Duration (33-50 msec) was given by Dumitru et al. (1999). Sixty-five MUs were used, consistent with the pick-up area of surface electrodes.

MUAPs were inserted at normally distributed intervals corresponding to ±20% of firing frequency. The MUAP trains were then summated to generate the IP. The result was passed through two transfer functions (Lindström and Magnusson, 1977). The first (eq. 3), accounted for low-pass tissue filtering. It is the ratio of two modified Bessel functions of the second kind and zero order (K_0), where ω is angular frequency, v (4.0 m/sec) is muscle fiber conduction velocity, h (2.0 mm) is distance from the electrode, and a (100 µm) is muscle fiber radius.

$$\Psi(\omega) = \frac{K_0(\omega h / v)}{K_0(\omega a / v)} \qquad \text{eq. 3}$$

The second function (eq. 4), accounted for the filtering properties of bipolar surface electrodes. The variable d (1 cm) is the inter-electrode distance. This function acts as a "comb" filter canceling out some frequencies while allowing others through.

$$\Psi(\omega) = \sin^2\left(\frac{\omega d}{2v}\right) \qquad \text{eq. 4}$$

Experimental Validation: Six subjects (2 males and 4 females) performed 5 maximal voluntary contractions (MVCs) of the elbow flexors on the Biodex System III (Biodex Medical Systems, Shirley, NY). The MVCs were 2 seconds in duration at 1-minute rest intervals. Biceps SEMG was monitored with DE-2.1 (Delsys Inc., Boston, MA) electrodes. The SEMG signals were amplified (1000×) and band-passed filtered (20-450 Hz) using the BAGNOLI-4 (Delsys Inc.) bioamplifier, before A/D conversion at 2 kHz (CODAS, DATAQ Instruments Inc., Akron, OH) on a Pentium III IBM-PC. Mean power frequency (MPF) was calculated on a 512 msec stationary portion of the signal in MATLAB (The Math Works, Natick, MA).

RESULTS AND DISCUSSION

The average MPF for the sample was 75 ± 7 Hz. The range was from 65 to 92 Hz. These values are slightly lower than the 89 ± 13.3 Hz to 123 ± 23.5 Hz reported by Moritani and Muro (1987) for ramp isometric contractions of the elbow flexors. However, the two distributions certainly overlap. The discrepancy may be explained by differences in body composition due to the inclusion of female subjects in the present study, who were in the majority.

Figure 2 illustrates a representative power spectrum from one subject, and for a synthetic biceps SEMG signal. Since the strongest contributor to the power spectrum is MUAP duration, all other variables were held constant and the proportion of MUs between the 35 and 50 msec range was manipulated. The resulting synthetic SEMG signals had MPFs that ranged between 62 and 88 Hz. Clearly, these values are comparable with that of the experimental data. The close similarity between experimental and simulated power spectra suggests that the model was able to faithfully generate synthetic SEMG signals.

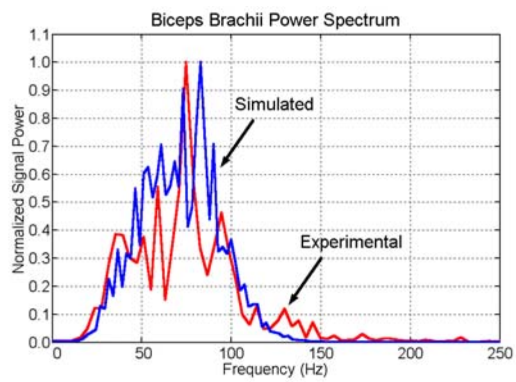

Figure 2: Power spectrum from one subject (red) and from simulated SEMG (blue).

SUMMARY

A volume conduction model of SEMG activity with physiological parameters for the biceps brachii can produce realistic power spectra.

REFERENCES

DeLuca, C.J. (1975). *Biol. Cyber.*, **19**, 159-167.
Dumitru, D. et al. (1999). *Clin. Neurophysiol.*, **110**, 1876-1882.
Lindström, L.H., Magnusson, R.I. (1977). *Proc. IEEE*, **65**, 653-662.
Moritani, T., Muro, M. (1987). *Eur. J. Appl. Physiol.*, **56**, 260-265.
Plonsey, R. (1974). *IEEE Trans. Biomed. Eng.*, **21**, 371-381.

A FIVE LINK BRACHIATION MODEL WITH LIFE-LIKE MOTIONS

Mario W. Gomes[1] Andy L. Ruina[2]

Department of Theoretical and Applied Mechanics
The Human Power, Biomechanics, and Robotics Laboratory
Cornell University, Ithaca, NY, USA
http://www.tam.cornell.edu/ ruina/hplab
[1]mwg1@cornell.edu [2]ruina@cornell.edu

INTRODUCTION

We use a periodic solution of a simpler rigid-body model as a starting point to find periodic motions of a system with one more degree of freedom. Unlike a method based on relaxing a spring from infinity, the method is non-singular. A new degree of freedom is added sequentially, with periodic solutions being found at each step in the process: first a point mass is added at a hinge, which has no effect on the complexity of the governing equations; then the point mass is changed to a rigid body with center of mass at the hinge, again with no effect; and then the center of mass is moved slowly away from the hinge, with periodic solutions being found during the growth, a non-singular homotopy process. Alternatively, to add a degree of freedom by breaking one link into two, the new hinge degree of freedom is endowed with a relative-motion inertia of infinity, causing no change to the dynamics from the one-link case. The inertia is then slowly relaxed to zero in a smooth process, with periodic motions being found at each step of the relaxation.

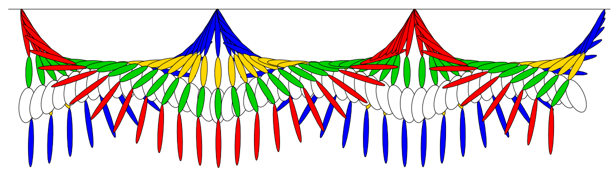

Figure 1: A ricochetal collisionless motion for the 5 link model

DISCUSSION AND RESULTS

A central part of some biomechanics locomotion simulations is the finding of periodic orbits of. This search can be difficult in itself. And, as the number of degrees of freedom increase, the problem of finding the biologically relevant solutions, for example solutions that are not double or triple flips, becomes increasingly difficult. We describe here a method for adding degrees of freedom to a system in a continuous manner so that one can find periodic solutions of interest in these higher degree of freedom systems based on solutions of a lower-degree-of freedom model.

The method was applied to a series of brachiating ape models in order to find a realistic collisionless periodic motion for a ricochetal 5 link brachiating ape. We implemented a rigid body simulation in C++ capable of handling a variety of

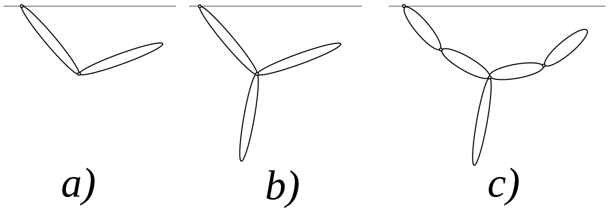

Figure 2: Progression of collisionless brachiation models, from the two arm model(a), to the two arms with torso model(b), to the two forearms with two uperams with torso model (c)

brachiating ape models. Using this simulation we first conducted a brute force search for periodic collisionless motions in a 2 link model (two arms and a point mass body). Having mapped out all of those solutions we used our homotopy method to grow additional degrees of freedom in a continuous manner while tracking the relevant solution. First a torso was added to the middle of the 2 link system thereby increasing the degrees of freedom from 2 to 3. Next both arms were broken in half with both pieces of each arm linked to each other through a rotary inertia (shown in Figure 3) which resists relative motion of the two arm segments, resulting in the final 5 link system. Periodic solutions were found for this five-link model (9 dimensional map) that maintained the pleasing simplicity of the two-link solutions. (As a point of comparison, 2D kneed passive dynamic walking models with 4 links are described with a 5 dimensional map.)

CONCLUSION

This homotopy method seems to be an improvement over trial and error using root-finding routines applied directly to the higher degree of freedom system. The method yielded a path to a relevant periodic solution in a reasonably complex biomechanical system and shows promise for yet-more complex systems.

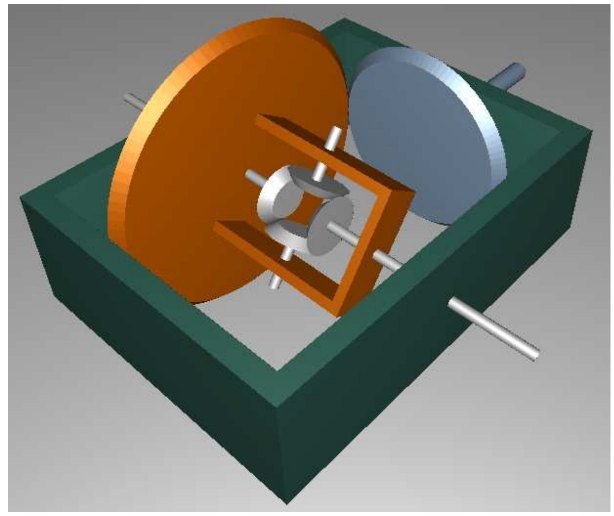

Figure 3: Schematic of a differential used for growing situations requiring a coupling inertia as the continuation parameter

REFERENCES

Bertram, J., Ruina, A., Cannon, C.,Chang Y., Coleman, M. (1999), Journal of Experimental Biology, v202, 2609-2617.

Chatterjee, A., Reddy, C., Ruina, A. (2002), International Journal of Robotics Research, v21, No 7, 621-634.

ACKNOWLEDGEMENTS

This work was partially funded by an NSF biomechanics grant and NSF IGERT program.

Metabolic Cost and Muscle Contraction during Human Leg Swing

Jiro Dokeh and Arthur D. Kuo
Biomechanics Research Laboratory, University of Michigan, Ann Arbor, MI, USA
E-mail: jdokeh@umich.edu

INTRODUCTION

Leg swing is an important part of human locomotion. Evidence suggests that pendular dynamics may be responsible for much of the swing phase of gait (Mochon, McMahon, 1980). As it would require mechanical energy to swing a pendulum fast, it may require metabolic energy to swing a leg at a high frequency. Studies have shown that short, intermittent contraction of muscles cost more energy than long, sustained contractions (Hogan et al. 1998). We hypothesize that the increase in metabolic cost of leg swinging at high frequencies may be linked to short bursts of muscle contractions. In this study, we measured the metabolic cost of swinging the leg, isolated from walking.

We constructed an ergometer that measured metabolic, kinematics, and kinetics data as subjects stood on one leg and swung their other leg at various frequencies. Metabolic cost increased sharply as swing frequency increased, while muscle contraction time decreased with swing frequency.

METHODS

Twelve healthy young adults (6 males, 6 females; body mass = 64.8 ± 8.3 kg, leg length = 0.88 ± 0.07 m, mean ± SD) consented to participate in this study. Seven different swing frequencies, ranging from approximately 0.5 to 1.1 Hz, were tested on each subject's left leg. For each frequency, metabolic, kinematics, and kinetics data were collected. At a later session, electromyographic (EMG) data were collected on the same 6 male subjects during the leg swing conditions.

The leg swing apparatus consisted of a metal frame that supported the upper body of the subject, and was placed on a force plate to measure the kinetics (Figure 1). An optical encoder was attached to the swing leg to record the kinematics of the leg. The subjects wore a mouthpiece connected to an open circuit respirometry system for measuring metabolic data.

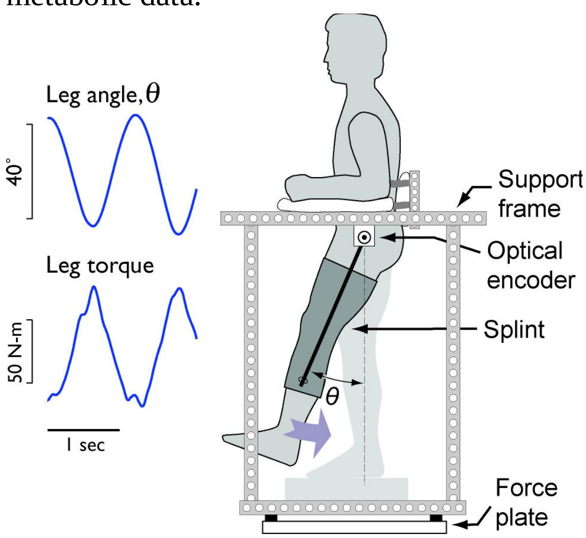

Figure 1: Leg Swing Apparatus. The graphs show sample of leg angle and computed leg torque data.

Subjects received visual feedback of their leg angle against a constant target amplitude, with frequency enforced by a metronome. Each trial ran for six minutes to allow oxygen consumption to reach steady state, with the last three minutes used for analysis. For EMG measurements, we recorded muscle activity from one hip flexor (Rectus Femoris) and two extensors (Medial Hamstring and Gluteus Maximus) using surface EMG electrodes, as subjects swung their leg at the same range of frequencies for 1 minute each.

RESULTS AND DISCUSSION

One possible cause for an increase in metabolic cost is the amount of mechanical work done on the leg during leg swing. Assuming constant muscle efficiency, we can expect the metabolic cost to increase in proportion to the mechanical work (*work hypothesis)*. Pendular mechanics suggest that metabolic power would increase roughly with the 3rd power of the swing frequency. Yet another cause for metabolic increase is the cost for the muscle to produce short bursts of force (Roberts et al., 1997), proportional to force divided by burst duration (*force/time hypothesis)*. With this hypothesis, we predict the metabolic power to increase roughly with the 4th power of the swing frequency.

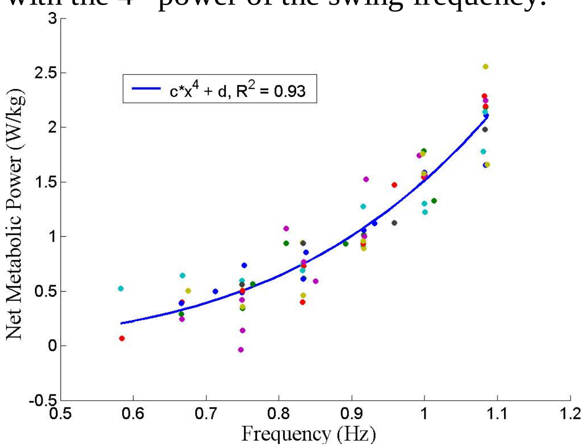

Figure 2: Net metabolic power increased by roughly (freq)^4. Cost of standing quietly was subtracted from overall power to yield net.

We found that the metabolic cost increased sharply with leg swing frequency. Metabolic power also increased to the 4th power of swing frequency (R^2 = 0.93; Figure 2). This suggests that the metabolics of leg swinging at high frequencies may be governed by the *force/time hypothesis*, more so than by the cost of producing work.

EMG measurements showed that contraction durations decreased with increasing swing frequency (Figure 3). Burst magnitudes also increased with frequency. Metabolic cost has been shown to increase with force magnitude, and inversely with burst duration (Roberts et al. 1997), and both may be responsible for the metabolic cost increases observed here.

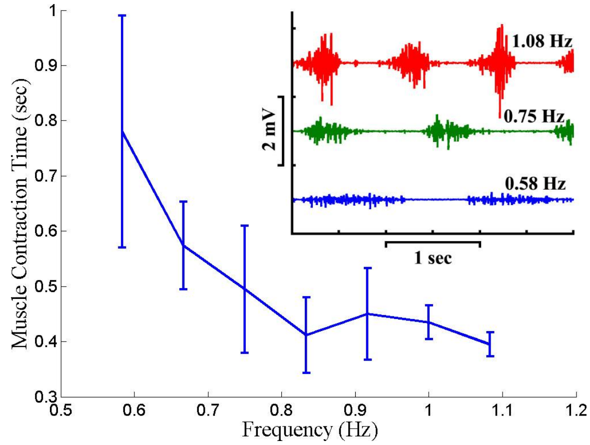

Figure 3: Medial hamstring (MH) contraction duration per cycle. The data is the average of all subjects. The inset displays samples of raw EMG signals from the MH at 3 different frequencies. As the frequency increases, the peak amplitude increases and the contraction time decreases.

These results suggest that much of the metabolic cost of swinging the leg is due to muscles producing high forces for short durations. Some of the mechanical work may be performed by elastic hip tendons, similar to the function of other tendons in running (Roberts et al., 1997). Further comparisons of metabolic cost with the mechanical work performed by muscle will provide more insight as to the relative contributions of muscle work and force to the energetic cost of leg swinging.

REFERENCES

Mochon, S., McMahon, T.A. (1980). *J. Biomech.*, **13**, 49-57.

Hogan, M.C. et al. (1998). *Am. J. Physiol. Endocrinol. Metab.*, **274**, E397-E402.

Roberts, T.J. et al. (1997). *Science*, **275**, 1113-1115.

ACKNOWLEDGEMENTS

This work was supported in part by NIH grant 1R29DC02312.

METABOLIC COST OF HUMAN WALKING AS A FUNCTION OF STEP FREQUENCY

J. Maxwell Donelan [1] and Arthur D. Kuo [2]
[1] Centre for Neuroscience, Dept. of Physiology, University of Alberta, Edmonton
[2] Dept. of Mechanical Engineering and Applied Mechanics, University of Michigan, Ann Arbor
Email: mdonelan@ualberta.ca Web: www.ualberta.ca/~mdonelan/

INTRODUCTION

What determines the metabolic cost of walking? A major contributor is the mechanical work of step-to-step transitions (Donelan, et al., 2002b). During each transition, negative mechanical work is required to redirect the center of mass velocity from one inverted pendulum-like stance phase to the next, and positive work is required to restore the energy lost. The amount of work depends strongly on step length and it exacts a proportional metabolic cost (Donelan, et al., 2002a).

It is unlikely that transition costs are the only major determinant of metabolic cost. Otherwise, cost would be minimized by walking with short step lengths and high step frequencies. Instead, humans typically walk faster by increasing step length and step frequency in almost equal proportion (Kuo, 2001). At a given speed, longer or more frequent steps are penalized by a higher metabolic cost. While transition costs may explain the increase in metabolic cost with longer steps, it cannot explain the increase in cost with more frequent steps. This suggests that there are additional determinants of metabolic cost that depend on step frequency.

We tested for the presence of frequency dependent determinants by studying the metabolic cost of walking at different speeds but with the same step length. Our models of step-to-step transitions predict that under these conditions, transition costs depend upon the third power of step frequency. A stronger dependence of metabolic cost on step frequency is evidence for additional determinants of the metabolic cost of human walking.

METHODS

Model predictions: The simplest two-dimensional passive dynamic walking model predicts that transition costs increase with the third power of step frequency (Equation 1 and Figure 1; Kuo, 2001). During single support phases, the model behaves as an inverted pendulum. Each transition to a new stance limb, modeled as a collision, requires negative work by the leading limb. An equal amount of positive work is required to replace the energy lost. The average rate of both positive and negative mechanical work, $\dot{W}_{\text{trans}}$, scales according to:

$$\dot{W}_{\text{trans}} = f^3 \cdot l^4, \tag{1}$$

where f is step frequency and l is step length. Keeping step length fixed predicts that the average rate of mechanical work increases with the third power of step frequency. This prediction also holds true for a passive dynamic walking model with more anthropomorphic features (Figures 1 and 2). Transition mechanical work exacts a proportional metabolic cost (Donelan, et al., 2002a). As a result, these models predict that the metabolic cost due to transition work will also increase with the third power of step frequency.

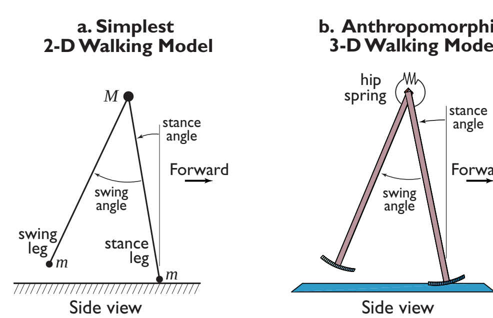

Figure 1. Passive Dynamic Walking Models.

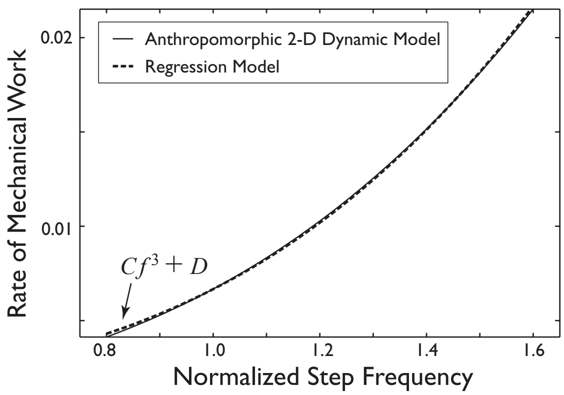

Figure 2. Predicted step-to-step transition work as a function of step frequency.

Experimental Procedures: Nine healthy subjects (4 male, 5 female, body mass 66.0 kg ± 8.4; leg length 0.93 m ± 0.05; mean ± s. d.) provided informed consent. They then walked on a treadmill at 1.25, 1.50, 1.75, 1.90 and 2.00 m/s while matching a metronome set to 1.0, 1.2, 1.4, 1.52 and 1.6 f^*, where f^* is their preferred step frequency at 1.25 m/s (1.81 Hz ± 0.07). This protocol kept step length constant (0.70 m ± 0.03). Simultaneously, we measured metabolic cost using an open circuit respirometry system (Physio–Dyne Instrument Co., Quogue, NY). Following a 3 minute period to allow subjects to reach steady state, we measured the average rates of O_2 and CO_2 production over 3 minutes, and then calculated metabolic rate (Donelan, et al., 2002a). We subtracted the metabolic rate for standing from all walking values and divided by body mass to derive net metabolic rate, $\dot{E}_{\text{met}}$ (W/kg).

RESULTS AND DISCUSSION

Metabolic power depended strongly on step frequency (Figure 3). Increasing step frequency by 60% (1.0-1.6 f^*) caused a 222% increase in metabolic power (2.3-7.3 W/kg). Assuming an equation of the form:

$$\dot{E}_{\text{met}} = C' \cdot f^e + D', \qquad (2)$$

and maximizing R^2, yielded the coefficients C' = 0.78±0.05 W/kg (± 95% c.i.) and D' = 1.52±0.41 W/kg (R^2=0.97). The exponent (e = 4.23±0.39) is statistically greater than expected from the dependence of power on transition work (e = 3).

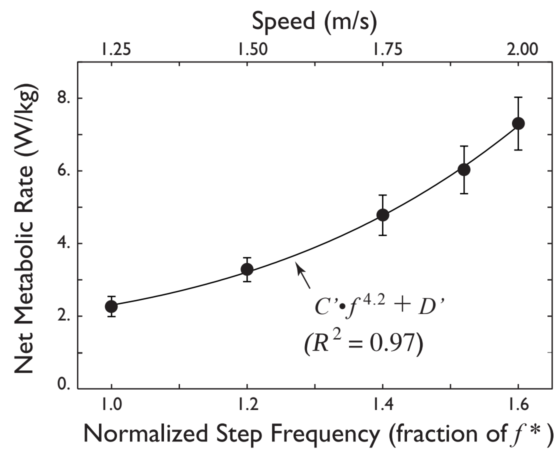

Figure 3. Measured net metabolic rate as a function of step frequency. Plotted values are means ± s.d.

These results indicate that there is at least one determinant of the metabolic cost of walking that depends strongly on step frequency. Due to its frequency dependence, it will have a major contribution to metabolic cost when walking at fast speeds. Two possible determinants are the cost of generating force to swing the legs (Kuo, 2001) and to support body weight (Kram, et al., 1990). The former is predicted to increase with the fourth power of frequency (Kuo, 2001), consistent with our present empirical findings. We are currently studying the metabolic cost of limb swing.

REFERENCES

J. M. Donelan, et al. (2002a) *J Exp Biol* 3717-3727.
J. M. Donelan, et al. (2002b) *J Biomech* 117-124.
R. Kram, et al. (1990) *Nature* 265-267.
A. D. Kuo (2001) *J Biomech Eng-T ASME* 264-269.

ACKNOWLEDGEMENTS

We gratefully acknowledge helpful discussions with R. Kram. This research was supported in part by an NSERC fellowship to J. M. Donelan, NIH grant AR44688 to R. Kram, and NIH grant DC0231201A1 to A.D. Kuo.

REDUCING VERTICAL CENTER OF MASS MOVEMENT DURING HUMAN WALKING DOESN'T NECESSARILY REDUCE METABOLIC COST

Keith E. Gordon[1], Daniel P. Ferris[1] and Arthur D. Kuo[2]

[1]Department of Movement Science and [2]Department of Mechanical Engineering, University of Michigan, Ann Arbor, MI, USA; E-mail: kegordon@umich.edu

INTRODUCTION

In 1953, Saunders, Inman and Eberhart published a highly influential and controversial paper relating the mechanics and energetics of human walking. It proposed that minimizing displacements of the center of mass (COM) during gait minimizes metabolic cost, and listed six kinematic characteristics that reduce center of mass motion. Recent research has questioned the ability of the kinematic characteristics to decrease COM movement.

The purpose of this study was to directly test the hypothesis that minimizing COM displacement leads to minimal metabolic cost during human walking. We tested two cases where a decreased COM displacement might result in increased metabolic cost. In the first experiment, subjects walked at a constant speed but with different stride lengths. Reducing stride length is one way to decrease vertical COM movement but requires swinging the limbs at a faster rate. Increasing leg swing frequency could increase metabolic energy costs because of higher muscle forces (Kuo 2002). In the second experiment, subjects walked at a constant speed and stride length, but reduced their vertical COM motion through visual feedback of pelvis position. Farley et al. (2003) found that subjects increase their metabolic cost under this condition with visual feedback. Increasing limb flexion during stance would decrease COM displacement but would also require greater muscle forces due to a decreased mechanical advantage (Biewener 1989).

METHODS

Seven young healthy adult subjects walked on a treadmill at 1.2 m/s during five conditions: 60, 80, 100 and 120% of their preferred stride length, and 100% of their preferred stride length with visual feedback about position of their sacrum. Subjects altered stride length by matching stride frequency to a metronome. During the visual feedback condition, we projected a real time display of the position of a reflective marker placed on the subject's sacrum onto a grid displayed in front of the subject.

We recorded data from each subject during a 6-minute period. For each condition we collected oxygen consumption and carbon dioxide production data to calculate metabolic cost (W/kg) during three minutes of steady state walking. We also collected kinematic data using a full body marker set to calculate vertical COM displacement over a twenty second period coinciding with steady state. As the treadmill rested on force platforms, we also collected kinetic data to calculate vertical COM displacement over a 2-minute period of steady state walking. We found no significant differences in vertical COM displacement between the two methods.

RESULTS AND DISCUSSION

In experiment 1, vertical COM displacement increased with stride length. Metabolic cost increased as stride length deviated from the subject's preferred stride length (Figure 1).

Maximum metabolic cost occurred when vertical COM displacements were at a minimum. In experiment 2, vertical COM displacement decreased with visual feedback about sacrum position but metabolic cost significantly increased (Figure 2.). During the visual feedback condition most subjects selected a "Groucho" walking pattern in order to minimize vertical COM displacement without altering stride length.

The metabolic cost of human walking is not directly proportional to vertical COM movement. Decreasing vertical COM movement beyond that which occurred at one's preferred walking pattern resulted in increased energetic cost. These results suggest that factors other than minimizing COM displacement are important in determining the metabolic costs of gait.

SUMMARY

We have demonstrated that the most energetically efficient gait pattern is not the same as the pattern that minimizes COM displacement. Clearly, humans are capable of walking in a manner that will minimize COM displacement beyond what they will

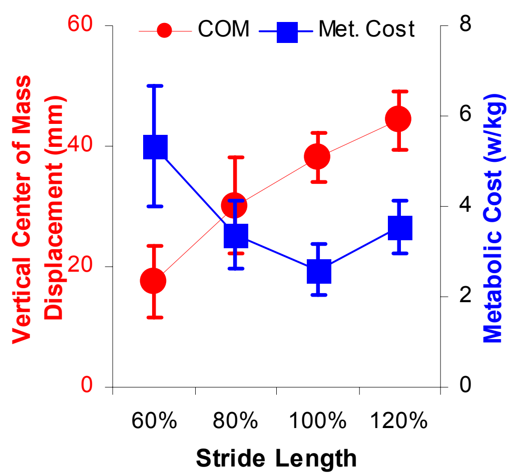

Figure 1: Mean vertical center of mass displacement and metabolic cost are plotted during walking at 1.2 m/s at varying percentages of preferred stride length.

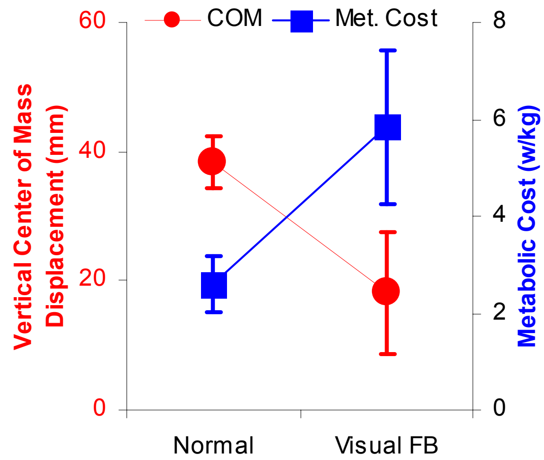

Figure 2: Mean vertical center of mass displacement and metabolic cost are plotted during walking at 1.2 m/s and a given stride length either with or without visual feedback.

normally choose to do. The fact that humans do not choose to minimize COM displacement suggests that 1) factors other than COM displacement play an important role in the metabolic costs of human walking and 2) factors other then minimizing COM displacement may determine why humans select the gait patterns that they do.

REFERENCES

Biewener, A.A. (1989). *Science* **245**:45-8.
Farley, C.T. et al. (2003). *Proc. ASB,* Toledo OH.
Kuo, A.D. (2002). *J Biomech Eng.* **124**:113-20.
Saunders, J.B., Inman, V.T., Eberhart, H.D. (1953). *J Bone Joint Surg Am* **35,** 543-58.

ACKNOWLEDGMENTS

The authors would like to thank Tanisha Tate for their contribution to this project.

METABOLIC COSTS OF HUMAN BOUNCING

Jesse C. Dean[1] and Arthur D. Kuo[2]

[1]Department of Biomedical Engineering, University of Michigan, Ann Arbor
[2]Department of Mechanical Engineering and Applied Mechanics, University of Michigan, Ann Arbor

INTRODUCTION

In running, hopping, or bouncing, humans have been modeled as mass-spring systems, with an associated natural frequency for each task. The passive elasticity of the musculo-tendon complex may store and return energy to the system, decreasing the amount of muscular work required. A simple example of humans exhibiting spring-like activity is bouncing about the ankle joint. We hypothesize that the energetic cost of this bouncing is influenced by two major factors. Energy is expended when muscles perform work, leading to a certain metabolic cost. When muscles contract isometrically, there is no work performed, but there is still an energetic cost, increasing with the average force and potentially inversely with the contraction time. These two factors together may explain the total metabolic cost of bouncing.

METHODS

Four subjects (2 male, 2 female) participated in this study. The subjects bounced vertically using only the ankles over a range of frequencies. Bounce amplitudes were kept small, so the subjects never left the ground. We collected ground reaction force and ankle height data for all trials. Subjects first bounced at seven frequencies (1 – 4 Hz) while we collected electromyographic (EMG) data from the left medial gastrocnemius. Oxygen consumption data was then collected with the subject at rest, and while bouncing at four frequencies (1 – 4 Hz). In each trial, the bounce amplitude was adjusted to keep the positive mechanical work constant across frequencies.

The filtered EMG, ground reaction force, and ankle height data were fit with modified sinusoids. We calculated the gain and phase differences from the EMG to the reaction force and ankle position. These gain and phase values were then fit to a mechanical model representing the action of the ankle plantarflexors (Fig 1, after Bach et al., 1983) by adjusting the model parameters. This model was used to calculate positive muscle work performed on the center of mass at the various frequencies. Metabolic cost was calculated from steady state oxygen consumption data.

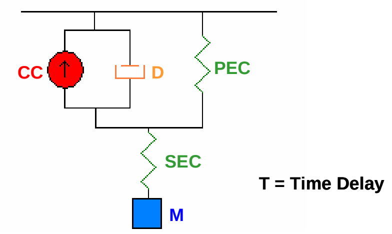

Figure 1: Mechanical model of musculo-tendon system including a contractile component (CC), damper (D), parallel elastic component (PEC), series elastic component (SEC), and time delay (T).

RESULTS AND DISCUSSION

The calculated experimental gains and phases were qualitatively a good fit with the model bode plot for each subject. An example for one subject is shown in Figure 2. Between the four subjects, the average model parameter values were SEC = 30175 kg/s^2, PEC = 24202 kg/s^2, D = 3909 kg/s, and T = 0.109 s, comparable to values found in earlier studies (Bach et al, 1983).

For each subject, we used the model to calculate the theoretical positive muscle work and total system positive mechanical work for each frequency. The model parameters were identified from experimental force data and then compared with the corresponding metabolic data. We also calculated the duration of active muscle contraction at each frequency from the fit EMG data. This was used to calculate the average force per contraction time under each condition.

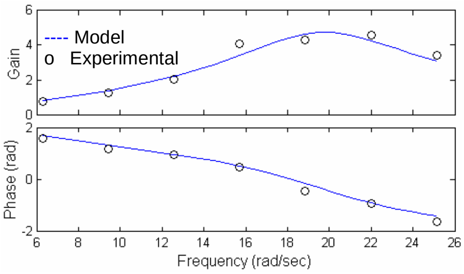

Figure 2: Comparison of experimental and modeled gain and phase data from EMG (input) to ground reaction force (output).

If muscular work is the major determinant of metabolic cost, the expected cost can be calculated by assuming a constant work efficiency of 25% (Hill, 1938). But if the metabolic cost is determined by the rate of force application, as in running (Kram & Taylor, 1990), the expected cost will be proportional to the average force per contraction time. This proportionality was calculated to be 0.183 JN^{-1} in running (Kram and Taylor, 1990), a task similar to bouncing in that the primary cost is supporting body weight.

The theoretical metabolic costs from these two sources were calculated for each frequency and compared with actual metabolic costs (Fig. 3). It appears that if both of these costs are present in bouncing, the cost of doing positive muscle work dominates at low frequencies, while the cost of generating force with a short time course dominates at high frequencies. The theoretical combined metabolic cost is minimized around 3 Hz, the same frequency at which the subjects' actual metabolic cost was minimized.

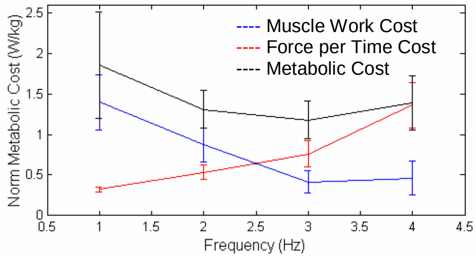

Figure 3: Theoretical costs from positive muscle work, force per contraction time, and actual metabolic cost.

Total mechanical work was kept constant at all frequencies, and therefore does not explain the observed variations in energetic cost. Muscle work alone also does not explain energetic cost, because the calculated efficiency (mechanical power per metabolic power) exceeded 25% at 3 Hz in all subjects. Instead, it is likely that at higher frequencies, the muscle is contracting more isometrically, and the tendon is responsible for much of the positive work (Kubo et al, 2000).

SUMMARY

Humans bouncing about their ankle joint can be treated as a mechanical system, in which the passive dynamics influence the metabolic cost. At low frequencies, the cost of muscular work dominates, while at higher frequencies, the cost of generating force quickly is more important. Metabolic cost is minimized at an intermediate frequency.

ACKNOWLEDGEMENTS

J.C.D. supported in part by a fellowship from the UM Institute of Gerontology.

REFERENCES

Bach, T.M. et al. (1983). *J Biomech.* **16**, 85-90.
Hill, A.V. (1938). *Proc. Roy. Soc. Lond.* **B126**, 136-195.
Kram, R., Taylor, C.R. (1990). *Nature*, **346**, 265-267.
Kubo, K. et al (2000). *Act Phys Scand*, **170**, 127-135.

OXYGEN CONSUMPTION AND THE PREFERRED FREQUENCY SPEED RELATION IN HUMAN WALKING

John E.A. Bertram[1] and Andy Ruina[2]

[1] Nutrition, Food & Exercise Sciences, Florida State University, Tallahassee, FL, USA
[2] Theoretical and Applied Mechanics, Cornell University, Ithaca, NY, USA
Email: jbertram@fsu.edu ruina@cornell.edu

INTRODUCTION

It has long been recognized that, at different speeds, an individual will, roughly, select the step length and step frequency that minimizes energy expenditure per unit distance travelled. We discovered (Bertram and Ruina 2001) that, roughly, an individual will also choose the speed and step frequency that minimizes energy expenditure if step length is constrained, or the speed and step length that minimizes energy expenditure if step frequency is constrained. A schematic of the three preference curves and their relation to a prototypical set of oxygen consumption contours are shown in Fig. 1.

How might an individual control walking to minimize metabolic cost? One possibility is that the neural system constantly monitors the energetics of walking, processes that derived information and implements an appropriate optimization. This direct internal control seems to formidable task for big-brained bipeds. Alternatively, the neural system could implement a simpler control strategy that has evolved so that it has the observed minimization property.

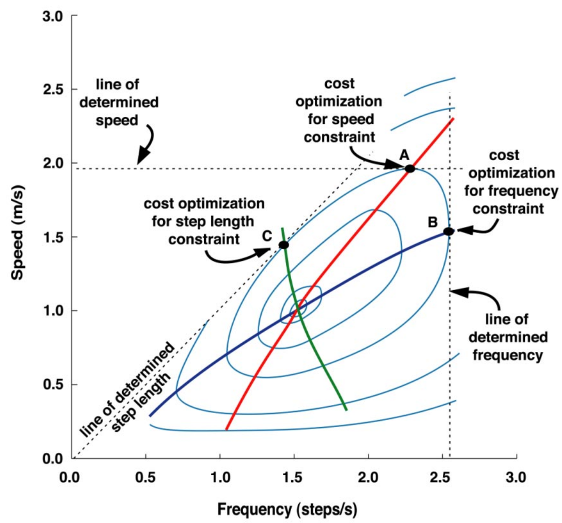

Figure 1: Description of the constrained optimization hypothesis. The concentric blue lines indicate iso-cost curves that have greater magnitude as they expand outward.

Here we further investigate the relation between oxygen consumtion and the various constrained preference tests for several subjects. Rather than using published VO2 data this work uses VO2 data from the same subjects as are used in the preference tests.

METHODS

A metabolic cost surface is generated from oxygen consumption rate at 49 speed-frequency conditions for 10 subjects. Energy optimization using this surface predicts the results of the preference tests, which we can compare to the results of the actual preference tests for the same individuals (constrained speed walking on a standard treadmill; constrained frequency level walking to a metronome beat; constrained step length level walking on evenly spaced markers).

RESULTS

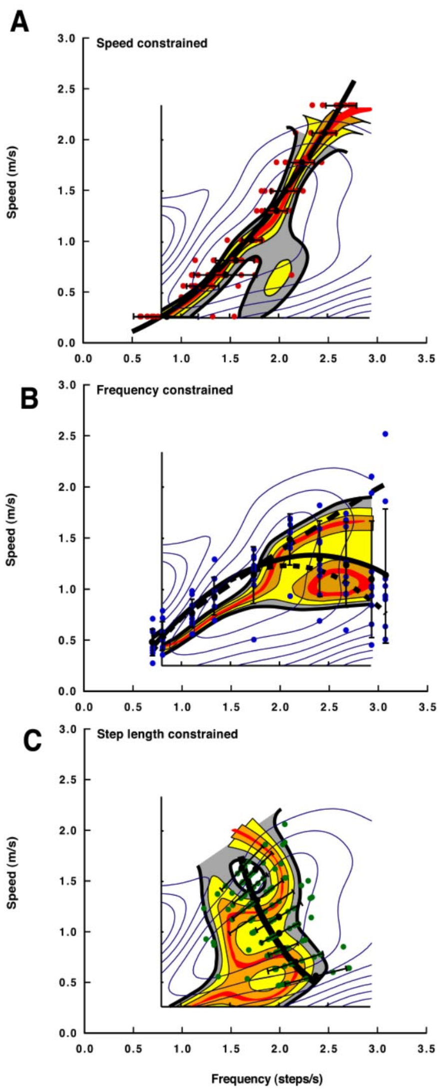

Figure 2: Observed walking of 10 subjects compared to the predictions from metabolic cost of movement (blue contours). Shaded areas show ranges around optimum: red ± 1%, orange ± 5%, yellow ± 10%, gray ± 15%. Solid black circles indicate mean (±1 sd). Plots A and C are fit with least-squares power function regressions (applied to the independent variable and mathematically manipulated to match the variables shown in these plots). Plot B is fit with least-squares quadratic regressions, solid line, all data; long dashed line, the subgroup that selected high speed optimum; short dashed line, subgroup that selected low speed optimum.

DISCUSSION

The correlation between the preference tests and energy optimization observed in Bertram and Ruina (2001) is maintained when VO2 data is used for the same subjects as are used in the preference tests (as opposed to old published VO2 data). Although minimization of cost per distance appears to dominate walking control, differences from predicted behavior suggest that other factors are also relevant.

REFERENCES

Bertram, J.E.A., Ruina, A. (2001) *J. Theor. Biol.* **209**, 445-453.

MECHANICAL ENERGY FLUCTUATIONS DURING HILL WALKING: REDUCED ROLE OF ENERGY EXCHANGE

Jinger S. Gottschall and Rodger Kram

Locomotion Laboratory, University of Colorado, Boulder, CO, USA
E-mail: gottscha@mail.colorado.edu

INTRODUCTION

An egg will repeatedly roll, end over end, on a level, rigid surface. A rolling egg conserves total mechanical energy despite the fluctuations in kinetic and gravitational potential energies. Similarly, humans conserve a substantial amount of mechanical energy when we walk on the level (Margaria, 1976). During the first half of the stance phase, the kinetic energy (KE) decreases while the gravitational potential energy (GPE) increases. So, KE is converted to GPE. In contrast, during the second half of the stance phase, GPE decreases while KE increases, resulting in a conversion of GPE into KE. The GPE and KE curves are out of phase so that fluctuations in total energy (GPE + KE) are attenuated and the muscles perform less work (Cavagna et al., 1977). However, an egg does not roll uphill and it accelerates downhill. The purpose of this study was to investigate the mechanical energy fluctuations during hill walking.

Many researchers have studied a variety of metabolic and kinematic variables of hill walking (e.g. Kawamura, et al., 1991, Minetti, et al., 1993, Kuster, et al., 1995, Kang & Chaloupka, 2002). But none have quantified the fundamental fluctuations of the mechanical energies of the center of mass during hill walking.

We tested three hypotheses regarding the mechanics of downhill and uphill walking. First, we hypothesized that during the stance phase, the pattern of GPE fluctuations would be asymmetrical with a net decrease in energy for declines and a net increase for inclines. Second, we hypothesized that, during the stance phase, the pattern of KE fluctuations would be similar to level walking. Third, we hypothesized that the total (GPE + KE) energy fluctuations during both downhill and uphill would be dominated by GPE.

METHODS

We measured the fluctuations of the mechanical energy of the center of mass for five males and five females walking downhill and uphill on a force measuring treadmill mounted at 3, 6, and 9 degrees (Figure 1).

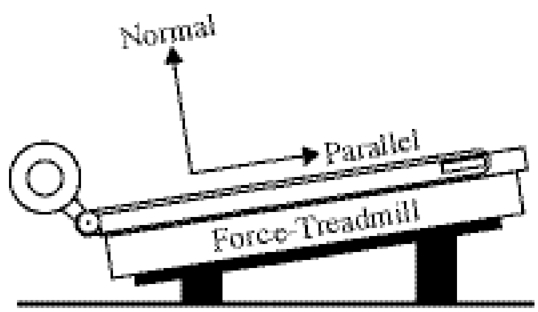

Figure 1: Force measuring treadmill mounted on 9 degree wedges.

We calculated the mechanical energy exchange by integrating the ground reaction force signals, taking into account the angle of the hill (Cavagna, 1975). GPE and KE fluctuations were calculated by determining the position and velocity changes of the center of mass. The positive increments in the total center of mass energy (GPE + KE) fluctuations equal the total external work performed and was calculated per step.

RESULTS AND DISCUSSION

As hypothesized, for downhill and uphill walking, the GPE fluctuations were asymmetrical (Figure 2a, b, c). With increasing hill grade, the center of mass vertical displacement per step increased. The KE fluctuations during stance were more similar to level walking (Figure 2d, e, f). Thus, positive vertical work against gravity was smallest during downhill walking and largest during uphill walking, while work associated with velocity fluctuations did not substantially change.

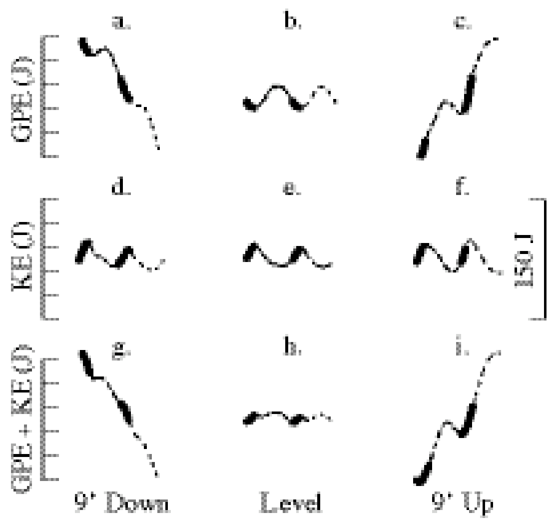

Figure 2: Fluctuations in GPE, KE, and GPE + KE of the center of mass for a typical subject (69 kg) walking at 1.25 m/s. Thick lines indicate double support. Dashed lines indicate single support.

Overall, the fluctuations in total energy (GPE + KE) increased incrementally with hill grade (Figure 2g, h, i). The external work per step during 9 degree downhill walking was one seventh that of level walking. But during 9 degree uphill walking, the external work was 5 times greater than for level walking. Although this method does not take into account the individual limbs method of Donelan, et al. (2002), it seems likely that there is less simultaneous positive work and negative work during walking on steep hills.

SUMMARY

The exchange of gravitational potential and kinetic energy is greatly diminished during both downhill and uphill walking.

REFERENCES

Cavagna, G.A. (1975). *J. Appl. Physiol.*, **39**, 174-179.

Donelan, JM. (2002). *J. Biomech.*, **35**, 117-124.

Kang, J., Chaloupka, E.C. (2002). *Eur. J. Appl. Physiol.*, **86**, 503-508.

Kawamura, K. et al. (1991). *Acta Medica Okayama,* **45**, 179-184.

Kuster, M. et al. (1995). *Clin. Biomech.,* **10**, 79-84.

Margaria, R. (1976). *Biomechanics and Energies of muscular exercise.* Oxford University Press.

Minetti, A.E. et al. (1993). *J. Physiol.,* **471**, 725-735.

ACKNOWLEDGEMENTS

We thank Sid Gustafson for helpful advice on the construction of the force treadmill wedges.
Supported by a United States National Institutes of Health Grant AR44688.

PROBLEMS WITH SOME HISTORICAL LOCOMOTION ENERGY ACCOUNTING

Andy Ruina[1] and John E.A. Bertram[2]
[1]The Human Power, Biomechanics, and Robotics Laboratory, Cornell, Ithaca, NY, USA
[2]Nutrition, Food & Exercise Sciences, Florida State University, Tallahassee, FL, USA
http://www.tam.cornell.edu/~ruina/hplab jbertram@fsu.edu

INTRODUCTION

The analysis and interpretation of human and other animal locomotion are facilitated by a few key observations which are central in the minds of many researchers interested in comparing the performance of different species or different gaits.

a) Bodies are bigger than legs, so the approximation of a point mass connected to the ground with massless legs is often reasonable,
b) The body motions in the single stance phase of walking are similar to the motions of an inverted pendulum,
c) The body motions in human running are similar to those of a point mass bouncing on a massless spring.

Starting with these ideas, as supplemented with some simple dynamics theory, a group of common terms have been developed over the past century (starting roughly with Fenn 1930). Now-a-days, however, we feel the usage of these terms can be counter productive; they obscure basic mechanics concepts. Here we review some of these word's definitions and critique their utility using simple mechanics examples.

"EXTERNAL WORK"

The center of mass energy is all of the gravitational potential energy plus that part of the kinetic energy associated with translation of the center of mass. The "external work" is defined as the sum of positive increments in the center-of-mass energy. The "external work" is zero for a simple point-mass pendulum, leading to the oft-used generalization that the external work is a measure of the essential cost of the observed motions due to their not being pendulum-like.
*But the external work is *not* zero for most other passive conservative rigid body systems, even for a pendulum if the pendulum-mass is not concentrated at a point (e.g., a swinging stick). Although the "external work" has the same units as work (and energy) it is generally not the work of any identifiable subset of actuators. Most especially, it is *not* the work of the external forces. Thus the "external work" is not external, it is not work, and it is not well correlated to the degree to which a system is passive (but for the one special case of a point mass pendulum).

"INTERNAL WORK"

The kinetic energy of any system can be written as kinetic energy of the center-of-mass motion (called "the external kinetic energy" perhaps because it can be measured "externally" with a load cell) plus the remainder (due to motion of the parts relative to the center of mass) called, as a complement, "the internal kinetic energy". The "internal kinetic energy" varies in time. Internal work is sometimes defined as the sum of positive increments in the "internal kinetic energy" and sometimes as the sum of the positive increments in various terms that contribute to the "internal kinetic energy".

*Although "internal work" has the same units as work, work by an internal actuator need not show up in the "internal work" accounting. And even when there is no actuator work at all, say for a passive double pendulum with constant total energy, there can be both "internal work" and "external work".

"RECOVERY"

The abstract term recovery is defined as (A+B-C)/(A+B) where A is the sum of positive increments of gravitational potential energy, B is the sum of positive increments in the "external kinetic energy" and C is the "external work". Recovery is defined *ad hoc* to yield a value of 100% for a point-mass pendulum, and has thus been described as a measure of the extent to which a moving animal employs pendulum-like motion.
*However, recovery measured in this way is not 100% even for a distributed mass pendulum (a swinging stick), for a double pendulum (either with or without gravity), for a rolling wheel with an eccentric mass, or for most any passive mechanisms onto which one might add actuators as a model for animal locomotion. Thus “recovery” does not seem to measure anything fundamental or even indicate anything but the extent that a system is literally like a *point-mass* pendulum.

"EFFICIENCY"

Technical definitions of efficiency are usually constructed as the ratio of a benefit to a cost; for an engine it's (work out)/(fuel energy in). But for terrestrial locomotion where the energetic benefit is zero (the gravity force is orthogonal to the direction of net motion) simple definitions of efficiency give an efficiency of zero. One attempt to remedy this inappropriateness of an energetic efficiency define an "efficiency" as ("external work" + "internal work")/(metabolic cost).
*However, this efficiency has no relation to thermo-dynamic efficiency. And it is not even well correlated to intuitive notions of efficiency: a) for most passive systems it goes to infinity and b) it is close to zero, say, for a car that gets 100 miles per gallon.

SUMMARY

Each quantity above serves as a reduction of complex temporal data to a single number and thus might aid in detecting trends within or between subjects. But they seem to be of little help in explaining energetics of locomotion.

In this light it is perhaps unsuprising that the monumental four-part paper using the concepts above has this penultimate sentence (Heglund et al 1982) "We have found that the rate at which muscles of running animals perform mechanical work during locomotion does not provide a simple explanation for either the linear increase in metabolic rate with speed, or the regular change in cost of locomotion with body size."

Of more direct value perhaps, is accounting based on the observation that positive muscle work is equal to the net dissipation (e.g., through collisions and negative muscle work).

REFERENCES

Fenn,W.O., (1930) Am. J. Physiol., **93,** 433-462.
Heglund,N.C., Fedak,M.A., Taylor,C.R, Cavagna,G.A., (1982) *J. Exp Biol.*, **97**, 57-66.

MECHANICS AND ENERGETICS OF WALKING AT DIFFERENT STRIDE RATES

Brian R. Umberger [1] and Philip E. Martin [2]

[1] Exercise & Sport Research Institute, Arizona State University, Tempe AZ, USA
[2] Biomechanics Laboratory, The Pennsylvania State University, University Park, PA, USA
E-mail: brian.umberger@asu.edu

INTRODUCTION

Metabolic energy expenditure depends on walking stride rate in a nonlinear manner, with minimum energy occurring near the preferred stride rate (Zarrugh & Radcliffe, 1978). Kram (1997) has suggested that the energetic cost of repetitive movements reflects the combined costs of generating muscular force and doing mechanical work. In a task such as walking, the cost of generating force is likely to dominate the total metabolic cost. The purpose of this study was to determine how well variations in energy demand, due to altered stride rate, correspond to variations in muscle mechanical demand, as reflected by lower limb joint moments.

METHODS

Ten male (n = 6) and female (n = 4) subjects (M_{age} = 26.7 ± 3.6 yr; M_{ht} = 173.9 ± 9.6 cm; M_{mass} = 67.9 ± 11.9 kg) walked at one speed (1.3 $m \cdot s^{-1}$) using five different stride rates (preferred, ± 10% of preferred, and ± 20% of preferred). Measurements were made of pulmonary gas exchange, ground reaction forces, and body segment positions. Metabolic measurements were made on a motorized treadmill, while kinematic and kinetic data were collected as subjects walked along a 12 m walkway. Stride rate was matched to a metronome on the treadmill, and to marks placed on the floor for overground trials. Subjects walked with arms folded across their chest, to control for the effects of arm swing.

The rate of metabolic energy expenditure was estimated from pulmonary gas exchange, and sagittal plane joint moments were calculated at the hip, knee, and ankle using a standard inverse dynamics approach (Winter, 1990). Body segment parameters were based on de Leva (1996). Average absolute moments across the gait cycle were computed, then summed over the lower limb joints to estimate total mechanical demand.

Cubic polynomials were fit to the energy rate and summed moment data, and stride rates corresponding to minimum cost were determined from the resulting equations. A paired t-test was used to test for differences between the stride rates at which energy and mechanical demand were minimized.

RESULTS AND DISCUSSION

Preferred stride rate was 54.3 ± 3.1 str/min. Energy expenditure and mechanical demand were minimized at stride rates 0.1% above and 8.1% below the preferred, respectively (Figure 1). This difference was significant at $p < .01$ For both dependent variables, it was relatively more costly to walk at stride rates lower than the optimal, compared to stride rates higher than optimal.

The mechanical demand on the lower limb muscles, as reflected by net joint moments, was minimized at a stride rate lower than energetically optimal, and the energetically optimal rate was coincident with the preferred rate. This is in contrast to the case in cycling, where joint moments are

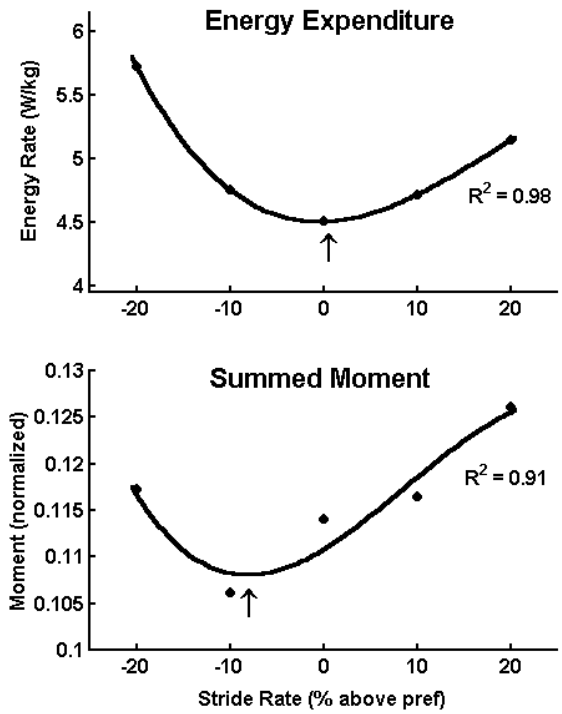

Figure 1: Trends in energy and mechanical demand in walking at different stride rates. Arrows indicate minimum cost stride rates relative to preferred stride rate.

minimized close to the preferred pedaling cadence, which is substantially higher than the energetically optimal rate (Marsh & Martin, 1993, Marsh et al., 2000). While mechanical and energetic demand were minimized at significantly different stride rates, the absolute difference was still quite small (~ 4 str/min). In cycling, mechanical demand is minimized at pedaling cadences 30-40 rpm higher than energetically optimal. The relative proximity of preferred rates to the rates resulting in minimal mechanical demand in both walking and cycling suggests that the demand placed on the active limb muscles is probably a more general predictor of self-selected movement patterns than global energy cost. There are, however, other differences between walking and cycling that likely affect preferred rates, such as a substantially higher work rate in moderate intensity cycling than in walking.

Important limitations of the present work are that net joint moments can not account for muscle cocontraction, storage of elastic energy, or biarticular muscles. Global energy expenditure also may not adequately reflect the metabolic demands placed on the leg muscles. To address these issues, we are extending the current project using computer models based on muscle thermodynamics (Umberger et al., 2003).

SUMMARY

Both energetic and mechanical demand exhibited similar trends, such as U-shaped responses and a steeper slope at stride rates below the optimum. Findings were generally consistent with the hypothesis that the cost of generating muscular force dominates metabolic demand in walking. Mechanical demand, however, was minimized at a lower stride rate than energy expenditure, suggesting a mechanical benefit to taking slightly longer strides.

REFERENCES

de Leva, P. (1996). *J Biom*, **29**, 1223-30.
Kram, R. (1997). *J Appl Biom*, **13**, 460- 463.
Marsh, A., Martin, P. (1993). *Med Sci Sp Ex*, **25**, 1269-74.
Marsh, A. et al. (2000). *J Biom*, **33**, 173-80.
Umberger, B. et al. (2003). *Comp Method Biom Biomed Eng*, **6**, 99-111.
Winter, D. (1990). *Biomechanics and Motor Control of Human Movement*. Wiley.
Zarrugh, M., Radcliffe, C. (1978). *Eur J Appl Physiol*, **38**, 215-223.

ACKNOWLEDGEMENTS

Support was provided by NSF IGERT grant DGE9987619 and the ASU Kinesiology Conley Memorial Research Scholarship.

EFFECT OF CEREBRAL CONCUSSION ON THE COMPLEXITY OF CENTER OF PRESSURE TIME SERIES IN COLLEGIATE ATHLETES

James T. Cavanaugh, MS, PT[1], Kevin M. Guskiewicz, PhD, ATC[1], and Nicholas Stergiou, PhD[2]

[1] Department of Exercise and Sport Science, University of North Carolina, Chapel Hill, NC
[2] HPER Biomechanics Lab, University of Nebraska at Omaha, Omaha, NE
Email: jimcavanaugh@nc.rr.com Web: http://www.unc.edu/depts/exercise/SMRL.html

INTRODUCTION

Athletes with cerebral concussion, i.e., mild head injury (MHI), may be at increased risk for recurrent brain trauma, especially when returning to competition immediately after an initial injury (Guskiewicz et al., unpublished manuscript). Postural steadiness appears to be a reliable marker of recovery after cerebral concussion, with unsteadiness in athletes typically resolving within 3-5 days (Guskiewicz et al., 1996). Researchers have suggested, however, that the amount of center of pressure (COP) variability in subjects standing as still as possible may not reflect subtle postural control abnormality, and therefore, is inadequate for certifying that an athlete is free of impairment. (Guskiewicz et al., 1997).

An alternative approach for discriminating between healthy and brain-injured states is to measure the effect of injury on COP time series complexity. Approximate Entropy (ApEn) is a complexity measure that quantifies the ensemble amount of randomness in a time series (Pincus, 1991). ApEn measures the logarithmic probability that a series of points a certain distance apart will exhibit similar relative characteristics on the next incremental comparison (Harbourne & Stergiou, in press). ApEn generates values from 0-2, with higher values indicating greater complexity. Our purpose was to examine the effect of cerebral concussion on COP complexity in collegiate athletes.

METHODS

We analyzed a convenient sample of 5 male and 3 female collegiate athletes, 17-24 years old, with unsteadiness after cerebral concussion. Subjects had no other medical pathology. Postural steadiness was measured during pre-season, within 24 hours post injury, and every other day thereafter until steadiness returned to pre-season levels. For comparison, we analyzed data from 8 non-athlete control subjects, matched by age and gender, who were tested on 3 occasions.

Postural steadiness was evaluated using the Smart Balance Master System 8.0 (NeuroCom International, Inc., Clackamas, OR, USA), which measured vertical ground reaction forces at 100 Hz using dual force plates. COP location was estimated during 20-second trials. An equilibrium score was generated based on the average peak-to-peak amplitude of COP excursion measured during 6 sensory conditions. Athletes had greater than 5% decline in equilibrium score at 24 hours after injury. Many athletes also had complaints of headache, fatigue, dizziness, confusion, and / or blurred vision.

ApEn ($m=2$, $r = .2 \times$ process s.d., $N = 2000$) was calculated on the A/P and M/L components of COP time series data from two visual conditions (fixed platform, eyes open and eyes closed). Athlete data were analyzed from preseason (Day 1), 24 hours post injury (Day 2), and from the day on which equilibrium scores returned to preseason levels (Day 3). A mixed model (Group x Day) ANOVA was used for data analysis ($\alpha = .05$).

RESULTS AND DISCUSSION

On Day 1, athlete and non-athlete subjects displayed similar ApEn values for all time series (Figs. 1 & 2). On Day 2, athletes with MHI displayed a marked decline in time series complexity in both visual conditions. Even after steadiness returned to preseason levels (Day 3), ApEn values for injured athletes remained depressed.

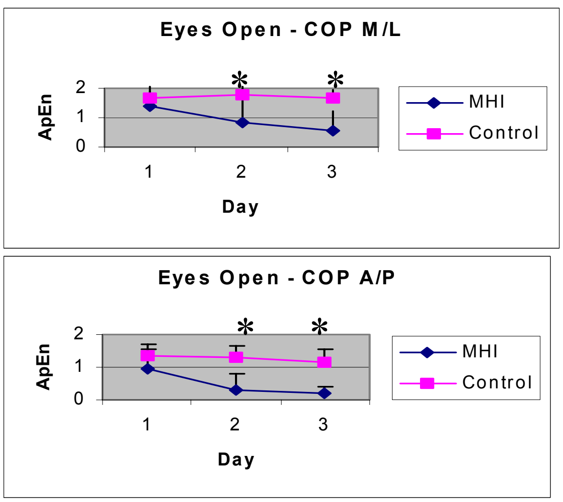

Figure 1: ApEn values for M/L and A/P COP time series in MHI and Control subjects standing with eyes open. * Between group comparison $p < .05$.

The data supported the hypothesis that pathology produces a loss of physiologic complexity (Lipsitz & Goldberger, 1992). More importantly, ApEn revealed postural control system disturbance that persisted despite the return of pre-injury steadiness, as measured by the amount of COP variability. Given the risk of recurrent concussion associated with returning to play before complete recovery, the failure of athletes with MHI to recover pre-injury levels of postural control system complexity might predispose them to further injury.

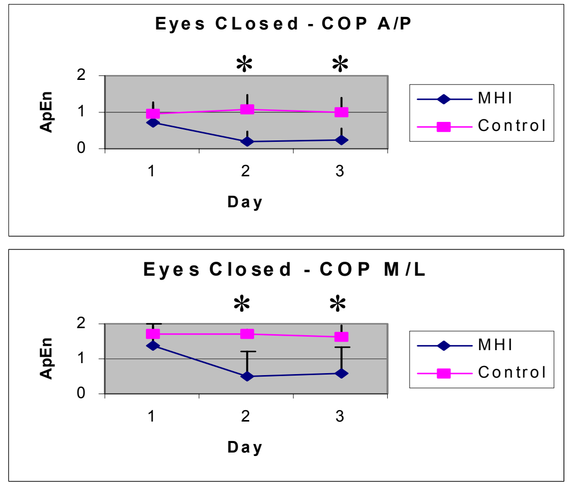

Figure 2: ApEn values for M/L and A/P COP time series in MHI and Control subjects with eyes closed. *Between group comparison $p < .05$.

SUMMARY

In contrast to measures of the amount of COP variability, ApEn may reveal subtle postural control system change resulting from MHI. ApEn shows promise as a valuable post-concussion assessment tool.

REFERENCES

Guskiewicz, K. M. et al. (unpublished manuscript).

Guskiewicz, K. M. et al. (1996). *Journal of Athletic Training, 31*(4), 300-306.

Guskiewicz, K. M., et al. (1997). *Med Sci Sports Exerc, 29*(7 Suppl), S213-221.

Lipsitz, L. A., Goldberger, A. L. (1992). *JAMA 267*(13), 1806-1809.

Pincus, S. M. (1991). *Proc Natl Acad Sci U S A, 88*(6), 2297-2301.

Harbourne R.T. , Stergiou, N. (in press). Dev Psych.

ACKNOWLEDGEMENT

J.T. Cavanaugh was supported by an award from the Foundation for Physical Therapy, Inc.

WORK ANALYSIS OF DUTY CYCLE EFFECTS FROM INJURIOUS STRETCH-SHORTENING CONTRACTIONS *IN VIVO* OF SKELETAL MUSCLE

Kenneth B. Geronilla [1], Brent A. Baker [1], Ian Hover[2], Mike L. Kashon[1], Robert G. Cutlip
[1] National Institute of Occupational Safety and Health 1095 Don Nehlen Drive
[2] West Virginia University, Division of Physical Therapy

INTRODUCTION

Muscle damage and concomitant changes in performance due to stretch-shortening contractions (i.e., reciprocal eccentric/concentric contractions) is one of the major concerns in sports and occupational-related activities. Stretch-shortening exercise has been shown to produce muscle damage in humans. However, the dynamics of the movement were not controlled and muscle response was not quantified during the movement in these studies (e.g. Kyrolainen et al., 1998). Further, excitation-contraction fatigue has been shown to play an important role in skeletal muscle injury resulting from eccentric contractions (Warren et al., 2001). We hypothesized that (1) the stretch-shortening exercise would affect work output of muscle both during and 48 hours after exposure and (2) very short duty cycles (the time between contractions) would further disrupt excitation-contraction coupling, thus creating a larger work decrement than those associated with a longer duty cycle.

METHODS

All testing was performed with anesthetized male Sprague-Dawley rats (N=48) on a custom-designed rat dynamometer (Cutlip et al., 1997). The response of the dorsiflexor muscles to isometric and stretch-shortening contractions (SSC) were quantified *in vivo*. Rats were randomly assigned to three groups (N=8) having either 10-seconds, 1-minute, or 5-minute duty cycles. The testing consisted of 7 sets of 10 SSC performed at an angular velocity of 500°/s from 90° to 140° ankle angle for a total of 70 SSC (see Table 1). A single SSC was used as a test of work performance before, immediately after, and 48 hours after exposure to SSC sets. Negative work (eccentric contraction), positive work (concentric contraction), and net work (difference between negative and positive work) were examined. Work was calculated as the integration of force over ankle angle change. There was a 2 minute rest period between steps in the experimental protocol to minimize excitation-contraction fatigue.

Table 1. Experimental Protocol

Step	Type	Duty Cycle
1	Single SSC	2min
2	7 SSC Sets of 10 Cycles	10s, 1min, 5 min
3	Single SSC	2min
4	Cage Recovery	48 Hour
5	Single SSC	2min

Negative, positive, and net work were calculated in the second SSC of each injurious SSC to examine performance decrements during the seven sets of SSC and to compare to work parameters from single SSC time points. The second SSC was used to minimize excitation-contraction coupling fatigue between sets.

RESULTS AND DISCUSSION

There was a pronounced decrement in single SSC negative and net work 48 hours after exposure for all groups, but these decrements were not specific to duty cycle (Figs. 1, 2). However, positive work was not affected 48 hours after exposure (Fig 3). During the 7 sets of SSC, net work showed a large decrement but was not specific to duty cycle (Fig. 4). In contrast, positive work and negative work of the 10 second group was most affected during the 7 sets of SSC (Figs. 5, 6). While duty cycle had an affect on real-time performance, it was not reflected in the single SSC performance 48 hours after exposure.

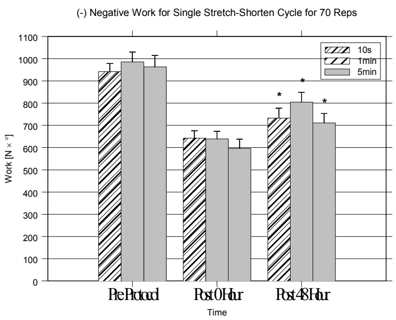

Figure 1: Single SSC Negative Work

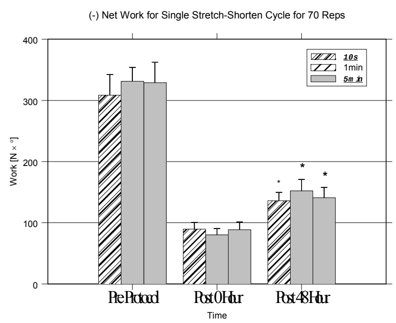

Figure 2: Single SSC Net Work

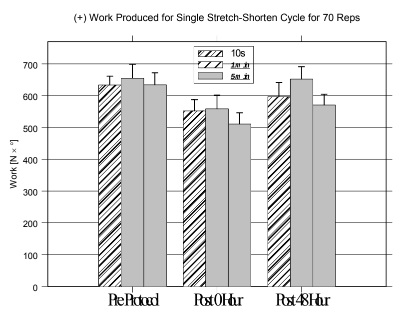

Figure 3: Single SSC Positive Work

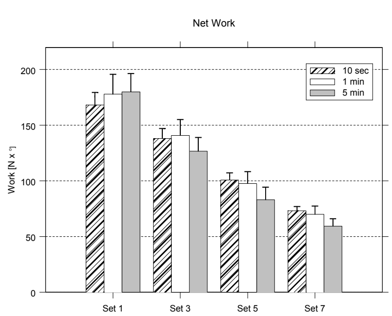

Figure 4: SSC Sets Net Work

Note: * indicates statistical significant difference

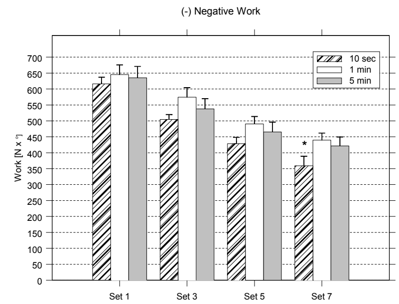

Figure 5: SSC Sets Negative Work

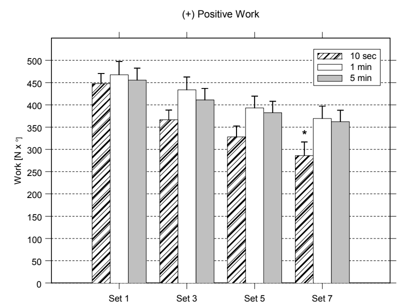

Figure 6: SSC Sets Positive Work

SUMMARY

Duty cycle appeared to have little effect on SSC 48 hours after exposure, but duty cycle did have an effect on real-time performance during the 7 sets of SSC. More contractions may give more pronounced results 48 hours after exposure. In addition, the similarity between single SSC and SSC sets indicated a good relationship between work parameters during and 48 hours after SSC.

REFERENCES

H.T. Kyrolainen, T.E.S. Takala, P.V. Komi, "Muscle damage induced by stretch-shortening cycle exercise," *Med. Sci. Sports Exerc*., Vol. 30, No. 3, pp. 415-420, 1998.

Warren, G. L., Ingalls, C. P., Lowe, D. A., and R. B. Armstrong. Excitation-Contraction Uncoupling: Major Role in Contraction-Induced Muscle Injury. Exerc. Sport Sci. Rev. 29(2): 82-87, 2001

R.G. Cutlip, W.T.Stauber, R.H. Willison T.A. Mcintosh, K.H. Means. "Dynamometer for rat plantar flexor muscle *in vivo*," *Med. Biol. Eng. Comput*., 35, 540-543, 1997.

FORCES IN THE LOWER LIMBS DURING ERGOMETER ROWING

Suzanne E. Halliday [1], Amy B. Zavatsky [1], and Kazunori Hase [2]

[1] Department of Engineering Science, University of Oxford, Oxford, UK
[2] Department of Mechanical Engineering, Nagoya University, Nagoya, Japan
E-mail: amy.zavatsky@eng.ox.ac.uk Web: www.eng.ox.ac.uk/~kneabz/

INTRODUCTION

Indoor ergometer rowing has long been used by competitive rowers as a training method, but it has also been widely adopted by non-rowers as an exercise for general fitness. Paraplegics can now reap the cardiovascular benefits of rowing by using a specially adapted ergometer, along with functional electrical stimulation of the leg muscles (Davoodi *et al*. 2002; Wheeler *et al*. 2002).

To estimate the potential risk of injury to ergometer rowers, particularly paraplegics, it is important to know the mechanical loads on the muscles, ligaments, and bones of the legs. This study uses mathematical modelling in conjunction with non-invasive *in vivo* measurements to calculate the forces in the anatomic structures of the lower limb during ergometer rowing.

METHODS

With institutional review board approval, five male subjects [23.4 yrs of age (20-27), 91.6 kg (83-97), 195 cm (191-198)] with an average 9.6 years (8-13) of competitive rowing experience participated in the study. Seventy-four 15 mm diameter markers attached to the upper extremities, lower extremities, trunk, and head were used to define seventeen segments and segment-based co-ordinate systems (Halliday et al. 2001). Subjects rowed at 20, 24, 28, and 32 strokes per minute (spm) while kinematic data were collected at 100 Hz with 12 MII cameras run by a Vicon 612 (Vicon Motion Systems, Oxford, UK).

The ergometer used in this study (Model C; Concept2, Inc., VT, USA) was instrumented with a six component force transducer (MC36-6-250; AMTI, MA, USA) beneath the right foot cradle. The rowing ergometer itself was used as a custom calibration object, allowing the integration of the kinematic and kinetic data to an accuracy of 3.05 mm. The chain joining the ergometer handle to the flywheel was modified to include a uniaxial force transducer (DDE–2500; Applied Measurements Ltd., UK). Kinetic data from both force transducers was sampled at 1000 Hz, as was EMG data from ten muscles (tibialis anterior, gastrocnemius, soleus, rectus femoris, vastus medialis, semimembranosus, gluteus maximus, adductor magnus, erector spinae at the fifth lumbar vertebrae and rectus abdominus) using an MA 100 (Motion Lab Systems, Louisiana USA).

A sagittal-plane model of the lower limb with revolute hip and metatarsalphalangeal joints and four-bar linkage knee and ankle joints was used to calculate articular contact, ligament, and muscle forces from the net joint forces and moments (Lu *et al*. 1998; Halliday *et al*. 2002; Halliday 2003). The model included 10 muscles and 4 ligaments. The indeterminate problem was solved in two ways: a Dynamically Determinate One-Sided Constraint method (DDOSC; Collins 1995) and static optimisation (minimize muscle force, minimize cube of muscle force, minimize ligament forces, minimize joint contact forces). A parameter sensitivity study was performed on 36 input variables and 40 model parameters.

RESULTS AND DISCUSSION

Ranges of lower limb joint motion did not differ at different rowing cadences. Sagittal plane angles and forces at the handle and foot cradle of the ergometer were all similar to those published previously. At least one EMG consistent DDOSC solution throughout 100% of the rowing cycle could be found for 17 of the 20 trials analyzed. For the remaining three trials, a solution was not found in the early recovery phase. The optimization criterion that resulted in the best agreement with EMG (37%) was to minimize the sum of the joint contact forces.

Force magnitudes calculated using the DDOSC method increased with increasing cadence and showed peak values that were not anatomically reasonable, although mean values of muscle and joint contact forces were comparable to reported *in vivo* measurements in other athletic activities. Optimization using any of the four criteria resulted in anatomically reasonable force magnitudes that also increased with increasing cadence. Fig. 1 shows an example of calculated gastrocnemius forces (24 spm) compared to EMG activity for one rower.

The parameter sensitivity study showed, for example, that gastrocnemius force calculated by the DDOSC method increased by 9% with an anterior shift of the lateral malleolus marker. It increased by 15% with an anterior shift of the muscle insertion on the heel. The overall uncertainty in the calculated gastrocnemius force ranged from –39% to +43%. This resulted in a predicted gastrocnemius force range of 4194 - 9834 N.

SUMMARY

Both DDOSC and optimization methods predicted anatomically reasonable joint, muscle, and contact forces in the lower limbs during ergometer rowing, although each method has certain weaknesses. A parameter sensitivity study showed that care must be taken in the interpretation of force results, given the range of errors possible.

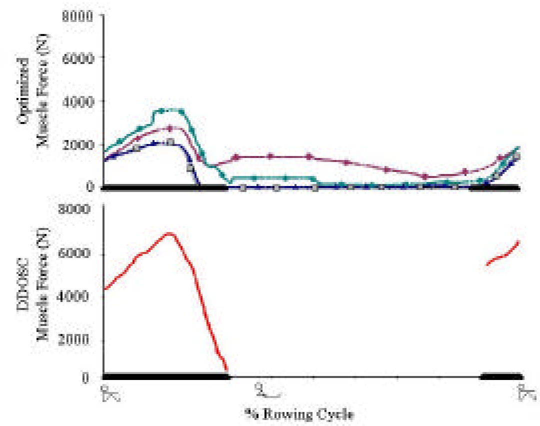

Figure 1: Model gastrocnemius muscle forces. Optimizations: linear muscle force (blue triangles), cubic muscle force (teal circles), ligament force (plum diamonds), joint contact force (gray squares). EMG activity indicated by thick black lines.

REFERENCES

Collins, J. J. (1995) *J Biomech* **28,** 251-267.
Davoodi, R. et al. (2002) *IEEE Trans Neural Syst Rehabil Eng* **10**, 197-203.
Halliday, S.E. et al. (2001) *Proc XVIIIth Conf ISB*, 52.
Halliday, S.E. et al. (2002) *Acta Bioengng Biomech* **4** (Suppl 1): 209-210.
Halliday, S.E. (2003) D.Phil. thesis, University of Oxford.
Lu, T-W. et al. (1998) *JBiomech* **31,** 63-69.
Wheeler, G.D. et al. (2002) *Arch Phys Med Rehabil* **83**, 1093-1099.

ACKNOWLEDGEMENTS

The authors wish to thank Prof. Brian Andrews and the Tolkien Trust for their generous support.

EFFECTS OF SPEED AND CADENCE ON THE LOWER EXTREMITY JOINT REACTION FORCES AND TORQUES DURING WALKING

T. W. Kernozek[1,2], Jessica Woodworth[1], Kimberly Harbst[1]
[1]Physical Therapy Department, University of Wisconsin-La Crosse, La Crosse, WI, [2]Gundersen Lutheran Sports Medicine, La Crosse, WI
E-mail: kernozek.thom@uwlax.edu

INTRODUCTION

Lower extremity modeling may yield useful information for injury prevention (Novacheck 1999; Winter 1992). A relationship between gait velocity and joint forces has been suggested by previous research. The speed of walking affects the ground reaction forces that may affect joint kinetics. Devita and Hortobagyi (2000) reported that the lower extremity joint torques were reduced with aging. Furthermore, Devita (2000) stated that elderly adults select a slower gait velocity with a shorter step length. However, the relationship between cadence and gait velocity and the resultant effect on joint forces has not been examined previously. The terms “Gait velocity” and “cadence” have often been used interchangeably in the literature. Thus, the effect of isolated alteration of cadence or gait velocity on resultant joint kinematics and kinetics are unknown. The purpose of this study was to examine these effects.

METHOD

Fifteen healthy, 20-25 year-old female subjects were studied. Fifteen reflective markers placed on the subjects on the pelvis and lower extremities prior to testing using the Helen Hayes marker set (Kadaba et al.1990). Markers were tracked by a 3-D motion analysis system (Motion Analysis Corporation, Santa Rosa, CA) at 60 Hz. Static data were collected to establish hip, knee and ankle joint centers. Subjects walked along a 15-meter walkway using photocells to monitor walking speed. A digital metronome provided auditory feedback on the specified walking cadence. During each walking trial, subjects contacted a force platform (Bertec, Columbus, OH) located flush with the walkway surface to capture ground reaction force data at 1200 Hz. OrthoTrak software (Motion Analysis Corporation, Santa Rosa, CA) was used to create the link segment model and calculate the joint reaction forces and torques at the right hip, knee and ankle.

Standing height, weight and bilateral foot lengths were recorded. The subject’s normal walking speed was measured using photocells and averaged over ten trials. The subject’s normal walking cadence was matched to a digital metronome. Five combinations of gait speed and cadence were measured: normal speed-cadence, normal cadence-speed 15% above (+15% speed), normal cadence-speed 15% below (-15% speed), normal speed-cadence 15% above (+15% cadence), and normal speed-cadence 15% below (-15% cadence). Each subject was instructed to walk along a 15-meter walkway at a specified speed while matching her cadence to the auditory cues of the metronome. The subject was required to contact a force platform with her right foot.

Kinematic and kinetic data were time-normalized and average data were presented for each condition. A 2-way ANOVA with repeated measures (alpha = 0.05) was used to analyze the data.

RESULTS AND DISCUSSION

Range of Motion during Gait Cycle

Subjects demonstrated the least ankle and hip joint excursion in the preferred cadence condition with walking speed reduced by 15% (-15% speed). Conversely, knee range of motion was maximized at a walking speed of 15% below normal (-15% speed) and minimized at a walking speed of 15% above normal (+15% speed). There were no changes with cadence either 15% above or below (±15% cadence).

Joint Compression Forces during Stance

Ankle joint and knee joint compression forces were minimized at a walking speed of 15% below preferred with preferred cadence (-15% speed). Increased cadence at preferred gait speed reduced ankle, knee and hip joint compression forces (+15% cadence) (see Figure 1).

Anterior Shear Joint Forces during Stance

Anterior ankle, knee and hip joint forces were minimized at a speed 15% below preferred walking speed (-15% speed).

Posterior Joint Forces during Stance

Reducing either walking speed or cadence by 15% (-15% speed or –15% cadence) resulted in a reduction in the posterior ankle joint forces.

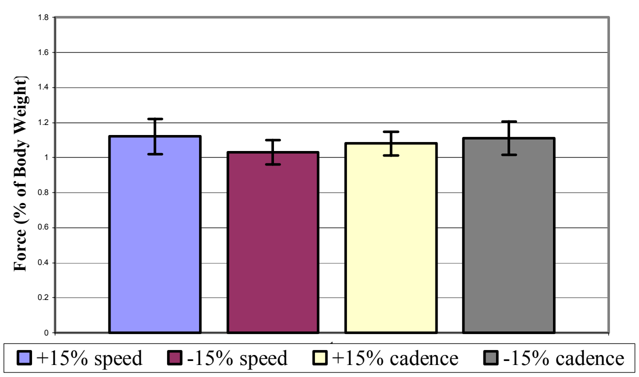

Figure 1: Compression at the Knee during Stance

Moments during Stance

Peak flexor and extensor moments at the ankle, knee, and hip were minimized when the subject walked at a speed 15% below preferred (see Figure 2).

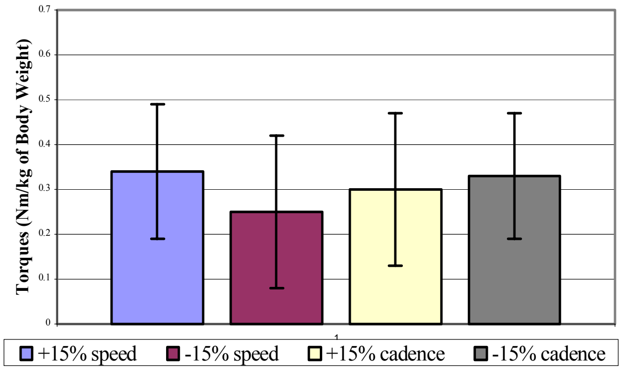

Figure 2: Knee Extension Moment during Stance

SUMMARY

The greatest reduction in lower extremity joint reaction forces and torques occurred when subjects walked reduced speed (-15% speed) rather than cadence (-15% cadence). Lower extremity compressive forces were minimized when the subject walked at a cadence that was faster than preferred (+15% cadence). The combined effects of reducing walking speed and increasing cadence results in a shorter stride length. Overall, reducing walking speed has a slightly greater effect on reducing joint compression and peak muscle moments during walking than altering cadence.

REFERENCES

Devita, P., Hortobagyi, T. (2000). *J Appl Physiol*. **88**,1804-1811.

Devita, P. et al. (1997). *MSSE*. **29**,853-859.

Kadaba, M.P et al. *J Orthop Res*. **8**,383-392.

Novacheck, T.F. (1999). *J Bone Joint Surg*. **80**,1220-1223.

Winter, D.A., Bishop, P.J. (1992). *Sports Med*. **14**,149-156, 1992.

ACKNOWLEDGEMENTS

Jessica Woodworth received a Dean's Distinguished Summer Fellowship from the College of Science and Allied Health at UW-L to work on this project.

ACCURACY OF USING MULTIPLE ZONES FOR THE DLT IN SWIMMING

Bryan J. Morrison and Richard N. Hinrichs
Department of Kinesiology, Arizona State University, Tempe, AZ, USA 85287-0404
E-mail: bryan.morrison@asu.edu

INTRODUCTION

Thee-dimensional analyses of swimming usually involve separate calibrations above and below water. For example, Cappaert and colleagues (1995) used the DLT to calibrate above and below water and found that predictions from above and below water did not match or had a discontinuity at the interface. They attempted to solve this problem by computing the location of the shoulder from both pairs of cameras and translating the underwater coordinates to match the above water coordinates. The purpose of this study was to investigate the nature of discontinuities of this type.

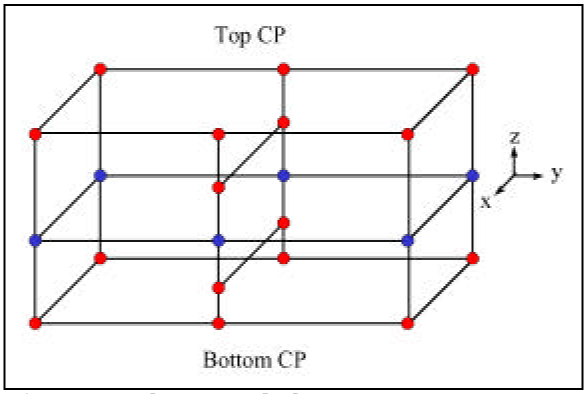

Figure 1: The control object containing 22 points, the middle 6 points (blue) were used in both the top and bottom zones with the red points being used in their respective zones. This object was displaced horizontally (with overlap) to create a larger control volume using the MDLT.

METHODS

A 22-point control object made out of 2-cm diameter PVC pipe was calibrated and used for this study (Figure 1). The multiphase DLT (MDLT, Challis, 1995) was used to join a second zone and create a larger volume with more points, with dimensions of 129.5 cm (x), 208.0 cm (y), and 95.2 cm (z). The top and bottom were not identical in the z direction when two zones were used; the top was 47.2 cm, and the bottom was 48 cm.

<u>Experiment 1 – Baseline accuracy, single calibration</u>. Four cameras, a top pair and a bottom pair, along with two positions of the control object (left and right) were used. First, the MDLT technique was used to determine camera parameters and known locations for the larger set of 44 points using two sets of camera pairs separately then averaged together. Keeping the larger volume the same, 22 points (out of the 44) were selected as control points (CP) to compute camera parameters for the MDLT. Six points of known location not used in the calculation of camera parameters were used as non-control points (NCP). These six NCP always fell in the middle (see blue points in Figure 1) because of our interest in the accuracy of points that lie on the water surface and can be seen above and below water at the same time. Computed NCP locations were compared for each camera pair to known NCP locations and expressed as “errors”.

<u>Experiment 2 – Two calibrated zones, one camera pair</u>. The original 44 MDLT points were then split into top and bottom zones with 12 points in the central plane being common to both zones. Of these 12, six were considered CP and six were used as NCP for each zone. This resulted in 22 (16 separate + 6 common) CP and 6 (common)

NCP in each zone. These CP were referred to as "zone control points" or ZCP. Camera parameters were computed for top and bottom zones separately for each camera pair. Errors in NCP locations were computed as above for each camera pair.

Experiment 3 – Two calibrated zones, two camera pairs. The "multiple-zone DLT" (ZDLT) set-up was done by using the ZCP, but using 2 pairs of cameras, one for each set of ZCP. Errors in NCP locations were computed between the top camera pair using the top ZCP and the bottom camera pair using the bottom ZCP (to simulate an actual above-water and underwater situation). This differs from Exp. 2 in which a single camera pair was used to compare the accuracy of the top and bottom zones.

The error analysis consisted of average location resultant (ALR), NCP difference (NCPD), and average resultant (AR) (Figure 2). The errors were normalized as a percentage of the longest diagonal of each individual control volume. The NCPD was used to determine how far the points actually were from each other (reflecting the discontinuity between zones), while the AR and ALR looked at the resultant error of the known point positions. In each case the reported errors are the means computed over the six NCP.

RESULTS AND DISCUSSION

The AR increased from Exp. 1 to Exp. 2 to Exp. 3, but not by much (0.04%, 0.13 cm total change). The ALR was always less than the AR and increased at a slower rate. The NCPD jumped from 0.08% (0.21 cm) to 0.22% (0.55 cm) to 0.27% (0.67 cm) for Exp. 1, Exp. 2, and Exp. 3, respectively. This was mainly due a shortened z dimension.

The greatest increase in error was caused by using different control volumes (Exp. 2). An example of this would be using periscopes to see both zones with a single camera pair. Only a small amount of additional error resulted from using two different camera pairs (Exp. 3). The results of this study could also apply to other situation where different DLT calibrations are used for different parts of the body (e.g. the left and right sides of the body during running).

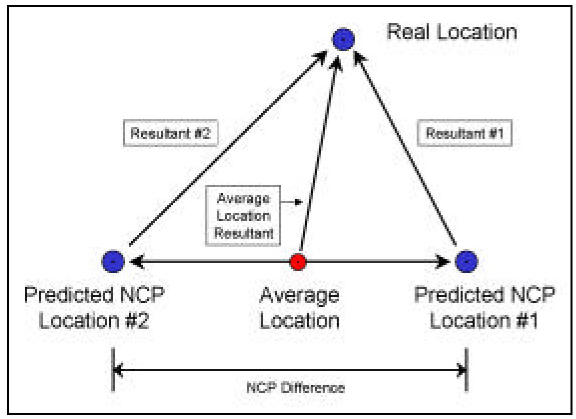

Figure 2: When using multiple camera zones to recreate an image, the errors can be identified as resultant, average location resultant, or NCP Difference.

SUMMARY

Discontinuities at the interface between zones of a multiple-zone DLT appear to result primarily from calibrating different zones and not from using different camera pairs.

REFERENCES

Cappaert, J.M. et al. (1995). *J Appl Biomech*, **11**, 103-112

Challis, J.H. (1995). *J Appl Biomech*, **11**, 351-358.

DO BODYSUITS FROM DIFFERENT MANUFACTURERS AID A SWIMMER'S BUOYANCY?

Richard N. Hinrichs[1], Bryan J. Morrison[1], and Scott P. McLean[2]
[1]Department of Kinesiology, Arizona State University, Tempe, AZ, USA 85287-0404
E-mail: hinrichs@asu.edu
[2]Department of Kinesiology, Southwestern University, Georgetown, TX, USA 78627-0770

INTRODUCTION

The new full-body swimsuits that became popular during the 2000 Olympic Games appear to provide swimmers with an advantage over conventional suits as evidenced by the sudden popularity of bodysuits and the onslaught of recent world records set in these suits. The reasons for such an advantage are unclear, however. Perhaps the suit material provides a reduction in frictional resistance (surface drag) compared to conventional suits or bare skin. Many swimmers claim that they feel that these suits allow them to "ride higher in the water" implying increased buoyancy. Previous research has looked at buoyancy characteristics and how they affect swimmers (Cordain & Kopriva, 1991; McLean & Hinrichs, 1998, 2000; Toussaint et al., 1989; Yanai, 2001). Cordain and Kopriva (1991) demonstrated a 3-5% time drop with a reduction in body density of 0.027 g/ml while wearing neoprene wetsuits. Toussaint et al. (1989) suggest that this is due to increased buoyancy and less frontal area in the water. Toussaint et al. (2002) observed a non-significant 2% drag reduction due to a full-body swimsuit, and two recent studies demonstrated no buoyant effects of the Fastskin™ (Benjanuvatra et al., 2002; Roberts et al., 2003).

The purpose of this study was to measure the buoyant forces and center of buoyancy locations of competitive swimmers wearing full bodysuits compared to conventional lycra suits and to see if the buoyant effects change with time in the water.

METHODS

Bodysuits were obtained from five different manufacturers. Of the many designs available, we tested the most popular variety from each manufacturer—those that covered full legs and torso but not the arms (or in one case only to the elbow). Thirty competitive swimmers (14 men, 16 women, ages 18-36) were used as subjects. Informed consent was received from each subject prior to testing. Each subject's **center of mass** (CM) was located relative to the malleolus in a prone body position with the arms fully extended above the head (hereafter referred to as the streamline position) using a two-dimensional reaction board (Hay, 1993). The distance between malleolus and the bottom of the foot was used to express all distances relative to the bottom of the heel. The **center of buoyancy** (CB) was determined using procedures similar to those we have followed in previous studies (McLean & Hinrichs, 1998, 2000). During these tests the subjects assumed a prone position underwater while being suspended by two tethers each attached through force gauges to a wooden beam placed above the water. They were asked to get into position as quickly as possible, and hold that position for a few seconds while we measured the forces in the tethers. The subjects then stayed attached, but with their heads above water, until they were tested again at one- minute intervals. This was done for the conventional suit first and then for each of the five bodysuits in random order.

RESULTS AND DISCUSSION

We found a significantly greater buoyant force (as a % of body weight) in women than men for all suits ($p<.05$) (Figure 1). We also found smaller CB-CM distances in women compared to men for all suits. These results are consistent with our previous data on conventional suits (McLean & Hinrichs, 1998, 2000). Bodysuits from three of the five manufacturers provided a significant increase in buoyant force compared to conventional suits. One additional suit had a non-significant trend in this direction. The increases in force were approximately 0.1 to 0.3% of body weight at minute 1 and tended to decrease over time. At minute 4 this effect had all but disappeared. While there were trends for all suits, we found only one suit that provided a significant reduction in the CB-CM distance compared to the conventional suit. Overall, the bodysuits had the greatest "buoyant effects" on the men. This may be because men have a higher body density and their legs tend to sink more than women's (McLean & Hinrichs, 1998, 2000).

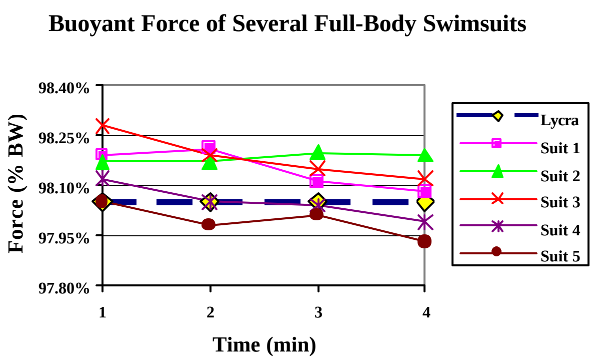

Figure 1: The suits provided a buoyant force that was reduced over time. Suits 1-3 provided significantly greater buoyant force than the conventional lycra suit.

SUMMARY

FINA rule SW 10.7 states "No swimmer shall be permitted to use or wear any device that may aid his speed, buoyancy or endurance during a competition . . ." It is this rule that makes wetsuits illegal. Why are bodysuits being treated differently than wetsuits? Our results show that at least three of these bodysuits do indeed aid in a swimmer's buoyancy compared to conventional suits. Perhaps this rule should be changed or else these suits should be disallowed.

REFERENCES

Benjanuvatra N. et al. (2002). *J Sci Med Sport*, **5**:115-23.

Chatard, J.C. et al. (1995). *Med Sci Sports Exerc*, **27**, 580-586.

Cordain, L., Kopriva, R. (1991). *Br J Sports Med*, **25**, 31-33.

FINA. (http://www.fina.org/swimrules_10.html)

Hay, J.G. (1993). *The Biomechanics of Sports Techniques* (4th ed.). Englewood Cliffs, NJ: Prentice-Hall.

McLean, S.P., Hinrichs, R.N. (1998). *J Sports Sci*, **16**, 373-383.

McLean, S.P., Hinrichs, R.N. (2000). *J Appl Biomech*, **16**, 248-263.

Roberts B.S. et al. (2003). *Med Sci Sports Exerc*, **35**, 519-24.

Toussaint, H.M. et al. (1989). *Med Sci Sports Exerc*, **21**, 325-328.

Toussaint H.M et al. (2002). *Sport Biomech*, 1, 1-10.

Yanai, T. (2001). *J Biomech*, **34**, 235-243.

ACKNOWLEDGEMENTS

This study was funded by a grant from USA Swimming.

A SIMPLE COMPUTER SIMULATION MODEL OF THE DEFORMATION CHARACTERISTICS OF GYMNASTIC LANDING MATS

Chris Mills, Matt Pain and Fred Yeadon

School of Sport and Exercise Sciences, Loughborough University, UK
E-mail: M.T.G.Pain@lboro.ac.uk

INTRODUCTION

The International Gymnastics Federation (FIG) has specific guidelines for tolerance levels of landing mats. However the criteria are based on threshold values obtained from vertical drops of a 20 kg mass with a contact area of 10 cm^2 and a landing velocity of 3.96m/s. If the mat properties are to be included in future inverse or forward dynamics analyses of gymnastics landings then the mechanical properties and responses to the requisite horizontal and vertical loading regimes needs to be quantified.

Spring-damper models have been used to represent the foot-ground interface (Lui & Nigg, 2000) and have included a variety of structures within a single lumped model (heel pad, mid sole, snow, tumbling track) Little experimental evidence is available to support the justification of a single 'lumped' model in all cases. In gymnastics the type of landing mat can vary and this has a distinct effect on gymnast landing perception. The modelling of the mat separately from the gymnast's foot would appear to be justified in these landings.

Landing mats are bulky, have a number of component layers and undergo large area visco-elastic deformations. To produce an accurate model of them would require an array of masses interconnected by spring-dampers. (Peikenkamp, Fritz & Nicol, 2002). This could prove computationally time consuming.

The purpose of this paper was to develop a simple model of a sample gymnastic landing mat that can be incorporated into future research involving injuries during landing.

METHODS

The force F measured by a force plate beneath the mat may be expressed as:

$$F = - kx - rvx - ma$$

The additional 'ma' term represents the mass of the mat accelerated during the impact. In this study an attempt was made to model the measured force F without including an effective mat mass m. using a linear spring damper model developed using Matlab MathWorks Inc. An impactor of mass 24 kg, contact area (25cm by 25cm) was used to represent a gymnast landing. The 24 kg mass of the impactor was determined via subject testing. The landing mat was a custom made Continental mat weighing 6.1 kg measuring 0.9 m by 0.6 m by 0.2 m. It was partially constrained to the force plate (Kistler 9281B) and two accelerometers (PCB Piezotronics) were securely attached to the impactor. Two Phantom high-speed cameras (1000Hz) were used to record the vertical deformation and the area deformation of the landing mat, based upon the methodology of Yeadon and Nigg (1988).

Five different drop heights were used to produce vertical impact velocities between 4.5 and 6.5 m/s. Additional oblique tests were carried out at five different angles (45°, 50°, 55°, 60° and 65°) on a custom built rig. Angles and landing velocities covered the range of those seen in competition landings (Takei 1998).

A static loading test was used to determine the approximate vertical stiffness coefficient of the landing mat. A series of weights were placed on the mat's surface and the amount of vertical deformation recorded. Simulated Annealing used the static stiffness as an initial guess of the spring stiffness parameter. Two points on the impactor were manually digitised using the Phantom software. DLT and reconstruction was performed in Matlab using the KineMat toolbox.

Markers on the impactor were used to calculate impact velocity and landing surface deformation. The damping coefficient was adjusted using Simulated Annealing to minimise the difference between the force time characteristics recorded via the force plate and the corresponding characteristics from the spring damper model and the high-speed video data.

RESULTS AND DISCUSSION

With an impact velocity of 5.5 m/s (Takei, 1998) the maximum vertical mat deformation was 0.083 m with a vertical peak force on the force plate of 7054 N at 0.20 s. Firstly a 3 spring damper model was used to simulate the impact. The three spring damper simulation produced a peak force of 7045 N at 0.20 s (Figure 1) with a vertical deformation of 0.086 m.

Secondly a single spring damper system was used to simulate the impact. The resulting force-time trace was virtually identical to that in Figure 1.

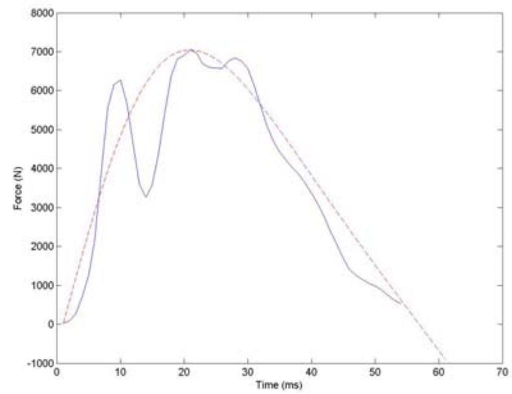

Figure 1: Force time trace. Raw data (continuous) plotted over simulation (dashed) three spring dampers.

The single spring damper model produced a peak force of 7060 N at 0.20 s with a vertical deformation of 0.086 m.

SUMMARY

A single spring damper has been used successfully to simulate the loading characteristics for an impact at 5.5 m/s. At an impact velocity of 4.5 m/s the model overestimated the peak force by 3.4%. At 6.5 m/s the model underestimated the peak force by 13.0%. This is probably due to the increase in the mass of the mat being accelerated at the higher velocities.

REFERENCES

Lui, W., Nigg, B.M. (2000). *Journal of Biomechanics,* **33**, 219-224.
Peikenkamp, K., Fritz, M. & Nicol, K. (2002). *Journal of Applied Biomechanics,* **18**, 122-134.
Takei, Y. (1998). *Journal of Applied Biomechanics*, **14**, 190-210.
Yeadon, M.R., Nigg, B.M. (1988). *Medicine and Science in Sports and Exercise,* **20**, 403-407.

VERTICAL JUMP KINETICS IN YOUNG CHILDREN

Kurt R. Neelly [1,2] and Carol J. Zebas [2]

[1] Department of Physical Therapy and Health Sciences, Bradley University, Peoria, IL, USA
[2] Biomechanics Laboratory, University of Kansas, Lawrence, KS, USA
E-mail: kurtn@bradley.edu

INTRODUCTION

Research suggests a link between physical and cognitive development in children exists (Diamond, 2000, Krombholtz, 1997). Developmental experts believe that motor delays negatively influence future development (Gallahue, 1996). A common motor skill frequently observed in children is the vertical jump (VJ). Many VJ studies have assessed kinematic and kinetic performance variables and training techniques on adults. Several kinematic studies have assessed the vertical and horizontal jumping performance of young children. However, no kinetic studies of very young children performing a VJ have been published. The purpose of this study was to compare kinetic, performance, and temporal measures of kinetically more and less efficient 3-5 year old children performing two VJ techniques. Kinetic efficiency (KE) represented the magnitude, direction, and duration of the forward-backward Y-forces.

METHODS

Eighty-six normal 3-5 year-old children (mean age of 4.6 years old) volunteered to participate in this study. All children had their standing height, reach height, and weight measured, along with completing the locomotor subtest of a developmental screening tool (Peabody Developmental Motor Scales – 2) to determine that their locomotor skill development was comparable to their peers.

Subjects were videotaped (JVC 9800 DVL at 30 fps) performing three maximal countermovement vertical jumps with upper extremity (UE) use ($CMVJ_{UE}$) and three maximal jumps without UE use ($CMVJ_{NoUE}$) on a force plate system (AMTI sampling at 500 Hz.). To facilitate maximum height jumps in the children, a balloon was suspended near the maximum jump height (Clark et al., 1989, Jensen et al., 1994) as assessed during practice trials.

VJ height was determined by digitizing the video performance of all trials. For the $CMVJ_{UE}$, VJ height was defined as the difference between standing reach and jump and reach heights, while the $CMVJ_{NoUE}$ height was the difference between standing height and the top of the head at the apex of the jump. Peak net force and power, normalized per body weight, peak velocity, and the time from peak kinetic values to takeoff were obtained from the force plate data from each respective maximum jump height trial. KE was calculated as the net normalized propulsive phase Y-impulse (fore-aft) produced during the jump.

The subjects were then placed in quartiles based on the KE of their $CMVJ_{NoUE.}$ The 1st quartile (n = 21), defined as kinetically more efficient, consisted of those jumpers with the largest negative directed KE. The 4th quartile (n = 21), defined as kinetically less efficient, consisted of those jumpers with the largest forward directed KE.

Two repeated measures MANOVA's were run to determine if there were differences between the dependent variables, based on UE use and KE. The first R-MANOVA utilized the performance variables as the dependent variables, while the second R-MANOVA utilized the temporal measure between occurrence of peak values and takeoff as the dependent variables. Significant R-MANOVA's were followed by R-ANOVA's for each dependent variable, with secondary pairwise and main effect comparisons being conducted. Familywise error rates were controlled by using a Holm's sequential Bonferroni technique to adjust the alpha levels.

RESULTS

Kinetically more efficient jumpers had a 19% higher $CMVJ_{UE}$ compared to their $CMVJ_{NoUE}$, while less efficient jumpers jump height did not differ between jumping techniques. In addition, the more KE group's $CMVJ_{UE}$ height was 30% higher than the less KE's $CMVJ_{UE}$ (Figure 1).

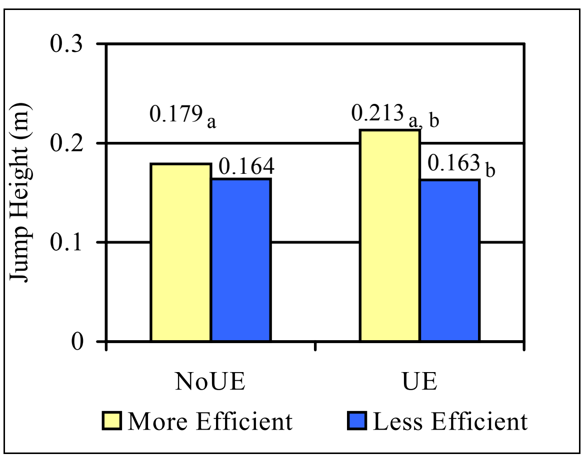

Figure 1: VJ height compared between UE Use and Kinetic Efficiency. Means with same subscripts are different at $p \leq 0.025$.

Regarding the timing (kinetic coordination) of peak kinetic values to takeoff, the less KE took 12% longer from peak power to takeoff than the more KE jumpers (Figure 2).

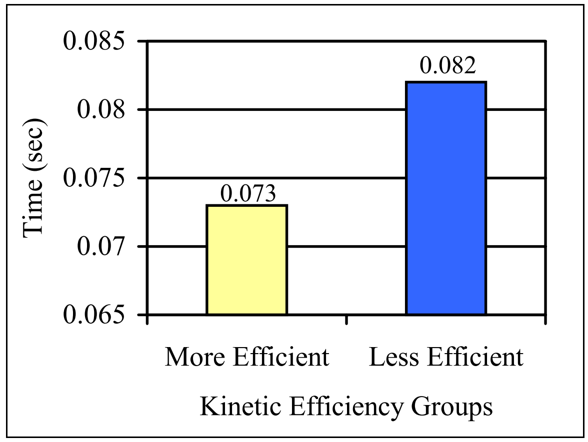

Figure 2: Time from peak power to takeoff, no difference between $CMVJ_{NoUE}$ and $CMVJ_{UE}$, data collapsed across techniques. Significant difference between more and less efficient jumpers, $\underline{p} = 0.006$.

CONCLUSION

The results of this study indicate that when performing a VJ, those children able to efficiently control and direct their kinetic forces (more KE) were able to integrate UE use more effectively from a performance and temporal coordination perspective than the less efficient group. These findings could potentially be implemented into an instructional program designed to improve jumping and ultimately future development.

REFERENCES

Clark, J.E. et al. (1989). *Dev Psychol*, **25**, 929-935.

Diamond, A. (2000). *Child Dev*. **71**, 44-56.

Gallahue, D. L. (1996). *Developmental Physical Education for Today's Children* (3rd ed.). Brown & Benchmark Publisher.

Jensen, J.L. et al. (1994). *Res Q Exerc Sport*, **65**, 258-268, 1994.

Krombholz, H. (1997). *Percept Mot Skills*, **84**, 1168-1170.

ENDPOINT INSTANTANEOUS RADIUS OF ROTATION MAGNITUDES IN SOCCER AND VOLLEYBALL PLAYERS

John DeWitt [1] and Peter Vint [2]

[1] Exercise & Sport Research Institute, Arizona State University, Tempe, AZ, USA
[2] Research Integrations, Tempe, AZ, USA
E-mail: john.k.dewitt1@jsc.nasa.gov

INTRODUCTION

Subjects with greater and lesser skills are often compared to identify components of expert performance. Those gross features found only in the experts are usually concluded to be vital to successful skill execution. It is also apparent, however, that fine differences exist within experts. Although two athletes may seem to perform a task in an almost identical manner, the outcomes may be different. In sport, slight differences in performance may separate success and failure. It is sometimes difficult to determine what causes those differences in an expert population due to similar methods of execution. A novel approach may identify intersubject differences within a homogenous group.

Soccer and volleyball players attempt to develop large foot/hand velocities to obtain large ball velocity magnitudes (BV). The kicking and striking tasks are similar in that many muscle groups act to coordinate multiple segments to achieve optimal contact surface velocity at impact. Although maximal endpoint velocity is desirable, it is only useful if achieved at the instant of impact. Therefore, these skills require muscular strength and fine motor control.

A particle's linear velocity (**v**) is determined by its angular velocity (**AV**) and radius of rotation. If the foot/hand center of mass (CM) is modeled as a single point in space, regardless of the segments involved in the action, it possesses an instantaneous **?** and instantaneous radius of rotation (IRR) at any given time. The IRR is an imaginary segment that connects the endpoint CM to some location in space about which it rotates. An examination of the IRR may offer insight about something that greater skilled athletes do to maximize their performance. Since segment **AV** occurs due to muscular action, coordinating segmental motion to increase the IRR will result in a greater endpoint **v** for a given muscular force. It is possible that experts manipulate their segments to increase the overall IRR to optimize the endpoint CM velocity at impact.

The purpose of this investigation was to determine if those experienced athletes who obtain greater BV than other experts also have different peak magnitudes of the IRR (pIRR). Separate but identical analyses were performed with soccer kicking and volleyball spiking. It was hypothesized that those athletes with higher BVs will have greater pIRR magnitudes than their counterparts.

METHODS

Two separate data collections were conducted. 16 experienced soccer players (SP) kicked a soccer ball as hard as possible, and 8 experienced volleyball players (VP) spiked a volleyball as hard as possible. Multiple trials of each task were videotaped at 60 Hz. Video data were digitized to identify the 3-D location of the CM of the striking endpoint and ball during each picture. Digitizing occurred from the beginning of hip flexion/shoulder flexion until impact. The trial for each subject that resulted in the greatest BV was chosen for further analysis. The trials were arranged in sequential order of BV, and divided into two equal groups of F (fast) and S (slow). An initial dependent t-test ensured that the BVs differed between each group (p<.05).

For each trial, the CM **v** and **AV** magnitudes were computed for each picture. The IRR magnitude was found as

$$|\mathbf{IRR}| = |\mathbf{v}| / |\mathbf{AV}|$$

The trial was then examined to find peak |**IRR**| (pIRR), peak |**v**| and peak |**AV**|. Dependent t-tests were used to compare the F and S groups for the three dependent variables. Alpha was set at p<.05 to determine significance.

RESULTS AND DISCUSSION

It was unexpected to find that for the pIRR, S and F group trends were different for each sport. Experienced SP tended to have a lower pIRR while VP tended to have greater pIRR values (Table 1, Figure 1). Although statistical significance was not reached, trends indicate that there may be differences within each group. The peak values for each variable did not necessarily occur at the same picture.

The large pIRR in SK in each group may occur because the **v** is affected by rotation and translation. The whole body translation during approach may increase the pIRR.

It is possible that SP attempt to minimize the pIRR to reduce the moment of inertia of the moving segments, thereby increasing **AV** for a given amount of muscular force. They sacrifice rotational radius for increased rotational velocity. In contrast, VP may not need to reduce their pIRR because of the smaller relative mass to move. They can afford to increase their pIRR to increase **v**.

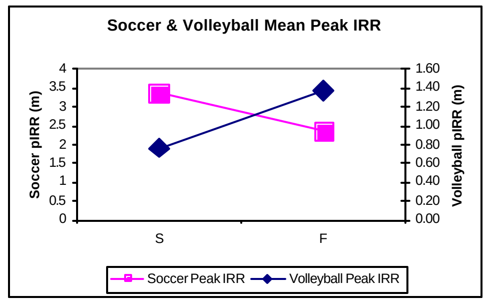

Figure 1: SP and VP pIRR means.

It might also be that because SP were kicking a resting ball, while VP struck an airborne ball, the task environment resulted in different control strategies. SP freely chose their speed and direction of approach, whole VP were required to react to the flight of the ball. These constraints may have resulted in different control strategies.

SUMMARY

We found that SP may tend to decrease their foot CM IRR, while VP may increase their hand CM pIRR to obtain higher ball velocities. Further study should be conducted with greater subject sizes to increase statistical power.

Table 1. Mean (SD) Magnitude of SP and VP BV, pIRR, Angular and Linear Velocity

	|**BV**| (m/s)		Peak |**IRR**| (m)		Peak |**AV**| (rad/s)		Peak |**v**| (m/s)	
	S	F	S	F	S	F	S	F
SP (n=16)	24.91 (1.34)*	28.48 (1.35)	3.39 (1.31)**	2.37 (0.72)	17.99 (2.77)	19.29 (2.26)	14.37 (1.39)*	15.91 (0.75)
VP (n=8)	20.01 (0.70)*	22.66 (0.58)	0.76 (0.17)**	1.38 (0.68)	61.68 (9.77)	50.38 (14.46)	11.66 (1.14)	12.79 (0.92)

*p<.05, **p<.13

RELATIONSHIP BETWEEN PHYSIOLOGICAL AND TECHNICAL PARAMETERS DURING AN EXHAUSTIVE TEST IN HIGH LEVEL SWIMMING

AUJOUANNET Y[(1)](✉), BONIFAZI M[(2)], HINTZY F[(1)], ROUARD AH[(1)]
[(1)]LMAS, Université de Savoie, Le Bourget du Lac, France
[(2)] Istituto di Fisiologica Umana, Sienna, Italy
E-Mail : yannick.aujouannet@univ-savoie.fr

INTRODUCTION

In swimming, numerous articles focused on the physiological aspect of fatigue (Keskinen and Komi 1988, 1993; Keskinen 1989) although only few authors studied the kinematic aspect of fatigue (Deschodt 1999). As concluded by Deschodt (1994;1999) who observed only sagittal view of the hand trajectory, fastest swimmers had the greatest fingertip coordinate on antero posterior (F) and on vertical axis (D). Under fatigue, a decrease of stroke velocity (SV), stroke rate (SR), stroke length (SL) was observed (Craig and Pendergast 1979; Keskinen 1989; Keskinen and Komi 1988 and 1993) and in hand displacement for F and D (Deschodt 1999). In order to understand the evolution of kinematic parameters under fatigue, the aim of this study was to investigate the relationship between fatigue and the 3-D kinematic parameters in elite swimmers.

METHODS

Ten male international swimmers (1.87 m ±7.54, 79 kg ±6.53, 22.5 yrs ±2.29) participated in this study. The 100m freestyle performance ranged from 49,07s to 53,98 (50,63s ±2,12). Each athlete performed 4*50 m in freestyle at maximal velocity separated by a 10 s rest period corresponding to a broken 200 m. Capillary blood sample (5 µl) was taken before and immediately after the test. Two digital cameras filmed frontal and sagittal views of aquatic stroke. Right hip joint and fingertip were digitized frame by frame to determine the swimmer displacement and the hand trajectory. Stroke parameters measured were SR, SL and SV. According to Maglischo (1986), different maximal coordinates of the fingertip trajectory were studied (F) on the antero-posterior axis, (D) on the vertical axis, maximal outward (O) and inward (I) on the transversal axis. The effects of fatigue was evaluate from the comparison of the different parameters between the 1st and the 4th50 using a Wilcoxon test ($p<0,05$). The parameters significantly different were computed into a principle component analysis (PCA).

RESULTS AND DISCUSSION

[Lmax] attained 12.98 ±2.79 mmol.l^{-1} at the end of the test and was comparable to 200m race (Bonifazi and Carli, 1993). This physiological parameter indicated a peripheral fatigue (Hermansen 1981) and the decrease in velocity between the 1st and the 4th 50m (14,02% ±6,06) attested the reaching of fatigue (Bonnard et al. 1994). At the end of the test, SR, SV, O(t) and I(t) decreased significantly (Table 1). In agreement with Toussaint and Beek (1992), the SR decrease could result from a decrease in force production engendered by a peripheral fatigue (Hermansen 1981) or by a failure in neural activation (Keskinen and Komi 1993). At the opposite, spatial parameters did not changed under fatigue. The maintaining of the hand trajectory suggested the existence of a robust spatial pattern in accordance with Rodacki et al. (2001). The closed position of [Lmax], SR and SV in the PCA diagram indicated that the fastest swimmers presented the higher [Lmax] associated to higher SR (Figure 1). These results confirmed previous studies (Keskinen and Komi 1988 and 1993; Cappaert et al. 1995). Weiss et al. (1988) underlined the importance of SR and lactate tolerance capacity for high level swimming. The opposite situation of SV, SR, [Lmax] to O(t), I(t) indicated that best swimmers presented the lower duration of the insweep phase. They spent less time for similar spatial trajectory, and as a result presented higher hand velocity. Schleihauf et al. (1983) observed that elite swimmers were characterized by the most rapid hand actions during the insweep phase. The present study confirmed this result in fatigue situation.

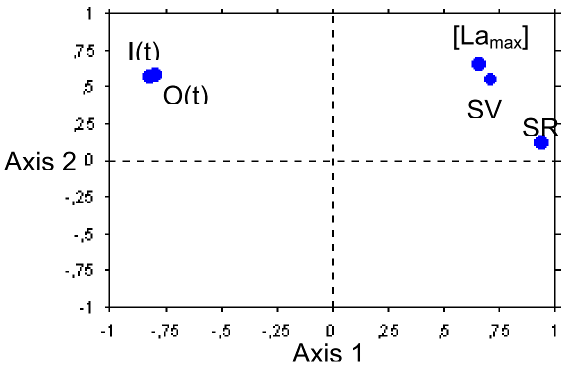

Figure 1: PCA representation of stroke and physiological parameters.

Table1 : Mean and standard deviation for physiological and stroke parameters during the 1st and the 4th 50m. (*p<0.05; **p<0.01).

Parameters	1st 50m	4th 50m	z	p
Lactate ($mmol.l^{-1}$)	1.03±0.13	12.98±2.79	-2.80	0.005**
SR ($cyc.min^{-1}$)	34.5±5.91	31.45±4.4	-2.19	0.023*
SL (m)	2.26±0.29	2.08±0.2	-1.58	0,114 N.S.
SV ($m.s^{-1}$)	1.29±0.2	1.08±0.9	-2.80	0.005**
Forward (X) (cm)	68±24	68±26	-0.18	0.086 N.S.
Depth (Z) (cm)	-67±8	-68±8	-0.51	0.610 N.S.
Outward (Y) (cm)	-1±12	-10.3±23.7	-1.07	0.284 N.S.
Inward (Y) (cm)	-23±15	-24±23	0.15	0.878 N.S.
Forward (t) (s)	0.47±0.16	0.5±0.15	-0.81	0.414 N.S.
Depth (t) (s)	0.70±0.16	0.73±0.20	-0.56	0.575 N.S.
Outward (t) (s)	0.82±0.15	0.93±0.16	-2.17	0.03*
Inward (t) (s)	0.59±0.13	0.70±0.16	-2.24	0.025*

SUMMARY

The fatigue of highly skilled swimmers was characterized by a stable spatial hand pattern associated with an increase of time pattern for O and I. The maintaining of the hand trajectory even the fatigue suggested the existence of a robust spatial pattern.

REFERENCES

Bonifazi M, Martelli G, Marugo L, Sardella F, Carli G (1993) *Blood lactate accumulation in top level swimmers following competition. J Sports Med Phys Fitness* **33**: 13-18

Bonnard M, Sirin AV, Oddsson L, Thorstensson A (1994) *Different strategies to compensate for effects of fatigue revealed by neuromuscular adaptation processes in humans. Neur Lett* **166**: 101-105

Cappaert JM, Pease DL, Troup JP (1995) *3-dimensional analysis of the men's 100m freestyle during the 1992 Olympic Games. J Appl Biomech* **11**: 103-112

Craig AB, Pendergast DR (1979) *Relationships of stroke rate, distance per stroke, and velocity in competitive swimming. Med Sci Sport* **11(3)** :278-283

Deschodt V, Rouard AH, Monteil KM (1994) *Relationships between the 3 coordinates of the upper limb joints with swimming velocity. In Biomech Med Swim Sci VII, 1st edition, E&F Spon* 52-58

Deschodt V (1999) *Modifications de la trajectoire aquatique du poignet liées à l'apparition de la fatigue en natation. Sc Mot* **37** : 19-25

Hermansen L (1981) *Effect of metabolic changes on force generation in skeletal muscle during maximal exercise. In: Hum Muscl Fatigue: Physiol Mech. Symp, London, Pitman*,.75-88.

Keskinen KL, Komi PV (1988) *The stroking characteristics in four different exercises in free style swimming. In: Biomech Med Swim. Int Series on Sports Sci* 9: 219-226

Keskinen KL, Komi PV, Rusko H (1989) *A study of blood lactate tests in swimming. Int J Sports Med* **10(3)**:197-201.

Keskinen KL, Komi PV (1993) *Stroking characteristics of front crawl swimming during exercise. J Appl Biomech* **9**: 219-226

Maglischo CW, Maglischo EW, Higgins J, Hinricks R, Luedtke D, Schleihauf RE, Thayer A (1986) *A biomechanical analysis of the 1984 US Olympic swimming team: the distance freestylers. J Swim Res* **2(3)**: 12-16

Rodacki ALF, Fowler NE, Bennett SJ (2001) *Multi-segment coordination: fatigue effects. Med Sci Sp Exerc* **33(7)**: 1157-1167

Schleihauf RE, Gray L, DeRose J (1983) *Three-dimensional analysis of hand propulsion in the sprint front crawl stroke. In: Biomech Med Swim. Int Series on Sports Sci* **14** : 173-183

Toussaint HM, Beek PJ (1992) *Biomechanics of competitive front crawl swimming. Sports Med* **13(1)**: 8-24

Weiss M, Reischle K, Bouws N, Simon G, Weicker H (1988) *Relationships of blood lactate to stroke rate and distance per stroke in top female swimmers. In: Swim Sci V Champaign: Human Kinetics Pub* **18**: 295-303

Acknowledgements to the swimmers of the Italian Swimming Federation.

RELATIONSHIP BETWEEN TECHNICAL PARAMETERS AND PERFORMANCE IN FRONT CRAWL SWIMMING IN CHILDREN

B. POUJADE[1], Y.AUJOUANNET[1], C.A. HAUTIER [2], A. ROUARD[1]
[1].LMAS, Université de Savoie, Le Bourget du Lac, [2].CRIS, Université C. Bernard Lyon1, Villeurbanne, France
E Mail: bastien.poujade@univ-savoie.fr

INTRODUCTION

Performance in adults swimmers was linked to morphological characteristics (Chatard et al., 1987) and technical abilities (Zamparo et al. 1996) determined by kinematic measures (Schleihauf et al., 1986). The underwater observation of swimmers showed that the sinusoidal trajectories for each spatial plane of the hand was very important in the swimmer's propulsion. Deschodt et al. (1994) proved that kinematic parameters such as the forward, depth and backward movements of the hand during the aquatic stroke of swimming accounted for the swimmer's velocity. In regard to these previous results, the aim of this study was to analyse the relationships between performance and kinematic parameters in young swimmers.

METHODS

Seventeen swimmers (12.3 yrs ±0.46; 1.57 m ±7.05; 47.36 kg ±6.8) volunteered to take part in the study. Subjects carried out a 400m in front crawl swimming at maximal velocity to determine maximal aerobic velocity (V400) (Costill et al., 1985). During the 400m, two digital cameras were used to film the underwater movements. Right hip joint and fingertip were digitalised. The fingertip entry was taken as spatial and temporal reference (0, 0, 0, 0). The length (SL), the duration (SD), the velocity (SV) of the whole stroke were studied as different points of the fingertip trajectory : the maximal coordinates in the forward direction (F), in the External direction (E), the Internal one (I) and the maximal depth (D). For the lengths, the points were noted Fm, Dm, Em, Im and for the durations, the points were noted Fs, Ds, Es, Is. Mean, standard deviation were calculated and a principal component analysis (PCA) was used to analyse the relationships between the studied parameters.

RESULTS AND DISCUSSION

The mean time for the V400 was 1.16 m.s^{-1} (± 0.11). The mean values of SL, SD and SV were respectively 1.95 (± 0.34) m.stroke^{-1}, 0.55 (± 0.08) stroke.s^{-1} and to 1.08 (± 0.1) m.s^{-1}. For adult swimmers at sub-maximal velocities (1.26 m.s^{-1}), Keskinen and Komi (1988) obtained similar SD (0.52 stroke.s^{-1}) and higher SL (2.38 m.stroke^{-1}). These differences could be explained by lower force production for children (Vrijens, 1978). The lower SL observed for young swimmers could be also linked to slower neuromuscular characteristics (Belanger et al., 1983). The averages of spatial and temporal coordinates of each significant point of the trajectory of the fingertip were shown in Figure 1.

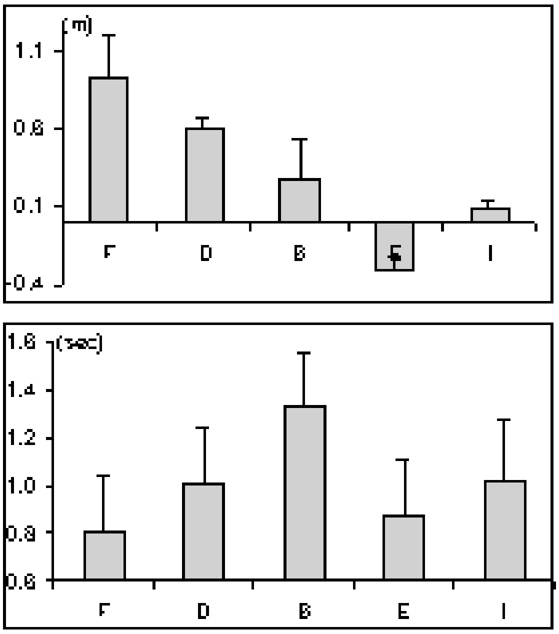

Fig 1: Characteristics of length (meter) (a) and of duration (second) (b) of the underwater fingertip trajectory: F forward, D depth, B backward, E external, I internal.

Even spatial parameters were not correlated to the height of the swimmers, children presented great differences with adults swimmers (Deschodt, 1994). The forward hand displacement was longer for the children compared to adults for a shorter duration. Children reached more quickly an equivalent maximal depth. On the transversal axis, they presented opposite results to adults swimmers with greater external outsweep and shorter insweep movement.. Children decreased all the phases that need forces due to their poorer strength.

On PCA the first factor (axis1) was mainly defined by Em located on the left side of the axis. This variable was negatively correlated to the group of variables located on the right of the axis (SD, Fs, Ds, Es, Fm, SL and V400). The 2nd factor (axis2) was defined by SV (Fig.2).

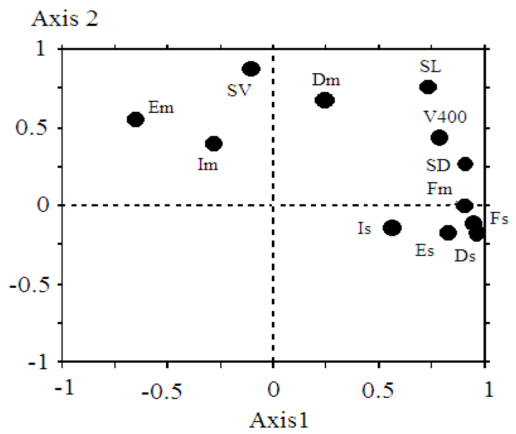

Fig.2: Variables representation with V400 (maximal performance on a 400-meter), SL (Stroke Length), SD (Stroke Duration), SV (Stroke Velocity), the length and duration of the maximal point were respectively noted Fm and Fs (Forward direction), Dm and Ds (Depth direction), Em and Es (External direction), Im and Is (Internal direction).

The performance on a 400m test was correlated to temporal parameters (SD, Fs, Ds and Es ($r=0.893$, $P<0.001$; $r=0.632$, $P<0.01$; $r=0.632$, $P<0.01$ and $r=0.586$, $P<0.05$). These relationship hasn't been found in any other study as well as for SD (Craig and Pendergast, 1979) as for parameters of hand trajectory (Deschodt et al., 1994). V400 was also correlated with SL and Fm ($r=0.787$; $P<0.001$ and $r=0.593$; $P<0.05$). The relationship between V400 and SL was in line with previous studies (Craig and Pendergast, 1979) when previous study proved that Fm was a weighty factor to the inter-individual differences of maximal velocities among international swimmers (Deschodt et al., 1994).

SUMMARY

This study of high-level young swimmers indicated that the variations of performance on a 400-meter could be explained by kinematic factors such as the time parameters (SD, Fs, Ds, Bs, Es) and spatial parameters (SL, Fm and Bm). Many authors proved that performance could be linked to other factors such as underwater torque (Zamparo et al., 1996) and muscular parameters. It is therefore necessary to carry out other tests in order to determine the precise influence of these factors on the young swimmer's performance.

BIBLIOGRAPHY

Belanger AY, Mc Comas AJ, Elder GBC. (1983). *Physiological properties of two antagonistic human muscle groups. Eur J Appl Physiol*, **51**, 381-393.

Chatard JC, Padilla S, Cazorla G, Lacour JR. (1987). *Influence de la morphologie et de l'entraînement sur la performance en natation. STAPS,* **8** (15): 23-27.

Costill DL, Kovaleski J, Porter D, Kirwan J, Fielding R, King D. (1985). *Energy expenditure during front crawl swimming: predicting success in middle-distance events. Int J Sports Med* , **6**, 266-270.

Craig BA and Pendergast DR. (1979). *Relationships of stroke rate, stroke length and velocity in competitive swimming. Med Sci Sports and Exerc*; **11**, 278-283.

Deschodt VJ, Rouard AH, Monteil KM. (1994). *Relationships between the three coordinates of the upper limb joints with swimming velocity. Biomechanics and Medicine in Swimming Science VII, , E & FN Spon, Troup JP, Hollander AP, Strasse D, Trappe SW, Cappaert JM (eds),* 52-58.

Keskinen KL, Komi PV. (1988). *The stroking characteristics in four different exercises in free style swimming. In De Groot, Hollander, huijing, Van Ingen Schenau (eds). Biomechanics XI-B. International Series on Biomechanics* ; **7**, 839-843.

Schleihauf RE, Higgins J, Hinrichs R, Luedtke D, Maglischo CW, Maglischo EW. (1986) *Models of aquatic skill sprint front crawl. N Z J Sports Med*; **1**,7-12.

Vrijens J. (1978). *Muscle strength development in the pre- and post-pubescent age. Med and Sport*; **11**, 152-158.

Zamparo P, Capelli C, Termin B, Pendergast DR, di Prampero PE. (1996) *Effects of the underwater torque on the energy cost, drag and efficiency of front crawl swimming. Eur J Appl Physiol*; **73**, 195-201.

EFFECTS OF FATIGUE ON SWIMMERS FORCES PRODUCTION

ROUARD AH[1], AUJOUANNET Y[1], BONIFAZI M[2], HINTZY F[1]
[1]LMAS, Université de Savoie, Le Bourget du Lac, France
[2] Istituto di Fisiologica Umana, Sienna, Italie
E-Mail : Annie.Rouard@univ-savoie.fr

INTRODUCTION

Performance in swimming was strongly related to the arm power (Sharp et al, 1982, Costill et al, 1983,). High correlation was reported between isometric strength of pull arm and swimming velocity (Miyashita, 1975). For Troup (1999), performance appeared to be more linked to the ability to maintain a high percentage of peak power throughout the race related to the swimming technique and the mechanical efficiency. In regard to these previous investigations, the aim of this study was to examine the influence of fatigue on power, isometric and propulsive forces production and on their relationships among elite swimmers.

METHODS

Ten male international swimmers (1.87 m ±7.54, 79 kg ±6.53, 22.5 yrs ±2.29) participated in this study. The 100m freestyle performance ranged from 49,07s to 53,98 (50,63±2,12). Three tests allowed to measure swimmers' forces before and after an exhaustive swimming test (pre and post conditions). Maximum isometric force in dryland situation was recorded for an arm-trunk angle of 30°, 90° and 120° (F30, F90, F120) according to Fomitchenko (1999). The maximal propulsive force (Fmaxp) was measured during a full tethered swimming on 5s (Rouard et al. 2001). The maximum Power (P) and corresponding Force (Fp), velocity (Vp) were measured on 5s during the central portion of a maximal 25m semi-tethered swimming (Rouard et al, 2001) in which an added resistance of 5% of Fmaxp was applied to the swimmer. After these initial forces tests (pre-condition), each swimmer performed an exhaustive test of 4*50 m in freestyle at maximal velocity separated by a 10 s rest period corresponding to a broken 200 m. Capillary blood sample (5 µl) was taken immediately after the test. The velocity (V) of the 4th 50m was taken as the indicator of performance in fatigue situation. At the end of the 4th 50m, the swimmer repeated the 3 forces tests (post-condition).

Mean and standard deviation were calculated for each parameter. The effects of fatigue on each variable was evaluated with a Wilcoxon test (p.<0.05). A principle component analysis (PCA) was computed to examine the relationships between the parameters before and after fatigue.

RESULTS AND DISCUSSION

[Lmax] attained 12.98 ±2.79 mmol.l^{-1} at the end of the 4*50m was comparable to 200m race (Bonifazi and Carli, 1993) and the decrease of performance (14.02% ± 6.06) between the 1st and the 4th 50m indicated a fatigue at the end of the exhaustion test.

Forces and power results in pre-conditions confirmed previous findings. All the parameters decreased significantly after fatigue excepted the Fmaxp. (figure 1).

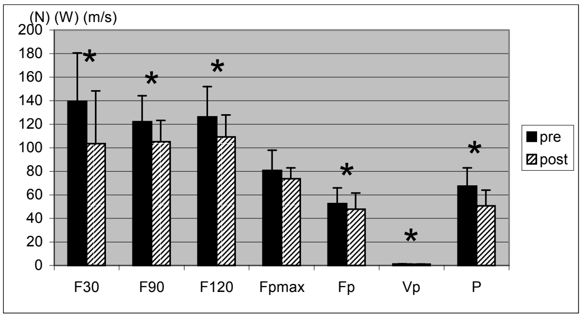

Figure 1-forces, velocity and power before (pre) and after fatigue (post). p<0.05

Before fatigue, power was linked to Fmaxp and Fp which were related to isometric forces (F30, F90, F120). All forces were opposite to velocity (Vp) which confirmed the F*V negative relationship observed in different human situations (figure 2) (Bouisset, Maton, 1999). The Fpmax represented 59.77 % (± 10.54) of F30 reflecting the use of general strength in the specific swimming force production (Fomitchenko, 1999). Fp represented only 38.92 % (± 9.52) of F30. This low ratio reflected the compromise between force and velocity in the power production.

Swimmers with higher swimming velocity (V) at the end of the exhaustion test presented the greater power (figure 3). The power appeared to be strongly related to the isometric forces and not to specific swimming forces (Fmaxp and Fp). These results suggested that under fatigue, best swimmers were characterized by greater force capacity and not by their technical ability.

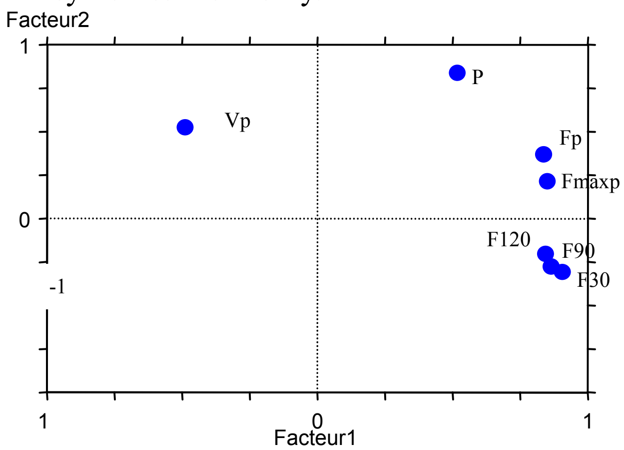

Figure 2 –ACP of forces, velocity and power parameters before fatigue.

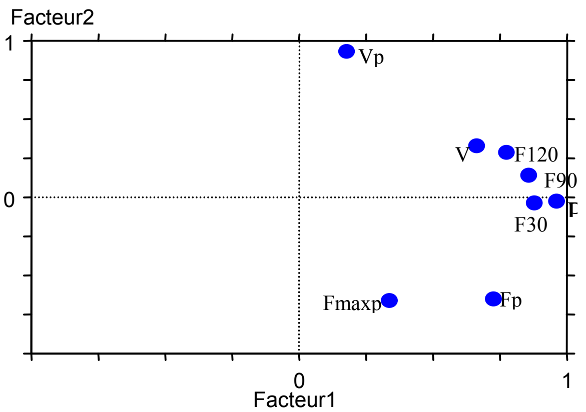

Figure 3 –ACP of forces and power parameters and velocity after fatigue.

Fomitchenko (1999) concluded that performance for young swimmers were limited by their general and specific strength development. The present results indicated that elite adults swimmers were limited by their isometric forces under fatigue conditions.

SUMMARY

The study of the effects of fatigue on force production indicated a decrease of maximal isometric forces, maximal power and the corresponded Fp and Vp. Before fatigue, power was related to specific swimming forces (Fmaxp and Fp) when after fatigue, power and velocity were determined by general forces. These results suggested that under fatigue, best swimmers were characterized by greater force capacity and not by their technical ability.

REFERENCES

Bonifazi M, Martelli G, Marugo L, Sardella F, Carli G (1993). *Blood lactate accumulation in top level swimmers following competition. J Sports Med Phys Fitness* **33**, 13-18.

Bouisset S., Maton B. (1999) *Muscles, posture et mouvements.*, Hermann (eds.).

Costill DL, King DS, Holdren A., Hargreaves M. (1983). *Sprint speed vs .swimming power. Swimming Technique*, **20**, 20-22.

Fomitchenko TG (1999). *Relationship between sprint swimming speed and power capacity in different group of swimmers. In Biomechanics and Medicine in Swimming VIII, eds K. Keskinen, P. Komi, P. Hollander*, University of Jyrväslylä, 203-207.

Miyashita M (1975). *Arm action in the crawl stroke. Int Series on Sports Sciences, vol 2, Swimming II, eds L. Lewillie, J.P. Clarys*, University Park Press, Baltimore, 167-173.

Rouard A.H., Bahuaud P.,.Boyer J.C. (2001). *Force, power and velocity in loaded tethered swimming. International Society of Biomechanics, XVIII congress, Zürich.*

Sharp RL, Troup JP, Costill DL (1982). *Relationships between power and sprint in freestyle swimming. Med&Sc in Sports Exerc.*, **14** (1), 53-56.

Troup JP (1999). *The physiology and biomechanics of competitive swimming . Clinics in Sports Medicine*, vol 18, **2**, 267-285.

A PERFECTIONIST LOOKS AT SPORTS TECHNIQUES: A TRIBUTE TO JIM HAY

INTRODUCTION

The biomechanics community lost one of its founding fathers on August 1, 2002. After a long battle with cancer, James G. (Jim) Hay died at his home in New Zealand. He was only 65 years old. Jim helped form the American Society of Biomechanics and hosted the very first ASB meeting in the Fall of 1977 at the University of Iowa. While at Iowa, Jim trained some of the finest scholars in biomechanics today, including Walter Herzog and Kit Vaughan. Jim was a phenomenal teacher and researcher of sports biomechanics, particularly track and field and swimming. He also developed a method to compute total body angular momentum and published two highly successful textbooks that will continue to be updated after his death. This symposium will highlight some of Jim Hay's greatest contributions to biomechanics.

HAY'S DETERMINISTIC MODELS AND THEIR USE IN SPORT BIOMECHANICS

Richard Hinrichs

Dept. of Kinesiology, Arizona State University, Tempe, AZ, USA
E-mail: hinrichs@asu.edu
Web: http://www.public.asu.edu/~hinrichs/

The Biomechanics of Sports Techniques (first published in 1973) contains chapters on different sports. In each chapter, Jim presented what he would eventually call "deterministic models" (DMs) or block diagrams that outlined the relationships between the result of a given motor skill (e.g., time, height, or distance) and various factors that determine that result (e.g., step length, forces exerted). The models have been used for both quantitative and qualitative purposes. One of the first quantitative studies used a DM to examine the critical factors in the performance of a vertical jump (1976). In the 1980s Jim and his students used DMs to quantify the critical factors in the long jump, and resulted in improvement in performance of elite U.S. long jumpers. With the debut of Jim's second book *The Anatomical and Mechanical Bases of Human Motion* (1982), the DM became an integral part of improving human performance qualitatively (e.g., "by eye"). This method of Qualitative Analysis has revolutionized the way coaches and teachers evaluate and eliminate faults in performance. DMs ("Hay-o-grams") may be Jim's greatest contribution to biomechanics.

THE EARLY DAYS: COMPUTATION OF ANGULAR MOMENTUM AT IOWA

Barry Wilson

School of Physical Education,
University of Otago, Dunedin,
New Zealand.
E-mail: bwilson@pooka.otago.ac.nz

In the 1970's there was an active Biomechanics "think tank" centered at the Fieldhouse. The interests of the group were diverse to the extent of working on, and even concocting, novel track and field techniques: the somersault long jump (Tom Ecker) and the dive high jump (Jim). Questions posed to Jim by his good friend George Nissen, of Nissen Gymnastics, often resulted in studies, eg: toppling of gymnastics vaulting horses, rotation of a gymnast who had missed a vault, analysis of gymnastics giant circles, and gymnastics tumbling. Many reports describing and explaining angular motion were written for Nissen before the methods used were presented by Jim at ACSM in 1975. Determining an appropriate set of segment parameters to use in calculations and validating the computation process kept the lab on task for a further two years. A comparison of three methods of calculating angular momentum was presented in Jyvaskyla in 1975, and a paper on the toppling dive was published in early 1977. The culmination of Jim's work on angular motion was the *Journal of Biomechanics* paper "A computational technique to determine the angular momentum of a human body", published in 1977.

HAY'S RESEARCH ON THE BIOMECHANICS OF THE LONG JUMP

Jesús Dapena

Biomechanics Laboratory, Indiana University, Bloomington, IN, USA
E-mail: dapena@indiana.edu
Web: http://www.indiana.edu/~sportbm/home.html

Jim's research on long jumping covered three main topics: description of the mechanics of the jump, correlational analysis, and analysis of the strategies used to achieve accuracy in the placement of the takeoff foot. This work was based on two-dimensional motion analysis of elite long jumpers in competitions. He found that long jumpers, on the average, start making adjustments for accurate placement of the takeoff foot about five steps before takeoff. His work also suggested the features of the optimum technique. Long jumpers should have a large horizontal velocity two steps before takeoff. In the next step, they should lower the center of mass (CM), and plant the foot slightly further ahead than in normal running. This preparation causes some loss of horizontal velocity, but it is overall beneficial. In the last step, they should maintain the CM height, and plant the takeoff foot clearly ahead of the CM. The low CM height and the forward position of the takeoff foot will produce a larger loss of horizontal velocity during the takeoff, but the associated increase in vertical velocity will more than compensate for it.

METHODOLOGICAL DEVELOPMENTS FOR BIOMECHANICAL ANALYSIS OF SWIMMING TECHNIQUES

Toshimasa Yanai

School of Physical Education, University of Otago, Dunedin, New Zealand.
E-mail: tyanai@pooka.otago.ac.nz

Biomechanical analyses of swimming techniques are especially difficult to conduct, due to the medium in which the techniques are performed. Dr. Hay and his students at Iowa devoted their energies to this challenging task in order to improve the understanding of the biomechanics of swimming. A series of innovative research methods were developed for kinematic analysis: the inverted periscope, the half periscope and the panning periscope. A method was also developed to record the details of the water flow. Dr. Hay hoped to deduce the forces acting on the swimmer from the observed motions of the water around the swimmer's body. A doctoral student adopted a totally different approach, pressure analysis, for the determination of the propulsive hand forces. These attempts at kinetic analysis were made in response to a previous doctoral study in which the most widely recognized method for the determination of propulsive lift and drag, devised by Schleihauf, was found to be invalid for unsteady flow conditions.

A SIMPLE 1$^+$ DIMENSIONAL MODEL OF ROWING MIMICS OBSERVED FORCES AND MOTIONS

David Cabrera and Andy Ruina

Human Power and Robotics Laboratory, Cornell University, Ithaca, NY, USA
E-mail: dsc16@cornell.edu Web: www.tam.cornell.edu/~ruina/hplab

INTRODUCTION

The first attempt to make a reasonable mechanical analysis of sliding-seat "sweep" rowing was presumably that of Alexander (1925). He neglected vertical motions of the centers of mass of the rower and boat as well as the yawing and pitching motions of the boat. He assumed one dimensional mechanics (momentum balance in the fore-aft direction), a point mass rower, an infinitely stiff oar, and quadratic force-velocity relationships to model drag forces on the boat and oar blade. He did take account of the 2D (looking down) kinematics and forces of the oar. Alexander prescribed made-up velocity vs. time patterns for the rower's legs, back, and arms to predict, using numerical integration (1925!), the motions of the system. Comparison with the scant data available was somewhat favorable. Pope (1973) used a similar but less complete model that had less good agreement with physical measurements.

Recent models (e.g. Brearley and de Mestre (1996) and Lazauskas (1997)) reasonably predict Olympic race times at the expense of producing or assuming force profiles which differ in many respects from on-water data. Atkinson (2001) uses a model in the same spirit, but with several extra kinematic variables, and gets better agreement with observed measurements.

METHODS

Our model is the same as Alexander' s with some minor elaborations that are allowed by our access to faster computation (Fig 1). We can use more general drag laws on the oar and boat. The length vs. time curves of the various body parts (*the coordination strategy*) are somewhat arbitrary. The oar goes in and out of the water so that it generates thrust while in the water and stays out when it would backsplash.

For a given coordination strategy, person, and boat parameters, we use shooting to find periodic solutions.

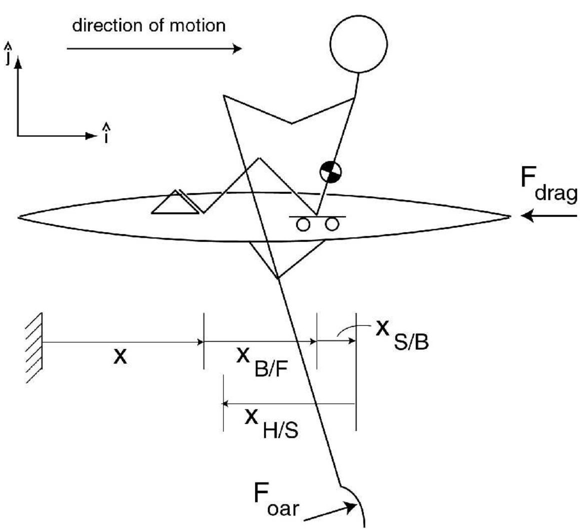

Figure 1: A sketch of the boat-oar-rower system is shown (top view of boat and oar, side view of rower). The various x' s are the

controlled and measured kinematic variables.

RESULTS AND DISCUSSION

Using numerical optimization on the coordination strategy, also allowing variation of some of the drag and rigging constants, we attempted to match some kinematic and force data from rowing (Fig 2). Note the presence of zero force during the recovery in our model. This is due to the assumption of a massless oar. The work rate of one rower was about 502 watts. The total negative work of all body parts was (a small) 5% of the total work thus supporting the claim that the leg-back-arms rowing coordination strategy is constructed so as to minimize negative work (the positive work of the arms at the end of the drive eliminates the need for negative work to stop the relative motion of the boat and body).

We also checked the possibility of improving our model by adding oar mass flexibility and got only small improvements. On the other hand neglecting oar slip seems significant.

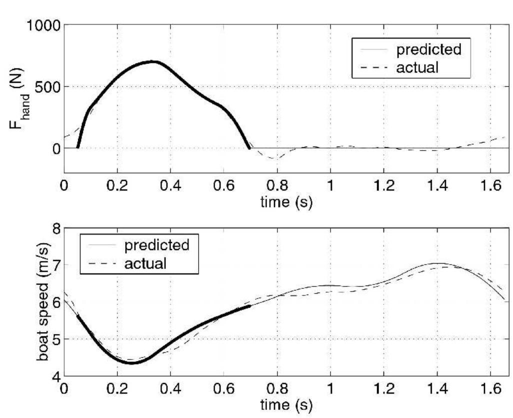

Figure 2: This plot shows a comparison of our model results (solid) with data from Kleshnev (dashed). The bold portions of the predicted curves indicate the drive sequence.

SUMMARY

We have constructed a model of rowing that seems to have the minimal complexity to well model the sport. The model seems promising for the investigation of the following questions: What kind of performance optimization will recreate observed rowing patterns? How can rigging be adjusted for various strength and height rowers to row together optimally? Can a moving coxswain make a boat go faster? What aspects of the coordination strategy are most central for maximizing performance?

REFERENCES

Alexander, F.H. (1925). *Proc. of the Univ. of Durham Phil. Soc.,* 160-179.

Pope, D.L. (1973). *ASME Report , Mechanics and Sport,* 113-130.

Brearley, M.N. and de Mestre, N.J. (1996). *Proc. of the Third conf. On Maths and Comp. In Sport, Bond Univ*., 35-46.

Lazauskas (1997) *Dept. Appl. Math. Tech. Report, Univ. of Adelaide.*

Atkinson (2001) *Technical Report,* unpublished

Kleshnev, V. (rowing data)

THE EFFECT OF VENUE ON THE DISTANCE OF A HAMMER THROW

Iain Hunter
Physical Education Department, Brigham Young University, Provo, UT, USA
iain_hunter@byu.edu

INTRODUCTION

In track and field, the hammer can travel over 70 meters and be in the air for over three seconds. While the implement is relatively massive (4 kg for women and 7.260 kg for men), the effects of air resistance and non-constant gravity throughout the earth need to be considered in how the hammer is affected at various venues. As release angle and speed increase, flight time will increase leading to more substantial altitude effects. In a throw of 44 deg that travels a throwing distance of the current men's world record, the differences due to an increase of 1000 m over sea-level is 55 cm (Mizera & Horvath, 2002).

A computer simulation of a hammer throw similar to that used by Dapena (1982) investigated the effects of gravity and air resistance at a range of venues around the world. With large enough differences, adjustments may need to be made in qualifying for certain meets according to which venue qualifying marks were made.

METHODS

A computer simulation was created to model the path and horizontal distance of the hammer during its flight. The average release velocity and angle used by finalists during 2002 USA Track and Field nationals were used as initial release conditions (Table 1). Release height was set at 1.3m which has been used previously in similar studies (Dapena, 1982). Estimates were made of gravitational accelerations and air densities for University of California Los Angeles, Brigham Young University, Gunnison, CO., Olso, NOR, and Mexico City, MEX for use in the simulation. Since air density varies with temperature, typical high temperatures for the location during July were used.

Table 1: Initial release conditions based upon the average throws of the 2002 USA Track and Field Meet finalists.

	Release Speed (m/s)	**Release Angle (deg)**
Men	26	36
Women	25	37

The simulation took into account characteristics of the hammer, gravitational effects, and air resistance. Atmospheric conditions for the various venues tested were found in the Weather Almanac (Ruffner, 2001) and the acceleration due to gravity was predicted for each venue using equation 1 (Jursa, 1985).

$$g(\mathrm{m/s}^2) = 9.780356\,(1 + 0.0052885\sin^2\varphi - 0.0000059\sin^2(2\varphi)) - 0.003086H$$

Equation 1: Prediction of gravitational acceleration based upon latitude and elevation.

where g is the acceleration due to gravity, φ is the latitude in degrees, minutes, and seconds, and H is the elevation in meters.

RESULTS AND DISCUSSION

Differences were found of up to 0.63 m for women and 0.54 m for men between the most extreme situations of Olso, NOR being the shortest throws and Gunnison, CO. and Mexico City, MEX being the longest (Table 1). Overall, variations in air density account for 70% of the differences in throws, while gravitational variations make up the other 30%.

The venue differences of 0.63 m and 0.54 m are relatively large considering the differences between athletes throws in competition; for example, the differences between medallists in the 2000 Olympic Games were 1.88 m and 0.85 m for women and men respectively. However, during a given competition, everyone throws under similar conditions, other than perhaps windspeed. While there are benefits to throwing at high altitude, other considerations such as: temperature, wind speed and direction, throwing direction, and other weather conditions should be taken into account before applying any conversions to throwing events by governing bodies of track and field.

Although equal release conditions were used in the simulations, the lower air density may also allow for increased release velocities further increasing the differences between venues.

Table 2: Distances thrown at various venues with the initial release velocities shown in table 1.

	Men's Distance (m)	**Women's Distance (m)**
Gunnison, CO	66.63	62.00
Los Angeles, CA	66.34	61.64
Mexico City, MEX	66.71	62.06
Oslo, NOR	66.17	61.43
Provo, UT	66.54	61.83

SUMMARY

Substantial differences are found between venues due to the differences in gravitational acceleration and air density, assuming similar release conditions. While the differences shown here appear to provide an advantage to throwing at relatively high altitude and certain latitudes, considerations of competition level at the meet, weather conditions for the day and time of day, and wind speed and direction.

REFERENCES

Dapena, J., & Teves, M. A. (1982). *Res Q Exerc Sport,* ***53***, 78-85.
Jursa, A. S. (1985). Handbook of Geophysics and the Space Environment, *Handbook of Geophysics and the Space Environment* (4 ed., pp. 14-17): Air Force Geophysics Laboratory.
Mizera, F., & Horvath, G. (2002). *J Biomech,* ***35***, 785-796.
Ruffner, J. A. (2001). *The Weather Almanac*. Detriot: Gale Research Company.

A COMPARISON OF LOWER EXTREMITY POWER BETWEEN GENDER FOR MAXIMAL VERTICAL SQUAT JUMPING AND HANG POWER CLEANS

Jeffrey B. Casebolt, Alan Hreljac, and Mitell Sison

Biomechanics Laboratory, California State University, Sacramento, Sacramento, CA
E-mail: sinewsport@onemain.com

INTRODUCTION

An outcome that has steadily increased, since the inception of Title IX in 1972, is the amount of knee injuries that have occurred in female athletics. It is well documented in research that women are more susceptible to knee injuries when compared to men, some reporting two to eight times greater (Rochman, 1996). There are several theories attempting to explain this phenomena ranging from a woman's Q-angle to hormonal effects on ligamental laxity. One such theory is the difference in lower extremity mechanics for males versus females during jumping movements. Also, Olympic-style lifting considered by many to be the "gold-standard" in training an athlete to become more ballistic in a vertical direction (NSCA, 1985). Power production at the major joints of the lower body assist in lifting an athlete from the ground into the air. An athlete with the greatest amount of power production in the shortest amount of time will create the largest impulse, therefore reaching a greater height. Power at a joint is a product of net joint moment and angular velocity. Therefore, the purpose of this study was to compare average and peak power outputs of the three major joints of the lower extremity between gender for three conditions during the propulsion phase: Maximal Vertical Squat Jump (MVSJ), 50% Hang Power Clean (50HPC), and 75% Hang Power Clean (75HPC). Also, the time to peak power and total time of the condition were investigated across gender for the three conditions.

METHODS

Ten highly trained and competitive Olympic-style lifters (five males average age = 27.4 $\pm$ 4.5 years and training years = 5.8 $\pm$ 3.1 years, and five females average age = 31.6 $\pm$ 5.7 years and training years = 9.6 $\pm$ 6.7 years) volunteered for the study. Each lifter performed each of the three conditions with his/her right foot on a single AMTI force plate recording at 600 Hz. Digital video recorded the movements from the right sagittal plane at 120 Hz. During the movement, reflective markers were placed on the right side of the body: mid-thoracic (inferior to the 12th rib), the greater trochanter, knee joint line superior to the fibular head, lateral malleolus, and styloid process of the 5th metatarsal. Digital video data were smoothed using a 4th order, zero lag, Butterworth filter. Every fifth sample of the AMTI force plate data were exported and synchronized with the data from the digital video. Ankle, knee and hip power were calculated using an inverse dynamics model. Prior to analysis moments and power were normalized by body mass. Dependent variables included average and peak power for ankle, knee and hip, and time to peak power compared to total time to complete the condition. A two-way ANOVA was used to compare males versus females for the three conditions MVSJ, 50HPC and 75HPC for variables related to power at the ankle, knee and hip ($p<0.05$).

RESULTS AND DISCUSSION

No significant differences were found between power or time variables related to the ankle and hip. However, average (Fig. 1) and peak power (Fig.2) and time to peak power variables associated with the knee differed significantly between gender for MVSJ, but not for the 50HPC and 75 HPC conditions ($P < 0.05$).

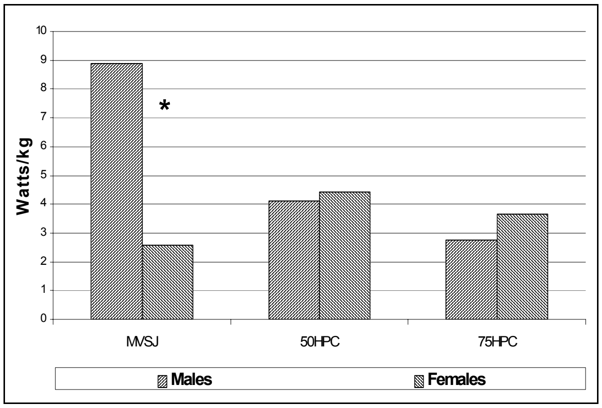

Figure 1: Average Knee Power. Conditions from left to right are MVSJ, 50 HPC, and 75HPC for males versus females.

There appears to be a different strategy being employed for females when compared to their male counterparts for MVSJ. Although, average and peak power outputs appear similar for 50HPC and 75HPC, female MVSJ power outputs are 29.1 and 31.2 percent to that of male average and peak power outputs, respectively.

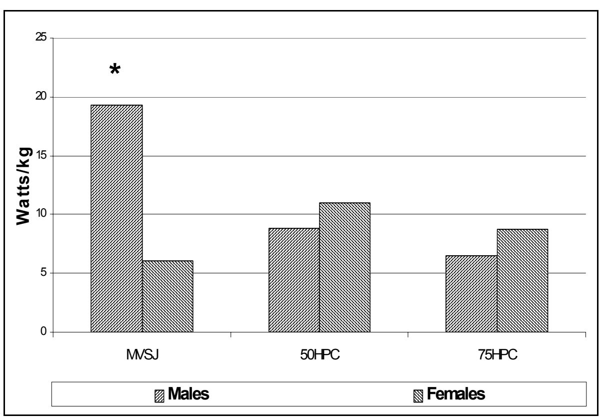

Figure 2: Peak Knee Power. Conditions from left to right are MVSJ, 50 HPC, and 75HPC for males versus females.

Females time to peak (Fig. 3) and total time (Fig. 3) to complete the condition were greater when compared to males. There was a significant difference between time to peak power and total time to completion for MVSJ when comparing males to females.
* indicates significance ($p<0.05$)

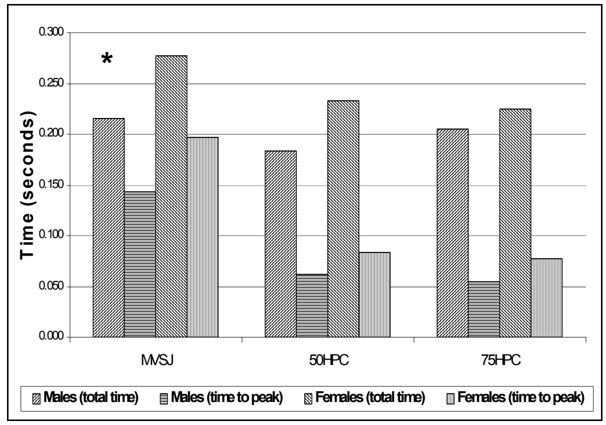

Figure 3: Time to Peak and Total to Time to complete the condition. Conditions from left to right are MVSJ, 50HPC, and 75 HPC for males versus females.

SUMMARY

All subjects were considered highly trained and competitive Olympic-style lifters; therefore no difference in MVSJ performance should have been evident, yet female subject produced significantly different power outputs at the knee. Thereby, lending some credibility to the argument that lower body mechanics for females may be a contributing factor to knee injuries in athletics. Also, the difference in MVSJ time to peak power and total time to completion indicates an increased ramping strategy is needed for the female subject's vertical impulse.

REFERENCES

NSCA (1985). Power clean. *NSCA Journal,* 7(2), 10-25.

Rochman, S. (1996). Gender Inequity. *Training and Conditioning.* VI, 5, 10-20.

CADENCE EFFECTS ON IN-SHOE PLANTAR PRESSURES IN SUBJECTS WITH DIABETES

T. W. Kernozek[1,3], M. Maher[2], K. Kalfas[1], A. Bellmeyer[2], J. Strasser[2]
[1]Physical Therapy Department, [2]Biology Department, University of Wisconsin – La Crosse, La Crosse, WI, [3]Gundersen Lutheran Sports Medicine, La Crosse, WI
E-mail: kernozek.thom@uwlax.edu

INTRODUCTION

Sensory neuropathy and ischemia are the main factors in the development of plantar ulcerations associated with diabetes (Birke, 1992; Caputo, 1994). Higher plantar pressures exist during gait in individuals with diabetic neuropathy (Pitei, 1999). The most common mechanism of injury with diabetic foot ulcers come from unperceived, excessive, and repetitive pressures on plantar bony prominences (Birke, 1992; Ctercteko, 1981; Caputo, 1994). Perry et al. (1995) demonstrated that the highest pressure in the neuropathic diabetic foot was under the 2nd metatarsal head, followed by the lateral metatarsal heads, 1st metatarsal head, and the heel. Contact time may also be a risk factor for plantar ulceration. The greatest contact time during gait was under the central forefoot and the metatarsal heads in diabetic patients (Giacomozzi, 2002). The most frequently ulcerated area of the diabetic foot is under the 3rd metatarsal head, followed by the 1st metatarsal head and toes, then the 2nd metatarsal head. The heel and the 4th metatarsal head have the least incidence of pressure ulcers (Veves, 1992; Stess, 1997).

Zhu et al. (1995) examined the plantar pressures of healthy subjects with changes in cadence. As cadence increased, the pressure-time impulse (PTI) and contact time (CT) decreased and the peak pressure (PP) increased. Perhaps the increased contact time as well as the increased pressure under the plantar bony prominences are risk factors for plantar ulceration.

Our purpose was to examine the changes in in-shoe pressures and contact time in diabetic subjects that have no sensory neuropathy with changes in their walking cadence.

METHODS

Twenty subjects with Type 2 DM, age 40-65, were used. Factors for exclusion from this study included current ulcerations, history of cardiac problems, and greater than Grade 2 obesity. In-shoe plantar loading was measured by the Pedar system (Novel GMBH, Munich, Germany). Each insole consists of 99 pressure sensors that measure the load normal to the insole interface. In-shoe loading was measured bilaterally at a sampling rate of 50 Hz. Contact time (ms) peak pressure (N/cm^2) and pressure-time impulse ($N/cm^2 \cdot s$) served as the dependent variables in this study while the independent variable was percentage of preferred stride frequency (PSF) (-10% of PSF, -5% of PSF, PSF, +5% PSF, and +10% PSF). A digital metronome was used to aid the subjects in maintaining the appropriate stride frequency while they walked on a treadmill.

A repeated measures multivariate analysis of variance (RM MANOVA) was used to determine differences in PP, PTI, and CT between the 5 cadences in 7 plantar regions ($p < 0.05$). A Bonferroni post hoc test was used to determine where those differences existed.

RESULTS

No differences were found in any plantar region in PP between the preferred cadence and the altered cadences. In the heel region, no significant differences were found in PP, PTI, or CT between the preferred cadence and the altered cadences. PTI in the medial forefoot, central forefoot, medial toe, and lateral toe were significantly higher for –10% of PSF than the preferred cadence, and the CT values were significantly higher in all of these regions plus the lateral forefoot. Additionally, with -5% of PSF, the PTI was higher than preferred cadence in the medial forefoot (table 1).

DISCUSSION

These findings are partially consistent with Zhu et al's (1995) study, but as cadence decreased, the PTI and CT increased with no change in PP. Therefore, changes in PTI were due to changes in CT, not PP. The fact that PP was unchanged between cadences, but PTI and CT showed significant differences indicates that CT may be the impetus behind the differences in PTI, not PP. Therefore, PTI and CT may be just as important in determining the risk of plantar ulceration as measuring PP. Stess (1997) reported that PTIs were higher in diabetic subjects with history of ulcers than in diabetic subjects with no history of ulceration or neuropathy. However, the same researchers also reported significantly higher PP in diabetic ulcerated feet than the diabetic non-ulcerated and non-neuropathic controls. Stess (1997) did not report a greater CT in the diabetic ulcerated feet than the diabetic non-ulcerated and non-neuropathic controls.

REFERENCES

Birke, J.A. et al. (1992). *J Prosthetics and Orthotics,* **4**, 13-22.

Caputo, G.M. et al. (1994). *N Engl J Med,* **331**, 854-860.

Ctercteko, G.C. et al. (1981). *Br J Surg,* **68**, 608-614.

Giacomozzi, C. et al. (2002). *Diabetes Care,* **25**, 1451-1457.

Perry, J.E. et al. (1995). *J Bone and Joint Surg,* **77A**, 1819-1828.

Pitei, et al. (1999). *Diabetes Care*, **22**, 1966-1970.

Stess, R.M. et al. (1997). *Diabetes Care,* **20**, 855-858.

Veves, A. et al. (1992). *Diabetologia*, **35**, 660-663.

Zhu H. et al. (1995). *Arch Phys Med Rehabil,* **76**, 1000-1005.

ACKNOWLEDGEMENTS

This study was funded by a UW – La Crosse research grant.

Table 1: PP, PTI, CT among four regions of the foot for all cadences. The percentages indicate the percentage of PSF.

	Medial Forefoot					**Central Forefoot**				
	-10%	*-5%*	*PSF*	*+5%*	*+10%*	*-10%*	*-5%*	*PSF*	*+5%*	*+10%*
PP (N/cm^2)	20.49 (4.82)	20.09 (4.66)	19.56 (4.11)	20.12 (4.37)	19.70 (4.26)	22.02 (5.55)	22.70 (5.17)	22.89 (5.53)	23.08 (5.38)	22.87 (5.57)
PTI (N/cm^2·s)	7.66* (1.64)	6.81* (1.45)	6.03 (1.42)	6.42 (1.40)	6.20 (1.42)	8.35* (1.73)	7.77 (1.61)	7.25 (1.78)	7.47 (1.66)	7.30 (1.67)
CT (ms)	732.69* (100.31)	676.60 (93.78)	631.54 (97.93)	659.10 (106.02)	635.25 (92.24)	765.84* (108.50)	711.31 (106.40)	666.50 (94.73)	688.73 (116.67)	657.97 (96.30)
	Lateral Forefoot					**Medial Toe**				
	-10%	*-5%*	*PSF*	*+5%*	*+10%*	*-10%*	*-5%*	*PSF*	*+5%*	*+10%*
PP (N/cm^2)	18.01 (5.396)	18.20 (4.81)	19.03 (5.31)	18.60 (4.96)	18.51 (5.21)	20.14 (6.38)	18.10 (6.25)	17.63 (6.74)	17.67 (5.71)	16.54 (5.00)
PTI (N/cm^2·s)	7.11 (1.88)	6.71 (1.63)	6.49 (1.79)	6.49 (1.68)	6.44 (1.71)	6.08* (2.34)	4.88 (1.94)	4.27 (1.75)	4.41 (1.63)	3.96 (1.23)
CT (ms)	767.51* (113.72)	709.30 (114.26)	680.35 (95.88)	685.81 (129.68)	662.78 (91.79)	636.34* (103.36)	582.51 (88.34)	541.98 (115.32)	566.48 (105.11)	539.28 (103.58)

* Indicates a significant difference from the preferred stride frequency (PSF).

AREA DEFORMATION CHARACTERISTICS OF GYMNASTIC LANDING MATS

Fred Yeadon, Chris Mills and Matt Pain

School of Sport and Exercise Sciences, Loughborough University, UK
E-mail: M.T.G.Pain@lboro.ac.uk

INTRODUCTION

Most sports landing surfaces are area elastic, for example, pole vault / high jump beds and gymnastic landing mats. The area of surface deformation is greater than the contact area. Loading of the human body is defined as the production of forces acting on the human musculo-skeletal system. When such loading is too large the internal structures will become damaged (Yeadon & Nigg, 1988). Area elastic surfaces help to reduce injury by increasing the time over which the force is applied. Initially the landing surface deforms locally and progressively throughout the impact the area of the surface involved in the impact increases. This introduces a problem in analysis because of the lack of a consistent area of deformation. Simple models may find it difficult to reproduce the complex deformation characteristics of an area elastic landing surface.

The purpose of this paper was to assess the area deformation of a gymnastic landing mat.

METHODS

An impactor of mass 24 kg, contact area (25 cm by 25 cm) was used to represent a gymnast landing. A total of five vertical trials with landing velocities between 4.5 m/s and 6.5 m/s were performed. Additional oblique impacts were carried out at five different angles (45°, 50°, 55°, 60°, 65°) using a custom built rig. Angles and landing velocities covered the range of those seen in competition landings (Takei, 1998).

The landing mat was a custom made Continental mat weighing 6.1 kg measuring 0.9 m by 0.6 m by 0.2 m. It was partially constrained so that the edges could not rise off from the force plate (Kistler 9281B) and all the force had to go through the force plate. Two PCB Piezotronics accelerometers were attached to the impactor. Two Phantom high-speed cameras (1000 Hz) were used to record the vertical deformation and the area deformation of the landing mat, based upon the methodology of Yeadon and Nigg (1988). All data were synchronized to within 1 millisecond.

28 markers placed in 4 rows and 7 columns. The row markers were 150 mm apart and 75 mm from the mat's edge. The column markers were 85 mm apart from the centre line of the mat. All 28 markers plus two markers on the impactor were manually digitised using the Phantom software. DLT and reconstruction was performed in Matlab using the KineMat toolbox.

Markers on the impactor were used to calculate impact velocity and landing surface deformation. The 28 markers were used to determine the area of deformation.

RESULTS AND DISCUSSION

During the vertical impact testing, data from the high-speed cameras showed that the entire area of the mat's surface was involved during the impact. With an impact velocity of 5.5 m/s and a peak vertical force of 6360 N the maximum vertical mat deformation was 0.083 m (Figure 1). The vertical positions of the markers nearest the centre line were 0.21 m, 0.20 m, 0.17 m, 0.15 m, 0.15 m, 0.17 m, and 0.21 m. The initial marker positions were 0.20 m above the ground. The volume of the mat involved during peak deformation was estimated to be 0.015 m^3.

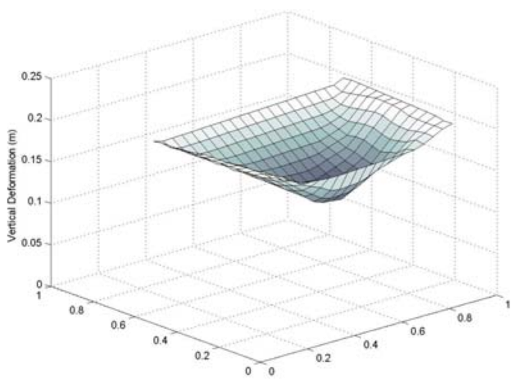

Figure 1: This graph illustrates the amount of area and vertical deformation of the landing surface during a vertical impact at 5.5 m/s.

During a 60° oblique impact at 6.5 m/s vertically and 4.5 m/s horizontally the landing mat deformed 0.093 m vertically and 0.017m horizontally (Figure 2). The peak vertical and horizontal force was 6595 N and 3910 N respectively.

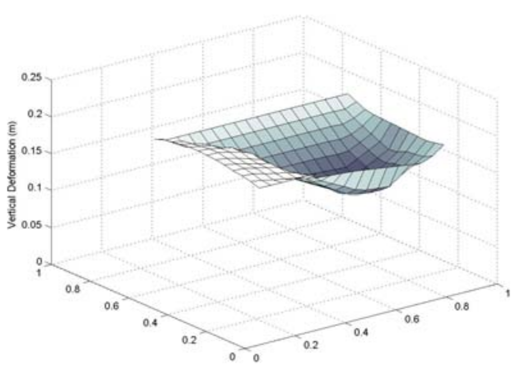

Figure 2: This graph illustrates the amount of area and vertical deformation of the landing surface during a 60° oblique impact.

The positions of the markers nearest the centre line in the vertical direction were 0.19 m, 0.21 m, 0.20 m, 0.17 m, 0.14 m, 0.13 m, and 0.16 m. The initial marker positions were 0.20 m above the ground. The volume of the mat involved during peak deformation was estimated to be 0.017m^3.

The acceleration data was filtered at 20 Hz (Fritz & Peikenkamp, 2003) and the video data gave filtered accelerations within 1% of the directly measured filtered accelerations. However the filtering process can underestimate the acceleration by approximately 8%.

SUMMARY

This high-speed video data allows the calculation of the vertical and horizontal deformation of the landing mat, the area of deformation and an estimate of the volume of the mat involved in the impact.

REFERENCES

Fritz, M. & Peikenkamp, K. (2003). *Medical and Biological Engineering and Computing,* **41**, 11-17.
Takei, Y. (1998). *Journal of Applied Biomechanics*, **14**, 190-210.
Yeadon, M.R., Nigg, B.M. (1988). *Medicine and Science in Sports and Exercise,* **20**, 403-407.

ACKNOWLEDGEMENTS

KineMat was produced by C. Reinschmidt & T. van den Bogert (1997).

THE EFFECT OF FOOT POSITION ON HIP FORCES DURING THE FULL GOLF SWING

Heather Gulgin, Isoa Okuda, and Charles Armstrong

Applied Biomechanics Laboratory, University of Toledo, Toledo, OH, USA
Email: hgbuckeye@yahoo.com

INTRODUCTION

Although golf is not considered a high-risk sport, participants are not immune from injuries. Overuse injuries, involving such areas as the low back, wrist, and hip, may develop from the repetitive loading that occurs during the golf swing. Recently there have been several cases of professional golfers with chronic hip pain who have required arthroscopic procedures for a torn acetabular labrum. Since the lower body acts as a closed kinetic chain during the full golf swing, the position of the foot may influence the magnitude of the forces that act on the hip. Thus, foot position may be a factor influencing the development of hip pathology. Therefore, the purpose of this study was to examine the forces at the hip during a full golf swing and determine if an alteration in foot position at address will change those forces.

METHODS

Eleven subjects (5 male, 6 female) from the University of Toledo golf teams volunteered for the study. A six-camera motion analysis system (Motion Analysis Inc.) recording at 120 Hz, and two (AMTI Inc.) force plates, recording at 960 Hz were used to track thirty-five retroflective markers and measure the involved ground reaction forces. Joint kinetics and kinematics were evaluated using the Kintrac software (Motion Analysis Inc.). Three different sets of 5 swings (using a driver) were measured, with each set having a different foot position (natural, left foot externally rotated 30°, and left foot square) at address.

RESULTS AND DISCUSSION

Preliminary results indicated that the left hip lateral shear force was least when the left foot was in a square position (Fig.1).

Fig 1 – Left Lateral Shear Force

Additionally, the external rotation moment (longitudinal axis) was least for left hip when the left foot was in the square position.

Fig 2 – Hip Rotation Moment

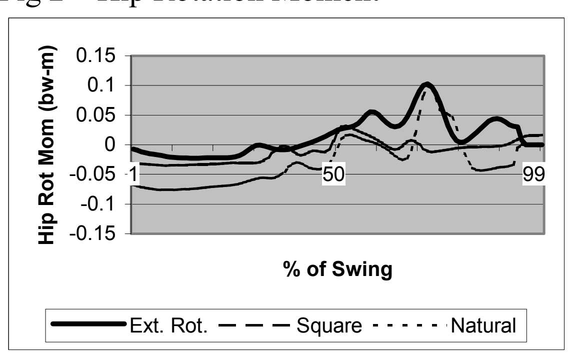

Associated with both of these, maximum IR of the left hip occurred when the feet were in the natural setup position at address. It was hypothesized that externally rotating the left foot would allow for easier hip rotation, or "clearing the hips," thereby diminishing the torque acting on that hip.

Fig 3 Hip Rotation ROM

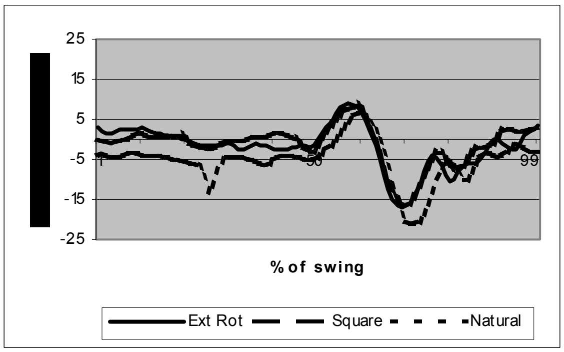

However, the preliminary results in this study show that there is a greater moment when the left foot is in the ER position at address. Completion of data analysis may further support or refute this.

SUMMARY

In sports involving similar rotational movements of the hip, such as soccer and tennis, a link has been hypothesized between foot position and hip joint stress. In addition, Buckwalter et al., 1997 stated that high levels of torsional loading increases the risk of articular cartilage degeneration. Thus, examination of the hip joint kinetics during a full golf swing is certainly worthwhile. Based on the results, recommendations may be made as to how the golfer could diminish those forces and still maintain the biomechanics necessary for desired performance.

REFERENCES

Buckwalter , J.A., Lane, N.E. (1997). *Am. J. Sports Med.*, **28**(6), 873-881.

WEIGHT TRANSFER PATTERNS DEPENDING ON GOLF SKILL LEVEL

Isao Okuda [1], Sema Kalaian [2], Charles Armstrong [1], and Hiroaki Yoshiike [3]
[1] Applied Biomechanics Laboratory, University of Toledo, Toledo, OH, USA
[2] Research and measurement, University of Toledo, OH, USA
[3] Institute of Physical Research, Co Ltd, Tokyo, Japan
E-mail: okudai2@aol.com

INTRODUCTION

Biomechanical studies of golf, although limited in number, have demonstrated that skilled golfers show more efficient patterns of motion and force application than less skilled golfers (Richard et al., 1985). Since the down swing in golf lasts only a fraction of second, golfers must rely on the stored memory of the motion to determine this phase of the swing, rather than on sensory feedback. This suggests that the phase that precedes the down swing, the preparation phase (address to top of the swing), may be crucial in creating the optimum conditions for a successful down swing. Information about this phase, relating to the involved movement patterns and the associated weight shift, may be of great practical value. Therefore, the purpose of this study was to examine the weight shift pattern associated with the preparation phase of a full-shot golf swing to determine how it differs between expert and novice golfers.

METHODS

Subject: Fourteen right-handed JPGA touring professional golfers (skilled group-SG) and twelve amateur golfers (unskilled group-UG, handicaps from 20 to 35 stokes), ranging in age from 22 to 45 years, volunteered to participate in this study.

Instruments: The weight transfer pattern during the golf swing was measured using a custom designed portable force platform (Kyowa-Dengyo, Tokyo, Japan). This platform system consisted of two separate footplates synchronized with a video camcorder, by which vertical ground reaction force (VGRF) was measured for each force plate. The VGRF data was collected at 1000Hz, while the associated video data was recorded at 30 fields per second. The camcorder was positioned perpendicular to the subject's frontal plane of motion and was used to identify the specific events during the swing.

Procedure: Data collection took place at an outside driving range so that the complete ball flight from each trial could be monitored. After a fifteen minute warm up, the subject performed three full-shot swings with their own driver while VGRF and video data were collected. The best shot in the three trials was determined subjectively and then used for data analysis. During post-processing of the data, the trial was analyzed at four specific points identified by the video data, which served as a basis for the analysis in this study. The four specific points were: (1) address, (2) back swing (club shaft horizontal to the ground), (3) top of the swing, and (4) ball impact.

Analysis of data: The subject's weight distribution between the two feet was converted into a percentage and analyzed at the four specific points. Because of this study's small sample size, applying a nonparametric statistical methods are needed. A nonparametric repeated measures ANOVA was used to identify the difference between the SG and UG group followed by nonparametric post-hoc tests to identify the points where the difference existed.

RESULTS AND DISCUSSION

Figure 1 illustrates right foot weight distribution across the four points, and the associated analysis revealed a significant ($p< .04$) difference between the two groups. The post-hoc tests indicated that there was a difference between the groups at the address ($p< .04$) and the top of the back swing ($p< .05$). The median value of right foot weight distribution at the address was 46.5% for the SG while that of UG was 40.0%. The median value of right foot weight distribution at the top of the swings was 77.0% and for the SG while that of UG was 66.0%.

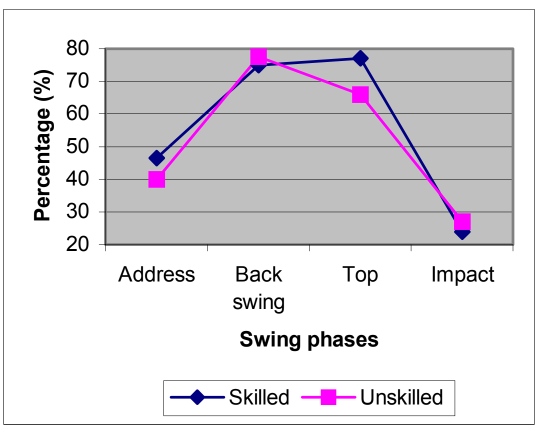

Figure 1: Changes in the right foot weight distribution.

In addition, as illustrated in Figure 2, the pattern of weight transfer was examined. This figure shows median values of the weight distribution change from the back swing to the top of the swing ($p< .012$).

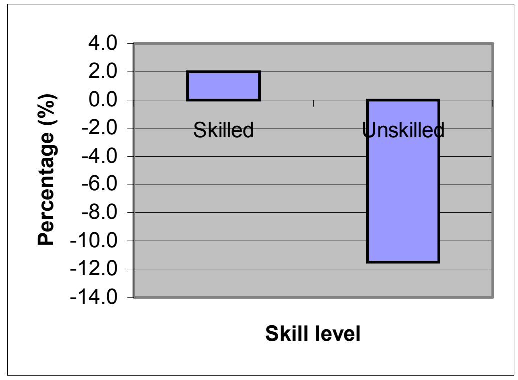

Figure 2: Changes in the right foot weight distribution from back swing to the top of the swing

Collectively these results demonstrate a pre-downswing weight shift pattern for the SG group that is characterized by increased loading on the rear foot and a weight shift to the left that is delayed until the club reaches the top of the backswing. This is in contrast to the reverse weight shift pattern that was observed in the US golfers. The pattern that was evident in the SG group may reflect trunk rotation and postural adaptations that ultimately enable optimization of the downswing.

SUMMARY

The weight transfer pattern from the back swing to the top of the swing clearly differs between the SG and the UG golfers, and may be a major factor influencing the downswing.

REFERENCES

Barrentine, S.W. et al. (1994). *Proceedings of the World Scientific Congress of Golf'94,* 33-39.

Richard, J. et al. (1985). *Research Quarterly for Exercise and Sport*, **56**, 361-365.

Thomas, J.R. et al. (1999). *Research Quarterly for Exercise and Sport*, **70**, 11-23.

KINEMATIC DIFFERENCES IN THE LACROSSE PASS WHEN PERFORMED WITH CROSSES OF VARYING DESIGNS

Lori A. Livingston, J. Steven LeBlanc and Saleema Karim

School of Health and Human Performance, Dalhousie University, Halifax, NS, Canada
E-mail: Lori.Livingston@Dal.ca Web: www.dal.ca/hahp

INTRODUCTION

The design of women's lacrosse sticks (or crosses) has evolved away from the traditional one-piece linear wooden frame to the now more popular composite stick consisting of a plastic head attached to an aluminum or graphite shaft (Figure 1). These new, lighter sticks have been heralded as a way to reduce injury in the game (Kulund et al., 1979). However, it is now suspected that offset and/or curvilinear crosse heads, with or without inverted-V shooting strings, increase the velocity with which the ball can be passed or shot (Ewell, 2002). Such increases in ball velocity would be problematic since minimal amounts of protective equipment are worn.

To date, there have been few biomechanical investigations of the lacrosse stick (Stevenson III, 1983) and none that have focused on throwing kinematics and changes in crosse design. The purpose of this study was to examine the effect of such changes on selected kinematic variables.

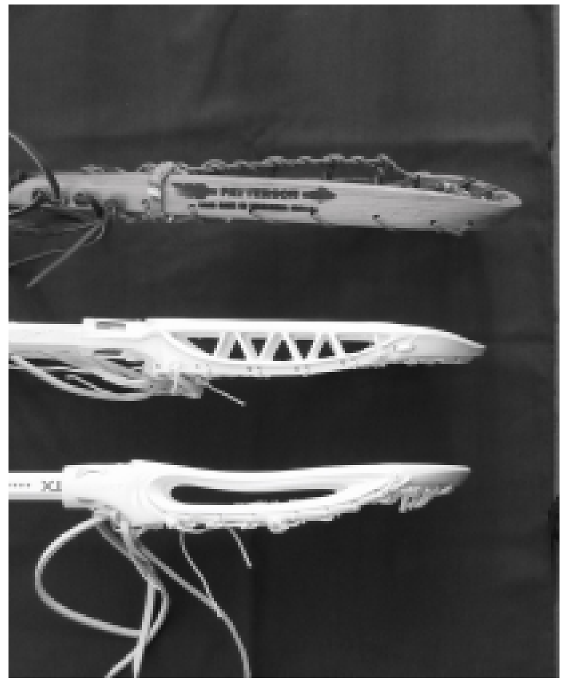

Figure 1: From top to bottom, a traditional wooden crosse, a composite crosse with a linear head aligned in the same plane as the stick shaft, and a composite crosse with a curvilinear head positioned out of plane (i.e., offset) with the stick shaft.

METHODS

One elite female lacrosse player, with international playing experience, completed all of the throwing trials. The athlete was positioned 10 meters from a target positioned 1.5-1.8 m above ground level. She was instructed to consistently complete a stationary throw simulating a hard pass to a teammate. She began with her feet positioned close together and was limited to striding forward with her lead foot. The order of testing was randomized and rest breaks were taken to control for practice and fatigue effects. Five throwing trials were completed for each of 24 different crosse models. Sagittal plane images were captured for each trial at a rate of 60 Hz and with a shutter speed of 1/1000 s using a digital video camera. Kinematic analyses were completed using Hu-M-An© software in conjunction with a microcomputer. The dependent variables were analyzed using standard ANOVA and ANCOVA procedures.

RESULTS AND DISCUSSION

Mean release angles ranged from 22.4° prior to the stick reaching a vertical position during the throwing motion, to 12.4° past the vertical. Differences in ball release angles were significant ($F(2,113)= 2.98$, $p<0.05$) with the ball releasing earlier from offset heads (M=179.7°-182.5°) than those aligned with the stick shaft (M=184.3°).

The mean peak angular velocity with which the crosse was rotated for any given model ranged from a low of 14.8 rad/s to a high of 17.4 rad/s, with lower velocities observed for the heavier wooden crosses. Ball release velocity data, adjusted for variations in angular velocity, are presented in Table 1. Statistical analysis revealed significant differences in ball release velocities according to material ($F(1,112)=30.99$, $p<0.0001$), crosse head alignment and shape ($F(2,112)=6.63$, $p<0.002$), and shooting string orientation ($F(1,112)=14.05$, $p<0.0001$). In general, ball release velocities were greater in composite versus wooden sticks, offset-aligned, curvilinear versus planar-aligned, linear heads, and with inverted-V shooting strings versus traditional shooting strings. Comparing the fastest composite crosse to wood, there is a 15% difference in ball velocity. Only 7% of this difference is explained in Table 1. This suggests that other factors (e.g., material properties of the crosse) contribute to the observed differences.

SUMMARY

Changes in the design of lacrosse sticks are leading to changes in the angle of release and the rate of release of the lacrosse ball from the crosse pocket. Such changes may have implications for player safety.

REFERENCES

Ewell, N. (2002). *Lacrosse*, **26**(4), 42-48.

Kulund, D.N. et al. (1979). *Phys. Sportsmedicine*, **7**(5), 83-90.

Stevenson III, J.R. (1983). *Doctoral dissertation*, Indiana University, Bloomington, IN.

ACKNOWLEDGEMENTS

Funding for this project was received from the International Federation of Women's Lacrosse Associations (IFWLA).

Table 1: Estimated means (SE) for ball velocity at release by material and crosse design.

Crosse Design (Head Alignment and Shape/ Shooting String Orientation)	Trials	Estimated Mean Release Velocity (m/s)	95% Confidence Intervals	
			Lower	Upper
Wood				
Planar Linear/Traditional	15	14.0 (0.2)	13.7	14.3
Offset Linear/Traditional	5	12.6 (0.3)	12.1	13.1
Offset Curvilinear/Traditional	5	13.5 (0.3)	12.9	14.0
Offset Curvilinear/Inverted-V	5	14.8 (0.3)	14.3	15.3
Composite				
Planar Linear/Traditional	45	14.7 (0.1)	14.5	14.9
Offset Linear/Traditional	15	14.8 (0.2)	14.5	15.1
Offset Curvilinear/Inverted-V	30	15.0 (0.1)	14.8	15.2

VELOCITY PROFILE IN STREAMLINE SWIMMING: DRAG QUANTIFICATION

Erin E. McIntyre, Noshir A. Langrana, Timothy Wei, Abram Voorhees

Rutgers, The State University of New Jersey
Department of Mechanical Engineering
Piscataway, New Jersey
E-mail: erinmcintyre721@yahoo.com

INTRODUCTION

The goal of studying the biomechanics of the streamline position is to find an optimal position of the head to produce the least amount of drag and the fastest time possible.

The fundamental questions addressed in this investigation are which arm position is optimal for sustaining maximum velocity during the glide streamline position after a start and turn, and is it possible to obtain velocity profiles of the flow around a swimmer. Our experiments examine the effects of two different head positions on passive drag measurements. It is extremely difficult to determine the frictional, wave making and/or eddy resistance because the swimmer's propulsion along the water surface is regarded as a collection of numerous traveling pressure points (Miyashita, 1978).

In addition, Digital particle image velocimetry (DPIV) method was used to create a two-dimensional field of velocity vectors describing the instantaneous fluid motions for streamline swimming.

METHODS

Passive Drag Quantification

15 swimmers from California participated in this portion of the experiment. The protocol developed by Russell Mark, Biomechanics Coordinator at USA Swimming Inc. was used. It includes:

- Athletes hung from a towrope in a streamline position attached to a load cell and tensiometer in the flume.
- Measurements were taken when the athlete reached a stable streamline position (no lateral movement, body position fully adjusted)
- 3 x 10 seconds data of @ 1.5 m/s and 2.0 m/s flume velocity drag measurements for each head position were collected
- Anthropometric data was collected

Velocity Profile Measurement

The pool in the Sonny Werblin Recreation Center at Rutgers University was used to perform the experiment. The camera was located in an underwater viewing window located 5 feet below water surface level.

After warming up, the swimmer was tethered with elastic tubing to ensure that he/she would stay in front of the window. The swimmer was asked to swim at maximum velocity. A Kodak Mega plus 18-108 mm camera with computer zoom lens and video capture boards was used to collect 500 two-dimensional sagittal images taken from several trials. During each trial the swimmer completed an average 100 arm cycles. Anthropometrics body segment measurements of the swimmers arm were used to scale images. The time between picture frames was set at 0.03 seconds. In this manner, both time and distance were scaled appropriately to insure accurate velocity measurements.

A high-resolution video-based technique for obtaining two-dimensional fluid velocity field data known as the digital particle image velocimetry (DPIV) technique was utilized (Dong, 2001). Autocorrelations of individual video frames in an image pair yield two instantaneous velocity fields. Tecplot was used to graphically demonstrate velocity vector fields of each successive frame. Dimensional analysis was then used to validate results.

RESULTS AND DISCUSSION

Figure 1a displays the experimental setup and one of the parameters analyzed, the angle α. Figure 1b is a different view of the testing setup. The parameter α is graphically represented in Figure 2 with respect to the corresponding drag measurements. Comparison of the different drag values associated with the two head positions and other anthropometric measurements yielded insignificant differences.

Figure 3 displays a digital image and the corresponding velocity profiles. The velocity in yards per second of the hand position in the second arm position in Figure 1 corresponds to a speed of 1.79 yards per second, which is reasonable for the level of swimmer used in the experiment. Analysis of several stroke cycles indicated velocity magnitudes of the second arm position to yield consistent velocity magnitudes of 1.79 ± 0.2 yards per second. The swimmer in these images has the ability to swim at maximum speed of 1.9 yards per second.

SUMMARY

The drag force increased linearly with increase in flow velocity, but different head postures in the streamline position resulted in a determination that anthropometrics measurements do not affect drag.

Velocity profiles of a swimmer in freestyle motion, provides both qualitative and quantitative data summarizing the motion of the fluid particles displaced and surrounding the swimmer. Consequently, DPIV processing can be instrumental in the comparison of different swimmers motions and speeds. The next step in our experiment is to look at several members of the Rutgers University swim team velocity profiles for freestyle motion.

REFERENCES

Vorontsov, A.R., Rumyantsev, V.A. (2000). *Encyclopaedia of Sports Medicine*, **9**, 193-196.

Miyashita, M. & Tsunoda, R. (1978) *Swimming Medicing*, **4**, 395-401.

Dong, P., Hsu, T.-Y., et al. (2001) *Experiments in Fluids*, **30**, 626-632.

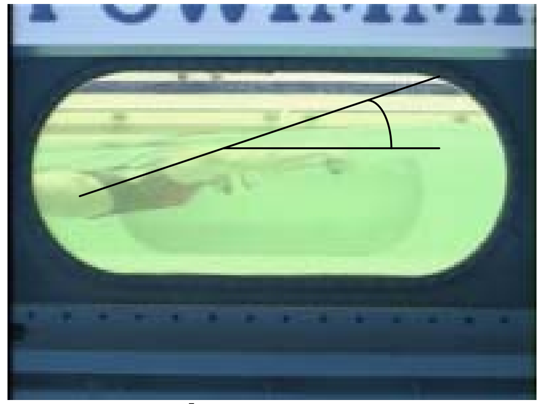

Figure 1a. Side view

Figure 1b. Top View

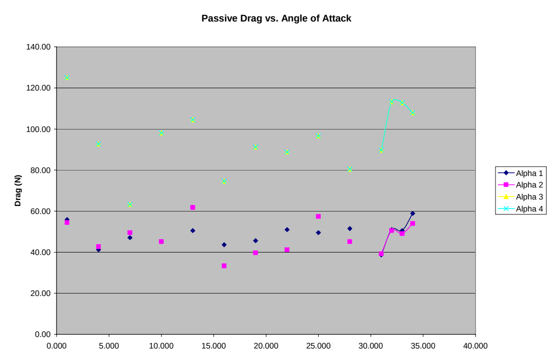

Figure 2. Angle of Attack vs. Drag

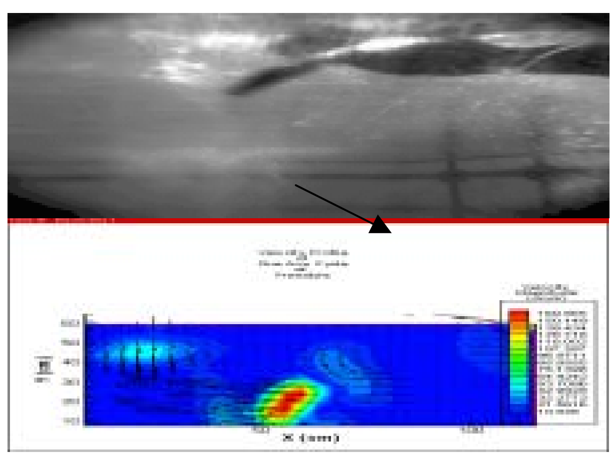

1.79 yds/s

Figure 3. Digital Image and Velocity Profile

DETERMINING SHOCK TRANSMISSION TIMES AND VARIABLE EFFECTIVE MASS OF GYMNASTICS LANDING MATS UNDER LOADING CONDITIONS PRODUCED BY MALE GYMNASTS

Matthew Pain, Chris Mills and Fred Yeadon

School of Sport and Exercise Sciences, Loughborough University, LE11 3TU, UK
E-mail: M.T.G.Pain@lboro.ac.uk

INTRODUCTION

Mats in gymnastics are now essential for the safe completion of landings from dismounts and vaults. The International Gymnastics Federation (FIG) has specific guidelines for tolerance levels of landing mats. However the criteria are based on threshold values obtained from vertical drops of a 20 kg mass with a contact area of 10 cm^2 and a landing velocity of 3.96 ms^{-1}. A more detailed knowledge of the mat properties and its responses to loading regimes that are observed with actual gymnasts is required for use in biomechanical analysis.

It is common to measure the landing forces using force plates positioned under the mat but this has a number of potential problems related to the construction and dynamics of the mat under impact and the mat-force plate interaction. Landing mats are bulky, have a number of component layers, transmit force relatively slowly (dependent on magnitude of compression) and undergo large area visco-elastic deformations. The forces of interest to the biomechanist are those acting at the mat-gymnast interface. These are different from those at the mat-force plate interface due to the slow transmission of force and the acceleration of mat mass.

The purpose of this paper was to use accelerometer data and force data to calculate shock transmission time and effective mass of the mat undergoing visco-elastic area deformation, for use in further studies.

METHODS

A solid impactor with a mass of 24 kg and a contact area of 25 cm by 25 cm was used to simulate a gymnast landing. The mass and area were chosen to represent the effective mass of a 72 kg gymnast landing, as determined by impulse, force and time to peak force.

Five vertical trials with landing velocities between 4.5 ms^{-1} and 6.5 ms^{-1} were performed. Additional oblique tests were carried out at five different angles (45°, 50°, 55°, 60° and 65°) on a custom built rig. Angles and landing velocities covered the range of those seen in competition landings (Takei, 1998). The landing mat was a custom made Continental mat weighing 6.1 kg and measuring 0.9 m by 0.6 m by 0.2 m.

The mat was partially constrained so that the edges could not rise off from the force plate (Kistler 9281B) and all the force had to go through the force plate. Two PCB Piezotronics accelerometers were attached to the impactor. All data were synchronized to within 1 millisecond.

Force-time, acceleration-time and position-time histories were recorded. The force data and the acceleration data were used to find the shock transmission time and the varying effective mass of the mat deforming during impact.

Fritz and Peikenkamp (2003) determined that elastic surfaces on force plates during impacts introduced 20 Hz or higher oscillations into the force data. Given this problem, that appeared to be observed here, all data were low pass filtered at 20 Hz to determine the effective mass of the mat and for comparisons with video data.

RESULTS AND DISCUSSION

There was a 6-8 millisecond time delay from initial impact to initial force development within the force plate (Figure 1). This appeared to decrease to 3-5 milliseconds at maximum compression. No delay was seen with a wooden blank. This needs to be taken into account if performing inverse or forward dynamics analysis since the accelerations has an initial spike with a peak of 210 ms^{-2} before any force was registered.

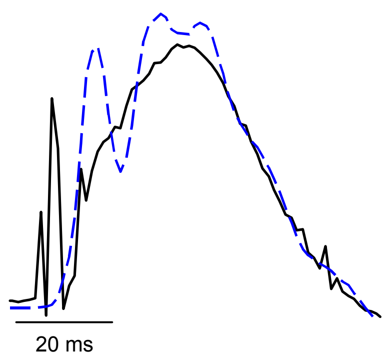

Figure 1: Scaled force (dashed) and accelerometer (continuous) curves showing non-linear delay in transmission of force through the mat.

The filtered peak vertical force was approximately 10 % less than the unfiltered force. The filtered peak acceleration values were about 8 % less than the unfiltered values. The following results are for a landing velocity of 5.5 ms^{-1}. Using unfiltered data the peak force and acceleration gave an effective mat mass of 2.7 kg. However due to the transmission times it was not certain if the values used were coincident in time.

Using the filtered data Figure 2 was obtained. The effective mass goes from that of the impactor only (24 kg) to 26.4 kg, representing 2.4 kg of mat mass. Given the percentage differences in filtered data to raw data this would correspond to a peak effective mass of 2.9 kg if obtained from unfiltered data.

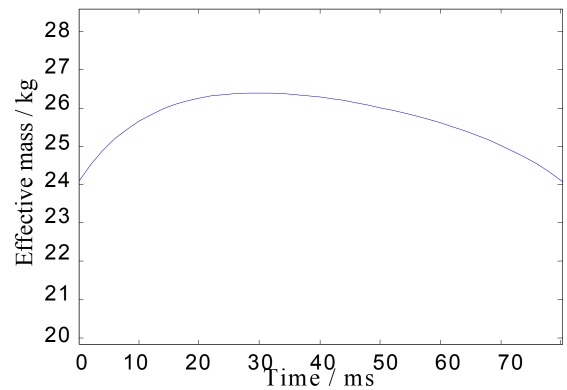

Figure 2: The effective mass of the mat changes with time.

SUMMARY

Forces at the different surfaces of the mat have been determined. Time delays as well as the effective mass of the mat have been calculated. Both of these need to be considered when utilizing force plate data in landings if the actual forces acting on the gymnast are to be obtained.

Further work has shown the change in mat shape during impact measured from the video indicated volume changes that were consistent with these effective mass values.

REFERENCES

Fritz, M. & Peikenkamp, K. (2003). *Medical and Biological Engineering and Computing,* **41**, 11-17.

Takei, Y. (1998). *Journal of Applied Biomechanics*, **14**, 190-210.

Knee Kinematic Sensitivity to Probed Anatomical Points

Lorin P. Maletsky and Junyi Sun

Experimental Joint Biomechanics Research Laboratory
University of Kansas, Lawrence, KS, USA
Email: maletsky@ku.edu Web: www.engr.ukans.edu/~biomech/research.html

INTRODUCTION

Kinematic investigations of the knee involve measuring rigid body motion and describing the three translations and three rotations between the pairs of bones (i.e. tibio-femoral and patello-femoral). Different open-chain models have been developed to describe this motion in familiar terms for clinicians such as adduction-abduction, anterior drawer, etc. (Pennock and Clark, 1990; Grood and Suntay, 1983). This abstract describes the effects on these kinematics from inaccuracies in probing the anatomical points that are used to define the coordinate systems.

METHODS

For a series of cadaveric tests in a dynamic knee simulator, eleven anatomical locations were identified and used to define the local coordinate systems on the three bones of the knee. These locations were identified using a three-camera system and probe. Three points were probed on the femur and used to define the femoral reference frame: the medial and lateral epicondylar points and a proximal point approximating the cross-section center of the bone. Four probed points on the tibia were the medial and lateral tibial plateau points, tibial origin, and a distal point. The four points used to define the patellar frame were the proximal and distal patellar ridge points, patellar origin, and lateral patellar point.

A series of perturbations that represented possible experimental errors were made to all eleven points. An experimental set of kinematics consisting of tibio-femoral and patello-femoral transformation matrices between rigid bodies fixed to the bones from a simulated walk cycle was used as the baseline. A computer program was used to test the anatomical perturbations. Six tibio-femoral and six patello-femoral kinematics were calculated and compared against the baseline results. The femoral epicondylar points were also moved with smaller steps. Comparisons of six different knees during a walk cycle were made to verify whether there were consistent changes under similar perturbations.

RESULTS AND DISCUSSION

Changes in the overall range of motion were compared to the baseline motion. For all kinematics investigated, the adduction-abduction showed the largest variation with 175.5% change from the baseline range for tibio-femoral motion (Table 1) and 144.9% in the patello-femoral system. The anatomical points whose perturbation had the largest effect on motions were found to be the two femoral epicondylar points. Proper and consistent identification of

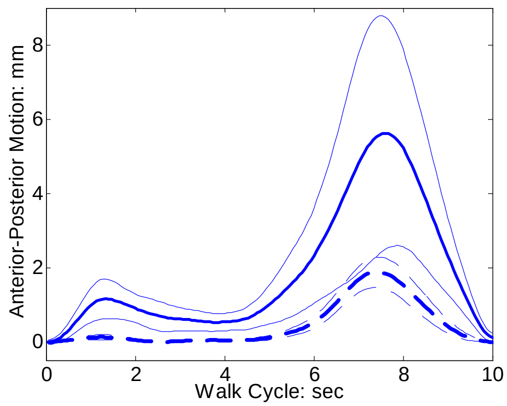

Figure 1: The baseline tibio-femoral ant(+)/post kinematics during walking (solid line) and change in motion with ant/post perturbation of epicondylar point (dashed line) [mean±SD].

these points are then the most critical anatomical locations to find. The kinematics most sensitive to the perturbations were adduction-abduction. Further investigation into the effects of the perturbations of the femoral epicondylar points showed that most of the changes of range from baseline were linear and maintained a similar shape if the perturbation also increased linearly. The only exception to this was ad-ab that showed a nonlinear change in range as well as a change in shape. Most of the kinematics were found to behave symmetrically when the anatomical points were perturbed (e.g. superior perturbation of lateral epicondylar point had same result as inferior perturbation of medial point). Comparison of six knees showed that there were consistent changes for most of the motions investigated during a complete walk cycle (Figure 1). Modifications to the kinematic testing protocol may reduce the sensitivity.

SUMMARY

An examination of the sensitivity of knee kinematics to anatomical probed points has shown that large changes may occur as a result of inaccuracies in locating the epicondylar points on the femur.

REFERENCES

Grood, E.S., Suntay, W.J. (1983). *J Biomech Eng*, **105**, 136-144.

Pennock, G.R., Clark, K.J. (1990). *J of Biomech*, **23**, 1209-1218.

ACKNOWLEDGEMENTS

Supported by DePuy Orthopaedics, Inc.

Table 1: Effect of perturbation of anatomical points on tibio-femoral knee kinematics. The two values in parentheses represent the effects when moving in the two different directions.

Kinematics	*Anat. points perturbed*	*Changed ratio*	*Changed range*
Adduction / Abduction (+)	Fem epicond, ant/post	(175.5%, -25.5%)	(3.65°, -0.53°)
	Fem epicond, sup/inf	(110.6%, -70.2%)	(2.30°, -1.46°)
Internal / External (+)	Fem epicond, sup/inf	(57.8%, -40.3%)	(3.03°, -2.11°)
	Fem epicond, ant/post	(41.0%, -23.3%)	(2.15°, -1.22°)
Medial / Lateral (+)	Fem epicond, ant/post	(41.8%, -29.1%)	(1.28mm, -0.89mm)
	Tibia origin, ant/post	(27.1%, -27.1%)	(0.83mm, -0.83mm)
Anterior (+) / Posterior	Fem epicond, sup/inf	(30.6%, -31.0%)	(3.26mm, -3.30mm)
	Fem epicond, ant/post	(21.0%, -20.8%)	(2.23mm, -2.21mm)

CONTACT CHARACTERISTICS OF THE KNEE JOINT IN DEEP KNEE FLEXION

Christian Spanu[1], Dumitru I. Caruntu[1,3], Mohamed Samir Hefzy[1,3], Vijay K. Goel[2,3], Henry T. Goitz[3] and Michael J. Dennis[4]

[1]Department of Mechanical, Industrial and Manufacturing Engineering, [2]Department of Bioengineering, The University of Toledo, Toledo, OH, USA
[3]Department of Orthopaedic Surgery, [4]Department of Radiology, The Medical College of Ohio, Toledo, OH, USA
E-mail: mhefzy@eng.utoledo.edu   Web : www.mime.eng.utoledo.edu/biomechanics_lab

INTRODUCTION

It appears that the challenge in developing a TKR that allows for deep knee flexion is the understanding of knee mechanics when it is maximally flexed. Only few biomechanical studies have been published to describe the knee response at this position. The objective of the present work is to determine the contact characteristics of the knee joint during a deep squat while the knee is maximally flexed, up to 150^o of flexion.

METHODS

An integrated human motion analysis system was employed to measure the relative spatial position of the right lower limb bones (foot, shank and thigh), and the ground reaction forces and moments for a subject performing a deep squat. The net equivalent external loads (forces and moments) at the knee joint for each position undertaken during the deep squat exercise were determined using inverse dynamics. Subsequently, and using a 2-D anatomical mathematical model, the knee joint internal loads including ligamentous forces, tibio-femoral contact force, and quadriceps and hamstrings equilibrating forces were calculated. For this purpose, the knee joint has been modeled as two rigid bodies, the tibia and the femur, undergoing general planar motion in the sagittal plane. The tibia was assumed fixed while the femur slides and rolls along the tibial plateau, without losing contact. Point of contact was enforced in the analysis. The model included ten ligamentous structures to represent the cruciate and collateral ligaments along with the posterior capsule, and two muscle forces: quadriceps and hamstrings. The quadriceps forces were applied through the patellar tendon. X-rays were obtained to determine the mathematical representation of the tibial and femoral articular surfaces. Polynomials of the second and third degrees were used to mathematically describe the different portions of the tibial plateau, the proximal posterior edge of the tibia, the different portions of the condyle, and the posterior and distal edge of the femoral shaft. Nissel's data ,1985, were used to account for the change of orientation of the patellar tendon force with respect to the tibia. This model also accounts for the wrapping of the patellar tendon around the tibia at flexion angles larger than 90 degrees. For each value of flexion angle the system of equations describing the joint behavior consists of six (6) equations in seven (7) unknowns. The system of equations consists of three equations describing the single point contact and three equilibrium equations. The seven unknowns include the tibial and femoral x-coordinates of the contact point; the X- and Y-coordinates of the origin of the femoral coordinate system with respect to the tibial coordinate system; the tibio-femoral contact force; and the magnitude of the patellar tendon and hamstring forces. To solve this system of equations the patellar tendon force was assumed as a known quantity, and the system of equations reduced to six (6) equations in six (6) unknowns. This approach simulated an isometric contraction of the quadriceps muscle associated with the co-contraction of the hamstring muscles.

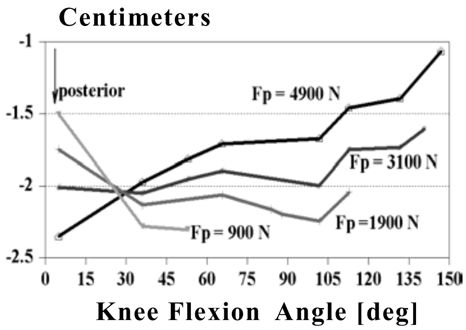

Fig. 1. Tibial antero-posterior contact location

RESULTS AND DISCUSSION

Results were obtained for 12 different positions of the knee joint during deep squat. Model calculations have shown that the path of the femoral contact point as the knee moved toward maximum flexion did not vary as the quadriceps force was changed. At maximum flexion, the contact occurred on the femur at the most proximal point of the femoral condyle. On the other hand, the path of the contact point on the tibia was found to highly depend on the level of quadriceps activation as shown in Fig. 1. In order to go beyond 135^{o} of flexion, a minimum quad force of 3100 N was required, and the contact point on the tibia moved anteriorly as the knee flexion angle increased. When the quad force was kept constant at 900 N, the knee could not go into deep flexion, and the contact point on the tibia moved posteriorly as the knee flexion angle increased. In agreement with Hefzy *et al.*, 1998, the results obtained from this study show that the contact point on the femur occurs on the most proximal point of the posterior condyle when the knee is in deep flexion. However, and while this study predicts that the contact occurs on the tibia anteriorly when the knee is maximally flexed, our previous work reports that it occurs posteriorly. This apparent discrepancy can be easily explained if one looks at the specific activity involving deep flexion. Figure 2.a shows the position assumed by the subject in the present study to achieve deep flexion, and Figure 2.b shows the position that was considered in our previous study.

(a) ***(b)***

Figure 2: Activities involving deep knee flexion
(a) squat - present study
(b) kneeling - previous study

In this study, and to maintain the position shown in Figure 2.a, large quadriceps and hamstring forces were required. These forces have a large posterior component acting on the tibia, causing the tibial contact point to be located anteriorly. In our previous study, the subject was in a kneeling position where quad and hamstrings appear to be dormant, causing the tibia not to be posteriorly dislocated, and hence the contact point to be posteriorly located on the tibia.

SUMMARY

These results suggest that in order to understand the contact characteristics of the knee joint in deep flexion, more detailed studies need to be undertaken to account for the different activities involving deep knee flexion. By taking this into consideration, future design of TKR capable for deep flexion could be achieved.

REFERENCES

Nissel, R. (1985). Acta *Orthopaedica Scandinavica Supplementum,* **216**(56), 5-42.
Hefzy, M.S. *et al.* (1998). *Medical Engineering and Physics,* **20**, 302-307.

THE INFLUENCE OF PATELLA ALTA ON KNEE EXTENSOR MECHANICS

Samuel R. Ward and Christopher M. Powers

Musculoskeletal Biomechanics Research Laboratory, Dept. of Biokinesiology and Physical Therapy, University of Southern California, Los Angeles, CA, USA.
E-mail: samuelwa@usc.edu Web: pt.usc.edu/labs/mbrl/

INTRODUCTION

Elevated patellofemoral joint stress is thought to be a contributing factor with respect to the development of patellofemoral pain (PFP) (Heino 2002). As stress is defined as force per unit area, elevated stress could occur as a result of increased joint reaction force and/or a decrease in contact area. It has been suggested that individuals with patella alta (a condition associated with PFP) have altered knee extensor mechanics that predispose them to increased joint reaction forces (Singerman 1994 and Yamaguchi 1989). This premise however, was based on data obtained from cadaveric and mathematical models and therefore may not have been representative of a population of persons with patella alta. Currently, there are no *in vivo* data to support the premise that patella alta is associated with abnormal knee extensor mechanics and larger patellofemoral joint reaction forces. The purpose of this study was to compare the knee extensor mechanics and the influence of these mechanics on joint reaction force potential in persons with and without patella alta.

METHODS

Twenty seven subjects (25 female and 2 male) with a mean age of 27 $\pm$ 4 years, mean height 164 $\pm$ 5 cm, and mean weight 58 $\pm$ 8 Kg were enrolled in the study after informed consent was obtained.

Subjects were screened for safety within the MR environment before being placed supine on the imaging table in a custom made loading device (Captain Plastic, Seattle, WA). This device (similar to a leg press) was loaded with 25% of body and simulated weightbearing knee extension. Sagittal plane images of the knee joint were obtained with a T1 weighted spin echo pulse sequence (TR 350 msec, TE 10 msec, NEX 1, Matrix 256 X 256, FOV 20 cm X 20 cm, slice thickness 10 mm) at 0, 20, 40, and 60 degrees.

Measurements of patellar ligament length (L_{pl}) and patellar length (L_p) were made on mid-sagittal images of the knee at 0 degrees of knee flexion. Subjects were then divided into patella alta (n=13) and normal patellar position (n=14) groups based on the Insall-Salvati criteria (L_{pl}/L_p ratio $\geq$ 1.2 equals patella alta) (Insall 1971).

Measurement of the quadriceps effective lever arm (M_{eff}) and calculation of the joint reaction force/quadriceps tendon force (F_r/F_q) ratio were computed using previously described methods (Yamaguchi 1989). Briefly, M_{eff} takes into consideration the influence of the pulley and pivoting actions of the patella in determining extensor mechanism leverage capability. The F_r/F_q ratio indicates the magnitude of the joint reaction force per unit quadriceps force and is estimated based on the orientation of the quadriceps tendon and the patellar ligament. This variable represents the patellofemoral joint reaction force potential (Yamaguchi 1989).

A 2 X 4 (group X knee flexion angle) repeated measures analysis of variance was used to test for group main effects for M_{eff}, and the F_r/F_q ratio with a significance level of 0.05.

RESULTS AND DISCUSSION

There was a significant group effect for M_{eff} (Figure 1) but no differences in the F_r/F_q ratio were found (Figure 2) across the range of knee flexion angles tested. When collapsed across all four knee flexion angles, the patella alta group had larger M_{eff} than the control group (4.40 cm $\pm$ 0.09 cm vs. 4.00 cm $\pm$ 0.09 cm, respectively).

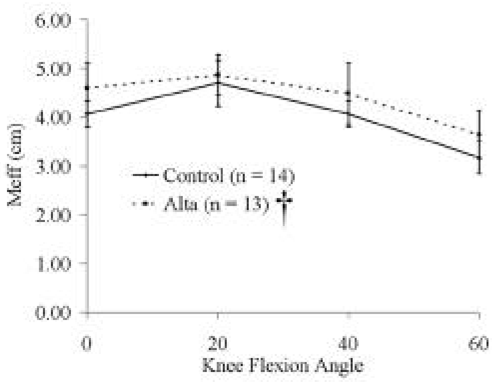

Figure 1. M_{eff} at each knee angle. † denotes alta > control when averaged across all knee angles, $p \leq 0.05$.

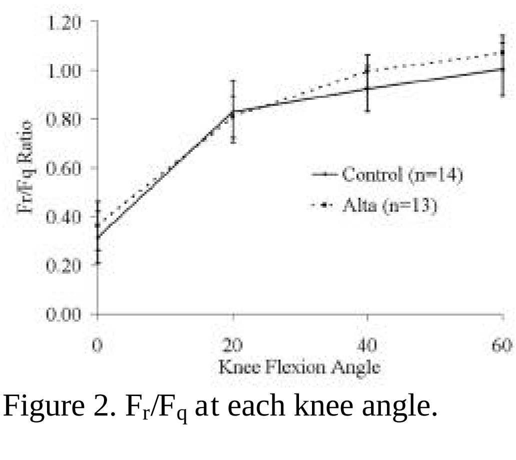

Figure 2. F_r/F_q at each knee angle.

The finding of a greater M_{eff} suggest an increased mechanical advantage in the quadriceps and indicates that subjects with patella alta would be expected to use less quadriceps force to overcome the same knee flexion moment compared to subjects with normal patellar position. The lack of a difference in F_r/F_q ratio indicates that persons with patella alta would be expected to have similar joint reaction forces per unit quadriceps force when compared to subjects with normal patella position.

SUMMARY

The observed differences in knee extensor mechanics suggest that individuals with patella alta have a more efficient knee extensor mechanism than subjects with normal patellar position. Given that these subjects would be expected to generate similar joint reaction forces per unit quadriceps force, subjects with patella alta may experience less joint reaction force to overcome the same knee flexion moment in the range of 0 to 60 degrees of knee flexion. These findings are contrary to previous in-vitro data suggesting that patella alta predisposes individuals to increased patellofemoral joint reaction forces.

REFERENCES

Heino-Brechter, J., Powers CM. (2002). *Med Sci Sports Exerc*. **34**, 1582-1593.

Insall, J., Salvati, E. (1971). *Radiology*, **101**, 101-109.

Singerman, R., *et al*. (1994). *J Biomech*, **27,** 1059-1065.

Yamaguchi, G.T., Zajack, F.E. (1989). *J Biomech*, **22**, 1-10.

ACKNOWLEDGEMENTS

Funding provided by the Foundation for Physical Therapy.

SPORT-DEPENDENT VARIATIONS IN ARM POSITION DURING SINGLE LIMB LANDING AFFECT KNEE LOADING: IMPLICATIONS FOR ACL INJURY

Ajit Chaudhari[1], Allyson Marquand[1], Brenna Hearn[1], Lise Leveille[1], Emilie Johnson[1],
Thomas Andriacchi[1,2]

[1] Biomotion Laboratory, Stanford University, Stanford, CA, USA
[2] Department of Orthopaedic Surgery, Stanford University Medical Center, Stanford, CA, USA
E-mail: ajit.chaudhari@stanford.edu   Web: biomotion.stanford.edu

INTRODUCTION

Non-contact injuries to the anterior cruciate ligament are most frequently reported during the deceleration phase of landing after a jump or in preparation for a cutting maneuver. Video observation and patient accounts have demonstrated that the knee is most often in a position near full extension and there is typically a valgus collapse of the knee associated with landing or deceleration (Colby 2000). Cadaver studies have shown that valgus knee moments place the ACL in greater danger near full extension (Woo 1999). Sidestep cutting maneuvers in particular can create higher valgus moments during deceleration, especially during unanticipated cutting (Besier 2001). Arm position has also been shown to affect lower limb dynamics (Ashby 2002). During single limb support, the arms are often used for balance and motion control. In sports, however, arm movement is often constrained for various reasons. Due to the role of the arms and upper body for balance and control, sport-dependent variations may cause changes in the loading of the knee that may lead to a higher risk of valgus collapse of the knee in some sports. The purpose of this study was to test this hypothesis, that sport-dependent variations in arm motion affect the potential for valgus collapse of the knee during cutting maneuvers.

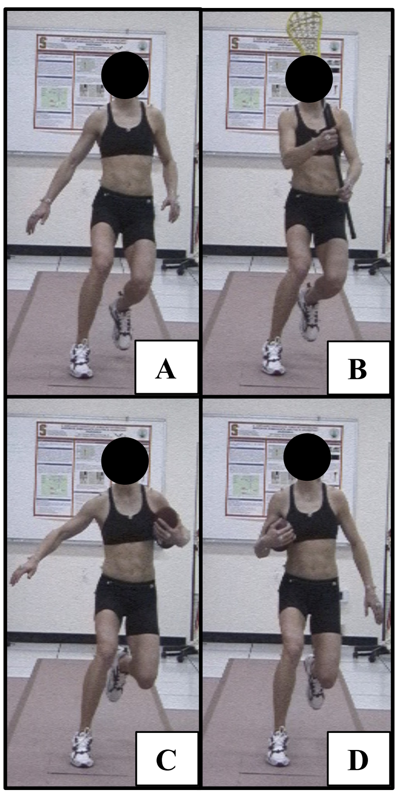

Figure 1: Examples of cutting maneuvers. (A) Normal, (B) Both arms constrained by holding a lacrosse stick, (C) Cutting side arm constrained by cradling a football, (D) Planting side arm constrained by cradling a football.

METHODS

Eleven subjects (6 females and 5 males, ages 18-29) without a history of lower limb injury and who exercise regularly were tested after providing informed consent. All subjects performed a 90-degree lateral run-to-cut maneuver on the side they felt more comfortable, first with no constraints to upper-body position and then in 3 arm-constraining positions (Fig. 1). Lower limb kinetic data was obtained using a three-dimensional opto-electronic system and a previously described 6-marker link model of the lower extremity (Andriacchi 1997). Upper body kinematic data was obtained using a full-body marker set with 30 markers. Arm position was quantified as the distance from the wrist to the centerline of the torso. Paired Student's t-tests (α=0.05) were used to compare the peak external knee abduction moment and arm positions between the normal maneuver and each of the 3 restricted maneuvers during deceleration.

RESULTS

The abduction moment at the knee was influenced by the arm position (Table 1). Holding a lacrosse stick caused a significant increase in the peak external knee abduction moment ($p<0.01$), and cradling a football in the plant-side arm caused an increase in the moment as well ($p<0.07$). In contrast, cradling in the cut-side arm did not cause a significant increase in the moment. The position of the plant-side arm was closer to the centerline of the body for most sport-dependent motion relative to unconstrained motion (Table 1), with the exception of cradling the football in the cut-side arm.

DISCUSSION

The results of this study indicate that sport-dependent arm position can have a substantial influence on the types of loads that can cause non-contact ACL injury. There appears to be an interaction between torso movement and arm position. When the plant side arm cannot be used for balance, athletes may compensate by accelerating the torso laterally to maintain balance, causing an increase in the abduction moment at the knee.

Previous studies have shown that a higher knee abduction moment places the ACL in greater danger (Woo 1999), so any condition that causes higher abduction moments during deceleration and landing may put athletes at greater risk of ACL injury.

This study provides a basis for understanding the multiple factors that lead to non-contact ACL injury. In addition, these results suggest that adopting training methods that consider arm position as a risk factor could help to reduce the probability of ACL non-contact injury.

REFERENCES

Andriacchi, T.P. et al. (1997). *Basic Orthopaedic Biomechanics, 2nd ed.*, 37-68.

Ashby, B.M., Heegaard, J.H. (2002). *J. Biomechanics,* **35**, 1631-1637.

Besier, T.F. et al. (2001) *Med. Sci. Sports. Exerc.,* **33,** 1176-1181.

Colby, S. et al. (2000). *AJSM*, **28**, 234-240.

Woo, S.Y. et al. (1999). *AJSM,* **27,** 533-543.

Table 1: Increase in peak external knee abduction moment, distance from body centerline to plant-side wrist, and distance from body centerline to cut-side wrist (mean ± SD). * denotes significant difference of $p< 0.05$, † denotes $p< 0.07$.

	Increase in Knee Abduction Moment [%bodyweight*height]	Distance from Centerline to Plant-side Wrist [%height]	Distance from Centerline to Cut-side Wrist [%height]
Normal	--	28 ± 3	22 ± 6
Lacrosse	1.58 ± 1.27 *	22 ± 3 *	20 ± 3
Plant-side Football	0.87 ± 1.42 †	20 ± 2 *	23 ± 3
Cut-side Football	0.49 ± 1.12	27 ± 5	20 ± 3

Validated Subject-Specific Model of Knee Joint Contact Force Distribution

Rose F. Riemer[1,2], Kenton R. Kaufman[1], and Tammy Haut Donahue[2]

[1]Motion Analysis Laboratory, Mayo Clinic, Rochester, MN, USA
[2]Mechanical Engineering, Michigan Technological University, Houghton, MI, USA
Email: Kaufman.Kenton@mayo.edu

INTRODUCTION

Biomechanical analysis of joints is an important indicator of joint health. Improper loading can cause progression of degenerative changes. Few models exist to predict articular surface loads during dynamic activities (Morrison, 1970; Johnson et al, 1980; Schipplien and Andriacchi, 1991). Therefore, the purpose of this study was to develop a flexible model which predicts unique tibial plateau load distribution based on an individual's joint geometry and dynamic loading pattern.

METHODS

The joint was modeled as two rigid bodies with spring elements representing the articular cartilage and collateral ligaments (Kawai,1977). The model uses subject-specific joint geometry and loads for predicting joint contact pressure distribution. Joint geometry is found from analyzing fluoroscopy-guided, weight-bearing radiographs. These radiographs are analyzed with Matlab's Canny edge detection algorithm (Mathworks, Natick, MA). Applied loads are calculated from individual gait data and translated to the knee joint center.

Ligaments and cartilage are assumed to have linear deformation. The model initially assumes the cartilage is loaded in compression and ligaments in tension. After initial displacement is calculated by the model, elements that experience an incorrect load are subtracted from the stiffness matrix and displacements are recalculated until equilibrium is reached. The joint space was modeled with 36 cartilage springs having a stiffness of 15.71Kgf/cm in the normal direction and 0.001Kgf/cm in the shear direction. The medial and lateral collateral ligaments were each modeled as individual springs with stiffness of 100Kgf/cm and 0.0, in the normal and shear direction.

The model was validated using a cadaver knee. Joint contact pressure readings were recorded using a calibrated sensor (TekScan, South Boston, MA) inserted into the knee joint distal to the menisci. A uniaxial load was applied through the fixed femur using a material testing machine, (MTS Systems Corp., Eden Prairie, MN) while the tibia was fixed to an xy table. The same forces were applied to the model as were applied during the experiment.

RESULTS AND DISCUSSION

The analytical model predicted that the contact forces are higher on the medial plateau(Fig1a). These results compare closely with the experimental measurements (Fig 1b).

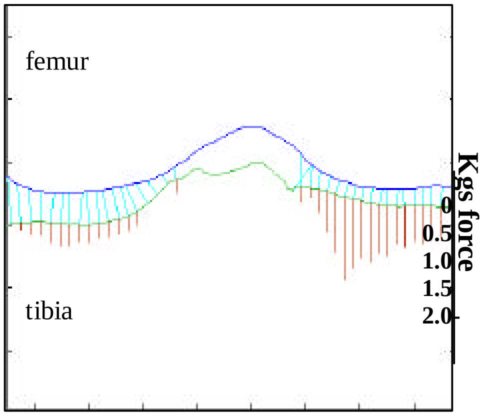

Figure 1a: Analytical force distribution across a right knee plateau resulting from a 34kg axial load; shown as vertical lines.

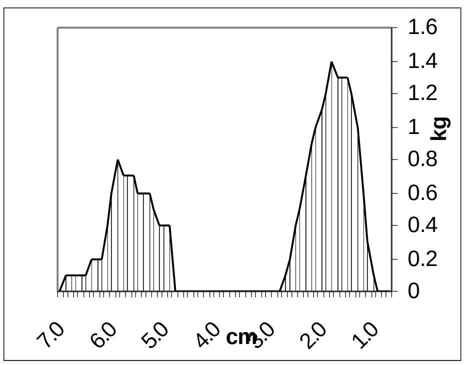

Figure 1b: Experimental force distribution across a right knee plateau.

This model has made several assumptions. The bones were assumed to be rigid. This assumption has been shown to be valid when computing contact variables of the tibial plateau (Haut Donahue et al, 2002). Further, it is known that cartilage is a biphasic material. However, during dynamic loading, .e.g <1 sec, the elastic solution does not deviate from the biphasic solution. (Garcia et al, 1988) Therefore the cartilage can be assumed to behave as an elastic material for the purposes of contact pressure computation during gait (Donzelli et al, 1999).

SUMMARY

An analytical model of the knee has been developed and validated to predict subject-specific load distribution on the tibial plateau.

ACKNOWLEDGMENTS

This study is funded by NIH grant # R01 AR048768.

REFERENCES

Donzelli PS. et al. (1999) *J Biomech* **32** 1037-1047
Garcia JJ. et al. (1988) *J Biomech Engr* **120(5)** 608-613.
Haut Donahue TL. et al. (2002) *J Biomech Enrg* **124** 273-280.
Johnson F, Leith S, Waugh W. (1980) *J Bone Jt Surg* **62[B],** 346-349.
Kawai, T., Toi, Y., (1977*). Seisan Kenkyu*, **29**, 204-207.
Morrison JB. (1970) *J. Biomechanics*, ***3***, 51-61.
Schipplein OD, Andriacchi TP. (1991) *J Orthop Res*, **9,** 113-119.

ANKLE AND KNEE JOINT KINETICS DURING RUNNING AND SPRINTING

Alan Hreljac[1], Nick Stergiou[2], Rodney Imamura[1], Jeff Casebolt[1], and Mitell Sison[1]

[1]Kinesiology and Health Science Department, California State University, Sacramento
[2]HPER Biomechanics Laboratory, University of Nebraska at Omaha
E-Mail: ahreljac@hhs4.hhs.csus.edu

INTRODUCTION

To an observer viewing a person running at a moderate pace and a person sprinting, there would be apparent differences between the two modes of locomotion beyond the obvious difference in speed. A gait has been defined as a pattern of locomotion characteristic of a limited range of speeds described by quantities of which one or more change discontinuously at transitions to other gaits (Alexander, 1989). Although there is agreement that there are differences between running and sprinting, it is not clear whether running and sprinting actually represent two distinct gaits, or whether sprinting is merely "fast" running. Previous studies (Mann & Hagy, 1980; Novacheck, 1995; Stefanyshyn & Nigg, 1997) have reported significant differences in joint moment and power patterns of the lower extremity joints between running and sprinting. All of these studies, however, have compared a single "running" speed to a single "sprinting" speed. It is not clear whether the observed differences occur on a continuum as speed increases, or if there is an abrupt change at some discrete speed. The purpose of this study was to compare ankle and knee joint moment and power patterns over a range of running and sprinting speeds. It was hypothesized that one or more variables would change abruptly as speed increases, thereby distinguishing a run from a sprint.

METHODS

Eleven male subjects, all of whom exhibited a heelstrike landing pattern at their preferred running speed, ran down a 25 m runway at seven different speeds, including their preferred running speed (0%), and speeds that were 15%, 30%, 45%, 60%, 75%, and 90% greater than this speed, landing with their right (dominant) foot on a floor mounted force platform. The randomly ordered trials were considered to be successful if the running speed was within ± 5% of the target speed, the landing foot completely contacted the force platform, and if there was no visible change in stride length (i.e. no targeting). Sagittal plane kinematics (240 Hz) of four relevant markers (greater trochanter, knee joint center, lateral malleolus, and head of the fifth metatarsal) were recorded and synchronized with ground reaction force data (960 Hz). After smoothing, using a fourth order, zero lag Butterworth filter, ankle and knee joint angular velocities, moments, and powers were calculated. Prior to analysis, all variables were normalized by dividing by body mass. Dependent variables (DVs) included maximum ankle plantarflexor and knee extensor moments, and maximum power absorption and generation at the ankle and knee. These DVs were compared between adjacent speed conditions using a repeated measures multivariate analysis of variance ($p = 0.05$).

RESULTS AND DISCUSSION

No significant differences were found between adjacent speed conditions in peak ankle or knee moments (Fig. 1).

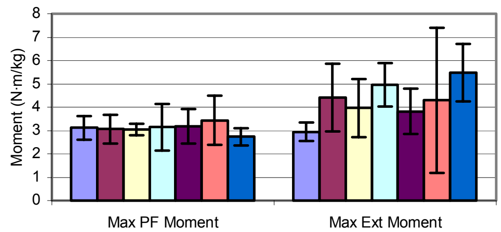

Figure 1: Peak ankle plantarflexor and knee extensor moments. Conditions range from 0% to 90% from left to right.

Although some differences existed between adjacent speed conditions in peak power absorption and generation at both the ankle (Fig. 2) and knee (Fig. 3), no variable could be identified as a "distinguishing" variable between running and sprinting.

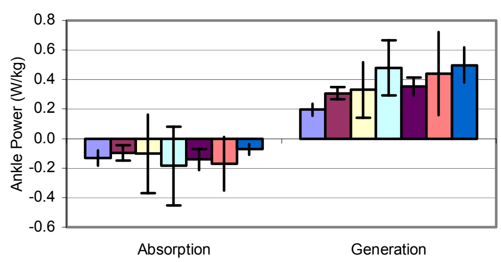

Figure 2. Peak power absorption and generation at the ankle. Conditions range from 0% to 90% from left to right.

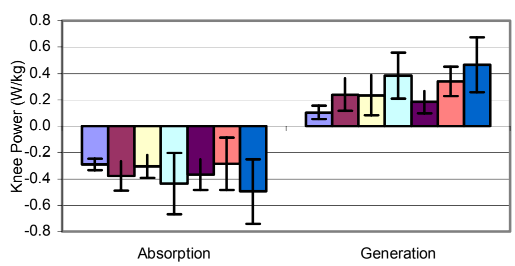

Figure 3. Peak power absorption and generation at the knee. Conditions range from 0% to 90% from left to right.

SUMMARY

As running speed increased to a sprint, maximum knee extensor moments (Fig. 1), peak ankle power generation (Fig. 2), and knee power absorption and generation (Fig. 3) generally increased. Increases in all of these variables occurred over somewhat of a continuum, indicating that none of these variables could be used to distinguish between a run and a sprint.

The walk to run gait transition has been shown to be "triggered" by high levels of dorsiflexor activity (Hreljac et al., 2001). In the present study, no variable was expected to trigger a change from a run to a sprint, but there was an expectation that variables would be found which could distinguish between a run and a sprint. None of the variables tested were able to do so. The discrete point analysis (i.e. maxima and minima) used in the current study might not have been adequate to identify differences between the run and sprint behaviors. It is possible that an analysis of intralimb coordination (see Stergiou et al., 2001) could be utilized to distinguish between a run and a sprint.

REFERENCES

Alexander, R.M. (1989). *Physiol. Rev.*, **69**, 1199-1227.
Hreljac, A. et al. (2001). *J. Appl. Biomech.*, **17**, 287-296.
Mann, R.A., Hagy, J. (1980). *Am. J. Sports Med.*, **8**, 345-350.
Novacheck, T.F. (1995). *Am. Acad. Ortho. Surg.*, **44**, 497-506.
Stefanyshyn, D.J., Nigg, B.M. (1997). *J. Biomech.*, **30**, 1081-1086.
Stergiou, N. et al. (2001). *Gait Posture*, **13**, 210-220.

COMPUTATIONAL MODELING OF THE EFFECT OF SKI BOOT DESIGN ON KNEE LIGAMENT INJURIES

Jerome Hausselle and A.J. (Ton) van den Bogert

Cleveland Clinic Foundation, OH, USA
E-mail: bogert@bme.ri.ccf.org

INTRODUCTION

While skiing, anterior cruciate ligament injuries (ACL) can occur when the skier lands from a jump and leans backward. The so-called "boot-induced" mechanism involves transmission of ground reaction forces from the tail of the ski through the boot, pushing the tibia forward. This puts stress on the ACL and can lead to rupture.

New ski boots have been designed to prevent this type of injury. They possess a backward release mechanism that is activated when the force exerted by the tibia on the boot is high enough, in order to prevent an excessive anterior translation of the tibia. The purpose of this study was to develop a forward dynamic model of a skier, optimize its muscles behavior to make it perform a safe landing, then perturb the initial conditions and look at the effect of the release mechanism.

METHODS

A 2D biomechanical model was used, based on the work of Gerritsen et al., (1996). Mechanical properties of two types of ski boot, a normal boot and a modified boot with a release mechanism, were obtained from Senner (2001). The model had 9 degrees of freedom and 16 muscles (8 in each leg). Equations of motion were generated using SD/FAST (PTC Inc.). Muscle activation patterns to perform a normal landing movement were found through optimization, with the goal to minimize the difference between simulation and kinematic data from Nachbauer et al. (1996).

Injuries were simulated through a Monte Carlo simulation in which the initial anatomical angles and the time of activation of the quadriceps muscles were randomly perturbed. 50,000 randomly perturbed landing movements were simulated. A 2D knee model (Herzog and Read, 1993) was used to calculate peak ACL force for each of these simulations and the ACL was considered injured if this force exceeded 2,000 N. All simulations were done for a classical boot and for the modified boot. The percentage of injuries was calculated in both cases.

RESULTS AND DISCUSSION

The optimization process produced multiple solutions, indicating that there are different muscle coordination patterns leading to almost the same movement. Figure 1 shows one of these results, comparing the simulated and measured kinematics.

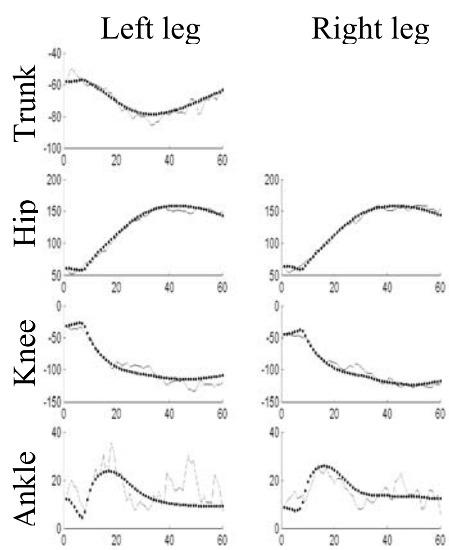

Figure 1: Simulated angles (dots) compared to the measured angles (continuous line), in degrees.

We selected two of these solutions, each simulating a normal landing movement, as a baseline condition for the Monte Carlo injury simulations. Both of these Monte Carlo simulations resulted in a higher rate of injury for the modified boot, one set of results is presented in Table 1.

Table 1: Percentages of injuries.

	Left leg	Right leg
Normal boot	2.0 %	6.7 %
Modified boot	4.1 %	14.1 %

In order to clarify the mechanisms responsible for this result, three simulations of a poor landing technique, all resulting in injury, were studied in detail. These situations can be described as a backwards balance disturbance with high quadriceps activation. In each of these cases the modified boot allowed the ankle to have a deeper plantar-flexion, which resulted in less knee flexion. In that position the quadriceps muscles pull the tibia forward (Herzog and Read, 1993) and stress the ACL.

The model was two-dimensional, which was thought to be appropriate for the backward fall injury mechanism. Valgus and internal rotation are important contributors to other ACL injuries in skiing, and these were not considered.

When searching for simulations of a normal landing movement, the optimization procedure found several solutions. This shows that unique muscle activation patterns are hard to find from kinematic data only. Nevertheless, the two solutions were found to produce similar conclusions on injury mechanics.

The release threshold of the boot should be adjusted to weight and height of the skier. In this study we used the moment-angle hysteresis curves from Senner (2001), which may not have been optimal for the skier and the movement represented by this model.

Benoit et al. (2001) showed that a rear release system decreases the shear force in the knee and should therefore decrease the stress on the ACL. But these experiments were done by fixing the boot to a force plate and asking the subjects to propel themselves backward. The dynamics and muscle activation during this task is different from skiing, and the ACL was not highly stressed. In human subject experiments, it is difficult to study movements that are close to injury, and this was an important motivation for our modeling work.

SUMMARY

We found that a release mechanism may not protect against ACL injuries in skiing, at least in the case of a backward fall or during a landing on the back of the skis. However, the boot may help prevent injury in other ways. When the release system activates, the skier will experience a powerful sensation of loss of balance. This sensory feedback signal may help skiers learn to avoid these situations. A definitive answer will have to come from injury surveys and from controlled studies on human subjects to detect any boot-induced learning effects.

REFERENCES

Benoit, D. et al. (2001). *Proc. of the 5th Symp. on Footwear Biomechanics* , Switzerland, (eds. E. Hennig, A. Stacoff).

Gerritsen K.G. et al. (1996) *J Biomech* **29**, 845-854.

Herzog W., Read L.J. (1993) *J Anat* **182**, 213-230.

Nachbauer W. et al. (1996). *J. Appl. Biomech.*, **12**, 104-115.

Senner, V. (2001) PhD thesis. Technische Universität München, Germany.

ACKNOWLEDGEMENT

We thank Dr. Werner Nachbauer (University of Innsbruck, Austria) for providing the kinematic data.

ACL INJURY: SAGITTAL PLANE BIOMECHANICS ARE NOT THE CAUSE

Scott McLean [1,2], Anne Su [1] and Ton van den Bogert [1,2]

[1] Dept. of Biomedical Engineering, The Cleveland Clinic Foundation, Cleveland, OH, USA
[2] The Orthopaedic Research Center. The Cleveland Clinic Foundation, Cleveland, OH, USA
E-mail: mcleans@bme.ri.ccf.org   Web: lerner.ccf.org

INTRODUCTION

Anterior cruciate ligament (ACL) injury is a common and potentially disabling sports related injury. Apart from the obvious acute short-term effects, long-term consequences such as osteoarthritis are likely. Non-contact ACL injuries typically occur during rapid execution of sports movements such as sidestepping. Abnormally large quadriceps forces during stance, resulting in excessive anterior tibial force, are touted as a primary injury mechanism (Delfico and Garrett, 1998). Testing this postulate is difficult however, as having subjects perform controlled systematic variations in these movements, or exposing them to injury experiments is not feasible. Current computer-based modeling techniques provide a fast and relatively inexpensive means to study acute musculoskeletal injuries while controlling all aspects of neuromuscular control (NMC). The purpose of this study was to determine the effects of NMC variability during sidestepping on resultant 3D knee joint loads. Using these data, the potential for sagittal knee loading associated with sidestepping as a mechanism of ACL injury was assessed.

METHODS

A previously validated 3D forward dynamic model of a sidestep cutting maneuver was implemented in the current study (McLean et al., 2003). Model inputs were obtained from initial contact 3D linear and angular kinematic positions and velocities, and GRF data measured across 10 sidestep trials in a single subject. A simulated annealing algorithm optimized muscle activation patterns (16 muscles) to reproduce the mean measured biomechanical data for the first 200ms of stance. Monte Carlo simulations were then performed on the optimized system to predict the effect of the subject's variability in pre-impact body kinematics, and a hypothetical 50% variability in peak quadriceps and hamstring activations on resultant 3D knee loads (Fig 1).

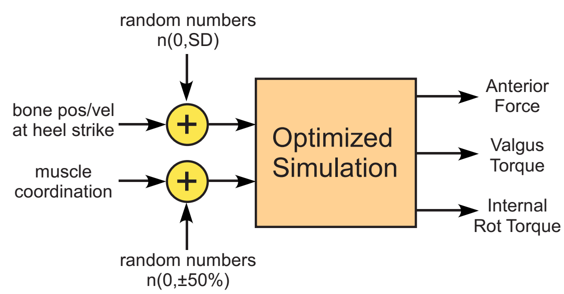

Figure 1: Monte Carlo simulation technique used to determine movement control variability effects on peak external knee loads.

In each simulated trial (N=200000), valgus and internal rotation torques were obtained directly from the SD/FAST multibody software used to develop the equations of motion for the forward dynamics simulation. Resultant anterior tibial force was calculated by combining the external joint reaction force with the quadriceps and hamstrings muscle forces acting across the joint.

RESULTS AND DISCUSSION

For the optimized solution, a peak anterior drawer force, valgus moment and internal rotation moment of 34.6 N, 19.15 Nm and 19.24 Nm were observed respectively. Both the magnitude and timing of these peaks were consistent with those reported previously for the stance phase of sidestepping (Besier et al., 2001). Monte Carlo simulations produced noticeable increases in each of these external knee loads (Fig 2).

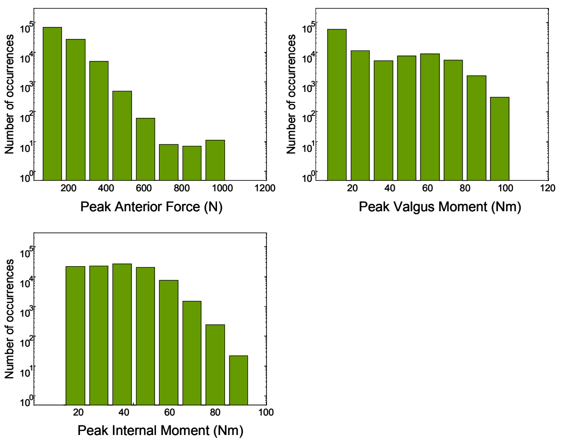

Figure 2: Effect of NMC variability on external knee loading (N=200000 simulations).

Specifically, peak anterior force, valgus and internal rotation moments as high as 1024.3 N, 101.2 Nm and 90.4 Nm respectively were observed. Maximum anterior tibial forces were well below failure loads reported previously (Approx. 2200 N) for the ACL (Woo et al., 1992). Perturbations applied to NMC variables, and in particular to peak quadriceps activations, represented "worst-case scenarios" in terms of sidestepping and resultant knee loading. Hence, sagittal plane biomechanics demonstrated during sidestepping, regardless of execution, appear unable to alone injure the ACL. The predominantly posteriorly directed joint reaction force evident through stance (Fig 3), in conjunction with hamstring activation, limits the resultant anterior tibial loading produced by the quadriceps, and negates the potential for injury via this mechanism. Excessive valgus and internal rotation torques therefore, which appear possible during sidestep execution (see Fig 2), are also essential for ACL injury to occur.

SUMMARY

The current study utilized 3D musculoskeletal modeling to determine whether stance phase sagittal plane knee loading could produce ACL injury during sidestepping. The observed interaction between quadriceps, hamstrings and joint reaction forces, negates the potential for injury via this mechanism. Rather, concomitantly large valgus and internal rotation knee joint torques appear necessary. Further work is required to determine the direct impact of combined 3D knee loading states on the ACL.

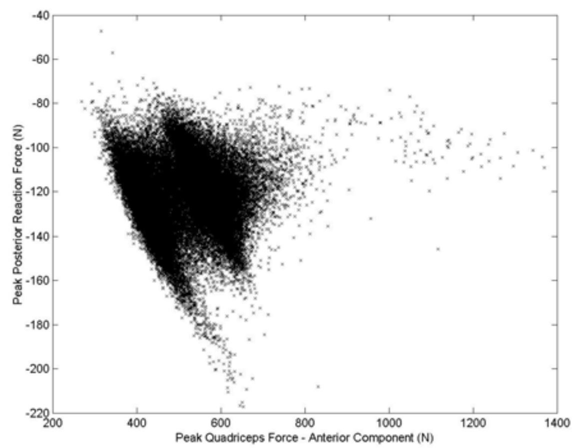

Figure 3: Relationship between peak quadriceps and posterior knee joint reaction forces demonstrated during simulated sidestepping trials.

REFERENCES

Delfico, A. and Garrett, W. (1998). *Clin Sports Med,* **17***, 779-785*.

McLean, S. et al. (2003). *Proceeding of the ORS*, New Orleans.

Besier, T. et al. (2001). *Med Sci Sports Ex*, **33**, 1168-1175.

Woo S.L. et al. (1992). Orthop Rev, **21**, 835-842.

ACKNOWLEDGEMENTS

This research is funded by NIH (AR47039).

EVIDENCE THAT QUADRICEPS MUSCLE CONTROL IS A KEY FACTOR IN COPING WITH ANTERIOR CRUCIATE LIGAMENT DEFICIENCY

Glenn N. Williams, Peter J. Barrance, Lynn Snyder-Mackler, Thomas S. Buchanan

Center for Biomedical Engineering Research, University of Delaware, Newark, DE. USA
E-mail: glennwms@udel.edu

INTRODUCTION

It is estimated that 250,000 anterior cruciate ligament (ACL) injuries occur in the United States each year (Boden, 2000). Most people cannot return to sports after an ACL injury without surgical intervention (Non-copers), but some people can (Copers). Coping with an ACL injury does not appear to be dependant on knee laxity or quadriceps strength; however, recent research suggests that the ability to cope with ACL injury is related to neuromuscular function (Rudolph, 2000). The purpose of this study was to evaluate the neuromuscular control strategies of ACL deficient (ACL-D) Non-copers, ACL-D Copers, and people with uninjured knees by assessing their specificity of muscle action using an established target-matching protocol (Buchanan and Lloyd, 1997) and circular statistics methods.

METHODS

Thirty-two subjects (12 ACL-D Non-copers, 8 ACL-D Copers, and 12 people with uninjured knees) volunteered to participate in this study. All subjects were regular participants in activities that required quick changes of directions and/or jumping. Subjects were seated on a small platform so that their thighs were unloaded. A fiberglass cylinder cast was applied to the distal shank and then rigidly clamped to a 6-axis load cell. The experimental task required subjects to position a circular cursor over a narrow target for one second. The cursor moved in response to isometric loads that the subjects produced against the load cell. Targets appeared in random order at one of 18 positions (located at every 20° of a circle in the flexion-extension-varus-valgus plane). Seventy-two trials (4 trials at each target) were performed bilaterally at each of three knee flexion angles: 50º, 70º, and 90º.

Electromyographic (EMG) signals were collected from the semitendinosus (ST), biceps femoris (BF), sartorius (SAR)*, rectus femoris (RF), tensor fascia lata (TFL)*, gracilis (GRA)*, vastus medialis (VM), vastus lateralis (VL), and the medial (MG) and lateral gastrocnemius (LG) muscles using surface or indwelling (*) electrodes. The EMG data were rectified, averaged, and normalized using maximum values collected earlier in the session.

Specificity of muscle action was analyzed by calculating a specificity index for each muscle using the formula:

$$\text{Specificity Index} = \frac{\left|R_{\underline{EMG}_i}\right|}{\sum_{i=1}^{18}\left|\underline{EMG}_i\right|}, \text{ where}$$

$\underline{EMG}_i$ is a vector describing the EMG magnitude in each target direction and $R_{\underline{EMG}_i}$ is the resultant vector determined by summing the EMG vectors in the 18 target directions. A multivariate ANOVA with each muscle as a dependent variable was used to test for significant differences in specificity of muscle action. *Post hoc*

Bonferroni multiple comparison tests were used to further define main effects.

RESULTS AND DISCUSSION

The muscles of the Non-coper's and Coper's involved knees always had specificity indices that were less than those of the uninjured subjects. The specificity indices for the RF, TFL, VL, and LG of the Non-coper's involved knees were significantly different ($p<.05$) from the respective values of the Uninjured subjects; the VM had a noteworthy trend toward significance (Figure 1). The only muscles with significant differences in the Copers were the VL and the LG.

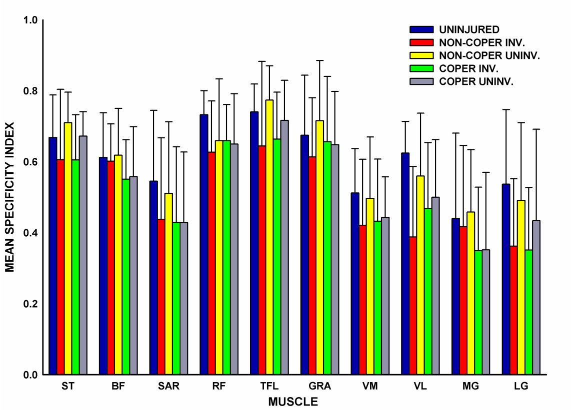

Figure 1: Mean specificity indices by group.

Although no statistically significant differences were observed between the Non-copers and Copers involved knees, the Copers exhibited greater neuromuscular control in their quadriceps muscles (Figures 1 & 2). The specificity indices for the RF, VM, and VL of the Coper's involved knees were 5%, 3%, and 21% higher than the respective values for Non-coper's muscles.

SUMMARY

The findings of this study indicate that ACL-D leads to reduced specificity of muscle action, especially in the quadriceps muscles and LG. Our findings also suggest that one of the key factors in the ability to cope with an ACL injury may be quadriceps muscle control. Poor quadriceps control may promote the giving-way episodes often observed in Non-copers (the primary factor leading to surgery), whereas good control may produce dynamic knee stability.

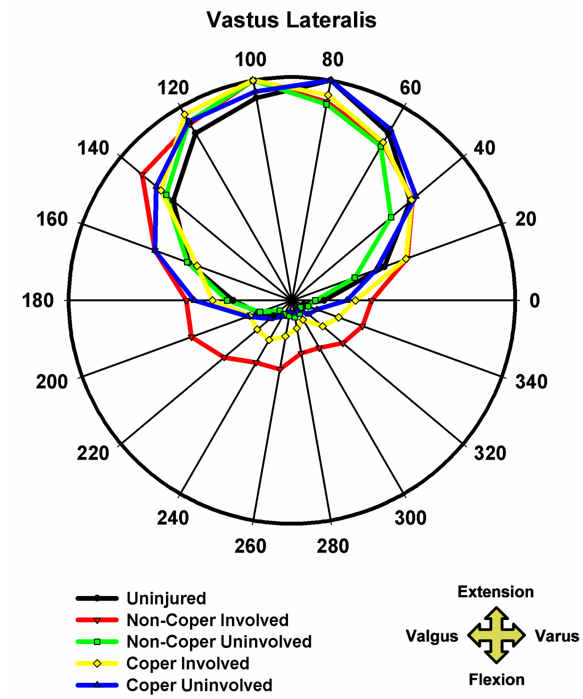

Figure 2: Mean vastus lateralis activity patterns. Note that the Copers involved limb activity patterns (yellow) are more similar to those of the uninjured/uninvolved limbs than the Non-copers involved limbs (red).

REFERENCES

Boden, B.P., Griffin, L.Y., and Garrett, WE, Jr. (2000). *Phys. Sports Med.*, **28**, 53-60.

Rudolph *et al*. (2001). *Knee Surg Sports Traumatol Arthrosc*., **9**, 62-71.

Buchanan, T.S. and Lloyd, D.G. (1997). *J Orthop Res*., **15**, 11-17.

ACKNOWLEDGEMENTS

NIH Grant RO1-AR46386 and the Foundation for Physical Therapy.

THE FUNCTION OF THE ANTERIOR AND POSTERIOR CRUCIATE LIGAMENTS IN KNEE EXTENSION EXERCISE

Dumitru I. Caruntu and Mohamed Samir Hefzy

Department of Mechanical, Industrial and Manufacturing Engineering,
The University of Toledo, Toledo, OH, USA
E-mail: mhefzy@eng.utoledo.edu   Web: www.mime.eng.utoledo.edu/biomechanics_lab

INTRODUCTION

Most of the anatomical three-dimensional models of the human knee are either static or quasistatic, and therefore they do not predict the effects of dynamic inertial loads, which occur in many locomotor activities. To the best of our knowledge, only two 3-D dynamic models of the human knee are available in the literature. First model, Abdel-Rahman and Hefzy, 1998, is a 3-D tibio-femoral joint model in which two spheres and two planes model the two femoral condyles and the two tibial plateaus, respectively. Yet, it accounts for a rigid contact formulation. Second model, Caruntu and Hefzy, 2001, is a 3-D model which includes both tibio-femoral and patello-femoral joints. It is an anatomically-based model accounting for deformable contact and allowing the wrapping of the quadriceps tendon around the femur, which occurs at large flexion angles.

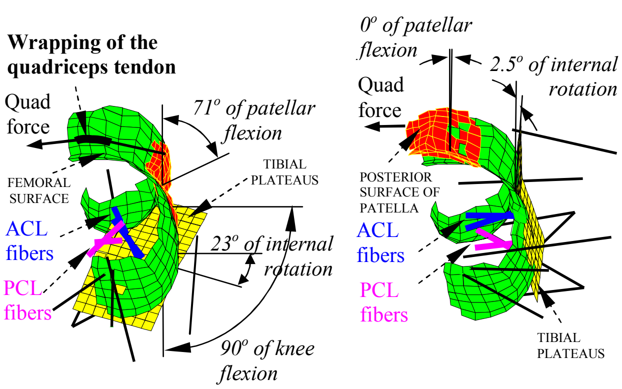

a. Initial position (*90° flexion*) ***b.*** Final position (*full extension*)

Figure 1: Initial and final positions

In this work, we present the 3-D dynamic response of the human knee using the model of Caruntu and Hefzy, 2001. Simulations were conducted to study the response of the anterior cruciate ligament (ACL) and posterior cruciate ligament (PCL) in the knee extension exercise. A good agreement has been found between the model predictions and published data.

METHODS

The femur was fixed, and both tibia and patella underwent a general 3-D motion while a forcing function has been applied to the quadriceps tendon. The twelve degrees of freedom describing tibio-femoral and patello-femoral motions were defined using two joint coordinate systems and include 3 rotations and 3 translations for each of the tibia and patella. A simplified contact theory was used to allow for deformable contact at the articular surfaces. The patellar tendon was modeled as a linear spring. Along with the posterior capsule, the lateral and medial collaterals, and the anterior and posterior cruciates were modeled using 12 nonlinear spring elements, Abdel-Rahman and Hefzy, 1998. Coons' bicubic surface patches were employed to allow for piecewise mathematical representation of the femoral, tibial and patellar articular surfaces, Hefzy and Yang, 1993. The dynamic response was obtained by solving a system of nonlinear differential algebraic equations using DASSL, a solver developed by Lawrence Livermore National Laboratory.

Model calculations were conducted to simulate the knee extension exercise and to predict the loads carried by the cruciate ligaments. Three quadriceps forcing functions have been considered. One of them has been specified using Grood *et al.*'s experimental data, 1984, as shown in Fig.2, the case of F^q=200 N. The other two forcing functions described a higher level of activation of the quadriceps, as shown in Fig.2, F^q=400 N and F^q=600 N.

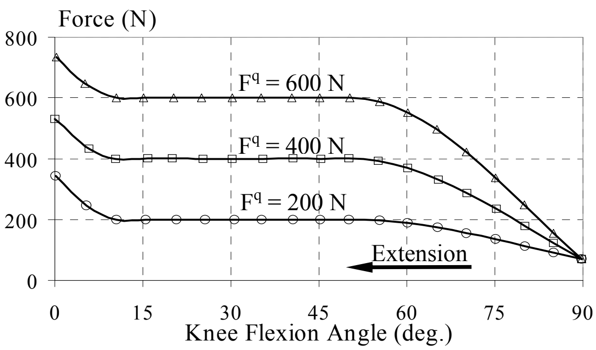

Figure 2: Forcing functions applied to the quadriceps tendon to simulate the knee extension exercise

RESULTS AND DISCUSSION

Model calculations for the knee extension exercise show that at full extension the ACL carries a larger force than the PCL, Fig. 3. Conversely, the force in the PCL is larger than the force in the ACL in the range of 75^o to 90^o of flexion. These results are in agreement with Wilk *et al.*'s data,1996, since they reported that maximum posterior and anterior tibio-femoral shear forces occurred around 90^o and 0^o of flexion, respectively, and it is well known that the posterior and anterior tibio-femoral shear forces are resisted by the PCL and ACL, respectively. Also, our model calculations have shown that the maximum forces carried by the ACL at full extension are larger than the maximum forces carried by the PCL near 90^o of flexion. These findings are consistent with other investigators' data reporting that the greatest amount of tibial displacement occurs within the last 30^o of knee extension in the knee extension exercise, Wilk *et al.*, 1996, Grood *et al.,* 1984.

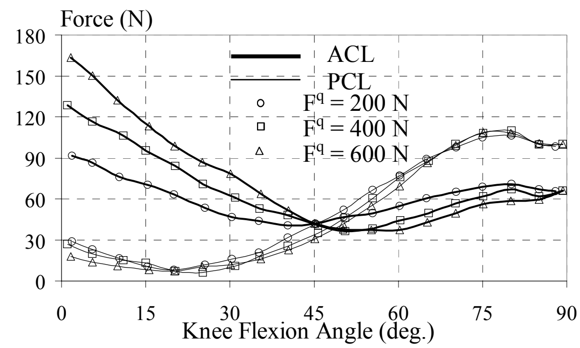

Figure 3: Forces of the ACL and the PCL versus knee flexion angle for different quadriceps forcing functions.

SUMMARY

Knee rehabilitation protocols are used to increase strength and improve range of motion. Different types of exercises are available for patients with ACL and PCL reconstructions. These results suggest that we need to limit initially the range of motion of the knee extension exercise to extensions (a) from 90^o to about 45^o of flexion for patients with ACL reconstructions and (b) from 45^o to full extensions for patients with PCL reconstructions.

REFERENCES

Abdel-Rahman, E.M., Hefzy, M.S. (1998). *Med. Engr.& Physics*, **20**, 276-290.

Caruntu, D.I., Hefzy, M.S. (2001). *Proceedings of MEDICON 2001,* 600-603.

Grood, E.S. *et al.* (1984). *J. Bone Joint Surg.* **66A**, 725-733.

Hefzy, M.S., Yang, H. (1993), *J. Biomed. Engr.* **15**, 289-301.

Wilk, K.E. *et al.* (1996). *Am. J. Sports Med.,* **24**(4), 518-527.

STANDARDIZED MEASUREMENT OF RESTING CALCANEAL STANCE POSITION AND TIBIAL VARUM IN HEALTHY CONTROLS AND PATELLOFEMORAL PAIN SUFFERERS

Shannon M. Mahar, Tera J. Winter, and Lori A. Livingston
School of Health and Human Performance, Dalhousie University, Halifax, NS, Canada
E-mail: Lori.Livingston@Dal.ca Web: www.dal.ca/hahp

INTRODUCTION

Increased amounts of calcaneal eversion and tibial varum are thought to predispose individuals to lower limb overuse injuries including patellofemoral pain syndrome (PFPS) (Powers et al., 1995; Tomaro et al., 1995). However, attempts to quantify resting calcaneal stance position (RCSP) and tibial varum (TV) have produced a broad range of values that are not always reliable or generalizable. (Buckley et al., 1997; Elveru et al., 1988). Observed differences in reported values may be partially explained by the use of differing samples and measurement error, yet it is hypothesized that the majority of the variation may be explained by methodological inconsistency (Guerra et al., 1994). Indeed, static measurement protocols often differ in terms of the overall positioning of participants (ie, supine, non-weight bearing vs erect standing, weight bearing), the use of self-selected versus fixed foot positions, and the measurement devices utilized.

The purpose of this investigation was to measure RCSP and TV using standardized weight bearing stance positions. The null hypotheses were that there would be no significant between-group (healthy controls, PFPS) or within-subject (limb, stance) differences, or interaction effects.

METHODS

Forty-six males (n=15) and females (n=31) ranging in age from 18 to 44 years (M=25.5) voluntarily participated in this study. The sample included 29 healthy controls and 17 PFPS sufferers. The latter had formal diagnoses of PFPS and were referred to the study by a physician, physiotherapist, or athletic therapist. All completed a general information questionnaire, while only those with PFPS completed a knee pain questionnaire.

The longitudinal axes of the calcaneus and distal one-third of the lower leg were defined by placing two circular adhesive markers on the midlines of the segments. In random order, each participant assumed four different upright static stance positions (ie, self-selected, Romberg, left and right single stance) while high-resolution digital photographs (Canon Digital Elph S300, Tokyo, Japan) were captured. The photos were printed using a high-resolution laser printer. Measures of RCSP and TV were derived from the photos using a manual goniometer (Sammons Inc., Burr Ridge, IL). The accuracy (ICC[2,1]=0.99) and intratester reliability (ICC[2,1]=0.72-0.90) of the measurement system was established in two preliminary investigations. The data were analyzed using mixed between-within repeated measures ANOVA procedures.

RESULTS AND DISCUSSION

The statistical analyses revealed no significant differences for RCSP by group ($F(1,44)=0.15$, $p<0.70$) or limb ($F(1,44)=2.10$, $p<0.15$). Similarly, there were no significant differences for TV by group ($F(1,44)=2,77$, $p<0.10$) or limb ($F(1,44)=3.09$, $p<0.09$). However, values for both measures differed significantly by stance position (ie, RCSP ($F(2,43)=33.13$, $p<0.001$; TV ($F(2,43)=229.75$, $p<0.001$) (Figures 1 and 2). For RCSP, a significant interaction effect of group by stance was noted ($F(2,43)=3.55$, $p<0.04$).

The data were also analyzed by non-injured (n=68) and injured (n=24) limbs. Similar results to those reported above were found, with significant differences by stance position ($F(2,89)=35.54$, $p<0.001$) and a significant stance by limb interaction effect ($F(2,89)=6.15$, $p<0.003$) for RCSP. For TV, significant differences were found by stance ($F(2,89)=218.63$, $p<0.001$).

SUMMARY

Observed values of RCSP and TV did not differ between healthy controls and those symptomatic for PFPS. Others have observed similar findings (Donatelli et al., 1999; Livingston et al., 2003). The measured angles were clearly altered by the stance position adopted during measurement. The Romberg and single limb positions, while repeatable, forced the calcaneus into a varus and somewhat unnatural position. This leads us to question the ecological validity of data collected under such circumstances. Clearly, standardized measurement protocols are warranted.

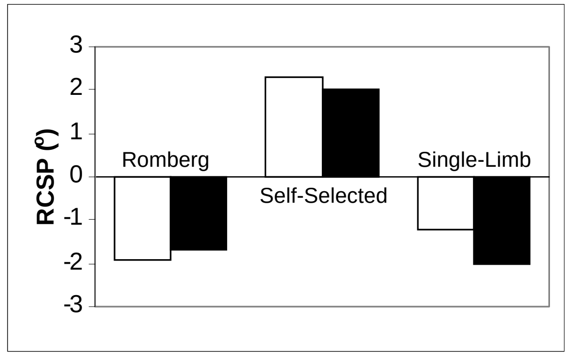

Figure 1: RCSP values (+ve valgus, -ve varus) for right (white) and left (black) limbs in three stance positions.

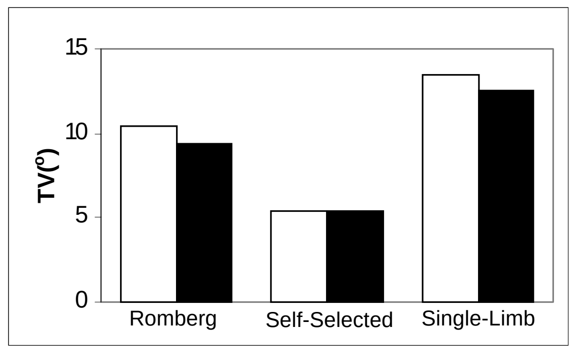

Figure 2: TV values for right (white) and left (black) limbs in three stance positions.

REFERENCES

Buckley, R.E., Hunt, D.V. (1997). *Foot Ankle Intl.*, **18**, 229-232.

Donatelli R.A. et al..(1999). *JOSPT*, **29**, 316-330.

Elveru R.A. et al. (1988). *Phys. Ther.*, **68**, 672-677.

Guerra J.P. et al. (1994). *JOSPT*, **19**, 200-205.

Livingston L.A., Mandigo, J.L. (2003). *JOSPT*, **33**, 48-55.

Powers C.M.. et al. (1995). *JOSPT*, **22**, 155-160.

Tomaro J. (1995). *JOSPT*, **21**, 86-89.

INCREASED ANTERIOR TIBIAL DISPLACEMENT IS OBSERVED IN ACL DEFICIENT PATIENTS DURING IN VIVO JOINT MOTION

Peter Barrance, Glenn Williams, Thomas S. Buchanan

Center for Biomedical Engineering Research, University of Delaware, Newark, DE, USA

E-mail: peteb@udel.edu

INTRODUCTION

Joint kinematics during activity are determined by a complex interaction between external loads, dynamic stabilization from muscle forces, and the internal joint loads in passive soft tissues and at contact surfaces. Changes in functional kinematics result in alterations of patterns of dynamic loading of the joint contact surfaces. These alterations in cartilage loading have been postulated as contributors to the degeneration cycle in articular cartilage which leads to osteoarthritis.

Injury of the knee's anterior cruciate ligament (ACL) results in a clinically observable increase in anterior-posterior joint laxity. The aim of this study is to assess the degree to which this injury may alter knee joint kinematics during activity. Specifically, changes in maximum anterior tibial translation during an open chain knee extension exercise are assessed. The methodology used is cine phase contrast (cine-PC) dynamic magnetic resonance imaging, combined with a rigid body model registration technique.

METHODS

Five subjects who had sustained an isolated complete tear of one anterior cruciate ligament, as well as five uninjured control subjects, participated in this study. All subjects read and signed a statement of informed consent which was approved by the University of Delaware's Human Subject Review Committee.

Subjects performed a repetitive knee flexion/extension exercise while lying supine within the bore of an MRI scanner (GE Signa LX.). The thigh was placed on a ramp to put the hip in a flexed position, and knee extensions were performed against the weight of the shank. The ramp was adjusted to achieve full knee extension when the toe touched the highest point of the imager's bore; this allowed flexion of the knee to approximately 30 degrees, depending on subject size. Subjects voluntarily synchronized their flexion/extension motions to the beat of a metronome set to produce a repetition frequency of 35 cycles per minute. An optical trigger, positioned below the ankle of the subject, was used to synchronize the acquisition of data with the motion. The scan duration was approximately six minutes.

Cine-PC MR is a flow imaging technique, yielding both anatomical and velocity data on the image plane. A sequence of 24 frames of cine-PC data was collected through the motion cycle on a sagittal image plane prescribed to pass through the joint center. At each data frame four images were reconstructed; one was an anatomical cross-section (magnitude image), and the others were encoded with velocity in the three principal directions of the image.

A high resolution static 3D scan was taken of each knee (1.0mm slice thickness, matrix size

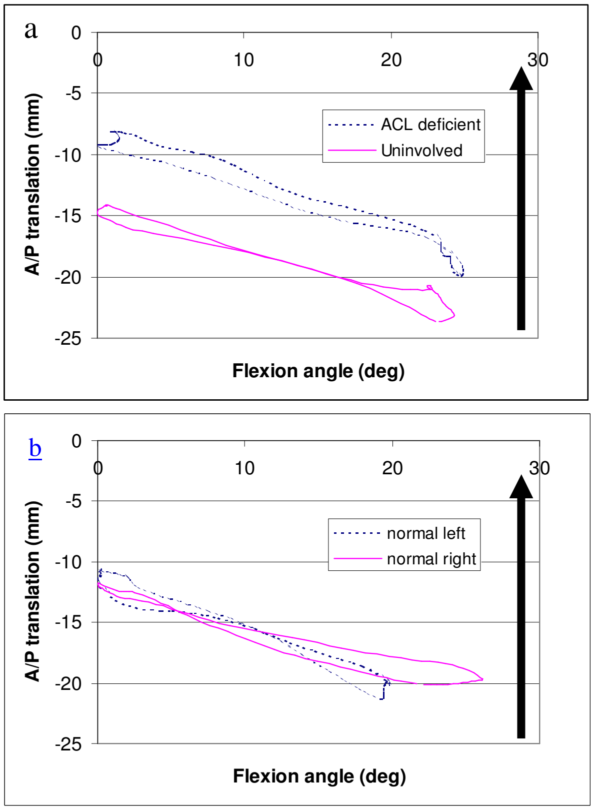

Figure 1: A/P translation parameters versus flexion angle. (a) Sample ACL deficient subject (b) sample control subject.

256x256, field of view=180mmx180mm). The peripheries of the distal femur and proximal tibia and fibula were traced on the images using a digitizing tablet. Custom developed software was used to reconstruct the 3D polygonal graphical models of each bone.

A previously described algorithm (Barrance et al. 2002) was used to develop a modeled trajectory for each 3D model, such that the agreement between simulated cross-section and velocity data most closely matched those observed in the cine-PC MRI dataset.

Anatomically based coordinate systems were fixed within each bone. Landmarks were digitized in the sagittal images in order to establish the directions of the long axes of the femur and tibia in that plane, and the graphical models were used to determine the other directions. The coordinates of the most distal point in the femoral notch and the tibial eminence were determined in the graphical models. The A/P position of the tibia relative to the femur was calculated as the projection of this vector along the anterior axis of the femur.

RESULTS AND DISCUSSION

Figure 1 shows sample translation parameters versus knee flexion angle, calculated for one of the ACL injured subjects, and one of the uninjured control subjects. The peak anterior translation of the injured knee (-8.1mm) of the injured subject is greater than that of the uninvolved side (-14.1mm), whereas the peak anterior translations are closer to equal side to side (-10.7 vs. -11.8mm). A paired t-test comparison between sides showed a statistically significant increase in peak A/P translation of 6.0mm of the ACL-deficient side relative to the uninvolved side ($p=0.037$.) No significant difference was found in the control group

SUMMARY

An increase in peak anterior translation was observed in the ACL-deficient knees during active joint function. This implies that the ACL is used during these simple flexion-extension movements in unimpaired subjects to reduce anterior translation and that the muscles of the ACL deficient knee do not control the knee so as to eliminate anterior translations.

REFERENCES

Barrance, PJ. et al, *Fourth World Congress of Biomechanics*, August 2002.

ACKNOWLEDGEMENT

Supported by NIH Grant R01AR46386.

ANATOMY OF THE EXTENSOR MECHANISM INFLUENCES TIBIAL TRANSLATION DUE TO QUADRICEPS CONTRACTION IN THE ACL DEFICIENT KNEE

Chris O. Dyrby [1], Joan E. Deffeyes [1], Mithun A. Vora [1], Thomas P. Andriacchi [1,2]

[1] Department of Mechanical Engineering, Stanford University, Stanford, CA
[2] VA Palo Alto RR&D Center, Palo Alto, CA
E-mail: cdyrby@stanford.edu

INTRODUCTION

Anterior tibial translation occurs during contraction of the quadriceps at certain knee flexion angles due to the geometry of the knee extensor mechanism, in particular the patellar ligament insertion angle (PLIA) (Figure 1). A greater PLIA can correspond to a greater component of force on the tibia in the anterior direction. The anterior motion of the tibia is restricted by soft tissue structures, in particular, the anterior cruciate ligament (ACL). In knees with a compromised ACL, the importance of the PLIA is hypothesized to be more significant in determining the amount of translation for a given quadriceps force. We tested the hypothesis that anatomical variations in the extensor mechanism (defined by the PLIA) would influence the amount of anterior tibial translation in the ACL deficient knee.

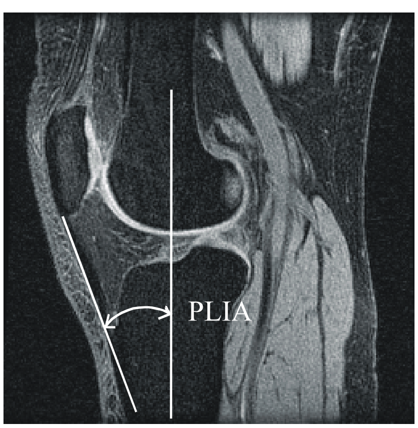

Figure 1: MRI image showing the PLIA

MATERIALS AND METHODS

The ACL deficient group consisted of five subjects (age = 32.4 ± 13 yrs, 1 female, avg. 103 mo. past injury). The control group consisted of six subjects with no musculoskeletal involvement (age = 27.5 ± 8, 4 females). Magnetic resonance imaging (3DSPGR) was used to measure the PLIA for each subject.

Each subject was tested bilaterally using a KT-1000 Knee Ligament Arthrometer in combination with a Cybex 350. The rotation axis of the Cybex resistance arm was aligned with the flexion-extension axis of the knee and the lower limb attached to the resistance arm with a foot plate. The KT-1000 was placed on the anterior aspect of the tibia with the tibial sensor pad placed on the tibial tubercle and the patella sensor pad resting on the patella. Measurements were obtained as the quadriceps produced a torque of 1% and 2% body-weight times height (BW*Ht), at joint angles of 10°, 20°, 40°, and 60°. These torques represented the physiological loads seen during the mid-stance phase of walking. With the subject's leg muscles relaxed, a manual 89N measurement of passive knee laxity was taken. Normalized knee motion was calculated by subtracting the passive tibial translation from the anterior tibial translation measured during quadriceps active translation.

RESULTS

The anterior tibial translation for ACL deficient knees showed a correlation between quadriceps activation at 10° and 20° knee flexion angle that was not seen in the control population (Table 1, Figure 2). At angles of 40° and 60°, there was no correlation for both ACL deficient and control populations.

Table 1: R^2 values for Controls and ACLD

1%BW*Ht

Knee Angle	Controls R^2	ACLD R^2
10°	0.01	0.91
20°	0.03	0.90
40°	0.01	0.03
60°	0.03	0.01

2%BW*Ht

Knee Angle	Controls R^2	ACLD R^2
20°	0.01	0.92
40°	0.02	0.06
60°	0.02	0.04

As Figure 2 shows, for ACL deficient subjects, as the PLIA increases, the amount of anterior tibial translation will also increase at 10° and 20°.

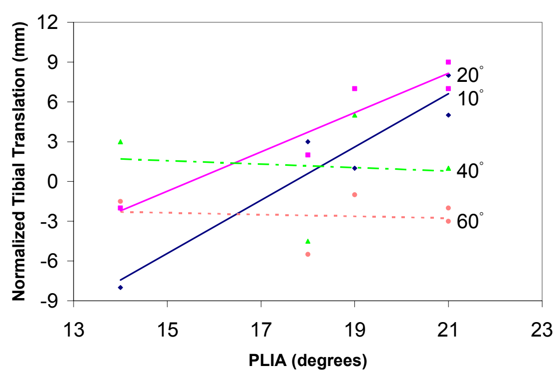

Figure 2: Relationship between normalized tibial translation and PLIA for 10°, 20°, 40°, and 60° knee flexion angle for 1% BW*Ht.

DISCUSSION

These results demonstrate that individual variations in the anatomy of the extensor mechanism influence the amount of quadriceps induced anterior tibial translation that occurs in the ACL deficient knee. Reducing tibial translation reduces shear at the articulating surfaces. Mechanical shear stress at a joint results in thinner cartilage (Carter and Beaupre 2001). A quadriceps avoidance gait may reduce the tibial translation, thereby reducing the individual's risk for osteoarthritis in the affected knee (Berchuck, et al, 1990). For an ACL deficient individual with a small PLIA, adopting a quadriceps avoidance gait may not be as critical, because less tibial translation will occur. However, it may be particularly important for an ACLD individual with a large PLIA to adopt the quadriceps avoidance gait in order to minimize tibial translation, thereby reducing risk for osteoarthritis.

REFERENCES

Berchuck, M., Andriacchi, T.P., Bach, B.R. and Reider, B. (1990). *JBJS-Am*, **72**, 871-877.

Carter, D.R. and Beaupre, G.S. (2001). *Skeletal Function and Form: Mechanobiology of Skeletal Development, Aging, and Regeneration.* Cambridge University Press 2001.

ACKNOWLEDGEMENTS

The authors gratefully acknowledge the support of NIH grant #AR39432, and the National Science Foundation Graduate Student Fellowship Program.

HIP AND KNEE FRONTAL PLANE MOMENTS IN PERSONS WITH UNILATERAL, TRANS-TIBIAL AMPUTATION

Todd D. Royer and Carolyn A. Wasilewski

Dept of Health and Exercise Sciences, University of Delaware, Newark, Delaware, USA
Email: royer@udel.edu

INTRODUCTION

Persons with unilateral, trans-tibial amputation demonstrate significant asymmetrical gait patterns. Their gait pattern results from an inability of the affected limb to function normally, most likely the result of pain, weakness, and/or instability. Specifically, the prosthetic limb displays a smaller push-off force, longer swing time, longer step length, and shorter stance time than the intact limb (Mattes et al., 2000). As a result, the intact limb experiences excessive joint loading (Sanderson & Martin, 1997); predisposing it to greater risk of developing degenerative joint disease, e.g., osteoarthritis (OA).

Current literature lacks adequate information to provide a clear understanding of the relationship between gait mechanics and osteoarthritis in amputees; however, previous research on osteoarthritic gait has demonstrated an important link between abnormal joint loading and osteoarthritis of the knee (Sharma et al., 1998) and hip (Hurwitz et al., 1998b).

The purpose of this study was to determine whether a significant difference exists between joint loading of the intact limb versus the prosthetic limb in unilateral, trans-tibial amputees. We hypothesized that peak net internal abduction moments of the intact limb would be significantly greater than the peak net internal abduction moments of the prosthetic limb at both the knee and hip.

METHODS

Five males and one female ($M_{age} = 39.9 \pm 11.0$ yrs; $M_{height} = 173.7 \pm 7.3$ cm; $M_{mass} = 87.3 \pm 19.5$ kg) with a unilateral, trans-tibial amputation served as subjects. All were recreationally active (able to comfortably walk for at least 30 minutes continuously without an assistive device, such as a cane or crutch), and utilized an energy storing prosthetic limb.

Freely chosen walking speed ($M_{speed} = 1.2 \pm 0.2$ m/s) was calculated from consecutive interruptions of photocells linked to a digital electronic timer. Walking speed was controlled ($\pm$ 5%) for all trials. To obtain data used in calculating gait mechanics, lightweight reflective markers were placed bilaterally on the legs and feet of the subject using the Cleveland Clinic marker set. Motion analysis cameras captured three-dimensional position data (60Hz) of these markers and a force platform captured ground reaction force data (480Hz) as the subject walked overground along a 20-meter walkway.

Peak net internal abduction moments for the knee (MK_{abd}) and hip (MH_{abd}) of both legs were determined using an inverse dynamics approach and normalized to body mass (Orthotrak software, Motion Analysis Corporation). Two dependent t-tests were used to test for significant differences in frontal plane joint moments between limbs ($p < .05$). Effect sizes (ES) were also calculated where differences existed.

RESULTS AND DISCUSSION

Between limb asymmetries existed for both the knee and hip (Figure 1). MK_{abd} for the intact limb was 66.1% greater than the prosthetic limb [$p < .05$; ES = 1.04]. MH_{abd} for the intact limb was 65.9% greater than the prosthetic limb [$p < .05$; ES = 1.35].

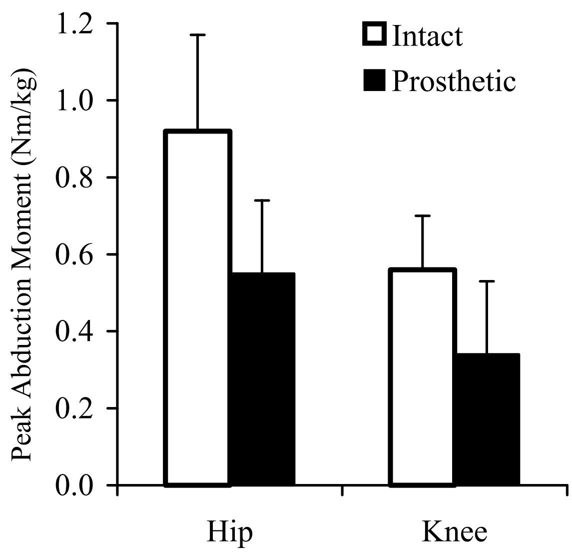

Figure 1. Peak abduction moments for the intact limb were larger ($p < .05$) than the prosthetic limb for both the hip and knee.

The internal knee abduction moment has been shown to reflect the force distribution between the medial and lateral compartments of the knee joint, where larger knee abduction moments correspond to greater loads on the medial knee versus the lateral knee compartment (Schipplein & Andriacchi, 1991). Sharma and colleagues (1998) reported a significant relationship between the frontal plane knee moment and osteoarthritis disease severity. In our study, MK_{abd} for the intact limb was 0.56 Nm/kg, which is 19.1% greater than normal (approximately 0.47 Nm/kg) reported by Hurwitz and colleagues (1998b). This suggests that the intact limb of unilateral, trans-tibial amputees is concomitantly made more susceptible to degenerative joint disease, specifically OA. Indeed, Melzer and colleagues (2001) reported 65% of unilateral, lower-extremity amputees had some degree of knee OA in the intact limb.

Hurwitz and colleagues (1998a) reported a significant positive correlation between hip joint loads and femoral neck bone mineral density, which may be associated with increased risk of OA. In our study, MH_{abd} for the intact limb was 0.92 Nm/kg, which is 9.5% greater than normal (approximately 0.84 Nm/kg) reported by Hurwitz and colleagues (1998a).

SUMMARY

Individuals with unilateral, trans-tibial amputation have approximately 65% larger peak frontal plane moments for the knee and hip compared to the prosthetic limb. Moreover, moment values for the intact limb are greater than normal values reported in the literature, which is problematic because the non-affected limb may be predisposed to premature degenerative joint disease.

REFERENCES

Hurwitz, D.E., et al (1998a) *J Biomech*, **31**, 423-30.
Hurwitz, D.E. et al (1998b). *J Biomech*, **31**, 919-25.
Mattes, S.J. et al. (2000). *Arch Phy Med Rehabil*, **81**, 561-68.
Melzer, I., et al. (2001). *J Rheumatol*, **28**, 169-72.
Sanderson, D.J., & Martin, P.E. (1997). *Gait and Posture*, **6**, 126-36.
Schipplein, O.D., & Andriacchi, T.P. (1991). *J of Orthop Res*, **9**, 113-9.
Sharma, L. et al. (1998). *Arthritis Rheum*, **41**, 1233-40.

ACKNOWLEDGEMENTS

Support from the University of Delaware Research Foundation is acknowledged.

GAIT STYLE AFFECTS EXTERNAL KNEE ADDUCTION MOMENT

Seiji Ueda, Chris O. Dyrby, Eugene J. Alexander, Thomas P. Andriacchi

Department of Mechanical Engineering, Stanford University, Stanford, CA, USA
E-mail: sueda@stanford.edu Web: stanford.edu/group/biomotion/

INTRODUCTION

The adduction moment has been shown to play an important role in the outcome of surgical treatment, such as high tibial osteotomy (HTO), for medial compartment knee osteoarthritis (Prodromos 1985). The HTO has been shown to reduce the adduction moment during walking, redistributing load from the arthritic compartment to the more normal compartment. In addition, braces have been shown to reduce the adduction moment during walking (Lindenfeld 1997).

Foot position (Wang 1990) and reduced walking speed (Stauffer 1977) have been suggested as methods to reduce the adduction moment during walking. The results of these studies suggest that a reduction in the adduction moment achieved through gait retraining could be an effective and efficient method of treatment for OA. The purpose of this study was to test the relationships between the adduction moment with walking speed and the relationship of the adduction moment with foot position (toe out angle).

MATERIALS AND METHODS

Fifteen healthy subjects (age: 33.9 ± 5.3 yrs, hgt: 171.6 ± 6.7 cm, wgt: 647.8 ± 112.7 N, 6F) were recruited for this study. All subjects signed an IRB approved informed consent. A previously described method was used to calculate kinematic and kinetic variables from gait analysis (Andriacchi 1997). Moments were normalized to percent body weight times height (%BW × Ht)(Prodromos 1985).

The subjects performed level walking using five different gait styles: normal speed, slow speed, fast speed, normal speed with intentional toe in, and normal speed with intentional toe out. Each gait style was performed three times and the average of these three trials was used for analysis. The first and second peaks of the adduction moment, walking speed, and toe out angle in each gait style were compared with normal walking speed by using Student's paired t-test ($\alpha < 0.01$). Multiple regression analyses were used to test for an association between the toe out angle and the first peak adduction moment and between the toe out angle and the second peak adduction moment.

RESULTS

During normal walking, the average speed was 1.29 ± 0.11 m/sec, toe out angle was 19.5 ± 7.4 degree, the first peak of the adduction moment was 2.73 ± 0.64 %BW × Ht, and the second peak was 2.27 ± 0.76 %BW × Ht. When the walking speed decreased, these were no significant differences with normal speed. When the walking speed increased, the first peak of the adduction moment was increased to 3.14 ± 1.03 %BW × Ht. The walking speed was not significantly different from normal when subjects walk with toe-in and toe-out styles. The first peak of the adduction moment was significantly lower than normal ($p < 0.01$) when subjects used a toe-in style. The toe-out style showed a significantly higher first peak adduction moment and lower second peak adduction moment than normal ($p < 0.01$) (Table 1). Figure 1 shows the correlation between toe out angle and first peak adduction moment and between toe out angle and second peak adduction moment. Although there was a significant correlation between toe out angle and first peak adduction moment ($R = 0.740$, $p < 0.01$), there was an inverse correlation between toe out angle and second peak adduction moment ($R = -0.704$, $p < 0.01$). Toe out angle at the cross point of each trend line was 12.4 degree, which is lower than normal (19.5 degree).

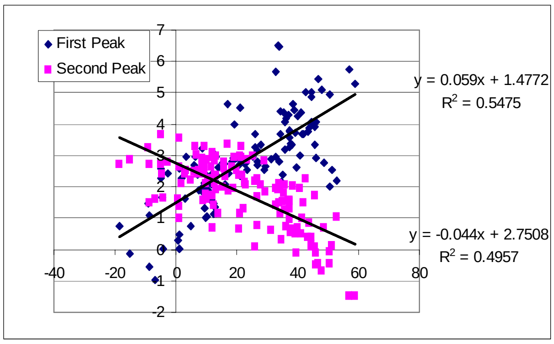

Figure 1: First peak increased but second peak decreased as toe out angle increased.

DISCUSSION

It is important for knee OA patients to reduce their adduction moment in order to slow or prevent the progression of OA. In the present study, it was shown that adduction moment was not reduced if gait speed was reduced. Some authors have reported that adduction moment decreased as toe out angle increased (Wang 1990), with the implication that toe out gait was able to reduce adduction moment during walking. However, our present results show that first peak adduction moment increased as toe out angle increases. Therefore, if the goal is to reduce both the first and second peak of the adduction moment a slight toe in gait would be better to reduce the total adduction moment sustained during the walking cycle, since the toe out angle at which both first and second adduction moment were equally low was 12.4 degree during walking.

Reducing gait speed is not necessary to decrease adduction moment during walking. An ideal toe out angle to reduce adduction moment is 12.4 degree, which is a slightly more toed-in than normal.

REFERENCES

Andriacchi, T.P. et al. (1997). *Basic Orthopaedic Biomechanics*, 2nd Ed., Lippincot-Raven, 37-68.

Lindenfeld T.N. et al. (1997). *Clin Orthop*, **344**, 290-297.

Prodromos C.C. et al. (1985). *J Bone Joint Surg [Am]*, **67**, 1188-1194.

Stauffer R.N. et al. (1977). *Clin Orthop*, **126**, 246-255.

Wang, J-W. et al. (1990). *J Bone Joint Surg [Am]*, **72**, 905-909.

Table 1: Values are compared with those of normal control walking (*$p < 0.01$) (Mean ± SD).

	Walking Speed (m/sec)	Toe Out Angle (degree)	First Peak (%BW × H)	Second Peak (%BW × H)
Normal Control	1.29 ± 0.11	19.5 ± 7.4	2.73 ± 0.64	2.27 ± 0.76
Slow Speed	* 0.94 ± 0.09	18.9 ± 7.5	2.74 ± 0.52	2.29 ± 0.64
Fast Speed	* 1.69 ± 0.21	19.1 ± 6.3	* 3.14 ± 1.03	2.25 ± 0.81
Toe In Walking	1.24 ± 0.14	* 4.10 ± 8.2	* 1.57 ± 1.00	2.29 ± 0.67
Toe Out Walking	1.26 ± 0.14	* 40.5 ± 5.6	* 3.87 ± 1.04	* 0.98 ± 0.79

GROUND REACTION FORCE PATTERN OF PATIENCES WITH BILATERAL TOTAL KNEE ARTHROUPLASTY SYSTEMS DURING CHAIR RISE

H. Wang[1], K. Simpson[2], M. Ferrara[2], S. Chamnongkich[2], S. Casto[2], T. Kinsey[3], O. Mahoney[3]
[1]Queens College, Flushing, NY. [2]University of Georgia, Athens, GA. [3]Athens Orthopedic Clinic PA, Athens, GA hewang@forbin.qc.edu

INTRODUCTION

There are mechanical differences between a single-radius (SR) total knee arthroplasty (TKA) and a multiple-radius TKA (MR) system. Compared to the MR, the SR has a longer quadriceps moment arm (D'Lima, et al., 2001) and has been shown to require less knee extensor (KE) muscle effort during a simulated stair climb (D'Lima, et al., 2001) and a chair rising movement (Wang, et al., 2003). While rising, the sum of all lower extremity extensor torques directly influence the amount of vertical and antero-posterior (AP) ground reaction forces (GRF) created to help propel a patient upwards and to control AP stability. Further, during chair rising, unilateral TKA patients with an MR used adaptive strategies, e.g., exhibited more trunk motion, that individuals with KE decrements typically exhibit (Wang, et al. 2003). However, it is not clear if bilateral TKA participants use different compensatory strategies that allow the SR limb to generate a greater proportion of the vertical and AP GRFs. Thus, the purpose of this study was to compare the GRF characteristics displayed during chair rising between the MR and SR limbs of bilateral TKA patients.

METHOD

Ten healthy participants each with an SR (Scorpio™, Stryker-Howmedica-Osteonics Inc.) and an MR (S-7000™, Stryker-Howmedica-Osteonics Inc.; and P.F.C.™, Johnson & Johnson Inc.) limb (mean $\pm$ SD: age = 73 ± 8 yr., post-operation time/limb: SR = 40 ±18 mo. MR = 81 ± 31 mo.) took part in this study. A force platform and high-speed video motion measurement system were used to collect the GRF and motion data during the chair rising maneuver. Participants performed four trials for each leg. Paired Student t-tests were used for overall statistical analyses ($\alpha = 0.05$); individual participant analyses also were performed.

RESULTS

Differences in postoperative time between the limbs may have influence the statistical results. For the SR vs. the MR leg, the SR leg exhibited greater change of the AP force in the seat unloading phase and a longer time to reach the vertical peak ($p = 0.049$) (eight out of ten subjects).

In addition, from the individual participant analyses, 6 – 7 of the 10 participants displayed the following by the SR compared to the MR limb: a) less minimum anterior-posterior (AP) force during the seat unloading phase, b) greater maximum AP force during seat liftoff, and c) greater peak vertical GRF.

DISCUSSION

It is suggested that some participants are utilizing the SR leg to generate more of the AP and vertical forces during various phases of the movement. First, the SR leg exhibited a greater change of AP force during seat unloading phase than the MR leg. Second, 7 out of 10 subjects also showed greater maximum AP force than the MR leg at the moment of seat-off. With greater AP force, the SR leg generated a greater magnitude of the momentum to transfer the body weight forward from the seat to the feet.

The SR limb of the majority of participants generated greater vertical impulse, hence greater upward vertical momentum, by generating greater vertical GRF for a longer period of time. This suggests that these participants might generate more of the total vertical GRF by their SR legs to perform chair rise during the initial ascending phase. This may have occurred due to their SR KE being able to generate more torque with less muscular effort (D'Lima, et al., 2001; Mahoney, et al., 2002). In our previous study performed with the same participants, we found that the SR legs demonstrated greater KE isokinetic strength than the MR legs.

This asymmetry for GRF patterns by limbs may have implications for maintaining balance while rising, especially as many TKA patients are older, rather than younger adults. In summary, the magnitude and timing of the GRF pattern of the SR leg is different from the MR leg for the majority of participants. These differences may signal that some bilateral TKA participants tend to favor their SR legs during daily activities, i.e., chair rising.

REFERENCES

H. Wang, et al. (2003) *Proceedings of the 70th AAOS*, 402.

O. M. Mahoney, et al. (2002) *Proceedings of the 69th AAOS,* 442.

D'Lima, et al. (2001) *Clin Orthop.* (392), 213-220.

ACKNOWLEDGEMENTS

This research was supported by a grant from Stryker-Howmedica-Osteonics, Inc.

STANCE PHASE MOMENT PATTERNS PRE AND POST TOTAL KNEE REPLACEMENT

David Mandeville, Louis Osternig, Li-Shan Chou, Michael Hahn, Sing-Jye Chen

Biomechanics and Sports Medicine Laboratory, University of Oregon, Eugene, OR, USA
E-mail: dmandevi@darkwing.uoregon.edu

INTRODUCTION

The antalgic gait in knee osteoarthritis (OA) patients is characterized by decreased walking velocity, stride length, single leg stance time, knee flexion angle, and peak internal extensor moment (Kaufman, 2001). Total knee replacement (TKR) is indicated for knee OA patients with disability due to pain when conservative treatment fails. Previous longitudinal gait analysis studies report that functional outcomes for TKR improve from pre-surgery levels, although post-TKR gait characteristics did not return to control values despite decreased pain (Skinner, 1993).

Two abnormal stance phase moment patterns were reported for TKR level walking: an external flexion moment pattern and an external extension moment pattern (Andriacchi, 1982). The external flexor moment pattern has been reported to be present in the gait of 50% and 40% of TKR patients by Simon et al (1983), and Andriacchi et al (1982), respectively.

Postulated causes for post-TKR gait adaptations are thought to include: decreased knee joint proprioception, decreased muscular strength, or a retained knee OA gait pattern (Andriacchi, 1982). The purpose of this study was to describe stance phase knee moment patterns of TKR patients from pre- to post surgical time periods, and to compare these patterns to that of an age-matched control group. Six month post-TKR gait characteristics were expected to resemble pre-surgery values more so than the gait characteristics of normal controls. This finding would suggest a residual knee OA gait pattern.

METHODS

Two groups completed this study: a TKR patient group (n = 5; mean age 65.8 yrs. ± 5.8), and a healthy control group (n = 5; mean age 67 yrs. ±12). Ground reaction forces, joint kinematics and kinetics were obtained for the involved (TKR group) and right (control group) lower extremity during a level walking protocol. TKR group data were collected over three periods: 2 weeks pre-surgery (PRE), three months post-surgery (3 MOS), and six months post-surgery (6 MOS).

For the level walking protocol, spatio-temporal and whole body kinematic data were obtained using a six camera Expert Vision HiRes motion tracking system. Ground reaction forces were obtained from two AMTI force plates and inverse dynamic calculations were computed using Orthotrak 4.0 software. Subjects performed level ground walking while barefoot at a self-selected pace. Peak internal knee extensor moment during stance (PEMst) and peak internal flexor moment during stance (PFMst) were evaluated.

RESULTS AND DISCUSSION

Table 1 indicates that PEMst increased from 7% of CON at PRE to 89% of CON at 6 MOS while PFMst decreased from 80% of CON at PRE to 40% of CON at 6 MOS. These data reveal a consistent trend toward an external flexion moment pattern during level walking and suggest a partial resolution of pre-surgical antalgic gait by 6 months post-surgery. This pattern of gait, although not physiologic, may not be pathologic, as joint compression forces are minimized with decreased PFMst values.

SUMMARY

Decreased PFMst values over time, combined with increased PEMst indicate an external flexor moment pattern during stance phase as described by previous work. The external flexion moment pattern may represent abnormal phasic muscle activity about the knee secondary to proprioception deficits. The presence of two stance phase moment patterns over a six month period argues against retention of a pre-surgery gait pattern. However, the trade off seen in the peak moments of the antagonist knee musculature may represent an attempt of the CNS to preserve an unloaded gait pattern.

REFERENCES

Kaufman, K.R. et al. (2001). *J Biomech*, **34**(7), 907-15.

Skinner, H.B. (1993). *Clin Orthop*, **288**, 78-86.

Andriacchi, T.P. et al. (1982). *J Bone Joint Surg Am*, **64**, 1328-35.

Simon, S.R. et al. (1983). *J Bone Joint Surg Am,* **65,** 605-613.

Table 1. Mean peak internal extension moment (PEMst) and peak internal flexion moment (PFMst) of the involved knee during stance phase for TKR and Con groups across periods

	TKR Pre		TKR 3mo		TKR 6mo	
	PEMst*	PFMst*	PEMst	PFMst	PEMst	PFMst
TKR	0.02	-0.28	0.15	-0.15	0.25	-0.14
Con	0.28	-0.35	0.28	-0.35	0.28	-0.35

Note: * All values are mean of three trials, units are NM/kg. Control values are shown across periods for comparison.

RELIABILITY OF DYNAMIC KNEE MOTION IN FEMALE ATHLETES

Kevin R. Ford [1], Gregory D. Myer [1] and Timothy E. Hewett [1,2]

[1] Human Performance Laboratory, SMBC, Cincinnati Children's Hospital, Cincinnati, OH, USA
[2] College of Medicine, University of Cincinnati, Cincinnati, OH, USA
E-mail: kevin.ford@chmcc.org Web: www.cincinnatichildrens.org/sportsmed

INTRODUCTION

The knee is one of the most commonly injured areas of the body in female athletes. Season ending knee injuries can occur at a rate as high as 1 in 10 athletes at the intercollegiate level, which can account for 15,000 female athletes lost each year to athletic participation (Hewett et al. 1999). Anterior cruciate ligament (ACL) ruptures are debilitating, often season-ending, knee injuries in female athletes that occur with a higher incidence than in male athletes. Numerous studies have found a 4-6 fold higher incidence of knee injuries in females compared to males participating in jumping and cutting sports (Hewett et al. 1999, Malone et al. 1993). This higher incidence of injury combined with the dramatic increase in female participation that has occurred since the inception of Title IX in 1972, has led to a gender gap in the number of ACL injuries over the last three decades.

Screening tests are needed to identify athletes at high risk for ACL injuries. It is likely that a significant proportion of the female sports population may demonstrate decreased dynamic knee stability measured during landing. Measures of dynamic knee stability in this study include medial knee motion, knee joint varus-valgus angle and flexion-extension angle. The purposes of this study were to examine the efficacy of a drop vertical jump in assessing dynamic knee stability and to identify differences between three different methods to calculate dynamic knee motion.

METHODS

Subjects consisted of 77 female high school basketball, soccer and volleyball players. Each subject was instrumented with 19 retroreflective markers. The drop vertical jump (DVJ) consisted of the subject starting on top of a box (31 cm in height) with their feet positioned 35 cm apart (distance measured between toe markers). They were instructed to drop directly down off the box and immediately perform a maximum vertical jump. Two force platforms embedded into the floor were positioned 8 cm apart so that each foot contacted a different platform during the maneuver. The first contact on the platforms (i.e. the initial landing from the box drop) was used for analysis. Three successful trials were recorded for each subject. The motion analysis system consisted of eight digital cameras (Eagle cameras, Motion Analysis Corporation) and sampled at 300Hz. Two force platforms (AMTI) were sampled at 1000Hz and time synchronized to the motion analysis system. Data was imported into KinTrak (Version 6.2, Motion Analysis Corporation) for data reduction and analysis. Prior to each data collection session the motion analysis system was calibrated to manufacturer recommendations.

Bilateral knee motion was calculated from the distance between the right and left lateral knee markers during the DVJ (knee distance 0.03s prior to initial contact minus minimum knee distance during contact phase). Three different calculations of knee motion were performed with the Cartesian coordinates of the lateral knee markers (X - medial/lateral;

XY – medial/lateral and inferior/superior; XYZ – all three planes). Varus-valgus angle was reported as positive numbers representing valgus and negative numbers representing varus orientation. Flexion-extension angle was reported as 0° representing near full extension with positive numbers representing flexion. Vertical ground reaction force was used to identify the time at initial contact with the ground (IC) and at toe off from the jump (TO). Knee angle at IC and the maximum angle during stance (IC – TO) were recorded.

RESULTS

Female athletes demonstrated high levels of medial knee motion during landing. Sixty-six out of 77 subjects demonstrated higher medial than lateral knee motion during the landing. The mean difference from initial contact to peak displacement was 5.7 ± 0.4 cm. Within session reliability was evaluated by calculating intraclass correlation coefficients (ICC[3,*k*]) for each variable from three trials. All variables showed high reliability with ICCs of greater than 0.93 (Table 1). There were no statistically significant differences between the three calculations of knee motion (Table 2).

Figure 1. Example of drop vertical jump

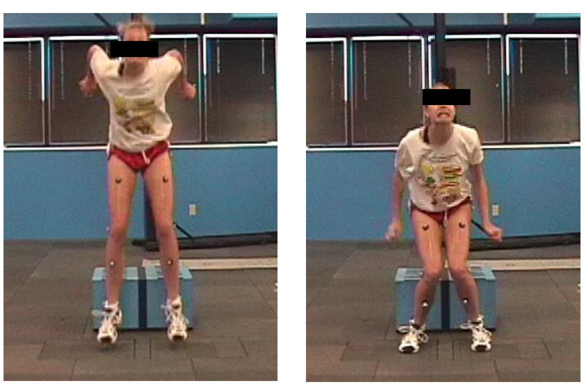

Knee distance is calculated from these two frames and the difference is defined as medial knee motion.

Table 1: Within session mean ± SE and Intraclass Correlation Coefficents (ICC[3,*k*])

Variable	**Mean ± SE**	**ICC**
Flex. Angle at IC	20.6 ± 1.4°	.935
Flex. Angle Max.	78.6 ± 1.3°	.953
Valgus Angle at IC	9.3 ± 1.4°	.982
Valgus Angle Max.	13.4 ± 1.3°	.986
Knee Motion - X	5.7 ± 0.4cm	.936
Knee Motion - XY	5.7 ± 0.4cm	.936
Knee Motion - XYZ	5.7 ± 0.4cm	.935

Table 2: Paired T-test and Intraclass Correlation Coefficients (ICC[3,1]) between different measurements of knee motion (mean of 3 trials for each subject)

Variable	**P-value**	**ICC**
Knee Motion X - XY	.614	.999
Knee Motion X - XYZ	.949	.998
Knee Motion XY - XYZ	.646	.999

SUMMARY

Gender differences in knee motion have been previously been identified (Myer et al. 2002). Female athletes show high levels of medial motion at landing. The results from this study suggest that three trials is adequate for reliable knee joint angle and knee motion measurements during the DVJ. The bilateral motion at the knee during the DVJ could be measured by tracking each knee in the medial/lateral direction. It has been suggested that a simplified 2-dimensional test could be utilized to replicate this measurement possibly on a larger scale outside of the laboratory. The authors are currently testing the reliability of this approach.

REFERENCES

Hewett, T.E et al. (1999) *American Journal of Sports Medicine*. **27**, 699-706.

Malone, T.R et al. (1993). *Journal of Southern Orthopaedic Association*. **2**,36-39.

Myer, G.D. et al. (2002) *Medicine and Science in Sports and Exercise*. 34:S5

ARTICULATED EXTERNAL FIXATION OF THE KNEE: THE EFFECT OF FIXATOR STIFFNESS ON CRUCIATE LIGAMENT PROTECTION

Daniel C. Fitzpatrick[2], Mark B. Sommers[1], Katrin Raudszus[1], Benjamin Kam[1], and Michael Bottlang[1]

[1] Biomechanics Laboratory, Legacy Clinical Research & Technology Center, Portland, Oregon
[2] Orthopedic Healthcare Northwest, Eugene Oregon
Email: mbottlan@lhs.org

INTRODUCTION

Knee fracture-dislocations typically involve rupture of the anterior cruciate (ACL) and posterior cruciate (PCL) ligaments. Treatment of these injuries requires reconstruction of the ligaments and fixation of the associated fractures. Due to the severe nature of this injury, immobilization with a rigid spanning external fixator is occasionally required to maintain stability and to protect the repair. Unfortunately, prolonged immobilization of the knee often results in stiffness, and may produce adverse effects on articular cartilage. Articulated external fixation holds the advantage of maintaining joint stability while allowing early controlled range of motion. However, the effect of articulated external fixation on the cruciate ligaments is unknown.

Currently available commercial articulated external fixators vary in design and construct rigidity. All utilize a single flexion-extension axis of rotation. Rigidity of the fixator construct likely has a significant effect on knee stability and the forces seen by the cruciate ligaments. This study was designed to investigate the protection provided to the cruciate ligaments by three different articulated external fixation constructs as measured by clinically relevant instrumented Lachman's and posterior drawer tests.

MATERIAL AND METHODS

Four fresh-frozen cadaveric specimens were prepared by dissecting away the soft tissues, while carefully preserving the joint capsule and supporting ligamentous structures. Each specimen was mounted horizontally on a custom-built frame. The frame rigidly held the femur and allowed translation of the tibia along a low friction x-y table. The knee and custom frame were aligned with the flexion-extension axis as described by Hollister et al. (1993) under lateral fluoroscopic guidance using the method described by Martin et al. (2002).

Small anterior and posterior arthrotomies were created to insert force probes (AIFP, Microstrain, Burlington, VT) into the ACL and PCL. For the Lachman's test, the femur was rigidly fixed with the knee flexed 30° and the tibia was allowed to move in pure anterior translation. Anterior loads of 50 N and 100 N were applied to the tibia and stress in the ACL was recorded as the AIFP output. Translation of the femur relative to the tibia was measured using two electromagnetic motion tracking sensors (Flock of Birds) mounted to the femur and tibia. In a similar manner, a posterior drawer test was performed with the knee flexed at 90°, and by measuring the forces and displacements in response to 50 N and 100 N posterior loading of the tibia. Measurements were performed for the unconstrained knee, after the application of a monolateral hinged fixator (EBI, Parsippany, NJ), a bilateral hinged fixator (Compass Hinge, Smith and Nephew, Memphis, TN), and a custom made, extremely stiff, bilateral rigid hinge (BRH). The commercial external fixators were placed on the specimens according to the manufacturer's specifications. Statistical analysis was performed using two-tailed, paired student t-tests with a 95% confidence level.

RESULTS

The Lachman's test for the unconstrained knee showed an average of 1.86 ± 0.39 mm of anterior translation for a 50 N load. The translation increased to 3.51 ± 0.39 mm in response to a 100 N load (Fig. 1). There was no significant difference between the two commercial external fixators and the unconstrained knee with respect to Lachman's testing ($p > 0.05$). However, there was a significant difference between the unconstrained knee and the custom bilateral rigid hinge (BRH) ($p < 0.05$).

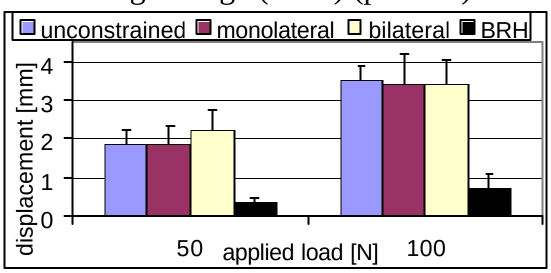

Figure 1: Displacement for Lachman's test

The AIFP probe results show a trend toward decreased forces in the ACL following Lachman's testing, for both the commercial frames and the custom bilateral rigid frame (Fig. 2). These data approached, but did not reach statistical significance.

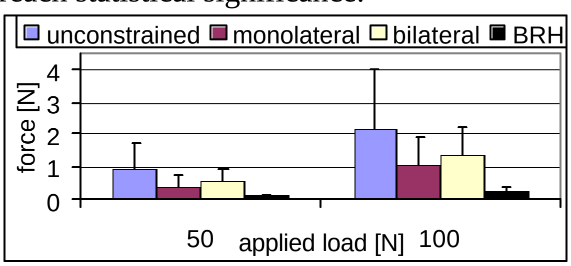

Figure 2: Lachman's test: AIFP forces in ACL

Posterior drawer testing for the unconstrained knee showed an average of 1.87 ± 0.56 mm posterior translation for the 50 N load (Fig. 3). This increased to 3.38 ± 1.10 mm in response to the 100 N load. There was significantly less posterior translation for the monolateral and custom bilateral rigid frame at both 50 N and 100 N. The bilateral compass hinge showed a significant decrease for the 50 N load only.

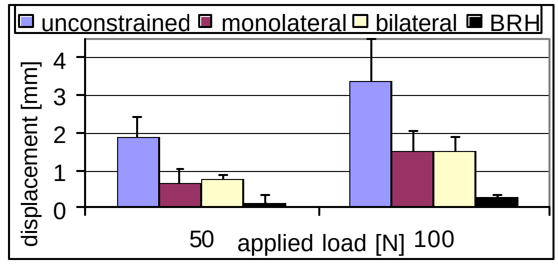

Figure 3: Posterior drawer test: tibial displacement

The AIFP probe showed significantly decreased PCL forces relative to the unconstrained knee in each of the fixators for the 100 N test (Fig. 4). The 50 N tests showed a trend toward decreased forces, but did not reach statistical significance.

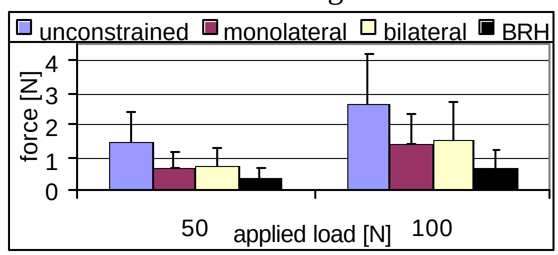

Figure 4: Posterior drawer: AIFP forces in PCL

CONCLUSION

None of the external fixator constructs decreased anterior tibial translation in response to an instrumented Lachman's test. However, the fixators were able to decrease the force detected in the ACL in response to anterior translation. This suggests that the fixator was able to act as a load-sharing device by absorbing a portion of the load normally borne by the ligament. Application of the fixator significantly decreased PCL translations and loads in response to a posterior drawer testing. These results demonstrate the utility of articulated external fixation in protecting the cruciate ligaments after severe injuries to the knee.

REFERENCES

Hollister, A.M. et al. (1993). Clin. Orthop., 290, 259-268.

Martin K, et al. (2002) Proc. of IV World Congress of Biomechanics, 1230.

ACKNOWLEDGMENTS

Funding provided by EBI, Parsippany, NJ

EFFECT OF MARKER SETS ON BETWEEN-DAY REPRODUCIBILITY OF KNEE KINEMATICS AND KINETICS IN STAIR CLIMBING AND LEVEL WALKING

Bing Yu, Robin M. Queen, and Lori A. Schrodt

Motion Analysis Laboratory, Center for Human Movement Science,
The University of North Carolina at Chapel Hill, Chapel Hill, NC, USA
E-mail: rqueen@med.unc.edu Web:med.unc.edu/chms

INTRODUCTION

External markers are commonly used in *in-vivo* human movement analysis. The Helen-Hays marker set is a commonly used external marker set for kinematic and kinetic analyses of the lower extremities. Reduced lower extremity kinematics and kinetics in level walking and stair climbing using the Helen-Hays marker set has satisfactory within-day reproducibility (Kadaba et al, 1991, Yu et al., 1997), but a low between-day reproducibility (Kadaba et al., 1991). The low between-day reproducibility is a major concern in clinical applications of motion analysis. The purpose of this study is to evaluate the between-day reproducibility of knee kinematics and kinetics in level walking and stair climbing reduced from (1) the Helen-Hay's marker set, (2) a modified Helen-Hays marker set, and (3) a UNC-CH marker set.

METHODS

Three male and three female volunteers without any known lower extremity disorders were recruited as subjects for this study. A Peak Performance real-time videographic data acquisition system (Peak Performance Inc., Englewood, CO) with six infrared video cameras, was used to collect the three-dimensional (3-D) coordinates of external markers at a sampling rate of 120 frames/sec. Two Bectec Type 4060A force plates (Bectec Cop. Worthington, OH) were used to collect ground reaction force data at a sampling rate of 1000 Hz. A staircase of four steps, with the lowest two steps attached to the force plates, was used for the stair climbing trials, (Yu et al., 1996).

Eleven reflective markers were placed at the joint space between the 4th and 5th lumbar vertebrae (L4-L5), and bilaterally on the anterior superior iliac spine (ASIS), thighs, knees, shanks, and ankles for the Helen-Hays marker set (Kadaba et al., 1990). Four additional reflective markers were placed bilaterally at the greater trochanter (GT) and below the tibial tuberosity for the UNC-CH marker sets. All of the markers listed above remained on the subject's body during testing. The modified Helen-Hays marker set and the UNC-CH marker set were created by adding a static calibration which consisted of four reflective markers placed bilaterally on the medial knee joint line and on the medial malleoli. The standing calibration was recorded following both the stair climbing and level walking trials.

Data were collected for three trials for each of ascending, descending, and level walking conditions on three different days. The 3-D coordinate data were filtered through a fourth-order low-pass digital filter at an estimated optimum cutoff frequency of 10 Hz (Yu and Andrews, 1998). The 3-D knee joint angles were calculated as Euler angles. The knee joint resultants were estimated using an inverse dynamic procedure and were transferred to the tibia segment reference frame. The within-day and between-day coefficients of multiple correlation (CMC) (Kadaba et al., 1991) were calculated for the kinematics and kinetics of the right knee joint during the stance phase of both stair climbing and level walking for each subject. Analyses of variance with repeated measures were conducted to compare the between-day CMC values of knee kinematics and kinetics among the three marker sets with an alpha level of 0.05 to indicate statistical significance.

RESULTS AND DISCUSSION

The UNC-CH marker set consisted of a standing calibration and the marker located at L4-L5, the bilateral GT, knee, tibial tuberosity, and ankles. The modified Helen-Hays and the UNC-CH marker sets had greater between-day CMC values for the knee valgus-varus angle than did the Helen-Hays marker set ($p < 0.01$ and $p < 0.01$). The UNC-CH marker set had a greater between-day CMC value for the knee valgus-varus angle than did the modified Helen-Hay's marker set ($p < 0.01$). The UNC-CH marker set had a greater between-day CMC value for the knee flexion-extension angle than did the Helen-Hays marker set and the modified Helen-Hays marker set ($p = 0.01$ and $p = 0.01$). The modified Helen-Hays marker set and the UNC-CH marker set had greater between-day CMC values for the knee internal-external rotation angle when compared to the Helen-Hays marker set ($p = 0.01$ and $p < 0.01$). These results suggest that the standing calibration improved the between-day reproducibility of knee kinematics, and that placing markers on well defined bony landmarks further improved the reproducibility of knee kinematics.

The UNC-CH marker set had a greater between-day CMC value for the knee anterior-posterior shear force than did either the Helen-Hays marker set ($p = 0.01$) or the modified Helen-Hays marker set ($p = 0.02$). The modified Helen-Hays marker set and the UNC-CH marker set had greater between-day CMC values for the knee medial-lateral shear force than did the Helen-Hays marker set ($p = 0.01$ and $p = 0.01$). The modified Helen-Hays marker set and the UNC-CH marker set had greater between-day CMC values for all three components of the knee resultant moment vector on the tibia than did the Helen-Hays marker set ($p = 0.01$). The UNC-CH marker set had greater between-day CMC values for all three components of the knee resultant moment vector on the tibia than did the modified Helen-Hays marker set ($p = 0.02$). These results suggest that standing calibration and placing markers on well defined bony landmarks also improved the between-day reproducibility of measured knee kinetics.

SUMMARY

The addition of a static standing calibration is recommended for improving the between-day reproducibility of lower extremity kinematics and kinetics in level walking and stair climbing. New marker sets where all the markers are placed on well-defined bony landmarks may need to be considered for further improvement of the between-day reproducibility.

REFERENCES

1. Kadaba, M.P., et al. (1989). *J. Orthopaedic Research*, **7**: 849-860.
2. Yu, B., Andrews, J.G. (1998). *J. Applied Biomechanics*,**14**: 223-237.
3. Yu, B., et al. (1996). *J. Biomechanics*, **29**: 1625-1628.
4. Yu, B., et al. (1997). *J. Orthopaedic Research*, **15**: 34

THE RELATIONSHIP BETWEEN HIP AND KNEE STRENGTH AND VALGUS KNEE POSITION DURING A SINGLE LEG SQUAT

T.L. Claiborne, V. Gandhi, D.M. Pincivero

Human Performance and Fatigue Laboratory, Department of Kinesiology, The University of Toledo, Toledo, OH
Claiborne@buckeye-express.com

INTRODUCTION

The control of knee motion in the frontal plane (varus/valgus) is achieved via three stabilizing mechanisms including tibio-femoral joint contact, as well as passive and active restraint systems. The active restraint system refers to the muscles that activate to control or produce motion (American Academy of Orthopaedic Surgeons, 1991). While muscular control of the knee in the sagittal plane has been well documented, it remains unclear what muscles contribute to varus and valgus control during functional weight bearing activities.

Dynamic control of the knee in the frontal plane, particularly in the valgus direction, has practical relevance with regards to injury prevention. A valgus knee angle not only places strain on the passive medial restraint system of the knee, but in combination with anterior tibial translation, strain on the anterior cruciate ligament is increased significantly (Berns et al., 1992). Consequently, understanding muscle contribution to the frontal plane active restraint system of the knee may have practical applications in strength training for sport and injury prevention.

The purpose of this investigation was to determine the relationship between hip and knee strength and valgus knee position during a single leg squat. Additionally, gender differences in knee joint kinematics and strength were determined.

METHODS

Thirty healthy adults (15 males, 15 females) participated in two separate testing sessions. During the first testing session, each subject was instructed to stand on their preferred leg, squat to approximately 1.05 rad of knee flexion, and return to the standing position. Frontal plane (varus/valgus) knee movement was evaluated kinematically using a Motion Analysis three dimensional system, at a sampling rate of 60 Hz. The SLS was repeated five times with two minutes of rest between each squat. During the second session, isokinetic concentric and eccentric hip and knee strength was tested using a Biodex isokinetic dynamometer at 1.05 $rad \cdot s^{-1}$. Motions tested included hip abduction (ABD), adduction (ADD), flexion (FLEX) extension (EXT), internal rotation (IR), external rotation (ER), knee flexion (KF), and knee extension (KE). Three maximal-effort reciprocal repetitions were performed for each movement with two minutes of seated rest between sets.

RESULTS

Absolute and body mass normalized peak torque values for concentric and eccentric ABD, ADD, FLEX, EXT, IR, ER, KF, and KE strength measurements were used for analysis. An independent t-test demonstrated that female subjects produced significantly less absolute peak torque than males for all strength measurements except eccentric IR ($p<0.05$). When normalized to body mass, gender differences were noted for concentric ADD, FLEX, KF, and KE, and eccentric EXT ($p<0.05$).

In the standing position, male and female subjects presented with a slightly varus knee position (males = 0.034 ± 0.071 rad, females = 0.011 ± 0.035 rad). During the SLS, the peak knee flexion angle for males and females was 1.09 ± 0.167 rad and 1.15 ± 0.136 rad respectively (mean ± SD). When performing the SLS, females demonstrated a peak knee valgus angle of 0.064 ± 0.080 rad, and males showed a peak knee valgus angle of 0.048 ± 0.092 rad (mean ± SD). During the SLS, females moved in the valgus direction 0.064 ± 0.080 rad (mean ± SD), while males moved toward the varus direction 0.012 ± 0.168 (mean ±SD). There were no significant gender differences noted for all measurements of frontal plane knee kinematics ($p>0.05$).

Linear regression analysis revealed that concentric ABD ($r^2 = 0.13$, SEE = 8.11), KF ($r^2 = 0.18$, SEE = 7.88), and KE ($r^2 = 0.14$, SEE = 8.10) peak torque were significant predictors ($p<0.05$) of frontal plane motion of the knee during a SLS. A Pearson product moment correlation demonstrated weak to moderate, but significant negative relationships between the concentric ABD ($r = -0.37$, $p<0.05$), KF ($r = -0.43$, $p<0.01$) and KE ($r = -0.37$, $p<0.05$) peak torque, and frontal plane knee motion. These data suggest that individuals with greater strength of these muscle groups, tend to demonstrate a lower amount of knee movement in the valgus direction. There were no significant relationships between peak torque and standing knee valgus or peak knee valgus.

When considering all of the strength variables collectively in a factor analysis, a regression analysis showed that only the knee factor ($r^2 = 0.22$, SEE = 7.85) was a significant predictor of frontal plane knee motion. When interpreting the knee factor, strength of all of the hip and knee muscle groups are taken together. High loadings of concentric and eccentric KF, KE, IR and concentric ABD suggest that strength of these muscle groups may contribute more than others when predicting motion of the knee in the frontal plane.

SUMMARY

These data suggest that increased frontal plane knee movement toward valgus direction may occur when ABD, KF, and KE peak torque values are relatively low. These findings are in agreement with previous work demonstrating a significant contribution of the quadriceps, hamstrings, hip abductors and hip adductors to the control of varus and valgus motion at the knee (Lloyd & Buchanan, 2001).

When normalized for body mass, females exhibited lower strength values in KF and KE strength when compared to males, possibly implying a gender predisposition to increased knee motion in the valgus direction during functional weight bearing activities.

REFERENCES

American Academy of Orthopaedic Surgeons (1991). *Athletic Training and* Sports Medicine (2nd ed). p. 332.

Berns, G.S., et al., (1992). *J Orthop Res, 10*, 167-176.

Lloyd, D.G. & Buchanan, T.S. (2001). *J Biomech, 34* , 1257-1267.

ARTICULATED EXTERNAL FIXATION OF THE KNEE JOINT: EFFECT OF FIXATOR STIFFNESS ON KNEE MOTION AND LIGAMENT STRESS

Katrin Raudszus[1], Benjamin Kam[2], Mark B. Sommers[1], J. Lawrence Marsh[3], Michael Bottlang[1]

[1]Biomechanics Laboratory, Legacy Clinical Research & Technology Center, Portland, OR, USA
[2] Oregon Health & Science University, Portland, OR, USA
[3]University of Iowa, Hospitals and Clinics, Iowa City, IA, USA
E-mail: mbottlan@lhs.org

INTRODUCTION

Severe knee injuries can be treated by rigid spanning external fixation. However, prolonged joint immobilization may produce degenerative effects on articular cartilage and connective tissue, resulting in post-traumatic morbidity such as joint contracture and osteoarthritis. Articulated external fixation can in theory provide both, joint stabilization and early controlled range of motion (ROM). Commercially available hinged knee fixators vary significantly in design and construct rigidity. This biomechanical cadaveric study investigated the effect of three articulated external fixators on the attainable ROM and on the stresses in the cruciate ligaments.

MATERIAL AND METHODS

Four fresh-frozen cadaveric leg specimens were sectioned 250 mm proximal and distal to the knee joint line. Specimens were dissected free from soft tissues, while retaining the capsulo-ligamentous structures. Each specimen was mounted horizontally on a custom-built frame connected to a biaxial material test system (Instron 8874, Canton, MA) (Fig. 1). Each specimen was aligned to the frame under lateral fluoroscopic guidance to ensure that the flexion-extension (FE) axis coincided with the frame axis, as described by Hollister et al. (1993). Passive knee motion was induced by the rotary actuator of the MTS, acting on the femur, while the tibia remained in a fixed position.

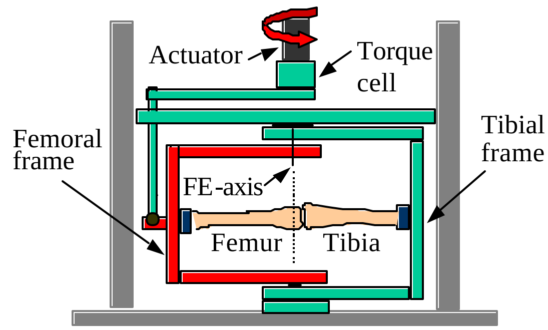

Figure 1: Experimental setup

Knee flexion and extension was induced at a constant angular velocity of 10°/s, starting at 30°, first toward extension and subsequently toward flexion. A torque cell was used to assess the resulting knee flexion moment as a measure for the motion resistance. Extension and flexion limits were set at –5° and 125°, respectively, or at 5 Nm, whichever was reached first. One force probe (AIFP, Microstrain, Burlington,VT) each was inserted through small arthrotomies into the anterior cruciate ligament (ACL) and posterior cruciate ligament (PCL). These sensors allowed to continuously monitor the stress in the cruciate ligaments. Motion resistance and ligament stress measurements were performed for the unconstrained knee, after subsequent application of a monolateral hinged fixator (EBI, Parsippany, NJ), a bilateral hinged fixator (Compass Hinge, Smith and Nephew, Memphis, TN), and a custom-made bilateral rigid hinge (BRH) of superior stiffness. Statistical analysis was performed using two tailed, paired Student's t-tests with α=0.05.

RESULTS

The experimental setup allowed continuous tracking of motion resistance (Fig. 2). The average range of motion (ROM) for a 1Nm threshold for the unconstrained knee was 125.4º ± 5.4º. Constraining the knee to the monolateral, bilateral, and BRH fixators reduced the ROM to 105.6º ± 16.8º, 100.8º ± 25.5º and 102.3º ± 19.7º, respectively. The ROM reduction caused by the monolateral fixator was statistically significant ($p<0.05$).

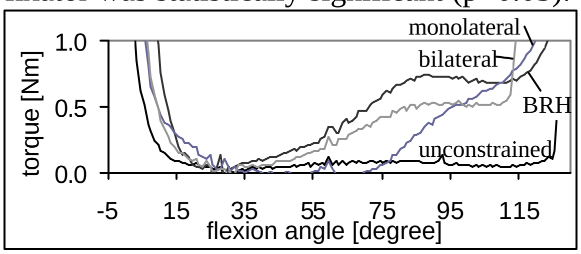

Figure 2: Average motion resistance

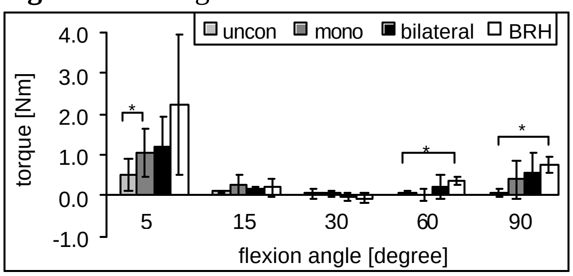

Figure 3: Motion resistance at specific flexion angles

Constraining the knee to rotate about a fixed axis resulted in increased motion resistance as compared to unconstrained motion (Fig.3). This trend was statistically significant for the monolateral fixator at 5º and for the BRH at 60º and 90º. The highest average torque of 2.21 ± 1.71 Nm was observed for the BRH at 5º. However, due to high standard deviations this was not statistically significant different to the unconstrained or the commercially available fixators.

The AIFP probes indicated increased PCL-stress towards flexion, and increased ACL-stress towards extension (Fig. 4). For both, flexion and extension, a trend was observed that constraining the knee increased the stress in the PCL and ACL. This was statistically significant at 90º flexion for the monolateral and bilateral external fixators. However, no significant differences were detected between different fixation constructs.

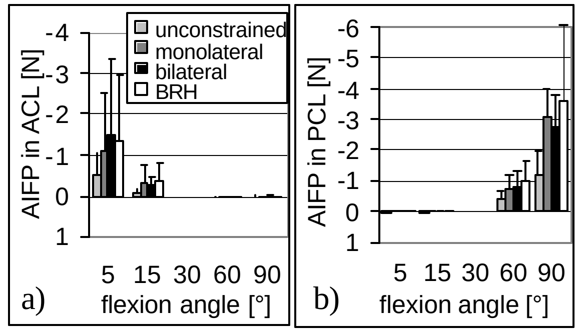

Figure 4: AIFP reports in ACL (a) and PCL (b)

CONCLUSION

The observed reduction in ROM of 18 % from the unconstrained to the BRH constrained knee was similar to previous investigations (Sommers, 2001). The increase in motion resistance was most pronounced towards full extension, and can be attributed to a mismatch between the external fixator axis and the inherent axis of the knee joint. Responsible for increase in motion resistance are in part the cruciate ligaments, which show a significant stress increase with applied fixators toward the end of the ROM. However, the observed ligament stress does not correlate to the fixator stiffness.

In conclusion, a limited but functional ROM can be achieved with proper application of an articulated external fixator to the knee joint. However, adequate motion limits should be applied to avoid increased stress in the cruciate ligaments.

REFERENCES

Hollister, et al. (1993). Clin. Orthop., 290, 259-268.

Sommers et al.(2001). Proceed. of ASB, 171.

ACKNOWLEDGMENT

Funding provided by EBI, Parsippany, NJ

CYCLIC LOADS POST SURGERY ARE BENEFICIAL FOR THE STRENGTH OF MENISCAL REPAIR DEVICES

**Mocniak, RL; **Nienberg, SM; **Prosser, MD; **Anthony, S; **Wasserman, N; +*Goitz, HT; **Goel, VK
+*Sports Research Center, Department of Orthopaedic Surgery, Medical College of Ohio, Toledo, Ohio
**Spine Research Center, Department of Bioengineering, University of Toledo, Toledo, Ohio

INTRODUCTION

Human knee is a complex joint and its menisci are vital for maintaining proper function. Tears of the meniscus are common, especially in young athletes. Tears in the peripheral meniscus regions with ample blood supply are usually repaired with either a suture or an implant. Numerous biomechanical studies dealing with the strength of the various suturing devices are reported in the literature but there is no comparative data, particularly the effects of cyclic loads. The present study was undertaken to assess the hypothesis that the cyclic loading of these devices will not lead to a decrease in repair strength or evidence premature failure. Six commercially available devices were tested: Arthrex Meniscal Dart, Bionix Contour Meniscus Arrow, Linvatec BioStinger, Mitek Rapidloc, Smith and Nephew Fast T-Fix and Surgical Dynamics Staple.

METHODS

Twenty-four fresh frozen porcine knee pairs (mid femur to mid tibia of either side leg), divided equally into four groups, were used for the study. Specimens were kept moist during the entire phase of the testing protocol by spraying 0.9% saline solution. Each specimen capsule was opened and lateral and medial collateral ligaments were dissected. One cm long meniscal tear located about 3mm from the peripheral edge of the posterior horn was created. The tear was repaired using one of the four devices as per manufacturer recommendations. One specimen of the pair was potted for mounting in a cyclic loading fixture (Figure 1), especially designed for the study while the other was used as a control. The loading fixture was placed within the MTS system to flex the specimen between 10 and 120 degrees with a preload of 450 N, (Figure 2). Menisci were removed from the cyclic and the control specimens. The cartilage surfaces and the condition of various devices were observed prior to cutting the repaired samples for further testing. These samples were then sutured at either end for holding in fixtures that helped pull the ends apart using the MTS machine at 12.5 mm/sec. Force-displacement data were recorded, and was analyzed and compared using appropriate statistical tools.

RESULTS

The average and one-standard deviation strength data for the four devices, from paired specimens with and without cyclic loading are shown in (Figure 3). Four of the six devices exhibited no statistical difference (student’s t-Test) in pull out strength before and after cyclic loading, while 2 devices exhibited statistical differences-i.e, Bionix Meniscal Arrow and Surgical Dynamics Staple (p of 0.007 and 0.000, respectively).

Interestingly, nearly all devices exhibited some degree of articular cartilage wear on the femoral condyle, particularly those devices with prominent ‘heads’ or ‘ends’ (Figure 4). Also, the gap from each artificially created tear in each tested meniscus did not widen with cyclic loading;

conversely, each tear was observed to increase approximation from such loading.

DISCUSSION

Although the specimens used were fairly uniform (about 4 to 4.5 months old pigs with weight between 260-270 lbs), the present study has several limitations. Porcine knees specimens were used due to lack of younger age group human cadaver knees. However, since the overall purpose of this investigation was to determine the effects of immediate post-operative activity of the repaired knee on the device strength, the number of cycles was kept to fifty. Furthermore, since literature data is mostly based on porcine specimens, the present data has provided some clinically relevant information. The devices produced wear on the femoral condyle surfaces, but extensive damage was inflicted by those devices which had plastic heads or plastic ends that were more difficult to be made flush with or be buried deep to the meniscal surface (Figure 4). Interestingly enough, despite the pull out strength data achieved, in no case did the meniscus tear either separate nor propagate with cyclic loading; in fact, the gross appearance of "tightening" of the repair site may suggest that early weight bearing and motion may be beneficial to the early rehabilitation of repaired meniscus of the knee.

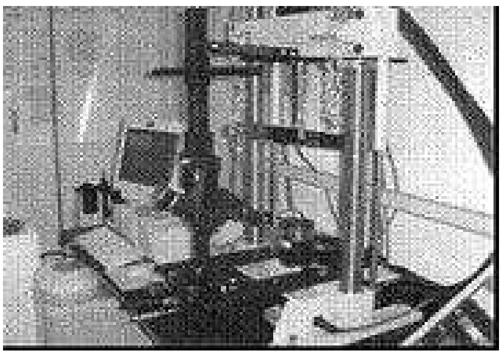

Figure 1: Cyclic loading fixture mounted to the MTS machine.

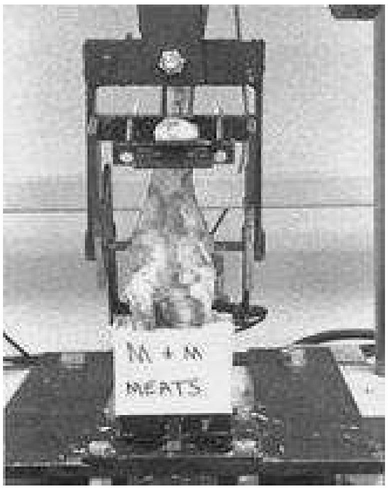

Figure 2: Porcine specimen mounted into the MTS loading fixture.

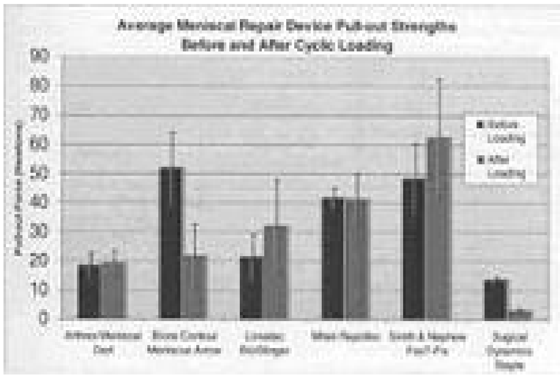

Figure 3: The graph illustrates the pull-out strengths of meniscal repair devices before and after cyclic loading.

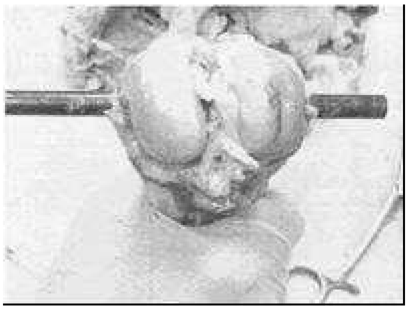

Figure 4: The femoral condyle surface experienced significant amounts of wear from repair devices with plastic heads/ends.

THE EFFECT OF LATERALLY WEDGED INSOLES ON STANDING ALIGNMENT

Stephanie Crenshaw[1], Todd Royer[1], Irene Davis[2], Emily Mika[2], Robert Butler[2]

[1] Dept of Health and Exercise Sciences, University of Delaware, Newark, Delaware
[2] Dept. of Physical Therapy, University of Delaware, Newark, Delaware
e-mail: sjcren@udel.edu

INTRODUCTION

Laterally wedged insoles (typically inclined 5-10 degrees) have been used as a conservative treatment for medial knee osteoarthritis (OA). The goal of wedged insoles is to alter the mechanical alignment of the lower extremity and redistribute forces at the knee. The mechanism of pain relief is unclear, however. Potential mechanisms include an alteration in static alignment and a decrease in knee adduction moment during stance phase of walking.

As the aim of the insole is to realign the limb to reduce a varus position of the knee, frontal plane radiographs of static alignment in patients with and without the insoles should reveal a significant difference between the two conditions. Reports have been conflicting as to whether or not static alignment changes. Toda et al. (2001) and Maly et al. (2002) did not find significant differences in tibio-femoral angle (TFA) between the two conditions, while Giffin et al. (1995) did find a significant varus to valgus alteration. Yasuda and Sasaki (1987) did not find a difference in TFA but did report a shift in the mechanical axis (MA).

The purpose of our study is to determine the effects of laterally wedged insoles on standing alignment in patients with medial knee OA. We hypothesized that TFA will shift towards valgus, and the MA will become more upright with respect to vertical with the addition of the wedged insoles.

METHODS

Two males and six females ($M_{age} = 59.4 \pm 4.0$ yrs; $M_{height} = 166.9 \pm 9.0$ cm; $M_{mass} = 92.4 \pm 16.3$ kg) with diagnosed medial knee OA of at least a grade II in the Kellgren-Lawrence scale volunteered as subjects in this study. Subjects were fitted with a full length laterally wedged foot orthoses for their affected knee side. The amount of wedging (10.4 ± 2.9 deg) was determined for each subject by a reduction in pain during a lateral step-down task.

Subjects were given two weeks to accommodate to the orthotic device. Full-length frontal plane radiographs were then taken of the subject's affected leg while they stood in bilateral stance, with and without the wedged insole in the shoe.

The TFA was determined from the intersection of the line joining the hip joint and knee joint centers and the line joining the knee joint and ankle joint centers. Zero degrees defines the neutral angle, while varus is positive and valgus is negative. MA was calculated as the angle that the line connecting the hip and ankle joint centers makes with the vertical. Positive angles represent a lateral tilt of the MA.

A two-factor, measure (TFA, MA) by condition (no wedge, wedge) within-subjects ANOVA was used to test for a significant interaction in alignment.

RESULTS AND DISCUSSION

Mean data for the eight subjects are provided in Figure 1. There was non-significant measure by condition interaction for alignment [F(1,7) = 0.008, p = 0.932]. For the wedge condition, the smaller TFA angle indicates a decrease in varus angulation, while the increase in MA indicates a more lateral tilt of the leg. Although the average values indicate a trend towards decreased varus and a more lateral MA tilt with the wedged insoles these differences were roughly one degree and resulted in a non-significant condition main effect [F(1,7) = 2.13, p = 0.185].

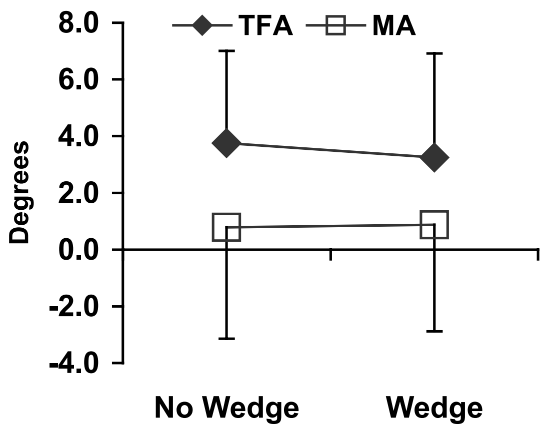

Figure 1: There were no significant differences between insole conditions. Zero degrees is vertical; positive angles are varus (TFA) and lateral tilt (MA).

Both TFA and MA are predictors of medial joint forces in the knee. The more acute the varus angle (TFA) or the greater the lateral tilt relative to vertical (MA), the greater the forces are on the medial side of the joint. Decreasing the varus angulation and tilting the MA into a more upright position should shift the knee joint load laterally and thus decrease load and ultimately pain on the medial side of the knee.

The TFA was not significantly altered in this study, which is consistent with three previous studies (Yasuda and Sasaki, 1987, Toda et al., 2001, Maly et al., 2002) but inconsistent with the results of Giffin et al. (1995). While our mean results are similar to Giffin and colleagues (1995), a closer examination of data showed that some of our subject's TFA improved while others worsened. This resulted in an average absolute angle change that was actually larger (1.8 ± 2.2 deg) than those of Giffin and colleagues (0.8 ± 1.1 deg).

Yasuda and Sasaki (1987) reported an improvement in MA measured during unilateral stance with the use of wedged insoles. Our MA, measured in bilateral stance, was not different between conditions. Perhaps MA measured during unilateral stance is more sensitive to the use of wedged insoles than MA measured during bilateral stance, which may explain the differences in results.

SUMMARY

The use of wedged insoles resulted in a decrease in knee pain during a lateral step down test; however, standing alignment measures (e.g., tibio-femoral angle and mechanical axis) did not differ between insole conditions as hypothesized.

REFERENCES

Giffin, JR. et al.(1995). *JPO*, **7**, 23-28.

Maly, MR et al.(2002) *Clin Biomech*. **17**, 603-10.

Toda, Y. et al. (2001). *J Rheumatol,* **28**, 2705-10.

Yasuda, K. & Sasaki, T. (1987). *Clin Orthop*, **215**, 162-172.

ACKNOWLEDGEMENTS

Support from NIH-RR16548 (Tom Buchanan, PI) is acknowledged.

A MUSCULOSKELETAL MODEL FOR SIMULATION OF ANKLE SPRAINS DURING TWO-LEGGED LANDING MOVEMENTS

Xuemei Huang, Scott G. McLean, Anne Su, A. J. (Ton) van den Bogert*

Department of Biomedical Engineering, Cleveland Clinic Foundation, Cleveland OH, USA
bogert@bme.ri.ccf.org, http://www.lerner.ccf.org/bme/

INTRODUCTION

Forward dynamic simulation is a fast and inexpensive way to study musculoskeletal injury mechanisms that can not be studied in human subjects within the limit of safety. Cadaver experiments are costly and technically challenging, especially when dynamic simulation of muscle forces is important for the injury mechanism.

Single-limb models have been used to simulate running (Neptune et al., 2000), ACL injury (McLean et al., 2003) and to study ankle sprain injury during a cutting or side-shuffle movement (Wright et al., 2000). In this paper we present a two-legged model to simulate ankle sprains during drop jumps. We optimize the muscle activation patterns to obtain a realistic movement simulation and then expose the model to injury-causing events.

METHODS

A 3-D two-legged model was developed, with 18 degrees of freedom and 31 muscles (Delp et al., 1990) on each leg, divided into 12 functional groups. Foot-ground contact was modeled using 91 contact points on each shoe. The forces from ground contact and muscle activity drive this musculoskeletal model through forward dynamics, using equations of motion derived with SD/FAST (PTC Inc.). An in-house software library was used to model muscles and ground contact forces. Simulations were done for the first 200 ms of ground contact.

The model is subject-specific, and results for one subject will be presented. 3-D coordinates of reflective markers were collected (Motion Analysis Corp., Santa Rosa CA) during a standing trial for automatic generation of the musculoskeletal model. The subject then performed ten drop jumps from a height of 61 cm, followed immediately by a forward running movement. Bilateral kinematic data and ground reaction forces (GRF) were collected.

Muscle stimulation patterns for the 24 muscle groups in the model were parameterized as stimulation values at 50 ms intervals. Simulated annealing was used with weighted least squares tracking (Neptune et al., 2000) to obtain muscle stimulation patterns that best reproduced the subject's movement and GRF.

A validation procedure was developed to test the ability of the optimized model to predict the effect of variations in initial conditions on the subsequent joint angles and ground reaction forces.

After validation, the model was exposed to a series of 50,000 uneven surfaces, each with a Gaussian "hole" at a random location in a 20x30 cm rectangle, a random width of 5-20 cm, and a random depth of 0-10 cm. Ankle sprain was defined to occur at a supination moment of 34 N m (Parenteau, 1998).

RESULTS AND DISCUSSION

The optimized model reproduced the subject data with an average RMS error of 1.1 times the between-trial standard deviation (Fig. 1). The fit tended to be better for the kinematic variables than for the forces. For instance, right ankle supination had an RMS fit error of only 0.68 times the between-trial standard deviation.

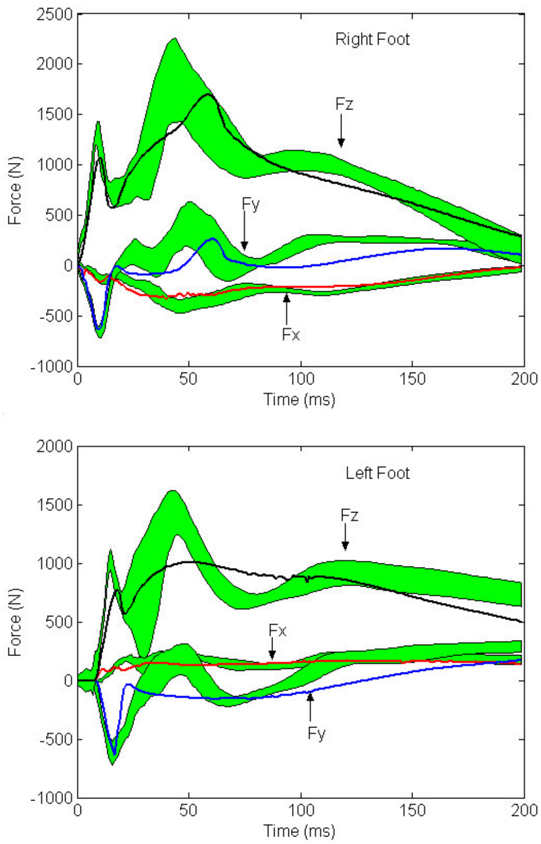

Figure 1: Simulated and measured ground reaction force. X is to the right, Y is to the front, and Z is vertical.

The optimization required 317,521 simulations (7.5 days on a 2.7 GHz Pentium IV). Repeated optimizations resulted in multiple solutions with similar tracking performance, indicating that different muscle coordination patterns could generate almost the same movement and ground reaction forces.

The validation indicated that the model could successfully predict the effect of variations in initial joint angles and velocities. The RMS error between predicted and measured between-trial variations in right ankle supination angle at 200 ms was 1.4 times the standard deviation.

In the 50,000 simulated landings on uneven surfaces, 199 right ankle sprains were seen. One example of a right ankle sprain is presented in Fig. 2. Injury occurred with a peak supination moment of 41 N m at 107 ms after landing on an uneven ground with a 9.4 cm deep and 19.7 cm wide hole.

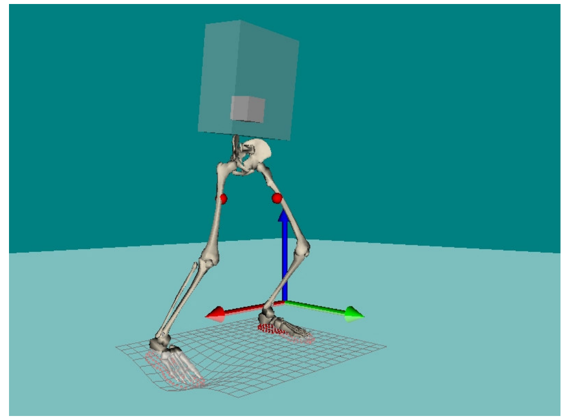

Figure 2: Example of a right ankle sprain on an uneven floor. Peak supination moment was 41 N m at *t* = 107 ms.

SUMMARY

The optimized 3D two-leg musculoskeletal model can successfully simulate the body kinematics and ground reaction forces during a landing movement. The model appears to be a useful tool to predict the effect of neuromuscular changes and protective equipment on the risk of ankle sprain during landing movements.

REFERENCES

Delp SL et al. (1990) *IEEE Trans Biomed Eng* **37**, 757-767.

McLean SG et al. (2003) *Proceedings of the Orthopaedic Research Society*, New Orleans, USA, Feb 1st-5th.

Neptune RR et al. (2000) *Comp Meth Biomech Biomed Engng* **3**:321-334.

Parenteau et al. (1998) *J Biomech Eng* **120**, 105-111.

Wright IC et al. (2000) *J Biomech* **33**:513-519.

ACKNOWLEDGEMENT

Supported by the U.S. Department of Defense.

THE FOOT- NO LONGER A SINGLE RIGID BODY: A DYNAMIC MRI STUDY

Tracy L. Rausch[1,2], and Frances T. Sheehan[1,2]

[1]Mechanical Engineering Department, The Catholic University of America, Washington, DC
[2]Physical Disabilities Branch, National Institutes of Health, Bethesda, MD
E-mail: trausch@cc.nih.gov

INTRODUCTION

Advancing the diagnoses, treatment and prevention of ankle injuries (or pathologies) has been hampered due primarily to an inability to non-invasively quantify individual bone dynamics. Currently most modeling and noninvasive measurement methods assume the entire foot (calcaneus, talus, etc) moves as a single rigid body. Yet, *in vivo* techniques have demonstrated that there is significant movement between the various bones (Lundberg, 1989). These methods unfortunately cannot be applied widely due to their invasive nature. A newly developed imaging sequence, fast phase contrast magnetic resonance imaging (fast-PC MRI), offers us the opportunity to quantify the *in vivo* 3D kinematics of individual bones within the ankle complex in both the healthy and impaired populations. This technique demonstrated excellent accuracy and precision in previous knee joint studies (Rebmann and Sheehan, 2003). Thus, the purpose of this study was to quantify, for the first time, the 3D *in vivo* kinematics of the tibia, talus and calcaneus non-invasively during dynamic activity.

METHODS

Three male subjects participated in this IRB approved study. Subjects were placed supine in a 1.5T GE magnet with the hip and knee maintained in full extension. A dual transmit-receive phase array MR coil was placed medially and laterally about the ankle. A sagittal-oblique imaging plane that bisected the Achilles' tendon and passed through the tibia, talus and calcaneus was determined from a static 3D axial gradient echo scan. Using this imaging plane a fast-PC MR scan (TR=9 ms, TE=min full, flip angle=30^o, V_{enc}=20 cm/s, 2NEX, imaging time=3min 48sec) was performed. With the aid of an auditory metronome, subjects maintained a repeated plantarflexion-dorsiflexion (PF-DF) movement at (35cycles/min). An elastic cord provided a small PF resistance. From this scan, 24 quasi-static anatomic images (representing the various phases of the PF-DF cycle) were obtained along with the 3D time dependent velocity vector for every pixel within the imaging plane.

From the velocity data, the orientation matrices of each bone were quantified, assuming that all bones began aligned with the laboratory coordinate system in the first time frame [**x** = transverse axis (+lateral), **y** = vertical axis (+superior), **z** = ant-post axis (+anterior)]. To begin, regions were graphically prescribed on tibia, calcaneus, and talus, in the first time frame. Using previously developed integration algorithms (Zhu, et al, 1996), 3D time-dependent positions of vertices of these regions were defined throughout the motion cycle. Based on these data, the orientation matrices were calculated and then simplified into three rotation angles using a xyz body-fixed rotation sequence. Thus, the order of rotation was PF-DF, internal- external (I-E) rotation, and supination-pronation (S-P).

RESULTS AND DISSCUSSION

All bones demonstrated 3D rotations, with transverse axis rotation (PF rotation) being the largest. For example, the calcaneus-talus joint demonstrated a total rotation of 11.3 ^{o} in PF, 6.9 ^{o} in I-E and 5.8 ^{o} in S-P (Figure 1). Based on the calcaneus-tibial joint kinematics, the cycle was divided into 3 primary movements, designated as pre-PF, PF, DF (Figure 2). During pre-PF large talus-tibial PF rotation was measured, but minimal calcaneus-tibial PF rotation was observed (Figure 2). The primary rotations of the calcaneus-tibial joint occurring during PF (+16.6^{o}) and DF (-16. 6^{o}).

The data from this preliminary study demonstrates the individual bones within the ankle complex experience alterations in their 3D orientations even when visible external movement is not present. If the change in ankle angle is approximated by the change in calcaneus-tibial transverse rotation, the ankle angle only begins to enter PF during time frame 10, whereas the talus begins to PF, relative to the tibia, at time frame 4 (beginning of pre-PF). Also, during this pre-PF phase large changes in calcaneus-talus orientation are observed.

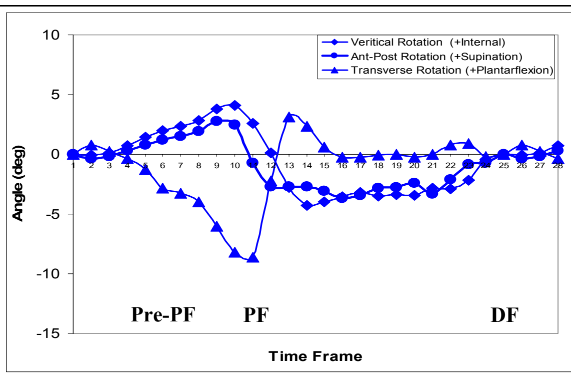

Figure 1: Calcaneus Rotation in Reference to the Talus (1 subject): Since DF started during time frame 21 and continued through time frame 4, time frames 1-4 were added to the end of the cycle as times frames 25-28.

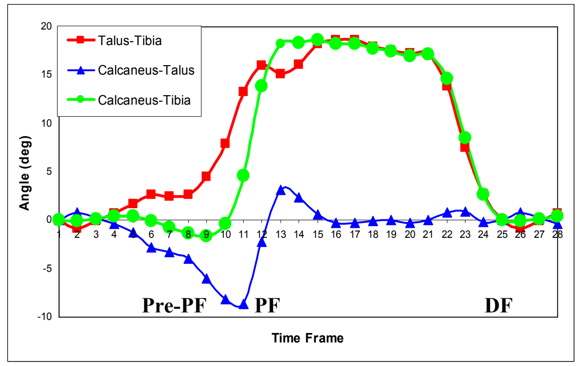

Figure 2: Rotation about the Transverse Axis (1 subject): Since DF started during time frame 21 and continued through time frame 4, time frames 1-4 were added to the end of the cycle as times frames 25-28.

SUMMARY

Quantifying the 3D kinematics *in vivo* and non-invasively has demonstrated that the individual bones of the ankle complex do not behave as a single rigid body. Further, the kinematics of these joints are likely to be much more complicated than reported in previous noninvasive studies. The planned advancements for this study are to develop anatomically-based coordinate systems for individual bones that can be consistently defined for all subjects, to build a device to allow more precise joint loading, and to compile a statistically significant normative database for ankle joint kinematics. Once completed, specific ankle pathologies will be investigated.

REFERENCES

Rebmann,A.J. and Sheehan,F.T. (2003). *J.Magn Reson.Imaging* **17,** 206-213.

Lundberg, A. et al. (1989). *Foot & Ankle* **9:**194-200

Zhu Y, et al. (1996)*Magn Reson Med.* **35**:471-480.

EFFECTIVENESS OF THE KINETIC WEDGE FOOT ORTHOSIS MODIFICATION TO REDUCE RELATIVE PLANTAR PRESSURE

Kerry K. Rambarran[1], Edward Lemaire[1,2] and D. Gordon E. Robertson[1]
[1]School of Human Kinetics, University of Ottawa, Ottawa, Canada, kerryram@netscape.net
[2]The Rehabilitation Centre, Ottawa Hospital, Ottawa, Canada

INTRODUCTION

Humans are the only species to successfully walk using an erect bipedal posture. The unique design of human feet, more so the first metatarsophalangeal (MTP) joint allows us to walk in a relatively upright position, to facilitate the efficiency of the inverted pendulum (Winter, 1995). An obstruction, inability or delay of the inverted pendulum to move through the sagittal plane is referred to as sagittal plane blockade. One source of sagittal plane blockage is the inability or delay of the first MTP joint to permit adequate dorsiflexion from late stance phase, to toe-off during gait. This condition is referred to as **Functional Hallux Limitus (FHL).** Podiatric clinicians suggest that FHL can result in slight disruptions of the inverted pendulum's centre of gravity (CoG) through the sagittal plane (Winter, 1995; Dananberg, 1986, 1993).

According to clinicians, FHL can produce momentarily elevated plantar pressures under the first MTP joint and Hallux. FHL can also lead to compensatory gait adaptations to restore the pendulum. One compensatory strategy used by individuals with FHL is to use the lesser MTP joints, rather than the first MTP joint to facilitate the inverted pendulum during stance. This strategy can be illustrated with elevated plantar pressures under the lesser metatarsal heads. Clinicians suggest this compensatory action may be a contributor to overuse injuries of the plantar tissues of the foot. Such inappropriate tissue stress can be expressed as plantar calluses under the metatarsal heads and hallux. The podiatric community uses custom foot orthoses (CFO) with the Kinetic Wedge modification (Langer) to improve MTP joint function and thereby reduce lateral forefoot plantar pressure. The purpose of this study was to determine if a CFO with a Kinetic Wedge modification reduces relative plantar pressures under the first MTP joint, the hallux and the fifth metatarsal during late stance.

METHODS

Fifteen subjects having moderate to severe FHL by a chiropodist were included in the study. Each subject was supplied a pair of CFOs manufactured with the Amfit CAD/CAM system. Plantar pressure data were recoded during multiple walking trials using the *F-Scan* system (Tekscan Inc.). Each subject was tested with the CFO without the Kinetic Wedge modification (NKW) and with the CFO plus the Kinetic Wedge modification (KW). Data for KW were collected after 30 minutes of practice. Plantar pressure data under the first MTP, hallux and fifth metatarsal for both conditions (NKW and KW) were compared. Relative peak plantar pressure under each of the three segments of the foot was used to represent maximum pressure.

RESULTS AND DISCUSSION

The average maximum plantar pressure under the first MTP joint achieved by all subjects during NKW was 1.871 kg/cm^2 ($\pm$0.459). The average maximum plantar pressure under the first MTP joint achieved by all subjects during KW was 1.554 kg/cm^2 ($\pm$0.409). Overall, application of the Kinetic Wedge modification to custom foot orthoses resulted in an average decrease of 0.317 (16.03%) kg/cm^2 in maximum plantar pressure under the first MTP joint during stance (SD = 0.326). The decrease in first MTP joint plantar pressure during stance was statistically significant ($p < 0.05$). Placing the first MTP joint in a relatively greater dorsiflexed position allowed the joint to avoid functional limitations. In addition to avoiding functional limitations, dorsiflexion of the first MTP joint may have established an anatomical forefoot rocker. Such a shaped surface would create a path of lesser resistance as the body centre of mass progresses forward over the first MTP joint.

Considering a significant reduction of first MTP joint plantar pressure, a significant reduction of hallux plantar pressure was expected. The average maximum plantar pressure under the hallux segment experienced by all subjects during NKW was 2.66 kg/cm^2 ($\pm$0.832). The average maximum plantar pressure experienced under the hallux segment by all subjects during KW was 2.28 kg/cm^2 ($\pm$0.781). Overall, application of the Kinetic Wedge modification to custom foot orthoses resulted in a decrease of 0.373 kg/cm^2 (14.05%) in maximum plantar pressure under the hallux segment during stance (SD = 0.743). The decrease in hallux segment plantar pressure during stance was not statistically significant ($p>0.05$).

Since the data showed an improvement first MTP joint plantar pressure, a reduction of plantar pressures experienced by the lesser metatarsal heads pressure was also expected (Dananberg, 1993 and Dananberg *et al*., 1996). The average maximum plantar pressure experienced under the 5th metatarsal segment by all subjects during NKW was 1.749 kg/cm^2 ($\pm$0.608). The average maximum plantar pressure experienced under the fifth metatarsal segment by all subjects during KW was 1.748 kg/cm^2 ($\pm$0.789). Overall, application of the Kinetic Wedge modification to custom foot orthoses resulted in a decrease of 0.0005 kg/cm^2 (SD = 0.363) in maximum plantar pressure under the fifth metatarsal segment during stance. The decrease in fifth metatarsal segment plantar pressure during stance was not statistically significant ($p>0.05$). According to the results, modified CFOs did not reduce the tendency of subjects to use the compensatory strategy of first MTP avoidance.

No significant change between treatments may have been related to the amount of practice time provided to subjects before KW data collection. Perhaps months, weeks, or even days of modified CFO use be required to result in significant kinetic changes at each site of the foot.

REFERENCES

Winter, D.A. (1995). *Gait & Posture*. **3**, 193-214.

Dananberg, H.J. (1993). *J.A.P.M.A.* **83**, 433-441.

Dananberg, H.J. (1986). *J.A.P.M.A.* **76**, 648-652.

Dananberg, H.J., Phillips, A.J., Blackman, H.E. (1996). *Ad. Pod. Med. Surg.* **2**, 67-87.

Dananberg, H.J. (1995). *Spine: State of the Art Reviews*. **9**, 389-405.

ACKNOWLEDGEMENTS

The chiropody staff of Total Foot Care, M. Louis Goudreau and staff of Rehabilitation Engineering of The Rehabilitation Centre, Ottawa Hospital and Mr. Graham Curryer

ESTIMATION OF EXTRINSIC FOOT MUSCLE FORCES USING A MUSCULOSKELETAL MODEL

Kristian O'Connor [1], Graham Caldwell [2], and Joseph Hamill [2]

[1] Biomechanics Laboratory, UW−Milwaukee, Milwaukee, WI, USA
[2] Biomechanics Laboratory, University of Massachusetts, Amherst, MA, USA
E-mail: krisocon@uwm.edu

INTRODUCTION

Excessive foot pronation is believed to lead to overuse running injuries by causing high stresses in the muscles of the leg. However, it remains unclear exactly how these muscles (particularly the extrinsic foot muscles) respond to foot pronation during running. The eleven extrinsic foot muscles originate proximal to the foot and insert on the foot. While forces in some of these muscles have been estimated through musculoskeletal modeling (e.g., Scott & Winter, 1990), there are no studies that have investigated the effect of perturbations on these muscle forces. This could be critical in understanding how interventions such as orthotics alter the muscular loading in the leg. The purpose of this study was to develop a musculoskeletal model to study the force contributions of the extrinsic foot muscles during the stance phase of running under perturbation conditions.

METHODS

One subject ran in shoes with a normal midsole, a varus-wedged midsole, and a valgus-wedged midsole (Milani et al., 1995). A four-segment, three degree-of-freedom model was developed using the SIMM software package. The thigh, shank, talus, and calcaneus were modeled with articulations at the knee, ankle, and subtalar joints. Knee data were used to more accurately estimate length changes in the medial and lateral gastrocnemius. Eleven Hill-type muscle-tendon actuators represented the extrinsic foot muscles. Muscle parameters were based on the work of Delp (1990).

Three trials (one in each shoe condition) from the single subject were used as input to the model. The subject was asked to run across a force plate while kinematic, kinetic, and EMG data (on six muscles) were collected. Three-dimensional kinematic and kinetic data for the knee, ankle, and subtalar (axis estimated) joints were calculated.

A static optimization approach was used to estimate the force in each muscle based on a criterion of minimization of muscle activation squared such that the net moments matched the experimentally derived ankle and subtalar moments.

Confidence in the model was evaluated using three criteria. First, the modeled muscle forces should result in joint moments that matched those calculated from the experimental data. Second, the model force profiles should be consistent with the EMG data. Third, the model and EMG should have responded similarly to the perturbation conditions.

RESULTS AND DISCUSSION

The model was successful in meeting the first two criteria (match joint moments and muscle forces consistent with EMG). However, there were some timing discrepancies between model activation and

EMG (Figure 1). There was general agreement in the relative magnitudes of model force and peak EMG across conditions, which supports the third criteria (Figure 1).

One interesting finding was that the soleus was a major contributor to foot supination, which is generally attributed mainly to the tibialis posterior. The soleus provided 60% of the peak supination moment about the subtalar joint. This strengthens the idea that excessive pronation of the foot may contribute to overuse injuries such as shin splints that have been associated with the origin of the soleus on the tibia.

SUMMARY

This model may be useful in examining the load sharing between the extrinsic foot muscles and allow estimation of energy absorption of muscle and tendon units. The next step in model development will be to perform a sensitivity analysis before proceeding with application to a larger population.

REFERENCES

Delp (1990). Stanford University.

Milani et al. (1995). *J. Appl. Biomech.*, **11**, 177-187.

Scott & Winter (1990), *MSSE*, **22**, 357-369.

ACKNOWLEDGEMENTS

The authors would like to acknowledge the International Society of Biomechanics, Life Fitness Corporation, and New Balance for the support of this project.

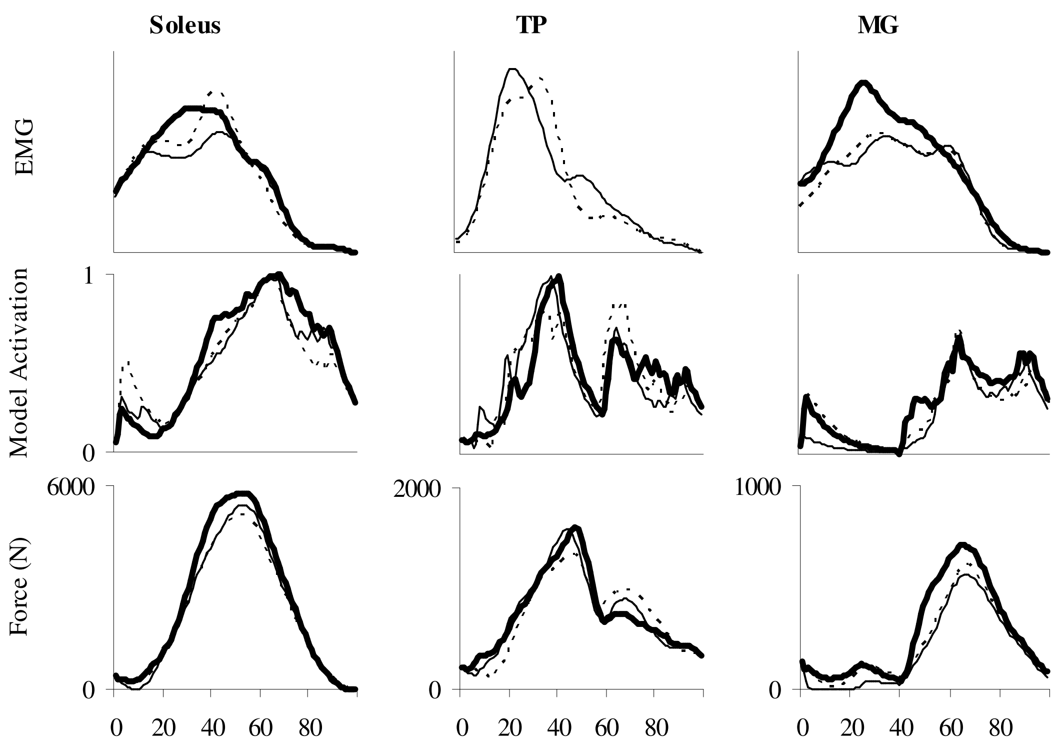

Figure 1: EMG profiles, modeled activations, and modeled forces for the soleus, tibialis posterior (TP), and medial gastrocnemius (MG) while running in each shoe condition. These muscles were the largest contributors to the joint moments. Legend: thin – varus, dashed – neutral, thick – valgus. Note: EMG profile for the tibialis posterior in the valgus shoe was not obtained. Temporal data are reported relative to percent stance.

LONGITUDINAL CHARACTERISTICS OF PLANTAR PRESSURE MEASUREMENTS OF A RUNNING SHOE

Songning Zhang, Michael Wortley, Kurt Clowers, and Charles Kohstall

Biomechanics/Sports Medicine Laboratory, The University of Tennessee, Knoxville, TN, USA
E-mail: szhang@utk.edu

INTRODUCTION

Fifteen to thirty percent of the North American population are active runners (Reinschmidt and Nigg, 2000). However, 37 – 56% of runners are injured every year (Nigg, 2001). The overall running injury rate is approximately between 25 to 75% (James, et al., 1978). Most footwear studies have concentrated on running shoes, one of the most popular recreational sports. Very few longitudinal studies of running shoes are available in the biomechanics literature (Cook, et al., 1985). Therefore, the purpose of the study was to examine longitudinal changes of plantar pressure and ground reaction force (GRF) measurements of a running shoe.

METHODS

Twenty healthy recreational male runners with no impairments to their lower extremities at the inception of the study participated in the study and nine of them completed the study.

Subjects ran in a pair of running shoes (Boston, adidas) for 400 miles and participated in five biomechanical test sessions: at 0 (beginning), 50, 100, 200, and 400 (end) miles during the study. Each subject performed five level running trials at 4.0 m/s during each testing session with simultaneous recording of sagittal and rear view kinematics (120 Hz, JVC 1980), ground reaction forces (1200 Hz, AMTI), and plantar pressure (120 Hz, Fscan). In the first test session (0 mile), each subject was asked to run in the testing shoes for 10 min on an outside track and then fill out a questionnaire immediately afterwards about the perception of comfort, fit, cushion, and stability of the running shoe. The subject was asked to fill out a weekly survey form during the study. Material properties of selected shoes were also tested using an Instron before and after the 400 miles run.

The plantar surface of the foot was divided up into six regions for data processing. The sensor area was divided into four rectangular regions based on longitudinal length: the heel region (the most posterior 30%), the midfoot region (the next 25% anterior to the heel), the ball region (the next 29% anterior to the midfoot), and the toe (the most anterior 16%). The heel and ball regions were further evenly divided into medial and lateral regions.

A one-way repeated measures analysis of variance (ANOVA) and post-hoc comparisons were performed on selected GRF and plantar pressure variables ($p < 0.05$).

RESULTS AND DISCUSSION

The subjects took an average of 17.9 weeks to complete the 400 miles. The ANOVA and post hoc comparisons showed no significant changes for the peak vertical GRF (Fmax), and maximum breaking (MaxBrk) and propulsive force (MaxProp) over the study period (Table 1). The plantar pressure data (Table 2) indicated that there was a significant increase from 0 to 200 miles, from 0 to 400 miles, and from 50 to 400 miles for the peak plantar pressure of the entire foot (PP). For the peak pressure of the toe region (Ptoe), an increase from 50 to 400 miles was significant. For the peak ball pressure (Pball), increases from 0 to 100, 200 and 400 miles were also significant. In addition, a significant increase from 0 to 400 miles was found for the peak heel (Pheel) and medial heel plantar pressure (Pmedheel). Finally, an increase from 0 to 100 miles was observed for the peak lateral heel pressure (Platheel).

Table 1. Selected GRF variables (mean ± SD).

Cond	Fmax	MaxBrk	MaxProp
0 miles	2.65 ± 0.23	-0.44 ± 0.08	0.34 ± 0.05
50 miles	2.67 ± 0.29	-0.45 ± 0.07	0.35 ± 0.05
100 miles	2.62 ± 0.27	-0.46 ± 0.11	0.34 ± 0.04
200 miles	2.69 ± 0.27	-0.45 ± 0.08	0.34 ± 0.06
400 miles	2.66 ± 0.30	-0.49 ± 0.09	0.32 ± 0.07

GRF unit is in N/kg. [a] – significantly different from 0 mile, [b] – significantly different from 50 mile, [c] – significantly different from 100 mile, [d] – significantly different from 200 mile.

Even though the GRF related variables showed no significant changes (Table 1), the plantar pressure data exhibited significant changes over the entire 400 miles of running. The peak plantar pressure of the entire foot, ball and heel regions at the 400 miles all demonstrated significant increases over the 0-mile condition (Table 2). These represent 64, 44 and 27% of increases in the peak plantar pressure for the whole foot, ball and heel regions respectively. Increases in the plantar pressure of these regions measured at some of the intermediate miles were also observed compared to the onset of the study, however, no statistical significances were found. These plantar pressure findings were supported by the results of the Instron testing. The rearfoot functional stiffness increased 39% and 11% over the reference shoes (new) for sizes of 12/12.5 and 9/9.5 respectively; the decreases in the rearfoot maximum deformation were 26% and 11% for the same two sizes. These results suggested that there was graduate deterioration in the cushioning capacity of the shoes over the run and are different from the results of the previous study (Cook, et al., 1985).

SUMMARY

We have documented a long-term profile of GRF and plantar pressure over a 400-mile run through this study. The results suggested a graduate breakdown in the cushion capacity of the running shoes from 50 – 400 miles.

REFERENCES

Cook, S. D., et al. (1985). *Am. J. Sports Med.*, **13**, 248-253.

James, S. L., et al. (1978). *Am. J. Sports Med.*, **6**, 40-49.

Nigg, B. M. (2001). *Clin. J. Sport Med.*, **11**, 2-9.

Reinschmidt, C. and Nigg, B. M. (2000). *Sportverletz Sportschaden*, **14**, 71-81.

ACKNOWLEDGEMENTS

Sponsored by adidas America, Inc.

Table 2. Average peak plantar pressure of selected plantar regions (mean ± SD).

Cond	PP	Ptoe	Pball	Pheel	Pmedheel	Platheel
0 miles	65.3 ± 25.1	69.3 ± 21.2	90.1 ± 31.5	94.0 ± 33.0	102.8 ± 34.9	84.3 ± 39.8
50 miles	62.8 ± 37.7	65.4 ± 25.6	92.1 ± 35.6	94.3 ± 49.9	102.7 ± 54.7	82.7 ± 44.3
100 miles	89.6 ± 41.8	81.1 ± 20.3	120.2 ± 38.5 [a]	108.7 ± 42.4	115.6 ± 45.2	100.3 ± 41.0 [a]
200 miles	96.7 ± 31.4 [a]	99.3 ± 47.5	133.1 ± 51.5 [a]	101.8 ± 39.5	107.0 ± 46.0	95.4 ± 41.6
400 miles	107.0 ± 56.3 [a,b]	97.4 ± 45.4 [b]	129.4 ± 66.1 [a]	119.1 ± 38.3 [a]	129.3 ± 39.5 [a]	104.0 ± 36.3

Pressure unit is in Kpa. See Table 1 for statistical comparison labels.

FOOT DEFORMITIES RESULTING FROM FORCES APPLIED TO THE TENDONS OF EXTRINSIC FOOT MUSCLES IN A CADAVER MODEL

Gregg E. Davis[1,3], James O. Sanders[6], and Stephen J. Piazza[1-5]
[1]Center for Locomotion Studies, The Pennsylvania State University, University Park, PA, USA; and Departments of [2]Kinesiology, [3]Mechanical Engineering, [4]Bioengineering and [5]Orthopaedics and Rehabilitation, The Pennsylvania State University, University Park, PA, USA and Hershey, PA, USA
[6]Shriners Hospital for Children, Erie, PA, USA
E-mail: *steve-piazza@psu.edu* Web: *www.celos.psu.edu*

INTRODUCTION

Various gait abnormalities result from inappropriate activations of extrinsic foot muscles whose principle actions are documented in standard anatomy texts. When the muscles act in combination with one another, however, decisions regarding which muscle to treat surgically become more complicated. The ability to predict the effects of spastic muscle synergies would have a profound impact on treatment decisions, but it is currently very difficult to determine these actions *in vivo*. The purpose of this study was to examine the degree of the three most common spastic foot deformities in the presence of varying levels of force applied to the tendons of the tibialis anterior, tibialis posterior, and to the Achilles tendon in a cadaver model.

METHODS

The soft tissues of six adult cadaver foot specimens (3 M, 3 F; 3 R, 3 L) were dissected 3 cm above the ankle, leaving the tendons of all extrinsic foot muscles intact. The tibia and fibula were sectioned 23 cm above the plantar surface of the foot.

Each specimen was rigidly mounted in an aluminum frame by fixing the proximal end of the tibia and allowing the foot to hang below with the tibia vertical. Steel cables were attached to the tendons of tibialis anterior and tibialis posterior and to the Achilles tendon using custom-designed clamps and sutures. The cables were routed around pulleys mounted in the frame that simulated physiological lines of action. Each cable was attached serially to a linear spring scale and an elastic cord that could be stretched and secured to prescribe individual tendon tensions.

A five-camera motion analysis system (Vicon 370; Oxford, UK) was used to record the locations of markers rigidly attached to the foot. Marker triads were fixed to the inferior aspect of the calcaneus and the medial aspect of the first metatarsal head using wood screws. An additional marker triad was attached to the aluminum frame. Homogeneous transformations between coordinate systems defined by the marker triads were decomposed into Euler angles (Craig, 1986). These Euler angles were taken to represent (a) hindfoot varus/valgus, measured with respect to ground; (b) forefoot supination/pronation, measured relative to the hindfoot; and (c) forefoot abduction/adduction, also measured relative to the hindfoot. Calculations of joint angles from marker coordinates were performed using custom-written routines in MATLAB (Mathworks; Natick, MA).

Eight loading patterns were applied in a random order to the tendons of each specimen. The loading patterns were achieved by systematically loading or unloading the three tendons of interest. The Achilles tendon was either unloaded or loaded to 100 N and tibialis anterior and tibialis posterior were either unloaded or loaded to 50 N. A greater force was applied to the Achilles tendon to reflect the larger cross sectional area of the triceps surae. One-way, repeated-measures analyses of variance (ANOVA) were performed to determine if significant differences in foot angles resulted from the eight loading scenarios. Each ANOVA was followed by Tukey mean comparison tests between individual patterns. The level of statistical significance was set at $\alpha = 0.05$.

RESULTS

Loading of the Achilles tendon was associated with levels of hindfoot varus that were significantly greater than the unloaded case (all $p \leq 0.003$) regardless of the tibialis anterior and tibialis posterior tensions (Figure 1). Tibialis posterior acting alone similarly contributed to hindfoot varus ($p < 0.001$) but tibialis anterior acting alone did not produce a significant difference in hindfoot varus ($p = 0.257$).

Tibialis anterior and tibialis posterior, acting either alone or in concert, produced significant forefoot supination relative to the unloaded case (all $p < 0.001$) (Figure 2). Addition of Achilles tendon tension did not significantly alter forefoot supination in any case (all $p \geq 0.464$). Only minimal changes in forefoot abduction-adduction were noted in any loading scenario.

DISCUSSION

These results suggest that forces transmitted by the Achilles tendon may be instrumental in producing hindfoot varus. Hindfoot varus may also result from the actions of tibialis posterior, but this effect may be masked by plantarflexor overactivity. Our results also suggest that clinicians should consider the function of tibialis posterior, as well as that of tibialis anterior, when treating patients with excessive forefoot supination. Future work will examine the effects of additional muscles that have the potential to affect foot postures, such as the peroneals.

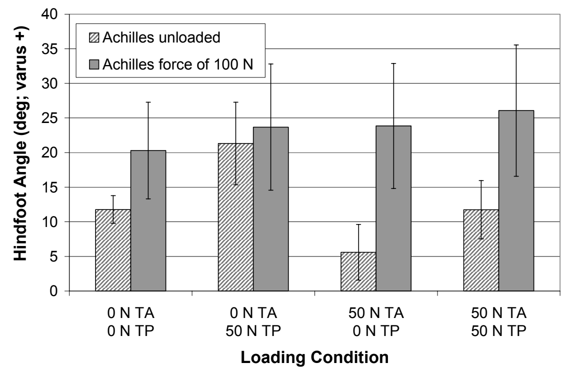

Figure 1. Mean ($n = 6$) hindfoot varus-valgus angle for all specimens at each loading condition. Error bars indicate plus and minus one standard deviation.

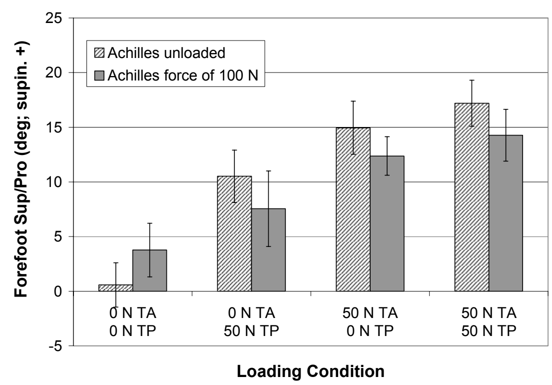

Figure 2. Mean ($n = 6$) forefoot supination-pronation angle for all specimens at each loading condition. Error bars indicate plus and minus one standard deviation.

REFERENCES

Craig, J.J. (1986) *Introduction to Robotics: Mechanics and Control.* Addison Wesley

ACKNOWLEDGMENTS

This work was supported by a grant from the Whitaker Foundation.

LOWER EXTREMITY MECHANICS BEHIND SUCCESSFUL ORTHOTIC INTERVENTION IN PATIENTS WITH ANTERIOR KNEE PAIN

Rachna Gupta[1] and Irene McClay Davis[1, 2]

[1]*Motion analysis laboratory, University of Delaware,* Newark, DE.
[1,2]*Joyner Sports Medicine Institute,* Harrisburg, PA.
Email: rachna@udel.edu

INTRODUCTION

Foot orthotic devices (FODs) have been widely used for the treatment of various running related injuries, including anterior knee pain. However, the mechanism behind their success is not yet clear.
During the gait cycle, a natural coupling of motion occurs between the rearfoot (RF) and the knee joint. Therefore, abnormal RF mechanics may cause abnormal knee mechanics and eventually lead to patellofemoral pain (PFP) (McClay et al. 1998) For example, in the frontal plane, increased RF eversion can lead to increased knee abduction (valgus) and hip adduction. In the transverse plane, increased tibial internal rotation (IR) can cause increased femoral and hip (IR). Along with increased movements, there may be an increase in the associated moments. If FODs control RF pronation, they might increase knee adduction and external rotation (ER) and hip abduction and ER.

Therefore the purpose of this study is to assess the effect of FODs on the kinematics and kinetics of the knee and the joints. It was hypothesized that in the frontal plane, FODs will increase knee adduction (PKAdd) and peak knee abduction moment (PKAbdMom) as well as decrease peak hip adduction (PHAdd) and peak hip abduction moment (PHAbdMom). In the transverse plane, it was expected that FODs will decrease peak knee internal rotation (PKIR) and peak hip internal rotation (PHIR).

METHODS

Patients reporting running-related PFP of 5/10 on visual analogue scale and demonstrating increased foot pronation, knee valgus and hip adduction and internal rotation on a single leg squat maneuver were included in the study. Patients were prescribed inverted FODs between 15-25º depending upon the degree of their malalignment. Once the subjects had accommodated to FODs for a period of at least 2 weeks, they underwent instrumented gait analysis.
Subjects were tested with and without their orthoses. Retroreflective markers were placed on their pelvis, thigh, shank and rearfoot. Subjects ran at a speed of 3.6m/s (±5%) along a 25 m runway, traversing a force plate at its center. Kinematic data were collected at 120 Hz frequency with a 6 camera VICON motion analysis system. Kinetic data were collected with a BERTEC force plate at 960 Hz. At least 10 trials were collected for each condition to obtain at least 5 good trials for analysis. The primary variables of interest were calculated from these data using MOVE3D software (NIH, Bethesda, MD). Percent changes in the variables were calculated as:

$$\%\text{Change}= \frac{[\text{NoOrth-Orth}]}{\text{Range of NoOrth Signal}} *100$$

One-tailed -dependent t-tests were conducted on each set of dependent variables with significance set at $\alpha = 0.05$.

RESULTS AND DISCUSSION

This is an ongoing study and the results for 13 subjects have been presented. The average decrease in pain with orthotic intervention was 65% (range: 30-100% range). Table 1 provides the comparison of means between orthotic and non-orthotic conditions. Overall, only the RF variables eversion excursion (EvExc) and peak eversion velocity (Evvel) were decreased, which is consistent with the literature (Smith et al.1986, Bates et al. 1979). No differences were found in the hip and knee variables, likely due to high variability in response to orthotic intervention. Figures 1-3 demonstrate the %changes in the hip and knee variables of interest. The ★ indicates when a patient exhibited a ≥15% change in the value of the variable in the hypothesized direction.

Table 1: Results for the statistical analyses on RF, knee and hip variables. ★ indicates a significant change.

Variable	Mean-NO	Mean-With	p-value
PEv	5.83	3.63	0.064
EvExc	13.68	11.69	0.005★
EvVel	229.87	216.6	0.022★
InvMom	-0.15	-0.11	0.14
PKAdd	0.87	1.21	0.39
PKAbdMom	-0.539	-0.543	0.151
PKIR	2.83	2.47	0.321
PHAdd	7.64	7.96	0.523
PHAbdMom	-1.237	-1.254	0.637
PHIR	5.957	6.707	0.277

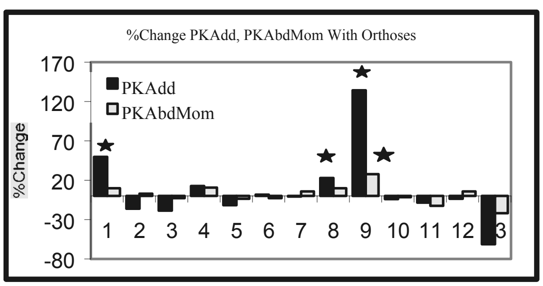

Figure 1: % Change in Peak Knee Adduction and Knee Abduction Moment with orthoses.

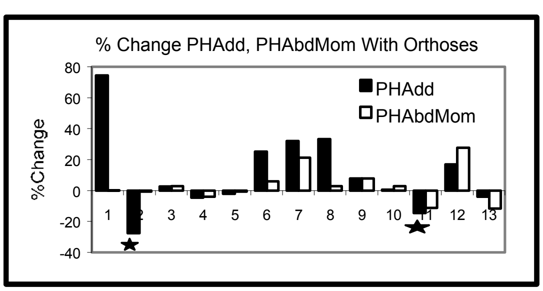

Figure 2: % Change in Peak Hip Adduction and Hip Abduction Moment with orthoses.

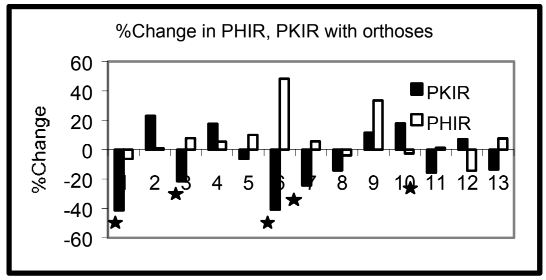

Figure 3: %Change in Peak Hip Internal Rotation and Knee Internal Rotation as a result of orthoses.

No significant changes were found in the hip and knee variables of interest. This is in contrast to a study by Eng et al. (1994) that found a surprising increase in the frontal and tranverse planes knee motion of runners with PFP during running with orthotics. However, they used standard orthotics in their study, which could have contributed to the results. In the present study, though no significant changes were observed in the knee and hip variables, it should be noted that 8 out of 13 subjects showed a ≥15% change in the expected direction in at least one of the knee and hip variables. This suggests that the mechanisms of pain reduction may be different in different subjects. As additional subjects are added more obvious trends might become evident in the data.

SUMMARY:

Inverted FODs were effective in the treatment of PFP. While FODs significantly altered RF kinematics, the mechanical response at the knee and hip were much more variable. With additional data, further trends might be noted.

REFERENCES:

1. McClay and Manal., *Clin Biomech*, 1998; **13**(3) 195-203
2. Smith, LS et al., *Podiatric Sports Medicine*, 1986; **76**(4) 227-233.
3. Bates, BT et al.. *American Journal of Sports Medicine*, 1979; **7**; 338-342.
4. Eng et al. *Physical Therapy*, 1994; **74**(9) 836-844.

ANKLE FOOT ORTHOSIS CONTRIBUTION TO NET ANKLE MOMENTS IN GAIT

Kelly McClenathan Nelson[1], Thomas M. Kepple[1], Karen Lohmann Siegel[1], Lauro S. Halstead[2], Steven J. Stanhope[1]

[1] Physical Disabilities Branch, National Institutes of Health, Department of Health and Human Services, Bethesda, MD, USA
[2] National Rehabilitation Hospital, Washington, DC, USA
E-mail: knelson@cc.nih.gov   Web: http://pdb.cc.nih.gov

INTRODUCTION

Understanding how an ankle foot orthosis (AFO) contributes to ankle joint mechanics is a basic step toward improving functional outcomes in brace design. Stiffness of traditional thermoplastic AFOs has been difficult to characterize because they tend to twist and deform differently in bench testing and walking conditions. New AFO designs and materials such as carbon fiber may deform more consistently across bench testing and walking trials. The goals of this study were to model the stiffness of a carbon fiber AFO, to demonstrate that similar deformation patterns occur during bench tests and walking conditions, and to determine the AFO contribution to net ankle moments in gait.

METHODS

The dynamic AFO investigated in this study (Advanced Prosthetics and Orthotics Inc., Encinitas, CA) (Figure 1a), is made from continuous carbon fiber and consists of semi-rigid tibial cuff and footplate components connected by two deformable posterior longitudinal struts. The material properties and the design of the orthosis limit primary deformation of the struts - characterized by rotation (θ_x) of the cuff relative to the footplate - to the sagittal plane.

The AFO stiffness was modeled as a torsional spring ($M=K*\theta_x$) during bench testing. Three reflective markers were located on both the cuff and footplate segments in order to measure displacements between two initially coincident (when $\theta_x=0$) coordinate systems. The AFO was mounted horizontally (Figure 1b) over a strain gauge force platform, (AMTI, Newton, MA) and a point force was manually applied normal to the surface of the cuff to bend the AFO struts in "dorsi-flexion" only - incrementally increasing θ_x from 2-20° for each of ten static trials. Data were collected for each trial using the force platform and a six camera Vicon 612 motion capture system (Oxford Metrics, Inc., Oxford, England). Visual3D (C-Motion, Rockville, MD) was used to calculate kinematic and kinetic variables.

Figure 1a. Dynamic AFO. **1b.** Test rig.

To compare the AFO deformation patterns, the 3D displacements of two markers located on the struts were measured in the footplate coordinate system for one bench test trial in which the brace was slowly loaded/unloaded to a θ_x of 20°, and during the walking trial.

Using the same target configuration, braced and unbraced walking trials were collected from a 66-year-old male diagnosed with post-polio syndrome. Bilateral dynamic braces had previously been prescribed to reduce the muscular strength demands of gait.

RESULTS AND DISCUSSION

Bench testing established a linear (r = 0.99) torsional spring model for the AFO with a spring stiffness (K) of -4.8 Nm/deg.

Analysis of the strut marker displacements shows that the AFO deformation patterns in both the bench test and walking conditions were very similar. The primary displacements were linear, had very similar slopes (-1.17mm/deg bench test, -1.19 mm/deg walking) with respect to θ_x, and occurred in the sagittal plane in both conditions. The deformations in other directions were very small (less than 1.5mm), non-linear, and followed similar trajectories in both conditions.

The rotations of the cuff coordinate system with respect to the footplate system about the Y and Z axes were also similar and small in magnitude in both test conditions (Table 1). These data combined with the strut displacement data show that the brace deformed in a predictable and similar pattern (primarily about θ_x) during both test conditions. Therefore, it appears valid to use the model established in bench testing to predict the moment contribution from the dynamic AFO in gait.

Table 1. Off-Axis Rotations (mean ± SD)

θ_y Walk	-1.41 ± 0.25º	θ_z Walk	-1.56 ± 0.86º
θ_y Bench	-0.44 ± 0.19º	θ_z Bench	-1.69 ± 0.98º

During one representative braced walking trial, the AFO was loaded in “dorsi-flexion” (across the interval B - D in Figure 2) to a maximum θ_x of 12°. Figure 2 shows the net braced ankle moment (Braced), the AFO only moment calculated from the model (Model), the Braced moment minus the Model moment – i.e. the contribution provided by the subject (Subject), and the net ankle moment from an unbraced walking trial (Unbraced). Compared to Unbraced walking, the Braced condition resulted in larger plantar-flexor moments during the loading period (B-C). Also, the transition from dorsi-flexion to plantar-flexion moment occurred earlier in the gait cycle in Subject than in Unbraced. In the later stages of stance (C-D), the peak moment was reduced for Subject compared to Unbraced despite a large Braced moment.

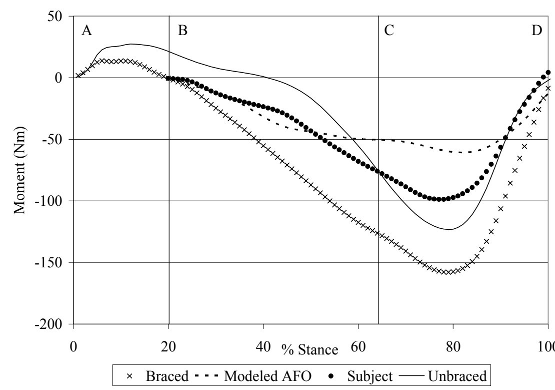

Figure 2. Ankle Moments

When comparing walking speeds for the two walking conditions, (1.22m/s unbraced, 1.14 m/s braced) minimal functional differences were noted. These data combined with the decrease in the Subject moment compared with the Unbraced moment values indicate that this AFO may benefit this subject by reducing the level of muscle activity needed to maintain the same walking speed.

CONCLUSIONS

The deformation patterns of this dynamic AFO were similar in bench and walking test conditions allowing the model created in bench testing to predict the dynamic AFO contribution to the Braced moment values. Further work is needed to establish a valid model for the entire stance phase and to develop advanced analyses that will extend our understanding of AFO contributions to limb and whole body control – ultimately improving brace design and outcomes.

Non-Parametric Analysis of the Ankle Joint in Inversion Eversion

S. Russell[1], G. Kauffman[2], and K. Granata[1]

[1] Motion Mechanics Laboratory, ESM, Virginia Tech, Blacksburg, VA, USA
[2] Motion Mechanics Laboratory, ME, Virginia Tech, Blacksburg, VA, USA
E-mail: Granata@vt.edu

INTRODUCTION

Most ankle injuries occur too quickly for reflex or higher level motor control to actively increase the stiffness of the joint by increasing muscle activation. The passive stiffness of the ankle joint contributes significantly to stability in both static and dynamic situations. Passive stiffness is able to control motion for smaller perturbations at near zero energy consumption. Knowing the most common mechanism for ankle sprains is during inversion the stiffness during inversion and eversion will be studied (Zinder 2002).

A number of investigations have studied ankle stiffness in plantar/dorsiflexion using various control schemes for force or position control (Weiss 1986, Hunter 1982, Zinder 2002). These studies modeled the ankle joint (plantar/doriflexion) as a second order system dependent on inertia damping and stiffness. The increase in mean ankle torque in axis of interest has also been demonstrated to increase the stiffness in the ankle (Hunter 1982).

It is hypothesized that an increase in plantar/dorsiflexion will result in an increased stiffness in the inversion eversion directions.

METHODS

Six subjects (five male one female) with ages ranging from 21-26, with no history of ankle injuries were selected. The subjects were asked to stand with one foot placed on a cradle, attached to a force plate, where the axis of rotation was aligned with the ankles, with each foot supporting approximately half the body weight. Three plantar/dorsiflexion ankle moments were examined; 1) subjects stood in a normal position 2) dorsiflexed the ankle until the ball of the foot was just touching the cradle 3) plantarflexed until the heel was just touching the cradle.

The cradle was actuated by a servo motor operating in a torque control mode. Torque impulses of 20 ms were applied in random directions and at random time intervals ranging from 0-500 ms (Figure 1). Input force was collected through an inline torque cell, with the position data collect using a potentiometer. The torque, position, and force plate data were all collected at 200 Hz.

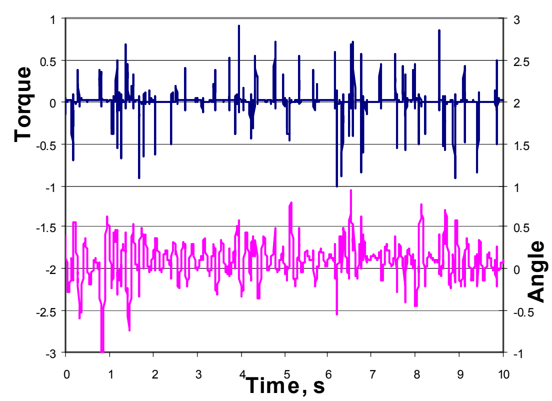

Figure 1: Torque input and resulting position Response

A non-parametric analysis was used to deconvolve the force and position data. The FFT of the resulting transfer function (impulse response) was then calculated and the peak frequency found. As the natural frequency is a direct function of the joint stiffness one is able to show an increase in stiffness by simply proving an increased natural frequency.

The transfer function of the experimental system is given as:

$$I\ddot{\theta} + \beta\dot{\theta} + \left(mL + F_z L + K\right)\theta = T$$

here I is the inertia of the system, β the damping ratio, m is the mass of the foot, L is the length from the pivot point to the center of mass, F_z body weight supported by foot, and K is the stiffness of the ankle joint in plantar/dorsiflexion. The effect of damping on the natural frequency is small so we calculate the natural frequency as:

$$\omega_n = \sqrt{\frac{mL + F_z L + K}{I}}$$

If I, m, L, and, F_z, are constant then changes in the natural frequency can be attributed to changes in the stiffness of the system.

RESULTS AND DISCUSSION

Using the testing system as described below the torque applied by the motor and the resulting position response were recorded (Figure 1). The FFT of the input and the output were then calculated in preparation for the deconvolution (Figure 2). The FFT of the applied torque has a broad

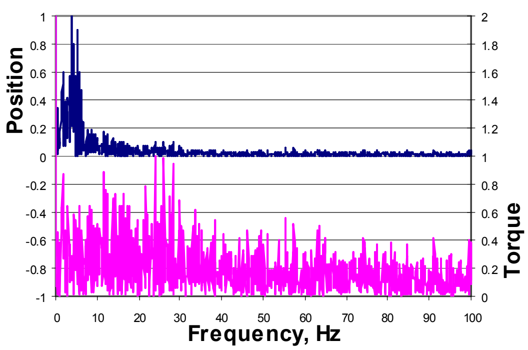

Figure 2: FFT of the input torque and the resulting position response

bandwidth of 0-100 Hz, justifying the 20 ms pulse duration used in the testing. The non-parametric analysis results in a graphical representation of the transfer function ie. impulse response (Figure 3). The FFT of the impulse response was used to determine the natural frequency of the transfer function (Table 1).

The increase plantarflexion and dorsiflexion resulted in a significant increase

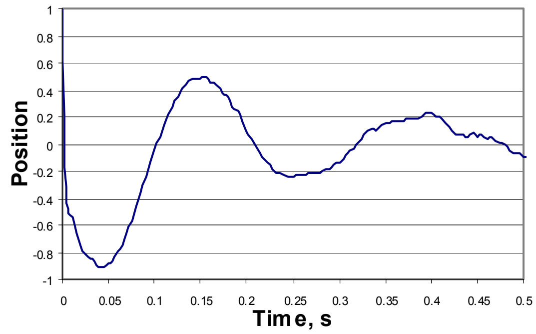

Figure 3: Transfer function (impulse response)

($p<0.05$) in the natural frequency. Based on the equations above we can conclude that the inversion/eversion stiffness of the ankle has increased with plantar/dorsiflexion moment.

Table 1: Increase in natural frequency

Subject	Ball/Neut	Heel/Neut
1	0.2333	0.0000
2	1.1667	0.1167
3	0.3500	-0.5833
4	0.8167	0.2333
5	0.4667	1.6333
6	0.7000	0.2333

SUMMARY

Although the results are based on a pilot study of six subjects the significance of the results warrants a more in depth investigation of the relationship between plantar/dorsiflexion and the increased stiffness of the ankle joint. It also validates the experimental process and data analysis method for future experiments. Results suggest plantarflexion moments as in walking or running may help to stabilize the ankle against inversion injury.

REFERENCES

Weiss. P.L.et.al.(1986). *J. Biomechanics,* **19**, 737-751.

Hunter, I.W., Kearney, R.E. (1982). *J. Biomechanics*, **15**, 747-752

Zinder, S.M. et. al. (2002). *Submitted to J. Biomech. On 10 Feb 2002*

ACKNOWLEDGEMENTS

This study was supported in part by a grant from the Carilion Biomedical Institute.

CAN NEUROMUSCULAR REFLEXES STABILIZE THE KNEE DURING VALGUS LOADING?

Yasin Y. Dhaher[1,3], Anastasios Tsoumanis[2,3], Maria Deloria-Knoll[4], W. Z. Rymer[1,2,3]
[1]Department of Physical Med. and Rehab., Northwestern University, Chicago, IL
[2]Department of Biomedical Engineering, Northwestern University, Evanston, IL
[3]Sensory Motor Performance Program, Rehabilitation Institute of Chicago, Chicago, IL
[4]Department of Prev. Med., Northwestern University, Chicago, IL
E-mail: *y-dhaher@northwestern.edu*

INTRODUCTION

We have previously shown that reflex activity mediated by periarticular tissue afferents can be elicited consistently in knee muscles by applying valgus angular perturbations to the human knee joint (Dhaher et al., 2003). Although a stabilizing role for these reflexes is widely proposed, there are as of yet no quantitative studies describing the contribution of such a system to joint stiffness in humans.

In the present study we estimated the mechanical contribution of muscle contractions mediated by periarticular tissue afferents to joint stiffness. We hypothesize that these reflex muscle contractions will significantly increase knee joint stiffness in the varus/valgus direction and enhance the over-all stability of the joint.

METHODS

Ten normal subjects (mean age 26 +/- 2 yrs; height 179 +/- 5 cm; weight 82 +/- 4.5 kgs), were tested. After securing the subject's limb in a single-degree of freedom servomotor system, the knee joint was pre-loaded (4° of valgus) to insure initial stretch of passive joint tissues (see Dhaher et al., 2003 for details). The subject was asked to maintain different knee muscle co-contraction levels as a percent of the valgus passive torque (VPT) measured at the joint's pre-loaded position with acquiescent knee muscles (η_o). The five different contraction levels were $\eta_1 \equiv$ 5-10, $\eta_2 \equiv$ 10-20, $\eta_3 \equiv$ 20-30, $\eta_4 \equiv$ 30-40, and $\eta_5 \equiv$ 40-50% of VPT measured with a six-degree of freedom load-cell (Figure 1).

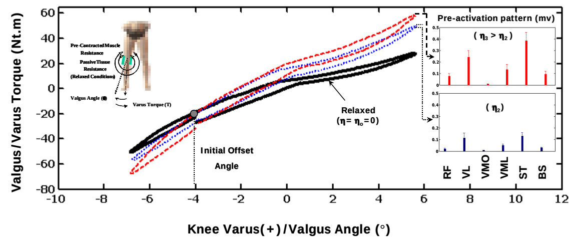

Figure 1: Torque-Angle relation in the varus /valgus direction on a representative subject.

Valgus positional perturbations were applied at the knee at 60°/s ramp speed with an amplitude of 7° (Figure 2).

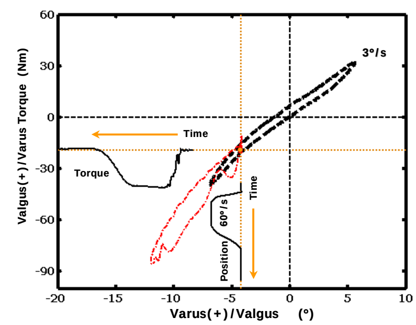

Figure 2: Torque-Angle relation with the mechanical perturbation superimposed. Note that the superimposed time-torque and time-position signals were scaled down by a factor of three. The cross plot, however, reflects the accurate amplitudes.

Surface EMG electrodes were used to record the muscle activity of knee flexor and extensors (see Figure 1). For each subject, only trials/conditions that exhibited consistent reflex response in all six muscles were used in the stiffness estimation procedure. This is to insure that stiffness estimates are due to reflexes and are not corrupted by non-reflex components.

A second order system describing the knee and lower limb musculoskeletal model was used and takes the following form:

$$
\begin{aligned}
I \cdot \ddot{\theta} &+ (B(\eta) + B_r(t \geq t_d; \eta)) \cdot \dot{\theta} \\
&+ (K(\eta) + K_r(t \geq t_d; \eta)) \cdot \theta = \mathrm{T}
\end{aligned} \tag{1}
$$

where η defines the varus/valgus torque level at the joint as a percent of VPT; t_d is the average periarticular reflex delay, estimated as the minimum reflex delay observed across all muscles for each subject (t_d ~ 70 ms, Dhaher et al., 2003) ; T is the joint's measured varus/valgus torque (output), and θ is the knee varus/valgus angle (input). In this model, the intrinsic and reflex based joint's musculoskeletal varus/valgus dynamic properties are separated and are assumed to be a function of the background varus/valgus torque. The inertia, I, stiffness, $K(\eta)$, and damping, $B(\eta)$ represent the intrinsic mechanics, including the pre-perturbation muscle contractions, contribution to the knee joint dynamics. $K_r(\eta)$ and $B_r(\eta)$ are the stiffness and damping reflex contributions, respectively. A nonlinear least squares optimization technique (Gill et al., 1981) was used to estimate a total of 5 parameters. The model was cross-validated with simulations based on fresh data not used in the estimation procedure. The linear association between K_r and $\hat{\eta} = 100 \cdot ([\eta_i - \eta_o]/\eta_o)$ was estimated using repeated measures linear regression to account for the multiple measurements taken from each subject (SAS version 8.02, Cary, NC). The method used to fit the data was restricted maximum likelihood (REML) with an unstructured covariance structure.

RESULTS AND DISCUSSION

Estimates of varus/valgus knee stiffnesses in ten subjects are shown for up to six joint valgus/varus torque levels in Figure (3-top). Reflex stiffness (K_r) was significantly greater than zero (mean=82.2 N.m/rad; 95% confidence interval: 67.7, 96.8) at relaxed condition ($\eta = \eta_o$), and increased on an average of 5.3 N.m/rad for every 10% increase in background varus torque (p = 0.015). When compared to the intrinsic joint stiffness, reflex mediated stiffness accounted for as much as 20% (mean across all subjects) of the over all joint varsus/valgus stiffness (Figure 3-bottom).

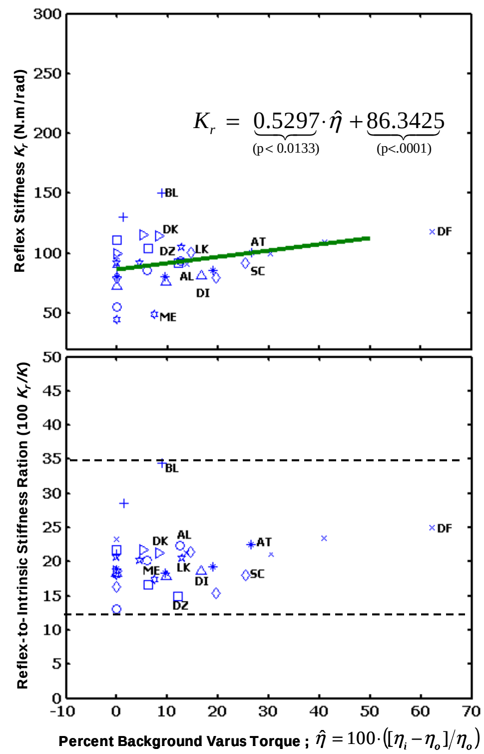

Figure 3: Reflex stiffness estimates (top) and Reflex-to-intrinsic stiffness ratio (bottom) as a function of the percent background varus torque in ten subjects.

SUMMARY

Based on our preliminary data, reflex activation of knee muscles is sufficient for active neuromuscular stabilization in the varus/valgus direction, where knee medial-lateral loading arises frequently in the course of normal locomotion (Andriacchi and Strickland, 1985).

REFERENCES

Andriacchi, T., and A. Strickland. 1985. *In* Biomechanics of Normal and Pathalogical Human Articulating Joints. **93**. N. Berme, A. Engin, and K. Correia Dea Silva, editors. 83-102.

Dhaher, Y.Y., A.D. Tsoumanis, and W.Z. Rymer. 2003. *Journal of Biomechanics*. **36**, 199-209.

Gill, P.E., W. Murry, and M.H. Wright. 1981. San Diego, CA, Academic Press.

DISTAL FAT PAD DISPLACEMENT AND ELEVATED PLANTAR PRESSURE IN DIABETIC NEUROPATHIC PATIENTS WITH TOE DEFORMITY

Sicco A. Bus [1], Ton de Lange [3], Mario Maas [2], Robert P.J. Michels [1], and Marcel Levi [1]

Departments of [1]Internal Medicine and [2]Radiology, Academic Medical Center, University of Amsterdam, The Netherlands.
[3] Fontys University for Professional Education, School for Podiatry, Eindhoven, The Netherlands
Email: s.a.bus@amc.uva.nl

INTRODUCTION

Elevated dynamic plantar pressure is as a major risk factor for plantar ulceration in diabetic feet with loss of protective sensation (Veves, 1992). Through the distal migration of the sub-metatarsal head (MTH) fat pad cushion, hyperextension (claw toe) deformity of the metatarsal phalangeal (MTP) joint has been suggested to play an important role in explaining these increased pressure levels (Ellenberg, 1968). However, objective quantitative evidence for such an association does not exist. Therefore, the aim was to assess the relationship between MTP joint hyperextension deformity, sub-MTH fat pad status and dynamic plantar pressure in diabetic neuropathic feet.

METHODS

Thirteen diabetic subjects (eight males) with peripheral sensory neuropathy and MTP joint hyperextension and 13 age and gender matched diabetic controls with neuropathy but no toe deformity were examined (Table 1). In 9 subject pairs the second ray and in 4 pairs the third ray of the foot was examined.

Table 1. Subject specific data (mean (SD))

Variable	Deformity	Controls
Age (yrs.)	56.3 (8.6)	57.2 (6.5)
BMI (kg/m^2)	27.2 (2.9)	26.4 (4.1)
DM[1] duration (yrs.)	32.8 (12.0)	31.1 (12.8)
VPT[2] (Volts)	33.5 (12.2)	36.2 (10.6)
MTP joint angle (α)	-57 (12)	-31 (6)

[1] Diabetes mellitus, [2]vibration perception threshold (>25 = indicator for neuropathy)

A 1.5 Tesla magnetic resonance imager (Siemens, Germany) was used to acquire high-resolution (512x512 pixels) T1-weighted spin-echo sagittal plane images of the metatarsal region of the foot. From these images the MTP joint extension angle was measured (Figure 1) in order to distinguish between deformed and normally aligned toes. Additionally, sub-MTH and sub-phalangeal fat pad thickness was measured.

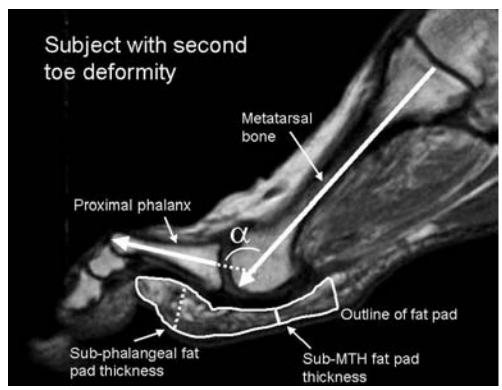

Figure 1: Assessment of MTP joint extension angle (α) and fat pad thickness in the forefoot.

Dynamic plantar pressures were measured at 70 Hz using an EMED-NT pressure platform (Novel*gmbh*, Germany). Five trials per subject using a 'two-step' gait approach were collected. From an anatomically referenced regional division of the foot (Figure 2), peak pressure (PP), force-time integral (FTI), and contact area (CA) were calculated.

All outcomes were analyzed statistically using independent t-tests (SPSS, $p<0.05$).

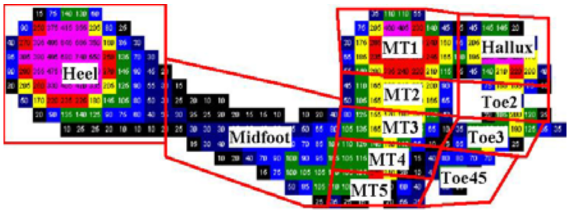

Figure 2: Schematic example of the division of the foot in 11 regions for pressure analysis.

RESULTS

Sub-MTH fat pad was significantly thinner and sub-phalangeal fat pad was significantly thicker in the subjects with toe deformity when compared to the controls (Table 2). The thickness ratio was substantially lower in the deformed feet reflecting distal fat pad displacement. Peak pressure at the MT region of interest (ROI) was significantly higher in the patients with deformity whereas PP at the toe ROI was not different between the groups. The toe-loading ratio, which is a ratio of FTI in the toes and in the MTs was significantly lower in the group with toe deformity. MT PP was significantly correlated with degree of toe deformity (α) ($r=-0.76$), sub-MTH pad thickness ($r=-0.59$) and thickness ratio ($r=-0.60$) ($p<0.005$).

Table 2: Results (mean (SD))

Variable	Deformity	Controls
Pad thickness (mm)		
Sub-MTH	2.7 (1.5)	6.3 (1.8)[b]
Sub-phalangeal	10.9 (2.4)	8.9 (1.4)[a]
Thickness ratio	0.26 (0.16)	0.70 (0.16)[b]
PP MT (kPa)	627 (236)	374 (111)[b]
PP toe (kPa)	110 (74)	145 (68)
Toe-loading ratio	0.036 (0.017)	0.072 (0.030)[b]
CA toes (cm^2)	8.1 (1.9)	12.1 (1.5)[b]

[a] $p<0.05$; [b] $p<0.005$

DISCUSSION

The results clearly show a distal migration of the sub-MTH fat pads when deformity of the MTP joint is present, which can be explained by the fact that the fat pads are physically connected to the proximal phalanges via flexor tendons and plantar ligaments (Bojsen-Moller, 1979). As a result of this migration, the fat pad lost its function as principal shock absorber of the MTHs, which was demonstrated by the significantly increased metatarsal peak pressures in the subjects with deformity. Within these interrelationships, the degree of MTP joint deformity was a strong independent contributor to elevated plantar pressure explaining 58% of its variance.

Due to the characteristic ‘cocked-up’ position of the clawed toe, the contact area of the toes during load bearing was reduced (Table 2); the toes had become less functional and as a result the MTHs bore an increased amount of weight as evidenced by a significant reduction in the toe-loading ratio in the patients with deformity. These findings confirm suggestions made by Boulton et al. (1987). Thus, while the fat tissue migrates *distally* in the foot, the load ‘migrates’ *proximally* in the foot. For diabetic patients who have lost protective sensation this is of major importance because it increases the risk for ulceration of the plantar surface of the foot. Therefore, these patients should be prescribed with adequate pressure-relieving footwear.

In conclusion, this study confirms the long held belief that MTP joint hyperextension deformity leads to a distal displacement of the sub-MTH fat pad cushion and to elevated dynamic plantar pressures in diabetic patients with neuropathy.

REFERENCES

Bojsen-Moller, F. (1979) *Clin. Orthop. Rel. Res.,* **142**, 10-18.
Boulton, A.J.M. et al. (1987). *Diabet. Med.* **4**, 225-228.
Ellenberg, M. (1968). *J Mt Sinai Hosp N Y,* **35**, 585-94.
Veves, A. et al. (1992). *Diabetologia* **35**, 660-663.

REPEATED INTELLIGENT STRETCHING OF THE SPASTIC ANKLE OF STROKE PATIENTS: PRELIMINARY DATA

Ruud W. Selles [1,2], Fang Lin [1,2], Xiaoyan Li[1], and Li-Qun Zhang [1,2]
[1] Rehabilitation Institute of Chicago, Chicago, IL, USA
[2] Northwestern University, Chicago, IL, USA
E-mail: rselles@northwestern.edu Web: http://p3.smpp.northwestern.edu/

INTRODUCTION

Spasticity and contracture are major sources of disability in stroke patients, disrupting the remaining functional use of muscles and impeding motion. Spasticity may cause severe pain and result in a reduction in joint range of motion (ROM), clinical contracture, and muscle weakness (Rymer and Katz, 1994). While controversial, many investigators believe that changed joint properties in spasticity not only result from hyperactive stretch reflexes, but also from non-reflex changes like structural changes of muscle fibers and connective tissue.

Physical therapy treatment for most spastic ankles may involve manual stretching of a joint with the intent of restoring movement and reducing spasticity and contracture. However, this therapy is labor intensive and strenuous, while the amount of force used may differ between therapists. We have developed a device to stretch the spastic ankle to its extreme positions with accurate control of the stretching torque and velocity (Zhang et al., 2002). The purpose of this study was to investigate biomechanical changes over multiple sessions of stretching treatment of the spastic ankle in stroke.

METHODS

The spastic ankle of a 69 years old male stroke patient with severe spasticity in his left ankle due to a cerebrovascular accident in October 1999 (Ashworth scale 3, tendon reflex scale 3) was stretched during 7 sessions of 45 minutes with 2 or 3-day intervals.

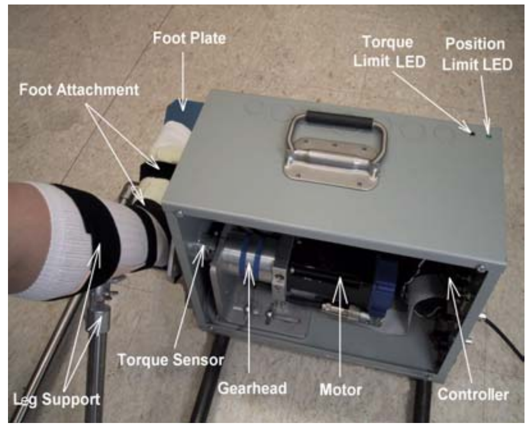

Figure 1: Intelligent ankle stretcher.

The treatment and evaluation were done using a custom-designed ankle stretching device (fig 1). The ankle was stretched to extreme dorsal and plantar flexion by a servomotor controlled digitally based on position, velocity and torque feedback. More specifically, the stretching velocity was inversely proportional to the resistance torque, stretching the ankle at higher speed when the resistance torque was small and slowing down near extreme dorsal flexion (DF) or plantar flexion (PF) positions until predefined torque limits were reached. At the extreme positions, the joint was held for several seconds before the stretching direction was reversed.

RESULTS AND DISCUSSION

Figure 2 shows angle and torque during two stretching trials, allowing maximally 5 and 10Nm resistance torque in both directions. Velocity of stretch was high in the middle ROM, and slowed down when resistance torque increased. It was found that the range of motion was significantly larger at 10Nm than at 5Nm, suggesting that this passive range was not limited by bony structures but by resistance due to stretch of the spastic muscles. Overall, the maximal resistance torque allowed in this subject during the treatment was 10Nm in PF direction and 20Nm in DF direction.

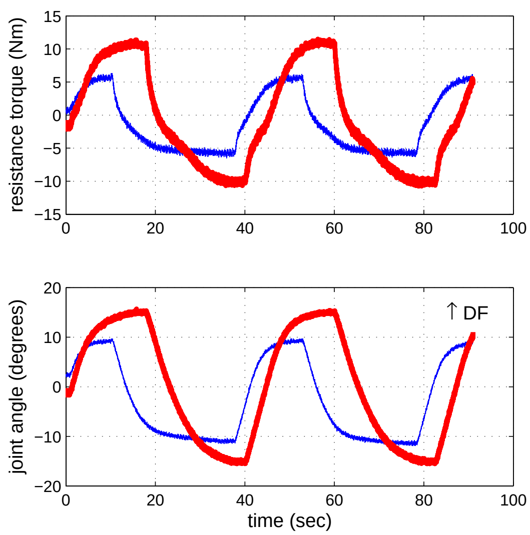

Figure 2: Joint torque (positive corresponds to a resistance torque in PF direction) and angle and during two stretching trials allowing maximally 5 (blue line) and 10Nm (thick red line) resistance torque.

The angle-torque curves of similar stretching sessions as in Figure 2 are shown in Figure 3. It can be seen that the ankle moved further into DF before 5Nm resistance torque was measured. Figure 3 illustrates the general finding that after 2 weeks of stretching, the joint ROM was changed considerably under the same amount of torque, indicating that the joint became less stiff.

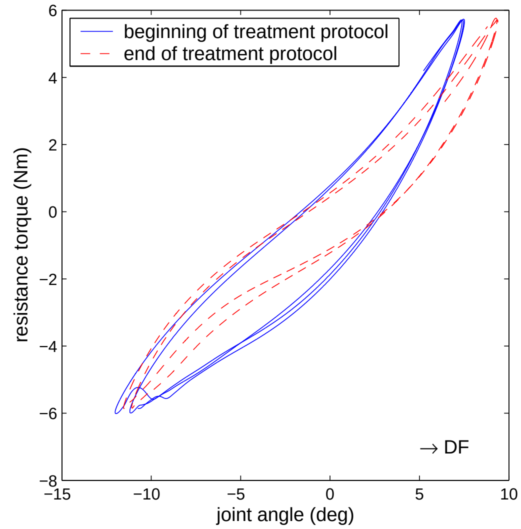

Figure 3: Angle-torque curve of stretching session at the beginning (blue line) and end (red dotted line) of a two-week period. Maximal resistance torque of 5 Nm was allowed in each direction in these trials.

SUMMARY

Preliminarily data of a study stretching the spastic joints of stroke patients using an intelligent stretching device were shown, suggesting positive effects in terms of range of motion and joint stiffness. Evaluation of more subjects in this study is needed to further validate the device and the treatment.

REFERENCES

Rymer, W. Z. and Katz, R. T. (1994) *Physical Medicine and Rehabilitation: State of the Art Reviews,* **8,** 441-454.

Zhang, L.-Q., Chung, S. G., Bai, Z., van Rey, E. M., Rogers, M. W., Johnson, M. E. and Roth, E. J. (2002) *IEEE Trans. Neural System Rehab. Eng.,* **10,** 149-157.

ACKNOWLEDGEMENTS

The authors acknowledge the supports of the National Institute of Disability and Rehabilitation Research and NIH.

INTER-MARKER DISTANCE CHANGES AT THE FOOT DURING THE STANCE PHASE OF WALKING

Arik S. Wiest, Shing-Jye Chen and Li-Shan Chou

Department of Exercise and Movement Science, University of Oregon, Eugene, OR
E-mail: chou@oregon.uoregon.edu

INTRODUCTION

In gait analysis there is neither standard nor reliable method for dynamic measurements of the foot (Carson 2001). Movement analysis is contingent upon marker locations being rigid to underlying bony landmarks. Markers attached to a segment, however, may not always represent true skeletal locations. The use of stereophotogrammetry for motion analysis is therefore limited by experimental errors associated with skin marker movement artifact. An increased understanding of the factors that influence skin movement artifact will assist kinematic investigations at the foot.

General trends in regard to skin movement artifact do exist. A static radiograph study shows the largest relative movements on the proximal markers (malleoli, calcaneus and navicular) and the smallest relative movements on the most distal markers (metatarsals) (Tranberg, 1998). Dynamic bone pin studies show a general overestimation of joint motion using superficial markers versus bone-anchored markers throughout the stance phase of walking (Westblad 2002). These bone pin studies also agree with static studies in that larger relative movements exist at the more proximal markers than the distal markers (Cappozzo 1996).

Current research addressing absolute measurement errors due to skin movement artifact have relied upon invasive techniques (static and dynamic studies) that may not be available in every gait laboratory. Multiple markers are needed to define motion of a rigid body segment. A better understanding of relative movement occurring at markers placed on the same body segment could provide an alternative assessment on skin movement artifact. The purpose of this study was to quantify changes in inter-marker distances at a foot between quiet standing and walking during different periods of the stance phase.

METHODS

Seven healthy young adults, including six males and one female (mean age, 24.9 ± 3.2 years) were recruited for this study. Nine 8-mm superficial skin markers were placed on the foot to create a rearfoot (3 markers), midfoot (3 markers) and forefoot (3 markers) regions (Fig. 1). Kinematic data was collected at the foot from each subject using a six-camera ExpertVision^{TM} system (Motion Analysis Corp., Santa Rosa, CA) during a double support static standing and 6 trials of level walking. Subjects were asked to walk with barefoot at a comfortable self-selected speed.

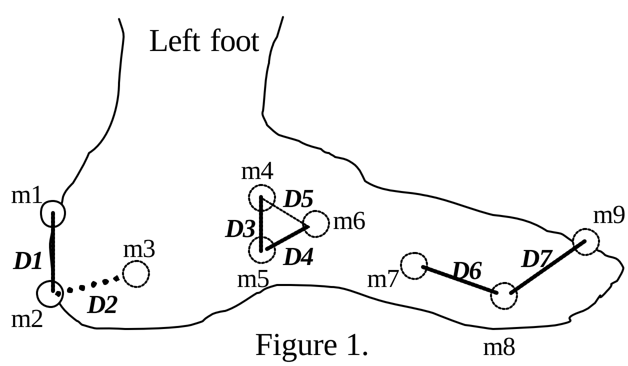

Figure 1.

Seven inter-marker distances were calculated from both standing and walking trials. Distances from the static trial was used as the baseline for comparison to those of dynamic walking trials. The seven inter-marker distances D1~ D7 (see Figure 1) were: D1: top-down calcaneus, D2: down-lateral calcaneus, D3: top-down navicular, D4: down-front navicular, D5: top-front navicular, D6: 1st metatarsal base – 1st metatarsal head, and D7: 1st metatarsal head – 5th metatarsal head. The stance phase was divided into 3 intervals: early stance (P1, heel strike to foot flat), mid-stance (P2, foot flat to heel off), and late stance (P3, heel off to toe off). Any changes from static measurements, whether by shortening (+) or elongating (-), was reviewed for each inter-marker distance and expressed as a percent change. A 2 x 3 within-subjects ANOVA was used to test for type of activities or stance phase effect on inter-marker distances.

RESULTS AND DISCUSSION

Table 1 summarizes findings for each inter-marker distance throughout each activity and period of the stance phases.
The 1^{st} metatarsal head to base (D6) and 1^{st} – 5^{th} metatarsal head (D7) both demonstrated significant simple main activity effect on the inter-marker distance changes during early and late stance (p < .05). The top-down calcaneus (D1), 1^{st} metatarsal head to base (D6), and 1^{st} – 5^{th} metatarsal head (D7) all demonstrated significant changes in inter-marker distance changes throughout all three intervals of the stance phase (p <.05). No significant changes were found in inter-marker distances of the down-lateral calcaneus (D2) and three distances calculated from navicular markers (D3, 4, and 5).

During early stance, the inter-marker distance of the rearfoot (D1) was shortened as well as those of the forefoot (D6 & 7). During the late stance, the rearfoot (D1) marker distance was significantly elongated. The forefoot marker distance (D6) become shorter compared to the distance measured during early stance, however the D7 was elongated.

SUMMARY

Our results demonstrate distal markers (forefoot) are affected most during walking by skin movement which is opposite to a static radiograph study (Tranberg, 1998). Significant activity effects (standing vs. walking) were only identified for inter-marker distances at the forefoot during early and late stance.

REFERENCES

Cappozzo et al. 1994. *Clinical Biomechanics*, 11(2): 90-100

M.C. Carson et al. 2001. *Journal of Biomechanics*, 34: 1299-1307

R Tranberg, D Karlsson. 1998. *Clinical Biomechanics*, 13(1): 71-76

Westblad et al. 2002. *Foot & Ankle International*, 23(9): 856-863.

Table 1: Means (Standard Deviation) of % Inter-maker Distance Change during The Stance Phase. '+': shortening; '-': elongating.

	Rearfoot region		Midfoot region			Forefoot region	
Period	D1[a]	D2	D3[a]	D4	D5	D6[a]	D7[a]
I	3.04 (4.21)[c]	1.58 (2.10)	-4.19 (9.86)	1.76 (5.70)	2.50 (6.26)	2.15 (2.23)[b c]	6.54 (0.78)[b c]
II	0.21 (4.21)[c]	1.63 (2.09)	-2.64 (8.50)	0.86 (7.01)	3.26 (6.86)	0.90 (2.30)[c]	0.74 (2.05)[c]
III	-3.23 (4.02)[c]	0.33 (1.03)	-0.48 (7.36)	1.88 (8.72)	3.86 (6.39)	4.18 (2.39)[b c]	2.96 (1.24)[b c]

[a] Significant activity x phase interaction effect. [b.] Significant simple main effect for the activity within phases.
[c.] Significant simple main effect for the interval within activities. N = 7 subjects. p < .05.

A NOVEL ARCH HEIGHT INDEX MEASUREMENT SYSTEM (AHIMS): INTRA- AND INTER-RATER RELIABILITY

CJ Richards[1], K Card[1], J Song[1], H Hillstrom[1], R Butler[2], IM Davis[2]
1. Temple University, School of Podiatric Medicine, Philadelphia, PA, USA
2. University of Delaware, Newark, DE, USA
Corresponding Author, crichards@tuspm.temple.edu

INTRODUCTION

The purpose of this study was to demonstrate the intra- and inter-rater reliability of the Arch Height Index Measurement System (AHIMS).

Assessment of the longitudinal arch of the foot has long been recognized as an important parameter in the classification of foot type. It has implications in research, as well as in the clinical prediction and treatment of pathology. Due to varying degrees of repeatability and reliability however, no single method or definition has been accepted as the standard for arch assessment. Saltzman et al reported that a clinically measured ratio of navicular height to foot length could yield reliable approximations of arch structure that closely correlate to radiographic reports. Using a different approach, Williams et al demonstrated reliability for measurement of dorsum height divided by truncated foot length across multiple loading conditions. While each method was found valid and repeatable, the above studies relied upon tester ability to locate and measure an exact anatomical landmark and did not account for all foot architectures.

Recently, the AHIMS was developed and proven to be highly intra-rater reliable by Richards et al. Initial testing involved repeated measures of select foot parameters at several loading conditions and postures using the AHIMS. This helped to identify which measurement values are most pertinent to arch height assessment. From these findings, two ratios were defined. The Arch Height Index, similar to how Williams et al described it, is determined as the ratio of Arch Height to Truncated Foot Length. The Arch Rigidity Index is formed as a ratio of the Arch Height Index during standing to the AHI during sitting. Values nearer to 1 indicate a stiffer (less flexible) foot.

The current study expands upon the previous, and demonstrates a clinical method that is reliable between labs, to objectively quantify the structure and function of the longitudinal arch for all foot types.

METHODS

To evaluate the intra- and inter-rater reliability of the AHIMS, 22 feet (the right and left foot of 11 subjects) were measured twice each by two raters, one from Temple University (TU), and one from University of Delaware (UD). Utilizing the AHIMS, measurements of total foot length (FL), truncated foot length (TFL), and arch height (AH) were made in the sitting condition (loading the foot to ~10% body weight) and standing condition (~50%bw).

- To measure arch height, a horizontal bar, in the frontal plane, was suspended at one half the total foot length from the heel. The bar was then lowered, allowed to rest with its own weight on dorsum of the foot. The height, with respect to heel and forefoot height, was recorded.

• The effect of foot elongation during load bearing was addressed by recording truncated foot length during both the sitting and standing condition.
• To account for extremely flexible feet, weight-bearing measurements were recorded with the mid-foot unsupported (removing the middle third of the floor support from beneath the foot).

RESULTS AND DISCUSSION

The AHIMS was evaluated for inter- and intra- rater reliability. ICC values were calculated within and between raters and, through all parameters polled, measurements were found to be highly repeatable, as is evident in Tables 1 and 2.

The Arch Height Index and Arch Rigidity Index have implications on foot type assessment. By objectively assigning a value to arch height and foot rigidity, a valuable characterization is made. This classification may influence orthotic design, taping styles, and footwear choices, as well as allow for further foot-type identification. This knowledge may also allow the clinician to better diagnose and treat patient pathology.

At present, a multi-site study is being conducted to determine normative Arch Height values, and to correlate these with other accepted and proven parameters of foot type.

SUMMARY

A portable, intuitive, low-maintenance instrument for quantification of the arch height was designed and built. The intra- and inter- rater reliability was tested, and the device was found to be highly reliable. Two parameters were developed to quantitatively assess arch height as a characteristic of foot type. The Arch Height Index evaluates normalized arch height, and the Arch Rigidity Index indicates foot flexibility.

REFERENCES

Denegar, C.R., Ball, D.W. (1993). *J. Sport Rehabil*, **2**, 35-42

Richards, C.J. et al (2003). Pres. at the 6th Symp. on FootWear Biomech., 07/03-05.

Saltzman, C.L et al (1995). *Arch Phys Med Rehabil*. **76**, 45-49

Williams, D.S., McClay I.S. (2000). *Phys Ther.* **80**, 864-871

Table 1.	**FL (10%BW)**		**Truncated FL (10%BW)**		**Arch Height (10%BW)**		**Arch Height (50%BW)**	
Locations Polled	TU	UD	TU	UD	TU	UD	TU	UD
Average (mm)	25.2	25.2	18.4	18.4	6.8	6.7	6.5	6.5
ICC(2,1)	0.914	0.997	0.961	0.963	0.961	0.953	0.955	0.949
ICC(2,k)	0.999		0.989		0.989		0.992	

Table 2.	**AH(10)/TFL(10)**		**AH(50)/TFL(10)**	
Locations Polled	TU	UD	TU	UD
Arch Height Index	0.371	0.367	0.351	0.353
ICC(2,1)	0.806	0.877	0.832	0.919
ICC(2,k)	0.977		0.983	

Tables 1 and 2. Arch Height Measurement: Conditions polled and their inter/intra rater correlation values.

A VALIDATION OF 1-D and 2-D DESCRIPTIONS OF FOOT TYPE USING 3-D COMPUTERIZED TOMOGRAPHY DERIVED ANGULAR MEASUREMENTS

William R. Ledoux [1,2,3], Eric S. Rohr [1], Randal P. Ching [1,3], Bruce J. Sangeorzan [1,2]

[1] RR&D Center for Excellence in Limb Loss Prevention and
Prosthetic Engineering, VA Puget Sound, Seattle, WA, USA
Departments of [2] Orthopaedics and Sports Medicine, and
[3] Mechanical Engineering, University of Washington, Seattle, WA, USA
Email: wrledoux@u.washington.edu Web: www.seattlerehabresearch.org

INTRODUCTION

Foot type is an architectural concept in which feet are categorized as pes cavus (high arch), neutrally aligned (normal arch) or pes planus (low arch). Often, foot type determination is based on clinical examination or on an arch index (*i.e.*, a measure of arch height based on the shape of the contact area of the foot). These measures are typically 1-D or 2-D and may have a subjective component. Furthermore, there is no universally accepted gold standard. Our group has developed a 3-D objective means of quantifying foot type based solely on the angular relationships between coordinate systems embedded in the foot bones (Camacho *et al.* 2002; Rohr *et al.* 2003). These coordinate systems are generated from weight-bearing computerized tomography (CT) scans. The purpose of this research was to use the Euler angle relationships from the CT scans to validate several accepted 1-D and 2-D measures of foot type.

METHODS

Subjects were recruited from the VA Puget Sound and the University of Washington medical centers. The inclusion criteria were: self-ambulation, between the ages of 18 and 75, and having either a pes cavus, neutrally aligned or pes planus foot type. The exclusion criteria were a current foot ulcer or partial foot amputation. Foot type was determined via clinical examination by an orthopaedic surgeon and verified with radiographic measurements. Enrolled subjects had a weight-bearing CT scan of their feet. The CT data were used to develop an embedded coordinate system for each foot bone by assuming uniform density and calculating the inertial matrix (Camacho *et al.* 2002; Rohr *et al.* 2003). Euler angles were calculated between several of the bones, including the talus-1st metatarsal (Tal-1st Met) (Figure 1) and the calcaneus-talus (Calc-Tal). For both relationships, the alpha, beta and gamma angles represented motion approximately in the frontal, transverse and sagittal planes, respectively. The CT data were also used to calculate the height of the navicular (the distance from the navicular tuberosity to ground). The subjects also had their feet scanned while they stood on an acrylic frame over a digital scanner. These scanned images were employed to calculate two arch indices (Cavanagh and Rodgers 1987; Staheli *et al.* 1987). An analysis of covariance (ANCOVA) was used to determine if the Euler angles, navicular height and arch indices differed between foot types and Fisher's Protected Least Significant Difference was used for post hoc analysis.

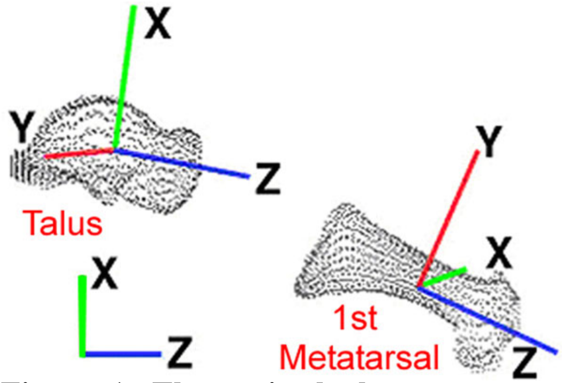

Figure 1: The sagittal plane relationship of the talus and 1st met.

RESULTS

There was no significant difference in age between the foot types, however, BMI was significantly less for the neutrally aligned feet. Therefore, all remaining calculations were adjusted for BMI. The navicular height measurement and both the arch indices were significantly different between all three foot types. The Euler angle relationships were also significantly different between foot types. In particular, there were significant differences between all foot types for the transverse and sagittal (beta and gamma) relationships between the talus and 1st metatarsal. Additionally, each of the calcaneus - talus angular relationships discriminated between foot types.

DISCUSSION

The Euler angle relationships presented in this study are 3-D, objective descriptions of foot shape. For our limited data sample (*i.e.*, 5 pes cavus feet) the significant differences between foot types for various 3-D measures demonstrates that these feet are structurally distinct. These data were used to validate the classification of foot type based on other 1-D or 2-D measures of foot type, namely navicular height and the arch indices developed by Cavanagh and Staheli. Thus, these other measures of foot type are able to distinguish between foot types.

ACKNOWLEDGEMENT

Department of Veterans Affairs project no. A2180R. We would like to thank Glenn Lee for help with the data analysis.

REFERENCES

Camacho, D. L. A., Ledoux, W. R., et al. (2002). *J of Reh Res & Dev* **39**(3): 401-10.

Cavanagh, P. R. and Rodgers, M. M. (1987). *Journal of Biomechanics* **20**(5): 547-51.

Rohr, E. S., Ledoux, W. R., et al. (2003). *49th ORS*, New Orleans, LA.

Staheli, L. T., Chew, D. E., et al. (1987). *J Bone Joint Surg [Am]* **69**(3): 426-8.

Table 1: Age, BMI, as well as 1-D, 2-D and 3-D measures of foot type.

	pes cavus (n=5)	neutral (n=18)	pes planus (n=14)	p-value	post-hoc
age (years)	40.6 ± 6.07	48.2 ± 6.00	46.4 ± 8.19	0.1085	na
BMI	33.7 ± 8.52	27.5 ± 3.70	32.7 ± 6.13	0.0168	cavus v neut., neut. v planus
navicular height (mm)	59.6 ± 9.81	44.9 ± 4.99	35.3 ± 7.07	< 0.0001[a]	all 3
Cavanagh Arch Index	0.263 ± 0.057	0.298 ± 0.034	0.342 ± 0.024	0.0002[a]	all 3
Staheli Arch Index	1.274 ± 0.136	1.052 ± 0.211	0.819 ± 0.078	< 0.0001[a]	all 3
Tal-1st Met alpha	-75.3 ± 20.4	-90.3 ± 11.6	-88.2 ± 13.7	0.1533[a]	na
Tal-1st Met beta	42.5 ± 21.6	-5.19 ± 9.08	-17.3 ± 5.50	< 0.0001[a]	all 3
Tal-1st Met gamma	23.8 ± 10.7	14.0 ± 5.92	0.45 ± 4.55	< 0.0001[a]	all 3
Calc-Tal alpha	-11.3 ± 7.66	-21.1 ± 9.29	-31.2 ± 15.9	0.0044[a]	cavus v planus, neut. v planus
Calc-Tal beta	-17.5 ± 11.4	-34.5 ± 5.23	-38.1 ± 6.01	< 0.0001[a]	cavus v neut., cavus v planus
Calc-Tal gamma	-23.7 ± 9.23	-24.1 ± 7.56	-14.8 ± 11.4	0.0364[a]	neut. v planus

[a] adjusted for BMI

BIOMECHANICAL FAILURE IN IMMATURE SPONDYLOLYTIC SPINE: LOAD-DISPLACEMENT BEHAVIOR OF CALF SPINE MODEL IN SHEAR

Koichi Sairyo [1], Vijay Goel [2], Shinsuke Katoh [1], Natsuo Yasui [1]

[1] Department of Orthopedics, University of Tokushima, JAPAN
[2] Department of Bioengineering, University of Toledo, OH, USA
E-mail: Vijay.Goel@utoledo.edu

INTRODUCTION

Slippage in patients with spondylolysis occurs mostly during the growth period and is rare afterward [1]. It was hypothesized that forward slippage in the pediatric population happened due to epiphyseal separation [2]. Our *in vitro* and *in vivo* investigations also lend support to this hypothesis [3,4,7,8]. However, the literature on the biomechanics of immature spondylolytic spines, especially in terms of kinematics, is sparse [5].

The purpose of this study was to investigate the effects of spondylolysis on the lumbar kinematics under anterior shear forces until failure.

METHODS

Three immature calf whole spines were harvested, and stored at –20° Celsius. The spines were separated into functional spinal units (FSUs) and ten ligamentous FSUs were obtained. The FSUs were randomly assigned into two groups; with (WD) or without pars defects (WOD). In the WD group, bilateral pars defects to the rostral vertebra of each FSU were created. An MTS machine (Test Star IIs, MTS Systems Corporation, MN), was used to apply anterior-posterior (AP) shear forces to the specimen as described elsewhere [3]. The AP shear force was applied at a rate of 25.0 mm/min until failure. The load-displacement curve for each specimen was recorded. From the load-displacement curve, initial rigidity, failure load and ultimate displacement at failure were calculated. The site of failure was confirmed radiographically.

RESULTS

The load displacement curve in WD showed single peak-pattern. The initial rigidity was 155.5 +/- 20.3 (N/mm), and it failed through the growth plate of the vertebral body (see figure 1) with displacement of 6.8 +/- 0.3 (mm). The corresponding ultimate strength was 734.1+/-65.3 (N). On the other hand, the curve in WOD group showed two peak-pattern. When the cranial vertebra displaced forward, the facet joints contacted and the strength became high. At this time, the initial rigidity was 225.3 +/- 22.3 (N/mm). Then, the facet joint dislocated at the displacement of 3.5 +/- 0.5 (mm) with the ultimate strength of 964.0 +/- 87.1 (N). With further displacement, the anterior shear force was applied to the anterior component like the WD group. Therefore, the second peak was derived due to resistance from the

anterior components of the segment.
The FSU failed through the growth plate of the vertebral body (as shown in figure 1) with displacement of 7.2 +/- 0.5 (mm). The corresponding ultimate strength was 750.5 +/- 72.3 (N).

Table 1. Biomechanical Parameters

		WOD	WD
	Initial	1st peak	2nd peak
Stiffness	155.5	225.3	
Strength	734.1	964.0	750.5
Displacement	6.8	3.5	7.2

DISCUSSION and CONCLUSIONS

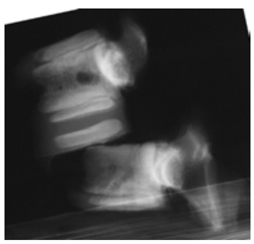

Figure 1. A calf spine after failure.

Slippage of spondylolytic spine is highly prevalent during the growth period. It has been widely considered that the pathogenesis of slippage is disc degeneration. However, if its pathogenesis is disc degeneration, the incidence of slip may increase with age since degree of degeneration is related to age. Thus, the plausible hypothesis could be that the pathogenesis of isthmic spondylolisthesis in children is due to the fracture of the physis [2]. Biomechanically, we clarified that the growth plate of vertebral body was the weakest-link under the anterior shear force as shown in the figure [3]. Furthermore, we created *in vivo* immature rat model producing vertebral slippage through the growth plate [4]. For the next step, we needed to clarify how kinematics changes or how mechanical stress concentrates in the pediatric lytic spine. In this study, the load-displacement behavior was shown to be different in the spine with or without pars defects. Under anterior shear load, facet joints protect the intact spines from failure; whereas, in the spondylolytic spine anterior spinal components support the entire load. Accordingly in the present study, the anterior components including growth plate would always be loaded and stressed in the shear mode; indicating biomechanical failure in the lytic spine. The previous FEM analysis also indicated the biomechanical failure in the lytic spine by predicting that about 90% of mechanical stress was concentrated at the growth plate in immature lytic spine under anterior shear stress [6].

Based on the results from the previous and present studies, we hypothesize the pathomechanism of slippage in pediatric spondylolysis as follows. First, spondylolysis changes kinematics of spine leading to stress concentration at the growth plate. Then, physis stress fracture occurs at the vertebral body, and finally cranial vertebral body slips forward through the growth plate after the physis separation.

REFERENCES

1. Sairyo K, et al.(2001). Spine J **1**: 171
2. Farfan H, et al.(1976). CORR **117**: 40
3. Sairyo K, et al.(1998). Spine **23**: 1442.
4. Sairyo K, et al.(2002). Proceedings of ISSLS. **113**.
5. Goel V, Weinstein J(1990). CRC Press.
6. Konz R, et al.(2001). Spine **26**: E38.
7. Sairyo K, et al.(2003). JNS **98**: 288.
8. Sairyo K, et al.(2003). Am J Sp. Med.

THE EFFECT OF *rh*BMP-2 ON ALLOGRAFT UNION AND REMODELING IN A CORPECTOMY MODEL

[1, 2]Mahar AT; [2]White KK; [2]Bawa M, [3]Ahn JS, [?]Farnsworth CL; [2]Faro FD; [1]Oka RS; [1]Wedemeyer MA; [?1,2]Newton PO; [2]Garfin SR;
[1]Children's Hospital & Health Center – San Diego, San Diego , CA; [2?]University of California San Diego, San Diego, CA; [3]Chungnam National University, Daejeon, Korea
amahar@chsd.org

INTRODUCTION

Anterior corpectomy with instrumentation and fusion is common in the treatment of fractures, tumors, infections, and kyphotic deformities of the thoracic and lumbar spine. Both autogenous as well as allogenous strut grafts are utilized in the reconstruction. One of the advantages of autogenous bone is thought to be the endogenous cells and growth factors present within the graft to promote union. Recombinant human BMP-2 (*rh*BMP-2) in a collagen matrix has been evaluated as a means of increasing the likelihood of arthrodesis in an interbody (single motion segment) allograft reconstruction. However, we are unaware of similar studies of cortical strut allograft healing after vertebral corpectomy. The purpose of this study was to evaluate healing and incorporation of strut allografts after lumbar corpectomy, and to evaluate the use of *rh*BMP-2 to augment graft union and remodeling.

METHODS

This study was approved by the Animal Subjects Committee and complies with all regulations for the humane treatment of animals. Sixteen calves (age 3 weeks) underwent L3 corpectomy and strut allograft reconstruction. Tibial allografts were harvested from 4 additional animals and stored at 0°C prior to implantation. *rh*BMP-2 impregnated collagen sponges were placed to fill the empty medullary canal of the allograft in eight animals (5-6 sponges per graft, 0.6mg/sponge). Eight "control" animals had the allograft filled with autogenous cancellous bone from the excised vertebral body. The graft was stabilized with an ATL Z plate (Medtronic Sofamor Danek, Memphis, TN) construct between L2 and L4. The average length of the allograft strut was 36 ± 3 mm. The procedures were performed in an alternating order between groups. After a four-month survival period, the lumbar spines were harvested en bloc from L2-L4 for radiographic and biomechanical evaluation. Computed tomographic (CT) spiral scans were obtained with 1 mm cuts. Coronal and sagittal reformatted images were also obtained and evaluated for the presence or absence of strut allograft union. Contact radiographs were made during histological evaluation for evaluation of fusion quality and bone remodeling (Figures 1A/1B).

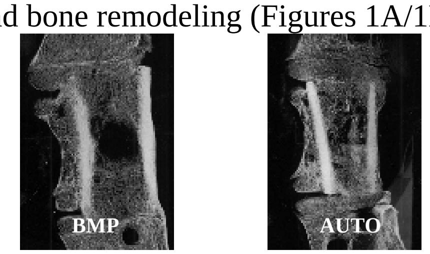

Figures 1A/1B: Contact radiography for use in assessment of fusion/remodeling.

Digital transverse CT images underwent image analysis (Scion Image software, NIH) to determine the volume of bone within the inner borders of the allograft strut. Greyscale thresholds for normal vertebral cancellous bone within each body were used to determine the volume percentage of bone present in sequential CT slices within the allograft (Figure 2).

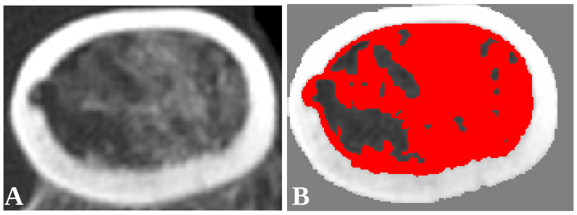

Figure 2(A): CT scan showing mid-graft section of autograft specimen in greyscale. (B) Red region represents "bone area".

Six spines from each group were mounted in an MTS 858 Mini-bionix biaxial testing machine (MTS Systems, Eden Prairie, MN) for biomechanical evaluation. Non-destructive testing of the spines in flexion (5 Nm), extension (5 Nm), lateral bending (5 Nm) and torsion (5 Nm with 100 N axial load) was performed. Ultimate load to failure was assessed by a single torsional loading test (0.5 deg/sec). Range of motion and stiffness were measured for the cyclic tests, while stiffness and ultimate failure torque were measured for the failure tests. The data were analyzed using a one-way ANOVA and comparisons of the 95% confidence intervals.

RESULTS AND DISCUSSION

The CT scans reveal allograft incorporation into the vertebral endplates in all specimens with the exception of one pseudoarthrosis in the control (autograft-filled) group. Image analysis demonstrated significantly different patterns of bone formation within the strut allografts. The BMP-treated group had more bone at the ends of the graft, while the autograft-filled struts maintained a uniform distribution of bone throughout the length of the strut (Fig. 3).

Biomechanical testing suggested possibly greater construct stability in the BMP-treated group compared to the control. The 95% confidence intervals for all modes of testing confirmed that the stability of the fusion in the BMP group was at least as great as the controls. (Fig. 4).

Figure 3. Percent Bone Within Graft

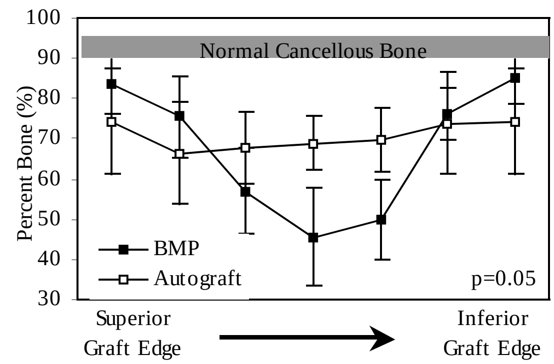

Figure 4. Physiologic Biomechanics

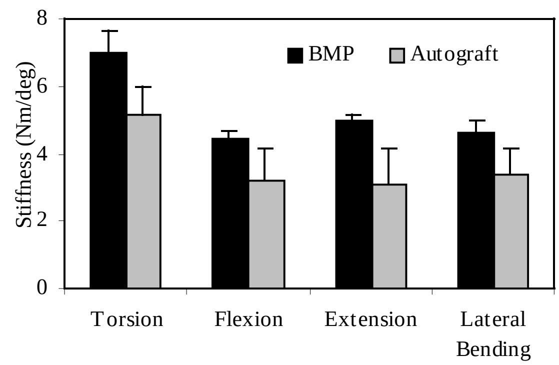

SUMMARY

This study confirms the healing and incorporation of large cortical strut allografts supplemented with *rh*BMP in a corpectomy model. The fusion in the BMP group appears to start at the vertebral endplates, with progressive bone formation toward the center of the allograft. When comparing rhBMP-2 impregnated allografts to those filled with autogenous bone graft, the formation of bone within the allograft as well as the structural integrity of the host-allograft junction appears to be equivalent between treatments. These results are similar to those previously seen in shorter interdiscal grafts and spacers, suggesting the efficacy of BMP in these large segment reconstructions performed after a vertebral corpectomy.

ACKNOWLEDEGEMENTS

Funded by Medtronic Sofamor Danek

This document was created with Win2PDF available at http://www.daneprairie.com.
The unregistered version of Win2PDF is for evaluation or non-commercial use only.

ENDOSCOPIC MECHANICAL HEMIEPIPHYSIODESIS MODIFIES SPINE GROWTH

Eric Wall [1]; Donita Bylski-Austrow [1]; Ronald Kolata [2]; David Glos [1] and Alvin Crawford [1]

[1] Children's Hospital Medical Center, 3333 Burnet Ave., Cincinnati, Ohio, USA 45229-3039
[2] Ethicon Endo-Surgery, Inc., Cincinnati OH, USA 45242
E-mail: Donita.Bylski-Austrow@cchmc.org

INTRODUCTION

Current surgical procedures for correcting scoliosis are among the most invasive and expensive in orthopaedics. Advances in thoracoscopy have decreased surgical trauma. However, the benefits of thoracoscopy are severely limited by the subsequent use of conventional instrumentation. Staple hemiepiphysiodesis is a well-established method for treating lower limb deformities. Combining thoracoscopy with growth control may lead to much less invasive treatment. In a pilot study of 5 staple designs, the most successful (Figs. 1, 2) resulted in a 40^{o} curve in 8 weeks in a porcine model (Bylski-Austrow 2000, Wall 2001). Growth plate histological changes suggestive of direct physeal compression were noted. The purpose of this study was to determine if spine growth was consistently altered using this spine staple.

METHODS

In 7 live skeletally immature domestic pigs, custom spine staples were implanted into the left side of the mid-thoracic vertebrae using video-assisted thorascopic procedures approved by an IACUC. Six staples were implanted per pig from T6-7 to T11-12. The staples were placed just anterior to the rib heads and spanned the intervertebral discs and two adjacent growth plates (Fig. 2). The staples were fixed to the vertebral bodies using two bone screws. The custom stainless steel staples were designed based on porcine thoracic spinal anatomy and were made using digital solid modeling, stereolithography, and micro-investment casting.

The animals were maintained for 8 weeks and anesthetized biweekly for radiography. Ventral-dorsal (VD), lateral, and right oblique radiographs were taken immediately after surgery, at 2, 4, 6 and 8 weeks, and again after spine harvest. Cobb angles were measured by standard methods. Paired t-tests were used to determine differences between initial and final post-operative curvatures. After euthanasia, the thoracic spine was removed. In vitro VD x-rays were taken twice, first with no load, then with a manually applied moment that simulated right side bending. CT scans were used to show staple and screw locations (Figs. 3, 4).

RESULTS

Five of the seven animals were followed for the entire 8-week period. These grew well with no notable clinical symptoms; they gained an average of 413 N (92.9 lbs) or 149% of their starting weight. Cobb angles at 0 (Fig. 5a), 2, 4, 6, and 8 (Fig. 5b) weeks were 0.8^{o} (± 1.8) 5.1^{o} (± 2.0), 7.3^{o} (± 1.1), 9.1^{o} (± 2.3), and 16.4^{o} (± 5.4), respectively. Cobb angles at 8 weeks were significantly different than the immediate post-operative values ($p=0.006$). With clearer radiographic views after spine harvest, the angles were 22.4^{o} (± 2.8), markedly different than initial values ($p=0.0001$) (Fig. 6). Mean angles in the lateral view did not change with time; the variability reflected that individuals exhibited changes from hyperkyphosis to lordosis (Fig. 7). The greatest curvatures were in the oblique plane (Figs. 8, 9), the plane of the staples.

CONCLUSION

This study showed that hemiepiphysiodesis using a relatively simple implant and minimally invasive surgery repeated induced spine curvature in a porcine model. If eventually successful clinically, these techniques may allow the highly desirable outcome of slowing the progression, and perhaps even correction, of spine deformity without spinal arthrodesis.

REFERENCES

Bylski-Austrow DI, et al (2000) *Proc. 46th Orthopaedic Research Society*, 265.

Wall EJ, et al (2001). *Proc. American Academy of Orthopaedic Surgeons*, 52.

ACKNOWLEDGEMENTS

Support from DePuy/AcroMed and Ethicon Endo-Surgery, Inc. is gratefully acknowledged.

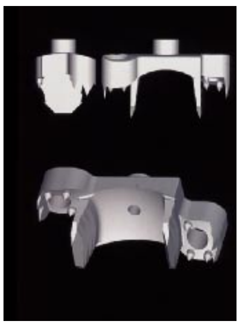

Fig 1. Staple.

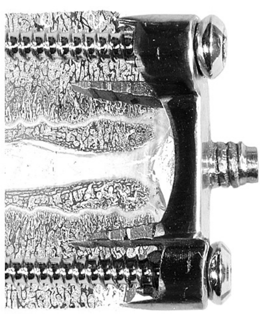

Fig. 2. In vertebrae.

Fig. 3. Blade in vertebra

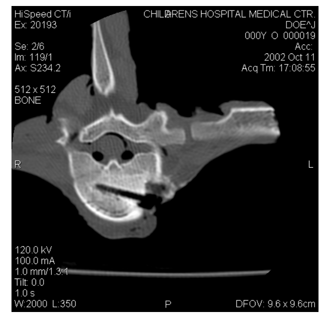

Fig. 4. Screw in vertebra.

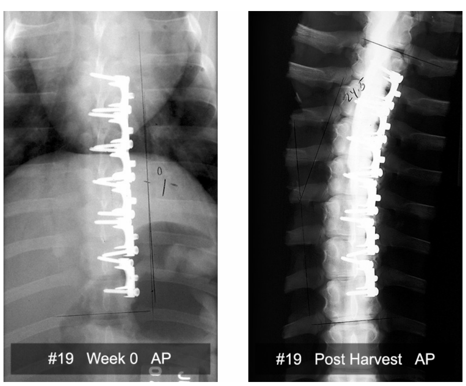

Fig. 5 a. Post-operative. **b.** 8 weeks.

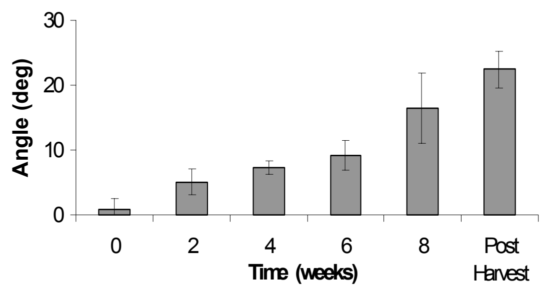

Fig. 6. Ventral-dorsal spine curvature increased with time after surgery.

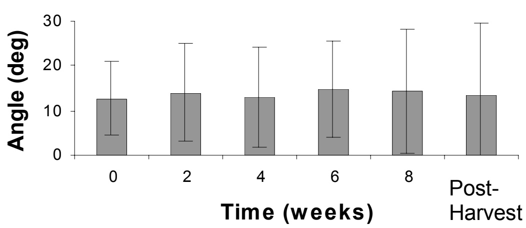

Fig. 7. Lateral curvature. Changes ranged from increased kyphosis to local lordosis.

Fig. 8. Oblique, 8 weeks.

Fig. 9. Oblique, 8 weeks.

AN APPARATUS FOR DETERMINING THE MULTI-DIRECTIONAL BENDING STIFFNESS OF THE HUMAN LUMBAR INTERVERTEBRAL DISC

David Spenciner P.E.[1], David Greene M.D.[2], James Paiva B.A.[1], Mark Palumbo M.D.[2], and Joseph Crisco Ph.D.[2]

[1]RIH Orthopaedic Foundation, Inc., Providence, RI, USA
[2]Department of Orthopaedics, Brown Medical School, Providence, RI, USA
E-mail: dspenciner@lifespan.org Web: www.rihof.org

INTRODUCTION

A wide variety of unconstrained systems for determining the biomechanical properties of the spine have been described (Crawford, 1995; Panjabi, 1981; Stokes, 2002; Wilke, 1994). These systems and others have been used to generate a substantial amount of biomechanical data relating to the human lumbar intervertebral disc along the three principal anatomic axes (axial rotation, lateral bending, and flexion/extension). However, physiologic motion typically comprises complex combinations of two or more of the principal axes. The biomechanical properties of the intervertebral disc have not been reported along complex axes.

Our objective was to develop an unconstrained apparatus for testing the multi-directional bending stiffness of spinal segments along 13 moment axes including the three principal anatomical axes, six axes that combine each pair of principal axes, and four axes that combine all three principal axes. This apparatus was then used to test the hypothesis that the bending stiffness of the human intervertebral disc does not differ with the direction of the moment axis.

METHODS

A multi-directional, unconstrained apparatus was constructed to interface with a biaxial servohydraulic load frame. The apparatus contained a custom specimen holder that was indexed in 45° increments along two perpendicular axes.

Validation was performed by testing an Ultra High Molecular Weight Polyethylene (UHMWPE) "dogbone" specimen. Testing involved applying pure moments (± 4 Nm at 0.1 Hz) about the 13 specified moment axes.

Additionally, seven human spinal specimens (L2/3 and L4/5) were tested (mean age 63.3 ± 3.0 years). Anterior column units (ACUs) were prepared by removing the posterior elements from functional spinal units (FSUs), potting, and then mounting in the apparatus. In all cases, the torque and rotation about the loading axis were recorded as well as the load and torque about the other orthogonal axes. Pure moments were applied to the ACUs at ± 8 Nm at 0.1 Hz for five cycles (four cycles of preconditioning and then one for which data were acquired). Bending stiffness, as defined by the slope of the linear least-squares fit of the torque vs. rotation curve, was calculated. For the ACUs, the bending stiffness values across all directions were compared using a repeated measures analysis of variance (ANOVA) with Tukey post-hoc test.

RESULTS AND DISCUSSSION

Tests on the UHMWPE specimen resulted in a final stiffness of 0.42 Nm/deg in pure rotation (one axis), 0.63 to 0.67 Nm/deg in pure bending (four axes), and 0.52 to 0.55 Nm/deg in combinations of pure rotation and pure bending (eight axes). The difference among axes expected to have equal stiffnesses was less than 7%.

The bending stiffness values of the ACUs demonstrated a statistically significant dependence on the direction of the moment axis (Figure 1). There was a statistically significant difference in the mean stiffness between flexion (FLE) and left lateral bending (LLB) ($p<0.001$), FLE and right lateral bending (RLB) ($p<0.001$), FLE and right axial rotation (RAR) ($p<0.001$), and FLE and left axial rotation (LAR) ($p=0.001$). Likewise, there was a statistically significant difference in the mean stiffness between extension (EXT) and RLB ($p<0.001$). Lateral bending and axial rotation were not statistically different from each other ($p = 0.115$).

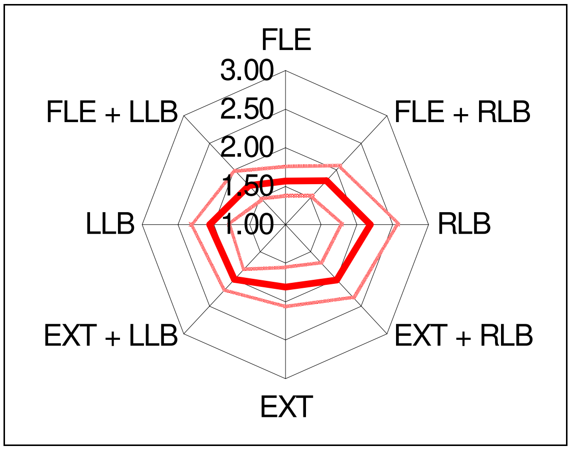

Figure 1: Mean (± SD) moment axis stiffness (Nm/°) in flexion/extension, lateral bending, and their combinations.

SUMMARY

An apparatus was designed to determine the multi-directional bending stiffness of the ACU. This system can also be used to measure other bending properties such as neutral zone and range of motion as well as the shear properties. At this time, only single levels of lumbar discs (i.e. ACUs) have been studied and it is unknown whether FSUs would provide similar results.

The results of this study provide novel data on the multi-directional bending stiffnesses of the intervertebral disc. We conclude that the bending stiffness of the human lumbar intervertebral disc depends on the direction of the moment axis and that the stiffness values of the principal axes may not be interpolated to determine the stiffness values along complex axes.

REFERENCES

Crawford, N. R., et al. (1995). "An apparatus for applying pure nonconstraining moments to spine segments in vitro." *Spine* **20**(19): 2097-100.

Panjabi, M. M., et al. (1981). "A technique for measurement and description of three-dimensional six degree-of-freedom motion of a body joint with an application to the human spine." *J Biomech* **14**(7): 447-60.

Stokes, I. A., et al. (2002). "Measurement of a spinal motion segment stiffness matrix." *J Biomech* **35**(4): 517-21.

Wilke, H. J., et al. (1994). "A universal spine tester for in vitro experiments with muscle force simulation." *Eur Spine J* **3**(2): 91-7.

ACKNOWLEDGEMENTS

Douglas C. Moore, M.S. provided invaluable advice during the design and construction of the spine tester. This work was supported by the RIH Orthopaedic Foundation, Inc.

INVESTIGATION OF THE LUMBAR SPINE PASSIVE TISSUE RESPONSE TO REPETITIVE LIFTING.

Rob Parkinson, Tyson A.C. Beach, and Jack P. Callaghan.

Biomechanics Laboratory, University of Guelph, Guelph, ON, CANADA
E-mail: jcallagh@uoguelph.ca

INTRODUCTION

The time varying changes that occur in the spine can alter both the potential for injury and the injury mechanisms. Conflicting findings from in vitro testing have been reported in the literature, Adams and Dolan (1996) reported decreased stiffness and Callaghan and McGill (2001) reported increased stiffness during repeated flexion protocols. This discrepancy in the literature and a lack of knowledge regarding the *in vivo* passive tissue response to dynamic flexion prompted this study.

METHODS

Ten male subjects (age 25±2 yrs, height 1.83±0.037 m, mass 84.7±10.69 kg) were recruited from the student population at the University of Guelph. Flexion stiffness was measured on a jig with the subject lying on their right side while the upper body was moved through a full range of flexion. The shoulders, pelvis and legs were restrained with straps. The jig was constructed of a large plexiglass surface upon which nylon ball bearings were set. The cradle supporting the upper body was lined with plexiglass and placed on top of the bearings.

Lumbar spine motion was measured using a 3-SPACE Isotrak system with the magnetic field source secured over the sacrum and the sensor over the spinous process of L1. 3-SPACE output was sampled at 20.5 Hz.

A cable fitted with a load cell was attached to the cradle to apply the bending moment. The cable was pulled until the experimenter could no longer move the subject, or the subject expressed discomfort.

To isolate the passive tissues during testing, electrodes were placed over the thoracic (T9) and lumbar (L3) erector spinae groups bilaterally. Maximum voluntary contractions (MVC) were performed for normalization. Throughout testing, trials during which muscle activity exceeded 5% MVC were recollected. EMG and force data were collected at 2048 Hz.

The lifting task required the subject to lift a 4.5 kg weight from the ground over a 55 cm high barrier, turn, walk 1.2 meters and lower the weight back down to the ground over another barrier. Lifting was performed at a rate of 7 times a minute.

Prior to any lifting, an initial stiffness testing session was performed with a minimum of three trials collected to allow subjects to practice the motion without activating the extensor musculature. The subjects then lifted for a thirty-minute interval followed immediately by another session of stiffness testing. This cycle was repeated three times for a total of 1.5 hours lifting, four flexion testing sessions and twelve trials. Typical stiffness vs. angle curves are illustrated in figure 1. Stiffness was calculated using the methods reported by McGill et al. (1994).

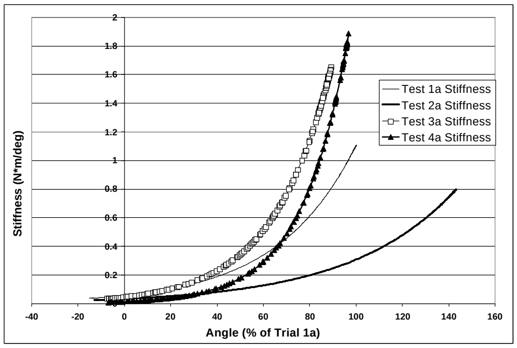

Figure 1: Stiffness vs. angle curves for one subject for the four sessions at 30-minute intervals. Only trial 1 is shown.

Moment at the highest common angle, angle at the highest common moment, and stiffness at 10, 30, 60, and 80% of flexion were compared with repeated measures ANOVAs.

RESULTS AND DISCUSSION

Statistical analysis revealed a significant difference ($p<0.05$) between trial 1 and trials 2 and 3 (figure 2) potentially due to an initial passive stretching of the tissues.

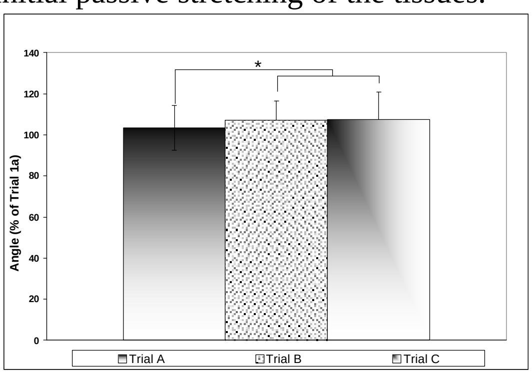

Figure 2: Angle averaged across subjects for each trial. The angle for trials 2 and 3 were significantly higher than trial 1.

Analysis also revealed that stiffness in session 2 was significantly lower than that of session 1 (figure 3). The initial decrease in stiffness may be due to creep in the ligaments and intervertebral disc. This decrease in stiffness was followed by a recovery, possibly due to an inflammatory response or increase in the passive stiffness of the musculature.

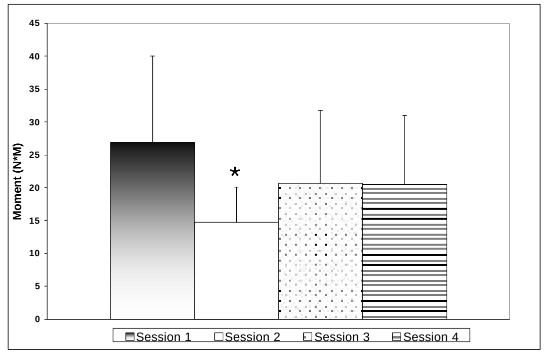

Figure 3: Moment for each session at the highest common angle across subjects.

SUMMARY

The passive lumbar spine tissue response to dynamic lifting revealed a two-phase response. The initial phase of decreasing stiffness is likely due to creep in the ligaments and intervertebral disc from exposure to repeated flexion. The second phase with a recovery of stiffness may be due to an inflammatory response, proposed as a mechanism for a similar “rebound” effect observed in the spine exposed to vibration (Sullivan and McGill, 1990). This rebound could also be due to an increase in the passive stiffness of the musculature, as has been shown in eccentric exercise (Howell et al., 1993). Due to the confounding factors of respiration, blood flow, inflammation and musculature, this in vivo assessment cannot be used to clarify the conflicting in vitro results.

REFERENCES

Adams, M.A., Dolan, P. (1996).*Clin Biomech*, **11**, 194-200.
Callaghan J.P., McGill S.M. (2001).*Clin Biomech*, **16**, *28-37.*
Howell J.H., Chleboun G., Conatser R. (1993).*J Physiol*, **464**, 183-196.
McGill S., Seguin J., Bennett G. (1994).*Spine*, **19**, 696-704.
Sullivan A., McGill S.M. (1990).*Spine,* **15**, 1257-1260.

HIP POSTURE AND PRE-ACTIVATION LEVELS MODULATE REFLEX CONTRACTIONS ELICITED BY KNEE LIGAMENT LOADING

Anastasios D. Tsoumanis [23] and Yasin Y. Dhaher [13]

[1]Department of Physical Medicine & Rehabilitation, Northwestern University Medical School, Chicago, IL, USA
[2]Department of Biomedical Engineering, Northwestern University, Evanston, IL, USA
[3]Sensory Motor Performance Program, Rehabilitation Institute of Chicago, Chicago, IL, USA
E-mail: *y-dhaher@northwestern.edu*

INTRODUCTION

We have previously shown that muscle contractions can be elicited by the application of valgus perturbations at the human knee (Dhaher et al., 2003). Based on several experimental qualifiers, we concluded that these contractions are reflex in nature and are mediated by periarticular tissue afferents. In this study we investigated the effect of posture (defined as change in hip angle) and neural state (defined by the pre-activation levels in knee muscles) on the intensity of this class of reflex. We hypothesize that both posture and neural state play a significant role on the modulation of periarticular tissues afferents mediated reflex at the human knee.

METHODS

A total of *9* normal subjects were tested. The experimental set-up and procedure has been thoroughly presented previously (Dhaher et al, 2003) and will be briefly described below. After securing the subject's knee in a single-degree of freedom servomotor system, the joint was pre-loaded at 4° in the valgus direction to ensure initial stretch of passive joint tissues. Each subject was asked to provide two knee muscle co-activation levels as a percent of the varus passive torque (VPT) (*0, 5-10*%). The VPT was measured with no muscle contractions using a load cell attached to the servo system. Multiple 8° rapid (*60º/sec*) valgus step inputs (stretch-hold and release paradigm; see Dhaher et. al. 2003) were applied at the knee joint at two different hip flexion angles (90° and 50°) repeated at both co-activation levels. EMG activity was recorded from a flexor, semitendinosus (ST), and an extensor, vastus medialis longus (VML) using surface electrodes. The elicited sustained reflex response (SR) measured over *500 ms*, was the EMG activity during the hold period of the valgus position stimulus (see Dhaher et. al. 2003)**.** The SR was quantified as follows:

$$SR = EMG_{mean}^{reflex} - EMG_{mean}^{baseline} \qquad (1)$$

where EMG_{mean}^{reflex} is the time average of the rectified and smoothed EMG during the reflex activity and $EMG_{mean}^{baseline}$ is the time average of the baseline activity calculated over *500 ms* prior to the onset of the mechanical perturbation.

RESULTS AND DISCUSSION

The sustained reflex response (SR) amplitude of both the VML and ST muscles exhibited a statistically significant increase ($p<0.001$) with increase in hip flexion angle. Specifically, in Figures 1-4 we observe a significant increase in SR activity of both muscles across all four subjects with change of hip flexion angle. Seven out of nine subjects showed a similar trend in the extensor muscle (VML) ($p<0.001$) and nine out of nine for the flexor muscle (ST) ($p<0.001$). As shown in Figures 1 and 2, for both hip angles (90º and 50º of hip flexion) this dependency was a function of muscle activation prior to the perturbation. Pre-activation of knee extensors exhibited both an increase (Figure 1) and decrease (Figure 2) as a function of pre-activation levels. This was also observed in the knee flexors

(Figures 3 and 4). However, for a given hip angle and across all nine subjects, six of the subjects demonstrated an increase ($p<0.001$) of the extensor and flexors reflex intensity as a function of knee muscles pre-activation level.

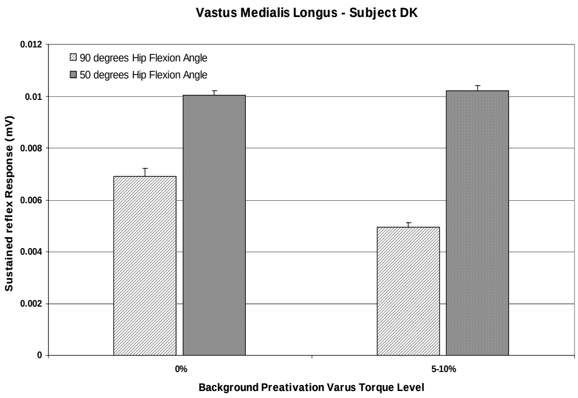

Figure 1: SR reflex activity of VML as a function of hip angle and pre-activation level for subject DK.

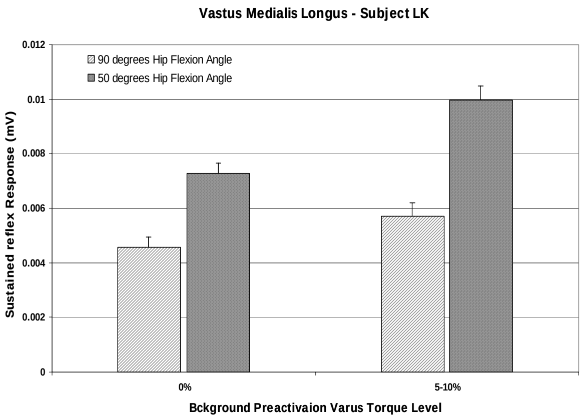

Figure 2: SR reflex activity of VML as a function of hip angle and pre-activation level for subject LK.

SUMMARY

Our preliminary results show that hip extension results in an increase of the sustained reflex response. The observed increase was consistent in both the flexor and extensor muscles. Our data also showed that the pre-activation state of knee muscles significantly alters the intensity of muscle contractions mediated by periarticular tissue afferents. This effect can be attributed to one of three potential factors: *1)* vestibular input, *2)* hip joint proprioceptors input, and *3)* input from muscle spindles of the pre-activated muscles. All these factors taken together indicate that other sensory layers derived from global sensory modalities could potentially influence the local varus/valgus-stabilizing role of reflexes mediated by the joint's periarticular tissue afferents.

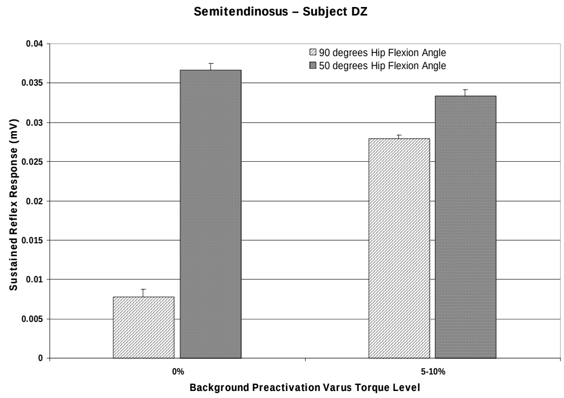

Figure 3: SR reflex activity of ST as a function of hip angle and pre-activation level for subject DZ.

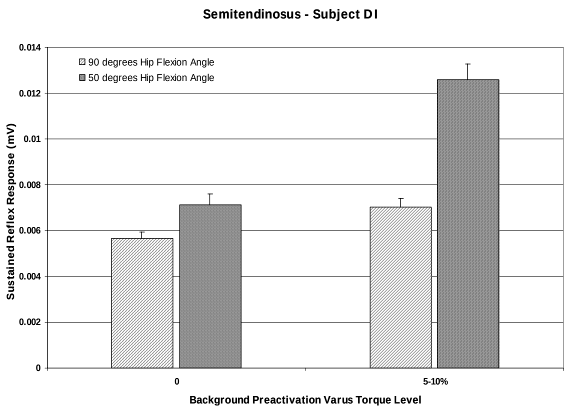

Figure 4: SR reflex activity of ST as a function of hip angle and pre-activation level for subject DI.

REFERENCES

Dhaher et al. (2003)., *J. of Biomechanics*, **36**(2),199-209

ACKNOWLEDGEMENTS

This work was supported by the Dr. Ralph and Marian C. Falk Medical Research Trust, the National Institute of Health (AR46422-02; 5P60AR30692; 5T32HD07418), and the Whitaker Foundation.

WHOLE CERVICAL SPINE MODELWITH MUSCLE FORCE REPLICATION FOR WHIPLASH SIMULATION: DEVELOPMENT AND EVALUATION

Paul C. Ivancic,[1] Manohar M. Panjabi,[1] Shigeki Ito,[1] Peter A. Cripton[2] and Jaw-Lin Wang[3]

[1] Biomechanics Laboratory, Yale University School of Medicine, New Haven, CT, USA
[2] Exponent Failure Analysis Associates, Biomechanics Practice, Philadelphia, PA 19104, USA
[3] Institute of Biomedical Engineering, National Taiwan University, Taipai, Taiwan
E-mail: paul.ivancic@yale.edu

INTRODUCTION

A variety of modeling strategies have been investigated to further understand the whiplash injury mechanisms, including human volunteer tests, mathematical models, anthropometric test dummies, whole cadavers and isolated whole cervical spine (WCS) specimens. Although the WCS model has shown its many advantages, e.g. injury quantification via pre- and post whiplash flexibility testing, it is not biofidelic with respect to spinal loads and postural stability. The goals of the current study were to develop a new dynamic WCS model for whiplash simulation that will incorporate muscle force replication, and then to evaluate its performance experimentally and compare the results with the available in vivo data.

METHODS

A WCS model is constructed from a fresh frozen whole cervical spine specimen consisting of the occiput (C0) through T1. Six specimens were carefully dissected of all non-osteoligamentous soft tissues and C0 and T1 were set in two parallel horizontal mounts.

In order to enhance the dynamic biofidelity of the whiplash model, a new WCS model with muscle force replication (MFR) was developed (**Figure 1**). The MFR system consisted of anterior, posterior and lateral cables attached to tension springs anchored to the base. Four anterior cables were anchored to the occipital mount such that two cables were fixed bi-laterally and two cables were fixed anteriorly. The anterior cables ran through posts at C4 (two cables per post), through pulleys within the T1 mount, and were connected to the two springs (two cables per spring). The preload in each anterior spring was 15 N. Two posterior MFR cables were connected bi-laterally to the occipital mount and ran through wire loops attached to the spinous processes, to a pulley within the T1 mount and connected to a preloaded 30 N spring. Bi-lateral MFR cables originated from C0, C2, C4 and C6. The cables passed around lateral guide rods, alternately anteriorly and posteriorly and through pulleys at the T1 mount. The eight lateral cables were each connected to a separate spring, preloaded to 30 N. A C0-C2 flexion limiter, consisting of a steel wire connected to the occipital mount and to the C2 spinous process, was developed to allow physiologic flexion of C0-C1 and C1-C2. The resulting intervertebral compressive pre-loads due to all MFR cables were: 120 N (C0-C1, C1-C2); 180 N (C2-C3, C3-C4); 240 N (C4-C5, C5-C6); and 300 N (C6-C7, C7-T1). A surrogate head with 3.3 kg mass and 0.016 kg m^2 sagittal plane moment of inertia was fixed to the occipital mount.

To evaluate the dynamic biofidelity of the WCS+MFR model, whiplash simulations were performed using a bench-top apparatus (Panjabi et al., 1998) and the incremental trauma protocol at nominal T1 maximum horizontal accelerations of 3.5, 5, 6.5 and 8 g.

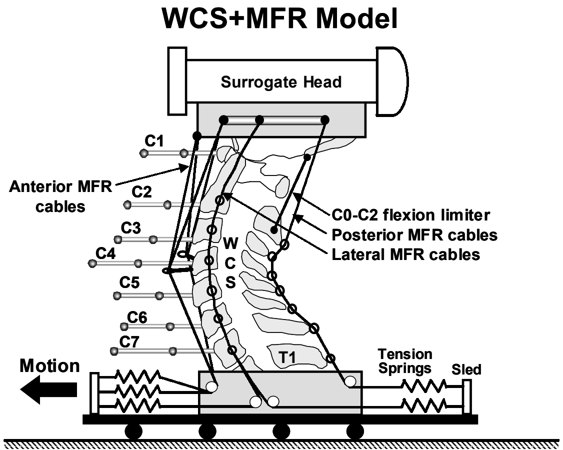

Figure 1. Whole cervical spine model with muscle force replication (WCS+MFR).

RESULTS

The average peak head-T1 extension of 37.1° during the 3.6 g acceleration (9.1 kph velocity) whiplash simulation was within the in vivo corridor (**Figure 2**) (Davidsson, 2000).

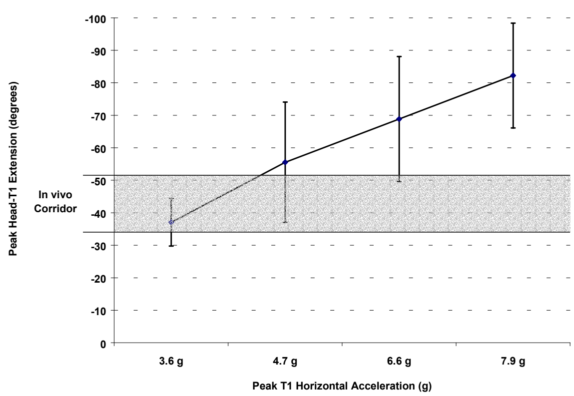

Figure 2. Average (SD) peak head-T1 extensions of the WCS+MFR model and the in vivo corridor (Davidsson, 2000).

During the 4.7 g whiplash simulation of the current study, the average peak intervertebral extensions compared favorably with the corresponding in vivo data (**Figure 3**).

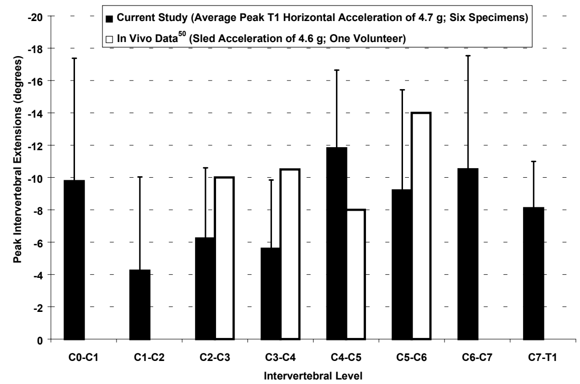

Figure 3. Average (SD) peak intervertebral rotations during the 4.7 g impact and in vivo data (4.6 g) (Kaneoka et al., 1997).

SUMMARY

A new in vitro WCS+MFR model for whiplash simulation has been developed and evaluated experimentally. The model behavior is similar to the data observed during whiplash simulation of volunteers. The peak head extension during the 3.6 g impact was within the in vivo corridor. The peak intervertebral extensions also compared favorably with the corresponding in vivo data. The WCS+MFR model is capable of generating important biomechanical data which may help improve our understanding of the whiplash injuries.

REFERENCES

Davidsson, J. (2000). Ph.D. thesis, Chalmers University of Technology.

Kaneoka, K. et al. (1997). *Int Conf on New Frontiers in Biomech Eng*, 265-268.

Panjabi, M.M. et al. (1998). *Spine,* **23**, 17-24.

ACKNOWLEDGEMENT

The financial support of the NIH (Grant 1 R01 AR45452 1A2) is gratefully acknowledged.

LUMBAR ARTHRODESIS: HOW MUCH RADIOGRAPHIC MOTION IS PRESENT WITH SOLID FUSION?

[1, 2] Mahar, A, [1] Bono, CM, [1] Bawa, M, [1] White, K, [1] Vives, M, [1] Garfin, S
[1] Department of Orthopaedics, University of California – San Diego
[2] Orthopedic Biomechanics Research Center, Children's Hospital – San Diego
amahar@chsd.org

INTRODUCTION
Radiographic assessment of lumbar fusion healing remains challenging. While static films reflect fusion mass, dynamic flexion/extension (F/E) views are an indicator of stability. Numerous authors have published "criteria" for declaring an anterior interbody fusion solid, ranging from 1° to 5°, while more motion is accepted for posterior fusion methods.[1, 2] Though these values are useful parameters, they have not been previously validated in a scientific investigation. The purpose of this study was to characterize the radiographic amounts of detectable motion on F/E views after various methods of simulated fusion in a cadaveric model.

METHODS
Eight cadaveric spines (L1 to L4) were tested in a radioluscent jig fixed to a MTS 858 Mini-bionix servohydraulic testing apparatus (Eden Prairie, MN). L4 was fixed to the machine base; L1 was fixed to the actuator via a cantilever bending apparatus. Sagittal K-wires were inserted adjacent to the superior and inferior endplates of L2 and L3, respectively, to facilitate radiographic measurements. Flexion/extension moments of $\pm$ 15Nm were applied, simulating physiologic loads, over 10 cycles. Following cyclic testing, the spines were held under maximal load for 3 minutes to assist with acquisition of lateral radiographs. First, spines were tested intact and after anterior discectomy and cage placement. They were then randomly tested with one of the following constructs simulating a solid L2-L3 fusion: plates fixing the transverse processes, plates fixing the spinous processes, pedicle screw-rod construct, and anterior vertebral body plating. While the pedicle and anterior plating methods are most common today, the other repair methods were included since clinical data exists with these techniques. Lateral radiographs were taken at the extremes of motion for each repair method. Range of motion measurements were repeated three times per film to ensure accuracy and repeatability. Flexion/extension data from the MTS were not used in this study. Values were averaged within repair methods across spines and statistically compared using a repeated measures ANOVA test with a Tukey's *post-hoc* multiple comparison correction when statistical differences were found.

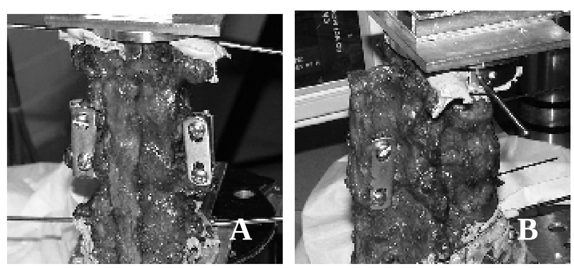

Figure 1A/B: Transverse and spinous process fixation techniques, respectively.

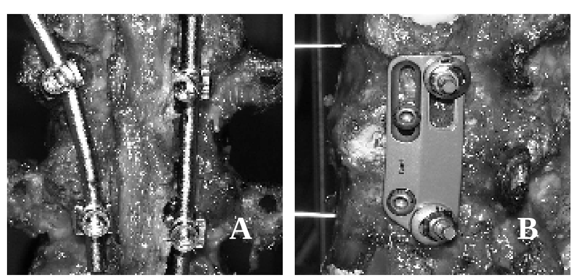

Figure 2A/B: Pedicle screw and anterior fixation techniques, respectively.

RESULTS AND DISCUSSION

The following F/E differences were measured: intact specimens, 13±2°; discectomy and interbody cage, 9±2°; spinous process fusion, 9±4°; transverse process fusion, 13±3°; pedicle screws, 5±3°; anterior plating, 3±2°. Statistical analysis demonstrated no difference between pedicle and anterior plating systems ($p=0.52$), though they both allowed statistically less radiographic motion than any of the other fixation constructs ($p<0.05$). The transverse process fusion did not statistically differ from intact ($p=0.99$). The cage and interspinous process constructs had significantly less motion than either the transverse process fixation method or the intact group ($p<0.05$) (Table 1). The cage, transverse process and interspinous process fixation methods each demonstrated end ranges of motion of about 10 degrees, indicating a high potential for psuedarthrosis.

Table 1: Range of Motion for different surgeries.

SURGERY	ROM (Deg) Mean $\pm$ SD	Range (Min-Max)
Intact	13 $\pm$ 2	(10-16)
Discectomy + cage	9 $\pm$ 2	(5-14)
Interspinous Process	9 $\pm$ 4	(4-19)
Intertransverse Process	13 $\pm$ 3	(9-19)
Pedicle Fixation	4 $\pm$ 2	(2-8)
Anterior Fusion	3 $\pm$ 2	(1-8)

SUMMARY

The amount of radiographically detectable motion is influenced by the type, location, and quality of fusion. The current study documents a range of values measureable on F/E views of simulated lumbar fusions. As anticipated, the anterior plating fusion method yielded the lowest dynamic motion, averaging 3 ± 2 degrees, resembling those previously proposed. In contrast, simulated TP fusion alone resulted in a range of motion not dissimilar to unfused specimens, while the common posterior methods (pedicle screw displayed significantly less. These data may be helpful in establishing more accurate criteria for pseduarthrosis rates based on flexion/extension radiographs. These data only represent a subset of available fusion constructs used clinically. A follow-up radiographic study should be conducted that explores single rod and dual rod anterior systems for dynamic fusion assessment. Also, further investigation of the radiographic mobility of known fused lumbar segments in vivo is warranted.

REFERENCES

[1]Frymoyer JW, et al. *Spine.* 1979; 4: 435-440.
[2] Brodsky AE, et. al. *Spine.* 1991; 16: S261-265.

ACKNOWLEDGMENTS

An unrestricted educational grant from the P.H. and Ruth Dickinson Foundation

This document was created with Win2PDF available at http://www.daneprairie.com.
The unregistered version of Win2PDF is for evaluation or non-commercial use only.

QUANTIFYING SAGITTAL MOTION ACROSS A SOLID LUMBAR INTERBODY FUSION USING FINITE ELEMENT MODELING

Ashutosh Khandha [1], Sasidhar Vadapalli [1], Scott Holekamp [1], Vijay Goel [1]
Christopher Bono [2], Steven Garfin [3]

[1] Department of Bioengineering, University of Toledo, Toledo, OH, USA
[2] Boston University Medical Center, Boston, MA, USA
[3] University of California, San Diego, CA, USA

E-mail: akhandha@eng.utoledo.edu

INTRODUCTION

Dynamic flexion/extension (F/E) radiographs are commonly used to assess lumbar fusion. They are intended to detect sagittal motion, which should be greater with pseudarthrosis and minimal with solid fusion. Despite widespread use, it is unclear what the appropriate "cut-off" criteria to declare a fusion solid should be, with recommendations ranging from 0 to 5°.

While observer variability may influence radiographic measurements, a fundamental mechanical question still remains: Does a solid fusion actually permit motion, and if so, how much? It was this study´s purpose to characterize the amount of angular sagittal motion permitted across simulated lumbar interbody fusions (IF) using a Finite Element Model (FEM).

METHODS

A validated 3-D, nonlinear FEM of an intact L3-L5 segment was developed. Various scenarios of healed anterior and transforaminal lumbar interbody fusions (ALIF and TLIF) were simulated. Fusion was represented as bridging cortical bone with a cancellous core. Degrees of "fusion completeness" (% disc space area) were tested, including solid bridging bone in the entire (100%) disc space (excluding the retained posterior annulus for ALIF and anterior annulus for TLIF) and the anterior or posterior 75%, 50%, and 25% disc space, simulating solid but "incomplete" fusion.

TLIF was tested with a unilateral facetectomy (UF) as well as bilateral facetectomy (BF). A 400N axial preload approximated conditions of a standing radiograph. Next, the model was stressed with 10.6 N-m F/E moments to simulate bending. The change in angulation between the adjacent vertebrae was recorded.

RESULTS AND DISCUSSION

The 100% complete ALIF and TLIF (UF or BF) allowed less than 0.5° of motion. Results for ALIF are shown in Table 1, indicating that motion varies from 0.5 to 2.15° in different cases.

Table 1. Results for ALIF.

Percentage and Location of Fusion Mass									
	Intact	100%	75% ant	50% ant	25% ant	100%	75% pos	50% pos	25% pos
L3-L4 Extension	4.32	0.47	0.90	1.36	2.15	0.47	1.19	1.27	1.28
L3-L4 Flexion	5.94	0.28	0.52	0.79	1.25	0.28	1.67	1.96	2.00

Results for TLIF are shown in figure 1 below. TLIF using a UF approach of the anterior 75%, 50% and 25% of the disc space yielded 1.08, 1.22 and 1.25° respectively.

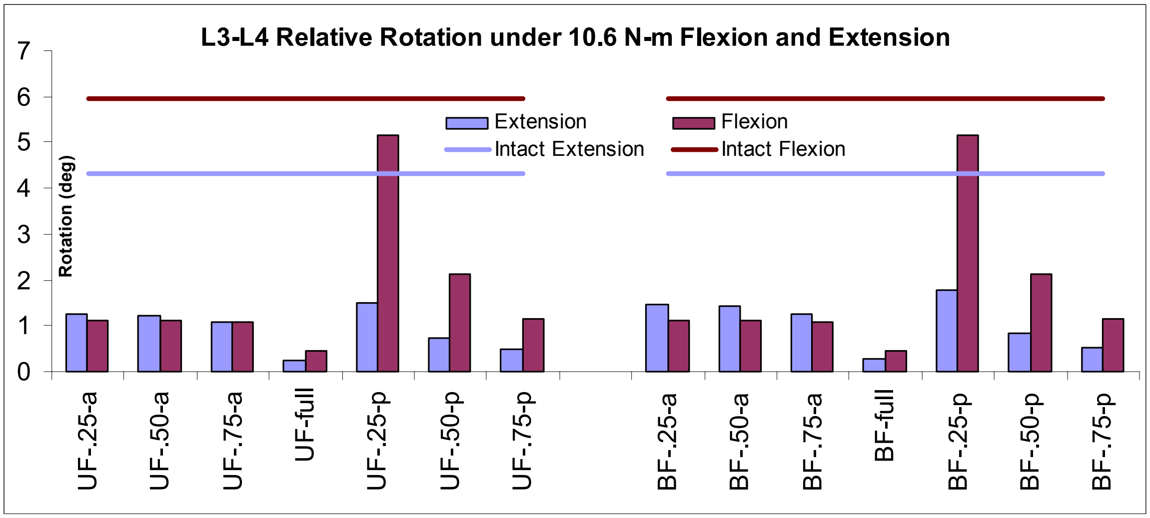

Figure 1. Results for TLIF. (a = anterior fusion, p = posterior fusion) (UF = Unilateral Facetectomy, BF = Bilateral Facetectomy)

TLIF using a BF of the anterior 75%, 50% and 25% of the disc space yielded 1.25, 1.44 and 1.48° respectively. TLIF using a UF as well as BF of the posterior 75%, 50% and 25% of the disc space indicated a wider range of motion.

The current analysis suggests that sagittal angular motion can be produced across a solid interbody fusion under physiologic F/E moments. Depending on fusion technique, location and completeness, 0.5 to 5.14° of angular motion can occur. More than 2.15° of motion would suggest pseudarthrosis after an uninstrumented ALIF attempt, while more than 5.14° would be suggest the same following uninstrumented TLIF. It should be noted that a solid but incomplete (25%) TLIF allowed substantially more motion than other situations. Excluding these cases, no more than 2.12° of motion should be allowed by 50%, 75%, or 100% fused TLIFs. Considering known radiographic measurement error, which may be as much as 2°, the authors suggest that up to 4.5° of sagittal motion may be demonstrable on F/E views of most solid ALIFs and TLIFs. The observed F/E values are similar to previously purported criteria. To the authors´ knowledge this is the first supportive mechanical study of this issue. The data suggests that residual motion after solid TLIF is more sensitive to % of fusion completeness than ALIF. Additional in vitro and in vivo studies are needed to validate these findings.

REFERENCES

Kowalski. R. J., Ferrara. L. A., Benzel. E. C. (2001). *J. Neurosurgery*, **10,** 4.

ACKNOWLEDGEMENTS

Research supported by DePuy AcroMed.

BIOMECHANICAL EVALUATION OF EXPULSION FORCES FOR PAIRED AND SINGLE PROSTHETIC DISC NUCLEUS DEVICE DESIGNS

Joseph E. Hale, Ph.D. [1], Britt K. Norton, B.S.[1], Sara E. Ross, B.S.[1] and William C. Hutton, D.Sc.[2]

[1]Raymedica, Inc., Minneapolis, MN
[2]Emory University School of Medicine, Atlanta, GA
E-mail: j.hale@raymedica.com

INTRODUCTION

A prosthetic disc nucleus (PDN® device), consisting of a hydrogel core encased in a woven polyethylene jacket, has been developed as an alternative to fusion in the treatment of degenerative disc disease. The core of the device is dehydrated when implanted, and subsequently absorbs fluid and swells within the disc. Previous studies have reported the ability of the device to restore disc height and biomechanical function *in vitro* (Eysel 1999; Wilke 2001).

The PDN device was originally designed to be implanted in a paired configuration (Figure 1). A new single device design has recently been developed for use in smaller discs that cannot accommodate two devices. The objective of this study is to evaluate the likelihood of device expulsion from the intervertebral disc space for both the paired and single device designs.

Figure 1: Illustration of paired device placement within intervertebral disc cavity.

METHODS

Twelve intact motion segments (L2–L3 and L4–L5) from six fresh frozen cadaveric lumbar spines (ages 33–69 years) were implanted with fully hydrated devices. For each spine, paired devices were implanted at one level and a single device was implanted at the other; levels were alternated with each successive spine to minimize the effect of implantation level on the results. Device models used were properly sized to the disc height.

The protocol for expulsion testing was similar to test methods employed for intervertebral body fusion devices (ASTM Standard 2077-00). An axial compressive preload of 500 N was applied to each implanted motion segment. A stainless steel wire threaded through the woven polyethylene jacket of the device was then used to pull the device out of the intervertebral disc space through a posterior opening in the anulus. The force required to pull the device out of the intervertebral space was applied (constant displacement rate of 1.27 mm/sec) and measured using a servo-hydraulic materials testing system.

RESULTS AND DISCUSSION

The maximum expulsion force for the paired devices ranged from 210 N to 316 N, with a mean maximum force of 251.0 N (± 47.2 N). The maximum expulsion force for the single device design ranged from 183 N to

541 N, with a mean maximum force of 364.5 N (± 119.1 N). In five of the six spines tested, the maximum expulsion force for the single device exceeded that of the paired device (Figure 2). When analyzed by motion segment, the mean maximum expulsion force for the single device was greater than that of the paired device at both lumbar levels, with the difference being more evident at L4–L5.

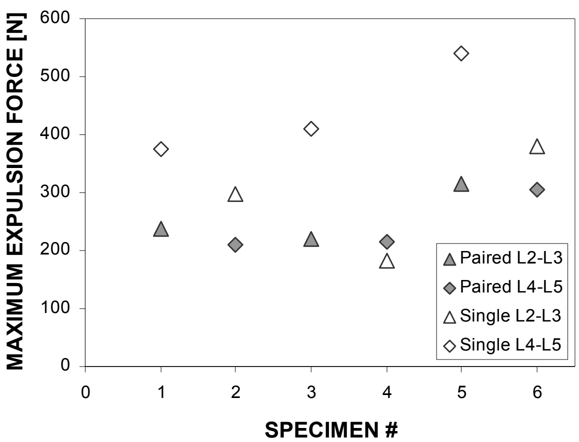

Figure 2: Maximum expulsion force data for paired and single device designs as a function of implant level.

Statistical analysis of maximum expulsion forces for paired and single devices was performed using an unpaired Student t-test ($P \leq 0.05$). The difference between groups, although notable, was considered to be not quite statistically significant ($P = 0.0551$).

This study was designed to assess the propensity of a prosthetic disc nucleus device to migrate out of the intervertebral disc space. Although the standardized test method employed in this study does not necessarily recreate the mechanism responsible for expulsions seen in clinical use and cannot be used to predict the frequency of expulsion, it is able to reproduce the expulsion failure mode and provide an accurate, quantitative measurement of the forces required to extract a device from the disc cavity.

SUMMARY

Expulsion of both paired and single prosthetic disc nucleus devices was reproduced using a standardized test method. The single device design required an average of approximately 44% more force to remove than did the paired design, which was implanted at another level in the same spine. These data suggest that the single device is no more likely, and may be less likely, to migrate compared to the paired devices and are consistent with the migration complication rate reported for these two designs in clinical use.

REFERENCES

Eysel, P. et al. (1999) *Acta Neurochir* 141:1083-1087.

Wilke, H.J. et al. (2001) *J Neurosurg* 95:208-214.

A PROPOSED MECHANISM OF SAGITTAL MOTION INDUCED BY MANUAL POSTERIOR TO ANTERIOR MOBILIZATION: ASSESSMENT OF LUMBAR SPINE KINEMATICS USING DYNAMIC MRI

Kornelia Kulig, Rob Landel, and Christopher M. Powers

Musculoskeletal Biomechanics Laboratory, Department of Biokinesiology and Physical Therapy, University of Southern California, Los Angeles, CA, USA
E-mail: kulig@usc.edu   Web: http://pt.usc.edu/labs/mbrl

INTRODUCTION

Posterior to anterior (PA) mobilization is frequently employed to assess spinal mobility, and involves a manual application of a force to a single spinous process with the individual lying in the prone position. It is still unclear how this manual technique influences inter-vertebral motion of the lumbar spine. An in vivo study, using an apparatus to deliver a PA force to the L4 spinous process (Lee et al 1997), identified bidirectional sagittal intervertebral motions at all segments with maximal extension at L2-L3. A mathematical model, of force application to L3, predicted linear posterior-anterior displacement, and only minimal sagittal rotation (Keller et al .2003). Considering the morphology of the lumbar vertebrae and their structural relationship, neither of the two studies appears to present a comprehensive model. The purpose of this study was to 1) describe the segmental motion of the lumbar spine during a PA mobilization procedure using dynamic imaging techniques and 2) to propose a mechanism of the lumbar spine's motion as a result of a PA force to a lumbar spinous process. We postulated that the unique structure of the lumbar spine would dictate the intervertebral responses to a PA force on a single spinous process.

METHODS

Twenty healthy individuals (12 male and 8 female) between the ages of 22 to 43 and with no history of back pain participated.

Dynamic imaging of the lumbar spine was performed using a vertical MRI system (0.5 Tesla, Signa SP, General Electric Medical Systems, Milwaukee, WI) with an opening that allowed the examiner access to the subject during testing. Sagittal plane imaging of the spine was performed using a flexible receive-only surface coil. Imaging parameters were: TR 200ms; TE 18 ms; matrix: 256 x 256; FOV: 28 x 21 cm; and a 7 mm section thickness with an interslice spacing of 1 mm.

The manual force was aimed at reaching the end range of vertebral motion and was comparable in magnitude to that of a "grade IV" (Maitland, 2001). Forces were applied at each subject's vertebrae starting at L5 and moving to L1.

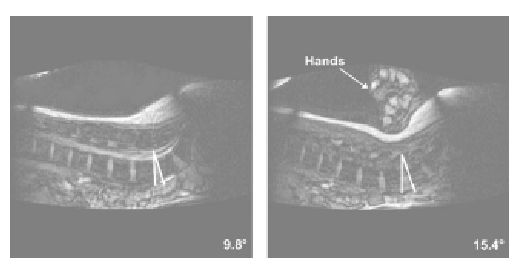

Figure 1: Sagittal images taken during a PA force applied to L4 spinous process.

The intervertebral angle, defined as the angle formed by lines delineating adjacent vertebral endplates, was measured (Figure 1). Segmental motion was defined as the difference between the intervertebral angles as measured from the resting and the end-range images. An increase in intervertebral angle between those positions was indicative of segmental extension. The superior vertebra was used to define the target segment.

RESULTS AND DISCUSSION

The results of this study revealed a consistent pattern of lumbar spine motion during a PA mobilization procedure. Specifically, motion at the targeted and adjacent segments always was directed towards extension (Figure 2, Figure 3 top).

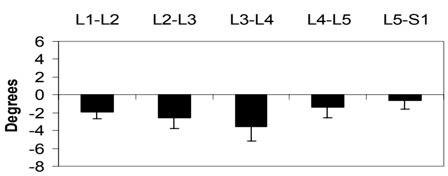

Figure 2: Mean motion at each lumbar segment during a PA force on L3.

A theoretical explanation for this pattern of segmental motion can be proposed based on the morphology of the lumbar spine. For example, when a PA force is applied to the spinous processes of L3, the facet of the tested (L3) vertebra approximates the facet joint of the adjacent caudal (L4) vertebra and imposes motion to it (Figure 3, bottom). It is conceivable that this approximation would result in the L3 facet "pushing" on its L4 counterpart (bone on bone contact), causing a bending moment rotating L4 away from L3 (Figure 3, bottom). The facet of L3 moves away from the facet of L2 causing tension in the joint capsule, which in turn also results in a bending moment of L2 on L3 into extension, but of lesser magnitude.

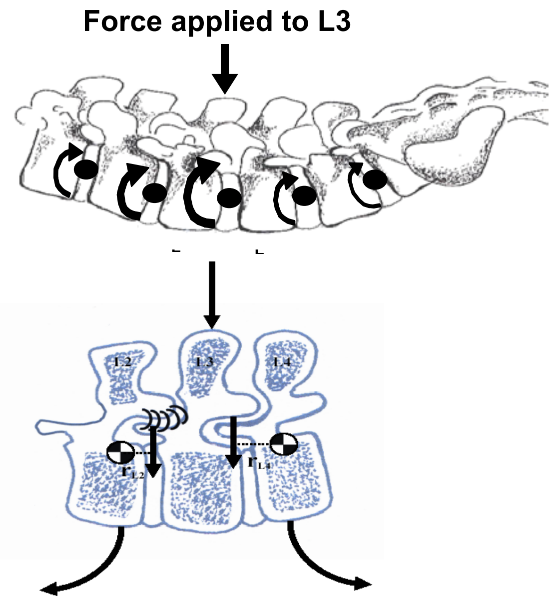

Figure 3: Segmental motion as a result of PA at L3 represented graphically (top) Artist's conception of the proposed mechanisms of intervertebral motion resulting from PA force on L3 (bottom).

SUMMARY

The findings suggest that a PA force at one spinous process causes motion at the target vertebra and the neighboring vertebrae. Secondly, we propose a mechanism by which a PA force applied to a spinous process propagates motion caudally and cranially.

REFERENCES

Keller T.S., et al. (2002). *Clin Biomech.* **17**, 185-196.
Lee R., Evans J. (1997). *Clin Biomech.* **12**, 400-408.
Maitland G.D., et al. (2001) Vertebral Manipulation. 6th ed. London: Butterworth-Heinemann.

ACKNOWLEDGEMENTS

This research was funded by the Foundation for Physical Therapy.

EFFICACY AND KINEMATIC CHARACTERISTICS OF TWO SPINAL ORTHOSES

Songning Zhang, Kurt Clowers, and Michael Wortley

Biomechanics/Sports Medicine Laboratory, The University of Tennessee, Knoxville, TN, USA
E-mail: szhang@utk.edu

INTRODUCTION

Patients with spinal injuries are often prescribed to receive various spinal orthoses. The objectives for spinal orthoses applications include combination of the following: support, maintaining a specific spinal posture, segmental immobilization, protection from damaging stresses, or correction of spinal malalignment (White and Panjabi, 1990). Most research studies have concentrated on the effect of the tested orthoses on limiting the gross range of motion (ROM) in the vertebral column using motion analysis and/or x-ray whereas some researchers focused on other measures such as electromyography, intra-abdominal pressure, forces and moments. Positive effectiveness of the tested orthoses has been shown in many studies (Jorgensen and Marras, 2000; McGill, et al., 1994). A lumbar orthoses (LO) and a lumbosacral orthoses (LSO) are designed to restrict motions of these two different regions. Therefore, the purpose for this study was to examine effectiveness of a LO and LSO orthoses in altering spinal kinematics.

METHODS

Seventeen healthy recreational male subjects (age: 23 ± 2 yrs, body mass: 83 ± 12 kg, height: 1.82 ± 0.06 m) with no impairments to their spine at the time of the data collection and no history of major spinal pathology, participated in the study.

A digital video camera (60 Hz, JVC) was used to obtain kinematic data from the right sagittal and posterior views of the subject. For the sagittal view, three retroreflective markers were placed on the right side of the body at the mid-trunk, the hip, and the knee and three customized marker wands were placed on the spinal process at the 1st thoracic vertebra (T1), and the 1st (L1) and 5th (L5) lumbar vertebrae. For the posterior view, three flat retroreflective markers were placed on the spinal process of T1, L1 and L5. The subjects were instructed to perform three trunk flexion trials, three trunk extension trails, and three lateral (right) flexion trials in an un-braced condition and each of the two braces of a total nine test conditions.

Two orthoses tested included a lumbar orthoses (ProLign, DeRoyal) and a lumbosacral orthoses (UltraLign, DeRoyal). Selected ROM and percent ROM variables were evaluated using a one-way analysis of variance with post hoc comparisons and significant level set at $p < 0.05$.

RESULTS AND DISCUSSION

A positive ROM is observed during trunk flexion and a negative ROM during trunk extension. For intervertebral segment tilting in the sagittal plane, a positive angle represents a posterior tilt and/or its ROM and a negative angle represents an anterior tilt and/or its ROM. The statistical results indicated that both ProLign and UltraLign orthoses significantly reduced L5, L1 and T1 anterior tilt compared to the un-braced condition (Table 1). The UltraLign showed a greater reduction of L1 and T1 ROM than the other two test conditions during the trunk extension. The UltraLign and ProLign orthoses showed significantly reduced ROM than the control condition for the lumbar and thoracic lateral flexion, and lateral trunk flexion (Table 1).

Table 1. Average ROMs (deg) of the examined segments (mean±SD).

	Device	L5 Tilt	L1 Tilt	T1 Tilt
Flex	No Brace	-13.2±11.8	-37.8±17.7	-65.1±14.9
	ProLign	-3.6 ±2.6[a]	-25.7±9.2[a]	-53.2±6.5[a]
	UltraLign	-3.9±2.2[a]	-14.7±9.2[a b]	-42.2 ±9.8[a b]
Ext	No Brace	6.7±7.0	17.1±6.2	39.7±9.1
	ProLign	4.6±10.6	14.2±5.2	33.7±9.0[a]
	UltraLign	4.5±11.6	9.2 ±5.9[a b]	28.0±11.4[a]
		Lateral Lumbar Flexion	Lateral Thoracic Flexion	Lateral Trunk Flexion
Lat. Flex	No Brace	-17.9±8.3	-39.1±11.3	21.7±4.2
	ProLign	-12.7±7.0[a]	-29.2±9.5[a]	16.7±4.1[a]
	UltraLign	-9.9±4.6[a b]	-21.1±6.3[a b]	11.4±3.5[a b]

[a] – significantly different from No Brace.
[b] – significantly different from ProLign .

These results were further verified by the percent ROM reduction data; the UltraLign and ProLign both limited significantly more intervertebral joint ROM with 42% and 43% reduction for L5 and with 16% and 48% for L1 compared to the control conditions during trunk flexion movements (Table 2). Similarly, the UltraLign LSO provided more restrictions than the ProLign LO on the motion of the lumbar, thoracic, and trunk segments during the lateral trunk flexion. The UltraLign is a lumbosacral LSO with greater support in both lumbar and lower thoracic regions whereas the ProLign is a lumbar orthoses with the support mainly concentrated on the lumbar region. The support frame in the lumbosacral brace is also more rigid than the ProLign LO.

Table 2. Average percent ROM changes of spinal segments vs the unbraced condition (mean±SD).

	Device	L5 Tilt	L1 Tilt	T1 Tilt
Flex	ProLign	41.9	16.4	14.9
	UltraLign	42.6 *	47.6 *	29.9 *
Ext	ProLign	-8.2	-4.8	18.4
	UltraLign	-5.3	40.6 *	29.1 *
		Lumbar Lateral Flexion	Thoracic Lateral Flexion	Trunk Lateral Flexion
Lat. Flex	ProLign	17.0	23.1	22.8
	UltraLign	20.4 *	42.8 *	46.2 *

* - significantly different from ProLign .

SUMMARY

The results suggested that both UltraLign and ProLign are effective in restricting the trunk movements. The UltraLign provided greater support and restricted more ROM in all three spinal movements and can be used when a strictest control of the lumbosacral region is warranted. The ProLign LO offered less support for the lumbosacral region and restriction on the movement, but was effective in providing such restriction to certain extents while offering functional flexibility for performing daily activities.

REFERENCES

Jorgensen, M. J. and Marras, W. S. (2000). *Clin. Biomech.*, **15**, 292-294.

McGill, S., et al. (1994). *Spine*, **19**, 696-704.

White, A. A. and Panjabi, M. M. (1990) *Clinical Biomechanics of the Spine.*

ACKNOWLEDGEMENTS

This study was sponsored by DeRoyal Industries, Inc.

BIOMECHANICAL ANALYSIS OF ANTERIOR INSTRUMENTATION FOR LUMBAR SPINAL CORPECTOMY

[1,2]Mahar A; [2]Faro F;[2]White K; [3]Ahn J; [1]Oka R; [1]Farnsworth C; [1]Newton P
[1]Children's Hospital & Health Center – San Diego, San Diego , CA; [2]University of California San Diego, San Diego, CA; [3]Chungnam National University, Daejeon, Korea
amahar@chsd.org

INTRODUCTION

Vertebral corpectomy is common in the treatment of spinal canal compromise from fractures, tumors, infections, and degenerative deformities of the thoracic and lumbar spine. Reconstruction of the vertebral body with a strut graft and anterior instrumentation allows restoration of the mechanical integrity of the anterior spinal column. Two basic design concepts are commonly implemented for anterior spinal instrumentation: plate constructs and rod constructs. Plate systems offer graft compression with a relatively low instrumentation profile. Rod systems are higher profile but offer rigid rod-screw connections. The purpose of this study was to compare the biomechanical properties of these two different design concepts for anterior spinal instrumentation after lumbar corpectomy, specifically evaluating the Antares 5.5 dual rod system and the Anterior Thoracolumbar Locking (ATL) Z-plate, which are distributed by a single manufacturer, Medtronic Sofamor Danek.

METHODS

Twenty lumbar spines (L2-4) from 3-week-old calves were dissected, removing all muscular tissue and leaving the anterior and posterior ligamentous structures intact. A corpectomy of the L3 vertebral body was performed and a previously harvested, fresh-frozen tibial allograft was placed in the corpectomy defect. Each spine was then instrumented on the left side with either the ATL Z-plate (n=10) (Figure 1) or the Antares dual rod system (n=10) (Figure 2) according to manufacturer instructions.

Figure 1: Z-plate stabilization

Figure 2: Anteres stabilization

Instrumented spines were then potted in an epoxy resin (Bondo; Mar-Hyde Corp., Atlanta GA), reinforced with screws and mounted in a MTS 858 Mini-bionix biaxial testing machine (Eden Prairie, MN) for biomechanical testing. In random order, the spines underwent non-destructive testing in flexion (5 Nm), extension (5 Nm) and lateral bending (5 Nm) using a cantilever bending apparatus. Torsional stability was tested between +/-5 Nm with a 100 N compressive axial load. Five loading cycles were completed with three cycles of pre-load followed by two cycles of data acquisition. Ultimate torque to failure was performed at a rate of 0.5 deg/sec (to the maximum torque cell capacity of 25 Nm). Force, displacement, torque and angular rotation data were collected at 10 Hz. Range of motion and stiffness were calculated for the cyclic tests while stiffness and ultimate failure torque were calculated for the failure tests. All data was analyzed using a one-way ANOVA ($p<0.05$).

RESULTS AND DISCUSSION

There was greater stiffness ($p<0.05$) in all directions of bending for the Antares construct. The Antares system was stiffer than the Z plate system in flexion (1.1 ± 0.7 Nm/deg vs 0.5 ± 0.2 Nm/deg) and extension (1.4 ± 0.8 Nm/deg v 0.6 ± 0.3 Nm/deg). Similar trends were noted in right and left lateral bending with greater stiffness noted in the dual rod Antares system. No significant difference was noted in the torsional testing (both nondestructive and torque to failure). There was no evidence of hardware failure or distortion following the failure tests except one instance of screw loosening in a Z plate specimen. Most failures initially occurred due to disruption of the facet joint capsule.

Figure 3. Non Destructive Biomechanical Testing

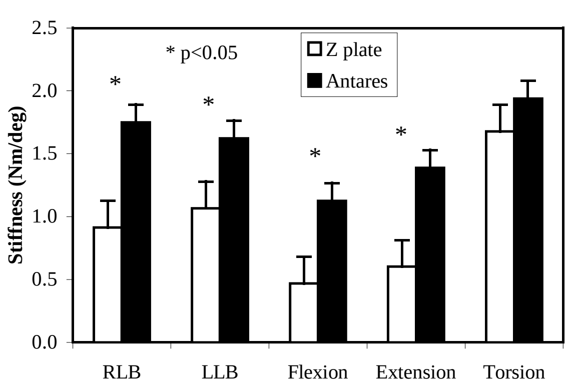

Figure 4. Torque to Failure

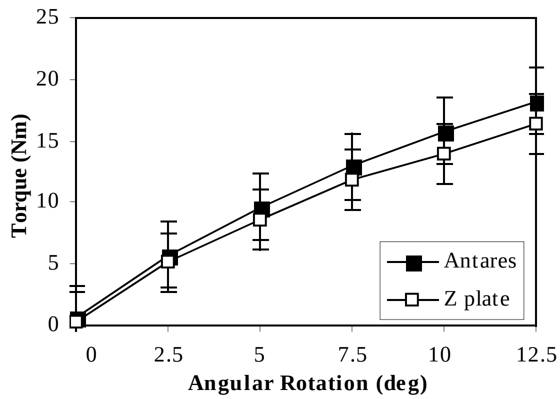

SUMMARY

Although there was significantly greater resistance to bending with the dual rod construct, the ultimate selection of a system will require an individual analysis of implant profile, construct demand, and ease of use. The plate system is low in profile but requires careful selection of the proper length plate to accommodate compression of the graft. The rod system allows a rigid connection between the rods and all of the vertebral screws (as opposed to only 2 of the 4 screws in the plate system). Both systems provided secure initial fixation following lumbar corpectomy; however, the Antares system may increase the likelihood of graft incorporation in cases with marked instability or greater external loading.

ACKNOWLEDGEMENTS

This study was funded by a research grant from Medtronic Sofamor Danek.

This document was created with Win2PDF available at http://www.daneprairie.com.
The unregistered version of Win2PDF is for evaluation or non-commercial use only.

CALCULATION OF DYNAMIC SPINAL SOFT TISSUE DEFORMATIONS

Paul C. Ivancic, Shigeki Ito, Adam M. Pearson, Manohar M. Panjabi and Wolfgang Rubin

Biomechanics Research Laboratory, Yale University School of Medicine, New Haven, CT, USA
E-mail: paul.ivancic@yale.edu

INTRODUCTION

To better understand the spinal injury mechanisms, the deformations of the spinal soft tissues during simulated trauma must be determined. The main purpose of the current study was to describe a technique to calculate the sagittal spinal soft tissue deformations due to either static or dynamic loading. The methodology is illustrated via an example to determine the deformations and strains in the C5-C6 capsular ligaments (CLs) of a whole cervical spine model during a simulated frontal impact. Additionally, the errors of the technique, and the rigid body assumption associated with the technique, are investigated.

METHODS

A fresh-frozen human osteoligamentous whole cervical spine specimen was mounted at the occiput and T1. Motion tracking flags, consisting of two white, spherical, radio-opaque markers, were rigidly attached to the C5 and C6 vertebral bodies (VBs) and lamina in the mid-sagittal plane. The C5 VB and lamina flags were denoted as flag 1 (with markers 1A and 1B) and flag 2 (with markers 2A and 2B) respectively, while the C6 VB and lamina flags were denoted as flag 3 (with markers 3A and 3B) and flag 4 (with markers 4A and 4B), respectively (**Figure 1**). A sagittal x-ray of the specimen was taken and digitized.

To prepare the specimen for frontal impact simulation, a surrogate head was attached to the occipital mount and the T1 mount was rigidly fixed to the sled. The surrogate head and spine were stabilized using the compressive muscle force replication system (Ivancic et al., 2002). Frontal impact simulation was performed using a previously developed bench-top apparatus at a peak nominal T1 horizontal acceleration of 5 g. A high-speed digital camera recorded the spinal motions at 500 f/s.

The lateral radiograph was used to establish rigid body relationships between the centroids of flag markers (1A to 4B) and the CL origin and insertion points, defined by vectors $\boldsymbol{u_1}$ to $\boldsymbol{u_4}$ (**Figure 1**) (Panjabi et al., 1991a; Panjabi et al., 1991b). The geometrical rigid body relationships were superimposed onto the first frame of the high-speed movie. Custom motion-tracking software was used to calculate the flag rotations and flag marker translations at each subsequent frame in the ground coordinate system z-y. The translation vectors of the CL origin ($\boldsymbol{t_O}$) and insertion ($\boldsymbol{t_I}$) at each subsequent frame were calculated in two ways, first using the VB flag rotations and VB flag marker translations:

$$(\boldsymbol{t}_O)_{VB} = \boldsymbol{t}_{3B} + R\,\boldsymbol{u}_3 - \boldsymbol{u}_3\,,$$

$$(\boldsymbol{t}_I)_{VB} = \boldsymbol{t}_{1B} + R\,\boldsymbol{u}_1 - \boldsymbol{u}_1\,,$$

and second using the lamina (L) flag rotations and lamina flag marker translations:

$$(\boldsymbol{t}_O)_{L} = \boldsymbol{t}_{4B} + R\,\boldsymbol{u}_4 - \boldsymbol{u}_4\,,$$

$$(\boldsymbol{t}_I)_{L} = \boldsymbol{t}_{2B} + R\,\boldsymbol{u}_2 - \boldsymbol{u}_2\,,$$

where the rotation matrix, R, was defined as:

$$R = \begin{bmatrix} cos(\theta) & -sin(\theta) \\ sin(\theta) & cos(\theta) \end{bmatrix}.$$

The sagittal length change, Δl, between the CL origin and insertion was calculated for each frame in two ways:

$$\Delta l_{VB} = \sqrt{(z_O - z_I)_{VB}^2 + (y_O - y_I)_{VB}^2} - l_0\,,$$

$$\Delta l_L = \sqrt{(z_O - z_I)_L^2 + (y_O - y_I)_L^2} - l_0\,,$$

where l_o was the CL length in the neutral posture. The CL strain was calculated by dividing the change in length by the original CL length (expressed in percent).

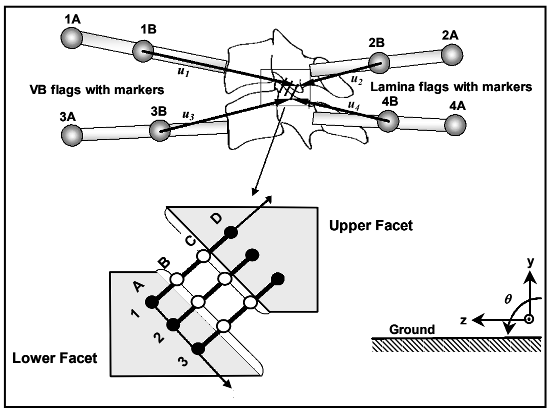

Figure 1. Schematic showing functional spinal unit with flags and facet points.

A jig was constructed to determine the overall system error. The jig consisted of two motion-tracking flags with three markers per flag. The flags were connected by a hinge joint. An automated digital micrometer was used to apply a known translation between the lower markers on the flags in 50 increments of 0.1 mm each, and a digital image was recorded at each motion step. The custom software was used to track the positions of the all markers. Using the mathematical technique, the length change between the markers was calculated. The average (SD) error in the length change was 0.3 mm (0.2 mm).

RESULTS

The C5-C6 CL strain during the 5 g frontal impact simulation exceeded 20% and was greatest at CL 3 (**Figure 2**). The difference between the VB and lamina length change calculations was 0.5 mm at peak CL elongation.

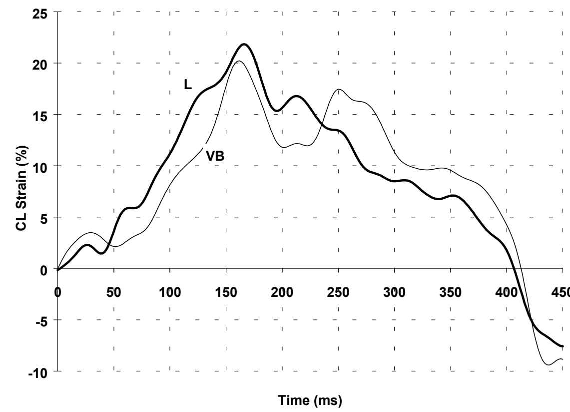

Figure 2. C5-C6 CL 3 strain calculated using the vertebral body (VB) and lamina (L) flags during the frontal impact.

DISCUSSION AND SUMMARY

A mathematical technique to calculate the spinal soft tissue deformations during either static or dynamic loading has been presented. The technique may be extended to three-dimensions to determine the spinal kinematics during side and head-turned simulated impacts.

REFERENCES

Ivancic, P.C.et al. (2002). *CSRS*, 180-182.

Panjabi, M.M. et al. (1991a). *Spine,* **16**, 861-869.

Panjabi, M.M. et al. (1991b). *J Spinal Disord,* **4**, 277-285.

ACKNOWLEDGEMENTS

The financial support of the NIH (Grant 1 R01 AR45452 1A2) and the Doris Duke Clinical Research Foundation is gratefully acknowledged.

COUPLING EFFECT OF AXIAL ROTATION AND LATERAL DEVIATION OF MOTION SEGMENTS IN IDIOPATHIC SCOLIOSIS

Behnam Heidari[1], David FitzPatrick[1], Keith Synnott[2] and Damien McCormack[2]

[1]Department of Mechanical Engineering, University College Dublin, Dublin, Ireland
[2]Spinal Unit Research Group (SURG), National Spinal Centre, Mater Misericordiae Hospital, Dublin, Ireland
E-mail: bheidari@yahoo.com

INTRODUCTION

Scoliosis is a complex three-dimensional deformity that is usually considered in the frontal plane without references to curvature in other planes. An important feature of idiopathic scoliosis deformity is the horizontal plane rotation (vertebral axial rotation). This rotation is thought to be significant for initiation and progression of idiopathic scoliosis (Adams W, 1865). Somerville's (1952) studies suggested that scoliotic spine exhibits lordosis as well as lateral curvature and horizontal rotations. Raof (1958) maintained that the deformities of idiopathic scoliosis could be explained on the basis of a primary rotation alone.

There is a lack of clear biomechanical analyses to explain the interaction of the lateral and axial deformity of the spine in idiopathic scoliosis and their coupling effect has yet to be effectively studied. This will allow description of scoliosis pattern and quantification of the deformity.

In the present study, only the geometry of scoliosis was of concern. Therefore, force and force-determination relationships were not considered. They undoubtedly play a significant role in the mechanics of scoliosis, but it seems reasonable to study first the kinematics of spinal deformity.

OBJECTIVES

The purpose of the present study is to investigate the relationship between axial rotation of the vertebral body and the resulting lateral deviation, sagittal deformity, and overall deformity of thoracic spine in scoliosis.

METHODS

Investigating the coupling effect of vertebral axial rotation and lateral deviation is essential in understanding the mechanism of scoliosis aetiology, progression, and correction. In this study a mathematical analog of the human thoracic vertebral column is constructed to model vertebral axial rotation and the associated lateral deviation and overall deformity of the spine. Thoracic spine curvature, with simplified cylindrical vertebral body geometry, is modeled by the use of anatomical data (Panjabi MM, 1991). In this model we assumed equal motion segments along the thoracic spine and the position of T-7 is considered at the apex of the curve.

We have adopted a global coordinate system for the thoracic spine and a local coordinate system on the vertebral body centroids. Geometrical data of the normal model is stored in a three-dimensional matrix. A homogeneous transformation matrix is employed to apply the vertebral rotation in each motion segment to the model. Different axial vertebral rotations were applied to the model to study the influence of rotational displacement on the overall configuration of thoracic spine and to investigate the required changes to bring a normal thoracic spinal column into the geometrical configuration of idiopathic scoliosis.

RESULT AND DISCUSSION

This study addresses a hypothesis that the development of scoliosis deformity is in association with the axial rotation of spinal motion segments. The initial results of the model demonstrate that: 1) vertebral axial rotation can deform the normal spinal curvature, 2) increase in the amount of axial rotation within spinal motion segments will increase the scoliosis deformity of the spine, and 3) the vertebral axial rotation before and after the apex of the curve are in opposite directions (i.e. clockwise and counter-clockwise direction) which is in accordance with the Raof (1958) findings.

Figure 1 illustrates the model with axial rotation of +5°(CW) and –5°(CCW) below and above the apex of the normal spine respectively. The three-dimensional results of the model demonstrate the important relationship between the axial rotation and the size of the scoliosis. The result shows the geometrical characteristics of the scoliotic spine and agrees with the studies of Kanayan et al. (1996).

Increasing axial rotation of the motion segments within the thoracic curve results in an increase in the lateral deviation of the spine in the coronal plane. In the thoracic region, our findings were in agreement with literature that scoliosis is accompanied by loss of sagittal curvature (Stokes IAF et al., 1987; Adams W, 1865).

Therefore, regardless of the precise aetiology of the scoliosis, results of our study demonstrate that the axial rotation of the motion segments directly affects the spatial curvature of the spine (i.e. the three-dimensional deformity produced) and implies that axial rotation could be a primary factor in development of scoliosis deformity.

Improved knowledge of the influence of axial rotation and the resulting lateral deviation will help in understanding the mechanism of scoliosis aetiology, progression and correction.

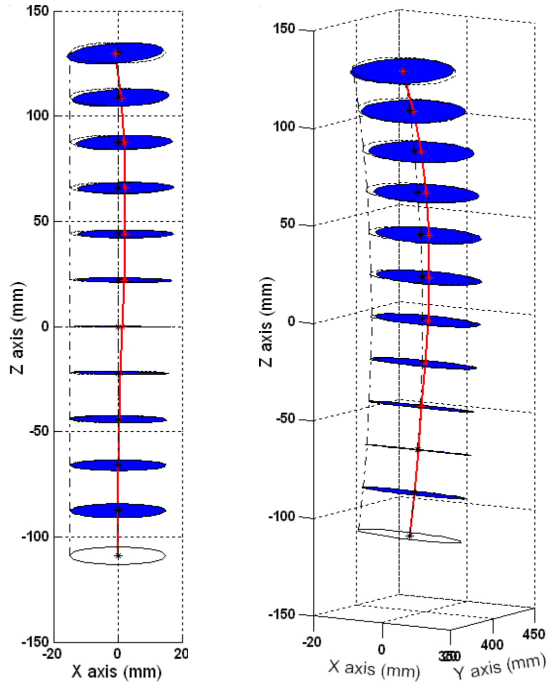

Figure 1: Frontal view (left) and 3D view (right) of thoracic spine with axial rotation of motion segments.

REFERENCES

Adams W. (1865). *Lectures on the Pathology and Treatment of Lateral and Other Forms of Curvature of the Spine.* John Churchill and Sons.

Somerville E. W. (1952). *J. Bone Joint Surg.*, **34-B**, 421-427.

Raof, R. (1958). *J. Bone Joint Surg.*, **40-B**, 312-332.

Panjabi MM, Takata K, et al (1991). *Spine,* **16**, 888-890.

Kanayama M, Tadano S, et al (1996). *ASME J. Biomech Eng.*, **118**, 247-252.

Stokes I.A.F., Gardner-Morse M. (1991). *J. Biomech.*, **24**, 753-759.

ACKNOWLEDMENTS

This research project is supported by a grant of the fund from Enterprise Ireland. First author wishes to thank Mr. Atid Shamaie for the computer programming assistance.

THE EFFECT OF A THIN COATING OF A BIOADHESIVE ON THE IMPACT PERFORMANCE OF THE CEMENT – IMPLANT INTERFACE IN THR

Ashokkumar Balasubramaniam[1], David W. Nicholson[1], Larry P. Chew[1], Simon Raab[2]

[1] Department of Mechanical, Materials and Aerospace Engineering,
University of Central Florida, Orlando, FL, USA
[2] Xenon Corporation, Lake Mary, FL, USA
E-mail: ashok_balu@hotmail.com

INTRODUCTION

The aging of the world population has led to the growth of the orthopaedics market, particularly in implants. However, most implants only last about 10 to 15 years. Loosening of the femoral stem remains the major mode of long-term failure of Total Hip Arthroplasty (THA). It has been postulated that the loosening of the prosthesis is initiated by debonding of the stem-cement interface, followed by bulk failure of the cement mantle itself [Jasty et al, 1991]. Debonding is promoted by repeated subcritical impacts. Precoating the stem of the prosthesis with a thin film of Poly Methyl MethAcrylate significantly improved the strength of the cement-prosthesis interface [Ahmed et al, 1984]. But the failure then shifted to the cement-bone interface [Dowd et al, 1998].

A precoating of the prosthesis that can absorb the strain energy and impede transfer of unwanted stresses to the cement-bone interface when subjected to impact load will be an ideal candidate material for Total Hip Replacement (THR). The objective of this research is to analyze the performance of a new copolymer of 2-Hydroxy Ethyl MethAcrylate (HEMA) and Methyl MethAcrylate (MMA) as an interface material used in THR under impact, using the explicit finite element code LS-DYNA, to see if this copolymer has the potential of eliminating the long term loosening in THR. To validate the model, a configuration for dynamic testing of the interfacial strength has been developed.

METHODS

The structure sample for testing is a simplified model of the actual artificial hip joint. Two steel rods, each coated with HEMA/MMA copolymer at the ends to be embedded, are joined together with bone cement. These samples are impacted coaxially with two spherical steel balls, causing shear at the interfaces (bone cement-copolymer and copolymer-steel rod interface). After the rods have been coated with the copolymer layer, they are soaked in 0.85 % NaCl solution for about 30 to 35 days in order to saturate the samples.

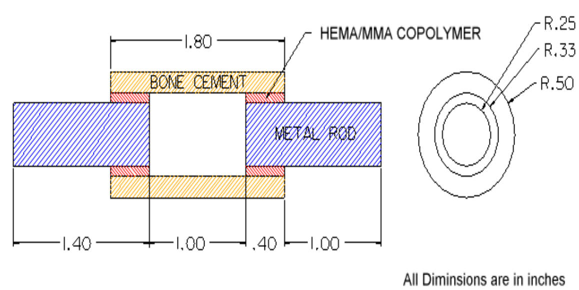

Figure 1: Structure Sample

A finite element model of the structure sample and the spherical steel balls was developed in the LS-INGRID modeling package. For the rods, the bone cement and the spherical balls, a linear elastic material model was used. The copolymer layer was modeled using piecewise linear plastic material model. LS-DYNA, an explicit nonlinear finite element code, was used for the analysis. The main reason for using LS-DYNA is its element killing capability, which few other codes do not have. When the effective plastic strain reaches the failure strain, the element loses its ability to carry tension and the deviatoric stresses are set to zero, i.e., the element behaves like a fluid.

The material properties for the copolymer layer have been obtained from experimental tensile test results of the material sample. Spherical balls delivering the impact were given an initial velocity while the structure sample was held stationary. The energy absorbed by the structure sample was noted. The composition of the copolymer was varied from 0% HEMA to 60% HEMA so as to show the effect of increase in the percentage of HEMA. Both the dry and the wet samples were analyzed. With the help of a specially designed set-up for dynamic strength testing, testing was performed on several compositions of the copolymer.

RESULTS AND DISCUSSION

Results of the validation exercises indicate satisfactory consistency between the analytical and the computational solutions.

Results of analysis without failure indicate an increase in energy absorption from 0% to 20% HEMA and a gradual drop after that till 60% HEMA. This is the same with both the wet and the dry samples. Computations with failure indicate a decrease in the energy absorbed by the structure sample at break from 0% to 20% HEMA and an increase in the same from 20% to 60% HEMA for the wet samples. However, there is not much difference between the energy absorption by 0% and 40% HEMA. On the other hand, in case of the dry samples, the energy absorbed at break is totally scattered.

Results of the experimental analysis indicate satisfactory consistency with the energy absorbed at break using finite element analysis, but for 40% dry HEMA and for 0% wet HEMA. The difference in the values of these two compositions of HEMA may be attributable to the fact that the material properties for the copolymer layer were obtained from the static results. Since four of our six finite element results matched with the experimental ones, the finite element results are believed to be reliable.

Also of importance is that the test procedure is reproducible and capable of discrimination between different adhesives, and different specimen preparations.

CONCLUSIONS

Varying the percentage of HEMA in the copolymer appears to improve the performance of the structure sample under impact loading conditions, below the breaking limit. A reliable finite element model, which can be used for further analysis, has been developed, and a discriminating experimental set-up for dynamic testing of the specimen has been designed.

REFERENCES

Ahmed A.M. et al. (1984). *Metal/cement interface strength in cemented stem fixation, J Orthop Res.* **2**, 105-118.

Jasty, M. et al. (1991). *The initiation of failure in cemented femoral components of hip arthroplasties, J Bone Joint Surg [Br],* **73,** 551-558.

Dowd, J.E. et al. (1998). *Failure of Total Hip Arthroplasty With a Precoated Prosthesis. J Clinical Orthopedics and Related Research,* 123-136.

Livermore Software Technology Co. (1993). *LS-DYNA-3D Manuals.*

SARCOMERE NUMBER ADAPTATION IN THE RABBIT TIBALIS ANTERIOR AFTER CHRONIC ECCENTRIC EXERCISE

Tim Butterfield and Walter Herzog

Human Performance Laboratory, University of Calgary, Calgary, Alberta, Canada
E-mail: timb@kin.ucalgary.ca

INTRODUCTION

It has been well documented that a bout of eccentric exercise causes subsequent pain and discomfort within days of the exercise. However subsequent eccentric exercise fails to produce the same discomfort. One proposed theory used to explain this repeated-bout effect links fiber damage produced through the popping of weak sarcomeres on the descending limb of the force-length relationship (FLR) to a subsequent increased serial sarcomere number within the fibers. This would result in a rightward shift of the FLR, allowing the adapted muscle fibers to operate over the ascending limb and plateau of the FLR with subsequent exercise bouts (Proske and Morgan, 2001). This mechanism is based on damage as a precursor to adaptation, and thus should only occur with eccentric exercise performed on the descending limb of the FLR. Although studies have shown a significant increase in serial sarcomere number with an *in-vivo* animal model (Lynn et al., 1998) as well as a controlled eccentric training protocol (Koh and Herzog 1998), pre and post-exercise FLRs have not been reported.The purpose of this study was to assess the adaptation of the ankle dorsiflexors in conjunction with the FLR, before and after a chronic eccentric exercise protocol.

METHODS

Nerve cuff electrodes were implanted bilaterally on the peroneal nerves of nine adult New Zealand white rabbits. The left nerve cuff electrode was attached to a custom made subcutaneous electrical interface that allowed the formation of temporary connections to an external stimulator (Koh and Leonard, 1996). The interface was connected to a stimulator, and the anesthetized rabbits were placed supine in a sling with their left foot attached to a foot plate connected to the cam of a servo motor. Supra-maximal stimulation was determined (voltage 3x α-motoneuron threshold, 150 Hz) and the isometric FLR of the ankle dorsi-flexors was assessed on day one. Subsequently, an eccentric exercise bout of 5 sets of 10 repetitions was performed (stimulus train duration = 500 ms) from a tibiotarsal joint angle of 70^o-105^o at 70^o sec^{-1}. The eccentric exercise protocol was repeated 3 times per week for 6 weeks, with at least 48 hours rest between bouts. One week after the last exercise bout, the FLR was repeated, and the rabbits were euthanized 48 hours later. Left and right tibialis anterior (TA) muscles were excised, weighed and processed. Six fascicles were teased from the superficial and deep layers of the central third, and placed on glass slides. Fascicle and sarcomere lengths were measured and analyzed.

RESULTS AND DISCUSSION

Seven rabbits were used in the final analysis. Mean weight of the TA between trained ($6.19 \pm .591$g) and contralateral control ($5.10 \pm .579$g) limbs using a paired t-test showed a significant training effect of the exercise protocol (p<.001). The FLR showed no rightward shift after the 6 week training protocol (Fig.1). There was a small (3.6%) but significant increase in serial

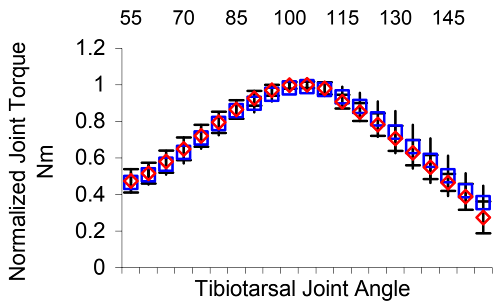

Figure 1. Isometric FLR pre (◊) and post (□) exercise (mean ± SD)

sarcomere number in the superficial fibers of the central portion of the exercised TA (p<.05). Sarcomere number was not significantly different between the deep fibers of the trained and control TA (Fig. 2). Normalizing sarcomere number to 1 mm

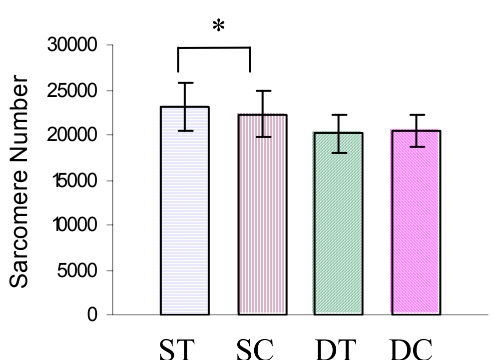

Figure 2. Graph of serial sarcomere numbers for superficial trained (ST), superficial control (SC), deep trained (DT), and deep control (DC) fascicles. (Mean ± SD)

Table 1. Values are Mean ± SD

	Sarcomere # / mm (density)		Fascicle Length (mm)	
	TA Superficial	TA Deep	TA Superficial	TA Deep
trained	479.09 ± 20.97	467.71± 33.57	48.44 ± 7.40	43.51 ± 6.33
control	474.84 ± 28.56	461.98 ± 32.55	47.37 ± 7.69	44.20 ± 4.46
difference	4.25	5.73	1.07	-0.69
P- value	.443	.253	.042*	.530

of fascicle length showed the actual number of sarcomeres/mm (density) remained unchanged with no significant differences between the measures. Superficial fascicle lengths were significantly longer (2%), compared to the controls (p<.05) (table1), suggesting sarcomere density remains constant, and fascicle lengths increase in response to chronic eccentric exercise.

SUMMARY

Although there was a significant increase in serial sarcomere number, this appeared to be due to an increasing fascicle length, as sarcomere numbers per length of fascicle (density) remained unchanged. The exercise protocol was performed through a ROM consistent with the ascending limb and plateau of the FLR, which may account for the small increase in sarcomere number and lack of shift in the FLR. Future studies using eccentric exercise over a greater ROM may help explain these findings.

REFERENCES

Koh, T.J., Herzog, W. (1998). *J Biomech,* **31**, 499-501.

Lynn, R. et al. (1998). *J. Appl. Phys.* **85**, 98-104.

Proske, U., Morgan, D.L. (2001). *J Physiol.* **537.2**, 333-345.

Koh, T. J., Leonard, T. (1996). *J. Neurosci Methods.* **70**, 27-32.

ACKNOWLEDGEMENTS

Tim Leonard, Dr. David Corr, Dr. David Longino, Hoa Nguyen, NSERC of Canada.

FAILURE MODE OF SUTURE ANCHORS AS A FUNCTION OF INSERTION DEPTH

[1,2]Mahar, A; [3]Bynum, C, [2]Lee, S , [3]Tasto, J,[2,3]Pedowitz, RP

[1]Orthopedic Biomechanics Research Center, Children's Hospital San Diego, CA
[2]Department of Orthopedics, University of California, San Diego, CA
[3]San Diego Arthroscopy and Sports Medicine Fellowship, University of California San Diego
amahar@chsd.org

INTRODUCTION

A high proportion of successful rotator cuff repairs are left with residual deficiencies in the cuff. Previous biomechanical studies reported failures via suture cutting through bone tunnels, suture breakage, knot slippage, suture anchor pull out, and soft tissue failure at the suture- tendon junction. Due to the clinical failures discussed above, surgeons often "bury" the anchor or place the anchor at twice the normal depth to improve pullout strength. It is unclear, however, if the depth of anchor insertion may have an influence on failure characteristics. New modes of failure could be either weakening of the suture at the tunnel entrance or anchor eyelet during cyclic loading with abrasion and mechanical degradation of the suture, or suture cut out through the bone. The purpose of this study was to determine if anchor insertion depth has an effect on the failure characteristics of sutures and suture anchors used in rotator cuff repairs.

METHODS

Thirty metallic OBL (Smith and Nephew, Memphis, TN) 5.0 mm screw-in suture anchors loaded with a single number 2 braided nonabsorbable polyester suture were randomly inserted at 3 depths (proud, standard, and deep) in four, 12 week old bovine humerii. Immature bovine bone has reported a bone density of 0.8g/cm^3, similar to the value reported for young humans[1], making the bovine model a viable biomechanical testing option.

Anchors were placed in the rotator cuff insertion site of the infraspinatus tendon after soft tissue resection. Anchors were placed 1 cm away from an adjoining anchor in a random pattern. The "proud" anchors were inserted with the shallowest part of the threaded portion of the anchor flush with the bone surface in the middle of the hole. The "standard" anchors were inserted according to the manufacturer's guidelines with the first laser line flush with the bone surface (threads 3mm counter sunk). The "deep" anchors were inserted at twice the depth of the standard anchors (6 mm) (Figure 1).

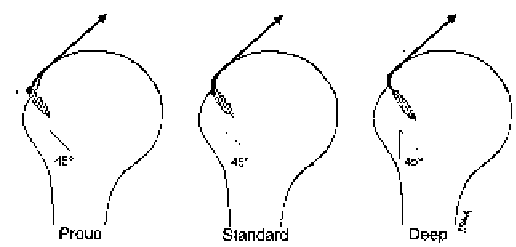

Figure 1: Anchor insertion techniques.

The anchor was placed into the bone at an angle of 45 degrees to maximize purchase. Each shoulder was tested with an equal number of proud, standard, and deep anchors (n=3). Surgical knots were used to create a closed loop and concentrate the failure mechanism at the suture-bone-anchor interface. The loop was then attached to a MTS 858 machine (Eden Prairie, Minnesota) over a smooth metallic rod. The humerus was held in place with a custom fixation rig. Sutures were marked at the eyelet and within the rig to accurately determine the location of failure. The direction of suture pull was perpendicular to the angle of insertion of the suture anchor. The sutures were then placed under 10 N of pre-load and cyclically loaded from 10 to 90N at 0.5 Hz to a maximum of 500 cycles. If still intact after 500 cycles, the sutures were loaded at 0.5mm/sec to failure. The number of cycles, mode of failure and maximal failure load were recorded for each specimen. All data were compared with a one-way ANOVA ($p<0.05$), employing a Tukey's *post-hoc* test for multiple comparisons.

RESULTS

There was a significant difference in the number of cycles to catastrophic failure between the deep and both the standard and proud sutures ($p<0.0004$) (Table 1). No deep construct failed early via suture breakage. Four out of eleven standard depth and 6/9 proud depth anchors failed early during cyclic testing. All early failures in these groups occurred by suture failure at the anchor eyelet. There was no statistical difference in cyclic failure between the proud and standard anchors (Table 1). Using 3 mm of displacement as a standard for clinical failure, the sutures in the deep anchor group failed earlier than the standard and proud anchor groups. In 9/10 of the deep specimens, failure via gross cutting through the cortical margin of the bone was observed and occurred at an average of 8 ± 6 cycles. The standard anchors failed to the 3 mm level at an average of 12 ± 2 cycles with a variable degree of bone cut through. The proud anchor sutures failed at the 3mm clinical level at an average of 30 ± 31 cycles. There was no statistical difference between the deep and standard anchors in number of cycles to 3mm of failure. In evaluating ultimate load failure, the deep anchor had a statistically greater failure load than either the even anchors or the proud anchors. In all deep construct specimens, ultimate failure occurred at the knot at a mean of 165 ± 18N. For the even constructs the mean ultimate failure was 133 ± 38N, while the proud anchors had the lowest failure load of 112 ± 36N.

SUMMARY

Based upon these data, burying suture anchors beyond the specified insertion depth is inadvisable. Excessive anchor depth may lead to early clinical failure by the suture cutting through bone, and is of specific concern for osteoporotic bone. It is clear that suture abrasion at the anchor eyelet may result in catastrophic failure of the repair construct. There are two potential solutions for this phenomenon. Anchor eyelets should be designed to lessen the possibility of abrasive degradation of the suture, and abrasion-resistant materials should be developed in order to decrease the risk of suture fretting.

REFERENCES

[1] Gibson, L, Ashby, M. **Cellular solids**. 1987, 316-331.

ACKNOWLEDGEMENTS

This study was funded by a research grant from Stryker Howmedica.

Table 1: Biomechanical data from cyclic and failure testing.

Anchor Depth	Cycles to Catastrophic Failure *	Cycles to 3mm of Failure **	Max Failure Load (N)***
Deep	**500** $\pm$ 0 *	**8** $\pm$ 6	**165** $\pm$ 18 ***
Even	**377** $\pm$ 197	**12** $\pm$ 2	**133** $\pm$ 38
Proud	**259** $\pm$ 207	**30** $\pm$ 31 **	**112** $\pm$ 36
	* $p<0.0004$	** $p<0.02$	*** $p<0.005$

This document was created with Win2PDF available at http://www.daneprairie.com.
The unregistered version of Win2PDF is for evaluation or non-commercial use only.

ADAPTIVE FINITE ELEMENT ANALYSIS FOR ORTHOPAEDIC CONTACT PROBLEMS

Roarty C.M. and Grosland N.M.

University of Iowa, Iowa City, Iowa, USA

INTRODUCTION

Finite element and other computational techniques are widely applied in the analysis and design of hip and knee implants, with additional joints (ankle, shoulder, wrist) attracting increased attention. Recently, a growing interest has developed in the orthopaedic biomechanics community, allowing numerical models to be constructed for the optimal solution of contact mechanics problems. Improving upon implant design is just one example of why new developments in this area are of such importance.

The process of creating a finite element (FE) mesh can prove to be a constant negotiation between refining the mesh and keeping the model within a reasonable size. As a solution, an adaptive method has been developed to locally refine the mesh in areas of computational instability (point contact areas) while keeping the majority of the mesh less refined. The devised adaptive meshing scheme introduces additional elements exclusively within the critical areas of the mesh and only for the necessary duration.

METHODS

The Universal total wrist implant (Universal, Kinetikos Medical Inc. San Diego, CA) is the prosthesis used in this adaptive analysis. The Universal implant is composed of carpal, radial, and polymeric components. The carpal and radial components were modeled as rigid bodies represented by 4-noded quadrilateral elements (1600 elements) and 3-noded triangular elements (2108 elements), respectively. The polymeric component was modeled via 6,400 8-noded hexagonal elements (E = 634.92 MPa, v = 0.45). All FE analyses were performed with ABAQUS (Version 6.2 & 6.31, HKS Inc., Pawtucket, RI), and coupled with the custom-written adaptive meshing algorithm.

Initiating with a relatively coarse base grid generated in PATRAN, a rotational (or translational) displacement is assigned (i.e., 5 degrees (4mm)). As the solution proceeds, the resisting moment (force) is tracked. Once oscillatory behavior is observed, the FE solution is halted and the elements with high von Mises stresses are identified. Refined subgrids are then invoked in only those regions. The FE solution is re-started from its pre-oscillatory position with the new locally refined mesh. If need be, additional subgrids are added recursively until either a given maximum level of refinement is reached or until the oscillatory behavior ceases.

The subgrids are generated automatically by decomposing the pre-existing elements. This allows for the preservation of the hexahedral element shape that is preferable for contact problems. Twenty-five adjacent elements are identified within each highly stressed region. Each of these elements is decomposed into smaller hexahedral elements. As a result, 100 new elements lie on the articular surface of the polyethylene mesh, replacing the original 25 elements. Two different constraining techniques, to secure the refined mesh to the original coarse base mesh, were considered in this investigation: the multi-point constraint (MPC) and the tie constraint (both available in ABAQUS).

RESULTS AND DISCUSSION

Results have shown that increasing the mesh density within these regions of high stress does in fact decrease oscillatory behavior. Furthermore, additional increases in refinement lead to better results. Figure 1 illustrates a comparison between FE Results obtained from original coarse mesh 1(a) to two different sets of data obtained. The first set of data was taken following a single refinement 1(b). A double refinement introduces a second subgrid, with greater mesh density, within each critical area.

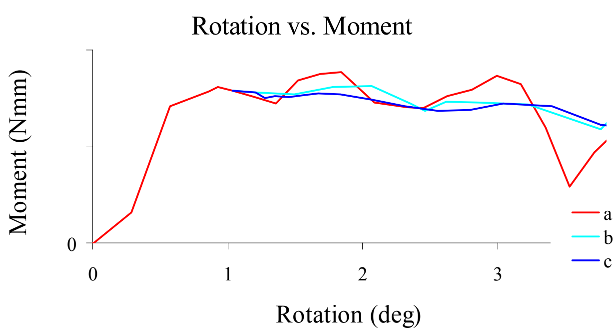

Figure 1: Resistive moment data obtained during axial rotation simulation: from (a) the original coarse mesh, (b) the singly refined mesh, and (c) the doubly refined mesh.

SUMMARY

Axial rotational results are promising when compared to experimental data. The quality of solution improves with each level of local refinement. Additionally, the adaptive nature provides an efficient means to offer multi-level refinements. This method has also been successfully applied to the model during translational displacement.

ACKNOWLEDGEMENTS

University of Iowa College of Medicine Research Grant

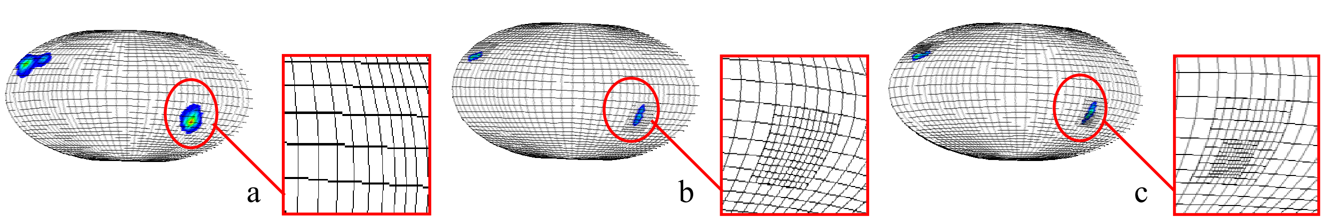

Figure 2: Articular surface of poly component throughout two stages of refinement. The (a) original mesh undergoes the two possible levels of refinement: (b) single and (c) double refinement.

LUMBAR-PELVIC COORDINATION IS ALTERED WITH HEAVY LIFTING TASKS

Anupama Maduri, Bethany Anderson and Sara Wilson

Department of Mechanical Engineering, University of Kansas, Lawrence, Kansas, USA
E-mail: anupama@ku.edu, sewilson@ku.edu

INTRODUCTION

Low back pain is a significant health concern. Incidences of low back injuries are reported to be high for industrial workers operating in flexed postures and lifting heavy objects [1]. As a person moves, a range of lumbar curvatures is available for any torso posture. For example, one can slouch ("Kyphotic") or stand up straight ("Lordotic"). This range of curvature can be associated with the neutral zone of the vertebra motion [2]. At the limits of this zone ligaments and/or facet joints are engaged limiting further motion.

Earlier, several authors examined lumbar-pelvic coordination in lifting tasks[3]. However, none have examined how this coordination interacts with range of motion and its ligamentous limits. Postures engaging the ligamentous or facet structures may load these structures risking damage. Control of motion in these postures may also benefit from proprioceptive feedback from sensors in these structures [4,5]. In order to better understand low back injury risk, it is therefore important to understand the interaction with ligamentous limits during lifting tasks. In this study, a variety of lifting tasks were assessed as a function of lumbar range to examine what types of tasks most interact with the end ranges.

METHODS

Twelve healthy volunteers, with ages ranging from 22-32 years participated in the study. The study was approved by Human Subjects Committee, University of Kansas, Lawrence.

An electromagnetic motion analysis system (Motion Star, Ascension Tech., VT) was used to collect data. Three markers, one over the T-10 spinous process, one over the L5/S1 spinous process, and one on the manubrium were placed on the participant (Figure 1).

Lordosis was defined as the angle between the markers over the T-10 and L5/S1 spinous process (Figure 2a). Torso flexion was defined as the angle between the vertical and the plane containing the three sensors (Figure 2b).

Figure 1: Three markers attached to participant over manubrium, T10 and S1 spinous process. The EMG electrodes are placed over the erector spinae muscle group at L2/L3 level of lumbar spine.

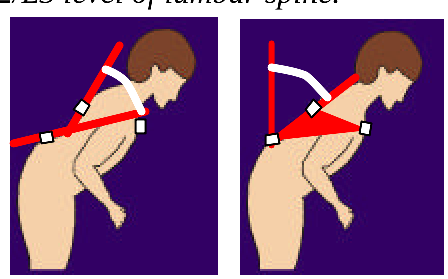

Figure 2. Lumbar angle was defined as the angle between markers over the T-10 and S1 spinous process (a). Torso flexion was defined as the angle between the vertical and a plane containing the 3 markers (b).

Subjects were asked to move from a minimum lumbar curvature to a maximum lumbar curvature three times at four flexion angles (0°, 30°, 60° and 90°). Subjects were then asked to perform heavy (40% of maximal effort) and light (no weight) lifting tasks at two lifting speeds (25 and 100 deg/sec). Each lifting task was repeated 3 times with speed controlled by having the subject follow a visual display. Finally subjects were asked to repeat the lumbar range measure again at the four flexion angles.

Coordination of the lumbar spine relative to torso motion was examined for the four types of lifting tasks. Lumbar lordosis was examined as a function of torso flexion. The limits of range of motion at 0°,30°,60°, and 90° were used to define the bounds of range of motion. Maximally lordotic was considered to be 0% of the range and maximally kyphotic was considered to be 100% of the range (Figure 3a).

RESULTS

During lifting tasks subjects remained near the middle of their range (54%) while descending. On ascent, subjects moved from the middle of their range (58%) to a highly kyphotic posture (92%) at 50 degrees of torso flexion ending at a slightly kyphotic posture (70%). Lumbar curvature was more kyphotic with heavy lifting tasks by 21% of the range and with slow lifting speeds by 14% of the range.

DISCUSSION

Lordosis was put in terms of the lumbar range of motion by initially measuring lumbar range at four flexion angles (0°, 30°, 60°, 90°). By moving to a more kyphotic lumbar curvature during ascent, particularly in heavy and slow lifting tasks, subjects put their lumbar spine into a greater degree of flexion, putting greater load on posterior spinal ligaments. These ligaments, in addition to providing support and reducing muscle forces, also have been found to be important proprioceptive elements. This sensory feedback is important in control and stability of the lumbar spine.

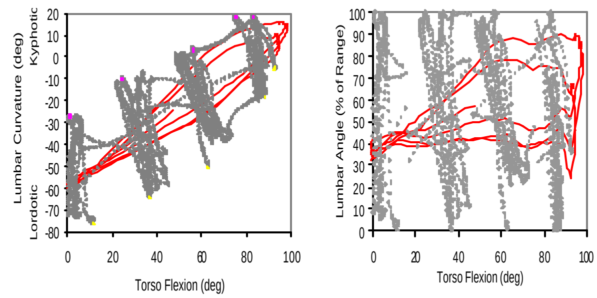

Figure 3(a and b): Lumbar curvature was examined as a function of torso flexion (a). Limits of the range of lumbar motion were projected on a 0 to 100% scale (b).

CONCLUSION

Subjects were found to have more kyphotic lumbar curvature during heavy, slow lifting tasks, particularly in ascent from a flexed position. Such lifting strategies may serve to improve spinal stability by engaging sensory feedback from the ligamentous structures but may also put the ligaments under strain, risking damage. Future work is needed to better understand the role of the spinal ligaments in motion control and mechanisms of injury to these ligaments.

REFERENCES

1. Marras WS et.al., (1995). *Ergonomics*, **38(2)**, 377-410.
2. Panjabi M.M., (1992). *J Spinal Disord*, **5(4)**, 390-6.
3. Granata, K.P. and Sanford, A.S. (2000). *Spine*, 25(11), 1413-8.
4. Khalsa, P.S. et.al., (2002). 4th World Congress on Biomechanics.
5. Solomonow M. et.al, (1998). *Spine*, **23**, 2552-62.

A PRECLINICAL TOOL TO MONITOR FATIGUE FAILURE OF FEMUR COMPONENT OF TOTAL HIP ARTHROPLASTY IN REAL TIME

Jihui Li [1] and Gang Qi [1, 2]

Medical Acoustic Research Laboratory
[1] Department of Biomedical Engineering, Joint program of The University of Memphis and University of Tennessee, Memphis, TN, USA
[2] Department of Mechanical Engineering, The University of Memphis, Memphis, TN, USA
E-mail: jihuili@memphis.edu Web: http://www.me.memphis.edu/mar_lab/mar_lab/home.htm

INTRODUCTION

Total hip arthroplasty (THA) has proven to be a procedure for the successful relief of pain and restoration of patients' daily activities. However, annually, 16 to 17% of the patients of 160,000 surgeries will need revision mainly due to loosening (Maloney, 2001 and Stat. 2001). A benchmark work conducted by Gruen and his coworkers 25 years ago revealed the "modes of failure" of cemented THA femoral components (Gruen et al, 1979). In their work, seven zones were identified to examine for loosening from their retrieved implants. In the past two decades, researchers have conducted studies in various approaches to better understand the mechanism of THA loosening: analytical (Mann et al, 1998), experimental (Davies et al, 1995), and clinical (Brumby et al, 1998). These experimental techniques used in orthopedic applications are somewhat limited, but the acoustic emission (AE) technique used in this experiment is unique in providing information on real time monitoring of cemented THA under fatigue process and in assisting the concurrent effort in analytical and clinical studies. This technique is utilized to study the behavior of a cemented hip stem under the in-vitro compressive cyclic loading condition.

METHODS

Composite femurs, a Cobalt Chrome (CoCr) cemented hip stem, and bone cement were used in this experiment. A CoCr hip stem (Spectron hip stem, Smith-Nephew, Inc, Memphis, TN) was implanted in a composite femur using Versabond bone cement. The composite femur was instrumented with eight resonant listening sensors as shown in Fig. 1. This construct was placed in a MTS loading machine using ball-joint fixtures on both proximal and distal ends of the construct. A compressive cyclic load of 60 to 600 lbf was applied at 8 Hz in air at room temperature for five million cycles. An eight-channel Vallen AMSY-5 AE system was used to collect and process AE data. AE characteristics including activity counts, energy, onset time and amplitude were monitored online and recorded for analysis.

RESULTS AND DISCUSSION

Based on the AE data, microcrack source locations were computed and displayed on screen in real time according to the relative locations of the sensors (Qi, 1999). Fig. 2 shows a sample of computed microcrack source locations as the fatigue process progresses. In this figure, computed massive microcracks were grouped by clusters (size of 5 x 5 mm) to illustrate the geo-center and intensity of microcracks. Microcracks first appeared after 2 - 3 hours of cyclic loading below the distal tip of the implant where high bending stress was experienced, as shown in Fig. 2(b). The majority of the microcracks were found on the medial aspect of the femur, which was under compressive cyclic loading. This condition continued for 30 hours. In this period, the intensity of accumulation of microcracks increased significantly on both medial and lateral aspects of the femur. After 40 hours (1.15 million cycles), microcracks began to expand towards the proximal-medial region. The number of microcracks was counted according to Gruen's zonal distribution. The results are summarized in Table 1. Significant microcrack accumulation was formed in Zone 4. This technique may provide a preclinical tool to correlate in vitro studies to clinical retrieval findings due to mechanical failures.

SUMMARY

In this study, the fatigue failure history of THA was monitored via the AE technique. This technique provides a real time monitoring means to detect and visualize microcrack initiation, accumulation history and their locations. This information could be used to enhance the design of cemented hip stems to increase their life expectancy.

REFERENCES

Maloney, W.J. (2001) *AAOS & AAOS Bulletin*, 49(1): 15-16.

Stat. (2001) *Orthopedics Today*, 21(5): 33-48.

Gruen et al, (1979) *Clin Orthop*, 141: 17-27.

Mann et al, (1998) *J Orthop Res*, 16: 370-378

Davies et al, (1995) *J Orthop Res*, 13: 335-338

Brumby et al, (1998) *Clin Orthop*, 355: 229-237

G. Qi, J. Pujol, and Z. F. Fan (1999) *J. Biomed Mat Res*, 52 (2): 256-260

ACKNOWLEDGEMENTS

This project was supported in part by the Whitaker Foundation. The authors would like to thank Mr. Andy Whitten and Dr. Abraham Salehi for assisting the experiments.

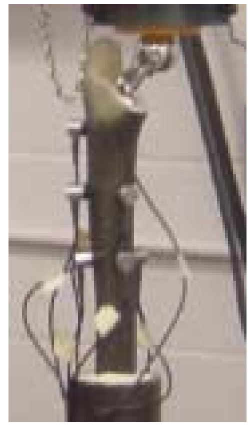

Fig. 1 THA specimen with eight sensors

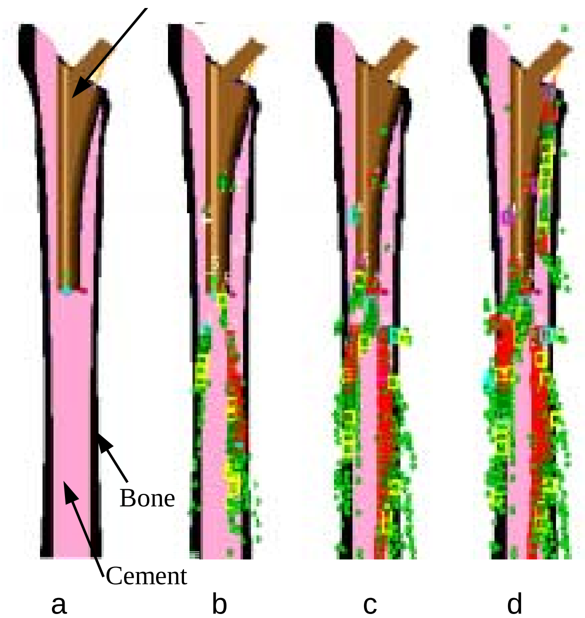

Fig.2 Microcracks accumulative history in THA from 0, 2, 30 and 40 hours

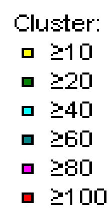

Table 1 Seven areas defined according to Gruen's method, number of patients suffered from THA loosening and microcracks happened in each area were listed.

Zone	1	2	3	4	5	6	7
Location	z>23; 2>x>0	23>z>20; 2>x>0	20>z>16; 2>x>0	16>z>6	20>z>16; -2<x<0	23>z>20; -2<x<0	z>23; -2<x<0
Gruen's	10	7	10	15	11	11	35
Microcracks	8	75	152	270000	17500	170	372

VHS - HIP SCREW - A BIOMECHANICAL STUDY

Terry Madsen M.D., [2] Despina Ciocanel M.D. [1, 2], Nabil Ebraheim M.D., [2]
Vijay Goel Ph.D.[1, 3], Kathleen Madsen R.N.[2],
and Richard Yeasting Ph.D.[2]
Spine Center[1], Medical College of Ohio[2] and University of Toledo[3], Toledo, Ohio
E-mail: dciocanel@mco.edu

INTRODUCTION

Intertrochanteric fracture represents almost half of all hip fractures; majority found in older female. Intertrochanteric fracture fixation with the VHS Vary-Angle Hip Fixation System (Biomet Orthopedics Inc.), in which the angle of lag screw placement can be varied, was biomechanically studied on twelve cadaver femurs. Although, the VHS system allows surgeons flexibility in dialing in angles other than 135 and 150 degree, our research aims to compare the failure strength of the VHS system implanted femurs only for high-angle screw (150 degrees) and low-angle screw (135 degrees).

METHODS

Twelve femurs (mean age 75.3 years, SD 8.85 years) were harvested from embalmed cadavers and intertrochanteric fractures were simulated. The femurs were DEXA scanned to ensure similar bone quality.
The angle at which the lag screw was inserted has been chosen randomly. After lag screw insertion the barrel of the side plate was engaged with the lag screw. Then, the six holes side plate was fixed with 3.5-mm cortical screws, using the manufacturers' recommended procedures and instruments.
Prior to biomechanically tests all specimens with the VHS system were radiographied to rule out bone pathology and to verify a satisfactory placement of the device. (Figure1)
The femurs were cut at the distal portion at the metaphyseal-diaphyseal junction and potted distally. The specimens were mounted in the MTS system at an angle of 23 degree to the anatomic axis simulating weight bearing, one leg stance. (Figure 2)

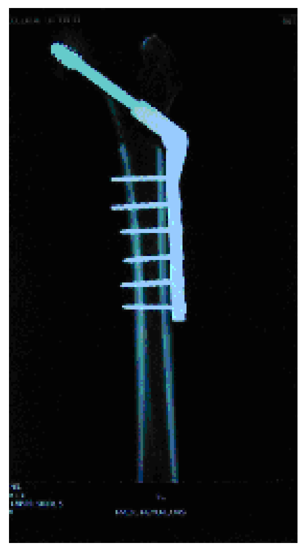

Figure 1: A/P radiograph before testing for one specimen at low-angle (135^0).

The reconstructed femurs were initially cyclically loaded to 444 N at a rate of 44 N/sec for 5 cycles. After cyclic loading, the reconstructed femurs were loaded to failure at a rate of 10-millimeters/ sec. The loading was applied on the femoral head through an acetabular cup. (Fig.2) The load and displacement until failure were recorded on a computer-based data acquisition system. Failure modes were identified.

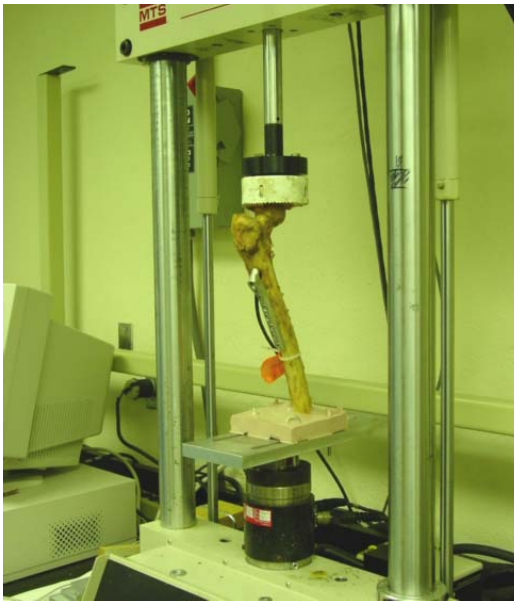

Figure 2: Specimen setup showing the VHS system on femoral specimen mounted in the MTS at 23-degree angle to the anatomical axis.

RESULTS AND DISCUSSION

The VHS - system for intertrochanteric fracture consistently failed in two distinct modes: either screw migration (33.3 per cent) or screw bending (58.3 per cent). The mean lag screw protruding on the femoral head for these two different angles was not considered to be a significant factor.

Table 1 A: Failure loads for matched specimens

Specimen ID	VHS system 135^0	VHS system 150^0
17 R/ 17 L	1700 N	2439 N
28 L/ 28 R	1944 N	1579 N
45 R/ 45 L	2795 N	1279 N
Mean	2146.3 N	1765.66 N
SD	469.36 N	491.61 N

Table1B: Failure loads for unmatched specimens

Specimen ID	VHS system 135^0	VHS system 150^0
29 L /38 L	918 N	1218 N
36 R /18 L	2331 N	1382 N
6L / 8 L	1569 N	2277 N
Mean for all trials	1876.16 N	1695.66 N
SD for all trials	1270.45 N	483.78 N

The mean load to failure for the VHS system at 135^0 for all trials was 1876.16 N, and the corresponding value for the matched specimens was 2146.3 N (tables 1A and 1 B). The mean load to failure for 150^0 fixation for all trials was 1695.66 N, and corresponding value for the matched specimens was 1765.66 N.

SUMMARY

The biomechanics of the intertrochanteric femoral fracture fixated with VHS Hip screw system at high angle (150^0) and low-angle (135^0) was studied. Mean compressive failure was found higher in low-angle VHS systems than for high-angle VHS systems suggesting that low-angle placement (135 degree) are more clinically relevant.

REFERENCES

R.C.Haynes, R.G.Poll, A.W. Miles, (1978): *Injury, **28***,337-341.

Sean McLoughlin, Donna Wheeler (2000) *Journal of Orthopedic Trauma,* **14,** 318-323.

Y.Gotfried (2002) *Journal of Orthopedic Trauma,* **16**, 644-650.

EFFECT OF ACETABULAR ORIENTATION ON HIP SUBLUXATION

George T. Rab

Dept. of Orthopaedic Surgery, University of California Davis, Sacramento, CA, 95817
E-Mail: george.rab@ucdmc.ucdavis.edu

INTRODUCTION

Surgical re-orientation of the acetabulum by peri-acetabular osteotomy (PAO) is used to treat hip subluxation caused by congenital or acquired acetabular dysplasia. Although surgeons use center-edge (CE) angles and false profile views to estimate the direction and degree of correction needed, there are no objective criteria for decision-making.

This study uses a rigid body spring method (RBSM) model of the hip to quantitate multidirectional subluxation as a function of acetabular orientation in the frontal and saggital planes. It provides insights into causes of subluxation by acetabular deficiency, treatment by re-orientation in multiple planes, and effect of re-orientation on contact areas and pressures as well as subluxation.

METHODS

An RBSM model of the hip was created to include a spherical femoral head model (255 nodal points) and a spherical acetabular surface with rim contours and orientation derived from bony adult acetabular measurements. Soft-tissue elements (e.g., labrum) were excluded. All simulations were in static single-limb stance, with loading force directed 18° medially and 3° anteriorly upward. Acetabular orientation was varied in 5° increments between 20° adduction and 50° abduction in the frontal plane, and from 20° backward flexion to 45° forward flexion in the saggital plane. Iterative model calculations were continued until the model reached equilibrium, at which point measurements of subluxation (degree and direction) and acetabular contact surface area were made.

RESULTS AND DISCUSSION

Composite graph of lateral subluxation (Figure 1) shows rapidly progressive instability as the acetabulum is adducted (tilted more vertically). Loss of as little as 10° CE angle from normal produced marked increases in lateral subluxation. As acetabulum is abducted 10° beyond neutral (increase of CE angle 10° above normal), lateral subluxation disappears, and this effect remains stable for all degrees of additional increases in lateral coverage.

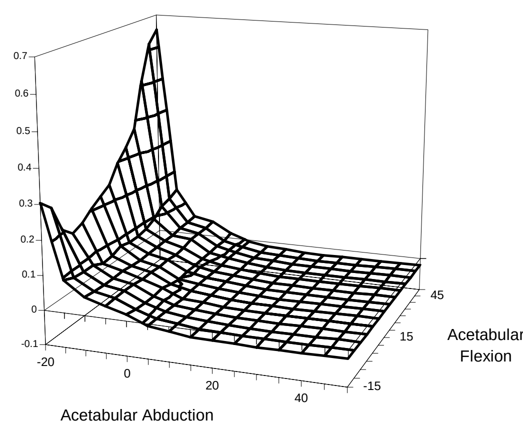

Figure 1: Lateral subluxation as a function of frontal (x axis) and saggital (y axis) acetabular orientation.

Composite graph of anterior subluxation (Figure 2) demonstrates progressive anterior subluxation as the acetabulum is rotated backwards (extended) more than 10°, corresponding to anterior acetabular dysplasia. As the acetabulum is flexed forward in this region, there is a strong tendency to counteract this, and to develop posterior subluxation instead (this might be interpreted as effective treatment for the subluxation noted in acetabular dysplasia). However, as the acetabulum is abducted 15°, increasing the CE angle, the sensitivity of the hip to acetabular flexion and extension diminishes, and stability occurs regardless of acetabular flexion.

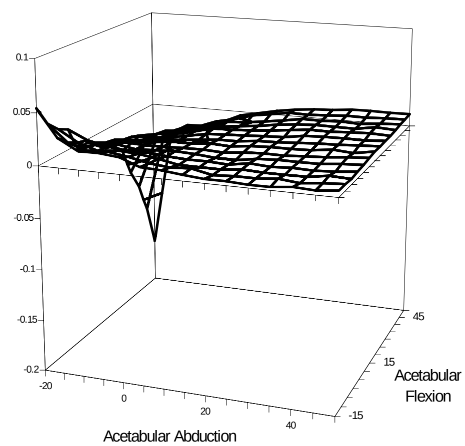

Figure 2: Anterior subluxation as a function of frontal (x axis) and saggital (y axis) acetabular orientation.

A potential advantage of PAO is that the medial-lateral position of the acetabulum may be adjusted along with the orientation, reducing joint contact pressure by medializing the joint center, or by providing greater superior articulating surface. The model allowed quantitive measurement of effective articular surface with reorientation, which is inversely related to joint contact pressure.

The effective weight-bearing surface of the acetabulum falls above the "equator" of the spherical femoral head that lies normal to the loading force. As the acetabulum is abducted, the contact area of the joint gradually increases (Figure 3) by about 3% for every additional 5° of abduction (increased CE angle). As contact area increases, joint surface contact pressure
decreases.

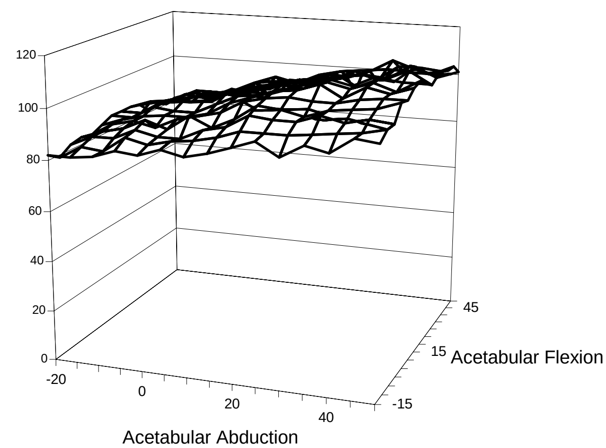

Figure 3: Effective acetabular contact area as a function of frontal (x axis) and saggital (y axis) acetabular orientation.

SUMMARY

Acetabular abduction is more effective than acetabular flexion at controlling the majority of clinical hip instabilities, and may allow reduced joint contact pressure. Relatively small degrees of anterior flexion (10-15˚) can compensate for significant anterior subluxation, but it is the increase in CE angle afforded by acetabular abduction that leads to the greatest stabilizing effect of PAO.

CROSS-SECTIONAL GEOMETRY OF HUMAN RIBS

Eduard Abrams, Marcus Mohr, Christine Engel, and Michael Bottlang

Biomechanics Laboratory, Legacy Clinical Research & Technology Center, Portland, OR, USA
Email: mbottlan@lhs.org

INTRODUCTION

This study describes geometric parameters of rib cross-sections along human cadaveric ribs three through nine. The shape, size, and cortex thickness apparent on rib cross-sections varies within each rib and between ribs. However, only limited information on cross-sectional geometry over the complete rib length is available to date [Roberts et al., 1970 and Yoganandan et al., 1998]. Results of this study provide geometric descriptors of human rib anatomy as a scientific basis for the advancement of hardware for rib fracture fixation. Such surgical fixation of multiple segmental rib fractures can aid restoration of pulmonary function in a timely manner to reduce mortality associated with prolonged mechanical ventilation [Lindenmaier et al., 1990].

METHODS

Right ribs three through nine were harvested from five non-embalmed human cadavers (59 ± 13 years, 71 ± 30kg, 3 male, 2 female). Using a custom circular saw, 2 mm thick cross-sections were excised at 5%, 25%, 50%, and 75% of rib length (Fig. 1a). The rib length was defined from the tubercle (0%) to the costo-chondral junction (100%) in each rib. The 5% cross-section was located between the tubercle and angle. Cross-sectional specimens were transferred directly onto an x-ray cassette. The outer cortex of each specimen was aligned parallel to the right edge of the cassette, and contact radiographs of each cross-sectional specimen were obtained. For quantitative image analysis with MATLAB (MathWorks, Natick, MA), contact radiographs were scanned in 8-bit grayscale mode at a resolution of 800 pixels per inch. Successive gray scale equalization and thresholding was applied to objectively discretize cortical and trabecular structures.

Cortex Thickness (t_C): To quantify the thickness of the superior (t_{sup}), inferior (t_{inf}), inner (t_{inn}), and outer (t_{out}) cortex of each cross-section, a bounding box was fitted to each cross-sectional image. The side lengths of the bounding box represented the height (h) and width (w) of each cross-section (Fig. 1b). t_C was measured at the intersections of the cortex with the horizontal and vertical symmetry lines of the bounding box. t_C was also measured 0.75 mm above and below at each intersection to obtain average t_C reports (t_{sup}, t_{out}, t_{inf}, t_{inn}) over 1.5 mm regions of interest.

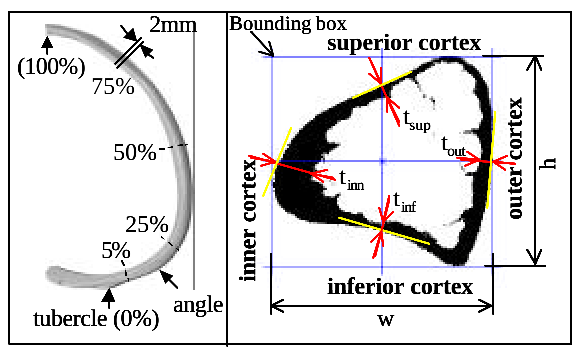

Figure 1: (a) Location of cross-sections; **(b)** Geometric parameters.

Cross-Sectional Area: The total area of each cross-section and the cortex area itself were computed with MATLAB. Finally, the area of the medullary canal was calculated by subtracting the cortex area from the total cross-sectional area.

RESULTS

The cross-sectional shape varied among specimens excised at the four locations along each rib, but remained similar for corresponding locations on ribs three through nine (Fig. 2). As determined by the bounding box, the average cross-sectional height among ribs three through nine was 10.3±1.8 mm, 13.5±3.1 mm, 12.1±2.9 mm, and 12.2±3.1 mm and the width was 7.5±1.8 mm, 7.1±2.1 mm, 6.9±2.1 mm, and 12.2±3.1 mm at 5%, 25%, 50%, and 75% locations, respectively. The inner cortices were on average the thickest (1.1±0.5 mm). The average thickness of t_{out}, t_{sup} and t_{inf} was 0.8±0.4mm, 0.5±0.4 mm, and 0.5±0.3mm, respectively. The outer, superior, and inferior cortices were thickest at 5 % rib length (Figure 2).

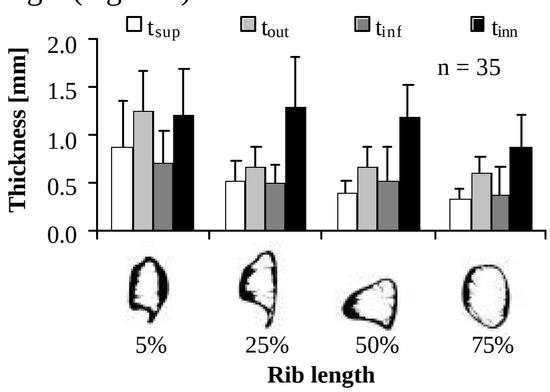

Figure 2: Average cortical thicknesses, and exemplary cross-sections

The cortical thickness and the rib height and width are listed in Table 1 for ribs three through nine. The average cortical area of ribs three through nine decreased from 26.3 mm^2 to 16.3 mm^2 from cross-sections at 5% to 75% rib length, respectively. The medullary area increased from 29.9 mm^2 at 5% to 41.2 mm^2 at 75% (Figure 3).

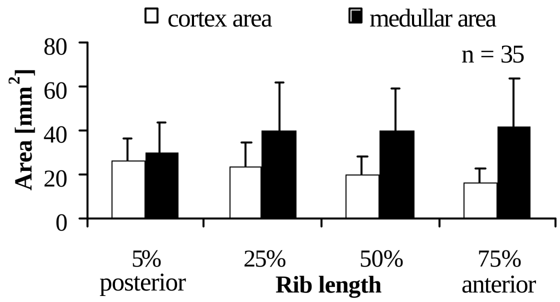

Figure 3: Cortical and medullary area

DISCUSSION

Results of this study expand the limited set of data available on cross-sectional rib geometry to date. Results quantify for the first time characteristic differences in cortex thickness distribution within rib cross-sections over the rib length. It shows the non-uniform distribution of cortex and the pronounced change of the cross-sectional rib shape over the rib length. This quantitative information has direct implications to advanced rib osteosynthesis and techniques.

REFERENCES

Yoganandan, N., Pintar, F.A. (1998). *J Biomech Eng*, **120**, 100-104.

Roberts, S., Chen, P. (1970). *J Biomechanics*, **3**, 527-545.

Lindenmaier, H.L., Kuner, E.H., et al. (1990). *Unfallchirurgie*, **16**, 172-177.

ACKNOWLEDGEMENTS

Supported by Legacy Research Foundation.

Table 1: Cortex thicknesses and outer dimensions in mm (n = 20)

	Rib 3	Rib 4	Rib 5	Rib 6	Rib 7	Rib 8	Rib 9
t_{sup}	0.6 ± 0.4	0.6 ± 0.5	0.4 ± 0.3	0.5 ± 0.3	0.5 ± 0.3	0.6 ± 0.4	0.6 ± 0.3
t_{out}	0.7 ± 0.3	0.7 ± 0.3	0.8 ± 0.3	1.0 ± 0.5	1.0 ± 0.4	0.9 ± 0.5	0.8 ± 0.4
t_{inf}	0.5 ± 0.3	0.5 ± 0.3	0.5 ± 0.3	0.5 ± 0.3	0.5 ± 0.2	0.6 ± 0.4	0.6 ± 0.3
t_{inn}	0.9 ± 0.4	0.9 ± 0.3	1.1 ± 0.4	1.4 ± 0.4	1.4 ± 0.4	1.2 ± 0.6	1.1 ± 0.4
h	11.3 ± 2.5	11.6 ± 2.6	11.4 ± 2.6	11.8 ± 2.6	12.8 ± 2.8	13.1 ± 3.6	12.0 ± 3.8
w	6.0 ± 2.0	6.8 ± 2.0	7.2 ± 1.9	7.6 ± 1.8	7.4 ± 1.7	6.5 ± 2.1	6.4 ± 1.9

STABILIZING POTENTIAL OF TRUNK MUSCLES

Stephen Brown and Jim Potvin

Department of Kinesiology, University of Windsor, Windsor, Ontario, Canada
E-mail: jpotvin@uwindsor.ca

INTRODUCTION

Without muscle activation, the lumbar spine is inherently unstable and will buckle under compressive loads of approximately 90N (Crisco et al., 1992). Further, it has been hypothesized that coactivation of trunk muscles serves the primary purpose of fulfilling stability requirements of the spine (Gardner-Morse & Stokes, 1998). However, the exact role of particular muscles in this regard is not fully understood. The purpose of this paper is to present a quantitative estimate of the static ability of individual trunk muscles to stabilize the L4-L5 joint about three separate axes.

METHODS

Anatomical data was taken from Cholewicki and McGill (1996). A two-dimensional measure of the stabilizing potential of muscles was taken about each of the flexion/extension (FE), lateral bend (LB) and axial twist (AT) axes. Nodal points were included on muscles where appropriate to present a more realistic view of the function of the spinal musculature about L4-L5. Joints above L4-L5 were considered to be rigid.

The minimum potential energy (V) approach was used to calculate stability. This method states that, in order for a system to be stable, the second derivative of the V of the system must be positive definite (Bergmark, 1989). V for a particular muscle was calculated as the elastic energy stored in the muscle plus the work done by the muscle for small rotations:

$$V_{mi} = \frac{1}{2} k_{mi} dl_{mi}^{\ 2} + F_{mi} dl_{mi} \qquad (1)$$

where: *mi* is a particlar muscle *i*, *k* is the muscle stiffness, *dl* is the small change in muscle length with a small rotation and *F* is the muscle force.

Substituting appropriate muscle length-change relationships into (1), applying a Taylor Series expansion to the second order and twice differentiating with respect to trunk angle yields:

$$\frac{dV_{mi}^{\ 2}}{d^2\theta} = k_{mi} r_{mi}^{\ 2} - \frac{F_{mi} r_{mi}^{\ 2}}{l_{mi}} \qquad (2)$$

where: *r* is the 2Dmuscle moment arm

From Bergmark (1989), we assume:

$$k_{mi} = q \frac{F_{mi}}{L_{mi}} \qquad (3)$$

where: *q* is a dimensionless multiplier and *L* is the entire 2-D muscle length

Substituting (3) into (2) gives:

$$\frac{dV_{mi}^{\ 2}}{d^2\theta} = \frac{qF_{mi} r_{mi}^{\ 2}}{L_{mi}} - \frac{F_{mi} r_{mi}^{\ 2}}{l_{mi}} = S_{mi} \qquad (4)$$

where S_{mi} is a measure of a given muscle's contribution to stability.

In muscles with nodal points, *r* and *l* are calculated based on the vector of the muscle as it crosses the L4-L5 joint.

To determine the stabilizing potential of each muscle, activations are set to 100% of maximum; muscles were assumed to be at resting length; q was set to 10 and the maximum muscle stress was set to 35 N/cm^2.

RESULTS AND DISCUSSION

Total stabilizing potential of the trunk muscles analyzed (N=9) is highest in the AT axis (S_{mN}=1213), followed by the LB axis (S_{mN}=1095) and the FE axis (S_{mN}=728).

Figure 1 shows the stabilizing potential of each muscle normalized to the total stabilizing potential of all muscles examined. External Oblique and Internal Oblique display the highest stabilizing potential in each of the LB and AT axes; while the LES and multifidus show the highest stabilizing potential in the FE axis.

The FE axis appears to be most vulnerable to instability as trunk muscles generally are less capable of stabilizing this axis. However, most industrial tasks, in which FE is the dominant axis of movement, require higher posterior than anterior levels of muscular activation. Thus, it is likely that the critical axis, in which buckling is most likely to occur for a given situation, is dependant on the action being performed.

SUMMARY

Trunk muscles are shown to have a higher stabilizing potential in the AT and LB than in the FE axis. This increased potential may serve to protect against instability in these axes, as the main AT and LB stabilizers (EO & IO) tend to activate to a lesser degree than the main FE stabilizers (erector spinae) in most industrial activities.

REFERENCES

Bergmark, A. (1989). *Acta Ortho Scan Supp*, **60**, 3-52.

Cholewicki, J., McGill, S. M. (1996). *Clinical Biomechanics,* **11**, 1-15.

Crisco et al. (1992). *Clinical Biomechanics*, **7**, 27-32.

Gardner-Morse, M.G., Stokes, I.A.F. (1998). *Spine*, **23**, 86-91.

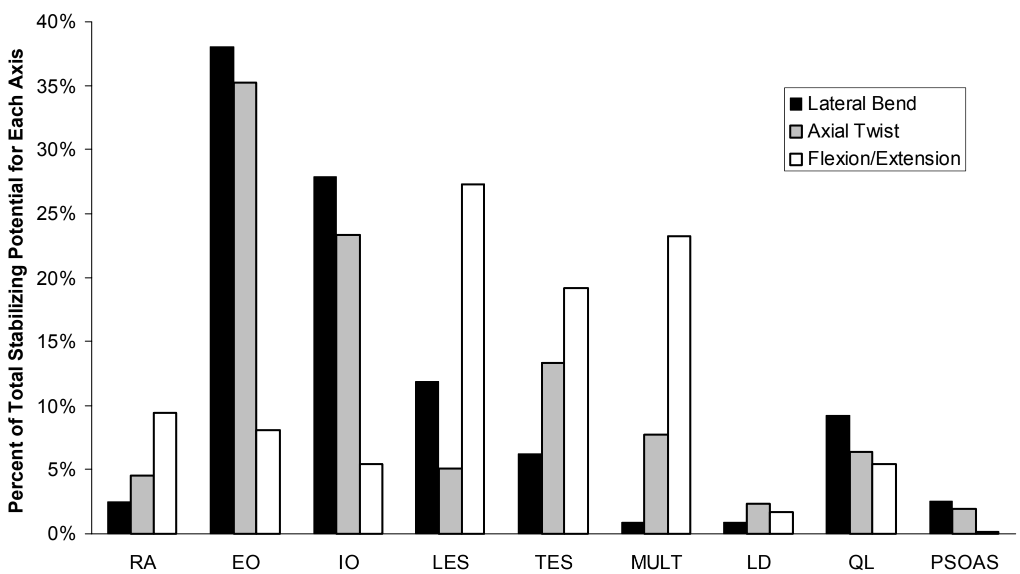

Figure 1. Normalized stabilizing potential, about each axis, for every muscle examined (one side of the body only) relative to the total stabilizing potential about each axis.

EFFECT OF BODY REPRESENTATION ON PERCEPTION OF AFFECT

Daniel O'Reilly [1], Jodi James [2], Barbara Fredrickson [3], Brad Smith [1] and Melissa Gross[2, 4]

[1] Biomedical Visualization Program, School of Art and Design, [2] Movement Dynamics Lab, Division of Kinesiology, [3]Positive Emotions and Psychophysiology Lab, Department of Psychology, [4]Institute of Gerontology, University of Michigan, Ann Arbor, MI, USA
E-mail: mgross@umich.edu Web: www.kines.umich.edu/facstaff/gross.htm

INTRODUCTION

Information about emotions is conveyed in body movements, and individuals can discern the emotions of others by observing their movements. Using point-light displays with only 6-12 points, observers have identified emotions in gait (Montepare et al., 1987), dance (Brownlow et al., 1997) and knocking movements (Pollick et al., 2001). Although perception of affect with such diminished body representations is remarkable, it is not yet known which aspects of the movement kinematics convey the emotion information or how body representation may affect perception.

The purpose of this project was to determine the effect of different body representations on perception of affect during a common movement. Motion capture data collected with five different emotions were used to animate four different body representations and observers rated the emotional content of each movement.

METHODS

<u>Motion data</u>. One subject with 8 years of performance experience volunteered to participate (female, 28 yrs) after giving consent. Thirty-four markers were placed on anatomical landmarks on the head, torso, right arm and right leg of the subject. Emotions were induced by asking the subject to recall events from her own life in which she felt angry, sad, content, joyful and neutral. The subject was then asked to perform a knocking movement against a vertical plexiglass surface with each of the emotions selected at random. Motion data were captured at 120 Hz with a 5 camera video system. The trial rated as "best" by the performer was chosen for analysis.

<u>Animations</u>. Three different geometries were constructed using Maya software (Fig. 1). Only the body representations differed; the underlying degrees of freedom were the same. The point-light display consisted of balls placed at joint centers of the toe, ankle, knee, hip shoulder, elbow, wrist, neck and spine. The stick-figure consisted of thin segments joining adjacent joint centers. The industrial geometry was constructed using multiple digital photographs of the subject to create a custom model similar to those used in engineering software applications. One set of motion capture data for each affect was used to animate the geometries. The video associated with each motion capture trial was used as the fourth geometry for each affect. Three different ensemble videos were produced in which each of the 20 different motion sequences (5 affects x 4 representations) were randomly ordered.

<u>Affect perception</u>. Twenty University of Michigan students volunteered to participate (8 men; 12 women; 21.4±3.4 yrs). The observers viewed each of the motion sequences and then filled out a questionnaire with 20 items, each of which described a different feeling. The observers rated the intensity of the feeling (0 "not at all"- 4 "extremely") that they thought the performer

experienced as they moved. Recognition rates were obtained from non-zero responses; intensity scores were tested for significant differences using ANOVA.

RESULTS AND DISCUSSION

Affects were recognized at rates greater than chance for all representations. Recognition rates with video were 100%, 75%, 45% and 65% for anger, sad, joy and content, respectively. Recognition rates for non-video representations were similar to video for most affects. For sad, however, video rates were greater than the non-video rates, and for content, recognition rates tended to increase with industrial. On average, our recognition rates for video (71%) and point-light (63%) were similar to those reported by Pollick et al. (2001) for knocking with a similar set of affects.

Anger produced the highest affect intensity scores; mean peak scores reached 3.75 for anger but did not exceed 2.10 for other affects. Our results are consistent with others that report anger is readily perceived from point-light (Montepare et al., 1987); further, observers' responses to anger did not improve with the other non-video representations. Joint amplitudes and velocities were much larger during anger which may have contributed to the higher overall scores.

For sad, scores were significantly different among displays ($p<0.026$). Responses to video (2.10) and point-light (1.75) were higher than responses to stick-figure (1.05) and industrial (0.95) representations. For joy, video scores were significantly higher for positive items ($p<0.001$) but non-video scores were higher for some inappropriate, negative questionnaire items ($p<0.001$). For content, the industrial display produced the highest scores for positive items ($p<0.018$); scores were not different for other displays. Neutral affect yielded low mean scores that were similar among representations.

SUMMARY

Although affect intensity was best perceived with video, non-video representations were also effective in communicating affect during movement. In some cases, however, industrial and stick-figure displays were associated with less accurate recognition of affect during movement.

REFERENCES

Brownlow S., et al. (1997) *Psychological Record*, **47**, 411-421.

Montepare J. M., et al. (1987) *J. Nonverbal Behavior*, **11**, 33-42.

Pollick, F.E., et al. (2001). *Cognition*, **82**, B51-B61.

ACKNOWLEDGEMENTS

Supported by a Rackham Interdisciplinary and Collaborative grant and the Graduate Program, School of Art and Design, UM.

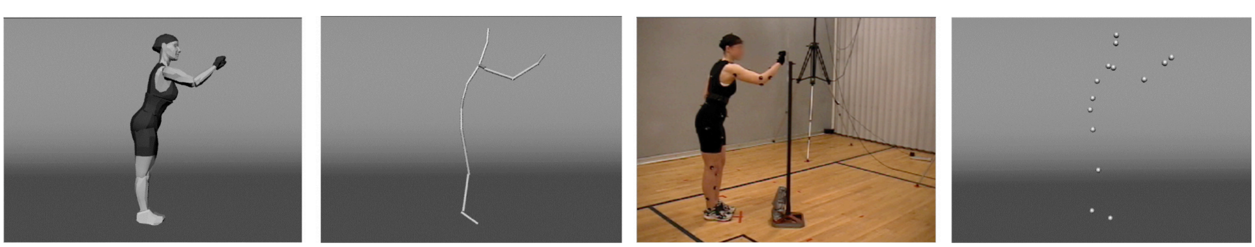

Figure 1: Body representations used to display movement with different affects. From left to right, industrial, stick-figure, video and point-light representations are shown for an anger trial.

FUNCTIONAL ABILITY IN MID-LIFE WOMEN

Melissa Gross [1,2], MaryFran Sowers[3,4], Kelly Lenard[1], and Anna Furniss[3]

[1]Division of Kinesiology, [2]Institute of Gerontology, [3]Department of Epidemiology and
[4]Department of Internal Medicine, University of Michigan, Ann Arbor, MI, USA
E-mail: mgross@umich.edu Web: www.kines.umich.edu/facstaff/gross.htm

INTRODUCTION

Functional disability in the elderly has been associated with both progressive decline and catastrophic change due to a medical event (Ferrucci et al., 1996). The progressive decline has been attributed to age-related factors as well as physical activity and chronic disease. Understanding the factors related to progressive functional decline provides the theoretical basis for design of appropriate therapeutic interventions.

That functional ability is diminished in old adults compared to young adults is well-established; however, the trajectory of functional ability across mid-life has not been described. It is important to understand the natural history of functional ability in mid-life to better understand mechanisms leading to progressive functional decline and to provide a basis for early detection. The purpose of this study was to assess function in a population of women at mid-life.

METHODS

Participants were pre- and perimenopausal women enrolled in one of two longitudinal studies - Michigan Bone Health Study (466 women) and the Detroit-area site of the longitudinal, population-based Study of Women's Health Across the Nation (306 women) (Sowers et al., 2000). Height and weight were measured and body mass index (BMI) was calculated (kg/m^2). Three performance-based measures of functional ability were obtained: timed 40-ft walk, timed stair climb and timed sit-to-stand. In the timed walk, participants were asked to "walk like you are trying to catch an elevator." In timed stair climb, subjects were asked to ascend, turn around, and descend a set of four stairs. In the timed sit-to-stand task, subjects rose from a standard height bench. Time was measured in all three timed tasks by an observer using a stopwatch.

To obtain gait measures, participants walked down a corridor over an instrumented mat (Gaitrite™). The gait mat was 4.6 x 0.9 m with an active sensor area 3.7 x 0.6 m (1.3 cm between sensors). Footsteps detected by the sensors were sampled at 80 Hz. Data from right and left legs were averaged. Spearman's correlations were used to detect significant relationships between variables.

RESULTS AND DISCUSSION

787 women participated in the study (77% Euro-American, 23% African-American). Mean age was 46.6±4.7 years. Mean BMI was 30.5±7.5 kg/m^2.

Gait speed varied greatly among the women (Table 1). Although the median velocity was similar to values reported for young adults (Cutlig et al., 2000), individuals in the lowest quartile walked at substantially slower speeds; velocity halved below the 25th percentile, to speeds similar to those reported for old adults (Alexander et al., 2000). Some women walked very quickly, however, and speeds doubled above the 25th percentile.

The median values for the gait cycle components, percent stance and percent double support, were similar to young adult values. In the lowest quartile, however, relative durations of stance and double support increased substantially, as has been reported for old adults (Winter et al., 1990). The relative durations of stance and double support decreased in the upper quartile as expected with an increase in gait velocity.

Gait velocity was most strongly associated with the timed performance tasks (Table 2). Not surprisingly, gait measures were most strongly correlated with timed walk. It is likely that other factors contributed to weakening the relationship between gait and the other performance tasks, such as the increased muscle strength demands in stair climb and sit to stand.

Table 3: Gait correlations with BMI and age

Measure	BMI	Age
Velocity (cm/s)	-0.36	-0.41
Stance (%)	0.48	0.25
Double support (%)	0.50	0.30

*p<0.0001 for all correlations

Gait speed and timing of gait cycle components were correlated with BMI and age (Table 3). Gait velocity decreased as age and BMI increased. Double support and stance times were particularly sensitive to BMI; the relative time that stance and double support phases occupied during the gait cycle increased with BMI.

SUMMARY

This study presents a normative dataset for mid-aged population of women in which multiple measures of functionality were assessed simultaneously. The range of performance was greater than expected, spanning a function continuum between young and old adult performance. Increasing BMI was associated with poorer function, and as much as 25% of the population was performing at less than adequate levels.

REFERENCES

Alexander, N.B. et al. (2000). *JAGS,* **44**, 434-451.

Ferrucci, L. et al. (1996). *J. Gerontol. Med. Sci*., **51A**, M123-M130.

Sowers, M.F. et al. (2000). In: Menopause: Biology & Pathobiology. Academic Press.

Winter, D. A. et al. (1990) *Physical Therapy*, **70**, 15-22

ACKNOWLEDGEMENTS

Supported by NIA grant R01-AG17104

Table 1: Percentile distribution of gait measures (n=599).

Gait Measure	1%	25%	50%	75%	99%
Velocity (cm/s)	76.0	115.8	144.6	172.3	230.9
Stance (%)	67.2	61.7	59.7	58.2	54.8
Double support (%)	32.5	23.4	19.7	16.9	10.9

Table 2: Correlations of performance measures and gait measures

Gait measure	40 ft walk	Timed stair climb	Timed sit to stand
Velocity (cm/s)	-0.60 (p<0.0001)	-0.40 (p<0.0001)	-0.29 (p<0.0001)
Stance (%)	-0.39 (p<0.0001)	-0.29 (p<0.0001)	-0.19 (p<0.0001)
Double support (%)	0.45 (p<0.0001)	0.34 (p<0.0001)	0.22 (p<0.0001)

,

CONTROL OF BALANCE DURING WALKING IN YOUNG AND ELDERLY ADULTS

Steven H. Collins, Catherine E. Bauby, and Arthur D. Kuo
Dept. Mechanical Engineering & Applied Mechanics, University of Michigan, Ann Arbor, MI
E-mail: shc@umich.edu Web: http://www-personal.engin.umich.edu/~artkuo/

INTRODUCTION

Balance ability decreases in older adults, due to age-related sensory, motor, and other changes. Human walking appears to be unstable in the lateral direction (Kuo, 1999; Bauby & Kuo, 2000), and relatively stable in the fore-aft direction. Age-related deficits in balance during walking may be most apparent in the lateral direction.

The stability of walking depends on the dynamics of the musculoskeletal system. The limb dynamics appear to be passively stable in the sagittal plane (McGeer, 1990). We developed a 3-d model incorporating roll motion (Kuo, 1999) and found that its fore-aft motion remained stable, but its lateral motion was unstable. This instability is controllable with feedback-driven lateral foot placement.

We previously presented a simple experiment measuring variability of foot placement during walking in young adults. We found that step variability was greater in the lateral direction and that walking with eyes closed had a greater effect on lateral variability (Bauby and Kuo, 2000), supporting the hypothesis that humans actively stabilize

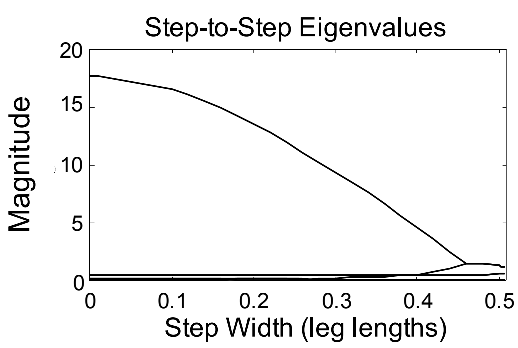

Figure 2: Eigenvalue magnitudes of the linear map as a function of step width. Instability decreases as step width increases, indicating a possible strategy for reducing lateral control requirements.

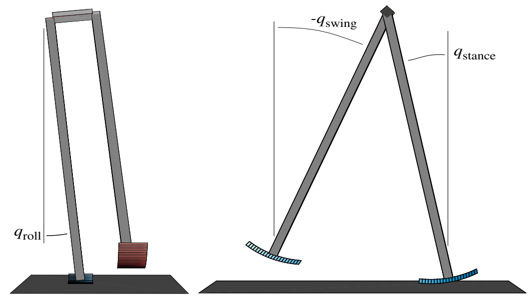

Figure 1: Three-dimensional passive dynamic walking model (Kuo, 1998). Left: Front view. Right: View from right.

lateral, but not fore-aft, motions. Here, we repeat the experiment with elderly subjects. Our results again implicate active control in lateral balance and highlight the difficulty of this control for older patients.

METHODS

3-D Passive Walking Model

Dynamics. The model consists of a pelvis and two legs (Fig. 1), with 3 degrees of freedom: a pin joint at the hip, rolling line contact with the ground, and a pin joint between the foot and leg allowing for lateral motion. Starting with the beginning of the swing phase, we forward integrated equations of motion until heel-strike, then modeled an inelastic collision using conservation of angular momentum. We employed 1st-order shooting to find a fixed point, signifying a limit cycle. Local stability was evaluated in a discrete linear approximation of the nonlinear mapping. There is one unstable eigenvalue, mostly limited to the roll states. The magnitude of this eigenvalue decreases with increasing step width (Fig. 2).

Control. We studied several methods for stabilization, and found lateral foot placement particularly attractive since small adjustments prior to heel strike have large ef-

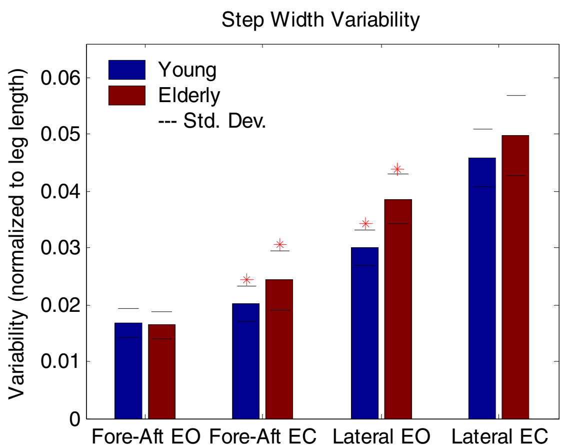

Figure 3: Foot placement variability under the eyes open (EO) and eyes closed (EC) conditions. * indicates significant difference (p < 0.01).

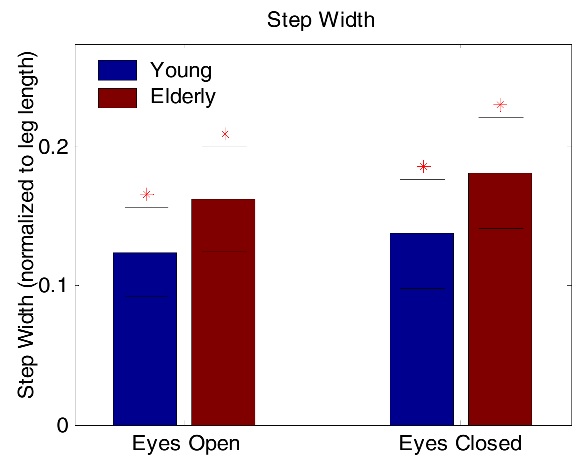

Figure 4: Mean step width. On average, elderly subjects' steps were 0.041 leg lengths (~1.52 inches) wider than those of young subjects.

fects on the trajectory of the next step, while other methods have a larger energy cost (Kuo, 1998). We used pole placement to design a stabilizing feedback control law for once-per-step splay angle adjustments.

Human Walking Experiments

Our model indicates that limb dynamics and local reflex loops may be sufficient to provide passive fore-aft stability, but the CNS should find it necessary to stabilize lateral motions. Reducing sensory input to the controller of an unstable system leads to poorer overall control, with greater variability in the control signal. If the CNS actively stabilizes lateral balance through feedback-driven lateral foot placement, closing one's eyes should result in greater variability in lateral, but not fore-aft, foot placement. Reduced sensory precision associated with age should also cause an increase in lateral variability.

We measured foot placement in the natural overground gait of 15 young adult subjects, aged 18-40, and 13 elderly subjects, aged 64-82. Step parameters were measured using a mobile kinematic tracking system (Bauby & Kuo, 2000) as subjects walked at a self-selected speed in a straight line for at least 400 contiguous steps.

RESULTS AND DISCUSSION

All subjects always had greater lateral than fore-aft variability ($p = 6.4e-8$). All subjects had increased lateral variability with eyes closed ($p = 1.7e-5$), with greater increases in lateral than fore-aft variability ($p = 0.009$, Fig. 3). Step width increased for all subjects with eyes closed ($p = 0.003$), and elderly subjects always took wider steps than young subjects ($p = 0.008$, Fig. 4), while maintaining similar step length.

These results are consistent with our hypothesis that the CNS utilizes sensory feedback to actively control lateral balance. Additionally, the increased step width of elderly subjects may indicate a strategy to reduce active control requirements, per Kuo (1999). The increases in fore-aft variability may be due to fluctuations in walking speed and the control coupling described by Bauby (2000).

ACKNOWLEDGEMENTS

Supported by NIH 1R29DC02312-01A1.

REFERENCES

Kuo, A.D. (1999). *Int'l J. Robotics Research*, **18(9)**, 917-930.
McGeer, T. (1990). *IJRR* **9**, 68-82.
Bauby, C.E., Kuo, A.D. (2000). *J. of Biomechanics*, **33**, 1433-1440.

A 3D MODEL OF MUSCLE REVEALS THE CAUSES OF NONUNIFORM STRAINS IN THE BICEPS BRACHII

Silvia Blemker[1] and Scott Delp[1,2]
Departments of [1]Mechanical Engineering and [2]Bioengineering, Stanford University
E-mail: ssblemker@stanford.edu Web: http://www.stanford.edu/group/nmbl

INTRODUCTION

Biomechanical models generally assume that muscle fascicles shorten uniformly. However, dynamic magnetic resonance (MR) images of the biceps brachii have recently shown nonuniform shortening along some muscle fascicles during low-load elbow flexion (Pappas et al., 2002.)

The purpose of this study was to uncover the features of the biceps brachii muscle's architecture and material properties that could cause the nonuniform shortening. To do this, we created a finite-element (FE) model of the biceps brachii and compared the tissue strains predicted by the model with dynamic MR data. We then used the model to explore the effects of the muscle's internal geometry and material properties on the strain distributions.

METHODS

We modeled muscle as a transversely isotropic, quasi-incompressible, hyperelastic material based on the model described by Weiss et al. (1996). In our model, the strain-energy function (W) was described by:

$$W = F_1(□, act) + F_2(□) + F_3(□) + F_4(□),$$

where □, □, and *act* represent the fiber stretch, volume stretch, and activation level, respectively. The along-fiber shear strain (□) and the cross-fiber shear strain (□) were derived from a physically-based strain invariant set for transverse isotropy proposed by Criscione et al. (2001). We defined F_1 to be consistent with the nominal force-length characteristic of a muscle fiber, scaled by the activation level (Zajac, 1989). F_2 provides the shear stress-strain relationship in the along-fiber direction, and F_3 provides the shear stress-strain relationship in the cross-fiber direction. F_4 was defined such that tissue was nearly incompressible. The 2nd Piola-Kirchhoff stress was determined by $\partial W/\partial E$, where E is the Green-Lagrange strain.

The finite-element brick mesh geometry represented the long head of the biceps muscle tissue and aponeuroses (Fig. 1A) and was axially symmetric about the centerline, creating a three-dimensional muscle model. A map for fiber directions (Fig. 1B) was created based on fascicle arrangement and aponeurosis dimensions measured from static MR and ultrasound images (Asakawa et al., 2002) and used to define the fiber direction for each element.

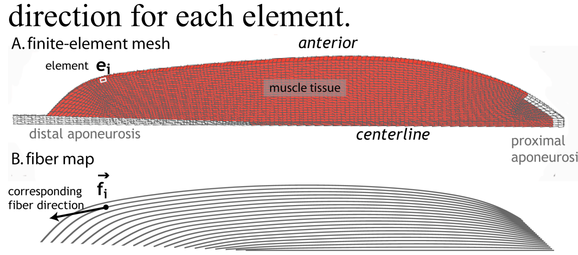

Figure 1: Sagittal-plane geometry of the FE mesh (A) and the fiber map (B).

We used NIKE3D, a nonlinear finite-element code (Puso et al., 2002), to generate simulations of the biceps muscle at 15% activation during a quasi-static 4cm length change. We compared the strains in the model to dynamic MR data (Pappas et al. 2002). These data describe the displacements of 1-cm regions in the biceps during elbow flexion in 12 subjects. To compare these data, we calculated average change in length along 1cm regions in the FE model.

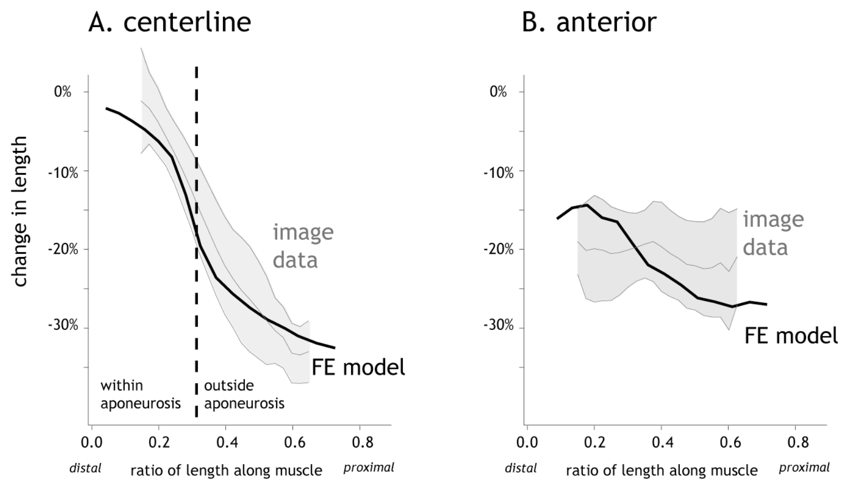

Figure 2: Change in length between 1-cm regions in the FE model (lines) and the image data (shaded regions, average ± one standard deviation from Pappas *et al*. 2002) along the centerline (A) and the anterior (B) regions of the biceps. Percent change in length is plotted as a function of distance from distal tendon, normalized by the length of the biceps brachii long head muscle belly. Negative values of % change in length indicate muscle shortening with elbow flexion. The degree of nonuniformity in the strains is indicated by the amount of variation in % change in length along the muscle (i.e., if the strains along each region were uniform, the curves would be horizontal.)

RESULTS AND DISCUSSION

The finite-element model predicted changes in length (or "strains") along both the anterior and centerline regions that were within one standard deviation of the average changes in length measured in 12 subjects (Fig. 2). The strains were not uniform along the centerline fascicles (Fig 2A); the greatest strains occurred at the proximal end of the muscle. The strains along the anterior fascicles (Fig. 2B) were more uniform than the strains along centerline fascicles.

Analysis of the model showed that the difference in lengths between the centerline and anterior fascicles was the primary cause of the nonuniform strain along the centerline fascicles. The presence of the distal aponeurosis also affected the strain distributions. Because of the aponeurosis, the centerline fascicles insert 6cm proximal to where the anterior fascicles insert. This "staggering" of the fascicles, coupled with the along-fiber shear stiffness, resulted in nonuniform strain along the fascicles.

The nonuniform strains in the biceps model are strongly influenced by the muscle-tendon architecture, suggesting that the degree nonuniform shortening will vary across muscles of various architectures. Continuum representations of muscle, combined with *in vivo* image data, are needed to deepen our understanding of how complex geometric arrangements of muscle fibers affect muscle force production.

REFERENCES

Asakawa et al. (2002) *J Mechanics in Medicine and Biology*, **2**, 1-7.

Criscione et al. (2001) *J Mechanics and Physics of Solids*, **49**, 871-897

Pappas et al. (2002) *J Appl Physiol* **92**, 2381-2389.

Puso et al. (2002) *Lawrence Livermore National Labs Technical Report*, UCRL-MA-105268.

Weiss et al. (1996) *Comput Methods Appl Mech. Engrg*, **135**, 107-128

Zajac (1989) *Critical Reviews in Biomedical Engineering*, **17**, 359-411.

ACKNOWLEDGEMENTS

G. Pappas, D. Asakawa, P.Pinksy, J.Weiss, J. Criscione, F. Zajac, LLNL, and the NIH.

COMPARISON OF DIFFERENT METHODS ON THE ESTIMATION OF HUMAN JOINT KINEMATICS

Mario Lamontagne[1,2], Lanyi Xu[1], Jonathan Singer[1], Dany Lafontaine[1,2] and Daniel Théoret[1,2]
Laboratory for Research on Biomechanics of Hockey[1] and School of Human Kinetics[2],
University of Ottawa, Ottawa, Ontario, Canada
E-mail: mlamon@uottawa.ca

INTRODUCTION

In joint kinematics studies, it is very important to estimate the relative rotations between the two body segments around the joint. The fundamental methods are based on rigid body mechanics. The most popular method for studying the rigid body rotation is the Euler angle method. However, one of the key pro-blems associated with this approach is that Euler angles are sequence dependent (Cole et al., 1993). In this study, human knee and ankle joint angle rotations based on six possible Euler angle se-quences and the Grood & Suntay (GS) methods (Grood, & Suntay, 1983) were compared using these methods of calculation of the 3D angular kinematics during walking, cycling and running.

METHODS

The definition of the femur, tibia and foot local coordinate systems are similar to Pennock, et al.(1990), i.e. the x axes is oriented medio-laterally, the y axes is oriented antero-posteriorly and the z axes is oriented inferior-superiorly in the standing position. All 17 skin markers (as shown in Figure 1) placed from foot to thigh were filmed with three digital video cameras in the standing position within the calibrated volume. The coordinates of all 17 markers relative to the global reference system (Laboratory Calibration frame) were obtained by the APAS system® (Ariel Dynamics Inc, San Diego, USA) during this standing trial. Subsequently the femur, tibia and foot embedded coordinate systems (local coordinate system) were obtained by using marker sets (12, 13, 17), (10, 11, 4), and (4, 5, 10) respectively. Afterwards, the relationships between the local coordinate system and the motion makers of the femur (14, 15, 16), tibia (7, 8, 9) and foot (1, 2, 3) were calculated using the method described by Challis (1995). These nine markers were maintained for the moving trials and the others were removed.

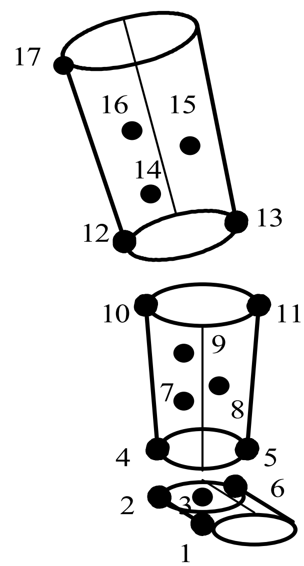

Figure1: The schematic diagram for placement of skin markers used for joint kinematic analysis of the knee and ankle.

A volunteer was filmed with three video cameras while wearing the three sets of markers on the femur, tibia, and foot respectively during walking, running, and cycling trials. During the test, the 3D coordinates of the nine markers relative to global frame were recorded with the APAS system ® or later with the SIMI system ®. Once the orientation matrices of the two segments (proximal and distal) of one joint with respect to the global frame were determined, the rotation matrix (or attitude matrix) of the joint can easily obtained (Woltring, H. J., 1992). Then based on the rotation matrix, the three angels, α, β and γ, which correspond to flexion/extension, adduction/abduction and internal/external for knee and dorsiflexion/plantarflexion, inverion/eversion and adduction/abduction for ankle, can be computed accordingly.

RESULTS AND DISCUSSION

From the computation results, it shows that there is not much difference which methods was involved to estimate angular movement of flexion/ extension of the knee joint during cycling and running. However, there is some difference for walking and particularly for the ankle joint. To quantitatively show the difference between these methods, we define the maximum deviation of different Euler sets from the GS method as

$$mDev = \frac{\max\left(\left|x^{e}(t) - x^{gs}(t)\right|\right)}{\max\left(\left|x^{gs}(t)\right|\right)} \qquad t \in T$$

where x^e (t) is the result of one of Euler sets, x^{gs} (t) is the result of GS method and T is one cycling or step period. After computing the results of MDEVs of 3D knee and ankle joint rotations during cycling, running and walking, we can conclude that the 3D joint rotation angles of the knee and ankle estimated by Eulerian sequence *xyz* are exactly the same as those estimated by the GS method. The only difference is the sign. For other Eulerian convention sequences, the deviation to the GS method varies depending on joints and movements. The deviations are small for knee flexion/ extension rotation for all six Euler sets with respect to the GS method, normally not exceeding 10%. This value is within the measurement error. The Euler sequences should be carefully selected for knee flexion/extension during cycling where the knee flexion angle may exceed 90^0 since this will cause the rotation matrices singular for those whose second rotation is around knee flexion. In this study, this will happen for sequences *yxz* and *zxy*. For the ankle joint, the *yxz* sequence is closest to the GS method except the *xyz* sequence.

REFERENCES

Cole, G. K., Nigg, B. M., Ronsky, J. L., and Yeadon, M. R., 1993, "Application of the joint coordinate system to three-dimensional joint attitude and movement representation: a standardization proposal," J Biomech Eng, Vol. 115, pp. 344-349.

Grood, E. S. & Suntay, W. J. (1983). A joint coordinate system for the clinical description of three-dimensional motions: Application to knee. *J. Biomech Eng. (Trans. Of ASME)*, 105, 138-144.

Pennock, G. R., & Clark, K. J. (1990). An anatomy-based coordinate system for the description of the kinematic displacements in the human knee. *J. Biomech.*, 23(12), 1209-1218.

Challis, J. H. (1995). A procedure for determining rigid body transformation parameters. *J. Biomech.*, 28(6), 733-737.

Woltring, H. J. (1994). 3-D attitude representation of human joints: a standard proposal. *J. Biomech.* 27(12), 1399-1414.

Pio, R. L. (1966). Euler Angle Transformations. *IEEE Trans. Automatic Control.* AC-11(4), 707-715.

INTERPOLATING THREE DIMENSIONAL KINEMATIC DATA USING QUATERNIONS

James C. Coburn[1] and Joseph J. Crisco[2]

[1] Department of Mechanical Engineering, Brown University, Providence, RI
[2] Department of Orthopedics, Brown Medical School/Rhode Island Hospital, Providence, RI
E-mail: jcc@brown.edu

INTRODUCTION

Multiple CT volume images can be used to noninvasively determine the normal and pathological kinematics of the carpal bones of the wrist (Crisco et al. 1999). Only a limited number of positions can be acquired with CT due to radiation exposure. Accurate interpolation of the kinematics between these positions permits a more thorough kinematic analysis, especially of *in vivo* data sets where it is difficult to precisely control an independent position variable. Quaternions, four-dimensional unit vectors describing rotations, are currently used in computer graphics to interpolate a smooth path between key frames. We report a method for interpolating any 3-D kinematic data set by combining cubic quaternion splines with Catmull-Rom interpolation for translations.

MATERIALS AND METHODS

A quaternion spline (Shoemake 1985, Kim 1995), coupled with Cartesian Hermite curve was implemented and examined using a test object and *in vivo* kinematic data.

Image and Data Acquisition: Gold standard data for verification was acquired using five sensors tracking a rigid body motion, collected with an Optotrak (Northern Digital, Waterloo, ON) sampling at 30 Hz. Test data was resampled at 6 Hz from the gold standard and interpolated. Ten distinct wrist positions of a subject were scanned using a GE Highspeed Advantage CT (GE Medical Systems, Milwaukee, WI). Kinematic data of each carpal bone were calculated using established markerless bone registration techniques (Crisco 1999).

C^1-continuous Piecewise Quaternion Spline: Quaternions are elements of the four-dimensional space Q formed by the real axis and three imaginary orthogonal axes, **i**, **j**, and **k** that obey Hamilton's rule:

$$\mathbf{i}^2 = \mathbf{j}^2 = \mathbf{k}^2 = \mathbf{ijk} = -1 \qquad \text{Eq. 1}$$

Each four-component quaternion is written as a unit vector:

$$\mathbf{q} = [\cos\theta, \mathbf{n}\sin\theta] \qquad \text{Eq. 2}$$

where **n** is the orientation of the helical axis of motion (HAM) and θ is twice the angle of rotation, ϕ, about that axis. Quaternions are therefore directly calculable from 3x3 Euler rotation matrices.

An interpolative spline was implemented using a cubic curve between quaternions with an iterative spherical linear interpolation (slerp) technique (Shoemake 1985). For compactness *slerp*($\mathbf{q}_0$, $\mathbf{q}_1$; t) is notated $(\mathbf{q}_0 : \mathbf{q}_1)_t$ and is defined as:

$$\mathbf{q}(t) = (\mathbf{q}_0 : \mathbf{q}_1)_t = \mathbf{q}_0(\mathbf{q}_0^{-1}\mathbf{q}_1)^t \qquad \text{Eq. 3}$$

for $0 \le t \ge 1$ where t is the fractional advance from $\mathbf{q}_n$ to $\mathbf{q}_{n+1}$.

According to this method the tangents, $\mathbf{a}_n$ and $\mathbf{b}_{n+1}$, at each quaternion, $\mathbf{q}_n$, must be calculated. Cyclic motions have tangents for all points, but single direction motions encounter discontinuities at endpoints. A simple end-point tangent solution (Kim 1995) was implemented. (Fig. 1)

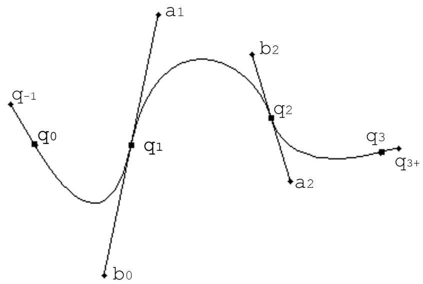

Fig. 1: An example curve showing the location of tangents $\mathbf{a}_n$, $\mathbf{b}_n$, $\mathbf{q}_{-1}$, and $\mathbf{q}_{3+}$.

The final equation for the cubic spline is:

$$(\mathbf{q}_0{:}\mathbf{a}_0)_t = \mathbf{p}_1 \quad (\mathbf{a}_0 : \mathbf{b}_1)_t = \mathbf{p}_2 \quad (\mathbf{b}_1{:}\mathbf{q}_2)_t = \mathbf{p}_3$$
$$(\mathbf{p}_1{:}\mathbf{p}_2)_t = \mathbf{p}_4 \quad (\mathbf{p}_2{:}\mathbf{p}_3)_t = \mathbf{p}_5$$
$$(\mathbf{p}_4{:}\mathbf{p}_5)_t = \mathbf{q}_0(t) \qquad \text{Eq. 5}$$

C^1- continuous Piecewise Cartesian Spline: Hermite curves, specifically Catmull-Rom curves, are well-described mathematical tools for interpolating smoothly between any set of three-dimensional points. After quaternion interpolation, the remaining HAM parameters (axis location in space, $\mathbf{Q}_L$ and translation along the axis, $\mathbf{t}_{\mathbf{ham}}$) were splined using these curves. $\mathbf{t}_{\mathbf{ham}}$ was interpolated directly. $\mathbf{Q}_L$ was calculated to minimize its displacement in the data set. The location, on the axis, nearest the origin was found for the first HAM, $\mathbf{Q}_{L1}$. Each subsequent axis location, $\mathbf{Q}_{Ln}$, was calculated to be the point closest to $\mathbf{Q}_{L1}$.

Combining Quaternion and Hermite Curves: Hermite curves operate in a linear space whereas quaternion curves operate in a spherical space. This causes a discrepancy in the length of each interpolated element. To compensate we interpolated the quaternions using a constant increment t, then constructed the Hermitian parameter t_n:

$$t_n = \frac{\sum \theta_n}{S} \qquad \text{Eq. 6}$$

where S is the quaternion segment arc length and θ_n is arc length for increment n.

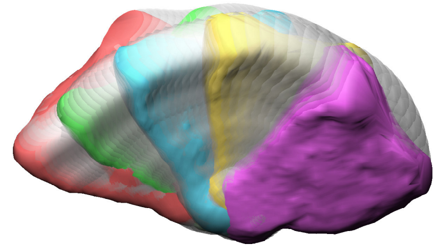

Fig. 2: Scanned capitate positions (colors) and interpolated positions (grey).

RESULTS AND DISCUSSION

- C^1-continuity was verified for all interpolated curves made from test data.
- When applied to the *in vivo* data set, bones maintained anatomically reasonable positions.
- Curves obtained from these splines allowed for selection of a constant independent variable across subjects.
- Large changes in data point increments cause artifacts from varied arc lengths.
- Interpolations are directionally dependent due to differences in tangent calculation.

Comparison of "gold standard" and "test data" HAM parameters yielded mean differences of 0.01° ± .06° in ϕ, 0.3 ± 1.8mm in $\mathbf{t}_{\mathbf{ham}}$, 0.55° ± .8° and 4.5 ± 7.4mm in HAM orientation and location.

With the mentioned limitations, this method gives an accurate path between a data set of kinematic transforms sampled at irregular intervals.

REFERENCES

Crisco, J. J., McGovern, R. D., and Wolfe, S. W. (1999). *J Orthop Res*, 17(1), 96-100.

Shoemake, K. (1985). *Proceedings of SIGGRAPH '85*, **19**(3), 245-254.

Kim, M.J. et al. (1995) *Proceedings of Computer Animation '95*, 72-81.

ACKNOWLEDGMENTS

Funded in part by NIH AR44005

BASELINE MEASURES ARE ALTERED IN BIOMECHANICAL STUDIES

Melissa M. Scott and Nicholas Stergiou

HPER Biomechanics Laboratory, University of Nebraska at Omaha, Omaha, NE, USA
Email: mmscott@mail.unomaha.edu Web: www.unocoe.unomaha.edu/hper/

INTRODUCTION

Often biomechanists measure the average performance within a group of individuals and generalize this information to a larger population without regard of how any given individual performed. Single Subject (SS) designs can be used to address this issue. For example, Dufek and Bates (1991) using such a design, found meaningful differences in performance between sport shoes, while previous investigations were unable to detect any differences. Although the need for SS designs in biomechanical studies has been well established by Bates and colleagues (Dufek et al., 1991, 1995; Bates, 1996), their work has not addressed the topic of Baseline adjustments. The evaluation and usage of Baseline data between conditions where an independent variable (speed, footwear, obstacle height, etc.) is manipulated can be critical to the evaluation of treatment effects. The primary purpose for establishing Baselines is to use the subject's performance in the absence of the independent variable as an objective basis for evaluating the effects of the independent variable (Heward, 1987). A multiple Baseline design allows the examination of these effects. This is also the case in any repeated measures type of experimental design (Heward, 1987). The purpose of our investigation is to examine if baseline measures are altered between conditions in biomechanical studies and to determine the need for Baseline measures in biomechanics.

METHODS

Ten subjects ran under two different experimental settings, speed changes and obstacle heights, while lower extremity sagittal view video (200Hz) and force platform (1000Hz) data were collected simultaneously. The speed setting consisted of the participants running at their comfortable self-selected pace, 10% faster, 10% slower, and 20% faster. The obstacle session consisted of participants running at the same self-selected pace over obstacles of three heights: 5%, 10%, and 15% of their standing height. Each speed and obstacle condition consisted of 10 trials and the order of presentation was randomized. Additionally, between conditions, 10 trials of unperturbed running were collected as Baselines for both settings. The above protocol is presented in detail in Stergiou et al. (1999). One kinetic variable (vertical Ground Reaction Impact Force; GRIF) and one kinematic (Maximum Knee Angle during stance; MKA) were identified for all trials of all Baselines. The Baseline group means from each setting (speed and obstacle) were analyzed using ANOVA with repeated measures ($p<0.05$) with a Tukey test as post-hoc. The Baseline subject means from each setting were analyzed with a single subject statistical procedure (Model Statistic; Bates, 1996).

RESULTS AND DISCUSSION

The ANOVA results showed no significant differences between the Baseline group means for both dependent variables in the speed setting (Table 1). However, in the obstacle setting, both the kinetic and the kinematic variable revealed significant differences. The post-hoc analysis showed significant differences between the first Baseline and the last two. It is interesting to notice a decreasing trend for both dependent variables (Table 1), which suggests an accumulative treatment effect (the varying obstacle height). The single subject comparisons for the kinematic variable produced 15% and 30% overall significant differences for the speed and the obstacle settings, respectively. For the kinetic variable, the corresponding results were 13.3% and 18.3%. These results are in agreement with the group results and indicate that the obstacle perturbation had a larger treatment effect. Furthermore, the single subject analysis showed that this effect was even larger for the kinematic variable.

The above results indicated that in biomechanical studies when a repeated measures design is being used, Baseline measures should be incorporated. This should be the case in both group and single subject designs, and especially when kinematics are used as dependent variables. Consideration is also warranted when evaluating different types of perturbations, since some of them, like obstacle heights during locomotion, may generate a larger treatment effect.

SUMMARY

Ten runners were asked to run at varying speeds and obstacle heights. Baseline measures were taken between all conditions. Right lower extremity kinematic data and kinetic data were collected for all trials and Baselines. The Baseline measures were then evaluated by both a group and a single subject analysis. The group analysis revealed significant differences for the obstacle setting, while the single subject analysis indicated that Baseline measures for kinematics are altered in a greater degree than kinetics. These findings suggested that Baseline measures are needed in biomechanical studies, when a repeated measures design is being used.

REFERENCES

Bates, B.T. (1996). *Med Sci Sports Exerc*, **28**, 631-638.

Dufek, J.S., Bates, B.T. (1991). *Med Sci Sport Exerc*, 23, 1062-1067.

Dufek, J.S., Bates, B.T., Davis, H.P. (1995). *Med Sci Sports Exerc*, **27**, 288-295.

Heward, W.L. (1987). In: Cooper, J. et al. (Eds): *Applied Behavior Analysis*, Merrill Publ.

Stergiou, N., Bates, B.T., James, S.L. (1999). *Med Sci Sports Exerc*, **31**, 1645-1655.

Table 1: Group Baseline means evaluated with superscripts indicating post-hoc differences ($p<0.05$).

	SPEED		OBSTACLE	
	MKA (deg)	**GRIF (Nt)**	**MKA (deg)**	**GRIF (Nt)**
Baseline 1:	138.62	1264.12	$139.95^{Bas3, Bas4}$	$1304.76^{Bas3, Bas4}$
Baseline 2:	138.24	1271.98	138.94	1256.34
Baseline 3:	137.95	1233.28	138.82	1230.45
Baseline 4:	138.37	1259.23	138.75	1225.67

HEAD IMPACT TELEMETRY SYSTEM (HITS™) FOR MEASUREMENT OF HEAD ACCELERATION IN THE FIELD

Richard M. Greenwald[1,2], Jeffrey J. Chu[1], Joseph J.Crisco[3], Jeffrey A. Finkelstein[4]

[1] Simbex , Lebanon, NH, USA
[2] Thayer School of Engineering, Dartmouth College, Hanover, NH, USA
[3] Department of Orthopaedics, Brown Medical School and Rhode Island Hospital, Providence, RI USA
[4] Microprocessor Designs, Shelburne, VT, USA
E-mail: rgreenwald@simbex.com

INTRODUCTION

Correlations between head acceleration measurements and concussions in sports have not been established. Current systems for measuring head accelerations are costly or not applicable for widespread use in sports. A telemetry based measurement and data analysis system incorporating a novel computational algorithm (Crisco et al., 2002) has been developed. Head Impact Telemetry System (HITS™) integrates this algorithm with a wireless sensor system and a large-scale database to provide simultaneous real-time continuous monitoring of head acceleration data from all players on the field. This paper describes the technical validation of the telemetry system in a football helmet.

METHODS

The HITS system provides data measurements for estimating linear acceleration magnitude and direction of the head. It has been initially applied inside of a football helmet (Figure 1). System components include: *Sensor Package* with single axis MEMS accelerometers, *Player Unit* with encoder hardware, analog front end and transceiver, *Sideline Controller* with decoder hardware, transceiver and *Software Interface* with PC interconnect, user interface, and access to impact database (Figure 2). Other sensors, including thermocouples and position transducers, can be added to the package.

Figure 1 – HITS embedded in helmet (left). Player Unit and Sideline Controller (right).

Wireless Sensor System Specifications

- Frequency Agile Radio (ISM Band 902-928 MHz)
- Small Size - 2.75" x 1.20" x 0.75"
- 10-bit Data Acquisition on 8 channels
- 100 Meter Range
- Up to 64 players / Sideline Controller
- All Channel Trigger Monitoring with user selectable threshold
- Up to 38.4Kbaud Data Throughput

Figure 2 – Schematic of HITS capability for wireless recording and capture of impacts and other data from up to 64 players at once

Field and laboratory testing was performed to validate the robustness of HITS for field applications in outdoor environments. Measures included: environmental signal strength of sideline controller across the ISM frequency band, communication range between Player Unit and Sideline Controller at the Dartmouth College football field, and durability of Player Unit in a football helmet under high g impact loading

RESULTS AND DISCUSSION

Field tests of the HITS telemetry hardware showed that environmental RF energy varied across the ISM band in an outdoor environment (Figure 3). Increases in environmental signal strength lowers the signal-to-noise ratio of HITS, leading to greater transmission errors and increased download times. HITS automatically switches to the frequency with minimal RF energy within the ISM band.

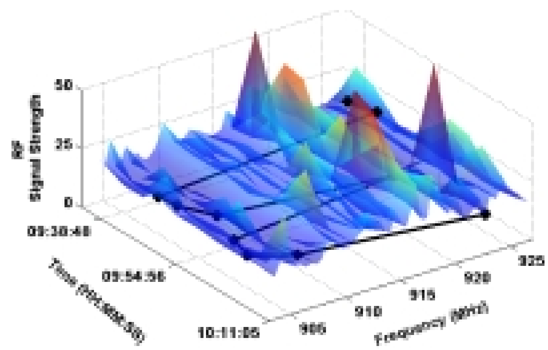

Figure 3 – RF signal strength varied as a function of both frequency and time over the ISM band. HITS automatically switches to the frequency with minimal RF signal strength (black circles).

Communication between Player Unit and Sideline Controller remained acceptable at distances up to 80 m, as measured by number of packet errors and communication retries. Download times per impact (500 bytes) averaged 500 msec, ensuring that if all 22 football players got hit simultaneously, data would all be downloaded before the next play.

Multiple impact testing of HITS hardware mounted in a commercially available football helmet demonstrated accurate transmission of accelerometer data at peak accelerations up to 140 g's within the defined specification requirements of 10% accuracy. No hardware damage was noted.

To date, there are no commercially available telemetry systems that meet our specifications for widespread use in sports applications. Specifically, we use automatic continuous frequency hopping, a marked improvement over fixed frequency devices, and a single Sideline Controller for up to 64 Player Units. Helmet-radio systems currently used for NFL quarterbacks use a fixed frequency, which if corrupted by other RF devices, prevents communication.

Currently, the Sideline Controller must be near the sideline at the 50-yard line to allow full coverage of the football field. Improved antenna construction will allow increases in transmission range and accuracy.

HITS was initially designed to be mounted inside a football or other sport helmet and can withstand high impact accelerations that might occur on the field during play. The system can also be used in non-helmeted applications, such as studies of head acceleration during the heading of soccer balls.

SUMMARY

A novel RF-telemetry system for measuring head acceleration in the field was developed and tested. This system provides a cost-effective method for studying head impacts and concussions that was heretofore not possible.

REFERENCES

Crisco J.J., Greenwald R.M., Chu, J.J. (2002) *Proceedings of World Congress of Biomechanics 2002.*

ACKNOWLEDGEMENTS

This work was supported in part by NIH 2R44HD40473

MORPHOLOGICAL CONTROL OF HYDROXYAPATITE WHISKERS FOR REINFORCED BIOMATERIALS

Huijie Leng and Ryan K. Roeder

Dept. of Aerospace and Mechanical Engineering, Univ. of Notre Dame, Notre Dame, IN, USA
E-mail: rroeder@nd.edu Web: www.nd.edu/~amebio

INTRODUCTION

Hydroxyapatite (HA), due to its resemblance to human bone mineral and excellent biocompatibility and bioactivity, has attracted increasing attention and use in orthopaedic surgery. Furthermore, single crystal HA whiskers are desirable as a reinforcement for bulk biomaterials (Roeder, *et al*., 2002). In reinforced polymers, the use of HA whiskers over particulate reinforcements results in an improved biocomposite stiffness, strength, toughness and anisotropy that is more like that found in native bone tissue.

Several reports have appeared in the literature for hydrothermal synthesis of HA whiskers. E.g., Suchanek, *et al*. (1995) studied the effects of the reactant concentrations on the HA whisker morphology. Fujishiro, *et al*. (1993) investigated the effects of the solution pH and reaction temperature on the morphology. In the present work, HA whiskers were prepared by the decomposition of a calcium-lactic acid complex and the precipitation of HA under hydrothermal conditions. The effects of the heating and stirring rates on the whisker morphology were examined, providing new insights into the reaction mechanism.

METHODS

HA whiskers were prepared from aqueous solutions containing 0.1 M lactic acid ($C_3H_6O_3$), 0.03 M phosphoric acid (H_3PO_4) and 0.05 M calcium hydroxide ($Ca(OH)_2$). HA whiskers were precipitated from the solution under hydrothermal conditions using a 2 L, Teflon®-lined pressure vessel with a heating assembly and temperature controller. The reactor heating and stirring rates were independently controlled. All reactions were heated to 200°C and held for 2 h. Reactions were heated to this temperature in 1, 2, 4 and 8 h, corresponding to heating rates of 3.33, 1.67, 0.83 and 0.42°C/min, respectively (Fig. 1). For the 1.67°C/min heating rate, stirring rates included 0 (static), 50, 150 and 250 rpm.

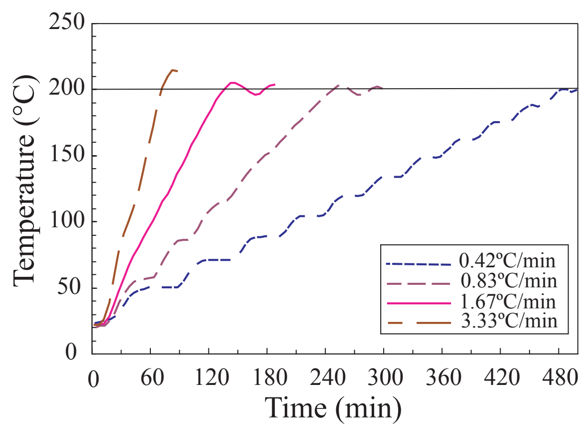

Figure 1: Reaction heating rates.

The whisker morphology was characterized using an optical microscope and digital camera. Whisker lengths and widths were measured, and the aspect ratio calculated. 500 whiskers were randomly selected and measured for each sample. One-way ANOVA was used to compare group means.

RESULTS

The morphology of the as-prepared HA whiskers is shown by the optical micrograph in Figure 2. The morphology of the HA whiskers was significantly affected by the reaction heating rates. Decreased heating rates resulted in increased whisker length (Fig. 3) and aspect ratio. Differences between each heating rate were statistically significance ($p < 0.05$). The aspect ratio was 17.5, 13.2, 10.1 and 8.1 for heating rates of 0.42, 0.83, 1.67 and 3.33°C/min, respectively. The mean whisker length (and aspect ratio) was 33.5 μm (13.6) and 19.8 μm (10.0) for stirring rates of 0 and 50 rpm, respectively. Stirring rates of greater than 50 rpm resulted in submicron, particulate HA (Fig. 4).

DISCUSSION

The heating and stirring rate effects on the HA whisker morphology were governed by nucleation kinetics. For increasing heating rate, the number of HA nuclei increased due to rapid decomposition of the Ca chelates. An increased number of nuclei for fixed solution concentration resulted in a smaller mean whisker length, regardless of the growth rate. Similarly, increased stirring rate during the reaction disrupted stable growth of HA whiskers. Therefore, compared with static reaction, stirred reactions resulted in shorter whiskers or no whiskers at all.

SUMMARY

HA whiskers of controlled morphology were prepared by hydrothermal synthesis. Decreased heating rates and stirring rates resulted in whiskers of greater length and aspect ratio.

REFERENCES

Fujishiro, Y., *et al*. (1993). *J. Chem. Tech. Biotechnol.* **57**, 349-353.

Roeder, R.K., *et al*., (2001). *J. Biomed. Mater. Res*., submitted Aug. 2002.

Suchanek, W., *et al*., (1995). *J. Mater. Res.* **10,** 521-529.

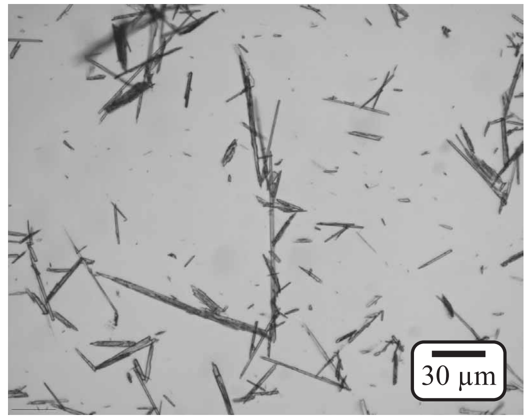

Figure 2: Optical micrograph of HA whiskers synthesized at a 0.42°C/min heating rate without stirring.

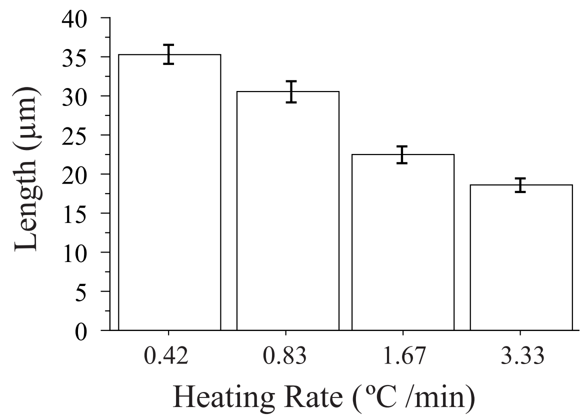

Figure 3: The mean length of HA whiskers for each reaction heating rate. Error bars span the first standard error.

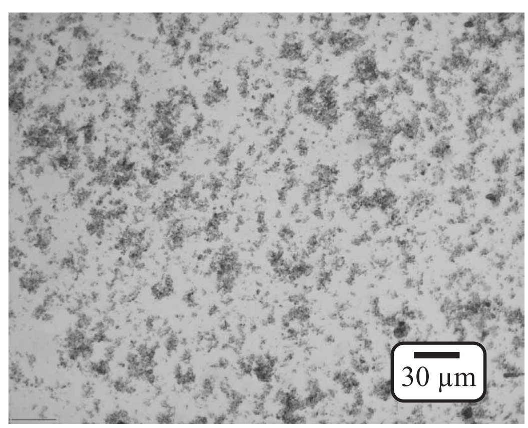

Figure 4: Optical micrograph of HA synthesized at a 1.67°C/min heating rate and 250 rpm stirring rate.

LASER DISPLACEMENT SENSOR REPORTS ARE AFFECTED BY SURFACE COLOR AND OPACITY

Mark B. Sommers, Kara J. Martin, Oliver K. Erne, and Michael Bottlang

Biomechanics Laboratory, Legacy Clinical Research & Technology Center, Portland, OR
E-mail: mbottlan@lhs.org

INTRODUCTION

Laser displacement sensors (LDS) provide for high-resolution, non-contact assessment of linear distances in an economical fashion and find increasing use in biomechanical research applications [Rydmark, 1999]. In combination with a two-axis motion platform, LDS are used for three-dimensional scanning of anatomic geometries, such as articular cartilage and bony surfaces [Haut, 1998]. While LDS rely on adequate reflective properties of the surface of interest, great variability in specimen surface preparation persists among published studies [Haut, 1998, Sommers, 2001, Heuer, 2001]. This study investigated how LDS reports are affected by the color and opacity of the target surface. Specific for biomechanical applications, this study tested if accurate LDS measurements can be obtained on articular cartilage in the absence of a reflective coating.

METHODS

A commercially available laser-based displacement sensor (NAIS; ANR 12821, San Diego, CA) with an accuracy of 4 µm, a measurement range of 80 ± 20 mm, and a wavelength of 670 nm was utilized. This sensor was suspended 80 mm above a reference surface, with the laser beam perpendicular to the reference surface. Four repetitive laser displacement reports were obtained before and after placing solid gauge blocks of height h_O= 8976 ± 7µm on the reference surface under the laser beam.
To determine the LDS accuracy for relative height measurements h_r on surfaces with same colors, displacement records were obtained for gauge blocks with white, red, green, blue, and black surfaces on white, red, green, blue, and black reference surfaces, respectively (Fig. 1a). The resulting height differences h_r between same-colored surfaces were computed and compared to h_O to quantify the effect of surface color on LDS accuracy.
To determine the LDS accuracy for measurement on objects with different colors, displacement records were obtained for gauge blocks with white, red, green, blue, and black surfaces with respect to a white reference surface (Fig. 1b).

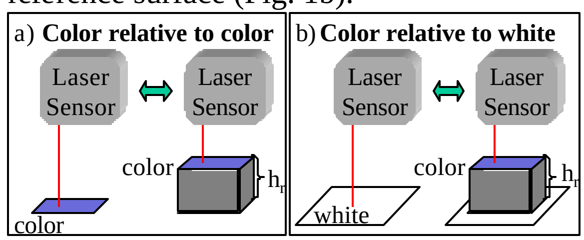

Figure 1: Color sensitivity assessment

To evaluate the effect of surface opacity, geometric profiles across a cadaveric bovine femoral head were obtained by translating the LDS with a motorized linear slide over the specimen. Four line scans (LS) across the specimen were obtained: LS_C, on cartilage in the absence of surface coating; LS_{CC}, after application of a white, diffuse reflective coating of nominally uniform thickness of 50 µm; LS_B, on dry subchondral bone surface after chemically dissolving the articular cartilage; and LS_{BC}, on subchondral bone after application of the white coating. All scans were obtained over the identical region of interest, and the nominal thickness of the coating layer was subtracted from LS_{CC} and LS_{BC}.

The effect of coating on LDS reports on cartilage and bone specimens was assessed in terms of the average difference between LS_C and LS_{CC}, and between LS_B and LS_{BC}, respectively. Cartilage thickness was estimated in terms of the average distance between 10 data points on the apex of the articular cartilage and subchondral bone. Statistical analyses were conducted at a confidence level of α=0.05 using a two-tailed Student's t-tests for unpaired samples.

RESULTS

The height difference h_D between LDS measurements on the white gauge block and white reference surface was 8976 ± 1.9 µm, and was not statistically different from h_O = 8976 ± 7µm. However, h_D assessment on same-colored red, green, blue, and black surfaces differed from h_O (Fig. 2a). The highest error was observed for h_D on the black gauge block and black reference surface, which yielded an overestimation of h_O by 65 ± 9.2µm.
For different colored surfaces the error in h_D was more pronounced (Fig. 2b). With respect to the white reference surface, measurement on red, green, blue, and black gauge blocks resulted in errors of 24 ± 1.2 µm, 130 ± 2.5 µm, 154 ± 4.4 µm, and 207 ± 4.4 µm, respectively.

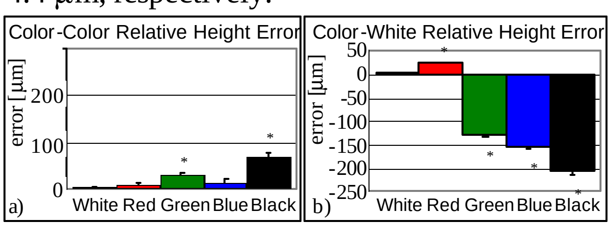

Figure 2: Accuracy effected by surface color

All four line scans LS_C, LS_{CC}, LS_B and LS_{BC} over the femoral head specimen closely reflected the gross geometry (Fig. 3). The average difference between three reproducible scans on innate cartilage (LS_C) after specimen repositioning was 23 ± 15 µm. The average difference between the line scans obtained on innate (LS_C) and coated (LS_{CC}) cartilage surfaces was 667 ± 148 µm. The average difference between the line scans obtained on non-coated (LS_B) and coated (LS_{BC}) subchondral bone was 222 ± 44 µm. The average cartilage thickness in apex vicinity derived as distance between coated cartilage and subchondral bone surfaces was 1147 ± 35 µm. Without coating the cartilage thickness measurement was 29% smaller, i.e. 812 ± 52 µm.

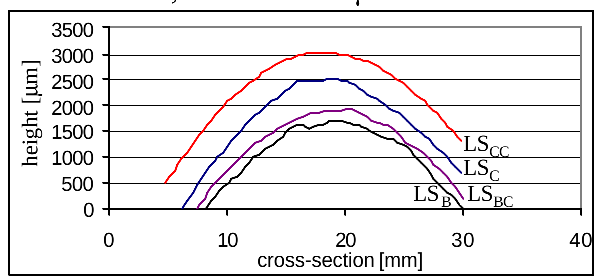

Figure 3: Effect of surface opacity

DISCUSSION

Laser displacement sensors constitute a highly precise research tool in the presence of target surfaces with adequate reflective properties. This study demonstrated that diffuse reflective, white target surfaces provide the highest accuracy. LDS measurements on dark, non-uniform colored, or semi-opaque surfaces can be obtained with high repeatability, but may exhibit considerable measurement errors. Innate articular cartilage, albeit inherently white in color, is semi-opaque, and in the absence of appropriate coating, is unlikely to provide adequate reflective properties for LDS employment.

REFERENCES

[1] Rydmark et al., Stud Health Technol Inform 62, 315-20, 1999
[2] Haut et al., J Biomech 31, 571-577, 1998
[3] Sommers et al., ASME Bioeng. Conf., BED-Vol. 50, 555-556, 2001
[4] Heuer et al., ASME Bioeng. Conf., BED-Vol. 50, 569-570, 2001

TOWARD AN MRI-BASED METHOD TO DETERMINE NON-UNIFORM DEFORMATIONS THROUGHOUT THE VOLUME OF ARTICULAR CARTILAGE

Corey Neu [1], Maury Hull [1], Jeffrey Walton [2] and Michael Buonocore [3]

[1] Orthopaedic Biomechanics Laboratory, University of California at Davis, Davis, CA, USA
[2] UC Davis NMR Facility, University of California at Davis, Davis, CA, USA
[3] UC Davis Research Imaging Center, University of California at Davis, Davis, CA, USA
E-mail: mlhull@ucdavis.edu

INTRODUCTION

The experimental study of the non-uniform deformation of articular cartilage throughout the volume of the tissue (hereafter termed three-dimensional (3D) deformation) in response to compressive loading is important to provide a comprehensive understanding of the properties of the normal and diseased tissue. Such 3D deformation of cartilage is expected due to the anisotropic and inhomogeneous properties of cartilage. Importantly, investigations of 3D deformation may provide an increased understanding of the process of mechanical signal transduction (Guilak 1995).

The realization of an MRI-based method to measure 3D cartilage deformation requires the fulfillment of several objectives, including the design of (1) a unique MRI pulse sequence to apply features throughout the volume of the cartilage, (2) an apparatus to load the tissue within the MRI scanner, and (3) software to compute deformation from MR images. This paper describes how these objectives were satisfied.

METHODS

A phantom material (Sylgard 527 Silicone Dielectric Gel, Dow Corning, Midland, Michigan) was used to demonstrate the new MRI-based method. A phantom material rather than articular cartilage was used because the phantom material can also be used to ultimately verify 3D strain calculations. The thickness of the phantom was approximately 6 mm (representing the maximum thickness expected in human cartilage on the tibial plateau).

The MRI pulse sequence was designed to visualize the phantom material when imaged in both undeformed and deformed states. Determining deformations in the phantom sample required imaging in both states to directly observe changes in geometry. Importantly, conventional MRI of the phantom material only identifies surface shape and volume changes and not internal features required for 3D deformation throughout the volume of the tissue. Thus, prior to imaging features were superimposed onto the material using MRI to allow for tracking of individual tissue points.

The DANTE pulse sequence was used to generate a grid of features (i.e. *tag lines*) in the phantom (Mosher and Smith 1990) using a Biospec 70/30 MRI system with microgradients (7.05 Tesla (T), Bruker Medical GMBH, Ettlingen, Germany). In each orthogonal direction 20 RF pulses were applied (duration of 4 μs, inter-pulse duration = 100 μs) during the application of a 20 Gauss/cm magnetic field gradient.

The fast spin echo pulse sequence was used to image the phantom in the undeformed and deformed states. Fast spin echo imaging parameters were: TR = 5000.0 ms; TE = 6.8 ms; number of echoes per TR = 8; field of view = $2.00 \times 2.00 \times 0.05$ cm^3; image matrix size = 256×256 pixels^2; number of excitations = 1; slice thickness = 1 mm.

The time available for image acquisition was limited by the time duration of the tag lines superimposed by the DANTE technique. The contrast between the tag lines and the phantom decays according to the T_1 of the material (approximately 1.5 s), which is much less than the 80 s total acquisition time for two images (i.e. one slice) representing the undeformed and deformed phantom.

The stringent time limits on image acquisitions motivated the need for a custom apparatus with loading cycles synchronized to the MRI pulse sequence thus providing a method for observing changes in deformation by acquiring image data over many loading cycles.

An apparatus composed of electronic and pneumatic components was constructed to load a tissue sample within the bore of an MRI scanner. The apparatus regulated pressure to a loading mechanism that included a double-acting pneumatic cylinder to apply load-controlled compression cycles to material samples. In addition, the apparatus allowed gating for MR image acquisition. For the phantom material, the cyclic loading apparatus was configured for a 20 N cyclic load magnitude (for the soft gel) with a 5-second total cycle duration.

An automated image processing algorithm was used to calculate deformations of specific cartilage material regions from the MR volume images. This algorithm mathematically and automatically determined the transformation needed to "morph" undeformed images into deformed images using a free-form deformation-based formulation (Rueckert, et al. 1999).

RESULTS AND DISCUSSION

Images of a phantom material were successfully captured by integrating the cyclic loading apparatus and MRI pulse sequence (Figure 1). The DANTE parameters in conjunction with the fast spin echo technique resulted in a grid pattern of tag lines initially spaced approximately 1 mm apart and voxel dimensions of $78 \times 78 \times 500$ microns^3. The timing of the apparatus and MRI scanner allowed for the acquisition, assembly, and visualization of images depicting the material in undeformed and deformed states. From these images, the 3D deformations were computed using the image processing algorithm.

This study was motivated by the need for detailed 3D articular cartilage deformation under compressive loading. The key results were that 1) a phantom material was imaged in undeformed and deformed states and 2) the deformation was determined from these images, thus demonstrating the potential of this unique method to measure 3D deformation in cartilage. To realize this potential, the phantom used for demonstration can now be replaced by cartilage. The foundation is now laid to acquire images of cartilage in the undeformed and deformed states and mathematically determine the corresponding 3D deformations. This will represent a major advance in our ability to analyze the behavior of articular cartilage when compressively loaded.

(A)

(B)

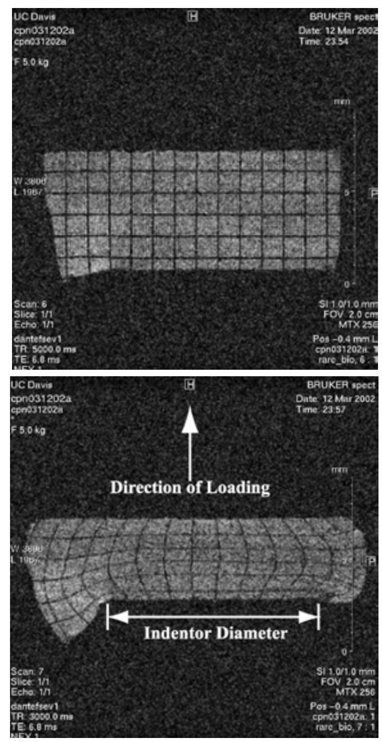

Figure 1. A set of phantom material images in undeformed (A) and deformed (B) states. DANTE tag lines are seen to deform with the tissue, thus permitting the calculation of deformation on the material surface and throughout the interior.

REFERENCES

Guilak, F. (1995). *J Biomech*, **28**, 1529-41.

Mosher, T.J. and Smith, M.B. (1990). *Mag Res Med*, **15**, 334-9.

Rueckert, D., et al. (1999). *IEEE Trans Med Imag*, **18**, 712-21.

MODELING THE ANISOTROPIC MECHANICAL PROPERTIES OF HYDROXYAPATITE WHISKER REINFORCED BIOCOMPOSITES

Weimin Yue and Ryan K. Roeder

Dept. of Aerospace and Mechanical Engineering, Univ. of Notre Dame, Notre Dame, IN, USA
E-mail: rroeder@nd.edu Web: www.nd.edu/~amebio

INTRODUCTION

The ideal bone substitute biomaterial should have mechanical properties similar to that of human bone tissue. Hydroxyapatite (HA) alone suffers from low fracture toughness, and most polymers alone lack sufficient stiffness and strength, limiting applications in load-bearing implants. Synthetic HA whisker reinforced polymer biocomposites provide a means to overcome these deficiencies (Roeder, *et al*., 2002).

HA reinforced polymers were modeled as short-fiber reinforced composites. The elastic modulus in any orientation of the composite was modeled according to three critical factors: 1) the contribution of each material phase, 2) the morphology of the reinforcement phase, and 3) the degree of preferred orientation in the reinforcement phase. Typical theoretical models in the literature consider, at most, two of these factors. The model presented here accounts for all three factors, assuming linear elasticity of both phases and that all HA reinforcements are uniformly dispersed in the polymer matrix. Similar models have been used to model bone tissue properties (Sasaki, *et al*., 1991).

METHODS

The model was based upon and verified by experimental data for the elastic modulus of HDPE reinforced with either oriented HA whiskers or particulate HA (Roeder, *et al*., 2002). Voigt and Reuss averages were used to calculate the upper and lower bounds for HA-polymer at varying volume fractions. The Halpin-Tsai equations (Halpin, *et al*., 1976) were used to account for the reinforcement aspect ratio, R, in calculating the longitudinal modulus, E_L, transverse modulus, E_T, and shear modulus, G_{LT}, of a representative volume element (RVE) containing perfectly aligned whiskers.

The HA whisker preferred orientation was considered transversely isotropic and simulated by two-dimensional orientation distribution functions (ODFs), $f(\chi)$, for all orientations rotated about any transverse axis, where χ is the angle of HA whisker inclination to the longitudinal composite axis. The degree of preferred orientation was quantified in multiples of a random distribution (MRD), where MRD = 1 corresponds to a random distribution. Simulated ODFs for MRD at the transverse axis of 1, 2, 5 and 10 were used to model preferred orientation of HA whiskers in the polymer matrix (Fig. 1). Note that each ODF has the same area which represents the same reinforcement volume.

To account for the preferred orientation of reinforcements, the RVE with perfectly aligned reinforcements was misoriented at angles, χ, from the longitudinal composite axis, and the modulus of the RVE in the longitudinal composite axis was calculated as,

$$E(\chi) = \left[\frac{\cos^4(\chi)}{E_L} + \frac{\sin^4(\chi)}{E_T} + \ldots \right.$$
$$\left. \sin^2(\chi)\cdot\cos^2(\chi)\cdot\left(\frac{1}{G_{LT}} - \frac{2\cdot\nu}{E_L}\right)\right]^{-1},$$

where ν is Poisson's ratio. Each RVE was weighed over an ODF to get the overall composites elastic modulus in the longitudinal direction as

$$E = \sum_{\chi}\left(f(\chi)\cdot E(\chi)\right)\Big/\sum_{\chi} f(\chi).$$

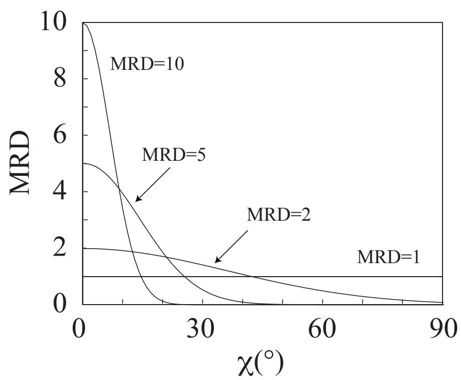

Figure 1: Simulated ODFs used in the model for MRD = 1, 2, 5, and 10.

RESULTS AND DISCUSSION

Within the Voigt and Reuss averaged upper and lower bounds for the elastic modulus of HA reinforced HDPE, various results were simulated with HA volume fraction from 0 to 0.5, HA reinforcement aspect ratio (*R*) of 1 and 10, and ODFs with MRD of 1, 2, 5, 10 (Fig. 2). Predictions for *R* = 10 and MRD = 2, closely fit experimental data for HA whisker reinforced HDPE. Note that HA whiskers were known to have a mean aspect ratio of 8 and a preferred orientation which has not yet been fully quantified. Predictions for *R* = 1 and MRD=1 underestimated experimental data for the particulate HA reinforced HDPE, warranting further investigation.

The model was used to design new biocomposites which may match the stiffness and anisotropy of bone tissue. For HA whisker reinforced HDPE with MRD > 2 (Fig. 2) or *R* > 10 (not shown), the longitudinal elastic moduli are predicted to reach those shown for bone tissue (Fig. 3). HA whisker reinforced polyetheretherketone (PEEK) is also predicted to match bone tissue (Fig. 3).

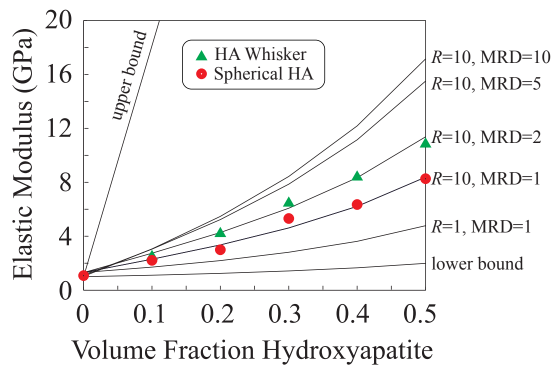

Figure 2: Model predictions for the elastic modulus of HA reinforced HDPE versus experimental data.

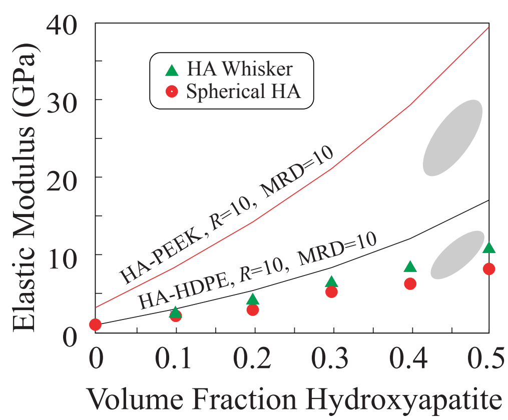

Figure 3: Model predictions for HA whisker reinforced PEEK composites. Shaded areas show the longitudinal (upper) and transverse (lower) elastic moduli for human bone tissue.

REFERENCES

Halpin, J.C., *et al*. (1976). *Polym. Eng. Sci.* **16** [5] 344-352.

Roeder, R.K., *et al*., (2001). *J. Biomed. Mater. Res*., submitted Aug. 2002.

Sasaki, N., *et al*., (1991). *J. Biomechanics.* **24** [1] 57-61.

DEVELOPMENT OF A HALL EFFECT MEASUREMENT SYSTEM TO MONITOR HYDRAULIC ACTUATION JOYSTICK KINEMATICS

Michele Oliver, Greg Northey, Toby Smith, Carrie Wilson, and Gord Hayward

School of Engineering, University of Guelph, Guelph, ON, CAN
E-mail: moliver@uoguelph.ca

INTRODUCTION

Hydraulic actuation joystick controlled machinery is commonly used in mobile North American construction, forestry and mining operations. Operators often make as many as 20,000 motions with one joystick over the course of a 10 hour shift (Golsse, 1989). Research is currently being conducted to quantify the dynamic forces exerted by operators of these types of machines in a laboratory mock-up of a heavy machinery cab. The ultimate objective of this work is to develop joystick design protocols which seek to minimize the risk to the operator of developing repetitive strain injuries such as carpal tunnel syndrome. In order to quantify the forces and torques exerted by an operator, knowledge of the joystick kinematics is required (Oliver et al., 2002a,b). The purpose of this paper is to describe the development of a joystick kinematics monitoring system which uses an array of four Hall Effect sensors. This system is intended to provide an inexpensive alternative to the previously used optoelectric motion analysis system, which, due to the low sampling frequency capabilities (60 Hz), does not allow for the accurate prediction of velocity and acceleration from displacement data when the joystick is moved quickly and forcefully into the hard endpoint at the end of the range of motion.

METHODS

As pictured in Figure 1, the design consisted of four Hall effect sensors (Honeywell SS495A1 miniature ratiometric semiconducting Hall effect sensors) fixed with epoxy to the cover plate. Each sensor was coupled with a rare earth magnet (Lee Valley rod shaped NIB 6.34 mm diameter, 12.69 mm long) and fixed with epoxy to the bottom of the swash plate. The magnet length was chosen so as to bring the magnet close to the sensor without actually touching it thus producing a larger magnetic field and

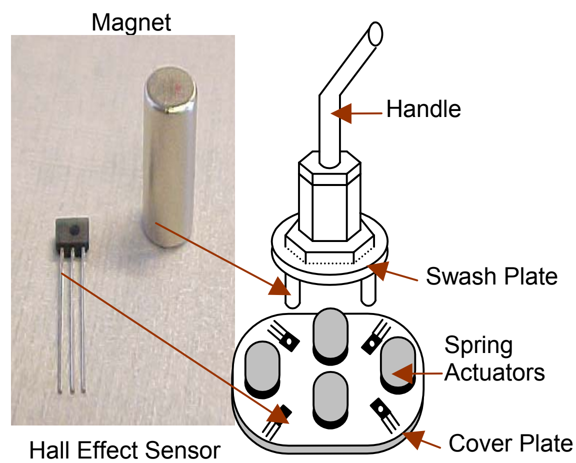

Figure 1: Illustration of sensor and magnet placement

output voltage. The sensors were located between the joystick spring actuators and onto the cover plate. The magnets were located directly above the Hall effect sensors when the joystick was in the neutral position. Given that the structure of the bottom of the joystick is a true universal joint which permits rotation about two orthogonal axes, as the joystick is moved, the magnets move toward and away from the sensors in an arc-like pattern causing a change in the Hall effect induced voltage.

An amplification circuit powered by a 12 volt source was used to amplify the sensor outputs which were then taken through analog to digital conversion into a computer for further analysis.

Calibration of the joystick involved the creation of an anchoring wooden frame and cover. Two tracks were cut in the cover to allow the joystick handle to move in two perpendicular axes. The angle of the joystick as it moved through the tracks was marked on the top of the cover. For each axis, this provided a relationship between the joystick angle and the Hall effect sensor output.

RESULTS AND DISCUSSION

While an excellent correlation between the angle and the output voltage from the Hall sensor was achieved, it was found to be non-linear and was therefore modeled using a third order polynomial (Figure 2). The calibration procedure was time consuming and quite cumbersome. In addition, the procedure did not allow for any indication of off-axis movement, which is required for the assessment of unintended operator motion in future studies.

Due to the small size of the joystick and the sensitivity of the Hall effect sensors, it was found that all four sensors would be activated for any movement of the joystick, thus creating a redundant system. The proximity of the four sensors also caused cross-talk as all the magnets would affect any one sensor.

Due to the nature of the sensors and the need for more accurate off-axis joystick orientation information, it is apparent that a more sophisticated calibration system is required, one that can utilize the specific subtleties of the sensors.

The Hall effect sensors give a clean signal and do not interfere with telemetered EMG. In addition, unlike camera based motion analysis systems, Hall effect sensors allow higher sampling frequencies, which is required for the analysis of impact loading which can occur if the operator moves the joysticks quickly and hits a hard endpoint at the end of the range of joystick motion.

SUMMARY

An inexpensive, hydraulic actuation joystick kinematics monitoring device was successfully developed. However, a more extensive and efficient calibration procedure needs to be developed in order to be able to shorten calibration time as well as accurately monitor off-axis joystick motion and orientation.

REFERENCES

Golsse, J.-M. (1989). Technical Note TN-134, *Forest Engineering Research Institute of Canada-Wood Harvesting*.

Oliver, M., Biden, E., Rogers, B., and Rickards, J. (2002a). *Proceedings of World Congress of Biomechanics'02* Paper #79.

Oliver, M., Rogers, B., Garland, P., Gallant, T., and Biden, E. (2002b). *Proceedings of World Congress of Biomechanics'02* Paper #78.

ACKNOWLEDGEMENTS

This research was funded by the Natural Sciences and Engineering Research Council of Canada.

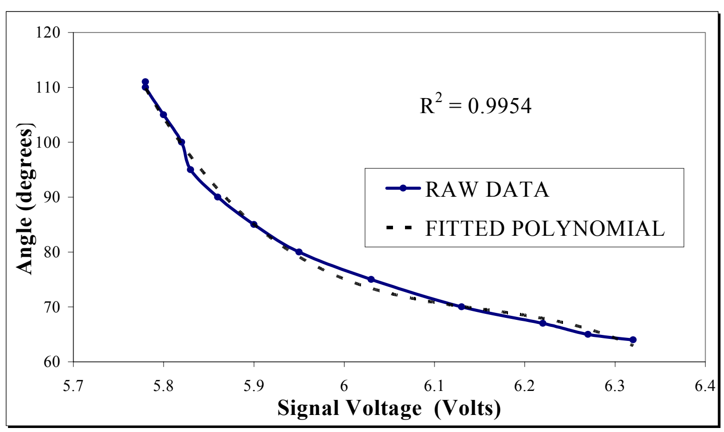

Figure 2: Non-linear relationship between one Hall effect sensor and joystick angle.

DETERMINATION OF EFFECTIVE MASS IN IMPACT TESTING

Cathie L. Kessler, Ismail El Maach, Jean-Philippe Dionne, Aris Makris

Med-Eng Systems Inc., Ottawa, Ontario, Canada
E-mail: ckessler@med-eng.com Web: www.med-eng.com

INTRODUCTION

The concept of effective mass (m_{eff}) is useful for determining impact force using an accelerometer on the impactor, based on Newton's law (F=ma) [Bir, 2000]. Effective mass is not always the actual mass of an impacting object, as in the case of a blunt impact simulator [Dionne et. al, 2002]. This impact simulator has a pneumatically-driven cam, which swings a baseball bat in an arc at various energy levels. Since some of the weight of the baseball bat is taken at the fulcrum, $m_{eff}<m_{actual}$, but there is also a rotational inertia component that must be considered.

With the intent of determining m_{eff} of a particular baseball bat, initial tests were performed using a blunt impactor and the assumption that m_{eff}=F/a (using the peak values from the force and acceleration signals, respectively). It became apparent that the value of m_{eff} was strongly dependent on the material being hit, thus identifying the need for more fundamental type testing.

METHODS

In the drop tower tests, the drop object had a steel cylindrical impacting surface (8.0 cm x 2.2 cm) with an accelerometer (PCB Piezotronics 353B18) attached. The total drop mass of 5.0 kg was dropped on a platform supported by three force transducers (PCB Piezotronics 208C05) (see Figure 1). The platform was covered with various protective layers, as discussed below. The acceleration signal and the three force signals were acquired at 10 000 Hz using a PC-based data acquisition system. The signals were filtered in accordance with the SAE J-211 CFC 1000 standard. The three force signals were summed, and 'force signal' henceforth refers to this sum.

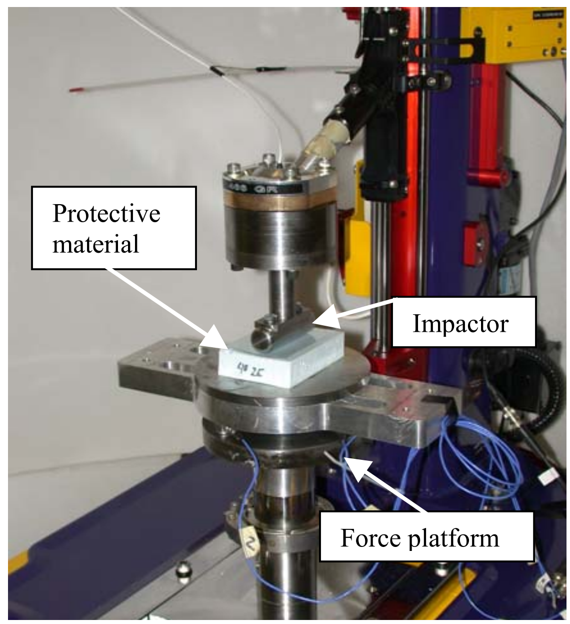

Figure 1: Test apparatus

For comparison, three different materials were impacted with the same drop weight: HL34 foam (2 layers of 12.7 mm), standard Dow Styrofoam insulation (25.4 mm), and HD80 foam (25.4 mm). For each set of tests, the protective layer consisted of a 76 mm x 102 mm piece of material covered by a centred 64 mm x 89 mm piece of 1 mm lexan sheet. Five drops were made on each material from a drop height of 80 cm, and five more were made on each material from a drop height of 40 cm. For each drop, both the foam and the lexan sheet were replaced.

The effective mass was determined using two different methods. In the first, the peak value of the force signal and the peak value of the acceleration signal were used in m_{eff}=F/a. For the second, the peak value of the force signal was found, and the signal was searched backward and forward from the peak to the points at which it became zero. The force signal was integrated between these points to get impulse (I), the acceleration signal was integrated between the same two time indices to get velocity (V), and these were used in m_{eff}=I/V (see Figure 2).

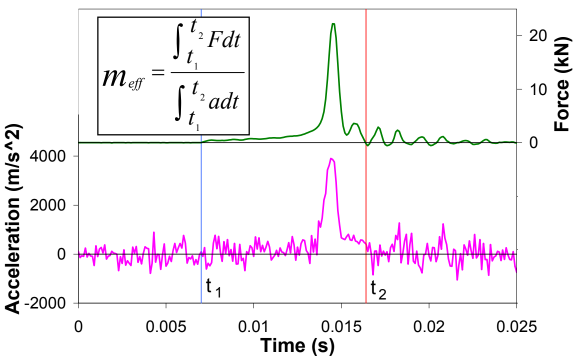

Figure 2: Example of a set of force and acceleration signals, showing the integration limits for determining impulse and velocity

RESULTS AND DISCUSSION

Results from the testing are presented in Table 1 and in Figure 3. For each set of test conditions (drop height, protective material), Table 1 shows the average m_{eff} as calculated with the above methods, including standard deviation among the five trials. In Figure 3, the averages are plotted to compare calculation methods.

In general, the values for m_{eff} were lower than the actual mass of the drop object, due to the fact that some energy was absorbed by the protective foam layers. This indicates that using an instrumented impactor may not be a suitable method of measuring forces transmitted through protective layers of energy-absorbing materials. Since the test sample composition my affect the measurement, this should only be used when there is no alternate method available.

Table 1: Tabulated results of testing, with average values and standard deviations from five trials in each configuration (actual mass: 5.0 kg)

Drop Height	Foam	m_{eff}=F/a (±SD)	m_{eff}=I/V (±SD)
80 cm	HL34	5.2 (0.1) kg	4.7 (0.4) kg
	Dow	4.5 (0.2) kg	4.6 (0.3) kg
	HD80	3.6 (0.4) kg	4.4 (0.2) kg
40 cm	HL34	3.7 (0.2) kg	4.3 (0.2) kg
	Dow	2.7 (0.5) kg	4.5 (0.3) kg
	HD80	3.1 (0.3) kg	4.8 (0.3) kg

The results also indicate that using impulse and velocity rather than peak force and acceleration gives a much more consistent value of effective mass, which is closer to the nominal value of 5.0 kg.

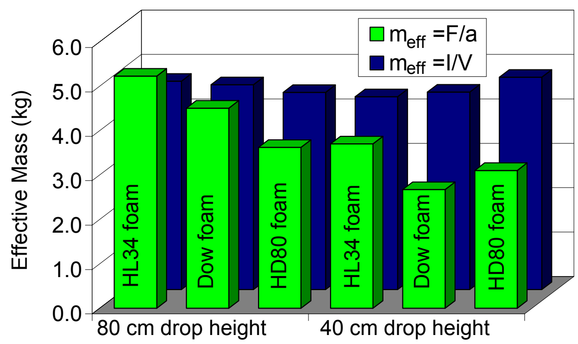

Figure 3: Comparison of average values of m_{eff} for various drop heights and protective materials as calculated by the two different methods (actual mass: 5.0 kg)

REFERENCES

1. Bir, C.A. (2000). *The Evaluation of Blunt Ballistic Impacts of the Thorax*, Ph.D. Thesis, Wayne State University, Detroit, Michigan
2. Dionne, J.P. et al. (2002). *Proceedings of European Society of Biomechanics*, Wroclaw, Poland

WALKING SPEED AND EXTERNAL KNEE ADDUCTION MOMENT IN HEALTHY KNEES AND IN KNEES WITH OA: CAUSE OR EFFECT OF OA?

Anne Mündermann[1], Chris Dyrby, Debra Hurwitz, Leena Sharma, Thomas Andriacchi
Division of Biomechanical Engineering, Stanford University, Stanford, CA
Rush Presbyterian St. Luke's Medical Center, Chicago, IL
[1]amuender@stanford.edu

INTRODUCTION

Osteoarthritis (OA) of the knee has been associated with increased mechanical load on the medial compartment of the knee (Baliunas et al. 2002), typically assessed as increased external knee adduction moment (Schipplein & Andriacchi 1991). Previous research indicated that patients with knee OA walk at slower speeds compared to asymptomatic individuals (Stauffer et al. 1977). However, it is not clear whether slower walking speed is associated with reduced knee adduction moments and whether patients with medial compartment knee OA reduce the loading on the medial compartment of the knee by reducing walking speed. We hypothesized that (a) when walking at the same speed, the knee adduction moment in OA patients is greater than in healthy controls, (b) when walking at normal speed, the knee adduction moment in OA patients and healthy controls are the same, and (c) the external knee adduction moment is correlated with walking speed in healthy controls and in patients with knee OA.

METHODS

Forty-four patients (88 knees) with OA of the medial compartment of the knee participated in this study (24 female, 20 male; age: 65.4 ± 10.0 yrs; height: 169.3 ± 9.8 cm; mass: 78.4 ± 13.1 kg). Patients were diagnosed to have knee OA in one or both knee joints based on clinical and radiographic data, and mechanical axis and K-L grades for both knees were determined. For each patient, an asymptomatic control subject matched for gender, age, height and weight (24 female, 20 male; age: 63.3 ± 10.7 yrs; height: 169.2 ± 8.5 cm; mass: 76.4 ± 12.7 kg) was selected. A six-marker link model was used to obtain walking speed and kinematic and kinetic data (Andriacchi et al. 1997). Subjects wore their own low top, comfortable walking shoes. Marker and force data was captured using four Qualisys MCU240 cameras (Sweden) and a Bertec force platform (Columbus, OH). Each patient was instructed to walk at three self-selected speeds: slow, normal, and fast. Due to missing markers, data for ten knees were excluded resulting in 78 control-OA knee pairings. Linear regression analysis was used to relate the external knee adduc-tion moment during the support phase of walking to walking speed. Comparisons between the control and OA groups were performed using repeated measures t-tests. Differences between the control, less severe OA (Kellgren-Lawrence grade ≤ 2) and more severe OA (Kellgren-Lawrence grade ≥ 3) were determined using repeated measures analysis of variance (ANOVA; $\alpha = .05$).

RESULTS

Only 6.0 and 11.6% of variance in adduction moment, respectively, were explained by differences in walking speed (Table 1). The linear regressions between walking speed and external knee adduction moment was not significantly different between the two groups. No significant differences in walking speed and external knee adduction moment were found between the control and the OA groups (P = .396 and P = .421, respectively). A statistically significant increase in knee adduction moment was found for knees with K-L grade 3 or 4 compared to asymptomatic matched control knees (P = .039) and for knees with K-L grade 3 or 4 compared to knees with K-L grade equal or smaller than 2 (P < .001; Figure 1). The mechanical axis varus alignment was significantly greater for knees with K-L grade 3 or 4 (6.0 ± 0.6˚) compared to knees with K-L grade equal or smaller than 2 (0.0 ± 0.5˚; P < .001).

Table 1: Results of linear regression analysis: Knee adduction moment dependent on walking speed.

Group	Control	OA
Slope	.724	.933
Intercept	2.373	2.126
R^2	.060	.116
P-value	< .001	< .001

DISCUSSION

The results of this study do not support the hypothesis that knee adduction moment and walking speed are directly related in asymptomatic controls and patients with knee OA. Previous research that did not control for gender, age, height or weight reported slower walking speeds in OA patients compared to healthy controls (Stauffer et al. 1977). Other studies (e.g. Baliunas et al. 2002) compared the knee adduction moment at a controlled speed of 1 m/s, which is more than 20% slower than the values for self-selected walking speed in our study. Differences in adduction moments at such slow walking speeds may not truly represent the mechanical loads most frequently placed on the knee. Based on the results of the current study, walking at slower speed appears not to be a strategy utilized by OA patients to reduce mechanical loading of the knee. The fact that walking speed and knee adduction moment did not differ between the control and OA groups and that the knee adduction moment and mechanical axis varus alignment was significantly greater in patients with more severe OA (K-L grade 3 and 4), similar to results reported by Sharma et al. (1998), suggests that differences in adduction moment are less likely the initial cause for OA but rather the effect of morphological changes in the pathological joint such as medial compartment joint space narrowing. This increase in adduction moment at later stages of OA may lead to an accelerated rate of disease progression.

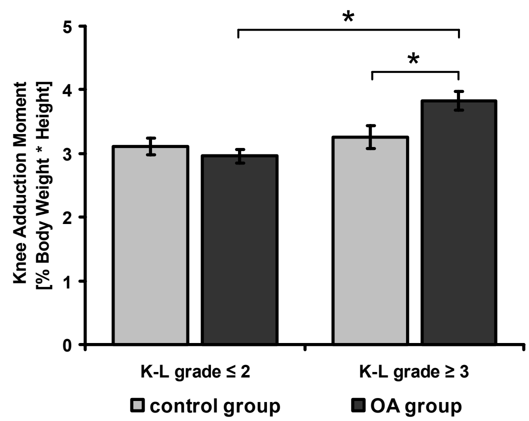

Figure 1: Estimated marginal mean (SEM) for knee adduction moment (K-L grade ≤ 2: n = 50; K-L grade ≥ 3: n = 28). * = significant difference.

REFERENCES

Andriacchi T.P., et al. (1997). *Basic Orthopaedic Biomechanics.* Lippincott-Raven Publishers.

Baliunas A.J., et al. (2002). *Osteoarthritis Cartilage*, **10**, 573-579.

Schipplein O.D., Andriacchi T.P. (1991). *J. Orthop. Res.*, **9**, 113-119.

Sharma L., et al. (1998). *Arthr. Rheum.*, **41**, 1233-1240.

Stauffer R.N., et al. (1977). *Clin. Orthop. Rel. Res.*, **126**, 246-255.

ACKNOWLEDGEMENTS

This project was funded by NIH grant # AR 39239.

REALISTIC RIOT HELMET IMPACT TESTING

Cathie L. Kessler, Ismail El Maach, Jean-Philippe Dionne, Steve Truttmann, Aris Makris

Med-Eng Systems Inc., Ottawa, Ontario, Canada
E-mail: ckessler@med-eng.com Web: www.med-eng.com

INTRODUCTION

Helmet standard testing [CSA, 2002] is performed with a drop tower, with either helmeted headforms dropped on fixed anvils, or with stationary helmets being hit by an impactor. Neither case is representative of typical threats for which the helmet was intended, in which the wearer would be moved bodily upon impact, absorbing a fraction of the energy through inertia. In the current testing, a more realistic case of a mannequin wearing a Riot Helmet being hit by a baseball bat is considered.

METHODS

All testing was performed on a Hybrid II mannequin representing the 50th percentile. Baseball bat blows were generated with a blunt impactor simulator [Dionne et. al, 2002], which consists of a pneumatically-driven cam swinging the baseball bat in an arc. One accelerometer (PCB Piezotronic 350A03) was installed on the baseball bat (plane of motion) and three were located in the head of the mannequin (oriented with its Frankfort plane horizontal), positioned along the axes of a right-handed coordinate system. The origin of the coordinate system was at the nasal root. Data was collected through a computerized data acquisition system at a rate of 10 kHz.

The mannequin was hung from a crane by a yoke between the shoulder blades connected to a quick-release mechanism, consisting of several relays and a solenoid-operated pneumatic cylinder (Fig. 1). As the bat swung, a lever passed through an optical sensor, triggering both the release mechanism and the data acquisition. Impacts were aimed at three locations (crown, sellion and tragion, Fig. 1), with the mannequin either unprotected (no helmet) or protected. In the unprotected case, five impacts were performed at each location. For the protected case, each site was impacted three times (only one helmet used throughout). All impacts were delivered with a bat angular velocity of 28.8 rad/s (or 16.8 m/s).

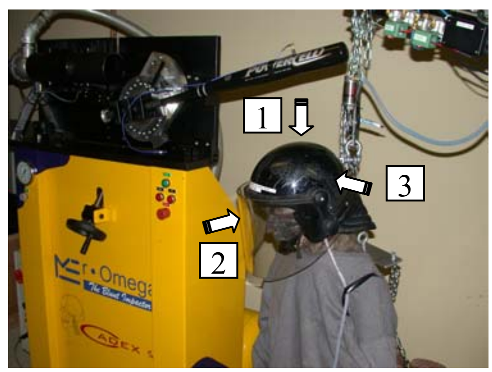

Figure 1: Experimental apparatus and impact sites: 1) Crown, 2) Sellion 3) Tragion

The Head Injury Criterion (HIC) was used to assess the probable level of injury due to head acceleration [Versace, 1971]. The HIC is calculated as follows:

$$HIC = \left\{ (t_2 - t_1)^{-1.5} \left[\int_{t_1}^{t_2} a(t)dt \right]^{2.5} \right\}_{\max}$$

where t_1 and t_2 are chosen to maximize the HIC parameter. This value was then used to calculate the scores for the Abbreviated

Injury Scale (AIS), which gives the probability of the injury falling into various levels of severity [Prasad et. al, 1985]. A weighted average of the AIS values obtained for the given HIC was also calculated.

RESULTS AND DISCUSSION

Values of the peak acceleration, HIC, and average AIS are shown in Table 1. For the unprotected impacts, the average of the five impacts and the standard deviation are shown. For the protected cases, values are given for all three impacts, showing that the results did not change significantly, despite using the same helmet for all impacts. Figure 2 shows the full set of AIS values for the protected and unprotected cases of impacting the mannequin directly in the face (sellion). Without head protection, there was a 40% probability of sustaining a critical injury (AIS 5) and a 21% chance of sustaining a fatal injury (AIS 6), whereas wearing a helmet provided enough protection to ensure a 100% probability of no injury (AIS 0).

SUMMARY

A free-falling mannequin was impacted in the head, with and without head protection. The head injuries sustained from these blows were estimated using the Head Injury Criterion (HIC) and the Abbreviated Injury Scale (AIS), and a comparison was made between unprotected and protected injuries. The results show that for impacts from all directions tested, wearing a helmet makes the difference between sustaining a potentially lethal injury and remaining virtually unharmed. These tests differ from those required by most helmet standards, in that an unrestrained mannequin was used, thereby accounting for imparted inertia. Further, a realistic impact was generated. These, together, make the testing much more representative of actual use, and also make comparisons with the unprotected case possible.

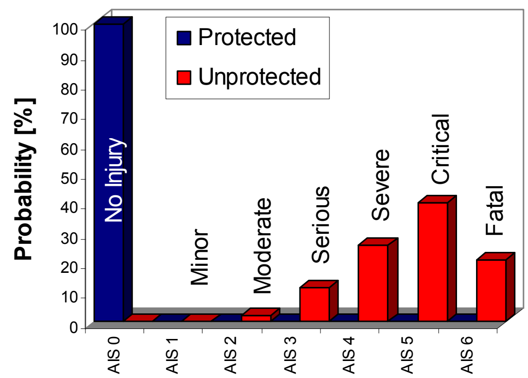

Figure 2: Injury levels for protected and unprotected impacts in the face (sellion).

REFERENCES

1. Canadian Standards Association (2002), Standard Z611-02
2. Dionne, J.P. et al. (2002). *Proceedings of European Society of Biomechanics*, Wroclaw, Poland
3. Versace, J. (1971). *Proceedings of 15th Stapp Car Crash Conference*, 771-796
4. Prasad P, Mertz HJ (1985), *Society of Automobile Engineers*, SAE Paper Number 85-1246

Table 1: Results for Impacts of Protected and Unprotected Mannequin Heads

	Unprotected – Average of 5 (± SD)			Protected								
Impact Site	Avg. Peak Acc. (g's)	Avg. HIC	Avg. AIS	Peak Acc. (g's)			HIC			Avg. AIS		
Tragion	500 (10)	1854 (67)	4.4	60	58	57	41	41	37	0.0	0.0	0.0
Sellion	502 (15)	1946 (180)	4.7	42	35	48	34	18	29	0.0	0.0	0.0
Crown	538 (27)	2115 (187)	5.1	87	97	95	129	140	144	0.0	0.0	0.0

QUANTIFICATION OF ANATOMICAL SHAPES IN TERMS OF THEIR SPATIAL CURVATURE PROFILE: AN ACCURACY VALIDATION

Barbara Schweizer, Sven Claes, Larry W. Ehmke, Marcus Mohr, and Michael Bottlang

Legacy Clinical Research & Technology Center, Portland, OR; *email: mbottlan@lhs.org*

INTRODUCTION

Quantitative descriptors of complex anatomic shapes provide the basis for geometric characterization of the skeletal system. A host of tools for 3-D rendering of anatomical shapes are readily available, providing accurate graphical representation at the expense of large data sets (Eckhoff 2001; Spitzer, 1998). Planar radiographic projections remain an attractive alternative to generate descriptive representations of 3-D anatomical shapes in terms of simple geometric entities, such as radii of curvature, but lack spatial information (Hollister, 1993; Testi, 2001).

This study introduces a parametric approach to completely describe the trajectory of an anatomic shape in terms of its spatial curvature profile. Furthermore, the accuracy of this algorithm has been determined for trajectory source data from a common 3-D digitizing system. Finally, this approach has been used to quantify the 3-D shape of a human rib in terms of its spatial curvature profile.

METHODS

Spatial curvature profile: Three non-collinear points P_{i-1}, P_i, and P_{i+1} distributed along a curve segment define a unique circle in space with an apparent radius vector $\underline{\boldsymbol{R_i}}$ (fig. 1a). $\underline{\boldsymbol{R_i}}$ is found by determining the intersect P_C of two lines, which bisect vectors $\underline{P_{i-1}P_i}$ and $\underline{P_iP_{i+1}}$, and which lie in the plane defined by P_{i-1}, P_i, and P_{i+1}, where $\underline{\boldsymbol{R_i}} = \underline{P_iP_C}$. Assuming that small segments along an anatomical curvature approximate regular arcs, the entire curvature can be described by a sequence of n arc segments in terms of the corresponding vectors $\underline{\boldsymbol{R_i}}$. The sequence of all $\underline{\boldsymbol{R_i}}$ constitutes a spatial curvature profile, which uniquely defines the shape of the anatomical curvature by means of the amount and direction of apparent radii, and which is independent of the orientation of the anatomical curvature.

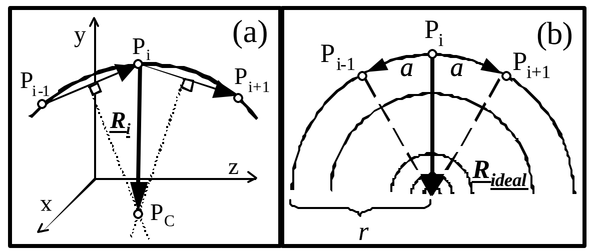

Figure 1: a) mathematical model of curvature determination and b) accuracy evaluation setup

Accuracy Evaluation: $\underline{\boldsymbol{R_i}}$ was computed from P_{i-1}, P_i, and P_{i+1} in an exact closed-form solution. However, errors in digitization of P_{i-1}, P_i, and P_{i+1} affect the accuracy of $\underline{\boldsymbol{R_i}}$. Source data was used from a commercially available digitizer with known accuracy of 0.23 mm (MicroScribe G2X, San Jose, CA). The accuracy of $\underline{\boldsymbol{R_i}}$ was determined for point triplets, digitized on arcs of known radii as a function of two variables: the radius, r, and the angle, a, of arc segments between adjacent points, P_{i-1}, P_i and P_{i+1} (fig. 1b). To determine the effect of r and a on the accuracy of $\underline{\boldsymbol{R_i}}$, point triplets were digitized along arcs, ranging from r=10 to 200 mm and a=10° to 90°. Each point triplet was digitized three times. For each point triplet, the apparent radius vector $\underline{\boldsymbol{R_i}}(r,a)$ was computed and compared in magnitude and orientation to the known radius vector $\underline{\boldsymbol{R_{ideal}}}$ on the digitization template. The error in radius magnitude, ε_m, was expressed as percentage of $\underline{\boldsymbol{R_{ideal}}}$. The error in radius orientation, ε_o, was calculated as the angle between $\underline{\boldsymbol{R_i}}(r,a)$ and $\underline{\boldsymbol{R_{ideal}}}$.

Application to rib geometry:
Points along the centerline of the periosteal surface of a human cadaveric rib (right, 9th) were digitized in 2-mm increments using the MicroScribe system. A sequence of n=19 radii vectors, $\underline{\boldsymbol{R_i}}$ were then computed.

RESULTS

ε_m decreased exponentially for increasing a values (fig. 2). On the arc with r=100mm, ε_m decreased from 6.3 ± 4.1% to 0.1 ± 0.1% for a=10° to 90°, respectively. For constant a, ε_m decreased exponentially for increasing r values. For a=10°, ε_m ranged from 76.2 ± 34.7% (r=10mm) to 2.5 ± 2.1% (r=200mm).

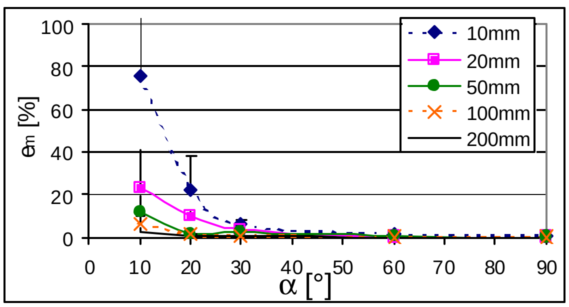

Figure 2: ε_m for varying a and r.

ε_o decreased exponentially for increasing a values (fig. 3). On the arc with r=100mm, ε_o decreased from 1.4 ± 0.8° to 0.1 ± 0.03° for a=10° to 90°, respectively. For constant a, ε_o decreased exponentially for increasing r values. For a=10°, ε_o ranged from 20.3 ± 7.1° (r=10mm) to 1.1 ± 0.8° (r=200mm).

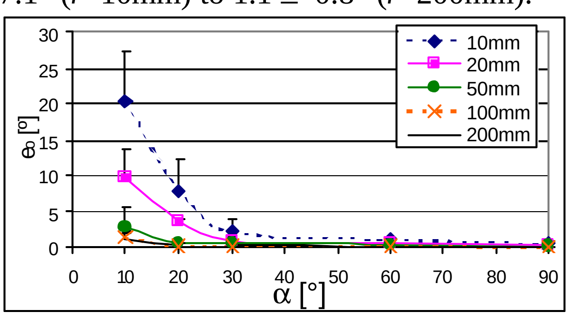

Figure 3: ε_o for varying a and r.

The spatial curvature profile of the human rib demonstrated the changes in magnitude and orientation of rib curvature in graphical and quantitative means in terms of apparent radii, $\underline{\boldsymbol{R_i}}$, vectors along the rib.

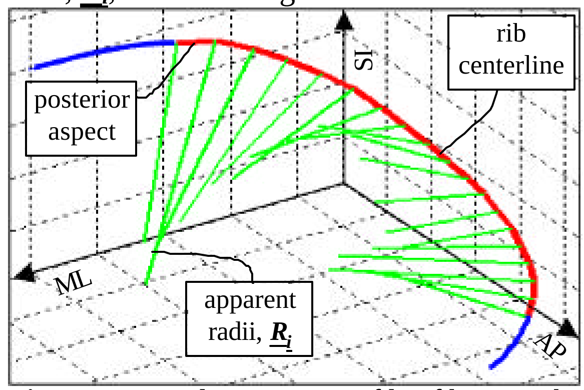

Figure 4: spatial curvature profile of human rib

DISCUSSION

Expressing the 3-D curvature of an anatomical trajectory in terms of a spatial curvature profile delivered an intuitive, quantitative, and complete characterization of its shape. Increasing the angle α over which point triplets are acquired will increase the accuracy of $\underline{\boldsymbol{R_i}}$, but will decrease the sensitivity by which local changes in curvature can be detected. The presented method constitutes a direct extension of curve fitting procedures on planar radiographs into 3-D space. In combination with the accuracy evaluation for source data of a common 3-D digitizing system, results of this study are pertinent to a host of biomechanical and clinical research applications, which seek to extract quantitative descriptors of spatial geometry.

REFERENCES

Eckhoff et al. (2001) *JBJS*, **83**-A:2 43-50
Spitzer et al. (1998) *Anat Rec.*, **253**:2:49-57
Hollister et al. (1993) *Clin Orthop.*, **290**:259-68
Testi et al.(2001) *Comp Meth Prog Biomed*, **65**:175-182, 2001.

AN INDEX FOR EXAMINING MOMENT INDUCED ACCELERATIONS

John H. Challis

Biomechanics Laboratory, Department of Kinesiology, The Pennsylvania State University,
University Park, PA, USA
E-mail: jhc10@psu.edu

INTRODUCTION

The moments generated by a muscle are capable of accelerating joints in addition to any it crosses (Zajac & Gordon, 1989). One way of examining this effect is to perform an induced acceleration analysis. Kepple et al. (1997) experimentally computed the resultant joint moments during human gait, and then computed the angular accelerations these moments induced. Zajac et al. (2003) also examined gait, but used a simulation model which estimated the forces produced by the muscles to generate gait, the angular accelerations induced by these muscle forces were computed.

The purpose of this study is to introduce a induced acceleration index (IAI) which permits quantification of the relative potential of accelerations produced at joints in the system to accelerate other joints in the kinematic chain.

THEORY

For a system of articulated rigid bodies the equations of motion can be written in matrix form, Craig (1989), as follows,

$$T = M(\theta).\ddot{\theta} + v(\theta,\dot{\theta}) + G(\theta) \qquad (1)$$

where T - vector of joint moments, $M(\theta)$- inertia matrix, $v(\theta,\dot{\theta})$- vector of centrifugal and Coriolis terms, $G(\theta)$- vector of gravity terms, $\theta,\dot{\theta},\ddot{\theta}$ - generalized coordinates and their first and second derivatives.

For an induced acceleration analysis accelerations caused by the centrifugal, Coriolis, and gravity terms are ignored as the focus is the accelerations caused by the moments acting at the joints. In T the moments are set to zero except for those at the joints considered active, and the acceleration computed at the other joints, the induced accelerations. For simplicity the joints will be classified as active for those considered to be generating a moment, and inactive for those not generating a moment but with the potential to be accelerated by the active joints. For this analysis equation 1 is rewritten as,

$$\begin{bmatrix} T \\ [0] \end{bmatrix} = [M].\begin{bmatrix} \ddot{\theta}_A \\ \ddot{\theta}_I \end{bmatrix} = \begin{bmatrix} M_{AA} & M_{IA} \\ M_{AI} & M_{II} \end{bmatrix}.\begin{bmatrix} \ddot{\theta}_A \\ \ddot{\theta}_I \end{bmatrix} \qquad (2)$$

where $\ddot{\boldsymbol{\theta}}_A$ - vector of accelerations at active joints, $\ddot{\boldsymbol{\theta}}_I$ - vector of accelerations induced at inactive joints, M_{AA} - sub-matrix relating active moments to active joints accelerations, the other sub-matrices are similarly named, T_A - vector of moments applied at active joints, $[0]$- vector of zeros. The induced accelerations at the inactive joints can be computed from,

$$M_{AI}.\ddot{\theta}_A + M_{II}.\ddot{\theta}_I = [0] \qquad (3)$$

Therefore,

$$\ddot{\theta}_I = -M_{II}^{-1}.M_{AI}.\ddot{\theta}_A \qquad (4)$$

so a matrix (M_{IAI}) can be defined which dictates the induced accelerations,

$$M_{IAI} = M_{II}^{-1}.M_{AI} \qquad (5)$$

This matrix is a function of the joint angles and segmental inertial properties only. The inertia matrix is symmetric and positive semi-definite, and the sub-matrices maintain these properties so are always invertible. If one joint only is active this matrix, M_{IAI} , is a scalar and a number can be produced which shows for a given system how the induced accelerations vary with joint angles. If more than one joint is considered active the condition number of the matrix can be used as the index (Lawson & Hanson, 1974).

METHOD

To illustrate the IAI the upper limb was examined for planar motion. For 11 subjects anthropometric data were collected. These data were used to model the upper arm, forearm, and hand as series of geometric solids. From this modeling the inertial properties of the segments were determined, and used to compute the IAI for the shoulder and elbow joints. The equations for the IAI for these joints depends on the elbow joint angle only, which was varied from full extension to full flexion.

RESULTS

The IAI for elbow demonstrates the shoulder can cause significant angular acceleration of the elbow joint (figure 1). In contrast elbow moments have relatively small influences on the shoulder angular acceleration. The ability to accelerate an adjacent joint is greatest when these joints are near to fully extended.

DISCUSSION

In human movement the ability of muscles to cause significant acceleration at joints they do not cross is exploited to a large extent (Zajac et al., 2003). The proposed

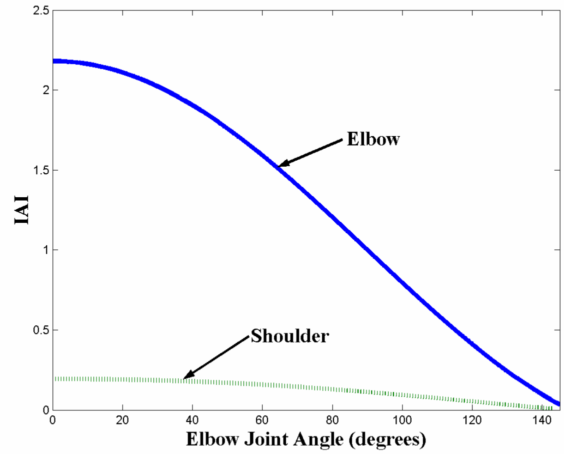

Figure 1: IAI for the shoulder and elbow joints.

induced acceleration index permits quantification of the relative potential of accelerations produced at joints in the system to accelerate other joints in the kinematic chain. The index can also be computed to examine how this coupling may change due to inertial changes to the system, for example if the inertial properties of a prosthetic are changed, or if a tool is held in the hand.

REFERENCES

Craig, J.J. (1989). *Introduction to Robotics: Mechanics and Control*. Addison-Wesley Publishing Company, Inc.

Kepple, T.M., et al. (1997). *Gait & Posture* **6,** 1-8.

Lawson, C.L., Hanson, R.J. (1974). *Solving Least Squares Problems*. Prentice-Hall, Inc.

Zajac, F.E., Gordon, M.E. (1989). *Exerc. Sport Sci. Rev*. **17,** 187-230.

Zajac, F.E., et al. (2003). *Gait & Posture* **17,** 1-17.

ACKNOWLEDGEMENTS

This research was in part supported by a grant from The Whitaker Foundation.

ESTIMATING THE SPECIFIC TENSION OF MUSCLE IN VIVO: A SIMULATION STUDY

Samantha L. Winter and John H. Challis

Biomechanics Laboratory, Department of Kinesiology, The Pennsylvania State University, University Park, PA, USA
E-mail: slw294@psu.edu

INTRODUCTION

The specific tension of muscle is an intrinsic property of muscle; it is defined as the maximum muscle force normalized with respect to muscle cross sectional area. Several authors have reported values for specific tension measured *in vivo*. These values vary widely, for example from 62 kPa (Ikai & Fukunaga, 1962) to 155 kPa (Maganaris et al., 2001). *In vivo* estimates rely on imaging procedures for the estimation of cross-sectional areas and external measures of joint moments.

There are a number of methodological problems with *in vivo* specific tension estimation including: not all muscles may be fully activated, co-activation of agonists and antagonists, variations in force output due to the force-length properties of muscle, and accounting for the moment arms of the muscles.

The purpose of this study is to demonstrate the variation in specific tension of the gastrocnemius and soleus with ankle and knee joint angles during plantar flexion using a model of the human triceps surae.

METHOD

When specific tension is estimated *in vivo* muscle cross-sectional areas and maximum muscle moments are measured. Then given the muscle moment arms the muscle forces can be estimated, assuming that the contributions of the muscles to the moment are proportional to their cross-sectional areas. In this study a simulation model was used to provide estimates of muscle moments at the ankle joint during isometric plantar flexions.

The force produced by the muscle model (F_M) can be described by,

$$F_M = q.F_{\max}.F_L$$

Where q is the active state of muscle, which was assumed to be 1, (i.e. maximal) for the simulated maximum isometric efforts. The maximum isometric force $(F_{\max})$ is based on the cross-sectional data presented in Out et al. (1996). The force-length properties (F_L) of the muscles are modeled as a parabolic function (Gallucci & Challis, 2002), with the optimum fiber length based on the number of sarcomeres comprising fibers in the muscles (Out et al., 1996).

The muscle model comprises a contractile component and a series elastic component for a muscle that crosses both the knee and the ankle joint (gastrocnemius) and a muscle that crosses only the ankle joint (soleus). The series elastic component is assumed to have a linear stress-strain curve, and an iterative process was used to estimate the muscle force for the soleus and gastrocnemius for a range of ankle and knee angles (Gallucci and Challis, 2002).

The maximum specific tension of these muscles was based on the data of

Lannergren and Westerblad (1987), who presented a value of 375 kPa based on an isolated single fiber preparation. Muscle specific tension was estimated for a range of ankle and knee angles, and compared to this criterion value.

RESULTS

The model moment-angle data in figure 1 is representative of experimental data (Sale et al., 1982). There were significant variations in specific tension with ankle and knee angle (figure 2). In this figure a 90° ankle angle and a 180° knee angle would represent the normal anatomical position.

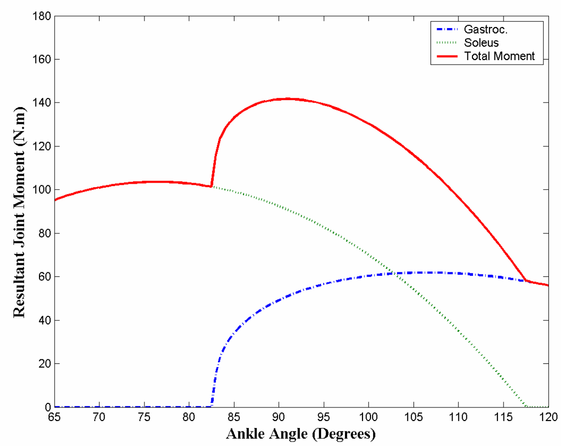

Figure 1: Variation in moment-ankle angle relationship with knee flexed to 90 degrees.

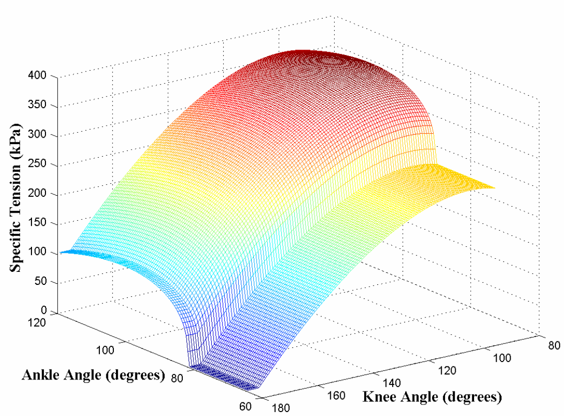

Figure 2: Relationship between angle and knee angles and specific tension.

DISCUSSION

The model demonstrates that the joint angles at which the moment measures are made strongly influence the estimated specific tension. This factor could easily account for the variations in specific tension measured *in vivo* that are reported in the literature. Further variability could be introduced *in vivo*: the model did not take into account sub-maximal effort on the part of subjects or inaccuracy in cross-sectional area, and moment arm measurements. The results presented here are specific to the model used, but represent a similar physiological system, and highlight the some of the problems of estimating specific tension *in vivo*.

REFERENCES

Gallucci, J.G., Challis, J.H. (2002). *J. App. Biom.*, **18**, 15-27

Ikai, M., Fukunaga, T. (1962). *Int. Z. Angew. Physiol.*, **26**, 26-32.

Lannergren, J., Westerblad, H. (1987). *J Physiol.*. **390**, 285-293.

Maganaris, C. N. et al. (2001). *J. Appl.Physiol.*, **90**, 865-872.

Out, L., et al. (1996). *J. Biomech. Eng.*, **118**, 17-25.

Sale, D.G., et al. (1982). *J. Appl. Physiol,*. **52**, 1636-42

ACKNOWLEDGEMENTS

This research was in part supported by a grant from The Whitaker Foundation.

DEVELOPMENT OF AN LS-DYNA FINITE ELEMENT MODEL OF THE CRANIO-CEREBRAL COMPLEX FOR UNDERSTANDING BIOMECHANICS OF TRAUMATIC BRAIN INJURY

Binu Oommen[1], David Nicholson[1], Ted Conway[1], Alexandra Ahlqvist[1], Gerald Bertetta[2]

[1] Department of Mechanical Engineering, University of Central Florida, Orlando, FL, USA
[2] Department of Physical Therapy, University of Central Florida, Orlando, FL, USA
E-mail: boommen@ucf.edu

INTRODUCTION

Traumatic Brain injury (TBI) is a leading cause of death and disability among children and young adults in United States, with an estimated 1.5 million Americans sustaining TBI (CDC, 1999). The cranio-cerebral complex is the most severely affected region during an automobile accident. This is because of transfer of high amount of kinetic energy to the upper extremity of the body during an accident. Pressure variations with respect to space and time cause brain tissue to deform beyond the level of recovery. Pressure gradients are produced as a result of linear acceleration involving both the absolute motion of the brain and its relative displacement with respect to the skull during a head impact (Goldsmith, 1992). Accurate modeling of the cranio-cerebral complex is necessary to predict the correct distributions of strains during an injury to the brain. Computational techniques such as the finite element method provide a means to study the tolerance level for the head during an impact.

This paper describes the development of a three-dimensional hexahedral LS-DYNA finite element model for the cranio-cerebral complex, based on fresh CT scans for the skull model and MRI images for the brain model. The components modeled to study the injury mechanism are brain, cerebrospinal fluid (CSF), dura and the skull. LS-DYNA is a finite element code with special features for modeling shock and impact.

METHODS

For modeling the three dimensional geometry of the skull and brain, horizontal slices of fresh CT scans and MRI data of a living Human Head, are used, at an incremental distance of 2 mm in the superior-inferior direction. The CT data are imported into MIMICS, a software used for the visualization and segmentation of CT and MRI data. The combination of manual segmentation and automatic discretization based on threshold values is used to create the regions of interest for the skull. The same methodology is adopted to create the outer contours of the brain using MRI data.

The geometric data of the skull and brain are exported as IGES files into I-DEAS, a general-purpose solid modeling and finite element software code. The data from MIMICS are used to create three-dimensional solid model of skull and brain in I-DEAS. The surface that forms as the interface between the skull and the brain is used to represent the cerebrospinal fluid (CSF). A constant thickness of 1.5 mm is assumed for the CSF. In real life the distance between the dura and brain is negligible, but for modeling purposes a realistic thickness for CSF needs to be assumed to avoid numerical instabilities during the solution phase.

The surface data of the brain, skull, CSF and dura are exported from I-DEAS as STL files into GeoMagic Studio, an imaging software which enables the surface data to be edited and smoothed. Non-uniform Rational B-Spline (NURBS) surfaces are created at the final stage and are imported in IGES format into TRUEGRID, a meshing software. The surfaces are used to create the hexahedral mesh for the brain and CSF and 4 noded shell elements for the dura.

RESULTS AND DISCUSSION

Figure 1 shows several views of the developed hexahedral Finite Element (FE) model for the brain, to be used for the impact analysis. The brain model consists of 19894 elements and 24096 nodes.

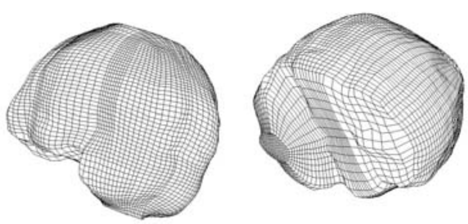

Figure 1: Finite Element Model of Brain

Figure 2 shows the FE model of CSF, which surrounds the brain and is primarily responsible in attenuating the shocks. The CSF consists of 4998 elements and 10876 nodes. Also modeled is the Dura matter using 4 noded shell elements. The Skull is modeled as hexahedral elements, which represent three layers of bone material, with the inner and outer layer representing the compact bone of skull and middle layer representing the diploe layer of the cranium (Kleiven, 2002).

The brain will be modeled as a homogeneous material using the Non-Linear

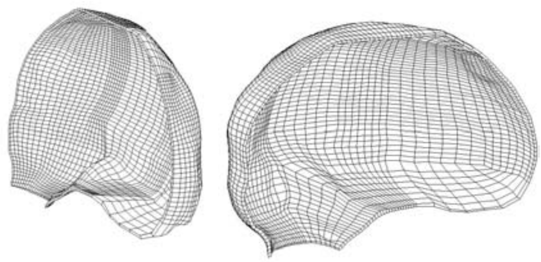

Figure 2: Finite Element Model of CSF

Viscoelastic constitutive model developed by Mendis et al (Mendis et al, 1992). A summary of the properties which used in the simulation, is shown in Table 1.

Table 1 Properties used for FE Modeling

Tissue	Modulus (GPa)	Density (Kg/m^3)	ν
Outer Table	E =15	2.00	0.22
Inner Table	E =15	2.00	0.22
Diploe	E =1	1.30	0.24
Brain	Hyperelastic	1.04	0.499
Dura	E =0.0315	1.13	0.45
CSF	K = 2.1	1.00	0.5

The explicit non-linear finite element code LS-DYNA is used to evaluate the shock and stress underlying brain damage mechanics. The broad goal of this research is to predict the extent of cognitive neurologic dysfunction and understand the overall role of impact conditions in the pathophysiology of TBI.

REFERENCES

Traumatic Brain Injury In the United States, *A report to Congress*, CDC, December 1999.

Goldsmith, W. (1972), *Biomechanics-Its foundation and Objectives*, Prentice-Hall, NJ

Kleiven, S., Von Holst, H. (2002), *J. of Biomechanics*, **35**, 153-160

Mendis et al (1995), *J. of Biomechanical Engineering*, **117,** 279-285

A RULE BASED APPROACH TO IMPROVE CARTILAGE THICKNESS MEASUREMENT REPRODUCIBILITY FROM KNEE MRI

Seungbum Koo[1], Apratim N. Dixit[1], Eugene J. Alexander[1] and Thomas P. Andriacchi[1,2,3]

[1] BioMotion Laboratory, Stanford University, Stanford, CA, USA
[2] Department of Orthopedic Surgery, Stanford University, Stanford, CA, USA
[3] VA Palo Alto RR&D Center, Palo Alto, CA, USA
E-mail: koosb@stanford.edu Web: biomotion.stanford.edu

INTRODUCTION

Osteoarthritis (OA) occurs in a substantial portion of the population over the age of fifty, yet, the causes of the disease and reasons for varying progression rates are not well understood. Quantitative imaging of articular cartilage is potentially a valuable tool to study both disease progression and treatment outcome. Imaging methods have been developed to reconstruct three-dimensional cartilage volumes (Stammberger, 1999, Lynch, 2000) that can be used to evaluate morphological changes associated with OA. However, the majority of these techniques require user intervention during the segmentation process, which can reduce the precision of the final measurement. A rule based approach to segmentation has the potential to improve the precision of the segmentation process. The purpose of this study was to test the inter- and intra-observer segmentation reproducibility and to determine if rule based segmentation can increase inter-observer reproducibility.

METHOD

Three knees were examined using an MRI sequence with a SPGR, 3DFT, fat-saturated sequence with a slice thickness of 1.5 mm and a pixel size of 0.55mm x 0.55 mm after IRB approval and informed consent. One knee was used for intra-observer reproducibility testing, two knees were used for inter-observer testing.

Intra-observer reproducibility was tested by two observers. Each observer segmented one MRI set five times on separate days. The first observer segmented the lateral and medial femoral cartilage, while the second observer segmented only the lateral side.

Inter-observer reproducibility was tested by four observers. One was a medical doctor, two were familiar with knee MRI, and one had no background in knee MRI and was trained for one hour prior to segmenting the knee MRI. The first test was conducted without any rules for selecting cartilage boundaries. The second test was conducted with a rule based protocol. In the second test, the testers were all trained in the rule based protocol as shown in Figure 1.

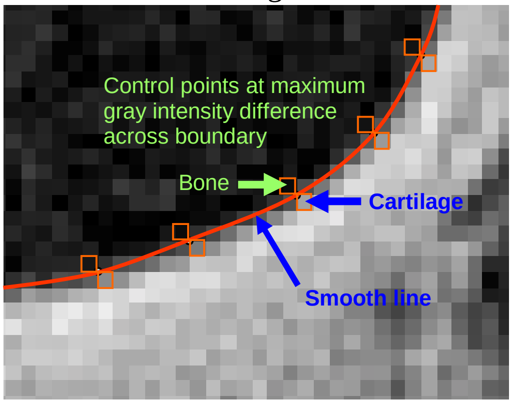

Figure 1: A rule base protocol to segment cartilage in MRI.

In the rule based protocol, it was assumed that the healthy femoral cartilage had a smooth surface and consistent gray intensity to prevent the users from putting a segmentation line on other soft-tissues. In the rule base protocol, techniques to put boundaries exactly in the middle of the bone and cartilage interface, and also in the middle of the cartilage and outer soft tissues, were provided. This was designed to increase the consistency in segmentation between observers. The same observers performed both tests on different MRI data sets.

The initial segmentation used a B-spline snake (Kass, 1987) which is a semi-automatic boundary detecting tool. After application of the initial snake technique, the segmentation is manually corrected.

Femoral cartilage was divided into six regions, three functional regions each on lateral and medial side, as shown in Figure 2.

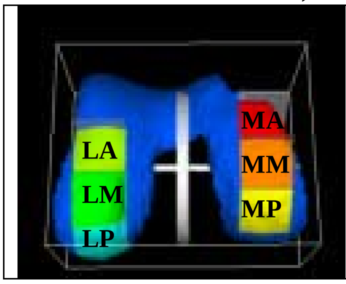

MA : Med. Ant.
MM: Med. Mid.
MP: Med. Post.
LA: Lat. Ant.
LM: Lat. Mid.
LP: Lat. Post.

Figure 2: Functional regions on cartilage used to measure average thickness.

The average thicknesses of the load bearing regions and the volumes of whole femoral cartilage were calculated for every trial. The coefficient of variance (CV) was used to measure the reproducibility and calculated by dividing the standard deviation with the mean value. This metric increases as there is larger variation in segmentation.

RESULTS AND DISCUSSION

The intra-observer test showed a very low CV as shown in Table 1. The average thickness of the load bearing regions had a CV of 2.1%, and CV of the volume was 1% for first observer and 2.9% and 1.5% respectively for the second observer. The Inter-observer test without the rule based protocol showed high a CV for average thickness and volume measurements, 8.3% and 5.7% respectively, as shown in Table 1. The high CV for the non rule based approach reflects each observer was using different rules. The second inter-observer test with the rule based protocol showed a decreased CV for the average thickness and volume measurements, 6.6% and 5.5%.

	Thickness	Volume
Intra-observer (first observer)	2.1 %	1 %
Intra-observer (second observer)	2.9 %	1.5 %
Inter-observer (w/o protocol)	8.3 %	7.5 %
Inter-observer (/w protocol)	6.6 %	5.5 %

Table 1: Coefficient of variance (CV) of intra- and inter-observer reproducibility test

CONCLUSION

Intra-observer tests were very reproducible based on the low CV in Table 1 indicating that individual observers are very consistent. But the inter-observer test without the rule based protocol shows that the results are highly observer-dependent. The inter-observer test with a rule based protocol showed that the rule based approach in segmentation can decrease variability between observers. Most cartilage reconstruction from MRI requires a segmentation step so a rule based approach can be important in building consistent cartilage models. Larger studies will be conducted by multiple observers in the future to more full examine the reproducibility of this rule based approach. This study does show that a rule based approach can increase the reproducibility of cartilage segmentation from MRI.

REFERENCES

Kass, M. et al. (1987). *Int. J. Computer Vision*, **1**, 321-331.
Lynch, J. et al (2000), *Proc. SPIE*, **3979**, 925-935.
Stammberger, T. et al. (1999). *Magn. Reson. Imaging*, **17**, 1033-1042.

EFFECT OF SPECIMEN/PLATEN FRICTION IN UNCONFINED COMPRESSION OF SOFT TISSUES IS NON-NEGLIGIBLE

John Z. Wu, Ren G. Dong, W. Paul Smutz, and Aaron W. Schopper
National Institute for Occupational Safety and Health, Morgantown, WV, USA
E-mail: jwu@cdc.gov(John Z. Wu)

INTRODUCTION

The mechanical characteristics of soft tissues in compression have traditionally been obtained via unconfined compressions. In such tests, frictionless specimen/platen contact in unconfined compression tests has usually been assumed in determining material properties of soft tissues via an analytical solution. Armstrong et al. (1984) and Brown and Singerman (1986) observed that their peak reaction forces in the unconfined stress-relaxation experiments of articular cartilage exceeded the corresponding maximum values predicted analytically. These authors suggested that this discrepancy might have resulted from the friction between the specimens and the platens. Spilker et al. (1990) analyzed the effects of the platen-specimen friction on the mechanical response of cartilage in unconfined compression using a finite element (FE) method. In their study, only two extreme cases in the unconfined compression were analyzed; the specimen either adhered to or was in frictionless contact with the end-platens. In addition, the cartilage was assumed to be linearly biphasic, and an infinitesimal deformation assumption was applied in their analysis.
The goal of the present study was to analyze the effect of the specimen-platen friction on the mechanical characteristics of soft tissues in unconfined compression tests via a FE model.

METHODS

The unconfined compression tests of soft tissues were simulated using a FE model. The tissue specimen was unconstrained laterally and squeezed between two steel platens. The bottom platen was fixed, while the upper platen was displaced downward at a constant speed. The friction coefficient (*f*) of the contact between the tissue specimen was assumed to be 0.0, 0.1, 0.3, or 0.5. The mechanical behavior of the soft tissue was considered to be nonlinear and viscoelastic (Wu et al., 2003).
Two numerical tests (A and B) were performed to investigate the effects of specimen-platen friction. Numerical tests were conducted on unconfined compression tests of pig brains (Test A) (Miller and Chinzei, 1997) and human calcaneal fat pads (Test B) (Miller-Young et al., 2002). All material parameters in the constitutive equation were obtained by fitting the nonlinear viscoelastic skin model (Wu et al., 2003) to the published experimental data (Miller and Chinzei, 1997; Miller-Young et al., 2002).

RESULTS AND DISCUSSION

The deformation pattern of flat specimen (Fig. 1A) is compared to that of slim specimen (Fig. 1B). Without friction, the tissue specimen is deformed in a uniform stress/strain and expands uniformly in the lateral direction with increasing axial nominal strain. When there is friction between the specimen and platens, the strain distribution in the specimen becomes non-uniform, and the specimen buckles externally in the middle of the lateral side (Fig. 1).
The effects of specimen/platen friction on the stress responses were analyzed quantitatively (Fig. 2). The unconfined compression tests were performed at loading strain rates of 0.64×10^{-5} and 35.0 1/s, for tests A and B, respectively. Our analysis indicated that the effect of the specimen/platen friction on the stress responses is independent of the loading rate (results not shown).
For "flat" specimen (Test A), the difference of the stress response increases dramatically with increasing friction coefficients. The

stress response in the experiment with a specimen/platen friction of 0.5 could be greater than that obtained in the idealized frictionless test condition by more than 100 %. For "slim" specimen (Test B), the effect of friction on the stress response does not increase significantly with increasing friction coefficients. Even when the specimen/platen friction reaches values as large as 0.5, differences in the stress response are limited to 60 % from that in idealized condition.

SUMMARY

The present study represents the first systematic analysis of the effects of specimen/platen friction on the deformation behaviors of soft tissues in unconfined compression tests. Our simulation results indicate that friction at the specimen/platen interface has significant effects on the measured stress response of soft tissues. Even under well-controlled test conditions, the specimen/platen friction may easily exceed 0.3; consequently, the tissue stress can be overestimated by over 50 %.

REFERENCES

Armstrong, C.G., W.M. Lai, and V.C. Mow (1984). An analysis of the unconfined compression of articular cartilage. J Biomech Eng. 106:165-73.

Brown, T.D. and R.J. Singerman (1986). Experimental determination of the linear biphasic constitutive coefficients of human fetal proximal femoral chondroepiphysis. J Biomech. 19:597-605.

Miller, K. and K. Chinzei (1997). Constitutive modelling of brain tissue: experiment and theory. J Biomech. 30:1115-21.

Miller-Young, J., N. Duncan, and G. Baroud (2002). Material properties of the human calcaneal fat pad in compression: experiment and theory. J Biomech. 35:1523-1532.

Spilker, R.L., J.K. Suh, and V.C. Mow (1990) Effects of friction on the unconfined compressive response of articular cartilage: a finite element analysis. J Biomech Eng. 112:138-46.

Wu, J.Z., R.G. Dong, W.P. Smutz, and A.W. Schopper (2003) Nonlinear and viscoelastic characteristics of skin under compression: experiment and analysis. Bio-Med Mater Eng. In Press.

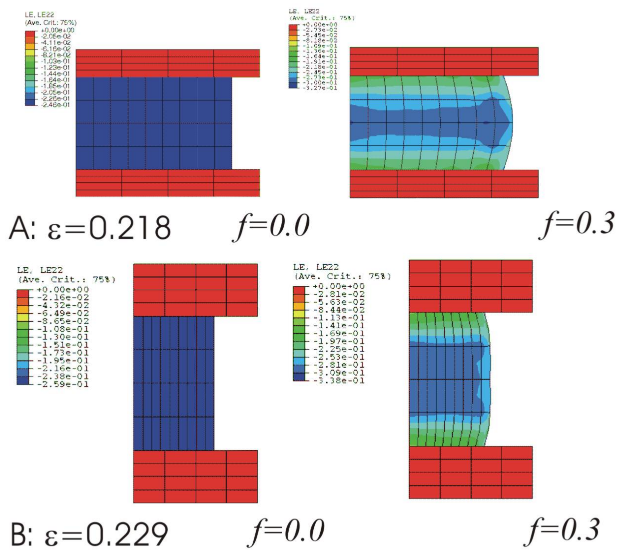

Figure 1: Simulated deformation behaviors of the soft tissue samples under unconfined compressions. **A:** Test A (pig brain sample; Miller and Chinzei, 1997), d/h=2.31. **B:** Test B (human calcaneal fat sample; Miller-Young et al., 2002), d/h=0.80. d/h = diameter/height

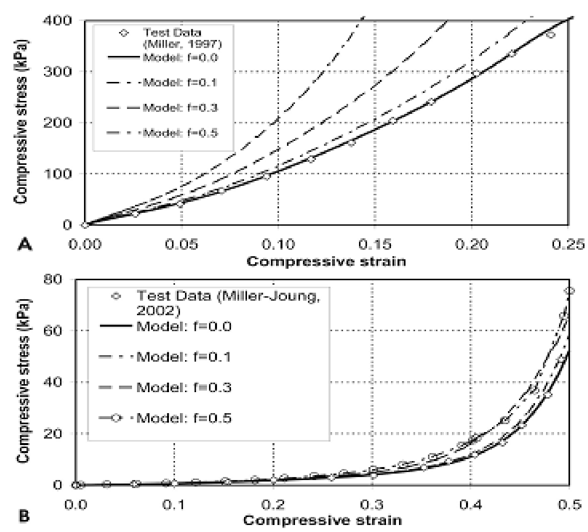

Figure 2: Simulated stress/strain relationships of soft tissue samples with the effect of friction. A: Test A; B: Test B.

THE STRAIN RATE SENSITIVITY OF THE PLANTAR SOFT TISSUE

William R. Ledoux [1,2,3], Joanna J. Blevins [1], Bruce J. Sangeorzan [1,2]

[1] RR&D Center for Excellence in Limb Loss Prevention and
Prosthetic Engineering, VA Puget Sound, Seattle, WA, USA
Departments of [2] Orthopaedics and Sports Medicine, and
[3] Mechanical Engineering, University of Washington, Seattle, WA, USA
Email: wrledoux@u.washington.edu Web: www.seattlerehabresearch.org

INTRODUCTION

Mechanical testing of the plantar soft tissue has primarily consisted of structural tests on the heel pad (Ker *et al.* 1989; Bennett and Ker 1990; Aerts *et al.* 1995; Kinoshita *et al.* 1996). Recently, one group has determined the material properties of the subcalcaneal tissue in compression (Miller-Young *et al.* 2002). However, there has been little research on rate sensitivity or on other locations, and often factors such as temperature, age, and diabetes are not taken into account. The purpose of this study was to control for temperature, age and diabetes while quantifying the material properties and strain rate sensitivity of the plantar soft tissue at six locations: the subcalcaneal, subhallucal, lateral submidfoot and the first, third and fifth submetatarsal.

METHODS

Specimens were obtained from 10 fresh frozen, nondiabetic, cadaveric feet (36 ± 8.7 years, 798 ± 131 N). The plantar soft tissue was dissected free, cut into 2 cm x 2 cm specimens, and the skin was removed. The tissue was placed between two platens in an environmental chamber in an ElectroForce 3400 materials testing machine (Figure 1). Hot moist air was circulated to keep the specimen at 35˚ C and near 100% humidity. The top platen was lowered until a force of 0.5 N was applied; the distance between the platens was the initial thickness. The target load (0.2 times body weight) was based on normative ground reaction force and contact area data (Ledoux and Hillstrom 2002), specimen cross sectional area and cadaveric weight. In load control, the specimen underwent ten 1 Hz sine waves from 10 N to the target load; this displacement was the target for subsequent tests. In displacement control, the tissue underwent a series of three triangle waves to the target displacement at frequencies of 10 Hz, 1 Hz, 0.1 Hz, 0.01 Hz and 0.005 Hz. The measured parameters included peak stress, modulus and energy loss. A linear mixed effects statistical model was used to determine the effect of location and frequency.

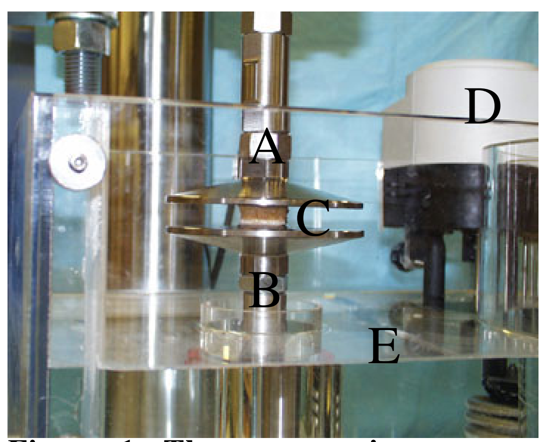

Figure 1: The compression apparatus. top (A) and bottom (B) platens, specimen (C), heater (D), environmental chamber (E).

RESULTS

There were significant differences in the stress between all locations, with the subcalcaneal having the highest values (Table 1). Thus, the modulus and energy loss were adjusted for force. The stress also increased significantly with each increase in frequency (Table 2 and Figure 2). The subcalcaneal location had a significantly larger modulus. Energy loss also varied significantly across locations, with the subcalcaneal location having the lowest, followed by the 5th submetatarsal, and then the remaining areas. Both stiffness and energy loss significantly increased at high frequencies of 1 and 10 Hz.

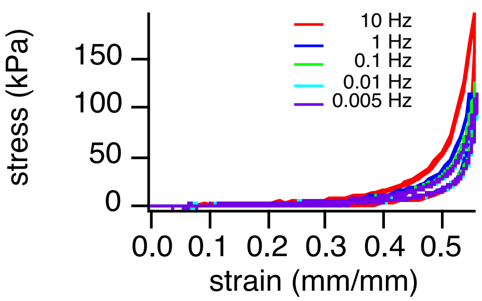

Figure 2: The strain sensitivity of one subcalcaneal specimen.

DISCUSSION

These data demonstrate that the material properties of the plantar soft tissue are dependent on specimen location and testing frequency. The subcalcaneal tissue had different material properties from the other locations, with a significantly greater modulus and less energy loss. The tissue was found to be rate sensitive, as the peak stress, modulus and energy loss were significantly greater for the 1 and 10 Hz tests. These results have important implications for computational foot models, as material models of the plantar soft tissue need to account for location and frequency.

ACKNOWLEDGEMENT

Department of Veterans Affairs project no. A2362R. We would like to thank Jane Shofer, M.S. for the statistical analysis.

REFERENCES

Aerts, P., et al. (1995). *Journal of Biomechanics* **28**(11): 1299-1308.

Bennett, M. B. and Ker, R. F. (1990). *Journal of Anatomy* **171**: 131-8.

Ker, R. F., et al. (1989). *Proc. Inst. Mech. Eng. <H>.* **203**(4): 191-6.

Kinoshita, H., et al. (1996). *Eur. J. of Appl. Physio. & Occ. Physio.* **73**(5): 404-9.

Ledoux, W. R. and Hillstrom, H. J. (2002). *Gait Posture* **15**(1): 1-9.

Miller-Young, J. E., et al. (2002). *Journal of Biomechanics* **35**(12): 1523-31.

Table 1: Stress, modulus and energy loss as a function of tissue location (all frequencies included).

location	subcalcaneal	subhallucal	lat submidfoot	submet1	submet3	submet5	p-value
stress (kPa)	92.75 ± 3[a]	79.25 ± 2.5[a]	75.75 ± 2.25[a]	72.5 ± 2[a]	74.75 ± 2.75[a]	76.5 ± 2[a]	<0.0001
modulus (MPa)	1.05 ± 0.05[a]	0.73 ± 0.03	0.66 ± 0.04	0.65 ± 0.03	0.69 ± 0.04	0.69 ± 0.03	<0.0001[b]
energy loss (J/J)	0.37 ± 0.01[a]	0.49 ± 0.01	0.46 ± 0.01	0.46 ± 0.02	0.50 ± 0.01	0.42 ± 0.01[a]	<0.0001[b]

[a] significantly different from others, [b] adjusted for force

Table 2: Stress, modulus and energy loss as a function of frequency (all locations included).

frequency (Hz)	0.005	0.01	0.1	1	10	p-value
stress (kPa)	61.5 ± 1.25[a]	65.75 ± 1.5[a]	74 ± 1.5[a]	76.75 ± 1.5[a]	117.5 ± 2.5[a]	<0.0001
modulus (MPa)	0.50 ± 0.02	0.54 ± 0.02	0.64 ± 0.02	0.77 ± 0.03[a]	1.32 ± 0.04[a]	<0.0001[b]
energy loss (J/J)	0.39 ± 0.01	0.37 ± 0.01	0.38 ± 0.01	0.46 ± 0.01[a]	0.63 ± 0.01[a]	<0.0001[b]

[a] significantly different from others, [b] adjusted for force

BIOMECHANICAL AND BIOCHEMICAL CHANGES WITHIN TENDON EXPLANTS IN RESPONSE TO COMPRESSIVE INJURY, FOLLOWED BY REHABILITATIVE LOADING AND NSAID TREATMENT

Flick, J [1,2]; Devkota, A [1,2]; Tsuzaki, M [1]; Banes, A [1,2]; Almekinders, L [1]; Weinhold, P [1,2]

[1] Dept. of Orthopaedics, University of North Carolina, Chapel Hill, NC, USA
[2] Dept. of Biomedical Engineering, University of North Carolina, Chapel Hill, NC, USA
Email: Paul_Weinhold@med.unc.edu

INTRODUCTION

The administration of non-steroidal anti-inflammatory drugs (NSAID's) is a common prescriptive therapy for acute and overuse tendon injuries. Although this class of drugs is known to inhibit the formation of inflammatory mediators, the primary therapeutic mechanisms have yet to be isolated. It has been hypothesized that NSAID's may also possess additional beneficial mechanisms beyond the suppression of systemic inflammatory responses. This study utilizes a cultured tendon explant model to characterize the biomechanical effects of NSAID administration, in conjunction with daily rehabilitative loading, following a controlled compressive midsubstance tissue injury.

METHODS

Flexor digitorum profundus tendon specimens were sterilely isolated from the middle digit of White Leghorn chicken feet (48 day old). All tendon explants were clamped in serpentine grips, cultured in standard medium supplemented with antibiotics, and allowed to recover for 48 hours following isolation and handling.

Immediately following this recovery period, all samples were subjected to a calibrated 20 lb. (~4.0 MPa), 10 second, midsubstance compressive crimping injury (Minns and Muckle, 1982). At this time point, the specimens were divided into two treatment groups; one receiving daily rehabilitory regimens (2 hrs., 0.25 - 3 MPa cyclical load at 0.5 Hz) and the other remaining in a continuous non-loaded condition. Tendons subjected to daily rehabilitation underwent treatment within a tissue loading device receiving waveforms produced via a pneumatic servo-valve.

The rehabilitation treatment group was further divided into two subsets (n=7/group): controls and Celebrex treated (5 μM). The non-loaded treatment group was divided into three subsets (n=7/group): controls, Celebrex treated (5 μM), and Piroxicam treated (5 μM). Media was supplemented with 2 μM arachidonic acid for 48 hrs. following crimping, with daily samples recovered during this time period being analyzed in duplicate for inflammatory mediators, prostaglandin E_2 and nitric oxide, by ELISA and colorimetric assays. Following this period of arachidonic acid supplementation, media was replaced every 48 hours.

Tissue culture strain measurements were performed using video dimensional analysis of midsubstance suture markers immediately following injury, on day 8, and on day 14. Histological specimens were divided into 10mm segments and incubated with MTT for 4 hours to evaluate cell viability by colorimetric assay. Mechanical properties of the tendon specimens were evaluated by tensile failure tests utilizing cryogrips in conjunction with video strain analysis of midsubstance suture markers.

RESULTS

In tests of nonviable tendons, the immediate effect of crimping was found to cause a significantly ($P<0.05$) higher strain at the failure load relative to uncrimped controls. Loaded Celebrex samples indicated a significantly lower strain at the immediate post-injury time point relative to the loaded controls. Collectively, all crimped samples revealed a significant increase in strain from the time point of injury through day 14. Non-loaded controls and Celebrex samples displayed significantly higher values in failure stress (Figure 1) and elastic modulus, relative to non-loaded Piroxicam specimens. MTT assays showed significantly higher cellular viability in compressed tissues relative to uninjured tissues, presumably due to cell proliferation. Specimens receiving NSAID treatment displayed significantly lower PGE_2 concentrations relative to controls.

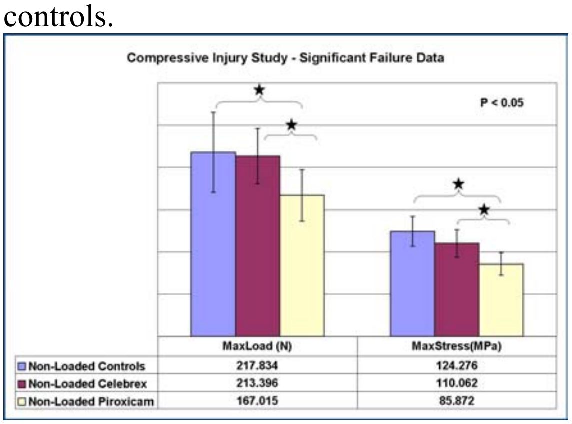

Figure 1: Average Failure Loads and Stresses Among Non-Loaded Treatment Groups

DISCUSSION

The administered compressive injury was found to have measurable effects in that a cellular response was observed via the MTT assay, as well as inducing mechanical changes within the tissue by increasing failure strains and decreasing the elastic modulus. Furthermore, independent of drug treatment, increases in midsubstance strain were found to occur across the measured time points, indicating possible mechanical alterations due to the crimping injury.

Biomechanical failure data revealed no effects due to the daily rehabilitation loading, in contrast to earlier studies indicating decreases in mechanical properties due to stress deprivation (Hannafin et al, 1995). Failure data did reveal adverse drug treatment effects due to the NSAID Piroxicam, and displayed no changes resulting from Celebrex treatments. This data contradicts previous in vivo ligament studies (Elder et al, 2001; Dahners et al, 1988), indicating a need for further studies characterizing the effects of NSAID treatments on soft tissue injuries.

NSAID treatment was effective, in both loaded and non-loaded conditions, in inhibiting the production of the inflammatory mediator PGE_2, as seen in the significant decreases in concentration immediately following the compression injury.

REFERENCES

Dahners, L.E. et al. (1988). *American Journal of Sports Medicine*. **16**(6):641-6.

Elder, C.L. et al. (2001). *American Journal of Sports Medicine.* **29**(6):801-5.

Hannafin, J.A. et al. (1995). *Journal of Orthopaedic Research.* **13**(6):907-14.

Minns, R.J., Muckle, D.S. (1982). *Journal of Biomechanics.* **15**(10):783-7.

ACKNOWLEDGEMENTS

Funding provided by the Whitaker Foundation and a UNC IRC award.

CHANGE OF CONSTITUTIVE MATERIAL PROPERTIES IN ORGANOTYPIC BRAIN CULTURES IN VITRO

Y.H. Chu[1], M.B. Sommers[1], W.E. Rochefort[2], J. Miesch[1], Z. Xiong[1], M. Bottlang[1]

[1]Legacy Clinical Research & Technology Center, Portland, OR, USA
[2]Department of Chemical Engineering, Oregon State University, OR, USA
E-mail: **mbottlan@lhs.org**

INTRODUCTION

Over the past decade, organotypic brain slice cultures emerged that allow preservation of the *in vivo* heterogeneous cell population and cytoarchitecture in a controlled culture environment over a prolonged period of time. Most recently, organotypic brain slice cultures have been employed for *in vitro* modeling of traumatic brain injury to study long term injury cascades and potential therapeutic interventions (Miesch et al., 2001, Morrison et al., 1998). Such injury models induced a mechanical insult to organotypic brain cultures to determine the consequential biological injury cascade. To characterize the mechanical insult on the tissue level, accurate knowledge of the viscoelastic constitutive properties of brain tissue is essential. While numerous studies have investigated material properties of fresh brain tissue, no study to date has determined the material properties of organotypic brain cultures, and their change over time *in vitro*.

In this study, we used a parallel plate measuring system (Bohline CS Rheometer, Cranbury, NJ) to investigate the shear material properties of organotypic mouse brain tissues up to six days in culture. We hypothesized that the material properties of organotypic mouse brain tissues change over time of culture.

METHODS

Organotypic Culture: Whole brains (excluding the cerebellum) were removed from 8 days old Swiss mice pups after sacrifice with the use of halothane. The brains were placed in sterile, chilled dissecting media and cut coronally to 400*mm* with a vibratome (Leica VT 1000). Each slice was then transferred on a cell culture membrane (Millipore, Millicell-CM) containing neuro-basal nutrient medium. Slices were maintained in an incubator at 37°C with a 5% CO_2 enriched atmosphere.

Oscillatory frequency sweep tests: For dynamic shear tests, 32 brain slices were randomly selected and tested at day 0 (n=6), and after 1 day (n=7), 2 days (n=8), 3 days (n=6), and 6 days (n=5) in culture. For each test, a brain slice sample was placed in between a 6mm diameter cylindrical spindle and a 50mm diameter base plate of the rheometer (Fig. 1). The Millipore substrate was securely attached to the based plate of the rheometer with super glue. All brain slices were subjected to a prescribed oscillatory frequency sweep between 0.1 Hz and 1 Hz, with a target strain of 1%. The strain applied was defined as the plate displacement at the edge of the sample divided by the sample height. The sample height was adjusted by the distance between the spindle and base plate to fit sample thickness. To prevent slip between the spindle and the brain slice surface, a sandpaper disk of 6mm diameter was glued to the spindle. During each test, a chamber encapsuled the brain culture to minimize potential for dehydration.

Three repeatability frequency sweep tests were performed on each specimen to ensure result consistency, but only measurements from each first test were used for result compilation. The complex shear modulus (G*) was calculated from $G^* = \sqrt{G'^2 + G''^2}$, where G′ represents the elastic modulus and G″ represents the viscous modulus. Statistical analyses were performed using a student's t-test with a 95% confidence interval.

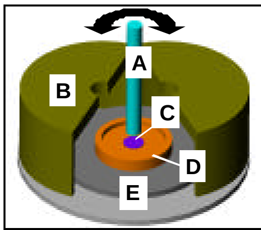

Fig.1: Experimental setup for frequency sweep tests.

RESULTS
Complex shear moduli (G*) from *day 0* through *day 6* in culture are depicted in Figure 2.

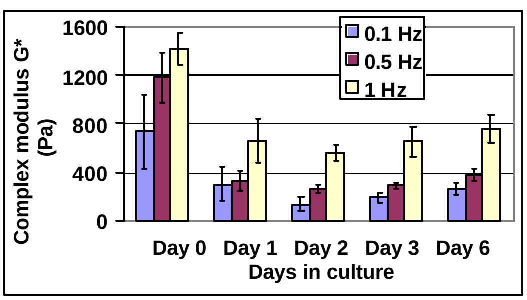

Fig. 2: Complex shear modulus (G*) of organotypic brain cultures at 0.1, 0.5 and 1 Hz frequency versus days in culture.

For all days in culture, brain samples became stiffer with increasing frequency. Acute brain slices (*day 0*) demonstrated the highest shear stiffness and the shear modulus reached 1416±150 Pa at a frequency of 1 Hz. At *day 1*, the average values of complex shear moduli at 0.1 Hz, 0.5 Hz and 1 Hz dropped significantly (p<0.005) by 61%. The least shear stiffness was observed at *day 2* in culture. From *day 3* to *day 6 in vitro*, the shear stiffness gradually increased. However, this increase was not statistically significant.

DISCUSSION
The observed complex shear moduli of acute mouse brain slices is comparable to that of porcine brain (608 Pa at 0.1 Hz, 715 Pa at 1 Hz, Brands et al., 1999) and bovine brain (2500 Pa at 0.1 Hz and 3162 Pa at 1 Hz, Bilston et al., 2001). Variations among shear modulus reports may be due to differences in specimen species, age, and interface conditions during shear testing.

This study documented for the first time changes in shear modulus over time *in vitro*. The decrease in shear modulus may be attributed, in part, to an increase in water content as brain slices observed maximum swelling at day two *in vitro* (Sommers et al., 2002).

REFERENCES
Bilston, L.E., et al. (2001). *Biorheology*, **38**, 335-345.
Brands, D.W., et al. (1999). *Proceedings of the Stapp Car Crash Conference*.
Miesch, J., et al., (2001). *Proceedings of 32th Neuroscience Society*.
Morrison, B., et al. (1998). *J. Neurotrauma*, **15**, 911-928.
Sommers, M.B, et al. (2002). *Proceedings of IV WCB*, #1165.

ACKNOWLEDGEMENTS
This study was supported by the NIH, NINDS R01 NS 42946.

EFFECT OF AGE ON DETECTING A LOSS OF BALANCE IN A SEATED WHOLE-BODY BALANCING TASK

Alaa A. Ahmed[1], M.S. and James Ashton-Miller[1,2], PhD.

Biomechanics Research Laboratory
Departments of [1]Biomedical and [2]Mechanical Engineering
University of Michigan, Ann Arbor, MI, U.S.A.[aaahmed@umich.edu]

INTRODUCTION

Falls in the elderly are associated with considerable morbidity and mortality. All unintentional falls are attributable to a 'loss of balance' (LOB). However, a precise definition of a LOB is lacking. It has earlier been proposed that a LOB is required for the central nervous system to trigger a compensatory response to prevent the ensuing fall (Ahmed, 2002). The LOB is posited as a *loss of effective control*, detectable, both internally and externally, as a control error signal anomaly (CEA).

A model-reference adaptive controller and failure-detection algorithm were used to represent central nervous system decision-making based on input and output signals obtained during a challenging whole-body planar balancing task. Control error was defined as the residual generated when the actual system output is compared to the predicted output of a simple model of the system. A CEA is hypothesized to occur when the error exceeds a threshold three standard deviations (3Σ) beyond the mean baseline signal. The quality of the signals involved is inherently dependent on the accuracy of the afferent signals which is known to decline with the neuropathic changes associated with aging. This deterioration could result in an inability to detect a CEA and respond appropriately.

Our goal was to (a) detect CEA in both healthy young (YA) and older (OA) subjects performing a challenging seated balancing task, and (b) compare the performance of the 3Σ detection algorithm in predicting any impending compensatory response. We tested the null hypothesis (H1) that there would be no age effect on the successful detection of CEA using a 3Σ threshold criterion on the controller error signal. The secondary (null) hypothesis (H2) was tested that age would not affect the performance of the 3Σ threshold in predicting the occurrence of any compensatory reaction by 100 ms.

METHODS

Twenty YA (10 females) and 20 OA (10 females) volunteers were tested (ages were 18-25 and 65-80 years, respectively). Seated subjects were asked to balance a custom high-backed chair for as long as possible over its rear legs, P (Fig. 1). Each performed five trials with eyes open. The ground reaction force under the dominant foot, which constituted the sole input to the system, was measured using a two-axis load cell. The position of three LEDs on the head and two on the chair were tracked using an Optotrak 3020 system. The error signal formed from the difference between the expected system output due to the given force input and the actual output, chair acceleration was calculated. CEA was defined to have occurred once the error signal crossed a

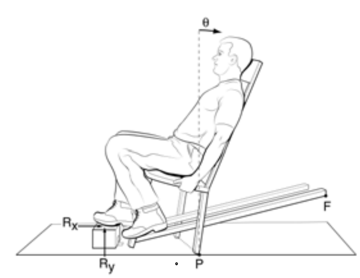

Figure 1: Experimental Setup

threshold level set at three standard deviations (3Σ) above the mean value in a 2-second-wide moving window, **b**, which lagged the current time instant, **t**, by 100 msec (Fig 2: The threshold calculation begins at '**Start**', initially using data in **a** as baseline data. Points 'F' on the chair must strike the ground within **c**, a two-second post-CEA interval.) The occurrence of a natural righting response, a large acceleration of the head in flexion (relative to the chair), was defined as a compensatory response, and evidence of CEA perception. Reaction time (RT) was defined as the latency of this response and could occur no earlier than 100 ms after CEA.

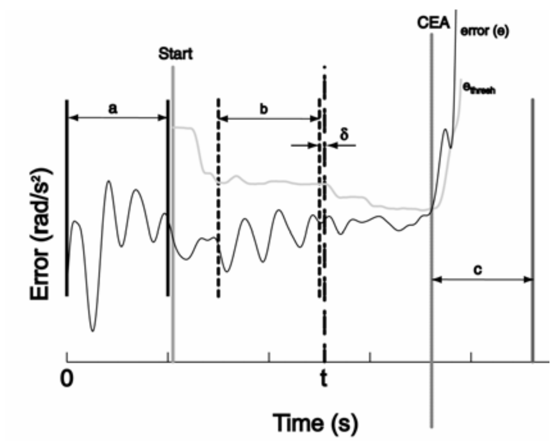

Figure 2: Sample time history of the control error signal (black) along with the moving threshold (gray) from one trial

RESULTS

The primary hypothesis (H1) was supported in that the 3Σ algorithm successfully detected CEA in 91.6% of the 99 YA trials and in 91.9% of the 95 OA trials (no significant age difference: χ^2: $p>0.995$). The secondary hypothesis was rejected in that a compensatory reaction was successfully predicted using the 3Σ algorithm in 92.7% of the 82 YA trials with reactions, and in 67.5% of 80 OA trials with reactions (age effect significant: χ^2: $p<0.005$). Applying a lower threshold (2Σ) to the H2 trials in which 3Σ was unsuccessful did successfully predict reactions in a further 2% of YA trials and 10% of OA trials. However, a sensitivity analysis in both YA and OA demonstrated that the optimal threshold level was 3Σ; lower levels resulted in more false positives, while higher levels resulted in delayed CEA detection times (Fig. 3).

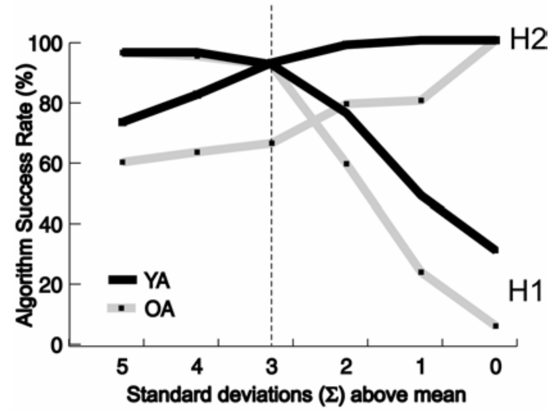

Figure 3: Sensitivity analysis results

DISCUSSION

The results suggest that a CEA is detectable by an external observer in both YA and OA. There are, however, age-related changes in a healthy subject's ability to internally detect a CEA. The 3Σ threshold did not predict a reaction in OA as accurately as in YA. Two OA in particular seemed to respond to a lower threshold, or perhaps another signal due to decreased sensor accuracy (manifested as a lower error threshold for CEA detection in OA), and/or a more conservative strategy. CEA detection provides a novel approach to understanding and quantifying the effect of aging on postural control.

REFERENCES

Ahmed, A.A., Ashton-Miller, J.A..(2002) WCB & Gait & Posture, *accepted*.

ACKNOWLEDGEMENTS

PHS Grants AG 08808, 10542 & 00116

MECHANICAL RESPONSE OF TENDON SUBSEQUENT TO RAMP LOADING TO VARYING STRAINS

Aaditya Devkota[1] and Paul Weinhold[1, 2]

[1]Department of Biomedical Engineering, University of North Carolina, Chapel Hill, NC
[2]Department of Orthopaedics, University of North Carolina, Chapel Hill, NC
E-mail: aaditya@unc.edu

INTRODUCTION

Acute strain and cumulative trauma injury to tendon are a growing clinical problem. While the pathophysiology following these injuries is complex, it is believed that loading of the tissue beyond specific mechanical limits (4% Strain) can cause irreversible damage to the extracellular matrix and the tendon's mechanical properties (Rigby et al., 1959). However, the methods used to characterize these limits may have adversely influenced the results. Recent studies applying subfailure stretches of 80% of the failure deformation to bone-ligament-bone complexes have shown little differences in mechanical properties (Panjabi et al., 1996).

In an effort to reexamine the results of classic tendon studies while utilizing current testing methodologies, the following study was carried out to characterize mechanical changes in avian flexor tendon with subfailure ramp loading to varying strain limits.

METHODS

Feet from unprocessed chickens were acquired from a local poultry processing plant, and the flexor *digitorum profundus* tendon was isolated from the middle toe. Tendons were clamped by liquid nitrogen fed cryo-clamps and mechanically loaded by a materials testing system. Two black sutures were stitched transversely, approximately 13mm apart at the longitudinal center of the tendon for midsubstance strain analysis. The suture displacement was monitored by a video strain analysis (VSA) system and the grip displacement was monitored by a LVDT within the actuator of the Instron. The load level, monitored by a 250lb load cell, and the two displacements were collected simultaneously at 60Hz for all mechanical tests.

Mechanical testing was preceded by first pretensioning the tendon at 0.25N, then preconditioning with 10 cycles of a 0.5% strain havertriangle waveform. The specimens were again pretensioned, then taken to a predetermined grip strain-level (1,2,3,4,6,8,10,12&14) by a 1% strain/sec ramp. A subsequent -1% strain/sec ramp brought the tendon back to the original rest state, where it was wrapped in saline soaked gauze and allowed to rest for 5 minutes to recover from any viscoelastic effects.

After the rest period, the specimens were again pretensioned to 0.25N, and then taken to failure by the same 1% strain/sec ramp. From the paired strain-limited and failure ramp loadings, differences in mechanical properties were evaluated based on suture marker (midsubstance) strains, grip strains and load level.

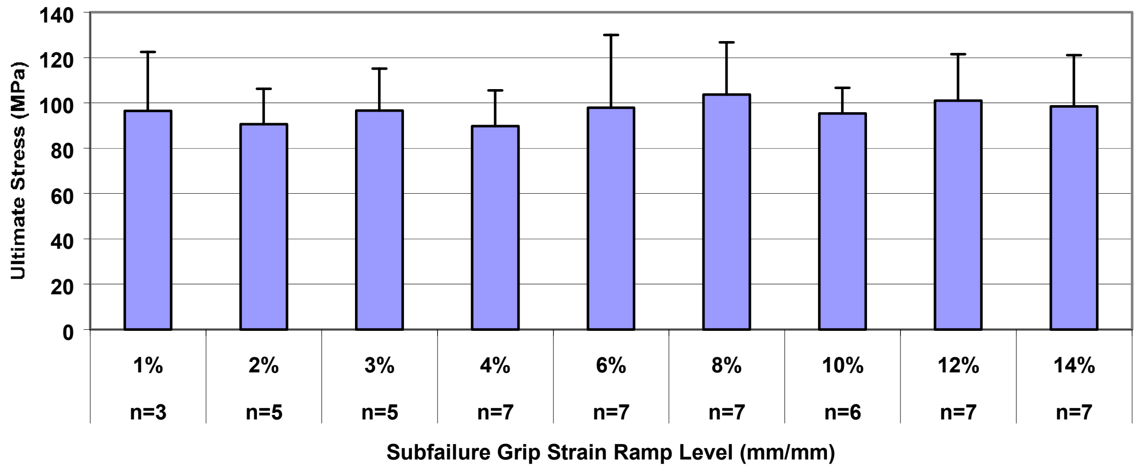

Figure 1: Average ultimate stress of tendons following various subfailure strain ramps.

RESULTS AND DISCUSSION

Varying the strain-limit of the subfailure ramp loading did not influence (P>0.05) the ultimate stress of the tendons (Fig 1). In addition, the elastic modulus based on midsubstance or grip strain was not found to differ (P>0.05) with the level of the strain-limit applied. The elastic modulus based on the midsubstance strain was found to be significantly stiffer then the modulus based on the grip strain (P<0.05). The midsubstance residual strain 5 minutes after each strain-limited subfailure ramp loading was not found to differ from zero (P>0.05), and this strain was not found to differ with the level of the strain-limit applied (P>0.05).

However, there was a minor change (P<0.001) in midsubstance strain between the strain-limited and failure ramp loadings when 10MPa of stress was applied, but this change in strain was not influenced by the level of the strain-limit applied. Neither the midsubstance and grip strain at failure (ultimate stress), nor the energy density at failure were influenced by the level of the strain-limit applied.

Overall averages at failure across all groups were 96.7 MPa for max stress, 16.4% for grip strain and 12.2% for midsubstance strain. One specimen did fail during the 14% ramp loading, and its data was discarded.

SUMMARY

In contrast to earlier reports, this study provides strong evidence that the basic tendon matrix displays an elastic response with minimal to no change in its mechanical properties when subjected to a single ramp loading to subfailure strain levels below 14%, and that tendon changes observed after such ramp loading *in vivo* may be due to the cellular response to load and not due to physical damage of the matrix.

REFERENCES

Rigby, B.J. et al. (1959). *J General Physiology*, **43**, 265-283.

Panjabi, M.M. et al. (1996). *J Orthop Res* , **14**, 216-22.

ACKNOWLEDGEMENTS

Whitaker Foundation Research Grant.

NON-LINEAR ELASTIC PARAMETERS OF BOVINE PATELLAR CARTILAGE

Ravi Namani [1], Narendra K. Simha [1] and Jack L. Lewis [2]

[1] Department of Mechanical Engineering, University of Miami, Coral Gables, FL 33124
[2] Department of Orthopaedic Surgery,University of Minnesota, Minneapolis, MN 55455

INTRODUCTION

Articular Cartilage (AC) primarily facilitates the load-transfer between bones in a joint. Mechanical properties such as elastic parameters characterize the load carrying ability of materials. Hence elastic parameters can be used to obtain a functional characterization of AC. Diseases that afflict AC, such as osteoarthritis, degrade its mechanical properties. Hence elastic parameters can be treated as markers to study the progression of disease processes. Currently, there is an extensive effort to develop engineered tissues. In addition to satisfying physiological requirements, replacement tissue will have to withstand in vivo mechanical loads in joints. Elastic parameters can be used to establish relevant functional criterion for engineered tissues. Also, tracking the evolution of elastic parameters during tissue growth will aid in the development of functional tissues.

From the viewpoint of elastic properties, AC can be treated as a composite consisting of collagen fibrils embedded in a hydrated proteoglycan gel. The volume fraction and orientation of fibrils have significant variation, and hence AC has highly inhomogeneous mechanical properties. Microindentation can measure elastic parameters with a spatial resolution of ~10μm. Moreover, it does not require standard-shape specimens and can use mm-size specimens. Recently, we have developed methods to extract nonlinear elastic parameters from microindentation data, where the load applied by the indenter is measured continuously as a function of the indenter displacement [Namani03, Simha03]. This paper will describe novel microindentation tests and methods to extract the nonlinear elastic parameters of bovine patellar cartilage.

METHODS

Microindentation tests were performed using a Nanoindenter XP (MTS Inc) and conical diamond indenters with an included angle of 57.5^0. Bovine patellar cartilage specimens had a thickness of ~2mm and surface area of ~1cm^2 . Five specimens from the same patella were used. Phosphate buffered saline (PBS) drops placed on the specimen surface ensured hydration. Loads (p) were increased at a constant rate until displacement (d) reached a maximum, held constant briefly and then unloaded.

The basis of the methods is to simulate the experiment and extract parameters by minimizing the difference between measured and predicted p-d curves. Cartilage is treated as an incompressible nonlinear hyperelastic Mooney-Rivlin (MR) material with a strain energy density:

$$W=C_1(I_1-3) + C_2(I_2-3) \qquad (1)$$

where I_1, I_2 are invariants of the Cauchy-Green Stretch tensor. The elastic material parameters C_1 and C_2 will be extracted using the following procedure:

1. Estimate (C_1+C_2).
Asymptotic results indicate that the p-d relation is quadratic [Beatty75, Costa99]. Based on this a series of simulations have established the following correlation

$(C_1+C_2)=(0.2092)\beta$ (at an *arbitrarily assumed* ratio $C_1/C_2 = 1/8$). Here the quadratic fit coefficient β ($mN/\mu m^2$) provides (C_1+C_2) in MPa. For an experimental p-d curve, β is obtained and (C_1+C_2) is estimated.

2. Optimal parameter ratio C_2/C_1.

Starting with a range $2 \leq C_1/C_2 \leq 80$, use Golden Section Search to obtain optimal parameter ratio by minimizing a non-dimensional area error ε.

3. Final Values of (C_1, C_2).

Estimate from step 1 and optimal ratio from step 2 provide three starting points for Simplex minimization. Final values obtained by minimizing area error ε.

RESULTS AND DISCUSSION

The measured force-displacement curves for two tests (from different specimens) are well described by quadratic curve fits (Figure 1a) for indentation depths that are about 10% of specimen thickness. The quadratic fit coefficient β ranges from 2.106 to 3.451 (10^3 X $mN/\mu m^2$) for tests 1-4 and 8 which were conducted at a load rate of 4mN/s (Table 1). There is a measurable difference at higher load rates, since the values range between 4.331 to 4.715 (10^3 X $mN/\mu m^2$) for tests 5 and 6 which were performed at 10 mN/s.

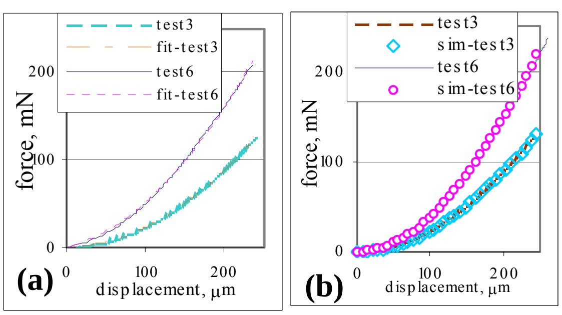

Figure 1. (a) Experimental (p-d) curves for Bovine AC compared with quadratic fits. **(b)** Comparison of simulated and experimental (p-d) curves for two tests.

The MR parameter C_1 and C_2 range from 0.362 to 0.588 Mpa and from 0.192 to 0.335 MPa for the 4mN/s tests; this quantifies variations due to material inhomogeneity. In contrast, the ranges are 0.725-0.755 Mpa and 0.391-0.449 Mpa for the 10mN/s tests. These higher values indicate the dependence of elastic parameters on the loading rate. In contrast, the parameter ratio C_1/C_2 has a remarkably small variation with an average value of 2.04. This suggests that there is a possibility of eliminating step 2 of the methods, which considerably simplifies parameter extraction. The sum C_1+C_2 is equal to one-fourth of the linear elastic Young's modulus. Table 1 shows that this is ~0.687Mpa at 4mN/s and increases to ~1.160 Mpa at 10mN/s.

Table 1. Fit coefficient and MR parameters

#	$\beta x10^3$	**C1**	**C2**	C_1+C_2	$\varepsilon x\ (10^{5})$
1	3.451	**0.588**	**0.335**	0.923	3.00
2	2.709	**0.474**	**0.192**	0.666	5.30
3	2.288	**0.387**	**0.235**	0.622	1.97
4	2.106	**0.362**	**0.225**	0.587	2.79
8	2.122	**0.371**	**0.221**	0.639	2.02
5	4.331	**0.725**	**0.391**	1.116	2.88
6	4.715	**0.755**	**0.449**	1.204	1.84

The area error was of the order of 10^{-5} (Table 1) indicating that the proposed methods are successful in extracting nonlinear elastic parameters. Also the negligible error suggests that the MR hyperelastic material model is a reasonable continuum description of AC, at least in the context of microindentation tests.

REFERENCES

Beatty, M. F. and Osmani, S. A. (1975). *Quart. J. Mech. Appl. Math.*, **28**, 47-62.

Costa, K. D. and Yin, F. C. P. (1999). *ASME J. Biomech. Engineering,* **121,** 462-471.

Namani, R. and Simha, N. K. (2003).submitted to *J. Biomech. Eng.*

Simha, N. K. et al. *Abstract submitted to ASME 2003 Bioengineering Conference*.

NONLINEAR ELASTIC PROPERTIES OF ARTICULAR CARTILAGE VIA MICROINDENTATION

N.K. Simha [1], N. Ravi [1] and J.L. Lewis [2]

[1] Department of Mechanical Engineering, University of Miami, Coral Gables, FL 33124
[2] Department of Orthopaedic Surgery, University of Minnesota, Minneapolis, MN 55455
nsimha@miami.edu

INTRODUCTION

Microindentation has significant advantages for characterizing the mechanical properties of Articular Cartilage (AC) and other soft tissues, e.g. it requires minimal specimen preparation, can use mm-size specimens and provides spatial distribution of properties with a resolution that is a hundred times more than that of conventional tension tests. This has two important consequences: First, the strong inhomogeneity of AC can be characterized. Second, specific regions near lesions can be examined, and thus the mechanical properties of osteoarthritic AC can be quantified.

In indentation tests, the indenter displacement is measured continuously as a function of the applied force and standard methods exist for extracting the linear elastic modulus [Doerner86, Oliver92]. However, due to the non-linear, large-deformation and time-dependent behavior of AC, existing methods cannot be extrapolated to AC and other soft tissues [Namani03]. Hence, this talk will propose new microindentation methods for extracting the nonlinear elastic properties of AC and other soft tissues.

METHODS

For brevity, this abstract will treat AC as a Mooney-Rivlin (MR) material. The talk will describe results for Polynomial and Exponential hyperelastic models as well. In simple terms, the proposed method extracts material parameters by comparing the force-displacement predictions from model based simulations with measurements from an indentation test. Simulations of the indentation of a ~2mm thick cartilage specimen lying on a rigid substrate are performed using ABAQUS (HKS, Inc.). All contact is frictionless. The indenter is rigid and conical with an apex angle of 67^o. Cartilage is treated as an incompressible nonlinear hyperelastic Mooney-Rivlin (MR) material with a strain energy density

$$W=C_1(I_1-3) + C_2(I_2-3) \qquad (1)$$

where I_1 and I_2 are invariants of the Cauchy-Green Stretch tensor. The MR material is characterized by the parameters C_1 and C_2. An asymptotic relation between the indentation force p and indenter displacement d is [Costa99]

$$p = (4/\pi)\, E \tan\alpha\, d^2 \qquad (2)$$

where α is the indenter half-angle and the linear elastic modulus $E=4(C_1+C_2)$. This is valid only for small indentation and is used here only to aid parameter extraction.

The steps for parameter extraction are:

1. <u>Establish a correlation $E=h(\beta)$</u>. Fix $C_2/C_1=1/8$. Based on (2), fit quadratics $p=\beta d^2$ to curves predicted by FEM. Relate known E to predicted β.
2. <u>Minimize using Golden Section Search</u>. For given p-d measurement, obtain fit coefficient β and an initial estimate $\hat{E}=h(\beta)$. Fix $(C_1+C_2)= \hat{E}/4$. Minimize a non-dimensional error ratio ε to get an optimal parameter ratio C_2/C_1.

3. Minimize using Simplex method. Using optimal ratio and Ê obtain three initial points. Minimize area error ε to obtain final values of (C_1, C_2).

Indentation measurements were performed under load control using a ~67° conical diamond tip and a Nanoindenter XP (MTS, Inc.). Bovine patellar cartilage specimens with thickness ~2mm, surface area ~1cm^2 were used and drops of PBS buffer solution were frequently placed on the cartilage to prevent drying. The load increased at a constant rate (4mN/s) until the displacement reached a maximum, held constant for 10s and then decreased at the constant rate.

RESULTS AND DISCUSSION

Although the predicted force-displacement curve is quadratic, it deviates from the asymptotic relation (2). The difference is small for d<0.1T (T is tissue thickness), but can be as large as 20% for d=~0.5T. This indicates the limitations of the asymptotic relation (2) for finite indentation depths. Using predicted p-d curves with fixed C_2/C_1=1/8 and quadratic fits for d<0.1T, the correlation h(β) was found to be E=1.048 β.

The parameter extraction method is validated by treating the p-d curve predicted by FEM for C_1=1.067 and C_2=0.133 MPa as a benchmark. In step 2, the fit-coefficient was β=4.58 x10^{-3} mN/μm^2, and the correlation E=1.048β resulted in C_1+C_2=1.2 MPa. Then starting with the range $2 \leq C_1/C_2 \leq 80$, the golden section search gave the optimum parameter ratio as C_1/C_2=7.99. In step 3, starting with the three initial points of (C_1, C_2) = (0.9603,0.1197), (0.9603,0.1463) and (1.1737,0.1463), the MR parameters were extracted as C_1=1.070 and C_2=0.131 MPa. The error between the benchmark and extracted values are 0.28% for C_1, 1.50% for C_2 and 0.08% for E.

Parameters were then extracted for five tests on bovine AC (Table 1). The average (st. dev.) values are C_1=0.496 (0.047), C_2=0.283 (0.013), E=3.115 (0.220) MPa and C_2/C_1=0.575 (0.045). These are preliminary; the talk will present more extensive data.

Table 1. Quadratic fit parameter β, estimates for C_1+C_2, Step 2 results for C_2/C_1, and final values of C_1 and C_2 and corresponding area error from step 3.

#	βx10^3 (mN/ μm^2)	C_1+C_2 MPa	C_1/C_2	**C_1 MPa**	**C_2 MPa**	ε x 10^5
2	3.451	0.722	2.036	**0.555**	**0.278**	1.97
3	3.217	0.673	2.036	**0.538**	**0.303**	4.54
4	2.708	0.566	2.036	**0.453**	**0.275**	3.55
5	2.841	0.594	2.036	**0.458**	**0.271**	5.05
8	2.928	0.613	2.036	**0.474**	**0.289**	3.75

SUMMARY

Methods to extracts material parameters by comparing the force-displacement predictions from model based simulations with measurements from an indentation test are proposed. These methods extracted the benchmark values with errors of less than 1.5%. This is well within the range of experimental errors, indicating that the proposed method can successfully extract nonlinear elastic parameters. Preliminary data provide the following results: bovine patellar cartilage can be modeled as a Mooney-Rivlin material with parameters C_1=0.496 and C_2=0.283 MPa.

REFERENCES

Doerner, M.F., Nix, W.D. (1986). *J. Mater. Res.*, **1**, 601-609.
Oliver, V.C., Pharr, G.M. (1992). *J. Mater. Res.,* **7**, 1564-1583.
Namani, R., Simha, N.K. (2003). submitted to *J. Biomech. Eng*.
Costa, K.D., Yin, F.C.P. (1999). *J. Biomech. Eng.,* **121,** 462-471.

BIOMECHANICAL EVALUATION OF A POLYMER SCAFFOLD FOR USE IN A TISSUE ENGINEERED NUCLEUS PULPOSUS

Huntzinger, JL[1]; Phares, TL[1]; Goel, VK[1]; Fournier, RL[1]; Kuroki, H[1]; McGowan, D[2]

[1]The University of Toledo, Toledo, OH 43606;
[2]Kearney Bone & Joint Clinic, Kearney, NB 68847
E-mail: vijay.goel@utoledo.edu

INTRODUCTION

One approach for an alternative method to fusion is to add cells to a tissue engineered biodegradable polymer scaffold to replace the degenerated nucleus pulposus. A three-dimensional polymer scaffold houses NP cells during extracellular matrix material (ECM) development and provides stability under spinal loads. This 3-D scaffold should restore destabilized spinal motion to the intact state following a discectomy. Scaffold strength is a function of the number of polymer casts and concentration and we hypothesize that the scaffold with higher concentration and number of casts will restore spinal motion.

METHODS

Scaffolds of four compositions were developed using a biodegradable polymer, poly(lactide-co-glycolide) (PLGA: 12%-18% concentrations, 2-3 casts)(Ma, 2001). Rabbit spines were tested intact, destabilized across L5-L6, and with scaffolds in L5-L6 using the Optotrak® motion measurement system (Grauer, 2000). Physiologically relevant loads were applied sequentially through pure moments in four steps from 0-0.15 Nm. The spines were tested in flexion (Flex), extension (Ext), right and left lateral bending (LB), and right and left axial rotation (AR) with LB and AR being an average of the right and left bending motions. The scaffolds were tested for 3-D load-displacement behavior in seven spines each for the 2 casts scaffolds and 6 spines each for the 3 casts scaffolds. The motion data of the scaffolds were compared with the intact spine and analyzed for significance using the student t-test.

RESULTS AND DISCUSSION

The average percent change in motion of L5 with respect to L6 following the implantation of the scaffold wrt the intact case for loads to 0.15 Nm is shown in Table 1. Figures 1-3 show the load displacement curves used to compute the % change seen in Table 1. The exterior longitudinal ligaments are cut to insert the scaffold and therefore extension data does not well represent conditions seen *in vivo*. The scaffold made of 18% PLGA and 3 casts best mimics the motion of the intact spine overall. In axial rotation, the scaffold motion, as indicated by percent change, is less than that of the intact spine. The 18%, 3 cast scaffolds perform better than the other scaffolds in all motion directions except left lateral bending. Based on the statistical analysis ($p<0.05$), motion values of the 18%, 3 cast scaffolds are not significantly different from the intact spine ($p=0.22$). This data suggests that with continued research, a tissue engineered scaffold can be developed that can restore flexibility to the spine following a discectomy.

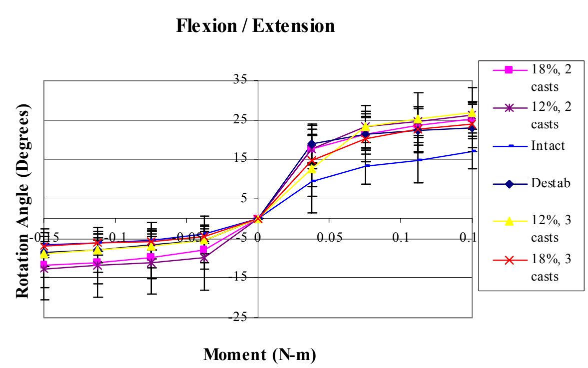

Figure 3: Average load displacement data for L5 wrt L6 in flexion/extension for 4 equal load steps to 0.15 Nm. Standard deviations are shown for each loading step.

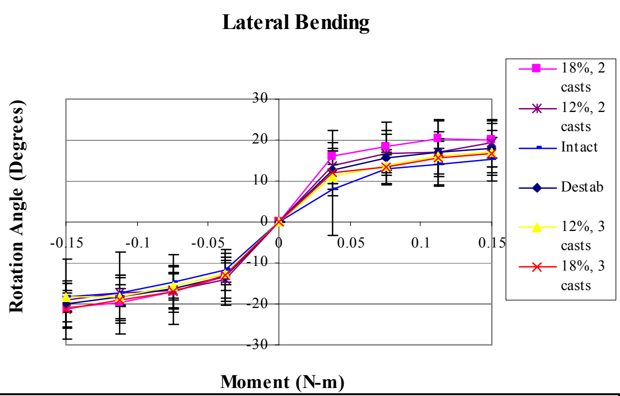

Figure 2: Average load displacement data for L5 wrt L6 in lateral banding for 4 equal load steps to 0.15 Nm. Standard deviations are shown for each loading step.

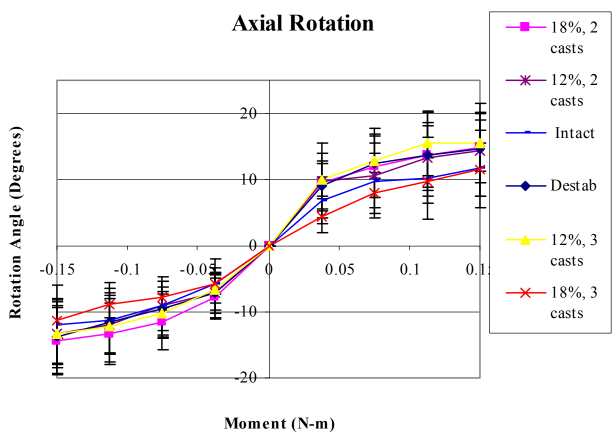

Figure 3: Average load displacement data for L5 wrt L6 in axial rotation for 4 equal load steps to 0.15 Nm. Standard deviations are shown for each loading step.

Table 1: Average % change from intact for L5 wrt L6 for 0.15Nn for each bending motion in the 3 planes of movement. A negative corresponds to an increase in motion from the intact case while a number corresponds to a decrease in motion from the intact case.

	Flex	Ext	LLB	RLB	LAR	RAR
Destabilized	-31.98	-34.67	-7.85	-17.51	-14.09	-24.86
12%, 2 casts	-91.01	-52.54	-2.42	-25.72	-10.02	-23.02
12%, 3 casts	-35.85	-55.85	0.72	-10.57	-11.62	-33.83
18%, 2 casts	-77.69	-47.46	-13.68	-31.64	-19.99	-27.43
18%, 3 casts	-4.68	-39.54	-16.38	-9.95	6.06	1.51

REFERENCES

Grauer et al. (2000). *European Spine Journal,* **9,** 250-255.
Ma et al. (2001). *Tissue Engineering,* **7,** 23-33.

CELL VIABILITY WITHIN A 3-D SCAFFOLD STRUCTURE

Rebecca Long[1], Janet Huntzinger[1], Tamara Phares[1], Hiroshi Kuroki[2], Vijay Goel. PhD[1], Ron Fournier, PhD[1], Ashok Biyani, M.D.[3], Dennis McGowan, M.D.[4]

[1]Spine Research Center, University of Toledo and Medical College of Ohio, Toledo, OH, USA
[2]Miyazaki Medical College, Miyazaki, Japan
[3]Department of Orthopedics, Medical College of Ohio, Toledo, OH, USA
[4]Kearney Bone and Joint Clinic, Kearney, NB, USA
E-mail: rlong@eng.utoledo.edu

INTRODUCTION

Intervertebral disc degeneration and associated spinal disorders are a leading source of morbidity, resulting in substantial pain and increased health care costs [Borenstein, 1992, Greenberg, 1996, MacDonald, 1997, Waddell, 1996, Webster, 1994]. Evidence suggests that disc degeneration can begin in the nucleus pulposus (NP). This is attributed to a decrease in proteoglycan content leading to the dehydration of the NP [Adler, 1983, Hirsch, 1953, Pearce, 1987, Silberberg, 1979]. The swelling pressure resulting from high concentrations of proteoglycans in the NP helps to maintain disc height and contributes to the load-bearing ability of the disc. A loss of proteoglycans may directly affect the biomechanical function of intervertebral discs [Butler, 1990, Urban, 1985, Urban, 1988]. It has been suggested that because the disc is the largest avascular tissue in the body, one reason for degeneration is a fall in transport of nutrients into the disc.

A biodegradable artificial disc has been developed using standard tissue engineering techniques, injecting NP cells into this scaffold, and culturing the cells in the scaffold. This bioartificial NP can then be inserted into the vertebrae to replace the degenerated disc [Huntzinger, 2003]. The growth of intervertebral disc cells possess an essential role in maintaining disc health because they make and maintain the extracellular matrix (ECM) [Bao, 1996]. Therefore, the viability of the cells within the scaffold is crucial for the success of a biodegradable artificial disc. The purpose of this study is to quantify the cell viability within the scaffold.

METHODS

Development of the Scaffold: Biodegradable polymer scaffolds were made according to the procedure outlined by Ma[30]. The scaffolds were developed using a pore size of 425 µm [Huntzinger, 2003].

Cell Isolation: Nucleus pulposus cells were isolated from the rabbit discs by enzymatic digestion from recently euthanized mature New Zealand white rabbit lumbar discs with testicular hyaluronidase (1600 u/ml, 60 minutes) followed by collagenase (0.25 mg/ml) and protease (0.1 mg/ml, 16 hours). Cells used for seeding the scaffolds are cultured using standard tissue culture techniques in Dulbecco modified Eagle medium (DMEM) with 10% fetal bovine serum (FBS).

Glucose Assay: Cell viability was monitored through the use of glucose assays (Sigma-Aldrich Corp.). In a 12-well culture plate, NP seeded scaffolds, and NP cells, both in triplicate, were placed in DMEM (10% FBS, 1μl antibiotics) and cultured for 1 week. The media was changed at 3 days.

Daily samples were taken of the culture media and centrifuged to extract the supernatant. A standard curve is formulated utilizing a 0.2% glucose stock solution. The glucose assay is performed in triplicate and analyzed using the media samples as reference points.

RESULTS AND DISCUSSION

Figure 1 summarizes the data collected from the glucose assays.

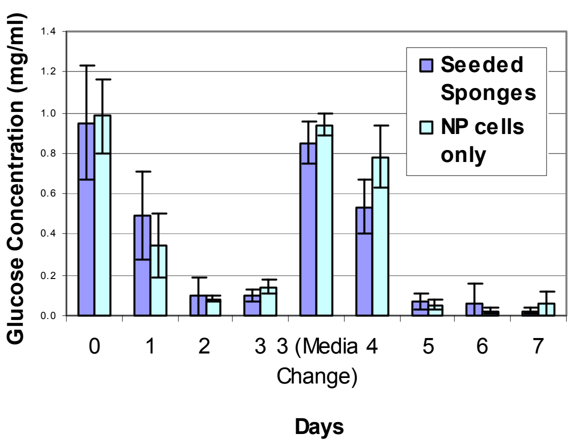

Figure 1: Glucose consumption

The theory behind the glucose assay is that if the cells are alive, they will consume the glucose at a steady rate both in standard culture and within the scaffolds. Due to the glucose consumption in the seeded scaffolds, it is concluded that the NP cells are viable in the scaffolds. This data suggests that the biodegradable scaffold will provide an environment that will maintain disc health.

REFERENCES

Adler, J.H., Schoenbaum, M. (1983). *Vet Pathology*, **20**, 13-22.

Bao Q.B. et al. (1996) *Biomaterials*, **17**, 1157.

Borenstein, D. (1992) *Curr. Opin. Rheumatol*., **4**, 226-232.

Butler, D., et al. (1990) *Spine*, **15**, 111-113.

Greenberg, S.N., Bello, R.P. (1996) *J. Orthop. Sports.* Phys. Ther., **24**,37-45.

Hirsch, C. Schajowica, F. (1953) *Acta Orthop. Scand.*, **22**, 184-231.

Horner, Heather A., Urban, Jill P.G. (2001) *Spine*, **26**, 2543-2549.

Huntzinger, Janet., et al (2003) *49th ORS Conference Proceedings,* New Orleans, LA.

MacDonald, M.J., et al. (1997) *J. Occup. Environme. Med.*, **39**, 35-43.

Maroudas, A., et al. (1975) *J Anat*, **120(1)**, 113-30.

Pearce, R.H. et al. (1987) *J. Orthop. Res.*, **5**, 198-205.

Silberberg, R. et al. (1979) *Arch. Pathol. Lab. Med.*, **103**, 231-235.

Urban, J.P., Mullin, J.F. (1985) *Biorheology*, **22**, 145-157.

Urban, J.P., Mullin, J.F. (1988) *Spine*, **13**,179-187.

Waddell, G. (1996) *Spine*, **21**, 2820-2825.

Webster, B.S., Snook, S.H. (1994) *Spine*, **19**:1111-1115.

EXERCISE CAN REVERSE THE PHENOTYPE OF BIGLYCAN-DEFICIENT MICE

Wallace JM[1]; Rajachar RM[1], Chen X[2]; Shi S[2]; Allen MR[3]; Bloomfield SA[3]; Robey PG[2]; Young MF[2]; Kohn DH[1,4]

[1] Department of Biomedical Engineering, University of Michigan
[2] National Institute of Dental and Craniofacial Research/National Institutes of Health
[3] Department of Health and Kinesiology, Texas A&M University
[4] Department of Biologic and Materials Sciences, University of Michigan
E-mail: dhkohn@umich.edu

INTRODUCTION

The strength and toughness of bone are derived from the organized mineralization of the organic constituents of the ECM. Small leucine-rich proteoglycans (SLRPs) help regulate ECM organization and mineralization by interacting with other matrix macromolecules and regulating their function (Boskey, et al., 1997). Biglycan (Bgn) is a SLRP that is highly expressed in bone and involved in the regulation of postnatal skeletal growth (Bianco, et al., 1990). Bgn knockout mice exhibit a lower peak bone mass than wild type mice (Xu, et al., 1998) and, at the cellular-level, osteoblasts and bone marrow stromal cells are altered, suggesting that the reduction in bone mass is due to a deficiency in bone formation (Chen, et al., 2002). Since mechanical loading is recognized as a viable strategy to maintain peak bone mass and structural integrity, we hypothesized that mechanical stimulation could rescue the phenotype of these knock-outs. In this study, the effects of exercise on the geometric and mechanical properties of bones from Bgn knockouts were compared to the corresponding wild types.

METHODS

Bgn-deficient and wild type male mice were bred on a C57BL6/129 background as previously described (Xu, et al., 1998). Forty mice (2 genotypes x 2 exercise groups x 10 mice/group) were housed in standard cages and given unrestricted access to food, water and cage activity until skeletally mature (NIDCR animal approval protocol # NIDCR 001-151). At 2 months, mice were randomly assigned to exercise or control groups. Exercise consisted of running at 10 m/min on a treadmill at a 5° incline, 30 min/day for 21 days. Mice were sacrificed on day 24. Femora and tibiae were harvested, stripped of soft tissue and stored in a Ca-buffer. QCT analysis was performed on right bones. Left bones were tested to failure in 4 point bending in a custom-designed, solenoid driven apparatus at a rate of 0.01 mm/sec. Femora were tested in the AP direction (posterior surface in compression) and tibiae were tested in the ML direction (lateral surface in compression). Load and deflection were recorded, from which strength, energy, stiffness and deformation properties were derived. After fracture, bones were sectioned at the fracture site. Geometric parameters were determined using an inverted light microscope and digital analysis software (Nikon Eclipse 300T, Image Pro-Plus v4.1, Matlab v5.3). Statistical analyses were performed using 2-way ANOVA.

RESULTS AND DISCUSSION

Biglycan-deficient males ($Bgn^{-/0}$) exhibited phenotypic changes in their tibiae (Table I) with differences in the femora being less.

No femoral geometric properties were affected, though yield energy (p=0.033) and yield stress (p=0.026) were significantly decreased. Bgn$^{-/0}$ tibial ML width (p=0.007) and MOI (p=0.031) were significantly increased. These geometric changes were accompanied by significant decreases in elastic deformation (p=0.038), yield energy (p=0.044) and yield stress (p=0.048). These results imply that Bgn$^{-/0}$ mice have more tissue present, and this tissue is more isotropically distributed. However, because of the Bgn deficiency, the tissue is of lower quality, causing the bone to have lower strength and energy dissipation. This mechanical phenotype may be due to an upregulation of other non-collagenous proteins responsible for promoting matrix mineralization, causing over-mineralization and leading to a weaker, more brittle bone. This hypothesis is supported by QCT data showing a significant increase in BMC in the Bgn$^{-/0}$ tibial diaphyses. Exercise increased Bgn$^{-/0}$ tibial cortical thickness (p=0.002), and this geometric change was accompanied by increases in yield force (p=0.0048), post-yield displacement (p=0.044), total displacement (p=0.045), and ultimate energy (p=0.045) with marginal increases in ultimate force and yield energy. These geometric and mechanical properties were equal to or greater than the wild type control values, and the percent increase in these properties due to exercise was at least as large in knock outs as in wild types. Therefore, our data indicates that exercise was able to rescue the skeletal phenotype of Bgn knockouts.

REFERENCES

Bianco, et al. (1990). *J Histochem Cytochem*, **38**, 1549-1563.

Boskey, et al. (1997). *Calcif Tissue Int*, **61**, 298-305.

Chen, et al. (2002). *J Bone Min Res*, **17**, 331-340.

Xu, et al. (1998). *Nat Genetics*, **20**, 78-82.

ACKNOWLEDGEMENTS

NIH IPA Award, Tina Kilts for help with mouse genotyping

Table 1: Tibiae Geometric and Mechanical Properties (mean ± SEM)

Property	Bgn$^{+/0}$ Control	Bgn$^{+/0}$ Run	Bgn$^{-/0}$ Control	Bgn$^{-/0}$ Run
C/S Area (mm^2)	0.519 ± 0.042	0.633 ± 0.033	0.616 ± 0.031[b]	0.649 ± 0.024
Cortical Thickness (mm)	0.197 ± 0.012	0.210 ± 0.013	**0.197 ± 0.007**	**0.225 ± 0.005**[c]
ML Width (mm)	**0.899 ± 0.054**	1.043 ± 0.344	**1.093 ± 0.038**[a]	1.072 ± 0.034
AP/ML	1.232 ± 0.030	1.195 ± 0.320	1.140 ± 0.030[b]	1.135 ± 0.019
Section MOI (mm^4)	**0.037 ± 0.008**	0.058 ± 0.006	**0.061 ± 0.006**[a]	0.063 ± 0.006
Yield Force (N)	23.134 ± 2.808	15.963 ± 1.011	**17.310 ± 2.155**	**23.303 ± 1.919**[c]
Ult. Force (N)	24.343 ± 2.639	22.448 ± 2.753	23.169 ± 2.092	28.489 ± 2.051[d]
δ (elastic) (mm)	**0.075 ± 0.136**	0.046 ± 0.005	**0.049 ± 0.004**[a]	0.058 ± 0.005
δ (plastic) (mm)	0.024 ± 0.008	0.086 ± 0.028	**0.019 ± 0.004**	**0.036 ± 0.007**[c]
δ (total) (mm)	0.093 ± 0.158	0.115 ± 0.024	**0.071 ± 0.005**	**0.099 ± 0.107**[c]
Yield Energy (mJ)	**1.176 ± 0.350**	0.501 ± 0.072	**0.578 ± 0.092**[a]	0.884 ± 0.124[d]
Ult Energy (mJ)	1.584 ± 0.438	1.877 ± 0.461	**1.148 ± 0.146**	**1.807 ± 0.260**[c]
Yield Stress (N/mm^2)	**150.54 ± 33.34**	85.02 ± 8.63	**90.39 ± 11.63**[a]	118.12 ± 11.51

[a]Significant effect of genotype (**Bold**, p<0.05)
[b]Marginal effect of genotype (0.05<p<0.10)
[c]Significant effect of exercise (**Bold**, p<0.05)
[d]Marginal effect of exercise (0.05<p<0.10)

STOCHASTIC ANALYSIS OF ANATOMICAL DATA SUGGESTS THREE CHARACTERISTIC KINEMATIC DESCRIPTIONS OF THE THUMB

Veronica J. Santos [1] and Francisco J. Valero-Cuevas [1,2]

[1] Neuromuscular Biomechanics Laboratory, Cornell University, Ithaca, NY, U.S.A.
[2] The Hospital for Special Surgery, New York, NY, U.S.A.
E-mail: vjl4@cornell.edu Web: www.mae.cornell.edu/nmbl

INTRODUCTION

A realistic biomechanical model of the thumb would be instrumental to the study of the functional consequences of orthopedic and neurological diseases, and treatment outcomes. Our modeling work has shown, however, that assuming a kinematic description of the thumb with five orthogonal and intersecting axes of rotation at the carpometacarpal (CMC) and metacarpophalangeal (MP) joints cannot predict realistic thumbtip forces (Valero-Cuevas et al., In press).

An alternative kinematic description proposes five axes of rotation that need not be orthogonal or intersecting (Giurintano et al., 1995). This kinematic description, however, is not in a format amenable for use in robotics-based models. Moreover, it is not known if the large variability in the anatomical data used to derive this description (Hollister et al., 1992, 1995) is informative of kinematic differences among individual thumbs. That is, the mean axis location and orientation values may not be representative of any one thumb.

The objective of this work was twofold: to describe this alternative kinematic description in Denavit-Hartenberg (DH) standard robotics notation for use in robotics-based models; and to establish the effects of the reported anatomical variability on this kinematic description of the thumb.

METHODS

We calculated the four DH parameters (θ, d, a, and α describing the location and orientation of the axes of rotation) from the 2D projections of the axes reported by Hollister et al. (1992, 1995) by interpreting them as rotations and translations in 3D.

We explored the effects of the reported anatomical variability of these axes using Monte Carlo (MC) simulations. To determine the DH parameters, at each of 2,700 MC iterations, a set of anatomical parameters was randomly selected from uniform distributions bounded by reported mean value ± one standard deviation (Valero-Cuevas et al., In press; Hollister et al., 1992, 1995).

RESULTS AND DISCUSSION

The MC simulations reveal that the reported anatomical variability results in three characteristic descriptions of thumb kinematics. In 64.4% of the simulations (sets 1 and 2), the MP FE axis was distal to the MP AA axis. In all others (set 3), this order was reversed. Sets 1 and 2 differed in that the MP FE axis was slightly dorsal to the IP FE axis in set 1 (30.6% of cases) and slightly palmar in set 2 (33.8% of cases). Figure 1 shows a sample case from set 1.

The change in the relative location between the MP FE and AA axes among iterations is not surprising given the overlapping distributions of reported MP axis parameters

(Hollister et al., 1995).

Monte Carlo simulations are affected by the number, distribution-type, range, and covariance of the variables to be randomly drawn. The large variability in the DH parameters (Table 1) may reflect the relatively large variability in the reported anatomical data (Hollister et al., 1992, 1995) and/or the fact that we did not set any parameter covariances. Not including these currently unknown covariances likely produced some unrealistic parameter combinations.

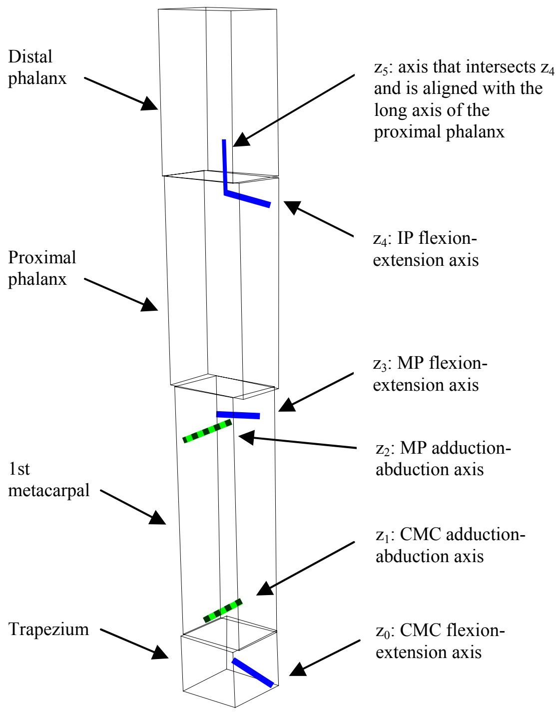

Figure 1. Representative instantiation of the five axes of rotation, depicted by the bold lines, for set 1. (Not to scale)

This work provides the Denavit-Hartenberg notation for a kinematic description of the thumb with five axes of rotation that need not be orthogonal or intersecting. We are currently investigating the biomechanical consequences of the three sets of kinematic descriptions found. We now pose the question, Are multiple types of kinematic descriptions necessary to faithfully account for the natural anatomical variability of the thumb?

REFERENCES

Giurintano, D. J. et al. (1995). *Medical Engineering and Physics*, **17**, 297-303.

Hollister, A. M. et al. (1992). *Journal of Orthopaedic Research*, **10**, 454-460.

Hollister, A. M. et al. (1995). *Clinical Orthopaedics and Related Research*, **320**, 188-193.

Valero-Cuevas, F. J. et al. (In press). *Journal of Biomechanics*.

ACKNOWLEDGMENTS

This material is based upon work supported under a National Science Foundation Graduate Research Fellowship.

Table 1. The three characteristic sets of DH parameters, mean (std). For parameters that distinguish the sets, three sets of values are listed, one per line (sets 1,2,&3 in Roman, *italics*, and **bold**, respectively). The θ values are not specified because they are rotational degrees of freedom.

	Frame #				
DH param	1	2	3	4	5
a (cm)	1.21 (0.26)	3.22 (0.74)	0.38 (0.27)	0.11 (0.08) *0.11 (0.08)* **3.96 (0.37)**	0 (0)
d (cm)	-0.25 (0.26)	3.31 (2.20) *3.31 (2.20)* **0.71 (0.77)**	-3.02 (2.09) *-3.02 (2.09)* **0.62 (0.36)**	14.54 (3.79) *14.54 (3.79)* **-0.92 (0.41)**	-14.35 (3.87) *-14.35 (3.87)* **-0.76 (0.22)**
α (rad)	-1.40 (0.13)	-0.58 (0.15) *-0.58 (0.15)* **1.35 (0.13)**	1.87 (0.08) *1.87 (0.08)* **-1.87 (0.08)**	-0.31 (0.07) *0.32 (0.07)* **1.82 (0.08)**	1.69 (0.04)

THE FUNDAMENTAL THUMB-TIP FORCE VECTORS PRODUCED BY THE MUSCLES OF THE THUMB

Jonathan L. Pearlman[1], Michal Weisman[1], Francisco J. Valero-Cuevas[1,2] and Stephanie Roach[1]

[1] Neuromuscular Biomechanics Laboratory, Cornell University, Ithaca, NY, U.S.A.
[2] The Hospital for Special Surgery, New York, NY, U.S.A.
E-mail: fv24@cornell.edu   Web: http://www.mae.cornell.edu/nmbl

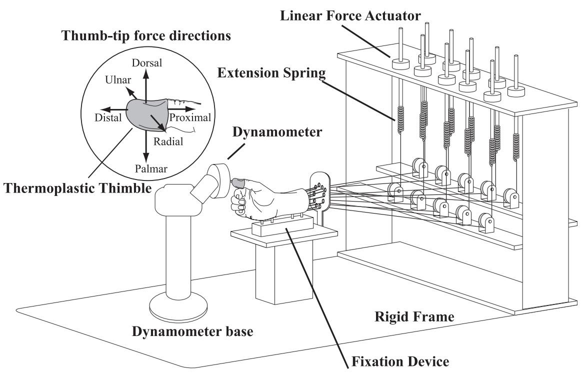

Figure 1: Experimental Apparatus.

INTRODUCTION

A rigorous description of the magnitude and direction of the 3D force vector each thumb muscle produces at the thumb-tip is necessary to understand the biomechanical consequences to pinch of a variety of paralyses and surgical procedures. Available descriptions of the biomechanical function of thumb musculature include muscle architectural parameters and moment arms; and graphical descriptions of the relative lines of action of intact and transferred tendons at each joint (Brand and Hollister, 1999). These descriptions, however, do not translate directly or unequivocally into descriptions of the 3D force vector each muscle produces at the thumb-tip—where pinch forces occur and where force vectors need to be restored by tendon transfers, for example. In this study, we characterized the 3D force vector each muscle produces at the thumb-tip, and investigated if these thumb-tip force vectors scaled linearly with tendon tension.

METHODS

We measured the output 3D thumb-tip force vector produced by each tendon acting on the thumb, plus two common tendon transfers, as a function of input tendon tension (n = 13). After fixing the hand to frame (Fig 1), we mounted the thumb by configuring it in standardized key or opposition pinch posture and coupling the thumb-tip to a rigidly-fixed 3D force/torque sensor. Computer-controlled linear actuators applied tension to the distal tendons of the four extrinsic thumb muscles, and to six Nylon cords reproducing the lines of action of i) the four intrinsic thumb muscles and ii) two tendon transfers commonly used to restore thumb opposition following low median nerve palsy. Transfer A (TRa), is performed by routing the *extensor indicis proprius* muscle to the insertion of the failed *abductor pollicis brevis* (AbPB) via the pisiform bone. Transfer B (TRb) is done by routing the *flexor digitorum superficialis* of the ring finger to the insertion of the failed AbPB via a slip in the *flexor carpi ulnaris* (Hentz and Leclercq, 2002). We measured the 3D force vector at the thumb-tip while each actuator ramped tendon tension from 0 to 1/3 of predicted maximal muscle force expected at each tendon, and back to zero.

RESULTS AND DISCUSSION

Many thumb-tip force vectors act in unexpected directions (e.g., the *opponens* force vector is parallel to the distal phalanx, Fig 2). This underscores how standard anatomical nomenclature can be of little value in describing fingertip force production for the purposes of the clinical restoration of pinch function. The two tendon transfers produced patently different force vectors, demonstrating how alternative (but presumably equivalent) tendon transfers to restore thumb opposition can be compared and contrasted by analyzing the 3D thumb-tip output force they produce. TRb better reproduces the radial component of force lost after low median nerve palsy (i.e., previously provided by AbPB). For most muscles, the increase of the thumb-tip force vectors with tendon tension is best described by a quadratic function ($p<0.05$)—likely due to load-dependent viscoelastic tendon paths and joint seating. Thumb-tip force vectors were sensitive to mounting procedure, as the moderate sensitivity to joint seating was compounded by inaccuracies in thumb posture. We are now studying the effect of these nonlinearities and sensitivities on the production of thumb-tip forces by the simultaneous action of multiple muscles.

REFERENCES

Brand, P. W. and Hollister, A. (1999) *Clinical mechanics of the hand* (3rdEdn). Mosby, St. Louis, Mo.

Hentz, V. R. and Leclercq, C. (2002) *Surgical rehabilitation of the upper limb in tetraplegia*. W B Saunders.

ACKNOWLEDGEMENTS

This material is based upon work supported under a National Science Foundation Graduate Research Fellowship (JLP) and a Whitaker Foundation Grant (FVC).

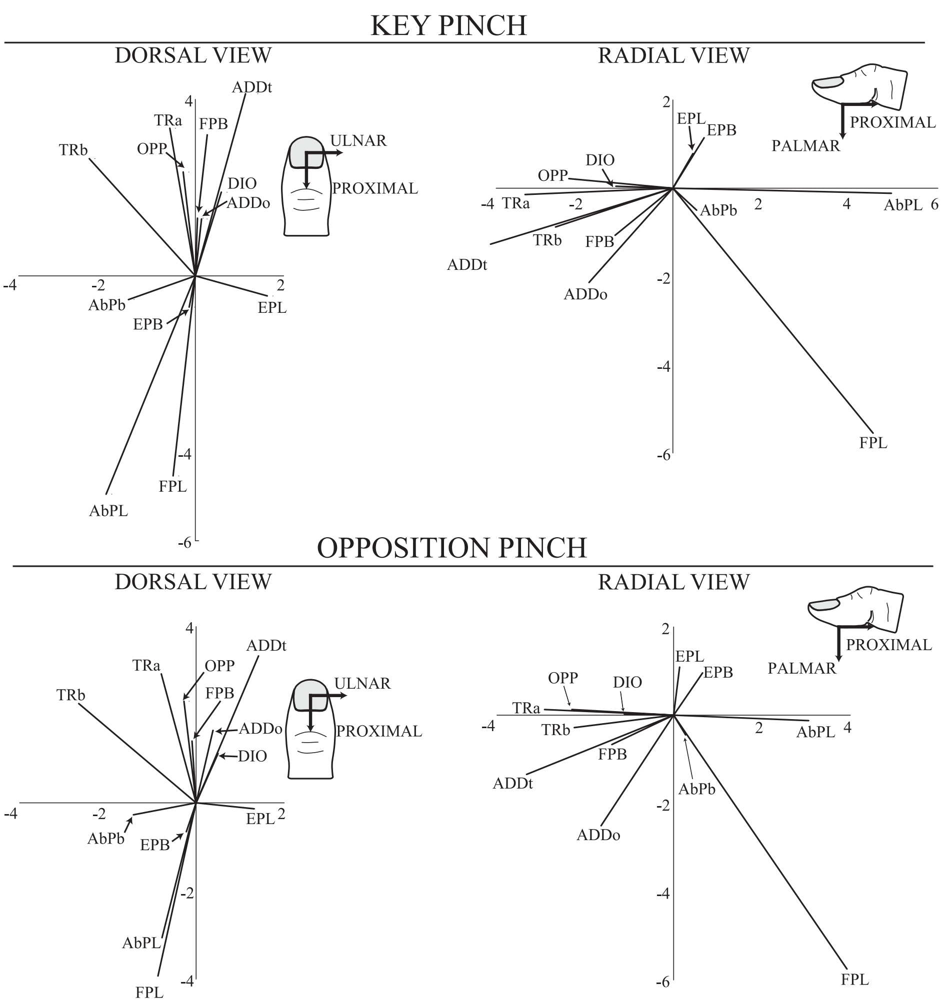

Figure 2. Average thumb-tip output vectors (N) for each functional posture in anatomical projections. *Flexor Pollicis Longus* (FPL), *Extensor Pollicis Longus* (EPL), *Extensor Pollicis Brevis* (EPB), *Abductor Pollicis Longus* (AbPL), *Abductor Pollicis Brevis* (AbPB), *Flexor Pollicis Brevis* (FPB), *Opponens Pollicis* (OPP), *Adductor Pollicis* oblique and transverse heads (ADDo and ADDt), and *first dorsal interosseous* (DIO). Transfers A and B (TRa and TRb, respectively) are also shown.

PREDICTING THUMB FORCE CHANGES WITH ULNAR NERVE IMPAIRMENT

Laurel Kuxhaus[1], Jonathan L. Pearlman[1], Michal Weisman[1], and Francisco J. Valero-Cuevas[1,2]
[1] Neuromuscular Biomechanics Laboratory, Cornell University, Ithaca, NY, USA
[2] The Hospital for Special Surgery, New York, NY, USA
E-mail: lck8@cornell.edu Web: www.mae.cornell.edu/nmbl

INTRODUCTION

There is no "gold standard" to objectively and sensitively quantify the impairment in 3D force-production caused by palsies. For example, in nerve entrapment syndromes leading to low ulnar or low median nerve palsies, clinicians must prescribe treatment based on sensory tests, the patient's reported clumsiness in grasp, and measures of maximal force in one or two directions. As each muscle uniquely contributes to the force-production capabilities of a digit (Valero-Cuevas, 2002), measuring the magnitude of thumbtip force in a variety of 3D directions may be informative of the impairment level.

A thumb's *Feasible Force Set* (FFS) represents the relative force production in every 3D direction (Figure 1). The size and shape of this polyhedron will naturally change with impairment (Valero-Cuevas, 2002). The FFS is directly calculated by combining all possible combinations of muscle forces. The goal of this study is to use the actions of thumb muscle measured in cadaver hands to calculate the 3D FFS and its changes with complete low ulnar and low median nerve palsies. This approach avoids assumptions needed in biomechanical models, and the confounding effects of adaptive strategies and muscle control variability in live people.

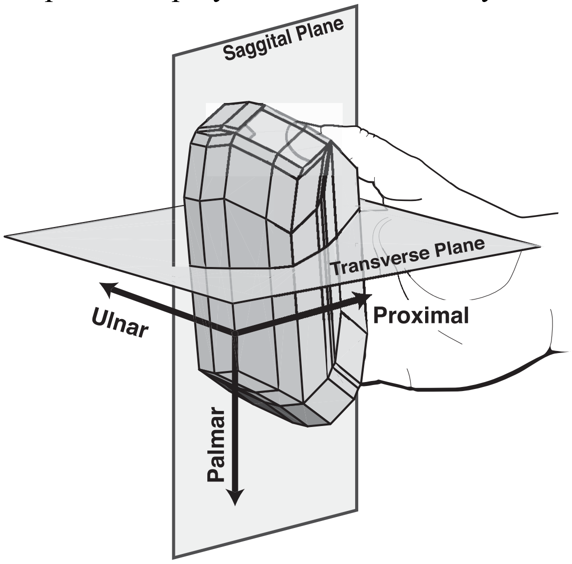

Figure 1: A FFS and Two Planes of Interest.

METHODS

Nine fresh-frozen cadaver hands were dissected, and nylon strings fixed to the following muscles: *abductors pollicis brevis* and *longus* (AbPB, AbPL), *adductors oblique* and *transverse* (ADDo, ADDt); *first dorsal interosseus* (DIO); *extensors pollicis brevis* and *longus* (EPB, EPL); *flexors pollicis brevis* and *longus* (FPB, FPL); *opponens pollicis* (OPP). The hand was mounted to a custom-fixture and the thumbtip rigidly fixed to a six-degree-of-freedom load cell (ATI Nano17, Apex, NC). The nylon strings joined each muscle's tendon to its own stepper motor via a spring. The computer-controlled motors pulled each tendon to one-third of its maximal force while the others were slack in both key and opposition pinch. Nine hands yielded data sets for key pinch, and 6 yielded data sets for opposition pinch (Pearlman et al., In review) Assuming linear scaling, the convex hull of the data is a one-third scale FFS of the thumb.

Changes in the FFS were calculated for each palsy by omitting the contributions of the affected muscles (low ulnar nerve palsy: ADDo, ADDt, DIO removed, FPB reduced to 50% of the intact case; low median nerve palsy: AbPB and OPP removed, FPB reduced to 50% of the intact case). The transverse and saggital cross-sections were selected for further study. Each FFS was appropriately "sliced" and its area and aspect ratio (characterized by the ratio of its principal moments of inertia) calculated in MATLAB (The MathWorks, Natick, MA). We compared these cross-sections across conditions using an Analysis of Variance followed by Tukey's post-hoc procedure in SPSS (SPSS Inc., Chicago, IL).

RESULTS AND DISCUSSION

For the transverse plane, the area of the cross-section did not change with any impairment in key pinch, ($p=0.646$), but did in opposition pinch ($p=0.024$), though the palsies were not distinguishable form each other ($p=0.996$). For the saggital plane in key pinch, the area of the low ulnar palsy cross-section was statistically different from the other two cases ($p=0.00031$). In opposition pinch, this plane can distinguish the low ulnar palsy from the intact case ($p=0.033$), but cannot tell either from the low median nerve palsy ($p=0.390$).

The aspect ratio of the transverse cross-section of the FFS is insensitive to posture for all cases ($p>0.422$). The aspect ratio of the saggital cross-section is sensitive to posture for the low ulnar nerve palsy only ($p=.048$). In addition, the aspect ratio of the transverse cross-section can distinguish the median nerve palsy case ($p=0.013$) regardless of posture. The saggital cross-section aspect ratios statistically distinguish between the low ulnar and low median nerve palsy cases ($p=0.018$), but neither from the intact case ($p=0.662$). Slight variations in hand posture could have clouded these differences in the FFS.

This study is limited in that it assumes that thumb muscle actions scale and superimpose linearly. Our goal was to simulate the worst-case FFS changes with complete palsies to guide the development of clinical measures of force impairment. We expect that the sensitivities to impairment found are robust against the system nonlinearities.

The transverse cross-section's sensitivity suggests that measuring it in patients may be an objective and sensitive measure of partial and evolving decrements in force production, as in nerve entrapment syndromes. The results of this study motivated and guided the development of a clinical method to quantify changes in force production in palsies affecting the thumb.

REFERENCES

Chvátal, V. (1983). Linear Programming. New York, W.H. Freeman and Company.

Pearlman, J. L., et al. (In review). Journal of Orthopaedic Research.

Valero-Cuevas, F. J. and V. R. Hentz (2002). Journal of Orthopaedic Research **20**(5): 902-9.

ACKNOWLEDGEMENTS

This material is based upon work supported under a National Science Foundation Graduate Research Fellowship (LK, JLP) and a Whitaker Foundation Grant (FVC).

HAPTIC FEEDBACK IMPROVES UPPER EXTREMITY CONTROL OF RESONANCE

Felix C. Huang, R. Brent Gillespie, Arthur D. Kuo
Dept. of Mechanical Engineering, University of Michigan, Ann Arbor
E-mail contact: fhuang@umich.edu

INTRODUCTION

Humans experience reaction forces in common motor tasks such as bouncing a ball (Schaal et al., 1996) or swinging a leg. These reaction forces may be useful feedback when resonance detection and maintenance are important. Our goal was to test whether haptic feedback complements visual feedback in the continuous manual control of a resonant sprung mass (Dingwell et al. 2002). We hypothesized that subjects would perform better in this when given combined visual and haptic feedback than with either feedback channel alone. We designed an apparatus with a motorized handle that would simulate the dynamics of a sprung mass. Comparing errors in the power spectrum of the input motion, subjects demonstrated better performance with visual and haptic feedback than with visual feedback alone (paired t-test: $p<0.002$) and haptic feedback alone ($p<0.04$).

METHODS

Ten healthy adults (7 male, 3 female) participated in this study after providing informed consent. The task was to repeatedly turn a handle connected to one end of a virtual torsional spring, with a virtual torsional mass at the other end, so that the mass was actuated to resonance. Using the dominant hand, each subject grasped a motorized handle and operated the handle using wrist pronation and supination (See Figure 1). Three feedback conditions were presented: Vision-Only, Haptic-Only, and Vision-Haptic. For each condition, four undamped resonant systems were presented: (7, 9, 11, and 13 rad/s), each with a spring stiffness of 0.0125 N-m/rad. Three trials of each combination were presented in random order for a

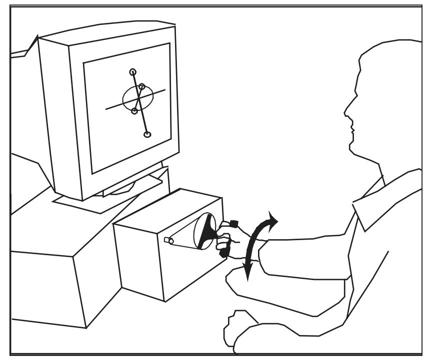

Figure 1. Operation of virtual sprung mass resonance task may include visual and haptic feedback.

were presented in random order for a total of 36 trials, each lasting 30 sec. In each trial, the computer released the sprung mass from an initial stretch, and the subject attempted to find and maintain a resonant motion of the mass, relying on available feedback to do so. Visual feedback consisted of a computer animation of the motion of the handle and sprung mass. Haptic feedback consisted of a torque produced by the motor and felt through the handle, simulating the reaction of the sprung mass.

Using collected handle input data (100 Hz sample rate) from each trial, we determined the power spectrum of the input motion. As a metric for the input error, we calculated the sum of squared differences (SSD) be-

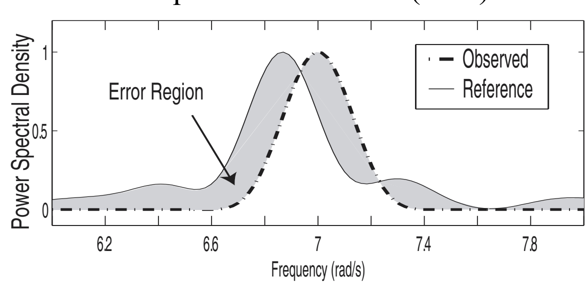

Figure 2. These frequency distributions of handle input motion show an error between the observed and a reference spectra at a target 7 rad/s. Data are sample from one subject.

tween the observed and reference frequency distributions in a band of 2 rad/s centered about the target frequency (See Figure 2). The reference distributions were determined from simulated handle input data (also sampled at 100 Hz) operating at the target natural frequencies.

RESULTS AND DISCUSSION

Our metric SSD demonstrated significantly better performance when both feedback channels were available. See Figure 3 for mean results of frequency distribution sum-squared errors for each condition. Vision-Only trials produced significantly more error than Vision-Haptic trials for all frequencies tested (paired t-test, $p < 0.002$). Haptic-Only trials produced significantly more error than Vision-Haptic trials in only the highest and lowest frequencies tested (paired t-test, $p < 0.04$ for 7 and 13 rad/s).

For this experiment design, haptic feedback was the dominant channel of sensory information. However, vision contributed to significant gains in performance, suggesting that both feedback channels aid control. Visual inspection of the handle input phase portraits showed that most subjects had faster convergence to resonance when haptic feedback was provided. The scatter in the phase portraits typically occured earlier in the trial (see sample plot in Figure 4, left). With haptic feedback, discontinuities in the phase typically occur, due possibly to force coupling between the hand and the virtual sprung mass. A plot of the input velocity versus the spring torque shows that, with haptic feedback, more positive work is done to the system, as evidenced by more consistency in the first and third quadrants of the sample power traces (Figure 4, right).

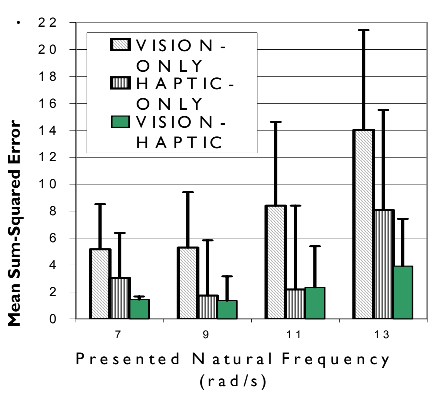

Fig. 3. Sum-squared errors (n=10, +1 s.d.) for each feedback condition and natural frequency.

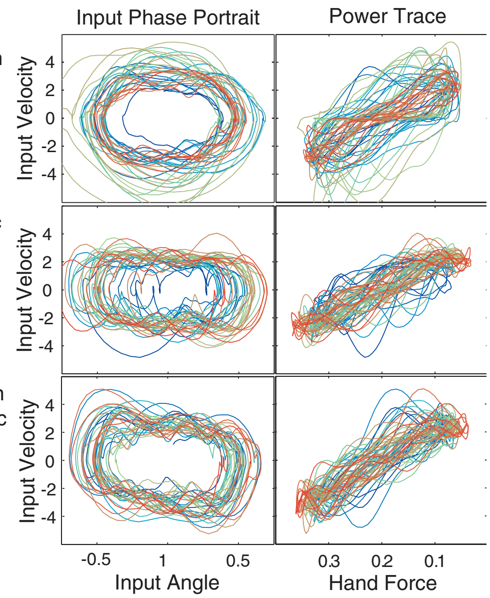

Fig. 4. Sample phase portraits (left) and power traces (right) for each feedback condition.

In the manual control of resonant systems such as a sprung mass, haptic feedback costs mechanical work and may affect input motion. Yet it may improve performance by providing information to complement vision for control or identification purposes. Haptic feedback may aid resonant tasks since it is energetically advantageous for a human to be aware of effort and thus minimize negative work while achieving the task goals.

ACKNOWLEDGEMENTS

This work supported in part by the Midwest Regional Rehabilitation Network (R24).

REFERENCES

Schaal S. et al. (1996) J. Mot. Behav. 28: 165-183.

Dingwell, J.B. et al. (2002) J. Neurophysiol. 88: 222-235.

DEPTH-DEPENDENT RELAXATION OF ARTICULAR CARTILAGE IN UNCONFINED COMPRESSION

Oliver K. Erne[1]; John Reid[2]; Larry W. Ehmke[1], and Michael Bottlang[1]
[1]Legacy Clinical Research & Technology Center, Portland, OR; *email: mbottlan@lhs.org*
[2]Oregon Health & Science University, Portland, OR

INTRODUCTION

Articular cartilage (AC) is an in-homogeneous, anisotropic and multiphasic composite. Depth-dependent strain distribution in full thickness AC has previously been investigated with optical methods (Guilak, 1995; Schinagl, 1997; Wang, 2003). Depth and time-dependent compressive strain has been predicted with theoretical models (Li, 2000; Wang, 2001). Most recently, Electronic Speckle Pattern Interferometry (ESPI) has been employed to measure depth-dependent strain on AC cross-sections in response to incrementally applied strain (Erne, 2003).

In this study, we used ESPI to measure depth and time-dependent strain over the cross-section of AC. We hypothesized, that the strain in the superficial zone of AC will increase during relaxation, while strain in the deep zones will decrease.

METHODS

Specimens: Osteochondral plugs (∅ 9mm) were harvested from fresh-frozen porcine patello-femoral joints of skeletally mature animals. Plugs, extracted from the medial aspect of both joint members, were cut with a diamond saw to cubes with a base of 5x5mm, including full thickness AC and subchondral bone. These osteochondral cubes were stored in phosphate buffered saline and protease inhibitors (PBS+PI) at -40°C. At the day of testing, each specimen pair (n=5) was thawed in PBS+PI, and stained with Hematoxylin and Eosin to ensure adequate reflective properties for ESPI measurements.

Experimental setup: Each pair of corresponding specimens was subjected to unconfined compression in a custom cartilage compression setup (Fig. 1). Displacement was induced using the actuator of a servo-hydraulic material test system (8841, Instron, Canton, MA). Each specimen remained submersed in PBS+PI, and optical access to the specimen cross-section for ESPI measurements was provided by a glass window. An ESPI system (Q100, Ettemeyer, Nersingen, Germany) in combination with a custom magnification optics was used to assess full-field compressive strain on the specimen surface with 42 pixel/mm spatial resolution. After alignment of the specimen, the femoral and patellar AC thickness of each specimen pair was optically assessed. Prior to testing, a pre-strain of 4% was applied and the AC was allowed to relax for 60 minutes.

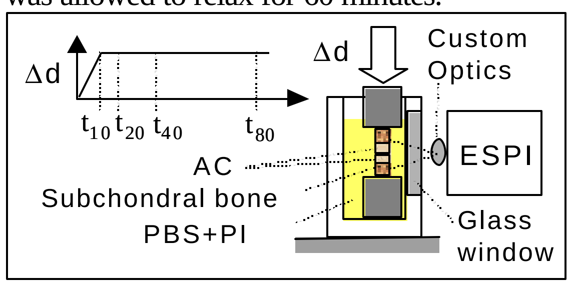

Figure 1: Section view of cartilage compression setup with ESPI sensor

Loading protocol: All specimens were subject to incremental compression by *Dd*=0.5µm over a ramp duration of 10s, followed by 90s relaxation. Full-field ESPI strain distributions of the femoral cartilage cross-section were recorded directly after *Dd* was applied (t_{10}=10s), and subsequently at t_{20}=20s, t_{40}=40s and t_{80}=80s. This sequence (i.e., application of *Dd*, followed by four ESPI recordings) was repeated 100 times until a total displacement d=50µm was applied.

Data evaluation: The cumulative strain reports over 100 steps were computed for t_{10}, t_{20}, t_{40}, and t_{80}. These strain reports were normalized to account for differences in femoral cartilage thickness. To reduce the full-field strain maps, average strain values over the specimen width (i.e., parallel to the articular surface) were computed to obtain compressive strain profiles e_{t10}, e_{t20}, e_{t40}, and e_{t80}. To further reduce the strain profiles, averaged zonal compressive strains e_s, e_m, and e_d, were extracted from the superficial (20%), middle (50%), and deep (30%) cartilage zones, respectively, for e_{t10}, e_{t20}, e_{t40}, and e_{t80}. Differences in strain magnitudes obtained at specific times were statistically analyzed using two-tailed paired Students T-tests.

RESULTS

ESPI strain reports at specific times, t_{10} to t_{80}, yielded time-dependent compressive strain distributions over the cartilage thickness (Fig. 2). At the articular surface, e_{t80} was 11% higher compared to e_{t10}.

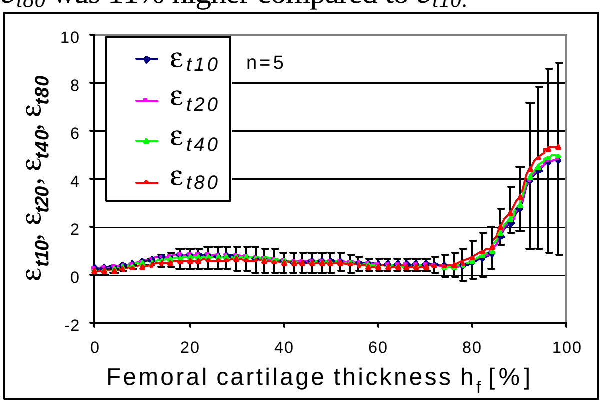

Figure 2: Time-dependent strain over femoral cartilage thickness (h_f=100% indicates articular surface).

At all times, strain at the superficial zone was larger as compared to the middle and deep zone (Fig. 3). During relaxation (i.e., t_{10}-t_{80}) strain e_s at the superficial zone increased significantly, while strain e_d at the deep zone decreased.

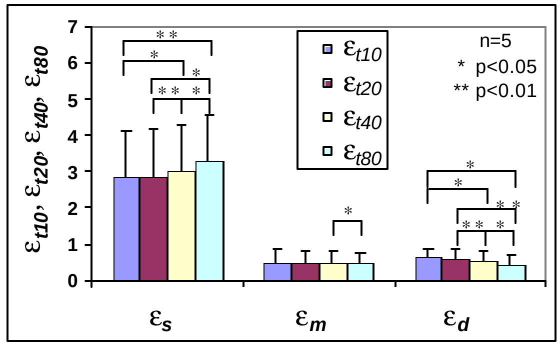

Figure 3: Time-dependent zonal strain across articular cartilage.

DISCUSSION

This study demonstrates direct measurements of time-dependent strain distributions over the cross-section of AC in response to small incrementally applied compression. Results are in line with previously reported equilibrium strain distributions (Guilak, 1995; Schinagl, 1997; Wang, 2003). In addition, the high sensitivity of ESPI allowed to detect subtle and consistent changes in the strain distribution during relaxation. Similar results were predicted in a fibril reinforced non-homogeneous poroelastic model (Li, 2000) and measured using ultrasound (Zheng, 2002). While ultrasound measurements are affected by material properties, ESPI captures full-field strain independent of the material. However, since ESPI can only capture relatively small strain increments per measurement step, 100 serial measurements were used to determine strain in response to 50µm compression.

REFERENCES

Erne, O., et al. (2003). 49th ORS, 292
Guilak, F., et al. (1995). J Orthop Res **13**(3): 410.
Li, L., et al. (2000). J BioMech **33**: 1533.
Schinagl, R., et al. (1997). J Orthop Res **15**(4): 499-506.
Wang, C., et al. (2001). J BioMech **34**: 75.
Wang, C., et al. (2003). J BioMech **36**: 339.
Zheng, Y., et al. (2002). Phys Med Biol **47**: 3165-3180.

INFLUENCE OF ARTICULAR GEOMETRY ON PROSTHETIC WRIST STABILITY

Nicole M. Grosland[1] Renee D. Rogge[2] and Brian D. Adams[1]

[1]The University of Iowa, Iowa City, IA, USA
[2] Mercer University, Macon, GA
E-mail: nicole-grosland@uiowa.edu

INTRODUCTION

Despite advances in joint arthroplasty, wrist arthrodesis is typically favored by hand surgeons over total joint replacement, because of high complication rates and early failures associated with most implants. Implant fracture, loosening, and imbalance have been the primary failure modes. Although wrist arthrodesis effectively relieves pain and corrects deformity, the sacrificed motion may substantially impair function, especially when multiple joints in the extremity are afflicted. Procedures that preserve some degree of wrist motion have become increasingly popular including renewed interest in joint replacement. We hypothesize that an ellipsoidal distal articulation would provide greater articular contact area through a larger range of motion and better prosthetic stability than a toroidal articulation. Using both computational modeling and experimental testing we compared the stability of the two geometries.

METHODS

Computational Model A three-dimensional finite element (FE) non-linear contact analysis was performed. A CAD (Pro/ENGINEER, PTC, Needham, Massachusetts) model of the Universal prosthesis was created based on the manufacturers dimensional specifications and imported into PATRAN (MSC Software, Los Angeles, CA; version 8.5), enabling a FE mesh to be generated for each component. The carpal and radial components were each modeled as rigid bodies, represented by 4-noded quadrilateral elements (6,710) and 3-noded triangular elements (1,366), respectively. The polymer component was modeled via 20,130 8-noded hexagonal elements (E = 634.92 MPa, ν = 0.45). In addition to the aforementioned user defined elements, 14,370 elements were defined internally by ABAQUS 6.2 (Hibbitt, Karlsson & Sorensen, Inc., Pawtucket, RI) for contact purposes.

An ellipsoidal distal articular component was similarly modeled. Maintaining the major and minor radii of the toroid, an ellipsoid was created by revolving the large radius of curvature about an axis established by the smaller radius.

Initiating in the anatomic 'neutral' position, the radial component was free to translate in the radial-ulnar and volar-dorsal directions, while the carpal-poly complex was unconstrained along the vertical axis. A compressive load was maintained while the prescribed rotation (in increments of 0.1 degrees) was applied about a central axis parallel to the stem of the carpal component. The compressive load was varied between models from 10N to 110N, in 20N increments, to simulate various degrees of soft tissue tension. The articulating interface was assumed frictionless.

Experimental Testing Experimental validation was performed on a BIONIX 858 Test System (MTS, Eden Prairie, MN). Initiating in the neutral prosthetic position, the polyethylene-carpal component was rotated +45 degrees with respect to the radial component, after which it was swept back through the neutral position to an angle of –45 degrees, at a rate of 1 deg/sec. An x-y stage was used to provide translational freedom to the radial component. Six replicate trials were performed for each of the six compressive loads (10N – 110N; 20 N increments).

The Modified Radial Articulation The volar-dorsal width of the distal radial component was increased by 5 mm, thereby increasing the articular capture between the components. Using the same experimental and computational methods above, the effects of the modified radial component were tested. Experimentally, the following conditions were tested: a 30N and a 500N compressive load coupled with a rotation rate of 1 deg/sec. In each case, the device was positioned in neutral alignment.

RESULTS AND DISCUSSION

Toroidal Carpal Articulation The experimental and computational results were in good agreement. The results show an extreme sensitivity to rotational malalignment at even sub-degree rotations. On average, the maximum resisting moments were encountered experimentally within 2-3º of rotation. Once neutral alignment was lost, there was a shift in the contact area, of both position and surface area. This was accompanied by a substantial increase in peak contact stress.

Ellipsoidal Carpal Articulation
The ellipsoid produces a more consistent contact area (Figure 1). With less than 4 degrees of extension, or flexion, it is apparent that the toroidal articulation is no longer contacting the depths of the radial surface (Figure 1). The severity of incongruency is accentuated by rotation. As the alignment deviates from neutral there is an accompanying decrease in resistance to dislocation. The rotational and translational resistances of the ellipsoidal design were approximately 144 N-mm and 23.5 N, respectively. The rotational resistance of the ellipsoidal articulation permitted greater rotation (10.87º) prior to attaining the maximum resisting moment.

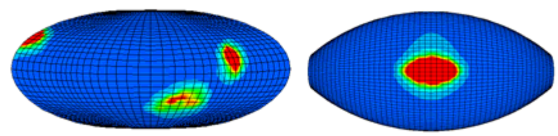

a. b.

Figure 1. Stress contours resulting from 4 degrees of flexion for the (a) toroidal and (b) ellipsoidal carpal articulations in the original radial concavity.

An increase in rotational resistance accompanied the increase in the width of the radial articular surface. An average resisting moment of 305 Nmm was observed at approximately 11 degrees of rotation.

SUMMARY

Ellipsoid and toroid-shaped articulations for total wrist prosthesis were evaluated using computational models and laboratory experiments. An ellipsoidal design was found to accommodate a concave proximal component of greater width, resulting in better capture and prosthetic stability than a toroid shape. An ellipsoid articulation also provides greater contact area through the available arc of motion. We conclude that an ellipsoidal articulation is a reasonable design for total wrist arthroplasty.

CINERADIOGRAPHIC ASSESSMENT OF ROTATOR CUFF FATIGUE ON GLENOHUMERAL KINEMATICS

JM Miller[1], TW Randle[1], EJ Kane[1], A Kelly[1], DS Teyhen[1,2]

[1]Physical Therapy Research Center, U.S. Army-Baylor University Graduate Program in Physical Therapy, Fort Sam Houston, TX, USA
[2]Department of Kinesiology & Health Education, The University of Texas, Austin, TX, USA
E-mail: deydre.teyhen@us.army.mil

INTRODUCTION

Superior migration of the humeral head with respect to the glenoid has been found to occur during humeral elevation with shoulder impingement syndrome, with rotator cuff (RTC) tears (Deutsch et al, 1996), and with fatigue (Chen & Chen, 1998). However, only minimal humeral head migration was found to occur in those without shoulder pathology (Chen & Chen, 1998, Poppen & Walker, 1976). These analyses of the arthrokinematics utilized repetitive static standard radiographs to quantify the glenohumeral positions under isometric conditions. Dynamic analysis of frontal plane arthrokinematics during elevation has not been reported. The purposes of this study were to analyze humeral head migration during humeral elevation (0-135^o) in those without shoulder pathology 1) to assess the test-retest reliability, 2) to describe normal humeral head migration patterns, and 3) to investigate the effect of RTC fatigue on superior humeral head migration.

METHODS

A convenience sample of 20 males without shoulder pathology, 18-35 years of age (27.95 $\pm$ 3.69 years), completed this study.

Three cineradiographic images (Dynamic Motion X-Ray, DMX-Works Inc., Palm Harbor, FL) of humeral elevation in the plane of the scapula were collected at 30 Hz for each subject. Two pre-fatigue humeral elevation trials were used to assess test-retest reliability at 0, 45, 90, and 135^o of humeral elevation.

Subjects then performed a RTC fatigue protocol adapted from Chen & Chen (1998) and Blackburn & Wofford (1990). Fatigue was estimated when the subject could not continue to lift the arm past 45^o on three consecutive trials and was confirmed by a least a 40% strength decrement as measured by a hand held dynamometer with humeral elevation. After fatigue was established, a final set of images was obtained.

The digital images were analyzed according to the methods described by Chen & Chen (1998) from 0-135^o. An ICC (3, 1) was used to establish test-retest reliability at the pre-selected angles. The first pre-fatigue and the post-fatigue trials were compared to assess the difference in humeral head migration due to RTC fatigue. This study utilized a 2x4 (fatigue by position) repeated measures ANOVA in order to contrast humeral head migration at 0, 45, 90, and 135^o with and without fatigue (α = .05).

RESULTS AND DISCUSSION:

The test-retest reliability among this sample ranged from good to excellent (.77 to .92) with a SEM ranging from .54 to .657 mm (approximately 1.6 pixels).

Repeated measures ANOVA revealed a main effect for angle ($p<.001$). Pair-wise t-test with a Bonferroni Correction revealed that superior migration at 0^o was significantly different ($p<.001$) from superior migration at 45, 90, and 135^o (Figure 1). Of the 40 pre- and post- fatigue trials analyzed, 33 demonstrated this trend. However, 7 demonstrated either inferior or relatively no migration.

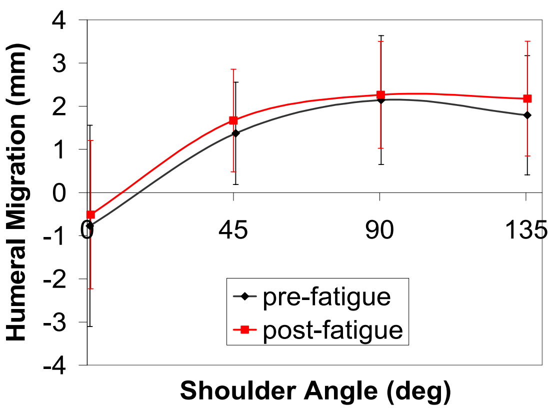

Figure 1: Mean superior migration of the humeral head with elevation during both pre- and post-fatigue for all subjects.

There was no significant effect for pre-to post-fatigue ($p=.224$) and no interaction between angle and fatigue state ($p=.956$). These results indicate that the humeral head migration was associated with humeral head position and not the state of fatigue. Pre-fatigue and post-fatigue maximal elevation occurred at 90^o with 2.14 ± 1.49 mm and 2.26 ± 1.24 mm superior migration, respectively.

The combined findings of superior migration of the humeral head in those without shoulder pathology and the finding of no significant difference between due to RTC fatigue are in contrast to prior reports (Chen & Chen, 1998). In our study, it does not appear that the amount of fatigue could be an explanation for this contradiction. The fatigue strength of the subjects was $53\% \pm 8.6\%$ of the original strength. Chen & Chen (1998) defined fatigue as a 40% reduction in strength. Further, there was no correlation ($r = .152$, $p=.592$) between the percent fatigue and the amount of migration change post-fatigue. Additionally, the time from the end of the fatigue protocol to the post-fatigue assessment was also controlled (16.64 ± 1.96 s). It is hypothesized that a measurement difference between the static radiographs versus cineradiographic imaging techniques, or the difference between RTC activation during isometric and concentric conditions, may explain this discrepancy. Further study is needed to address these questions.

SUMMARY:

Cineradiographic assessment of shoulder kinematics provides a reliable tool for studying the underlying arthrokinematics during humeral elevation. Further, during humeral elevation there is superior migration of the humeral head that does not increase with RTC fatigue in subjects without shoulder pathology. The effect of RTC fatigue on those with shoulder pathology is unknown and currently under investigation in our laboratory.

REFERENCES:

Blackburn, T.A., Wofford, W.B. (1990). *Athletic Training*, **25**, 40-45.

Chen, Y.C., Chen, S.K. (1998). *J. Shoulder Elbow Surgery*, **7**, 164-7.

Deutsch, A. et al. (1996). *J. Shoulder Elbow Surgery*, **5**, 186-93.

Poppen, N.K., Walker, P.S. (1976). *J. Bone Joint Surgery*, **58**, 195-201.

The opinions and assertions contained herein are the private views of the authors and are not to be construed as official or as reflecting the views of the Departments of the Army or Defense.

THE EFFECTS OF TOTAL SHOULDER REPLACEMENT GEOMETERY ON THE JOINT KINEMATICS AND CONTACT MECHANICS

John E. Novotny, Yingxin Gao

Dept. of Mechanical Engineering, Center for Biomedical Engineering Research
University of Delaware, Newark, Delaware, E-mail: novotny@me.udel.edu

INTRODUCTION

Total shoulder replacement resurfaces the glenoid and humeral head, perhaps changing their dimensions and orientations (inclination and retroversion angle) relative to the scapula and humerus. These changes in anatomy will alter articular contact, muscle lever arms and soft tissue tension, and may result in abnormal kinematics. This study will investigate the effects of changing glenohumeral joint geometry on kinematics and contact mechanics. This includes the radius, thickness, inclination and retroversion angle of the humeral head and the radius and the depth of the glenoid. A mathematical model will observe the response to an external moment loading pattern where the humerus is abducted, extended and externally rotated, similar to reaching to comb the hair. Sensitivity of humeral translations and rotations to variation of the geometry parameters will be explored, along with the response of contact force, area and stress. By understanding the sensitivity of joint kinematics and contact mechanics, identification of important design parameters for total shoulder replacement can be made.

METHODS

To describe humeral head motion relative to the glenoid, coordinate systems were defined. The extent and orientation of the articular surfaces were determined from four in vitro specimens [Novotny, 2000]. The glenoid surface was a partial sphere with radius, r_G, with **g**(x, y, z), for $g_x \leq 0$, as:

$$r_G^2 = (g_x - d)^2 + g_y^2 + g_z^2$$

and d as the distance its center. Glenoid depth is r_G-d. The humeral head was also a partial sphere with radius r_H, as:

$$r_H^2 = (c_{ix} - p_x)^2 + (c_{iy} - p_y)^2 + (c_{iz} - p_z)^2$$

where p is the origin of the sphere. Points, c_i, on the sphere also satisfied a description of the partial sphere:

$$r_C^2 \geq (c_{ix} - c_{rx})^2 + (c_{iy} - c_{ry})^2 + (c_{iz} - c_{rz})^2$$

where $\mathbf{c_r}$ is the center of the rim and r_C is the radius of the rim. The inclination angle was between the x-axis of the humeral coordinates system and the vector c_r. The retroversion angle was the angle between the frontal plane and epicondylar axis, which is the z-axis of the humeral coordinate system. Three external moments were applied to move the humerus in abduction, extension and external rotation. Contact forces were calculated with a deformable contact model. Five glenohumeral ligaments and forces applied through four rotator cuff muscles were represented. The ligament and muscle elements might run linearly from origin to insertion or wrap around the head surface. The path was found assuming the shortest length. The ligament tension was applied if its length was greater than an initial length and the muscle forces were applied in relation to their cross-sectional areas [Veeger, 1991]. Forces and moments on the humerus were those from articular contact, ligament elements, muscles and those externally applied. The model was solved for the position (X, Y, Z) and (RZ, RY, RX) orientation resulting in force and moment equilibrium, using a hybrid-form of Powell method for non-linear equations. The sensitivity of the humeral translations and rotations and contact forces, stress and areas to the geometric variables was determined. All geometric parameters were varied through a common range of values for total shoulder replacement: humeral head radius (21.9-26.3 mm); humeral head thickness (12.3-19.5 mm); inclination angle (115-145^0); and retroversion angle (0-30^0); glenoid radius (25.5-29.5 mm); glenoid depth (3.9-6.9 mm).

RESULTS AND DISCUSSION

The radius of the humeral head. The increase in the radius of the humeral head sphere resulted in less translation, less extension and more abduction with the external rotation unchanged. The contact area decreased. The magnitude of the contact force did not change, though, so the stress on the surface increased.

The radius of the glenoid. Increasing the radius of glenoid sphere allowed the humeral head to translate more, extend less and externally rotate more. The contact area and the contact stress were unchanged.

The thickness of the humeral head. More superior-inferior translation was found by increasing the humeral head thickness. Also the humerus externally rotated more and extended less. Although increasing thickness increased the overall area of the humeral head surface, the contact area did not change. A small increase in contact force did not result in greater contact stress.

The depth of the glenoid. Increasing the depth of the glenoid resulted in the less anterior-posterior and superior-inferior translation, more extension and less external rotation. Increasing the humeral head thickness did not make the contact area increase but the increasing in the depth of the glenoid did. Due to the more centered location of the humeral head in the glenoid, the magnitude of the contact force decreased. This resulted in a large decrease in the contact stress.

The retroversion angle. There was increased posterior and inferior translation with increased retroversion angle. There was also an increased contact force. The contact area decreased, and so the contact stress increased. The increase in the retroversion angle externally rotated the humerus more with less extension.

The inclination angle of the humeral head. No changes in translations were found with increasing inclination angle, but there was less extension and more abduction. The contact area and contact stress were unchanged.

Overall. Ligament tensions were not needed for equilibrium to be met, due to the presence of the constant rotator cuff muscle forces. Only when the thickness of the humeral head was increased do the soft tissues show tensions at equilibrium.

This sensitivity analysis using analytical modeling methods provides information about how changes in the humeral head and glenoid geometries can affect glenohumeral kinematics for a common activity of daily living. This is in contrast to other modeling efforts that have mainly been concerned with implant fixation. These results give some indication of how changes to modular implants may change the loads transmitted to the glenoid component also, and thus could be coupled with current finite element models of glenoid component fixation. Future work on soft tissue loading and more realistic joint surfaces may lend greater understanding to the relationships between implant design, kinematics and functional results.

REFERENCES

Novotny JE, et al. (2000). *J Biomech*, **33**, 345-54.

Veeger HE, et al. (1991). *J Biomech,* **24**(7), 615-29.

OPTIMUM FINGER FORCES IN PRONATED AND SUPINATED POSTURES

Todd Pataky [1], Vladimir Zatsiorsky, and Mark Latash [2]

[1]Biomechanics and [2]Motor Control Laboratories, Penn State University, State College, PA, USA
E-mail: tcp120@psu.edu

INTRODUCTION

Deterioration of hand function with age and pathology has promoted many finger coordination research efforts. Most of these have focused on normal forces (F_n) during tasks that require a vertical orientation of the handle (i.e. with F_n acting horizontally). When an object is held in a vertical orientation, the basic mechanics are simple: the tangential forces (F_t) act vertically to support the object weight (W), and the F_n act horizontally to prevent slip and to balance moments. The summed F_n must be zero, and the summed F_t must equal W. However, when the object is rotated with respect to the gravity field, the task mechanics are changed: both F_t and F_n either contribute to W support or 'add' to W. Moreover the sums of F_t and F_n become trigonometric functions of the orientation angle θ (with respect to the vertical). The central nervous system (CNS) must somehow account for these changes. Other studies have investigated finger forces for θ≠0 (e.g. Johansson et al., 1999, Goodwin et al., 1998), but have not incorporated optimization. The purposes of this study were: 1) To document how finger forces change with θ, and 2) To attempt to account for the observed force patterns with optimization of a simple mechanical model.

METHODS

Eight students (4 female, 4 male) from the Pennsylvania State University volunteered to participate in this study. Five multi-component force/torque transducers (ATI Industrial Automation, Garner, NC, USA) were topped with 100-grit sandpaper (μ=1.4) and attached to a 580g aluminum handle (Figure 1) that was free to rotate about a horizontal axis orthogonal to the normal-tangential plane.

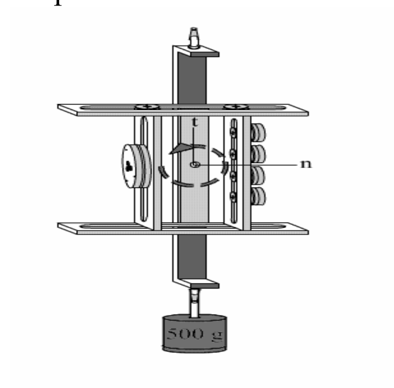

Figure 1: Experimental apparatus.

Loads of 250, 500, and 750 g were suspended from the bottom of the handle. Subjects were required to hold the handle. in 13 orientations (twice each) between θ=±90° in increments of 15°. Either two (IM) or four (IMRL) fingers were used, where I, M, R, and L refer to the index, middle, ring, and little fingers, respectively. The measured F_n and F_t were averaged over three seconds. A simple model that incorporated only the F_n and F_t and the experimental geometry was created in Matlab (MathWorks Inc., Natick, MA, USA). Optimization was performed using different objective functions (f) including, among others: f = norm($[F_n]_{IMRL}$) where $[F_n]_{IMRL}$ is the four-component vector of finger normal forces. The difference between the observed and predicted F was termed 'optimum-observed discrepancy' (OOD). The standard deviation of the OOD

(sd_{OOD}) was used to reflect how closely the observed F paralleled the predicted F.

RESULTS AND DISCUSSION

All finger forces changed in a sine-like manner with θ. Both the F_n and F_t tended to parallel the optimum results (sd_{OODn}= 0.063, sd_{OODt}= 0.028), but the average OOD_n for the fingers was more than five times greater than the average absolute OOD_t (Figure 2). This was due mainly to a peak in OOD_n for θ near zero. Similar results were obtained for the IM tasks, but are not presented here.

The f that produced the minimum sd_{OOD} (out of the functions tested so far) was f = norm($[F_n]_{IMRL}$). The fact that F_t are predicted quite well without incorporating F_t in f might suggest that the CNS coordinates only the 'grasping' forces, and that the F_t are 'passive' consequences of the F_n.

The reasons for the relatively constant OOD_t (with the exception of the thumb) are also not clear. Further explorations with various objective functions and/or including anatomical and physiological features in the model might explain the OOD.

SUMMARY

Optimization of a simple mechanical model could predict some of the main features of the experimental data collected when humans rotated a hand-held object through 180° in the gravity field. The OOD might be a useful tool for exploring motor control strategies employed by the CNS.

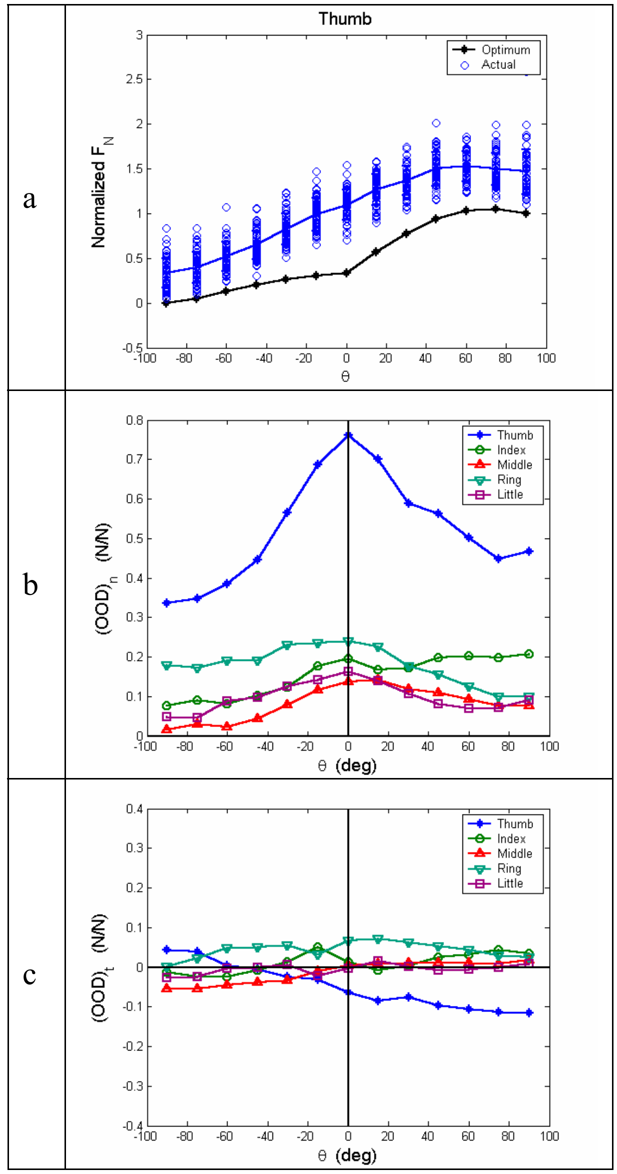

Figure 2: Comparison of observed and optimum results for f=norm($[F_n]_{IMRL}$); (a) $(F_n)_T$, (b) $(OOD)_n$, and (c) $(OOD)_t$.

REFERENCES

Johansson, et al. (1999). *Exp. Br. Res.*, **128**, 20-30.

Goodwin, A.W., et al. (1998). *J. Neurosci.*, **18**, 10724-34.

ACKNOWLEDGEMENTS

This research was supported in part by NIH grant AR048563.

MODELING THE SENSITIVITY OF GLENOHUMERAL KINEMATICS, LIGAMENT TENSION AND ARTICULAR CONTACT TO ROTATOR CUFF MUSCLE ACTIVITY

John E. Novotny, Yingxin Gao

Dept. of Mechanical Engineering, Center for Biomedical Engineering Research
University of Delaware,Newark, Delaware, E-mail: novotny@me.udel.edu

INTRODUCTION

Mathematical models can provide the means to investigate rotator cuff muscle function, glenohumeral kinematics, mechanics and external loading conditions that are difficult to experimentally measure or simulate. A previous study modeled ligament element tensions and contact forces [Novotny, 2000]. The goal of the current study is to analyze the effects that the rotator cuff muscles have on humeral kinematics, contact forces and ligament tensions during the cocked phase of throwing or overhead reaching. Sensitivity to variations in rotator cuff muscle forces is explored to describe their roles in joint stabilization. Since the rotator cuff muscles have been shown to act synergistically, their effects alone will be compared to their effects when varied with the other rotator cuff muscles activated.

METHODS

To describe humeral head motion relative to the glenoid, coordinate systems and joint surfaces were defined. Their extent and orientations were determined from in vitro specimens [Novotny, 2000]. The contact forces were calculated using a deformable contact model. The model included five ligaments (superior, middle and anterior, axillary pouch and posterior band of the inferior glenohumeral ligaments) and rotator cuff muscles (supraspinatus, infraspinatus (3 elements), subscapularis (3 elements) and teres minor. The origins and insertions of the muscles were obtained from the literature [Van der Helm, 1994]. The ligament and muscle elements could run linearly from origin to insertion or wrap around the humeral head surface along the shortest possible path. Ligament forces were applied if the ligament was stretched beyond its initial length. Forces and moments acting on the humerus were those from articular contact, ligament element tension, muscle forces and external application. Equilibrium resulted in six equations solved for the position (X, Y, Z) and (RZ, RY, RX) orientation minimizing the summed forces and moments using a hybrid form of Powell method for non-linear equations. The external loading pattern applied to the humerus simulated the cocked phase of throwing or overhead reaching. Initially the rotator cuff muscles were loaded to a level defined in this study as the 100% force in proportion to their cross-section areas [Veeger, 1991]. The magnitudes were varied to 0, 25, 50, 75, 125, 150 and 200% of the initial level both with the other muscles all at 100% and 0% force levels. This resulted in eight solutions for position and orientation at equilibrium for the eight loading conditions over the four cuff muscles with the other muscles activated or inactivated. Along with the kinematic parameters, the tensions in the five ligament elements and the contact force, area and stress on the glenoid joint surface were determined for each muscle loading combination.

RESULTS AND DISCUSSION

<u>Total Rotator Cuff Activation:</u> In the cocked phase of throwing, the humeral head is abducted, extended and externally rotated,

with an inferior and posterior location on the glenoid surface. Increasing to forces to the entire rotator cuff from 0%-200% resulted in centering of the humeral head with less extension and external rotation, but more abduction. Contact force and stress initially decreased from 0-25% and contact area increased. Then contact force, area and stress all increased from 25-200%. Ligament element tensions were only evident at 0%, with the MGHL and IGHL loaded.
Individual Muscle Activation with Other Muscles Inactive: *Infraspinatus*. The increase from 0-200% resulted in greater extension and external rotation. For translations, an initial increase in inferior and posterior translation occurred with the application from 25-50% force. Contact stress was also increased.
Subscapularis. Subscapularis activation moved the humerus into flexion, greater abduction and internal rotation. Centering the humeral head and decreased contact force resulted. The contact area, though, decreased and thus stress was increased.
Supraspinatus. Increasing supraspinatus force resulted in less extension and more external rotation. Anterior and superior translation occurred. Contact stress decreased and contact area increased. Ligament tension was noted in the anterior band of the IGHL only at 25%.
Teres Minor. There is no significant change in kinematics, contact force, area and stress with teres minor increase. Tensions in MGHL and IGHL were noted and they decreased with increasing teres minor force.
Individual Muscle Activation with Other Muscles Active: *Infraspinatus*. The infraspinatus had a strong effect on joint rotation when increasing its force from 100-200%, with the humerus moved into greater flexion, adduction and external rotation further cocking the arm. More inferior and posterior translation was evident. Contact force and stress were increased with a decrease in contact area. Decreasing the infraspinatus force from 100-0% did not strongly affect kinematics or contact.
Subscapularis. Increasing subscapularis force from 0-200% resulted in increased humeral flexion, internal rotation, and more anterior and superior translation. No large changes in contact mechanics were evident with increasing subscapularis load from 100-200%. The contact stress was increased and contact area decreased from 100-0%.
Supraspinatus. Increasing supraspinatus loading from 0-200% caused increased external rotation coupled with forward flexion. When decreased to 0%, a notable posterior translation occurred. Contact area decreased and stress increased only at 0%.
Teres Minor. Teres minor slightly flexed and externally rotated the humerus with its increase from 0% to 200%. Contact mechanics were unchanged.
Overall. The subscapularis and supraspinatus both played roles in centering the humeral head by moving it anteriorly and superiorly. Subscapularis alone was primary in resisting both extension and external rotations. Infraspinatus further aided the cocking motion when activated and pulled the humeral head inferiorly and posteriorly. More posterior-inferior translations resulted in higher contact stress with smaller contact area. Balance between infraspinatus and subscapularis is significant in limiting rotational motion, while supraspinatus joins them in balancing translations by centering the humeral head on the glenoid.

RERFERENCES

Novotny JE, et al. (2000). *J Biomech*, **33**, 345-54.
Van der Helm FC, et al. (1994). *J Biomech*, **27**(5), 527-50.
Veeger HE, et al. (1991). *J Biomech,* **24**(7), 615-29.

EFFECT OF ROTATOR CUFF PATHOLOGY ON SHOULDER RHYTHM

A.G. Mell[1], S. LaScalza[1], P. Guffey[1], J.E. Carpenter[2], R.E. Hughes[1]

[1]Orthopaedic Research Laboratories, University of Michigan, Ann Arbor, MI USA
[2]MedSport, University of Michigan, Ann Arbor, MI USA
E-mail: rehughes@umich.edu

INTRODUCTION

Shoulder rhythm, which is the coordinated movement of the scapula and humerus during arm elevation, may be affected by shoulder pathology. Ludewig and Cook have reported that impingement syndrome affects shoulder rhythm. Others have reported no difference in scapular orientation between patients with cuff pathology and controls (Graichen et al. 2001). Previous studies have focused on elevation in the scapular plane, and little work has been done to explore differences in shoulder rhythm between patients having impingement syndrome and full thickness rotator cuff tears (RCTs). The purpose of this study was to test the hypothesis that shoulder rhythm is affected by rotator cuff pathology (tendinopathy and RCT) during arm elevation in the sagittal and scapular planes.

METHODS

Forty-two subjects were divided into three groups for this study. Group 1 consisted of 15 healthy volunteers (9 F, 6 M, 47.8 ± 14.6 years) who had no history of shoulder pain or trauma in either shoulder, group 2 included 13 patients (3 F, 10 M, 52.5 ± 8.3 years) with chronic (more than 3 months) rotator cuff tendinopathy but without a full thickness tear as seen during imaging of cuff tendons, and group 3 consisted of 14 patients (4 F, 10 M, 54.7 ±8.3 years) with chronic (more than 3 months) full-thickness rotator cuff tear greater than 1 cm^2 in size as seen during imaging of the cuff tendons.

Sensors from the MotionStar electromagnetic tracking system (Ascension Technology, Burlington, VT) were placed at subject's sternum, scapula (Karduna et al. 2001), humerus (LaScalza et al. 2002), and forearm. Subjects were seated in a wooden chair and performed 3 trials of flexion in the sagittal plane and elevation in the scapular plane. The order of the trials was randomized.

Shoulder and arm kinematics were computed from the MotionStar sensor data. The digitized landmarks were used to construct anatomic coordinate systems (van der Helm and Pronk 1995), and these were represented in the local coordinate systems of each electromagnetic sensor. At each point in time, the anatomic coordinate systems were rotated using the rotation data of the electromagnetic sensors. Thus, at each point in time the anatomic coordinate systems were computed in the global coordinate system of the MotionStar transmitter. Euler angles were computed. For the scapula, the three angles were protraction, elevation, and AP tilt. For the humerus, the angles were plane of elevation, elevation, and axial rotation. Both scapula and humeral angles were computed with respect to the torso coordinate system.

Data was divided into three equal phases based on minimum and maximum humeral elevation. Linear curves were fit to each phase of the scapular elevation versus humeral elevation curve. The dependent

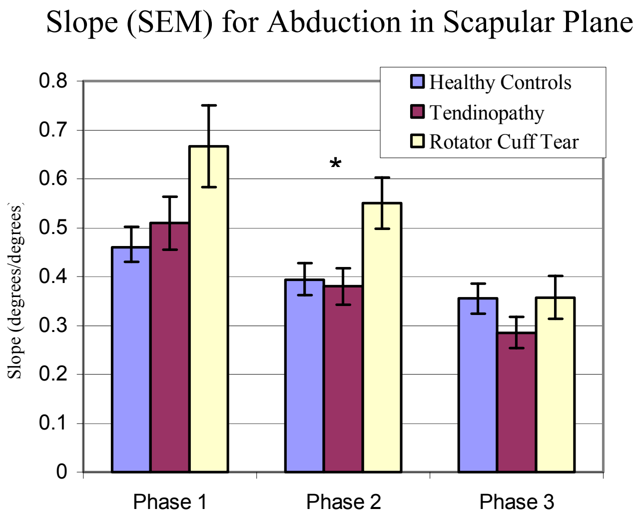

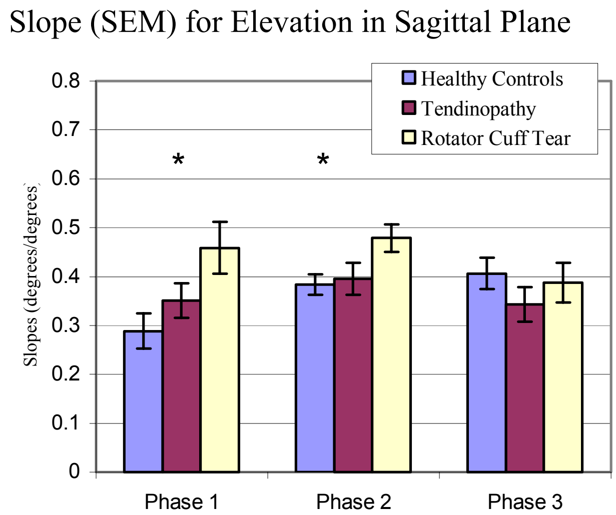

Figure 1: Average slope (SEM) of scapular elevation versus humeral elevation for each group during abduction in scapular plane. * indicates $P<0.05$.

Figure 2: Average slopes (SEM) of scapular elevation versus humeral elevation for each group during sagittal flexion. * indicates $P<0.05$.

measure used in the analysis was the slope of the linear fit in each phase. A one-way ANOVA model was used to test for differences between experimental groups.

RESULTS AND DISCUSSION

Statistically significant differences in scapular contribution to arm elevation were found between experimental groups. The RCT group had higher slopes in Phases 1 and 2 for elevation in the sagittal plane and for Phase 2 during abduction in the scapular plane. No statistically significant differences were found between the tendinopathy group and healthy controls. Differences were found between the tendinopathy and RCT groups. These results suggest that for the RCT group, the scapula moves more for the same amount of humeral elevation. The difference in slopes between the tendinopathy and RCT groups suggests the change in shoulder rhythm is caused by loss of cuff function rather than pain, as both the impingement and RCT groups were symptomatic. It may be that the scapula is elevated more by the RCT group in the initial two-thirds of movement to change the length of remaining muscles so they operate on a more effective part of their length-tension curve. Scapular anterior-posterior tilt and protraction were also analyzed. However, no statistically significant differences were found between groups.

REFERENCES

Graichen, H. et al. (2001). *J. Ortho. Res.*, **19**, 1192-1198.

Karduna, A.R. et al. (2001). *J. Biomech. Eng.,* **123**(2), 184-190.

LaScalza, S. et al. (2002). *J. Applied Biomechanics,* **18**, 374-383.

Ludewig, P.M. and Cook, T.M. (2000). *Physical Therapy*, **80**, 276-291.

van der Helm, F.C.T. and Pronk, G.S. (1995). *J. Biomech. Eng.,* **117**, 27-40.

ACKNOWLEDGEMENTS

This research was supported by the Clinical Research Partnership Fund grant from the University of Michigan.

IN-VIVO AND *EX-VIVO* DETERMINATION OF ELBOW FLEXOR OPTIMAL MUSCLE LENGTHS

Joseph Langenderfer[1], Suzanne LaScalza[1], Amy Mell[1], James E. Carpenter[2], John E. Kuhn[2], Richard E. Hughes[1]

[1]Orthopaedic Research Laboratories, University of Michigan, Ann Arbor, MI USA
[2]MedSport, University of Michigan, Ann Arbor, MI USA
E-mail: rehughes@umich.edu

INTRODUCTION

Optimal muscle length (OML) is one of the most important parameters for modeling the force generating characteristics of skeletal muscle. OML, coupled with joint range of motion and tendon compliance, determines where the muscle acts along its length-tension curve. The purpose of this study was to determine the optimal muscle lengths of elbow flexors by *in vivo* and *ex vivo* methods and to compare the results.

METHODS

Optimal muscle lengths of the biceps, brachialis, and brachioradialis were determined two ways: (1) numerically fitting *in vivo* isometric strength profiles, and (2) dissecting cadavers and measuring muscle length and sarcomere length.

In Vivo: Elbow flexor OMLs were estimated from isometric strength data using a least squares approach (Chang et al. 1999). Maximum isometric elbow flexion torque was measured for 13 angles. Body segment (torso, scapula, upper arm, and forearm) position and orientation was collected with a MotionStar electromagnetic tracking system (Ascension Technology, Burlington, VT) and used as inputs to a SIMM musculoskeletal model to predict muscle-tendon lengths and moment arms. Moment arms in the SIMM model were fit to 95% confidence intervals for moment arm data available in the literature (An, K.N. et al. 1981, Murray, W.M. et al. 1995, 2000, Amis, A. A. et al. 1979, Schuind, F. et al. 1994). Muscle force was estimated with a Hill muscle model. Parameters for the model (PCSA, tendon length, index of architecture) were taken from the literature (Chang et al. 1999). OMLs were predicted by minimizing the sum of square errors between predicted and experimentally measured torques. The minimization problem was solved using a sequential quadratic programming (SQP) algorithm in MATLAB (Mathworks, Inc., Natick, MA). Equal specific tension was assumed for all muscles, bounded in the range 400 KPa to 5 MPa, and solved for by the SQP algorithm. Passive elastic muscle torque at 10 degrees flexion was constrained to less than or equal to 2 N-m, and long and short head biceps forces were constrained to be of equal order of magnitude at each angle.

In Cadavera: Musculoskeletal data was collected from 2 fresh-frozen human cadaver upper extremities (from separate bodies). Muscle belly length and average muscle fascicle length were measured with a digital caliper to the nearest millimeter**.** Following fixation, thin slips of fascicles were dissected from the muscle interior, using fine sharp dissection. A pilot study was conducted to assess the interrater reliability of sarcomere measurements. Sarcomere lengths were determined using laser diffraction (Lieber et al. 1990).

Optimal fascicle lengths were determined by normalizing measured fascicle length to the optimal sarcomere length of 2.8 μm (Walker and Schrodt 1974). OML was estimated as measured muscle length normalized to sarcomere length of 2.8 μm.

RESULTS AND DISCUSSION

Optimal muscle lengths determined by the two methods were similar (Table 1). However, the small sample size of cadaver measurements makes it difficult to make a strong statistical statement that there are no differences.

Each method has limitations. For the *in vivo* estimation, musculoskeletal parameters (PCSA, tendon length, index of architecture) for the Hill model were from a single source and not scaled to individual subjects. Scaling is an obvious improvement and might reduce variances in results. The quality of kinematic input is also a limitation, since the SIMM model depends on *in vivo* measurements of torso, and upper extremity kinematics.

A strength of the cadaver data was that we performed a reliability experiment as part of the study and determined that the intraclass correlation for sarcomere lengths measured by two people was 0.99. Interestingly, no sarcomere lengths were found to be excessively greater than the optimal sarcomere length, suggesting that muscles operate near their optimal muscle lengths. Although *in vivo* measurement of sarcomere length using laser diffractometry is ideal, the exposure necessary to achieve that for the shoulder is unrealistic. Thus, cadaver measurements are the most feasible method available.

SUMMARY

OML is an important musculoskeletal parameter for modeling muscle force. This study furthers our knowledge of OML for the elbow flexors and suggests that OML may be similarly determined using either method.

REFERENCES

Chang, Y.W. et al. (1999) *Clin. Biomech.,* 14, 537-42.
Lieber R.L., et al. (1990) *J. Hand Surgery,* 15A, 244-50.
Walker S.M. and Schrodt G.R. (1974) *Anat. Rec.,* 178, 63-91.
An, K.N., et al. (1981) *J. Biomech*., 14, 659-669.
Murray, W. M. et al. (1995) *J. Biomech.,* 28, 513-525.
Murray, W.M. et al. (2000) *J. Biomech.,* 33, 943-952.
Amis, A. A. et al. (1979) *Eng. in Med.,* 8, 41-48.
Schuind, F. et al. (1994) *J.S.E.S.,* 3 191-199.

ACKNOWLEDGEMENTS
This research was supported by grants from the Whitaker Foundation and the Rackham Graduate School of the University of Michigan.

Table 1: OML determined *in vivo* and *in cadavera* (mean and S.E.M.) (meters)

OML method	**Biceps LH**	**Biceps SH**	**Brachialis**	**Brachioradialis**
in vivo (n = 13)	0.2559 (0.0066)	0.2405 (0.0045)	0.1577 (0.0027)	0.2182 (0.0232)
in cadavera (n = 2)	0.1741 (0.0086)	0.2070 (0.0012)	0.1594 (0.0044)	0.1887 (0.0241)

EFFECTS OF SCAPULAR ORIENTATION ON SUBACROMIAL CONTACT FORCES

Andrew Karduna [1], Paul Kerner [2], and Mark Lazarus [3]

[1] Department of Exercise and Movement Science, University of Oregon, Eugene, OR, USA
[2] Departement of Orthopaedic Surgery, Drexel University, Philadelphia, PA, USA
[3] Department of Orthopaedic Surgery, Thomas Jefferson University, Philadelphia, PA, USA
E-mail: karduna@uoregon.edu

INTRODUCTION

There appears to be a general consensus among clinicians that abnormal control of scapular motion may be associated with an increased risk of subacromial compression of the rotator cuff tendons. For example, Fu et al. proposed that if the synchronous pattern of motion between the scapula and humerus is disrupted, the rotator cuff tendons might become impinged under the coracoacromial arch (1991). Differences in kinematics between patients with impingement syndrome and healthy individuals have also been documented in scientific studies (eg, Ludewig and Cook, 2000 and Lukasiewicz et al, 1999). The purpose of this study was to investigate the effect of scapular rotation on subacromial contact forces due to superior translations.

METHODS

Eight human glenohumeral joints (mean age = 76 years) were harvested from fresh cadavers and dissected to the level of the rotator cuff. On the humerus, all soft tissue between the rotator cuff and distal condyles was removed. On the scapula, the inferior-medial portions of the infraspinatus, teres minor and subscapularis were resected. The glenohumeral capsule was vented. Both the scapula and humerus were potted in appropriately sized fixtures with quick setting epoxy. Joints were tested on a mechanical testing machine (Instron, Canton, MA), with the humerus maintained horizontally at 90 degrees of elevation in maximal internal rotation. The scapula was potted in a rotation jig that allowed for accurate and reproducible angular positioning of the scapula based on the standard Euler angle sequence of external rotation, upward rotation and posterior tilting. This rotation jig was mounted on top of a biaxial translational table fixed to the Instron actuator, thus allowing off-axis translations. The ML and AP axes were aligned with the table axes and the SI axis was aligned with the Instron actuator.

Four muscle forces were simulated in this experiment: subscapularis, supraspinatus, combined infraspinatus-teres minor complex and middle deltoid. A constant load of 25 N was maintained for each muscle line of action with a hanging weight. Prior to each test, the humeral head was centered in the glenoid. The experimental procedure consisted of loading the simulated muscles and then translating the joint superiorly to 125 N of force. At the end of each trial, the scapula was reoriented and the test repeated. Scapular rotations were varied by +/- 5 and +/- 10 degrees from a neutral position determined from *in-vivo* data collected in our laboratory (McClure et al., 2001).

In order to isolate the forces due to impingement at the subacromial space, specimens were re-tested after the completion of the experiment with the coracoacromial ligament cut and the entire acromion removed. The differences in forces between these trials and the experimental trials was used to determine the forces due to impingement with the subacromial arch. By looking at the amount of translation that occurs when the impingement force develops (set at 20 N in this study), a so-called subacromial clearance was determine for each test.

RESULTS

There was no significant effect of either external rotation (p=0.32) or posterior tilting (p=0.52) on subacromial clearance (figure 1A,C). However, there was a significant effect of upward rotation (p = 0.004) on subacromial clearance (figure 1B). A follow up contrast reveal a significant linear relationship, with a decrease in subacromial clearance resulting from an increase in scapular upward rotation (p = 0.04).

DISCUSSION

Despite previous discussion in the literature, our data do not support the concept that changes in scapular external rotation and posterior tilting significantly affect clearance in the subacromial space. We did find a shift in clearance with upward rotation; however, it was not consistent with what was expected. Our original hypothesis was that increasing upward rotation would serve to increase clearance in the subacromial space. However, our results run contrary to this hypothesis. Based on these results, the decease in upward rotation found in patients with impingement syndrome could serve to open up the subacromial space, thus acting as a compensating mechanism to the pathology. However, this speculation is probably premature and needs to be confirmed by other models.

REFERENCES

Fu et al (1991). *CORR*, **269**, 162-73.
Ludewig and Cook (2000). *PT*, **80**, 276-91.
Lukasiewicz (1999). *JOSPT*, **29**, 574-83.
McClure et al (2001). *JSES, **10***, 269-77.

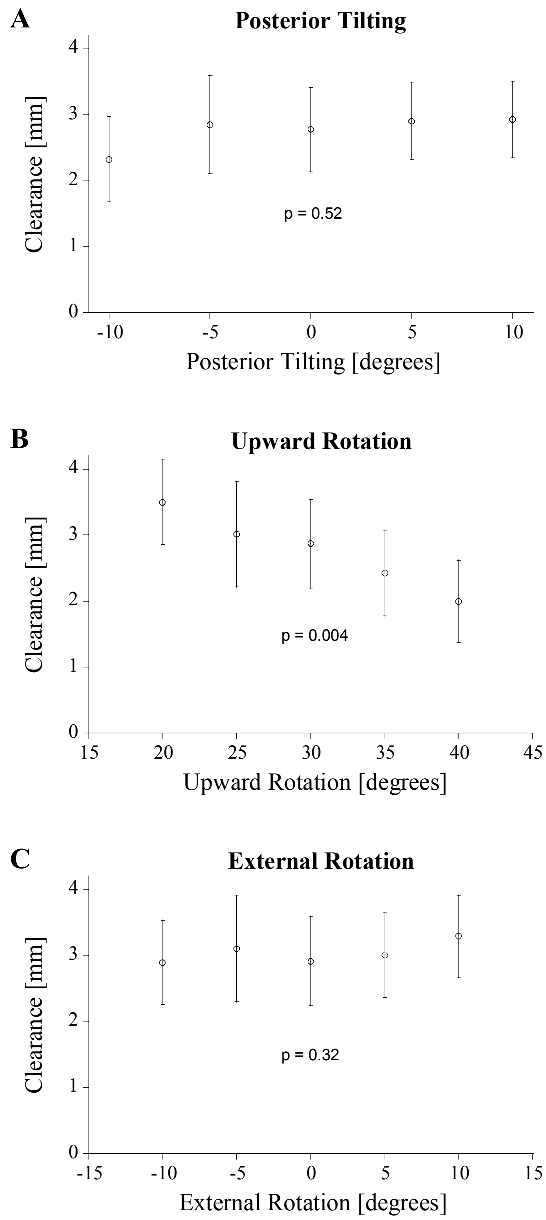

Figure 1 Mean ± SD of subacromial clearance as a function of (A) posterior tilting, (B) upward rotation and (C) external rotation.

ACKNOWLEDGEMENTS

Funding provided by a grant from the Whitaker Foundation.

SCAPULAR KINEMATICS IN ADULTS AND CHILDREN

Sudarshan Dayanidhi [1], Margo Orlin [1], Susan Duff [2], Scott Kozin [2], and Andrew Karduna [3]

[1] Department of Rehabilitation Sciences, Drexel University, Philadelphia, PA, USA
[2] Shriners Hospital for Children, Philadelphia, PA, USA
[3] Department of Exercise and Movement Science, University of Oregon, Eugene, OR, USA

E-mail: karduna@darkwing.uoregon.edu

INTRODUCTION

During humeral elevation, the mobile scapula acts as a stable base on which glenohumeral motion occurs (Paine & Voight, 1993). Appropriate motion of the scapula is important for dynamic positioning of the glenoid and three-dimensional scapular kinematics plays an important role in shoulder motion.

A number of studies have described scapular kinematics during humeral elevation in adults in both healthy individuals as well as those with shoulder pathologies (McClure et al., 2001, Graichen et al., 2000, Ludewig et al., 1996). The typical patterns of scapular movement in adults are documented in these studies. However, children and adults have morphological and physical differences. To our knowledge, no study has been performed examining scapular kinematics in children with either typical or atypical development. Consequently the influence of age and development on scapular motion is currently unknown. The aim of this study was to describe and compare the kinematic patterns of the scapula during humeral elevation in children with typical development and healthy adults.

METHODS

<u>Kinematics</u> Kinematic data were collected using a magnetic tracking device (Polhemus 3Space ® Fastrak, Colchester, VT), with a 3-dimensional motion sensor on the lateral humerus, T3 spine and the top of the acromion. The sensors for the thorax and scapula were attached with double sided tape, while the humeral sensor was placed at the deltoid tuberosity using an elastic band around the arm. The acromial method, with the sensor stuck directly over the flat acromion was used for the scapular sensor (Karduna et al., 2001).

<u>Protocol</u> Fifteen adults (7 F/ 8 M), 25-37 years of age, and fourteen children (8 F/ 6 M), 4-9 years of age, participated in this study. The independent variables were age and humeral elevation. The dependent variables were scapular angles of upward rotation, posterior tilt, and external rotation. Three trials of humeral elevation in the scapular plane were collected and averaged across the trials. The data were pooled in each of the groups and the maximum range that was common among all the subjects was selected (25º-125º of humeral elevation). The data were divided into three divisions within each group: 25º-60°, 60° - 90°, and 90°-125º of humeral elevation. For each of the scapular variables, an ANOVA was used to test significance (α=0.05). Also, glenohumeral (gh): scapulothoracic (st) ratios were determined.

RESULTS

Significant differences were observed between adults and children for all three scapular variables. During humeral elevation, both adults and children demonstrated the expected patterns of upward rotation, posterior tilt. In addition the adults showed decreasing external rotation, while the children showed increasing external rotation. During scapular plane rotation from 25°-125°, children showed greater upward rotation ($43.9^{\circ} \pm 6.39^{\circ}$) than adults ($29.1^{\circ} \pm 10.1^{\circ}$). The mean glenohumeral to scapulothoracic ratio was 2.4:1 for adults and 1.3:1 for children.

DISCUSSION

The present study demonstrated that there are significant differences in scapular kinematics between children with typical development and healthy adults. These results suggest that age and development might influence scapular kinematics. Children seem to have a greater contribution from the scapulothoracic joint, specifically upward rotation during humeral elevation. The clinical importance of these results is the incorporation of the scapulothoracic joint during exercises for a child, for improving shoulder function.

REFERENCES

Graichen et al. (2000). *CORR, **370***, 154-163.
Ludewig et al. (1996). *JOSPT, **24***, 57-65.
Karduna et al. (2001). *J Biomech Eng, **123***, 184-190.
McClure et al. (2001). *JOSPT, **10***, 269-277.
Paine and Voight (1993). *JOSPT, **18*** (1), 386-391.
Price and Goodman (1995). *Hand Clinics, **11***(4), 607- 617.
Sundholm et al. (1998). *Dev Med Child Neurol, **40***, 4-11.

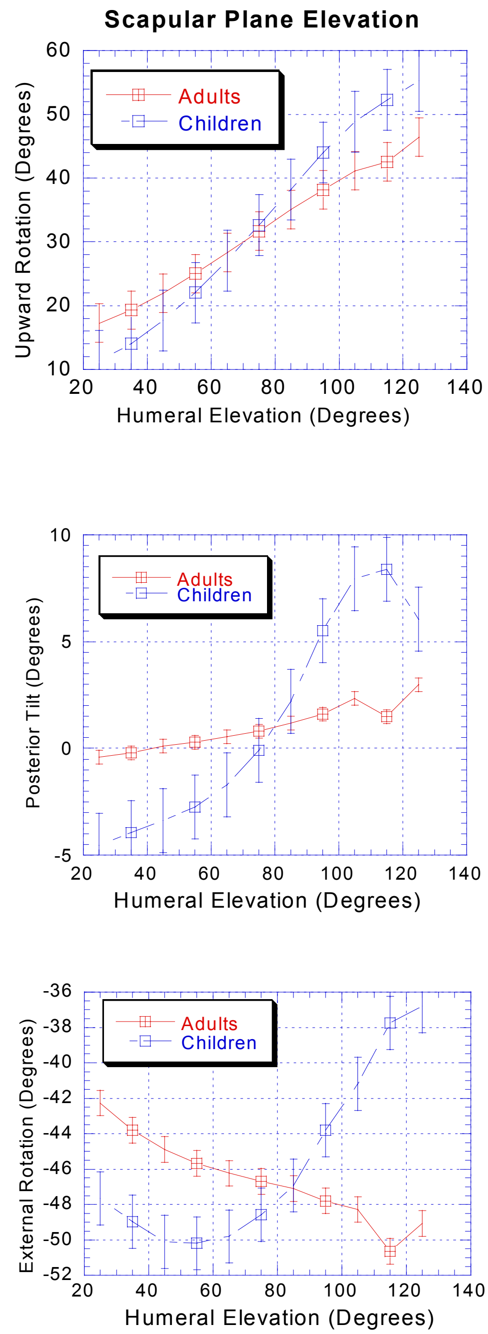

Figure 1 Scapular rotations of upward rotation, posterior tilt and external rotation during scapular plane elevation, in children and adults (means ± sem).

EFFECTS OF TASK INTENSITY ON CHANGES IN SCAPULAR KINEMATICS

David Ebaugh [1], Phil McClure [2], and Andrew Karduna [3]

[1] Department of Rehabilitation Sciences, Drexel University, Philadelphia, PA, USA
[2] Department of Physical Therapy, Acrcadia University, Glenside, PA, USA
[3] Department of Exercise and Movement Science, University of Oregon, Eugene, OR, USA
E-mail: debaugh@drexel.edu

INTRODUCTION

Muscle fatigue and shoulder pain are commonly reported in manual laborers whose job requires repetitive hand use at or above shoulder level. Fatigue of the shoulder girdle musculature may result in altered kinematics of the shoulder complex (McQuade, 1998), which could lead to the development of abnormal forces and stresses being placed upon the tissues associated with the shoulder girdle. The purpose of this study was to investigate the effects of two protocols for shoulder girdle muscle fatigue on three-dimensional scapular kinematics.

METHODS

Kinematics The 3Space Fastrak (Polhemus, Colchester, VT) was used to collect kinematic data. A thoracic receiver was placed over T3 with double sided tape, a humeral receiver was placed at the deltoid tuberosity using an elastic strap, and a scapular receiver was fixed to a scapular tracking device attached to the scapular spine and acromion using Velcro strips (Karduna et al., 2001). Data were collected during three trials of elevation in the scapular plane, with data averaged over the three trials. Data for 3 scapular rotations were analyzed: posterior tilting, upward rotation, and external rotation.

EMG The MyoSystem 1200 (Noraxon, Scottsdale, AZ) was used to collect surface EMG data. Passive electrodes were applied to the upper and lower trapezius, lower serratus anterior, anterior deltoid, and infraspinatus muscles. Data were collected during a 30 second isometric contraction and the mean power frequency (MPF) of each muscle was determined.

Protocol Sixteen subjects (10 male, 6 female; mean age = 22 years) without a history of shoulder injury volunteered to participate in the study. The first step was to collect baseline measurement of EMG and kinematics during scapular plane elevation. Subjects then went through a fatigue protocol, classified as either "high" or "low" intensity. Immediately afterwards, EMG and kinematic data collection was repeated. After a one-hour rest period, each subject repeated the protocol (baseline testing and post-fatigue testing) at the other intensity level. Order of performance of the high or low intensity protocol was determined randomly.

Fatigue Tasks The first task required subjects to stand and manipulate a puzzle with their arms in an elevated position for a defined period (high = 1 min at 115^o, low = 2 min at 45^o). The second task required them to elevate their arm in the scapular plane against resistance (high = 10 reps at 40% MVC, low = 20 reps at 20% MVC). The third task required them to raise their arm in a diagonal pattern against resistance (high = 10 reps at 40% MVC, low =20 reps at 20% MVC). Subjects cycled through the three tasks until they were unable to complete two tasks in a row.

RESULTS

The MPF decreased across all muscles for both the low (2 - 22%) and high (7 - 25%) intensity protocols. Significant increases in scapular rotations were noted following both fatigue protocols for all three rotations. For upward and external rotation (figure 1 A and B), the low load protocol resulted in greater changes, approaching 10° at some elevation angles. For posterior tilting (figure 1C), the effects of fatigue were greater for the high load protocol, however, for both protocols, the changes were small.

DISCUSSION

Scapular rotations were found to be affected by fatigue regardless of the intensity level of the fatiguing protocol. The low load, high repetition protocol resulted in greater changes than the high load, low repetition protocol. This finding is particularly interesting, since a NIOSH report concluded that although there is evidence of a link between high repetition and shoulder injuries, there is insufficient evidence to link force and shoulder disorders (Bernard, 1997). Particularly important are the increases in upward rotation, since we recently demonstrated in a cadaver model that an increase in upward rotation may resulted in a decrease in subacromial clearance (Karduna et al., 2002). Consequently, shoulder fatigue may be associated with increased compressive forces on tissues within the subacromial space due to changes in scapular kinematics.

REFERENCES

Bernard (1997). *NIOSH Report*.

Karduna et al (2001). *J Biomech Eng,* **123**, 184-190.

Karduna et al (2002). *International Shoulder Group Meeting,* Cleveland, 49.

McQuade et al. (1998). JOSPT, **28**, 74-80.

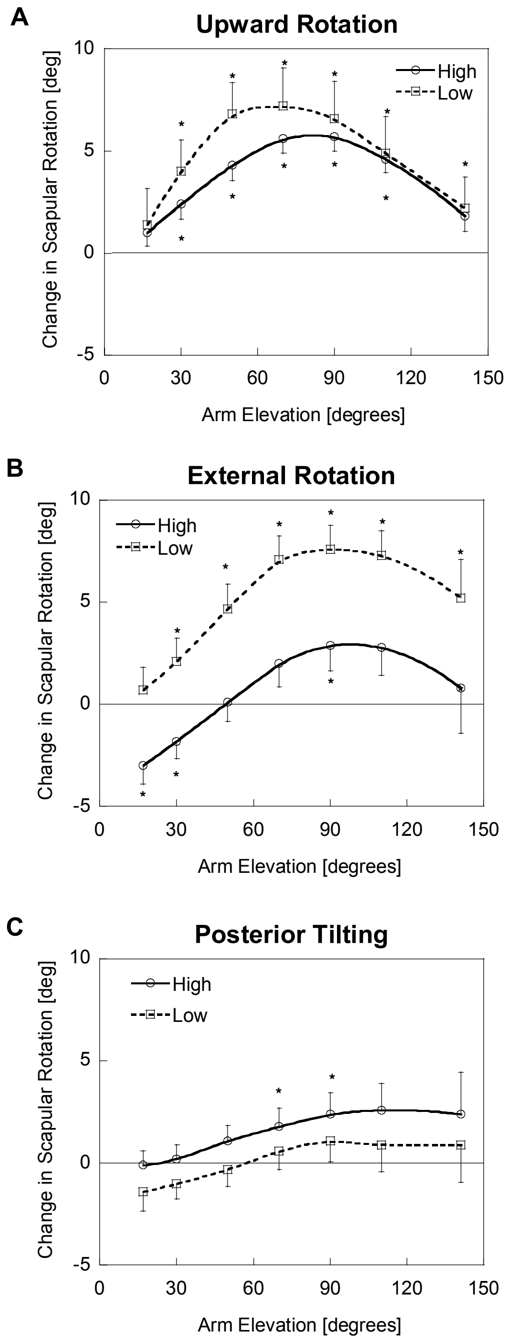

Figure 1 Changes in scapular rotations after the fatigue protocols (means ± sem).
* $p < 0.05$ comparing pre to post fatigue

ACKNOWLEDGEMENTS

Funding provided by a grant from NIOSH (5R030H03869-2)

CALIBRATION OF A HALL EFFECT JOYSTICK POSITION MEASUREMENT SYSTEM USING A NEURAL NETWORK

Greg Northey, Matheson Rittenhouse, and Michele Oliver

School of Engineering, University of Guelph, Guelph, ON, CAN
E-mail: gnorthey@uoguelph.ca

INTRODUCTION

Biomechanics studies often utilize camera based systems for the prediction of position and orientation, however, as a more cost-effective alternative, Hall effect sensors have also been used (Korhonen, 1991; Kyberd and Chappell, 1993). However, for many applications, their non-linear behavior and cross-talk effects make these sensors difficult to utilize and calibrate for effective and accurate position and orientation determination. This paper discusses the calibration of an array of Hall effect sensors used to measure the orientation and position of a hydraulic actuated joystick used for repetitive motion analysis of heavy equipment operators. The system utilizes four sensors that are all active during any joystick movement. This built-in redundancy allows the calibration to use a fully connected feed forward neural network in conjunction with a Microscribe™ 3D digitizer, allowing an infinite number of joystick orientations and positions to be found within the range of joystick motion.

METHODS

A hydraulic actuated joystick was instrumented with four Hall effect sensors (Honeywell SS495A1 miniature ratiometric semiconducting Hall effect sensors) and rare earth magnets (see Figure 1 of ASB Companion paper). The sensors and magnets were placed in the same vertical plane to produce a measurable voltage in each sensor proportional to joystick position. At each position, a Microscribe™ 3D digitizer (Immersion Corporation, San Jose, CA, USA, 0.23 mm accuracy) was used to determine the x, y and z co-ordinates of the tip of the joystick relative to the center of the universal joint about which the tip rotates. The outputs from the Hall effect sensors were collected using a Noraxon 16 channel A/D card. A total of 261 points were taken to digitize the curved surface created by joystick motion, 101 were used for initial training and the remaining points were used to validate the network. The voltages from the four Hall effect sensors were used as inputs into the neural network while the outputs were the x, y and z co-ordinates of the joystick.

To make the calibration procedure as simple and efficient as possible, the neural network was designed to optimize both the training time and the amount of training data needed. The sigmoid activation function was used in each neuron. It was determined that a single hidden layer with five neurons in the hidden layer was sufficient to predict accurately the x, y and z coordinates of each point. The data points used for training the network were determined by taking points on a variable number of circles projected onto the surface of the sphere representing the possible location of the tip of the joystick. The number of points used for training and the number of neurons in the hidden layer were varied until the squared difference between the predicted location of the joystick and the measured location of the joystick was minimized.

Once the design of the neural network was established, the system was validated using the remaining point data.

RESULTS AND DISCUSSION

Table 1 describes the statistics used to describe the quality of the neural network used to predict the x, y and z coordinates of the tip of the joystick.

Table 1: Average Absolute Error (AE) and Standard Deviation of the AE for each Network Used to Predict the x, y and z Position of the Joystick.

	Average AE	Standard Deviation of the AE	r^2
X	3.79	3.00	0.99
Y	2.71	2.04	0.99
Z	1.31	1.02	0.96

The neural network successfully predicted the x, y and z coordinates of the joystick Correlation between predicted and measured values was above 0.95 for all three coordinates and was above 0.98 for the x and y coordinates.

Figure 1 depicts the correlation found for the coordinates in the x direction. The average AE and the standard deviation of the AE show that the magnitude of the error between predicted and measured coordinates was minimal.

SUMMARY

The preceding work developed a neural network for calibrating a joystick displacement measurement system. Results indicate that the optimal neural network had five neurons per hidden layer and required approximately 100 data points for training. The small number of data points required to train the network coupled with the ability of the network to predict accurately the coordinates of the joystick show that a neural network is a suitable approach for calibrating an array of Hall effect sensors used to determine the spatial location of joysticks used in ergonomic studies.

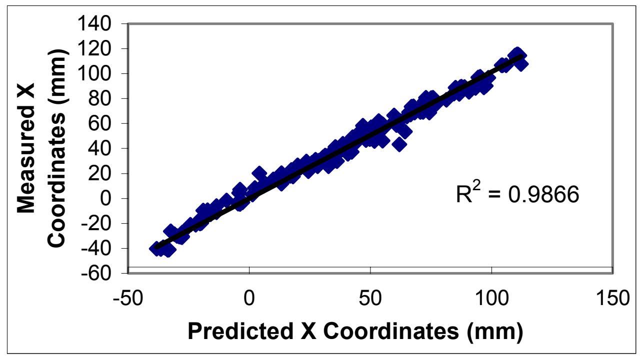

Figure 1: Neural network predicted x coordinates vs. the actual measured x coordinates.

REFERENCES

Korhonen, T. (1991). *Physiology & Behavior*, **49**, 651-652.

Kyberd, P. J. and Chappell, P. C. (1993). *Measurement Science and Technology*, **4**, 281-287.

ACKNOWLEDGEMENTS

This research was funded by the Natural Sciences and Engineering Research Council of Canada.

TOWARD UNDERSTANDING MECHANICS OF THE CARPAL TUNNEL: A COMPUTER GENERATED MODEL

Jeremy P.M. Mogk and Peter J. Keir

School of Kinesiology & Health Science, York University, Toronto, ON, Canada
Email: pjkeir@yorku.ca Web: http://www.yorku.ca/kahs

INTRODUCTION

Carpal tunnel (CT) pressure is known to increase with deviations from a neutral wrist posture. This may be due to altered CT volume and/or a change in the volume of its contents. It is often assumed that CT volume may be determined by integration of the cross-sectional area (CSA) of contiguous CT "slices". However, unless the magnetic resonance (MR) image slices provide a perfect cross-section, there is a potential confound due to parallax error. MR images have been used to reconstruct CT volume, but only for a neutral wrist posture, and assuming specific CT boundaries (Richman et al., 1987). However, it is unknown whether boundary definitions are constant between individuals, or even between postures. While non-neutral volume reconstruction is essential to understanding mechanisms of CTS, parallax error and tunnel boundaries must be evaluated.

An objective evaluation of the potential changes in CT shape and volume was performed using a computer-generated model. Analysis included the effect of parallax error, as well as the effect of tunnel boundaries on CSA and volume.

METHODS

A 3D model of the CT was created using Maya™ software (v4.5, Alias|Wavefront, Toronto, Canada) by merging two surfaces to form a polygonal cylinder. One surface represented the bony carpal arch and the other represented the transverse carpal ligament (TCL). CT shape and volume were altered only according to the Newtonian properties embedded in the software, with the tunnel ends remaining perpendicular to the carpal surface in all postures. Wrist posture was manipulated using a four-segment model (radius, proximal carpal row, distal carpal row and metacarpal), linked by a series of universal joints (Figure 1). Segments and joints were not tangible surfaces which could alter the shape or volume of the CT, but served only as visual cues about spatial orientation and the points about which rotation occurred. The segment model was aligned with the center of the cylinder, positioned above the dorsal surface (of the cylinder) to simulate the anatomical relationship between the joint centers and the CT. The global coordinate system was defined such that the x-axis was medial-lateral, the y-axis palmar-dorsal, and the z-axis proximal-distal. Rotation was limited to flexion-extension (about the x-axis), and occurred only at the 2 most proximal joints. Cylinder dimensions measured 4 units (z-axis) by 1 unit (y-axis) by 1.5 units (x-axis).

CT volume was calculated in each of seven wrist postures, from 45° flexion to 45° extension, in 15° increments. CSA was also determined at 0.1 unit increments to simulate transverse plane MRI slices (perpendicular to the radius). As with MRI, CSA could only be calculated as long as both the carpal surface and the TCL were transected by the vertical cut-line. Any volume beyond the last calculable CSA was also determined, as an estimate of the volume, which may be overlooked in 3D reconstruction (Figure 1). Wrist angle was measured as the angle between the radius and metacarpal segments. Flexion angle was the result of equal rotation at the radio-carpal and mid-carpal joint, while the mid-carpal joint accounted for 3/5 of each extension angle (Sun et al., 2000). Length of the TCL was assumed to remain constant, while carpal arch width decreased by 4% with flexion and 2% with extension (Garcia-Elias et al., 1992). Despite these changes in width, uniform dimensions were maintained throughout the length of the tunnel for any given posture.

RESULTS AND DISCUSSION

Moving distally, cross-sectional area increased by 1-3% at each 0.1 unit increment, resulting in a 30.3% increase in 45° of flexion, and a 41% increase in 45° of extension. This would act to overestimate CT volume in a typical 3D reconstruction, with an even greater effect expected with a longer tunnel than used. As stated previously, CSA could only be calculated along the length of the tunnel for which both the carpal surface and TCL were transected. Relative to the neutral wrist posture, total CT volume increased by 31.5% in 45° wrist extension, and decreased by 20.2% in 45° of flexion. Volumetric changes can partially explain the reported CT pressure in flexion but not for wrist extension. While our calculations examined the entire CT volume, the slice orientation depicted in Figure 1 may result in exclusion of volume beyond the most distal CSA. This would amount to 20.8% in extension and 30.9% in flexion.

SUMMARY

This study represents the initial stages of developing a simulation of the carpal tunnel and its contents. Although rudimentary, this model indicates that volume alone cannot account for reported changes in CT pressure with wrist deviation. It also provides insight into the importance of establishing boundary definitions for the CT, as well as dynamics of the TCL, to assist with 3D reconstruction and modelling of the tunnel. Such a model could be key in determining the mechanical consequences of non-optimal postures and forces on the median nerve in the carpal tunnel. Further development will include full carpal kinematics, muscle belly incursion, and pressure dynamics within the tunnel.

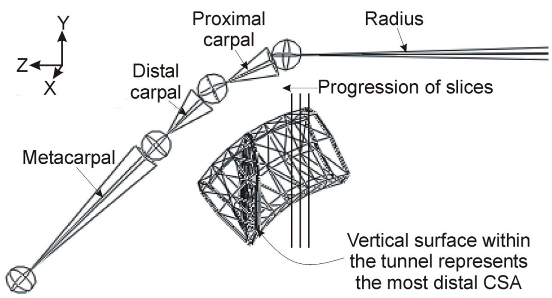

Figure 1: Maya wire frame representation of the carpal tunnel and bony structures in 45° wrist flexion.

REFERENCES

Garcia-Elias, M. et al. (1992). *J. Hand Surg.*, **17A(6)**, 1017-1019.

Richman, J.A. (1987). *J. Hand Surg.,* **12A(2)**, 712-717.

Sun, J.S. et al. (2000). *Clin. Biomech.,* **15(3)**, 212-216.

ACKNOWLEDGEMENTS

Special thanks to Cory Mogk for his invaluable assistance and expertise with Maya. This research was supported by NSERC (Canada) grant # 217382-00.

THE EFFECTS OF GRIP FORCE AND A MENTAL TASK ON MAXIMUM ISOMETRIC SHOULDER EXERTIONS

Christopher MacDonell and Peter J. Keir

School of Kinesiology & Health Science, York University, Toronto, ON, Canada
Email: pjkeir@yorku.ca Web: http://www.yorku.ca/kahs

INTRODUCTION

Muscle activation and force development at the shoulder joint is influenced by its structure. Due to its shape and large range of motion, stability of the shoulder joint is maintained primarily through muscular activation. This muscle activity varies with the task, changing in response to both postural and movement demands.

The shoulder girdle musculature has been shown to increase in activity to rapid and/or precise movement (Laursen, 1998), task complexity (Waersted et al., 1991), gripping (Sporrong et al., 1996) and hand load (Palmerud et al., 2000). In addition, mental "load" has been shown to affect shoulder muscle activity. Shoulder muscle activity has been shown to increase in response to tasks with increased mental demands. The upper trapezius muscle appears to be particularly sensitive to this increase in mental load (Lundberg et al., 2002).

The relationship between arm posture, stability, hand activity and mental load may be additive, or multiplicative, when experienced in combination. The purpose of this study was to investigate the individual and combined influence of grip force and mental effort on maximal isometric shoulder contractions.

METHODS

Five male and five female volunteers participated in two sessions. The first session consisted of laboratory orientation, isometric shoulder and grip strength testing, as well as, practice sessions. A 30% relative grip force level was calculated and used for the grip force condition. Pilot work identified a learning effect during trials where gripping and shoulder contractions were paired, thus a practice session was introduced to reduce the effect of learning. On a separate test day, maximal isometric shoulder exertions were performed under four different conditions: 1) alone 2) with a 30% maximum grip force 3) during a mental task (the Stroop task) and 4) with both grip force and the mental task. All exertions were performed at 30°, 60°, and 90° in shoulder abduction and flexion. Force and torque were measured as the participants pushed the distal part of the humerus against a six-degree of freedom force transducer (MC3A 500, AMTI, MA) attached to the terminal end of the torque arm on a Cybex II dynamometer. A grip force dynamometer (MIE Medical Research LTD, UK) was used with a grip span of 5 cm. To control joint rotation during exertions, the elbow was slightly flexed (approx. 20°) and the hand oriented with thumb pointing upwards.

Mental demands were increased using the Stroop test. In this task, the nouns "red", "green", "blue", and "yellow" are presented in one of the other (incongruent) colours. The task requires the participant to verbally state the colour of the print rather than the noun itself. The use of this task was to create a mental "load" and, while subjects were encouraged to be as accurate as possible, the number of errors was not recorded.

Electrical activity of the left and right trapezius, infraspinatus, latissimus dorsi, anterior, medial, and posterior deltoid, and the biceps brachii were collected on the second day of testing. Ag-AgCl electrodes with an inter-electrode distance of 3 cm were placed over the respective muscle belly. EMG data were sampled at 1000 Hz, and analyzed with custom software (LabView, National Instruments, TX).

Participants sat with their hips secured, and performed three shoulder exertions in each shoulder plane and angle. The order of trials was randomized. In order to reduce processing demands an audible beep ensured participants were at the 30 % grip force level (within +/- 5% of the target). The Stroop task was presented on a monitor positioned in front of the participant. A repeated measures ANOVA ($p<0.05$) was used.

RESULTS AND DISCUSSION

Preliminary data indicated a decrease in torque during the relative grip task, the Stroop task, and the combination of both, compared to maximum exertions alone (Fig. 1). Thus, participants were unable to maintain the same torque output when physical (grip) and mental (Stroop) demands increased. Also, there was no difference in EMG between tasks, indicating that the same activation was required despite lower torque output.

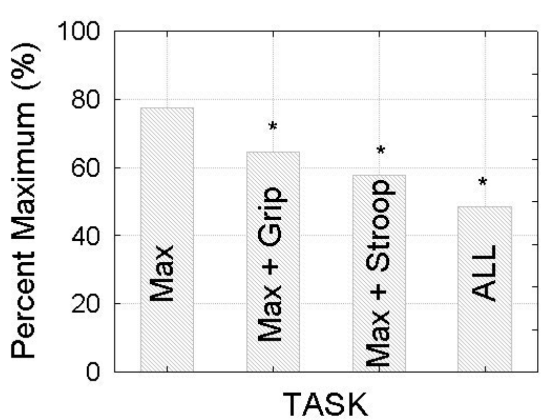

Figure 1. Torque output across tasks (*p<0.05).

Pilot work has demonstrated an interesting interaction between task and angle during isometric flexion trials (Fig. 2). Flexion trials that included grip force showed a linear increase in activation, while trials without grip seem to decrease or plateau after 60°. Although interpretation of this pilot data is guarded, it appears that there may be an important interaction between physical and mental tasks on muscle activity of the shoulder. This research may help explain the complex interaction of factors involved in work-related injuries of the shoulder musculature.

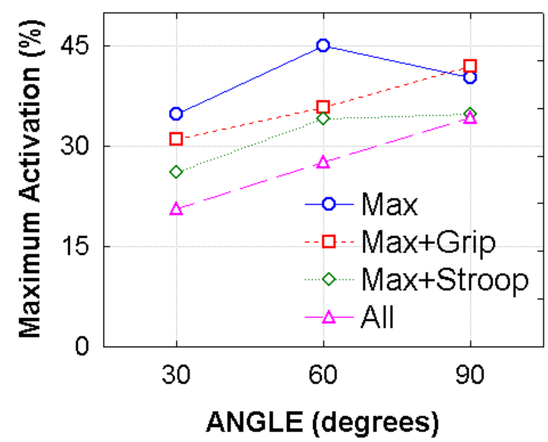

Figure 2. Interaction between angle and task during maximum shoulder exertions

REFERENCES

Laursen, B et al., (1998). *Eur.J.Appl.Physiol Occup.Physiol* 78: 544-548.

Lundberg, U. et al. (2002). *Work and Stress* 16: 166-178.

Palmerud, G. et al. (2000). *Eur. J. Appl. Physiol* 83: 223-230.

Sporrong, H. et al. (1996). *Acta Orthop. Scand*. 67: 485-490.

Waersted, M et al. (1991). *Ergonomics* 34 (2): 137-150.

ACKNOWLEDGEMENTS

This research was supported by NSERC (Canada) grant # 217382-00.

DYNAMIC LOADING AND EFFORT PERCEPTION DURING ONE-HANDED LOADED REACHES

Clark Dickerson and Don Chaffin

HUMOSIM Laboratory, University of Michigan, Ann Arbor, MI, USA
E-mail: cdickers@umich.edu   Web: www.engin.umich.edu/dept/ioe/HUMOSIM

INTRODUCTION

Currently, analysis of occupational shoulder loading and potential discomfort is based upon models that use static worker postures as their input. These models provide useful information about working postures, however, they do not address the overall effect of performing a task. Cumulative joint and tissue loading are dependent upon the motions and postures associated with all aspects of performing a task. Fidelity of task analysis could be improved through a dynamic loading model. This study seeks to determine if the amount of effort perceived while performing a reach is more closely related to overall joint loading, rather than to the loading occurring during commonly studied 'extreme' static postures. It also addresses the utility of shoulder torque as a predictor of perceived effort.

METHODS

Ten Subjects (six male [Age 38 +/- 21], four female [Age 23 +/- 5]) participated in this study. Subjects were asked to perform a randomized series of one-handed reaches to specified targets. The target locations were varied for each subject according to the maximum reach distance that subject. Targets were arranged in the work envelope of the right arm, with targets located along five azimuths. Targets were also distributed along three elevation angles from the hip point. Further, targets were placed at two distances along these projections (Figure 1). Reaches were performed to each target using three hand weights (0%, 25%, and 50% of

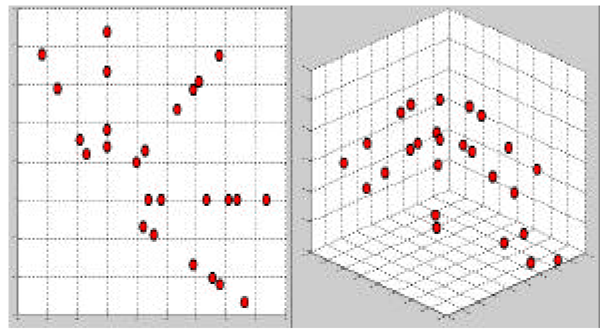

Figure 1: Target Locations. A. Top View; B. Perspective View

extended arm abduction strength). Some trials were repeated to examine intrasubject variability. During each trial, a combination optical/electromagnetic position tracking system was used to record a set of surface markers placed on body landmarks. After each trial was completed, the subjects reported their perceived effort score using an input device. Scores were calibrated to pre-experimental exertions of known muscular effort. A continuous modified Borg scale (0-10) was used to report shoulder effort.

The recorded motions were translated into joint center locations using an existing algorithm (Nussbaum & Zhang, 2000). Dynamic shoulder moments were calculated using a custom software program (Dickerson et al, 2001). These data were used to predict perceived effort through a multiple regression statistical model that included as factors: age, gender, stature, target location, and cumulative shoulder torque loading. Peak shoulder torque loading (i.e. a 'worst posture' scenario) was also used in place of cumulative loading for comparison. A model that relied solely on subject and task information (age, gender, stature and target location) was also made.

RESULTS AND DISCUSSION

It was immediately clear that task and subject characteristics alone do not predict perceived effort adequately across subjects. The resulting model explained a minimal portion of the data's variability ($R^2 = 0.15$).

Similarly, cumulative shoulder torque data alone did not create a model of compelling accuracy ($R^2 = 0.32$).

Inclusion of subject and task variables in the analysis improved the prediction accuracy dramatically (R^2 rose from 0.32 to 0.67). The leverage plot of this combined model is shown in Figure 2. The composition of the factors of this model suggests that mental evaluation of the difficulty of a reaching task may be a multifactorial event, which combines both physical loading, as well as mediating task and subject characteristics.

There was a minimal difference between the quality of prediction achieved using the cumulative and maximum torque values in the regressions ($R^2 = 0.67$ and $R^2 = 0.66$, respectively). This suggests that static and dynamic models could provide comparable task effort predictions, if they are able to identify the positions when maximum torques occur.

SUMMARY

This investigation has affirmed several characteristics of perceived effort for loaded reaches. First, subject and task data can not produce a model that is sufficient to explain the variability in perceived effort data. Second, shoulder torque data alone cannot produce an adequate predictive model of perceived effort. Third, when the two data sources are combined, a more accurate prediction model is produced. Finally, it was shown that both cumulative and maximum shoulder torque loading exhibit the same predictive ability in a combined regression model. Care should be taken, however, when using static postures to evaluate working tasks, in that the postures used represent maximum torque situations. The relationship between internal muscle forces and perceived effort ratings is also being investigated in a related study, which may provide a stronger predictive ability.

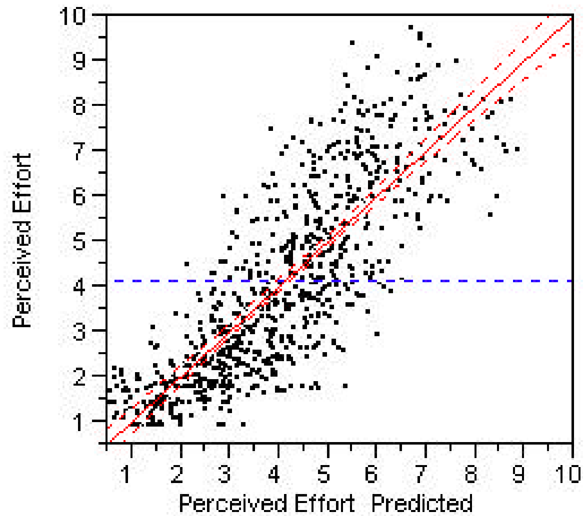

Figure 2: Combined Whole-Model Leverage Plot using cumulative loading and task and subject characteristics.

REFERENCES

Dickerson CR, Chaffin DB, Kim K, Martin BJ, & Womack N, *ASB, San Diego*, 2001.

Nussbaum MA and Zhang X, *Human Movement Science* **19**:797-816, 2000.

ACKNOWLEDGEMENTS

The authors would like to thank HUMOSIM consortium partners and the Automotive Research Center for funding this research.

KEYSWITCH DESIGN AND FINGER POSTURE AFFECT JOINT IMPEDANCE WHEN TAPPING ON COMPUTER KEYSWITCHES

Devin L. Jindrich, Aruna D. Balakrishnan, and Jack T. Dennerlein
Department of Environmental Health, Harvard School of Public Health, Boston, MA.USA
(jax@hsph.harvard.edu)

INTRODUCTION

A possible risk factor for the development of computer work-related musculoskeletal disorders (MSDs) is mechanical load to the tissues resulting from extensive keying. Mechanical impedance (i.e. stiffness and damping) may be an indication of internal load to the tissues of the musculoskeletal system during dynamic tasks (Hajian et al., 1997). Both external loading and finger posture affect the mechanical impedance of the finger (Milner et al., 1998). We tested the hypothesis that net joint torques and joint impedance were different when tapping in the postures associated with typing on different keyboard rows, and different when tapping on different keyswitch designs.

METHODS

Sixteen human subjects tapped with the index finger of the right hand on a computer keyswitch mounted on a two-axis force sensor with miniature finger goniometers (Model S720 Shape Sensors, Measurand, Inc.) across each joint (Figure 1). Output from the force, position and angle sensors were sampled at 10 KHz.

Figure 1: Experimental apparatus

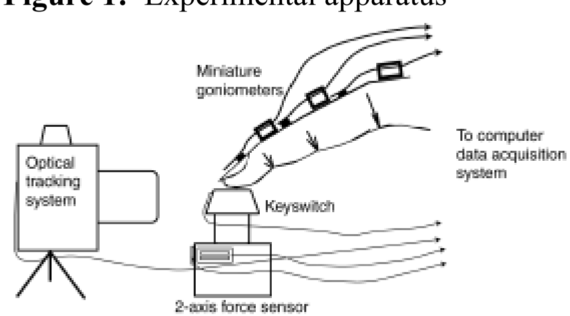

Subjects tapped on four different keyswitch designs (Table 1) in three different postures emulating typing on the upper, middle and lower rows of a keyboard.

Table 1. Keyswitch design parameters

	A	B	C	D
Type	Spring	Spring	Dome	Dome
Activation				
Force	0.31 N	0.49N	0.58N	0.96N
Travel (mm)	4.1	3.75	3.9	2.55

Approximately 20 taps were recorded for each subject per condition, resulting in a dataset of 3,900 taps.

An inverse dynamic model of the finger was used to calculate joint torques from forces and kinematics. A linear spring-damper model was fit to the kinematic and torque data for each joint during the loading portion of each tap. Repeated-measures ANOVA with Tukey post-hoc tests were used to test for differences due to posture or keyswitch.

RESULTS AND DISCUSSION

Subjects employed different joint postures when tapping on different rows of a computer keyboard (Fig. 2).

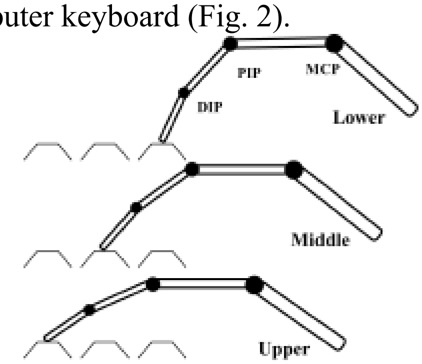

Figure 2: Finger postures employed to tap on three keyboard rows. Finger postures

represent least-squared mean joint angles at mid-tap.

All postures showed significantly different joint angles for the PIP and DIP joints, and Upper and Lower postures were significantly different for the MCP joint. Lower postures were associated with increased flexion of the finger joints.

Upper postures were associated with 40%, 240%, and 450% higher torques than Lower postures for the MCP, PIP, and DIP joints, respectively. Joint posture also had a significant effect on joint stiffness for the MCP and DIP joints (Table 2).

Table 2: Mean (± S.E.M.) Joint Spring Constant (N-m/rad). Positive values indicate energy production during finger loading, and negative values indicate energy absorption by joints during loading.

	Lower	Middle	Upper
MCP	401 ± 159	472 ± 160	772 ± 160
PIP	-82 ± 84	-219 ± 84	-252 ± 85
DIP	-35 ± 15	-108 ± 15	-168 ± 15

Subjects modulated finger stiffness during tapping across different keyswitch designs (Figure 3). Stiffness provided different information than tip force.

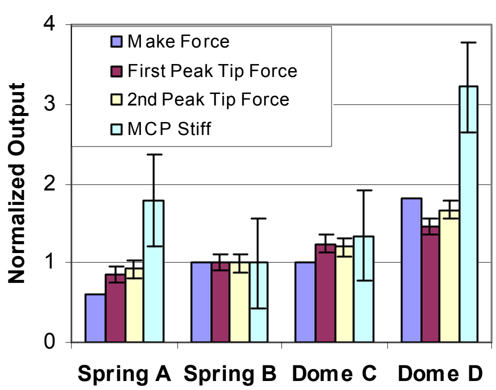

Figure 3. Stiffness parameters varied across different key switch designs.

All three finger joints showed similar trends in finger stiffness, but joint stiffness was not directly related to keyswitch activation force (Figure 4).

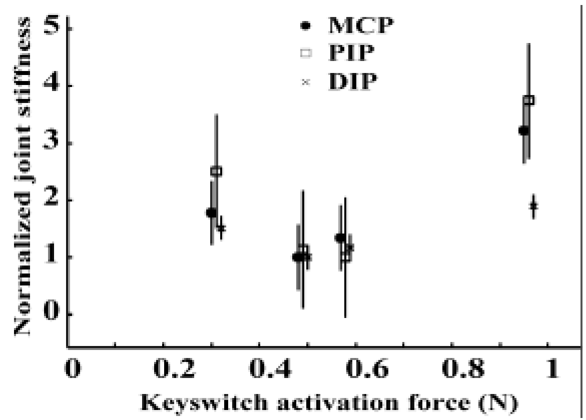

Figure 4. Joint stiffness (relative to minimum joint stiffness) as a function of keyswitch activation force for three finger joints. MCP and DIP symbols are offset by 0.01 N along the abscissa for clarity.

These findings support the hypotheses that finger posture and keyswitch design affect joint impedance during tapping on a computer keyswitch. Net joint torques and joint impedance were up to four times higher when tapping using different postures, with highest joint stiffness parameters in the extended/Upper posture. Joint stiffness exhibited over a three-fold range when tapping on different keyswitch designs.

REFERENCES

Hajian, A. Z. and Howe, R. D. (1997). *Journal of Biomechanical Engineering* **119**, 109-114.

Milner, T. E. and Franklin, D. W. (1998). *IEEE Transactions on Biomedical Engineering* **45**, 1363-1375.

ACKNOWLEDGEMENTS

This project is supported by the Whitaker foundation.

THEORETICAL AND COMPUTATIONAL ANALYSIS OF THE MECHANICS OF HYPER-ELASTIC WRIST BRACES

Taeseung D. Yoo[1] and Daniel K. Bogen[2]

[1]Department of Mechanical Engineering, [2]Department of Bioengineering
University of Pennsylvania, Philadelphia, PA USA
E-mail: tyoo@seas.upenn.edu

INTRODUCTION

A computational model is developed to analyze the mechanical behavior of an elastic wrist brace (soft orthopaedic orthosis). This model uses a finite element geometrical model of the wrist and the brace, and a hyper-elastic constitutive relation for the brace material. Calculations of brace stiffness (moment-deflection relations) are carried out to study the effects of material anisotropy and buckling of the elastic brace material. The model demonstrates that buckling behavior has a significant effect on the mechanical behavior of the brace.

Work-related injury to the wrist from over-use – cumulative trauma disorder (CTD) or repetitive strain injury (RSI) – is widely prevalent and can cause permanent impairment of the wrist. It is commonly treated with an elastic brace that restricts the motion of the joint. Braces are available in a range of stock sizes, but are not otherwise constructed for individual patients, who have different needs in terms of wrist anatomy and motion restrictions. Ideally, each patient would receive a brace constructed according to a "mechanical prescription" that would indicate the mechanical behavior of the brace for the four basic wrist motions: flexion, extension, abduction, and adduction. Before such customized braces can be constructed, however, it is first necessary to understand more about the basic mechanical behavior of elastic braces than is presently known. Therefore, a computational model of the elastic brace was developed to investigate how the geometry and the material composition of the brace influence brace stiffness; i.e., the moment-deflection relations for the four wrist motions.

APPROACH

The model consists of five steps. (1) Finite element geometrical models for the wrist and brace are constructed. (2) The "wearing" of the brace on the wrist is modeled as a mathematical mapping from the wrist surface to the brace surface. (3) Wrist motion is modeled as simple bending of the model. Because of the mapping between wrist and brace, this causes deformation of the brace. (4) Local deformation (strain) of brace is calculated; and from the strains, strain energy density (SED) is calculated. (5) SED is integrated over the brace surface to give the total strain energy (TSE). This model approach is repeated over a range of deflections to give the ΔTSE-deflection relation. The slope of this relation is the brace "stiffness."

Finite Element Models (FEM)

A mathematical description of wrist geometry is developed based upon imaging data obtained from a Cyberware™ PS 3D Range Scanner. 12-node, isoparametric, rectangular, cubic, serendipity interpolation functions in a 3D rectangular Cartesian coordinate system are used to represent wrist surface geometry. The FEM is least-squares fit to measurements of wrist surface geometry obtained with the scanner. The brace model is tubular in shape and is formed (mathematically) by wrapping a sheet of elastic material around the wrist model. Wrapping is described by a 2D-to-3D mapping function.

Local Deformation Field

Wrist bending is modeled by embedding the high-order, multi-element wrist model inside a low-order single-element beam model, and then bending the beam by displacing its nodes. The resulting nodal displacements of the "captured" wrist model are then used to describe the deformation of the wrist. The deformation gradient, **F**, is calculated from the set of nodal displacements using the FEM interpolation functions for the wrist model.

Strain Energy Density

SED is obtained from the right Cauchy-Green deformation tensor **C**, which is calculated from **F** (Humphrey and Yin, 1987). For a rubber-like hyper-elastic brace material, SED can be described by the function (Treloar, 1975):

$$SED = \tfrac{1}{2} G (I_1 - 3)$$

where G is the rigidity modulus of the material and I_1 is the first strain invariant -- the trace of the tensor **C**. This function is modified for a 2D isotropic membrane and 1D anisotropic fibrous material.

Total Strain Energy

To obtain TSE, SED is integrated over the model surface using a 2D Newton-Cotes Closed formula. Bending stiffness results from the increase in TSE that occurs when the wrist is deflected by an angle θ, and is described by the ΔTSE-θ relation.

Buckling Laws

A thin elastic sheet may buckle when placed in compression. Three buckling conditions were investigated. The first buckling condition is the "No-Buckling Model", where it is assumed that buckling of the brace material does not occur. The second model assumes that buckling occurs when at least one principal stress is compressive, causing the local strain energy (SE) to go to zero. The third buckling model assumes: that SE is reduced, but not zero, when one principal stress is compressive; but SE is zero when both principal stresses are compressive.

RESULTS AND DISCUSSION

The most significant finding is that the calculated TSE, based upon the no-buckling condition, is approximately twice that observed in either of the buckling conditions. Thus, the computational model indicates that buckling reduces elastic brace stiffness by about 50%. This occurs because about one-half of the elastic material under deformation is in a buckled state. Computations also show that buckling behavior can be influenced by how tightly the brace is initially placed on the wrist. This is because a tight brace can force the elastic brace material into tensile pre-stress, and thus prevent buckling when the brace is later deformed.

Finally, when the brace is constructed from an orthogonal fiber material, the brace is about four times stiffer when the fiber axis parallels the wrist axis, compared to when fibers lie at 45° to the wrist axis.

REFERENCES

Humphrey, J.D. and Yin, F.C.P. (1987), *A New Constitutive Formulation for Characterizing the Mechanical Behavior of Soft Tissues, Journal of Biophysics*, Vol. 52, pp. 563-570.

Treloar, L. R. G. (1975*), The Physics of Rubber Elasticity*, 3rd ed., Clarendon Press.

MATRIX ANALYSES OF INTERACTION AMONG FINGERS IN STATIC FORCE PRODUCTION TASKS

Fan Gao[1], Sheng Li[2], Zong-Ming Li[3], Mark L. Latash[4], Vladimir M. Zatsiorsky[1]

[1] Biomechanics Laboratory, Depertment of Kinesiology, The Pennsylvania State University
[2] Rehabilitation Institute of Chicago, Northwestern University
[3] Musculoskeletal Research Center, University of Pittsburgh
[4] Motor Control Laboratory, Depertment of Kinesiology, The Pennsylvania State University
E-mail: fug101@psu.edu

INTRODUCTION

When a person produces a force with a fingertip, other fingers of the hand also show an increase in their force. This phenomenon has been termed enslaving (Li et al. 1998a; Zatsiorsky et al. 2000). When several fingers are activated simultaneously, the relations among fingers can be described with an inter-finger matrix (IMF). We suggest using the IMFs to quantify individual differences among humans. An IFM for a hand contains 16 numbers. Hence, in general, individual differences in finger interaction, as reflected in IFMs, may require 16 variables to be fully described. We hypothesize, however, that a significantly smaller number of variables may be sufficient to describe differences among individuals without special skills. Hence, a major goal of this study has been to discover such variables and relate them to indices of finger interaction introduced in earlier studies.

METHODS

Twenty right-handed university male students (age 29.4±4.3 yr; body mass 78.8±13 kg, height 1.80±0.09 m) served as subjects. The subjects had no previous history of neuropathies or trauma to the upper limbs. All subjects gave informed consent according to the procedures approved by the Compliance Office of The Pennsylvania State University. Four uni-directional piezoelectric sensors (Model 208A03, Pizeotronic) were used for force measurement. Subjects were instructed to press downward maximally with various combinations of the four fingers: the index (I), middle (M), ring (R), and little (L) fingers. Ten combinations were performed: I, M, R, L, IM, MR, RL, IMR, MRL, and IMRL.

DATA ANALYSIS

Neural network model: A three layer network described in Zatsiorsky et al (1998) was used. Normalized *IFMs* were computed by dividing the elements of a non - normalized IFM by the sum of its elements. The differences between IFM's: The dissimilarity of the matrices was computed as a square root of the trace of a matrix, $\delta_{ij}= \{\text{trace } [(\mathbf{A}–\mathbf{B})^T(\mathbf{A}–\mathbf{B})]\}^{0.5}$
Multi-dimensional scaling: The proximity matrices were used to perform MDS analysis. The goodness of fit of stress are: 0.2 - poor, 0.1 - fair, 0.05 - good (Kruskal and Wish 1978). Correlation: Individual coordinates of the subjects along the 2D/3D (using both non - normalized and normalized *IMFs*) were correlated with 18 parameters. For n=20, the critical values of the Pearson product-moment correlation coefficient equal r=0.561 at p = 0.01 and r=0.444 at p = 0.05 (a two - tailed test).

RESULTS AND DISCUSSION

The stress versus dimensions (scree plot) is presented in Fig 1.

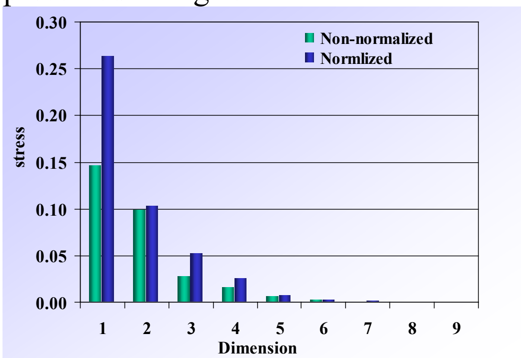

Fig 1. Scree plot (Stress vs dimension).

The non-normalized *IFMs* can be represented well in 2D. _Mapping_:The outcome of an MDS is presented as a map, similar to the map shown in Fig 2.

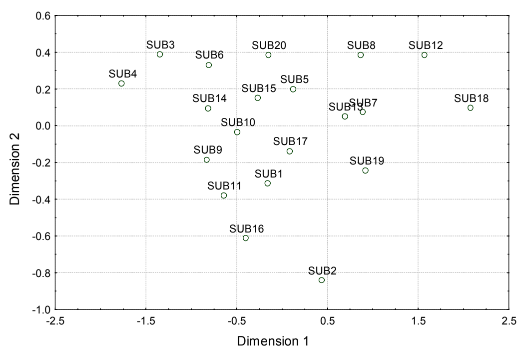

Fig 2. Final configuration of the non-normalized IFM's in two dimensions.

Interpretation of the dimensions: The coefficients of correlation between the coordinates of the studied objects (subjects) in the 2D and 3D spaces and a set of pre-selected parameters were calculated. _Non-normalized matrices:_ The first dimension correlated highly with the finger forces. For the 2D, the highest coefficient of correlation (r=0.978) was observed with the traces of the non - normalized IFMs. The correlation with the sum of the finger forces in single finger tasks and four finger task were also large: 0.86 and 0.82. The correlation with the individual finger forces varied from 0.64 (little finger) to 0.80 (index finger). Hence, the first dimension represents the total finger force. In the 2D representation and 3D representation the second dimension correlated with the force sharing pattern. _Normalized matrices:_ In the 3D representation, the first dimension correlated with the force sharing pattern. The third dimension was highest correlated with the sum of the non - diagonal elements which can be interpreted as the total amount of enslaving. The second dimension did not correlate significantly with any of the studied variables.

SUMMARY

The similarities/dissimilarities among the individual inter-finger matrices can be represented in 2D/3D Euclidean spaces. Hence, the differences among the subjects can be described by the values along just two or three dimensions. For the non - normalized IFMs the main measure that distinguishes individual subjects is the total finger force; for the normalized IFM's two dimensions have been revealed and interpreted: (1) the force sharing pattern reflected in a displacement of the point of resultant force application along the latero - medial axis and (2) the amount of enslaving.

REFERECNES

Kruskal JB, Wish M (1978). *Multidimensional Scaling.* Sage Publications, London

Li ZM et al. (1998a) *Exp Brain Res*, 122, 71-78.

Zatsiorsky VM et al. (1998) *Biol Cybern*, 79, 139-150

THE EFFECT OF PROSTHETIC SPINAL RODS ON SHOULDER COMPLEX MOVEMENTS

Tania B. Straczek [1] and Les G. Carlton[1]
[1]Department of Kinesiology, University of Illinois, Urbana, IL 61801
E-mail: lcarlton@uiuc.edu

INTRODUCTION

During elevation of the arm, whether for reaching and grasping or pushing a wheelchair, movement at the glenohumeral joint is accompanied by scapulothoracic movement. The focus of this study was to examine the effects of spinal rods on movements of the shoulder complex in individuals with thoracic spinal cord injury by measuring the individual's scapulohumeral rhythm and maximum reach. It was hypothesized that the presence of spinal rods, commonly located in the thoracic region, will affect the scapulohumeral rhythm in individuals with spinal cord injury, and ultimately affect the movement of the arm.

METHODS

The participants for this study included individuals in one of three groups: 11 individuals with thoracic spinal cord injury and spinal rods (age 23±4.17 years; 5 male, 6 female), 4 individuals with thoracic spinal cord injury without spinal rods (age 21.5±2.64 years; 2 male, 2 female), and 12 individuals without spinal cord injury serving as controls (age 23.4±2.94 years; 6 male, 6 female). Scapulohumeral rhythm and maximum reach were measured for each individual. Scapulohumeral rhythm was measured by asking the individual to abduct his or her dominant arm in the transverse plane in 30° increments from 0-180°. At each increment, the inferior angle of the scapula was palpated and the angle of deviation with respect to inferior angle and the vertical line between T1 and T9 was measured using a manual goniometer (Figure 1). For the maximum reach measurement, the participant was asked to reach in two different directions (anterior and lateral) at two different heights from the floor (70 cm and 150 cm) while sitting in a chair. Distance was measured using a meter stick.

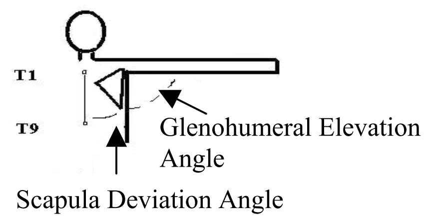

Spinohumeral Angle = Scapula Deviation + Glenohumeral Deviation Angle

Figure 1: Measurement of Scapulohumeral rhythm

Data were analyzed using a mixed-model ANOVA, with glenohumeral elevation and reaching direction treated as within-subjects factors, and participant group the between-subjects factor. Level of spinal cord injury (T2-T8, T9-T12, controls) was used as a between-subjects factor in a separate analysis. Post-hoc tests using Tukey analysis were used when significant differences were found, with the significance level set at 0.05.

RESULTS AND DISCUSSION

Spinohumeral angle was calculated by adding the scapular deviation angle to the glenohumeral elevation angle. This was plotted against the glenohumeral elevation angle for each group (Figure 2). The results showed that there was a statistically significant difference between groups of individuals (p<0.05). Post-hoc analysis indicated that there were significant between the individuals with rods and the control group. There were no significant difference between individuals without rods and the controls. These results suggest that the presence of spinal rods within the torso does in fact affect movement at the shoulder complex. An analysis based on spinal cord injury level indicates that there was a statistically significant difference between groups according to spinal cord injury levels (p<0.05). Post-hoc analysis showed that there was a significant difference between controls and low level spinal cord injury (T9-T12, Figure 1), but there were no difference between high spinal cord injury (T2-T8) and either controls or low level spinal cord injury (Table 1). This suggests that the level of injury plays a large role in the functioning of the shoulder complex. Further analysis using gender as a between-subjects factor revealed that gender was not a significant factor when measuring scapulohumeral rhythm.

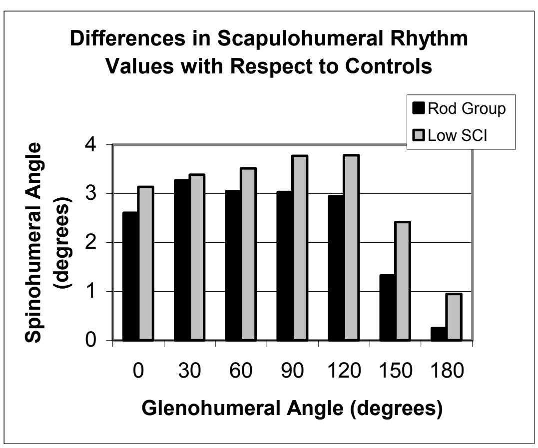

Figure 2: Differences in mean scapulohumeral values for the rod and low SCI groups with respect to control values.

Analysis of the maximum reach showed that there were no significant differences in maximum reaching distance between groups of individuals based on either rod presence or spinal cord injury level. Further analysis of gender showed that there was a statistically significant difference between males and females with respect to reaching distance (p<0.05). The results suggest that presence of spinal rods do not affect the ability to reach large distances, regardless of direction or height.

	Rod SCI		Low SCI		Control	
	Mean	SD	Mean	SD	Mean	SD
0°	31.27	2.72	31.80	2.04	28.66	3.02
30°	63.18	2.63	63.30	2.75	59.91	2.74
60°	95.63	1.74	96.10	2.13	92.58	2.10
90°	128.36	1.85	129.10	2.92	125.33	2.87
120°	162.36	2.54	163.20	3.15	159.41	3.57
150°	195.90	2.87	197.00	3.33	194.58	3.14
180°	228.00	3.25	228.70	3.09	227.75	3.10

Table 1: Summary of means and standard deviations at each angle increment for the rod group, low thoracic SCI group, and controls.

SUMMARY

Prosthetic spinal rods in individuals with thoracic spinal cord injury affect the scapulohumeral rhythm, but do not affect the person's reaching distance. An abnormal scapulohumeral rhythm affects the mechanics of how a person moves, and may also alter the strategies used to control upper extremity movements. For individuals with spinal cord injury, the movement of the upper extremity is extremely important, and must be explored further.

REFERENCES

Inman, V.T. et al. (1944). *The Journal of Bone and Joint Surgery,* **26**, 1-30.

IMPACT OF IMPAIRED WRIST MOTION ON HAND AND UPPER EXTREMITY PERFORMANCE

Matthew McCullough, David Murphy, Brian Adams, and Nicole Grosland

University of Iowa, Iowa City, IA, USA
E-mail: matthew-b-mccullough@uiowa.edu

INTRODUCTION

In the treatment of wrist arthritis, motion-preserving procedures are commonly preferred over complete arthrodesis because it is perceived these procedures provide higher patient satisfaction. Potential reasons for higher satisfaction include better function and reduced impact on other joints. Reported risks with these procedures include further arthritic changes, failure of fusion, and implant loosening. To justify the risks and added technical challenges associated with these procedures, the benefits should be objectively measurable.

Our goals were to quantify and compare the impairments caused by reduced and absent wrist motion using objective measurements of task performance and perceived impairment, and to assess the compensatory motions of the shoulder, elbow, forearm, and trunk imposed by impaired wrist motion.

METHODS

Twenty-one subjects (average age 23.8 years) without upper extremity compromise were recruited. After informed consent was obtained from all subjects, each subject's dominant side was tested on three consecutive days.

A custom brace (Figure 1) containing a single hinge at the wrist was made for each subject.

Figure 1: A Rolyan Incremental Wrist

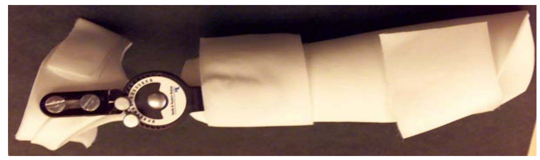

Hinge (Rehabilitation Division, Smith and Nephew, Germantown, WI) joined the components.

The mini-BIRDS® electromagnetic tracking system (Ascension Technology, Inc., Burlington, VT) was used to track wrist, forearm, elbow, and shoulder motions of the tested extremity and trunk. The Disabilities of the Arm, Shoulder and Hand (DASH) and Patient Rated Wrist Evaluation (PRWE) standardized patient questionnaires were administered to each subject to assess the difficulty of completing various tasks.

Task performance was measured under three conditions: 1) unrestricted wrist motion 2) fully restricted wrist motion, and 3) partially restricted wrist motion. Each subject performed the Jebsen hand function test, then a series of 13 tasks obtained from questions in the DASH, PRWE, and previous studies on wrist and elbow motions. Time was recorded in seconds and perceived difficulty of task completion was measured by the completion of a modified version of the DASH and PRWE, as well as a study specific questionnaire regarding tasks in the Jebsen test and the 13 Activities of Daily Living.

The process began with the subject completing a baseline DASH and PRWE surveys. After a practice run of all the activities, subjects were then braced, randomly assigned an order of bracing method, and instructed to wear the brace until testing the next day.

On reporting the next day for testing, the subject completed the DASH and PRWE. The Jebsen test and the 13 ADL were then performed, with each task timed in seconds and joint motions recorded. Subjects then completed the Jebsen and ADL surveys. The brace was removed and the protocol repeated. The subject was dismissed wearing the brace set for the other condition of restricted motion. The third day, the protocol was repeated as on the second day.

Mixed-model, analysis of variance (ANOVA) techniques were run using the SAS system (version 8.2; SAS Institute Inc., Cary, NC). Statistical analyses were conducted for individual joints and planes of motion. Both the brace and task orders were considered "nuisance" conditions, and analyzed for their effects. Repeated baseline measurements on days 2 and 3 assessed learned-effects.

RESULTS AND DISCUSSION

Times to complete the Jebsen test were significantly increased ($p<0.05$) for both the fully and partially restricted wrists. The times were highly variable among subjects, with standard deviations of 4.8, 5.8, and 9.4 seconds respectively.

The times for the ADL test also significantly increased ($p<0.05$) for both the fully and partially restricted wrists (Figure 2), and times were highly variable among subjects.

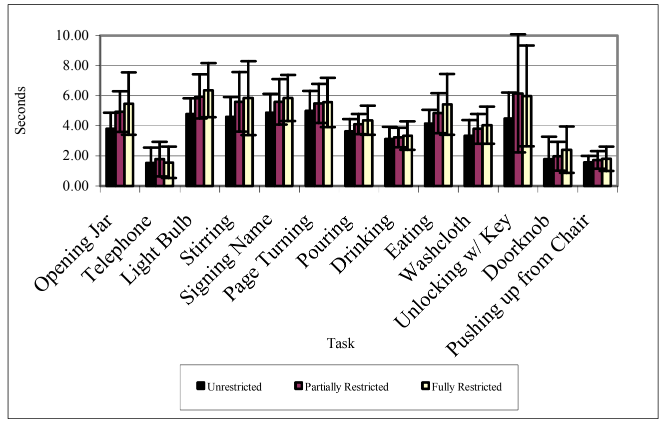

Figure 2: Average ADL times per task

DASH, PRWE, and ADL survey scores significantly worsened ($p<0.05$) for the partially and fully restricted wrists. The differences between the partially and fully restricted wrists were also significant, with the fully restricted wrist having worse scores. The Jebsen survey scores significantly worsened for the partially and fully restricted wrists, but did not statistically differ from each other.

Both restricted wrist motion conditions were associated with small increases in ipsilateral forearm, elbow, shoulder, and trunk motions, of which some were statistically significant. The average differences between the partially and fully restricted wrists were not statistically significant, however the changes in motions were highly variable among subjects and tasks.

SUMMARY

An individual's perceived impairment with performance of common tasks appears to be influenced by their available wrist motion. Simulated motion preserving procedures rated better than simulated arthrodesis by several parameters but the differences were not as great as we had anticipated. Thus, it may be hard to predict a patient's response to reduced wrist motion.

THE ASSOCIATION BETWEEN HAND ACCELERATION AND WHEELCHAIR PROPULSION KINETICS

Yusheng Yang[1,2], Alicia Koontz[1,2], Rory A. Cooper[1,2], Michael L. Boninger[1,2]
[1]Dept. of Rehab. Science and Technology, University of Pittsburgh, Pittsburgh, PA , USA
[2]Human Engineering Research Laboratories, VA Medical Center, Pittsburgh, PA, USA
E-mail: yuy7@pitt.edu Web: www.herlpitt.org

INTRODUCTION

Previous studies indicate that the prevalence of carpal tunnel system (CTS) among MWUs is approximately 49% (Gellman et al., 1988). A higher rate of force loading on the pushrim during propulsion may lead to the development of CTS (Boninger et al., 1999). Recent studies showed that during wheelchair propulsion, the major cause of a higher rate of impact loading on the pushrim was related to the coupling of the hand to the pushrim (Richter et al., 2002; Yang et al., 2003). Yang et al. (2003) found that a larger difference between the hand speed and the pushrim speed resulted in a higher rate of loading and greater forces imparted to the pushrim as well. To further evaluate the coupling of the hand to the pushrim, we investigated the relationship between hand acceleration immediately before impact with the pushrim and wheelchair propulsion kinetics. We hypothesized that the forces generated during propulsion would be correlated to the hand acceleration prior to contact with the pushrim.

METHODS

Subjects: Thirty-two MWUs (24 men and 8 women) with thoracic or lumbar spinal cord injuries ranging from T1 to L2 provided informed consent prior to participation in the study. Their mean age and years post injury were 42.17±10.71, and 13.46±7.46 years respectively. Their average weight was 79.95 ±17.13 kilograms.

Experimental protocol: Subjects' own personal wheelchairs were fitted bilaterally with SMART^{wheels}, force and torque sensing pushrims, and secured to a dynamometer with a four point tie down system. IRED (infrared emitting diode) markers were placed on the subject's third metacarpalphalangeal joints to record the hand position in a global reference frame via a three-dimensional motion analysis (OPTOTRAK, Northern Digital Inc.). Subjects were instructed to propel at a steady-state speed of 0.9m/s. Propulsion speed was displayed on a 17-inch computer screen placed in front of the subjects. Upon reaching the target speed for one minute, data collection was initiated and continued for 20 seconds. SMART^{wheel} data were collected at 240 Hz and filtered with an 8th order Butterworth low-pass filter, zero lag and 20 Hz cut-off frequency. Afterwards, the kinetic data were linearly interpolated for synchronization with the kinematic data collected at a rate of 60 Hz.

Data analysis: The hand speed $\vec{V}=(V_x,V_y,V_z)$ prior to contact with the pushrim was determined by differentiating the hand position $\vec{P}=(x,y,z)$ in the global reference system. The hand acceleration $\vec{A}=(A_{ht},A_{hr},A_{hz})$ prior to contact with the pushrim was determined by differentiating the hand speed $\vec{V}$ in the hand segment reference system, and the hand acceleration (the scalar form of the vector acceleration) was given by: $A_{hand} = \sqrt{A_{ht}^2 + A_{hr}^2 + A_{hz}^2}$. Since previous data have shown that the user's weight is correlated with propulsion forces, the kinetic data were normalized by the subject's weight (Boninger et al., 1999). A coordinate transformation was performed to convert the resulting forces from a global reference frame to a local one with respect to the pushrim where the forces are denoted as radial (F_r), tangential (F_t), and lateral (F_z) forces (Boninger et al., 1999). Five consecutive strokes were used in the data analysis. Peak forces, and the maximum rate of loading (slope of the force curves) were calculated for each stroke. For each parameter, data from all five strokes on the right side were averaged to provide a single kinetic value for the trial.

Statistical Analysis: The Pearson correlation test statistic was used to determine the relationship between the hand acceleration and propulsion kinetic parameters (α=0.05).

RESULTS AND DISCUSSION

Users with a greater mismatch in hand/pushrim speed showed increased hand acceleration prior to contact (r=0.37, p<0.05) (**Table 1**). This increase in hand acceleration just prior to hand contact was an attempt by the users to try and match the pushrim speed. The data analysis also showed that the tangential hand acceleration had a significant positive relationship with the rate of loading on the pushrim (r=0.501, p<0.05), while the radial hand acceleration did not. On average, the tangential acceleration (16.40 ± 7.24 m/sec^2) was approximately five times the radial component (6.74 ± 2.65 m/sec^2). This further indicates that before contacting the pushrim, the hand accelerated faster in the tangential direction than in the radial direction in order to match the wheel speed. However, the large acceleration in the tangential direction resulted in a significantly increased rate of loading on the pushrim which has been linked to the development of CTS (Boninger et al., 1999).

SUMMARY

Increased hand acceleration in an effort to compensate for slow hand speed results in a high rate of loading on the pushrim during wheelchair propulsion predisposing the user to injury. Manual wheelchair users may be less prone to wrist injuries if their hand speed prior to contact closely matches the wheel speed.

REFERENCES

Gellman H. et al. (1988). Carpal tunnel syndrome in paraplegic patients. *J. Bone Jt Surg*, **70(A),** 517-519.

Boninger M.L. et al. (1999). Wheelchair pushrim kinetics: body weight, and median nerve function. *Arch Phys Med Rehab*, **75**, 513-518

Richter W.M. et al. (2002). Kinematic state of the hand at impact with wheelchair handrim as a function of handrim compliance. *Proceedings of the RESNA'2002*. 377-379.

Yang Y. et al. (2003). The effect of hand contact speed on wheelchair propulsion kinetics. *Proceedings of the RESNA'2003*. Atlana, GA: RESNA in press

Table 1: The correlation between kinetic variables and relative hand acceleration movement in prior to contact.

Kinetic variable (n=32)	Hand acceleration	Tangential hand acceleration	Radial hand acceleration
Relative hand velocity to pushrim	r = 0. 370 p=0. 037*	r = 0. 419 p= 0. 017*	r = -0. 075 p = 0. 682
Peak tangential force	r = 0. 051 p = 0. 784	r = -0. 035 p = 0. 848	r = 0. 263 p = 0. 145
Peak radial force	r = 0. 368 p = 0. 038*	r = 0. 258 p = 0. 155	r = 0. 240 p = 0. 185
Peak total force	r = 0. 433 p = 0. 013*	r = 0. 338 p = 0. 059	r = 0. 176 p = 0. 335
The rate of rise tangential force	r = 0. 589 p = 0. 000*	r = 0. 501 p = 0.004*	r = 0. 052 p = 0. 777
The rate of rise radial force	r = 0. 253 p = 0. 163	r = 0. 183 p = 0. 317	r = 0. 151 p = 0. 409
The rate of rise total force	r = 0. 465 p = 0. 070	r = 0. 360 p = 0. 043*	r = 0. 147 p = 0. 421

* denotes a significant difference (p<0.05)

TEMPORAL CHARACTERISTICS OF REAL-WORLD WHEELCHAIR PROPULSION

Alicia Koontz[1,2], Kazuaki Ebihara[2], Rory Cooper[1-3], Michael Boninger[1,3], Brad Impink[2]
[1]Dept. of Rehab. Science and Technology, University of Pittsburgh, Pittsburgh, PA 15261
[2]Center of Excellence in Wheelchairs & Related Technology, VAMC Highland Dr., Pittsburgh, PA
[3] Department of Physical Medicine and Rehabilitation, University of Pittsburgh, Pittsburgh, PA
Email: akoontz@pitt.edu Web: www.herlpitt.org

INTRODUCTION

The high prevalence of upper extremity pain and injury reported among individuals with spinal cord injury (SCI) has been attributed to everyday wheelchair propulsion (Boninger et al., 1999). Several researchers have conducted biomechanical studies of wheelchair propulsion to investigate the relationship with pain/injury. However, most of these studies are limited to testing wheelchair users in a controlled laboratory environment with wheelchair ergometers and dynamometers designed to simulate various surfaces and slopes. While these systems have been shown to produce rolling resistances very close to that experienced on an actual surface, users are still confined to testing in an unfamiliar and unrealistic environment. Recently, we conducted a kinetic study of wheelchair propulsion over 'real' surfaces and inclines using a new wireless 3D force and torque measurement system called the SMART^{Wheel} (Three Rivers Holding, Mesa, AZ) (Ebihara et al., 2003). The preliminary analysis provided insight into the forces required to transverse common indoor/outdoor terrain and ramps. The purpose of this study was to expand the analysis to investigate temporal characteristics (e.g., push/recovery time, cycle time, stroke cadence and velocity) as well as distance traveled per stroke.

PROCEDURES

The study took place at the National Veterans Wheelchair Games in Cleveland, Ohio. Eleven (10 men and 1 woman) with a spinal cord injury (ranging from T12 to C6/7) provided written informed consent to participate in this study. The average age and years post injury were 53 and 22 years, respectively. The SMART^{Wheel} was secured to each subject's own wheelchair and he/she was asked to push the wheelchair at a self-selected comfortable speed, over an assortment of surfaces which included shag carpet, indoor tile, hardwood flooring, grass, outdoor concrete tile, smooth, level concrete flooring, and smooth pile carpeting. Subjects were also asked to push up and coast down an outdoor sidewalk with a 5^{o} slope. While coasting down, the subjects were asked to keep pace with a study researcher who walked along their side. The total distances traveled for each surface, ramp up and coast down conditions ranged from 20 to 60 feet. Subjects also popped a wheelie and traveled forward for 10 feet on the smooth, level concrete flooring. Each trial lasted less than 2 minutes with a 5-minute rest break in between. Force and wheelchair position data (via an on-board encoder) from the SMART^{Wheel}'s were recorded at 240 Hz for each trial and post-processed to determine, push time, recovery time, total cycle time, stroke frequency, stroke velocity and distance traveled per stroke. Push time was defined as the amount of time per stroke when force and torque were imparted on the handrim. Thus, recovery time occurred when the hand was off the handrim. Stroke cadence (strokes/second) was calculated as the inverse of the total cycle time.

Peak temporal and distance values were determined for five strokes and averages were computed. Due to occasional technical difficulties with the new instrumentation some trials could not be analyzed and some subjects did not complete all the trials within a condition. The average temporal and distance values were compared across surfaces, wheelie and the two slope conditions (pushing up and coasting down) using a repeated-measures ANOVA test ($\alpha < 0.05$).

RESULTS AND DISCUSSION

Mean temporal and distance data are shown in Table 1. The ANOVA test revealed significant differences between conditions for dependent variables: recovery time ($p=0.035$), total cycle time ($p=0.037$), stroke cadence ($p=0.028$), velocity ($p=0.000$), and distance ($p=0.01$). Individual comparisons among the conditions revealed that subjects spent the least amount of time in recovery when wheelie-ing, pushing over grass and up the ramp. Likewise, stroke cadence was higher for these same conditions. The wheelchair users pushed with slower self-selected speeds when propelling over the shag carpet and grass, wheelie-ing and while pushing up the ramp. Distance traveled per stroke was shorter for the wheelie, ramp up, grass, and indoor tile conditions.

High stroke cadence and force during wheelchair propulsion at slow speeds (0.8-1.9 m/s) has been correlated to upper extremity injuries (Boninger et al. 1999). The self-selected speeds in this study fall within this range. In addition, our previous analysis (Ebihara et al. 2003) showed that subjects imparted higher propulsion forces during the same conditions found in this study to involve higher cadences. As these conditions are often performed on a daily basis and are necessary for functional mobility, the risk for developing upper extremity problems is likely higher than if propulsion only occurred on level, even surfaces. Interestingly, users made adjustments in their self-chosen speed and technique, propelling slower and spending less time in recovery during the more challenging conditions (grass, ramp up, wheelie, shag carpet). Chow et al. (2000) also found that wheelchair racers who pushed on a roller system with increasing resistance spent less time in recovery and pushed with a slower self-selected speed when faced with a higher resistance.

REFERENCES

Boninger M.L. et al. (1999). *Arch Phys Med & Rehabil,* **80**, 910-915.

Chow J.W. et al. (2000). *J Biomech,* **33**:601-608.

Ebihara, K. et al. (2003). *Proceedings 2003 Annual RESNA Conference*, in press.

ACKNOWLEDGEMENTS

This study was supported by the Paralyzed Veterans of America (PVA), and Eastern Paralyzed Veterans of America (EPVA).

Table 1: Mean temporal and distance data for each of the test conditions

	A (n=9)	B (n=10)	C (n=11)	D (n=11)	E (n=11)	F (n=11)	G (n=10)	H (n=11)	I (n=11)	J (n=9)
Push time (sec)	0.46	0.66	0.54	0.54	0.62	0.99	0.50	0.63	0.48	0.50
Recovery time (sec)	0.22	0.40	0.51	0.55	0.23	0.69	0.47	0.19	0.51	0.55
Cycle time (sec)	0.68	1.06	1.05	1.09	0.85	1.68	0.97	0.82	0.99	1.05
Cadence (stroke/sec)	1.52	0.97	1.0	0.97	1.2	0.93	1.08	1.31	1.05	1.0
Velocity (m/sec)	0.68	1.04	1.43	1.51	1.01	1.62	1.45	0.75	1.37	1.41
Distance (m)	0.36	0.69	0.73	0.76	0.60	1.79	0.67	0.48	0.61	0.64

Key: A: wheelie 10 feet; B: shag carpet; C: smooth pile carpet; D: smooth level concrete flooring; E: 5° ramp up; F: 5° ramp down; G: outdoor concrete tile; H: grass; I: indoor tile; J: hardwood floor

THE DYNAMIC SENSORIMOTOR REGULATION OF FINGERTIP FORCE VECTORS IS INDEPENDENT OF HAND STRENGTH

Madhusudhan Venkadesan[1], Francisco J. Valero-Cuevas[1,2] and John M. Guckenheimer[3]

[1] Neuromuscular Biomechanics Laboratory, Cornell University, Ithaca, NY, U.S.A.
[2] The Hospital for Special Surgery, New York, NY, U.S.A.
[3]Department of Mathematics, Cornell University, Ithaca, NY, U.S.A.
E-mail: mv72@cornell.edu Web: http://www.mae.cornell.edu/nmbl

INTRODUCTION

We currently lack quantitative and objective measures of sensorimotor ability for dynamic manipulation. Such measures are essential for quantifying hand impairment and comparing treatment outcomes. The dynamical behavior of the brain-hand system during manipulation is extremely complex and nonlinear. Fortunately, bifurcation theory (a branch of nonlinear dynamics) shows that even complex systems behave like low-order systems at the verge of instability (*Guckenheimer et. al, 1983)*. Activities of daily living often involve dynamic regulation of fingertip forces to stabilize objects (e.g., rolling a pen, sliding grasps, etc) (*Valero-Cuevas et. al, 2003*). Thus, we propose that bifurcation analysis can be used to grade sensorimotor ability of the brain-hand system. In this study, we characterize the performance of the brain-hand system at the boundary of instability. We establish that the ability to control or postpone instability is a consistent measure of the sensorimotor ability to dynamically regulate thumbtip force. This motivates the future use of bifurcation analysis to understand sensorimotor function in dynamic manipulation, and clinically grade its impairment.

METHODS

As in our previous work, (*Valero-Cuevas et. al, 2003*), we have developed a task that consists of asking subjects to use their thumbtip to compress a slender spring prone to buckling. We now instrument the spring to measure <u>how</u> the brain-hand system fails to fully compress the spring. We selected a spring that buckled at very low loads with little shortening to maintain a near constant thumb posture, as in key pinch. The calculated buckling loads (*Haringx, 1948*) for the 1st, 2nd and 3rd modes of this spring are (buckling load / shortening): 1.6 N / 2.3mm, 7.0 N / 10mm and 15.2 N / 21.7 mm, respectively.

All subjects read, understood and signed the consent form approved by Cornell's "University Committee on Human Subjects." All 11 participants were unimpaired young adults (age: 29±7 years, 6 females). They placed their dominant hand on a table with the palm perpendicular to the tabletop and positioned their thumb pulp on a flat pad attached to the free end of the vertical slender spring attached to ground. The instructions to the subjects were to "*compress the spring as far as you can, even if the spring oscillates or is not straight, and hold the spring at this shortest length for a few seconds*." The free end of the spring was instrumented with a miniature 3-axis accelerometer to measure $\ddot{\underline{x}}(t)$. The fixed end was attached to ground via a uni-axial load cell to measure the compressive spring force. In five subjects, a 12-camera vision system (Vicon, Inc) tracked the 3D position and orientation of the free end of the spring to measure $\underline{x}(t)$. We also recorded the maximal static pinch strength of all subjects using a pinch meter in key and opposition pinch postures.

RESULTS AND DISCUSSION

Pinch strength varied considerably (mean±coefficient of variance: Key: 87.7 N ± 24%, Opposition: 70.7 N ± 29%), but the variability in maximal compressive spring force was much smaller (23.8 N ± 11%). This suggests that the ability of the brain-hand system to control the buckling instability is consistent across individuals, and independent of their strength.

Moreover, the brain-hand system actively postponed buckling by stabilizing the first 3 modes (cf. mean compressive load vs. spring buckling loads). Stiffening the thumb by co-contraction was likely not the strategy used to reach and hold the boundary of stability, as it is not an effective approach. Co-contraction results in greater fingertip force noise due to increased variability in force production associated with higher muscle recruitment. In contrast, minimizing noise in fingertip force is instrumental to maximizing the shortening of a slender spring past its 3rd buckling mode, as it is in a highly unstable state. Using the lowest possible level of muscle activity is, therefore, a more effective strategy than co-contraction. Although EMG will be collected in future to quantify the degree of co-contraction, it is most likely that subjects had to actively regulate fingertip force to control the unstable spring past its 3rd buckling mode.

Lastly, a clear onset of instability was observed both in position and acceleration data at a critical load (Fig 1). This is strongly indicative of the occurrence of a bifurcation. Future studies will fit low order models (normal forms) to the time-varying

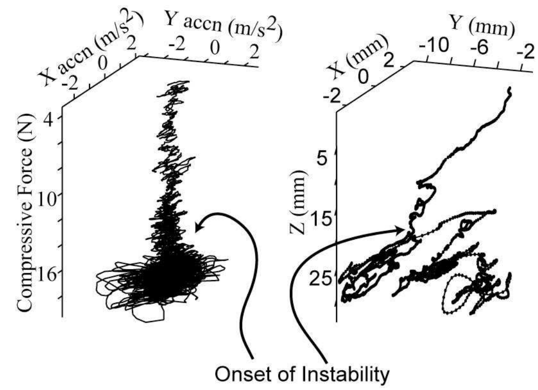

Figure 1: This graph shows representative acceleration (left) and position (right) data as the subject compresses the slender spring and reaches the verge of instability (bifurcation).

data to characterize the exact type of bifurcation that occurs.

We conclude that the maximal compression of the spring is consistent across people of different strengths, and could be used as a measure of the sensorimotor ability to dynamically regulate fingertip force. These results also motivate future work to use normal forms to quantitatively characterize the contribution of passive tissue properties and sensorimotor ability of the brain-hand system during dynamic manipulation in able and impaired hands.

REFERENCES

Haringx, J.A. (1948) *Philips Research Reports* **3**(6), 401-449.

Guckenheimer, J. and Holmes, P. (1983) *Nonlinear oscillations, dynamical systems and bifurcations of vector fields*. Springer-Verlag.

Valero-Cuevas, F.J., et al. (2003). *J* Biomech **36** , 265-270.

ACKNOWLEDGEMENTS

Prof. Jessica Hodgins and Jin-Xiang Chai at CMU for use of their motion capture system.

EFFECT OF A VINYL-COATED HANDRIM ON WHEELCHAIR USE

Mark Richter and Peter Axelson
Beneficial Designs, Minden, Nevada, USA
mark@beneficialdesigns.com www.beneficialdesigns.com

INTRODUCTION

There is a high occurrence of upper extremity injuries in the manual wheelchair user population. In a study of 239 manual wheelchair users, Sie *et al*. (1992) found that 64% of patients with paraplegia reported upper extremity pain. In a study of 34 manual wheelchair users, Boninger *et al*. (1999) found that incidence of injury was related to biomechanical loading during propulsion and concluded that reducing demands on the user should reduce the likelihood of developing injuries. Handrims are the primary interface by which the wheelchair user pushes, brakes, and turns the wheelchair. The standard handrim is an anodized aluminum tubing hoop, mounted offset to the side of each wheel. A vinyl-coated handrim is a standard handrim coated with vinyl. The coating provides increased friction between the hand and the handrim. Use of a vinyl-coated handrim was found to reduce the peak force applied to the handrim during propulsion by 10% (Koontz *et al*., 1998). Unfortunately, the vinyl coating is a very poor conductor of heat. As a result, the heat generated during braking quickly exceeds the tolerance threshold of the user and the user has to let go of the handrim.

This study will focus on quantifying the potential advantages and disadvantages of the use of a vinyl-coated handrim for propelling and braking the wheelchair.

METHODS

Nine subjects were randomly recruited from an internal database of local wheelchair users and participated in the evaluation of the vinyl-coated handrim. There were eight male participants and one female. The average subject body weight was 159±39 lb. Subject disability consisted of eight spinal cord injuries ranging from L5 to T3 and one Spina Bifida.

<u>Propulsion</u> - Subjects propelled their wheelchairs on a treadmill for five minutes continuously using a standard handrim and a vinyl-coated handrim in a randomized order. Each propulsion bout on the treadmill consisted of a ramping profile with four grade/speed combinations. The treadmill profile involved the following stages: 1) 2% grade at 2.1 mph (0.94 m/s) for 2 minutes, 2) 4% grade at 1.1 mph (0.49 m/s) for 1 minute, 6% grade at 0.7 mph (0.31 m/s) for 1 minute, and finally, 3) 8% grade at 0.5 mph (0.22 m/s) for 1 minute. Subjects had a 15-minute rest period between trials.

Handrim forces and moments were measured during propulsion using a wheelchair propulsiometer (Figure 1). When using a propulsiometer, loads applied to the handrim pass through a load cell and are transferred to the wheel. Metabolic demand

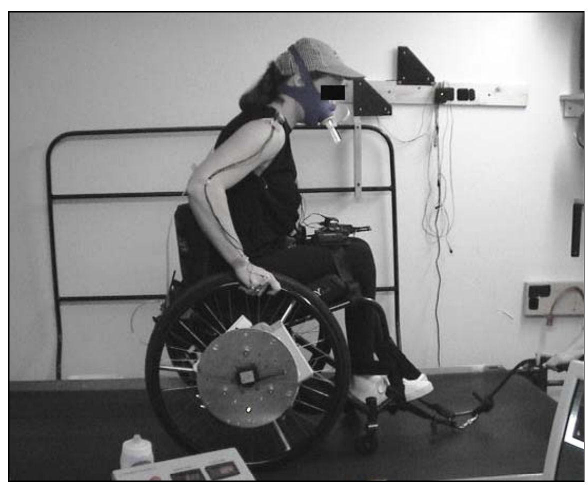

Figure 1. Demand on the user was measured using a propulsiometer, a portable gas analyzer, and a heart rate monitor.

during propulsion was measured using a portable metabolic gas analyzer and a heart rate monitor.

Braking - Subjects were asked to brake their wheelchairs on a treadmill using a standard and a vinyl-coated handrim in a randomized order. The treadmill grade was set to a 10% decline and the braking speed was set to 5.5 mph (2.46 m/s). Subjects were instructed to continue to brake until they were uncomfortable, or unable to continue. Braking duration was measured using a stopwatch.

Analysis - Both metabolic and kinetic data were averaged over the last four minutes of the propulsion bout as a representative characteristic of performance over the spectrum of grades. Propulsion kinetics including peak force and moment, push frequency, push angle, work per push, and the fraction of the applied force in the tangential direction (FEF) were assessed for each push and then averaged over each trial. Propulsion metrics and braking time were compared between the handrim conditions using a paired samples t-test and determined to be statistically significant for $p<0.05$.

RESULTS AND DISCUSSION

Each of the subjects was able to complete the protocol without undue stress, discomfort, or fatigue. The resulting propulsion kinetics and timing characteristics are shown in Table 1.

Oxygen consumption (VO2) was reduced by 9% when using the vinyl-coated handrim. The percentage contribution of the tangential force component to the resultant force when using the vinyl-coated handrim was increased by 33%. Braking time for the vinyl-coated handrim was reduced by over 91% from the standard handrim. Trends identified included a decrease in peak force on the handrim, as found by Koontz et al., as well as an increased push angle, decreased push frequency, increased work per push, and decreased heart rate.

Table 1. Handrim performance. *=$p<0.05$

Performance Metric	Standard	Vinyl
Peak Force (N)	76.3	70.2
Peak Moment (Nm)	16.14	16.20
Push Angle (deg)	85.8	87.3
Push Frequency (Hz)	1.04	1.00
FEF (Ft^2/F^2)	0.54	**0.83***
Work (J)	12.8	13.8
Heart Rate (bpm)	105	101
VO2 (L/min)	0.80	**0.73***
Braking Time (s)	103	**9***

SUMMARY

This study provides evidence that use of a high friction handrim reduces demand on the wheelchair user during propulsion. However, results also show an unacceptable decrease in braking performance due to the low heat conduction characteristics of the vinyl-coating. Improvements in handrim design, which incorporate the advantages of vinyl-coating for propulsion without its adverse effects on braking would be a beneficial technological advancement.

REFERENCES

Boninger ML, *et al*. (1999). Wheelchair handrim kinetics: body weight, and median nerve function. *Arch Phys Med Rehabil*, **(80)**, 910-915.

Koontz AM, *et al*. (1998). Effect of vinyl coated handrims on wheelchair propulsion kinetics. *Proceedings of RESNA '98 Annual Conference*. (pp. 131-133). Arlington, VA: RESNA Press.

Sie IH, *et al*. (1992). Upper extremity pain in the post rehabilitation spinal cord injured patient. *Arch Phys Med Rehabil*, **(73)**, 44-48.

EFFECT OF SHOULDER IMPINGEMENT ON SCAPULAR KINEMATICS DURING SELECTED TASKS IN WHEELCHAIR USERS

Margaret A. Finley, PhD., PT, Kevin J. McQuade, PhD., PT, Mary M. Rodgers, PhD., PT
University of Maryland School of Medicine, Baltimore, MD
Baltimore Veterans Administration Medical Center, Baltimore, MD
mfinley@som.umaryland.edu

INTRODUCTION

Manual wheelchair users (MWCU) depend on their upper extremities for mobility, transfers, pressure relief and a variety of other daily functional activities. As many as 78% of MWCU report experiencing shoulder pain since the onset of wheelchair use, with shoulder impingement diagnosed as the most commonly occurring pathology (Bayley,'87 Curtis,'99). While scapular movement patterns and scapulothoracic muscle function have been reported in open chain (non-weight bearing) humeral elevation in groups with and without shoulder impingement pathology, to date, no one has assessed the scapula during upper extremity loaded tasks that individuals who use a wheelchair must perform on a daily basis. Therefore, the **purpose** of this research was compare scapular kinematics and muscle function during selected activities of daily living (ADL) in groups of MWCU with and without shoulder impingement.

METHODS

Twenty- six MWCU (mean age=42 $\pm$ 11yrs; wheelchair use = 16 $\pm$ 8yrs) participated. Twelve subjects showed signs and symptoms of shoulder impingement. Disabilities of the subjects in the sample included spinal cord injury, multiple trauma, congenital birth injuries, cerebral palsy, and spina bifida. Kinematics of the thorax, humerus and scapula were measured (100Hz) during transfers, propulsion and scapular plane elevation via the MotionMonitor™(Innsport, Chicago, IL) electromagnetic tracking system. Segmental and global coordinate system definitions and Euler rotation sequences for the description of shoulder motions (recommended by the International Shoulder Group of the International Society of Biomechanics) were used. Surface EMG (Noraxon, USA, Inc. Scottsdale, AZ) from selected upper extremity and scapular muscles was collected at 1000Hz. Kinematics and EMG were synchronized and time normalized. Tasks were divided into phases of 30^{O} increments based on humeral elevation angle. Two-way analysis of variance ($p \leq 0.05$) was used to determine if differences existed in the scapular kinematics and EMG between the groups and among the tasks of lead limb and trail limb transfers.

RESULTS

There was no difference in age, or duration of wheelchair use between the groups. The impingement group (n=12) demonstrated reduced maximal humeral elevation angles, increased scapular medial rotation and decreased posterior tipping during the elevation task, compared to the group without shoulder pathology (n=14). No difference was found between the groups for other kinematic variables, so data was collapsed across groups for task comparisons (n=26). Significant differences were found to exist in maximal angles of thoracic flexion, scapular axial rotation, upward rotation, and posterior tipping, among the four tasks. Joint excursion was found to be greater for scapular upward and posterior rotations during the lead limb transfer and elevation compared to trail limb transfer and propulsion. The elevation task had the greatest amplitude of all three tasks in the upper trapezius muscle, and lowest amplitude in the bicep muscle. The trail limb transfer task demonstrated greater peak amplitude than the lead limb transfer and propulsion in the anterior deltoid and the lower trapezius muscles, with greater peak serratus anterior activity compared to activity during the propulsion task. (Table 1)

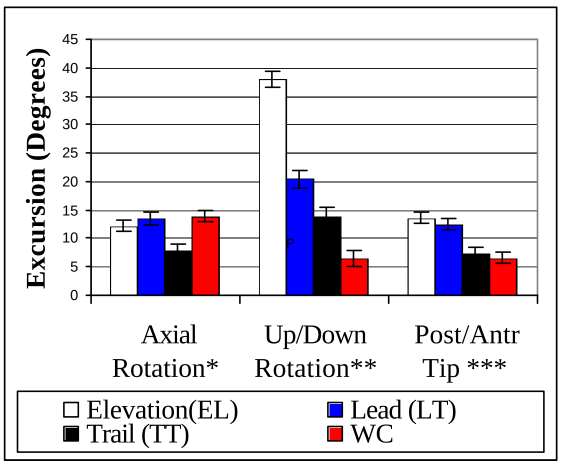

Figure 1: Scapular excursion among tasks (*EL&LT&WC> TT ** EL>LT>TT>WC *** EL&LT> TT&WC, p≤0.05.)

DISCUSSION/CONCLUSION

Shoulder impingement does affect humeral elevation task performance in MWCU, similar to that shown in a sample of people without disabilities (Ludewig, 2000). For both groups, the scapula is placed in positions that have been associated with impingement in open chain tasks. This is particularly true in the trial limb transfer where the scapula demonstrated increased medial, downward and anterior rotation with increased thoracic flexion. These mechanics may potentially place the MWCU at risk for development of the pathology.

REFERENCES

Bayley, et al (1987) *JBJS*,69 (5),676-8

Curtis, et al. (1999) *Arch Phys Med Rehabli,* 80(4)*l* 453-7.

Ludewig PM, Cook TM. (2000) *Phys Ther* 80(3):276-91

ACKNOWLEDGEMENTS

Funding provided by VA Pre-Doctoral Associated Health Rehabilitation Research Fellowship and the International Society of Biomechanics Dissertation Grant

Table 1: Peak EMG Amplitude during Performance of Selected Tasks (mean %MVC, se)
* = (p≤0.05)

Muscle		Elevation (EL)	Lead (LT)	Trail (TT)	Propulsion (WC)
Biceps	***TT & LT > EL**	8% (3)	22% (3)	24% (3)	15% (3)
Anterior Deltoid	***TT > LT &WC**	32% (4)	24% (4)	40% (4)	23% (4)
Upper Trapezius	***EL > LT&TT&WC**	28% (2)	12% (2)	8% (2)	11% (2)
Serratus Anterior	***TT > WC**	45% (6)	35% (6)	52% (6)	24% (6)
Lower Trapezius	***EL&TT &LT, WC**	28% (3)	13% (3)	26% (3)	15% (3)

TISSUE PERFUSION AND BLOOD FLOW RESPONSE IN A WHEELCHAIR WITH ADJUSTABLE ISCHIAL AND BACK SUPPORTS

MAKHSOUS M., LIN F., PATEL, J., HENDRIX, R.W., ZHANG L., RYMER, W.Z.
Rehabilitation institute of Chicago, Northwestern University, Chicago, IL 60611
E-mail: m-makhsous2@northwestern.edu Web: http://www.smpp.northwestern.edu

Introduction: Wheelchair use in spinal cord injury and MS patients was found to be associated with an increased risk of pressure ulcers (Pinchovsky-Devin 1986), primarily due to prolonged sitting, which causes excessive pressure over the ischia and coccyx, and thus poor local blood circulation. Therefore, proper pressure relief is important for wheelchair riders. The pressure relief benefits of altering ischial and back-support using a new sitting design, of which the back part of the seat (BPS) can be dynamically tilted downward with respect to the front part of seat, have been reported (Makhsous 2003). The purpose of this study is to evaluate the changes in local blood flow in terms of transcutaneous oxygen and carbon dioxide, interface contact pressure, and contact area across the buttock-thigh over an extended period of sitting while adjusting ischial and lumbar support in the wheelchair.

Materials and Methods: Six healthy office workers (31.2±9.3 years old (mean±SD); 72.7±8.8 kg in weight, and 177.0±10.5 cm in height) were tested. An instrumented X2™ wheelchair, of which the BPS can be tilted downward 18°, was used. Tilting the BPS and changing the shape of the backrest were precisely controlled via two motors. A pressure-mapping device (Xsensor™, Calgary, Canada) was used to measure the pressure distribution on the seat and backrest. The total contact area (TCA), total contact pressure (TP), peak pressure (PP) and average pressure (AP) were then calculated. Four surface electrodes from two monitoring systems (TCM400 & TCM3 Radiometers, Copenhagen, Denmark) were used to measure transcutaneous partial pressures of oxygen ($tcPo_2$) and the transcutaneous partial pressure of carbon dioxide ($tcPco_2$). The $tcPo_2$ and $tcPco_2$ were measured at the left ischial tubercles (IT) and $tcPo_2$ was also measured at the left posterior and middle thigh. One electrode was used as a reference and was placed on chest above carotid artery. The defined postures for sitting in this study were **Normal** (with the BPS at the level and without lumbar support) and sitting with the lowered BPS and with lumbar support **(WO-BPS).** Two 60 minute trials were performed for each subject: one with the posture of the seat was changed from **Normal** to **WO-BPS** at ten-minute intervals; the second trial with the chair kept at the **Normal** position for an hour, during which the subject was asked to perform the clinically recommend push-up every 20 minutes. To analyze the data for specific sitting area, three evenly divided regions, identified as anterior, middle, or posterior, were defined horizontally on the seat, in addition to being divided into left and right sides. The TCA, TP, AP and PP were calculated for each region of the seat. Data collected was normalized for each subject to the initial frame when the subject sat down for both pressure and perfusion data. Paired Student's t-test was used to evaluate the significance of the difference between **Alternate** and **Normal+Push-ups** sitting postures. Pearson's product moment was calculated between perfusion data and contact pressure.

Results: Typical results of changes in the $tcPo_2$, $tcPco_2$, TCA, TP and AP are shown for the **Alternate** and **Normal+Push-ups** sitting protocols from one subject in Fig 1. Under **Alternate** sitting, the $tcPo_2$ and $tcPco_2$ and all pressure parameters changed cyclically with the changing of the postures. The $tcPco_2$ was increased and $tcPo_2$ was decreased under **Normal** sitting condition. When changed to the **WO-BPS,** pressure on the IT was largely reduced and shifted to the thighs. At the same time, both $tcPo_2$ and $tcPco_2$ returned to the starting levels (Fig. 1). Under the **Normal+Push-up**, the TP and AP were not changed as much as under the **Alternate** protocol. The $tcPo_2$ was decreased to zero and it was hardly recovered by push-ups. The $tcPco_2$ was increased and slightly decreased by push-ups. **Alternate** sitting conserved more oxygen than **Normal+Push-**

ups did (0.56±0.06 vs 0.05±0.01, P<0.001) for the same length of sitting time (1 hour). For the **Alternate** sitting the change in $tcPo_2$ was significantly correlated to changes in $tcPco_2$, TCA, TP, AP, and PP ($P < 0.001$). Additionally, $tcPco_2$ was also correlated to TCA, TP and AP ($P<0.001$). $tcPco_2$ was not significantly correlated to PP. For the **Normal**+**Push–ups**, $tcPo_2$ was significantly correlated to $tcPco_2$ ($P<0.001$), TCA ($P=0.002$) and AP ($P=0.01$). The $tcPco_2$ was significantly related to TCA, TP, and AP ($P<0.001$).

Discussion: The hypotheses of this study were: 1) When the BPS is tilted down and lumbar support is used, pressure on the IT will be reduced and local tissue perfusion will be promoted. 2) Sitting alternately between the **Normal** and **WO-BPS** postures will reduce and redistribute the contact pressure in a cyclic fashion and decrease CO_2 accumulation and increase O_2 perfusion in the tissue around the sitting area, versus sitting with the **Normal**+**Push–ups**. Results from 6 subjects confirmed what was hypothesized. Although both $tcPo_2$ and $tcPco_2$ are sensitive to the release of pressure, they have different response patterns to the pressure changes. Primarily, $tcPco_2$ is more rapid in response to the pressure release, as shown by the greater drop of $tcPco_2$ than the rise of $tcPo_2$. Despite this high sensitivity, the push-up was not good enough to increase $tcPo_2$. This is most likely due to the brief duration of the push-up and the sudden return of pressure when the subject returns to **Normal** sitting. $tcPo_2$ is affected substantially by external pressure, as shown by its sharp decrease as the load started, while the $tcPco_2$ rose more gradually. This may be related to the fact that $tcPo_2$ is brought to and $tcPco_2$ is brought away from tissue by blood flow. When blood occlusion happens under the pressure load, the $tcPo_2$ supply is stopped at once, while the $tcPco_2$ will accumulate gradually as the waste of tissue metabolism.
It was reported that the posterior thighs are believed capable of sustaining more than 80mmHg without trauma, the ischia less than 40mmHg, and the coccyx less than 14mmHg (Bennett 1981). According to these values, shifting of the pressure from the IT to the middle thighs by changing the posture to **WO-BPS** would be helpful for better tolerating long-term sitting and preventing pressure ulcers in wheelchair riders.
Further experiment need to be done and the amount of time spent sitting in the **Normal** position should be shortened when using **Alternate** protocol. This could possibly lead to increased $tcPo_2$ and decreased $tcPco_2$ accumulation.
It can be concluded that **Alternate** sitting significantly promotes tissue perfusion, compared with **Normal + Push-ups**.

References:

Pinchovsky-Devin GD, Kaminski MV. J Am Geriatr Soc. 1986;34:435-40.
Makhsous M, Lin AF, Hendrix RW, Hepler M, Zhang L-Q. Spine. 2003;June.
Bennett L, Kavner D, Lee BY, Trainor FS, Lewis JM. Arch Phys Med Rehab. 1981;62:392-8.

Acknowledgements: Falk & NIOSH Award #R21 OH007737. We would like to thank MEDTRON Chicago Inc. for their support with the Radiometer products.

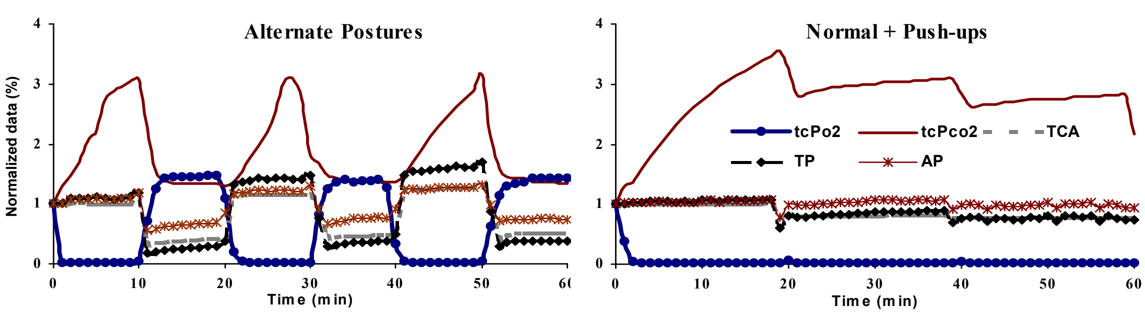

Fig. 1. Representative results from one subject. The $tcPo_2$, $tcPco_2$, TCA, TP and AP are shown for the **Alternate** and **Normal + Push-ups** sitting postures. The **Alternate** protocol was started with **Normal** sitting posture and the posture of the seat was change from **Normal** to **WO-BPS** at ten-minute intervals. The subject performed a push-up every 20 minutes under the **Normal + Push-up** protocol.

3D KINEMATICS AND KINETICS OF RUNNING IN THE OSTRICH (*Struthio camelus*)

Jonas Rubenson [1], David G. Lloyd [1], Thor F. Besier[1], Denham Heliams[2] and Paul A. Fournier[1]

[1] School of Human Movement and Exercise Science, University of Western Australia
Crawley, WA, Australia
[2] Fauna Technology, Gosnells, WA, 6990, Australia
E-mail: rubenson@cyllene.uwa.edu.au   Web: www.hm.uwa.edu.au

INTRODUCTION

Birds represent the majority of obligatory striding bipedal species. Birds therefore hold valuable information regarding the mechanics and energetics of bipedal locomotion (Gatesy and Biewener, 1991) and can provide insight into the specific nature of human bipedalism. Studies on the mechanics of avian bipedalism have typically focused only on locomotor kinematics and have been limited to 2D analysis. In the present study we examine both the 3D kinematics and kinetics of locomotion in the largest avian bipedal species, the ostrich.

METHODS

A 5 segment, 3D-kinematic model of the ostrich lower limb was developed from cadaver specimens. Numerically optimized joint axes of rotation and joint centers were computed from motion data of marker clusters placed on the cadaver limb segments. The joint axes and centers were used to develop anatomical coordinate systems (ACS) for each segment (pelvis, femur, tibiotarsus, tarsometatarsus and phalanges) following similar methods to those of Besier et al. (2003). We identified several key anatomical landmarks (ALs) on the cadaver segments that could also be located on the living animal and expressed them relative to their cadaver segment ACS. This allowed the use of ALs on the living bird, and appropriate scaling factors, to establish the ACS for each segment. The center of mass of each segment was located in 3D space using a suspension technique and expressed relative to its ACS. Moments of inertia were determined using a pendulum method.

Simultaneous video (Peak; 200Hz) and force data (Kistler, 9281 A; 1000Hz) were collected from 4 ostriches (72.5 ± 4.2 kg; mean ± S.D.) running on a high-density rubber-topped runway. Clusters of markers placed on the limb segments were used to determine their 3D position and orientation. In static trials, segment ALs were located relative to the segment marker clusters with a pointer and were used to reconstruct each segment ACS across running strides (Fig. 1).

These techniques were used to compute 3D joint angles of running ostriches. Inverse dynamics analysis was used to calculate flexion/extension (FE), adduction/abduction (AA), varus/valgus, VV (at the knee) and internal/external (IE) joint moments and powers.

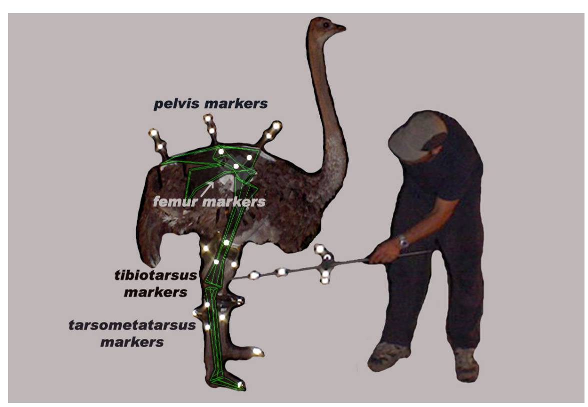

Figure 1: Segment clusters and AL location.

RESULTS AND DISCUSSION

Table 1 shows the maximum range of motion of each joint during running at 3.5 m/s. As was expected, the greatest motion occurs in FE. However, non FE motion is considerable. Given the limb orientation of the ostrich, a substantial frontal plane component it is likely as this reflects the complex task of re-orienting the foot (toe) position during the swing-phase in these animals.

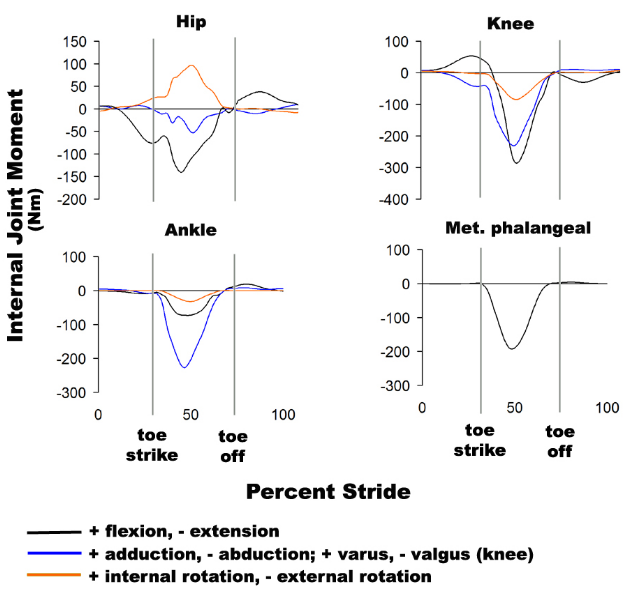

Figure 2: Internal joint moments of running ostriches

Figure 2 shows the internal joint moments over a typical running stride (3.5 m/s). The total support moment (SM; sum of individual moments required to support the body against gravity) is considerably higher in ostriches compared to similar size humans due to their more splayed and crouched posture. A large part of their SM is comprised of a valgus moment at the knee and an abduction moment at the ankle. These are likely produced not only by muscle forces but also by joint articular and ligament forces. This load sharing would help in improving locomotor economy, but only at the expense of an increased reliance on passive joint structures to protect against injury.

The major contribution to propulsive power (45%) comes from the metatarso-phalangeal joint and may be provided nearly entirely by storage and release of tendon elastic strain energy. This, together with specialized muscle properties (e.g. short fibers, large moment arms), may help to explain why ostriches use nearly 40% less energy when running compared to humans, despite their much larger SM (Rubenson et al., 2002).

A next step in understanding the mechanics and energetics of locomotion in this species is to estimate muscle and tendon force and work. To this extent we are currently developing a 3D musculoskeletal model of the ostrich lower limb.

REFERENCES

Besier, T. et al., (2003) *J. Biomech,* in press.

Gatesy, S.M., Biewener, A.A. (1991). *J. Zool. Lond.* **224:** 127-147.

Rubenson, J. et al., (2002). *Proceedings of IV WCB '02,* Cd-Rom.

Table 1: Maximum joint range of motion during running.

	Hip	Knee	Ankle	Met.-phalangeal
Flexion/Extension	15°	65°	100°	120°
Adduction/Abduction	12°	25° (varus/valgus)	17°	-
Internal/External Rot.	10°	12°	15°	-

COLLISIONAL ACCOUNTING OF ENERGY IN HORSE GALLOPING

Manoj Srinivasan, Andrew Dressel, Andy Ruina†, and John E.A. Bertram‡,
†The Biorobotics Laboratory, Cornell University, Ithaca, NY, USA,
http://www.tam.cornell.edu/~ruina/hplab, ruina@cornell.edu
‡Dept. of Nutrition, Food & Exercise Sciences, Florida State University, Tallahassee, FL, USA,
jbertram@fsu.edu

INTRODUCTION

Terrestrial legged locomotion requires repeated, generally dissipative, collisions with the ground. Any dissipation is necessarily an energetic cost. One mechanism useful for reducing collisional dissipation is through elasticity in the tendons, muscles and ligaments. We have found another. Whether or not the legs have some elasticity, sequencing leg collisions, as in the three beat (Lone Ranger) "pa-da-dump" of a slow horse gallop, can substantially reduce collisional losses over a one-beat gait with the same speed and period.

METHODS

Start by considering a seemingly unrelated springless locomotion system, brachiation. The gaits used by some arm swinging apes (Fig. a; 1) allows the making and breaking of contact without collisional loss by a smooth matching of the flight velocity with the swing velocity. The second inspiration is purely mechanical, although based on an apparently a new mechanical discovery (5). A rolling ellipse (or ellipsoid) that rolls too fast will leap in the air. If the speed is just right it will leap and flip in a manner so that the landing is symmetric with the take-off and the contact is at zero relative velocity (Fig. b). Thus even with no elasticity there is no dissipation and the ellipse can passively 'bounce', recovering all potential energy in each cycle, but without the requirement of a spring. Numerical simulation of this model confirms this motion. We have found that a horse seems to employ mechanics similar to these models in order to bounce better with incompletely elastic legs.

In more detail, first consider a particle collision mediated by a single massless leg. Conservation of momentum orthogonal to the leg yields $v_0 = v_i \cos \alpha$, where v_i and v_0 are incoming and outgoing speeds and α is the deflection angle caused by the contact. The post-collisional energy is $E_0 = E_i \cos^2\alpha$ and the fractional energy loss is $\Delta E/E_i = \sin^2\alpha \approx \alpha^2$ (for small α). By the same reasoning, a collision at a shallower angle ($\alpha/2$) has a fractional energy loss of $(\alpha/2)^2$, a quarter of that for α. Thus with a given incoming velocity, two successive collisions of deflection $\alpha/2$ together accomplish a net deflection of α but with only half the total energy loss of a single collision. More generally, taking the net interaction of an animal with the ground as a sequence of n such inelastic collisions, each collision has a deflection angle of α/n and $v_0 = v_i \cos^n(\alpha/n)$ so $E_0 = E_i \cos^{2n}(\alpha/n)$ and fractional energy lost $\Delta E/E_i \approx \alpha^2/n$ which goes to zero as $n \to \infty$. That is, an infinite sequence of plastic collisions makes up a fully elastic collision. Taking 3 as an approximation of ∞, we get the 3-collision model of horse galloping in Fig. c.

A similar analysis can be performed using elastic legs but keeping track of the work in restitution. The net restitution cost goes to zero as the number of legs goes to infinity.

RESULTS AND DISCUSSION

Following through this mechanics and using $g=10m/s^2$, $T=0.5s$, $v=7m/s^2$ from (6) we predict a (dimensionless) specific cost of transport of c_s = (power)/mgv=gT/8v=0.1 for a pronk and c_s = gT/8v=0.03 for a 3 beat canter. Assuming 25% muscular efficiency the VO2 data in (6) shows c_s=0.05. Thus our one-beat pronk is too costly (0.1>0.05) and our model for a three beat canter accounts for 60% of the measured cost of locomotion (0.03/0.05=60%), leaving some energy to swing the legs around and so on. With the given oxygen consumption even more energy is available to the horse for various "internal work" if the collision has some elasticity. Note also that ground force orientations predicted from this model agree qualitatively with the observations of a cantering horse (Fig. c, d, 3) and differ markedly from previous models of smaller animal galloping where the landing of the forelegs cock a spring that is released for the later push-off of the legs (4). Note also that both this model and real horses have a *maximum* horizontal speed at mid-stance, the opposite of that predicted by a "pogo-stick" model where the *minimum* horizontal speed is mid-stance.

These arguments are made more precise by numerical optimization of a simple model of a horse consisting of a point mass with elastic legs and a metabolic cost proportional to the restitution work done by the legs at each collision. Fitting this model to kinematic data of a horse gives a good prediction of the measured metabolic cost. Given that the horse can do a maximum of 3 footfalls per stride, the strategy that minimizes this metabolic cost is the one that uses 3 footfalls per stride as opposed to one (pronk) or two (trot). This timing of the footfalls and the metabolic cost at the optimum are well correlated to experimental data (6).

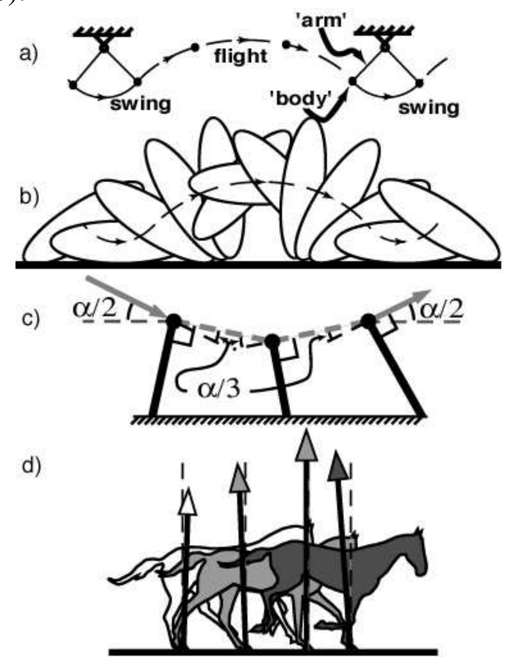

a) brachiation, **b)** bouncing ellipse, **c)** the model, **d)** horse.

REFERENCES and FOOTNOTES

1. Bertram, J.E.A., Ruina, A., Cannon, C.E., Chang, Y-H., Coleman, M.J. (1999) *Journal of Exp. Biol.*, 202, 2609-17.
2. Minetti, A.E. (1998) *Proc. R. Soc.* B 265, 1227-35.
3. Merkens, H.W., Schamhardt, H.C., van Osch, G.J., Hartman, W. (1993) *Am. J. Vet. Res.* 54, 670-74.
4. Alexander, R.McN. (1993) *Am. Zool.* 28, 237-45.
5. Haggerty, P, (2001) PhD thesis, U of Michigan independently constructed a similar model.
6. Minetti, A.E., Ardigo, L. P., Reinach, E. Saibene, F. (1999), *J Exp Bio*, 202, 2329-2338,

LOADING CONFIGURATIONS AND GROUND REACTION FORCES DURING TREADMILL RUNNING IN WEIGHTLESSNESS

John DeWitt[1], Grant Schaffner[2], Kristi Blazine[1], Jason Bentley[2], Mitzi Laughlin[2], James Loehr[2], and Donald Hagan[3]
[1] Bergaila Engineering Services, Houston, TX, USA, [2] Wyle Life Sciences, Houston, TX, USA
[3]NASA Johnson Space Center, Houston, TX, USA
E-mail: john.k.dewitt1@jsc.nasa.gov

INTRODUCTION

Studies have shown losses in bone mineral density of 1-2% per month in critical weight bearing areas such as the proximal femur during long-term space flight (Grigoriev et al., 1998). The astronauts currently onboard the International Space Station (ISS) use a treadmill as an exercise countermeasure to bone loss that occurs as a result of prolonged exposure to weightlessness.

A crewmember exercising on the treadmill is attached by a harness and loading device. Ground reaction forces are obtained through the loading device that pulls the crewmember towards the treadmill surface during locomotion. McCrory et al. (2002) found that the magnitude of the peak ground reaction force (pGRF) during horizontal suspension running, or simulated weightlessness, was directly related to the load applied to the subject. It is thought that strain magnitude and strain rate affects osteogenesis, and is a function of the magnitude and rate of change of the ground reaction force. While it is not known if a minimum stimulus exists for osteogenesis, it has been hypothesized that in order to replicate the bone formation occurring in normal gravity (1G), the exercise in weightlessness should mimic the forces that occur on earth. Specifically, the pGRF obtained in weightlessness should be comparable to that achieved in 1G.

While exercising on the treadmill, the crewmembers currently utilize various bungee configurations to create specific loads. These configurations are derived from a load prediction table based on weight and leg length measurements during static testing. We do not know how the various configurations affect the pGRF during running onboard the ISS.

Therefore, the purpose of this investigation was to determine the pGRFs that occur during locomotion in weightlessness utilizing the various loading configurations used by crewmembers onboard ISS.

METHODS

Three subjects (172.67 ± 13.65 cm; 76.56 ± 15.06 kg) ran at 5 mph (2.24 m/s) during weightlessness onboard the KC-135 aircraft and on the ground (1G). The number of available KC-135 flights limited subject size. The KC-135 flies in a parabolic trajectory allowing for approximately 25 sec of weightlessness. Vertical GRF data were collected during 2 trials at each load with a force treadmill (Kistler Gaitway, Amherst, NY) at 250 Hz for 25 sec. Each loading configuration was tested separately in a predetermined order of 1 bungee - 2 clips (1B2C), 1 bungee - 1 clip (1B1C), 1 bungee - 0 clips (1B0C), 2 bungees - 4 clips (2B4C), and 2 bungees - 3 clips (2B3C). Clips are used to decrease the length of the bungees, reducing the applied load based on the bungee's stiffness. Each arrangement is described as the bungee/clip setup attached to the hip on each side of the harness. One-bungee configurations used bungee and clips in series, while two-bungee configurations had both bungees in parallel, with the clips in series with the combined pair. One data set (1B1C, Sub 1) was lost due to hardware malfunctions during data collection.

Stride Rate (SR), stride length (SL) and pGRF data were processed using software included with the treadmill. For each trial, the mean of each variable was computed using all recorded footfalls. Any partial footfalls measurements were eliminated from the analysis.

RESULTS AND DISCUSSION

SR, pGRF, and SL means were normalized to 1G values to allow comparison between weightlessness and 1G, (see Figure 1). Estimates of loading levels obtained from static load tests indicate that subjects were loaded at 55-95% BW when using one bungee, and at 95-144% BW when using two bungees.

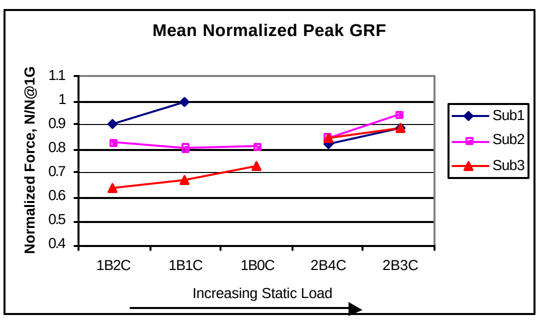

Figure 1: Mean Normalized Peak GRF values for each subject, for all bungee/clip configurations and 1G

The normalized force data show that for the two-bungee configurations producing vertical subject loads greater than 1 BW, pGRF was less than that observed during 1G running.

Examination of mean SR and SL suggest that when loaded with two-bungees, SR tended to increase and SL tended to decrease with increasing load and approached those typically observed during 1G (see Figure 2). The spread of individual curves suggest that normalized pGRF, SR and SL are less dependent on subject size and weight for the two-bungee configurations than for the one-bungee configurations.

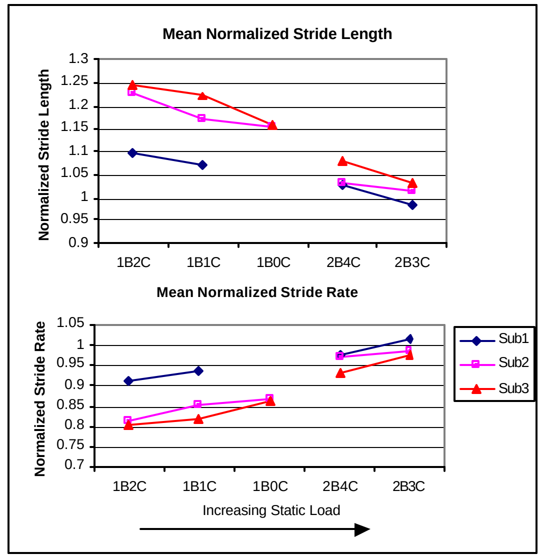

Figure 2: Mean Normalized SL and SR for all configurations for each subject.

SUMMARY

Our findings suggest that for the loading configurations studied, even though SL and SR may replicate that measured during 1G, pGRF is less than that produced in 1G. This occurs even when predicted loads are greater than 1BW. Variations are greater in pGRF, SR and SL between subjects during one-bungee running than during two-bungee running, suggesting that subject mass and height may affect pGRF, SR and SL when using one-bungee configurations.

REFERENCES

McCrory, J.L. et al. (2002). *Aviat Space Environ Med*, **73(7)**,625-631.
Grigoriev, A.I. et al. (1998). *Aviaksom Ekolog Med*, **32(1)**,21-25.

Treadmill Running in Simulated Microgravity

Kerim O. Genc and Peter R. Cavanagh

Department of Biomedical Engineering, The Cleveland Clinic Foundation, Cleveland, OH, USA
E-mail: genck@bme.ri.ccf.org   Web: www.lerner.ccf.org/bme/

INTRODUCTION

During treadmill exercise on the International Space Station (ISS) a subject load device (SLD) provides a restoring force to bring the runner back to the treadmill surface. The SLD interfaces with a shoulder and waist harness worn by the crew member. The function of this harness is critical for effective and comfortable use of the treadmill as a countermeasure to musculoskeletal changes during prolonged space flight. This study in simulated microgravity was designed to evaluate the comfort and function of a new SLD and harness design that allows controlled distribution of the load between the waist and shoulders during treadmill running.

METHODS

Twelve subjects (6 M, 6 F, age: 24.9 ± 5.5 yrs, height: 1.72 ± 0.09 m, body mass: 64.3 ± 10.1 kg) who were recreational runners (at least 4x per week for 20 minutes at a pace of 3.35 ms^{-1}) gave their informed consent to participate in the experiment.

The Zero Gravity Locomotion Simulator (ZLS) was used to simulate treadmill running in microgravity (Davis et al., 1996, McCrory et al., 2002). A new SLD was developed using a servomotor that minimized the variation in applied loads during running (Mandes, 2002). The SLD incorporated devices that allowed alteration in the load distribution between the waist and shoulders (McCrory et al., 1999).

Subjects completed nine, five minute running trials in the ZLS at a constant speed (3.35 ms^{-1}) using 3 SLD loads (50%, 75% and 100% of BW) and 3 shoulder-to-waist loading ratios (50:50, 60:40 and 70:30) presented at random. Ground reaction forces (GRFs) were recorded from a force platform under the treadmill belt and SLD loads were measured with in-line force transducers. Subjects were asked to assess the level of discomfort in five categories (neck, shoulders, back, waist, and overall) after 30 seconds and 3 minutes of running during each trial. A modified Borg scale was used to assess discomfort: 0 "no discomfort at all," 5-6 "somewhat uncomfortable," and 10 "extreme pain."

The following GRF variables were derived: mean active peak force (MAPF), mean impact loading rate (MILR), maximum loading rate (MaxLR), stride frequency (SF), and stance time (ST). Two-way analyses of variance (SLD loads x loading ratios, $\alpha = 0.05$) followed by Tukey pairwise comparisons were used to explore differences in the comfort and GRF response variables between loading conditions.

RESULTS AND DISCUSSION

The level of discomfort increased significantly ($p < 0.05$) in all categories as the SLD load increased. The maximum average discomfort at 100% BW load (across all loading ratios) was 3.1 at the neck, 4.9 at the shoulders, 3.4 at the back, and 4.7 overall. Shoulder discomfort was always significantly higher ($p < 0.05$) than neck, back, and waist discomfort at all SLD loads and loading ratios. After 3 minutes of running, the comfort level at the waist, but not the shoulders, was dependent on the loading ratio ($p < 0.05$). Waist discomfort was significantly lower ($p < 0.05$) at the 70:30 shoulder-to-hip loading ratio compared to a 50:50 distribution.

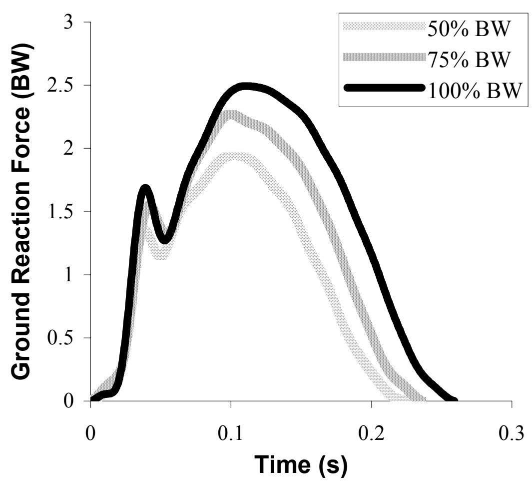

Figure 1. Typical example of ZLS GRF profiles at different SLD loads. The 100% BW data exhibits typical characteristics of 1G running (see Table 1).

The GRF variables were all significantly affected by the magnitude of the SLD load ($p < 0.05$) but not by the loading ratio. 100% BW loading in the ZLS resulted in similar GRF profiles to those obtained from the literature for overground running (Table 1).

Although increased SLD loads resulted in greater subject discomfort, the average maximum discomfort under all conditions was only rated as "somewhat uncomfortable". This study indicates that 100% BW loading can be achieved in short bouts of running in simulated microgravity and that a shoulder-to-hip loading ratio of 70:30 minimizes subject discomfort. Future research will use these settings for a prolonged exercise program on the ZLS in order to provide information on comfort and lower extremity loads in conditions similar to those that might be used for an in-flight exercise program.

Table 1: Comparison of GRF variables [mean (SD)]

Response	ZLS	Literature
MAFP (BW)	2.5 (0.15)	2.56 (.17)[1]
MILR (BWs^{-1})	64.0 (26.1)	77.4 (19)[1]
MaxLR (BWs^{-1})	110 (38.4)	100.0[2]
SF (Hz)	1.43 (0.06)	1.4 (.08)[3]
ST (ms)	253 (23.0)	258 (18)[1]

Results from the ZLS at 100% SLD load were compared with those at a similar speed from the literature ([1]Munro et al., 1987; [2]Chang et al., 2000; [3]Cavanagh and Kram, 1989).

REFERENCES

Cavanagh and Kram. *Med Sci Sports Exerc*. 1989;**21**:467-479.

Chang et al. *J Biomech.* 2000;**34**:679-685.

Davis et al. *Aviat Space Environ Med.* 1996;**67**:235-242.

McCrory et al. *J Appl Biomech*. 1999;**15**:292-302.

McCrory et al. *Aviat Space Environ Med.* 2002; **73**:625-31.

Mandes *MS Thesis* The Pennsylvania State University. 2002

Munro et al. *J Biomech.* 1987;**20**:147- 155.

ACKNOWLEDGMENTS

This research was supported by NASA grant NAG 9-1264. The authors also acknowledge V. Mandes, J. Strella, D. Tubbs, and A. Erdemir for their support.

MEDIOLATERAL SYMMETRY OF THE SWING LEG DURING RUNNING

G.D. Heise, M. Bohne, C-T. Hsieh, and R. Jorden

School of Sport and Exercise Science., University of Northern Colorado, Greeley, CO 80639
e-mail: gary.heise@unco.edu

INTRODUCTION

Researchers who study running traditionally examine sagittal plane motion, and often assume that the kinematics of gait are symmetrical. Iliotibial (IT) band syndrome, an injury which is manifested in lateral knee pain during the latter part of swing, may be influenced by nonsagittal motion of the lower extremity. For example, Fredericson et al. (2000) showed that runners with IT band syndrome had significantly weaker hip abductors on their affected side when compared to controls.

Those who do study nonsagittal motion of the leg and foot often examine the stance phase of running. Studies which focus on rearfoot motion usually attempt to identify connections between frontal plane mechanics with a person's predisposition to leg and foot injuries (e.g., Williams et al., 2001). Focusing on the stance phase of running makes sense because of the high forces encountered by the single support leg, however, an analysis of lower extremity motion outside the sagittal plane during swing phase is often not addressed.

The latter part of swing has been identified as a crucial phase of locomotion with respect to injury. Radin and colleagues (1991) went so far as to say that uncoordinated motion prior to foot contact ("microklutziness") may predispose persons to knee pain and ultimately, osteoarthritis. This suggests the motion of the leg during swing may contribute to poor mechanics during stance. This connection and the paucity of 3-D analyses examining swing leg motion were motivations for this experiment. Specifically, we tested the hypothesis that mediolateral motion of the leg during swing would be symmetrical.

METHODS

Three men volunteered as subjects. All were right-leg dominant. Each participant attended one test session. An injury questionnaire was completed and Q-angle was measured on both legs as subjects stood quietly on a flat surface. Prior to running, reflective markers were placed for each leg on the greater trochanter and the lateral epicondyle of the femur, the lateral malleolus of the fibula, and two locations on the shoe (heel and over the 5th metatarsal head). After a sufficient warm-up, participants ran on two different treadmills at 3.5 m/s (9 min/mile pace) for a total of 20 min. Treadmills were located next to each other, but faced opposite directions (see Fig 1). Two 60-Hz video cameras recorded the motion of the right leg on one treadmill and then after a brief rest, the motion of the left leg on the adjacent treadmill.

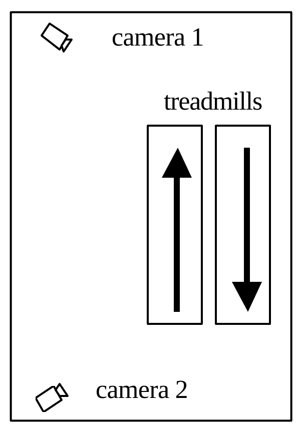

Fig 1. Experimental set-up showing two cameras and treadmills

Direct linear transformation (DLT) was used to calibrate a 1.25 m x 0.80 m x 0.90 m volume, which included both treadmills. A 13-point calibration object was used resulting in an overall error of 0.22%.

After digitizing, coordinate data were filtered and 3-D coordinates were calculated using DLT methods (Abdel-Aziz & Karara, 1971). Mediolateral linear kinematics were calculated and compared between right and left legs for each subject.

RESULTS AND DISCUSSION

All participants were experienced runners, but symmetrical mediolateral swing leg motion was noticed in only one runner. An in-phase pattern was noticed for both legs of one subject displaying symmetry, and from the left leg of the other two subjects (see Fig 2). The in-phase pattern is characterized by the knee and ankle traveling laterally in early swing and then, together, moving medially late in swing.

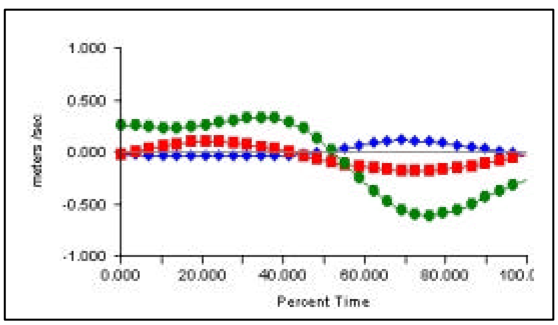

Fig 2. In-Phase mediolateral linear velocities of the hip (◆), knee (■), and ankle (●) for the swing phase of running. positive = lateral: negative = medial

Data from the right legs of the two asymmetrical subjects show a distinctly different pattern (see Fig 3). Here, during the second half of swing, the knee moves laterally while the ankle moves medially.

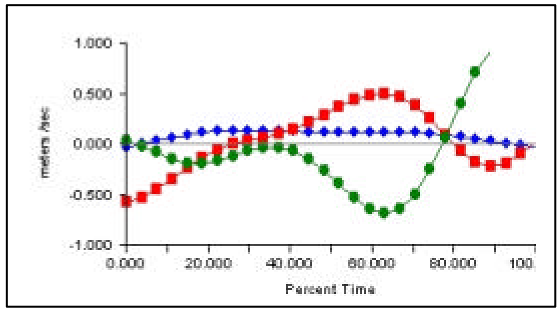

Fig 3. Out-of-Phase mediolateral linear velocities of the hip (◆), knee (■), and ankle (●) for the swing phase of running. positive = lateral: negative = medial

Similar to the findings of Radin et al. (1991), no gross, qualitative, discernible differences were noted by a trained eye, however, stark kinematic differences were noted as outlined above. In addition, neither Q-angle nor running experience appeared to help explain differences in mediolateral swing leg symmetry among the runners. At present, we have no alternative explanations for our findings. Future work will examine mediolateral symmetry in women and in inexperienced runners.

REFERENCES

Abdel-Aziz, Y.I. & Karara, H.M. *Proc of the ASP/UI Symposium on Close-Range Photogrammetry*, Amer Soc Photogr, pp. 1-18, 1971.

Fredericson, M. et al. *Clin J Sport Med*, 10, 169-175, 2000.

Radin, E.L. et al. *J of Ortho Res*, 9, 398-405, 1991.

Williams, D. S., et al. *J of App Biomech*, 17, 153-163, 2001.

DISCRETE AND CONTINUOUS JOINT COUPLING DURING RUNNING

Tracy A. Dierks[1] and Irene McClay Davis[1,2]

[1]Department of Physical Therapy, University of Delaware, Newark, DE, USA

[2]Joyner Sportsmedicine Institute, Harrisburg, PA, USA

E-mail: tdierks@udel.edu

INTRODUCTION

Abnormalities in joint coupling between the rearfoot and the knee may lead to overuse injuries in runners (Bates et al., 1978). Joint coupling has been assessed using discrete timing differences as well as excursion ratios. However, neither of these methods consider joint coupling throughout the entire stance phase of running. Therefore, the continuous relative phase (CRP) has been borrowed from the Dynamical Systems Theory (DST) to assess joint coupling throughout the stance phase (Hamill et al., 1999). Due to possible limitations in the CRP method, Heiderscheit et al. (2002) used coupling angles (CA) from a vector coding method to assess continuous joint coupling. Little is known regarding the boundaries of normal joint coupling, outside of which may predispose a runner to injury. In addition, sample sizes for most studies have been relatively small and contained primarily males. Therefore, the purpose of this study was to describe normative data for various joint coupling relationships using measures of timing differences, excursion ratios, CRP, and CA in a group of recreational runners.

METHODS

Forty recreational runners (20 males, 20 females) ran along a 25 m runway at a speed of 3.65 m/s (±5%). Ground reaction force (GRF) data (960 Hz) and kinematic data (120 Hz, filtered at 8 Hz) were collected. Coupling variables were averaged over 5 individual trials and then across subjects. Within-subject variability (WSD) was calculated for each subject and averaged across subjects and presented as the standard deviations for the coupling variables. A normal interval based on the between subject variability (BSD) was calculated for each variable as the group mean ±1SD. Timing differences were calculated for: 1. rearfoot eversion and tibial internal rotation (EV-TIR), 2. TIR and knee flexion (TIR-KF), 3. EV and KF (EV-KF), 4. EV and knee internal rotation (EV-KIR), and 5. TIR and KIR (TIR-KIR). Excursion ratios were calculated for EV/TIR and EV/KIR. CRP and CA were calculated for: 1. rearfoot eversion/inversion and tibial rotation ($RF_{(ev/in)}$-$T_{(rot)}$), 2. $T_{(rot)}$ and knee flexion/extension ($T_{(rot)}$-$K_{(f/e)}$), 3. $RF_{(ev/in)}$-$K_{(f/e)}$, 4. $RF_{(ev/in)}$ and knee rotation ($RF_{(ev/in)}$-$K_{(rot)}$), and 5. $T_{(rot)}$-$K_{(rot)}$. The CRP was constructed from the angles and velocities of two segmental motions, while CA were constructed from angle-angle diagrams. Continuous relationships were assessed over 4 phases that were based on events of the vertical GRF.

RESULTS AND DISCUSSION

EV-TIR, EV-KF, and TIR-KF all exhibited timing differences relatively close to zero, indicating synchronous coupling (Table 1). EV-KIR and TIR-KIR were both negative, suggesting that KIR reached its peak after both EV and TIR. For KIR to continue after tibial external rotation has begun, the femur must be externally rotating to a greater degree than the tibia during this period. Both EV/TIR and EV/KIR were 2.0,

Table 1. Joint Timing & Excursion Ratio Means, WSD, & BSD Intervals.

Timing	Mean	WSD	±1 BSD	Ratios	Mean	WSD	±1 BSD
EV-TIR^	0.8	(9.1)	-12.8 to 14.5	EV/TIR	2.0	(0.5)	1.2 to 2.9
EV-KF^	2.1	(4.1)	-4.4 to 8.7	EV/KIR	2.0	(0.6)	0.7 to 3.3
TIR-KF^	1.3	(8.5)	-11.5 to 14.1				
EV-KIR^	-14.8	(9.5)	-30.6 to 0.9				
TIR-KIR^	-15.7	(12.5)	-33.7 to 2.3				

^Negative indicates the distal segment reached peak displacement first.

indicating that every 2° of EV is coupled with 1° of TIR or 1° of KIR. All CRP angles were between –43.74° and 48.28° across the 4 phases of stance, indicating relatively in-phase couplings (<90°) (Figure 1). However, relationships involving $K_{(rot)}$ had the highest CRP angles and, thus, were the most out-of-phase. This may be related to the differences in the timings, as EV and TIR reached their peaks prior to KIR, resulting in asynchrony in both position and velocity. Increased CRP angles and variability were seen in all relationships during phases 1 and 4. Increased variability at transitions, such as heel strike and toe-off, is believed to provide the system with more flexibility to better adapt to a changing environment (Kelso, 1984). Conversely, phases 2 and 3 had the least variability, which is when the environment is relatively stable and less coupling patterns would be needed. CA were lowest for both relationships involving $K_{(f/e)}$, due to greater knee motion (Figure 2). CA were highest between $RF_{(ev/in)}$ and both $T_{(rot)}$ and $K_{(rot)}$, due to greater rearfoot motion. $T_{(rot)}$ and $K_{(rot)}$ were about 45° throughout stance, indicating equal motion. However, all CA were about 45° at midstance, where joint reversals occurred. Variability was relatively constant throughout stance.

SUMMARY

The results of this study have provided a normative reference for joint coupling measures. Deviations outside the ±1SD interval may place runners at a greater risk for lower extremity running injures. However, prospective injury studies are needed to lend further insight into the relationship between coupling and injury.

REFERENCES

Bates, B.T. et al. (1978). *Running*, Fall, 24-30.
Hamill, J. et al. (1999). *Clin. Biomech.*, 14, 297-308.
Heiderscheit, B.C. et al. (2002). *J.A B.*, 18, 110-121.
Kelso, J.A. (1984). *Am. J. Phys.*, 246, R1000-R1004.

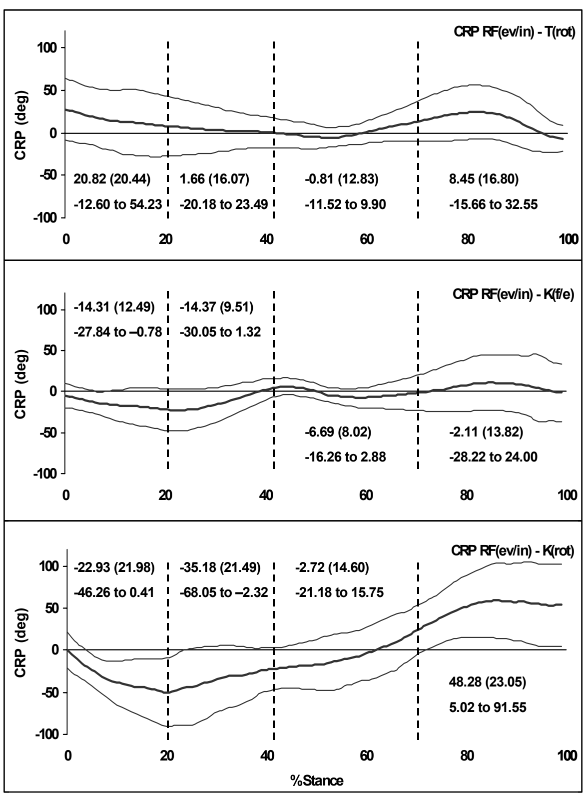

Figure 1. Selected CRP curves (mean ±1BSD). 0° is in-phase coupling, 180° and –180° are out-of-phase. The mean, WSD, and normal interval are displayed by phase.

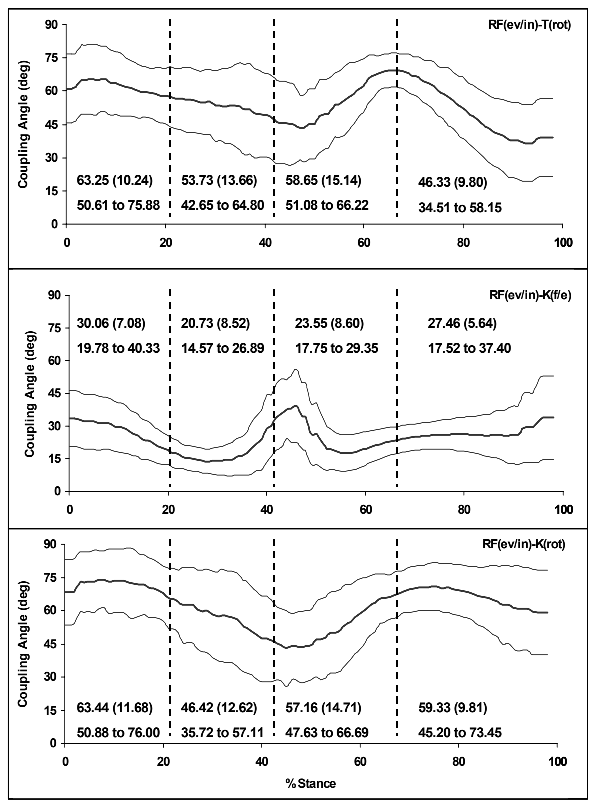

Figure 2. Selected CA curves (mean ±1BSD). 45° is equal motion, >45° is more distal motion. The mean, WSD, and normal interval are displayed by phase.

STEPPING UP AND ONTO A LATERALLY-COMPLIANT STRUCTURE: FRONTAL PLANE RESPONSES IN YOUNG ADULTS

Bing-Shiang Yang and James A. Ashton-Miller

Biomechanics Research Laboratory
Department of Mechanical Engineering
University of Michigan, Ann Arbor, MI, USA.
E-mail: bsyang@umich.edu

INTRODUCTION

Falls from raised surfaces such as stepladders, chairs and stools cause injuries across the age spectrum, but especially in the elderly. In the case of a stepladder, a lateral fall is the most common type of accident (Björnstig and Johnsson, 1992). One reason for this may be that stepladders, chairs, and stools are not usually rigid, but have structural compliance, often in the mediolateral (ML) direction. This study examines the interaction between that structural compliance and the strategy used to step onto the structure. Although lateral balance recovery under external perturbations has been described (Maki et al. 1996 and Rietdyk et al. 1999), responses to the self-induced ML perturbations that can occur when stepping up and onto a compliant structure have not been reported. The purpose of this study, therefore, is to test the null hypothesis that stepping strategy does not change when stepping up and onto rigid and compliant structures.

METHODS

Twenty healthy young adults (25.6±2.2 yrs) standing on firm ground were asked to step forward and up onto a seven-inch high step at a comfortable speed. The ML compliance of the structure supporting the step could be covertly assigned one of three different values: low compliance (C_1= 1×10^{-3}m/N measured at the step surface), high compliance (C_2= 2×10^{-3}m/N) and rigid (C_0<10^{-4}m/N).

Body segment and step kinematics were recorded using an Optotrak 3020 system at 100 Hz with 10 IRED sensors on the dorsal surface of the trunk and legs. The whole-body center of mass (COM) location was estimated using three body segments—head-arm-torso (HAT) and two legs. Two F-scan foot-pressure sensors, larger than the feet, were placed on the step surface to capture, at 100 Hz, the time history of normal reaction force under each foot. Six trials were run with each compliance. Trial order was C_0, C_1, and C_2 interspersed by different numbers of blocks of six C_0 trials to prevent subjects knowing when a change occurred.

Phases of stepping movement (Figure 1). The stepping movement was divided into four phases: (1) weight transfer preparation phase, (2) structural compliance identification phase, (3) unipedal support phase, and (4) bipedal recovery phase

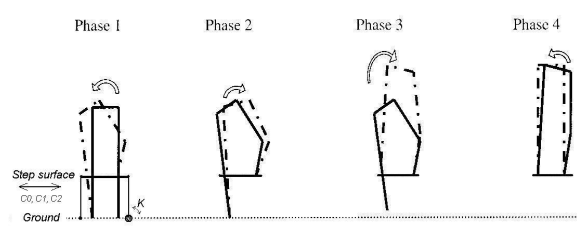

Figure 1: Four phases of forward stepping movement onto a raised structure. Solid lines illustrate initial leg states while broken lines illustrate final states of phases. Arrows indicate the directions of weight transfer.

RESULTS AND DISCUSSION

Only data from the first trial of each test condition are reported here. Changes in compliance did not significantly affect Phase 1 kinematic parameters. Table 1 shows the parameter changes in Phases 2 - 4 for the three structural compliances. The time used in Phase 2 for identifying structural properties and initiating stepping onto the compliant structure (C_1 or C_2) was significantly longer than onto the rigid structure (C_0) (t_{id} increased 15% with C_1 and 21% with C_2). This difference indicates that subjects needed more information and time to transfer their weight onto compliant structures.

Lateral COM velocity at the time of trailing-foot push-off (between Phase 2 and 3) decreased significantly with increasing structural compliance (COM_{vpf} decreased 20% with C_1 and 38% with C_2) apparently to prevent inducing unnecessary lateral oscillations in the human-structure system.

In Phase 3, subjects significantly shortened their unipedal support period (t_u decreased 15% with C_1 and 17% with C_2), and lateral COM excursion (COM_{uex} decreased 35% with C_1 and 45% with C_2) on compliant structures. Moreover, lateral COM velocity decreased with increasing structural compliance (COM_{vm} decreased 19% with C_1 and 37% with C_2).

In Phase 4, the bipedal recovery phase, average lateral weight transfer rate (dRy_2) decreased significantly (37%) on the most compliant structure compared with the rigid structure.

These results suggest that, without any practice, these healthy young adults naturally slow their lateral weight transfer once they have identified the compliance of the structure that they are stepping onto. Failure to do so may be one mechanism for a fall from a stool, chair, or stepladder. Future studies might address this situation in older adults.

SUMMARY

Young adults adapted to the presence of unexpected structural compliance as they stepped up and onto the structure by identifying its compliance, slowing their lateral motion, decreasing lateral COM excursion, and shortening the unipedal support phase.

REFERENCES

Björnstig, U. and Johnsson, J. (1992). *J. Safety Research*, **23**, 9-18.

Maki, B.E. *et al.* (1996). *J. Biomechanics*, **29**, 343-353.

Rietdyk, S. *et al.* (1999). *J. Biomechanics*, **32**, 1149-1158.

Table 1: Effect of compliance on mean (SD) movement parameters. Percentage differences (Diff) between test conditions are also shown.

Parameters (units)	C_0	C_1	Diff C_1 to C_0	C_2	Diff C_2 to C_0
t_{id}^{*} (sec)	0.52 (.05)	0.60 (.20)	+15%	0.63 (.13)	+21%
COM_{vpf}^{**} (BH/sec)	0.113 (.033)	0.090 (.019)	-20%	0.070 (.031)	-38%
t_u^{*} (sec)	0.41 (.06)	0.35 (.02)	-15%	0.34 (.05)	-17%
COM_{uex}^{*} (BH)	0.020 (.011)	0.013 (.005)	-35%	0.011 (.006)	-45%
COM_{vm}^{**} (BH/sec)	0.062 (.026)	0.050 (.016)	-19%	0.039 (.018)	-37%
dRy_2^{+} (BW/sec)	1.245 (.297)	1.334 (.608)	+7%	0.786 (.179)	-37%

t_{id}: time used in Phase 2; COM_{vpf}: COM velocity at trail-foot push-off; t_u: time used in Phase 3; COM_{uex}: lateral COM excursion in Phase 3; COM_{vm}: average COM velocity in Phase 3; dRy_2: average lateral weight transfer rate in Phase 4; BH: body height; BW: body weight.

**: ($p<0.05$ across 3 conditions); *: ($p<0.05$: C_0 vs C_1, and C_0 vs C_2); +: ($p<0.05$: C_0 vs C_2, and C_1 vs C_2)

MULTIPLE FEATURES OF MOTOR-UNIT ACTIVITY INFLUENCE FORCE FLUCTUATIONS DURING ISOMETRIC CONTRACTIONS

Anna M. Taylor, Evangelos A. Christou, and Roger M. Enoka

Neural Control of Movement Laboratory, University of Colorado, Boulder, CO, USA
E-mail: anna.taylor@colorado.edu Web: www.colorado.edu/kines/research/ncm.html

INTRODUCTION

The time and frequency structure of force is often used to assess the neural mechanisms that control muscular contractions. Recent literature (Enoka et al. 2003; Jones et al. 2002) suggests that the amplitude of force fluctuations declines with the amount of force produced. Furthermore, it appears that the primary contribution to force variability is the variation in the discharge rate of the motor units involved in the task. However, other possible causes of force fluctuations include low-frequency oscillation in drive (Vaillancourt et al. 2002) to the motor units, motor unit synchronization (Yao et al. 2000), and motor unit discharge rates (Patten and Kamen 2000). One of the limitations of the extant literature is that most studies have used low-force contractions. Thus, comparatively little is known about the structure of force produced during high intensity contractions. The purpose of this study was to identify the mechanisms that influence the structure of isometric force across the entire operating range of a muscle. To achieve this aim, a combined experimental and computational approach was used.

METHODS

Isometric force was recorded during contractions of the first dorsal interosseus in ten young (29.4 ± 4.4 years) subjects (5 men and 5 women). Force and EMG were recorded for 6 s (3 s with visual feedback and 3 s without) at 9 levels of contraction intensity (2, 5, 15, 30, 50, 70, 85, 95, and 98% of MVC force). Two trials were completed per force level. The order of the force levels was randomized for each subject.

The experimental data were compared with the isometric force produced by a model of a motor unit population (Fuglevand et al. 1993). The model comprised 120 motor units, each of which had individual twitch properties and force-frequency relations. The model motor units are activated according to the Size Principle, and their properties are designed to approximate the first dorsal interosseus.

To address the research question, multiple parameters were varied in the model. These included: (1) the rate-excitation functions for the individual motor units; (2) the maximal discharge rates of individual motor units and the pattern of maximal rates across the population; (3) range of recruitment levels; (4) discharge variability; (5) synchronization of the motor units; and (6) oscillating drive to the motor units in the population.

The variability of the experimental and model forces were analyzed in the time domain by quantifying the amplitude of the fluctuations in force using the coefficient of variation of force. The frequency structure of the forces was quantified with power density spectra, expressed as a percentage of the total power in the signal. The results for the no-vision force trials were compared to the model data.

RESULTS AND DISCUSSION

The results from this study indicated that there was a decline in force fluctuations between 2 and 30% MVC, but that the amplitude of force fluctuations then increased and plateaued at forces greater than 30% MVC.

Of the parameter changes that were made to the model, four could approximate the experimental data at a minimum of four out to the nine force levels (Figure 1).

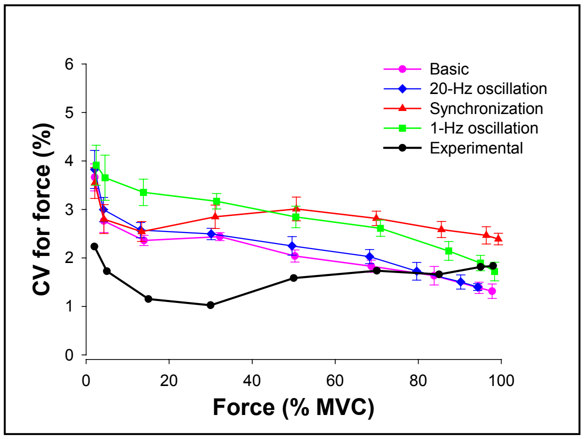

Figure 1: The models that matched the experimental coefficient of variation for force were significantly different at moderate force levels (15 and 30% MVC).

The maximal power in the experimental force spectra occurred at 1.4 ± 1.1 Hz, with 43 ± 6% of total power at this frequency. The 1-Hz model exhibited a similar peak frequency (0.99 ± 0.53 Hz) and peak power (38 ± 2.3%). The peak frequencies for the other models were higher (basic: 5.1 ± 5.5; 20-Hz: 5.2 ± 5.3; synchronization: 3.6 ± 1.7 Hz). Furthermore, the models had secondary peaks at higher frequencies, with the exception of the synchronization model.

Of the four models that matched the time-domain variation in force, only the synchronization model showed an increase at higher forces. However, this did not occur at the same point as in the experimental force. The secondary peaks in the power spectra for the models were likely related to the mean rates of the model motor units. The prominent low-frequency peaks in all models suggested that the low-frequency power in human force signals was largely unrelated to oscillating activation of motor units.

SUMMARY

The results from this study indicate that the variability in motor output changes across levels of excitatory drive. The two most explanatory mechanisms for force variability are a low frequency oscillation in the activity of the motor units and motor unit synchronization. The inability of the model to reproduce the decline and subsequent plateau in force fluctuations at moderate forces suggests that a more complex theoretical model of the neural control of force is needed.

REFERENCES

Enoka, R.M. et al. (2003) *J Electromyogr Kinesiol* **13**, 1-12

Fuglevand, A.J. et al. (1993) *J Neurophysiol* **70**, 2470-88.

Jones, K.E. et al. (2002) *J Neurophysiol* **88,** 1533-44.

Patten, C. and Kamen, G. (2000) *Eur J Appl Physiol* **83,** 128-43

Vaillancourt, D.E. et al. (2002) *Clin Neurophysiol* **113**, 1325-38.

Yao, W. et al. (2000) *J Neurophysiol* **83,** 441-52

ACKNOWLEDGEMENTS

Supported by an NIH grant (AG09000) awarded to RME and an NSF Graduate Fellowship awarded to AMT.

A KINEMATIC ANALYSIS OF THE EFFECTS OF AGE ON TURNING STRATEGIES IN HEALTHY FEMALES

Peggy Meinhart, Carol Persad, and James A. Ashton-Miller

Biomechanics Research Laboratory, University of Michigan, Ann Arbor, MI, USA
E-mail: pmeinhar@umich.edu

INTRODUCTION

The costs of falls and fall-related injuries in the elderly exceed $20 billion per year [Englander 1996]. One third of community-dwelling elderly fall each year, and 5% of these will experience fracture or significant injury requiring hospitalization [Tinetti 1988]. Due to the serious costs and consequences of falls, locomotion in the elderly continues to warrant further analysis.

While level gait has been extensively studied, turning, another feature of locomotion, has received limited attention despite its relationship with falling and with hip fractures in the elderly. For example, Lipsitz et al. found that fallers took 40% longer and 6 more steps to complete a 360^{o} turn than did non-fallers [Lipsitz 1991]. In addition, a fall while turning was shown to be 7.9 times more likely to lead to a hip fracture than a fall while walking straight [Cumming 1994]. We therefore tested the (null) hypothesis that age alone, uncomplicated by disease, has no effect on the kinematics of a 180^{o} turn executed in a confined space.

METHODS

Ten healthy young females and 10 healthy elderly females (ages 21.8$\pm$1.99 and 72.5$\pm$5.82 yrs) participated in the study. The heights of the young and elderly were not significantly different. Upon arrival, subjects were asked to turn in a circle. The turn direction chosen was designated as the "preferred turn direction". Subjects were outfitted with an over-head safety harness system to guard against injury. They performed 62 trials in which a 180^{o} turn to the right or left was required to move a bowl between two tables. Forty-eight of the trials consisted of normal 180^{o} standing turns and 14 trials consisted of "catch" turns, or an initiation of a turn followed by a sudden direction reversal. Trials were organized in a pre-determined random order unknown to the subjects and initiated by a visual cue. The direction reversal in catch turns was triggered by an audible cue activated by a 90% weight shift as measured by two force plates.

The total time and number of steps required to complete the task were recorded. The timing of each step was determined from thin pressure sensors placed inside the shoes (F-Scan System, Tekscan, Inc., South Boston, MA). Body segment kinematics were recorded at 100 Hz by an optoelectronic camera system utilizing infrared-emitting diode triads placed on each side of each shoe and on each iliac crest (Northern Digital Inc., Waterloo, Ontario). Finally, the outline of each shoe was digitized in order to quantify the foot separation distance for each trial, an indicator of risk for foot-foot interference.

RESULTS

General turning strategies and characteristics are compared for young and elderly subjects in Table 1. While the elderly tended to take more steps and more time to complete each trial, the only significant age difference occurred in the number of steps required to complete a catch trial.

Table 1: General turning characteristics (ave ± SD).

	# of Steps		Total Time (sec)		Preparatory Stepping Strategy
	Normal	Catch	Normal	Catch	
Young	3.93 ± 0.67	5.47 ± 1.13	3.97 ± 0.60	4.87 ± 0.62	23.4%
Elderly	4.45 ± 0.89	6.54 ± 0.53	4.40 ± 1.19	5.68 ± 1.09	65.3%

It was found that the elderly are more likely to use a conservative, preparatory stepping strategy whereby the first step is taken with the foot contralateral to the turn direction as shown in Figure 1. Young and elderly used this strategy in 23.4% and 65.3% of the trials, respectively.

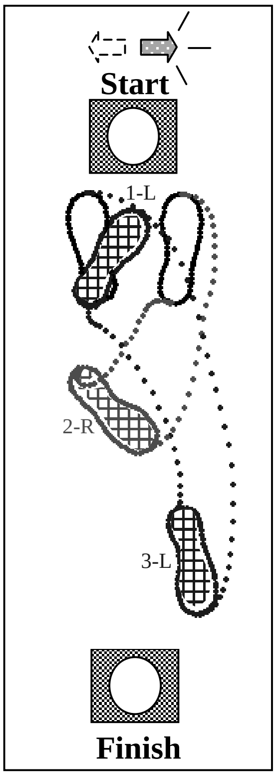

Figure 1: Stepping pattern and trajectory for single normal turn
1-L: First step, left foot
2-R: Second step, right foot
3-L: Third step, left foot

To express the foot separation distance, an overall minimum distance for each trial was determined. Values for normal turns were grouped by subject age and turn direction preference (Figure 2). A repeated measures analysis showed that irrespective of the turn type, the direction of the turn and the interaction between age and direction significantly affected the results ($p=0.043$ and $p=0.047$, respectively). The foot separation distance was significantly more variable in the elderly than in the young ($p=0.049$) with the difference in variability reaching a significance level of $p=0.025$ for normal turns. Therefore, differences in foot kinematic characteristics for young and elderly were found. Other measures examined were base of support dimensions and angular versus linear motion of the subject.

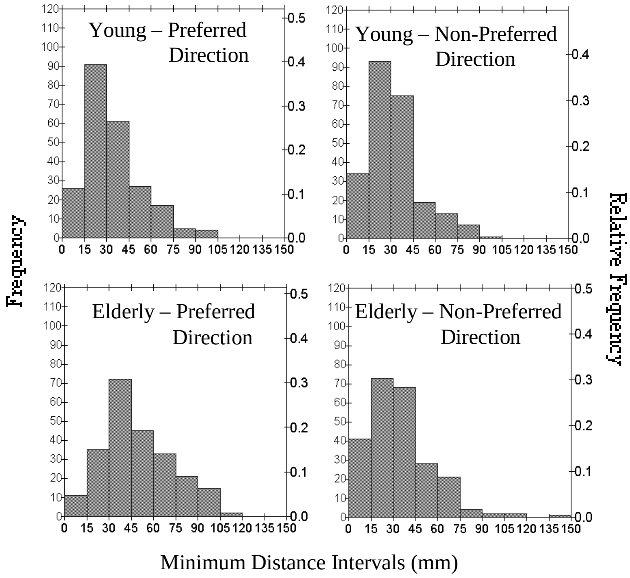

Figure 2: Minimum foot separation distance grouped by age and preferred turning direction.

DISCUSSION

In general, elderly tend to use conservative strategies by taking more steps and time to complete the task and utilizing a preparatory stepping strategy. However, in elderly adults, minimum foot separation distance is more variable and more affected by turn direction. These differences between healthy populations give insight into turning tendencies of elderly who may be at risk for falling while turning.

REFERENCES

Englander, F., et al., (1996). *J. of Forensic Sci.*, **41**, 733-746.

Tinetti, M.E., et al., (1988). *N. Engl. J. Med.*, **319**, 1701-06.

Lipsitz, L.A., et al., (1991). *J. Gerontol. Med. Sci.*, **46**, M114-M122.

Cumming, R.G., Klineberg, R.J., (1994). *J. Am. Geriatr. Soc.*, **42**, 774-8.

A COMPARISON OF C-LEG® AND 3R60 PROSTHETIC KNEE JOINT PERFORMANCE

M. R. Meier, PhD, CPO[1], S. A. Gard, PhD [1,2], A. H. Hansen, PhD [1], D S. Childress, PhD [1,2]

[1]Northwestern University, Feinberg School of Medicine, Prosthetics Research Laboratory and
[2]VA Chicago Health Care System, Lakeside Division, Chicago, IL 60611, USA
E-mail: m-meier@northwestern.edu Web: www.repoc.northwestern.edu

INTRODUCTION

The C-leg® is an advanced microprocessor-regulated knee mechanism. It is thought to enhance function in a wide range of locomotion modes due to the stance and swing phase monitored gait cycle. It has been suggested that the C-leg® improves the amputee's ability to walk down ramps and descend stairs (Stinus, 2000; Michael, 1999; Dietl, 1998; Zahedi *et al*., 1998). In this study the C-leg is compared with the 3R60 knee joint.

METHOD

General: Each participant wore each prosthetic knee joint for a period of four weeks. Test prostheses were fabricated using a duplication of the participant's current prosthetic socket and a Dynamic Plus foot. *Participants:* Persons with unilateral transfemoral amputation, ages between 40 and 60 years, with a body-weight less than 220 lbs, were included in the study if they presented with no serious complications that interfered with their walking ability; had six or more months of experience with a definitive prosthesis; were able to walk unassisted at a comfortable speed without undue fatigue and without health risk; and were able to climb stairs. *Protocol:* Quantitative gait analysis was performed at the VA Chicago Motion Analysis Research Laboratory (VACMARL). Participants were requested to walk at their preferred and fastest speed, with and without mental loading. The mental loading test consisted of a mathematical calculation task where the participant had to count vocally backwards in three-step increments (first visit) and in 7-step increments (second visit). An obstacle course was set up at VACMARL being composed of a foam session (10 feet), narrow slaloms around three chairs, a vacuumized bean-bag section (10 feet) simulating sand, a rock section (10 feet), a short ramp (5 feet), a 90-degree turn, and a final step. Participants completed the obstacle course twice, once without mental loading, once with mental loading. They were timed. The stair task included one-flight with 10 steps; participants were requested to climb up and down the stairs in their usual manner, once without mental loading, once with mental loading. Heart rate was measured during all conditions in order to calculate the Total Heart Rate Index (THBI) (Hood *et al*., 2002). The THBI is calculated by dividing total heartbeats during an exercise period by the total distance traveled and is an indicator of energy efficiency. All of the participants gave written consent approved by the Institutional Review Board of Northwestern University.

RESULTS AND DISCUSSION

To date, data of three participants have been analyzed. The participants' characteristics are shown in Table 1. Table 2 presents their walking speeds on level walking with and without mental loading. Due to the small number of participants analyzed, statistical tests have not been carried out. When comparing the two knee joints the mental task had a negative impact on all walking speeds in all participants while wearing the

Table 1: Anthropometric and Social Data of the Participants. TK= Transfemoral; KD=Knee disarticulation

Participants n=3	Gender	Age (years)	Height (m)	Weight (kg)	Years since Amputation	Amput. Level	Current Foot	Current Knee	Current Socket
A	male	54	1.73	87.5	28	TF	Flex-Walk	SNS	IC-type
B	female	44	1.64	60.0	43	KD	Ceterus	Total Knee	IC-type
C	male	54	1.71	88.7	3	TF	Multiflex	SNS	IC-type

3R60 joint; with the C-leg®, two participants increased their fast walking speed under the mental loading condition, one also at normal speed. In Table 3 the results of the THBI are summarized. Better energy efficiency, as indicated by the THBI, was achieved by the C-leg® only during normal walking speed without mental loading. In all the other conditions, the energy efficiency was the same or better with the 3R60 joint.

Table 2: Walking Speeds [a]Average of 9 trials (min 4 trials; max 21 trials) MT= Mental Task

Participants (n=3)	3R60				C-leg			
	Normal Speed (m/s)		Fast Speed (m/s)		Normal Speed (m/s)		Fast Speed (m/s)	
	w/o MT	w MT	w/o MT	w MT	w/o MT	w MT	w/o MT	w MT
A	1.13[a]	1.12	1.64	1.62	1.04	0.91	1.70	1.82
B	1.10	0.97	1.34	1.16	1.10	0.96	1.30	1.04
C	0.76	0.48	0.88	0.72	0.82	0.89	1.01	1.08
Median	1.10	0.97	1.34	1.16	1.04	0.91	1.30	1.08

Table 3: Total Heart Beat Index (THBI)
[a] Median; MT= Mental Task

THBI	3R60	C-leg
Walking:		
Normal w/o MT	24.85[a]	15.43
Normal w MT	22.27	24.45
Fast w/o MT	19.72	21.26
Fast w MT	22.07	22.06
Obstacle Course:		
w/o MT	34.66	41.64
w MT	34.57	43.19
Stairs:		
w/o MT	142.26	156.66
w MT	141.80	198.30

The C-leg® demonstrated the tendency to facilitate fast walking speed, especially under the mental loading condition. This suggests that once the participants' main focus was not on walking, the C-leg® increased their confidence, so that they were able to walk faster with almost the same energy efficiency as with the 3R60 knee joint. However, in almost all other conditions energy efficiency was worse with the C-leg®, especially during the obstacle course and on the stairs. Under the mental loading condition, the C-leg® did not demonstrate energy efficiency improvement, like the 3R60 knee joint. The overall performance on the stairs was the same with both knee joints; thus performance change cannot explain the C-leg®'s THBI difference during stair negotiating. The THBI results stand in contrast with the results of Buckley *et al*. (1997) who observed reductions in the physical energy cost using an "Intelligent Prosthesis" (IP) from Blatchford. But our results regarding the mental loading are in support with the results of Heller *et al*. (2000) who also demonstrated that the IP was not shown to be less cognitively demanding than a conventional knee joint.

SUMMARY

In the given circumstances, the C-leg® seemed to produce mixed results. It tends to facilitate fast walking speed, especially under a mental loading task. However, the C-leg® energy efficiency, as estimated by the THBI, is generally worse than that of the 3R60 knee.

REFERENCES

Buckley JG, Spence WD et al. (1997) *Arch Phys Med Rehabil*. **78**,330-3

Dietl H. (1998) IXth *World Congress of ISPO, Amsterdam*, NL, 51-52

Heller BW, Datta D et al (2000) *Clin Rehabil*. **14**, 518-522

Hood VL, Granat MH et al.(2000) *Arch Phys Med Rehabil.* **83**,1266-73

Michael JW. (1999) *Clin Orthop*. **361**,39-47

Stinus H (2000) *Z Orthop Ihre Grenzgeb*. **138**, 278-282

Zahedi S, Sykes A, et al. (1998) IXth *World Congress of ISPO, Amsterdam*, NL, 612-614.

ACKNOWLEDGMENTS

This work was supported by the Department of Veterans Affairs, Rehabilitation Research and Development Service and is administered through the VA Chicago Health Care System, Lakeside Division, Chicago, IL, USA.

IDENTIFYING MUSCULAR CHALLENGE DURING LOCOMOTION IN THE ELDERLY: AN EMG STUDY

Heng-Ju Lee, Michael E. Hahn, Sentaro Koshida and Li-Shan Chou

Department of Exercise and Movement Science, University of Oregon, Eugene, OR, USA
E-mail: chou@oregon.uoregon.edu

INTRODUCTION

Adequate muscle strength in the lower extremities is essential for effective responses to maintain balance during locomotion. However, skeletal muscle strength involved in balance control and locomotion declines with age (Fiatarone et al., 1993). The loss of muscular strength may limit functional capacity and contribute to falls in the elderly. Age related reductions in strength are greatest in the lower extremity muscles (McDonagh et al., 1984).

To better examine the level of challenge imposed on a muscle group, a quantitative index that takes both the strength availability (capacity) and strength requirement (demand) during performance into account is needed. Dynamic EMG data allows us to examine the timing and relative intensity of the muscle effort (Perry, 1993). Difference in the EMG magnitude of a single muscle represents varying levels of effort. The ratio between the EMG amplitudes collected during functional tasks and the peak EMG amplitude collected during the maximum effort manual muscle testing (MMT) can be used to quantitatively identify the utility of available strength of a muscle group, which can allow us not only to monitor muscle recruitments during different phases of gait but also to examine the instantaneous level of neuromuscular challenge imposed on the selected muscle. The purpose of this study was to test the hypothesis that this EMG ratio is able to quantitatively reflect a relatively higher challenge in lower extremity muscles of elderly adults when compared to young adults during balance challenging tasks, such as obstacle crossing.

METHODS

Ten young adults (5 males/5 females; mean age 25.2yrs) and twelve elderly adults (8 males/4 females; mean age 72.7yrs) were recruited for this study. All participants were determined to be free of neuromuscular or orthopedic pathologies. Pre-amplified surface electrodes were attached bilaterally to bellies of the gluteus medius (GM), vastus lateralis (VL) and gastrocnemius (medial head, GA). These muscle groups were previously shown to be substantially challenged during obstacle crossing (Chou et al., 1998). Maximum effort MMT was performed for isometric hip abduction, knee extension, and ankle plantar flexion. Subjects were then asked to walk at a self-selected pace during level and obstructed gait tasks. A light-weight crossbar was set to a single obstacle as height of 2.5, 5, 10, and 15% body height (BH). Obstacle heights were randomized with 3 trials being collected for each condition. Data were analyzed from the heel-strike of the trailing limb before stepping over the obstacle to its next heel-strike when crossing the obstacle. The leading limb was defined as the first limb to cross the obstacle followed by the trailing limb.

EMG signals were collected at 960Hz using the MA-300™ system (Motion Lab Systems, Baton Rouge, LA). Filtered and rectified signals from the gait trials (demand) were then normalized to the MMT signal maximum (capacity) for each muscle to indicate their relative activation levels. The gait cycle was divided into 4 phases according to the trailing limb: 1st double support, 1st single support, 2nd double support, and swing phases. Similarly 4 phases were defined for the leading limb: swing, 1st double support, single support, 2nd double support. The mean EMG ratios of both limbs during each phase were then analyzed for the effects of age group and obstacle heights with a two-factor ANOVA with repeated measures of obstacle height.

RESULTS AND DISCUSSION

Compared to young adults, elderly adults demonstrated greater relative activation levels in both lower limbs for all four phases. Average EMG ratios of GM and VL were significantly greater in the elderly (p=0.039 and p=0.031, respectively) and were activated up to 50% and 40% of their peak MMT magnitudes, as compared to 30% and 25% in the young (Fig. 1). The GA of the elderly was activated up to 43% of its peak MMT magnitude, as compared to 36% in the young.

Each of obstacle crossing condition required higher activation levels than level walking for all muscles in both limbs. Increasing obstacle height resulted in significantly greater relative activation for all muscles of both limbs (p=0.023). Peak relative activation of GM and VL of both limbs occurred during the 1st double-support phase (weight acceptance). The results can be interpreted as during double-support, weight transfer and acceptance required GM to maintain lateral balance and VL to maintain anterior balance. The GA peak mean relative activation occurred at single-support phase. Maintenance of dynamic stability and forward progression is required during the single-support phase of gait.

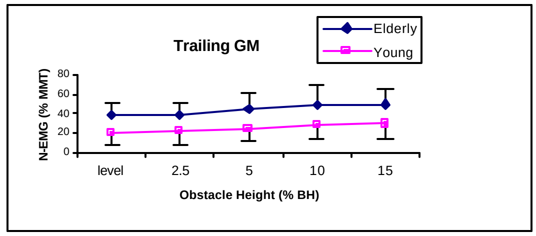

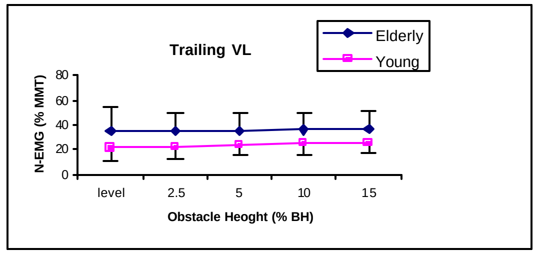

Figure 1: Average EMG ratios of the trailing limb GM and VL

SUMMARY

These findings indicate that elderly adults require a greater proportion of their muscular capacity during level walking and obstacle crossing tasks than young adults. As the task of crossing obstacles poses a greater challenge to dynamic balance control, it may be inferred that decreased lower extremity muscle strength likely puts the elderly population at greater risk for imbalance or falling. This EMG ratio may further allow us to better identify the timing for the onset of falls (maximum instability) in the elderly.

REFERENCES

Chou, L.S. et al. (1998). *Gait Posture* **8**, 186-204.
Fiatarone, M.A. et al. (1993). *J Gerontol* **48S**, 77-83.
McDonagh, M.J. et al. (1984). *Gerontology* **30**, 49-54.
Perry, J. (1993) *Gait Analysis*. Thorofare, NJ, Slack Inc.

ACKNOWLEDGEMENTS

This work was supported by the University of Oregon and the Oregon Medical Research Foundation.

POTENTIAL THERAPEUTIC BENEFITS OF SELF-ASSISTED STEPPING

Pei-Chun Kao and Daniel P. Ferris

Department of Movement Science, University of Michigan, Ann Arbor, USA
E-mail: kaop@umich.edu

INTRODUCTION

Body weight-supported treadmill training is a new approach in gait rehabilitation that can substantially improve walking capacity of patients with spinal cord injury or stroke. Disadvantages to the technique are that it is labor intensive and it relies on therapists' manual assistance. More active participation by the patient during therapy may increase neuromuscular recruitment and coordination. An ideal gait therapy would allow a patient to actively practice stepping motions without the need for therapist intervention.

The NuStep recumbent stepping machine (Ann Arbor, MI) may be able to provide beneficial gait therapy with minimal therapist labor. It has two pedals and two handles that move in a simplified one-degree of freedom stepping motion. Pedals and handles are contralaterally coupled and patients can drive the motion with their legs and/or arms. As a result, patients that cannot step independently can use their own arms to assist the stepping motion. This may benefit neuromuscular recruitment due to inherent links between upper limb and lower limb control during locomotion (Dietz 2002). The handle/pedal coupling of the stepping machine also allows patients to increase the frequency of their stepping motion during therapy beyond what they are capable of with legs alone. Walking at higher speeds produces greater muscle activity, more normal EMG patterns, and better walking capability after training in neurologically impaired patients (Harkema 2001; Hesse et al. 2001; Sullivan et al. 2002).

To provide insight into potential benefits of self-assisted recumbent stepping as a gait therapy, we examined young healthy subjects stepping at four frequencies under three conditions. The three conditions were: (1) active stepping using both arms and legs, (2) self-driven motion with passive legs (i.e. using arms to propel the stepping motion and allowing legs to move passively on the pedals), and (3) externally-driven motion with passive legs (i.e. both arms and legs are totally passive and the stepping motion was propelled by another person moving the handles). We tested two hypotheses: (a) increasing stepping frequency results in increased left-right symmetry in muscle activation patterns during active stepping (condition 1), and (b) self-driven lower limb motion (condition 2) results in greater muscle activation than externally-driven lower limb motion (condition 3).

METHODS

Four healthy female subjects stepped at four different frequencies (30, 60, 90, 120 bpm) at a constant resistance. Before data collection, subjects stepped with a range of resistances to self select the hardest resistance they could maintain with their arms only. We recorded lower limb joint angles and EMG from six muscles on each leg. We analyzed EMG root mean square (RMS) amplitude for each muscle across conditions and calculated the correlation coefficient between left and right side low-pass filtered EMG for condition 1.

RESULTS AND DISCUSSION

During active stepping using both arms and legs, symmetry between left and right muscle activation patterns increased with stepping frequency (ANOVA $p < 0.001$; Fig. 1). In addition, muscle activation amplitude increased with frequency for all conditions ($p < 0.001$; Fig. 2). These results suggest that higher stepping frequencies may benefit neurologically impaired subjects by increasing motor symmetry and neuromuscular recruitment.

Self-driven lower limb motion resulted in greater leg muscle activation amplitude compared to externally driven lower limb motion (THSD, $p < 0.05$; Fig. 2). This supports the idea that self-assisted stepping may increase neuromuscular recruitment in neurologically impaired subjects compared to externally-driven stepping.

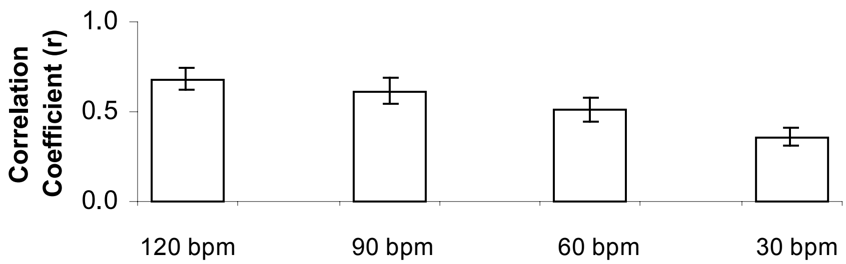

Figure 1: Mean correlation coefficient values of EMG patterns between left and right side for the six muscles during active stepping. Error bars represent the standard error of mean.

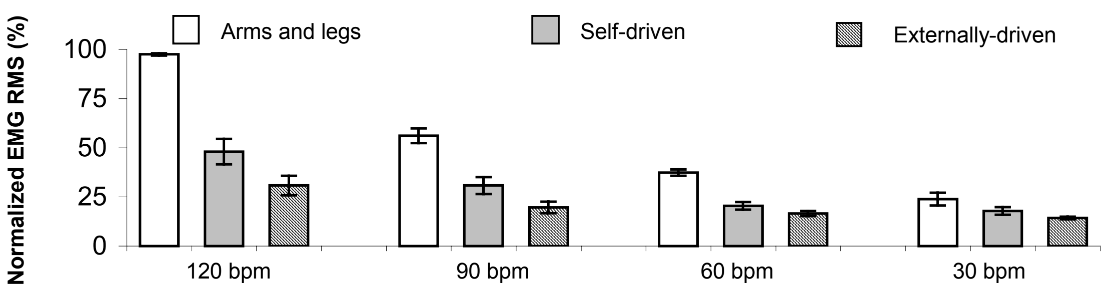

Figure 2: Mean EMG RMS amplitudes for the six muscles averaged together. We normalized amplitudes to the maximum value recorded in each muscle in each subject across conditions. Error bars represent the standard error of mean.

SUMMARY

This study on healthy subjects suggests that neurologically impaired patients may benefit from self-assisted stepping on a recumbent stepping machine. The stepping device may allow patients to achieve increased neuromuscular recruitment and bilateral coordination due to higher stepping frequencies and inherent neural coupling between the arms and legs.

REFERENCES

Dietz V. et al. (2002). *Trends Neurosci.* **25**:462-7.

Harkema S.H. et al. (2001) *Prog Clin Neurosci.* **7**:455-68.

Hesse S. et al. (2001). *Arch Phys Med Rehabil.* **82**:1547-50.

Sullivan K.J. et al. (2002). *Arch Phys Med Rehabil.* **83**:683-91.

FORCE CHANGES WHEN WALKING CONTINUOUSLY WITH EXTRA WEIGHT

Scott White, Chiung-Yu Cho and Laura Malczewski

Biomechanics Laboratory, Exercise & Nutrition Sciences
State University of New York at Buffalo, Buffalo, NY, USA
E-mail: swhite@acsu.buffalo.edu

INTRODUCTION

It has been hypothesized that long duration walking (20 minutes) will cause quadriceps fatigue resulting in an increase rate of loading and an increase in the magnitude of ground reaction forces (Syed & Davis, 2000). Quadriceps act as shock absorbers, reducing the rate of loading on the knee during the weight acceptance phase of gait (Whittle, 1999). Quadriceps strength is predictive of both radiographic and symptomatic evidence of osteoarthritis (OA) of the knee, and a strong correlation exists between quadriceps strength, knee OA, and obesity (Slemenda et al., 1997; Slemenda et al., 1998). Syed and Davis (2000) theorized that the obese would reach a point of quadriceps fatigue sooner than normal when walking resulting in higher loads and rates of loading. The link between body weight and changes to limb loading measures for continuous walking has not been shown. An experimental model of weight manipulation is proposed to investigate changes to ground reaction forces over a continuous, 32-minute walk. We hypothesized that force measures during the weight acceptance phase of gait would increase over time, and that the increase would be more pronounced when walking with extra weight.

METHOD

Five subjects (3 males, 2 females, mean age = 33 years) with a body mass index (BMI) in the normal weight category (BMI between 20 and 25) walked at a constant treadmill speed (between 1.34 ms^{-1} and 1.51 ms^{-1}) on two occasions; once with, and once without additional weight. Weight was added via a weight vest and weight belt to achieve a BMI equivalent to Obese I (BMI between 30 and 35). A minimum of 8 steps (right and left) of vertical ground reaction force data were collected within the first 3 minutes of walking on a force measuring treadmill, and at 8-minute marks over a 32-minute interval. Peak loading force during the first half of stance (F1) and the rate of rise of the loading force ($F1_R$) were calculated from the vertical force records. Dependent measures for the 8 steps were averaged for each subject treating right and left limbs separately. F1 and $F1_R$ from the original data sample were subtracted from each 8-minute sample, plotted against time and fit with a linear best-fit trend line. A paired t-Test was used to test for significant differences ($p < .05$) between the original and the last data sample.

RESULTS

There were no significant increases in end-point values (32-minute sample) and the original values for the normal weight condition (F1: $p = .08$; $F1_R$: $p = .21$) or the extra weight condition (F1: $p = .41$). The loading rate for the weighted condition was significantly less ($F1_R$: $p = .02$). The peak force during loading and the loading rate did not tend to increase over the duration of the walk (Fig. 1 & 2). There were no differences in this trend when walking with or without the extra weight.

DISCUSSION

Peak force and loading rate did not increase over time as had been predicted. (Syed & Davis, 2000). Subjects in this study were healthy, active and normal weight. It may be that the protocol did not fatigue quadriceps enough to affect the force measures. Knee extensor strength was measured within 3 minutes of completing the walk. It decreased for all subjects for the weighting condition (average = 8.5%); however, the change is low considering the reliability of retesting a maximum voluntary contraction. There was substantial between-subject variability in dependent measures. Forces are influenced by how an individual changes their "effective mass" to achieve greater shock absorption and lower impacts. The ability to adapt to fatigue is a factor and has been shown to influence impact forces when running (Derrick, et al., 2002). It may be that overweight individuals have insufficient strength or muscular endurance to adjust to loading. A treadmill was used to control walking speed but fatigue effects could have been masked if changes in the force measures reflect gait accommodation. All subjects had prior experience walking on a treadmill and force signals were collected about 3 minutes into the trial to account for accommodation. A previous study reported no significant within-day accommodation changes to vertical force measures over a 20-minute run after 30 seconds (White et al., 2002). Accommodation should not have had a major effect on the data.

The present study suggests that peak weight acceptance force and loading rate do not increase when healthy, normal weight individuals walk continuously over 32 minutes with or without extra weight. These results may not reflect changes that might be expected for overweight individuals.

REFERENCES

Derrick, TR et al. (2002). *Med. Sci. Sport, Exerc.* **34**, 998-1002.
Slemenda, C. et al. (1997). *Annals of Internal Med.* **127**, 97-104.
Slemenda, C. et al. (1998). *Arthritis & Rheum*. **41**, 155- 159.
Syed, IY, Davis, BL. (2000). *Medical Hypotheses*. **44**, 182-185.
Whittle, MR. (1999). *Gait, Posture*. **10**, 264-275.
White, SC, et al. (2002). *J. Appl. Biomech*. **18,** 74-82.

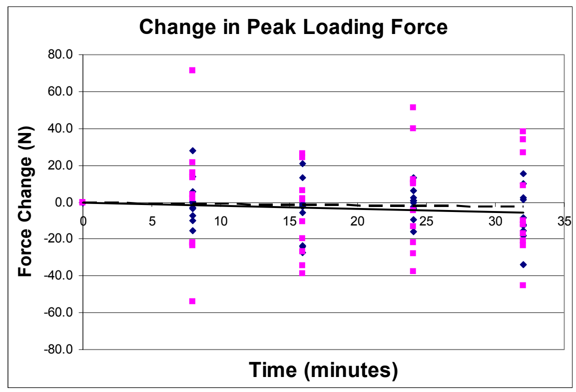

Figure 1. Change in peak force for normal (solid) and weighted condition (dashed). Measures are relative to initial data trial.

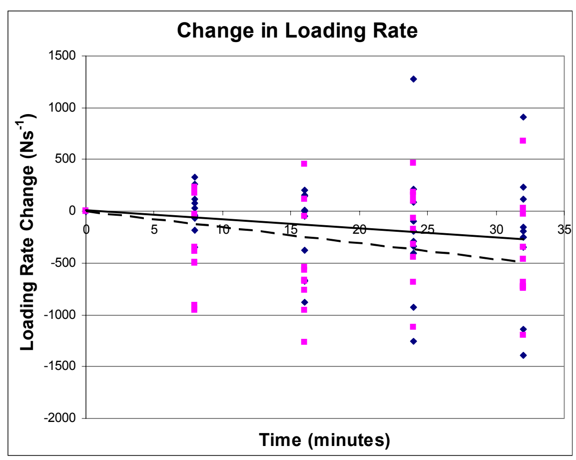

Figure 2. Change in peak loading rate for normal (solid) and weighted condition (dashed). Measures are relative to initial data trial.

AN EMPIRICAL INDEX OF STEP INITIATION IN YOUNG, OLDER, AND BALANCE-IMPAIRED OLDER FEMALES

Brian W. Schulz[1,2,3], James A. Ashton-Miller[1,3], and Neil B. Alexander[2,3,4]

[1]Department of Biomedical Engineering Biomechanics Research Laboratory,
[2]Department of Internal Medicine Mobility Research Center, and
[3]Institute of Gerontology, University of Michigan, Ann Arbor, MI, USA
[4]Ann Arbor VA Medical Center GRECC, MI, USA
Email: bwschulz@umich.edu Web: http://me.engin.umich.edu/brl/

INTRODUCTION

Earlier work on compensatory stepping responses to waist-pull perturbations indicates that age- and balance impairment-related differences in the initiation of initial and successive steps may be associated with the control of whole-body center of mass (COM) velocity (i.e., Schulz et al., 2002). Indeed, a velocity-based step initiation model has proven to be more accurate for predicting initial steps than the traditional displacement model (Pai et al., 1998 & 2000). However, this model has yet to be applied to step prediction beyond the initial step. This study therefore seeks to extend the Pai dynamic step initiation model to predict both initial and subsequent compensatory stepping reactions in response to waist-pull balance perturbations.

METHODS

Maximal unipedal stance time (UST) was used to divide women over 64 years into unimpaired old (O, N=12, UST > 30s) and ìbalance-impairedî old (BI, N=16, UST < 10s). Healthy young women (Y, N=13, UST > 30s) served as controls. Randomized anterior (A) and posterior (P) pulls of 1-5% body weight were applied to the waist while kinematic and kinetic measures of recovery responses were recorded for three seconds at 100 Hz. Subjects were instructed to ìrecover balance normallyî.

A dynamic model based on Pai et al. (1998) was used to predict all compensatory steps, not just the initial step. This model used the COM velocity and the distance of the COM from the margin of the base of support (BOS) along the velocity vector to determine a ìstep indexî:

$$\text{Step Index} = \frac{\text{COM velocity vector}}{\begin{array}{c}\text{Distance from COM to BOS margin}\\ \text{along COM velocity vector}\end{array}}$$

after projecting all vectors onto the transverse plane.

The optimal index for correct prediction of stepping was determined across all trials for step direction, for subject group, and for subject group in specific step directions.

RESULTS

Stepping was less predictable in the BI than in the O and slightly less predictable in O than in Y. Stepping in A direction was more predictable (highest % correct) than in P direction, but P direction had the most defined threshold (predictivity peaks at a specific threshold value for P but not for A). Between 72% and 95% of all trials could be correctly predicted, depending on the subset of trials analyzed. The likelihood of a correct prediction generally decreased with subsequent steps - it was reduced 5-17% per each additional step for the most and least specific optimal thresholds, respectively.

Table 1: Optimal step index and predictivity by group and step direction

		Step Direction		
		A	P	Both
Optimal index	Y	3.0	1.2	1.3
	O	2.3	0.9	1.4
	BI	1.9	1.0	1.2
	All	1.9	0.9	**1.3**
Correct prediction by optimal index	Y	95%	81%	85%
	O	94%	81%	83%
	BI	86%	75%	78%
	All	90%	72%	**82%**

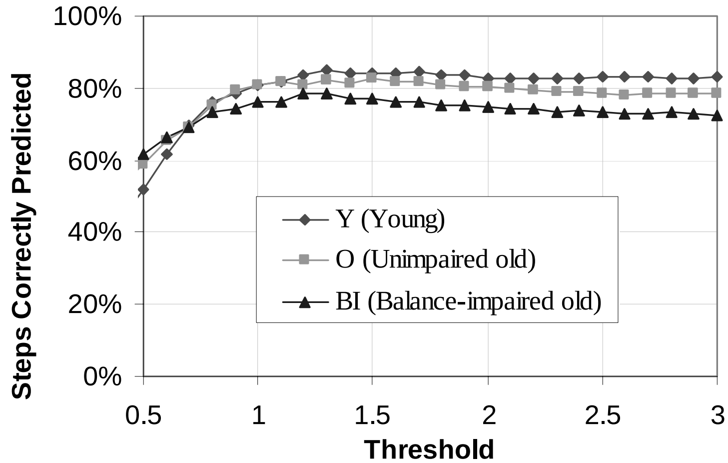

Figure 1: Step index predictivity by threshold for both A & P pulls

DISCUSSION

This step prediction model appears to be applicable to all three subject groups, although age and especially impairment did reduce its accuracy. Both A and P steps can be predicted, although A steps are more likely to be correctly predicted and P steps are more sensitive to the threshold used. The initial and all subsequent steps could be predicted, although the accuracy declined with each additional step. This may in part be due to the uncertainty at the end of the trial - we had no reasonable way of knowing if an additional step would have occurred after the data collection stopped.

Elderly persons tend to use multiple steps to recover their balance, rather than a single step (Luchies et al., 1994). Although the Pai dynamic step initiation model works well for initial steps, it does not account for the subsequent steps that may be the vital determinant of a fall or a recovery in this at-risk population. Thus, this variant of the Pai dynamic stepping model may provide some insight into multiple stepping and why the elderly are more frequently injured by falls.

SUMMARY

A step prediction model for anterior and posterior stepping in response to standardized waist pulls was developed and validated for healthy young and older women, and for balance-impaired older women. Multiple steps were predicted, not just the initial ones. There were slight group and step direction differences in the model, but it correctly predicted 72%-95% of all steps or non-steps, depending on the subset of trials analyzed.

REFERENCES

Luchies CW, et al. (1994). ***J Am Geriatr Soc*** 42(5): 506-12.

Pai YC, et al. (1998). ***J Biomech*** **31**(12): 1111-8.

Pai YC, et al. (2000). ***J Biomech*** **33**(3): 387-92.

Schulz BW, et al. (2002). Annual GSA Meeting, Boston.

ACKNOWLEDGEMENTS

NIA AG 00114 & 08808 grants

BIOMECHANICS OF ASCENDING AN INCLINE

Jon Singer [1] and D. Gordon E. Robertson [1]

[1] School of Human Kinetics, University of Ottawa, Ottawa, ON, Canada
E-mail: jon_singer@hotmail.com and dger@uottawa.ca

INTRODUCTION

This project was initiated to determine the differences between the work and power requirements of the net moments of the lower extremity during ramp ascent compared to level walking. Ramps are a common means of ambulation or the transportation of materials (Robertson & Ellwood, 1995) from one level surface to another. Yet little research has ever been done on this type of activity. To permit an assessment of this activity comparison with established normative data from level walking is possible based on the data presented by Winter (1987). One useful tool for comparing walking on a level surface and to walking up an incline is the support moment. Winter (1987) outlined this concept, that during the stance phase of walking people produce a characteristic bimodal impulse that is the sum of the three extensor moments of the lower extremity. The support moment ($M_{support}$) was defined as, $M_{support} = -M_{hip} + M_{knee} - M_{ankle}$ where the negative signs reverse the polarities of the hip and ankle moments so that extensor moments at each joint are positive while flexor moments are negative.

METHODS

Eight subjects were recruited to walk across a laboratory walkway and ascend a 10-degree ramp. After informed consent, the subjects were filmed walking at a self-selected pace up the incline. They stepped so that one foot landed on a level force platform, the other foot landed on the bottom of the incline and the first foot stepped onto a second force platform imbedded in the ramp.

Video data were reduced using the APAS system and then processed with the Biomech Motion Analysis System (www.health-.uottawa.ca/biomech/software). The video data were filtered and then kinematics of the three segments of the lower extremity computed. The force platform data were rotated to compensate for the 10-degree incline and then combined using inverse dynamics with the kinematic data to obtain the net moments of force and their associated powers at the ankle, knee and hip (Winter & Robertson, 1978). Lastly, the three moments were added, as presently previously, to obtain the support moment. For comparative purposes the moments were normalized to body mass.

RESULTS AND DISCUSSION

Figure 1 shows a typical subject's support, hip, knee and ankle moments during the step immediately before the ramp and the same foot's moments while on the ramp (second step on ramp). Notice that the first (ground level) support moment was approximately the same as normal level walking but the support moment on the ramp was twice as large. Notice also the dominant role of the hip extensors to the production of the support moment.

Figure 2 shows the powers produced by the same subject as in Figure 1. The powers during the first step were not different from what occurs during normal level gait. All subjects exhibited similar patterns.

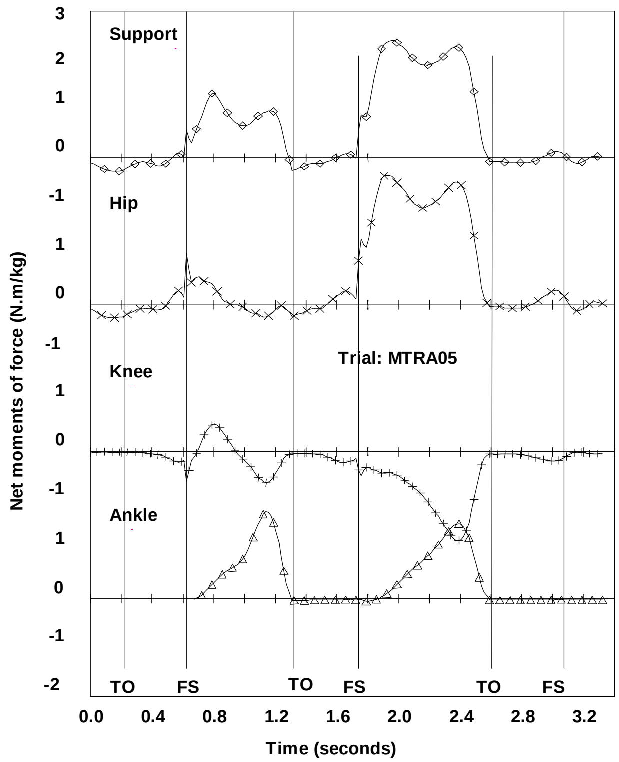

Figure 1: Moments of force during ramp ascent. The first step (leftmost) was done while on a level surface while the rightmost step was produced during the second step on the ramp. (TO=toe-off, FS=foot-strike)

The powers during the step on the ramp were considerably different from level walking for the knee and hip moments but not the ankle. The knee power during the stance phase on the ramp was exclusively flexor with an initial burst of positive work, followed by negative work during midstance and concluding with positive work immediately before toe-off. Essentially, the knee flexors flex the knee at the beginning and end of stance but resist extension during midstance. At the hip, the extensors dominate throughout stance continuously doing positive work. They provide the necessary energy to extend the hip and knee while the knee flexors act to prevent full knee extension during midstance.

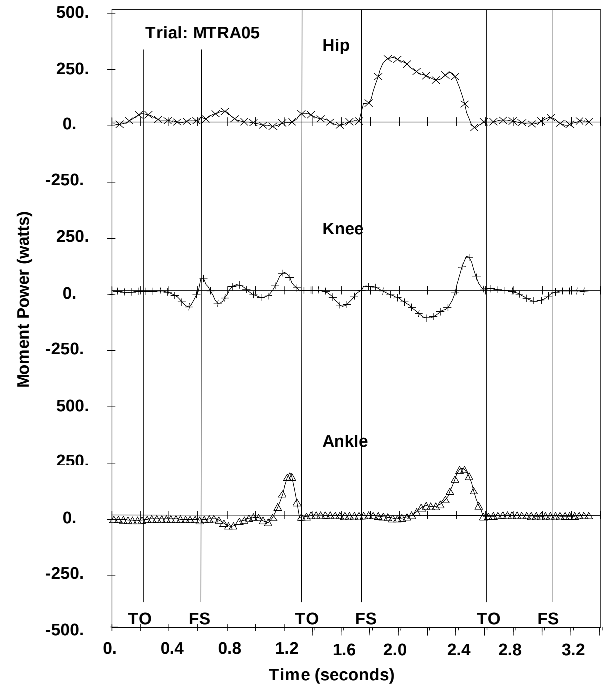

Figure 2: Hip, knee and ankle moment powers during ramp ascent. Data are from same subject and trial as Figure 1.

SUMMARY

The ankle moments during ramp ascent provide the same functions as normally occur during level walking. The flexor knee moment of force produce bursts of positive work during ramp ascent that are different compared with level gait. The extensor hip moment is the dominant working group during ramp ascent producing positive work throughout the stance phase that is quite unlike what occurs during level gait.

REFERENCES

Robertson, D.G.E., Ellwood, D.M. (1995). *Proceedings of ISB 15*, 774-775.

Winter, D.A., Robertson, D.G.E. (1978). *Biological Cybernetics*, **29**, 137-142.

Winter, D.A. (1987). *Biomechanics and Motor Control of Human Gait*. Waterloo: Waterloo Biomechanics.

CHANGES IN MUSCLE ACTIVATION PATTERNS DURING ROBOTIC-ASSISTED GAIT TRAINING

Joseph Hidler[1, 2], Jessica Cisper[1], and Anji Wall[1]
[1]Department of Biomedical Engineering, Catholic University, Washington, DC, USA
[2]National Rehabilitation Hospital, Washington, DC, USA
Email: hidler@cua.edu Web: http://engineering.cua.edu/biomedical/faculty/hidler

INTRODUCTION

Manual-assisted, body-weight supported gait training is a promising neurorehabilitation intervention for restoring walking ability following stroke and spinal cord injury (Wernig, 1992, Visintin, 1989). Recent advances in robotics are attempting to overcome the limitations associated with this therapy, such as therapist fatigue, training inconsistencies, and the duration of training sessions. One of the potential limitations with robotic-assisted gait training is the necessary limitation of the degrees of freedom through which the patient can move. Such restrictions may influence natural muscle recruitment patterns in both the temporal and spatial sense, which in turn may influence the effectiveness of the therapy.

The objective of this study was to investigate whether there are differences in muscle activation patterns between unrestricted and robotic-assisted treadmill ambulation.

METHODS

A single healthy subject participated in this study. Surface EMGs were recorded differentially from the gastrocnemius, rectus femoris, vastus medialis and lateralis, adductor longus, hamstrings, and gluteus medius and maximus muscles using a DelSys (Boston, MA) Bagnoli-8 EMG system. Knee and hip angles were measured using twin-axis goniometers (XM100, Motion Labs, Baton Rouge, LA), while foot-switches (MA151, Motion Labs, Baton Rouge, LA) were placed on the subject's heel to detect heel-strike.

The subject first walked on a treadmill at a self-selected walking speed during which 60-seconds of stepping was recorded. The subject was then placed into the Lokomat (Figure 1) with no body-weight support. The Lokomat restricts motion of the lower limbs to the sagittal plane and has a single DOF in the vertical direction. Small DC motors actuate the hip and knee joints through a kinematic pattern that is adjustable. Foot straps are placed on the subject's forefoot to assist with dorsiflexion during swing. The leg kinematics of the Lokomat were adjusted to match the subject's natural kinematic pattern.

The subject was allowed to walk in the Lokomat at the same self-selected speed for up to 5 minutes to acclimate to the device. Data was then recorded for 60-second step sequences. EMG patterns during both conditions were broken up into individual steps, time-normalized, and the RMS was calculated using a 10 ms window.

Figure 1: Lokomat robotic-orthosis (Hocoma, Inc, Zurich, Switzerland)

RESULTS AND DISCUSSSION

Comparisons between unrestricted treadmill ambulation and Lokomat treadmill ambulation found that there were significant differences in the spatial and temporal muscle activation patterns across nearly all muscles. For example, during Lokomat stepping, there was minimal activity in the gastrocnemius, presumably because the foot straps prevent significant plantarflexion and push-off (Figure 2). Conversely, there was over-activity in the adductor longus in Lokomat stepping, perhaps attributable to the leg being restricted to the sagittal plane as well as the inability to weight shift.

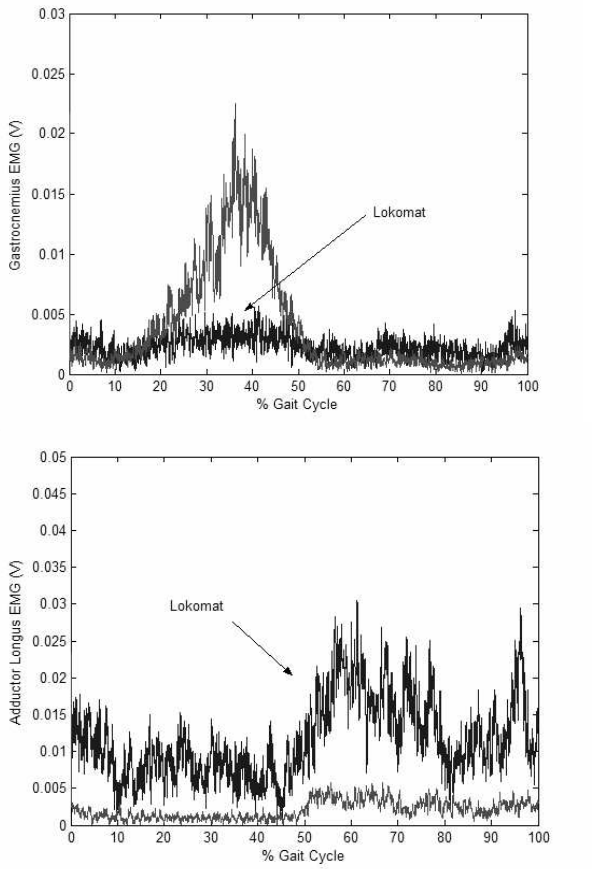

Figure 2: Muscle activation patterns in the gastrocnemius (upper trace) and rectus femoris (lower trace) during treadmill stepping and Lokomat stepping.

Mean RMS values were compared at 0, 20, 40, 60, and 80% of the gait cycle for each muscle, where it was found that at each phase across a number of muscles, there were statistical differences between the two walking conditions.

SUMMARY

While robotic-assisted gait training overcomes many of the limitations associated with manual-assisted gait therapy, restrictions in the walking patterns appear to influence muscle activation patterns from what would normally be observed in over-ground walking. These changes include over-activity and under-activity, as well as shifts in the phase of burst patterns. We are currently running more subjects, and investigating whether the changes described here are affected by walking speed as well as the foot-strap used to provide dorsiflexion.

REFERENCES

1. Visintin, M. and Barbeau, H. (1989). *Can. J. Neurol. Sci*., **16**, 315-325
2. Wernig, A., and Muller, S. (1992). *Paraplegia*, **30**, 229-238.

ACKNOWLEDGMENTS

We would like to thank the National Rehabilitation Hospital for sponsoring this work.

ASSESSMENT OF PRESSURE MEASUREMENT SYSTEMS ON FLAT SURFACES

Mitchell A. Fergenbaum [1], Joan M. Stevenson [1], Evelyn Morin [1], J.Tim Bryant [2], Lindsay Hadcock [1] and Sue A. Reid [1]

[1] Biomechanics Laboratory, Queen's University, Kingston, Ontario, Canada
[2] Human Mobility Research Centre, Queen's University, Kingston, Ontario, Canada
Email: mitchellfergenbaum@hotmail.com Web: http://www.phe.queensu.ca/ergbio/

INTRODUCTION

Anytime the human body comes in contact with another object, compressive forces are applied to a given area of the skin, exerting a pressure. When repetition, duration and/or level of pressure are too great, skin tissue damage may occur. Understanding how pressure on the skin affects human comfort and performance has relevance to applications such as to understand how pressure exerted by prosthetic limbs may affect patient comfort and mobility and to better understand how pressure causes tissue breakdown in bed-ridden patients (bedsores) or long-term wheelchair patients. To study skin contact pressure, accurate and repeatable equipment is required. The goal of this research was to evaluate the latest pressure-sensing technologies using standardized flat surface tests, to determine which system is suitable for pressure-related research.

METHODS

Three pressure technologies were tested, including: a resistive ink technology by Tekscan Inc., (F-Scan F-socket model); a capacitance technology by Xsensor Technology Corp., (X2 seat system); and a piezoresistive technology by Vista Medical Ltd., (Medical Seat UT Model). Each pressure pad was placed on a 3 mm Bocklite® cushion and marked by the researcher, to ensure that loads were placed on the same part of each pressure pad, to maintain testing consistency.

Three protocols were performed in a randomized order. An incremental protocol was used to test accuracy and repeatability by placing loads between 9.392 kg to 19.627 kg on each pad for 2 minute intervals. Each loaded interval was followed by a 2 minute unloaded condition before the next load was placed on the pad. A low threshold protocol was used to test light load accuracy by placing a predetermined load on the pad for 20 minutes. The load created a light pressure that was 1 unit of pressure above the manufacturer's lowest recommended threshold. A creep test protocol was used to study the accuracy and creep characteristics of each pad, by placing an 18.627 kg load on each pad for 1 hour. All data were collected at 1 sample/s and normalized by dividing the measured pressure gathered by the pressure system by the theoretical predicted pressure, to allow comparison of accuracy between different pressure systems.

RESULTS AND SUMMARY

Normalized incremental results (Table 1) showed that the Xsensor and FSA continually underestimated the predicted pressures by approximately 25%; however, this accuracy was much better than the F-Scan, a finding consistent with others

(Hochmann, et al., 2002). The F-Scan continually overestimated pressures by more than double the theoretical predicted pressure; a value which was higher than others who reported inaccuracies as high as 62 % (Sih, 2001). For all systems, there was no basic pattern of repeatability, even though loading methods were highly controlled and standardized. The repeatability of the FSA and Xsensor needs further investigation; however, poor repeatability for the F-scan has been reported in the past (Woodburn & Helliwell, 1997). At low pressure thresholds, the Xsensor was highly accurate compared to the FSA and F-Scan (Table 1). The FSA may have performed poorly because the loaded sensors required a charge amplifier to measure the charge emitted from the piezo-material (capacitance sensor measure stored charge between the sensing plates); thus, amplification may be the source of error for the FSA at low pressures (Cavanagh et al., 1992). Last, the FSA and Xsensor showed a 9.7% and 12.7% creep, respectively, although both systems underestimated the predicted pressure (Table 1). F-Scan showed the smallest creep (2.7%) which is less than other reports in the range of 12% to 15% (Polliack et al., 2000 Woodburn, J. & Helliwell, 1997); however, the F-Scan system dramatically overestimated the actual predicted pressure.

SUMMARY

In summary, the Xsensor and FSA systems were superior to the F-Scan for accuracy; however, the Xsensor appears to be more suitable for research that requires measurement of a variety of pressures (low through high). Future work still needs to address repeatability and creep concerns for all systems tested.

REFERENCES

Cavanagh, P. R., et al. (1992). In-shoe Plantar Pressure Measurement: A Review. *Foot,* **2**, 185-194.

Hochmann D. et al. (2002). Evaluation of Measurement Systems for Determining Therapeutic Effectiveness of Anti-decubitus Ulcer Devices. *Biomediziniche Technik,* **47** Suppl 1 Pt 2, 816-9.

Polliack, A.A. et al. (2000). Scientific Validation of Two Commercial Pressure Systems for Prosthetic Socket Fit. *Prosthetic and Orthotic International,* **24** (1), 63-73.

Sih, B.L. (2001). *Modeling for Military Operational Medicine Scientific and Technical Objectives (Improving Accuracy of the F-Scan Sensor).* Contract number DAMD17-00-1-0031. JAYCOR, San Diego, CA.

Woodburn, J., Helliwell, P.S. (1997). Observations on the F-Scan In-shoe Pressure Measurement System. *Clinical Biomechanics,* **12**(3), S16.

ACKNOWLEDGEMENTS

This study was supported by a grant from Defence Research and Development Canada. The authors would like to thank Mohammad Abdoli for his technical assistance.

Table 1: Normalized pressures for pressure systems.

Protocol	**Normalized FSA**	**Normalized F-Scan**	**Normalized Xsensor**
Incremental	0.745 ± 0.05	2.47 ± 0.38	0.751 ± 0.04
Low Threshold	$1.81 \pm 7.6\times10^{-8}$	2.92 ± 0.32	1.03 ± 0.02
Creep	0.768 ± 0.019	2.29 ± 0.31	0.778 ± 0.051

FORCE PLATE CONSIDERATIONS IN STUDIES INVOLVING RAMPS AT DIFFERENT ANGLES

Andrew Post and D.G.E. Robertson PhD.

Biomechanics Laboratory, University of Ottawa, Ottawa, ON, CAN
E-mail: APOST033@uottawa.ca

INTRODUCTION

A fair amount of research has gone into the biomechanical aspects of gait on various surfaces. The most recent and interesting area of gait has been focused on how humans negotiate ambulation on ramps. It has been shown that gait on inclines have a noticeably different force reading than those found during level ground gait (Kuster et al. 1995).

This project was concerned not so much with the description of the kinematics of ramp negotiation but more with the force curves and vectors present during gait up ramps. With ramp gait there are unique considerations that need to be assessed in ramp design and force curve and vector analysis. The force plate readouts need to be adjusted so that the force vectors are set to a proper inclination. This requires the use of axis transformation.

METHODS

Three subjects participated in the trials. Reflective markers were placed on the tip of the toe, ball of the foot, calcaneus, lateral malleolus and greater trochanter of the right side.

A VHS camera was used to record the marker trajectories with a sampling rate of 60 Hz. Kistler 9261A (force plate 1 inset into the ground) and 9286AA model (force plate 2 inset into the ramp) force plates sampling at 200 Hz were used in collecting the force data. The ramp was constructed of hollow iron and set to 10 degrees. Panels of 1 inch plywood pieces fill in the border of the ramp so that the force plate and the ramp surface were even.

Following the filming of a control points the subjects walked across the gait laboratory. Each subject walked over level ground and then walked up the ramp 5 times each.

The data were collected with BioWare software for force plate recording. The VHS data were collected and processed using APAS software. The force data were analyzed using the Biomech Motion Analysis software.

RESULTS AND DISCUSSION

The force curves for the ramp and level gait are noticeably different. They both have the typical double hump, however, the ramp curve has a higher push-off force (peak 2) than the first. This is different from level gait where the first peak is usually marginally higher than the second (Winter, 1991).

Analysis showed there was noise found in the force recording of force plate 2, as shown in Fig. 1. This noise was attributed to the structure of the ramp itself. At time 0.00 to 0.20 the ipsilateral foot makes contact with the ramp and causes a vibration through the structure that is recorded by the force plate. It is possible to run a fourier analysis to discover the power of the signal and then set a digital filter to eliminate this noise.

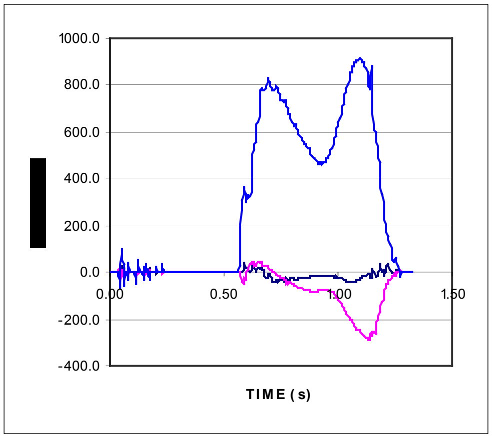

Figure 1: Force plate recording of a force plate inset into a 10 degree ramp.

Another consideration shown by this study is in relation to the force vectors recorded. In figure 2 it is shown how the computer interprets the force vectors from the force plate on a ramp. The vectors are noticeably off angle.

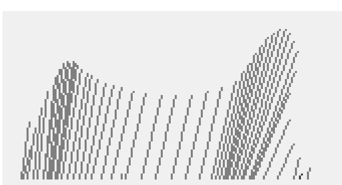

Figure 2: Ramp force vectors without inclination adjustments.

In figure 3 the adjustment using the following transformation:

$$X` = x \cos \theta - y \sin \theta$$
$$Y` = x \sin \theta + y \cos \theta$$

The vectors now show a properly angled push off while on the ramp. The vectors in figure 3 show a more oblique push-off phase vector.

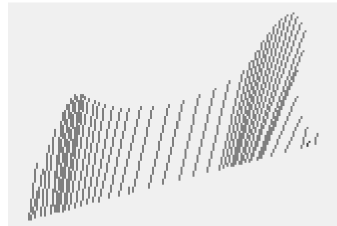

Figure 3: Ramp force vectors with inclination adjustments.

SUMMARY

The considerations that need to be made when designing a lab ramp are that the researcher must consider how to limit resonance that can interfere and cause noise in the data recorded (Post & Robertson, 2002). The angles of the force vectors also need to be adjusted in the data analysis phase of the research. Stiff surfaces will be preferable to limit the resonance and transfer of forces can be limited using damped surfaces. The angle of inclination is easily dealt with using a transformation.

REFERENCES

Winter, D.A. (1991). The biomechanics and motor control of human gait. Waterloo: Waterloo Biomechanics.

Post A. & Robertson, D.G.E. *Proceedings of the IV World Congress of Biomechanics*, p 594.

Kuster, M., Sakurai, S., & Wood, G.A. (1995). *Clinical Biomechanics*, **10**, 79-84.

MULTIPLE FEATURES OF MOTOR-UNIT ACTIVITY INFLUENCE FORCE FLUCTUATIONS DURING ISOMETRIC CONTRACTIONS

Anna M. Taylor, Evangelos A. Christou, and Roger M. Enoka

Neural Control of Movement Laboratory, University of Colorado, Boulder, CO, USA
E-mail: anna.taylor@colorado.edu Web: www.colorado.edu/kines/research/ncm.html

INTRODUCTION

The time and frequency structure of force is often used to assess the neural mechanisms that control muscular contractions. Recent literature (Enoka et al. 2003; Jones et al. 2002) suggests that the amplitude of force fluctuations declines with the amount of force produced. Furthermore, it appears that the primary contribution to force variability is the variation in the discharge rate of the motor units involved in the task. However, other possible causes of force fluctuations include low-frequency oscillation in drive (Vaillancourt et al. 2002) to the motor units, motor unit synchronization (Yao et al. 2000), and motor unit discharge rates (Patten and Kamen 2000). One of the limitations of the extant literature is that most studies have used low-force contractions. Thus, comparatively little is known about the structure of force produced during high intensity contractions. The purpose of this study was to identify the mechanisms that influence the structure of isometric force across the entire operating range of a muscle. To achieve this aim, a combined experimental and computational approach was used.

METHODS

Isometric force was recorded during contractions of the first dorsal interosseus in ten young (29.4 ± 4.4 years) subjects (5 men and 5 women). Force and EMG were recorded for 6 s (3 s with visual feedback and 3 s without) at 9 levels of contraction intensity (2, 5, 15, 30, 50, 70, 85, 95, and 98% of MVC force). Two trials were completed per force level. The order of the force levels was randomized for each subject.

The experimental data were compared with the isometric force produced by a model of a motor unit population (Fuglevand et al. 1993). The model comprised 120 motor units, each of which had individual twitch properties and force-frequency relations. The model motor units are activated according to the Size Principle, and their properties are designed to approximate the first dorsal interosseus.

To address the research question, multiple parameters were varied in the model. These included: (1) the rate-excitation functions for the individual motor units; (2) the maximal discharge rates of individual motor units and the pattern of maximal rates across the population; (3) range of recruitment levels; (4) discharge variability; (5) synchronization of the motor units; and (6) oscillating drive to the motor units in the population.

The variability of the experimental and model forces were analyzed in the time domain by quantifying the amplitude of the fluctuations in force using the coefficient of variation of force. The frequency structure of the forces was quantified with power density spectra, expressed as a percentage of the total power in the signal. The results for the no-vision force trials were compared to the model data.

RESULTS AND DISCUSSION

The results from this study indicated that there was a decline in force fluctuations between 2 and 30% MVC, but that the amplitude of force fluctuations then increased and plateaued at forces greater than 30% MVC.

Of the parameter changes that were made to the model, four could approximate the experimental data at a minimum of four out to the nine force levels (Figure 1).

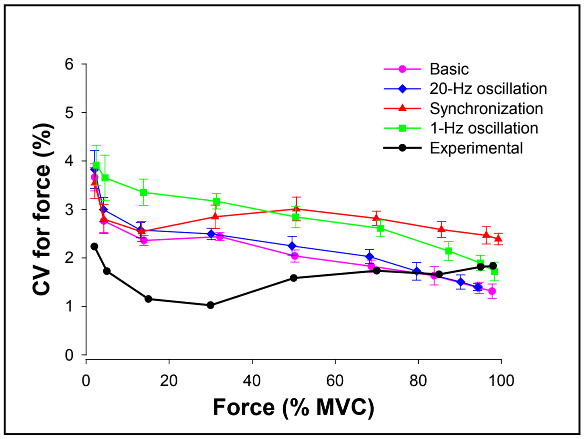

Figure 1: The models that matched the experimental coefficient of variation for force were significantly different at moderate force levels (15 and 30% MVC).

The maximal power in the experimental force spectra occurred at 1.4 ± 1.1 Hz, with 43 ± 6% of total power at this frequency. The 1-Hz model exhibited a similar peak frequency (0.99 ± 0.53 Hz) and peak power (38 ± 2.3%). The peak frequencies for the other models were higher (basic: 5.1 ± 5.5; 20-Hz: 5.2 ± 5.3; synchronization: 3.6 ± 1.7 Hz). Furthermore, the models had secondary peaks at higher frequencies, with the exception of the synchronization model.

Of the four models that matched the time-domain variation in force, only the synchronization model showed an increase at higher forces. However, this did not occur at the same point as in the experimental force. The secondary peaks in the power spectra for the models were likely related to the mean rates of the model motor units. The prominent low-frequency peaks in all models suggested that the low-frequency power in human force signals was largely unrelated to oscillating activation of motor units.

SUMMARY

The results from this study indicate that the variability in motor output changes across levels of excitatory drive. The two most explanatory mechanisms for force variability are a low frequency oscillation in the activity of the motor units and motor unit synchronization. The inability of the model to reproduce the decline and subsequent plateau in force fluctuations at moderate forces suggests that a more complex theoretical model of the neural control of force is needed.

REFERENCES

Enoka, R.M. et al. (2003) *J Electromyogr Kinesiol* **13**, 1-12
Fuglevand, A.J. et al. (1993) *J Neurophysiol* **70**, 2470-88.
Jones, K.E. et al. (2002) *J Neurophysiol* **88,** 1533-44.
Patten, C. and Kamen, G. (2000) *Eur J Appl Physiol* **83,** 128-43
Vaillancourt, D.E. et al. (2002) *Clin Neurophysiol* **113**, 1325-38.
Yao, W. et al. (2000) *J Neurophysiol* **83,** 441-52

ACKNOWLEDGEMENTS

Supported by an NIH grant (AG09000) awarded to RME and an NSF Graduate Fellowship awarded to AMT.

MEASURING MOMENT OF INERTIA IN THE FIELD: DEVELOPMENT AND ACCURACY OF A PORTABLE PHYSICAL PENDULUM DEVICE

Jeffrey M. Schiffman, Leif Hasselquist, Karen P. Norton, Louis P. Piscitelle, Carolyn K. Bensel

Center for Military Biomechanics Research,
U.S. Army Natick Soldier Center, Natick, MA, USA
E-mail: Jeffrey.Schiffman@Natick.army.mil

INTRODUCTION

Previous research has shown that center of mass (COM) is an important characteristic of loads that individuals must handle, particularly when the load must be carried on the back (Obusek et al.1997). More recently, research has suggested that moment of inertia (MOI) may also be an important characteristic. (Norton et al. 2003). A project was undertaken to fabricate a low-cost, portable device that can be used to take measurements of MOI in the field. The device is described here and data comparing measurements made on the portable device with those made on a laboratory MOI instrument are presented.

METHODS

A physical pendulum, improving on one previously built (Hinrichs et al.1982), was constructed to take field measurements of the MOI of objects. The physical pendulum consists of a rigid, wooden frame that supports a fixed axle from which a bar (2.11 kg) swings freely. An angular displacement transducer (ADT) series 600 (Trans-Tek Inc., Ellington, CT) is attached to the axle and measures the period of oscillation as the bar swings. A custom cage (0.41 m x 0.47 m x 0.58 m, 5.55 kg), securely attached to the bar, contains the test object. The bar and cage comprise the holder (7.66 kg).

To start a measurement trial, the holder is displaced 3° and released. Oscillation data are collected for 30 s from which the average period is determined. Mass and COM measurements are made using a forceplate; model OR6-5, 908 kg Fz capacity (AMTI, Watertown, MA). The COM of the test object is determined for each coordinate.

For each test case, measurements are made of the period (T_i), mass (M_i) and COM distance (x_i), where the subscripts denote the specific component, o ~ the object whose MOI is to be determined, h ~ the holder used in the swing device and s ~ the system comprised of the holder and the object. The MOI of the system and of the holder is determined relative to the axis of rotation by

$$I_i^{cm} = \frac{M_i g x_i T_i^2}{4\pi^2} \qquad (1)$$

where (g) is the acceleration due to gravity.

The parallel-axis theorem is then utilized to determine the MOI about the object's COM, see Equation 2.

Error Analysis
Bench testing for the physical pendulum device involved measuring the MOI of either one or two 10-kg steel blocks, with known dimensions, in different positions relative to the cage. These results were compared to values obtained using a laboratory instrument for measuring MOI; model XR250 (Space Electronics, Berlin, CT). The procedures employed and precision of the Space Electronics device

have been discussed elsewhere (Norton et al., 2003).

The object's MOI about its mass center, $I_o^{cm} = f(z_1,...,z_n)$, where z_i's are the measured quantities, is given as,

$$I_o^{cm} = \frac{(M_h + M_o) g x_s T_s^2}{4\pi^2} - \frac{M_h g x_h T_h^2}{4\pi^2} - \frac{[x_s(M_h + M_o) - x_h M_h]^2}{M_o} \quad (2)$$

The most likely error in the MOI, $I_o^{cm}\Delta$, based upon errors in the measurements made during the experimental procedure, can be expressed as

$$\Delta I_o^{cm} \cong \sqrt{\sum_{i=1}^{n} \left(\frac{\partial f}{\partial z_i}\right)^2 (dz_i)^2}. \quad (3)$$

Using Equation 3, one can calculate the most likely error bounds for I_o^{cm}.

RESULTS AND DISCUSSION

The accuracy of COM, mass, and period were determined by taking repeated measurements and obtaining the maximum error bounds. The accuracy data were 0.003 m, 0.05 kg, 0.003 s, respectively.

By incorporating an ADT to quantify the period of a physical pendulum, the precision of the swing has been determined and the error of measuring MOI with such a system has been characterized accurately. The bench test data, presented in Table 1, revealed that the MOI values obtained using the physical pendulum (i.e., Measured) differed from the values obtained using the laboratory MOI device (i.e., Actual). Measurements made on objects close to the axis of rotation revealed less error than those made on objects further away. Larger object MOIs exhibited smaller relative likely error.

This project was initiated to develop a low cost, portable device for measuring the MOI of objects. The aim was to have a means of measuring MOI in field environments where it would not be practical to transport bulky and expensive laboratory equipment. The physical pendulum described here that incorporates an ADT to quantify the period of oscillation fulfills the requirement, within the constraints revealed through the error analysis.

Table 1. Error Analysis Results

Test Condition	X_o (m) From Axis of rotation	Actual I_o^{cm}	Likely Error I_o^{cm}	Measured I_o^{cm}	Actual % Error	Most Likely % Error
1 block, cage bottom[1]	0.6985	0.0195	0.0511	0.0622	218.9	262.9
1 block, cage top[1]	0.1028	0.0195	0.0211	0.0188	-3.59	108.2
2 blocks, cage bottom[2]	0.6472	0.6024	0.0683	0.7058	17.16	11.34
2 blocks, cage top[2]	0.0968	0.6024	0.0330	0.6540	8.56	5.472

[1]10 kg [2]20 kg (Object Mass) (Unit of measure for I = kg·m^2)

SUMMARY

A simple swing device for field measurements of MOI can provide reasonably accurate data for objects with large MOI. The error analysis gives a priori estimates that may be used to decide how best to employ the technique. In general, objects with small MOI that can only be placed far from the pendulum's axis of rotation should be measured with a more accurate device.

REFERENCES

Hinrichs, R. N., et al. (1982). *An investigation of the inertial properties of backpacks loaded in various configurations* (Tech. Rep. TR-82/023). Natick, MA: U.S. Army Natick Res. & Dev. Labs.

Norton, K., et al. (2003). *Inertial properties of an external-frame backpack device* (Tech. Rep. TR-03/020). Natick, MA: U.S. Army Natick Soldier Center.

Obusek, et al. (1997). *Med Sci Sports Exerc*, *29,* S205.

DIABETIC FEET AT RISK OF PLANTAR ULCERS: A NEW METHOD OF ANALYSIS OF STANDING FOOT PRESSURE IMAGES WITH VARIATIONS IN FOOT SOLE PROPERTIES

V. Jacob Thomas[1], K. M. Patil[1], S. Radhakrishnan[1], V.B.N. Murthy[2] and R. Parivalavan[2]

[1] Biomedical Engineering Division, Indian Institute of Technology, Madras-36, India.
[2] Diabetic Foot Clinic, Sundaram Medical Foundation Hospital, Madras-40, India.
E-mail: jacobmec@hotmail.com Web:iitm.ac.in

INTRODUCTION

The most feared lower extremity problem among patients with diabetes is amputation, and the sequences of events leading to amputation are initiated by skin ulceration combined with sensation loss (Birke, J.A. *et.al.*1995). Therefore, it is essential to detect the foot at risk of plantar ulceration, at an early stage of sensation loss, so as to prevent complications and amputation, (Armstrong, D.G. *et.al* 1998). It is found that the foot pressure parameters are functions of the mechanical properties of foot sole soft tissue and also different levels of sensation loss. Therefore, this paper presents the results of the research study undertaken to find the relationship between the foot pressures characterized by a new parameter known as Power Ratio, PR (the ratio of high frequency power to the total power in the power spectrum of the foot pressure image) at different levels of sensation loss and the foot sole mechanical property (in terms of hardness of foot sole soft tissue characterized by its Shore level, Sh).

METHODS

In this study, the foot pressures are measured using the optical pedobarograph. The sensation levels on the foot sole are measured by scanning ten standard areas of the foot sole (Figure 1 a) using the Semmes-Weinstein nylon monofilaments of specified diameters to determine quantitatively the degree of neuropathy (characterized by sensation levels S, ranging from 3 gm to 10 gm). The mechanical properties of foot sole, in the above ten foot sole areas, are measured using the Shore meter which measures the hardness of the foot sole soft tissue- lesser the Shore value, softer is the soft tissue (Pigassesi, A. *et.al* 1999). The Shore meter works on the principle of indentation using a truncated cone tipped indenter; indentation depth being inversely proportional to the modulus of elasticity. The standing foot pressure images are obtained from the optical pedobarograph. Spatial frequencies (cycles per degree, cpd) and their distributions in these images are analyzed by performing the 2-D Discrete Fourier transform (DFT) using MATLAB. The magnitudes of the power spectrum, in each of the foot sole areas, are obtained by squaring the absolute magnitudes of Fourier spectrum of light intensity variations of foot images. Now, the power ratio PR is calculated by using the equation as follows.

$$PR = \left(\frac{HFP}{TP} \right) \text{X } 100$$

where, HFP- High Frequency Power and TP – Total Power in Foot pressure image. Multiplication by 100 is to express the PR value as a whole number. The parameter, PR is evaluated for normal and diabetic feet with different levels of loss of sensation and different hardness values of the soft tissue.

RESULTS AND DISCUSSION

Analysis of the standing images of foot on 7 normal and 18 diabetic subjects show that in diabetic neuropathy, as the sensation loss increases from diminished light touch (sensation level S=4.5 gm, early stage of sensation loss) to loss of protective sensation (sensation level S=10 gm), the foot pressure parameter PR, increases in all the foot sole areas (Figure1 b). The increase in PR values for diabetic subjects in the upper sensation loss region (S=7.5 to 10gms) compared to the corresponding increase in lower sensation loss (S= 3 to 4.5gms) are of the order of 5 times in lateral heel and big toe and 4 times in the first metatarsal regions of the foot sole. Figure 2 presents the variations of mean PR values in the ten foot sole areas for different Shore levels. The increase in PR values for diabetic subjects in the upper Shore value regions (30 to 40) compared to the corresponding increase in lower Shore value regions (20 to 25) are of the order of 4 times in lateral heel, 5.4 times in the first metatarsal regions and 2 time in big toe.

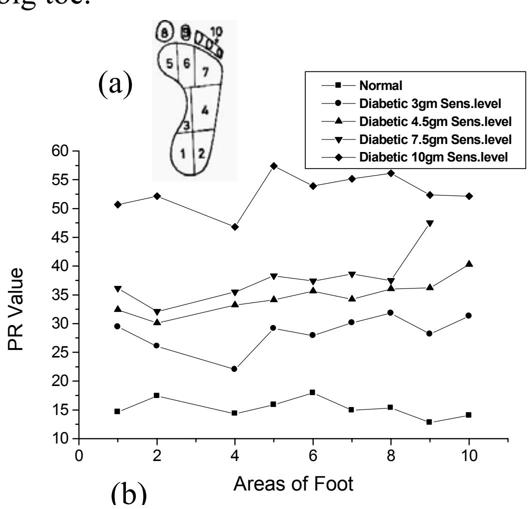

Figure 1. (a) Areas of foot. (b) PR values vs areas of foot with sensation levels 'S'.

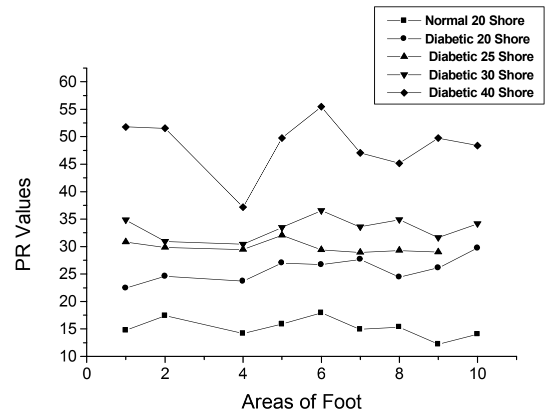

Figure 2. PR values vs areas of foot with different Shore levels

SUMMARY

It is seen that the foot pressure parameter PR values in diabetic subjects increase by (i) 4 to 5 times in higher sensation loss regions and (ii) 2 to 5.4 times in higher Shore regions compared to the corresponding lower sensation loss and Shore regions of the foot sole, respectively that are ulcer prone (namely areas of lateral heel, big toe and first metatarsal heads). Therefore, it may be concluded that both the increase in sensation loss and Shore (hardness) levels of the foot sole soft tissues may be responsible for plantar ulcers.

REFERENCES

Birke, J.A. et al. (1995) "A Review of causes of foot ulcerations in patients with diabetes Mellitus" *J. Prosthetic and Orthotics",* **4** , 13-22.

Pigassesi, A. et al. (1999), "Hardness of Plantar Ulcers in Diabetic Neuropathic Feet", *J.Diabetics and its Complications*, **13**, 129-134.

Armstrong, D.G. et al.(1998), "Validation of diabetic wound classification", *Diabetes Care*, **21**, 855-867.

NUMERICAL APPROACH TO SKIN ARTIFACTS CORRECTION IN STEREOPHOTOGRAMMETRY

Stefano Corazza, Gianluigi Pillonetto, Ruggero Frezza and Claudio Cobelli

Department of Information Engineering, University of Padova, Italy.
e-mail: stefano.corazza@unipd.it web: www.dei.unipd.it

INTRODUCTION

Stereophotogrammetry represents one of the most useful tools for reconstruction of human movement body kinematics in several areas including rehabilitation, mobility assessment sport performance analysis and computer animation. However estimation of bone segment movement is corrupted by experimental errors that have been studied by many authors [Cappozzo 1996, Fuller 1997, Sati 1996]. They are mainly due to: i) marker position reconstruction, ii) calibration errors and iii) skin artifacts due to relative movement of skin markers and bone. This last factor is relatively more important than the two others which are also more repeatable and subject invariant. The present work deals with the correction of skin artifact in the acquisition of thigh kinematics i.e. location in space of femoral segment. The analyzed movement is a hip flexion-extension. The knee is held fully extended in order to permit the use of articular skin marker as reference. A numerical simulation through Finite Elements method is used to identify more promising regions for markers placement in the thigh. Numerical algorithms and in particular a Kalman smoothing filter are employed to improve measurement precision and accuracy.

METHODS

We have first identified the best region on the thigh for skin markers positioning (i.e. minimal skin stretching during hip joint movements) by FEM numerical simulation. Bony parts are assumed to be rigid while thigh soft tissue nonlinear elastic. The subject previously acquired kinematics is used as dynamic load applied in the simulation to bony segments, obtaining as output the deformation of thigh soft tissue. This allowed the identification of a region in the central part of the thigh in which skin stretching is minimal during flexion-extension movement of hip joint.
Once acquisition protocol and marker position on the thigh (firstly, a grid of 8 markers, then reduced to 4) are defined, several motor acts are acquired on three different subjects. The hip joint center is identified with functional method [Stagni 2000, Leardini 1999, Camomilla 2002]. The acquisition of femur movement using articular skin markers (anatomical landmarks are lateral and medial epicondyles) can be considered as reference movement because the knee is maintained fully extended during motor act.
The movement of femoral segment obtained from grid markers placed on the thigh skin is compared with the reference frame. Once the former is properly corrected to adhere with the latter, it can be used also for more general movement because perturbations on markers grid on the thigh due to knee flexion is negligible.
Correction algorithms utilize geometric constraints to make the movement of grid markers frame the more similar to the reference one. Adopted constraints are the mutual distance of the markers from each other and the distance of them from the hip joint center (HJC) previously identified. The

optimal corrected position of the grid markers in relation to experimentally acquired data is found by minimizing a cost function. Once the optimal position of the 4 grid markers is identified, it is used to estimate useful reference point on the femur (e.g. LE-ME intermediate point). The point trajectory is finally reconstructed by employing a Kalman smoothing filter [Kitagawa 1985] containing unknown parameters that are estimated via a maximum likelihood strategy.

RESULTS AND DISCUSSION

The efficacy of skin artifact correction algorithm goes from about 45% reduction in the vertical direction to only about 5% in the mediolateral direction (pelvic bone-embedded anatomical frame is used). The most important consequence of the use of this protocol is that errors will remain of the same magnitude once the movement start varying, e.g. during gait analysis, because knee flexion doesn't affect thigh markers data as occurs for articular markers.

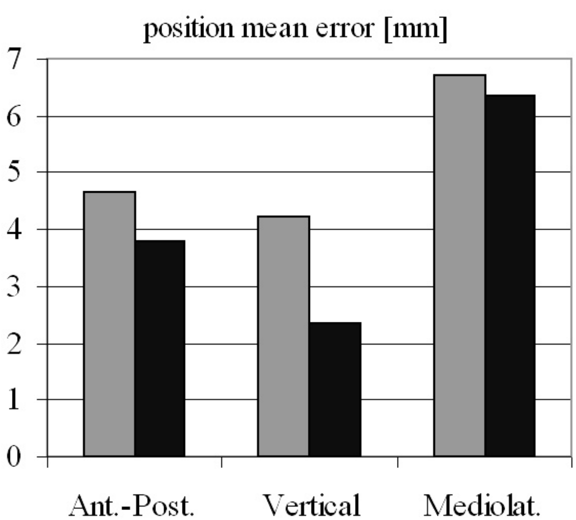

Figure 1: Mean position error for the 4 markers of the grid before (gray) and after (black) the use of correction algorithm.

The smoothing algorithm gives a further improvement of trajectory data quality and estimates the measurement standard deviation through maximum likelihood algorithm.

SUMMARY

A new approach for correction of thigh skin artifacts has been proposed, based on numerical methods that involve both geometrical constraints and statistical approaches. An acquisition protocol is formulated that guarantees smaller artifact errors. Moreover these errors are much less correlated with lower limb joints angles.

REFERENCES

Cappozzo A., Catani F., Leardini A., et al., (1996), *Clinical Biomechanics*, **11**, N.2, 90-100.

Fuller J., Liu L.J., Murphy M.C., (1997), *Human Movement Science*, **16**, 219-242.

Sati M., De Guise, J.A. et al., (1996) *The knee*, **3**, 121-138.

Stagni R., Leardini A., Cappozzo A., Benedetti M.G., Cappello A., (2000) *Journal of Biomechanics*, **33**, 1479-1487.

Leardini A., Cappozzo A., et al. (1999), *Journal of Biomechanics*, **32,** 99-103.

Camomilla, V., Cereatti, A., Cappozzo, A.(2002) *Gait and Posture,* **16** S.1, 182-183.

Kitagawa, G., Gersch, W., (1985), *IEEE transactions on Aoutomatic Control*, **30** N.1, 48-56.

ACKNOWLEDGEMENTS

Authors want to thank Prof. Aurelio Cappozzo for the precious help and eMotion company for supporting the research.

DIFFERENCES BETWEEN VICON CLINICAL MANAGER AND VISUAL3D WHEN PERFORMING GAIT ANALYSES USING THE HELEN HAYES MODEL

Michael Rainbow, Frank L. Buczek, Ph.D., Kevin M. Cooney, P.T., Matthew R. Walker, M.Sc., James O Sanders, M.D.

Motion Analysis Lab, Shriners Hospitals for Children, Erie, PA, USA
E-mail: mrainbow@shrinenet.org

INTRODUCTION

Although the majority of clinical gait analyses have been accomplished using the Helen Hayes (HH) biomechanical model (Kadaba et al., 1989), newer, mathematically optimized techniques (6DOF) are emerging and may well overcome mathematical weaknesses in the former technique (Buczek et al., 1994). While HH is clinically easy to implement due to its basic marker set, markers used to track motion are shared by adjacent segments, and several of these are virtual. This is thought to cascade errors from the pelvis to more distal segments. 6DOF techniques avoid these limitations and may prove to be more accurate as a result. Our ultimate goal is to compare results of gait analyses using these two modeling techniques. Two building blocks for this overall project involve validation of HH and 6DOF techniques in commercial software used in our MAL. HH will be validated by comparisons with Vicon Clinical Manager (VCM) and Visual3D (V3D). 6DOF techniques will be validated through comparisons of Move3D, validated software developed at the National Institutes of Health, and V3D. The purpose for this abstract is to present results from the first step in this process, the comparison of clinically relevant data output from Helen Hayes models in both VCM and V3D.

METHODS

A single stride was analyzed in both VCM and V3D for each of 25 patients in this IRB exempt, retrospective study. Each signal was normalized to 51 data points. A custom program was developed to scan each program's output for a given stride. The custom program extracted 20 variables commonly used to make clinical decisions in our case reviews. We hypothesized that no significant difference would be detected between the two programs. Paired t-tests were used to detect differences in means for these 20 variables, using a Bonferroni adjusted, two-tailed, alpha of 0.05/20 (i.e., $p < 0.0025$). Because it is difficult to determine VCM smoothing techniques, this process was repeated four times producing four families of data. For a given family, VCM remained unaltered while the filtering steps of V3D were changed (Table).

Table: Smoothing parameters used in V3D.
POS = position data filtered at 6Hz,
GRF = ground reaction forces filtered at 15 Hz,
Link Model = output variables filtered at 15 Hz.

Family	POS	GRF	Link Model
1	X		
2	X		X
3	X	X	
4	X	X	X

RESULTS AND DISCUSSION

Families one through three showed no significant difference for fifteen out of twenty variables. Family four, the most heavily smoothed family, had no significant difference shown for sixteen out of twenty variables. It should be noted that no significant difference was found for all seven of the kinematic variables tested. The variables showing a significant difference were four out of six joint moments tested, specifically, max knee extension moment in late swing (Figure), max ankle plantar flexion moment, max hip abduction moment in early stance, and max hip extension moment in early stance.

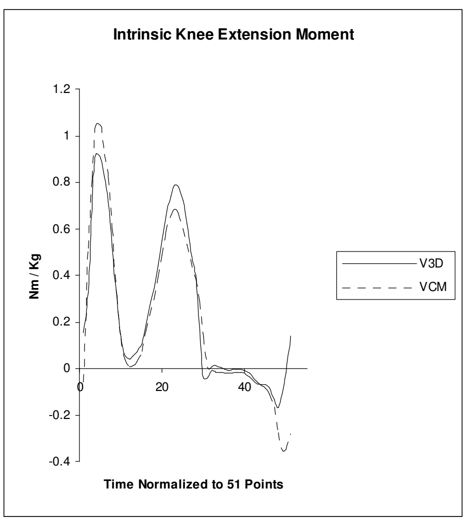

Figure: A representative example of one of the statistically different moment graphs.

Common trends in the discrepant variables were higher peaks and lower valleys as well as deviation at the end points. This can most likely be attributed to each program's smoothing and normalization techniques. VCM uses a bezier spline to perform both interpolation and filtering of force, position, velocity, and acceleration data (Roren, 2003). V3D uses a second order low pass Butterworth filter on position data and normalizes with a cubic spline.

SUMMARY

When switching biomechanical modeling software it is useful to note key differences between platforms. When using a given model like HH, it is important that clinical decisions remain unaffected by software platform changes. This study showed no statistical difference between the Helen Hayes modeling in VCM and V3D for 16 out of 20 variables key to our gait analyses. We are in the process of determining the clinical importance of the statistically significant differences. These findings allow us to move ahead with our validation of V3D against M3D, and 6DOF against Helen Hayes.

REFERENCES

Buczek FL, Kepple TM, Siegel KL, and Stanhope SJ (1994) *Journal of Biomechanics*, 27(12), 1447-1457.

Kadaba MP, Ramakrishnan HK, Wooten ME, Gainey J, Gorton G, and Cochran GVB, (1989) *Journal of Orthopaedic Research*, 7, 849-860.

Roren, L < lasse.roren@vicon.com > "RE: VCM Questions." Private e-mail message to Frank L Buczek, 06 Mar 2003.

STRUCTURED LIGHT GENERATION OF SUBJECT SPECIFIC HUMAN BODY MODELS FOR MOTION CAPTURE APPLICATIONS

Joonho Seo[1], Eugene J. Alexander[2] and Thomas P. Andriacchi[2,3,4]

[1] Department of Mechanical Engineering, Seoul National University
[2] Department of Mechanical Engineering, Stanford University
[3] Department of Orthopedics, Stanford University
[4] VA Palo Alto RR&D Center
E-mail: jhseo@cad.snu.ac.kr

INTRODUCTION

A number of areas of human motion research would greatly benefit from subject specific human body models. This type of information is particularly important for forward dynamic models, but can also be very useful in motion capture applications. Newer methods of motion capture require subject specific information on segmental shape and inertial properties. Many approaches to modeling of human posture and motion have been proposed; for example, silhouette based techniques use multiple camera views to approximate 3D human models (Bottino 2001). Other researchers approximate limb segments with simple primitives such as cylinders or ellipsoids to make articulated skeletal curves (Plankers 2001). These methods typically oversimplify the human body in order to generate a tractable model. To overcome this problem, another approach has been suggested, matching a generic human model to a silhouette of the subject (Chu 2003). This approach also has limitations, in that the general model doesn't adequately describe the unique shape of each human subject. Commercially available techniques such as the Cyberware® whole body scanners can generate detailed subject models, however, these methods are very expensive. The purpose of this project is to develop a cost effective method to generate subject specific 3D models of human subjects using a structured light approach.

METHODS

Equipments

The grid pattern is obtained by structured light projection. A commercially available slide projector is used, projecting a grid pattern printed on transparency film by a laser printer. Data is acquired with color DV cameras. Freely available camera calibration software (Bouguet J.Y) is used to calculate the distortion, internal and external camera calibration parameters. Red tags are attached to various points on the body, to be used as a seed point in the topology calculation.

Algorithms

- Preprocessing The red tags are extracted by a color filter to produce the seed points. The color images are then converted to gray scale and contrast enhanced. Erosion and H cut operators are applied to separate merged regions, then a thicken operator is applied to make a region with a smooth shape. The centroid of each blob is calculated. One image is selected arbitrarily as the 'base image', the other as the 'target image', and both images are processed.

- Tree for base image From the seed point in the base image, the algorithm detects neighbor points (< 5: Left, Right, Top, Bottom) within certain angle ranges and distances between blobs. Once all available neighbors are determined, the algorithm moves to one of the neighbor points, proceeding recursively until no untagged neighbor can be found. This topological information is stored in a tree structure; the initial node is the seed point and leaf nodes are its neighbors, which may have leaf nodes with their neighbors. Each edge connects between parent and leaf node and leaf nodes are sorted by orientation from their parent.

- Case of multiple trees Because the human body consists of several parts, in an arbitrary posture some segments may be partially occluded, possibly by shadows. In this case, after the recursion ceases, the algorithm moves on to the next red tag on the subject and multiple trees are generated.

- Corresponding points finding.
Correspondence between seed points is first determined between images. Usually two or three seed points are visible in each image and correspondence between these points can be determined through brute force methods. Once this correspondence has been determined, all of the points in the base trees can be corresponded to points in the target trees by following the tree structure.

RESULTS
An example result for the lower body is shown in Figure 1. Images were captured for each calibrated camera view in Figures 1a and 1b. The algorithm correctly generated 1458 points for the lower body (1c). Figure 1d shows the surface patches generated directly from the data. Commercial software, Rapidform®, was then used to merge and smooth the surface model (1e).

DISCUSSION
This research demonstrates a "low tech", inexpensive technique for producing subject specific human body models. The accuracy can be improved by increasing the density of the grid and the image resolution. This technique will be used for developing 3D body models for a markerless motion capture system.

REFERENCES
Chi-Wei Chu, Odest Chadwicke Jenkins. (2003) *ICRA.*
Andrea Bottino, Aldo Laurentini (2001). *Computer Vision and Image Understanding.* **83**,79-95
Ralf Plankers, Pascal Fua (2001). *Computer Vision and Image Understanding.* **81**, 285-302
Bouguet J.Y. *http://www.vision.caltech.edu/bouguetj*

Figure 1: (a), (b) Planar camera views; (c) 3D points on surface of the lower half body reconstructed from planar camera images; (d), (e) Shaded surfaces generated from point cloud.

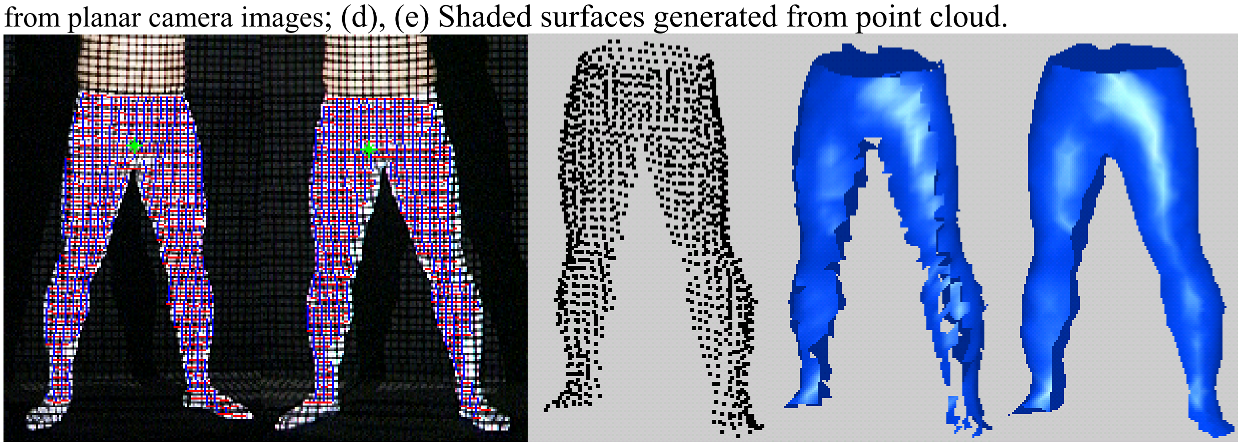
(a) (b) (c) (d) (e)

HUMAN HOPPING ON VERY SOFT SURFACES

Chet T. Moritz [1,2] and Claire T. Farley [1]

[1] Locomotion Laboratory, University of Colorado, Boulder, CO, USA
[2] Dept. of Integrative Biology, University of California, Berkeley, CA, USA
E-mail: ctmoritz@socrates.berkeley.edu

INTRODUCTION

Fast moving legged animals bounce along the ground with center of mass dynamics that are predicted by a spring-mass model (Cavagna *et al*. 1977). Humans hopping in place and running adjust stance leg stiffness to maintain similar center of mass dynamics on a range of elastic surface stiffnesses (Ferris & Farley, 1997; Ferris *et al.*, 1999; Kerdok *et al*., 2002). Surprisingly, humans hopping on heavily damped surfaces also adjust leg mechanics to maintain bouncing center of mass motions regardless of surface damping (Moritz *et al*., 2002).

This research explored the limits of leg adjustment by studying humans hopping on extremely soft elastic surfaces. Specifically, we tested the hypothesis that hoppers adjust leg mechanics to conserve center of mass dynamics even when surface stiffness decrease below the leg stiffness used on a hard surface. This hypothesis predicts that to maintain center of mass dynamics on very soft surfaces, the legs must extend during early stance and flex during late stance. This pattern is opposite to the spring-like leg mechanics used on hard surfaces. Leg extension in early stance may reduce muscle pre-stretch and elastic energy storage, thereby increasing muscle activation during hopping on very soft surfaces.

METHODS

Eight male subjects hopped in place on a surface with adjustable stiffness. We decreased surface stiffness from 81 kN/m (3 cm compression during hopping) to 11 kN/m (15 cm compression). Subjects hopped to a metronome at 2.2 Hz while we collected ground reaction force, surface position, high speed video, and surface EMG from eight leg muscles. We calculated overall mean EMG as the combined average of all muscles over the entire hop cycle.

RESULTS AND DISCUSSION

As predicted by our hypothesis, hoppers maintained similar center of mass movements despite a 7-fold change in surface stiffness. Downward center of mass displacement during stance varied by 10% on all surfaces (Figure 1), and the combined vertical stiffness of the legs and surface decreased by 22% from the hardest to softest surface. If each hopper had not adjusted leg mechanics, the center of mass would have moved downward twice as far during stance and the combined vertical stiffness would have decreased by 60% between the hardest and softest surface.

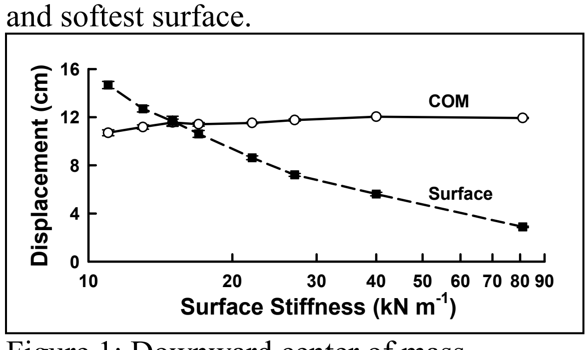

Figure 1: Downward center of mass displacement during stance (‘COM’) changed little despite a large change in surface stiffness and peak ‘surface’ compression.

To maintain similar center of mass movements on very soft surfaces, the legs *extended* during early stance and then *compressed* during late stance (Figure 2). This phase reversal of leg compression and extension caused the legs to produce positive mechanical work in early stance and absorb mechanical energy in late stance on very soft surfaces.

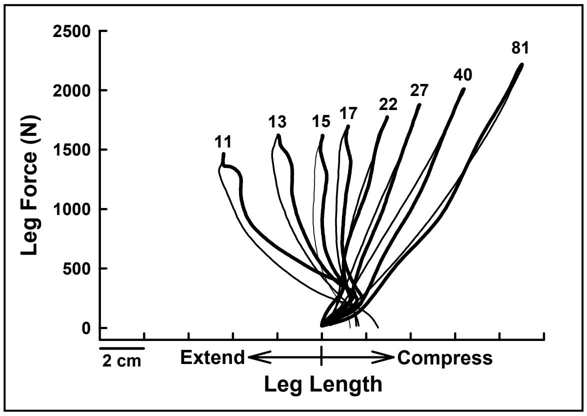

Figure 2: Leg force-displacement relation for hopping. Values above each curve are surface stiffness (kN/m). Note that during early stance (thick lines), the legs compressed on the 81 kN/m surface but extended on the 11 kN/m surface. In late stance (thin lines) the legs extend on the 81 kN/m surface but compressed on the 11 kN/m surface.

Hoppers performed zero net leg work for an entire hop cycle on all surfaces. However, performing positive mechanical leg work in early stance and then absorbing energy in late stance on the very soft surfaces may reduce muscle pre-stretch and the storage of elastic energy in muscle-tendon units. Thus, it makes sense that mean muscle EMG increased by an average of 2-fold from the hardest to softest surface (Figure 3). Net muscle moments at the joints did not increase on softer surfaces, suggesting that a greater EMG is required to produce a given net muscle moment on softer surfaces due to the reduction in muscle pre-stretch.

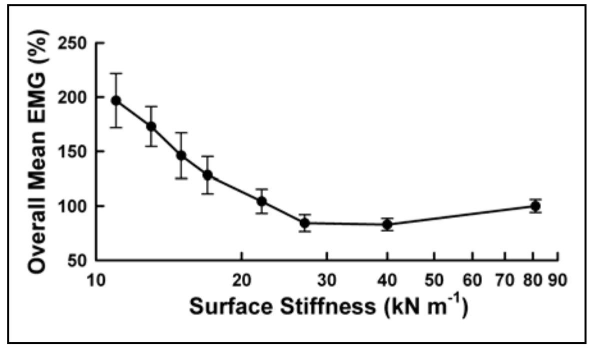

Figure 3: Overall mean EMG decreased 2-fold as surface stiffness increased.

SUMMARY

Humans maintained similar center of mass movements when hopping on a very large range of surface stiffnesses. On extremely soft surfaces with lower stiffness values than the leg stiffness used for hopping on a hard surface, the legs extended in early stance and compressed in late stance. This phase reversal of leg movements is an extreme strategy that prevents large changes in center of mass dynamics even on very soft surfaces. It also may dramatically reduce the amount of muscle pre-stretch during a hop cycle as evidenced by the large increase in muscle activation.

REFERENCES

Cavagna, G.A. et al. (1977). *Am. J. Physiol.* **233**, R243-R261.

Ferris, D.P., Farley, C.T. (1997). *J. Appl. Physiol.* **82**, 15-22.

Ferris, D.P. et al. (1999). *J. Biomech.* **32**, 787-794.

Kerdok, A.E. et al. (2002). *J. Appl. Physiol.* **92**, 469-78.

Moritz, C.T. et al. (2002). *Fourth World Congress on Biomechanics, 2002.*

ACKNOWLEDGEMENTS

This work was supported by an ASB–GIA to CTM and an NIH R29 AR-44008 to CTF.

THE ROLE OF CENTRAL AND PERIPHERAL VISION IN THE CONTROL OF UPRIGHT POSTURE DURING ANTERIOR-POSTERIOR OPTIC FLOW

Jeff G. Jasko[1,4], Patrick J. Loughlin[1,2], Mark S. Redfern[1,4], and Patrick J. Sparto [1,3,4]

[1]Department of Bioengineering, University of Pittsburgh, Pittsburgh, PA, USA
[2]Department of Electrical Engineering, University of Pittsburgh, Pittsburgh, PA, USA
[3]Department of Physical Therapy, University of Pittsburgh, Pittsburgh, PA, USA
[4]Department of Otolaryngology, University of Pittsburgh, Pittsburgh, PA, USA
E-mail: psparto@pitt.edu

INTRODUCTION

Numerous studies over the past several decades have investigated how the integration of the visual, vestibular, and somatosensory systems contributes to the maintenance of postural stability. Experiments using various oscillating visual environments have shown a marked increase of sway amplitude in response to the stimulus (e.g., Lee and Lishman 1975; Lestienne et al. 1977). Several theories have been developed in an attempt to characterize the functional roles of central and peripheral vision in maintaining postural equilibrium (Bardy et al. 1999). However, it is not clear which theory best reflects the available data since many different methodologies have been used. This study seeks to better understand how central and peripheral vision influence postural sway.

METHODS

Twenty healthy subjects (mean age: 24 ± 3 years) who were naïve to the specific purposes of the experiment participated after providing informed consent. The experiment was a repeated measures design consisting of 3 main factors: field of view (FOV) of the moving stimulus, frequency of the moving stimulus, and surface support. Postural sway of the head and pelvis in the antero-posterior (AP) direction was acquired using the Polhemus Fastrak™ system. Center-of-pressure (COP) data were also recorded in the AP direction from a NeuroTest™ force platform, which could rotate about an axis collinear with the subject's ankles.

During each 90-second trial, subjects were surrounded by a contiguous front screen and two side screens, encompassing 180 degrees horizontal field of view (Figure 1). The images were displayed on the screens using three LCD projectors. The central portion of the stimulus was a black-and-white target pattern comprised of a black center circle (5° in radius) and five alternating rings (each 5° wide), giving the entire target a diameter of 60°. The height of the target was adjusted so that its center was aligned with the subject's eye height. The periphery of the stimulus was a black-and-white checkered pattern.

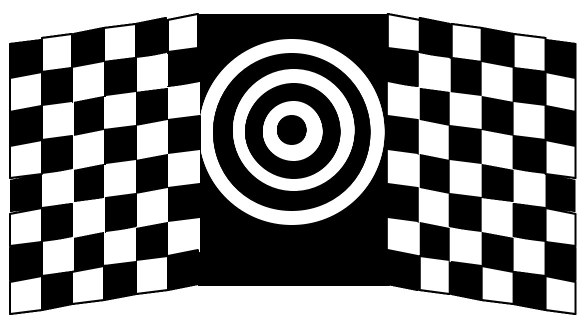

Figure 1: Unfolded schematic of the full visual stimulus. Side walls were folded around the subject to encompass the horizontal field of view.

The trials varied according to two independent visual parameters: (1) the frequency of sinusoidal visual oscillations (16-cm peak-to-peak amplitude) in the AP direction: 0.1 Hz and 0.25 Hz; and (2) the FOV of the stimulus: full, peripheral, and central. For the full FOV condition, both the central and the peripheral objects were present; for the peripheral FOV condition, only the side checkers were present; and for the central FOV, only the target was seen. Each subject observed all six visual stimuli during both fixed and sway-referenced surface conditions. (Sway-referencing was accomplished via the Neurotest to reduce somatosensory inputs from the ankle).

Data were sampled at 20 Hz. Root-Mean-Square (RMS) amplitudes of the AP head sway were calculated after the data were filtered with a 2nd-order Butterworth bandpass filter centered at the stimulus frequency (±0.05 Hz). Statistical analysis was performed using a repeated measures ANOVA to test for the effects of Frequency, FOV, and Surface condition ($\alpha = 0.05$).

RESULTS AND DISCUSSION

The RMS amplitude of head sway obtained from the experimental conditions is shown in Figure 2. For the fixed surface condition, the amplitude of sway was similar across visual conditions – except for a reduction in sway at 0.25 Hz when only the central target was presented. For the sway-referenced surface condition, again a reduction of sway is evident for the central FOV. Furthermore, the attenuation at 0.25 Hz is remarkable.

Repeated measures ANOVA revealed significant main effects of Surface condition ($p < 0.001$) and FOV ($p < 0.001$). The main effect of Frequency was not significant ($p = 0.06$), nor was the 3-way interaction. However, there were significant 2-way interactions between FOV*Frequency ($p = 0.001$), FOV*Surface ($p = 0.002$), and Frequency*Surface ($p = 0.02$). The FOV*Frequency and FOV*Surface interactions appear to be primarily related to the reduction in sway at 0.25 Hz when the central FOV was presented.

Thus, the data suggest that visual influences on posture are highly frequency dependent in the central field when somatosensory inputs are unreliable. However, the peripheral field appears to be influential along a broader frequency range when somatosensory cues are reduced. More testing at other frequencies is required to fully examine this effect.

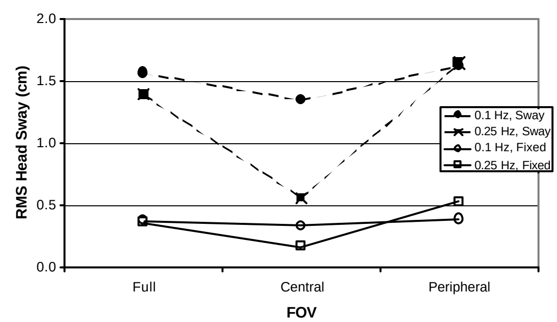

Figure 2: RMS head sway for each of the visual/surface conditions.

REFERENCES

Bardy B.G., et al. (1999). *Perception & Psychophysics*. **61**, 1356-68.

Lee D., Lishman J.R. (1975). *Journal of Human Movement Studies*. **1**, 87-95.

Lestienne F. et al. (1977). *Experimental Brain Research*. **28**, 363-84.

ACKNOWLEDGEMENTS

This research was supported by grants from NIH/NIA-1K25 AG01049, NIH/NIDCD-DC02490, and the Eye and Ear Foundation.

MOVING ROOM PARADIGM: ADAPTION DURING PROLONGED AND REPEATED EXPOSURES

Steven R. Torgerud and Shirley Rietdyk

Biomechanics Laboratory, Purdue University, West Lafayette, IN, USA

Email: srietdyk@purdue.edu

INTRODUCTION

During quiet standing body sway is relatively small. Lee and Lishman noted that sway can be increased by adding a perturbation such as a moving visual surround (see Loughlin et al. 1996 for review). Loughlin et al. (1996, 2001) have shown that subjects will sway at the frequency of the stimulus in addition to the quiet standing frequency. As the room continues to move, sway at the quiet standing frequency continues, while sway at the stimulus frequency decays. These studies have reported the change in sway frequency, but not the change in sway magnitude.

The purpose of this study was to determine if the magnitude of sway also decays as the subject stands inside a moving room.

METHODS

Four volunteer subjects (mean age = 24.5 years, SD = 2.9) have participated in the study to date. The walls of the moving room (2.3 m high, 1.2 m wide, 1.2 m deep) are aluminum. Twenty-five black dots per square meter, ranging in diameter from 1.3 cm to 11.5 cm, were placed randomly on the front and side walls. For the first trial subjects were instructed that the room was not going to move, and they were to stand quietly for 60 s. For the remaining 24 trials, the subjects were informed that the room would be stationary for 30 s, and then it would move for 60 s. The room translated sinusoidally for 60 s with a peak to peak displacement of 13 cm at a frequency of 0.23 Hz.

The subject was instrumented with a single IRED, placed posteriorly at the level of the umbilicus, approximating the COM. The moving surround was also instrumented with a single IRED. Marker position was collected at 60 Hz with the Optotrak motion analysis system (NDI). Root mean square (RMS) values of sway magnitude were measured for 30 s intervals: (1) when the subject knew the room was not going to move, (2) before the room began to move, (3) the first 30 s of room movement and (4) the remaining 30 s of room movement.

RESULTS AND DISCUSSION

As others have observed, sway significantly increased when the visual surround was moving (p=0.007, see Figures 1 & 2). We were surprised to find that the subject swayed considerably less when they knew the room was not going to move versus when they knew the room was going to move, although the difference was not signficant (see Figures 1 & 2). This is especially surprising because they also knew *when* the room would start moving (30 s from the beginning of the trial). The subjects are apparently responding to the potential room movement, possibly even perceiving movement that doesn't exist. All subjects were naïve and had not experienced a moving room before.

Comparison of the RMS for the first and last trial was not significantly different (p=0.767), so the effect did not diminish over time, and cannot be attributed to apprehension.

Contrary to the finding that sway frequency of the moving room decays during the trial

(Loughlin et al. 1996; Loughlin and Redfern 2001), no changes were observed in the sway RMS from the first 30 s to the last 30 s. Continued data collection and frequency analysis is in progress and will be presented at the meeting.

SUMMARY

It appears that the anticipation of motion in the peripheral field of vision increased sway, even in the absence of peripheral field motion. Subjects did not demonstrate an adaptation to the visual perturbation, either within a trial, or during multiple exposures, as measured by sway RMS.

REFERENCES

Loughlin P., et al. (1996). *IEEE Trans Neural Syst Rehabil Eng,* **4**(4): 416-424

Loughlin P., Redfern M. (2001). *IEEE Trans Neural Syst Rehabil Eng,* **9**(1): 24-30

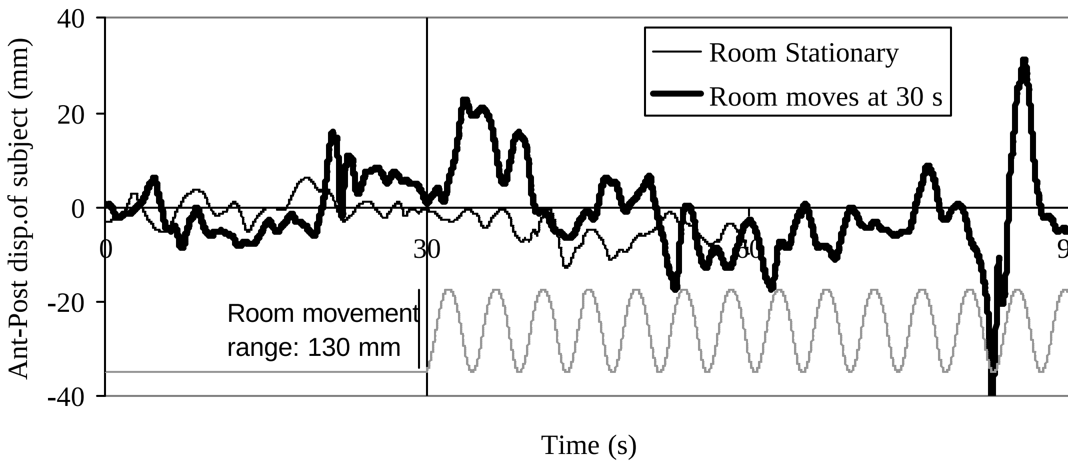

Figure 1: Time series data of body sway; note that room begins to move at 30 s, and is shown on a separate scale. The stationary room trial was collected at the beginning of the experiment (60 s duration), the moving room trial shown was the sixth trial.

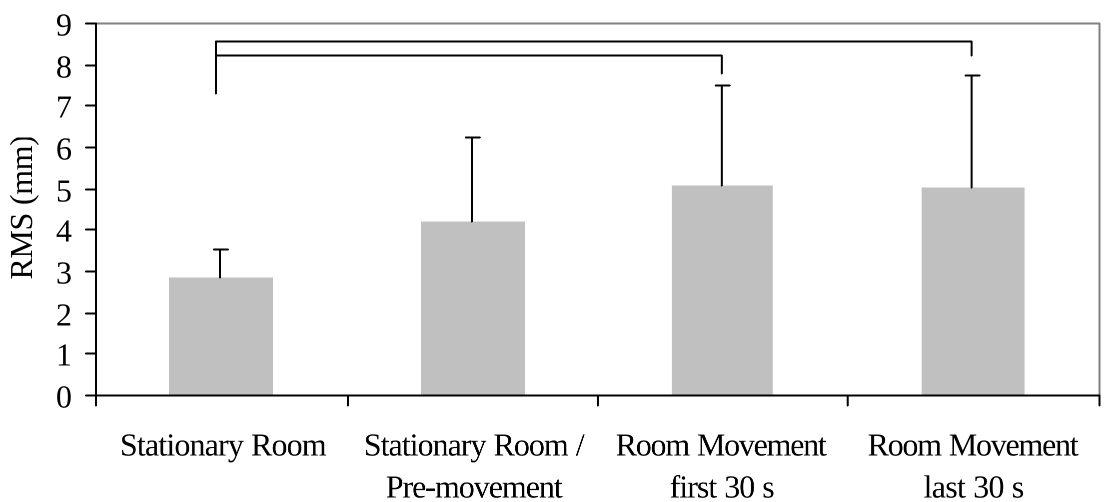

Figure 2: Mean RMS values for thirty second time periods.

GENDER DIFFERENCES IN MUSCLE RECRUITMENT PATTERNS DURING LANDING

Ross D. Hunter[1], Philip E. Martin[2], and Brian R. Umberger[1]
[1]Department of Kinesiology, Arizona State University, Tempe, AZ
[2]Department of Kinesiology, Penn State University, University Park, PA
E-mail: pmartin@psu.edu

INTRODUCTION

Female athletes have a higher non-contact anterior cruciate ligament (ACL) injury rate than male athletes (e.g., Arendt et al., 1999; Ferretti et al., 1992; Ireland, 1999). The most common mechanism for non-contact ACL injuries in female athletes is landing from a jump. Differences between males and females in recruitment patterns of knee flexor and extensor muscles have been proposed as one factor affecting the higher rate of ACL injury in females (Harmon and Ireland, 2000). The purpose of this study was to test the hypothesis that females display greater neuromuscular asynchrony and greater imbalance between hamstring (H) and quadriceps (Q) contributions during vertical landings.

METHODS

Eleven female (M_{age} = 20.2±1.7 yrs) and 11 male (M_{age} = 22.4±0.9 yrs) recreational athletes with no history of knee injury performed three drop landings onto a force platform for each of two relative heights (100% and 75% of individual maximum jump height) and one absolute height (25 cm). Electromyography (emg) signals from five muscles of the right leg (rectus femoris, RF; vastus lateralis, VL; vastus medialis, VM; biceps femoris, BF; and medial hamstrings, MH) and ground reaction force data were sampled at 1200 Hz. Emg data were subsequently normalized to voluntary isometric actions for each muscle.

Neuromuscular asynchrony was defined as the time lapse from the onset of hamstring excitation until the onset of quadriceps excitation. H/Q muscular imbalance was quantified as the average H/Q excitation ratio (H %MVC / Q %MVC) calculated for the first 100 ms following landing impact. Time of onset for the RF, VL, and VM muscles from each subject were averaged to represent the time of onset for the quadriceps group. Likewise, time of onset for the BF and MH muscles were averaged to represent that of the hamstrings.

RESULTS

The onset of H activity occurred prior to the onset of Q activity for all subjects. Consistent with our hypothesis, females displayed greater neuromuscular asynchrony by exhibiting a significantly greater amount of time between the onsets of their H and Q at each height (Figure 1). Females displayed greater H/Q imbalance by also exhibiting significantly lower H/Q excitation ratios than males over the first 100 ms following impact (Figure 2). The H/Q excitation results are explained by a higher relative excitation of the quadriceps in females compared to males at all three drop heights.

DISCUSSION

The quadriceps muscles have often been implicated for their role in pulling the tibia anteriorly in relation to the femur and stressing the ACL at knee angles close to full extension (Li et al., 1999). The small knee flexion angles typically observed at landing impact and corresponding tensile stress on the ACL, along with the results from the present study that females activate their quadriceps to a significantly higher degree than males during landing, may help to explain why females are at a greater risk of ACL disruption than males. The hamstring muscles provide dynamic stability to the knee joint by resisting mediolateral and anterior translational forces on the tibia. Studies have shown that coactivation of the hamstrings and quadriceps decreases total

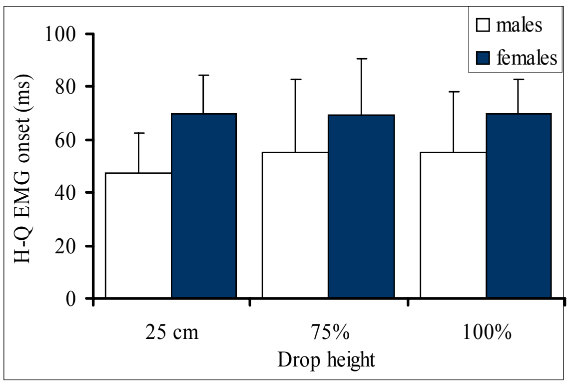

Figure 1: Females showed a significantly greater time lapse between the onset of hamstrings and quadriceps for all landing height conditions.

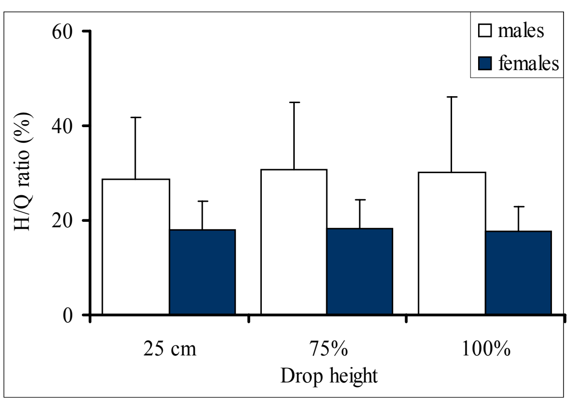

Figure 2: Females had significantly lower H/Q emg ratios during the first 100 ms following impact for all landing height conditions.

knee anterior shear force and thus the stress on the ACL (Li et al., 1999). In the present study, female subjects had a higher level of quadriceps excitation and an equivalent or slightly lower level of hamstrings excitation compared to the male subjects. The level of hamstring muscle activity is much lower than the level of quadriceps muscle activity for the females, and as such, may contribute to higher levels of anteriorly-directed loading.

In this study we made no attempt to quantify anterior tibial translation or ACL loading. Thus, we can only speculate about the contribution of gender differences in muscle recruitment patterns on ACL loading and injury rate. Nevertheless, our results support the conclusion that females display greater neuromuscular asynchrony and greater imbalance between hamstring and quadriceps contributions during vertical landings than males, and suggest this neuromuscular phenomenon should be examined more extensively.

REFERENCES

Arendt, E.A. et al. (1999). *J. Athletic Training*, **34**, 86-92.

Ferretti, A. et al. (1992). *Amer. J. Sports Med.*, **20**, 203-207.

Harmon, K.G., Ireland, M.L. (2000). *Clinics in Sports Med.*, **19**, 287-302.

Hodges, P.W., Bui, B.H. (1996). *EEG Clin. Neurophysiol.*, **101**, 511-519.

Ireland, M.L. (1999). *J. Athletic Training*, **34**, 150-154.

Li, G. et al. (1999). *J. Biomechanics*, **32**, 395-400.

ACKNOWLEDGEMENTS

This research was completed in the Exercise and Sport Research Institute, Department of Kinesiology, Arizona State University.

EFFECTS OF 'TONE-IN-NOISE' MOVING VISUAL SCENES ON POSTURAL SWAY

Mark Musolino[1,2,3], Pat Loughlin[1,2,4] and Mark Redfern[1,2,3]

Human Movement and Balance Laboratory[1]
Dept. of Bioengineering[2], Dept. of Electrical Engineering[3], and Dept. of Otolaryngology[4]
University of Pittsburgh, Pittsburgh, PA, USA (markmuso@pitt.edu)

INTRODUCTION

The use of moving visual scenes to evoke postural responses is a practical method of experimentally examining the sensory integration processes related to posture, as it provides a means of manipulating visual input in a controlled fashion. This approach has been utilized to investigate postural phenomena such as sensory conflict (Kuo et al. 1998) and sensory reweighting (Peterka, R. 2002), as well as *adaptation* – which is a transient decrease in postural sway that has been observed in subjects exposed to periodic moving visual scenes (Loughlin et al, 1996). Evidence of adaptive behavior in response to periodic inputs suggests that predictive mechanisms may exist in the postural control loop. A useful next step would be to determine if non-periodic inputs elicit similar adaptive behavior. As such, *the purpose of this study is to experimentally examine the effect of 'tone-in-noise' moving visual scenes on postural sway adaptation*.

METHODS

Postural sway responses to various moving visual scenes were examined in 6 healthy young adults. Tests were performed in the BNAVE, a custom built virtual environment that projects computer generated images onto several adjoining screens (Jacobson et al. 2001). Subjects stood comfortably in an upright position, with arms folded across the chest, and bare feet placed side-by-side on a force platform (NeuroCom Inc., Clackamas OR), while viewing a bullseye-and-checkerboard pattern that moved back and forth in a periodic or pseudorandom fashion (Fig 1). There were a total of six scene movements, each of which was a tone-in-noise time series that was created by combining a 0.3Hz sinusoid with gaussian white noise (bandpassed, 0.05-0.5Hz) at one of six signal-to-noise ratios (SNR): –inf (i.e. noise), 0dB, 3dB, 6dB, 12dB, and +inf (i.e. sinusoid). Each trial lasted 80 seconds: 60 seconds of scene movement bounded at beginning and end by 10 seconds of a stationary scene. The six movements were presented randomly, and shown only once. Subjects rested for 2 minutes after each trial.

Postural responses were examined through measurements of head, hip and center-of-pressure (COP) displacements (collected with a Polhemus electromagnetic tracking system (20Hz) and the NeuroCom platform (100Hz), respectively). The anterior-posterior (AP) root-mean-square (RMS) of these data was used to compare responses among the six tone-in-noise populations, and to determine if sway adaptation occurred.

Figure 1: Subject standing in the BNAVE

RESULTS AND DISCUSSION

Visual data inspection and cross-correlation analyses revealed that AP head, hip and COP displacements were in phase with one another for all trials, indicating that the body swayed as an inverted pendulum (Fig 2).

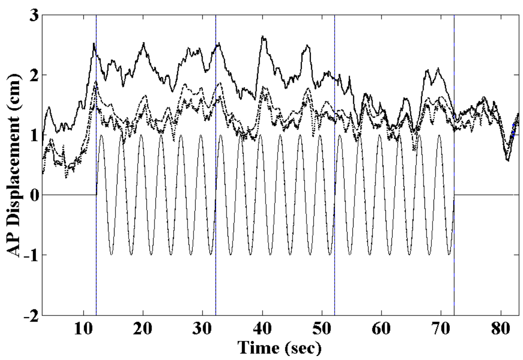

Figure 2: AP head (top), hip (mid) and COP (bot) responses to the 0.3Hz sinusoid (also shown).

Power spectra for the head data revealed that (1) the tone-in-noise moving scenes evoked sway responses near the stimulus frequency (primarily the 0.3Hz sinusoid), and (2) mean sway frequency appeared to decrease with decreasing SNR of the tone-in-noise scenes.

Prior to the onset of visual scene motion, RMS values were similar for all six tone-in-noise populations, likely because the motions that differentiate the scenes had not yet occurred (Fig 3). RMS values were higher and more varied among the tone-in-noise groups during periods of scene motion, but a consistent trend was not apparent. Overall, there was no discernable correlation between visual tone-in-noise SNR and sway RMS in any of the 20-second intervals.

Adaptation did not occur. RMS did not decrease over the course of the 60 second trial, for any of the tone-in-noise conditions (Fig 3). In fact, RMS values increased throughout the moving scene portion of the trials for three of the six tone-in-noise populations (sin, 12dB, and 0dB).

SUMMARY

There was no discernable correlation between tone-in-noise SNR and sway RMS. In addition, adaptation of the sway response was not observed, even in the sinusoidal scene population, which is in contrast to earlier findings (Loughlin et al. 1996). This may be due in part to the inability of a summary statistic like RMS (applied over 20 second intervals) to capture dynamic aspects of the time-varying adaptation process. A method such as time-frequency analysis is better suited to this task, and will be utilized in future analyses.

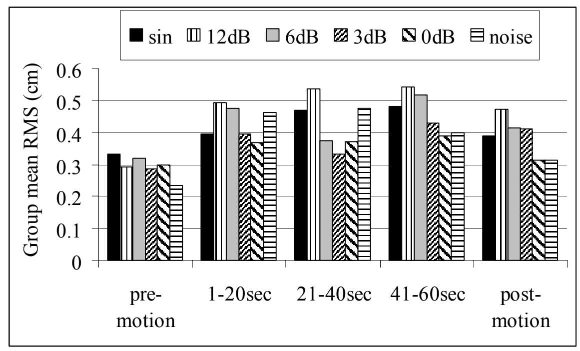

Figure 3: RMS values for AP head sway responses to each of the six tone-in-noise visual scenes. Head responses are representative of those for hip and COP as well. This plot summarizes data from 36 trials (6 subjects x 6 trials). RMS values are group means (n=6) in centimeters. Each 80 second trial was portioned into 5 intervals, as indicated on the x-axis. The pre- and post- intervals are 10 seconds long.

REFERENCES

Jacobson, J. et al. (2001). *Proceedings of the Virtual Reality Software & Technology Mtg.*

Kuo, A. et al. (1998). *Experimental Brain Research*. **122(2),** 185-95.

Loughlin, P. et al. (1996). *IEEE Trans. Rehab. Eng*. **4(4)**, 416-424.

Peterka R (2002). *J Neurophys,* **88**, 1097 1118.

ACKNOWLEDGEMENTS

This work was supported by NIH grant R01 AG14116.

FORCE VARIABILITY AND NULL SPACES IN HIERARCHICAL ORGANIZATION OF STATIC HUMAN PREHENSION

Jae Kun Shim[1, 2], Mark Latash[2] and Vladimir Zatsiorsky[1]
[1] Biomechanics Laboratory and [2] Motor Control Laboratory,
The Pennsylvania State University, University Park, PA, USA
E-mail: shimjaekun@psu.edu   Web: www.psu.edu/dept/biomechanics

INTRODUCTION

Both theoretical analyses (Iberall, 1997) and experimental evidence (Santello, Soechting 1997; Zatsiorsky et al., 2002) have suggested that prehension is controlled in a hierarchical fashion. The hierarchical organization is based on a virtual finger which is an imaginary finger that generates the same mechanical effect as a set of actual fingers. This study employed two hierarchical levels of finger control; virtual finger level (VF) and individual finger level (IF). The accuracy and stability of static force production has been the object of many research efforts. However, little is known about trial-to-trial variability in human prehension under different external torque conditions. We hypothesized that a) the variability of the variables would differ in different subjects and tasks, b) the variability of forces would depend on their magnitudes and c) there would exist more than one null space in the prehension tasks.

METHODS

Equipment: Four six-component (three forces and three moments) transducers (Nano-17, ATI Industrial Automation, Garner, NC, USA) were attached to an aluminum handle which had a beam affixed to the bottom. A load was attached to the beam at different positions to create different external torques: –1.0 Nm, –0.5 Nm, 0 Nm, 0.5 Nm, and 1.0 Nm.

Experimental Procedure: Subjects (n=6, male, right-handed) sat on a chair and positioned the right upper arm on a wrist-forearm brace fixed on the table. Subjects performed 25 trials at each torque condition. Subjects were instructed to stabilize the handle with the thumb and three fingers without the little finger. A planar static task was chosen with a prismatic grip.

Accuracy Measurement: The error propagation and uncertainty of indirect measurements were estimated from the data reported by the producer for individual sensors. The propagation of uncertainty in the elemental errors u_i to the uncertainty of the result u_R was computed as (Taylor 1997):

$$u_R = \pm\sqrt{\sum_{i=1}^{n}\left(\frac{\partial R}{\partial x_i}u_i\right)^2} \quad (1)$$

Statistics: Levene's homogeneity tests were performed to determine whether the trial-to-trial variability is affected by tasks and subjects. S.D. was used as a force variability measure. Pearson coefficients of correlation were computed and corrected for the noise and error propagation using the equation 2.

$$\frac{r_x}{r_{x+n}} = \sqrt{\left(1+\frac{\sigma_{n1}^2}{\sigma_{x1}^2}\right)\left(1+\frac{\sigma_{n2}^2}{\sigma_{x2}^2}\right)} \quad (2)$$

Principal component analyses were performed to reduce the dimension of variables and verify the null spaces.

RESULTS AND DISCUSSION

Trial-to-trial variability: The trial-to-trial variability of all the VF-level variables was affected by the tasks (P<0.001). The variability was also different in various subjects (P<0.001). The variability of the virtual finger normal force increased with the increased force magnitude as could be expected from earlier studies (Slifkin and Newell, 1999) (Figure 1). The variability of the tangential force showed a V-shape dependence on the force magnitude, which can be explained by the constant total load constraint. The variability of individual finger normal forces also showed increase with the increased magnitudes (r ranged from 0.72 to 0.86) although the tangential forces showed low correlations (r ranged from 0.01 to 0.36).

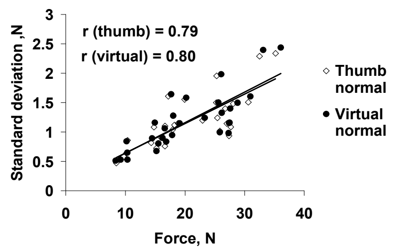

(A)

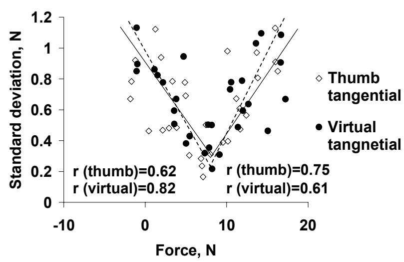

(b)

Figure 1. Variability of the thumb and virtual normal (a) and tangential (b) forces versus the force magnitude. Representative example.

It was found that individual performance variables are organized in two null spaces (Figure 2). Variables within one null space highly correlate with each other while there is no correlation among variables from the other null space. The discovery of the two null spaces supports the principle of superposition for human prehension (Arimoto, 2001). The variables in Figure 2a prevent the handle from slipping off the hand while the variables in Figure 2b are associated with the control of hand held object orientation. Principal component analyses confirmed that more than 90% of variability can be explained by two groups of VF-level variables (two null spaces) in all subjects.

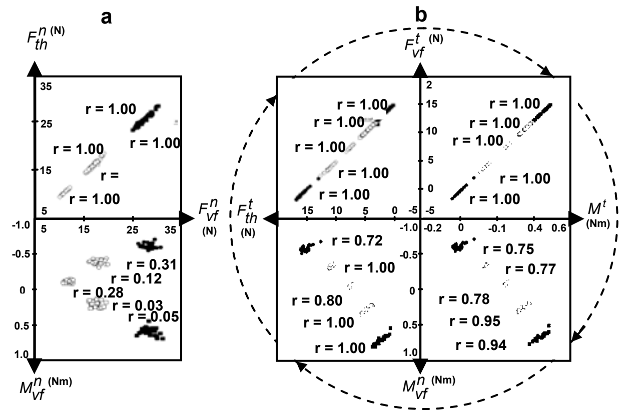

Figure 2. Interrelations among the VF-level variables. Representative example.

SUMMARY

In general, people do not perform the same prehension static task in an identical way. However, the variability of normal forces increases with their magnitude increase in both IF and VF levels of human prehension. The prehension synergy is comprised of two sub-synergies; *grasp control* and *torque control*.

REFERENCES

Arimoto, S. and Nguyen, P.T.A. (2001) IEICE, E84A, 39-47.

Iberall T (1997). International Journal of Robotics Research 16, 285-299.

Newell KM, Carlton LG, Hancock PA (1984). Psychol Bull 96: 133-151.

Santello M., Soechting JF (1997). Mot Res. 14(3): 203-12.

Taylor, J.R. (1997) An Introduction to Error Analysis. University Science Books.

Zatsiorsky VM, Gao F, Latash ML (2002). Exp Brain Res 148, 77-87.

EFFECTS OF INITIAL MUSCLE LENGTH IN STRETCH REFLEX EXCITABILITY IN PEOPLE WITH POST-STROKE SPASTICITY AND HEALTHY VOLUNTEERS

J de J Salazar-Torres[1], A D Pandyan[2], C I M Price[3], M P Barnes[1, 4], G R Johnson[1].

[1] Centre for Rehabilitation and Engineering Studies (CREST), University of Newcastle, UK.
[2] Dept. of Physiotherapy, Keele University, Staffordshire, UK.
[3] Department of Medicine (Geriatrics), Newcastle University, UK
[4] Hunters Moor Regional Neurological Rehabilitation Centre, Newcastle, UK.
E-mail: j.d.j.salazar-torres@ncl.ac.uk

INTRODUCTION

Stretch reflex excitability is influenced by neural (e.g. feed-forward and feedback mechanisms) and biomechanical components (e.g. muscle length). Spasticity is as a motor disorder resulting from hyper-excitability of the stretch reflex [Lance JW, 1980]. Measurements of spasticity predominantly focus on the velocity dependent property of the stretch reflex.

There are divided opinions whether the initial muscle length affects the stretch reflex properties [Yamamoto, 2000; Lin, 1999]. The objective of this work was to quantify the stretch reflex parameters of the biceps brachii at two different initial muscle lengths in non-impaired (NI) volunteers and stroke patients (SP) with elbow spasticity and objectively evaluate their differences

METHODS

A biomechanical device capable of eliciting a stretch reflex during a 50 ms controlled stretch perturbation to the elbow joint was designed. Stretch reflex response was measured at 75º and 105º flexion (full extension was 0º). Surface EMG electrodes were placed on the biceps brachii. The torque applied at the elbow was determined by presetting the tension of a spring, in this case of 13.68 Nm, which is the second maximum tension of the operational range in the device. A footswitch released the tension instantaneously stretching the biceps brachii. A potentiometer recorded the changes in angle. All signals were sampled at 4096 Hz.

Data analysis was set to commence 150 ms before (background activity) and to complete 450 ms after the footswitch was activated. EMG signals were full wave rectified and filtered at 15 Hz .The outcome measurements for this study were the reflex amplitude, latency, rise time and duration (figure 1). A one-way ANOVA was used to test for significant differences.

RESULTS AND DISCUSSION

Seventeen NI volunteers (mean age 35; range 24-55 years) and 14 SP with spasticity (mean age 67; range 52-86 years) resulting from a CVA six months previously were included.

The stretch reflex was elicited in all NI volunteers in the lengthened position (75º flexion) but only in 12 in the shortened position (105º flexion). It was elicited in all of the SP volunteers regardless of the muscle length.

In the NI population the reflex amplitude and the latency at the shortened position was significantly lower than that of the lengthened position ($p<0.05$). The duration of the reflex slightly increased at the shortened position ($p=0.087$). No significant differences were found in the rise time ($p>0.05$).

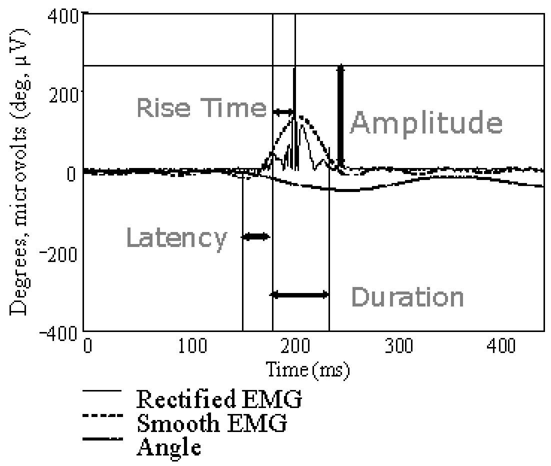

Figure 1: Typical signal and the parameters characterizing the stretch reflex activity.

In the SP population, the primary variables that were used to characterize the stretch reflex, i.e. the amplitude, latency, duration and rise time, did not significantly change with changes in muscle length ($p<0.05$).

Comparisons between the NI and SP populations, in the shortened position, showed no significant differences in the reflex amplitude, latency, duration and rise time ($p>0.10$). However, for the lengthened position the reflex amplitude and latencies were significantly smaller ($p<0.05$). No other significant differences were found in the rest of the variables

Length dependent changes in the reflex amplitude are consistent with the literature [Yamamoto, 2000; Nordin, 1996]. This suggests increased passive stiffness of the muscle reduces the required EMG activity to maintain the elastic properties of the muscle. [Lin, 1998].

Reduced latencies in NI at shorter lengths may suggest an increased sensitivity of the muscle spindles. The reasons for these differences are being explored.

The lack of differences in all reflex parameters in the SP population and the results between the groups suggest that there are indeed changes in the stretch reflex excitability after stroke but that muscle length may not have an influence it. This could be due to soft tissue changes that sometimes accompany spasticity.

SUMMARY

The characterization of the stretch reflex under different conditions is necessary to understand the neurophysiology and changes occurring after neural injury. This work was intended to clarify the influence of initial muscle length. Changes in the reflex properties due to different initial muscle lengths were more evident in the NI population, suggesting that the modulation of the reflex is lost with after stroke and remains at the same level regardless the muscle length. However biomechanical changes of the muscle may also have influence such modulation. Further work is being performed to observe other factors affecting the stretch reflex excitability and how to dissociate neural from non-neural components

REFERENCES

Lance J.W. Symposium Synopsis, in Spasticity: Disordered Motor control. Feldman RG, Young RR, Koella WP, editors. 485. 1980. Eds. Symposia Specialist. Miami.

Yamamoto S., Nakazawa K., Yano H., Ohtsuki T. *J Electromyogr Kinesiol* 2000; 10:135-142.

Lin J.P., Brown J.K., Walsh E.G. *Dev Med Child Neurol* 1999; **41**:534-548.

Nordin M., Hagbarth K.E. *Acta Physiol Scand* 1996; **156**:435-440.

Vattanasilp W., Ada .L, Crosbie J. *J Neurol Neurosurg Psychiatry* 2000; **69**:34-39.

Lin, DC, Rymer W.Z.. *J Neurophysiology*, 1998; **80**:3369-3372.

POSTURAL RESPONSES AND THE DEFENSIVE STARTLE REFLEX

Elizabeth T. Hsiao-Wecksler [1], Charles H. Hillman [2], and Karl S. Rosengren [2,3]

[1] Department of Mechanical and Industrial Engineering, [2] Department of Kinesiology,
[3] Department of Psychology
University of Illinois at Urbana-Champaign, Urbana, IL, USA
Email: ethw@uiuc.edu, Web: http://www.staff.uiuc.edu/~ethw/hdcl/hdcl.html

INTRODUCTION

Framed within the biphasic theory of emotion (Lang 2000; Lang et al., 1997), behavioral indices were investigated to examine the relationship between postural responses and the defensive startle reflex associated with an unexpected acoustic burst. Biphasic theory contends that emotion is fundamentally organized around two basic motivational systems: appetitive and defensive (Lang, 2000). The appetitive system is responsible for approach behaviors that underlie pleasant reactions (Bradley et al., 2001). The defensive system is responsible for withdrawal or avoidance behavior that is activated during threatening or unpleasant situations. In this context, emotions are considered to elicit behavioral responses that are organized along an approach-withdrawal dimension.

The defensive startle reflex is characterized by a response, which begins with a rapid eye blink (i.e., the startle-blink reflex). To date, no behavioral (or postural) measure of the defensive startle reflex has been identified in humans. Thus, this study attempts to identify and characterize behavioral indices of the startle reflex by examining variations in center-of-pressure (COP). It was hypothesized that, in response to an acoustic startle probe, individuals would demonstrate a defensive posture that involves a fetal-like response, which would be an anterior movement followed by movement away from the threat, i.e., forward-backward movement of the COP. It was also hypothesized that following this initial response, participants would continue to move backward due to a withdrawal behavior, i.e., a sustained posterior movement.

METHODS

Twenty-four undergraduate students (12 females, 12 males) provided informed consent. Participants stood in stocking feet on a force platform (9281B; Kistler Instruments, Amherst, NY) in their normal, comfortable stance with arms at the side. Participants were instructed to stand quietly for the entire length of the trial (40 s), and occasionally they may hear brief noises over headphones, which should be ignored. One practice startle trial was given. Participants completed two blocked conditions (baseline and startle), each consisting of 11 trials with a brief rest between each trial and block. During startle trials, participants received one acoustic startle probe (50 ms burst of 95 dB white noise with instantaneous rise time) between 4 to 8 s after trial onset. No noise probe was used in baseline trials. COP data were sampled at 100 Hz.

For the startle condition, COP data were reduced to an 11 s epoch of continuous data (from 1 s prior through 10 s after startle probe onset). Data were adjusted by the mean of the 1 s prior-to-startle period. For the baseline condition, an 11 s epoch were created from 5 to 16 s after trial onset. The 5-6 s period was used for mean adjustment. The 6 s time point was the average time for probe onset during the startle condition. For both conditions, the average response over all 11 trials was computed. Peak amplitude was scored in the anterior and posterior directions during the first second following probe onset to examine the initial response. The sustained response was measured by calculating the mean for each second following the initial response (i.e., 1-10 s after probe onset).

The eye-blink response was measured by placing electromyographic (EMG) electrodes on the lower arc of the left orbicularis oculi muscle using two adjacent 4-mm Ag-AgCl electrodes (In Vivo Metric, Ukiah, CA). An 8-mm Ag-AgCl electrode on the right collarbone served as ground. The startle eye-blink reflex was recorded with a Neuroscan Synamps amplifier and Acquire 4.2 software (Neuro, Inc., El Paso TX). The raw EMG signal was amplified and bandpass filtered from 30 to 500 Hz (24 dB/octave), rectified, and integrated using Neuroscan Edit 4.2 software. The eye-blink response was sampled at 2000 Hz from 50 ms prior to, and 250 ms after the onset of the acoustic startle probe. Average peak magnitude and latency of the eye-blink response were computed.

RESULTS

Analysis of the initial COP response, which occurred within approximately 500 ms following the startle probe onset, indicated that participants exhibited an immediate anterior movement, followed by a posterior movement; no effect was observed in the baseline condition ($p < 0.001$, 2×2 MANOVA; Figure 1a). No differences between the startle and baseline conditions were observed in the medial-lateral directions. Further, correlational analyses revealed a positive association ($r = 0.44$, $p = 0.036$) between the magnitude of the startle-blink response and initial posterior movement, such that increased blink magnitude was related to greater movement in the posterior direction. Multivariate analyses for the sustained COP response also differentiated startle and baseline conditions, with the startle condition eliciting sustained posterior movement over the course of 10 s following startle probe onset ($p = 0.01$, 2×3×3 MANOVA). This effect was not observed for the baseline condition (Figure 1b). No significant differences were observed in the medial-lateral direction for the sustained COP analysis.

SUMMARY

These results suggest that a measurable behavioral (postural) response may be observed following an acoustic startle probe. This defensive response has two succinct components, the first being an initial anterior-posterior movement to the startling noise, and the second being a posterior movement that may be associated with a withdrawal response. These data appear to be consistent with the biphasic theory of emotion (Lang, 1985, 2000), indicating that humans activate the defensive system in the context of threat and that this motivational system underlies withdrawal or avoidance reactions.

REFERENCES

Bradley, M.M. et al. (2001). *Emotion* **1**, 276-298.
Lang, P.J. (1985) *Anxiety and the anxiety disorders*; A.H. Tuma, J. Maser (Eds). Erlbaum Assoc.
Lang, P.J. (2000). *J Sport Exer Psych*, **23**, S122-140.
Lang, P. et al. (1997). *Attention and orienting: sensory and motivational processes*; P.J. Lang et al. (Eds). Erlbaum Assoc.

ACKNOWLEDGEMENTS

Thank you to Sarah Buck, Richard Doyle, Darin Smith, and Abner Satterthwaite-Phillips for their assistance. This project was partially supported by a UIUC Research Board Grant to CHH and KSR.

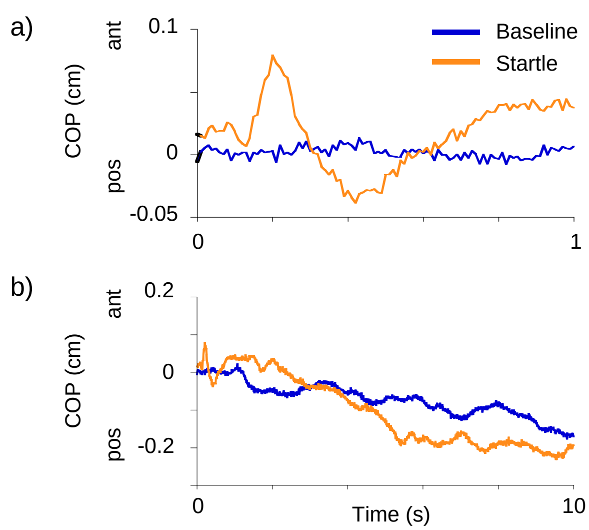

Figure 1. Ensemble averages of initial (a) and sustained (b) responses of anterior-posterior COP after startle onset.

COORDINATION OF LOWER LIMB JOINTS DURING LOCOMOTION:THE EFFECTS OF VESTIBULO-OCULAR REFLEX ADAPTATION

Chris Miller [1], Ajitkumar Mulavara [2], Jason Richards[1], Brian Peters[1], Jeremy Houser[3], Ann Marshburn[4], and Jacob Bloomberg[4]

[1] Neurosciences Laboratory, Wyle Laboratories, Houston, TX, USA
[2] National Space Biomedical Research Institute, Baylor College of Medicine, Houston, TX, USA
[3] Neurosciences Laboratory, Bergaila Engineering Services, Houston, TX, USA
[4] Neurosciences Laboratory, NASA Johnson Space Center, Houston, TX, USA
E-mail: chris.miller1@jsc.nasa.gov

INTRODUCTION

Controlling locomotion while maintaining a stable gaze requires precise coordination between several, interdependent full-body sensorimotor subsystems (Bloomberg and Mulavara, 2003; McDonald, et al., 1997). The overall goal of this study is to determine how this full-body gaze stabilization system responds to adaptive changes in vestibulo-ocular reflex (VOR) function.

Locomotion involves cyclical physical interactions (impacts) with the environment. Hence, focusing on a target and maintaining visual acuity during this activity may require mechanisms to manage the energy flow, so it does not disrupt the visual and vestibular sensory information processing that stabilizes gaze. It has been shown that increasing the difficulty of a gaze task (reading numbers on a screen as opposed to simply focusing on a central dot pattern) resulted in an increase in the amount of knee flexion movement during the critical phase immediately following the heel strike event (Mulavara and Bloomberg, 2003). The increase in knee flexion during the stance phase of the gait cycle has been suggested to function as a shock absorbing mechanism associated with the rapid weight transfer from the trailing to the leading leg during walking.

To understand this full-body coordination, the relative contributions of each component and the resulting effects should be assessed. In this study, we hypothesized that VOR adaptation would result in a reorganization of the lower limb joint coordination during treadmill walking in a manner to facilitate the gaze stabilization task and preserve locomotor function.

METHODS

Fifteen subjects participated in this study, which was approved by the NASA Committee for the Protection of Human Subjects. Footswitch data (Motion Lab Systems, Baton Rouge, LA), collected at 1000Hz, were used for calculating gait timing events. Retroreflective markers were affixed to the right lower limb in a configuration such that each segment's 3-D motion could be determined. Marker motion was collected at 60 Hz using six Hi-Res Falcon cameras (Motion Analysis, Santa Rosa, CA) set up in a split-volume configuration.

In this protocol, five walking trials were recorded before VOR adaptation as a "normal" baseline. For each 90 second trial, the subjects walked on a treadmill at 6.4 km/hr while reading 5-digit numbers on a computer screen placed 2 m from his/her eyes. Data were recorded for a 20-second epoch in the middle of each trial. The VOR adaptation consisted of the subject sitting and watching a movie while wearing minimizing lenses (0.5x mag.). The movie was projected onto a large screen (2.5 x 2.5 meters) positioned 2 meters in front of the subject. During the 30-minute viewing time, the subject was instructed to move his/her head slowly in pitch to incite the adaptation. Immediately after the adaptation period, five more walking/reading trials were recorded in the same manner as before adaptation.

Marker motion data were tracked using EVa system software (Motion Analysis, Santa Rosa, CA). Motion of the lower limb joints was determined using the convention detailed by Verstraete (1992). The following parameters were computed for each of the 20 gait cycles analyzed in each trial: the maximum, minimum, average and range of the joint angles. These parameters were used as input to a repeated-measures ANOVA (STATA 6, College Station, TX) with a significance level of $p<0.05$.

RESULTS AND DISCUSSION

The repeated-measures ANOVA showed that in the first walking trial after VOR adaptation, subjects significantly increased their average knee flexion ($p<0.001$; Figure 1). Average ankle angle tended to decrease (i.e., increased dorsiflexion) in the first trial post-adaptation, but did not quite attain statistical significance ($p=0.064$).

This coordinated increase in average knee flexion and decrease in average ankle angle appears to be part of a compensatory strategy by the lower limbs to stabilize gaze in response to modified VOR. Hence our subjects may have experienced gaze instability immediately after the adaptation period, and they evoked a strategic response to minimize perturbations to the head with increased knee flexion.

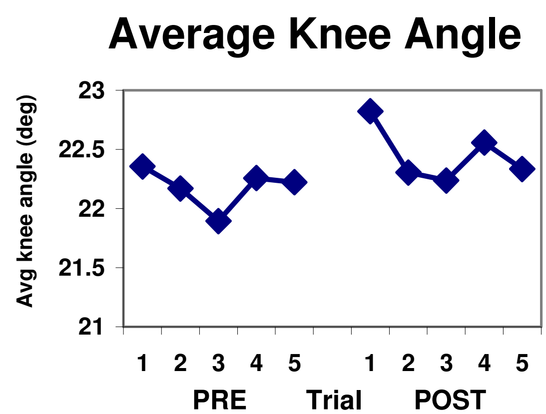

Figure 1: Representative average knee angle data for one representative subject before and after VOR adaptation.

SUMMARY

The adaptive modification of the VOR resulted in a reorganization of knee and ankle joint coordination during treadmill walking, specifically increased knee flexion. Hence the subjects were able to adopt a modified strategy for full-body coordination to maintain stable gaze.

REFERENCES

Bloomberg, J.J., Mulavara, A.P. (2003, In Press). *IEEE EMBS Magazine*.

McDonald, P.V., et al. (1997). *J. Vestib Res,* **7**, 239 – 50.

Mulavara, A.P., Bloomberg J.J. (2003, In Press). *J Vestib Res.*

Verstraete, M.C. (1992). *Med Sci Sports Exer.* **24**, 825 – 31.

NEUROMOTOR ADAPTATIONS USED BY UNILATERAL TRANSTIBIAL AMPUTEES DURING NORMAL WALKING

Michael Neal [1], Richard R. Neptune [2] and Andrew Gitter [3,4]

[1] Department of Biomedical Engineering, University of Texas, Austin, TX
[2] Department of Mechanical Engineering, University of Texas, Austin, TX
[3] Department of Rehabilitation Medicine, University of Texas Health Science Center, San Antonio, TX
[4] South Texas VA Medical Center, San Antonio, TX
E-mail: rneptune@mail.utexas.edu

INTRODUCTION

Unilateral transtibial amputation results in the loss of ankle muscle function and joint movement as well as modified mechanical properties in the residual limb. The muscles crossing the ankle joint have been shown to be important contributors to normal walking mechanics including body support, forward progression and swing initiation (Neptune et al., 2001). As such, significant neuromotor adaptations would be expected in order to restore normal walking mechanics, although it is not clear what adaptations would be necessary. Most, but not all amputees adapt their neuromotor strategies in such a way that they achieve relatively normal walking kinematics. Understanding how successful amputees achieve relatively normal walking mechanics may provide insight into designing effective prosthetic devices and rehabilitation strategies to improve their gait mechanics and accelerate recovery. Therefore, the objective of this study was to collect EMG data from the intact and residual limbs to identify how proficient amputee walkers adapt their neuromotor patterns to achieve relatively normal walking mechanics, which was defined based on symmetric walking kinematics.

METHODS

Eight traumatic unilateral transtibial amputees (seven males, one female) free from additional musculoskeletal disorders and five healthy normal subjects serving as controls (5 males) participated in this study. Informed consent was received before participation in the study. Muscle EMG activity in six intact limb muscles (tibialis anterior, soleus, medial gastrocnemius, vastus medialis, rectus femoris, biceps femoris long head) and three residual limb muscles (vastus medialis, rectus femoris, biceps femoris) were recorded using surface EMG electrodes. The subjects were asked to walk multiple trials at a speed of 1.3 m/s. The amputee subjects used their own prosthetic foot (7 energy storage and return, 1 SACH). The EMG signals were full-wave rectified, low-pass filtered and normalized to the maximum value observed in each muscle across all trials. Simultaneously, motion capture data was collected (Vicon 370 Workstation) using a modified Helen Hayes marker set to generate joint kinematic trajectories over the gait cycle. Foot switches were used to provide temporal timing for the EMG data. All data were averaged across trials for each subject, and then averaged across subjects. Both the group and individual average trajectories were analyzed to identify the neuromotor strategies used by the amputees.

RESULTS AND DISCUSSION

All subjects were proficient walkers with symmetrical and smooth kinematic trajectories similar to the healthy control subjects (Fig. 1). As a group, the primary neuromotor adaptations were 1) a larger and more prolonged burst of vasti (VAS) activity in both the intact and residual limbs beginning in pre-swing and 2) prolonged ankle plantarflexor activity during the stance-swing transition. These adaptations were consistent with the observed increase in the knee extensor moment in pre-swing (e.g., Nolan and Lee, 2002) and greater power output from the intact limb needed for forward propulsion, respectively. All other muscles were similar between the amputee and control groups.

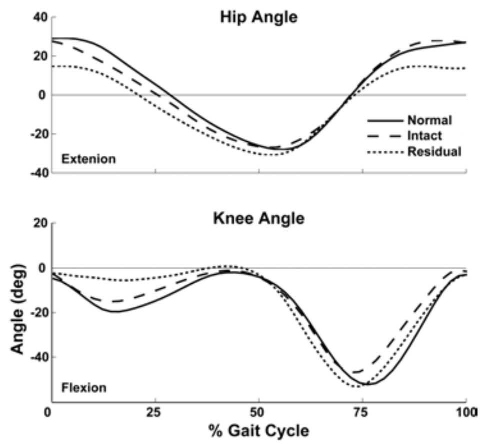

Fig. 1: Hip and knee joint kinematics for the amputee and normal groups. Differences were observed in the ankle joint during swing as expected (not shown).

Similar to normal subjects (Wootten, 1990), distinct variations in neuromotor strategies were present in individual amputees that were masked by the group averaging. For example, Subject A used a prolonged burst of intact limb soleus (SOL) activity in pre-swing, while using relatively normal intact limb VAS activity (Fig. 2). In contrast, Subject B used a different strategy with a relatively normal SOL pattern and a late burst of VAS activity in pre-swing (Fig. 2). SOL activity in pre-swing has been previously shown to provide body support and forward progression (Neptune et al., 2001). The present results suggest that VAS and SOL may be co-functional and have the same body segment energetic effect during this region, and thus provide an alternative strategy for the amputees to satisfy the task requirements. Differences in neuromotor strategies were also evident in both the intact and residual limb biarticular hamstring and rectus femoris muscles.

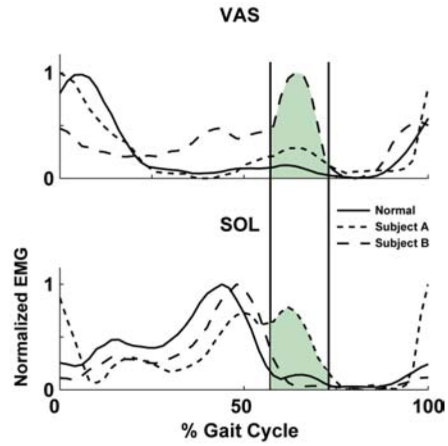

Fig. 2: SOL and VAS activity over the gait cycle for two amputees and the control group.

SUMMARY

The amputees analyzed in this study were proficient walkers with symmetric gait kinematics. Both as a group and individually, altered patterns of EMG activity were present reflecting the use of adaptive neuromotor strategies to compensate for the lost ankle function and altered mechanical properties in the residual limb. Individual amputees adopted differing neuromuscular strategies that all lead to the recovery of successful ambulation. The potential advantages associated with the different strategies are unknown, likewise it is unclear if adverse consequences exist that may increase metabolic cost or increase muscle/joint loading that may lead to musculoskeletal disorders. Future work will be directed at using musculoskeletal modeling and dynamic simulations to understand how these individual neuromotor strategies are used to satisfy the task requirements, potential consequences of using such strategies, and how they vary with prosthetic components.

REFERENCES

Neptune, R.R., et al. (2001). *J Biomech*, **34**: 1387-98.

Nolan, L and Lees, A. (2000). *Prosthet Orthot Int*, 24: 117-125.

Wootten, M.E. et al (1990). *J Orthop Res*, **8**: 259-265.

CONTROL OF HEAD MOVEMENT DURING WALKING

Gail F Forrest [1]and Ronita Cromwell[2]

[1]Kessler Medical Rehabilitation Research and Education Corporation, West Orange, NJ, USA
gforrest@ kmrrec.org
[2]Department of Physical Therapy, Center for Rehabilitation Sciences, and Sealy Center on Aging,
The University of Texas, Medical Branch Galveston.

INTRODUCTION

Researchers have been investigating movement profiles of the head, neck, trunk, and lower limbs during various activities since the 1960s (Murray, 1964). Previously, researchers have established that when the body moves, head position can be adjusted by: (a) the vestibulo-collic reflex (VCR), (b) the cervico-collic reflex (CCR), (c) vision, (d) higher order mechanisms, and (e) head in space movement.

Suggested strategies for head stabilization include:

1. The head remains stable in space as the body moves beneath it. (Di Fabio & Emasithi, 1997) Head displacements occur in anticipation of a change in the body's center of gravity and also that head movement is independent of trunk movement. This model has been termed as a top down or head first control mechanism (Berthoz & Pozzo, 1988)
2. The control of head stability is the cooperative interaction between linked body segments. They examined locomotion and established a strong dependence between body segment coordination in the control of head stability (Cromwell, Newton, and Carlton,in press).

Investigators have illustrated that intersegmental torques and gravitational torques (i.e., passive torques) can significantly contribute to control of movement of the non weight-bearing, unrestrained limb segment (Schneider & Zernicke, 1991).

The purpose of this study was to determine if head stability was directly related to coordination of linked body segments during gait.

METHODS

Fifteen participants (mean age 26.0 ± 2.0 years) participated in this study. Subjects were healthy students. Testing involved 4 repeated trials of a 10 meter walking task where participants walked at their preferred velocity and cadence. The normal condition was used to characterize head stabilization in a natural gait. Sagittal plane kinematic data were collected at 60Hz using Qualysis AB, 3-D motion tracking.

The head, neck, and trunk linked system was viewed as an unrestrained limb segment and modeled as three interconnected-planar segments where the head was most distal. The trunk was allowed to move freely to ensure that the resulting torques due to linear accelerations of the trunk were included in the equations of motion. At each joint, torques were partitioned into four categories: net joint torque, gravitational torque, intersegmental torque, and generalized muscle torque. Limb dynamics were calculated in the local moving plane with calculation of orientation angles for each segment relative to the right horizontal. Inverse dynamic modeling (Schneider and Zernicke, 1991) was used to quantify the net torque, gravitational and intersegmental torque and the residual term (muscle torque) for the trunk, neck and head. Net joint torque describes the joint motion. All torque data were inverted and appended to original torque data in order to filter the original data. These appended data sets were filtered using a low pass Butterworth filter with a cutoff frequency of 6 Hz (Winter, 1990).

Cross correlation functions (CCF) were performed and provided analyses of time series data for head, neck, and trunk multisegment movement.

RESULTS AND DISCUSSION

The torque data profiles were consistent with EMG profiles obtained in previous studies (Winter, 1984) At heel strike, there was major activity of the erector spinae and the splenius capitius muscles to stabilize each section of the trunk and the neck, respectively. The EMG activity was bimodal and consistent with each heel strike. Torque data (shown in Figure 1) demonstrated that, with heel strike, there was an increase in extensor muscle torque. This increased magnitude opposed the gravitational and intersegmental torques and its pattern was bimodal for 100% of stride length.

Cross-correlation z-transforms between trunk and neck gravitational torque profiles and head angular acceleration were greater than all other cross-correlations (0.89 ±0.11; 1.03 ±0.29) and different from each other ($p < .05$). Changes in trunk and neck orientation generated changes in trunk and neck gravitational torque, and produced changes in trunk and neck motion. Motion, orientation and configuration of the trunk and neck relative to the head determined head intersegmental torque. It was through head intersegmental torque, mechanics of connecting segments, and intrinsic motor control mechanisms that the trunk and neck segments were able to contribute to the control of head stability.

The cross-correlation z-transform mean between head muscle torque profile and head acceleration was greater than trunk muscle torque, head intersegmental torque, trunk net torque, and neck net torque z-transform means. The neck intersegmental z-transform mean was greater than trunk net torque and neck net torque. During walking the head muscle torque contributed more to head acceleration compared to other torques (excluding the gravitational torques). Head muscle torque, (Z transform correlation coefficient: 0.67± 16) - by definition, the residual term that included forces from active muscle contraction and passive deformation of muscle, ligaments, tendons and other periarticular tissues. If the gravitational torques were the major contributors to movements in this study, nervous system involvement or active muscle torque counterbalanced or continually adjusted the passive (gravitational torque) to further enhance control of head.

SUMMARY

Results demonstrate that it is possible to model the head, neck, and trunk linked segment as three interconnected-planar segments. Furthermore, muscle, gravitational, and intersegmental torques at each of the three segments did integrate to determine segmental joint net torque and coordinate to control movement at the head, neck, and trunk.

REFERENCES

Murray, M. P., Sepic, S. B., & Barnard, E. J. (1967) *Physical Therapy,* **47**, 273-284.

Di Fabio, R. P., & Emasithi, A. (1997*),Physical Therapy*, **77**, 458-475.

Berthoz, A., & Pozzo, T. (1988). In B. Amblard, A. Berthoz, & F. Clarac. (Eds.), *Development, adaptation and modulation of posture and gait* (pp. **189-99**). Amsterdam: Elsevier Science

Schneider , K., Zernicke, R.F. (1991). *Advances in Engineeering Software*, **12**,123-128

Winter, D. A. (1984). *Human Movement Science*, **3**, 51-76.

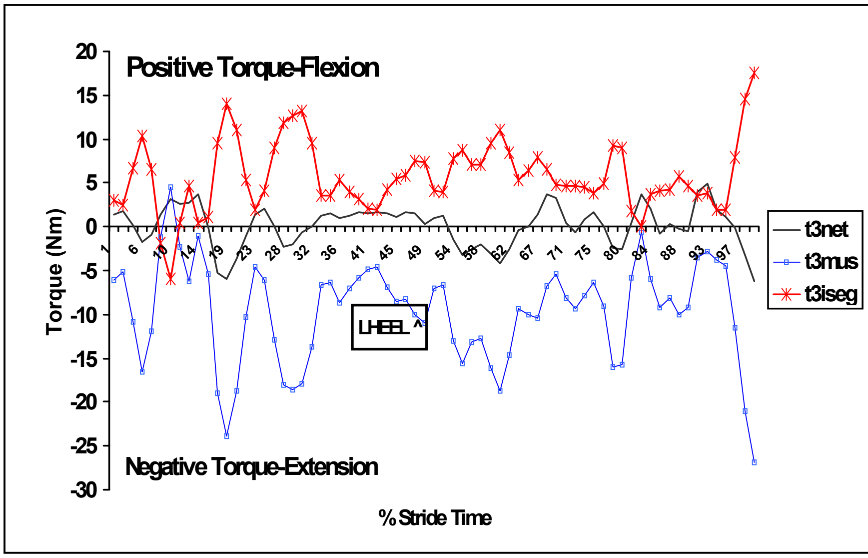

Figure 1 Trunk Torque Profiles

MULTIJOINT CONTROL STRATEGIES TRANSFER BETWEEN TASKS

J. L. McNitt-Gray,[123] Philip S. Requejo,[1] and Henryk Flashner[134]
Departments of Kinesiology[1], Biomedical Engineering[2], Biological Sciences [3]
and Aerospace and Mechanical Engineering[4]
University of Southern California, Los Angeles, CA, USA
mcnitt@usc.edu

INTRODUCTION

Multijoint movement represents the ongoing interaction between the control and dynamics of the human musculoskeletal system. Observation of complex whole body movements suggests the central nervous system organizes the human body into a number of operational subsystems that are coordinated by using some type of hierarchical control. We can advance our understanding of the relationships between functional components by determining differences in control between related tasks.

Experimental evidence suggests that humans take advantage of the learning capabilities of the nervous system and transfer movement strategies between related tasks. In this study, we hypothesized that related tasks could be performed by transferring multijoint coordination strategies between tasks with minimal modifications to other subsystems. Our specific aim was to determine whether the knee-hip coordination strategy used by an individual during one task could be used to generate the linear and angular momentum required to perform a related task. Experimental data collected during the take-off phase two types of backward rotating somersaults that translate in opposite directions (Back: translate and rotate backwards; Gainer: translate forward and rotate backwards) and an experimentally validated dynamic model were used to test this hypothesis.

METHODS

Two skilled male athletes (n=2) performed Back and Gainer somersaults from a force plate onto a foam landing pit in accordance with the Institutional Review Board. The knee-hip coordination strategies used by these subjects were representative of two distinct knee-hip coordination patterns often used by skilled performers. Reaction forces were recorded using a force plate (1200 Hz, Kistler, 0.4 x 0.6m force plate). Sagittal plane kinematics were recorded simultaneously using a digital video camera (200Hz, NAC C^2S). Each coordinate of the body landmarks (deLeva, 1996) were digitized (Motus, Peak Performance, Inc.) and filtered using a fifth-order spline (Woltring, 1986). The knee-hip coordination strategy for each subject was characterized using angular kinematics observed during the take-off phase of the Back somersault.

The dynamic model of the human body consisted of a 2-dimensional chain of six rigid segments interconnected by frictionless revolute joints actuated by moments about the joint centers. The elastic interaction between the plantar surface of the foot and the ground was modeled as proposed by Gerritsen et al., (1995). The equations of motion representing the human body dynamics were expressed as a set of seven second-order differential equations and two constraint equations expressing the interface of the foot with the platform:

$$\mathbf{M(q)\ddot{q}+H(q,\dot{q}) = Q} + \left[\frac{\partial P_f}{\partial \mathbf{q}}\right] l$$

$$\left[\frac{\partial P_f}{\partial \mathbf{q}}\right]\dot{\mathbf{q}} = 0$$

where $\mathbf{M(q)}$ is a 7×7 mass matrix, $H\mathbf{(q,\dot{q})}$ is a 7×1 vector representing centrifugal, Coriolis, and gravity terms, $\mathbf{Q}$ is an 7×1 vector of generalized forces, l is a 2×1 vector of the reaction constraint force at the foot/surface interface, $\left[\frac{\partial P_f}{\partial \mathbf{q}}\right]$ is a 2×7 matrix representing the Jacobian of the constraint force as a function of the generalized coordinates. Experimental kinematics and reaction force data were used to validate the dynamic model (ADAMS, Mechanical Dynamics, Ann Arbor, MI).

Simulations, incorporating the knee-hip coordination strategy used by the individual during the take-off phase of the Back somersault, were performed to identify the initial conditions that would produce the momentum conditions at departure consistent with those observed experimentally for Gainer somersaults.

RESULTS AND DISCUSSION

Simulation results incorporating the Back somersault based knee-hip coordination strategy, were successful in producing momentum conditions at departure required to perform a Gainer (Figure 1). The simulated reaction force curves replicated the bimodal vertical reaction force-time curve measured during the take-off phase of the Gainer. The net horizontal impulse generated during the take-off produced the forward directed horizontal velocity of the total body center of mass (TBCM) at departure required for the Gainer (Figure 1). These task specific momentum conditions at departure were achieved with minimal modifications in the initial shank position.

Coordinating knee and hip motion simplifies activation of muscles responsible for controlling motion during complex tasks. Maintaining knee and hip kinematics between tasks provides the same length and velocity conditions for generating muscle force.

SUMMARY

Experimental evidence suggests performers take advantage of the learning capabilities of the nervous system and transfer control strategies between tasks. In this study, we hypothesized that related tasks could be performed by using a common multi-joint strategy with minimal modifications to other subsystems. Simulations incorporating the knee-hip coordination strategy used by the individual during the take-off phase of the Back produced the linear and angular momentum conditions at departure consistent with those observed experimentally for Gainers. These results support the hypothesis that related tasks can be performed by transferring multi-joint coordination strategies between tasks with minimal modifications to other subsystems.

REFERENCES

deLeva (1996). J. Biomech.29(9),1223-30

Gerritsen, K. et al. (1995), J. Biomech., 28(6), 661-668

Woltring (1986), Adv. Eng. Soft.,8(2), 104-107

ACKNOWLEDGEMENTS Intel, USOC USA National Governing Bodies of Sport

Total Body Center of Mass Velocity During The Take-off Phase

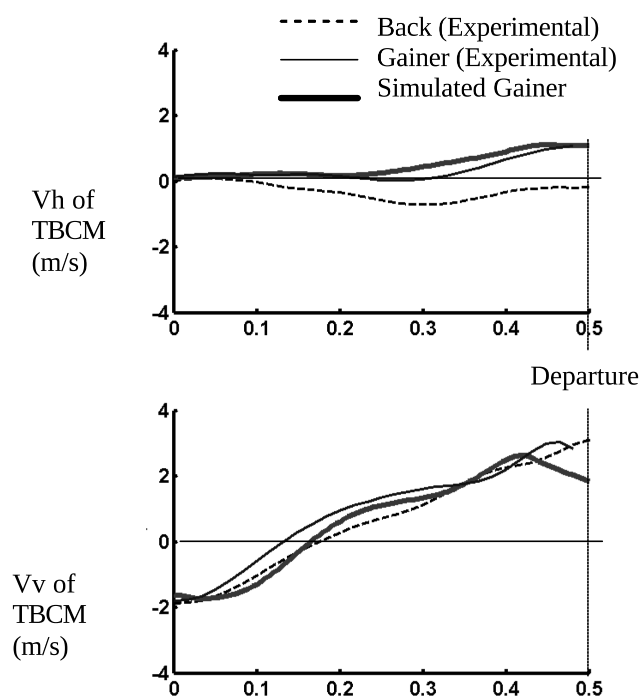

Figure 1. Comparison of the Horizontal (Vh) and Vertical (Vv) Total Body Center of Mass (TBCM) velocities measured during the Take-off phase of a Back somersault and Gainer somersault and the simulated TBCM velocities of a Gainer somersault incorporating the knee-hip coordination used by the individual during the Back somersault.

VECTORIAL FORCE COORDINATION AMONG DIGITS DURING GRIPPING

Zong-Ming Li
Musculoskeletal Research Center, Department of Orthopaedic Surgery
University of Pittsburgh, Pittsburgh, PA 15213. zmli@pitt.edu

INTRODUCTION

Manipulation of an object relies on the precise mechanical interaction at the object-digit interface and coordination among multiple digits. Previous research has mainly focused on thumb-index precision grip using single unidirectional force sensor. It is advantageous to study digit coordination using six degree-of-freedom force/moment sensors (Li 2002; Zatsiorsky et al. 2003; Rearick et al. 2003). Thus, the purposes of this study were (1) to develop an experimental method to investigate digit coordination utilizing five force/moment sensors, (2) to visualize force vectors at the object-digit interface, and (3) to investigate migration of force vectors of individual digits during sustained maximal gripping.

METHODS

Five force/moment sensors (4×Nano17, 1×Mini40, ATI Industrial Automation, NC) were attached to a rectangular plastic plate (180×73×12 mm, 282 g) via mounting tape (Fig. 1). Force and moment signals from the five sensors, were amplified, multiplexed and converged to a 12-bit analog-digital converter (Li 2002). A LabVIEW program was used for data acquisition. Sandpaper (Medium 80, 3M Construction and Home, MN) was attached to each sensor surface. Sensors for the individual fingers were positioned 25 mm apart in the radioulnar direction. The sensor for the thumb on the opposite side of the plate was positioned 6.0 mm ulnarly from the center of the sensor of the middle finger.

Ten college students who had no history of neuromuscular or musculoskeletal disorders related to the upper extremities participated in the study. Each subject maximally gripped the instrumented plate for a period of 15 seconds while holding the plate in the air. The task was repeated five times with a rest period of 5 minutes between trials. The 30-channel force/moment data were collected at a frequency of 100 Hz.

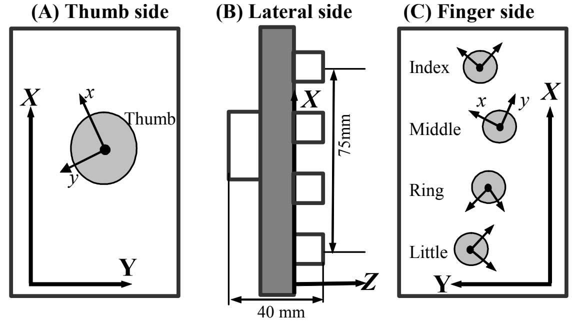

Fig. 1. A schematic diagram of the instrumented plate with five force/moment sensors

The raw forces and moments from each sensor were measured in its own coordinate system. The transformation matrices between the plate and individual sensors were established using the digitized 3D coordinates of points on the plate and sensors, which were subsequently used to express force components and center of pressure (COP) coordinates with respect to the plate coordinate system (Fig. 1). The coordinates of the COP were first calculated within each local sensor coordinate system: $x = -M_y/F_z$, $y = M_x/F_z$, and $z = 0$, and then converted to the plate coordinate system. COP migration of each digit was defined as the total distance traveled over time. Force vector migration of each digit was calculated as the sum of the magnitudes of force vector displacement over time, assuming a fixed COP. The data from the last 10 seconds of each trial were used to calculate migrations of the COP and components of the force vector.

RESULTS AND DISCUSSION

Force vectors (i.e. COP, direction and magnitude) showed considerable variations during static maximal gripping. However, the clusters of force vectors tended to converge towards the thumb (Fig. 2).

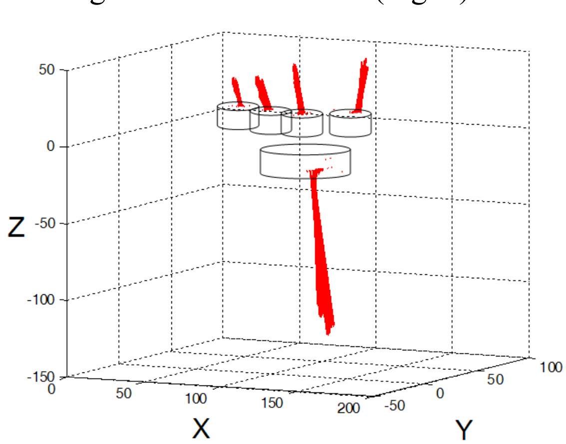

Fig. 2. Force vector visualization of a representative trial

The COP migrated in both X and Y directions. The total distances of the COP migration, averaged across subjects, were 128.5, 84.0, 63.3, 80.0, and 142.7 mm for the thumb, index, middle, ring and little fingers, respectively. In addition to COP migration, the magnitude and direction of each force vector also fluctuated over time. The amounts of force vector migration were 320.4, 181.8, 153.7, 58.1 and 142.7 N for the thumb, the index, middle, ring, and little fingers, respectively.

Table 1. Mean forces and SD in three directions

		Thumb	Index	Middle	Ring	Little
Fx	Mean	2.7	-5.0	-0.8	1.1	4.7
	SD	4.1	2.3	1.6	2.0	1.7
Fy	Mean	-10.4	2.9	4.7	3.6	0.2
	SD	4.9	1.6	2.6	1.9	1.9
Fz	Mean	85.5	-27.8	-28.0	-15.7	-12.2
	SD	18.3	7.8	9.4	3.4	2.2

The forces of individual digits at the instant of peak F_Z of the thumb are shown in Table 1. The index finger generated an ulnar force of 5.0 N, while the little finger produced a radial force of 4.7 N. In the longitudinal (Y) direction, the digits II-V tended to produce forces in the proximal direction, while the thumb produced force distally. The contributions of the index, middle, ring and little fingers to opposition of the thumb force in the normal direction were 33.2%, 33.5%, 18.7%, and 14.6%, respectively.

SUMMARY

An experimental method has been developed to simultaneously measure forces and moments at the digit-object interface of each of the five digits during a manipulation task. Visualization of force vector clusters could provide a valuable addition to the traditional time-series data considering a large number of signals from multiple force/moment sensors. The utilization of force/moment sensors for five digits has the potential to provide more detailed and subtle characteristics of manipulation mechanics than previous studies on thumb-index gripping using unidirectional force sensors, therefore, to advance our understanding of force coordination among multiple digits and mechanical interaction at the digit-object interface. In the future, measurements of forces/moments and hand/digit motion will be synchronized so that force vectors can be visualized and analyzed in real time together with dynamic hand configuration during various manipulation tasks. Experimental force outputs and derived internal joint forces/moments and muscular involvement can further our understanding of normal and patho-mechanics of the human hand.

REFERENCES

Li, Z.M. (2002) *Ergonomics* **45**: 425-440

Zatsiorsky, V.M. et al. (2003) *Exp Brain Res* **148**: 77-87

Rearick, M.P. et al. (2003) *J Neurophysiol* **89**: 1317-1326

ACKNOWLEDGEMENTS

The Whitaker Foundation

VISUALLY-INDUCED POSTURAL SWAY IN CHILDREN AGED 7-12: EFFECT OF FREQUENCY AND SURFACE SUPPORT

PJ Sparto [1,2], MS Redfern [2], JM Furman [2], EM Mandel [2], and ML Casselbrant [2]

[1] Department of Physical Therapy, University of Pittsburgh, Pittsburgh, PA, USA
[2] Department of Otolaryngology, University of Pittsburgh, Pittsburgh, PA, USA
E-mail: psparto@pitt.edu

INTRODUCTION

The integration of visual, somatosensory, and vestibular inputs for the control of balance develops throughout childhood. Initially, children demonstrate a strong visual dependence for control of balance (Lee and Aronson, 1974, Shumway-Cook and Woolacott, 1985, Wann et al., 1998). Adult patterns of sensory integration that include more veswtubular and proprioceptive weighting occur around 10-12 years (Wann et al., 1998), but can as early as 4-6 years (Shumway-Cook and Woolacott, 1985). However, we have observed visually-induced postural responses in children aged 7-12 that remain different from adults. The purpose of this study was to examine the sensory integration process in children aged 7-12 in altered visual and somatosensory conditions.

METHODS

Nineteen subjects between the ages of 7-12 participated in the study after parental consent and subject assent was obtained. Unequal distribution of subjects did not allow a full analysis of effects due to age.

Postural sway was induced by movement of a visual scene and by altering the stability of the flooring surface. Four frequencies of visual scene movement (0.1, 0.25, 0.4 and 0.7 Hz) were chosen. The surface upon which they stood was either fixed or sway-referenced in order to reduce the availability of proprioceptive information from the ankles. Sway referencing about the ankles attempts to keep them at a constant angle, thereby reducing proprioceptive inputs.

Prior to testing, electromagnetic sensors (Polhemus, Inc.) were secured over the crown of the head and the pelvis at the level of L4. A harness was worn by the subjects to prevent an impending fall. Subjects stood without shoes on the platform which recorded center of pressure displacements (COP). Only results from the head motion recordings are reported in this abstract.

Surrounding the subjects were 3 back-projected screens that entirely subtended the horizontal viewing plane (Figure 1). The visual stimulus consisted of a set of concentric rings that occupied the central 60^o field of view and an array of squares that extended peripherally beyond 180^o. This stimulus assured maximal stimulation of both the central and peripheral retina.

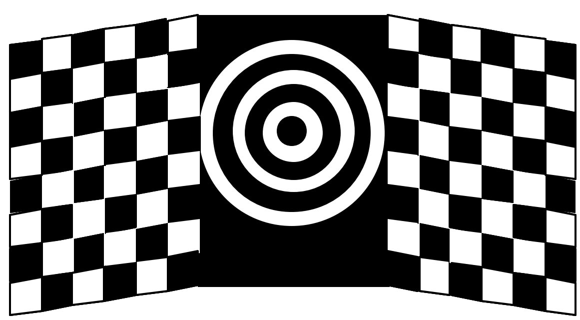

Figure 1. Unfolded view of the visual stimulus. Side walls were folded around subject to encompass full horizontal field of view.

Each trial consisted of a 30 s baseline during which there was no visual movement, followed by at least 9 cycles of visual field movement in the anterior-posterior (AP) direction (8 cm amplitude, Figure 2).

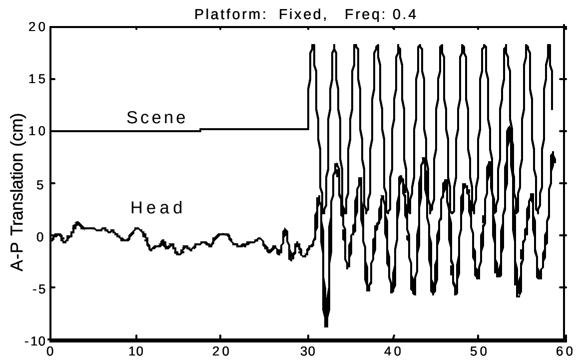

Figure 2. Anterior-posterior (A-P) translation of the head in response to 0.4 Hz stimulus with the surface fixed.

Head, pelvis and COP data were sampled at 20 Hz and stored for subsequent processing. The time series were filtered using a second-order Butterworth bandpass filter centered at the stimulus frequency ($\pm$ 0.05 Hz). The root-mean-square (RMS) of the AP translation of the head was computed during the period of scene movement and analyzed using a repeated measures ANOVA to test for the effects of movement frequency and somatosensory condition ($\alpha = .05$).

RESULTS AND DISCUSSION

Figure 2 shows a time series from a 9 year old female who had considerable visual dependence. Observe the immediate response when the visual stimulus began moving, as well as the strict phase-locking of the response. The effects of visual frequency and surface stability on the RMS head sway are shown in Figure 3. The main effects of frequency ($p = 0.006$) and surface ($p<.001$) were both significant, while the interaction was not. In comparison with patterns that have been found in adults, the following differences emerge. First, the amplitude of the sway in children aged 7-12 is approximately 1.5 - 3 times that of adults for similar conditions. Second, these children demonstrate a peak response at 0.25 Hz, whereas adults generally show a level to declining response at 0.25 Hz. Third, the children show significant postural responses at 0.4 and 0.7 Hz, which are rarely seen in adults. These findings may indicate that the vestibular control of posture, which is thought to stabilize posture at these intermediate frequencies in adults, may not be fully integrated by the ages of 7-12.

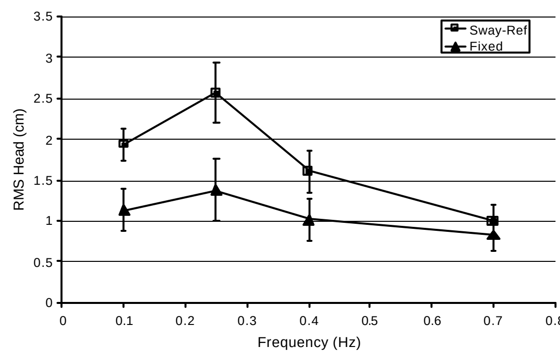

Figure 3. Mean + S.E.M. values of RMS anterior-posterior head translation due to frequency and surface conditions.

REFERENCES

Lee D. N., and Aronson E. (1974). *Percept. and Psychophysics*, **15**, 529-532.

Shumway-Cook A., and Woolacott M.H. (1985). *J Motor Behavior*, **17**, 131-137.

Wann J.P., et al. (1998). *Hum Movement Science*, 17, 491-513.

ACKNOWLEDGEMENTS

This research was supported by grants from NIH/NIA-1K25 AG01049, NIH/NIDCD-DC02490, and the Eye and Ear Foundation

EFFECTS OF WRIST POSTURE AND TENDON LOADING ON CARPAL TUNNEL DIMENSIONS: AN MRI EVALUATION

Jason A. Bower and Peter J. Keir

Occupational Biomechanics Laboratory, York University, Toronto, ON, CAN
Email: pjkeir@yorku.ca Web: http://www.yorku.ca/kahs

INTRODUCTION

Several mechanisms have been proposed to explain the nature of median nerve trauma in carpal tunnel syndrome (CTS), including increased pressure within the tunnel and contact forces on the nerve itself. However, greater understanding of the underlying mechanisms is necessary to advance management and prevention programs.

Wrist posture and tendon loading have been shown to increase carpal tunnel pressure, which may result in median nerve compression (Keir *et al*., 1998). This change in pressure may be due to a change in carpal tunnel volume or the volume of its contents. Thus magnetic resonance imaging (MRI) studies have been used to evaluate parameters such as cross-sectional area (CSA) and the relationship of space availability and the median nerve (Horch *et al*., 1997; Skie *et al*., 1990). While previous studies have evaluated the CSA in flexed and extended wrists, volume has only been addressed in neutral wrist postures (Cobb *et al*., 1992; Richman *et al*., 1987). By evaluating numerous parameters in both healthy and symptomatic wrists, mechanisms by which CTS develops may be elucidated.

The purpose of the study was to determine the effects of finger and thumb forces combined with wrist flexion and extension on carpal tunnel shape (defined by volume, CSA and the space available for the median nerve). Furthermore, we sought to identify the relationship between the space (CSA, volume) of the carpal tunnel and its contents.

MATERIALS AND METHODS

A total of ten wrists were imaged, 5 healthy controls and 5 volunteers diagnosed with CTS. Magnetic resonance images were collected with the use of a 1.5 Tesla Imaging System (Signa, Milwaukee, WI) at Sunnybrook & Women's College Hospital (Toronto, ON). To obtain high tissue contrast and resolution, 2-D axial images were acquired using fast gradient echo with fat suppression and a 17.5 cm diameter extremity coil. Repetition Time (TR) and Echo Time (TE) were 51 and 3 ms, respectively. A flip angle of 30^o was chosen along with contiguous 3 mm slices, 12x12 cm field of view (FOV), 256x256 matrix and 10 acquisitions. Total imaging time was approximately 5 minutes per series.

Participants lay prone with their dominant arm abducted and flexed above the head. Wrists were imaged in seven different conditions, including three postures (neutral, 30^o flexion and 30^o extension), with and without maintaining a sub-maximal pinch grip of approximately 10 N. Also, a closed fist in a neutral wrist posture was imaged.

Carpal tunnel cross-sectional areas, volumes and space adjacent to the median nerve were calculated for the entire tunnel for each condition.

RESULTS AND DISCUSSION

Although a full quantitative analysis has not yet been completed, preliminary qualitative data analysis has revealed several findings consistent with the literature. For example, in wrist flexion the carpal tunnel takes on a more circular appearance with the finger flexor tendons lining up against the transverse carpal ligament (TCL) (Fig.1). In wrist extension, the shape of the tunnel appears more flattened as it progresses distally (Fig.2). We have graphically outlined the carpal tunnel borders in the figures to illustrate part of the process. In addition to the area indicated in the figures, the same will be done for its contents, as well as linear measures of depth and width.

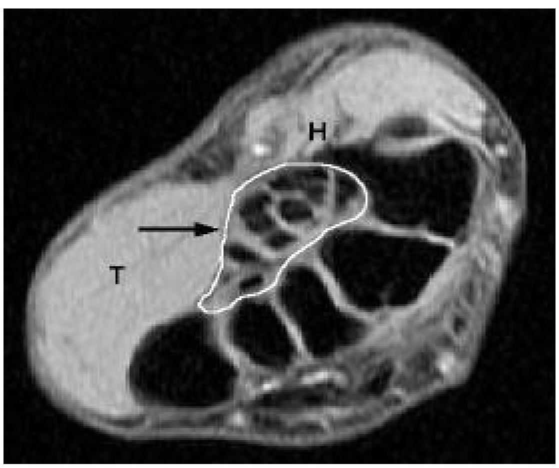

Figure 1: Axial image of the carpal tunnel. Flexed wrist at the level of the hook of the hamate (H). Thick arrow (TCL); thenar eminence (T); tunnel border outlined.

MRI slice orientation is typically aligned visually to the "best" fit. While this does not generally affect medical interpretation, it may introduce parallax error, which becomes important when calculating areas and volumes. This topic has not been discussed in the literature and, if considered, may result in changes in areas reported for the carpal tunnel. When calculating carpal tunnel CSA and volume, it is necessary to obtain perpendicular cross-sections, or account for this potential confound.

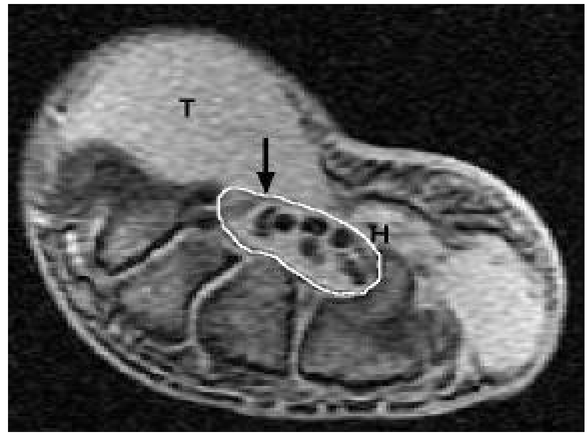

Figure 2: Axial image of the carpal tunnel with an extended wrist at the hook of the hamate (H). Thick arrow (TCL); thenar eminence (T); tunnel border outlined.

SUMMARY

Quantitatively examining carpal tunnel parameters in healthy and symptomatic wrists will help develop better strategies in prevention and rehabilitation of CTS.

REFERENCES

Cobb, T.K., et al. (1992). *J. Hand Surg*, **17A**, 843-849.

Horch, R.E., et al. (1997). *Neurosurgery*, **41**, 76-83.

Keir, P.J. et al. (1998). *J. Hand Surg*, **23A**, 1004-1009.

Richman, J.A., et al. (1987). *J. Hand Surg*, **12A**, 712-717.

Skie, M. et al. (1990). *J. Hand Surg*, **15A**, 934-939.

ACKNOWLEDGMENTS

This research was supported by NSERC (Canada) grant #217382-00. The authors also wish to thank Dr. G. Stanisz of Sunnybrook Hospital.

THE EFFECT OF WALKING SPEED ON MUSCLE EMG PATTERNS DURING NORMAL WALKING

Kevin Terry [1], Richard R. Neptune [2] and Kotaro Sasaki [2]

[1] Department of Biomedical Engineering, University of Texas, Austin, TX
[2] Department of Mechanical Engineering, University of Texas, Austin, TX
E-mail: rneptune@mail.utexas.edu

INTRODUCTION

Recent studies of walking at self-selected speeds have shown how individual muscles work in synergy to satisfy task demands including support, forward progression and swing initiation (e.g. Neptune et al., 2001; Anderson and Pandy, 2003). However, how muscle activity changes with increasing walking speed is not well understood, since all the task demands should not be expected to change in a same manner. Intuitively, increasing walking speed would necessitate an increase in activity for muscles that contribute to forward progression. However, since increasing walking speed is associated with longer stride lengths (e.g., Holden et al., 1997), which also increase the vertical excursion of the body's center-of-mass, increased output may be required from muscles contributing to swing initiation and vertical support. However, in addition to mechanically inspired increases in muscle force, muscle activity may increase due to intrinsic factors such as muscle force-length-velocity relationships. Previous studies have examined the effect of walking speed on muscle activity using EMG measurements, but these studies either examined a limited set of muscles or walking speeds (e.g., Yang and Winter, 1985). Therefore, the goal of the present study was to examine EMG patterns of the major lower extremity muscle groups across a wide range of speeds to assess whether all muscle activity systematically increases in response to increasing walking speed.

METHODS

Ten subjects walked at speeds of 0.7, 1.0, 1.3 and 1.6 m/s on a split-belt treadmill instrumented with force plates while simultaneous ground reaction force, EMG and 3D motion data were collected. EMG data from the gluteus maximus (GMAX), rectus femoris (RF), vastus medialis (VAS), biceps femoris long-head (BF), tibialis anterior (TA), soleus (SOL) and medial gastrocnemius (GAS) were collected at 1200 Hz and full-wave rectified, low-pass filtered and normalized to the maximum value observed for each muscle at the highest walking speed. For the motion data collection, a modified Helen Hayes marker set was used to establish lower extremity joint kinematics. At each speed, data were averaged across trials within each subject and then across subjects.

RESULTS AND DISCUSSION

As walking speed increased, muscle EMG also systematically increased in a mostly linear fashion from 0.7 to 1.6 m/s, although there was a more dramatic increase in GMAX, RF, BF and SOL from 1.3 to 1.6 m/s (Fig. 1). The only instances of muscles not increasing activity with speed were SOL and GAS, which showed a negligible increase in activity from 0.7 and 1.0 m/s. This is intriguing considering their importance in meeting the task demands of support, forward progression and swing initiation (e.g. Neptune et al., 2001). For 8 of 10 subjects, the difference in ankle angular velocity at the two slowest speeds was also negligible, suggesting that the SOL and GAS fiber velocities may be operating at the same contraction speeds at 0.7 and 1.0 m/s, and therefore do not have to increase activity to compensate for force-velocity effects to produce the same amount of force.

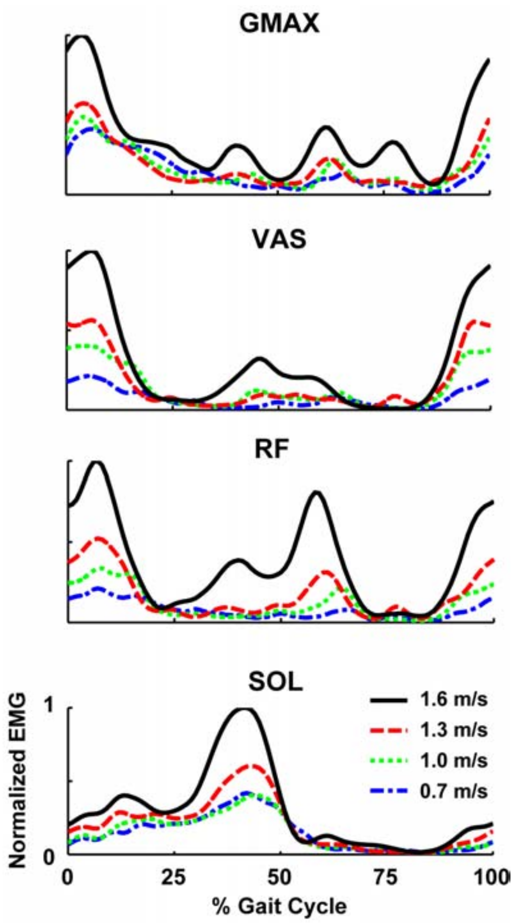

Fig. 1: Muscle EMG changes across increasing walking speeds.

The nonlinear increase in some muscles from 1.3 to 1.6 m/s is also noteworthy considering the preferred walking speed of normal healthy individuals is near 1.3 m/s (Perry, 1992). Greater muscle activation may be required as speed increases beyond the preferred walking speed, as muscle force production changes because of differences in muscle fiber length and velocity, as well as walking mechanics (e.g., increased stride length). Also, as walking speed increases, additional negative muscle work may occur during the loading response as stride length increases and because of activation dynamics that limits the rate at which muscle force can deactivate (Neptune and Kautz, 2001). Increased negative muscle work would necessitate additional positive work, and hence muscle activity in order to maintain a given energetic state of the system.

In addition, at the highest walking speed, secondary bursts of RF and VAS activity developed during late stance (Fig. 1). These bursts may be related to the inability of SOL to satisfy the energetic requirements during pre-swing, since RF, VAS and SOL act to accelerate the knee into extension in late stance phase. Interestingly, the secondary bursts of activity are also a phenomenon observed in transtibial amputees when the plantar flexors are absent (e.g., Winter and Sienko, 1988).

There are many factors that influence muscle activity including the force-length-velocity relationships, increased negative muscle work and changes in the energetic demands of the task. Future work will be directed at understanding these complex interactions and how they influence the required muscle activity as walking speed increases.

REFERENCES

Anderson, FC and Pandy, MG (2003), *Gait & Posture,* **17**: 159-69.

Holden, JP et al. (1997), *Clin Biomech*, **12**: 375-82.

Neptune, RR et al. (2001), *J Biomech*, **34**: 1387-98.

Neptune, RR and Kautz, SA (2001). *Exerc Sport Sci Rev,* **29**: 76-81.

Perry, J. (1992), *Gait analysis: normal and pathological function*. Thorofare, NJ, Slack Inc.

Winter, DA, and Sienko, SE, (1988), *J Biomech*, **21**: 361-7.

Yang, JF and Winter, DA, (1985), *Electroencephalogr Clin Neurophysiol,* **60***: 485-91.*

ACKNOWLEDGEMENTS

The authors are grateful to Julie Perry for help with the data collection and The Whitaker Foundation for financial support of this research.

TOE OUT EFFECTS FRONTAL PLANE KNEE MOMENTS AND ANGLES IN PATIENTS WITH KNEE OSTEOARTHRITIS

Robert J. Butler[1], Irene McClay Davis[1,2], Todd Royer[3], Stephanie Crenshaw[3] and Emily Mika[1]

[1] Department of Physical Therapy, University of Delaware, Newark, DE, USA
[2]Joyner Sportsmedicine Institute, Harrisburg, PA USA
[3] Department of Health and Exercise Science, University of Delaware, Newark, DE USA
Email: rbutler@udel.edu

INTRODUCTION

Knee osteoarthritis is a common problem facing the aging adult population. This condition is most prevalent in the medial compartment of the knee and is associated with increased varus (or adduction) alignment of the knee. Patients with medial knee osteoarthritis often exhibit increased medial joint space narrowing, increased external knee adduction moments, and increased compressive forces in the knee joint (Kaufman et al., 2001). It has been noted that patients may compensate for medial knee pain, associated with the knee osteoarthritis, by increasing toe out during gait. Although the correlation was not significant, Hurwitz et al. (2002) reported that as subjects increased toe out, the external knee adduction moment decreased. This may be related to decreasing the varus alignment of the knee during stance. However, the relationship between toe out and varus alignment during walking has not been assessed.

Therefore, the purpose of this study was to evaluate the relationship between toe out and frontal plane knee kinetics and kinematics in a group of patients with medial knee osteoarthritis. It was hypothesized that as toe out increases peak knee adduction and knee adduction excursion will decrease. It was also expected that an increased toe out would result in a decrease in the peak external knee adduction moment.

METHODS

This is an ongoing study of which eighteen subjects (11 women and 7 men) with medial knee osteoarthritis have been recruited. Subjects with knee osteoarthritis diagnosed by a Kellgren-Lawrence grade of 2-4 on an anterior-posterior flexed knee radiograph were included in the study. All subjects had a minimum of 3 on a 10 cm visual analog scale that rated pain during walking. 3D kinematics and kinetics were collected using a six camera VICON motion analysis system (sampling at 120 Hz) and a Bertec force platform (sampling at 960 Hz) as subjects walked across the 25 m runway at their comfortable walking speed. Data were collected on the limb with the greatest severity of knee osteoarthritis. Five trials were averaged for analysis.

The variables of interest included the toe out angle of the foot, peak knee external adduction moment, peak knee adduction angle, and adduction knee excursion (from foot strike to peak adduction) during the first half of stance. The toe out angle was calculated as the angle between the local anterior-posterior axis of the foot and the anterior-posterior axis of the lab coordinate system. Statistical analyses were performed using one way bivariate correlations with an alpha level of 0.05.

RESULTS AND DISCUSSION

Toe out was significantly correlated to a reduction in both knee adduction moment (Fig. 1; p=0.05) and peak knee adduction (Fig. 2; p=0.02). Knee adduction excursion also decreased with toe out, but the correlation was not quite significant (Fig. 3; p=0.07).

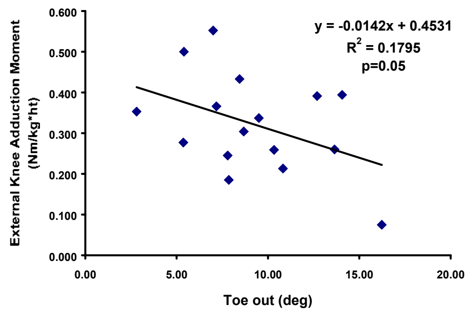

Figure 1. Correlation between Toe out and Frontal Plane Knee Moment

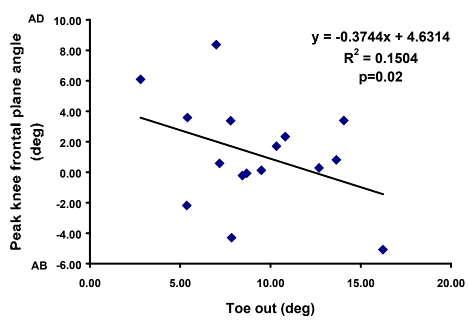

Figure 2. Correlation between Toe out and Peak Knee Adduction Angle

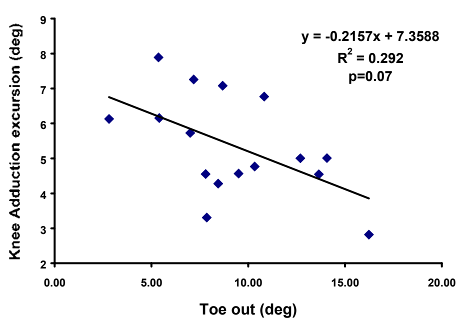

Figure 3. Correlation between Toe out and Knee Adduction Excursion

The results of our study are similar to those of Hurwitz et al. (2002) who observed a trend between the amount of toe out and the first peak adduction moment in a group of patients with knee osteoarthritis. As the patients increase their toe out, they decrease the amount of adduction at the knee and therefore decrease the amount of contact at the medial compartment of the knee joint. Decreased knee adduction likely alters the position of the vertical ground reaction force vector thereby ultimately decreasing the external knee adduction moment.

Therefore it does appear that increasing toe out is related to decreased knee moments and decreased knee adduction motion. However only 15-30% of the variance in the knee variables was explained by toe out, suggesting that other factors influence knee mechanics as well. As additional subjects are added, these correlations may be strengthened.

SUMMARY

The results of this study suggest that increasing toe out decreases the amount of peak adduction and adduction excursion that occurs at the knee joint this likely reduces the loading on the medial compartment of the knee joint. This may be a compensatory strategy in response to pain. Future studies might focus on training patients with knee osteoarthritis to walk with increased toe out to decrease peak knee adduction and external knee adduction moments. This may decrease compressive forces at the knee joint and slow the progression of knee osteoarthritis.

REFERENCES

Hurwitz et al. (2002). *J. Ortho Res.,* **20**, 101-107.

Kaufman et al. (2001). *J. Biomech.,* **34**, 907-915.

ACKNOWLEDGEMENTS

This study has been supported by NIH grant# P20 RR16458.

THE INFLUENCE OF THE SEVERITY OF PARKINSON'S DISEASE ON THE COP-COM MOMENT ARM DURING GAIT INITIATION

Chris J. Hass[1,2], Dwight E. Waddell[1], Richard P. Fleming[1], Jorge L. Juncos[2], Robert J.Gregor[1]

[1] Center for Human Movement Studies, Georgia Institute of Technology, Atlanta, GA, USA
[2] Department of Neurology, School of Medicine, Emory University, Atlanta, GA, USA
E-mail: chass@emory.edu Web: http://www.emory.edu/WHSC/MED/NEUROLOGY/CAM

INTRODUCTION

Transitions between states of static and dynamic equilibrium, such as during gait initiation, termination, or turning are phases of movements when patients with Parkinson's disease (PD) are particularly susceptible to perturbations and falls (Polcyn et al., 1998). Gait initiation (GI) is challenging because it is a volitional transition from a condition of static stable support to a continuously unstable posture during locomotion. Martin and colleagues suggest that an important approach to understand GI in the early stages of PD is to characterize the relationship between the whole body center of mass (COM) and the center of pressure (COP)(Martin et al., 2002).

The peak COP-COM moment arm measures how far the subject will tolerate the whole body COM to deviate from the ground reaction forces COP and is an index of dynamic balance control. Previously, the magnitude of the COP-COM moment arm during GI has been used to discriminate between healthy adults and those with disability. The purpose of this investigation was to examine whether patients with varying severity of PD disability possessed differences in dynamic balance control during GI.

METHODS

Twenty-eight patients with idiopathic Parkinson's disease volunteered to undergo motion analysis during GI tasks. Patients were stratified based on Hoehn and Yahr disability into two groups: **a)** H&Y $\leq$ 2.0 (n=13; age: 61$\pm$11 yrs; mass: 81.9$\pm$15.1 kg; height:178.0$\pm$ 9.2 cm) or **b)** H&Y $\geq$2.5 (n=15; age: 68$\pm$9 yrs; mass: 84.7$\pm$13.9 kg; height:172.0$\pm$ 5.3 cm).

GI trials began with the participant standing quietly on the force platform in a relaxed position. Initial positioning of the feet was self selected. In response to a verbal cue, the participants initiated walking with the instructed limb and continued walking for several steps. For each participant, three data collection trials were collected for each leg performed at a self selected pace.

Kinematic data were collected using a six camera 3D Optical Capture system (Peak Performance Technologies, Englewood, CO). The Helen Hayes marker system was utilized with the addition of 6 passive, retroreflective markers attached bilaterally to the subject's styloid process of the ulna, lateral epicondyle of the humerus, and the acromium process.

Ground reaction forces were sampled at 300Hz using a Kistler force platform mounted level to the walkway surface. The cameras and force plate were time synchronized using a Peak Motus video analysis system.

Force platform data were subsequently used to calculate the instantaneous COP. The 21 markers were used to construct a simple nine segment model. Estimates of segment mass centers were based on Dempster's anthropometric data and the calculation of the location of the whole body COM was calculated using the Peak Performance Software. The distance between the vertical projections of the COM and the COP in the transverse plane was calculated using software developed in the Center for Human Movement Studies and is referred to as the "moment arm" in this investigation.

The COP during GI was divided into three periods (S1, S2, S3) by identifying two landmark events (Figure 1).The first section (S1) began with the initiation command and ended with the COP located in its most posterior and lateral position toward the initial swing limb (Landmark 1). The second section (S2) was characterized by a translation of the COP towards the stance limb ending at Landmark 2. The third section (S3) extended from Landmark 2 until toe off of the initial stance limb.

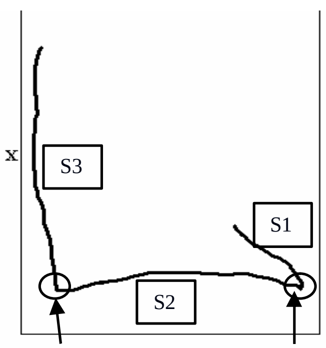

Figure 1: Landmark identification and the subsequent defined periods S1, S2, and S3 of the COP trace during GI.

The max moment arm distance during the S1, S2, and S3 were compared between the two H&Y groups using independent T-tests.

RESULTS AND DISCUSSION

The analysis revealed a significant difference in moment arm between the H&Y groups during the S3 section of the COP trace (Figure 2).

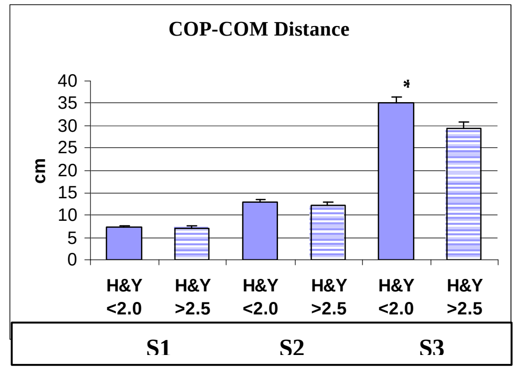

Figure 2: COP-COM distance during S1, S2, and S3 for the two H&Y groups.
* difference between groups $p<0.05$

The most challenging period in GI for stability occurs during S3 and is the instant prior to contact of the initial swing limb (Martin et al., 2002). The data suggest that the more disabled PD patients appear to limit the moment arm distance during this time to compensate for deficiencies in movement control. Martin et al. (2002) suggested this strategy may reflect a need for greater stability, impairments in momentum generation, or a combination of the two factors.

SUMMARY

These observed findings suggest that the relationship between the COP-COM during GI may provide a useful tool for identifying PD patients with gait and balance problems.

ACKNOWLEDGEMENTS
This project was supported by NIH grant # RO-1AT00612-01

REFERENCES

Polcyn et al. (1998). *Arch Phys Med Rehabil* **79**,1582-9.
Martin et al. (2002). *Phys Ther.* **82**(6):566-77.

THE EFFECT OF ALTERING WEIGHT DISTRIBUTION AND THIGH GIRTH ON LIMB LOADING FORCES

Scott White, Laura Malczewski and Chiung-Yu Cho

Biomechanics Laboratory, Exercise & Nutrition Sciences
State University of New York at Buffalo, Buffalo, NY, USA
E-mail: swhite@acsu.buffalo.edu

INTRODUCTION

Excessive body weight has been linked to a higher incidence of osteoarthritis (OA) (Felston et al., 2000), which is assumed to be due to overload. Epidemiological data suggests that overload by itself may be too simplistic an explanation (Lane et al., 1993). Abnormally directed forces may be a factor in cartilage degeneration. For example, differences in gait measures have been reported for obese adults, particularly with excessive thigh girth (Spyropoulos et al., 1991). A measure of fatness, the body mass index (BMI) has been correlated to varus alignment at the knee and OA severity (Sharma et al., 2000). The effect of extra weight, weight distribution and thigh girth on limb-loading patterns has received little attention. We hypothesize that weight distribution and thigh girth will significantly affect ground reaction forces during gait.

METHODS

Five subjects (2 males, 3 females, mean age = 30 years) with a body mass index (BMI) between 20 and 25 (normal weight) walked over force plates with and without additional weight. The extra weight conditions were equal and set to bring the subject's BMI to an obese 1 level (between 30 and 35). For weighted condition "A", subjects walked wearing a 10.9 kg waist belt and a weight vest (All Pro®). For condition "B", the waist belt was removed and subjects walked with thigh weight belts (All Pro®) of equivalent mass (10.9 kg) fixed to the upper thighs. The thigh weight belts added 13 cm of circumference to each thigh. For condition "C", subjects walked with the weight vest, waist belt (10.9 kg) and the thigh weight belts but with hollow wood dowelling in place of the thigh weights (< 0.5 kg total) to achieve an equal thigh circumference.

Subjects first walked on a treadmill for 3 minutes to determine a normal cadence for their self-selected speed within the range of 1.34 ms^{-1} and 1.51 ms^{-1}. Subjects were then asked to walk overground at the same cadence controlled by metronome. Ground reaction forces were measured for 6 right and 6 left foot contacts on force plates for the normal and the 3 weighted conditions. Four measures were calculated from the forces: peak medial (Fz) and peak posterior (Fx) force (relative to subject's foot), peak vertical force (Fy), during the first half of stance, and the rate of change of vertical force (Fy_R) from initial foot contact to the peak Fy. Dependent measures were averaged across trials for each subject with right and left limbs treated separately. Paired t-Tests were used to test for significant effects ($p < .01$).

RESULTS

Force patterns were altered and there were significant differences in the magnitude of dependent measures for the three conditions (Fig. 1; Table 1). Moving the 10.9 kg mass from the waist to the thighs (B) resulted in a significant decrease in vertical force (Fy) but a significant increase in medial force (Fz). Increasing the thigh circumference while maintaining all weight at the trunk (C) resulted in significantly greater values of peak vertical (Fy), posterior (Fx), and medial force (Fz), and loading rate (Fy_R).

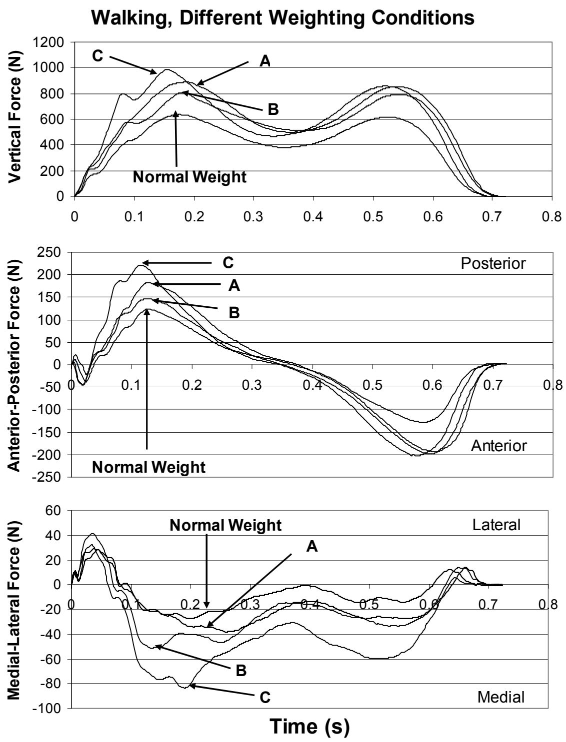

Figure 1: Force patterns for subject walking at normal weight and three equal weight conditions but different weight distributions.

DISCUSSION

Manipulating the distribution of weight affected ground reaction force patterns and the magnitude of selected force measures. Peak forces were greatest when the extra weight was carried in the trunk region and the thigh girth was increased (condition C). The greatest change in vertical oscillation occurs at the trunk during weight support; therefore, higher vertical forces and rates of vertical force loading were expected. Changing thigh girth affects vertical, posterior and medial forces. An increased thigh girth may change normal joint motion interfering with the ability to attenuate forces during limb loading. Peak medial forces were greatest when thigh girth was increased (conditions B & C). Greater medial forces and a varus knee alignment due to a wider gait, will likely result in higher adductor joint moments of force, which has been associated with OA of the knee (Hurwitz et al., 2000). The higher incidence of OA for the obese might not be a function of extra body weight alone; altered movement pattern due to weight distribution or a greater thigh girth may also contribute to greater joint loads.

REFERENCES

Felston, DT et al. (2000). *Ann. Int. Med.* **133**, 635-646.

Hurwitz, DE et al. (2000). *J. Orthop. Res.* **18**, 572-579.

Lane NE et al. (1993). *J. Rheumatol.* **20**, 461-468.

Sharma, L et al. (2000). *Arthritis Rheum.* **43**, 568-575.

Spyropoulos, P et al. (1991). *Arch. Physical Med. Rehab.* **73**, 1065-1070.

Table 1: Force magnitudes for different weighting conditions.

Extra Weight Conditions	FY (N)	FY_R (Ns^{-1})	FX (N)	FZ (N)
Vest & Weight Belt (A)	1167 (151)	8776 (2360)	176 (97)	75 (21)
Vest, & Thigh Weights^T(B)	1095 (165)*	8919 (2499)	241 (60)	94 (19)$^\#$
Vest, Waist Belt & Thigh Girth^T(C)	1223 (169)$^\#$	9931 (2331)$^\#$	275 (59)$^\#$	104 (17)$^\#$

Notes: Mean (N=10; 5 subjects, 2 limbs) presented with standard deviation in "( )"
^{T}thigh girth increase = 13 cm.*Significantly less than "A". $^\#$Significantly greater than "A"

A LEAST SQUARES INVERSE DYNAMICS APPROACH TO ESTIMATING MUSCLE ACTIVATIONS DURING GAIT

Darryl G. Thelen

Dept. of Mechanical Engineering, University of Wisconsin-Madison, Madison, WI, USA
E-mail: thelen@engr.wisc.edu

INTRODUCTION

Modeling can be used to quantitatively assess the function of muscles during movement. For example, forward dynamic simulation has been used to estimate muscle contributions to forward progression and vertical support during gait (Neptune et al. 2001, Anderson and Pandy 2003). While forward dynamic simulation represents an ideal consistent approach, it can be difficult to implement as a method to interpret experimental data. In particular, generating a simulation that replicates an inherently unstable movement, such as walking, is computationally challenging. An alternative involves using inverse dynamics to compute joint moments followed by static optimization to estimate muscle forces (Crowninshield and Brand 1981). Muscle forces can then be used to interpret function. A drawback of this approach is that some of the movement will be attributed to residual forces, which arise when using conventional methods for inverse dynamics computations.

The objective of this study was to develop a method for estimating muscle activities that reduces residual forces but retains the computational feasibility of inverse dynamics. The proposed method is an adaptation of a least squares estimation approach for inverse dynamics computations (Kuo 1998). Specifically, we incorporated muscles and a moving base of support. The methodology was used to estimate muscle activations that most closely replicate, in a least squares sense, measured accelerations and ground reactions during gait.

METHODS

A three-dimensional linked segment model of the human body with 23 degrees of freedom and 58 Hill-type muscle-tendon actuators was used (Anderson and Pandy 2003). Equations of motion were derived with SD/FAST (Parametric Technology Corp., Waltham, MA) and are given by:

$$\vec{\vec{M}} \cdot \ddot{\vec{q}} = \cdot \vec{\vec{R}} \cdot \vec{F}_m(\vec{a}) + \vec{G} + \vec{C} + \vec{E} \qquad (1)$$

where $\vec{q}$, $\dot{\vec{q}}$, and $\ddot{\vec{q}}$ are generalized coordinates, speeds, and accelerations; $\vec{\vec{M}}$ is a mass matrix; $\vec{\vec{R}}$ is a matrix of muscle moment arms, $\vec{F}_m$ is a vector of muscle forces, $\vec{a}$ is a vector of muscle activations, and $\vec{G}$, $\vec{C}$ and $\vec{E}$ are forces due to gravity, Coriolis and ground reactions, respectively.

Experimental gait data for three young adults walking at a comfortable speed was analyzed. At each time frame, generalized coordinates and speeds were set to experimental values. The stance foot (or stance feet during double support) accelerations were prescribed to measured values. Coupling these motion constraint(s) with (1) makes the estimated ground reactions and joint accelerations linear functions of muscle forces:

$$\vec{\vec{A}} \cdot \vec{F}_m(\vec{a}) = \vec{b} \qquad (2)$$

where $\vec{\vec{A}}$ depends on the generalized coordinates and $\vec{b}$ is a function of the states, accelerations and ground reactions (Kuo 1998). Equation (2) cannot usually be solved for activations that would simultaneously produce both the measured accelerations and ground reactions. As an alternative, nonlinear optimization was used to solve for activations that minimize a weighted sum of squared errors and squared activations:

$$J = \left|\vec{A}\cdot\vec{F}_m(\vec{a}) - \vec{b}\right|^2 + w\left|\vec{a}\right|^2 \qquad (3)$$

with the latter term included to resolve muscle redundancy (Crowninshield and Brand 1981).

RESULTS

The accelerations of the center-of-mass generated by estimated muscle activations were similar to that computed from ground reactions (Figure 1a). RMS errors in the COM accelerations over a gait cycle averaged 0.23, 0.45 and 0.20 m/s^2 in the forward, vertical and lateral directions, respectively. The muscle activations qualitatively agreed with the timing of EMG bursts for many of the lower extremity muscles (Figure 1b).

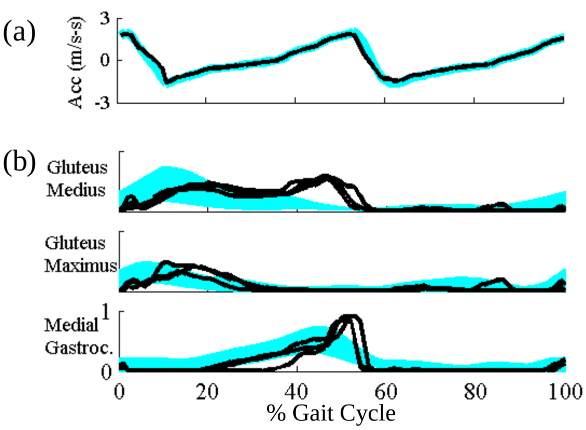

Figure 1: (a) Estimated (solid) and experimental (shaded) forward acceleration of the center-of-mass (b) Estimated activations (solid) and normalized EMG signals (shaded, Winter 1991).

DISCUSSION

The proposed least-squares methodology to estimating muscle activations has two notable advantages over conventional methods. First, a single consistent model can be used to directly estimate activations from measured kinematics and ground reactions. Conventional techniques often use an inverse dynamics model to compute joint moments and then a different musculoskeletal model to estimate muscle activities. The second benefit is the elimination of residual forces. Residuals can, in part, result from unmodeled dynamics. However, residuals can also result directly from differentiating noisy kinematic data. A least-squares approach to inverse dynamics was previously shown to make better use of all measurements so as to reject measurement noise and improve joint moment estimates (Kuo 1998).

A drawback of the proposed approach, compared to forward dynamics, is a lack of dynamic consistency between the estimated accelerations and states of the system. As a result, the muscle activations cannot be used to drive a forward dynamic simulation of a movement. However given the difficulty in generating stable forward simulations, the least squares approach may provide a feasible alternative for assessing muscle actions from experimental data.

REFERENCES

Anderson, F.C., Pandy, M.G. (2003). *Gait Posture*, **17**, 159-169.

Crowninshield, R.D., Brand, R.A. (1981). *J. Biomech.*, **14**, 793-801.

Kuo, A.D. (1998). *J. Biomech. Eng.*, **120**, 148-159.

Neptune, R.R. et al. (2001). *J. Biomech.*, **34**, 1387-1398.

Winter, D.A. (1991). The *Biomechanics and Motor Control of Human Gait*, Waterloo Biomechanics.

ACKNOWLEDGEMENTS

NSF BES-9702275; Center for Motion Analysis, Connecticut Children's Medical Center.

MECHANICAL IMPEDANCE IDENTIFICATION OF THE HUMAN LOCOMOTOR SYSTEM DURING ABLE-BODIED WALKING

Georgios A. Bertos[1], Dudley S. Childress[1,2] and Steven A. Gard[1,2]

[1] Rehabilitation Engineering Research Center, Northwestern University, Chicago, IL, USA
[2]VA Chicago Health Care System, Lakeside Division, Chicago, IL, USA
E-mail: gbertos@northwestern.edu Web: www.repoc.northwestern.edu

INTRODUCTION

A simple mass-spring-viscous damping model has been used by investigators mainly to model human bouncing (Zhang et al., 2000) and running (McMahon and Greene, 1979). Our laboratory has investigated a rocker-based inverted pendulum of walking without shock absorption on even terrain (Gard and Childress, 2001). The purpose of this investigation is to determine the impedance characteristics of the human locomotor system, based on a spring and viscous damper element added to the previous model of walking, as shown in Figure 1.

METHODS

Three able-bodied persons walked at different walking speeds ranging from 0.8-2.2 m/s. Kinematic and kinetic gait analysis data were collected. Since the vertical displacement of the Body Center of Mass (BCOM) during steady-state walking is approximately a sinusoid we decided to use steady-state sinusoidal analysis. Furthermore, because of the small vertical excursion of the BCOM we decided to assume a linear model. Thus, walking in the context of vertical shock absorption was modeled as a modified 2nd order linear vibration system (Figure 1). The terrain in Figure 1 is the approximate trajectory of the rocker-based inverted pendulum which we model by the trajectory's first harmonic.

For the proposed model we write the equations of a sinusoidal system (equations 1-4):

$$w_d = \sqrt{1-z^2} \cdot w_n \qquad (1)$$

where ω_d is the damped frequency of oscillation and can be derived from the walking cadence. ω_n is the natural frequency of oscillation and ζ is the damping ratio. We assume that the human is able to make neuromuscular adaptations of damping and stiffness parameters so that the frequency of stepping (cadence) is close to the damped frequency of oscillation ω_d. ($w = 2 \cdot p \cdot f_{cadence} \cong w_d$). If k is the stiffness and B is the viscous damping, then:

$$k = w_n^2 \cdot M_e \quad (2)$$

$$B = 2 \cdot M_e \cdot w_n \cdot z \quad (3)$$

where M_e is the effective mass during the stance phase of walking and is equal to 0.88M since the standing leg acts like a spring having a distributed mass (Stokey, 2002).

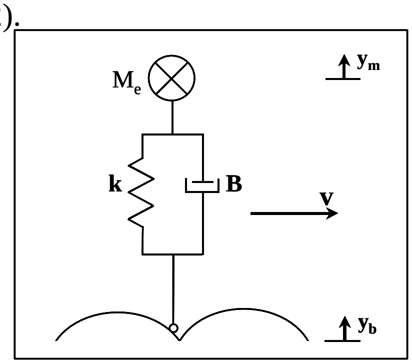

Figure 1: Able-bodied human walking was modeled with a 2nd order mechanical vibration system.

The equation of motion in the Laplace domain for the proposed mechanical model of walking (Figure 1) is:

$$\frac{y_m(s)}{y_b(s)} = \frac{\frac{B}{M_e}\left(s + \frac{k}{B}\right)}{s^2 + \frac{B}{M_e}s + \frac{k}{M_e}} \qquad (4a)$$

Since $y_m(s)$ is measured and $y_b(s)$ is approximated to a sinusoid with known minimums (heel-strike events) we can derive:

$$\text{Phase of}\left(\frac{y_m(jw_d)}{y_b(jw_d)}\right)$$

$$= \text{phase of}\left(\frac{\frac{k}{M_e}+\frac{B}{M_e}jw_d}{-w_d^2+\frac{k}{M_e}+\frac{B}{M_e}jw_d}\right) \quad (4b)$$

We then have a system of 4 equations (1-4) with 4 unknowns: ζ, k , B, ω_n. By solving this system of equations we can estimate the damping ratio ζ, stiffness k and damping B.

RESULTS AND DISCUSSION

Our results support the theory that the damping ratio $\zeta = [B/2(M_e k)^{1/2}]$ is fairly constant (ζ = 0.5-0.8) across different walking speeds of walking (Figure 2). Stiffness k appears to increase linearly with walking speed *V*, being around 15 kN/m at 1.2 m/s (Figure 3).

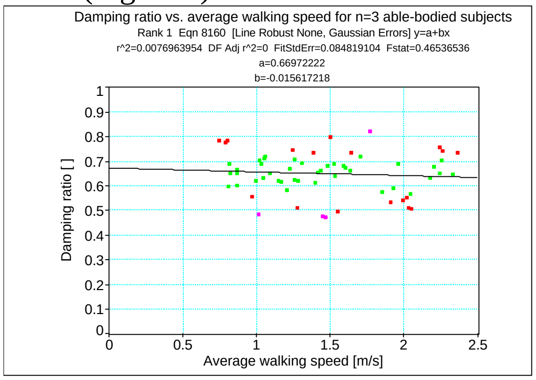

Figure 2: Estimated damping ratio ζ vs. *V*.

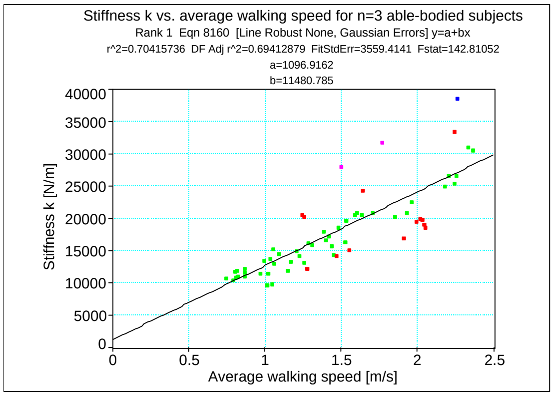

Figure 3: Estimated stiffness k vs. *V*.

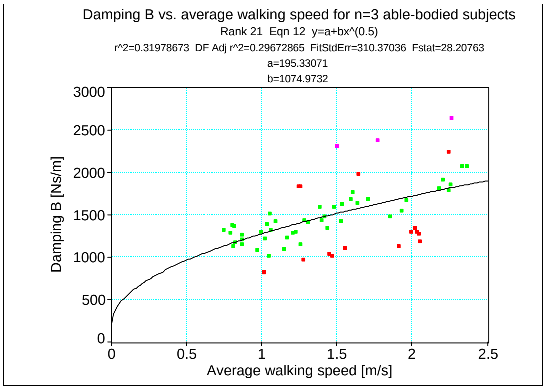

Figure 4: Estimated damping B vs. *V*.

Damping B appears to increase with the square root of walking speed, $\sqrt{V}$ (Figure 4). During able-bodied walking the system appears to be underdamped (0<ζ<1) having a high performance from a control theory standpoint with ζ between 0.5 and 0.8.

SUMMARY

Based on the proposed model the damping ratio of the locomotor system is maintained relatively constant, near high performance values (ζ = 0.5-0.8), with increasing walking speed *V*. The stiffness k and damping B vary with walking speed *V* in such a way that the damping ratio ζ remains in the ζ = 0.5-0.8 optimal value range.

REFERENCES

McMahon, T.A. and Greene P.R. (1979), *J. Biomechanics* **12**, 893-904.

Gard, S.A. and Childress, D.S. (2001), *J. Prosthetics and Orthotics*, **13(3)**, 64-65.

Stokey W.F. (2002) in *Harris' Shock and Vibration Handbook*, 5th ed., 7-5.

Zhang L.-Q. et al. (2000), *Proceedings of the 24th ASB*, 65-66.

ACKNOWLEDGEMENTS

The authors would like to acknowledge National Institute on Disability Rehabilitation Research (NIDRR), the Veterans Affairs Chicago Motion Analysis Laboratory (VACAMRL) and Steve C. Miff.

HUMANS ANTICIPATE SURFACE CHANGES DURING BOUNCING GAITS

Chet T. Moritz [1,2] and Claire T. Farley [1]

[1] Locomotion Laboratory, University of Colorado, Boulder, CO, USA
[2] Dept. of Integrative Biology, University of California, Berkeley, CA, USA
E-mail: ctmoritz@socrates.berkeley.edu

INTRODUCTION

Human hoppers and runners maintain center of mass dynamics by adjusting leg mechanics for changes in surface properties (Ferris et al, 1999). Surprisingly, runners perfectly adjust leg mechanics for abrupt but *expected* changes in surface stiffness (Ferris et al, 1999). Related work suggests that a combination of anticipation and reaction may contribute to stable locomotion. Anticipation of landing is seen when jumping down onto false floors (Duncan & McDonagh, 2000). In addition, mechanical reactions of active muscles and jointed limbs may act to stabilize the legs, as demonstrated by models of knee bends (Wagner & Blickhan, 1999). Finally, reflexive feedback may adjust muscle activation during stance. Cutaneous and stretch reflex gains are high during hopping and running (Duysens et al., 1993).

Based on the observation that runners perfectly adjust leg stiffness for expected surface changes, we hypothesize that humans anticipate changes in surface properties during bouncing gaits. This hypothesis predicts that humans will alter leg mechanics or muscle activation prior to contact when expecting a change in surface stiffness.

METHODS

Ten female subjects hopped in place on a sprung surface while we introduced surprise, expected and random changes in surface stiffness from soft (27 kN/m, 6 cm compression) to hard (411 kN/m, 0.5 cm compression). We designed a control system that changed the surface stiffness by locking the surface in place and preventing it from compressing. Subjects were completely surprised the first time the surface became hard. We collected ground reaction force, video kinematics, and surface EMG. From these data, we calculated center of mass and leg dynamics, joint angles, and mean EMG. We also determined the time within a hop when these parameters first deviated from the average curves on the continuous soft surface by more than 2 SD. All values are mean ± SEM.

RESULTS AND DISCUSSION

As predicted by our hypothesis, subjects began to change kinematics and muscle activation in the aerial phase before an expected surface change. Compared to the continuous soft surface, subjects hopped 50% higher and increased muscle activation in the aerial phase 31-55% before an expected hard surface. The knees were also $4 \pm 1^{\circ}$ more flexed at touchdown compared to the continuous soft surface. Subjects began to change kinematics and muscle activation 3-76 ms before landing when expecting a hard surface (Figure 1). Similarly, when the surface changed randomly, subjects landed with $3 \pm 1^{\circ}$ more flexed knees.

Hoppers adjusted leg stiffness similarly for expected and random hard surfaces, but did not fully decrease leg stiffness to the value used on a continuously hard surface in either case. As a result, center of mass vertical movement during stance decreased by 22%.

Subjects also did not fully decrease leg stiffness on the surprise hard surface. Although recent work showed that runners perfectly adjusted for surprise changes from hard to soft surfaces (Farley, 2002), Ferris et al (1999) found runners had more difficulty adjusting to expected soft to hard surface transitions (as used in this study). Transitioning to a hard surface may be more difficult because the legs completely dictate the center of mass movements on a hard surface. In contrast, on a soft surface the legs and surface each dictate ~50% of vertical center of mass movements.

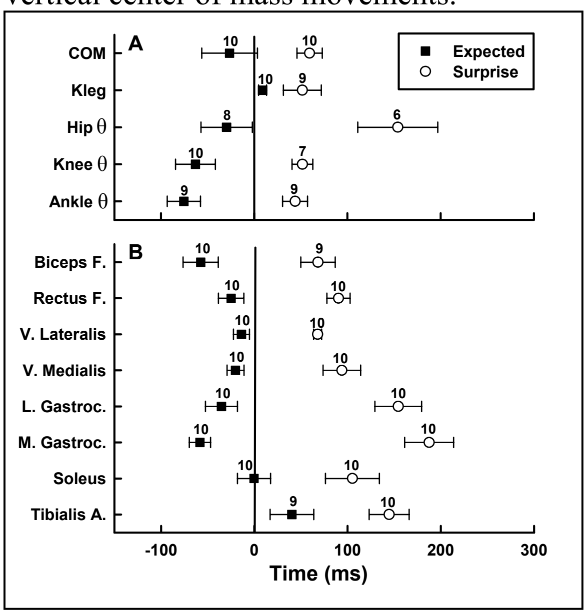

Figure 1: Time of first difference from the continuous soft surface for **(A)** kinematics and **(B)** muscle activation. Landing occurred at time zero. Values above each data point are the number of subjects (out of 10) whose data deviated by 2 SD from their continuous soft surface data. Abbreviations are center of mass trajectory ("COM"), the instantaneous slope of leg force vs. displacement ("k_{leg}"), and hip, knee and ankle angles.

Interestingly, when subjects landed on the surprise hard surface, leg stiffness and joint mechanics began to change before any change in muscle activation. The ankle and knee began to flex 47 ± 13 and 52 ± 11 ms after landing, respectively, on the surprise hard surface (Figure 1). In contrast, EMG in muscles crossing the ankle began to increase 108-160 ms after landing and upper leg muscle EMG began to increase 68-188 ms after landing (Figure 1). This early joint flexion was in the correct direction to adjust to the surprise hard surface, and suggests that passive mechanics of the leg may assist in stabilizing locomotion when the surface changes unexpectedly.

SUMMARY

Humans alter hopping mechanics and neural control before landing when expecting a change in surface compression. Similarly, hoppers land with more bent knees when the surface changes randomly. When subjects are surprised by a hard surface, joint flexion begins before any change in muscle activation. These results suggest that a combination of anticipation, passive mechanics, and neural feedback contribute to stable locomotion.

REFERENCES

Duncan, A., McDonagh, M.J.N. (2000). *J. Physiol.* **526**, 457-468.

Duysens, J. et al. (1993). *Brain Res.* **613**, 230-238.

Farley, C.T. (2002). *The Physiologist.* **45(4)**, 292.

Ferris, D.P. et al. (1999). *J. Biomech.* **32**, 787-794.

Wagner, H., Blickhan, R. (1999). *J. theor. Biol.* **199**, 163-179.

ACKNOWLEDGEMENTS

This work was supported by an ASB–GIA to CTM and an NIH R29 AR-44008 to CTF

PARASPINAL MUSCLE REFLEX DYNAMICS

K.P. Granata, Ph.D.   G.P. Slota   B.C. Bennett, Ph.D.

Musculoskeletal Biomechanics Laboratories, Virginia Tech, Blacksburg, VA USA

http://www.esm.vt.edu/~mmadigan/msbiolab/

INTRODUCTION

Reflex dynamics of the paraspinal muscles may influence spinal stability and low-back pain (Luoto, 1998). Although paraspinal reflex has been examined (Gardner-Morse, 2001), there are no studies to quantify response in terms of control dynamics. Reflex can be represented as the ascending vector on the feedback leg of a state-diagram (equation 1). Although inertia, I, is constant for a fixed posture; the stiffness, k, and damping, B, increase with muscle activation state, λ. The reflex loop adds additional dynamics of feedback gain, G, and delay $e^{-s\tau}$.

$$reflex = \left\{ \frac{G\, e^{-s\tau}}{I\, s^2 + B(\lambda)\, s + K(\lambda)} \right\} F \qquad (1)$$

The term in brackets is the system response, G_{IRF}. It can be empirically quantified from impulse response function (IRF) analyses.

Although this is a simple representation of neuromuscular control, we can predict two trends from this model. First, if the neuromuscular state, λ, is constant during the measurement trial, then it can be hypothesized that reflex amplitude must increase with perturbation force, F. Second, since muscle stiffness in the denominator increases with preparatory activation, it is hypothesized that response gain, G_{IRF}, must decrease with external trunk flexion preload. The goal of this study was to compute the influence of perturbation magnitude and preload on paraspinal reflex dynamics.

METHODS

Paraspinal EMG response to trunk flexion force perturbations were recorded from ten healthy males (27.3 ±8.4 years, 78.1 ±12.4 kg weight, 178.0 ±6.6 cm height). Subjects

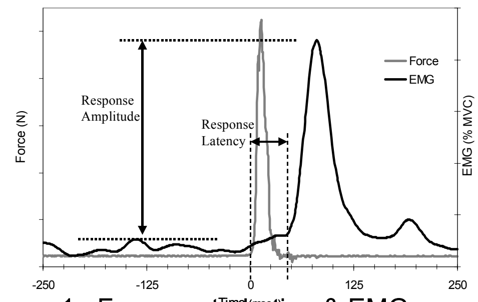

Figure 1. Force perturbation & EMG response

wore a chest harness to which a cable was attached anteriorly. Brief (11.2 ±2.0 msec) perturbation forces to the cable imparted force impulse levels of 6.2 ±1.6, 9.3 ±1.4, and 12.0 ±1.7 N sec (Figure 1). Subjects maintained an upright posture against an anteriorly directed preload of 0 or 110 N requiring paraspinal muscle preactivation.

EMG was recorded from bipolar surface electrodes over the paraspinal muscles as described in Granata et al (2001). EMG signals were band-pass filtered (20-450 Hz), rectified, integrated (6.3 Hz Hanning convolution filter) and normalized to levels recorded during maximum isometric exertions. Preparatory EMG was computed from a 250 msec mean recorded prior to each force impact (Figure 1). Reflex responses were identified by signals that exceeded two standard deviations greater than the preparatory activity.

The IRF, $h(\tau)$, was computed from the discrete convolution integral over lag time τ,

$$EMG\,(t) = \sum_{\tau} h(\tau)\, F(t-\tau) \qquad (2)$$

where F(t) is the input force at time t, and EMG(t) is the output myoelectric response. Response gain G_{IRF} was represented as the peak value of h(t). Statistical repeated measures analyses were performed to evaluate the influence of force impulse and preload on paraspinal reflex dynamics.

RESULTS

Peak perturbation force increased significantly, as much as 40% with impulse level (Table 1). The three levels of force impulse were significantly different from each other. Preload was associated with significantly increased peak force and impulse presumably because of increased trunk muscle activation and stiffness. Preactivation in the paraspinal muscles increased significantly with preload but was not influenced by force impulse.

Response latency was consistently observed at 30.7 ±21.3 msec following the force impact (Figure 1). EMG reflex amplitude increased with force impulse (Table 1). IRF gain, G_{IRF}, averaged 2.27 ±1.31 % / N sec and showed a trend wherein gain was reduced with preload. However, this trend failed to reach statistical significance ($p=0.096$). One subject demonstrated abnormally high G_{IRF}, 2 standard deviations more than others. If this subject were removed from analyses, a significant preload effect is observed ($p<0.037$). However, we chose to retain the full data set to assure conservative interpretation of results. Analyses demonstrated that G_{IRF}, declined 35% with force impulse ($p<.001$).

DISCUSSION

The model of reflex dynamics correctly predicted measured neuromechanical trends. EMG response increased with perturbation magnitude similar to a classical feedback system. This agrees with published paraspinal reflex data (Krajcarski, 1999). Open-loop mechanics dictate that increased force perturbation must cause greater kinematic disturbance. Thus, during high impulse trials, one expects greater stretch in the muscle spindle organs and spinal ligaments causing greater reflex response.

The model correctly predicted that trunk flexion preload reduces response gain. Increased paraspinal preactivation was necessary to maintain upright trunk posture against the external flexion preload. This recruitment causes greater trunk stiffness and reduced kinematic deflection (Gardner-Morse, 2001). Reduced trunk deflection will result in smaller neurosensor strain and reflex. Thus, for the same level of force perturbation, a trend toward reduced reflex response gain was observed when the trunk was preloaded.

In a linear system one would expect the response gain must be constant independent of the perturbation magnitude. Results indicate the reflex response of the trunk extensor muscles are highly sensitive to small movement disturbances whereas larger disturbances produce a less than linear increase in response.

ACKNOWLEDGEMENT

This research was supported by a grant R01 AR46111 from NIAMS of the NIH.

REFERENCES

Gardner-Morse M. and Stokes I.A. (2001) *J.Biomechanics* 34, 457-463.
Granata K.P.et al (2001) *J.Electromyo.Kinesiol.* 11, 247-254.
Krajcarski S.R. et al (1999) *Clin.Biomech.* 14, 54-62.
Luoto S.et al (1998) *Perceptual & Motor Skills* 87, 1283-1296.

Table 1. Statistical results of paraspinal reflex dynamics

	Peak Force *(N)*	Force Impulse *(N sec)*	Preactiv. *(% MVC)*	Reflex Ampl *(%MVC)*	Latency *(msec)*	G_{IRF} *(% / N sec)*
Perturbation	**p < .001**	**p < .001**	p = .537	**p < .001**	p = .186	**p < .001**
Preload	**p < .013**	**p < .043**	**p < .001**	**p < .005**	**p < .001**	p = .096
Pert x Preload	p < .249	p < .353	p < .686		p < .522	p < .811

Mechanical Properties Of The Support Tripod In Running Insects: The Role Of Preflexes In Dynamic Stabilization

Daniel M. Dudek, Dave Gilboa, Michael MacLafferty, and Robert J. Full

Poly-PEDAL Laboratory, University of California, Berkeley, CA, USA
E-mail: dmdudek@socrates.berkeley.edu Web: polypedal.berkeley.edu

INTRODUCTION

Despite variations ranging from leg number and shape to type of skeleton employed, terrestrial runners from mammals to arthropods produce ground reaction forces that can be modeled as a spring-mass system with the same dimensionless stiffness (Blickhan and Full, 1993). There are two major beneficial consequences of bouncing while running: 1) the ability to use springs to store and return elastic strain energy (Alexander, 1988) and 2) passive self-stabilization resulting from a well tuned mechanical (musculo-skeletal) system (Seyfarth *et al*, 2002; Schmitt *et al*, 2002).

The mechanisms which produce and control this amazingly stable bouncing behavior remain a mystery. Neural control relying on negative feedback is one obvious and important means of maintaining stability (Cruse, 1990), but without knowledge of the animal's musculo-skeletal system, such control can be counterproductive and even destabilizing (Full *et al*, 2002). This is due to preflexes, or the "zero delay, intrinsic response of a neuromuscular-skeletal system to a perturbation" (Brown and Loeb, 2000), which produces forces that could counteract the neural response.

The running deathhead cockroach, *Blaberus discoidalis*, can be modeled as a spring-mass system in both the horizontal and sagittal planes. It has been shown to be dynamically self-stabilizing in the horizontal plane (Kubow and Full, 1999) and capable of recovering from large lateral perturbations without a step transition (Jindrich and Full, 2002). Results from dynamic oscillations of the hind limb in the sagittal plane predict that the cockroach is under-damped during the stance phase of locomotion and over-damped during the swing phase (Dudek and Full, 2001). This leaves open the possibility that cockroaches possess a damped spring capable both of elastic energy storage during stance and perturbation rejection during swing. It remains to be seen whether the preflexes of live, actively running cockroaches are properly tuned in the sagittal plane to simplify control of locomotion via dynamic self-stabilization. The goal of this study was to determine the preflexive properties of the tripod of support of a running insect.

METHODS

Deathhead cockroaches, *Blaberus discoidalis* (2.56±0.32 g, N=4), were tethered to the arm of a servomotor by epoxying a candle (0.63±0.11 g) to the third thoracic tergum. The candle tether was shaved down to the wick at its center and therefore acted as a universal joint, providing the roach with a complete range of motion. They were then positioned above a Styrofoam ball (20 cm diameter, 6.61 g) that was floating on an air bearing and allowed to run freely. The rotational inertia of the ball is designed to match the translational inertia of the cockroach and therefore serves as an inertial treadmill.

Leg joint angles and body kinematics (yaw, pitch, and roll) were recording using 3 digital cameras at a frame rate of 500 Hz. Running speed was measured by two optical encoders aimed at the ball's surface, directed 90° apart. Roaches ran at their preferred speed (17.78±4.16 cm/s) and stride frequency (8.89±1.56 Hz) with the servomotor arm deflecting passively. The servomotor, acting in the sagittal plane, then imposed sinusoidal force oscillations ranging from 10-50 mN in amplitude (25 or 40 Hz) and the induced displacements were recorded. The resulting hysteresis loops were modeled as a spring and damper in parallel.

RESULTS AND DISCUSSION

Mechanical impedance (the time-dependent resistance of a material to deformation) of the support tripod varies with the magnitude of the imposed force and ranges from 25-100 N m^{-1}. This is 2-4 times the impedance of a single, ablated limb (Dudek and Full, 2001). The stiffness component of the impedance ranges from 20-60 N m^{-1}. This gives a dimensionless stiffness of 14.03±1.56, close to the 16.7 estimated from force plate data (Blickhan and Full,1993). The damping component of impedance ranges from 0.05-0.55 N s m^{-1} and is larger at a perturbation frequency of 40 Hz compared with 25 Hz.

Previous data from forced oscillations of individual limbs predicts that cockroaches should be underdamped during running, with a damping ratio (ζ) between 0.1 and 0.2. These data show that during low frequency perturbations the roach is underdamped (ζ = 0.63±0.15), but at high frequency perturbations the roach is actually overdamped (ζ = 1.59±0.57). This supports the hypothesis that for slow, small-scale perturbations, the cockroach relies on neural reflexes for control but for fast, large-scale perturbations the passive dynamics of the mechanical system play a larger role in controlling energy.

SUMMARY

Animals from humans to cockroaches bounce like a pogo-stick during running. These dynamics have the benefits of increasing mechanical efficiency by storing and returning elastic strain energy and also simplifying control using a well-tuned, springy musculo-skeletal system. The mechanical properties of the support tripod of running cockroaches appear to be well suited for both of these functions.

REFERENCES

Alexander, R. (1988). *Elastic Mechanisms in Animal Movement*. 141 pgs.

Blickhan, R., Full, R. (1993). *J Comp Phys A*, **173**, 509-517.

Brown, I., Loeb, G. (2000). *Biomechanics and Neural Control of Posture and Movement*, 148-163.

Cruse, H. (1990). *Trends in Neuroscience,* **13**, 15-21.

Dudek, D., Full, R. (2001). *Am Zool*, **41**, 1432-1433.

Full, R. *et al*. (2002). *Int & Comp Biol*, **42**, 149-157.

Jindrich, D., Full, R. (2002). *J Exp Biol*, **205**, 2803-2823.

Kubow, T., Full, R. (1999). *Philo. Trans R Soc London, Ser B*, **354**, 849-861.

Schmitt, J. *et al*. (2002). *Biol Cybernetics*, **86**, 343-353.

Seyfarth, A. *et al*. (2002). *J Biomech*, **35**, 649-655.

ACKNOWLEDGEMENTS

We would like to thank Sean Bailey, Mark Cutkosky, and members of the Poly-PEDAL lab. This research was supported by a grant from the Office of Naval Research.

PERFORMANCE OF ATTENTION-SPLITTING TASKS HAS DIFFERENT EFFECTS ON STATIC AND DYNAMIC STABILITY

Abby Walters[1], Tammy M. Owings[1] and Mark D. Grabiner[1,2]

[1]Department of Biomedical Engineering, The Cleveland Clinic Foundation
[2]School of Kinesiology, University of Illinois at Chicago
Email: grabiner@uic.edu

INTRODUCTION

Static and dynamic postural control requires allocation of attentional resources. Dual task, or attention splitting paradigms have been used to measure the influence of imposing secondary information processing tasks on postural control. Compared to the body of literature related to the influence of attention-splitting tasks on static postural control, there are substantially fewer studies related to performance of dynamic stability.

The purposes of this project were to determine if measures of static and dynamic stability are statistically correlated to one another and to determine if the performance of an attention-splitting task similarly influences measures of medial-lateral static and dynamic stability.

METHODS

Twenty healthy young adults participated in two separate protocols. One protocol assessed static postural stability with and without the addition of an attention splitting task. The second protocol assessed dynamic stability during locomotion on a motorized treadmill; also with and without the addition of an attention splitting task.

The attention-splitting task consisted of maintaining a light beam from a handheld laser pointer within a10 cm circular target placed approximately six feet in front of the subjects and approximately three feet off the floor.

During the trials that assessed static postural stability, subjects stood quietly on a force plate for three randomly ordered conditions. During condition 1 the subjects stood comfortably with their arms at their side while gazing at the 10 cm circular target. During condition 2 the subjects were instructed to aim a hand-held laser pointer at the target but without activating the laser pointer. During condition 3 the subject activated the laser pointer and attempted to maintain the laser beam within the 10 cm circle. The dependent variable of interest was postural sway amplitude in the medial-lateral direction.

During the trials that assessed dynamic stability, subjects walked on an instrumented treadmill at a self-selected velocity. Similar to the static postural stability trials there were three, randomly ordered, experimental conditions. Each condition lasted approximately 10-minutes during which at least 200 consecutive steps were collected. During condition 1 the subject walked with no restrictions at their self-selected velocity. During condition 2 the subjects were instructed to aim the inactive hand-held laser pointer at the target. During condition 3 the subject activated the laser and attempted to maintain the beam within the 10 cm circle. The dependent variable of interest was the variability of step width (Owings and Grabiner, in press).

The effect of the attention-splitting task on static and dynamic data was analyzed separately using 3 way repeated measures multivariate ANOVA. Post hoc multiple comparisons were conducted using Bonferroni-adjusted paired t-tests.

The relationships between measures of static and dynamic postural stability were measured using Pearson correlation coefficients

RESULTS

During conditions in which subjects did not hold the laser pointer, the relationship between static and dynamic stability was moderate ($r=0.53$, $p<0.05$). However, during the conditions in which attentional resources were directed at controlling the activated laser pointer, the correlation value was weak and did not achieve significance ($r=0.43$, $p>0.05$, respectively).

Performance of the attention-splitting task did not significantly influence static postural stability ($p=0.197$, Figure 1). Performance of the attention splitting task significantly influenced dynamic stability ($p<0.001$, Figure 1). Post hoc multiple comparisons revealed that dynamic stability during the condition performed with the activated laser was significantly smaller than the other two conditions. The dynamic stability of the control condition and the condition performed with the inactivated laser pointer were not significantly different from one another ($p=0.961$, Figure 1).

DISCUSSION

The results suggest that in young subjects, the relationship between measures of static and dynamic stability are moderate, at best, during conditions in which attention is not diverted and that performance of an attention splitting task dissimilarly influences measures of static and dynamic stability.

The finding that an attention-splitting task was associated with a decrease in the measure of dynamic stability may be consistent with an increased level of control.

Aging has generally predictable effects on measures of static stability and, to some extent, dynamic stability. Further study of the relationships between static and dynamic stability during conditions in which attention is diverted seems warranted in light of the need for effective and efficient means by which fall risk can be predicted and prevented.

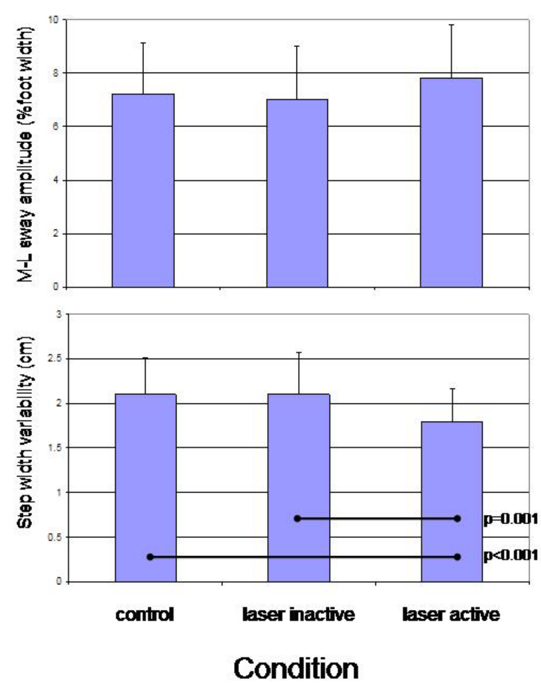

REFERENCES

Owings, T.M., Grabiner, M.D. (in press) J *Biomechanics*.

THE NEUROMECHANICAL EFFECTS OF PROPRIOCEPTIVE MODULATION OF REFLEXES ACROSS SPEED AND GAIT IN CAT LOCOMOTION

Young-Hui Chang[1], John P. Scholz[2] and T. Richard Nichols[1]

[1] Spinal Cord Research Center, Emory University, Atlanta, GA, USA
[2] Physical Therapy Department, University of Delaware, Newark, DE, USA
Contact: yhchang@physio.emory.edu

INTRODUCTION

Self-reinnervation (SR) of muscle following nerve transection and repair results in functional loss of stretch reflexes (Cope & Clark, 1993; Cope et al., 1994). Abelew et al. (2000) showed some deficits in limb coordination during walking after SR of cat triceps surae muscles. Our objective was to quantify the neuromechanical influence of short-latency proprioceptive feedback from cat ankle extensors over a range of speeds and gaits. Our rationale was that any deficits in single or multi-joint kinematics resulting from SR of a muscle correspond to reliance on proprioceptive feedback from that muscle in the context of biomechanical constraints. We also used the Uncontrolled Manifold (UCM) approach of Scholz and Schöner (1999) to study changes in global limb control after SR of a muscle.

METHODS

We used three adult cats in accordance with an approved IACUC protocol filed at Emory University. Triceps surae nerve (unilaterally, 2 cats) and soleus nerve (bilaterally, 1 cat) was transected and immediately reattached using sterile surgical procedures (described in Abelew et al., 2000). We present SR soleus muscle data here to illustrate our analysis methods. An approximate 1-2 month paralytic stage after nerve repair is followed by self-reinnervation of the muscle over post-surgery months 6-12. Full motor recovery is expected with some disruption of sensory afferents, in particular short-latency proprioceptive feedback related to functional loss of the stretch reflex (Cope et al., 1994). Hindlimb joint angles (Peak Motus 6.0, 125 Hz) were collected and analyzed for a range of walking and trotting speeds for control, 1 month (paralytic) and 6 months (SR) post-surgery. We quantified ankle yield for initial weight acceptance (E2) and knee-ankle coordination for stance. We calculated goal-equivalent variance (GEV) and non-goal-equivalent variance (NGEV) of joint angles relative to hypothesized locomotion-related variables (Scholz & Schöner, 1999).

RESULTS AND DISCUSSION

Ankle yield for control did not change with speed. Paralysis resulted in an increased ankle yield with no speed-effect. SR increased ankle yield only at high speeds (Fig. 1).

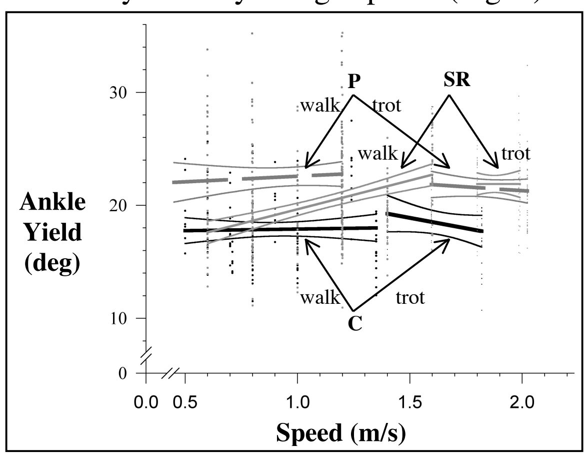

Figure 1: Ankle yield during E2 phase of stance. Linear regressions with 95% confidence intervals for walk and trot are shown for intact control (solid black lines, C), paralyzed soleus muscles (broken gray lines, P), and self-reinnervated soleus muscles (solid gray lines, SR). Same key used in Fig. 2. Data represent individual stance phases.

Paralysis and self-reinnervation of the soleus muscle resulted in substantial changes in knee-ankle coordination, but only during mid-stance for slow walking speeds (represented by the instantaneous slope of the knee angle-ankle angle plot, Fig. 2).

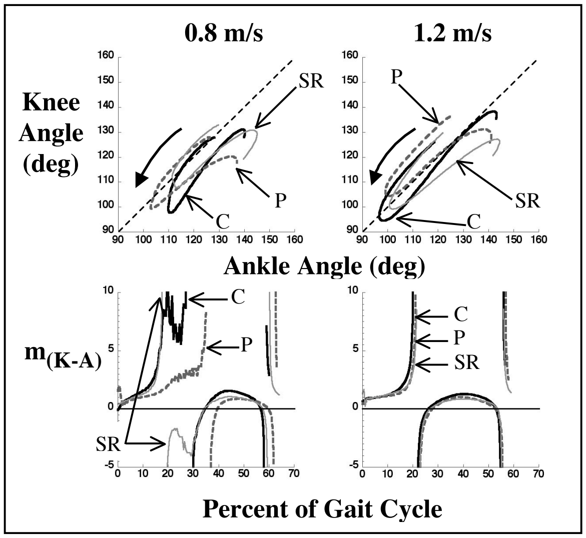

Figure 2: Angle-angle plots during stance (top, time flows CCW) with corresponding instantaneous slopes (m_{K-A}) vs. percent of gait cycle (bottom). Abnormal knee-ankle coordination emerged only in mid-stance for slow walking. Data are means of: 9 (C), 18 (P) and 25 (SR) steps for slow walk; 10 (C), 33 (P) and 32 (SR) steps for fast walk.

Hypothesizing the vertical component of the length vector between toe and hip (vertical limb length) as a task-related variable, we calculated the goal-equivalent variance (GEV) and the non-goal-equivalent variance (NGEV) of joint combinations at each percent of the gait cycle for all strides at a typical walking and trotting speed using the UCM approach (Fig. 3). GEV and NGEV were then averaged for stance and swing phases and compared. In general, self-reinnervation of the soleus muscle caused a shift in global limb control strategy toward more goal-equivalent joint combinations (i.e., GEV:NGEV >1) to achieve stable values of vertical limb length.

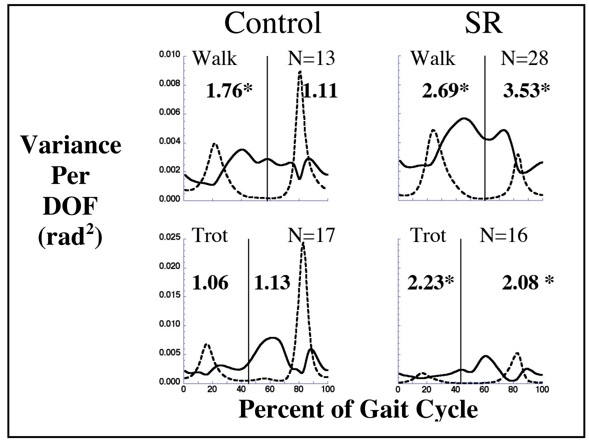

Figure 3: GEV (solid) and NGEV (broken) of joint angle combinations for hypothesized task variable, vertical limb length, in walk (1.0 m/s) and trot (1.8 m/s) for control and SR soleus muscles. Vertical line shows start of swing phase. GEV:NGEV for stance and swing phases are shown in bold. * indicates GEV:NGEV > 1 ($p<0.01$, paired t-test).

SUMMARY

Paralysis of extensor muscles likely resulted in a decreased ankle joint stiffness causing increased ankle yield at early stance. In SR soleus muscles, ankle yield increased only at the faster speeds. Our data suggest that short-latency proprioceptive feedback from soleus muscle is important for knee-ankle coordination only during mid-stance for slow walking, but not at faster speeds. Control of vertical limb length via goal-equivalent joint angle combinations emerges in response to loss of short-latency proprioceptive feedback from soleus muscle.

REFERENCES

Abelew, T.A., et al. (2000). *J. Neurophysiol.*, **84**, 2709–2714.

Cope, T.C. & Clark, B.D. (1993). *J. Neurophysiol.*, **70**, 1787–1796.

Cope, T.C., et al. (1994). *J. Neurophysiol.*, **71**, 817–820.

Scholz, J.P. and Schöner, G. (1999). *Exp. Brain Res.*, **126**, 289-306.

ACKNOWLEDGMENTS

Supported by NIH NS043893-01A1 to Y.H.C., NSF-0078127 to J.P.S. and NIH HD32571-06A1 to T.R.N.

CHANGES IN IMPACT FORCE AND JOINT TORQUES DURING A FATIGUING LANDING ACTIVITY

Michael Madigan[1] and Peter Pidcoe[2]

[1] Musculoskeletal Biomechanics Laboratory, Virginia Tech, Blacksburg, VA
[2] Department of Physical Therapy, Virginia Commonwealth University, Richmond, VA
Email: mlm@vt.edu Web: www.esm.vt.edu/~mmadigan/msbiolab/

INTRODUCTION

Past landing studies have investigated the effects of several performance factors on lower extremity loads in an effort to characterize their roles in injury development. Neuromuscular fatigue is another performance factor that may play a role in injury development, but its effect on lower extremity loads has received limited attention in the literature. Therefore, the objective of this study was to investigate the effects of LE fatigue on ground impact force and LE joint torques during landing.

METHODS

A fatiguing landing activity (FLA) was developed with two goals in mind: 1) the resulting muscle fatigue pattern should be "functionally realistic" in that it should not be limited to a single muscle group, 2) the protocol should allow frequent performance measurements as fatigue progresses to exhaustion. Frequent performance measurements allow not only the differences between unfatigued and fatigued landings to be quantified, but also their time history as fatigue progresses.

Twelve healthy male subjects were asked to perform the FLA until exhaustion. The FLA involved an alternating sequence of single-leg landings (25 cm height) and single-leg squats that was repeated until exhaustion. The landings were the biomechanical event of interest, and the squats were integrated into the activity to facilitate neuromuscular fatigue. Single-leg landings were used to avoid potential asymmetries in bilateral landings. Ground reaction force and lower extremity kinematics were sampled during the landings. Joint torques were estimated from an anthropometrically-scaled link-segment model and a recursive Newton-Euler inverse dynamics solution. Dependent variables included: peak value of the vertical component of the GRF (vGRF), vGRF impulse (calculated from impact to 200ms after impact), and joint impulse (calculated over same time interval). A repeated measures ANOVA with posthoc Dunnett's test was used to determine the significance of changes from initial values for each dependent variable.

RESULTS AND DISCUSSION

During the FLA, the vGRF peak decreased an average of 12.2% ($p<.01$), the vGRF impulse decreased an average of 5.9% ($p<.01$), and the vGRF peak loading rate did not change (Table 1). No statistically significant changes in joint impulse were found between unfatigued and fatigued landings. However, inspection of the time histories of the joint impulses as subjects performed the FLA (Figure 1) indicates statistically significant changes from initial values were found *during* the FLA (Madigan 2003).

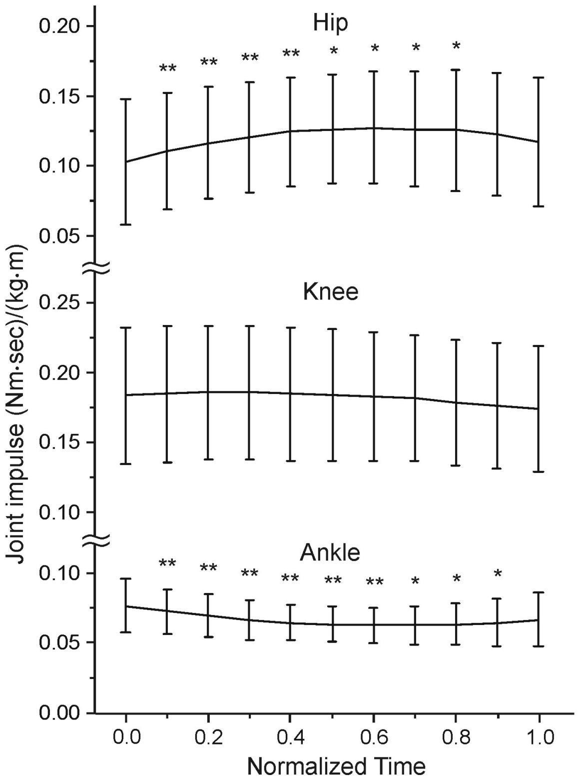

Figure 1: The average time history for joint impulses as subjects performed the FLA. Positive values correspond to an extensor (p-flexor) impulse. * significantly different from initial value (p<.05). ** significantly different from initial value (p<.01).

Changes in joint extensor impulse during the FLA included an increase at the hip and a decrease at the ankle (Figure 1). This pattern suggests a distal-to-proximal redistribution of extensor impulses. Changes in hip and ankle impulses became statistically significant early in the FLA. The subject fatigue level at this point in the activity was presumably low, so this raises the question: Are there other factors besides fatigue that contributed to the observed changes? One factor may involve an attempt by the subjects to alter their landing strategy in favor of reduced impact forces. The existence of a neuromuscular protective mechanism altering LE kinematics and stiffness characteristics to modulate impact forces has been suggested. If this was the case, the trend reversal that occurred later in the FLA may be associated with the progression of neuromuscular fatigue. Further research is needed to distinguish between changes caused solely by fatigue and changes caused other factors that occur with fatigue.

SUMMARY

A fatiguing landing activity was used to investigate the effects of LE fatigue on impact force, and joint torques during landing. The results suggest that fatigue decreases impact force and elicits a distal-to-proximal redistribution of joint extensor torques during landing. Time histories suggest that these changes may not occur in a linear or monotonic manner as fatigue progresses. The data also suggest that the changes may have resulted from other factors in addition to fatigue.

REFERENCES

Madigan, M.L., Pidcoe, P.E. *J. Electro. Kines (Accepted 3-10-03).*

Table 1: Summary of unfatigued and fatigued landings (mean±sd) (** p<.01).

Variables	Unfatigued	Fatigued
GRF peak (BW)	3.69 ± .30	3.24 ± .48 **
GRF impulse (Nm sec)/(kg m)	0.39 ± .02	0.37 ± .03 **
GRF max loading rate (KN/sec)	178.6 ± 58.5	186.7 ± 68.0
Hip extensor impulse (Nm sec)/(kg m)	.102 ± .045	.117 ± .046
Knee extensor impulse	.183 ± .049	.173 ± .045
Ankle extensor impulse	.076 ± .019	.066 ± .019

GENDER DIFFERENCES IN MUSCLE ACTIVATION PATTERNS DURING TWO STYLES OF DROP LANDINGS

Rhonda L. Boros[1] and John H. Challis[2]

[1] Applied Biodynamics Laboratory, Boston University, Boston, MA, USA
[2] Biomechanics Laboratory, The Pennsylvania State University, University Park, PA, USA
E-mail: rboros@bu.edu

INTRODUCTION

Landing from a drop has been identified as a movement challenging to the anterior cruciate ligament (ACL) (Lephart et al., 2002). Females have a much greater incidence of “non-contact” ACL injury compared with males, (Arendt and Dick, 1995) and studies have reported that females demonstrate muscle activation patterns potentially stressful to the ACL during certain landing tasks (Cowling and Steele, 2001). Females generally have a greater percentage of type I muscle fibers compared with males, and slowness of the quadriceps (QUAD) to de-activate as hamstring (HAM) and or gastrocnemius (GAS) activity begins to build during ballistic activities such as landing from a jump or drop may lead to a brief period where excessive anterior shear force is experienced by the tibia with respect to the femur, placing excessive stress on the ACL (Li et al., 1999).

The purpose of this study was to determine if females demonstrate ACL-compromising muscle activation patterns during two styles of landing from a drop.

METHODS

Vertical ground reaction force and EMG data on seven lower extremity muscles were measured as four female (mean±SD mass 63.1±4.9 kg, height 1.60±0.05 m) and four male (mean±SD mass 73.0±4.7 kg, height 1.79±0.05 m) subjects performed five trials each of flat-footed and toe landings onto a force plate from a 0.40-meter nominal drop height. All data were synchronously sampled at 1920 Hz. Event markers and landing phases were determined from the kinetic data. The filtered EMG data from the landings were normalized with respect to the EMG signals from maximum voluntary isometric contraction (MVIC) for each muscle, and expressed as a percentage of the maximum EMG signal recorded during the MVIC. Isometric knee extension and flexion strength tests were also conducted, with results normalized with respect to body mass. A repeated measures ANOVA ($P<0.05$) was performed.

RESULTS AND DISCUSSION

Males produced significantly greater knee extension moments during strength testing compared with females. Females displayed significantly greater HAM to QUAD strength ratios for most strength tests. Males exhibited greater body weight normalized vertical ground reaction force peaks (7.4±2.1 and 4.9±1.7 BW) compared with females (6.5±1.4 and 4.2±0.9 BW) for flat-footed and toe landings respectively, and demonstrated more rapid rates of loading.

EMG activation for the seven muscles for males and females during flat-footed and toe landings are presented in figures 1 and 2. The events of initial contact, peak force, bottom-most center of mass position, and end of movement are marked on each trace. Mean GAS activity onset occurred earlier and remained active significantly longer in females compared with males, and males exhibited significantly greater mean peak GAS EMG amplitude compared with females. Mean peak rectus femoris (RF), HAM and gluteus maximus (GLUT) EMG amplitudes were significantly greater in females compared with males across all landing conditions, and flat-footed landings resulted in significantly greater mean GLUT EMG magnitude for both genders.

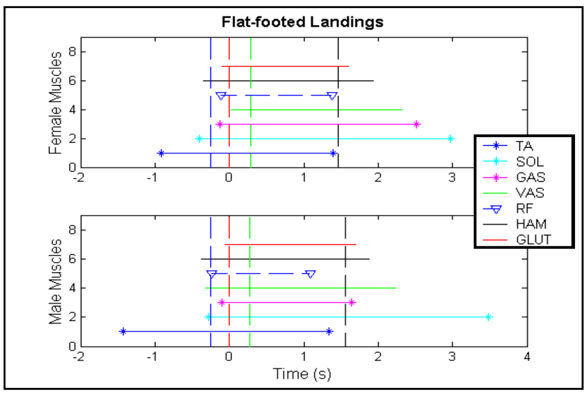

Figure 1: Mean EMG muscle activation patterns during flat-footed landings.

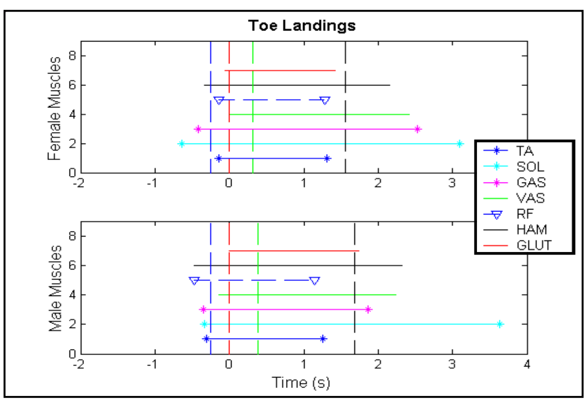

Figure 2: Mean EMG muscle activation patterns during toe landings.

SUMMARY

The results indicate that certain aspects of the muscle activation patterns observed in females differ significantly from those of males. Specific patterns of muscle activation have been associated with contributing to excessive stress on the ACL (e.g. Li et al., 1999). Such compromising muscle activation patterns were not observed in either landing style examined in this study. These data provide no direct evidence that women display muscle firing sequences potentially injurious to the ACL.

Consistent with the findings of Cowling and Steele (2001), males in the present study exhibited slightly delayed hamstring activation onset (+100 ms) across landing styles compared with females, although this delay was not statistically significant. GAS activation tended to occur earlier and remain active significantly longer in females compared with males, while males exhibited substantial bursts in GAS EMG amplitude that occurred slightly ahead of RF activity. These trends suggest that females may demonstrate ongoing GAS activity assisting the ACL in controlling anterior tibial translation relative to the femur, while males exhibit rapid bursts of GAS activity at times during landing possibly enhancing the protection of the ACL at critical instances of excessive anterior shear stress at the knee.

REFERENCES

Arendt, E., Dick, R. (1995). *Am. J. Sports Med.*, **23**, 694-701.

Cowling, E.J., Steele, J.R. (2001). *J. Electromyogr. Kinesiol.*, **11**, 263-268.

Lephart, S. A., Abt, J.P., Ferris, C.M. (2002). *Curr. Opin. Orthopedics*, **14**, 168-173.

Li, G., Rudy, T.W., Sakane, M., Kunamori, A., Ma, C.R., Woo, S.L.Y. (1999). *J. Biomech.*, **32**, 395-400.

EFFECT OF REGIONAL VARIATIONS IN MATERIAL PROPERTIES OF THE DISC ON THE CIRCADIAN VARIATION IN STATURE

Jamie Ryan Williams [1], Raghu N. Natarajan [2] and Gunnar B. J. Andersson [2]

[1] Department of Bioengineering, University of Illinois at Chicago, Chicago, IL, USA
[2] Department of Orthopedic Surgery, Rush-Presbyterian-St. Luke's Medical Center, Chicago, IL, USA
E-mail: jryan10@uic.edu

INTRODUCTION

It is the unique interaction between the solid and fluid components that provide the intervertebral discs the strength and flexibility necessary to bear the physiological loading of the spine. The current research is directed towards developing a numerical model of a lumbar disc including the fluid flow into and out of the intervertebral disc. The presence of the fluid is imperative in order to study the loading and unloading of the spine. This was accomplished by including the poroelastic behavior of the disc, the effect of the change in proteoglycan content in the disc and the effect of strain dependent permeability with respect to applied loads. It was hypothesized that the inclusion of regional variations in the material properties of the disc within the numerical model (i.e. permeability, porosity and water content) would better predict the diurnal change in disc height as compared to the model, which included only tissue specific properties.

METHODS

A three-dimensional finite element model of the L4-L5 motion segment, which was validated for static loading conditions [1], was modified to include the poroelastic components. Initial permeability and porosity values for the nucleus, annulus, endplate, cancellous bone and cortical bone were taken from the literature [2]. The drained elastic modulus and Poisson's ratios for all the disc components were also taken from the literature [2].

The effect of the change in the concentration of proteoglycans contained within the nucleus was modeled by incorporating a swelling pressure, which is dependent on the fixed charge density [3]. Similarly, the effect of change in permeability resulting from the axial strain in the tissue was included through an internal pressure acting on the disc, accounting for the dilatation of the pores as the tissue is compressed [3].

Two finite element model analyses were conducted. The original model included poroelastic material definitions specific for the nucleus and annulus (constant poroelastic material model – CPMM). However in this model, a single water content value was assigned to both tissues. In the second model, regional variations in the permeability, porosity and water content values were assigned to the inner and outer annulus as well as the nucleus (regional poroelastic material model – RPMM) [4].

In each analysis, the lumbar motion segment was loaded in order to observe the circadian variation in overall stature. The disc was loaded equivalent to normal daily activities without participating in physical work or exercise for approximately 16 hours and sleep was simulated for approximately 8 hours. Normal daily activity was modeled by applying a compressive load of 850 N [2] that was reduced to 440 N to simulate the load during sleeping. The results of overall height change from the two models, CPMM and RPMM, were then compared with measurements reported by Tyrrell et al. [5]. In the two models, the gross change in height of the subject was calculated by multiplying the measured height loss in a single motion segment by fifteen [5].

RESULTS AND DISCUSSION

The results from both finite element models, CPMM and RPMM, showed a gradual increase in disc height loss over the 16-hour period of activity. A 1.18 % loss of total stature (Figure 1) was predicted by the CPMM. Where as a 1.06 % loss of total stature was predicted by the RPMM. Both of the models predicted the resulting percent loss of stature accurately. However, the RPMM model was shown to follow the experimental curve more closely.

Upon releasing the load, a sudden recovery of height was observed with both finite element models, which compares well with the in-vivo results. During the first 4 hours of recovery, the CPMM predicted that 84% of the total loss of stature was recovered. This was reduced to 76% when the regional variations were included (RPMM). Again, the latter compared well with the results observed in vivo [5]. As the recovery time increased, the rate at which the stature was recovered decreased and began to plateau. A complete recovery of stature at the end of the 8 hours of recovery was predicted by the RPMM, which was in agreement with the in vivo data reported by Tyrrell et al. [5].

Throughout the 24-hour period, the variation in stature predicted by both finite element model analyses, CPMM and RPMM, was similar to the reported in vivo results. However, the RPMM provided an overall better prediction of the in vivo behavior particularly both during the initial loading and initial unloading of the spine. Complete recovery of total stature was also closely predicted by the RPMM.

A numerical model has been constructed that predicts the loading and unloading behavior of a lumbar motion segment over a 24-hour period. This numerical model can now be used to study the response of the disc to various cyclic loading conditions that occur during repetitive lifting.

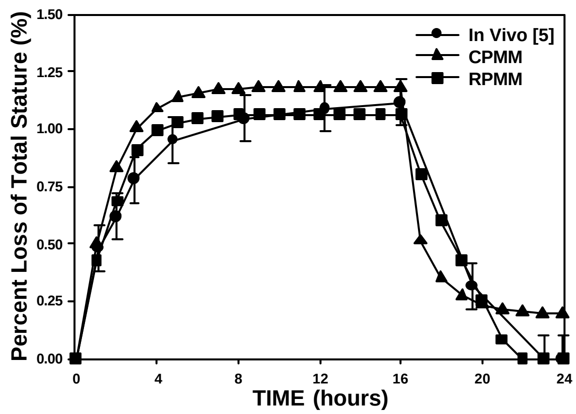

Figure 1: Circadian variation in stature as predicted by the CPMM and RPMM and compared to in-vivo results [5]

REFERENCES

[1] Natarajan RN and Andersson GBJ, (1999), *Spine*, 24: 1873-1881, [2] Agroubi M et al., (1996), *J. of Biomechanics*, 29: 1331-1339, [3] Williams, JR et al. (2003) ASME , [4] Gu W et al., (1999), *Spine*, 24(23): 2449-2455**,** [5] Tyrrell AR et al., (1985), *Spine*, 10(2): 161-164

ACKNOWLEDGEMENTS

NIH: AR48152-02, The first author wishes to acknowledge financial support from Rush-Presbyterian-St. Luke’s Medical Center.

FUNCTIONAL IMAGING REVEALS MODEST STRAIN CONCENTRATIONS ASSOCIATED WITH IMPLANT MICROMOTION USING MODIFIED BAK INTERBODY CAGES

Bay, B K[1]; Berry, D J[1]; Rutschman, S A[1]; Saucy, H[1]; Cunningham, B W[2]
[1]Department of Mechanical Engineering, Oregon State University, Corvallis, Oregon
[2]Orthopaedic Biomechanics Lab, Union Memorial Hospital, Baltimore, Maryland.
E-mail: bay@engr.oregonstate.edu

Introduction: Interbody fusion cages are increasingly used in the treatment of spinal disease and injury in order to stabilize movement and promote arthrodesis of the vertebral bodies, but the micromechanics of the interaction between the cage and the adjacent host bone is not fully understood. This information has bearing on post-surgical therapy protocols, prediction of long-term bone tissue changes, and optimization of cage design. In order to gain insight into this problem, we used functional microCT imaging to directly evaluate implant micromotion and full-field vertebral body strains in explanted motion segments from a baboon model. It is believed that functional fusion will be related to the extent of implant fixation, and that specific strain fields will be associated with fused and unfused samples.

Material and Methods: The study involved skeletally mature male baboons instrumented in the lumbar spine with one of three configurations of 11mm dia. x 20mm BAK interbody fusion cages (all procedures followed institutional and animal use and care guidelines). The cages, containing 2, 8, or 12 transverse holes, were randomized among the implant sites. Motion segments including the implants were retrieved 4-months post-op. In order to improve microCT imaging, posterior elements were removed from the specimens prior to testing. Specimens were mounted at the endplates in aluminum platens using PMMA, and placed within a microCT system that allows specimen loading during imaging. Projection images were obtained at approximately 1000 angular increments with no applied load, and at compressive loads of 150N, 300N, and 450N. Subsequent tomographic reconstructions were produced with a 50-micron voxel resolution. Mid-sagittal sections were extracted from the scans and animated through the loading sequence to assess relative motion between implant and vertebral bodies. The motion was quantified by measuring the change in distance between implant and adjacent bone from zero load to 450N compression at both the superior and inferior interfaces. Mid-frontal sections were also extracted in order to define a region of interest for making strain measurements. Digital volume correlation (Bay et al. 1999) was then used to measure continuum-level strains throughout three-dimensional volumes of interest immediately adjacent to the implant.

Results: MicroCT data sets revealed variable amounts of micromotion between the implant and adjacent bone (Figure 1). Presence of organized bone tissue in intimate contact with the implant was associated with fusion of the cage with the adjacent vertebral body (no motion), while radiolucency at the implant interface was associated with lack of fusion (motion). The 8-hole cage design appeared to provide the most consistent fusion (Table 1). Completely unfused and partially fused samples were associated with strain concentrations adjacent to the implant, while fully fused samples showed lower magnitude uniformly distributed strains (Figure 2).

Discussion: The unique aspect of this study is the functional tomographic imaging. In addition to providing detailed information about tissue morphology around the implants, it provides a means for quantifying both implant micromotion and trabecular bone strains. This indicates the immediate status of the implant and suggests adaptations that are likely to occur after longer implantation times.

Conclusion: In this model, fusion was variable. Lack of fusion and partial fusion were associated with scalloped radiolucency adjacent to the implant (motion), while full fusion was associated with intimate bone-implant interface (no motion). Partially and completely unfused samples exhibited higher magnitude strain concentrations adjacent to the implant while fully fused samples showed lower magnitude more uniform strains.

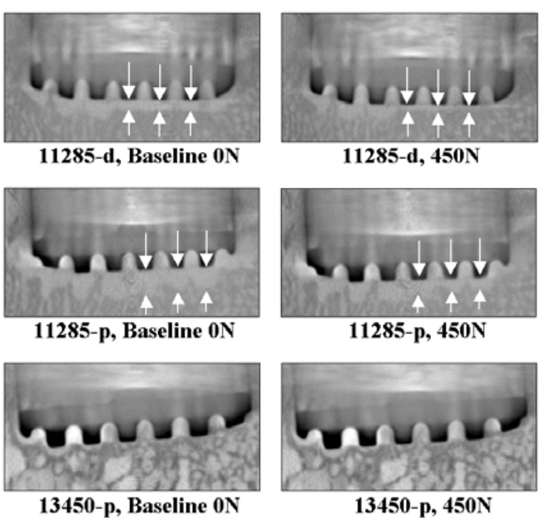

Figure 1 – Mid-sagittal slices through microCT data sets at the bone-implant interface for evaluating micromotion; (top) completely unfused, (middle) partially fused, and (bottom) fully fused.

Table 1 – Implant motion (mm) for each cage group based on functional imaging.

		Relative Micromotion Between Bone and Implant (mm)				
		Sample				
		1	2	3	4	Average
# of Cage Holes	**2**	1.30	0.55	N/A	N/A	**0.93**
	8	0.00	0.60	0.00	0.65	**0.31**
	12	1.00	0.85	1.05	0.00	**0.73**

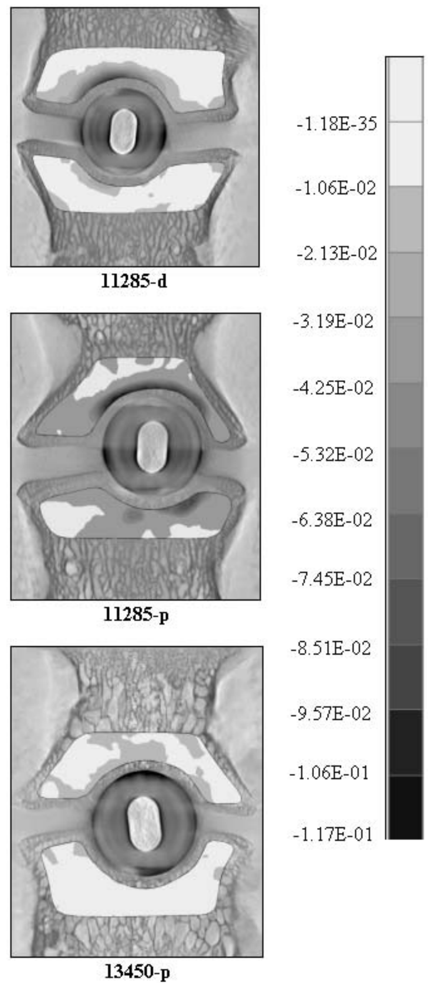

Figure 2 - Minimum principal strain superimposed on microCT data for (top) completely unfused, (middle) partially fused, and (bottom) fully fused specimens.

References:

Bay, BK, et al. (1999). *Experimental Mechanics*, **39**, 217-226.

CERVICAL INTERVERTEBRAL DISC INJURY MECHANISMS DURING SIMULATED WHIPLASH

Manohar M. Panjabi, Shigeki Ito, Adam M. Pearson and Paul C. Ivancic

Biomechanics Research Laboratory, Yale University School of Medicine, New Haven, CT, USA
E-mail: paul.ivancic@yale.edu

INTRODUCTION

Although clinical studies have thoroughly documented the occurrence of cervical disc injury in whiplash patients, there is a lack of biomechanical studies investigating the injury mechanisms of the intervertebral disc during whiplash. Thus, the goals of this study were to use the whole cervical spine model to determine the annulus fibrosus fiber strain and disc shear strain during simulated whiplash and compare these values with corresponding physiological data.

METHODS

Six fresh-frozen human osteoligamentous whole cervical spine specimens were mounted at the occiput and T1. Movie flags, each with two white, spherical, radio-opaque markers, were attached to each vertebra. A lateral x-ray of each specimen was used to develop geometrical rigid body relationships between the centers of the flag markers and points on the vertebral bodies (VBs) used to calculate the intervertebral disc deformations. The intact specimens underwent flexibility testing up to peak loads of 1.5 Nm to determine the physiological disc deformations.

To prepare a specimen for whiplash simulation, a surrogate head was attached to the occipital mount. The surrogate head and spine were stabilized using the compressive muscle force replication system (Ivancic et al., 2002).

Rear-impact whiplash simulations were performed using a bench-top sled apparatus at nominal T1 horizontal accelerations of 3.5, 5, 6.5 and 8 g (Panjabi et al., 1998). High-speed digital cameras recorded the spinal motions at 500 f/s.

The anterosuperior (point 1) and posterosuperior (point 5) corners of the lower VB of each functional spinal unit from C2-C3 to C6-C7 were selected on the x-ray (**Figure 1**). Three additional points (points 2, 3 and 4) evenly spaced between points 1 and 5 were also selected. The endplate coordinate system x-y had its origin at point 1, its positive x-axis was oriented posteriorly through point 5, and its positive y-axis was orthogonal to the x-axis and oriented superiorly.

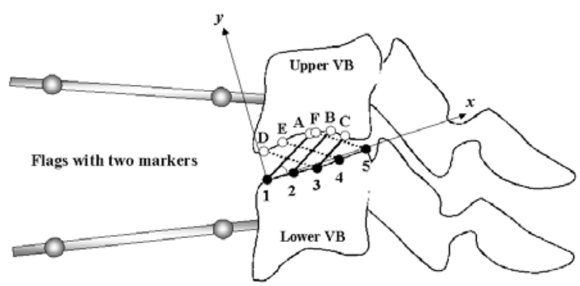

Figure 1. Schematic shows a functional spinal unit and points used to calculate disc strains.

The annulus fibrosus fibers were oriented posterosuperiorly at 30° to the x-axis (referred to as the 30°-fibers), with origins at points 1, 2 and 3 and insertions at the inferior surface of the upper VB (points A, B and C). Three points (1’, 3’ and 5’; not shown in Figure 1) were selected on the inferior surface of the upper VB such that points 1', 3' and 5' were directly superior to points 1, 3 and 5, respectively. The points were used to calculate the disc shear strain (γ) at each of the three points:

$$\gamma = \arctan(\Delta x / y_0)$$

where Δx and y_0 represented the x-axis translation and original disc height, respectively.

RESULTS

The peak 30°-fiber strains first exceeded physiological levels ($p < 0.05$) during the 3.5 g simulation at C4-C5 (**Figure 2**). At 5g, significant increases spread to C3-C4, C5-C6, and C6-C7. The highest strains tended to occur in the posterior fibers. Peak fiber strain generally increased with increasing acceleration and reached a maximum of 51.4% in the posterior fiber of C5-C6 during the 8 g simulation.

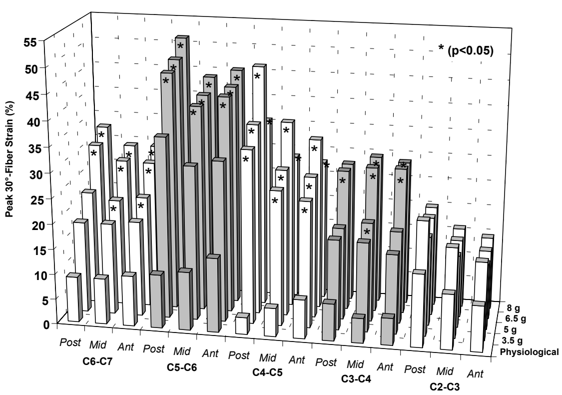

Figure 2. Average peak 30°-fiber strains in the anterior (Ant), middle (Mid), and posterior (Post) annulus fibrosus fibers.

Peak disc shear strains exceeding physiological levels were observed throughout the C5-C6 disc during the 3.5 g simulation and spread to C4-C5 and C6-C7 at 5 g (**Figure 3**). In general, the disc shear strain increased with increasing impact acceleration. The greatest disc shear strain occurred at the posterior region, reaching a maximum of 1.0 radian at C5-C6 during the 8 g simulation.

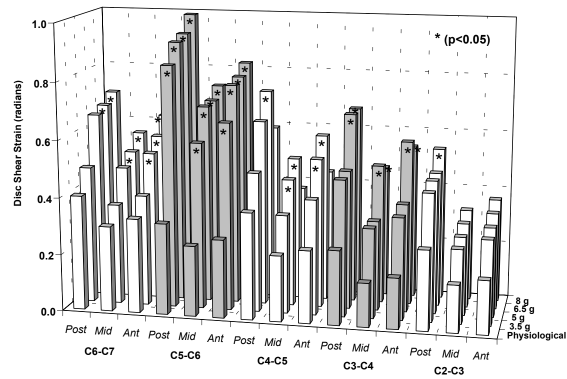

Figure 3. Average peak disc shear strains at the anterior (Ant), middle (Mid), and posterior (Post) disc regions.

DISCUSSION AND SUMMARY

The current study demonstrated that excessive 30°-fiber and disc shear strain occurred during simulated whiplash. These strains were greatest at the posterior region of the C5-C6 disc, and clinical data suggests that this is the most common location for disc herniation in whiplash patients. While disc injury may be the cause of acute pain and muscle spasm following the trauma, it could also lead to disc degeneration, facet osteoarthritis and chronic neck pain.

REFERENCES

Ivancic, P.C. et al. (2002). *CSRS*, 180-182.

Panjabi, M.M.et al. (1998). *Spine,* **23**, 17-24.

ACKNOWLEDGEMENTS

The financial support of the NIH (Grant 1 R01 AR45452 1A2) and the Doris Duke Clinical Research Foundation is gratefully acknowledged.

STABILITY OF A POSTERIOR LUMBAR INTERBODY FUSION CAGE WITH AND WITHOUT POSTERIOR INSTRUMENTATION

Sasidhar Vadapalli, B.S.; Ashutosh Khandha, B.S.; Ashok Biyani, M.D.; Matt Robon, M.D.; Vijay Goel, Ph.D.; Rebecca Long, B.S. and Melvin Malak, B.S.[1]

Spine Research Center, University of Toledo and Medical College of Ohio, Toledo, OH, USA
[1] Synthes Spine, Paoli, PA, USA
E-mail: svadapal@eng.utoledo.edu

INTRODUCTION

In order to promote solid fusion across a decompressed spinal segment, inter-body spacers are used with and without posterior instrumentation to provide an initial "rigid" fixation of the segment in proper alignment. Inter-body spacers of various shapes (e.g., rectangular, cylindrical) and materials are currently available on the market. In this study, the efficacy of a rectangular type spacer made of PEEK[+] (Synthes, Inc.) to stabilize the L4-L5 decompressed segment was evaluated using fresh ligamentous spinal segments.

METHODS

Six fresh ligamentous lumbar spine specimens (L1-S2) were radiographed and prepared for testing by fixing a base to the sacrum and a loading frame to the top-most vertebrae, using well-established protocols[1]. Each specimen was subjected to pure couples (maximum value of 6 Nm in steps of 1.5 Nm) using a system of weights, strings, and "frictionless" pulleys. The resulting spatial orientations of the vertebrae were recorded using Optotrak Motion measurement system. Each specimen was tested in six loading modes: flexion (Flex), extension (Ext), right and left lateral bending (RLB, LLB), and right and left axial rotation (RAR, LAR).

The load-displacement data for each specimen was collected in a sequential manner for the following case: 1) intact spine, 2) destabilization of the L4-5 segment involving laminotomy, and L4-5 complete discectomy, 3) insertion of the rectangular spacers (Synthes, Inc.), 4) posterior instrumentation consisting of Synthes pedicle screws and rods, and finally, 5) following flexion-extension cyclic loading for 5000 cycles. For cyclic testing, the specimen was placed in an MTS and subjected to ±3 Nm of flexion/extension moment at 0.5 Hz.

The spatial data was further processed to yield angular displacement for each vertebral body with respect to the fixed base as a function of the load step, surgical procedure (cases) and the loading modes. The angular data for each load step was normalized to the intact case by computing the percentage change in motion. A positive change indicated a decrease in stability with respect to the intact and vice-a-versa. In several specimens, decompression resulted in highly unstable structures and those were not tested prior to stabilization to avoid failure during loading. In two specimens, the motions for the intact case were very small and thus effectiveness of the cage and posterior instrumentation placements could not be quantified appropriately. Data for these cases were not included in further analyses.

RESULTS AND DISCUSSION

The motion increased following decompression, except in extension (Tables 1 and 2). In extension change in motion was minimal. After the cage placement, a significant increase in rotation was observed compared to intact in extension [77%; P<0.05] and axial rotation. With posterior fixation the motion significantly decreased when compared to intact in flexion [79%; P<0.05], extension [63%], right lateral bending [73%; P<0.05], left lateral bending [77.27%; P<0.05], right axial rotation [73%], and left axial rotation [61%; P<0.05]. The cyclic loading did change the outcome.

Table 1: Mean ($\pm$1 SD) of rotation in degrees across L4-L5 at 6.0 N-m load step in various cases.

	Flex	**Ext**	**RLB**	**LLB**	**RAR**	**LAR**
Intact	7.73 (1.70)	2.98 (1.50)	4.90 (1.58)	4.96 (1.80)	2.80 (1.87)	2.26 (0.94)
Destabilized*	11.42 (5.56)	2.58 (1.21)	7.18 (2.62)	5.75 (1.71)	4.02 (3.37)	3.19 (1.30)
2 Cages	7.16 (2.62)	4.89 (1.65)	5.06 (1.50)	5.97 (1.91)	3.53 (1.75)	3.20 (1.22)
2Cage & Posterior Fixation	1.49 (1.82)	1.11 (1.42)	1.34 (1.03)	1.10 (1.11)	0.77 (0.53)	0.92 (0.59)
After Fatigue	2.09 (2.06)	1.27 (1.50)	1.52 (1.01)	1.26 (1.13)	0.82 (0.62)	0.88 (0.78)

Table 2: Percentage average change in rotation with respect to intact for 6.0 N-m load step in various cases.

	Flex	**Ext**	**RLB**	**LLB**	**RAR**	**LAR**
Destabilized* wrt Intact	39.48	9.66	44.21	32.95	83.86	63.35
2Cage wrt Intact	-8.83	77.31	4.80	22.76	59.36	45.08
2Cage & Posterior Fixation wrt Intact	-79.14	-63.55	-72.97	-77.27	-73.40	-61.74
After Fatigue wrt Intact	-72.18	-53.04	-67.65	-73.22	-72.76	-65.50

* Based on three specimens.

SUMMARY

The change in motion in extension following destabilization was minimal, as compared to the intact case. Likewise, the cages alone brought the motion back to the intact case, except in extension. The facets were preserved during decompression and while inserting cages. This lead to the preservation of the motion in extension for the destabilized case. The cages were force fit in the disc space and thereby increased the range of motion in extension, as seen in our data. The cages alone did not provide full stabilization, underscoring the need to use additional instrumentation for a "solid" fixation. The use of PEEK+ material for the device did not reduce the effectiveness of the cage, as compared to the Titanium cages (Hitchon, 2000).

REFERENCES

Hitchon, P.W. et al. (2000). *J. Neurosurgery – (Spine 1)*, **93**, 102-108.

ACKNOWLEDGMENTS

Worked supported in part by an unrestricted grant from Synthes Spine, Inc.

+ The vertebral spacer is intended for use in the thoracolumbar spine (T1-L5) to replace a damaged or unstable vertebral body due to trauma or tumor. This is intended to be used with Synthes supplemental internal fixation systems e.g., ATLP, VentroFix and USS.

ASSESSMENT OF MUSCLE ACTIVITY AND SPINE COMPRESSION DURING CONSTRICTED AXIAL LOADING

Patrick Lee[1], Greg Slota[2], and K.P. Granata[2]

Musculoskeletal Biomechanics Lab, ME, Virginia Tech, Blacksburg, VA, USA
Musculoskeletal Biomechanics Lab, ESM,Virginia Tech, Blacksburg, VA, USA
Email: palee2@vt.edu Web: http://www.esm.vt.edu/~mmadigan/

INTRODUCTION

Occupational-related low back disorders are the leading cause of lost work days as well as the most costly occupational safety and health problem facing industry today. Twisting has been found to be associated with lower back pain (Frymoyer, 1983). Previous biomechanical measures of twisting allowed ancillary moments and forces in addition to the twisting exertion. This confounding makes it difficult to assess twisting. However, pure twisting adds neuromuscular constraints. Research suggests optimal control strategy allows variability in redundant or task-irrelevant directions (Todorov, 2002). This suggests control of ancillary degrees of freedom (sagittal and lateral moment during twist exertion) may require increase motor control effort and muscle co-contraction. Therefore, the goal of this study was to compare muscle activity of the lumbar spine during *pure* twisting with less constricted twisting. The term *pure* twisting refers to a situation where the lateral and sagittal forces are no more than 20% of the axial torque. We hypothesize that muscle activity will be greater during constrictive twisting when compared to less constrained twisting.

METHODS

Nine subjects were requested to perform isometric twisting exertions of ± 20%, ± 40%, and ± 60 of their maximum voluntary contraction (MVC) against a load cell placed an arms length away while standing on a ground-reaction force plate. Throughout the experiment EMG signals were collected on the left and right rectus abdominus (RA), external obliques (EO), internal obliques (IO), and erector spinae (ES) as described in Granata (1995).

Data collection consisted of two parts. First, the subjects were simply required to match the above mention percentages of their MVC. Second, the subjects were asked to match the torques as before, but with an added constraint requirement. This constraint required subjects to minimize forces in the non-axial directions (less than 20% of twist). This was achieved by displaying a real-time two dimensional graph which had the maximum allowed non-axial forces graphed as a box. The subjects were required to keep the forces inside the box while the desired twisting force was achieved. The protocol was performed while the subjects stood parallel to the wall and while standing with 30º left trunk rotation.

RESULTS AND DISCUSSION

Muscle activity increased for all muscle groups during constraint twisting exertions. This was statistical significance for RA, EO, and ES (Table 1).

During the twisting exertions there was a significant ($p<.0356$) difference between right and left EO. The EO were the only muscle group to display statistical significance under this relationship. This agrees with past research which has indicated that the EO are the primary muscles responsible for creating a twisting exertion (Pope 1986).

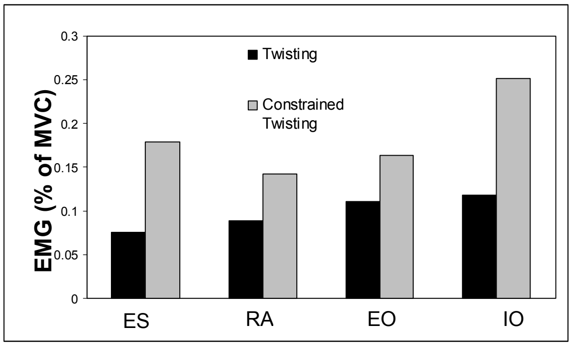

Figure 1. Muscle activity as a function of constriction.

SUMMARY

Muscle activity increased as constraints were added to twisting. As a result, stiffness and subsequently stability of the trunk are increased when muscle activity of the trunk increases. However, increased cocontraction has been associated with greater levels of spinal compression (Granata 95, Marras 1997). Recent evidence from motor control research suggests that neuromuscular variability can be mapped into task-irrelevant directions thereby improving performance in the critical task dimension (Todorov, 2002). Eliminating task-irrelevant dimensions by constraining ancillary degrees-of-freedom requires greater control effort from the neuromuscular system with potential influences in spinal load and risk of overload injury.

Future analysis will evaluate spinal compression during constrained twisting. The ground force plate data will be used to perform a bottom-up analysis to find the forces and moments at the S5/L1 region of the lumbar spine. Along with kinetic data, kinematic, and EMG data will be used to run an EMG-Assisted Model of Trunk Loading[3] which will output spine compression.

REFERENCES

1. Frymoyer JW, Pope MH, Clements JH, Wilder DG, McPhearson B, Ashikaga D: Risk factors in lower back pain, An epidemiologic study. *J Bone Joint Surg* [Am] 65:213-218,1983

2. Granata KP, Marras WS: An EMG-Assisted Model of trunk Loading During Free-Dynamic Lifting. J. Biomechanics 28:1309-1317, 1995

3. Marras, WS, Granata KP: The Development of an EMG-Assisted Model to Assess Spine *Loading During Whole Body Free-Dynamic Lifting.* J Electromyogr, Kinesiol 1997

4. Pope MH, Andersson BJ, Broman H, Svensson M, Zetterburg C: Electromyographic Studies of the Lumbar Trunk Musculature During the Development of Axial Torques. *Journal of Orthopedic Research* 4:288-297, 1986.

5. Todorov, E and Jordan, M *Optimal feedback control as theory of motor coordination.* Nature Publishing Group 2002.

Table 1. Statistical results of twisting

Muscle Group	**Constrained Twisting**	Twist Level	Forward/ Sideways	Gender	Moment Direction	Constrictive X Twisting
ES	**p<.01**	p<.05	p=.481	p=.246	p=.372	p<.01
RA	**p<.01**	p=.681	p=.584	p=.302	p=.731	p=.892
EO	**p<.05**	p<.05	p=.181	p=.707	p<.05	p<.05
IO	**p=.088**	p=.792	p=.531	p=.378	p=.321	p=.828

LOAD SHARING WITHIN A HUMAN THORACIC VERTEBRAL BODY: An In Vitro Biomechanical Study

Cumhur Kılınçer[1], Serkan Inceoğlu[1], Moon-Jun Sohn[1] and Lisa A. Ferrara[1]

[1]Spine Research Laboratory, The Cleveland Clinic Foundation, OH, USA
E-mail: ferrarl@ccf.org

INTRODUCTION

The spine play very crucial role in bearing body weight. The loads acting upon a vertebra are borne by vertebral bodies and facet articulations. The vertebra has a composite structure, composed of large trabecular bone surrounded by thin cortical bone. The cortical and trabecular components share the load when the vertebra undergoes axial loading. The distribution and transmission pathway of the load within a vertebral body is still not well understood despite of some studies in the literature (Rockoff 1969, Cao 2001). The strength of these two components of bone and distribution of the loads between them determines the capability of the spine to resist compressive fractures. In addition, the vertebra is affected severely by osteoporosis changing the load distribution across the vertebra and increasing likelihood of vertebral fracture. Therefore, it is very important to understand the contribution of cortical and trabecular bone to load bearing applying on a vertebra. The present study was thus designed to quantify the percentages of the load transmitted by the cortical and trabecular bone.

METHODS

Nine vertebra selected from T10, T11 and T12 levels was separated and surrounding musculature was removed. Then, each vertebra was circumferentially defatted and cleaned using alcohol and ether for strain gauge application at the mid level of the vertebral body. Four uniaxial strain gauges were laterally and anteriorly attached to the cortex in parallel to the longitudinal axis of each vertebra using cyanoacrylate. The specimens were then supported with polyester resin from superior and inferior endplates to generate even surfaces for compression. Each vertebra was placed in MTS Allience RT/10 materials testing machine and exposed to compressive load by two platens. The testing is conducted at 1 mm/min and 5 mm/min rate of loading until 400 N load for six cycles. After intact testing, the inferior endplate of each vertebra is partially removed leaving the cortical margin intact and tested again. Then, 25% of the trabecular bone was meticulously removed and the specimen was tested again. The area calculations were done using image analysis software (Scion, NIH) from the picture of the inferior crossection of each vertebra. The same procedure was repeated for 50%, 75% and 100% conditions.

The strain, load and displacement data were collected and the data from last cycle were used for analysis. Using the strain data from “100% removal” the percentage of the load at the cortical bone was calculated for each condition.

Descriptive analysis and Friedman test were used to detect the differences between the groups.

RESULTS AND DISCUSSION

The load sharing was calculated and analysis was done separately for each gauge. The mean of the data from four stain gauge showed that 35.94% and 34.60% of the total load was experienced by cortex in intact vertebra when loaded at the rate of 1 mm/min and 5 mm/min respectively.(Figure 1, 2)

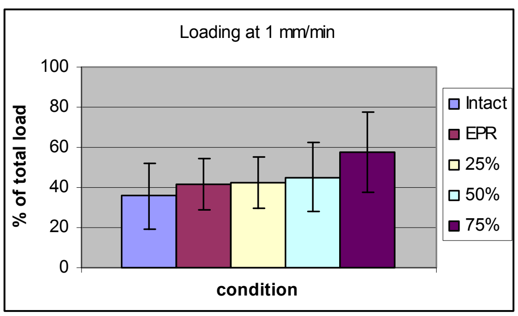

Figure 1: The mean of percentages of total load transmitted by cortical bone obtained from four different regions of vertebral body under different conditions when tested at the rate of 1 mm/min

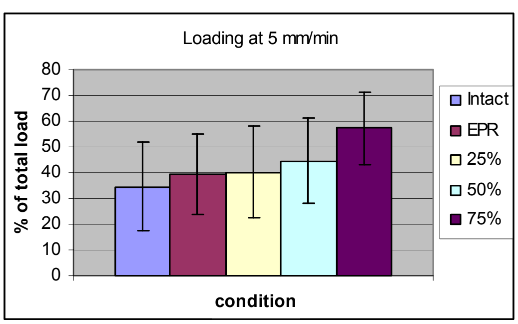

Figure 2: The mean of percentages of total load transmitted by cortical bone obtained from four different regions of vertebral body under different conditions when tested at the rate of 5 mm/min

At the rate of 1 mm/min, the gauges did not show significant changes in load sharing until 75% of trabeculae were removed ($p>0.05$). On the other hand, only two gauges detected significant changes in load at the cortex after 50% removal of trabecula when tested at the rate of 5 mm/min ($p<0.05$).

Statistical analysis did not show significant difference in load sharing among the four different region of strain measurement after the trabecular bone was removed ($p>0.05$). However, anterior gauges yielded significant difference in the amount of load borne by cortex in intact specimens ($p<0.05$).

SUMMARY

In this study, the authors investigated and quantified the contribution of cortical and trabecular bone to load bearing within the vertebral body when axially loaded.

Results suggested that the cortical bone took almost 35% of the total axial load acting upon a vertebra. Moreover, this percentage did not show significant change even though the trabecular bone vanished 50%.

REFERENCES

Rockoff S.D. et al. (1969). *Calcif. Tissue Res.*, 3(**2**):163-75.
Cao K.D. et al. (2001). *Spine*, **12**, E253-E260

MUSCLE MORPHOLOGY AFTER ANTERIOR CRUCIATE LIGAMENT RECONSTRUCTION WITH AUTOLOGOUS SEMITENDINOSUS-GRACILIS GRAFT

Glenn N. Williams, Peter J. Barrance, Lynn Snyder-Mackler, Thomas S. Buchanan

Center for Biomedical Engineering Research, University of Delaware, Newark, DE. USA
E-mail: glennwms@udel.edu

INTRODUCTION

It is estimated that 250,000 anterior cruciate ligament (ACL) injuries occur in the United States each year (Boden, 2000). More than half of those who sustain ACL injuries are treated surgically. Autologous semitendinosus-gracilis (ST-GRA) grafts have increased in popularity over the last decade and are rapidly becoming the graft of choice for many surgeons. Although there is a growing body evidence demonstrating that the short-term functional outcomes for this procedure are comparable to that which is observed with other grafts, the effect(s) that it has on the muscles of the injured person's limb remains unclear. The purpose of this study was to evaluate the effect that ACL reconstruction with autologous ST-GRA graft has on muscle volume and peak cross-sectional area (CSA) by digitally reconstructing participants' muscles from magnetic resonance images.

METHODS

Six subjects who sustained isolated ACL ruptures volunteered to participate in this study. Magnetic resonance imaging (MRI) of both limbs of each subject was performed shortly before surgery and after the subjects had returned to playing their sport of choice (6 to 9 months later). All subjects had been regular participants in activities that required quick changes of directions and/or jumping prior to their injuries and had been injured within 6 months of the date of enrollment in this study. Axial spine-echo T1-weighted scans were acquired with a 1.5-T GE SignaLX scanner from the level of the ankle mortise to the iliac crest while subjects lay supine in the scanner. The images were acquired in four sequences: lower leg, knee, thigh, and pelvis. Both limbs were imaged simultaneously using the scanner's body coil. The imaging protocol was as follows: repetition time (TR) = 350 ms, echo time (TE) = 9 ms, slick thickness = 10 mm except over the knee joint where it was 5 mm, gap between slices = 1.5 mm except over the knee joint where it was 1.0 mm, 256x160 matrix, and the field of view varied with the subjects size.

Each subject's semitendinosus (ST), semimembranosus (SM), biceps femoris longus (BF), sartorius (SAR), rectus femoris (RF), tensor fascia lata (TFL), gracilis (GRA), vastus medialis (VM), and vastus lateralis (VL) muscles were digitally reconstructed by tracing the contour of each muscle in each axial slice.

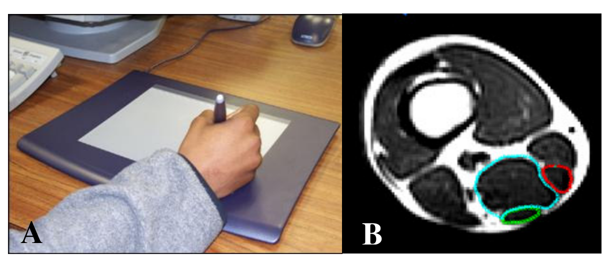

Figure 1: A) Tracing muscles with a digital palette. B) Axial image of the thigh with the ST (green), SM (blue), & GRA (red) traced.

The contours from all imaging sequences containing each muscle were grouped and used to build patient-specific polygonal models of each muscle with custom software. The volume and peak CSA of each muscle were calculated from these models.

RESULTS AND DISCUSSION

The ST and GRA muscles of the reconstructed knees exhibited markedly reduced muscle volume and peak CSA when pre-surgery and post-surgery data were compared (Figures 2 & 3). Conversely, the BF, SM, and TFL hypertrophied. The other muscles of the reconstructed knee displayed slight atrophy. Little change was observed in the muscles of the uninjured limbs.

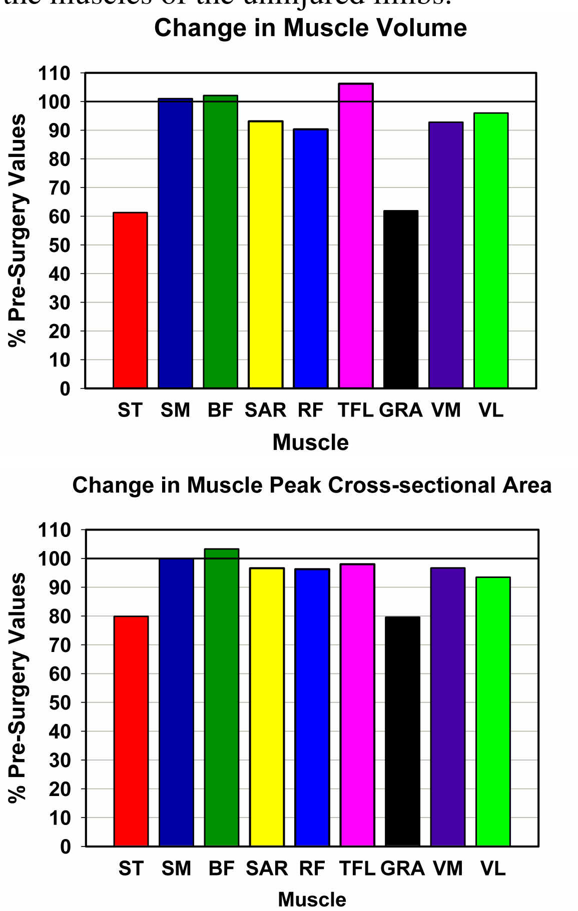

Figure 2: A) Change in muscle volume for the reconstructed limb. B) Change in peak CSA for the reconstructed limb.

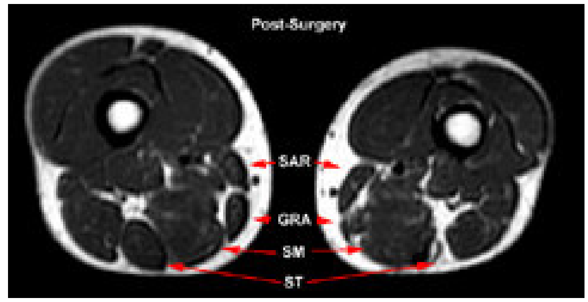

Figure 3: MRI image (mid-thigh) showing marked atrophy of the ST & GRA muscles.

The BF and SM hypertrophy observed in our subjects suggests that they used these muscles to compensate for their ST and GRA deficits. Using the BF to account for decreased medial flexor function may result in increased loading of the lateral compartment of the knee. This could be detrimental to articular cartilage health over the long term. The reasons for TFL hypertrophy are unclear. It is plausible that subjects compensated for decreased medial knee rotation with increased medial rotation of the hip (an action of the TFL).

SUMMARY

Semitendinosus and GRA muscle volume and peak CSA were markedly reduced. Our results suggest that people may compensate for autologous ST-GRA graft harvest with increased BF and SM use. Although subjects who undergo ACL reconstruction with autologous ST-GRA grafts appear to do well over the short-term, this procedure may not be as benign as is currently thought. More research is needed on this topic.

REFERENCES

Boden, B.P., Griffin, L.Y., and Garrett, WE, Jr. (2000). *Phys. Sports Med.*, **28**, 53-60.

ACKNOWLEDGEMENTS

NIH Grant RO1-AR46386 and the Foundation for Physical Therapy.

DOES TAI CHI AFFECT POSTURAL SWAY & MUSCLE ACTIVITY IN OLDER ADULTS?

E.T. Hsiao-Wecksler [1,5], K. Narayanan [2,5], B.S. Lee [5], C.A. Laughton [3,5], and L.A. Lipsitz [4]

[1] Department of Mechanical and Industrial Engineering, University of Illinois, Urbana, IL, USA
[2] Department of Bioengineering, Arizona State University, Tempe, AZ, USA
[3] Motion Analysis Laboratory, Shriners Hospitals for Children, Philadelphia, PA, USA
[4] Hebrew Rehabilitation Center for Aged, Harvard Medical School, Boston, MA, USA
[5] Center of BioDynamics, Boston University, Boston, MA, USA
Email: ethw@uiuc.edu, Web: http://www.staff.uiuc.edu/~ethw/hdcl/hdcl.html

INTRODUCTION

Tai Chi has been promoted to older adults as an intervention to improve physical and mental fitness (Kutner et al., 1997) and prevent falls (Wolf et al., 1996). Practitioners of Tai Chi (TC) report that their balance improves as a consequence of TC. Previous studies, however, have found mixed results as to whether elderly practitioners of TC demonstrate better standing balance as compared to non-practitioners (Hong et al., 2000; Tse & Bailey, 1992; Wu, 2002). Tai Chi also emphasizes complete relaxation, and has been called meditation in motion. This relaxed state may possibly reduce muscle activity.

Our study examined whether various center-of-pressure (COP) and muscle activity measures were capable of detecting differences between Tai Chi practitioners and non-practitioners during tests of quiet and mildly-perturbed stance. The purpose of this study was to better characterize the effects of TC experience on static (quiet-stance) and dynamic (perturbed-stance) postural control and lower limb muscle activity in elderly adults.

METHODS

A cross-sectional study was conducted with fifteen elderly TC practitioners (9 females; mean age 69 ± 4 yrs) and thirteen elderly controls matched by age, gender, and activity level (8 females; mean age 69 ± 2 yrs). Two TC practitioners (one male and one female) had 33 years of experience. The remaining practitioners averaged 3.2 ± 1.6 years of experience (range of 1.5 to 7 years). All subjects were community-dwelling, had no neurological, gait, or postural disorders. Informed consent was given by all subjects.

Twenty randomized trials were conducted: 10 quiet-standing trials and 10 perturbed trials, all 30 s in duration. To generate a weak impulse perturbation (a backward tug), the subject was tethered to a suspended 2.3 kg weight that was released after a delay of 10-20 s (Figure 1). The tug necessitated only a postural sway response. After the weight fell, the tether slackened and allowed the subject to readjust to an upright posture. The subject stood with both feet on a force plate, arms crossed at the chest, and eyes open.

COP data were determined from force plate recordings, which were originally sampled at 1500 Hz and then resampled to 100 Hz. Quiet-stance COP data were analyzed using techniques from both stabilogram-diffusion analysis (SDA) (Collins & De Luca, 1993) and more commonly-reported or traditional sway analysis procedures, e.g., maximum COP displacement, sway speed, and swept area. For the perturbed-stance trials, the maximum posterior COP displacement immediately after the tug was determined.

Surface electromyography (EMG) bilaterally monitored four lower extremity muscles: tibialis anterior, soleus, vastus lateralis, and biceps femoris. EMG data were collected at

1500 Hz. Raw EMG signals were bandpass-filtered (20-450 Hz, inverse Chebyshev), processed with a 40 ms moving RMS window to obtain a linear envelope, adjusted to mean baseline offsets from relaxed seated data, and finally normalized to maximum voluntary isometric contraction measurements. In addition, the percentages of muscle activation time and antagonist muscle pair co-activation times were also computed. For the quiet-stance data, the muscle activity parameters were first bilaterally averaged to determine mean values over each 30s trial and then averaged over all ten trials for each subject.

RESULTS AND DISCUSSION

For the quiet-stance data, no significant differences were found between TC practitioners and controls in any EMG or COP analysis parameters, except for a decrease in the SDA term for critical time interval in the radial direction for the Tai Chi group ($p = 0.03$). The critical time interval approximates the transition from open-loop to closed-loop postural control. Non-statistically significant trends in the data ($p > 0.05$) were, however, noted. SDA short-term diffusion coefficients tended to be larger for controls. Larger coefficients imply greater instability. Controls also tended to have their muscles active during more of the trial period than TC practitioners. Additionally, they had greater muscle activity and more co-activation in the thigh muscles and less activity in the shank muscles.

For the perturbed-stance data, an unexpected trend was found in the maximum amplitude of backward sway immediately after the tug. TC practitioners had significantly greater posterior sway than controls (32 ± 8 mm and 25 ± 6 mm, respectively; $p = 0.01$). These results may suggest that Tai Chi practitioners may be more willing to allow larger excursions within their base of support after a perturbation than their untrained counterparts. Older adults have been noted to have smaller backward excursions compared to young adults during a similar protocol (unpublished data) and voluntary sway (Blaszczyk, 1994).

SUMMARY

These results suggest that practicing Tai Chi may not necessarily reduce quiet-standing postural sway, but may influence static postural control mechanisms more subtly. The greater benefit of Tai Chi training may be that it influences how individuals respond to external disturbances to balance. Our future work will examine whether TC practitioners adopt different postural strategies and how these may influence postural control and stability. These studies may help to explain why Tai Chi appears be an effective intervention for preventing falls in older adults.

REFERENCES

Kutner, N.G. *et al.* (1997). *J Gerontol B Psychol Sci Soc Sci* **52**(5)**,** 242-6.

Wolf, S.L. *et al.* (1996). *J Am Geriatr Soc* **44,** 489-497.

Hong, Y. *et al.* (2000). *Br J Sports Med* **34**(1)**,** 29-34.

Tse, S.K., Bailey, D.M. (1992). *Am J Occup Ther* **46**(4)**,** 295-300.

Wu, G. (2002). *J Am Geriatr Soc* **50**(4)**,** 746-54.

Collins, J.J., De Luca, C.J. (1993). *Exp Brain Res* **95**(2)**,** 308-318.

Blaszczyk J.W. *et al.* (1994). *Gait Posture* **2**, 11-17.

ACKNOWLEDGEMENTS

Our gratitude to JJ Collins, Jennifer Kettell, Kunal Katdare, NIH, NIDRR, and NSF for their assistance and support on this study.

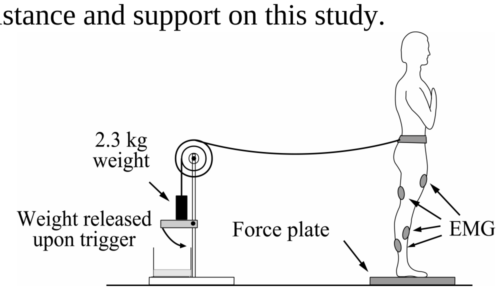

Figure 1. Experimental set-up.

TASK-DEPENDENT VARIABILITY IN HUMAN HAND EMG: EVIDENCE FOR OPTIMAL FEEDBACK CONTROL AT THE MUSCLE LEVEL

Francisco J. Valero-Cuevas [1,2] and Emanuel Todorov [3]

[1] Neuromuscular Biomechanics Laboratory, Cornell University, Ithaca, NY, USA
[2] The Hospital for Special Surgery, New York, NY, USA
[3] Department of Cognitive Science, University of California, San Diego, La Jolla, CA, USA
E-mail: fv24@cornell.edu Web: www.mae.cornell.edu/nmbl

INTRODUCTION

How the central nervous system (CNS) coordinates redundant actuators is a central problem in motor control. We have shown that the CNS can simplify the control of redundant muscles by selecting task-specific coordination patterns and scaling them to modulate the magnitude of the force output (Valero-Cuevas 2000). Moreover, we have recently argued (Todorov and Jordan 2002) that the CNS does not eliminate redundancy in a planning stage, but instead takes advantage of redundancy—by using a feedback control law to choose (online) the best motor pattern under the circumstances. We have found (Todorov and Jordan 2002) that such optimal feedback controllers obey a “minimal intervention” principle, which states that task-irrelevant deviations away from the average behavior should not be corrected. Such a controller allows variability to accumulate in dimensions that are redundant (task-irrelevant), and selectively constrains variability in task-relevant dimensions. This phenomenon has been repeatedly observed since Bernstein, and recently quantified via the “uncontrolled manifold” method (Scholz and Schoner 1999). However, existing observations are restricted to the levels of kinematics and kinetics. An important open question is whether muscle activity (the true output of the CNS) also exhibits such task-dependent variability. Here we ask that question, and answer it affirmatively.

EXPERIMENTAL METHODS

The data used in the analysis have been described previously (Valero-Cuevas 2000). We recorded fine-wire EMG signals from the seven muscles of the index finger and the 3D components of the fingertip force vector. The task consisted of producing isometric force plateaus at 50% and 100% maximal voluntary force. We studied five orthogonal directions of force, each in three finger postures. Eight unimpaired young adults wore a custom-molded thimble that defined a point-contact with the 3D force sensor that required well-directed forces and no fingertip torque to prevent slipping or rotation about the contact point (Fig 1). Filtered EMGs and force measurements were sampled at 100Hz. Each EMG was normalized so that its maximal observed activation was 1.

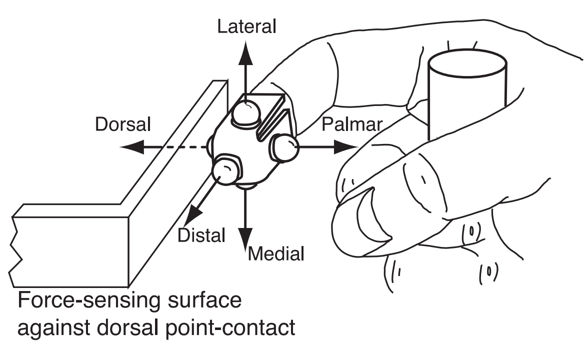

Figure 1: Producing isometric fingertip force in one of five directions (the “dorsal” direction). 3D force is produced across a point-contact defined between a polished force-sensing surface and a metallic bead embedded in the thimble.

DATA ANALYSIS

The usable dataset consisted of 1209 plateau periods (about 1.3 sec each), which were grouped so that all periods from the same subject and finger posture belonged to the same set (23 sets total). Within each set, we found the 3x7 matrix A that best relates the instantaneous 7D muscle activations $\mathbf{m}$ to the instantaneous 3D fingertip forces $\mathbf{f}$. The linear model $\mathbf{f}(t) = A * \mathbf{m}(t)$ accounted for about 85% of the force variance. We then decomposed the 7D muscle space into a 3D subspace R which is task-relevant, and a 4D subspace N which is task-irrelevant or redundant. R and N are computed as the range and null-space of the matrix A. The redundant subspace N has the property that if a vector $\mathbf{v}$ belongs to N, then $A * \mathbf{v} = 0$, and therefore $A * (\mathbf{m}+\mathbf{v}) = A * \mathbf{m}$. So if the 7D vector of muscle activations $\mathbf{m}$ is perturbed by adding the vector $\mathbf{v}$ to it, the new vector of muscle activations $\mathbf{m}+\mathbf{v}$ will generate exactly the same fingertip force. Such a perturbation is task-irrelevant, and according to the minimal intervention principle should not be corrected. Thus the minimal intervention principle predicts higher variability in subspace N compared to subspace R. To test this, we projected the 7D muscle activation vectors in the two (complementary) subspaces N and R, computed the corresponding variances V(N) and V(R), and compared them. Note that V(N) and V(R) are not scalars, but 4x4 and 3x3 covariance matrices, repectively. To obtain scalars v(N) and v(R) that represent overall variance, we computed the average variance per dimension: v = trace(V)/dim(V) for each subspace (Scholz and Schoner 1999). Although the coordinate systems of R and N are defined up to an arbitrary rotation, rotations do not affect the trace of V, and so v are independent of the choice of coordinates.

RESULTS AND DISCUSSION

The results are illustrated in Fig 2, which shows the average standard deviation per subspace dimension. We plot sqrt(v(R)) vs. sqrt(v(N)), and each data point corresponds to one of the 23 sets of plateau periods. The fact that 87% of points lie below the diagonal indicates that EMG variability in redundant dimensions is indeed higher than EMG variability in task-relevant dimensions. The ratio v(N)/v(R), averaged over the 23 sets, was 3 (Fig 2 shows statistics for the ratio of standard deviations). These results strongly suggest that the CNS regulates muscle activity in a manner equivalent to that of optimal feedback controllers.

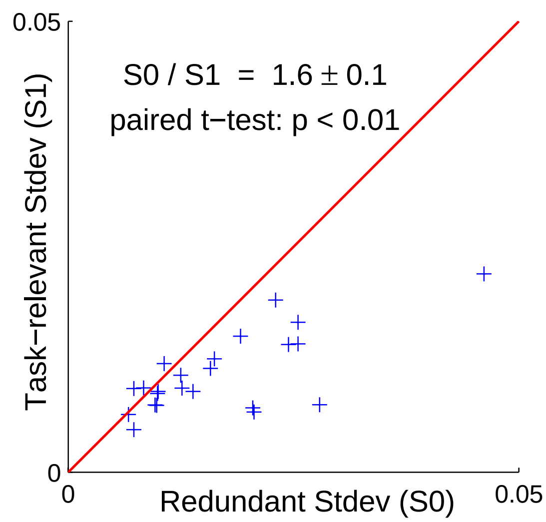

Figure 2: Comparison of EMG average standard deviations in the redundant (abscissa) and task-relevant (ordinate) subspaces.

REFERENCES

Scholz, J. P. and G. Schoner (1999). *Exp Brain Res* **126**(3): 289-306.

Todorov, E. and M. I. Jordan (2002). *Nat Neurosci* **5**(11): 1226-35.

Valero-Cuevas, F. J. (2000).*J Neurophysiol* **83**(3): 1469-1479.

ASB Symposium: Modern Perspectives on the Six Determinants of Gait

Speakers: C. T. Farley, D. S. Childress, D. C. Kerrigan, A. D. Kuo (chair)

In 1953, Saunders, Inman, and Eberhart proposed that six kinematic features—the Six Determinants—were employed to reduce the energetic cost of human walking. These Determinants have long been featured in many clinical textbooks, and are considered a major paradigm for understanding gait. But like all successful scientific theories, the Six Determinants have been subject to rigorous testing and refinement. In this symposium, four speakers will reexamine this paradigm from clinical and/or scientific perspectives, and offer modern interpretations of this important theory.

Flattening the Center of Mass Trajectory Increases the Cost of Walking

Claire T. Farley and Justus Ortega
Dept. of Kinesiology and Applied Physiology, University of Colorado, Boulder, CO

This talk focuses on the hypothesis that minimizing the vertical movements of the center of mass will reduce the mechanical work and metabolic energy consumption of walking. Subjects walked normally and with minimal vertical excursions of the center of mass (i.e., 'flat trajectory walking'). Flat trajectory walking led to impaired inverted pendulum energy exchange. Consequently, although the mechanical work required to lift the center of mass was reduced by nearly 75%, this reduction was offset by the extra work needed to accelerate the center of mass in the second half of stance. For these reasons, the mechanical work of flat trajectory walking was not lower than in normal walking. Surprisingly, during flat trajectory walking, subjects consumed approximately twice as much metabolic energy to travel a meter as during normal walking. We conclude that minimizing the vertical excursions of the center of mass during walking does not reduce the mechanical work moving the center of mass, and it actually increases the metabolic cost.

When Some Gait Determinants Fail, Some Equations Can Eventuate

Dudley S. Childress, Steven A. Gard, and Steven Miff
Rehabilitation Engineering Research Center on Prosthetics and Orthotics,
Feinberg Medical School, Northwestern University, Chicago, IL

The six determinants of gait proposed by Saunders, Inman and Eberhart supposedly reduce peak-to-peak vertical motion of the torso during walking compared with their compass gait model. Gard and Childress have shown that pelvic obliquity and stance phase knee flexion, the 2nd and 3rd determinants, do not reduce this peak-to-peak movement. Consequently, the determinants are questioned. If the idea about what the determinants do is not valid, the measured peak-to-peak movement should be approximately the same as predicted by a compass gait model with a rocker foot. This approximation allows us to write an equation that predicts peak-to-peak vertical movement is proportional to walking speed, which has been observed. Another equation eventuates from differentiation to predict that peak-to-peak vertical acceleration is proportional to the square of the walking speed (over a limited region). Preliminary data tends to support the theory. Failure of several of the determinants is required in order for the theory to be developed.

The Heel Rise Determinant of Gait

D. Casey Kerrigan
Department of Physical Medicine and Rehabilitation
University of Virginia School of Medicine

Although the determinants of gait described by Saunders and Inman recently have been challenged, our group's data do agree with Saunders and Inman's report that the actual vertical displacement of the center of mass during walking is reduced to some portion of that predicted using a compass based model. Saunders and Inman had described this reduction in actual versus predicted vertical center of mass displacement as being due primarily to three phenomena or determinants of gait; pelvic tilt, pelvic rotation, and knee flexion in stance, although Gard and Childress effectively disproved two of these determinants (pelvic tilt and knee flexion) and we disproved another (pelvic rotation). In search of an alternative explanation for the reduction in actual versus predicted center of mass displacement, we explored the phenomenon of heel rise at the end of stance of the trailing limb. We modeled the effect of measured heel rise during normal walking on raising the center of mass while the center of mass is at its lowest point during the gait cycle. We found that this modeled effect of heel rise on center of mass position accounts for most, if not all, of the overall reduction during gait in actual versus predicted center of mass vertical displacement. We conclude that while indeed there is a reduction in center of mass displacement compared to that predicted with a compass gait model (as originally described by Saunders and Inman), this reduction can be largely, if not entirely, explained by the phenomenon or new determinant of heel rise occurring at the end of stance, which in turn, may be attributable to foot/ankle anatomy as well as ankle/foot muscle control.

Mechanistic Determinants of the Energetic Cost of Walking

A. D. Kuo
Depts. of Mechanical Engineering & Biomedical Engineering, Ann Arbor, MI

Muscles consume energy when performing mechanical work, and also when producing mechanical force even without work. The metabolic cost of walking might therefore depend more directly on kinetic, rather than kinematic, features. A mechanistic approach to walking, based on the physics of an inverted pendulum, shows that relatively little work is needed to produce the inverted pendulum motion. But substantial work is needed to redirect the body center of mass in the transition between inverted pendulum phases. We will show that this determines a substantial fraction of the metabolic cost of walking. In this mechanistic approach, metabolic cost depends not on center of mass displacement *per se*, but on center of mass redirection between steps. The overall metabolic cost of walking appears to be a result of the tradeoffs between this work, and the costs of moving the legs and supporting body weight.

MINIMIZING VERTICAL CENTER OF MASS MOVEMENT DOES NOT REDUCE METABOLIC COST IN WALKING

Justus Ortega and Claire Farley

Locomotion Laboratory, Department of Integrative Physiology
University of Colorado, Boulder, CO, USA
E-mail: ortegajd@colorado.edu

INTRODUCTION

In a classic paper titled "The Major Determinants of Normal and Pathological Gait", Saunders et al. (1953) hypothesize that minimizing vertical movements of the body's center of mass during walking will minimize the metabolic cost. Alternatively, the inverted pendulum view of walking suggests the vertical fluctuations of the center of mass trajectory provide a mechanism for mechanical energy exchange and reduce metabolic cost (Alexander, 1995; Cavagna et al., 1976). The purpose of this study is to examine the relationship between center of mass trajectory and metabolic cost in walking. We hypothesize that minimizing the vertical displacement of the center of mass does not minimize the metabolic cost of walking because the inverted pendulum mechanism of energy exchange is partially disabled.

METHODS

Eight healthy, young adults (5 female, 3 male) walked on a force-sensing treadmill (Kram et al., 1998) at five speeds (0.7, 1.0, 1.3, 1.5, 1.8 m/s). At each speed, subjects walked using a normal center of mass trajectory and a flat center of mass trajectory. Prior to testing, subjects were habituated to both normal and flat walking conditions. For each trial, subjects walked for seven minutes.

During the flat trajectory walking trials, we used real time video feedback of a reflective marker located in the lower lumbar region to help each subject minimize center of mass vertical movements. We measured ground reaction force, metabolic cost, and stride frequency during the last two minutes of each trial.

We used ground reaction force data to calculate center of mass vertical displacement, mechanical energy fluctuations, and external work.

Metabolic cost was determined using indirect calorimetry and standard equations (Brockway, 1997). We calculated net metabolic cost of transport by subtracting standing metabolic power from gross metabolic power and dividing by body weight and speed.

RESULTS AND DISCUSSION

In flat trajectory walking, the center of mass moved vertically by 72% less than in normal walking (Figure 1), while other aspects of the kinematics, including lateral displacement and stride frequency, remained similar.

Despite the reduction in vertical center of mass movement during flat trajectory walking, subjects consumed twice as much metabolic energy to walk a meter than during normal walking (Figure 2).

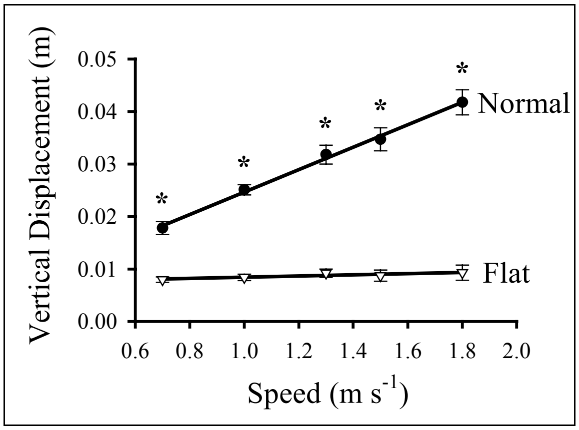

Figure 1: Center of mass vertical displacement versus speed. Asterisks (*) indicate $p<0.0001$

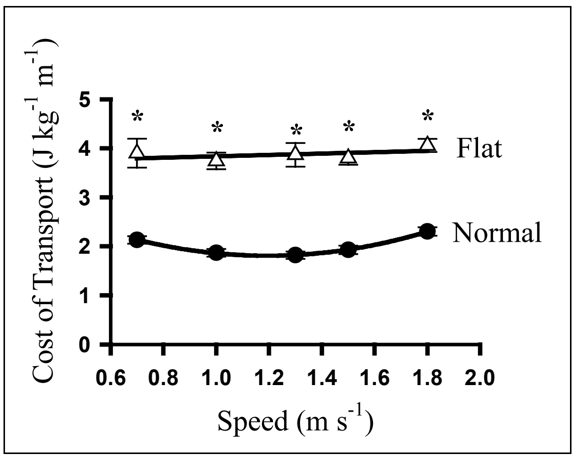

Figure 2: Net metabolic cost of transport versus speed. Asterisks (*) indicate $p<0.0001$

In flat trajectory walking, the fluctuations in gravitational potential energy and kinetic energy were mismatched and had a variable phase relation, partially disabling the inverted pendulum mechanism of energy exchange. As a result, in flat trajectory walking, subjects performed less work to lift the center of mass in the first half of the stance phase but performed additional work to accelerate the center of mass in the second half of the stance phase. Thus, despite the reduction in vertical movement in flat trajectory walking, individuals recovered about 50% less mechanical energy by the inverted pendulum mechanism but performed a similar amount of external work as in normal walking.

These observations suggest that other factors, such as greater muscle force generation due to a more flexed limb posture, may explain the high metabolic cost of flat trajectory walking (Biewener, 1989). In flat trajectory walking, stance limb posture appears to be more flexed than in normal walking, and as a result, individuals may have to generate greater muscle force to support body weight.

SUMMARY

Minimizing the vertical movements of the center of mass doubles the net metabolic cost of human walking but does not affect the external work. Although the inverted pendulum energy exchange is partially disabled, the high metabolic cost of flat trajectory walking is likely due to an increase in muscle force generation to support body weight.

REFERENCE

Alexander, R.M. (1995). *Appl. Mech. Rev.,* **48,** 461-470.
Biewener, A. A. (1989). *Science*, **245**, 45-48.
Brockway, J. M. (1987). *Hum. Nutr. Clin. Nutr.*, **41**, 463-71.
Cavagna, G.A. (1976). *J. Physiol., Lond.*, **262,** 639-657.
Kram, R. et al. (1998). *J. Appl. Physiol.*, **85**, 764-769.
Saunders, J. B. et al. (1953). *J. Bone Joint Surg. [Am].*, **35**, 543-558.

ACKNOWLEDGEMENTS
Supported by NIH AG00279-02.

WHEN SOME GAIT DETERMINANTS FAIL, SOME EQUATIONS CAN EVENTUATE

Dudley S. Childress[1,2], Steve C. Miff[1], and Steven A. Gard[1,2]

[1]Rehabilitation Engineering Research Center, Northwestern University, Chicago, IL, USA
[2]VA Chicago Health Care System, Lakeside Division, Chicago, IL, USA
E-mail: d-childress@northwestern.edu

INTRODUCTION: Saunders, et al. (1953) posed a "compass gait" model of human walking in which the leg of the compass represented the human leg length "L". We have used a similar model (Fig. 1), except we included a rocker base to represent the roll-over shape of the foot/ankle rocker system (Hansen, et al. 2000). To an approximation, this modification leads to a longer equivalent leg length "L_v'', which we call the virtual leg length ($L_v \cong 1.7 \cdot L$). This new model has been useful in deriving equations that relate a number of walking parameters (Gard & Childress, 2001).

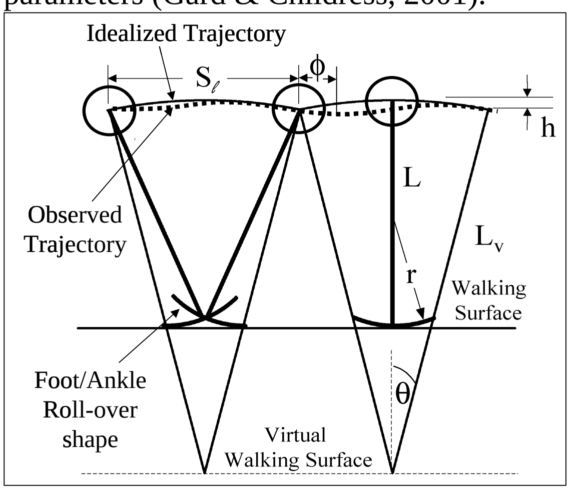

Figure 1: Rocker-based inverted pendulum model.

In opposition to the six determinants of gait, Gard and Childress (1997 & 1999) have found that pelvic obliquity and stance-phase knee flexion do not decrease vertical trunk excursion. Since these 2nd and 3rd determinants fail to alter the peak to peak vertical excursion of the body, and since our idealized model has been found to reasonably predict relationships between walking parameters, we have used "h" (see Fig. 1), as derived from the idealized model, to be the peak-to-peak value of a sinusoidal equation representing the trajectory actually observed, which appears sinusoidal with a phase shift. Other equations eventuate, one that relates to the kinetics of walking. This equation, Eq. 2, appears useful because it provides quantitative relationships between vertical acceleration and various gait parameters.

METHODS: The method is mainly to mathematically manipulate equations that come from relations and approximations concerning non-disabled human walking. We know from Koopman (1989) and others that $S_l = a \cdot f_{cad}$ and $f_{cad} = \sqrt{\frac{V}{a}}$ where f_{cad} is the cadence, a is the step ratio constant, S_l is the step length and V the walking speed. Using simple trigonometric relationships, small angle approximations for q, and an approximation for the cycloidal trajectory of the rocker-based inverted pendulum (Morawski & Wojcieszak, 1978) it can be shown that

$$h = \frac{a \cdot V}{8 \cdot L_v}$$

Substituting $h/2$ into a sinusoid function we obtain an estimate of vertical position "y".

$$y \cong -\frac{a \cdot V}{16 \cdot L_v} \cdot \cos(w \cdot t - f),$$

where f is the angular shift between the observed trajectory and the first harmonic of the idealized trajectory. Differentiating the vertical position twice and substituting

$w = 2 \cdot p \cdot f_{cad} = 2 \cdot p \cdot \sqrt{\frac{V}{a}}$, we obtain Eq. 1 for the vertical acceleration.

$$\ddot{y} \cong \frac{p^2 \cdot V^2}{4 \cdot L_v} \cdot \cos(w \cdot t - f) \qquad \text{Eq. 1}$$

If "g" is the gravitational constant, the acceleration "*Acc*" may be written as:

$$Acc \cong g + \frac{p^2 \cdot V^2}{4 \cdot L_v} \cdot \cos(w \cdot t - f) \qquad \text{Eq.2}$$

If walking makes a transition to jogging when *Acc* = 0, then V_T, the transition speed, can be estimated by Eq. 3.

$$V_T = \frac{2}{p} \cdot \sqrt{g \cdot L_v} \qquad \text{Eq. 3}$$

RESULTS AND DISCUSSION: A summed GRF for one subject from our lab's data files is shown in Fig. 2. The amplitude of the sinusoid is approximated as (mg – minimum). The GRF above "mg" is not very sinusoidal in shape but the impulse magnitude above "mg" equals that below. Data at three walking speeds is plotted in Fig. 3. A curve predicted by theory is shown along with the data. The preliminary data tend to be in agreement with the theory.

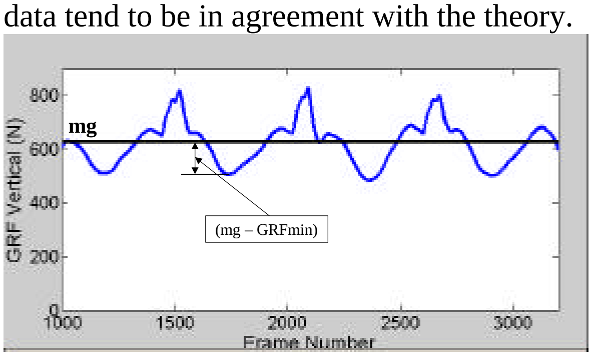

Figure 2: Vertical Ground Reaction Force.

SUMMARY: An interesting finding, if supported by more data, is that the peak vertical GRF increases about the body weight (mg) as the square of the walking speed. Sinusoidal analysis may be important to walking because it avoids the need for initial conditions. Some numeric results are that an 64 kg person with height of 1.73 m, leg length of 0.53 * height, L_V = 1.7 L, walking at 1.0 m/s 1.4 m/s, 1.8 m/sec and 2.5 m/s will have peak forces above "mg" of about 16%, 31%, 52%, and 100% respectively. Actual peak forces may be somewhat greater. The transition speed V_T is predicted by the model to be 2.49 m/s.

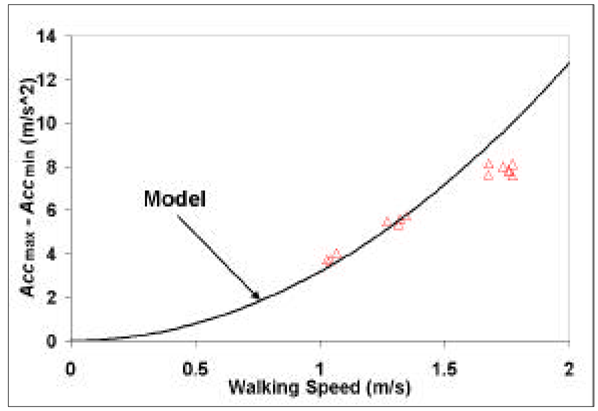

Figure 3.

REFERENCES: Gard SA & Childress DS, *Gait & Posture*, **5**:233-238, 1997.

Gard SA & Childress DS, Arch Phys Med Rehabil. **80**:26-32, 1999.

Gard SA & Childress DS, *JPO*, **13**:3,64-67, 2001

Hansen, A, Gard, S, & Childress, in *Pediatric Gait*, Eds., Harris & Smith, IEEE, pp. 159-165, 2000

Koopman, B, Ph.D. Dissertation, Univ. of Twente, The Netherlands, 1989

Morawski J.& Wojcieszak I, *Biomechanics **VI-A***, 445-451, 1978.

Saunders JB , Inman VT, Eberhart HD, *J Bone Joint Surg (Am)*, **35A**:543-558, 1953

ACKNOWLEDGEMENTS: The work was funded by the National Institute on Disability and Rehabilitation Research (NIDRR) of the Dept. of Education (grant # H133E980023). The opinions contained in this publication are those of the grantee and do not necessarily reflect those of the Dept. of Education. The authors acknowledge the use of the VACMARL, VA Chicago Health Care System, Lakeside Div, Chicago

DETERMINATION OF CONTACT STRESS DISTRIBUTIONS ON EMU FEMORAL HEADS

Karen L. Reed[1], Michael G. Conzemius[3], Thomas D. Brown[2,1]
Departments of [2]Orthopaedic Surgery and [1]Biomedical Engineering University of Iowa, Iowa City, IA
[3]Veterinary Teaching Hospital Iowa State University, Ames, IA
Email: karen-reed@uiowa.edu

INTRODUCTION Successful orthopaedic management of femoral head osteonecrosis remains problematic. Availability of an animal model, reliably mimicking the human disorder in terms of collapse, could provide valuable insight. Recently (Conzemius 2002), the emu has been established as such a model, in that cryo-induced osteonecrosis consistently progresses to femoral head collapse. Besides merely collapsing, however, another prerequisite to serving as a meaningful model for human osteonecrosis is that the patterns of load transmission through the emu hip be reasonably consistent with those in humans. Since forestalling juxta-articular collapse is such a major consideration in treating osteonecrosis, one aspect of load transmission of particular importance is the distribution of intra-articular contact stress. Contact stress mapping in the emu hip is therefore here reported, using a cadaveric Fuji-film preparation.

METHODS Recent contact stress measurement work for human hips (Bay 1997) has highlighted the importance of maintaining physiologically realistic peri-acetabular deformations. Key considerations in that regard are to simulate (muscle) traction loads on the pelvis, and to avoid artifactual reinforcement retro-acetabularly (i.e., no PMMA potting of the acetabulum). We have developed an “emu version” of the Olson/Bay loading apparatus (Bay 1997), augmented to include the capability for capturing contact stress data for various joint configurations spanning the stance phase of the emu gait cycle (Figure 1).

In the case of the emu, based upon exploratory dissections, plus on existing literature which describes the leg musculature (Patak 1998) and gait characteristics (Abourachid 2000, Gatsey 1991), two principal muscle groups needed to be included: hip abductors and hip extensors. The hip abductors were modeled with attachment points from distal to the greater trochanter, to three locations on the pelvis:

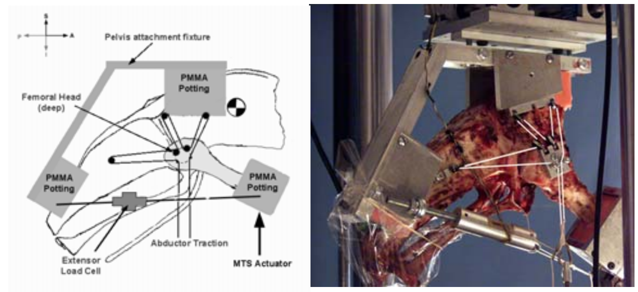

Figure 1 Schematic and photograph of emu hip loading fixture. The pelvis attachment fixture (aluminum struts, plus two PMMA pots) freely moves in A-P and M-L translation, and in rotation about A-P and M-L axes; S-I translation, and rotation about the S-I and M-L axes, are constrained. The distal femur potting block is subjected to S-I force from the MTS actuator and is allowed rotational freedom along the M-L axis; all other degrees of freedom are constrained. Abductor traction is applied by a pneumatic actuator.

anterior and superior to the acetabulum, directly superior to the acetabulum, and posterior and superior to the acetabulum.

Due to the high degree of femoral flexion occurring throughout the gait cycle in emus (early in stance phase the femur approaches 90° from vertical), the other muscle group modeled was the hip extensors, which run from the distal femur to the caudal end of the pelvis. Force plate recordings, combined with kinematic data obtained from digitized video recordings, were used to estimate the ground reaction forces (GRF) at ten-percent intervals during the stance phase of the emu gait cycle. The distal femur was PMMA-potted, and loaded with the calculated ground reaction force, while the pelvis was allowed translational freedom transversely, and rotational freedom in the coronal plane. A load cell was positioned in series with the hip extensor muscle group, to monitor muscle tension. To maintain balance, the abductors were tensioned with a pneumatic actuator (abductor force was measured with an additional load cell) as the hip was loaded. Both Super Low and Low range Fuji-film were used to record static joint contact stresses. Two independent sets of film (each containing one Low and one Super Low piece) were recorded at each ten percent increment of the gait cycle across the entire range of motion seen during stance phase. Identical gait-cycle tests were performed for two different pelvis/femur specimens, resulting in a minimum of four independent Fuji-films for each stance phase increment.

RESULTS It is apparent from these data that although emus load their hips with a high degree of flexion, the contact stress is superiorly concentrated, as in humans (Figure 2). This is due to the large flexion moments (loading at the knee) that the hip extensors must overcome to maintain stability, thereby axially compressing the femur into the acetabulum.

To validate the loads recovered from the Fuji film, a static free-body diagram (FBD) analysis of each loading configuration was performed. The calculated resultant joint reaction force was then compared to the total recovered force from the Fuji Film, obtained by numerical integration of the digitized film (data are summarized in Table 1). At all points except for 10% stance phase, average recovered force was within 13% of the average calculated resultant force. All films were qualitatively similar: each had a large contact patch located anterosuperiorly on the femoral head.

Table 1 Recovered and calculated joint reaction forces

% Stance (N)	GRF (N)	Flex Ang. (deg)	Avg Recov. Force (N)	Avg FBD Force (N)	P_{ave} (MPa)
0	0	62	0	0	0.00
10	160	62	608	771	2.92
20	241	66	977	970	3.28
30	301	58	1402	1377	3.63
40	335	65	1029	1183	3.28
50	353	67	1161	1180	3.77
60	370	71	1124	1081	3.33
70	280	74	630	676	3.11
80	172	76	392	414	2.54
90	65	75	182	168	2.02
100	0	76	0	0	0.00

A smaller contact patch was located on the posterior side of the femoral head. The location and size of the contact patches were very consistent between all films.

DISCUSSION The stress distributions recorded for emu femoral heads are generally similar to those seen in human femoral heads, in terms of anatomic engagement sites and contact stress magnitudes. The loading apparatus setup provides consistent results, verified by the similar magnitudes and articular contact distributions seen in duplicate films and between specimens.

The use of Super Low and Low Fuji film, loaded at the same time, allowed accurate measurement of a wider range of contact stresses than that obtainable with a single film range. When force recovery calculations were performed, Super Low film was used to estimate stresses and areas ranging from 0.5 MPa to 3 MPa. Low film was used to estimate stresses greater than 3 MPa.

SUMMARY Emu proximal femur articular contact stress distributions were mapped using a cadaveric fuji-film preparation. The fixturing and loading procedure mimicked *in vivo* loading seen during a typical gait stance phase. Emu femoral head contact stress distributions are generally similar to those in humans, in terms of stress magnitudes and contact patch locations.

ACKNOWLEDGEMENTS NSF Graduate Research Fellowship, NIH Grant #46601. & #49919. Dr. Wanda Gordon, Mr. Tom Baer, and Mr. Todd Howatt provided assistance.

REFERENCES Abourachid A and Renous S *Ibis* 142 p 538, 2000.
Bay BKet al. *J. Biomech* 10(2) p 193, 1997.
Caldwell et al., J. Biomech 26 p1001, 1993.
Gatsey SM, and Biewener AA *J Zool. Lond.* 224 p 127, 1991.
Patak AE and Baldwin J *J Morph* 238 p23, 1998.
Conzemius et al *J Orthop Res.* **20** pp303, 2002.

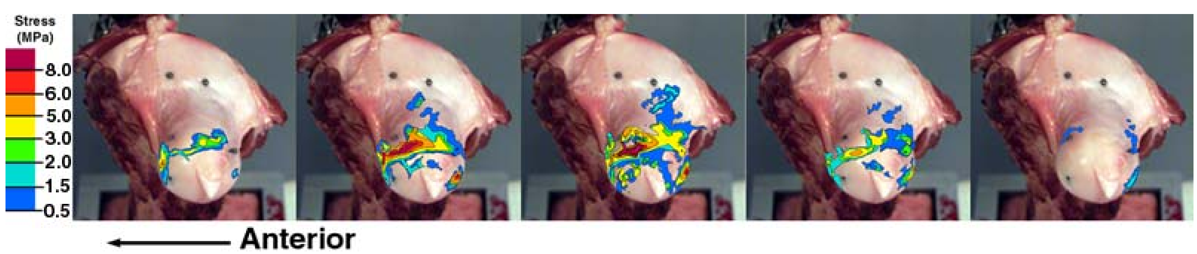

Figure 2 Contact stress distributions on the emu proximal femur at 10%, 30%, 50%, 70%, and 90% stance phase.

RELIEF OF PRESTRESSES WITHIN THE MINERALIZED COLLAGEN MATRIX UPON FRACTURE

Nicholas Wasserman[1], Fran Adar[2], Mitchell B. Schaffler[3] and Ozan Akkus[1]

[1] Department of Bioengineering, University of Toledo, Toledo, OH
[2] Jobin Yvon Inc., Edison, NJ
[3] The Leni & Peter W. May Department of Orthopaedics, The Mount Sinai School of Medicine, New York, NY
Email: ozan.akkus@utoledo.edu

INTRODUCTION

Bone is a biocomposite made of carbonated apatite crystals and collagen molecules. There is scant amount of information available as to how these components behave under deformation and fracture. Raman spectroscopy is becoming a popular method to observe molecular deformation and fracture mechanisms in bone (Akkus, 2003; Carden et al., 2003). Using this technique, we have previously studied changes in the mineral phase of bone following fracture. In this study we focused on the effects of the fracture process on the organic constituent of bone. Furthermore, we investigated the effects of loading mode and age on the fracture characteristics at the molecular level.

METHODS

Femurs were obtained from 13 female Sprague Dawley rats within the age range of 3 months to 24 months old. The left femora were loaded to failure in 3-point bending at 0.1 mm/s, which induced tension in the anterior quadrant and compression within the posterior quadrant. The right femora were cut at the mid-diaphysis with a low speed saw, polished and used as controls. Using a confocal Raman microscope (LabRam Infinity, Jobin-Yvon Inc.) with a 532 nm laser, spectra were obtained within the anterior and posterior quadrants of the specimens.

Using custom-written software (Matlab, The Mathworks, Inc.), the spectra were filtered for noise, baseline corrected for fluorescence and analyzed to determine the wavenumbers of collagen and mineral molecules in bone. An increase in the wavenumber indicates a shortening of the bond length, while a decrease would indicate a longer bond length. We focused on three molecular vibrations: $\nu_1(PO_4^{3-})$ at ~960 cm^{-1} and $\nu_1(CO_3^{2-})$ at ~1071 cm^{-1} within the mineral, and $\delta(CH_2,CH_3)$ at ~1451 cm^{-1} in the amino acid residues of collagen. The data were analyzed for statistical significance using a multivariate analysis of variance. This analysis took into account the age of the specimen, the failure mode (compression vs. tension) and the effects of fracture.

RESULTS

There was an overall decrease in all chemical bond lengths following fracture. The wavenumber was 2.30 cm^{-1} greater in the fractured specimens than in the control specimens for the $\delta(CH_2,CH_3)$ scissors band, (Figure 1) suggesting that the bond lengths between these atoms in collagen are becoming shorter. The wavenumber for the phosphate symmetric stretch ($\nu_1(PO_4^{3-})$) was 1.58 cm^{-1} greater for the fractured specimens (Figure 1). In addition, the carbonate

($\nu_1(CO_3^{2-})$) wavenumber increased 2.10 cm^{-1} in the fractured specimens. Another vibrational mode of phosphate, ν_4(PO) (~580 cm^{-1}), was examined and a positive shift of 2.81 cm^{-1} was found. The amount of wavenumber shift for the vibrational modes examined was found to be significantly different ($P<0.05$) between the fractured and control specimens. There wavenumber shift did not change significantly with age and failure mode (i.e. tension vs. compression).

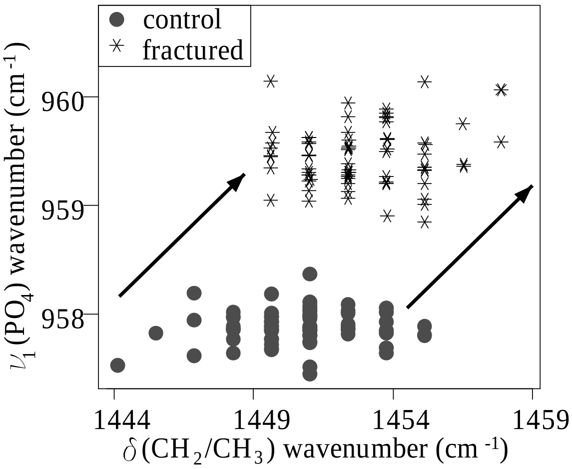

Figure 1: The wavenumber shift for the mineral ($\nu1(PO_4^{3-})$) and collagen ($\delta(CH_2,CH_3)$) phases with fracture.

DISCUSSION

In our previous work, we observed a positive wavenumber shift for the $\nu_1(PO_4^{3-})$ vibrational mode with fracture. Based on this result, we developed the following postulation. Mineral crystals nucleate and grow in the gap regions within the collagen matrix. The growth of mineral crystals along their lateral axes (a,b) is restrained by the adjacent collagen molecules (Fratzl, 1991). This restraint would cause residual compressive stress laterally within the matrix. This residual stress would elongate the crystals longitudinally due to Poisson's effect. Upon fracture, the residual stress is relieved, resulting in shorter chemical bond lengths within mineral crystals. If this postulation holds, then the collagen phase should also display a reduction in bond length due to the relief of residual compressive stress. In support of this, current results confirmed a positive shift in the wavenumber for $\delta(CH_2,CH_3)$, implying the shortening of bond lengths for the collagen phase as well.

Recently, Carden et al. (2003) reported similar wavenumber shifts in the collagen and mineral components of bone around locations of indentation. They attributed the shift in the phosphate band to the emergence of new mineral species as a result of pressure induced phase transformation. The shift in the organic component was assigned to rupture of the crosslinks within collagen.

SUMMARY

From this work and the work of others, it is obvious that some significant structural changes occur in the mineralized collagen matrix at the molecular level with damage. Whether the observed wavenumber shifts are due to the relief of the residual compressive stress or to phase transformation and crosslink rupture is not immediately clear. Further work that examines both of these possibilities is needed for a better understanding of the fracture process in bone.

REFERENCES

Akkus, O., et al. (2003). *Proceedings of ORS 2003*, 449.

Carden, A., et al. (2003). *Calcified Tissue Int.*, **72**, 166-175.

Fratzl, P., et al. (1991). *Calcified Tissue Int.*, **48**, 407-413.

EFFECT OF PAMIDRONATE TREATMENT ON *oim/oim* MOUSE FEMURS

S. H. Rao[1], R. B. Martin[1], K. D. Evans[2], and A. M. Oberbauer[2]

[1]Orthopaedic Research Labs, University of California, Davis, CA, USA
[2]Animal Science Department, University of California, Davis, CA, USA
Email: shrao@ucdavis.edu

INTRODUCTION

Osteogenesis Imperfecta (OI), a heritable disease affecting 1:20,000 to 1:60,000 live births, is caused by mutations in the genes that code for Type I collagen. OI is characterized by skeletal fragility, multiple fractures, and in some cases blue sclera, hearing loss, short stature, and dentinogenesis imperfecta.

Currently there is no cure for OI, however research and clinical trials involving a family of drugs known as bisphosphonates have shown ameliorating effects in children with OI. Bisphosphonates are analogs of pyrophosphate with a P-C-P structure. The mechanism of action of bisphosphonates is not entirely understood, however they are known to inhibit osteoclastic bone resorption, and may have a positive effect on osteoblasts as well. Pamidronate ((3-Amino-1-hydroxypropylidene)bis-phosphonate) is an amino-bisphosphonate of intermediate potency in terms of resorption inhibition.

We hypothesize that pamidronate treatment will inhibit ostoclastic resorption on the metaphyseal surfaces of growing OI patients, thereby creating larger diaphyses, and increasing the bone strength and stiffness. We tested this hypothesis in the *oim* mouse model.

MATERIALS AND METHODS

Oim mouse pairs from Jackson Labs (Bar Harbor, ME) were bred to obtain wildtype (+/+), heterozygous (+/o), and homozygous (o/o) offspring. The pups were randomly assigned one of 4 treatments. Initially three pamidronate doses were used: high (50mg/kg/mo), medium (10mg/kg/mo), and low (5mg/kg/mo). However, the high dose adversely affected the internal organs of the animals and was terminated. The fourth dose consisted of a phosphate buffered saline control. Tables 1 and 2 summarize the numbers of female and male animals in the experimental groups.

Table 1: Male Experimental Group

genotype	Control	Low	Medium
+/+	10	12	10
+/o	13	11	9
o/o	7	9	8

Table 2: Female Experimental Group

genotype	Control	Low	Medium
+/+	11	10	10
+/o	15	12	13
o/o	7	8	9

Treatments were started at age 4 weeks and ended at age 12 weeks, when the mice were sacrificed by CO asphyxiation, and stored frozen. The left femurs were dissected out and tested in 3-point bending such that the posterior surface was in compression. An Instron 8511 (Canton, MA) was used for the testing, with a 4mm span, and a 1mm/s loading rate. Using StatView (Cary, NC) software, the effects of gender, genotype, and treatment on stiffness, yield displacement, yield load, ultimate displacement, ultimate load, total energy, elastic energy, and plastic energy were determined.

RESULTS

The results were analyzed using 3 factor (gender, genotype, and treatment) ANOVA and Fisher PLSD for pair-wise comparison. Based on the results, there was a significant effect of gender on stiffness ($p=0.0017$), ultimate load ($p<0.0001$), total energy ($p=0.0381$), and elastic energy ($p=0.0004$). The genotype had a significant effect on all of the measured mechanical properties. Treatment had a significant effect on stiffness ($p=0.002$), yield displacement ($p=0.0282$), and yield load ($p=0.013$). Tables 3 and 4 summarize the properties affected by treatment. There was a significant ($p=0.0463$) interaction between gender and treatment for yield displacement. Fisher's PLSD showed significant stiffness differences between the controls and the low ($p=0.0203$), and medium ($p=0.0027$) treatment groups.

Table 3: Treatment Effects in Males

	Genotype		
Dose	+/+	+/o	o/o
Stiffness (N/mm)			
Control	357 ± 83	333 ± 85	196 ± 59
Low	406 ± 82 *	421 ± 78 *	270 ± 72 *
Med	403 ± 84 *	404 ± 103 *	260 ± 87 *
Yld. Disp. (mm)			
Control	.121 ± .024	.100 ± .039	.055 ±.072
Low	.090 ± .009 *	.088 ± .046	.014 ± .027 *
Med	.096 ± .020	.123 ± .019 †	.046 ± .067 †
Yld. Load (N)			
Control	25.2 ± 5.8	23.1 ± 9.8	4.8 ± 6.4
Low	24.5 ± 6.8	22.9 ± 13.0	2.3 ± 4.7
Med	24.4 ± 6.4	28.9 ± 7.6	7.6 ± 10.7

* significantly different than control dose
† significantly different from low dose

In the case of yield displacement, there was a significant difference between the control and low treatment ($p=0.0451$) and the low and medium treatment ($p= 0.0157$). For the yield load, Fisher PLSD analysis revealed significant difference between the low and medium treatments ($p=0.0301$). Both treatments increased the ultimate load however the change was not quite significant ($p=0.0626$).

Table 4: Treatment Effects in Females

Stiffness (N/mm)			
	Genotype		
Dose	+/+	+/o	o/o
Control	352 ± 71	293 ± 69	210 ± 98
Low	348 ± 75	319 ± 68	210 ± 60
Med	372 ± 93	370 ± 75 *	234 ± 68
Yld. Disp. (mm)			
Control	.091 ± .037	.103 ± .036	.029 ±.050
Low	.113 ± .037	.099 ± .028	.031 ± .043
Med	.096 ± .043	.102 ± .029	.087 ± .040
Yld. Load (N)			
Control	20.3 ± 8.5	18.1 ± 6.8	3.2 ± 6.1
Low	21.9 ± 4.0	21.6 ± 7.2	4.1 ± 6.0
Med	20.9 ± 6.1	23.4 ± 7.1 *	12.8 ± 7.4 *

* significantly different than control dose
† significantly different from low dose

DISCUSSION

During growth, resorption occurs on the metaphyseal surface to create the diaphysis. In OI, the bone is of inferior quality due to mutations in the collagen genes. By inhibiting the metaphyseal resorption using pamidronate, the diaphysis will be larger, compensating for the weaker OI bone material. The results of the 3-point bend testing support the hypothesis that inhibition of resorption via pamidronate treatment increases the strength and stiffness of OI bones. We are currently studying the effects of treatment on femoral diameter.

REFERENCES

Camacho, N. P., et al. (2001). *Calcified Tissue International*, **69**, 94-101.

Fleisch, H. (1997). *Bisphosphonates in Bone Disease: from the laboratory to the patient*. The Parthenon Publishing Group.

ACKNOWLEDGEMENTS

This work was supported by NIH grant AR4720501.

APPARENT MODULUS OF FUSED VS. UNFUSED FEMORAL IMPACTION GRAFTS

Anneliese D. Heiner, Thomas D. Brown and Nicole M. Grosland

Departments of Orthopaedic Surgery and Biomedical Engineering,
University of Iowa, Iowa City, IA, 52242, USA
E-mail: anneliese-heiner@uiowa.edu

INTRODUCTION

Impaction grafting with morselized cancellous bone (MCB) is increasingly utilized in revision total hip arthroplasty (THA). In this procedure, MCB is impacted into the surgical site to build up bone stock which had been lost to osteolysis or during prosthesis removal (Figure 1a). Ideally, bone remodeling proceeds from the adjacent live host bone, into the bone graft, such that eventually the MCB graft is fused into a new, contiguous cancellous lattice. Contiguously fused MCB obviously behaves differently than in the unfused state, but to date there has been no way to assess an impaction graft both before and after fusion.

We have developed a method to simulate MCB fusion in the laboratory, by mixing defatted and dried MCB with an amine-based epoxy (Heiner & Brown, 2001). The mixture is impacted into a construct, then allowed to fuse. The MCB/epoxy mixture fuses into a contiguous structure whose apparent modulus in simple unconfined compression is comparable to that of virgin, unmorselized cancellous bone. The purpose of this current study was to evaluate the stiffness of fused vs. unfused impaction grafts under clinically representative circumstances of confined compression. This was done with MCB particles of a size used in human femurs during impaction grafting, using a fixture having a geometry representative of a human femur, and using impaction instrumentation and protocols representative of actual surgical practice.

MATERIALS AND METHODS

Fixturing was designed to replicate the nominal *in situ* confinement of MCB. The femoral endosteal cavity was simulated axisymmetrically from the isthmus to 20 mm below the lesser trochanter (Figure 1b); the fixture dimensions were based on normative cadaveric measurements (Noble et al., 1988). The MCB was in the form of cubes of 4.4 mm per side, and was defatted by saline rinsing. MCB cubes used for fused impaction grafts were further defatted with chloroform, and then dehydrated. The MCB:epoxy volume ratio (disregarding MCB porosity) was approximately 3.6:1. Impactions were performed with surgical cylindrical distal impaction instruments (DePuy Orthopaedics, Warsaw, IN), and a proximal axisymmetric cone having a taper representative of surgical proximal impaction instruments (and femoral stem tips). The impaction protocol was based on accelerometer quantification of femoral impaction grafting (Heiner et al., 2003).

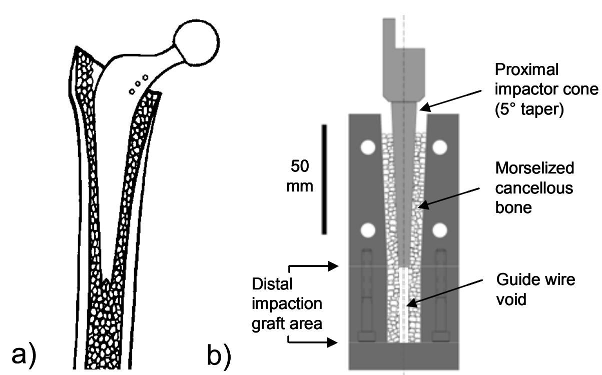

Figure 1: a) Femoral impaction graft (Gie et al., 1993), and b) schematic of femoral fixture and tapered proximal impactor cone.

Impactions were applied with a drop tower. Five unfused specimens and four fused specimens were tested.

The proximal impaction graft was tested by displacing the proximal impactor cone into the graft at 2 mm/min. The impaction graft was tested to either 1860 N or graft yield. Force/deflection stiffness was calculated. Proximal graft effective modulus was determined from the average graft stiffness, using an axisymmetric finite element model (run with ABAQUS 6.3) to account for the taper geometry of the specimens. The fixture and impactor cone were modeled as rigid bodies, fully bonded to the impaction graft, which was modeled as a linearly elastic continuum.

The distal impaction graft was tested by first removing the tapered proximal portion of the impaction graft, and then compressing the distal cylindrical portion of the graft with a flat platen at 1 mm/min. The impaction graft was tested to either 500 N or graft yield. Distal graft effective modulus was calculated from stress/strain curves computed from the force-deflection data.

RESULTS AND DISCUSSION

The fused impaction grafts formed a contiguous structure (Figure 2). The effective modulus of the unfused proximal impaction graft was 59 ± 2 MPa. MCB fusion increased the distal impaction graft effective modulus 20-fold, from 36 ± 4 MPa to 729 ± 343 MPa (Figure 3); this fused graft effective modulus is comparable to the compressive modulus of unmorselized cancellous bone (Linde et al., 1992). This MCB fusion simulation provides modulus data to be used with actual femurs, to further investigate biomechanical aspects of impaction graft fusion in revision THA.

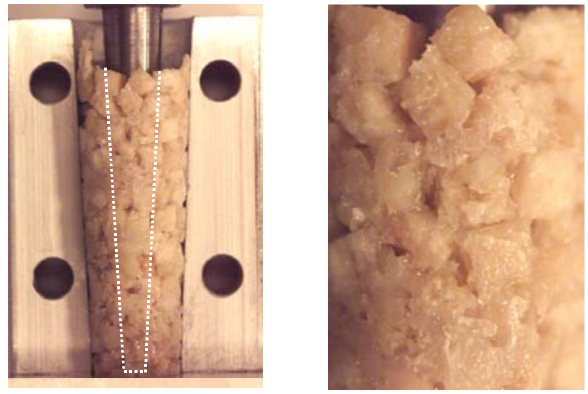

Figure 2: Fused proximal impaction graft in fixture, with impactor taper outlined (l); and close-up of graft (r).

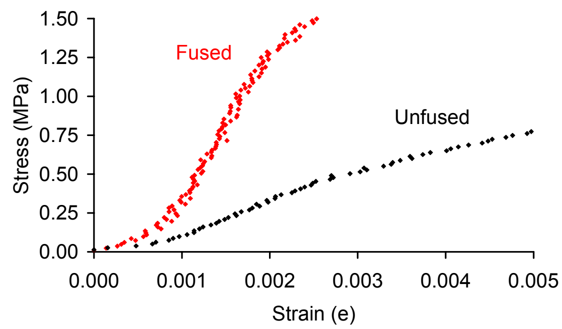

Figure 3: Representative stress/strain curves for fused vs. unfused distal impaction grafts.

REFERENCES

Gie, G.A. et al. (1993). *Orthop Clin N Am*, **24**, 717–725.

Heiner, A.D., Brown, T.D. (2001). *J Biomechanics*, **34**, 811–814.

Heiner, A.D. et al. (2003). *Proc 27th ASB,* (submitted).

Linde, F. et al. (1992). *J Biomechanics*, **25**, 359–368.

Noble, P.C., et al. (1988). *Clin Orthop* 235, 148–165.

ACKNOWLEDGEMENTS

This study was funded by NIH R03 AR46863. The authors wish to thank DePuy Orthopaedics for donating instrumentation, and Tom Baer, Liam Glennon, Jessica Leinen, and Jim Rudert for their assistance.

EVIDENCE OF SEPARATE DAMAGE AND PLASTIC BEHAVIORS IN HUMAN VERTEBRAL TRABECULAR BONE

Todd L. Bredbenner and Dwight T. Davy

Musculoskeletal Mechanics and Materials Laboratories
Case Western Reserve University, Cleveland, OH, USA
E-mail: todd.bredbenner@cwru.edu

INTRODUCTION

The understanding of nonlinear behavior (*i.e.* time-dependence, modulus degradation, and permanent stresses/strains) and the underlying mechanisms in trabecular bone remains limited. We follow the usual assumption that compliance increases are related to the development of damage and plasticity refers to the accumulation of non-recoverable strains or residual stresses. In experimental studies (Keaveny, *et al.*, 1997; Keaveny, *et al.*, 1999) or theoretical models (Zysset and Curnier, 1996) of trabecular bone, damage and plasticity are often linked explicitly. We investigated the separation of damage and plastic behaviors using experimental and analytical investigations by 1.) examining apparent specimen behavior and 2.) applying a constitutive model assuming independent plastic and damage variables along with finite element methods to specimen response.

METHODS

Using established testing methods (Morgan, *et al.*, 2001), cylindrical specimens of vertebral trabecular bone with anterior-posterior (AP), medial-lateral (ML), or superior-inferior (SI) primary orientation were subjected to 4 trapezoidal strain-controlled loading pulses. The first and third pulses had a peak strain of 0.1% and were "diagnostic" and intended to produce negligible damage. The second and fourth pulses had peak strain levels of 0.8% and 1.2% strain to produce successive levels of damage accumulation. Hold periods were 60 sec. and subsequent zero-strain recovery periods were 180 sec. for each pulse. Axial stress-strain data between 0.004% and 0.09% strain for each trapezoidal pulse was fit using a quadratic least-square regression and tangent moduli were defined as the slope of the regressions at zero strain (Bredbenner and Davy, 2003a).

A multiaxial constitutive model for vertebral trabecular bone was developed on the basis of an additive decomposition of strain with viscous, damage, and plastic strain components describing material time-dependence, stiffness degradation, and permanent deformation, in addition to linear elastic strain components. This unified model and an iterative solution scheme were implemented within finite element analyses (FEA) and applied to the experimental response for a typical SI specimen for the full first damaging trapezoid and reloading period of the second damaging pulse (Bredbenner and Davy, 2003b).

RESULTS

A total of 6 AP, 1 ML, and 9 SI specimens were successfully tested. Paired comparison between tangent moduli for all specimens showed a small but significant reduction following the first diagnostic pulse (0.75% mean modulus reduction, p-value = 0.008). Following unloading for the first diagnostic pulse, residual stresses relaxed to negligible levels when allowed to recover at zero strain (Fig. 1).

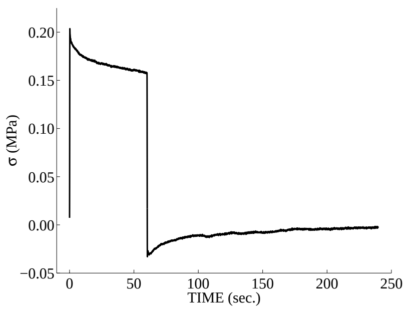

Fig. 1: Experimental response (SI specimen)

The finite element model predicted the experimental response to the first loading ramp quite well and captured the basic features of the reloading ramp, including the stress plateau (Fig. 2.). However, the FEA model did not fully represent the residual strain or hysteresis of the response.

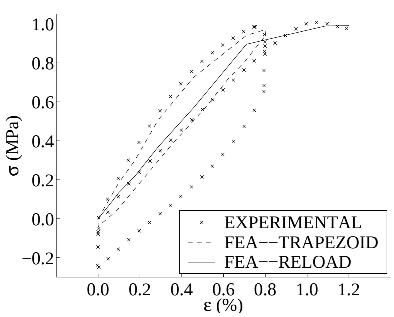

Fig. 2: Experimental vs. FEA response

DISCUSSION

Small, but significant, modulus reduction is demonstrated following the first diagnostic pulse with a peak strain magnitude of 0.1%, well below the yield strain. This evidence, along with studies of damage accumulation under fatigue loading in trabecular bone (Bowman, *et al.*, 1998; Haddock, *et al.*, 2000), calls into question the assumption of explicit coupling of damage and plastic response, at least prior to material yield.

The ability to predict damage measures, such as evolving and accumulated modulus degradation, was achieved despite less satisfactory prediction of permanent deformation, providing further evidence that apparent plastic and damage effects may not be intrinsically related, as often assumed. The actual relationship, particularly the possibility of both coupled and uncoupled damage accumulation, needs further study.

Distinction has been reported between brittle and ductile damage characteristics for trabecular and cortical bone (Keaveny, *et al.*, 1999; Norman, *et al.*, 1998). In continuum damage mechanics theory, unilateral constraints can be imposed on damage evolution (*i.e.* crack closure effects), so that modulus degradation varies with loading conditions, as well as damage accumulation. Although no such distinction is made in the present study, this type of restriction may also lead to improvement in modeling the residual (plastic) response and further work is necessary to determine whether such restriction on the damage description is warranted. It remains that the combined history and path dependence of the mechanical behavior provides a challenging set of problems, even with the controlled geometry and loading of experimental investigations.

REFERENCES

Bowman, SM, *et al.* (1998). *J. Biomech. Eng.*, **120**, 647-654.

Bredbenner, TL, Davy, DT. (2003a). *Trans. ORS*, **28**, 422.

Bredbenner, TL, Davy, DT. (2003b). *ASME Summer Bioengineering*, (accepted).

Haddock, SM, *et al.* (2000). *Trans. ORS*, **25**, 733.

Keaveny, TM, *et al.*, (1997). *J. Orthop. Res.*, **15**, 781-787.

Keaveny, TM, *et al.*, (1999). *J. Orthop. Res.*, **17**, 346-353.

Morgan, EF, *et al.* (2001). *J. Biomech. Eng.*, **123**, 1-9.

Norman, TL, *et al.*, (1998). *Bone*, 23, 303-306.

Zysset, PK, Curnier, A., (1996). *J. Biomech.*, **29**, 1549-1558.

BIOMECHANICAL AND BODY COMPOSITION FACTORS AS PREDICTORS OF OSTEOARTHRITIS AND POST-MENOPAUSAL OSTEOPOROSIS

Jean L. McCrory[1,3], Anne L. Harrison[2], and Jody L. Clasey[1]

[1] Department of Kinesiology and Health Promotion, [2] Department of Physical Therapy, University of Kentucky, Lexington, KY USA
[3] Neuromuscular Research Laboratory, University of Pittsburgh, Pittsburgh, PA USA
E-mail: mccroryjl@msx.upmc.edu web: http://www.pitt.edu/~neurolab

INTRODUCTION

Osteoporosis (OP) and osteoarthritis (OA) are recognized as major age-related health problems that disproportionately affect women. Anecdotally, many of the predictors for OP and OA appear to be inversely related, which has led to the theory that these diseases are mutually exclusive of one another (Dequecker et al., 1996).

Knee adduction moment and bodyweight (BW) were found to be predictive of medial tibial BMD (Hurwitz et al., 1998). In a comparison of women with OA to women with post-menopausal OP, no differences in gait mechanics were noted between groups when joint forces and moments were normalized to BW (McCrory, et al., 2002). However, when the variables were compared in units of Newtons, all gait kinetics were significantly different between groups, indicating that BW may be the mediating factor (McCrory et al., 2002).

The purpose of this investigation was to determine which kinematic, kinetic, and body composition variables were discriminators between primary OA and post-menopausal OP.

METHODS

Thirty-one post-menopausal women aged 50 to 85 received a standing bilateral A-P knee x-ray and a dual energy x-ray absorptiometry (DXA) scan of their femoral neck. Women with knee OA rated 2 or 3 on the Kellgren-Lawrence scale were placed in the OA group (n=12, 68.3±7.4yrs, 1.62±0.06m, 79.4±12.8kg). Women with proximal femoral BMD two SD below normal were placed into the OP group (n = 10, 74.4±7.9yrs, 1.64±0.06m, 61.2±10.0kg).

A gait analysis was performed on each subject using a 6-camera system (60 Hz) interfaced with a force plate (600 Hz). Five good trials of the most affected leg (OA group) or a random leg (OP group) were collected. Body composition measures were determined using total body DXA scans.

Gait analysis and body composition variables included in the statistical model are listed in Table 1. Stepwise discriminant function analyses were performed separately on the kinematic, body composition, ground reaction force, joint force, and joint moment data. Variables significant at the 0.10 level in the preliminary analyses were used in a subsequent discriminant function analysis to identify the factors that best discriminate between the injured and control groups.

RESULTS

Eight variables were found to be significant discriminators between the groups. Total body BMC (TB BMC) was the most predictive measure in the analysis, followed by impulse, knee range of motion, BW, age, hip extension, knee adduction moment during loading, and the active GRF peak. The mean values for these variables are listed in Table 2. The prediction equation is as follows:

D = -16.1 TB BMC +22.7 Impulse +7.6 Knee ROM + 9.21 BW –1.4 Age -10.1 Hip

Extension –3.3 Passive Knee Adduction Moment +2.0 Active Peak.

Table 1: Variables Included in the Statistical Model

Kinetics	**Kinematics**	**Body Composition**
Active and Passive GRF	Knee Flexion in Stance	Total Body Fat Mass
Active and Passive Hip Comp Force	Knee Flexion in Swing	Total Body Mineral-Free Lean Mass
Active and Passive Knee Comp Force	Knee Extension in Stance	Total Body Bone Mineral Ctnt
Active and Passive Hip Add Moment	Knee and Hip ROM	Total Body % Fat
Active and Passive Knee Add Moment	Hip Flexion in Stance	Height
Int and Ext Hip Rot Mnt	Hip Flexion in Swing	Body Weight
Int and Ext Knee Rot Moment	Hip Extension in Stance	Age

DISCUSSION

Our purpose was to determine which kinematic, kinetic, and body composition variables best discriminate between women with post-menopausal OP and those with primary OA. Eight variables were found to do this. It is not surprising that TB BMC is the most significant predictor because the OP group, by definition, had low bone density and the OA group did not.

Our results confirm those of Hurwitz et al. (1998) in that a greater knee adductor moment and BW were predictors of medial tibial bone mineral density in individuals with knee OA.

Previously in the same subjects, ANOVAs were performed on the kinetic and GRF data and significance was only found when compared in units of actual force, not bodyweight normalized (McCrory et al., 2002). Only age, weight and TB BMC ($p < 0.05$) were found to be significantly different between the groups in the present study.

Future studies that include the use of a healthy control group will allow researchers to determine if, compared to a healthy population, the eight discriminators are able to predict whether women are likely to develop OA or OP.

Table 2: Mean ± SD measures of variables that best discriminate between the OA and OP groups.

Variable	**OA**	**OP**
TB BMC (kg)	2.62 ±0.57	1.74±0.51
Impulse (BW sec)	0.52±0.04	0.57±0.08
Knee ROM (º)	57.3±6.9	60.1±8.7
Weight (kg)	79.5±12.7	63.0±11.3
Age (yrs)	69.9±8.2	74.1±6.9
Hip Extension (º)	5.1±8.0	11.6±10.6
Passive Knee Add Moment (Nm/kg)	0.33±0.17	0.30±0.14
Active Peak (BW)	1.07±0.08	1.12±0.12

SUMMARY

Eight of the gait and body composition variables significantly discriminated between OA and OP.

REFERENCES

Dequecker, J et al. (1996). *Br. J Rheum*. **35**: 813-29.
Hurwitz DE et al. (1998). *J. Biom*. **31**: 423-30.
McCrory JL et al. (2002). *Proc. WCB2002*. Calgary, AB, August 3-9.
Stewart A and Black AJ (2000). *Cur. Opin Rheum*. **12**: 464-467.
Wardlaw GJ. (1988). *Am. Dietc Assn*. **88**: 17-25.

ACKNOWLEDGEMENTS

This research was supported by the University of Kentucky, and by the UK GCRC Grant NIH/NCRR MO1 RR02602.

WORKSITE TRIPS AND FALLS: EFFECT OF AGE AND HANDLING SMALL LOADS

Shirley Rietdyk[1], James D. McGlothlin[2] and Steven R. Torgerud[1]
[1]Biomechanics Laboratory, [2]School of Health Sciences, Purdue University, IN, USA
E-mail: srietdyk@purdue.edu

INTRODUCTION

Gait is a complex, unstable task: the inertial load of the upper body must be controlled while the lower limbs are coordinated to provide forward movement and adequate ground clearance. Skilled locomotor behavior in the workplace is challenged by factors such as uneven walkways, handling loads, and the health of the sensory and neuro-muscular systems. Therefore, it is not surprising that pedestrian-fall accidents are the second largest cause of unintentional workplace fatalities (Leamon and Murphy 1995).

Handling loads compounds the inertia and momentum of the trunk and obstructs the view of the feet relative to the environment; information critical for appropriate foot placement and clearance (Patla, 1998).

The purpose of this study was to highlight age-related and load handling-related factors that may predispose workers to trips and falls while accommodating a raised surface.

METHODS

Participants were ten younger males (27.2 ± 4.3 yrs.) and eight older males (55.1 ± 4.9 yrs.), who worked as roofers for the previous two years, and were free from any known neuromuscular disorder. Subjects walked at a self-selected pace down a 10 m walkway, and accommodated a raised surface (0.15 m high, 1 m wide, 3.7 m long). Ten trials of the following load handling conditions were observed: (1) no load, (2) an empty box (negligible mass) and (3) the same box loaded with the equivalent of 5% body mass.

Infra-red emitting diodes were placed bilaterally on the toe, heel, ankle, knee, hip, shoulder, elbow and head and recorded with Optotrak (NDI).

RESULTS AND DISCUSSION

This paper will focus on the foot clearance, foot placement, trunk motion and the momentum of the head, arms and trunk (HAT) about the hip. Load handling effects on the risk of tripping are described first, followed by age effects. There were no interaction effects (load by age).

The visual obstruction due to carrying the load did not alter foot clearance or placement, but did alter the trunk vertical position for both younger and older workers. The three conditions observed: no box, empty box and box with weight allowed us to differentiate between the effects of carrying a weight versus obstructed vision. Foot clearance and placement for the no box condition were not significantly different from the empty box condition. Therefore, obstruction of the view of the foot relative to the environment did not alter foot control. Patla (1998) showed that young non-construction workers with similar, but slightly larger, loss of visual information increased their toe clearance. The differences across workers and non-workers could result from either the magnitude of the visual information obstructed and/or the chronic exposure of workers to load handling in a cluttered environment: workers may not rely on a combination of visual and somatosensory cues, rather they may rely on somatosensory cues alone. The only observed change due to the visual loss was a more vertical trunk position as each foot crossed the surface edge (1.5 deg. decrease, $p < 0.001$).

Handling the load did not alter toe clearance or foot placement, but did increase trunk control for both younger and older workers. Although the load was relatively small (5% body mass), the workers significantly decreased trunk angular range and trunk angular velocity range (Table 1) when carrying the load. A more stable trunk minimized visual and vestibular disturbances. Because the stride length and hip horizontal velocity were not altered, it appears that the trunk angular motion is controlled directly rather than resulting from significantly slower gait or shorter step length. An interesting finding is the lack of change in HAT angular momentum about the hip joint when handling the load, despite decreases in angular velocity (Table 1). As inertia increased due to the load, it appears that the nervous system determined the required reduction in trunk angular velocity to maintain a constant momentum. Therefore, HAT angular momentum appears to be a well-controlled variable in younger and older roofers.

When accommodating raised surfaces, older workers demonstrated greater control of trunk angular movement, but had an increased risk of tripping, and they adopted a foot placement strategy which reduced the chance of recovery if a trip occurred. Visual and vestibular disturbances were minimized in the older roofer due to decreased range of trunk angular displacement and velocity (Table 2). Again, it appears that the nervous system reduced the trunk angular velocity as inertia increased, in order to maintain HAT angular momentum about the hip (Table 2). The older subjects had a lower foot clearance, which increased the risk of tripping. The older subjects placed the trail foot farther away from the edge of the step (Table 2): although this placement kept the center of mass closer to the supporting foot, it reduced correction time and potential sites for foot placement in the event of tripping with the lead foot. The changes in foot control are similar to non-construction older females (Begg and Sparrow, 2000), although the clearance by roofers is almost 2 cm smaller. Because many roofers scuffed their shoe on the surface edge, we feel the decrease in toe clearance does not reflect more precise foot control by the roofers, rather it may be due to accumulated injury and fatigue factors. Comparison of clearance magnitude and variability with non-construction workers is in progress and will be presented at the meeting.

SUMMARY

The non-optimal foot clearance and foot placement puts the older worker at a greater risk of tripping than the younger worker. To reduce the possibility of a fall should tripping occur, both younger and older roofers controlled the angular momentum of the upper body and the load by minimizing trunk angular velocity. The older worker adopted a single strategy for enhancing safety beyond that of the young workers: they demonstrated greater trunk control.

REFERENCES

Begg, Sparrow (2000) *J Geron,* **55A**: M147-54
Leamon, Murphy(1995)*Ergonomics*,**38**:487-98
Patla (1998) *Ecolog Psych,* **10**:284-302

ACKNOWLEDGEMENTS

The authors would like to thank Tonya Adkins, Alex Baria, Mark Knezovich, Abby Mitchell, Scott Potts, Sarah Scheu and David True for their assistance during data collection and analysis. This research was supported by the National Institute for Occupational Safety and Health Pilot Project Research Training Program of the University of Cincinnati Education and Research Center Grant #T42/CCT510420.

Table 1: Effect of load: variables which describe the tripping risk and trunk control for 18 subjects.

Variable	**No Box**	**Loaded Box**	**Sig.**
Foot clearance	7.1 ± 1.9	7.5 ± 1.9	p = 0.194
Placement of trail foot (% of step length)	29.8 ± 4.3	30.7 ± 4.5	p = 0.148
Range of trunk angle in one stride (deg.)	17.2 ± 3.0	16.4 ± 3.1	p < 0.001
Range of trunk angular velocity (deg./s)	92.0 ± 13.6	87.6 ± 14.5	p = 0.001
Range of HAT angular momentum ($kg.m^2/s$)	15.2 ± 4.1	15.1 ± 4.1	p = 0.698

Table 2: Effect of age: variables which describe the tripping risk and trunk control.

Variable	**Younger (N=10)**	**Older (N=8)**	**Sig.**
Foot clearance	7.7 ± 1.9	6.9 ± 1.9	p < 0.001
Placement of trail foot (% of step length)	28.8 ± 4.2	32.0 ± 3.6	p < 0.001
Range of trunk angle (deg.)	17.9 ± 3.1	16.1 ± 2.8	p < 0.001
Range of trunk angular velocity (deg./s)	92.2 ±12.7	89.1 ± 16.0	p < 0.001
Range of HAT angular momentum ($kg.m^2/s$)	15.3 ± 3.7	15.2 ± 4.4	p = 0.645

GENDER SPECIFIC RESPONSE TO EXERCISE IN C57BL6/129 MICE

Wallace, J.M.[1]; Rajachar, R.M.[1], Chen, X.[2]; Shi, S.[2]; Robey, P.G.[2]; Young, M.F.[2]; Kohn, D.H.[1,3]

[1] Department of Biomedical Engineering, University of Michigan
[2] National Institute of Dental and Craniofacial Research/National Institutes of Health
[3] Department of Biologic and Materials Sciences, University of Michigan
E-mail: dhkohn@umich.edu

INTRODUCTION

Adult peak bone mass is an important predictor of fracture risk (Akhter 1998). The decline in bone mass and strength in men and women with age may contribute to increases in skeletal fragility with age. Therefore, maximizing peak bone mass may protect against bone loss and fracture (Iwamoto 1999). Mechanical loading is recognized as a valuable way to maintain peak bone mass and structural integrity (Yingling 2001, Frost 1987). Exercised-based animal models have shown a link between mechanical loading and maintenance/increase of bone structural and mechanical properties (Yingling 2001, Sakakura 2001, Mosekilde 1999). However, most of these models apply an exercise regimen of 2-5 months, and few have documented gender-specific responses to exercise. The purpose of this study was to establish a physiologically-relevant murine exercise model and use this model to test the hypothesis that the geometric and mechanical properties of male bones are more responsive to exercise than female bones.

METHODS

Forty C57BL6/129 mice were bred in-house at the NIH (NIDCR animal approval protocol # NIDCR 001-151). Animals were housed in standard caging and given unrestricted access to food and water, and cage activity was unrestricted. At 2 months of age, mice were assigned randomly to 1 of 2 groups (exercise and control; 10 males and 10 females in each group). Exercise consisted of running at 10 m/min on a treadmill at a 5° incline, 30 min/day for 21 days (Columbus Instruments, Columbus OH, model 1055M). Mice were sacrificed on day 24. Left femora and tibiae were harvested, stripped of soft tissue and stored in a buffered calcium solution (with 0.01% sodium azide as an antibiotic) at -80º C for later use. Bones were tested to failure in 4 point bending using a custom-designed, solenoid driven loading apparatus (Rajachar 2003) at a rate of 0.01 mm/sec. Femora were tested in the AP direction (posterior surface in compression) and tibiae were tested in the ML direction (lateral surface in compression). Load and deflection were recorded, from which strength, energy, stiffness and deformation properties were derived (Turner, 1993). After fracture, the bones were sectioned at the fracture site. Geometric parameters (cross sectional area, ML and AP width, cortical thickness, centroid and moment of inertia) were determined using an inverted light microscope and digital analysis software (Nikon Eclipse 300T, Image Pro-Plus v4.1, Matlab v5.3). Statistical analyses were performed using 2-way ANOVA (SigmaStat v2.0).

RESULTS AND DISCUSSION

Male tibiae responded to exercise via an

increase and redistribution of the amount of tissue, as indicated by the significant increases in cross sectional area (p=0.045) and ML width (p=0.036), and marginally significant increases in AP width and moment of inertia (Table 1). These geometric changes were accompanied by a significant increase in post-yield displacement (p=0.018), but a decrease in yield force (p=0.027) and ultimate strength (p=0.026). Exercise did not alter the geometric properties of female tibiae, but there was a trend toward increased strength. No exercise-induced effects were seen in male femora, but female femora exhibited a significant increase in section modulus (p=0.011) and marginally significant increases in stiffness (p=0.072) and ultimate strength (p=0.082).
Although 3 weeks of exercise elicited a formation response, the tissue is still osteoid and does not have the mechanical integrity of fully organized and mineralized lamellar bone. It is possible that given more time between terminated exercise and sacrifice, bone would mature and increase in strength. Three weeks of exercise were able to elicit an osteogenic effect, compared to other exercise regimens, which prolonged exercise up to 8-18 weeks. This data establishes a simpler exercise protocol than those previously used. Gender-specific effects may generally be hypothesized to be hormonally related. A previous study demonstrated that the amount of load-stimulated bone formation in growing male rats is greater than in female rats (Mosley 2002). Our study represents the first report indicating that there is a gender-specific response to exercise in mice.

REFERENCES

Akhter, et al. (1998). *Calif Tissue Int*, **63**, 442-449.
Frost, (1987). *Bone Miner*, **2**, 73-85.
Iwamoto, et al. (1999). *Bone*, **24**, 163-169.
Mosekilde, et al. (1999) *Bone*, **24**, 71-80.
Mosley,Lanyon. (2002). *Bone,* **30**, 314-319
Rajachar. (2003). Ph.D. Dissertation, University of Michigan
Sakakura, et al. (2001) *J Bone Min Metab* **19**, 159-167.
Turner, Burr, (1993). *Bone*, **14**, 595-607.
Yingling, et al. (2001). *Calcif Tissue Int*, **68**, 235-239.

ACKNOWLEDGEMENTS
NIH IPA Award

Table 1: Geometric and Mechanical Properties of Tibiae (mean ± SEM)

Property	Male Control	Male Run	Female Control	Female Run
C/S Area (mm^2)	**0.519 ± 0.042**	**0.633 ± 0.033[a]**	0.574 ±0.048	0.586 ± 0.045
AP Width (mm)	1.102 ± 0.053	1.244 ± 0.047[b]	1.143 ± 0.084	1.117 ± 0.028
ML Width (mm)	**0.899 ± 0.054**	**1.043 ± 0.034[a]**	0.913 ± 0.078	0.953 ± 0.044
Section MOI (mm^4)	0.037 ± 0.008	0.058 ± 0.006[b]	0.046 ± 0.007	0.044 ± 0.005
Yield Force (N)	**23.13 ± 2.81**	**15.96 ± 1.01[a]**	16.91 ± 3.25	23.03 ± 4.32
δ (elastic) (mm)	0.075 ± 0.014	0.046 ± 0.005[b]	0.063 ± 0.024	0.065 ± 0.014
δ (plastic) (mm)	**0.024 ± 0.008**	**0.059 ± 0.010[a]**	0.038 ± 0.007	0.028 ± 0.010
Yield Energy (mJ)	1.176 ± 0.350	0.501 ± 0.072[b]	0.814 ± 0.430	1.067 ± 0.353
Yield Stress (N/mm^2)	150.54 ± 33.34	85.02 ± 8.63[b]	129.13 ± 48.52	194.14 ± 64.53
Ult. Stress (N/mm^2)	**197.37 ± 32.20**	**116.85 ± 11.28[a]**	150.96 ± 41.16	194.43 ± 119.98
Strain ($\mu\varepsilon$)	16887 ± 2576	28842 ± 5863[b]	13702 ± 1920	13697 ± 2682

[a]Significant effect of exercise (**Bold**, p<0.05) [b]Marginal effect of exercise (0.05<p<0.10)

KINETICALLY CRITICAL REGIONS OF FEMORAL HEAD ROUGHENING

Hannah J. Lundberg[2], Kristofer J. Stewart[1], Thomas D. Brown[1, 2]

[1]Department of Orthopaedic Surgery, University of Iowa, Iowa City, IA, USA
[2]Department of Biomedical Engineering, University of Iowa, Iowa City, IA, USA
E-mail: hannah-lundberg@uiowa.edu Web: poppy.obrl.uiowa.edu

INTRODUCTION

Polyethylene debris-induced aseptic loosening is the leading cause of total hip arthroplasty (THA) failure. THA wear is highly variable and can be accelerated by counterface roughening and third body ingress; up to 40% of clinical wear rate variance may be attributable to third body effects (Orishimo, 2003). Using a sliding-distance-coupled contact finite element (FE) model of THA wear (Maxian, 1996; Brown, 2002), we identified regions of the femoral head surface that, if roughened, result in maximal THA wear.

METHODS

The FE model implemented the Archard relation (Archard, 1953) for abrasive/adhesive wear. Per this relationship, the instantaneous local wear rate can be expressed as the product of a wear coefficient (tribologically determined), contact stress (calculated using the FE model), and sliding velocity, each functions of the instantaneous local position and time. One million duty cycles were simulated for each run by adaptively updating the acetabular component FE mesh at case-specific intervals (for this case, 4×10^4 cycles or approximately 15 days of in vivo service), so as to reflect conformity/contact changes accompanying progressive material removal.

Each element of the femoral head was assigned a wear coefficient. Elements not in a roughened zone were assigned a baseline wear coefficient of 1.07×10^{-6} mm^{3}N^{-1}m^{-1}, corresponding to typical undamaged THA implants. Elements in a region designated as roughened were assigned a wear coefficient 50 times that of the unroughened case (53.50×10^{-6} mm^3 N^{-1} m^{-1}).

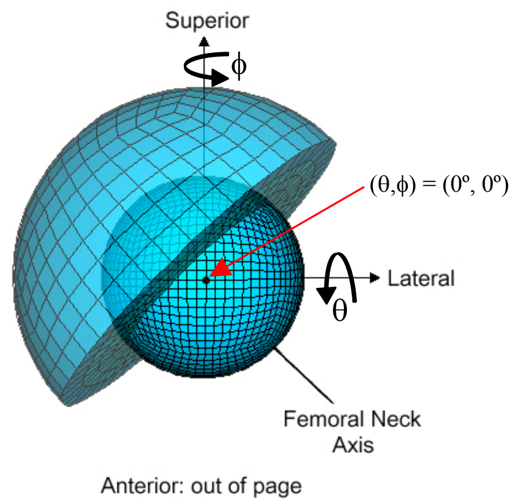

Figure 1: Sliding-distance-coupled contact finite element model. The model is of a left hip prosthesis. The femoral neck is omitted. The superior-lateral-anterior coordinate system centers at the center of the femoral head. Roughening patch centers are defined by angles θ and ϕ, where (θ,ϕ) = (0º, 0º) is on the surface of the femoral head along the positive anterior axis.

A parametric series was conducted to evaluate the effect of varying the area of roughened zones. Three zone sizes were investigated: corresponding to 4%, 10%, and 20% of the hemispherical femoral head area. The location of each roughened zone center, (θ,ϕ), was initially varied by 30º increments about the superior and lateral axes (see Figure 1). This coarse grid was used to search for kinetically critical roughened areas. A finer search grid with 10º increments then followed, concentrating on regions around local maxima identified by the coarse search.

RESULTS AND DISCUSSION

Volumetric wear (see Table 1) was approximately 3.5, 7.5, and 13 times that of a smooth femoral head for the respective 4%, 10%, and 20% roughening patch sizes. The volumetric wear propensity distribution (see Figure 2A) shows two main critical areas for all roughening sizes resulting in maximal wear, with a smooth gradient leading to each maximum.

Table 1: Results of wear simulations.

Patch Size (% hemispheric area)	Volumetric Wear (mm^3/year)	Linear Wear (mm/year)	Critical Patch Location (θ, °)	(ϕ, °)
0%	20.41	0.08	n/a	n/a
4%	70.54	0.21	-70	160
10%	155.40	0.37	-70	180
20%	268.02	0.58	-60	0

Wear directions, defined as the direction to the acetabular node of greatest linear wear, were also calculated for each roughened patch size (see Figure 2B). The angular spread between wear directions for the respective roughening patch sizes was 60.28º, 46.25º, and 55.27º.

SUMMARY

The above data demonstrate that varying the location of femoral head roughening increased the resulting volumetric wear by greater than 13 fold, depending on the area of the roughened zone. Dramatically different wear results were obtained depending on the location of femoral head roughening. Wear directions also varied greatly, depending on both the roughened zone size and location.

Kinetically critical locations for roughening on the femoral head have been identified. All three roughened patch sizes resulted in critical patch locations on the superior-most aspect of the femoral head, indicating that critical patch locations may be relatively independent of patch size. If possible, finding ways to restrict debris access to these areas would be especially beneficial for wear reduction.

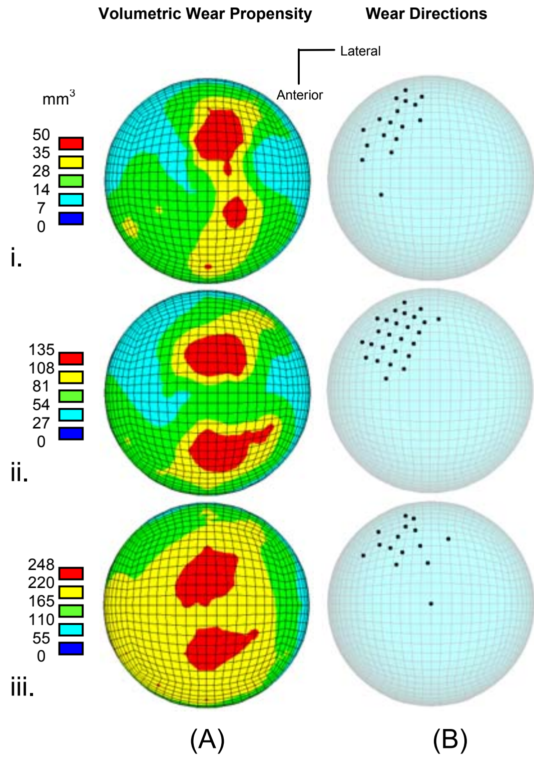

Figure 2: Volumetric wear propensity (A) and wear directions (B) for wear simulations with roughened zones constituting (i) 4%, (ii) 10%, and (iii) 20% of the hemispherical area of the femoral head. Volumetric wear propensity is defined as the wear increase above that of an unroughened femoral head, and is plotted at the center of the roughened patch from which it resulted. Wear directions are represented by black dots.

REFERENCES

Archard, J.F. (1953). *J. Appl. Phys.*, **24**, 981-988.

Brown, T.D. et al. (2002). *J. Biomech. Eng.*, **124**(6), 691-698.

Maxian, T.A. et al. (1996). *J. Biomech.*, **29**(5), 687-692.

Orishimo, K.F. et al. (2003) *J. Arthroplasty* **18**(2), 154-160.

ACKNOWLEGEMENTS

Supported by grants from the NIH (AR44106, AR47653) and DePuy, Inc. Helpful suggestions by John J. Callaghan were also appreciated.

BONE CHEMICAL STRUCTURE RESPONSE TO MECHANICAL STRESS STUDIED BY HIGH PRESSURE RAMAN SPECTROSCOPY

Olivia de Carmejane [1], Michael D. Morris [1], Rupak M. Rajachar [2,3], M. Kathleen Davis [4], Lars Stixrude [4], Mary Tecklenburg [5], David H. Kohn [2,3]

[1]Chemistry, [2]Biologic and Material Sciences, [3]Biomedical Engineering, [4]Geological Sciences, University of Michigan, Ann Arbor, MI, 48104
[5]Chemistry, Central Michigan University, Mt. Pleasant, MI 48859
E-Mail: dhkohn@umich.edu

INTRODUCTION

Age related skeletal fragility is a significant medical problem involving up to 250,000 fractures/year. Bone mass is not always an effective predictor of fragility, implying that measures of bone quality, such as composition, are also important variables.

We have reported Raman spectra showing the presence of both uncarbonated apatitic mineral and highly disordered carbonated mineral at the leading edge of fatigue-induced microcracks (Timlin et al., 2000) and at sites of catastrophic fractures in cortical bone subjected to bending (Morris et al., 2002). These studies, however, did not resolve whether the altered mineral phases were a cause or result of damage. Indentation/Raman spectroscopic imaging studies confirmed our hypothesis that changes in mineral composition result from deformation (Carden et al., 2003).

We now further hypothesize that phase changes in the mineral lattice of bone are pressure-dependent and occur concurrently with matrix changes. To address this hypothesis we assess Raman spectroscopic response of murine cortical tissue to hydrostatic pressure. These studies further demonstrate cause/effect relations between mechanical loading and compositional changes via collection of Raman data in real-time as a function of mechanical load.

METHODS

Specimens. Murine femora were harvested, stripped of soft tissue, wrapped in gauze soaked in Ca-buffered saline and stored at -30°C prior to handling. Both bone and deproteinated bone were analyzed. Bones were pulverized by snap freezing in liquid N_2 followed by grinding with mortar and pestle. Another set of bones was deproteinated in hydrazine with washing in ethanol. Powders were stored in Ca-buffered saline at 4°C (deproteinated bone) or-30°C (bone powder).

High Pressure Raman Spectroscopy. High pressure experiments (up to 3.8 GPa) employed a Bassett-type diamond-anvil cell with rhenium gaskets. The chamber was loaded with selected bone crystallites and a drop of deionized water (or deuterated water) was added as coupling fluid. At each pressure increment the hydrostatic pressure inside the cell was monitored as the 2.9 cm^{-1}/GPa shift of the diamond Raman band at 1332 cm^{-1}. In situ Raman spectra were collected in the 100-3800 cm^{-1} frequency range. Measurements were made under loading and unloading. Raman spectra were excited at 514.5 nm with Ar^+ laser operating at 2 W focused to a 2 µm spot through an epi-illumination microscope with a 50X objective. The scattered radiation was analyzed with a spectrograph operated at 2 cm^{-1} resolution and a cooled CCD detector.

Data Analysis. Spectra were baselined and bands were fitted to mixed Gaussian-Lorentzian line shapes to define band positions. Regression analyses were applied to mineral and matrix bands.

RESULTS AND DISCUSSION

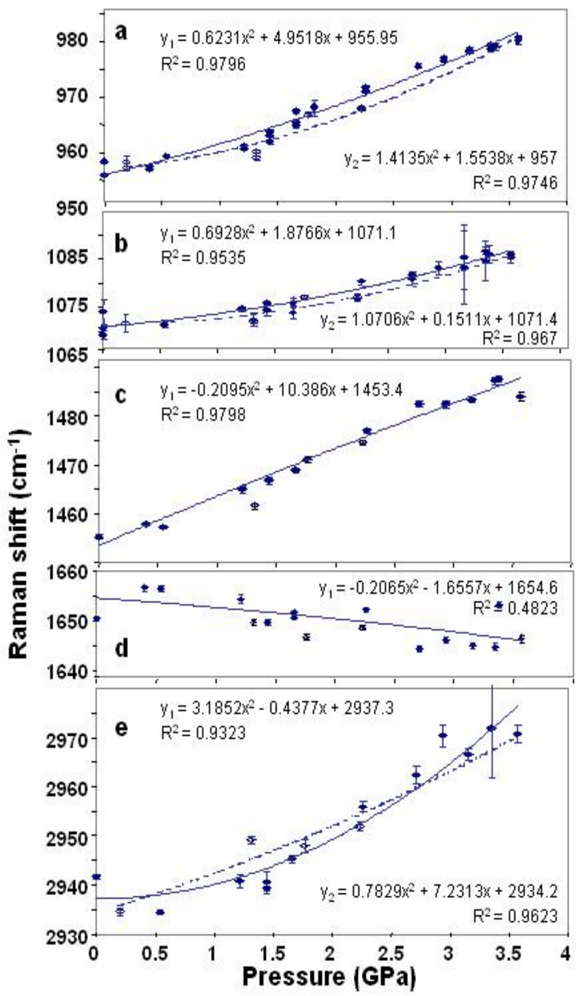

Figure 1: Pressure dependence of A) PO_4^{-3} ν_1, B) CO_3^{-2} ν_1, C) CH_2 wag, D) Amide I and E) CH_2 stretch Raman shifts for mouse bone. Loading: closed symbols and quadratic fit y_1; unloading: open symbols and quadratic fit y_2.

Shifts to higher wavenumbers were observed for most of the bands as pressure increased (Fig 1). Regression analyses determined that the pressure-dependence was a second-order relation. Since carbonate is a small, hard ion that cannot be deformed, we propose that the pressure dependence (Fig 1B) is due to movement of oxy-anions and cations within the apatitic unit cell. Amide I (Fig 1D) shows a small negative pressure dependence. The weak pressure dependence is surprising, because this band responds to changes in secondary structure and hydrogen bonding.

Unloading resulted in a return to the original band position. Comparison of band envelopes at atmospheric pressure before and after loading revealed no permanent changes such as band broadening or shoulders, implying that either the changes are reversible or the fraction of conversion is too small to measure in this experiment.

SUMMARY

Bone responds actively to mechanical stress at the lattice-level in a pressure-dependent fashion. This ultrastructural-level response is more complex than has been recognized. The spectral shifts are consistent with changes in unit cell parameter with little or no change in oxy-anion X-O bond lengths. The large changes in methylene wag are consistent with either changes in the pitch of the collagen helix or with changes in interfibril links.

REFERENCES

Timlin, J.A. et al., (2000). *Anal. Chem.*, **72**, 2229-2236.
Morris, M.D. et al., (2002). *Proc. SPIE*, **4614**, 47-54.
Carden, A. et al., (2003*). Calcif. Tissue Int.*, **72,** 166-175.

ACKNOWLEDGEMENTS

NIH P30 AR46024 (MDM), R01 AR047969 (MDM), T32 DE07057 (DHK).

BONE MORPHOLOGY CHANGES IN DDH HIPS THROUGHOUT ADULTHOOD

Heather M. Ralston and Douglas R. Pedersen

Orthopaedic Biomechanics Laboratory, University of Iowa, Iowa City, IA, USA

E-mail: doug-pedersen@uiowa.edu Web: http://mnypt.obrl.uiowa.edu/

INTRODUCTION

Development Dysplasia of the Hip (DDH) is a disease that is associated with progressive osteoarthritis at a much earlier age than the population norm. Infants diagnosed with unilateral DDH were conservatively treated throughout adolescence and are now in their fifth decade of clinical and radiographic follow-up. These patients provide a unique resource with which to quantify the natural history of bone changes following skeletal maturity. A previous study (Pedersen, 2002), showed measurable changes in bone parameters in the decade between individual 30-year and 40-year follow-ups. The differences in measurements were shown to be greater for the DDH affected hip with respect to time, than for the asymptomatic hip, which remained relatively constant between decades. With an increase in the radiograph database, the progression of morphology changes can now be observed from adolescence to current follow-ups. This study establishes a basis for comparison between asymptomatic hips and DDH hips and identifies trends in bone morphologic changes after skeletal maturity.

METHODS

Clinical and radiographic information from fifty-four patients afflicted with unilateral DDH were utilized for this study. Follow-up data were obtained from skeletal maturity (17 -20 years old) out to an average 40-year follow-up. Patients on average had a total of 3.2(±1.5) radiograph images. One hundred seventy-three radiographs were scanned at 300 dots per inch and 8-bit (256) gray scale. Assessment of radiographic information was performed with the use of a digitizing program (Lamb, 2002) written in PV~Wave (Ver. 6.1, Visual Numerics Inc.). Program users cursor-selected 32 landmarks on each radiograph, which were used to calculate common clinical measurements. Measured parameters include: Sharp's angle; the center-edge angle of Wiberg; articulo-trochanteric distance; acetabular depth, width, volume, and quotient (depth/width); percentage femoral head coverage; head-to-head ratio; and tear drop width. Data were output in spreadsheet form. Analysis began with computation of the mean and slope of each subject's values for each variable and side. These values were tested to see if the slopes and means were different with respect to affected vs affected by computing the subject differences (nonaffected – affected) and then doing 3 different tests on the differences: t test (this is the same as a paired t test since it is done on the differences), sign test, and signed rank test. Since the signed rank test is the most robust and will not be affected nearly as much by outliers, these test results are reported.

RESULTS AND DISCUSSION

A novel nonparametric statistical analysis (Pedersen, 1998) determined the temporal relationships between asymptomatic and DDH affected hips throughout adulthood.

The signed rank test confirms that there are significant differences in the rate of change (temporal slope) of the measured radiograph variables. The p-values for each parameter are provided in Table 1. These values relate the significance of measured variables to quantify morphologic changes in both asymptomatic and DDH affected hips. Ratios of variables, such as percentage of femoral head coverage and depth/width quotient, (Figure 1) are representative of the differences between asymptomatic and DDH affected hips. The individual measurements and group regression slopes are graphed in Figure 2.

SUMMARY

This study shows that there are significant measurable differences between the natural histories of unilateral DDH hips and their contralateral asymptomatic hips, evaluated over several decades after skeletal maturity.

REFERENCES

Lamb, C. A. et al (2002). *Trans. ORS*, 938.
Pedersen, D., et al (2002). *Trans. ASB*, 609.
Pedersen, D., et al (1998). *JOR,* 557-63.

ACKNOWLEDGEMENTS

The Whitaker Foundation

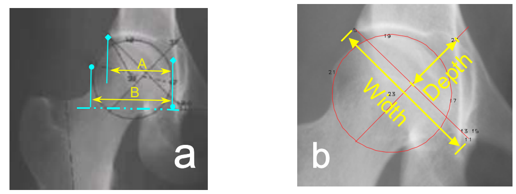

Figure 1: a) Percentage femoral head coverage; b) Acetabular quotient.

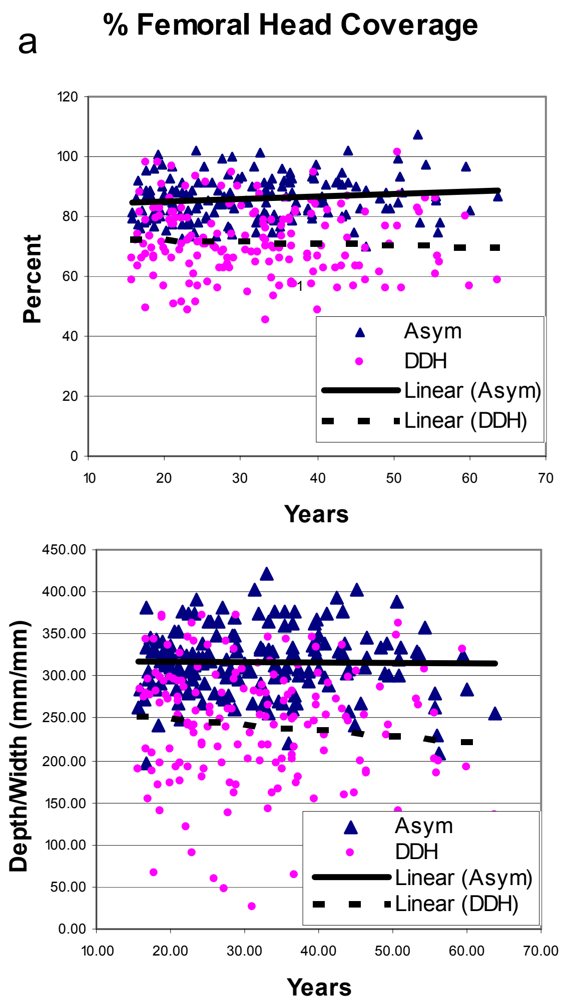

Figure 2: a) Percentage of femoral head coverage; b) Quotient; measured for all subjects.

Table 1: Probability values of the rate of change for the measured variables, ranked from most significant variable to least significant (left to right).

HHR	FemHead %	Quotient	Depth	Volume	Width	Lat. Dist.	CE Angle	ATD	Sharp Angle	Tear Drop
0.0002	0.0003	0.0023	0.0079	0.0502	0.2039	0.2231	0.2614	0.5776	0.5834	0.6928

THREADED END SHORT FIBER REINFORCEMENT OF BONE CEMENT

Y. Zhou [1], C. Li [1], J. E. Renaud [1], J. J. Mason [1]
[1] Department of AME, University of Notre Dame, Notre Dame, IN, USA
E-mail: yzhou1@nd.edu Web: www.nd.edu/~ame

INTRODUCTION

Poor interfacial properties between reinforcement fibers and a Polymethylmethacrylate (PMMA) matrix may result in debonding between them, which is a major failure mechanism for fiber reinforced bone cement. Optimization of the shape of the fibers can improve load transfer between the fibers and matrix. This paper presents a procedure for structural shape optimization of short reinforcement fibers using finite element analyses. The design objective was to improve the mechanical properties. The effects of fiber shape on the mechanical properties were evaluated in this paper.

METHODS

The composite is modeled by a representative volume element (RVE) composed of a single short fiber embedded in the PMMA matrix. Due to symmetry, only one quarter of the RVE was used in the finite element calculation (Figure 1). In contrast to most previous work on this subject, contact elements are employed between the fiber and matrix to model a low strength interface. Most models assume a perfect bond. Residual stress, due to matrix cure shrinkage and/or thermal stresses (Freund, 1992), is also included in the model. The interface is perfectly bonded before the fiber is subjected to loading. When the tensile stresses σ_N of the contact elements are larger than the residual stress σ_{Ns}, i.e. $\sigma_N > \sigma_{Ns}$, the interface will debond. It is assumed that the interface experiences Coulomb frictional contact after the debonding has taken place (Povirk and Needleman, 1993; Freund, 1992).

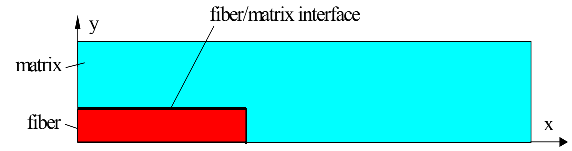

Figure 1 Model of short fiber in matrix

A procedure for structural shape optimization was developed in this study. Shape optimization was performed using the finite element software ABAQUS and the optimization software StudyWizard. In the process, StudyWizard retrieved ABAQUS results and calculated the constraint values and objectives. A new set of design variable values was then created with an optimization algorithm. These values were converted into new node coordinates by modifying the ABAQUS input file to realize shape optimization.

We examined two objective functions, stiffness-based and fracture toughness-based, with two different load conditions. To evaluate the stiffness of the model, the composite Young's Modulus was used as the objective function. The apparent composite modulus is calculated by:

$$F(X) = E_c = \frac{\sigma}{\varepsilon} = \frac{PL}{A(\Delta L)} \tag{1}$$

where ΔL is the displacement loading applied to the model of length L and cross-sectional area A, while P is the total reaction force at the right end of the matrix in direction X. To evaluate the fracture toughness of the composite, a pull out test was simulated. In this case, the concept of strain energy density (SED) was used to address crack initiation, stable crack growth and the onset of rapid fracture (Katoozian and Davy, 2000). And the total strain energy density U of the fiber was used as the objective function

$$F(X) = U = \sum U_i \qquad (2)$$

where U_i is the SED of the element. The displacement loading was applied to the left end of the fiber. In the optimization, the volume fraction of fiber is assumed to be 10% at the start and is limited to 15% in an attempt to limit fiber volume fraction effects during optimization.

RESULTS AND DISCUSSION

In the stiffness-based optimization, the objective function was improved by 62% when compared with the conventional straight short (CSS) fiber in the case of a weak bond interface and reached 92% of the composite stiffness with a perfect bond interface. While in the fracture toughness-based optimization, the objective function was improved from nearly zero to about 90% of the system with a perfect bond interface. The typical final geometry of the fiber looks like a threaded end short (TES) fiber (Figure 2b). As shown in Figure 2, the stresses generated in the TES fiber were much higher than those in the CSS fiber and were similar to the stresses generated in the CSS fiber with a perfect bond interface. This indicates that more load is transferred from the matrix to the TES fiber through the threads in the enlarged end. The shape reflects the fact that for discontinuous fiber reinforced composites with a weak interface, the total force needed to slide the fiber against frictional resistance is actually localized at the end of the fiber (Freund, 1992). Thus, to improve the efficiency of load transfer, most shape changes focus on the fiber end, which results in many threads at the end of the fiber. Obviously, the mechanism of load transfer between the fiber and matrix was changed for the TES fiber reinforced composites. The load transferred from the matrix to the fiber was not solely by friction force in the interface as in the CSS fiber but also by mechanical interlock between the fiber and matrix. In this case, the composite mechanical properties are not governed by the fiber/matrix interface but depend on the mechanical properties of fiber and matrix materials themselves.

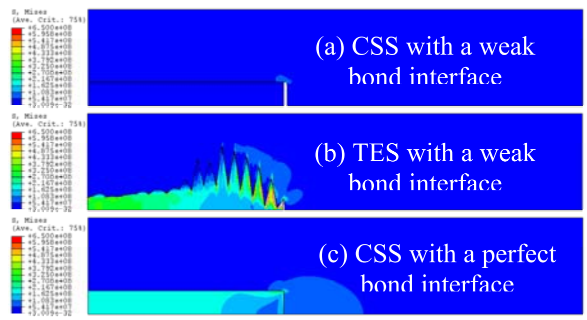

Figure 2 Mises stress in the stiffness models

SUMMARY

This study presents a procedure for structural shape optimization to improve the load transfer between short fibers and a PMMA matrix. The results demonstrate that a TES fiber can significantly improve the load transfer between the fibers and the matrix through the introduction of efficient mechanical interlock.

REFERENCES

Povirk, G.L., Needleman, A. (1993). *ASME Journal of Engineering Materials and Technology,* **115**, 286-291.

Freund L.B. (1992). *Eur. J. Mech., A/Solid,* **11** (1), 1-19.

Katoozian, H., Davy, D.T. (2000). *Medical Engineering & Physics,* **22**, 243-251

ACKNOWLEDGEMENTS

Supported by the Indiana 21st Century Research and Technology Fund.

A 3D METHOD FOR SEGMENTING AND REGISTERING CARPAL BONES FROM CT VOLUME IMAGES

Georgeta E Marai[1], David H Laidlaw[1], James C Coburn[2], Mohammad A Upal[3], Joseph J Crisco[2,3]

[1] Department of Computer Science, Brown University, Providence, RI
[2] Department of Mechanical Engineering, Brown University, Providence, RI
[3] Department of Orthopedics, Brown Medical School/Rhode Island Hospital, Providence, RI
E-mail: AUpal@LifeSpan.ORG

INTRODUCTION

The purpose of this study was to measure the accuracy of a new method to extract three-dimensional *in vivo* carpal kinematics from CT volume images. Recent advancements in three-dimensional imaging have offered the opportunity to examine *in vivo* carpal kinematics accurately and without invasive procedures. Our previous method requires manual segmentation of the CT volume for each wrist posture, which is labor intensive (Crisco et al. 1999). Our new method requires the manual segmentation of only one scan. Here, we report the kinematic accuracy of this new method in measuring 3D motion of ten bones of the wrist.

Our algorithm works in two stages. In the first stage, each CT volume image is automatically segmented by a tissue classifier that estimates each voxel's distance to the nearest boundary between tissues. The distance to a boundary between cortical bone and other tissues defines where the cortical bone surface lies within the CT data. This estimate accounts for the blurring or partial-volume effects inherent to CT imaging. In the second stage, a 3D polyhedral model of each wrist bone, reconstructed from the manually segmented neutral posture, is matched to the tissue-classified volume images to obtain the new bone position and orientation. For each vertex in the polyhedral model, its distance to a bone boundary is looked up in the tissue-classified CT volume. The bone position is then adjusted iteratively to minimize these distances.

MATERIALS AND METHODS

Specimen Preparation: We used one cadaveric specimen in four different positions to investigate the accuracy of this method. The cadaveric specimen was separated into two components: the hand, composed of the eight carpal bones, and the forearm, composed of the distal third of the radius and ulna. The skin and other soft tissues were removed, and then each component was encased in a plastic resin, to prevent relative motion between any bones. Seven radiopaque ceramic spheres of various high tolerance diameters (6.35 to 19.05 ± 0.002 mm) were then rigidly fixed to each component (Figure 1).

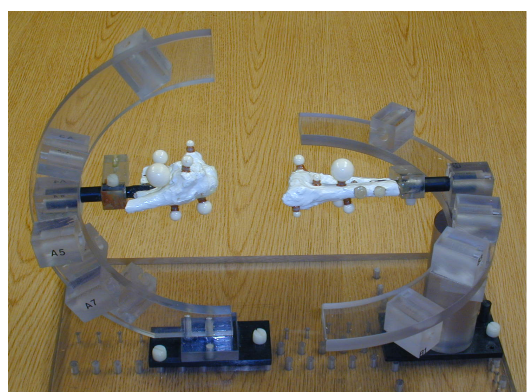

Figure 1: Cadaver positioning jig— hand and forearm components with affixed spheres

Image Acquisition: This specimen was placed in four different positions, and axially scanned using a GE Highspeed

Advantage CT (GE Medical Systems, Milwaukee, WI). Volume images were obtained with the voxel dimensions of 0.3125 X 0.3125 X 1 mm^3. Cortical bone contours from one single volume image were manually extracted using Analyze™ software (Mayo Foundation, Rochester, MN).

Data Analysis: For each specimen component, "gold standard" rotation and translation transformations were obtained using the sphere centroids. All seven spheres were used in the rigid body calculation by a method of least squares. Rotation and translation transformations were converted to helical axis of motion (HAM) parameters. The kinematic error of the algorithm was defined as the differences in the HAM parameters from the "gold standard" sphere values.

RESULTS AND DISCUSSION

Mean distance between all possible pairs of sphere centroids over the four scan positions was 0.52mm (S.D. 0.31mm, range 1.33mm). As a result of the small variation in intersphere distances, the specimen components were assumed to move as rigid bodies, allowing for direct comparison of sphere and bone motion. When comparing the registration algorithm with the "gold standard", the mean carpal bone rotational error was less than 0.5º for all bones (Figure 2). Mean bone translational error was less than 2.0mm, except for the pisiform and trapezoid (Figure 2).

The advantage of this algorithm is that it does not require the manual segmentation of each individual scan. The limitation is that manual segmentation must still be performed on one scan. The error analysis described evaluates the kinematic accuracy of the algorithm and all aspects of the scanning and image processing. As expected, the accuracy was better for larger bones and worse for smaller and more spherical bones. Our method dramatically reduces the user interaction time, while maintaining the accuracy and stability of the manual approach. The method would also be applicable to bones of other joints.

REFERENCES

Crisco, J.J., McGovern, R.D., and Wolfe, S. W. (1999). *J Orthop Res*, 17(1), 96-100.

ACKNOWLEDGMENTS

Funded in part by NIH AR44005 and NSF CCR-0093238.

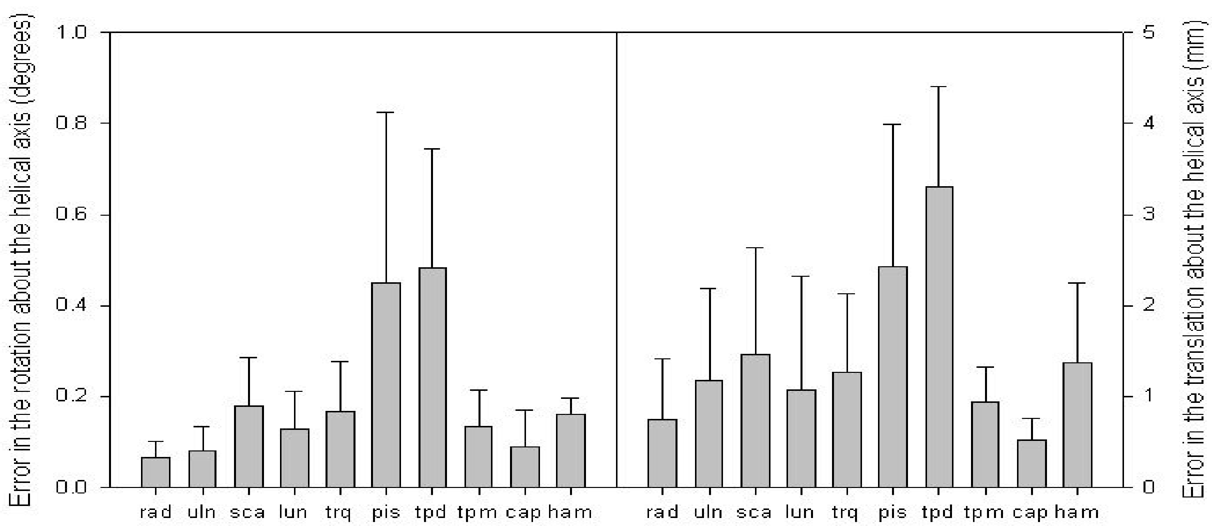

Figure 2: Mean (+ one S.D.) errors in HAM rotation and translation for the radius, ulna and the eight carpal bones

IN VIVO MEASUREMENT OF BONE STRUCTURAL PARAMETERS: ACCURACY AND PRECISION OF A DENSITOMETRIC TECHNIQUE

Tammy M. Cleek [1,2] and Robert T. Whalen [1]

[1] Musculoskeletal Biomechanics Lab, NASA Ames Research Center, Moffett Field, CA, USA
[2] Dept of Mechanical Engineering, Stanford University, Stanford, CA, USA
E-mail: Tammy.M.Cleek@nasa.gov

INTRODUCTION

We implemented a three-scan single-energy densitometric method to determine the accuracy and precision of measuring the cross-sectional structural parameters of the long bones of the lower leg in vivo.

METHODS

The in vivo setup consists of a foot fixture attached to an indexable rotating plate and an acrylic cylinder, aligned along the length of the table, that fits over the leg in the area to be scanned (Figure 1). The cylinder, with machined parallel flat surfaces, is fitted with an inner urethane bladder that is filled with saline to give a constant soft tissue baseline X-ray attenuation value in non-bone regions (Figure 1). All scans were taken with a Hologic QDR-1000/W bone densitometer using the spine scan mode (point spacing: 0.951 mm, line spacing: 1.003 mm).

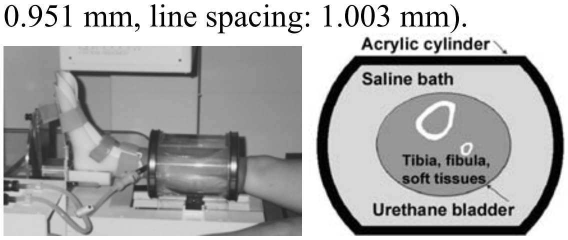

Figure 1: In vivo set up and cross-section.

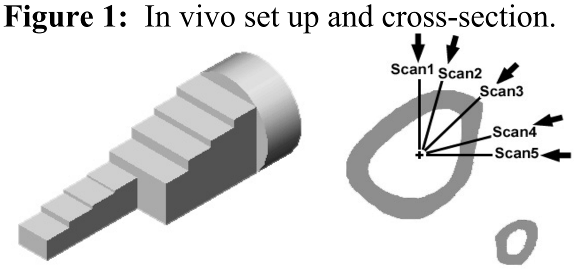

Figure 2: Aluminum phantom; lower leg scan orientations.

<u>Accuracy</u>: Accuracy was determined using an aluminum phantom (Figure 2), dimensioned to match a normal range in tibia and fibula cross-sectional area (*A*) and principal moments of inertia (*Imax*, *Imin*). The stepped end of the phantom was encased in a saline filled urethane tube; the other end held in a precision indexer.

The phantom, inserted into the cylinder in the manner of a leg, with the urethane bladder filled to eliminate air voids, was scanned in 15˚ increments of axial rotation spanning 90˚ (7 scans total). The principal axis of the phantom was initially set at 60° to the horizontal projection plane. A step phantom, machined from the same aluminum billet, was scanned in the same thickness of saline (plus acrylic) and used to convert X-ray attenuations to equivalent aluminum thickness values after subtracting a soft tissue (saline) baseline offset.

Cross-sectional structural parameters (*A*, *Imax*, *Imin*, and *J*= *Imax*+*Imin*, and principal angle) were computed for each section using three scans spanning included angles of 60° and 90°, respectively (Cleek and Whalen, 2002). Separate analyses using high and low DXA energies were performed.

<u>Precision</u>: In vivo precision of tibial structural parameters was computed from same day repeated measures of the tibial mid-diaphysis of fifteen female subjects aged 25 and older. The study was approved by NASA and Stanford University IRBs. Lead makers, marking start and stop scan

positions, were taped to the mid-diaphysis of the lower leg for registration of the scans during post processing. Five scans were taken. Between each scan, the leg was internally rotated to give scan sets which spanned included angles of 60° and 90°, in which the tibia and fibula did not overlap in the projected image (Figure 2). This entire procedure, with the subject getting off the table and markers removed, was repeated twice for a total of three independent measurements of structural parameters.

A set of dense bovine cortical bone steps was scanned and used to converted attenuations to equivalent cortical bone thickness. A simple thresholding program was used to detect bone edges. Structural parameters were computed as before from three scans spanning 60° and 90° *and* high and low energies, respectively (four combinations). Measurement averages for a 5 cm section centered at the mid-diaphysis were computed for each scan set at both included angles and at each energy level. Precision from triplicate measurements was calculated according to Gluer, et al. (1995).

RESULTS AND DISCUSSION

Accuracy: Estimated principal moments were within 4.1% and principal angles were within 1.2º for both energies and included angles (Table 1). Low standard deviations in error indicate little line to line variability. This is the "best case" in vivo accuracy to be expected with the current setup.

Precision: The low energy yielded slightly better precision than the high energy and the results for included angles of 60° and 90° were comparable at the low energy (Table 2). Better performance of the lower energy may be due to its larger dynamic range that can compensate for a decrease in signal to noise due to the large soft tissue thickness surrounding the bone in the in vivo setup. Our precision values from repeated measures incorporates errors in marker placement, initial foot position, and scan-to-scan misalignment. As a result, the measured precision is considered to be a "worse case", conservative estimate for the current setup.

In conclusion, we have validated a three-scan densitometric method for measuring structural parameters in long bones for use in future in vivo studies. The measured in vivo accuracy and precision establishes the confidence limits for measuring differences or changes in these parameters.

REFERENCES

Cleek, T.M., Whalen, R.T. (2002) *J. Biomechanics*, **35**, 511-516.

Glüer, C.C. et al. (1995) *Osteop. Int.,* **5,** 262-270.

Table 1: Errors (mean ± SD) in calculated section properties and principal angle for phantom.

Included angle, energy	Area (%)	Imax (%)	Imin (%)	J (%)	Pri angle (deg)
90º, hi energy	-4.80 ± 2.14	-4.07 ± 1.87	1.07 ± 2.13	-2.26 ± 0.99	0.33 ± 0.94
90º, lo energy	-5.03 ± 1.92	-3.65 ± 0.74	-2.91 ± 1.61	-3.43 ± 0.65	1.17 ± 1.44
60º, hi energy	-4.61 ± 1.88	-3.37 ± 3.40	1.07 ± 2.86	-1.72 ± 2.86	-0.76 ± 3.54
60º, lo energy	-5.34 ± 2.02	-2.85 ± 4.98	-3.38 ± 2.06	-3.12 ± 3.06	0.89 ± 1.99

Table 2: Calculated precision of structural parameters from triplicate measurements.

Included angle, energy	Area (cm^2)	Imax (cm^4)	Imin (cm^4)	J (cm^4)	Pri angle (deg)
90º, hi energy	0.046	0.083	0.033	0.084	7.040
90º, lo energy	0.025	0.053	0.022	0.051	3.098
60º, hi energy	0.017	0.086	0.068	0.108	13.823
60º, lo energy	0.013	0.071	0.019	0.077	6.164

TRUE MAGNITUDE OF DISPLACEMENT IN PELVIC RING FRACTURES

Michael Bottlang, Marcus Mohr, Frank Heuer, James C. Krieg, Steven M. Madey

Biomechanics Laboratory, Legacy Clinical Research & Technology Center, Portland, OR, USA
E-mail: mbottlan@lhs.org

INTRODUCTION

Accurate assessment of pelvic ring disruptions is an integral first step in the diagnosis and treatment of these potentially devastating injuries and is routinely obtained from initial plain radiographs or computer tomographic scans (Burgess et al., 1990). Treatment decisions are often predicated on the belief that certain degrees of injury severity can be inferred from the amount of displacement on plain radiographs and that once disrupted, the pelvic ring remains displaced (Tile et al., 1980). However, these static images, obtained post injury, cannot reveal the dynamic injury history and maximal fracture displacement. Therefore, estimation of injury severity and concomitant soft tissue injuries is largely confined to extrapolation of fracture displacement on an empirical basis. To gain better understanding of the correlation between maximal pelvic ring disruption and residual fracture displacement, we simulated distinct pelvic fractures in human cadaveric specimens and quantified the time-history of fracture displacement.

METHODS

Two distinct pelvic ring fracture scenarios were modeled in a biomechanical study on 15 fresh frozen human cadaveric specimens. In eight specimens, monolateral lateral compression fractures were induced, and in seven further specimens, monolateral open-book pelvic fractures were created.

Lateral Compression Fracture Model: Unilateral lateral compression fractures of the pelvis were created by means of a custom-built compression lever that allowed for controlled internal rotation of the hemipelvis (Fig. 1a). The femoral heads were replaced in the acetabula by the prosthetic heads of a lever device that applied a controlled lateral force through each acetabulum until defined and reproducible internal rotation of one hemipelvis occurred.

Open Book Fracture Model: Partially stable 'open book' pelvic fractures (symphysis diastasis=50 mm) were created by forced external rotation of each hemipelvis after symphysiotomy (Fig. 1b). These fractures were subsequently expanded into unstable pelvic fractures (symphysis diastasis=100 mm).

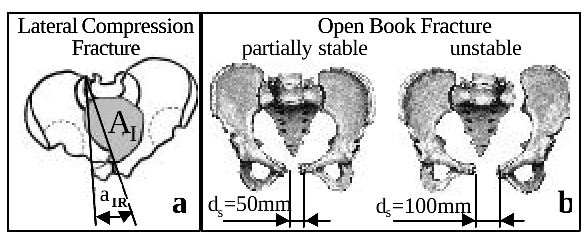

Figure 1: Pelvic fractures models: a) lateral compression fracture, characterized by A_I and α_{IR} and b) partially stable and unstable open book fracture.

Outcome Parameters: The pelvis of each specimen was instrumented with an electromagnetic motion tracking system (pcBird, Ascension Technology, Burlington, VT). The resulting data stream allowed computation of the initial pelvic orientation and the relative rotation of the unstable hemipelvis, expressed in terms of internal / external rotation (α_{IR}, α_{ER}).

Measurements of pelvic deformity, as well as standard radiographs (AP, inlet, and outlet views) were taken of each specimen prior to injury, at the moment of maximal displacement, and 60 seconds after cessation of the deforming force. Utilizing numerical image analysis software, we furthermore computed the inlet area (A_I) of the pelvis at each time point.

RESULTS

Clinically relevant pelvic ring injuries were created in all 15 specimens. The lateral compression fracture model was characterized by a 33 ± 7.5% decrease in A_I and by α_{IR} = 41 ± 6.8° (Fig. 2a). After removal of the compressive load, the collapsed pelvic ring passively expanded to a remaining decrease in A_I of 10.1 ± 4.3% and to α_{IR} = 7.5 ± 5.5°. This represents a passive correction of the maximal rotational deformity of > 80 %.

For the ‘open book’ injury, maximal symphysis diastasis d_s was 56.2 ± 6.4 mm (partially stable) and 99.0 ± 5.8 mm (unstable) (Fig. 2b). The unstable open-book fracture was furthermore characterized by a 33 ± 10.7% increase of the inlet area A_I and by α_{ER} = 37 ± 11.2° external rotation of the unstable hemipelvis. 60 seconds after removal of the disruptive force, the symphysis diastasis d_s decreased to 52% (partially stable) and 56% (unstable) of its maximal value. For the unstable open book fracture, the expanded pelvic ring relaxed to a remaining A_I increase of 25 ± 2.1% and α_{ER} = 25 ± 10.5°.

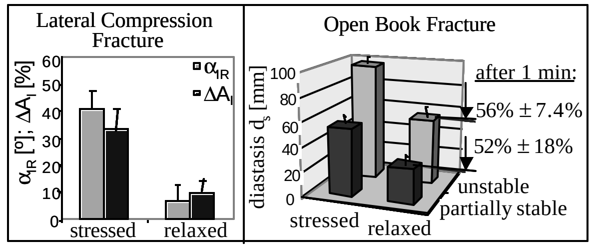

Figure 2: Rotational deformity of pelvic ring at maximal disruption (stressed) and after passive relaxation (relaxed).

DISCUSSION

This research demonstrates dramatically, that the degree of displacement seen on planar radiographs obtained post-injury represent only a portion of the maximal displacement at the time of injury. The displaced pelvis appears to retain residual elastic constraints, and therefore has an inherent tendency towards correction. This elastic re-coil effect was found more pronounced for lateral pelvic fractures as for open book type pelvic fractures. The complex pelvic anatomy, dependant on multiple ligamentous connections for it inherent stability, likely accounts for much of the observed elastic behavior. Albeit only two types of pelvic fractures have been modeled, these fracture models represent the two most common types of pelvic ring fractures. While, the type of injury pattern seemed to affect the amount of recoil that occurred, a significant passive correction of rotational pelvic deformity was observed in each fracture. This quantitative information on injury biomechanics of pelvic ring fractures is directly applicable to estimate injury severity in a clinical setting.

REFERENCES

Burgess et al. (1990). *J Trauma*, **30**, 848
Tile et al. (1980). *Clin Orthop*, **151**, 56

ACKNOWLEDGEMENT

Funded by the US Office of Naval Research

SYNCHRONOUS SIGNALING WITHIN THE OSTEOCYTE CELL NETWORK UNDERLIES THE OSTEOGENIC POTENCY OF REST-INSERTED LOADING

Brandon J. Ausk[1], Sandra L. Poliachik[2], Ted S. Gross[2], and Sundar Srinivasan[2]
[1]*Department of Mechanical Engineering, University of Washington, Seattle, WA, USA*
[2]*Orthopaedics and Sports Medicine, University of Washington, Seattle, WA, USA*
Email: bjausk@u.washington.edu

INTRODUCTION: We recently found that when a 10-s rest was inserted between low-magnitude mechanical loading cycles, these otherwise impotent regimens were transformed into stimuli perceived as potently osteogenic (over 8-fold increases in bone formation; Srinivasan et al, 2002). Considering that rest-insertion, per se, is a passive intervention, we hypothesize that this strategy derives its potency by amplifying signal coordination within the mechanosensory osteocytic cell network. Here, we explored this thesis by simulating the response of a population of osteocytic cells to both cyclic and rest-inserted loading utilizing a unique agent based modeling environment (NetLogo1.1; Wilensky, 1999).

METHODS: The response of a network of osteocytes to cyclic and rest-inserted stimuli was simulated within Netlogo 1.1. The Netlogo modeling environment allows exploration of connections between the micro-level behavior of individuals and the macro-level patterns that emerge from the interactions of many individuals. Specifically, within NetLogo, individual osteocytes were assigned localized sets of parametric rules (modeling micro-level behavior), permitted to interact with neighboring osteocytes, and global network (or population) level patterns allowed to emerge over time. For the simulations, each osteocyte was assigned the following parametric rules governing behavior: *1)* osteocytes were assigned internal clocks representing the time required to elapse before individual cells could activate (simulating rest intervals between stimuli; e.g., for a 5-s internal clock or rest interval setting, osteocytes can activate every 5-s); 2) each osteocyte can communicate with cells present within its immediate neighborhood (represented by the dimensionless 'communication length' parameter); 3) lastly, if an osteocyte perceives a given number (two) of simultaneously activated osteocytes within its neighborhood, the cell immediately activates (simulating signaling coordination between a localized grouping of 3 osteocytes). In this context, the activity of populations of 200 osteocytes (generated at random spatial locations and internal clock settings) were modeled and 5 simulations performed per experiment. First, parametric studies were performed for rest intervals of 2 to 30-s. Next, for rest intervals of 2 and 15-s, the influence of neighborhood size upon coordinated cell signaling was examined by varying communication lengths (from 15 to 50). For each simulation, the number of coordinated osteocytes as a percent of the entire population was recorded.

RESULTS: With respect to varying rest periods, synchronization of osteocyte activity displayed a normal distribution (Fig 1). Rest-intervals of 10- and 15-s induced the largest population of osteocytes to synchronize activity (70-80%). In contrast, rest-intervals of 2-, 5-, and beyond 20-s resulted in a markedly reduced and statistically similar number of coordinated osteocytes (50-60%). Additionally, protocols representative of cyclic loading (2-

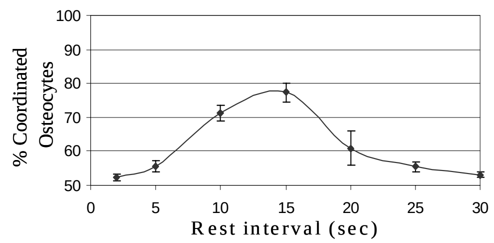

Fig 1: Percent coordinated osteocytes as a function of rest-intervals between stimuli.

s rest) and optimal rest-inserted loading (15-s) display markedly varied sensitivity to extents of osteocyte communication. Osteocytes exposed to cyclic stimuli (2-s rest) displayed reduced and invariant levels of coordination that was independent of communication lengths (Fig 2). In contrast, osteocytes exposed to 15-s rest inserted stimuli displayed markedly enhanced synchronicity (nearly 90%) beyond a threshold length (of 30), with saturation of coordinated activity occurring thereafter.

DISCUSSION: In support of our hypothesis, the presented model appears to indicate that rest-insertion between stimuli enables the osteocytic network to co-ordinate and synchronize its activity. Specifically, optimal synchronization of the network appears to occur beyond a threshold rest interval (~ 10-s), but with the benefits declining beyond 20-s of rest. In this context, *in vivo* observations suggest that while rest-insertion between mechanical load cycles enhances bone formation only beyond 7 – 10s (Srinivasan et al., 2002; Robling et al, 2001), the benefits of rest-insertion saturates between 10- and 20-s (Srinivasan et al, 2003). Further, if intervals of rest were too long (e.g., on the order of minutes), the protocol may cease to be perceived as a continuous train of stimuli that require a bone cell response. As such, the similarity of response trends between our model and *in vivo* data suggests that the ability to synchronize activity within the network of mechanosensory osteocytic cells may partly underlie the dramatic osteogenic potency of rest-inserted mechanical loading. Interestingly, our data indicates that synchronization of the osteocytic network in response to rest-inserted (but not cyclic) stimuli is enhanced and strongly dependent upon the ability of osteocytes to communicate with immediate neighbors. Importantly, this unique capacity of rest-inserted loading to utilize exquisite, interconnected networks of osteocytic cells arrayed *in vivo* may underlie its ability to transform mild mechanical stimuli into potent osteogenic regimens.

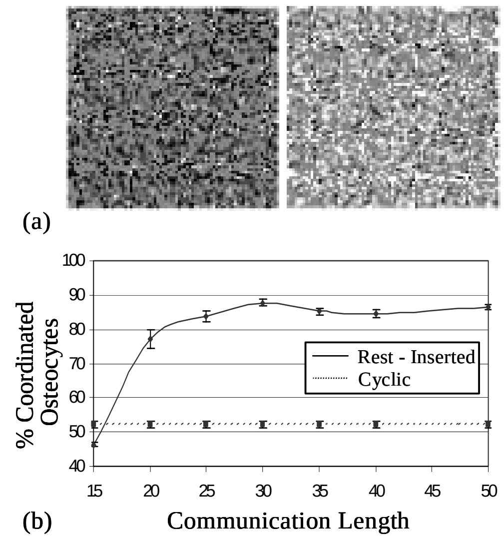

Fig 2: Typical model space screen captures displaying a larger population of activated (white) versus inactive (black) osteocytes when exposed to rest-inserted (15-s; right) versus cyclic stimuli at communication lengths of 30 (a). Similar response is evident in the coordinated activity of osteocytes plotted as a function of communication length (b).

REFERENCES: (1) Srinivasan et al. 2002 JBMR 17:1613; (2) Wilensky, U. 1999 http://ccl.northwestern.edu/netlogo; (3) Robling et al. 2001 J Exp Biol 204:3389; (4) Srinivasan et al. 2003 49th ORS.

ACKNOWLEGMENT: Support provided by the Whitaker Foundation (Rosslyn, VA).

FEMORAL INTRAMEDULLARY NAILING: GEOMETRY OF THE REAMED CANAL

Larry W. Ehmke[1], Britton Polzin[2], Christoph Roth[3], and Michael Bottlang[1]

[1]Legacy Clinical Research & Technology Center, Portland, OR; *email: mbottlan@lhs.org*
[2]Oregon Health Sciences University, Portland, OR; [3]Synthes (USA), West Chester, PA

INTRODUCTION

Intramedullary fixation with femoral nails is a standard treatment modality for femoral shaft fractures. Treatment success and the quality of reduction highly depend upon the geometric conformity between the implant and the reamed canal (Steriopoulos, 1997). Contemporary reaming systems with flexible shafts create reamed canals, which follow the path of least resistance through the intramedullary cavity. Depending on the reamer insertion site (greater trochanter or piriformis fossa), the reamed canal exhibits characteristic curvatures in the sagittal and coronal planes. The characteristic curvature of the intramedullary canal has previously been described only in terms of a single radius, fitted to 2-D radiographic projections of the femoral canal (Harper, 1987; Zuber, 1988). However, despite its crucial implication for implant design, no 3-D assessment of the reamed canal exist to date.

This study employed an experimental technique and mathematical algorithm to quantify the spatial curvature profile of the reamed femoral canal. The spatial curvature profile was quantified in paired femoral cadaveric specimens for reamer insertion through the greater trochanter and through the piriformis fossa. Results of this study provide a scientific basis relevant for implant design and implant insertion alike.

METHODS

Specimens: Eighteen paired, fresh-frozen, human femora from 5 female and 4 male specimens were obtained from Caucasian donors of age 64 ± 11 years.

Reaming: Specimens were reamed using a cannulated flexible reamer (SynReam, Synthes ,USA) over a guide wire to either 13 or 15-mm diameter in 0.5-mm steps depending upon specimen size. Reaming was done in accordance with standard reaming techniques aided by a C-arm fluoroscope (OEC 9600, OEC Medical Systems Inc.). The reamer was inserted through the greater trochanter (GT group, 12-mm lateral from tip) and through the piriformis fossa (PF group) in right and left specimens, respectively.

Intramedullary canal digitization:
Each specimen was aligned on a digitizing workstation, which consisted of a non-metallic table with an integrated electromagnetic motion tracking system (PcBird, Ascension Technology, Burlington, VT). A local coordinate system was defined by aligning the femoral shaft axis along the y-axis, the posterior aspects of the femoral condyles with the x-axis, and by placing the femur dorsal side down parallel to the x-y plane.

The centerline of the reamed femoral canal was traced by retracting a motion-tracking sensor through the reamed canal. For this purpose, the sensor was mounted on the tip of a flexible shaft while the outer diameter of the sensor was matched to the diameter of the reamed canal. Over 500 3-D data points were obtained per canal tracing.

Spatial Curvature Profile:
A custom Matlab software (Mathworks, Natick, MA) algorithm was generated to compute the apparent magnitude and orientation of curvature along the digitized canal pathway. A circle with center P_C was fitted to each triplet of points P_{i-1}, P_i, and P_{i+1} (fig. 1a). The radius vector $\underline{R_i} = \underline{P_C} - \underline{P_i}$ of the circle depicted the apparent magnitude and orientation of the reamed canal curvature at

point P_i. Plotting radius vectors for each successive P_i along the reamed canal pathway yielded the spatial curvature profile.
For result presentation, the curvature magnitude, $C_i = 1/|\underline{R_i}|$ and orientation, λ_i (fig. 1b), in the transverse plane were extracted from the spatial curvature profile over 5-95% of the reamed canal length.

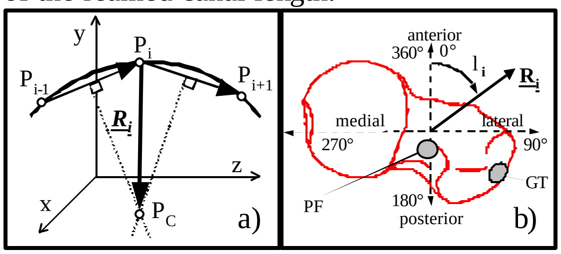

Figure 1: a) 3-D curvature calculation and b) definition of λ_i with PF and GT insertion sites

Differences between GT and PF groups were analyzed with a paired, two-tailed Student's t-test for both C_i and λ_i, along the canal length.

RESULTS

The spatial curvature profile yielded an antero-lateral curvature in the proximal region and an antecurvature in the diaphysis of the femur for GT specimens (fig. 2).

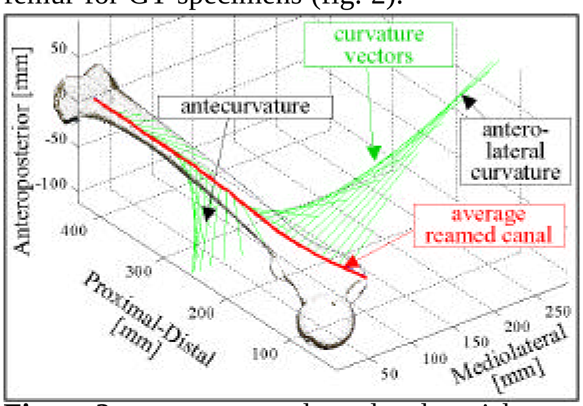

Figure 2: average reamed canal and spatial curvature profile for GT specimens

GT specimens yielded reamed canal radii of 604 ± 144 mm, 868 ± 190 mm and 2012 ± 2722 mm, while PF specimens yielded radii of 1674 ± 811 mm, 960 ± 266 mm and 1382 ± 760 mm at 25%, 50%, and 75% canal length, respectively. The corresponding curvature distribution along the reamed canal for both GT and PF specimens is depicted in figure 3.

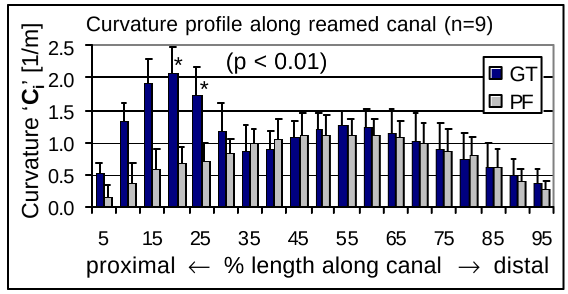

Figure 3: C_i distribution of GT & PF specimens

GT specimens yielded λ_i of 69 ± 16°, 176 ± 12° and 161 ± 60°, while PF specimens yielded λ_i of 236 ± 54°, 181 ± 13° and 175 ± 13°, at 25%, 50%, and 75% canal length, respectively (fig. 4).

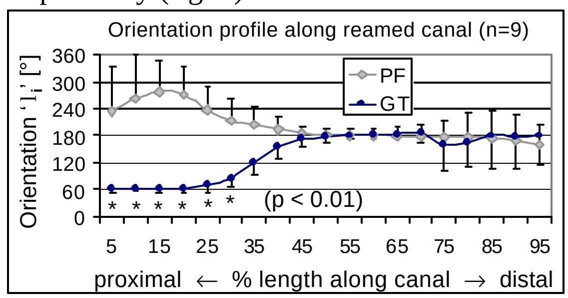

Figure 4: λ_i distribution of GT & PF specimens

DISCUSSION

The spatial curvature profile algorithm was able to quantify a complex canal trajectory in terms of two scalar parameters, C and λ, along the reamed canal. These outcome parameters are directly applicable for the design of intramedullary implants to optimize geometric conformity. The presented data suggest that the distinct insertion sites require intramedullary nails of different shapes to warrant optimal conformity between the implant and reamed canal. However, besides geometric conformity, femoral nail designs have to also account for ease of implant insertion and removal.

REFERENCES

Harper et al. (1987) *Clin Orthop,* **220**:155-161
Zuber et al. (1988) *Unfallchirurg,* **91**:314-319
Steriopoulos et al. (1997) *Acta Orthop Scand (Suppl 275),* **68**: 123-126

ACKNOWLEDGMENTS

Funding provided by Synthes (USA).

PASSIVE FORCE ENHANCEMENT AFTER STRETCH: EFFECTS OF BDM AND DATROLENE SODIUM

Dilson E. Rassier and Walter Herzog

Human Performance Laboratory, University of Calgary, Calgary, AB, Canada
*email: walter@kin.ucalgary.ca

INTRODUCTION

When skeletal muscles and isolated muscle fibers are actively stretched on the descending limb of the force-length relationship, the resulting force is higher than the isometric force at the corresponding length (Abbott and Aubert, 1952; Edman et al., 1982; Herzog and Leonard, 2002; Julian and Morgan, 1979). In whole muscles, when the stretch is performed at long muscle lengths, the extra-force is accompanied by an increase in the passive force after deactivation (Herzog and Leonard, 2002). Such “passive force enhancement” may underlie the intrinsic mechanism of the stretch-induced force enhancement, but it may also be a result of strain of elements between muscle cells when whole muscles are stretched. Therefore, it would be important to evaluate if the passive force enhancement is observed in single muscle fibers. The nature of the passive force enhancement is unknown, but there are two distinct possibilities to explain this phenomenon: (i) slow detachment of cross-bridges, and (ii) a Ca^{2+}-dependent engagement of a passive element upon fiber activation.

The purpose of this study was twofold. First, it was our intention to investigate if passive force enhancement was present in single muscle fibers. Since that was the case, we then proceeded to investigate the nature of the passive force enhancement. Specifically, we tested the hypotheses that (i) the passive force enhancement was related to slow detaching cross-bridges, and that (ii) the passive force enhancement was associated with a Ca^{2+}-induced engagement of a passive element upon stretch.

METHODS

Single fibers isolated from the flexor brevis muscle of frog were placed at a length 25% - 30% above the plateau of the force-length relationship (L_o). Passive and active stretches were performed with amplitudes of 5% and 10% L_o, and at a velocity of 40% fiber length/s. Isometric contractions at the corresponding initial and final lengths were also performed for comparison. All contractions had a duration of 4 s.

Two groups of fibers were used in this study. The first group was treated with 2 mM, 5 mM and 10 mM of 2,3-butanedione monoxime (BDM), a drug that decreases cross-bridge attachment to actin and force generation (Horiuti et al., 1988). The second group was treated with ~20 µm dantrolene sodium (DS), a drug that reduces Ca^{2+} release from the sarcoplasmic reticulum (Hainaut and Desmedt, 1974).

Total force enhancement was calculated as the difference in total force obtained after stretch and during isometric contractions at the corresponding final length. Passive force enhancement was calculated as the difference in force obtained after active stretch and subsequent deactivation of the fibers, and after passive stretch at the corresponding lengths.

RESULTS AND DISCUSSION

When active muscle fibers were stretched, active and passive forces were higher than the corresponding active and passive forces obtained during isometric contractions at the corresponding length. The passive force after the active stretch was also higher than the passive force after a passive stretch of identical magnitude and speed.

Therefore passive force enhancement was observed in single muscle fibers after deactivation, a result previously reported in whole muscles (Herzog and Leonard, 2002).

BDM significantly decreased tetanic force in a dose-dependent manner. However, the level of passive force enhancement was not decreased when fibers were exposed to different concentrations of BDM; it was increased (Figure 2). Since BDM decreases the proportion of cross-bridges strongly-bound to actin, this result suggests that the passive force enhancement is not associated with a high proportion cross-bridges attached to actin. The reason why passive force enhancement is actually increased after BDM application deserves further investigation.

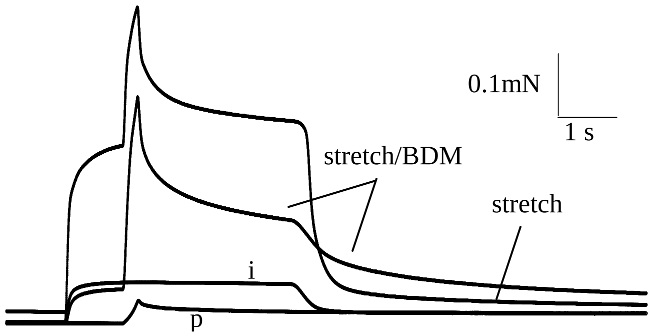

Figure 1: Total and passive force enhancement after stretch (amplitude: 10% fiber length, speed: 40 fiber length/s) in fibers before (stretch) and after 10 mM BDM (stretch/BDM). Isometric contraction at the corresponding final length (i) and passive stretch (p) after BDM are also shown.

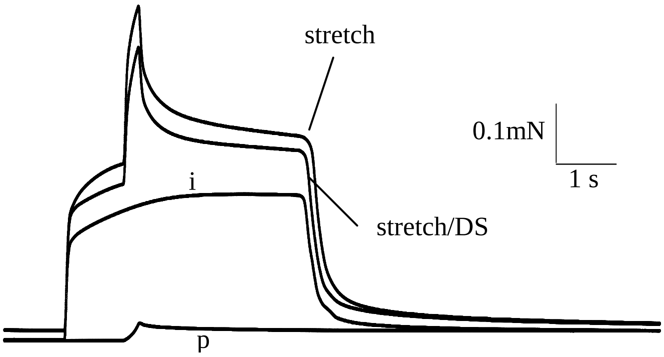

Figure 2: Total and passive force enhancement after stretch (amplitude: 10% fiber length, speed: 40 fiber length/s) in fibers before (stretch) and after (stretch/DS). Isometric contraction at the corresponding length (i) and passive stretch (p) after DS are also shown.

Dantrolene sodium decreased tetanic force, but the effects were not as prominent as those observed with BDM. After stretch and deactivation, the level of passive force enhancement was not significantly changed by DS. Therefore, reducing Ca^{2+} release from the sarcoplasmic reticulum did not affect passive force enhancement. Since the concentrations of DS used were not large enough to decrease the tetanic force substantially, there are two possible interpretations for these results: (1) Ca^{2+} concentrations during fiber activation and stretch does not affect the passive force enhancement, or (2) the decrease of Ca^{2+} release was not large enough to substantially inhibit the engagement of a passive element during stretch.

In summary, when muscle fibers are actively stretched along the descending limb of the force-length relationship, force enhancement is associated with a passive force enhancement, provided the stretch is initiated at long lengths. Such increase in passive force is likely not related to cross-bridges, and it does not seem to be associated with a Ca^{2+}-induced engagement of a passive structure, although this possibility needs further evaluation in future studies. By reducing Ca^{2+} release from the sarcoplasmic reticulum more substantially, it may be possible to test the influence of different degrees of activation on the passive force enhancement.

REFERENCES

Abbott, B.C., Aubert, X.M. (1952). *J. Physiol.* **117**, 77-86.
Edman, K.A.P. et al. (1982). *J. Gen. Physiol.* **80**, 769-784.
Hainaut, K., Desmedt, J.E. (1974). *Nature* **252**, 728-730.
Herzog, W., Leonard, T.R. (2002). *J. Exp. Bio.* **205**, 1275-1283.
Horiuti, K. et al. (1988). *J. Muscle Res. Cell Motil.* **9**, 156-164.
Julian, F.J., Morgan, D.L. (1979). *J. Physiol* . **293,** 379-392.

CAN BONE MINERAL DENSITY PREDICT FIXATION STRENGTH OF LAG SCREWS FOR PERTROCHANTERIC FRACTURE FIXATION?

Larry W. Ehmke[1], Benjamin C. Kam[2], Mark B. Sommers[1], and Michael Bottlang[1]

[1]Legacy Clinical Research & Technology Center, Portland, OR; *email: mbottlan@lhs.org*
[2]Oregon Health Sciences University, Portland, OR

INTRODUCTION

Fixation strength of pertrochanteric fractures treated with sliding hip screws highly depends on the bone quality in the proximal femur. The surgeon's perception of fixation strength determines the need for supplemental fixation by means of additional hardware or cement augmentation, and by the time-course of post-operative weight-bearing and patient mobilization (Bartucci, 1985). Bone mineral density (BMD) measurements from dual energy x-ray absorptiometry (DEXA) scans of the proximal femur are commonly used to estimate the quality of cancellous bone within the femoral head and neck (Lenchik, 1998). However, controversy remains regarding the value of BMD as a predictor for lag screw fixation strength (Stenström, 2000; Lin, 1999).

This biomechanical study investigated the relationship of BMD with lag screw insertion energy and fixation strength of a commonly used sliding hip screw. Results of this study depict the value of BMD as a quantitative tool to aid a surgeon's perception of lag screw fixation strength.

METHODS

Specimens: Eleven proximal femora from 6 female and 5 male fresh-frozen human cadavera with an average donor age of 77±6 years were obtained. The femoral heads were sectioned at the neck and potted into a steel shell (∅50mm) with low melting alloy.

BMD measurements: Prior to potting, DEXA scans were performed on all specimens to determine the BMD of the proximal femur using a fan beam x-ray bone densitometer (QDR 4500, Hologic, Waltham, MA). To ensure accurate BMD measurements, repeat recordings on one specimen were obtained in addition to measurements on contra-lateral specimens.

Insertion energy measurements: To determine the relationship between BMD of the proximal femur and the energy required to insert a lag screw, the insertion forces of a common lag screw (DHS, Synthes) were measured (fig. 1a).

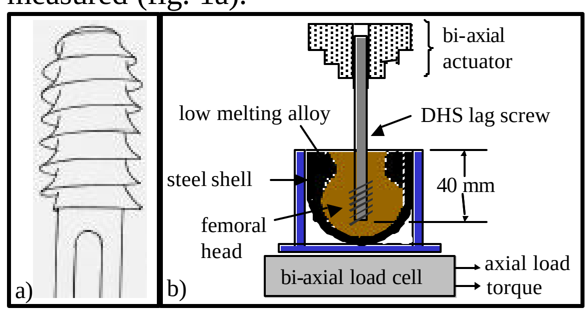

Figure 1: a) DHS lag screw, b) implant insertion setup

Specimens were mounted on a bi-axial load cell and implants were fixed to the bi-axial actuator of a material test system (Instron 8874, Canton, MA) (fig. 1b). Lag screws were advanced in concurrent linear and angular displacement to precisely reflect the pitch of its thread. Each lag screw was inserted to a depth of 40 mm, according to the manufacturer's insertion technique. The total amount of energy expended during lag screw insertion was computed as the area under the force-displacement curve (axial energy), plus the area under the torque-angle curve (torsional energy) (Heiner, 2001).

Fixation strength assessment: All specimens were subjected to a 3 Hz sinusoidal loading of 2 kN in a servohydraulic material test system (fig. 2a) (Sommers, 2001).

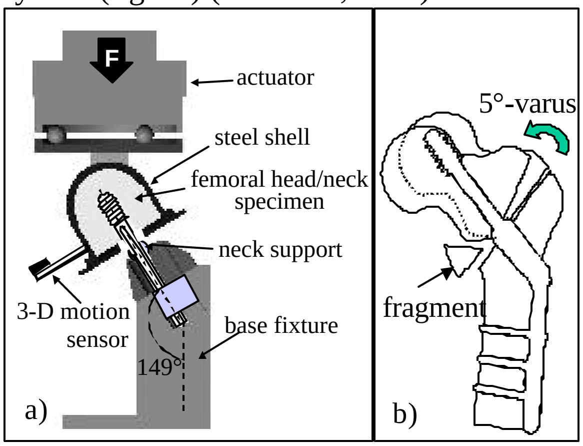

Figure 2: a) fixation strength test setup and b) varus collapse of specimen

An electromagnetic motion tracking system (PcBird, Ascension Tech., Burlington, VT) was used to record specimen migration into varus with respect to the lag screw. Loss of lag screw fixation was defined as 5°-varus collapse of the specimen (fig. 2b). Fixation strength under dynamic loading was quantified as the number of load cycles sustained at 5°-varus collapse ($NC_{5°\text{-varus}}$).

RESULTS

Specimens spanned the range from severely osteoporotic (0.25 g/cm^2) to normal bone (0.95 g/cm^2). As BMD increased so did the insertion energy required for DHS lag screws, although a considerable amount of variation was observed (fig. 3).

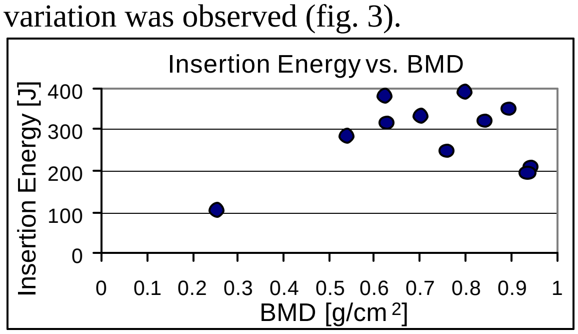

Figure 3: Insertion energy vs. BMD

BMD was a poor predictor for fixation strength. Although statistical evaluation did reveal a positive relationship between BMD and $NC_{5°\text{-varus}}$, a large amount of variation was observed (fig. 4).

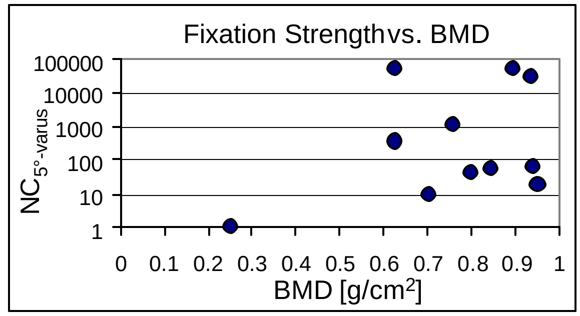

Figure 4: Prediction of $NC_{5°\text{-varus}}$ from BMD

Repeat BMD measurements on the same specimen were not significantly different and yielded a standard deviation of ± 0.01 g/cm^2. BMD measurements on 11 contra-lateral specimens yielded an average difference of 0.05 ± 0.03 g/cm^2, which was not significantly different (p=0.66).

DISCUSSION

Results of this study suggest that BMD does not closely correlate with either lag screw insertion energy or fixation strength.

The findings of this study may be in part explained since BMD is a measurement of mineral content and does not account for trabecular bone structure or mechanical properties.

REFERENCES

Bartucci et al. (1985) *JBJS*, **67**(7):1094-107
Lenchik et al. (1998) *Orthop Clin*, **29**:103-134
Stenström et al. (2000) *J Biomech*, **33**:289-297
Lin et al. (1999) *Osteoporos Int*, **9**:516-524
Heiner et al. (2001) *J Biomech*, **123**:629-634
Sommers et al. (2001) *Proceedings of ASME ‘01* **50**:721-722.

GAIT ADAPTATIONS TO FOOTWEAR ARE NOT TRANSIENT: IMPLICATION FOR THE TREATMENT OF KNEE OSTEOARTHRITIS

David Fisher[1], Anne Mündermann[1], Erez Morag[2], Tom Andriacchi[1,3,4]

[1]Biomechanical Engineering Division, ME Department, Stanford University, Stanford, CA, USA
[2]Nike Sport Research Laboratory, Beaverton, OR, USA
[3]Department of Orthopedic Surgery, Stanford University Medical Center, Stanford, CA, USA
[4]VA Palo Alto RR&D Center, Palo Alto, CA, USA
E-mail: fisherds@stanford.edu Web: biomotion.stanford.edu

INTRODUCTION

The knee adduction moment has been related to the load on the medial compartment of the knee (Andriacchi 1994) and has been shown to influence the treatment outcome of patients with osteoarthritis (OA) in the medial compartment of the knee (Prodromos 1985). Footwear intervention via shoe sole changes have been shown to modify this loading (Crenshaw 2000, Fisher 2002), but the benefit of the shoes is only useful if the effect of the intervention is not transient but rather sustained with usage. The hypothesis of this study was that using a more rigid lateral sole shoe results in a lower knee adduction moment and that this change continues with time.

METHODS

Six health subjects (3F, 3M, 32 ± 12 years, 167 ± 7 cm, 655 ± 95 N) were tested with Institutional Review Board approval and signed consent obtained for all subjects. Three different pairs of shoes, the subject's personal shoes, a pair of control shoes, and a pair of intervention shoes, were tested to determine usage effects on the knee adduction moment. The control shoes were a typical, flat, uniform stiffness sole shoe with the same thickness as the experimental shoes. The experimental shoes had a more rigid lateral side, while the medial side stiffness was the same as the control shoe. Subjects were first tested when the shoes were new to them. During this test, marker locations were marked on the body to assure the same marker placements for all future tests. The subjects were, then, given the control shoes to wear for a day before retesting. After this second test, they were given the experimental shoes to wear for five days before a final gait test was conducted. In each gait test, subjects performed five walking trials for each shoe at three different walking speeds, slow, normal, and fast.

To determine the effects of the intervention, the external joint moments were measured by gathering motion and force plate data during their gait trials. A three-dimensional optoelectonic system collected the motion data, while a multi component force plate was used to measure the ground reaction force. Inter-segmental forces and moments were calculated first at the ankle, then, propagated throughout the lower limbs using methods previously described (Andriacchi 1997).

The first peak of the knee adduction moment for each trial was recorded and ANOVA tests were used with subject, shoe type, test date, and walking speed as factors ($\alpha < .05$).

RESULTS AND DISCUSSION

There were statistically significant ($p < 0.05$) reductions in the knee adduction moment with the variable stiffness shoes that were sustained over time. However, the reduction in the knee adduction moment in the experimental shoes versus the control shoes was greater at higher walking speeds; at slow speeds (1.0 m/s ± 0.1m/s) there was no significant difference between the experimental and control shoes (Figure 1). This may be due to the fact that the variable stiffness soles, under the lower loads during slow walking, might have had less relative compression of the medial side. For normal speeds (1.3 m/s ± 0.2 m/s), significant reductions in the peak knee adduction moment on the second and third test days were observed. This shows that with continued usage the experimental shoes still showed reductions in the knee adduction moment. For fast speeds (1.7 m/s ± 0.2 m/s), there were also significant reductions for the second and third test days, again showing the continued reduction.

Additionally, the personal shoes were very repeatable in all tests (Table 1). This suggests that the data gathering method was reliable and indicates that subjects were accustom to their personal shoes. The control shoe, however, showed significant changes from the second to third tests suggesting that five days is a sufficient period of time to see some adaptation to the experimental shoes.

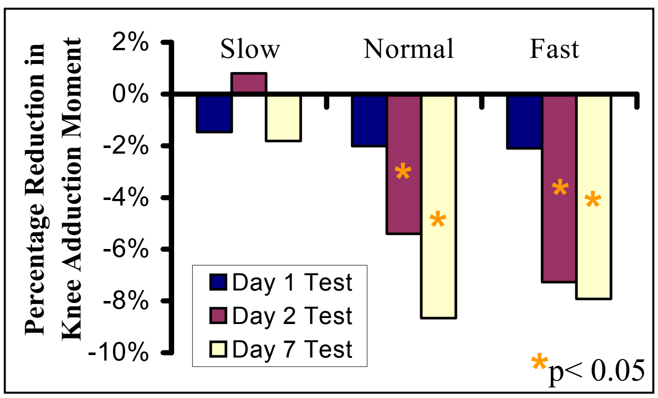

Figure 1: Percentage reduction in the peak knee adduction moment wearing the experimental shoes compared the control shoes

CONCLUSION

Shoe stiffness variation in the sole of the shoe can produce reductions in the peak knee adduction moment and this change is sustained with usage. Reductions of the knee adduction moment by approximately 8% are near the magnitude of effect of some high tibial osteotomies (Prodromos 1985), showing the clinically relevant potential for simple shoe sole modifications to avoid surgical procedures.

REFERENCES

Andriacchi, T.P. (1994). *Orthop Clin North,* **25**, 395-403.

Andriacchi, T.P. et al. (1997). *Basic Orthopaedic Biomechanics* 2nd ed., 37-68.

Crenshaw, S.J. et al. (2000). *Clin Orthop,* **375**, 185-192.

Fisher, D.S. et al. (2002). *48th Annual Meeting of the ORS,* **27**, 0700.

Prodromos, C.C. et al. (1985). *J Bone and Joint Surgery,* **67**, 1188-94.

ACKNOWLEDGEMENTS

This study was supported in part by Nike Inc.

Table 1: Average knee adduction moments for different test conditions (average ± SD).

	Control Shoe			Experimental Shoe			Personal Shoe		
	Slow	Normal	Fast	Slow	Normal	Fast	Slow	Normal	Fast
Day 1	3.1 ± .2	3.3 ± .2	3.6 ± .3	3.1 ± .2	3.2 ± .2	3.5 ± .3	3.0 ± .2	3.2 ± .2	3.6 ± .3
Day 2	3.0 ± .2	3.3 ± .2	3.6 ± .3	3.0 ± .2	3.1 ± .2	3.3 ± .3	3.1 ± .2	3.2 ± .2	3.5 ± .3
Day 7	3.1 ± .2	3.4 ± .2	3.7 ± .4	3.1 ± .2	3.1 ± .2	3.4 ± .4	3.1 ± .2	3.2 ± .2	3.6 ± .4

LOWER EXTREMITY MECHANICS IN PATIENTS WITH PATELLOFEMORAL JOINT PAIN: A PROSPECTIVE STUDY

Irene McClay Davis[1,2] , Tracy A. Dierks[1], Reed Ferber[1], and Joe Hamill[3]

[1]Department of Physical Therapy, University of Delaware, Newark, DE, USA
[2]Joyner Sportsmedicine Institute, Mechanicsburg, PA, USA
[3]Department of Exercise Science, University of Massachusetts, Amherst, MA, USA
E-mail: mcclay@udel.edu

INTRODUCTION

The knee is the most common site of injury in runners, with patellofemoral joint pain (PFP) being the most prevalent of knee pathology (Clement et al, 1986). Women have been noted to be twice as likely to experience PFP than their male counterparts. Women have also been consistently noted to have greater Q-angles. A greater Q-angle is thought to increase the lateral component of the quadriceps force vector, thereby increasing the tendency for lateral maltracking. The greater Q-angle noted in women is due to their greater hip width to femoral length ratios (Horton and Hall, 1989). This places the hip in greater adduction than males, putting females at greater risk for knee valgus as well.

These noted structural characteristics are likely to result in gender differences during movement. Ferber et al (2003) reported that females exhibited significantly greater hip adduction and internal rotation as well as greater knee abduction (valgus) during running than males. These differences could lead to abnormal patellofemoral alignment, placing females at greater risk for PFP. For example, increased knee abduction (associated with increased hip adduction) likely increases the functional Q angle and predisposes one to greater risk for patellar malalignment. In addition, femoral adduction is coupled with internal rotation. Excessive femoral internal rotation can also lead to a relative lateral malalignment of the patella. To date there are no studies comparing the 3D hip and knee kinematics of runners with PFP to that of healthy controls. In addition, while retrospective studies are informative, they do not lend insight into causative mechanisms.

Therefore, the purpose of this study was to compare, prospectively, the 3D kinematics of the hip and knee in female runners who later develop PFP to the mechanics of healthy controls who do not develop this pain. It was hypothesized that runners with PFP would exhibit greater hip adduction and internal rotation, lesser knee internal rotation (due to greater hip internal rotation) and greater knee abduction (valgus) than runners who do not develop PFP.

METHODS

These data are part of an ongoing prospective running injury study of female competitive distance runners. Female runners between the ages of 18 and 45 years and running a minimum of 20 miles per week are included in the study. All subjects undergo an instrumented gait analysis upon entry into the study. Subjects run along a 25 m runway at a speed of 3.65 m/s (±5%). Kinematic data are collected (120 Hz) with a 6-camera Vicon Motion Systems (Oxford, UK) motion analysis system. All kinematic data are filtered at 8 Hz. 3D angles of interest are calculated about a joint coordinate system using MOVE3D (NIH Biomechanics Laboratory, Bethesda, MD). Five trials were averaged for analysis. One-tailed independent t-tests were conducted on the data. Due to the preliminary nature of the data, an alpha of 0.10 was used for significance.

To date, 9 females have sustained PFP. All injuries were diagnosed by a medical professional. 9 healthy, uninjured females in the same study served as controls (CON). The PFP females were 33.4 yrs old (sd 8.2) and ran an average of 27 mpw. The CON were 29.9 yrs (sd 11.3) and ran 29 mpw.

RESULTS and DISCUSSION

Table 1 presents the comparison between the PFP and CON for the variables of interest. It is interesting to note that while excessive rearfoot eversion is thought to be associated with PFP, the values were identical between groups.

Table 1. Variables of interest (sd) for PFP and CON

(values in deg)	PFP	CON	p
Pk Eversion	8.7 (3.2)	8.7 (3.2)	0.50
Kn Add.	4.4 (3.2)	5.3 (3.3)	0.28
Kn IR	2.5 (5.7)	2.4 (6.9)	0.47
Hip Add	9.4 (5.4)	6.7 (2.9)	0.10*
Hip ER	5.1 (9.3)	10.2 (4.9)	0.08*
Q-Angle	16.1 (4.0)	13.0 (3.1)	0.05*

Peak knee adduction was not significantly different between groups. However, greater knee adduction excursion can be seen in Figure 1. The same is true for knee internal rotation excursion. When moving up to the hip, peak adduction was greater, as expected in the PFP subjects. In addition, the hip was in greater internal rotation at footstrike, and remained in greater internal rotation throughout stance (Figure 2).

Another interesting finding was the significantly greater Q angle noted in the PFP subjects. This structural difference coupled with the subtle kinematic differences could significantly alter the distribution of loading across the patellofemoral joint.

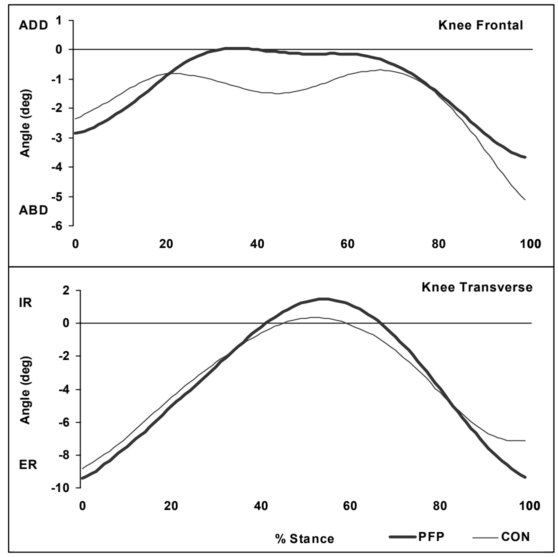

Figure 1. Knee Frontal and Transverse Motions (PFP vs CON)

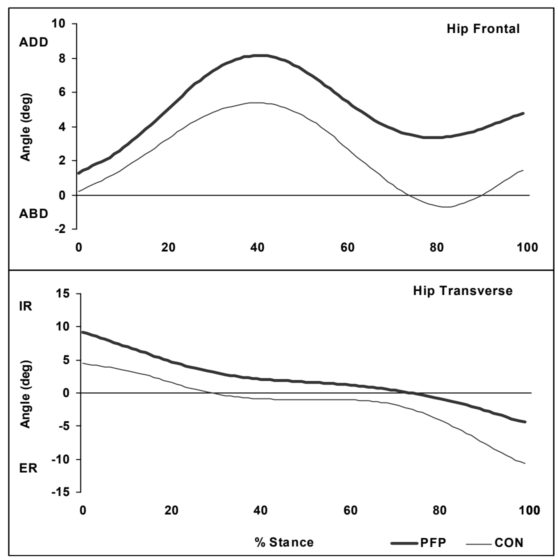

Figure 2. Hip Frontal and Transverse Motions (PFP vs CON)

SUMMARY

It is clearly difficult to infer patellofemoral kinematics and associated loading patterns from tibiofemoral kinematics. However, these preliminary data suggest there are some differences, noted prospectively, in the hip and knee mechanics of runners who develop PFP compared to those who do not. Additional differences may become evident as subjects are added to the study.

REFERENCES

Clement et al (1981) Phys Sports Med, 9(5):47-58
Ferber et al (2003) *Clin. Biom* (in press)
Horton et al (1989) *Phys. Ther.* 69:897-901

COMPARISON OF TWO TECHNIQUES OF FIGURE OF EIGHT TENSION BAND WIRING ON BIOMECHANICAL STABILITY OF PATELLAR FRACTURE

Despina Ciocanel M.D. [1, 2], Steve Haman M.D. [2], Richard Yeasting Ph.D. [2], Vijay Goel Ph.D. [1, 3] and Nabil Ebraheim M.D. [2]

Spine Research Center [1], Medical College of Ohio [2] and University of Toledo [3], Toledo, Ohio
E-mail: dciocanel@mco.edu

INTRODUCTION

Transverse fractures of patella are a common orthopedic problem with a relatively high rate of nonunion. This study aims to illustrate possible improvements in surgical technique, which may result in higher rate of fracture healing.
The objective is to compare biomechanical stability of two different techniques of patellar fixation using an established cadaveric model. Specifically, our research aims to study the effect of distance from the patellar poles of the tension band in the classic figure of eight construct on the separation at the fracture site in response to external loads applied through the tendon.

METHODS

Five pairs of embalmed knees (mean age 77.4 years, SD 10.15 years) were dissected, and transverse patella fractures were simulated. The knees were reduced and fixed with two distinct techniques. Both techniques employed the classic parallel k-wires and figure of eight tension band construct. In one group (left femurs), the tension band was placed at a distance of 1.0 cm from the proximal and distal pole of the patella (Fig. 1.a). In the other group (right femurs), the tension band was placed directly adjacent to the patellar poles (Fig.1.b). The knees were fixed by two parallel 2.3 mm Kirschner wires with a 1.0millimeter / Synthes titanium Cable with Crimp.

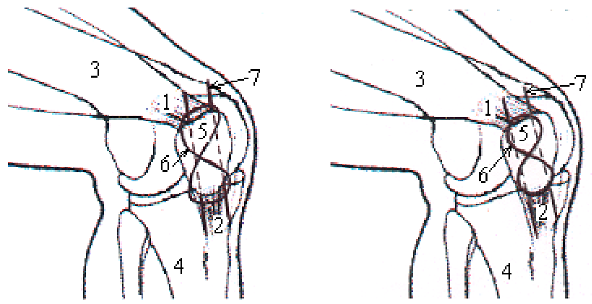

a) b)

Figure 1: Schematic of patella tension bend with figure of eight. 1–quadriceps tendon, 2-patellar tendon, 3-femur, 4–tibia, 5–patella, 6–tension bend, 7-Kirschner wires.

Knees were tested by applying a cyclic load through the quadriceps tendon between 20 and 300 N for 30 cycles.

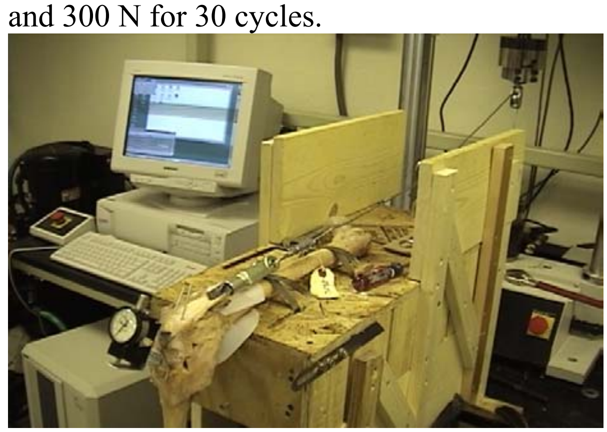

Figure 2: Specimen setup, showing the extensometer placement and the cable-and-pulley system assembly used to apply load to quadriceps tendon.

Force was applied to the quadriceps tendon through a cable-and-pulley system (Fig.2) and measured using an MTS load cell (1,000 Newton range). A mechanical extensometer was placed on the anterior surface, spanning the fracture to record the separation across the fracture site (Fig.2).

RESULTS AND DISCUSSION

The maximum fracture displacement increased with each cycle of loading for both techniques. (Fig. 3)
The average displacement at the thirtieth cycle was 1.078 millimeters (SD 0.82 mm) for patella tension band construct on the patella poles and 2.368 millimeters (SD 1.41 mm) for tension band construct 1 cm off the patellar poles.

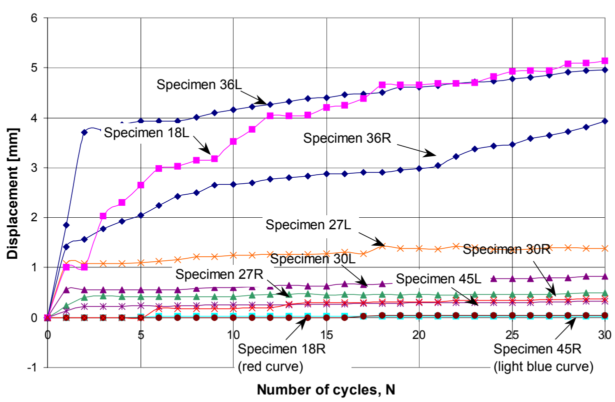

Figure 3: the maximum displacement (separation across fracture line) recorded during each cycle of loading for 10 specimens.

When comparing both methods for all cycles, the tension band placed on patellar poles allowed less fracture displacement than the tension band placed 1-cm off the patellar poles.

Fixations of transverse patellar fracture with figure of eight tension band have long been described. The position of the tension band in relation to the pole of the patella has not been biomechanically evaluated. We have demonstrated the importance of position of the tension band with relation to the pole of the patella. Soft tissue imposition between the pole of the patella and tension band is detrimental to maintenance of the reduction of the fracture.

SUMMARY

The effect of changing the distance from the patellar poles of the tension band with the figure of eight on the separation across the fracture was studied.

Comparing both methods for all cycles, the tension band placed on patellar poles allows lesser fracture displacement than the other tension band configuration. Thus, the placement of the tension band on both patellar poles may result in higher rate of fracture healing.

REFERENCES

A.P.Fortis, Z. Milis, V.Kostopoulos, et al: (*2002 Injury, p.489- 493) Experimental investigation of the tension band in fractures of the patella*

R. P. Grelsamer; C. H. Weinstein: (*2001 Clinical Orthopedics and related research, p.9-14) Applied Biomechanics of the Patella*

T. A. Scilaris, J. L. Grantham, M. J. Prayson, et al: *(1998 Journal of Orthopaedic Trauma, p.356-359) Biomechanical Comparison of Fixation Methods in Transverse Patella Fractures.*

ON STUDYING THE ONSET, ACCUMULATION, AND SOURCE LOCATION OF MICROCRACK IN BONE USING ACOUSTIC EMISSION TECHNIQUE

Jihui Li[1], Nicole Vos[2], and Gang Qi[1,3]

[1]Department of Biomedical Engineering and [3]Department of Mechanical Engineering

The University of Memphis, Memphis, USA

[2]Engineering Department, Dordt College, Sioux Center, IA, USA

E-mail: jihuili@memphis.edu   Web: http://www.me.memphis.edu/mar_lab/mar_lab/home.htm

INTRODUCTION

The accumulation and progression of microcracks in materials under loading is one of leading causes of mechanical failures. It is often believed that these microcracks coalesce into the final failure (O'Brien et al, 2000). Methods to study these failures include: numerical (Jacobs et al, 1996) and experimental (Keaveny et al, 1999). Most experimental techniques such as photomicrography, x-ray, and ultrasound have emphasized the detection of microcrack activities by performing offline experiments. The crucial advantage of these techniques is the relative accuracy. However, these techniques were not able to provide real time monitoring of the process of microcrack formation, progression, and source locations. As a result, the history of the micromechanical failures is yet well understood. This work is aimed to study the mirco-responses of materials under quasi-static loading by using the acoustic emission technique (AE). AE is a series of transient elastic waves generated inside a material due to a sudden stress/strain energy release. It is a very sensitive technique that can non-invasively monitor the deformation, fatigue, and fracture of materials. The objective of this study is to quantitatively measure microcrack activities of bovine cortical bone under quasi-static loading in real time. Quantitative indications such as onset time, intensity and source location of microcrack are sought to quantify the material failure process.

METHODS

A series rectangular beam specimens of cortical bone were harvested from the femurs of adult cow, oriented parallel to the bone's long axis with nominal dimension of 90 x 10 x 5 mm. A center notch of height 5 mm was machined to guide the fracture. Three-point bending tests on the specimens were performed using an Instron testing machine. All tests were performed as recommended by ASTM E399-90. Specimen was fixed and sustained constant speed loading at a rate of 0.08 mm/min. Each specimen was loaded until rapture. Five resonant sensors were installed on the surface of the specimen. An eight-channel Vallen AMSY-5 AE system was used to process the AE data. AE characteristics and waveforms from one channel were recorded for analysis.

RESULTS AND DISCUSSION

AE activities accumulation properties were widely used to decide the onset time of failure and destroy degree in the fatigue test (Wright et al, 1987). Figs.1 showed a cumulative relationship between AE activities and time. Three phases were identified: Phase I was the initial adjustment period, which took approximately 70% ~ 80% of the total test period. In this phase, the bone specimen experienced initial loading adjustment; steady elastic deformation associated with few insignificant AE activities. The Phase II, endured for 20% ~ 30% of the entire test period, was the material yielding period and characterized the onset of the microcracks.

In this period, the intensity of the AE activities formation was 51.2 counts/second. The last phase, known as the final rapture phase, was a sudden brief period. In this phase, the intensity of AE activities accumulation rate increased significantly to 1502 counts/second. One of the main advantages of AE technique is that it can compute the microcrack source location in real time and provide 3D visualization. Fig.2 indicated a typical microcrack source location result in x-y projection. The microcracks were clustered with square blocks of size 0.5 x 0.5 cm. The location of the cluster was defined as the geo-center of the microcrack cloud, could illustrate the distribution of the microcracks. Mean source location values of all the microcracks of each specimen were computed and compared with expected result (Table 1). Results showed that most calculated source location of those four specimens distributed on and around the actual failure location. This implied that AE is a unique technique to non-invasively localize the microcracks developing in biomaterials. In the source location calculation, noises and sensors condition were important issues that would induce errors (Qi et al, 1998); filters were used to block most noises and customized algorithm was developed.

SUMMARY

In this study, three points bending tests of bovine cortical bone specimens were performed. AE signals were received and analyzed. AE activities accumulation curve was used to identify the onset time of yielding and final fracture. Microcrack source locations were also calculated and error was discussed.

REFERENCES

J. O'Brien, et al., *J Anatomy*, vol. 197, 413-420, 2000.

Jacobs, C.R. et al., *J Biomech*, 30(6), 603-613, 1996.

Keaveny, TM, et al, *J Biomechanical Engineering*, 12, 99-107, 1999

Tim Wright (1987) *Nondestrctive testing handbook*

G. Qi, J. Pujol, and Z. F. Fan (1999) *J. Biomed Mat Res*, 52 (2): 256-260

ACKNOWLEDGEMENTS

This project was supported in part by NSF REU9912439 and the Whitaker Foundation. The authors would like to thank Dr. Eng T. Ng for assisting the experiments

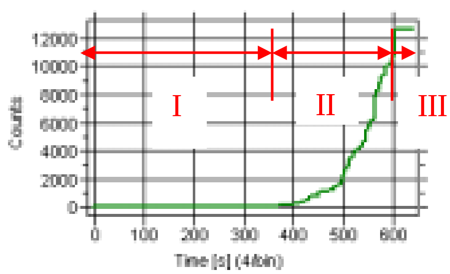

Fig. 1 Cumulative AE activities counts curve. Three phases are identified.

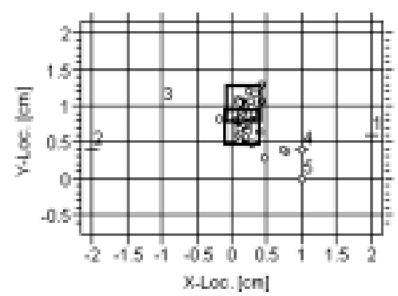

Fig.2 Computed microcrack source location in x-y projection. The expected microcrack locations are at x $\approx$ 0 and 5 < y < 10 mm.

Table 1. Calculated microcrack source location results and errors

Exp.Loc.	Test 1 (mm)		Test 2 (mm)		Test 3 (mm)		Test 4 (mm)	
(mm)	Computed	Error	Computed	Error	Computed	Error	Computed	Error
0	1.9	1.9	0.2	0.2	0.7	0.7	1.3	1.3
5 -10	8.3	0	4.5	0.5	6.2	0	6.4	0
±2.5	-0.9	0	-0.5	0	-5.3	2.8	-1.1	0

A BIOMECHANICAL ANALYSIS OF COMBINED INTERTROCHANTERIC AND FEMORAL SHAFT FRACTURE FIXATION CONSTRUCTS IN CADAVERIC FEMORA

Alison McConnell [1], Khalid Syed [2]
and Emil Schemitsch [1,2]

[1] Martin Orthopaedic Biomechanics Laboratory, St Michael's Hospital, Toronto, ON, CANADA
[2] Division of Orthopaedics, Dept of Surgery, University of Toronto, Toronto, ON, CANADA
E-mail: McConnellA@smh.toronto.on.ca, Schemitsche@the-wire.com

INTRODUCTION

Combined fractures of the proximal femur and femoral shaft are the result of high-energy trauma, such as motor vehicle accidents (MVA) and falls from heights. They comprise 28% of ipsilateral hip and shaft fractures (Alho, 1996).

In a biomechanical analysis of synthetic composite femora for fixation of ipsilateral femoral neck and shaft fractures, it was found that the reconstruction nail was stiffest in physiological bending whereas a dynamic compression plate with 3 cannulated screws was stiffest in torsion (Groebs *et al*, 2001).

Although the neck and intertrochanteric regions of the femur are close in proximity anatomically, the fixation constructs employed for these fracture combinations are different. Currently, there is no biomechanical evidence in the literature to support a particular construct combination from the numerous available options for ipsilateral intertrochanteric and femoral shaft fracture fixation.

The purpose of this study was to compare five common constructs for combined fractures of the intertrochanteric region and the femoral shaft in terms of bending and torsional stiffness in human cadaveric bone.

METHODS

Twenty-five fresh frozen adult femora were obtained from tissue donation centres, and were stripped of all soft tissues, and x-rayed to ensure absence of bony pathologies. Femora were positioned anatomically with the femoral head centred over the medial femoral condyle to simulate mid-stance orientation. To secure the distal femur, pointed screws were inserted through a jig into the bone. The jig simulating the acetabulum, a cup cut out of an obliquely sectioned stainless steel cylinder, was held in 15 degrees of anteversion. Additional screws were inserted into the femoral head when performing torsional loading.

To simulated physiological bending, an axial load was applied through the femoral head at 8 mm/min by a biaxial mechanical testing machine (8874 Instron, Canton, MA). The slope of the load-deflection curve was used to characterize the stiffness in physiological bending. Internal and external torsional loads were then applied to the head at 0.1 deg/s. The slope of the torque-angular displacement curve defined the torsional stiffness.

Baseline stiffness was determined by loading intact femora in physiological bending to 1500 N. Torsional baseline stiffness was determined by loading in both external and internal rotation to 12 Nm. The femora were block randomized to 5 construct groups based on bending baseline stiffness and constructs were applied. The construct groups were Dynamic Hip Screw (DHS) + retrograde intramedullary (IM) nail; Reconstruction nail (Recon); DHS + low contact dynamic compression (LCDC) plate; long DHS; long Intramedullary Hip Screw (IMHS).

Intertrochanteric fractures in concurrent hip and shaft fractures are usually transverse and seldom comminuted (Alho, 1996), simulated by osteotomizing between the trochanters. In addition, a transverse shaft osteotomy simulated the shaft fracture.

Fracture stiffness was measured by loading in bending to 750 N and 6 Nm. Bone loss at the shaft fracture was simulated by creating an 8-10 mm bone gap. Gap stiffness was retested by loading to 500 N and 3 Nm.

Fracture and gap stiffness data were expressed as a percent of baseline stiffness to account for between specimen differences in inherent bone quality. One way analyses of variance were performed on the data with a significance level of 0.05 to determine the effect of construct on physiological bending and torsional stiffness.

RESULTS

The baseline groups were balanced for bending stiffness, and were not statistically significantly different in average stiffness ($p=0.96$ for bending, $p=0.294$ for external rotation (ER), $p=0.295$ for internal rotation (IR).

There were no statistically significant differences between the percent baseline fracture bending nor torsional stiffnesses. ($p=0.447$ for bending, $p=0.299$ for ER, $p=0.665$ for IR).

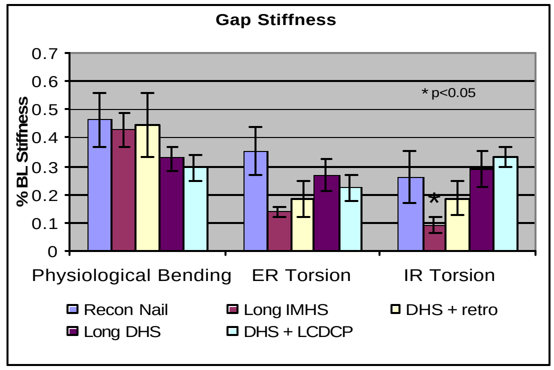

Figure 1: Mean values of stiffness, expressed as a percent of baseline stiffness, are shown for all constructs after testing with a shaft bone gap. Standard error of the mean values are shown.

Gap stiffnesses also did not vary for physiological bending nor ER ($p= 0.411$ for bending, $p=0.132$ for ER). There was, however, a statistically significant difference in percent baseline torsional stiffness, ($p= 0.048$), and post-hoc analysis showed that the DHS + LCDC plate was stiffer in IR torsion than the long intramedullary hip screw ($p=0.041$).

DISCUSSION

We did not find significant differences in in-situ bending stiffness among constructs tested; however, the long IMHS was found to be the least stiff in torsion with a shaft bone gap. The low polar moment of inertia of the IMHS, due to the distribution of the mass close to the examined axis of rotation, results in a low inherent torsional stability.

REFERENCES

Alho, A. (1996). *Acta Orthop Scand*, **67 (1)**, 19-28.

Groebs, A; Pugh, K; Seth, A; Chen, M; Litsky (2001) *Proc ORS*, 253.

ACKNOWLEDGEMENTS

Sincere thanks to Smith & Nephew for their generous donation of the implants.

EVALUATION OF FIXATION FOLLOWING PROXIMAL TIBIAL VALGUS OSTEOTOMIES IN CHILDREN WITH BLOUNT'S DISEASE

Michael Levy[1] and Brian Carney[2]

[1]Peninsula Center Consortium, Far Rockaway, New York, USA
[2]Shriners Hospitals for Children, Lexington, Kentucky, USA
E-mail: jemlevy1@juno.com

INTRODUCTION

Pathologic genu varum is progressive and rarely spontaneously resolves. Blount (1937) divided infantile (less than 5 years old) from the adolescent form (greater than 6 years old). A radiographic classification, developed by Langenskiőld (1981), demonstrated medial metaphyseal fragmentation, proximal beaking, varus, physeal depression, and osseous bridging.

Radiographic measurements differentiate infantile tibia vara from physiologic genu varum. Levine and Drennan (1982) measured the angle between the metaphysis and the diaphysis (metaphyseal-diaphyseal angle or MDA).

The purpose of proximal tibial osteotomy in Blount's disease is to prevent development of osteoarthritis by correcting of the mechanical axis. Pinkowski (1995) noted the complications of osteotomy to include, compartment syndrome, peroneal nerve palsy, infection, growth plate damage, iatrogenic fractures, vascular injury, recurrence of angular deformity, fixation failure, and nonunion. Loss of alignment may lead to complications such as nonunion and recurrence of deformity. Types of fixation include cast immobilization, rigid internal fixation with a plate and screws, limited internal fixation with pins, and varying constructs of external fixation. A literature review failed to produce a study on early loss of alignment.

METHODS

A retrospective analysis was conducted on children with a diagnosis of Blount's disease who underwent proximal tibial osteotomy during the period from January 1980 to December 1999. The medical record was reviewed for date of birth, date of surgery, sex, side of operation, and fixation type.

For each child the radiographic MDA described by Levine and Drennan (1982) was measured by a single investigator. The preoperative radiograph, the operative radiograph, and the early postoperative radiograph (taken on the first follow-up clinic date) were measured.

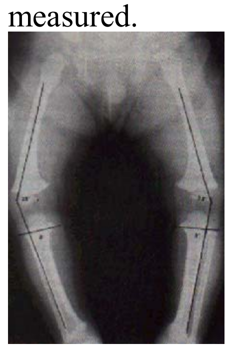

Figure 1: A radiograph of a child with bilateral Blount's disease, note the MDA.

Loss in alignment was defined as 5° change in MAD from the operative to the radiograph at follow up.

The data was then compiled and a statistical analysis was conducted accounting for age (less than 6 years versus 6years or more), sex, side of operation, preoperative deformity (less than 74° versus greater than or equal to 74°), and fixation method. Statically analysis was performed using chi square for normal data and an unpaired t-test for grouped continuous variables. A p-value <.05 was considered significant.

RESULTS AND DISCUSSION

The study consisted of 35 children with 49 osteotomies. There were 21 males and 14 females. The mean children's age at surgery was 9 years 10 months (range 2 years 5 months to 17 years 2 months). Of the thirty five children, 10 were less than 6 years old (infantile), and 25 were 6 years or older (adolescents). There were 26 right limbs and 23 left limbs. The mean preoperative MDA was 70° (range 50° to 85°). Preoperative MDA was more than 74° in 16 limbs while 33 limbs had a preoperative MDA equal to or less than 74°. Fixation was with pins in 20 limbs, plate and screws in 15 limbs, external fixation in 10 limbs, and cast in 4 limbs. The mean angle change from the operative radiograph to the early follow-up radiograph was 3° (range from 7° valgus to 14° varus).

There was no statistically significant difference in the mean MDA change versus age (infantile verses adolescent), sex, operation side, preoperative MDA. Plate fixation (mean MDA change of 1°) was found to be statistically better than pin fixation (mean MDA change of 4°) p-value .047.

This study evaluated early loss alignment following proximal tibial osteotomy in children with Blount's disease. Plate fixation was found to be statistically better than pin fixation.

SUMMARY

The goal of high tibial osteotomy, a surgical treatment for Blount's disease, is correction of the mechanical axis of the limb. 35 children with Blount's disease underwent 46 proximal tibial valgus osteotomies during the period from January 1980 to December 1999. A retrospective analysis for change in angular correction in the early postoperative period was conducted. The tibial metaphyseal-diaphyseal angles were measured preoperatively, at surgery, and at initial healing. Our data did not yield and statically significant change with respect to age, sex, side of operation, or preoperative deformity. Plate fixation was found to be statically superior to pin fixation.

REFRENCES

Blount, W.P. (1937). *J. Bone Joint Surg Am*, **19**, 1-29.
Langenskiőld, A. (1981). *Clin Orthop,* **158**, 77-82.
Levine, A.M., Drennan, J.C. (1982). *J. Bone Joint Surg Am*, **64**, 1158-1163.
Pinkowski, J.L., Weiner, D.S. (1995). *J. Pediatr Orthop*, **15**, 307-312.

EVALUATION OF BONE CEMENT AUGMENTATION IN PROXIMAL FEMUR

Chaodi Li [1], Yan Zhou [1] and James Mason [1]

[1] Department of Aerospace and Mechanical Engineering, University of Notre Dame, Notre Dame, IN, USA

E-mail: mason. 12@nd.edu   Web: www.nd.edu/~ame

INTRODUCTION

The prevalence of bone fractures increases markedly with age, which is correlated to osteoporosis, low bone mass and structural deterioration of trabecular bone. Infiltration of bone cement into vertebral bodies (vertebroplasty) has been shown to substantially increase the strength and stiffness of mechanically compromised trabecular bone. It was expected that a similar benefit might be realized in the proximal femur [Heini, et al, 2001]. Before clinical trails, the effects of this treatment technique should be investigated. The objective of this study was to investigate the effects of cement augmentation on the mechanical properties of the proximal femur. In the present paper, the relative effects of bone osteoporosis, femoral neck fracture and cement augmentation on the femur stiffness were evaluated using finite element simulations.

METHODS

A standardized femur (FE Mesh Repository, Istituti Ortopedici Rizzoli, Italia) was used as a basis for the finite element model of an intact femur (Figure 1). For simulating the osteoporosis effects on the femur stiffness, the Young's modulus of the cancellous bone was reduced, which was assumed to be 20% of the normal bone tissue [Silva and Gibson, 1997]. Bone fracture effects were simulated using a crack inserted in only the top portion cortical shell of the femur neck, i.e. only halfway through the neck. When modeling bone cement augmentation, a cement mantle was placed within the femur geometry with its shape shown in Figure 1. A perfect bond between cement and bone was assumed in the analyses. In the finite element simulations, the distal section of the femur was fully restrained. The structure was loaded at the hip joint (femoral head) with 3 kN at an angle of 20^o to the shaft of the femur. This loading corresponds to loads experienced by a person weighing 70 kg during normal walking [Akay and Aslan, 1996]. The properties of the normal bones (cortical bone and cancellous bone) and cement are shown in Table 1 [Lennon and Predergast, 2002]. The finite element models were generated using commercial software Hypermesh (Altair Engineering Inc., Troy, MI, USA) and analyzed with the finite element package ABAQUS (HKS Inc., Pawtucket, RI, USA).

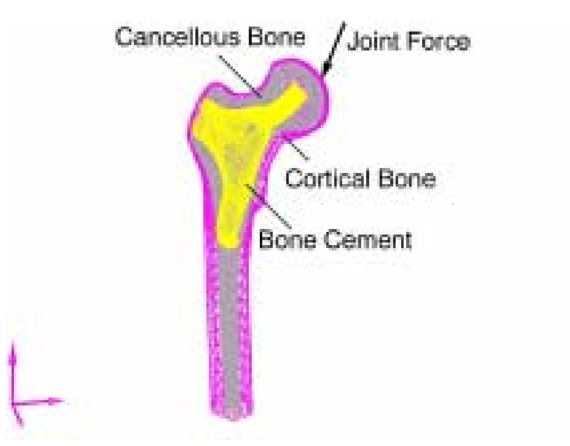

Figure 1: Finite Element Model of Bone Cement Augmentation in Proximal Femur

Table 1: Material Elastic Properties

Materials	Cortical Bone	Cancellous bone	Bone Cement
Young's Modulus (Gpa)	17	1.5	2.28
Poisson's Ratio	0.33	0.33	0.3

RESULTS AND DISCUSSION

The apparent stiffness of the proximal femur is shown in Figure 2 for several conditions, normal, fractured, and osteoporitic. For comparison, all the data were normalized with respect to the intact normal femur.

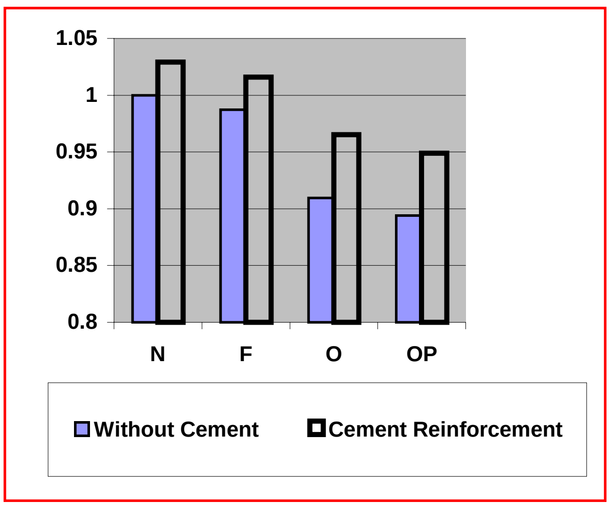

Figure 2: Apparent Stiffnesses of the Femur (N: Normal Bone Femur; F: Neck Fracture Femur; O: Femur with Osteoporosis Bone; OP: Femur with Neck Fracture and Bone Osteoporosis)

It is seen that femur stiffness with cement augmentation increased by 2.9%, 2.9% and 6.2% in normal bone, fractured bone and osteoporitic bone, respectively. This clearly demonstrates the efficacy of cement augmentation in reinforcement of the proximal femur. When the reinforced bone is osteoporitic, the stiffness of the femur was only 96% of the intact normal femur. This indicates that augmentation is not a replacement for bone loss and that prevention of bone loss is still desirable. Although the introduction of a partial neck fracture decreased the stiffness less than bone osteoporosis, it is expected that high stresses will occur near the neck fracture region, which will decrease the strength of the femur. Lastly, cement augmentation in the neck definitely improved stiffness in all cases and helps to reduce the concentrated stress around a fracture, which will likely strengthen the femur.

SUMMARY

The effects of bone cement reinforcement on femur stiffness were evaluated with three dimensional finite element analyses. This study shows that bone cement treatment is able to reinforce the osteoporitic femur and the neck-fractured femur. This is a preliminary study; further investigations are needed to provide more in-depth examinations before clinical application of cement reinforcement of the proximal femur is considered.

REFERENCES

Akay, M., Aslan, N. (1996*). J. Biomed. Mat. Res.*, **31**, 167-182.

Heini, P. F. et al. (2001). *Trans. 47th ORS*, 0898.

Lennon, A. B., Predergast, P. J. (2002). *J. Biomechanics*, **123** (6), 623-628.

Silva, M. J., Gibson, L. J. (1997) *Bone*, **21**(2), 191-199.

ACKNOWLEDGEMENTS

The research is supported by the Indiana 21st Century Research and Technology Fund and Zimmer, Inc.

EFFECT OF NAIL MATERIAL, NAIL SIZE AND "CANAL FILL" ON BIOMECHANICAL STABILITY OF COMMINUTED FRACTURES IN A PEDIATRIC-SIZED SYNTHETIC FEMUR MODEL

[1,2]Mahar, A, [3]Sink, E, [1]Oka, R, [2]Faro, F, [1,2]Newton, P

[1]Orthopedic Biomechanics Research Center, Children's Hospital – San Diego
[2]Department of Orthopaedics, University of California – San Diego
[3]Department of Orthopedics, Denver Children's Hospital
amahar@chsd.org

INTRODUCTION

The treating orthopaedic surgeon has many options available for the treatment of pediatric femur fractures. These include early spica casting, traction followed by spica casting, external fixation, open reduction and internal fixation, reamed intramedullary nails, and flexible non-reamed intramedullary (IM) nails. IM nails were mainly used to stabilize transverse fractures in pediatric populations. However, the frequency of use and types of fracture patterns stabilized by flexible intramedullary nails in the pediatric population has expanded over the last few years. Biomechanical data have supported their use. Lee et. al. (2000)[1] found that two 3.5mm stainless steel nails were effective in stabilizing both transverse and comminuted femur fractures in tests of torsion and compression using a pediatric sized synthetic model. In a subsequent study, titanium nails had improved biomechanical characteristics, during similar test conditions for torsion and compression, than stainless steel nails[2]. Clinical reviews at one facility (DCH) have reported that unstable fractures treated with 3.0mm titanium flexible nails were at risk for requiring an unplanned operative procedure, possibly related to inadequate "fill". Clinical questions remain as to the appropriate "canal fill" for maximum stabilization. Generally, a clinically optimal "fill" would be 80%. However, the biomechanical effects of increasing nail diameter; and therefore increasing "canal fill", have not been previously described. While comparison tests of materials have been conducted[2], a study comparing different materials across sizes has not been completed. The purpose of this study was to compare the biomechanical performance of increasing sizes of stainless steel and titanium intramedullary nails in tests of torsion, compression and valgus bending.

METHODS

Ten adolescent sized (38cm length) two-part composite synthetic femurs were randomly assigned to titanium or stainless steel repair groups (n=5/group). Each femur was then placed in a custom cutting rig and an identical 2cm section was removed from each diaphysis. For each type of material, the femurs were nailed in an ordered manner of increasing nail size. The available sizes for titanium were 3.0mm, 3.5mm and 4.0mm. The stainless steel sizes were 3.5mm and 4.0mm. Once fixed, the femurs underwent randomized testing in torsion, compression and valgus bending. For torsion and compression, femurs were tested with their mechanical axis in line with the MTS 858 Mini-bionix machine (Eden Prairie, MN). For torsion testing, cyclic torques between $\pm$ 2Nm were applied at 0.5 deg/sec over 5 cycles while maintaining 20N of compressive load, simulating passive muscle tension. For compression testing, a single test ramped to 5mm of failure at 0.5mm/sec. For each test, angle (deg), torque (Nm), displacement (mm) and force (N) were recorded at 10Hz. For torsion testing, range of motion (ROM) was measured. For compression testing, force values at 1mm increments were calculated. A custom fixation rig applied valgus bending loads directly to the femoral head at 0.5mm/sec until 15 degrees of valgus cantilever bending. Force and displacement were transformed into the bending moment required to induce a 15 degree valgus deformity. A one-way ANOVA (p=0.05) for multiple comparisons was used with a Tukey's *post-hoc* correction.

RESULTS

Fig 1: ROM During Torsion

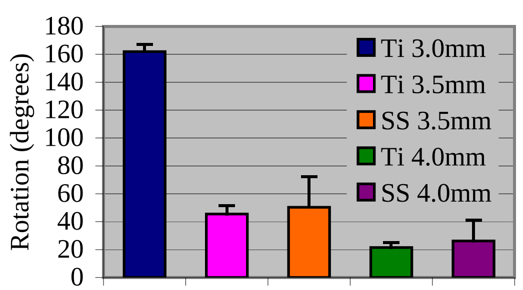

Data for range of motion during torsional testing indicated that the Ti 3.0 nails performed the worst ($p<0.000$), while the Ti 3.5 nails provided equal stabilization to the SS 4.0 nails (p=0.06) (Figure 1). Nails of equal size were equally stable.

Fig 2: Forces During Axial Loading

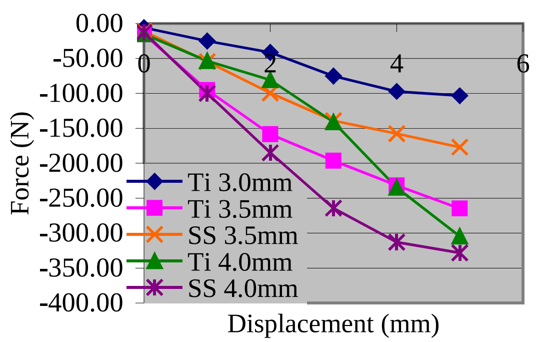

Data compressive forces during axial loading (Figure 2) showed that the Ti 3.0 nails had the lowest ultimate load at 5mm of compression ($p<0.02$). There were no differences between nails of equal sizes ($p\sim0.8$). There was no difference between the Ti 3.5 and SS 4.0 nails (p=0.37).

Fig 3: 15 Degree Valgus Torque

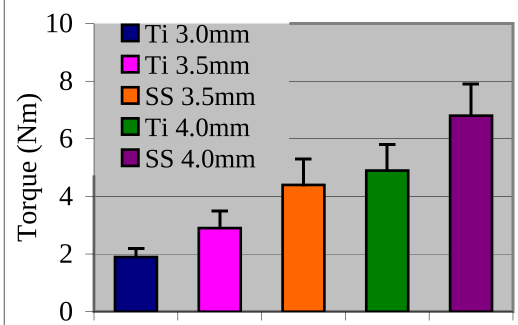

The bending torque required to create a 15 degree valgus deformity (Figure 3) was greatest for the SS 4.0 nails ($p<0.01$). The Ti 3.0 nails were weaker ($p<0.0001$) than all comparisons except the Ti 3.5 nails (p=0.2). For this test, the Ti 3.5 nails were weaker than the SS 4.0 nails ($p<0.008$).

SUMMARY

Data from this study demonstrate that a 67% canal fill (3.0 nails) provides little biomechanical stability. Increasing the fill from 77% (3.5 nails) to 89% (4.0 nails) increased stability; however there were no biomechanical differences between 3.5 titanium nails compared to 4.0 stainless steel nails for tests of torsion and compression.

REFERENCES

[1]Lee, SS, et. al., J Ped Orthop, 21, 442-445, 2001.
[2]Mahar, AT, et. al., Int. Soc. Biomech, P672, 2001.

ACKNOWLEDGEMENTS

This study was funded by a restricted research grant from the Denver Children's Hospital.

This document was created with Win2PDF available at http://www.daneprairie.com.
The unregistered version of Win2PDF is for evaluation or non-commercial use only.

BIOMECHANICAL COMPARISON OF THREE DIFFERENT FIXATION TECHNIQUES FOR TIBIAL EMINENCE AVULSION FRACTURES: SUTURES vs. BIOABSORBABLE NAILS vs. BIOABSORBABLE SCREWS

[1,2]Mahar, A, [3]Duncan, D, [1]Oka, R, [1,2]Chambers, H
[1]Department of Orthopedics, Children's Hospital, San Diego
[2]Department of Orthopaedics, University of California – San Diego
[2]Department or Orthopedics, Naval Medical Center, San Diego
amahar@chsd.org

INTRODUCTION

Tibial eminence fractures are relatively common injuries that range from minimally to completely displaced fractures. McKeever type II and III fractures represent 85% of all tibial eminence fractures and have poor outcomes using closed reduction techniques. Arthroscopic reduction may be accomplished using suture techniques or utilizing a variety of resorbable constructs[1]. Previous biomechanical studies have used human cadaveric femur-ACL-tibia complexes (FATC) for biomechanical testing of fixation constructs. Previous reports have shown that younger tissue has increased biomechanical strength.[1] However, this tissue still retains a great variation (~40%)[1], is difficult to obtain and very expensive. The immature bovine model has recently been used in rotator cuff research and does have a history in biomechanical studies of anterior cruciate ligament reconstruction.[2] Immature bovine bone has reported a bone density of 0.8g/cm^3, similar to the value reported for young humans[3], making the bovine model a viable biomechanical testing option.

Resorbable materials have an advantage over metallic devices since they do not require a secondary operation for implant removal. However, controversy exists as to the most appropriate fixation device. The purpose of this study was to compare the biomechanical performance of sutures, resorbable nails and resorbable screws for fixation of tibial eminence avulsion fractures.

METHODS

Twelve immature bovine knees from six animals (12-16 weeks old) were dissected of all soft tissue except the cruciate and collateral ligaments. This model and test method have been used previously for knee ligament research[2]. A tibial eminence fracture was created using standard osteotomes. The knees were then randomly assigned to one of three repair groups: #2 Ethibond sutures, bioabsorbable nail fixation (Smart Nails, Bionix Corp) or bioabsorbable screw fixation (BioCuff, Bionix Corp). The distal femur was potted in two-part epoxy resin and rigidly attached to the actuator of an MTS 858 machine (Eden Prairie, MN). The tibial diaphysis was also potted in two-part resin and secured to the load cell via a customized clamping rig at 35 degrees of flexion (Figure 1 A/B).

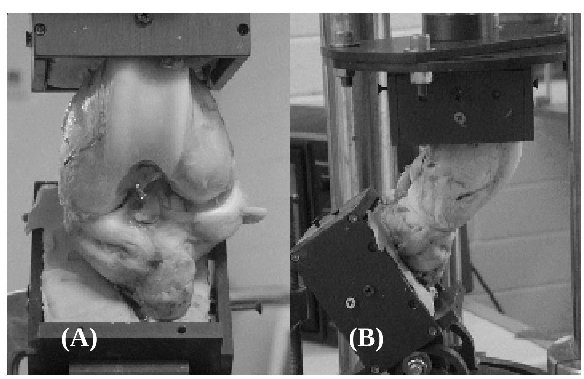

Figure 1A/B: Anterior and lateral views of test setup, respectively.

A pre-load of 5N was applied to reduce loads across the joint surface and isolate the eminence repair. A load control program applied physiologic cyclic loading between 5 and 150N at 1Hz for 200 cycles[4]. For repairs that withstood the cyclic testing, a single tensile failure test was then applied at a rate of 0.5mm/sec. Displacement (mm) and force (N) were collected at 10Hz for the duration of each test. Initial deformation was calculated over the first 5 cycles and initial stiffness from the load-deformation curve from the first 5 cycles. Failure load was taken from the final test. All data were averaged within repair groups and compared using a one-way ANOVA ($p<0.05$). A Tukey's *post-hoc* honest difference test was used when significance was found.

RESULTS AND DISCUSSION

Comparisons across groups did not yield significant biomechanical differences (Table 1). However, there was a potential clinical difference between repair techniques. Both sutures and screws resulted in a deformation that was more than 1mm greater than that for the nails. This 1mm of increased fracture separation indicates a potential loss in reduction during cyclic, physiologic loads. This deformation, along with stretching of the ACL during the time of injry, may also provide insight as to the post-operative ACL laxity reported previously. The nails and sutures had a similar initial stiffness and both were larger than the initial stiffness using screws. However, these differences were not significantly different.

While the sutures and screw groups had larger failure loads than the nails, each group could withstand up to an average of 380N of tensile force prior to failure. This minimum failure load likely exceeds those experienced during assisted weight bearing in the early post-operative period. However, clinicians should be aware that this failure load is lower than that during incidental/accidental weight bearing. The nail technique appears to offer two operative advantages. The nails are easier to insert arthroscopically than knot fixation. Also, nails are less likely to disrupt the open physis, compared to screws, in this population.

SUMMARY

The resorbable nail had lower initial deformation, comparable initial stiffness and lower failure loads than either screws or sutures fixation. Initial deformation and stiffness may be the most important clinical variables as they indicate the likelihood of fragment stabilization. Increased fragment stabilization reduces the problems associated with non-union or malunion. The biomechanical information gathered here necessitates an in-depth clinical review of tibial eminence fracture fixation techniques.

REFERENCES

[1]Noyes, RF, et. al. *JBJS [Am]*, 66, 1984.
[2] Hoffman, RFG, et. al. *J Arthro Rel Surg*, 15(4), 1999.
[3] Gibson, L, Ashby, M. **Cellular solids**. 1987, 316-331.
[4] Giurea, M, et. al. *AJSM*, 27(5), 1999.

Table 1: Biomechanical Data (**Mean** ± SD)

	Deformation (mm)	Stiffness (N/mm)	Failure Force (N)
Sutures	**2.96** ± 2.0	**27.17** ± 12.2	**466.74** ± 221.2
Screws	**2.96 ±** 1.2	**19.16** ± 4.7	**517.88 ±** 248.7
Nails	**1.77** ± 0.5	**26.37** ± 7.7	**383.62 ±** 131.6

This document was created with Win2PDF available at http://www.daneprairie.com.
The unregistered version of Win2PDF is for evaluation or non-commercial use only.

RELIABILITY OF MUSCLE ACTIVITY MEASURES DURING PERTURBED GAIT

Steven T. McCaw, J. Ty Hopkins, Todd A. McLoda, Deborah Birrer and Jeff G. Seegmiller

School of Kinesiology and Recreation, Normal, IL, USA
E-mail: smccaw@ilstu.edu Web: cast.ilstu.edu/mccaw

INTRODUCTION

Research investigating muscle response to sudden ankle inversion is popular because of the assumed role the muscles play in preventing ankle sprains. Most studies have measured responses when perturbations are induced from a position of quiet standing (i.e. Isakov et al, 1986). Since most ankle injury occurs during dynamic activity such as landing during running or from a jump, the clinical applicability of a static model is questionable. The purpose of this study was to quantify reliability in measures of ankle muscle activation collected during pilot testing of a methodology involving gait perturbation. A reliable and valid method of quantifying muscle response is imperative to study the neuromuscular aspects of ankle injury.

METHODS

Twenty-five healthy college age subjects (12 ♀ & 13 ♂) provided informed consent. Subjects completed 20 trials of walking at a controlled cadence (80 steps/min) along a 6m long raised walkway, custom made for our study. Sudden ankle inversion was induced on 5 randomly selected trials without notice to the subject. Dominant leg foot contact released a trapdoor concealed in the walkway, tilting the floor surface to 30° and allowing the foot to invert. Subjects were instructed to continue forward progression after trapdoor release.

An electrogoniometer was secured over the posterior shank and foot to measure ankle inversion. Muscle activity in the tibialis anterior (TA), peroneus longus (PL) and peroneus brevis (PB) was recorded (1000 Hz) using a commercially available EMG system (Biopac Systems, Inc.) and analyzed using custom software. For the peroneal muscles, latency was measured as the interval between trapdoor release and muscle activity onset. EMG linear envelopes were created and scaled to % of muscle activity measured from an isometric reference position (%IRP). The dependent variables (DV) describing EMG included latency, and peak %IRP and average %IRP values between onset and 200ms post trapdoor release.

The 5-trial mean value for each subject was calculated on each DV. Pearson's r was calculated between the DVs. Reliability of the muscle activity measures was quantified using procedures of Denegar & Ball (1993). The intraclass correlation coefficient designated as ICC (2,1) and the standard error of measurement were calculated (SEM= $SD\sqrt{1-ICC}$) for each measure across the repeated trials of the subjects. Statistical significance was set at α =.05.

RESULTS AND DISCUSSION

Ankle inversion following trapdoor release averaged 28±4° across all perturbed trials. This indicates the platform was capable of inducing the desired inversion.

There was a significant correlation between the PL and PB measures for latency (r =.84), but r was not significant between any of the muscles for average and peak %IRP values. Significant temporal similarity between PB and PL suggests that only one peroneal muscle needs to be monitored in future testing.

Table 1 presents the mean, SEM and ICC values for latency, average %IRP and peak %IRP.

Mean values for average and peak values range from 53 to 406 %IRP. The values for the PB and PL were significantly higher than those for the TA. Similarly, the SEM for both peroneal muscles was more than two times greater than the SEM for the TA. The SEM provides an estimate of the precision of measurement in units of the measurement (Denegar & Ball, 1993). This indicates the IRP used for the peroneal muscles (attempted eversion against manual resistance) did not sufficiently load the system to be used for scaling muscle activity.

The ICC value for latency was .90 for PL and .70 for PB. These values suggest acceptable reliability in our measured muscle onset, similar to Hopper et al (1998) and Benesch et al (2000). However, the ICC for both measures quantifying muscle activity level were lower across the three muscles (all ≤ .37), values unacceptable for purposes of our future investigations.

SUMMARY

The trapdoor mechanism in the walkway is appropriate for inducing sudden ankle inversion. However, the technique used to quantify muscle activity requires refinement. Use of a more demanding task to scale the EMG might reduce the variability and improve the precision of measured muscle activity.

REFERENCES

Benesch, S. et al, (2000). *Clin Biomech*., **15**, 21-28.

Denegar, C., Ball, (1993). D. *J. Sport Rehab.*, **2**, 35-42.

Hopper et al., (1998). *Clin. Ortho. Rel. Res.* **350**, 159-165.

Isakov, E. et al. (1986). *Acta. Ortho. Scand.* **2**, 100-109.

ACKNOWLEDGEMENTS

This project was funded by a *Jump Rope for Heart* grant to JTH & TAM from the Illinois Association for Health, Physical Education, Recreation and Dance.

Table 1. Means, standard errors of measurement (SEM) and intraclass correlation coefficients (ICC).

	Peroneus Longus			Peroneus Brevis			Tibialis Anterior		
	Latency	Average	Peak	Latency	Average	Peak	Latency	Average	Peak
Mean	57	232.6	367.0	60	280.2	405.8	NA	53.0	83.5
SEM	8	51.8	91.3	7	127.9	175.6	NA	15.4	23.7
ICC	0.90	0.16	0.13	0.70	0.25	0.24	NA	0.31	0.37

Note: Mean and SEM values are in absolute units (Latency: ms; Average & Peak: %IRP)

QUANTIFICATION OF SURGEON IMPACTION OF MORSELIZED CANCELLOUS BONE IN REVISION THA

Anneliese D. Heiner, Thomas D. Brown, and John J. Callaghan

Departments of Orthopaedic Surgery and Biomedical Engineering,
University of Iowa, Iowa City, IA, 52242, USA
E-mail: anneliese-heiner@uiowa.edu

INTRODUCTION

Impaction grafting with morselized cancellous bone (MCB) is increasingly utilized in revision total hip arthroplasty (THA). In this procedure, MCB is inserted and impacted into the surgical site, to build up bone stock which had been lost to osteolysis or during prosthesis removal. Ideally, bone remodeling proceeds from the adjacent live host bone, into the bone graft, such that eventually the MCB graft is fused into a new cancellous lattice that is contiguous with the host bone. Before this fusion occurs, however, the impaction graft must provide adequate mechanical stability, to prevent excessive prosthesis subsidence or migration during remodeling.

The structural properties of an impaction graft can depend on many variables, including MCB particle size, impaction magnitude (impulse, energy, maximum force), amount of MCB inserted per graft layer, number of impactions per graft layer, and longitudinal position within the graft. There is considerable variability in the impaction grafting literature among the type and magnitude of these impactions. The impaction grafting literature is also sparse on the issue of impacts per layer, and amount of MCB per layer used clinically. Therefore, the purpose of this study was to quantify the impaction grafting procedure as performed by an experienced orthopaedic surgeon, for use in subsequent studies of impaction grafting.

MATERIALS AND METHODS

The impaction grafting procedure was performed on bones from elderly human cadavers. Cavitary defects (the type of bone defect found in patients requiring impaction grafting revision THA) were created by removing cancellous bone. The MCB size was 4–6mm for the femur, and 8–12mm for the acetabulum. Impaction grafting instrumentation was provided by DePuy Orthopaedics (Warsaw, IN) (Figure 1). The orthopaedic surgeon (J.J.C.) was requested to perform the impaction grafting procedure using his regular protocol; this study was designed for minimal interference while quantifying the procedure.

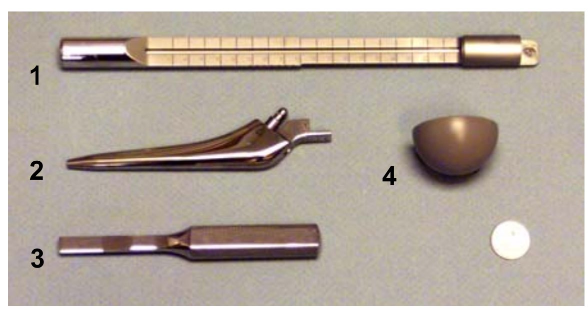

Figure 1: Distal femur impactor (1), proximal femur impactor (2), femoral tamp (3), and acetabular impactor (4). Scale indicated by quarter.

Impaction force was measured with a customized impulse force hammer (model 086C05, PCB Piezotronics, Depew, NY). The customization included mass extenders, to replicate the mass and inertia of a surgical impaction hammer, and a replaceable brass

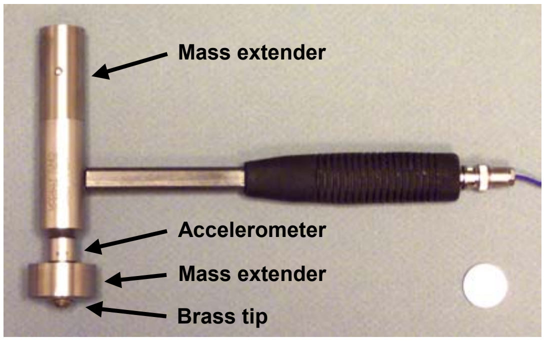

Figure 2: Customized impulse force hammer used for measuring impaction grafting impulse. Scale indicated by quarter.

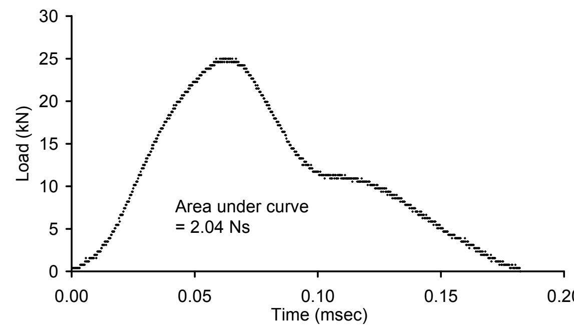

Figure 3: Representative proximal impaction impulse reading.

tip, to allow the force to be transmitted axially through the accelerometer (Figure 2). Impulse force hammer data were collected in 250 nanosecond intervals using a digital oscilloscope (model 54601A, Hewlett-Packard, Colorado Springs, CO). Impulse (integral of force vs. time) was calculated using Excel (Figure 3). Recordings which indicated that the force was not transmitted axially through the accelerometer (i.e., an off-axis hit) were not included. The number of impactions per layer, amount of MCB per layer, number of layers, and type and size of impaction instrument were also documented.

RESULTS AND DISCUSSION

Summary data on material utilization, numbers of impactions, and average impulse magnitudes for THA impaction grafting are reported in Table 1. The impulse values reported here are consistent with impulse values used in several recent bench studies of impaction grafting (Cornu et al., 2001; Grimm et al., 2001; Voor et al., 2000). The present data, to our knowledge, are the first available that fully characterize this specialized but important procedure.

REFERENCES

Cornu, O. et al. (2001). *Trans 47th ORS,* **26**, 1081.
Grimm, B. et al. (2001). *J Mater Sci: Mat in Medicine,* **12**, 929–934.
Voor, M.J. et al. (2000). *J Biomechanics,* **33(12)**, 1683–8.

ACKNOWLEDGEMENTS

This study was funded by NIH R03 AR46863. The authors wish to thank DePuy Orthopaedics for donating instrumentation, and Jessica Leinen for her assistance.

Table 1: THA impaction grafting procedure. Standard deviations of impulses are in parentheses. Femoral tamp was used on only one femur.

Instrumentation	Distal femur	Proximal femur	Femoral tamp	Acetabular
# layers	2–3	3–4	0–1	5
Impacts/layer	5–6	5–17	5	5–10
MCB/layer (ml)	10–20	5–35	10	7.5–15
Total impacts	10–16	38–41	5	36
Impulse (Ns)	1.70 (0.31)	2.05 (0.42)	0.54 (0.13)	1.56 (0.14)

QUANTIFYING FRACTURE ENERGY IN ORDER TO PREDICT POST-TRAUMATIC OSTEOARTHRITIS

Donald D. Anderson, Christina L. Beardsley, J. Lawrence Marsh, and Thomas D. Brown

Department of Orthopaedic Surgery, The University of Iowa, Iowa City, IA, USA
e-mail: don-anderson@uiowa.edu   web: poppy.obrl.uiowa.edu

INTRODUCTION

Bone and joint injuries with comminution (multiple small fragments) present a significant clinical challenge. There is a high incidence of post-traumatic osteoarthritis, likely linked to the initial trauma and to subsequent altered joint mechanics. The mechanical insult to articular cartilage is impossible to directly quantify, but bone fragmentation energy presents an indirect measure of the insult in situations such as tibial pilon fractures, for which the injurious forces are delivered to bone exclusively through joint loading.

We have developed novel measures of fracture energy absorption, using laboratory models predicated on fracture mechanics principles. The feasibility of an approach using CT-based assessments of freed fracture surface area was initially established using a dense polyetherurethane foam (Beardsley et al, 2002), followed by extension to bovine transcortical bone segments (Beardsley et al, 2001). Both series showed a statistically significant increase in measured *de novo* surface area with increase in fragmentation energy.

To demonstrate the feasibility of applying the CT-based techniques to bona fide patient fracture data, and to elucidate areas where further algorithm development may be necessary, bone free surface area was measured in tibias from a series of three clinical pilon fracture cases, as well as in seven intact tibias.

METHODS

CT studies obtained in standard clinical care from three fracture cases between 8/2001 and 9/2002 were analyzed in this preliminary investigation. The patients, all male, ranged in age from 19 to 59 years old. The fractures ranged from minimal to extensive comminution (Figure 1). Contralateral limb data were available to estimate pre-fracture endosteal and periosteal surface areas. Scans from the Visible Male and Female CT datasets were included in the analysis in order to assess side-to-side variability between bone surface areas in intact tibias.

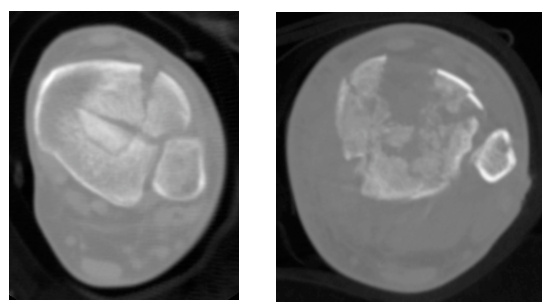

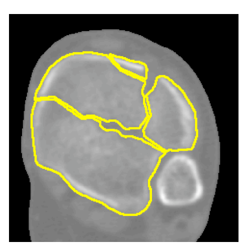

Figure 1: CT slices from two of the fracture cases analyzed (above) with identified bone edges in the tibia from the case on the left.

Bone surface area measurements were extracted slice by slice from the datasets, using validated digital image analysis routines executed in MATLAB. The amount of *de novo* surface area presumably liberated during fracture was calculated as the difference between areas calculated on the intact and fractured tibias of a given patient.

RESULTS AND DISCUSSION

The total free bone surface areas measured in the intact tibias (Table 1) ranged from 9300 to 17,828 mm^2. Between tibias in the Visible Male and Female dataset, there was a less than 3% side-to-side variation.

Table 1: Free bone surface areas measured in the three clinical cases and the visible male and female.

	bone surface area (sq mm)	% deviation from intact
Clinical Case 1 (intact)	16337.12	
(fracture)	19504.04	19%
Clinical Case 2 (intact)	9300.19	
(fracture)	12715.55	37%
Clinical Case 3 (intact)	9781.96	
(fracture)	25217.84	158%
Vis Male L (intact)	17791.71	
Vis Male R (intact)	17828.27	0%
Vis Female L (intact)	13438.42	
Vis Female R (intact)	13847.58	3%

In one illustrative fracture case (Clinical Case 1), there were eight distinct fragments identified in the patient's fractured tibia. The total surface area for the intact contralateral distal tibia was 16,337 mm^2. On the fractured side, surface area was 19,504 mm^2, yielding a net liberated surface of 3167 mm^2, a 19% increase over the intact.

In contrast, there were 70 measured fragments in the distal tibia of the most comminuted fracture case (Clinical Case 3). Among the fractured tibias, surface areas ranged from 19,504 to 25,218 mm^2, yielding net liberated surface areas ranging from 3167 to 15,436 mm^2. Expressed as % deviations from the intact side, *de novo* surface area thus ranged from 19 to 158%.

Because fracture toughness parameters are material-dependent, surface area measurements should ideally incorporate local material variability, available in the form of CT Hounsfield densities. Approximately 45% of Clinical Case 1 fracture's surface area was contributed by cancellous bone.

We have also been working to streamline our digital image analysis routines to run more quickly in an effort to enhance their clinical utility. Clinical case processing time has been reduced from two person-weeks initially, to now roughly six hours. This speed gain was achieved with a switch from a seeded fragment-growing algorithm (emphasizing fine spatial detail), to a custom thresholding approach requiring less user intervention yet yielding practically indistinguishable results.

SUMMARY

We have shown that we can quantify liberated bone surface area associated with clinical pilon fractures. Our previous work has shown that this parameter correlates closely with fragmentation energy. We can now, for the first time, quantify the mechanical insult associated with a clinical fracture, previously an immeasurable confounding factor in studies of post-traumatic OA.

REFERENCES

Beardsley, C.L. et al. (2002). *J Biomech,* **35**, 331-338.

Beardsley, C.L. et al. (2001). *Proceedings of 25th ASB Meeting,* 209-210.

ACKNOWLEDGEMENTS

Funded by the Arthritis Foundation, the Orthopaedic Research and Education Foundation, and the NIH (AR46601 and AR048939).

FREE RADICAL SCAVENGERS REDUCE THE BIOMECHANICAL AND BIOCHEMICAL IMPAIRMENT OF GAMMA IRRADIATED BONE ALLOGRAFTS

Ryan M. Belaney, Ozan Akkus

Orthopaedic Bioengineering Laboratory, University of Toledo, Toledo, OH, USA
E-mail: ozan.akkus@eng.utoledo.edu

INTRODUCTION

Prevention of viral and bacterial disease transmission by gamma radiation is widely used for sterilization of bone allografts (1). Despite its efficacy in sterility assurance, it has been shown that gamma radiation negatively affects the material properties of bone (2). The impairment in material properties is largely believed to stem from the cleavage of collagen molecules of bone via free radical attack(3). We hypothesize that the biochemical and biomechanical impairment of bone grafts during gamma radiation sterilization can be ameliorated via suppression of free radical generation using the free radical scavenger thiourea.

METHODS

Preparation of test specimens: Four fresh frozen bovine ulnae (3-4 years old) were machined into tensile test specimens. All specimens were obtained from the anterior mid-diaphyseal region. A low-speed metallurgical saw (South Bay Tech, San Clemente, CA USA) and a table-top milling machine(Sherline, CA USA) were used to machine specimens. The gage region measured 16 mm in length, 2 mm in width, and 1mm in thickness. Specimens were kept in calcium supplemented saline solution and stored at -40°C.

Treatment of Specimens: Thirty specimens were randomly placed into six treatment groups (n=5, each): control (C), irradiated (I), 0.5 [M] thiourea treatment (0.5 [M]), 1.5 [M] thiourea treatment (1.5 [M]), 0.5 [M] thiourea treatment and irradiation (0.5 [M] - I) and 1.5 [M] thiourea treatment and irradiation (1.5 [M] - I). Specimens were kept in aqueous thiourea solution supplemented with calcium at 4°C for two-weeks. The solution was supplemented with protease inhibitors to prevent microbial degradation and was changed every three days. Gamma radiation sterilization was performed using ^{60}Co source at an average dose of 30 kGy (Steris Corporation, Mentor, OH USA).

Biomechanical Tests: Specimens were monotonically loaded to failure under tension using an electromagnetic testing machine (ELF 3200, Enduratec, Minnetonka, MN USA). The loading was displacement controlled at a rate of 1%/s. Energy to fracture parameter was obtained from stress-strain curves.

Biochemical Analysis: The integrity of collagen molecules were assessed by SDS-PAGE analysis (n=2). The purification involved demineralization by formic acid, salt precipitation, dialysis to remove demineralization products, and solubilization of collagen molecules through pepsin digestion. In between purification steps of specimens, samples were lyophilized. Solubilized collagen molecules were loaded on 5% acrylimide-bis SDS-PAGE gels to determine the amount of intact alpha and beta chains.

RESULTS AND DISCUSSION

There were no statistically significant differences between the mechanical properties of any treatment groups for the bovine cortical bone. However, the trend in the data was as expected for most mechanical properties observed in the study such that (Fig 1.): The irradiated group demonstrated smaller energy to fracture than controls. Thiourea treated control groups were similar to controls suggesting that thiourea alone does not alter mechanical properties of bone. There was an apparent improvement in the mechanical properties of irradiated specimens treated with thiourea such that mechanical properties of irradiated specimens treated with 1.5 [M] thiourea was greater than irradiated specimens treated with 0.5 [M] thiourea and irradiated alone. Also the mechanical properties of irradiated specimens treated with 0.5 [M] thiourea were greater than those specimens irradiated alone. It appeared that the mechanical properties of irradiated specimens treated with 1.5 [M] thiourea were similar to the mechanical properties of unirradiated controls. This observation suggests that thiourea may have a radioprotective effect on the mechanical properties of bone.

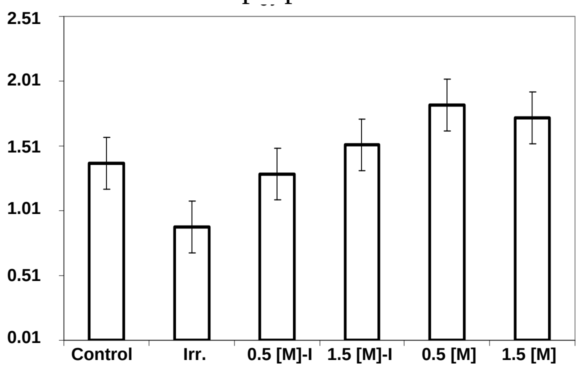

Fig. 1 Energy to fracture (Joules) of treatment groups. Error bars illustrate the standard error of the mean.

Biochemical results showed that there was a decrease in the intensity of α-chains following sterilization. It is shown in lane profiling that the irradiated samples treated with thiourea demonstrated intact α-chains (Fig. 2).

It is known that gamma radiation embrittles bone tissue by impairing the post-yield properties rather than the pre-yield properties (2,4). As bovine bone already suffers in terms of post-yield deformability in its natural state, further embrittlement due to gamma radiation sterilization is highly limited. Therefore, we do not suggest bovine ulna as a model for investigation of gamma radiation induced embrittlement.

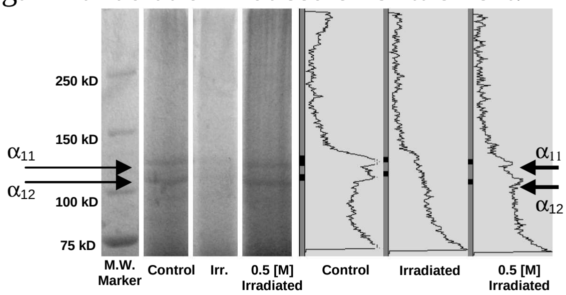

Fig 2:SDS-PAGE and lane profiles of the control, irradiated and 0.5 [M] irradiated samples.

SUMMARY

The trend observed in these results supports the hypothesis that the suppression of free radical generation has a radioprotective effect on the mechanical and biochemical properties of gamma radiation sterilized cortical bone tissue. The results of this preliminary study suggest that suppression of free radical damage via thiourea treatment may yield stronger and more durable grafts.

REFERENCES

1. Bright, R.W. et al. (1984). *Osteochondral Allografts: Biology and Clinical Applications*. Little and Brown Company.
2. Triantafyllou, N.(1975). *Acta OrthopBelg*, 41(S1), 35.
3. Hamer, A.J., Stockely, I. (1999). J. Bone Joint Surg, 81, 342.
4. Currey, J.D., Foreman, J. (1997). *J. Orthop Res*, 15, 111.

ACKNOWLEDGEMENTS

We thank the Musculoskeletal Transplant Foundation for funding this study.

THE ROLE OF ACCESSORY RESPIRATORY MUSCLE IMPAIRMENT IN THE MECHANISM OF RIB FRACTURE IN ROWERS

Jennifer A. Whitney[1,2]*, MPT and Joyce Campbell[2], PT, PhD
1 Rancho Los Amigos National Rehabilitation Center, Pathokinesiology Lab
2 California State University Long Beach, Department of Physical Therapy
E-mail: Jwhitney@dhs.co.la.ca.us,
* the author completed this study as a thesis project while a master's level graduate student in the Dept. of Physical Therapy

INTRODUCTION

The purpose of this study was to investigate the dual function of Serratus Anterior during 2000m rowing time trials relative to the mechanism of rib fracture previously reported in competitive rowers. The research presented in the literature has not conclusively established one mechanism of injury in the etiology of rib fracture, however, the most common location reported in the rowing and golf communities has been on the postero-lateral aspects of ribs 5-9**.** Serratus Anterior has been shown to be integral during several phases of the rowing stroke, as well as during respiration (Sliwinsky, 1996) with deep inspiration for increased ventilatory capacity by way of raising and expanding the rib cage (McConnell 1997, Smith 1994). Impaired function of the SA may be one risk factor for the development of rib fractures, an injury that is pervasive in the competitive rowing community with incidences reported as 32.6% in female rowers and ratio of 1.58:0.85 F:M (Hickey, 1997). The intent of this study was to obtain normative data related to pathomechanics of rib fracture in rowers in an effort to establish evidenced risk factors to augment preventative training techniques and rehabilitative strategies.

METHODS

The subjects included asymptomatic sweep rowers from California State University Long Beach rowing team and normal age-matched controls (mean age 22.9 SD 4.65, $P<0.05$) including 24 untrained rowers (UR,<3 yrs training, 14 females, 10 males), 9 trained rowers (TR>3 years, 5F:4M), and 12 controls (NR, 5F:7M). 1 subject had a prior history of rib fracture, postero-lateral rib 7 that was well healed by x ray. Subjects were cleared for participation by a physician and surveyed for exclusion secondary to injury, medical, or orthopedic pathology. Asthmatic rowers' (AR, N=4) data were analyzed separate from non-asthmatic rowers (NAR, N=29). The rowers participated in three test sessions. The first and second testing sessions were 1 week apart, at the same time of day, after 1 week of heavy work load training. Tests included a 2000m timed rowing trial (concept II ergometer) with measures collected of pre(I) and post(F) time trial: Heart rate (I, F), Forced Vital Capacity(I, F), and lactate measurement (I, F1min, F3 min). Additional measures of Maximum Inspiratory Peak Pressures (MIPP), MIPP80 (time maintaining 80% peak inspiratory pressures), and Maximum Voluntary Ventilation (MVV) for measures of accessory inspiratory muscle strength (MIPP, Rochester, 1988) and endurance (MVV, MIPP80) were collected at the second testing session. The final set of measures were electroneuromyography, and assessed innervation status and injury of Long Thoracic Nerve (LTN). The control group participated in tests 2 and 3 as above. Diagnostic EMG, was conducted by a licensed electrodiagnostician on subjects with history of rib fracture or determined neurologic impairment.

RESULTS AND DISCUSSION

The ENMG data demonstrated that while gender may influence the chronaxies (F 0.039, SD 0.024, M 0.24 SD 0.19 $P<0.05$) and sport development may influence the amplitude (peak to baseline mean R 4.5 SD 0.7, NR 2.14 SD 1.38, $p=0.057$), the subjects were neurologically intact. The time means data ($p<0.05$) indicated that the subjects were grouped appropriately R (7-7.5 min) (<) than NR (>9:30), TR(7-7:30) < UR (7:30-8), and AR (8-8:30)> NAR (7-7:30). All subjects utilized similarly amplified cardiovascular response. However, averaged MVV data indicated TR demonstrated proportionally higher increases in ventilatory volume (TR 35.4 to 37.9 BPM, 106.4 to 116.14 L/min), while UR increased rate and volume of ventilation, (UR 40.4 to 47 BPM , 98.8 to 184.3 L/min), as did AR (33 to 44 BPM, 98 to 108 L/min MVV), and NAR increased primarily volume (42.4 to 39 BPM, 101 to 157 L/min). Significant increases in lactate values from baseline were higher R>NR, TR > UR AR>NAR post erg. Significant drop of post erg MIPP80 was observed in all groups: 37%UR, 40%TR, 41%NR, AR 60%, NAR 39%. TR v. UR had no differences in baseline MIPP however, TR demonstrated greatest post erg decrease (TR 19.2% v. UR 1.8%). While all groups decreased in the MIPP 80 times, the TR demonstrated in the face of normal FVC and respiration, severe compromise in post erg MIPP.

SUMMARY

These data may suggest that at maximum fatigue trained rowers, controls, and asthmatic rowers may be at the highest risk for fatigue fracture secondary to impaired accessory respiratory muscle strength and endurance contributing to excessive rib bending forces leading to rib fracture. At end stage maximum fatigue, the SA may not maintain the stroke necessitated eccentric resistance, isometric stabilization at the catch, or may demonstrate impaired muscle length/tension relationship. These values may be underestimated as they lacked torsional and side bending forces of sweep rowing. Research has supported skeletal muscle warm-up phenomena in MIPP/MIPP 80 data, (Volianitis, 2000), increased tidal volume with entrainment (Steinacker, 1993), decline in inspiratory mm endurance after high intensity workload (Ker, 1996), and correlated workload fatigue with respiratory fatigue and decrease in MIPP values (McConnell, 1997). This data and previous literature implicate the necessity for pre-season workload respiratory muscle assessment, warm up, and inspirometry training for decreased risk of fatigue fracture, improved performance, and rehabilitative efficacy.

REFERENCES

Hickey, G.J. et al. (1997). *Med Sci Sports Ex*, 29(12),1567-72

Ker, J., Schultz, C.M. (1996). *Int J Sports Med*, 17(7):493-6

McConnell, A.K., et al. (1997) *Int J Sports Med*,18(3),169-73

Nava, S. (1998) *Monaldi Arch Chest Dis*, 53(6), 640-3

Rochester, D.F. (1988) *Clin Chest Med* Jun;9(2):249-61

Sliwinski, P. et al.(1996) *Pneum Aler Pol*, 64(9-10), 590-603

Steinacker, J.M. et al. (1993*). Int J Sports Med*. 14 Suppl 1:S15-9.

Volianitis, S., et al. (1999) *Int J Sports Med* , 20(8), 542-7

RIB GEOMETRY PERTINENT TO OPERATIVE CHEST WALL FIXATION

Marcus Mohr [1], Suresh Kasaraneni [2], Christine Engel [1], and Michael Bottlang [1]

[1] Biomechanics Laboratory, Legacy Health System, Portland, OR, USA
[2] Oregon Health & Science University, Portland, OR, USA
E-mail: mbottlan@lhs.org

INTRODUCTION

Plating of multiple segmental rib fractures can aid restoration of pulmonary function in a timely manner to reduce mortality associated with prolonged mechanical ventilation (Tanaka et al., 2002). Since no specialized or pre-contoured plates are commercially available, generic small fracture plates are commonly used for rib fracture fixation (Oyarzun et al., 1998). However, due to the complex geometry of ribs, intra-operative contouring of generic plates is time-consuming and difficult at best.

This study quantified the curvature of human ribs, the longitudinal twist along the rib diaphysis, and the unrolled shape of the outer cortical surface.

Results of this study are directly applicable to improve the accuracy and speed of intra-operative plate-contouring, and provide a scientific basis for the design of pre-contoured plates for rib fracture fixation.

METHODS

Right ribs three through nine were harvested from eight fresh frozen human cadavers (64 ± 13 years, 172 ± 10 cm, 64 ± 25 kg, 4 male, 4 female) and stripped of soft tissue. Three parallel lines l_M, l_S, l_I were marked along each rib between the tubercle and the costo-chondral junction (CCJ): at mid-height, 5mm superior and 5mm inferior of mid-height, respectively (Fig. 1).

A reference frame was defined for each rib with the origin in the center of the tubercle, the Y-axis crossing the CCJ, and the X-Y-plane coinciding with the midline at 0% (tubercle), 50%, and 100% (CCJ) of the rib length.

Points $P_{S,i}$, $P_{M,i}$, and $P_{I,i}$ were digitized in 2mm intervals along lines l_S, l_M, and l_I, respectively, using a 3-D digitizing system (MicroScribe, Immersion, San Jose, CA).

Rib curvature: The apparent radius R_i along the rib was calculated by fitting circles to sequential point triplets ($P_{M,i-20}$, $P_{M,i}$, $P_{M,i+20}$), using custom software code (MATLAB, Mathworks, Natick, MA). The apparent radius was then expressed as curvature $C_{\%} = 1/R_i$ for normalized locations along the rib length (0% = tubercle, 100% = CCJ).

Longitudinal twist: Ribs three through nine have in common a characteristic twist about their longitudinal axis. This twist was quantified by calculating angles α_i between the orientation of the outer cortical surface, defined by vectors $\underline{v}_{IS} = [P_{I,i}, P_{S,i}]$, and the Z-axis (Fig. 1).

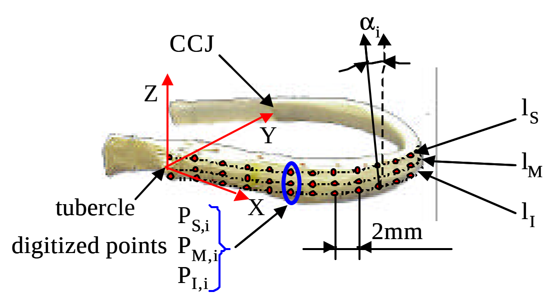

Figure 1: Rib coordinate system; inferior-, mid-, and superior lines l_I, l_M, l_S; and α_i between outer surface and vertical axis.

The total longitudinal twist α_{LT} was defined as the difference between α_i values obtained at 15% and 85% of the rib length.

Unrolled Shape: The outer surface of the rib was unrolled onto a plane (Fig. 2), in order to derive a two-dimensional shape that follows--upon bending--the outer surface of the rib. This was realized by outlining the rib contour on a flexible sheet conform with the rib's outer surface. Subsequently, this sheet was unrolled on a flat surface. The Matlab circle-fitting procedure was used to quantify the curvature C_u of the centerline of the unrolled contour.

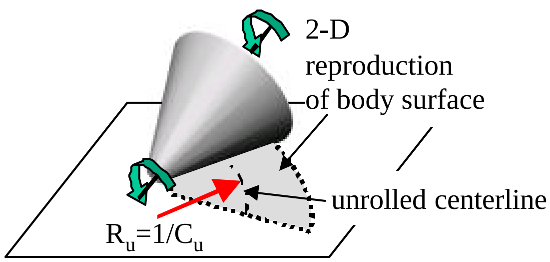

Figure 2: Unrolling a 3-D surface onto a plane.

RESULTS

The rib curvature $C_{\%}$ was similar among ribs three through nine at 15% and 85% rib length, respectively (Fig. 3). The posterior segment exhibited more than twice the curvature as compared to the anterior segment. The highest curvature was found in rib three at 15% length with C_{15} = 17.3 m^{-1}. The straightest portion was found in rib seven at 65% length with C_{65} = 3.8 m^{-1}.

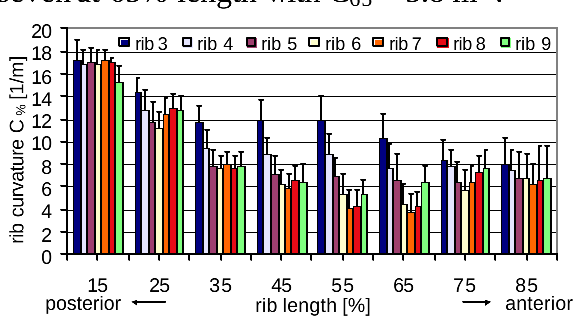

Figure 3: Rib curvature $C_{\%}$ for right ribs three through nine.

The longitudinal twist α_{LT} was counterclockwise in the right rib specimens. α_{LT} was smallest for rib three with 41 ± 14° and largest for rib eight with 60 ± 6° (Fig. 4). The observed variation in magnitude of α_{LT} between ribs three through nine was not statistically significant ($p>0.05$).

The curvature C_u of the unrolled centerline changed significantly in magnitude and direction from rib three through rib nine. C_u was most pronounced in rib three with a magnitude of 7.0 m^{-1} (Fig. 4). C_u was smallest in rib six with a magnitude of 1.1 m^{-1}. Ribs three through five were curved in opposite direction of ribs six through nine.

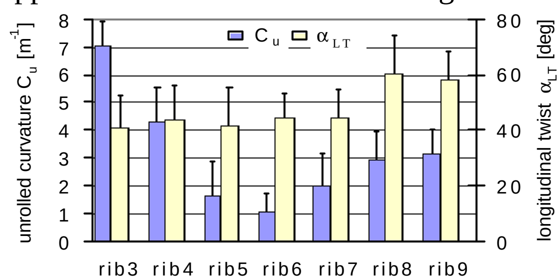

Figure 4: Unrolled curvature C_u and longitudinal twist α_{LT}

DISCUSSION

The presented study delineates complex spatial rib geometry into three basic parameters, which bear direct implications for pre- and intra-operative contouring of osteosynthesis plates used in chest wall fixation. While rib curvature, unrolled curvature, and magnitude of longitudinal twist can be assumed identical for right and left ribs, the direction of twist reverses to clockwise on left ribs, owing to para-saggital symmetry.

REFERENCES

Tanaka et al. (2002). *J Trauma*, **4**, 52

Oyarzun. et al. (1998). *Ann Thorac Surg*, **65**, 1471

ACKNOWLEDGEMENT

Supported by Legacy Research Foundation

COMPUTATIONAL ALGORITHM FOR ESTIMATING MUSCLE PROPERTIES

Brian A. Garner[1] and Marcus G. Pandy[2]

[1] Department of Engineering, Baylor University, Waco, Texas
[2] Department of Biomedical Engineering, University of Texas, Austin, Texas
E-mail: Brian_Garner@baylor.edu Web: www.ecs.baylor.edu/ecs

INTRODUCTION

Zajac (1989) proposed a generic, Hill-type model for musculotendon actuators that accounts for the force-length-velocity properties of muscles in musculoskeletal models. Zajac's model can be customized to a specific muscle by assigning values to five parameters: peak isometric force (F_o^M) and the corresponding fiber length (L_o^M) and pennation angle (α_o), maximum shortening velocity (v_o^M), and tendon slack length (L_s^T). Equipped with values for these parameters, the model can be used to calculate a muscle's force output as a function of the muscle-tendon length, velocity, and activation. Of particular importance are values of L_o^M and L_s^T, which determine where the muscle operates on its characteristic force-length curve over the range of joint motion (i.e. the muscle-tendon excursion).

Despite the importance of these parameters, determining appropriate values can be difficult because values reported in the literature vary significantly for even the same muscle. In addition, little data may be available for some parameters, such as L_s^T.

The aim of this study was to 1) develop a general method for estimating musculotendon properties, and 2) apply the method to estimate properties for forty-two muscles represented in a musculoskeletal model of the human upper limb.

UPPER LIMB MODEL

The upper limb model (Garner and Pandy, 2001) was derived from bone and muscle surface geometry reconstructed from the Visible Human Male (VHM) image set. Thirteen degrees of freedom describe motion of the bones from the sternoclavicular joint to the wrist joint. Forty-two muscle bundles representing the action of twenty-six muscle groups actuate the bones in the model. The path of each muscle bundle is modeled as an elastic band wrapping over simple geometric shapes. The fidelity of the modeled muscle paths was validated against experimental moment-arm data obtained from the literature (Garner and Pandy, 2001).

METHODS

A two-phase optimization scheme was used to estimate values of F_o^M, L_o^M, and L_s^T for all muscles in the model (Garner and Pandy, 2003). v_o^M was not calculated by the method as only isometric muscle contractions were considered in this study. α_o, considered to have a minor impact on model behavior, was assigned values obtained from the literature.

The parameter F_o^M was assumed to be proportional to physiological cross-sectional area (PCSA) by a constant (330 kPa) representing maximum muscle stress. PCSA was defined as the ratio between muscle belly volume and L_o^M. Because muscle belly volume was readily calculable from each muscle's reconstructed surface model, F_o^M was expressed as a function of L_o^M and eliminated as an unknown.

The remaining unknowns, L_o^M and L_s^T, were calculated simultaneously for all muscles using the optimization scheme. The procedure begins by assigning initial values to L_o^M and L_s^T for each muscle to ensure that the muscle operates within its active force region throughout the joint range of motion (i.e. its total muscle-tendon excursion). The total excursion of each muscle was calculated in advance using the model assumed for the muscle-tendon path.

The objective of the optimization scheme was to select values of L_o^M and L_s^T for all muscles such that the overall strength profile of the model matched as closely as possible the overall strength profile of human subjects. Each strength profile consisted of a total of 116 maximum isometric joint torque-angle trials representing the strength of flexion and extension at the shoulder, elbow, and wrist, abduction, adduction, and internal and external rotation of the shoulder, pronation and supination of the forearm, and radial and ulnar deviation of the wrist. Data representing the strength profile of human subjects was compiled from studies reported in the literature and from experiments performed with three healthy male subjects.

The model's strength profile was computed by simulating each of the 116 joint torque-angle trials during the first phase of the optimization scheme. During this phase the current values of L_o^M and L_s^T were held constant while muscle activation levels and joint position angles were computed to maximize joint torque for each trial.

In the second phase of the optimization scheme, values of L_o^M and L_s^T for all muscles were varied to achieve an optimum match between the simulated and experimental strength profiles. These two phases were repeated iteratively until no further improvement could be made.

RESULTS AND DISCUSSION

For the upper limb model the root summed square of normalized error averaged less than 15% for the 116 trials, with most trials falling below 10% error. The calculated values of muscle volume, PCSA, and F_o^M tended to be larger than corresponding values reported in the literature. These results may be due to the fact that the VHM subject was young and rather muscular, whereas subjects in cadaver studies are often elderly with less muscle mass. The calculated values of L_o^M and L_s^T compared much more favorably to data reported in the literature (when available). All muscles were found to operate within their active force region for a large portion of their muscle-tendon excursion.

SUMMARY

A method to estimate musculotendon properties was applied to forty-two muscles modeled in the upper limb. The method calculates values of L_o^M, L_s^T, and F_o^M for each muscle to reproduce human strength characteristics and to operate within the constraints of simulated muscle paths. The method requires knowledge of the volumes and total excursions of the modeled muscles, along with an experimental strength profile.

REFERENCES

Zajac, F.E. (1989) *CRC Critical Reviews in Biomedical Engineering*, **17**, 359-411.

Garner, B.A., Pandy, M.G. (2001). *Comput. Methods Biomech. Biomed. Eng.*, **4**, 93-126.

Garner, B.A., Pandy, M.G. (2003). *Annals Biomed. Eng.*, **31**, 207-220.

ACKNOWLEDGEMENTS

This work was partially funded by NASA Grant Nos. NGT-51025 and NAG9-805. Images provided by The National Libraries of Medicine, and support provided by the Visualization Laboratory at The University of Texas, are greatly appreciated.

FORCE ANALYSIS OF DUTY CYCLE EFFECTS FROM INJURIOUS STRETCH-SHORTENING CONTRACTIONS *IN VIVO* OF SKELETAL MUSCLE

Kenneth B. Geronilla [1], Brent A. Baker [1], Ian Hover[2], Mike L. Kashon[1], Robert G. Cutlip
[1] National Institute of Occupational Safety and Health 1095 Don Nehlen Drive
[2] West Virginia University, Division of Physical Therapy

INTRODUCTION

Stretch-shortening contractions (SSC i.e., reciprocal eccentric/concentric contractions) resulting in muscle damage and concomitant changes in performance are one of the major concerns in sports and occupational-related activities. Stretch-shortening exercise has been shown to produce muscle damage in humans. However, dynamic measurements of force and length were not precisely controlled, or recorded in real-time (Kyrolainen et al., 1998). In addition, excitation-contraction coupling has been shown to play an important role in skeletal muscle injury resulting from eccentric contractions (Warren et al., 2001). We hypothesized that very short duty cycles during SSC, defined as the time between contractions, will result in a more pronounced isometric force decrement 48 hours after exposure as compared to longer duty cycles.

METHODS

All testing was performed with anesthetized male Sprague-Dawley rats (N=24) on a custom-designed rat dynamometer (Cutlip et al., 1997). The response of the dorsiflexor muscles to isometric and stretch-shortening contractions (SSC) were quantified *in vivo*. Rats were randomly assigned to three groups (N=8) having either 10-second, 1-minute, or 5-minute duty cycles. The testing consisted of 7 sets of 10 SSC performed at an angular velocity of 500°/s from 90° to 140° ankle angle for a total of 70 SSC (see Table 1). An isometric force test was used as a measure of static muscle performance at the optimal ankle angle of 90°. Isometric force tests were performed before, immediately after, and 48 hours after the 7 SSC sets. There was a 2 minute rest period between steps in the experimental protocol to minimize fatigue.

Table 1. Experimental Protocol

Step	Type	Duty Cycle
1	F-L Curve	2min
2	7 SSC Sets of 10 Cycles	10s, 1min, 5 min
3	F-L Curve	2min
4	Cage Recovery	48 Hour
5	F-L Curve	2min

Dynamic force measurements were taken during the seven SSC sets to provide more quantitative information on real-time muscle performance. The force parameters used to evaluate the force changes between sets during the SSC were: 1) peak force (i.e, the maximum force achieved in the eccentric contraction), 2) minimum force (i.e. the force value prior to the eccentric contraction), and 3) cyclic force (i.e. the difference in the magnitude of force between the peak and minimum force). These force parameters were recorded for the second SSC in each set to evaluate the changes between sets. Force decrements were then compared between the static and dynamic tests.

RESULTS AND DISCUSSION

Compared to the 1-min group at 48 hours, the 10- sec and 5-min group showed a significant decrement in isometric force at an optimal ankle angle of 90° (Fig. 1). The dynamic force data showed a similar progression in performance between groups over the seven SSC sets (Figs 2, 3, 4). The peak and minimum force in the 10-sec group showed a more pronounced change than the other two groups. This was most likely the result of excitation-contraction coupling fatigue. However, this had no effect on the muscle's ability to produce eccentric force throughout the protocol as shown by the cyclic force (Fig 4).

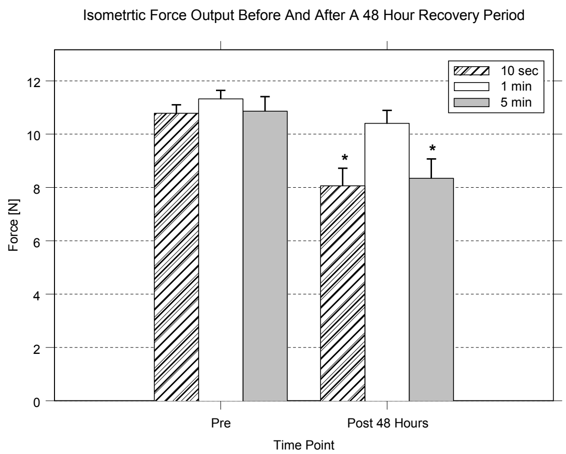

Figure 1: Isometric Force Test

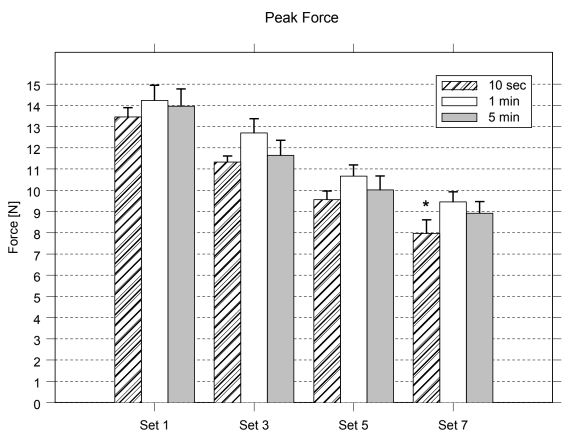

Figure 2: SSC Peak Force over 7 sets

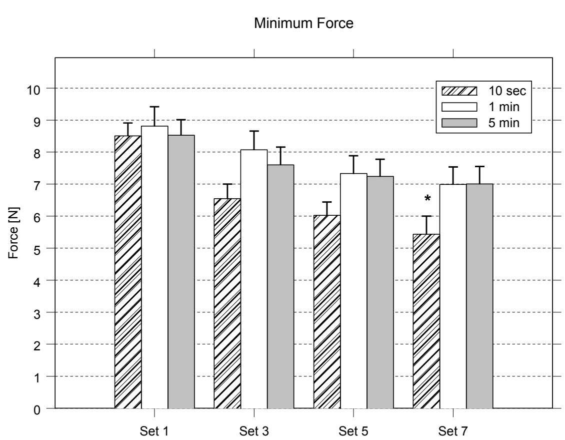

Figure 3: SSC Minimum Force over 7 sets

Note: * indicates statistical significant difference

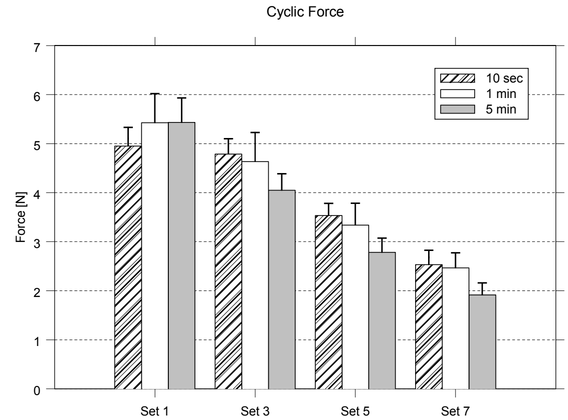

Figure 4: SSC Cyclic Force over 7 sets

SUMMARY

Duty cycle appeared to have a small but significant decrement on muscle performance in isometric force at long and short duty cycles at 48 hours. This small decrement in force at 48 hours indicated that the muscle was at the threshold of injury. More contractions may yield more pronounced differences. The dissimilarity between dynamic force decrements and static force decrements among groups indicated that eccentric force performance during stretch-shortening cycles was not predictive of isometric force output 48 hours later.

REFERENCES

H.T. Kyrolainen, T.E.S. Takala, P.V. Komi, “Muscle damage induced by stretch-shortening cycle exercise,” *Med. Sci. Sports Exerc.*, Vol. 30, No. 3, pp. 415-420, 1998.

Warren, G. L., Ingalls, C. P., Lowe, D. A., and R. B. Armstrong. Excitation-Contraction Uncoupling: Major Role in Contraction-Induced Muscle Injury. Exerc. Sport Sci. Rev. 29(2): 82-87, 2001

R.G. Cutlip, W.T.Stauber, R.H. Willison T.A. Mcintosh, K.H. Means. “Dynamometer for rat plantar flexor muscle *in vivo*,” *Med. Biol. Eng. Comput.*, 35, 540-543, 1997.

THE RELATIONSHIP BETWEEN SARCOMERE LENGTH AND FORCE IN RABBIT PSOAS MYOFIBRILS

Walter Herzog and Dilson E. Rassier

Faculty of Kinesiology, University of Calgary, Calgary, AB, Canada
E-mail: walter@kin.ucalgary.ca

INTRODUCTION

HE Huxley and Hanson (1954) and AF Huxley and Niedergerke (1954) showed that contraction in isolated myofibrils and single fibers, respectively, was not associated with an appreciable shortening of the A-band region of sarcomeres. They concluded independently that contraction in skeletal muscle occurs through the sliding of two sets of filaments, actin and myosin. In 1957, AF Huxley formulated a theory for contraction and force production in skeletal muscle, the cross-bridge theory, which explained how the relative sliding of actin and myosin was powered. The cross-bridge theory contains several basic assumptions including the idea that the cross-bridges are arranged uniformly on the myosin filament, and that they can attach to uniformly-spaced active sites on the actin filament. Also, on average, all cross-bridges are assumed to produce about the same amount of force and act independently of each other. These assumptions led to the prediction that the force in a sarcomere should be linearly related to the amount of actin/myosin overlap on the descending limb of the force-length relationship. In 1966, Gordon et al. tested this prediction and found it to be correct for single fibers of frog whose sarcomere lengths were controlled in the mid-portion of the fiber. Although individual sarcomere lengths could not be measured or controlled with this approach, the linearity of myofilament overlap and force has been accepted as fact in the muscle mechanics community. The purpose of this study was to test the relationship between sarcomere length and force in isolated myofibrils in which sarcomere lengths can be measured for each and all sarcomeres of the preparation.

METHODS

Myofibrils from rabbit psoas were isolated using standard chemical and mechanical isolation procedures. Myofibrils were attached to a nanolever force transducer (Fauver et al., 1998) at one end, and a glass needle at the other end. The glass needle was attached to a computer controlled micro manipulator to produce prescribed length changes of the myofibril. Individual sarcomere lengths were measured by projecting the striation patterns of the sarcomeres onto a linear photodiode array, and digitizing this area at 20 Hz (Blyakhman et al., 2001). Measurements were obtained from 8 myofibrils containing 7-30 sarcomeres in series. Typical recordings were made for isometric contractions of the myofibril on the descending limb of the force-length relationship, followed by stretches of approximately 10% of myofibril length.

RESULTS AND DISCUSSION

For all myofibrils, we observed that sarcomere lengths prior to stretching on the descending limb of the force-length relationship were non-uniform, but steady. During stretch, all sarcomeres of the myofibrils were stretched by varying amounts (Figure 1). In the isometric phase following the stretch, sarcomeres remained at non-uniform, but perfectly constant lengths. Differences in the sarcomere lengths following myofibril stretch typically exceeded 0.5 um. In the example shown in Figure 1, the shortest and longest sarcomere lengths following stretching are about 2.4 and 3.1 um, respectively, which, according to the myofilament overlap theory, corresponds to a difference in active force capability of 48% of the maximal isometric force at optimal length. The sarcomeres in a myofibril are arranged strictly in-series, therefore, the force at steady-state must be the same in each sarcomere. So, how can we possibly explain a difference of almost 50% of force between the shortest and longest sarcomere?

One explanation might be that the force deficit in the long sarcomere might be taken up by passive structures. However, we know that for sarcomere length of 3.1 um and less, passive force in rabbit psoas myofibrils barely reach 5% of the maximal isometric force (Bartoo et al., 1993), so passive forces are not sufficient to explain this discrepancy. Another explanation might be that sarcomeres in a myofibril have differing amounts of contractile proteins and that the difference in myofilament overlap might be accounted for by the number of contractile proteins. However, if this assumption was correct, the amount of overlap (or sarcomere length) before and after stretch should be exactly proportional, but it is not (Figure 1). At this point, we do not know why sarcomeres of vastly different length can produce identical forces, when the theory predicts that forces should differ by as much as 50%.

We propose that sarcomeres at different lengths can produce the same amount of force following active stretching because of the well-known force enhancement effect (Herzog, 1998). This theory needs rigorous testing in the future.

SUMMARY

We found strong evidence that sarcomere length does not uniquely determine sarcomere force. Future research will need to address systematically the origins of this highly unexpected result.

REFERENCES

HE Huxley and J Hanson, Nature 173:973-976, 1954

AF Huxley and R Niedergerke, Nature 173:971-973, 1954

AF Huxley Prog Biophys Biophys Chem 7:255-318, 1957

A Gordon et al. J Physiol 184:170-192, 1966

Rassier, Herzog and Pollack Proceedings of the Royal Society B (London) Submitted, 2003

M Fauver et al. IEEE Trans. 45: 891-898, 1998

F Blyakhman et al. Biophys J 81: 1093-1100, 2001

W Herzog, J Electromyo. Kines. 8:111-117, 1998

ACKNOWLEDGEMENTS

NSERC of Canada

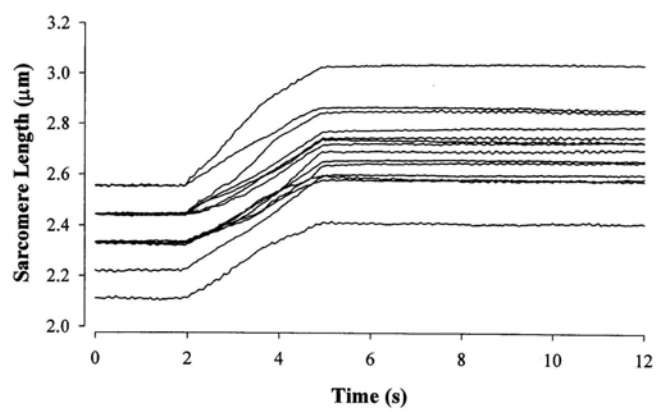

Fig. 1: Sarcomere lengths of a single myofibril as a function of time

EXPLORATORY SURFACE ELECTROMYOGRAPHY ANALYSIS USING PRINCIPAL COMPONENTS ANALYSIS

Miguel A. Perez [1] and Maury A. Nussbaum

[1] Industrial Ergonomics Laboratory, Virginia Tech, Blacksburg, VA, USA
E-mail: mperez@vt.edu

INTRODUCTION

Surface electromyography (sEMG) is frequently used to estimate active forces generated by muscular tissue. These estimates, often used in the development and evaluation of biomechanical models, are usually calculated for more than one muscle, making the resultant datasets multivariate in nature. However, analysis of the datasets is usually performed using univariate methods.

Among many different multivariate data analysis techniques, Principal Components Analysis (PCA) is commonly used as a data exploration method. PCA reduces the dimensionality of a dataset and allows for classification of participants by mathematically identifying and transforming the sources of variability in the data. Reductions in the dimensionality of the data may translate into simpler musculoskeletal injury risk models. Participant classification allows for generation of hypotheses suggesting possible reasons for observed differences between participant clusters.

In the field of biomechanics, PCA has been mainly used for dimensionality reduction (Wootten et al., 1990), patient vs. control classification (Lariviere et al., 2000), and multicollinearity adjustment (Hughes and Chaffin, 1997). The purpose of this work was to extend the application of PCA to trunk muscle activation patterns with the objective of identifying whether clusters of healthy individuals exist that differ in their trunk muscle activation patterns.

METHODS

sEMG readings from 14 different muscles (7 bilateral pairs) were analyzed with PCA. The methods for obtaining this activation are described in more detail in Perez and Nussbaum (2002). Sixteen participants (8 male and 8 female) with similar height and mass resisted static loads applied to their torso via a harness system. Eleven loading combinations were applied in two of three possible loading planes: sagittal/lateral, sagittal/horizontal, and lateral/horizontal. Each exertion in each plane combination was performed at magnitudes of 50 and 90 percent of each participant's maximum voluntary exertions (MVEs). All loading combinations were applied twice in randomized order. The final dataset contained 704 static loading trials.

PCA was applied in two different and sequential steps that used different arrangements of the same dataset. Initially (Step 1), PCA was performed on the complete dataset to determine whether further analysis of the data was required, a conclusion facilitated by two-dimensional plots of the first two PCs. Step 2 was triggered by the presence of outliers in the first step and had the main objective of identifying factors which could have caused these outliers. In Step 2, additional PCAs were performed on 22 distinct data subsets, separated by the loading magnitude (2 levels) and loading direction (11 levels) corresponding to each observation.

RESULTS AND DISCUSSION

PCA in Step 1, run on the complete dataset, resulted in the preliminary identification of outlying observations, mainly from participants 3, 7, and 9 (Figure 1), and prompting the execution of Step 2.

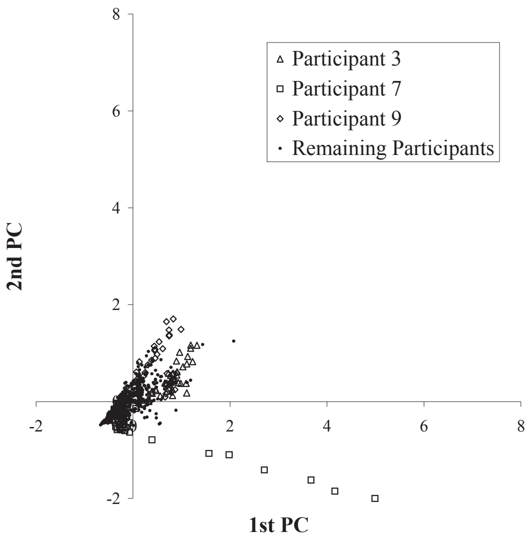

Figure 1: Plot of first and second principal component scores for the complete dataset. Scores for participants 3, 7, and 9 are easily distinguishable.

Step 2 confirmed the findings of Step 1, as participants 3, 7, and 9 again exhibited high outlier rates. In addition, this outlier detection process showed that a large number of observations from participants 5, 8, and 10 were outliers. No trends in outlier frequency were observed as a function of grouping by level of Loading Magnitude or Loading Direction. Four of the participants that exhibited outlier rates higher than 20% were female (participants 3, 5, 7, and 8), while two were males (participants 9 and 10).

PCA classified ~19% of experimental observations as outliers, most of these belonging to six participants. A similar proportion of 'differentially performing' participants was observed by Nussbaum and Chaffin (1997), who reported that 3-4 out of 10 healthy participants were clustered separately from remaining participants. These researchers suggested the idea, which our results support, that sEMG differences between both groups might be due to their use of different muscle coactivation patterns. This finding prompts caution in interpreting sEMG data based simply on means, especially when a large number of muscles are active, as the obtained mean may not be representative of any particular participant or group of participants.

SUMMARY

This investigation explored the use of PCA on electromyography data from healthy participants, with the objective of elucidating any between-participant differences in the multivariate patterns of muscle coactivation. Results indicated that, even between healthy participants, quantitative and qualitative differences in muscle coactivation patterns exist.

REFERENCES

Hughes, R. E., and Chaffin, D. B. (1997). *IEEE Trans Biomed Eng*, **44**, 639-642.
Lariviere, C., Gagnon, D., and Loisel, P. (2000). *J Electromyography and Kinesiology*, **10**, 261-273.
Nussbaum, M. A., and Chaffin, D. B. (1997). *Clin Biomech*, **12**, 97-106.
Perez, M. A., and Nussbaum, M. A. (2002). *Spine*, **27**, 1326-1335.
Wootten, M. E., Kadaba, M. P., and Cochran, G. V. (1990). *J Orthop Res*, **8**, 247-258.

A COMPARISON OF LOWER EXTREMITY MUSCLE ACTIVITY DURING EXERCISE ON A CYCLE ERGOMETER AND RECUMBENT STEPPER

Mark D. Tillman[1], John W. Chow[1], Gregory M. Gutierrez[1], Chris J. Hass[2]

[1]Center for Exercise Science, University of Florida, Gainesville, Florida
[2]Department of Neurology, Emory University School of Medicine, Atlanta, Georgia
Email: mtillman@hhp.ufl.edu

INTRODUCTION

Adults are encouraged to participate in aerobic activities that involve large muscle groups and are rhythmic in nature. Cycling and stair climbing are both activities that fit this recommendation and have been shown to enhance overall fitness and health. Further, cycling and stepping are currently prescribed during lower extremity orthopedic rehabilitation. These activities also help to reduce the risk of secondary injury because they reduce anterior shear forces in the knee due to their closed kinetic chain nature. Closed kinetic chain exercises are regularly used after ACL reconstruction surgery because they result in less strain on the ACL than open kinetic chain exercises like traditional knee extensions (Morrissey et al., 2000). Thus, bicycle ergometers are commonly used for rehabilitation after knee joint surgery. A recumbent stepper may provide the same exercise and safety benefits because it permits the user to perform a rhythmic closed kinetic chain exercise in a seated position.

Muscle activation is an important aspect of exercise and rehabilitation and can be quantified using electromyography (EMG). Following knee surgery proper lower extremity function is dependent on sufficient muscular activity and recruitment. Ergometer cycling has been shown to be an effective exercise for rehabilitating the thigh musculature. The high muscular activation and low knee joint loading associated with cycling exercise makes it an effective modality for successful rehabilitation. Since recumbent stepping has been shown to improve aerobic capacity and upper and lower body strength (Hass et al., 2001), one could hypothesize that it is also well suited for rehabilitation of the lower extremities. Apparently, the stepping activity requires a significant amount of muscle activation in the legs, but the extent of this activation has not been studied. The purpose of this study was to evaluate the muscular effort of a recumbent stepper compared to a traditional stationary cycle, using EMG. In addition, the influence of seat position was examined.

PROCEDURES

Ten male volunteers (age: 21.6 ± 1.9 y; height: 1.76 ± 0.05 m; mass: 74.1 ± 12.4 kg) with no history of lower extremity disorder or musculoskeletal trauma participated. To assess the myoelectric activitiy of selected lower extremity muscles, six pairs of surface electrodes were attached to the right side of the body over the following muscles: vastus lateralis (VL), vastus medialis (VM), rectus femoris (RF), biceps femoris (BF), medial gastrocnemius (MG), and soleus (SL). To obtain knee flexion angle (KFA), two 60 Hz video cameras were used to determine the 3D locations of the hip, knee, and ankle joints. Seat position was defined by the maximum knee flexion angle during exercise. Four seat positions (KFA = 0°, 15°, 30°, and 45°) were used and two trials were conducted at a stepping rate of 80 steps/min for each seat position and each exercise device. A metronome was used to control the stepping rate. Each subject was asked to exercise with a load that was perceived as “moderately heavy” for 30 s in each trial with a 1-min rest between trials. The order for the seat locations and exercise device was assigned randomly. A Peak Motus system and MESPEC 4000 8-channel radio telemetry EMG unit sampling at 900 Hz were used to collect EMG data during each trial.

Normalized average EMG data (expressed as %MVIC) were analyzed using separate two-way ANOVAs (2:device x 4:KFA) with repeated measures for each muscle during both the knee extension phase and the knee flexion phase (α=0.05).

RESULTS AND DISCUSSION

Several significant differences were detected during the extension phase. Increased muscle activation was observed in the thigh muscles (VL, VM, RF, BF) for the stationary bike compared to the recumbent stepper ($P<0.05$) (Figure 1). Muscle activation also varied with seat position for the VL and VM ($P<0.05$). More specifically, muscle activity increased with greater KFA.

For similar workloads, as measured with self-reported ratings of perceived exertion, stationary cycling requires greater muscular effort than recumbent stepping. In order to achieve comparable fitness improvements during rehabilitation, higher workloads should be used while recumbent stepping.

SUMMARY

Stationary cycles are commonly used during lower extremity rehabilitation. Recumbent steppers may be another effective device for rehabilitation although increased workloads may be necessary to achieve improvements in muscular fitness.

REFERENCES

Hass et al. (2001). *Eur J App Phys*, 85(1-2), 157-163.
Morrisey et al. (2000). *Knee Surg Sports Trauma Athr*, 8, 343-348.
29(3), 200-204.

ACKNOWLEDGEMENTS

This project was supported by NuStep, Inc. (UPN#01061905).

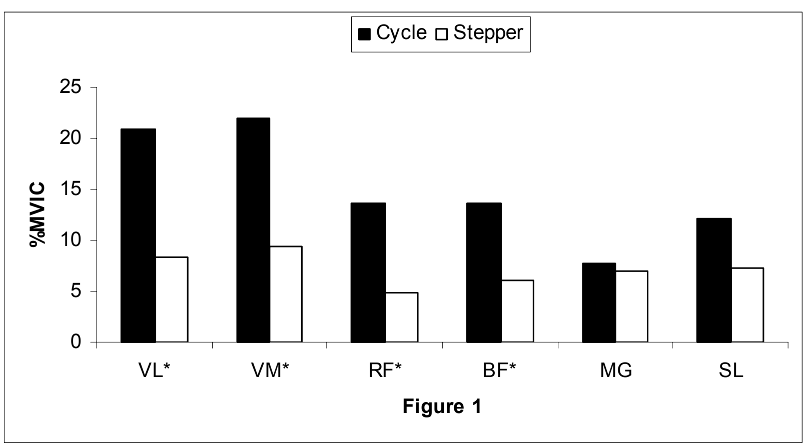

Figure 1. Average EMG values during the knee extension phase (VL=vastus lateralis, VM=vastus medialis, RF=rectus femoris, MG=medial gastrocnemius, SL=soleus). Significant differences (*$P<0.05$) exist between the cycle and stepper for the thigh muscles.

DEVELOPMENTAL SCALING OF THE POWER VELOCITY RELATIONSHIP

Randall L. Jensen[1,2] Andrew J. Harrison[2] and Ursula M. Barrett [2]

[1] Dept of HPER, Northern Michigan University, Marquette, MI, USA
[2] Dept of Physical Education and Sport Sciences, University of Limerick, Limerick, Ireland
E-mail: rajensen@nmu.edu Web: http://www.nmu.edu/hper/faculty/jensen.htm

INTRODUCTION

The force-velocity (F-V) and power-velocity (P-V) relationships are acknowledged as key factors in describing the isolated muscle's functional characteristics and have been described by the Hill equation.

$(P + a)(V + b) =$ Constant (Hill, 1938)

Where: P=force of contraction, V=velocity of shortening; *a* and *b* are constants. Constant *a*, describes force and depends largely on cross sectional area of the muscle (CSA); while constant *b*, relates to velocity and is proportional to muscle length (Hill, 1938).

Barrett and Harrison (2001) found that correction of peak power by thigh volume resulted in no differences between six year-old children and adults across velocities ranging from .524 to 5.24 rad · sec^{-1}. However, the peak force corrected for CSA was significantly different. In an effort to determine whether these findings hold true for older, but still pre-pubescent, children the current study compared peak force corrected for CSA and peak power corrected for thigh volume between adults and ten year old children.

METHODS

Twenty subjects evenly split according to age and further subdivided by gender were recruited from the community at large. The cohort of children was selected to be ten years of age, while adults were greater than 18 years of age (Mean 26.0±3.6).

Thigh volume of the subject's dominant (kicking) leg was determined via a series of anthropometric measurements of girths and lengths using a flexible steel tape. Skin fold measures were made with a Harpenden caliper and the lean circumference measures were calculated according to Jones and Pearson (1969). Lean thigh volume was calculated as a series of truncated cones by the methods of Katch and Weltman (1975).

Peak concentric knee extension torque was measured at 10 randomly ordered velocities (.524 to 5.236 rad · sec^{-1}) using a Con-trex isokinetic dynamometer (CVH AG Dübendorf, Switzerland), which was calibrated before each subject. Subjects underwent a five-minute warm-up on a stationary cycle ergometer and had several practice trials using the Con-trex prior to strength testing. During the test the subject was stabilized at the thigh, pelvis and trunk with Velcro straps. Three repetitions were performed at each velocity with two minutes rest between all velocities. All torque values were corrected for gravity effect on the limb.

Maximal torque values were corrected for cross sectional area. Peak power was calculated by multiplying force times the angular velocity. Angular velocity values were corrected by dividing them by the moment arm of the dynamometer arm. Peak power was then corrected for thigh volume.

RESULTS AND DISCUSSION

Three-way ANOVA (p=0.05) to compare age×gender×angular velocity for corrected power revealed main effects for speed and age, but not gender. In addition, all interactions were significant. Likewise torque corrected for CSA had main effects for speed and age, but not for gender. While corrected torque only showed an interaction of speed×age.

As shown in Figures 1 & 2, when corrected for thigh volume, peak power did not differ between the ages across angular velocities for females, however the males did vary. These findings are in contrast with those showing that six year olds did not differ from adults (Barrett and Harrison, 2001).

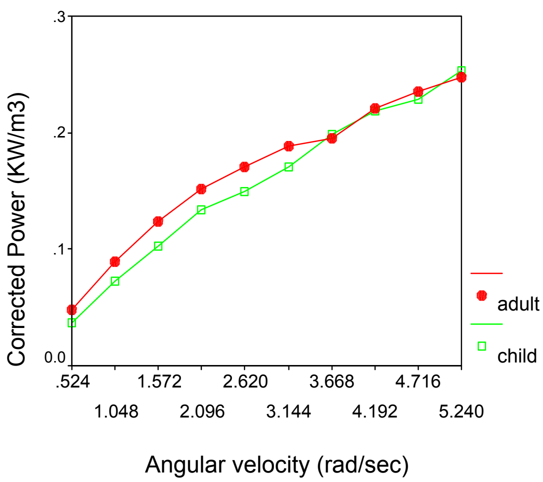

Figure 1: Peak power corrected for thigh volume in females (aged 10 and adult) at ten velocities.

These volume corrected differences in peak power may be due to training effects and/or sampling effects. Adult subjects were drawn primarily from an active population (students and members of a Physical Education Department), whereas the children were drawn from a local primary school. While the children may have been active, it is unlikely they were subject to the same levels of regular training as the adults. Rowland (2002) has noted a similarity of metabolic responses between children and untrained women and dissimilarity when comparing men who were more trained.

Volume correction for peak power brings the values closer together, however, training specificity has been shown to result in differences of peak power corrected for volume (Harrison and Coglan, 2002).

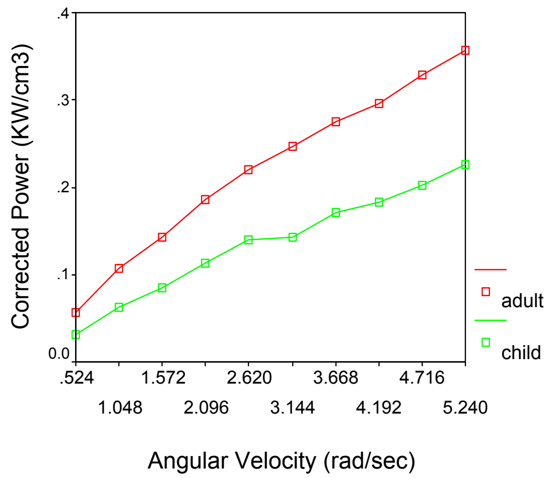

Figure 2: Peak power corrected for thigh volume in males (aged 10 and adult) at ten velocities.

SUMMARY

This study found significant difference in the volume corrected peak power between ten year-old children and adults. This may be due to higher training or as yet uninvestigated developmental differences.

REFERENCES

Barrett, U.M., Harrison, A.J. (2002). *Ped Exerc Sci,* **14**, 369-376.

Harrison, A.J. Coglan, J. (2002) *19th International Symposium on Biomechanics in Sports*, 68-71

Hill, A.V. (1938). *Proc Royal Soc London*, **126**, 136-195.

Jones, P.R.M., Pearson, J. (1969). *Proc Physio. Soc*. July

Katch, V., Weltman, A. (1975). *Human Biol,* **47**, 203-216.

Rowland, T.W. (2002). *Ped Exerc Sci,* **14**, 315-319.

REMOVAL OF MAGNETIC STIMULATION ARTIFACT FROM EMG USING A WAVELET SHRINKAGE-BASED METHOD

Ian Kremenic

Nicholas Institute of Sports Medicine and Athletic Trauma, Lenox Hill Hospital, New York, NY USA
E-mail: ian@nismat.org Web: http://www.nismat.org/

INTRODUCTION

Magnetic stimulation of peripheral nerves offers great opportunities for less-painful activation of muscles (relative to traditional electrical stimulation) in both rehabilitation and research settings. Study of muscle activation by magnetic stimulation, however, may be limited by the large stimulus artifacts that are induced into EMG recording systems. These are caused to a great degree by coupling of the large (up to 2 Tesla) magnetic fields that these systems use into the electrodes and cables of EMG systems. Removal of this artifact represents a non-trivial problem, as the stimulus artifact shares a great deal of its spectrum with the desired EMG.

Newer signal processing techniques, such as wavelet shrinkage (WS) (Donoho 1995), may prove useful in removing or reducing this artifact. The purpose of this study was to investigate whether a WS technique would be helpful in removing a known stimulus artifact from a known EMG signal. The goal is to validate a technique for removing magnetic stimulus artifact from EMG during magnetically-elicited contractions.

METHODS

Four male subjects volunteered for the study. Subjects were seated with their ankles fixed to the arm of an isokinetic dynamometer (Biodex, Shirley, NY). EMG electrodes were placed over their vastus medialis (VM) muscle. An additional pair of electrodes was placed slightly proximal to the VM electrodes, but still attached to their plastic backing—in this way, this electrode pair would pick up only coupled magnetic stimulation artifact, and not muscle activity. Subjects performed a 5-sec maximum voluntary isometric contraction (MVC) of their quadriceps to provide a clean EMG signal. Data were sampled at 1000 Hz using a Noraxon TeleMyo (Noraxon, Inc., Scottsdale, AZ) telemetered EMG system. Magnetic stimulation was then performed using a MagStim Rapid unit (Magstim Corp., Whitland, Wales) in order to obtain a sample of stimulus artifact. Stimulation of the femoral nerve was performed at 20 Hz at the maximum power output of the unit; a 3-sec train of pulses was administered.

Data were processed offline using MATLAB 6.5 and The Wavelet Toolbox (The MathWorks, Natick, MA). Each of the four artifact recordings (ARTIFACT) was added to the four MVC recordings, making a total of 16 noise-corrupted EMGs (NOISE). These noisy EMGs were decomposed using six-level discrete wavelet transform (DWT) using the Daubechies 4 wavelet (db4). The DWT is a time-scale transform, which gives simultaneous knowledge of both time and scale of a signal (scale is analogous to frequency in this context). It can be instructive to think of the DWT as the equalizer on a stereo: it splits a signal into several different signals (levels), each composing a different frequency range (scale) of the original signal. These separate signals may then be processed independently. The WS procedure involves taking each level of the DWT decomposition, applying a soft threshold to each level (decreasing the amount of the signal below the threshold rather than setting it to 0, hence the term "wavelet shrinkage"), and then performing an inverse DWT to obtain the denoised signal. In this study, an *a priori* examination of several EMG and artifact recordings suggested not applying any threshold to the lowest and highest scales, and a threshold of 70% of the maximum value in each scale at the other scales. Following inverse DWT, this yielded a signal that was almost entirely artifact, which could then be subtracted from the noisy signal to obtain a denoised signal (DENOISE).

To evaluate the denoising procedure, mean-square error (MSE) was calculated between the original MVCs and the NOISE signals, and compared with the MSE between the original MVCs and the DENOISE signals. Also, correlation coefficients were calculated between MVC and NOISE, MVC and DENOISE, ARTIFACT and NOISE, and ARTIFACT and DENOISE. Paired-samples t-tests were used to assess the effectiveness of the denoising procedure. Significance was set at $P < 0.05$.

RESULTS AND DISCUSSION

A sample of MVC, NOISE and DENOISE data is shown in Figure 1. The WS procedure decreased the MSE in the DENOISE signal by approximately 65% compared to NOISE ($P < 0.001$). Also, the correlation coefficient between DENOISE and MVC signals increased to 0.69 compared to 0.57 for NOISE and MVC ($P < 0.001$). Finally, the correlation between the ARTIFACT and DENOISE was decreased to 0.45 from 0.78 ($P < 0.001$). Thus, it can be seen that the WS technique is capable of removing significant amounts of magnetic stimulation artifact from EMG signals. Further adjustment of the parameters of the procedure may lead to improved performance.

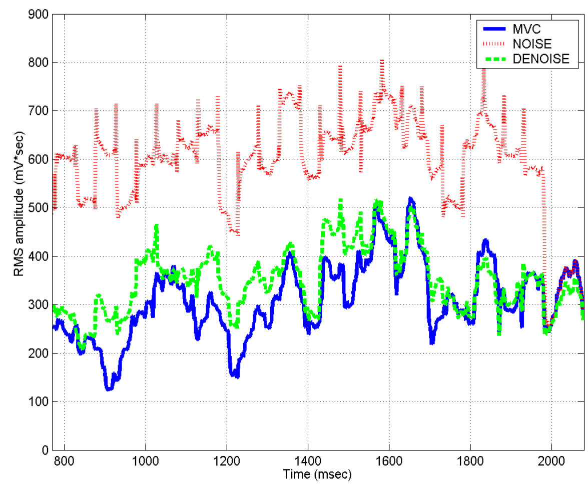

Figure 1: MVC (solid blue), NOISE (dotted red) and DENOISE (dashed green) signals for one subject.

SUMMARY

WS shows promise for the removal of magnetic stimulus artifact from EMG signals. Future work should involve tuning of the parameters of the noise-removal algorithm (e.g., threshold levels, wavelet type) and application of the procedure to EMG more like that elicited by stimulation rather than voluntary contractions (e.g., a tendon reflex response) in order to validate its effectiveness. Reduction or elimination of such artifact from EMG signals could allow for amplitude-based comparisons to be made between EMG signals recorded in the presence of such noise.

REFERENCES

Donoho, D.L. (1995). *IEEE Trans. On Inf. Theory*, **41**(3): 613-627.

TEST-RETEST RELIABILITY OF CARDINAL PLANE PRIMARY MOVER EMG DURING MAXIMAL-EFFORT ISOKINETIC HIP CONTRACTIONS

Mark K. Timmons, Tina L. Claiborne, and Danny M. Pincivero
Human Performance and Fatigue Laboratory, University of Toledo, Toledo, OH, USA
E-mail Mark.Timmons@utoledo.edu

INTRODUCTION

Numerous studies have employed isokinetic strength testing to determine joint torque produced during maximal muscular efforts, and have displayed high test-retest reliability (Gleeson, 1996). Specific to the prime movers of the hip joint in the cardinal planes, much less evidence is available regarding the reliability of electromyographic patterns during maximal effort strength testing. The purpose of this investigation was to examine test-retest reliability of hip joint primary mover electromyograms (EMG) during maximal effort concentric and eccentric isokinetic contractions through the cardinal planes.

METHODS

Subjects for this study included 13 healthy volunteers (7 males, 6 females, age 26.54 ± 3.80 years, height 172.15 ± 8.21 cm, weight 76.38 ± 17.78 kg). All subjects participated in two separate and identical testing sessions, separated by approximately one week.

Subjects were evaluated for three maximal-effort isokinetic concentric (CONC) and eccentric (ECC) contractions through the following motions: hip abduction (ABD)/adduction (ADD), hip flexion (FLEX)/extension (EXT), and hip internal (IR)/external rotation (ER). Measurement of hip ABD/ADD and FLEX/EXT were performed with the subjects in a standing position. Measurement of hip IR/ER was performed with the subjects in a seated position and their knees at a 90-degree angle. Electromyograms were obtained from the rectus femoris (RF), lateral hamstring (LH), medial hamstring (MH), adductor (AD), gluteus maximus (Gmax), and glueteus medius (Gmed) muscles during all contractions. The raw EMG signals were sampled at 2000 Hz, bandpass filtered (20-500 Hz), full wave rectified, and integrated (IEMG) over the middle portion of each contraction. Each IEMG value was divided by the duration of the analysis window. Average IEMG values were then determined by calculating the mean of the three consecutive contractions of each muscle during each contraction mode (CON and ECC) and motion. Test-retest reliability was determined through calculation of the intraclass correlation coefficient (ICC, model 2,K) and the standard error of measurement (SEM) normalized to the mean IEMG value (Bartko, 1966).

RESULTS AND DISSCUSSION

As a total of 144 ICC values were computed, only those values representing the muscles to be the primary movers for each contraction mode and direction are presented. The ICC value varied dependant upon the direction of motion (ABD, ADD, EXT, FL, ER, or IR), the mode of contraction (CONC, or ECC), and the muscle (AD, Gmed, Gmax, LH, MH, or RF). The ICC for the primary muscles involved in a particular hip action showed greater reliability (Table 1), ICC range 0.95 - 0.42, SEM range 0.086 - 0.007. The ICC for muscles not involved in movement production was 0.98 - 0.54, SEM range 0.114 - 0.001. CONC and ECC showed similar reliability ICC range, CONC 0.95 - 0.50, ECC 0.95 - 0.42. The Gmax (ICC 0.95 - 0.72) and the LH (ICC 0.93 - 0.81) showed the greatest reliability between muscles. Gmed (ICC 0.89 – 0.51) and MH (0.85 – 0.42) showed the lowest reliability. An aberrant reliability coefficient was noted for the AD muscle during the external rotation eccentric contraction.

SUMMARY

The findings of this study suggest that EMG activity of the prime movers during maximal-effort strength testing can be examined with a moderate to high degree of between-day reliability.

REFERENCES

Bartko,J.J. (1966). *Psychol. Reports,* **19**, 3-11.

Gleeson, N.P., Mercer,T.H. (1996). *Sports Med.*, **21**, 18-34

Larson, B. et al. (1999). *J. Electromyogr. Kinesiol.*, **9**, 351-357

Sleivert, G.G., Wenger, H.A. (1994). *Arch. Phys. Med. Rehabil.* **75**, 1315-1321

Yang, J.F., Winter, D.A. (1983). *Arch. Phys. Med. Rehabil*, **64**, 417-420

Table 1: Intraclass correlation (ICC) coefficients and standard errors of measurement (SEM) for cardinal plane hip muscle EMG.

Concentric					Eccentric				
Motion	**Muscle**	**R/L**	**ICC**	**SEM***	**Motion**	**Muscle**	**R/L**	**ICC**	**SEM***
EXT	G max	L	0.954	4.74	ER	AM	L	0.953	7.74
EXT	LH	R	0.933	7.37	FLEX	G max	L	0.943	14.19
EXT	LH	L	0.901	6.72	Ab	AM	L	0.942	7.79
IR	AL	R	0.887	8.19	EXT	RF	R	0.926	6.42
Ab	G med	L	0.878	9.2	Ad	G med	R	0.895	11.27
ER	G med	R	0.842	10.85	FLEX	LH	R	0.879	8.83
EXT	G max	R	0.830	9.8	IR	G med	L	0.858	12.92
Ad	AM	L	0.814	15.59	Ab	AL	R	0.849	12.7
IR	AL	L	0.814	11.37	FLEX	MH	R	0.849	8.59
ER	G med	L	0.812	12.35	FLEX	LH	L	0.817	9.03
FLEX	RF	R	0.759	11.61	Ad	G med	L	0.775	12.31
EXT	MH	R	0.755	8.93	EXT	RF	L	0.768	9.16
FLEX	RF	L	0.653	12.96	FLEX	G max	R	0.727	18.37
Ab	G med	R	0.592	10.49	IR	G med	R	0.513	16.98
Ad	AL	R	0.587	18.47	FLEX	MH	L	0.421	15.91
EXT	MH	L	0.501	12.24	ER	AM	R	-1.460	46.31

* % mean IEMG activity

THE INFLUENCE OF VIBRATION ON MUSCLE ACTIVATION AND RATE OF FORCE DEVELOPMENT DURRING MAXIMAL ISOMETRIC CONTRACTIONS

Humphries[1], B., Warman[2], G., Purton[3], J., Doyle[1], T., and Dugan[1], E.

[1]Biomechanics Laboratory, Ball State University, Muncie, Indiana, USA
[2] School of Human Movement Studies, University of Queensland, St.Lucia, Australia
[3] School of Health and Human Performance, Central Queensland University, Rockhampton, Australia
E-mail: bhumphries@bsu.edu Web: www.bsu.edu/web/biomechanics/

INTRODUCTION

Vibration is an oscillatory motion that has been applied to muscle contractions at various frequencies and amplitudes to facilitate muscular strength characteristics**.** Research has shown 30% improvements in dynamic explosive muscle strength (Issurin & Tenenbaum, 1999; Warman & Humphries, 2002), 10% improvements in isotonic muscle power (Bosco et. al., 1999), 10% increases in isometric torque and 50% changes in electromyographic amplitude (Gabriel et.al., 2002). In addition, early research on muscle strength has reported vibration generates high motor unit firing rates seen in the initial phase of maximal isometric contractions (Bongiovanni & Hagbarth, 1990). In contrast, researchers have shown a reduction in isometric leg extension strength and EMG median frequency (Rittweger et. al., 200) and a suppression in motor output of the muscle (Bongiovanni & Hagbarth, 1990).

The aim of this study is to examine the effects of a superimposed vibration at 50 Hz on muscular activation and torque for an isometric contraction.

METHODS

Sixteen participants (22 ± 4.4 years, 73.2 ± 11.7 kg and 173.1 ± 9.7 cms) were recruited for this study. Prior to participation each individual read and signed an informed consent document.

A modified four kilowatt, three phase electrical induction motor transfered vibration to the leg at 50.42 ± 1.16 Hz at 13.24 ± 0.18ms^{-2}.

Mechanical Force Data: Peak isometric force (N) was recorded via a load cell and analysed for RFD at times 0.05 s, 0.01 s, 0.1 s and 0.5 s, and RFD time at 50, 75 and 90% of peak force.

Electromyographic (EMG) Data: The EMG signals were collected from Rectus Femoris (RF) muscle via surface electrodes (10mm x 30mm).

Synchronisation of all Force, and EMG data collection was achieved via a software trigger set at 30 N force for the isometric contractions. Data was sampled at 1000 Hz.

Statistical Analysis: Mean ± standard deviations were calculated for subject characteristics. Statistical analysis involved a one-way analysis of variance (ANOVA) comparing vibration and no-vibration conditions. Statistical significance was accepted at or below 0.05

RESULTS AND DISCUSSION

A one-way ANOVA revealed no significant ($p < .05$) differences between the vibrated and no-vibration conditions for Peak isometric force, time peak force, time to

50%, 75% or 90% peak force, or rate of force development at times 0.05, 0.01, 0.1, 0.5 seconds, see Table 1.

A one-way ANOVA revealed no significant ($p < .05$) differences between the vibrated and no-vibration conditions for Peak normalised EMG_{RMS} (84.74% Vs 88.1%) values.

The present results indicate no significant changes to peak isometric force, isometric force characteristics, and peak normalised EMG_{RMS} in association with vibration. There was no simultaneous change in neuromuscular activity occurring with isometric force or rate of force development.

The non-significant response of the isometric contraction to vibration may reside in the responsiveness of the elastic and viscous properties of the muscle architecture, and or the length-tension relationship of the muscle. However, neither of these reasons appear to apply to the present study due to responses elicited using the same muscle groups, positioning and vibration frequencies (Warman & Humphries, 2002).

One possible explanation for the differences in response for isometric contractions may reside in contraction velocity. The contraction velocity of the isometric movement was limited by the nature of the contraction. In contrast the contraction velocity of a concentric isotonic movement is determined by the participant. The underlying mechanism/s behind the improvements previously reported in strength performances may rely on an individual optimal contraction velocity. Support for this explanation may be found in the recent studies reporting significant improvements in strength measures (Bosco et al., 1999; Issurin & Tenenbaum, 1999; Warman & Humphries, 2002). Each of these studies has examined isotonic contractions, with the participant contracting as hard and fast as possible, thereby having complete control over the contraction velocity. It is therefore possible that an unexamined reason behind these improvements may be in the selection of contraction velocity and its possible affect on the effectiveness of the vibration stimulation.

SUMMARY

The application of vibration stimulation at 50 Hz does not improve isometric force, or rate of force development in the initial phase of maximal isometric contractions.

REFERENCES

Bongiovanni. L.G., Hagbarth, K.E. (1990).*Jn. Physiol*. **423**, 1-14.

Bosco, C., Cardinale, M., Tsarpela, O. (1999). *Eur J Appl Physiol.* **79**:306-11.

Issurin, V.B., Tenenbaum, G. (1999). *Jn. Sport Sci.* **17**:177-82

Rittweger, J., Beller, G., Felsenberg, D. (2000). *Clin Physiol* **20**:134-42.

Warman, G., Humphries, B. (2002). *Avi. Space Environ. Med.* **73**:119-27.

Table 1. The mean(sd) characteristics of isometric force and rate of force development data.

	Peak RFD (N)	**Time Peak (s)**	**Time 50% (s)**	**Time 75% (s)**	**Time 90% (s)**	**RFD 0.01 s (N)**	**RFD 0.05 s (N)**	**RFD 0.1 s (N)**	**RFD 0.5 s (N)**
Vibration	581.8 (163.5)	2.5 (1.2)	.22 (.08)	.46 (.21)	.95 (.43)	983.3 (947.6)	1348.9 (300.9)	1525.4 (1006.5)	912.9 (268.6)
No-vibration	493.1 (163.9)	2.3 (1.2)	.18 (.13)	.49 (.48)	1.1 (.90)	657.9 (383.4)	1240.3 (300.9)	1620.4 (970.3)	785.9 (258.2)

AN ELECTROMYOGRAPHIC COMPARISON OF PARALLEL AND TRAP BAR SQUATS

John W. Chow [1], Mark D. Tillman [1], Gregory M. Gutierrez [1], Chris J. Hass [2]

[1] Center for Exercise Science, University of Florida, Gainesville, Florida
[2] Department of Neurology, Emory University School of Medicine, Atlanta, Georgia
E-mail: jchow@hhp.ufl.edu Web: www.hhp.ufl.edu/ess/CES

INTRODUCTION

The squat exercise is often referred to as the "king" of all weight-lifting exercises (O'Shea, 1985) and is considered the best exercise for the muscular development of the legs, hips and back (Weider, 1983). A squat is typically performed with an Olympic bar placed behind the neck with the load distributed across the upper back and shoulders and the bar parallel with the ground (parallel squat).

A trap bar is a diamond-shaped steel frame with sleeves extending from opposite corners and handles approximately 15 cm from the sleeves (Fig. 1). Its weight and sleeve size are identical to that of an Olympic bar. Performing free-weight squat exercises using a trap bar is thought to place a lesser load on the lumbar region because the center of gravity of the resistance is in closer alignment with the center of gravity of the lifter than the parallel squat using an Olympic bar (Gentry et al., 1987). This reduces the force placed on the lifter's stabilizing muscles while still providing sufficient resistance on the legs to provide an effective work-out.

Figure 1. Trap bar squat.

The purpose of this study was to compare the electromyographic (EMG) activity of the muscles of the thighs and lower back during a squat performed using an Olympic bar and a trap bar. It was hypothesized that reduced EMG levels in lower back muscles would be observed in the trap bar while no differences in thigh muscle activity would be found between bar types.

PROCEDURES

Twelve males and 4 females (age 25.4±6.1 yrs, height 177±13 cm, weight 751±190 N) with mixed strength training experience were asked to perform two trials of three repetitions using each of the two bars with a load approximately equal to 75% of their body weight. Subjects were asked to warm up by light jogging performed on a motorized treadmill at a self-selected pace.

Muscle activity was detected using a MESPEC 4000 radio telemetry EMG unit sampling at 900 Hz. Six pairs of surface electrodes were attached to the right side of the body over the following muscles: (1) rectus femoris (RF) – center of anterior surface of the thigh, approximately half the distance between the knee and iliac spine, (2) vastus lateralis (VL) – 3-5 cm above the patella, on an oblique angle just lateral to the midline, (3) vastus medialis (VM) – 2 cm superior to the rim of the patella at an oblique angle (≈55°) directed medially, (4) biceps femoris (BF) – lateral hamstring, 2/3 distance between the greater trochanter and the back of the knee, (5) semitendinosis (ST) – medial hamstring, half the distance between the gluteal fold and the back of the knee, and (6) erector spinae (ES) – approximately 2 cm lateral to the L3 level vertebrae oriented vertically. Electrode pairs were placed approximately 2 cm apart and parallel to the line of action of the muscle.

Maximum voluntary isometric contractions (MVIC) were performed for each of the muscle monitored for normalization purposes. To determine the descending and ascending phases of a repetition, a video-based Peak Motus® system was used to determine the vertical location of the right hip. For each subject, the middle repetition of each trial was analyzed and the average of the 2 repetitions for each bar type was used in subsequent statistical analysis. For the average normalized EMG levels during each phase for each muscle, a 2 (phases) x 2 (bar types) MANOVA with repeated measures was performed and Geisser-Greenhouse adjustments were used when the covariance matrix circularity was violated (using an a-priori alpha level of 0.05). Because the primary focus of this study was on the differences between bar types, results of the phase main effect are not reported here.

RESULTS AND DISCUSSION

No significant difference between bar types was found in the EMG levels of the muscles of the thigh (RF, VL, VM, BF, and ST) in the descending or ascending phase of the squat. However, significantly lower EMG activity was found in the ES during the descending phase (p=0.019). These results support our hypotheses.

Because muscle activity is a major contributor to forces acting on the spine (Schultz, 1990), the significantly lower ES activity during the descending phase of the squat indicates that a lesser load was placed on the anatomical structures of lumbar region. On the other hand, non-significant differences between bar types in the activity of thigh muscles confirm that thigh muscles received the same amount of stress with the Olympic and trap bars.

SUMMARY

Trap bar squats seem to be a good variation of squats for beginners because they will still receive the same workout for their legs with less risk of injury to the lumbar region. Also, they do not need to pick the bar up as high as in the parallel squat which makes it easier for someone with less experience working with free-weights to perform squat exercises. Furthermore, it is safe to perform trap bar squats without a spotter.

REFERENCES

Gentry, M., Pratt, D., and Caterisano, T. (1987) *NSCA Journal*, 9(3), 54-55.

O'Shea, J.P. (1985) *NSCA Journal*, 7(1), 4-6, 78.

Schultz, A.B. (1990) in Weinstein J.N. and Wiesel S.W., eds: *The Lumbar Spine*, WB Saunders.

Weider, J. (1983) *The Weider System of Bodybuilding*, Contemporary Books, Inc. (pp. 211-2)

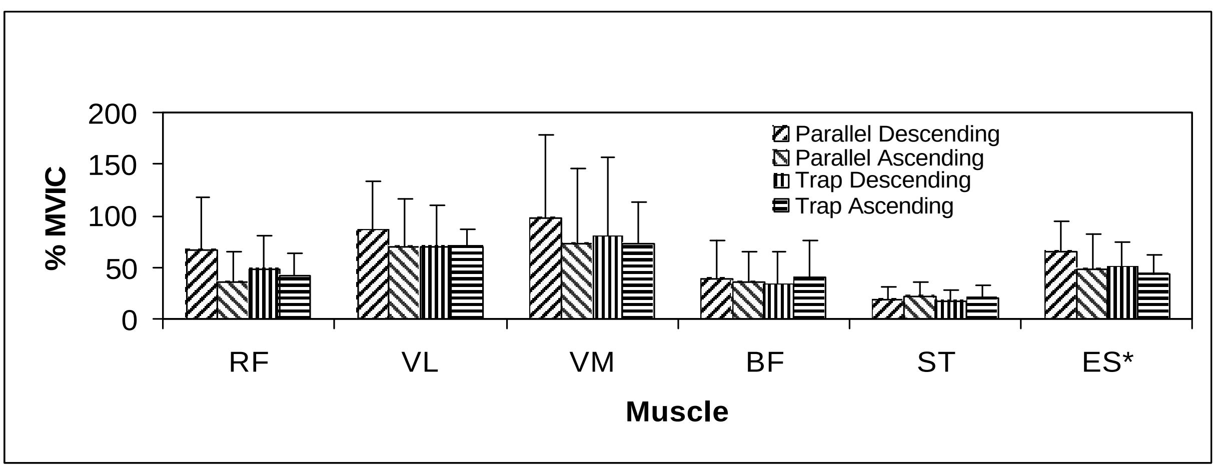

Figure 2. Average normalized EMG values during both phases of the parallel and trap bar squats. *Significant differences (p<0.05) exist between bar types in the descending phase.

RESOLVING CONFLICTS IN TASK DEMANDS DURING BALANCE RECOVERY: DOES HOLDING AN OBJECT INHIBIT COMPENSATORY GRASPING?

Hamid Bateni[1,2], Aleksandra Zecevic[1], William E. McIlroy[1] and Brian E. Maki[1,2]

1. Sunnybrook and Women's College Health Sciences Centre, University of Toronto, Toronto, Canada
2. School of Rehabilitation Sciences, McGill University, Montreal, Canada
Email: hamid.bateni@swchsc.on.ca Web: http://www.sunnybrook.utoronto.ca/~csia/CSiAInfo/

Introduction:

Ability to use the arms to reach and "grasp" (grip or touch) external structures for support in reaction to instability is an important element of the postural repertoire[1]. It is unclear, however, how the central nervous system (CNS) resolves the conflict in task demands that arises if an object is held in the hand, particularly if that object is perceived to provide stabilization, i.e. an assistive device. This study examined how initiation of "compensatory grasping" is affected when holding an object, and the influence of: 1) the nature of the held object, 2) prior activation of arm muscles, and 3) direction of the falling motion (forward or backward "loss of balance", LOB).

Methods:

Postural reactions were evoked in 16 healthy, right-handed young adults (23-34) via sudden, unpredictable platform translation. A handrail was mounted on the platform to the right of the subject. Subjects held: 1) no object, 2) a cane (instrumented to monitor loading), or 3) a "neutral" object (the top handle portion of a cane). The cane was either unloaded or loaded (10% body weight) prior to perturbation, and held in either the right or left hand. To create a clear conflict in task demands, foot motion was constrained by barriers and subjects were told not to move the feet. The intention was that successful balance recovery would require the held object to be released in order to use the right hand to contact the rail, in trials involving the largest perturbations, and that failure to do this would cause the subject to fall against a safety harness or padded barriers. Video recordings and biceps EMG latency and amplitude (first 100ms of initial burst) used to characterize the arm reactions evoked by the largest perturbations.

Results and discussion:

Right-arm grasping reactions were commonly used to recover balance when the right hand was free (70% of trials); however, holding an object in the right hand had a potent modulating effect. In reacting to backward LOB, subjects contacted the rail in only 41% of cane-top trials and 34% of cane trials. For forward LOB, the rail was contacted in just 19% of cane-top trials and only 7% of cane trials. Subjects released and dropped the cane or cane-top before contacting the rail in 39% of cases but more commonly (61% of cases) released the object partially (freeing 1-3 fingers to contact the rail). Although non-contact trials typically showed little evidence of any overt effort to reach toward the rail (93% of cases), the arm reaction was seldom completely inhibited. In fact, a reaction in right biceps was recorded in 96% of trials. There was, however, a substantial reduction in amplitude of biceps activation (27-36%), as well as a small delay in latency (13-

15ms), when the cane or cane-top was held in the right hand versus when that hand was free (p’s<0.001). Prior contraction (loading the cane) did not influence any of the findings.
The results indicate that holding an object can have a profound effect on the control of upper-limb balance reactions. Although arm reactions were seldom completely inhibited, arm-muscle activation was reduced and delayed and reaching movements to contact the rail became much less frequent when holding an object. In some trials, complex strategies (e.g. partial release of object) were adopted to allow the hand to contact the rail without dropping the object. It appears that the CNS may prioritize the ongoing task of holding an object, even when it has no stabilizing value (cane during backward LOB) or any intrinsic value whatsoever (cane-top). It seems remarkable that the CNS would prioritize this task, given the potential consequences (e.g. relying on a safety harness to prevent falling). The findings may have implications for fall prevention (e.g. guidelines for safer use of canes).

Summary:

Our findings indicate that holding an object has a significant effect on compensatory grasping. While grasping was used frequently to recover balance when the subject was not holding an object, it was often delayed or inhibited when the subject was holding an object. Our results indicate that, regardless of an object's usefulness, the CNS prioritizes the task of holding an object over the task of compensatory grasping in challenging balance situations.

Reference:

1. Maki BE, McIlroy WE. Phys Ther 1997;77:488-507.

RAMBLING, TREMBLING, AND RANDOM WALK IN POSTURAL CONTROL DURING SEATED BALANCE

Sheri P. Silfies[1], Peter N. Reeves[2], Jacek Cholewicki[3] and Theodore E. Milner[2]

[1]Rehabilitation Sciences Biomechanics Laboratory, Drexel University, Philadelphia, PA, USA

[2]Neuromuscular Control Laboratory, Simon Fraser University, Burnaby, BC, Canada

[3]Biomechanics Research Laboratory, Yale University New Haven, CT, USA

E-mail: silfies@drexel.edu

INTRODUCTION

Current evidence supports the hypothesis that at least two postural control subsystems work to maintain balance. Two proposed models include control through *open* and *closed-loops mechanisms* (Collins, 1993, 1995), and control of reference point migration (*rambling*) and movement around the reference point (*trembling*) by intrinsic muscle stiffness (Zatsiorsky, 1999). The purpose of this study was to compare stabilogram diffusion analysis parameters (Collins, 1993) during unstable seated postural control using center of pressure (CoP) and *trembling* (Zatsiorsky, 1999) trajectories. We hypothesized that *trembling* better reflects the *open* and *closed-loop* postural control mechanisms and therefore: 1) the long time interval, *trembling* trajectory would demonstrate significantly greater antipersistence than the CoP trajectory and 2) there would be no effect of visual input on critical point parameters or short term diffusion coefficients of the *trembling* trajectory in contrast to the CoP trajectory.

MATERIALS AND METHODS

Subjects and Protocol-Six healthy subjects (3 female, 3 male; mean: age 18.6 yrs, height 1.73 m, weight 67.2 kg) with no history of postural or skeletal disorders were studied with IRB approval. Subjects were placed on a seat equipped with leg and foot supports to prevent any lower body movement. A 30 cm diameter polyester resin hemisphere attached to the bottom of the seat created a liable surface. The seat was located on a force plate (Kistler, Germany, Model 9286AA) at the edge of a table (Fig. 1, insert). Subjects were instructed to maintain balance with arms crossed in both an eyes open and eyes closed condition. Force plate data (CoP, force) were collected at 124Hz over 70 seconds after the subjects had reached a state of balance control. Three trials of each condition were performed.

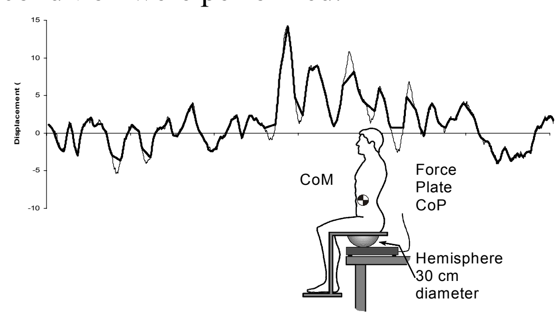

Figure 1: CoP trajectory (thin line) and interpolated CoM trajectory (thick line). Insert: Seated balance testing apparatus.

Data Analysis- Force plate data for the anterior/posterior and medial lateral directions were low pass filtered at 8Hz (4th order Butterworth) and zero referenced. The *trembling* component was then extracted from the CoP trajectory using the following steps. 1) Instances of $F_{hor} = 0$ (instant equilibrium point- IEP) were identified and the CoP position at those instances recorded. 2) The IEP trajectory (Fig. 1) was determined, linearly interpolated, and again low pass filtered at 8Hz. 3) *Trembling* was determined by subtraction of the IEP from the CoP position. Random walk analysis was performed to identify critical point (CP), scaling (Hr), and diffusion (Dr) parameters (Collins, 1993). Two-factor, repeated measures ANOVA ($p<0.05$) was used to address the hypotheses.

RESULTS

Both hypotheses were supported by the data. Anti-persistence in the long term region (Hr_{Long}) was significantly greater for *trembling* than CoP trajectories, with *trembling* demonstrating almost perfect antipersistence ($Hr_{Long} = 0.0004$). CP time was not significantly effected by visual input. However, significant interactions (visual input x trajectory) were demonstrated for CP displacement and short term diffusion parameters (Fig.2). This indicated that visual input significantly effected CoP, but not *trembling,* supporting the premise of *open-loop* control.

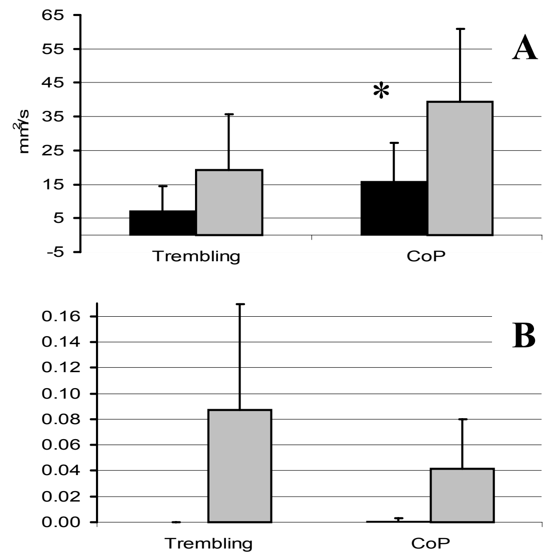

Figure 2: Mean and standard deviation of (a) short-term diffusion coefficients and (b) long term scaling exponents for *trembling* and CoP parameters (eyes open ■ and eyes closed ▢).

DISCUSSION

Stabilogram diffusion analysis of CoP trajectories was developed to extract parameters that reflected the mechanisms underlying postural control and to assist with determining relative contributions of different sensorimotor components. Collins (1993) hypothesized that the two regions represented *open and closed-loop* control mechanism. However, their interpretation has met with some challenge that is backed by data from several studies indicating that visual input affected this *open loop* parameter. Our postural challenge involved a liable surface that generated considerable reference point migration. In this case, decomposing CoP displacements into *rambling* and *trembling* may better represent postural control and serve to improve understanding of control mechanisms. The *trembling* trajectory in the short-term intervals represents *open loop* or pendulum like behavior that does not appear affected by visual input. The CP_{time} (0.51s) and displacements ($CP_r = 15.4$; $Dr_{short} = 15.8$) are reflective of the *open-loop* transition point and representative of the latency during which movement cannot be corrected. The long term region of the *trembling* trajectory was significantly more anti-persistent in comparison to the entire CoP trajectory, indicating that movement can be corrected through feedback in this region. *Trembling* may better reflect the mechanisms of postural control because it represents the control of the center of mass (CoM) over the CoP, which must be precisely maintained. On the other hand, the CoP does not have to be controlled precisely because it can be placed anywhere within the base of support or a range of support as in our seated balance case.

REFERENCES

Collins and De Luca. (1993). *Exp Brain Res,* **95**, 308-318.

Collins and De Luca. (1995). *Exp Brain Res,* **103**, 151-163.

Zatsiorsky and Duarte. (2000). *Motor Control,* **4**, 185-200.

ACKNOWLEDGEMENTS

This work was supported in part by NIH grant 5 R01 AR 46844.

PHASE SPACE INTERPRETATION OF THE LATERAL DYNAMICS OF THE TRANSITION FROM BIPEDAL TO UNIPEDAL BALANCE

Jaebum Son, M.S. and James A. Ashton-Miller, PhD

Biomechanics Research Laboratory
Department of Mechanical Engineering, University of Michigan, Ann Arbor, MI, USA
jaebum@engin.umich.edu

INTRODUCTION

The maximum time that an older human can balance on one leg is a predictor of the risk for an injurious fall within the next six months (Vellas 1997). It is not known how age may affect the mechanisms underlying the control of unipedal balance. In this paper we examine the dynamics of the bipedal-to-unipedal (BU) phase transition that initiates unipedal balance. We hypothesize that saturation of maximum ankle torque in the frontal plane limits the region of feasible phase space trajectories for a successful BU transition. This region could be conveniently expressed as an open set in the phase space, in agreement with recent studies emphasizing the importance of velocity in postural control (Pai 1997).

METHODS

The BU transition is modeled as a linearized 1-DOF collocated inverted pendulum. In general, it is assumed that the lateral unipedal balance system is (completely) controllable in the entire state space in the absence of the model "ankle" torque saturation. However, when we impose the saturation limitation on the model torque, we can find two different hyperbands: the weakly controllable (to the origin) band (B_{WC}) along the stable eigen-subspace of the passive dynamics, and the weakly reachable (from the origin) band (B_{WR}) along the unstable eigen-subspace. These bands are merely particular solutions of the differential equation describing the passive dynamics field effects. Then B_{WC} can be expressed as

$$B_{WC} = \left\{ (\theta, \dot{\theta}) \middle| -\frac{\tau_{e,\max}}{ml_c g} < \theta - \left(\frac{1}{\lambda_s}\right)\dot{\theta} < -\frac{\tau_{i,\max}}{ml_c g} \right\}$$

where λ_s is the stable eigenvalue and $\tau_{e,max}$ ($\tau_{i,max}$) are the maximum ankle everter (inverter) torques. B_{WR} is defined in a similar way.

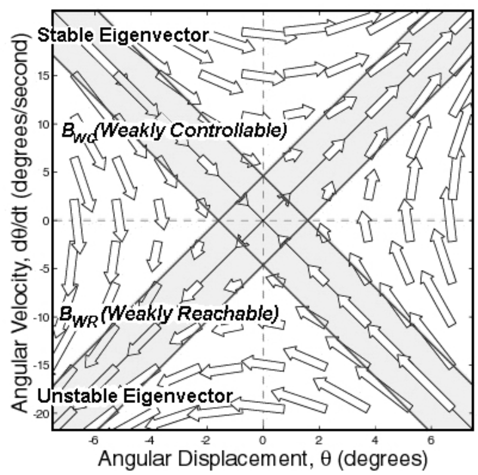

Figure 1: Phase space illustration of weakly controllable and reachable bands.

It can be inferred that a successful BU transition requires placing the state inside B_{WC}, and the state is moved to the $B_{WC} \cap B_{WR}$ region to maintain unipedal balance (Figure 1). It exits this region along B_{WR} if the subject ends (fails) the unipedal phase. The requirement that the state should remain in B_{WC} to access $B_{WC} \cap B_{WR}$ induces another hypothesis. That is, if the B_{WC} band becomes narrowed (e.g., by age or disease), then it constricts the distance from $B_{WC} \cap B_{WR}$ available for accessing $B_{WC} \cap B_{WR}$.

To validate the model four healthy young subjects (2 females), who could balance more than 1 minute with eyes open, were recruited. Subjects stood on various-sized narrow beams, oriented in the sagittal plane and ranging from 2 to 6 cm in width, presented in randomized order. These beams were used to constrain the maximum input torque and to control B_{WC} and B_{WR} by limiting the COP excursion. Subjects were asked to perform the BU transition and maintain unipedal balance for at least 30 seconds, or until they lost their balance. Signals were measured at 100 Hz from an AMTI™ OR-6 force plate under each foot and six OPTOTRAK® kinematic markers on the trunk and legs, and filtered using a two-way 4th-order Butterworth low-pass filter (4 Hz cutoff). A total of 27 successful trials were analyzed.

RESULTS AND DISCUSSION

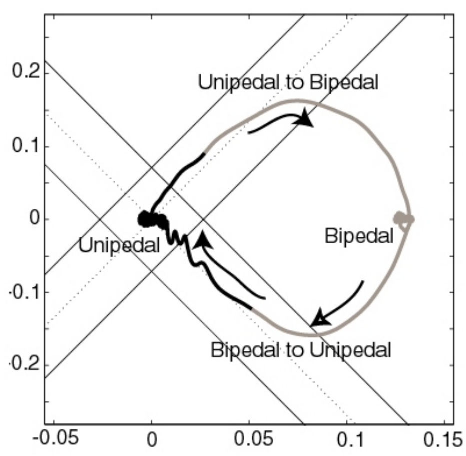

Figure 2: *Typical transition phase description in the state space* (τ_{max}=25 Nm; Ottaviani 1995)

More than 90% of the BU trajectories (27 of 29 trials) were well explained with our model (Table 1). On the narrowest beams (<3cm), 30% of the trajectories did not follow the expected band constraints, likely due to small-angle measurement error and the limitations of the 1-DOF model.

As B_{WC} was reduced, three of five subjects adapted by decreasing the transition speed (R^2= 0.6989~0.9613) defined as the COM velocity at the instant of contralateral leg lift-off, which is conceptually equivalent to the distance to $B_{WC} \cap B_{WR}$. One subject showed uncorrelated behavior.

Table 1: *Test of Model Validity. Based on COP data, the effective beam width is approximately 5mm narrower than the actual beam width.*

Beam Width	Trials	Valid Path w/ Actual Beam Width (%)	Validity w/ Effective Beam Width (%)
2cm	2	0 (0)	0 (0)
3cm	5	5 (100)	2 (40)
> 4cm	22	22 (100)	22 (100)

In the absence of torque saturation, both COM and COP displacements were unaffected by reducing the beam width. This implies that constraints in our analysis impose a boundary that does not affect the control system itself. However, the feedback control gain can result in earlier saturation, and the maximum torque rate (proportional to maximum torque, Thelen 1996) could indirectly change the boundary.

SUMMARY

The dynamics of the BU transition was interpreted in the phase space using a collocated inverted pendulum model. The maximum torque imposes a strict boundary for balance and this was verified experimentally.

REFERENCES

Pai YC (1997). *J. Biomech.* **30:**347-354.
Thelen DG (1996). *J. Gerontol.* **51:**M226-32.
Vellas BJ (1997). *J. Am. Geriatr. Soc.* **45:**735-8.
Ottaviani R (1995). *Am J Sports Med.* **23:**418-23.

ACKNOWLEDGEMENTS

PHS Grants AG 08808 & 10542

KINEMATICS OF THE SLIPPING FOOT

Sarah Margerum[1] (sem4@pitt.edu), Brian Moyer[1], Katie Bieryla[1], and Rakié Cham[1]
[1]Department of Bioengineering
University of Pittsburgh, Pittsburgh, PA, USA

INTRODUCTION

Accidental injuries and deaths are often a consequence of slip and fall incidents (Courtney 2001). The participant's a-priori knowledge of the floor's contaminant condition impacts his/her risk of slipping (Cham 2002). Thus, the goal of this study was to investigate the impact of a-priori knowledge of the floor's contaminant condition on (1) the kinematics of the leading foot at heel contact just prior to slipping and (2) on the severity of the slip.

METHODS

Equipment: Subjects were equipped with a safety harness to prevent injuries in case of a fall. Full body motion (Vicon 612 / M2-cameras system) was recorded at 120 Hz, while ground reaction forces (Bertec Force plates) were recorded at 120 Hz.

Subjects and protocol: Two healthy male and three healthy female subjects, aged 20 to 35 years (mean 24.8 years, SD 5.2 years), were screened for neurological, vestibular and orthopedic abnormalities prior to participation. Subjects were instructed to walk naturally across a vinyl tile walkway such that each foot hit one force plate. After collecting 2 dry trials, a diluted glycerol solution (75% glycerol by volume) was applied to the force plate without the subject's knowledge ("unexpected" slip), so that the left foot (leading) came into contact with the slippery area. Next, the subject was informed that he/she might encounter slippery conditions. Five additional dry trials were collected under this "alert" condition followed by an "alert" glycerol-contaminated trial. Finally, in the "no-doubt" condition, the subject was informed that the floor was contaminated.

Data processing and analysis: Position data of various markers on the foot and ankle were used to derive kinematic variables such as heel velocity and foot floor angle. In addition, slipping distance at the heel was calculated as a measure of slip severity. Finally, the outcome of the slip (no-slip, slip-recovery, slip-fall) was reported based on the heel's trajectory and visual video data. Within-subject repeated measures ANOVAs were conducted on the heel velocity and foot floor angle evaluated at heel contact as well as the sliding distance to investigate the impact of slippery surfaces anticipation.

RESULTS

At heel contact, the heel was moving in the forward direction as it was brought down onto the floor. There were no statistical significant differences in the horizontal heel velocity among anticipation conditions; however vertical heel velocity decreased significantly by 29% in the no-doubt condition compared to the unexpected slip (Figure 1).

Foot floor angle evaluated at heel contact was affected significantly by the anticipation condition (Figure 2). More specifically, the mean (SD) values of the foot-floor angles were 28.6^{o} (5.9), 27.3^{o} (4.72), and 21.1^{o} (3.58) during the unexpected, alert, and no-doubt slippery condition, respectively.

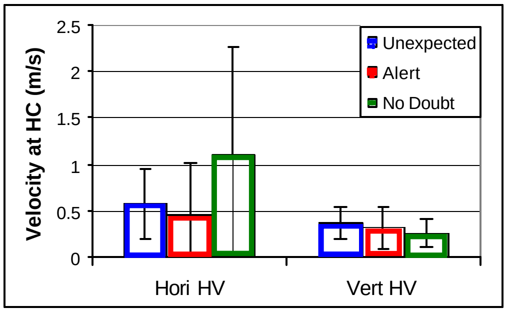

Figure 1: Heel velocity at heel contact (HC) (Error bars represent standard deviations). Hori HV is the heel velocity in the direction of travel and Vert HV is the negative vertical heel velocity.

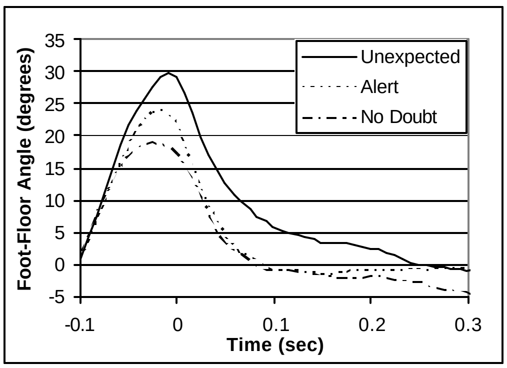

Figure 2: Left foot-floor angle for Subject 1(HC=0 s)

The slipping generated pronounced gait disturbances in the unexpected conditions. Three out of the 5 subjects lost their balance and were caught by the harness during the unexpected slippery condition, whereas only one fell during the alert-condition and all subjects were able to recover when informed of the slippery condition. Furthermore, 2 out of 5 subjects did not slip at all (slip distance < 1 cm) during the no-doubt condition. Another measure of slip severity is the slip distance of the left heel derived from the heel's horizontal trajectory (Figure 3). On average, unexpected slips resulted in slip distances greater than 15 cm (12) [distances during falls were calculated from heel contact to the recovery attempt] compared to average distances of 8 (6) and 3 (4) cm during the alert and no-doubt conditions, respectively.

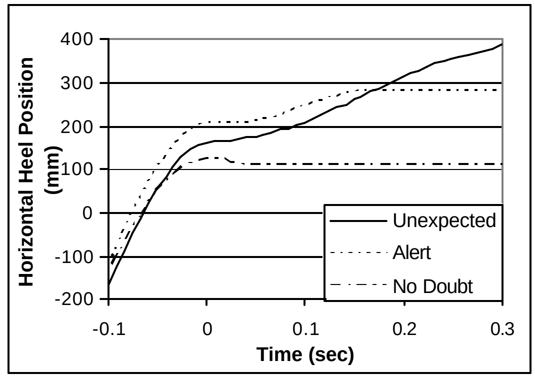

Figure 3: Typical profile of the left heel's horizontal trajectory (HC = 0 s)

DISCUSSION AND CONCLUSIONS

The a-priori knowledge of the floor contamination condition caused participants to adapt their gait when they suspected or knew the floor was contaminated. Those postural adaptations decreased not only slipping risk as reported in Cham and Redfern (2002), but also gait disturbances during slipping. Finally, it is important to acknowledge other gait adaptations, e.g. changes in knee and hip angles, which are beyond the scope of this paper and reported in another ASB submission (Chambers 2003).

REFERENCES

Courtney TK, et al. (2001) *Ergonomics*; **44**:1118-37.

Cham R, Redfern MS. (2002) *Gait and Posture*; **15**(2):159-71.

Chambers et al. (2003) Submitted to American Society of Biomechanics.

ACKNOWLEDGEMENTS

Funding was provided by the National Institute of Occupational Safety and Health (NIOSH R03 OH007533). We would also like to thank Dr. J. Furman for conducting the neurological screening.

SLIP ANTICIPATION EFFECTS ON HIP/KNEE KINEMATICS
PART I: GAIT ON DRY FLOORS

Kathleen Bieryla (kab35@pitt.edu), April Chambers and Rakié Cham
Human Movement and Balance Laboratory, University of Pittsburgh, Pittsburgh, PA, USA

INTRODUCTION

Slips and falls are among the leading generators of non-fatal injuries and deaths at work and among the elderly (Courtney T.K., 2001). Slips are often the cause of multidimensional environmental and human factors. Biomechanical gait studies are an important component of slips/falls prevention research (Redfern M.S., 2001). The goal of this study is to investigate the strategies of maintaining balance when anticipating slippery surfaces. More specifically, this study will examine hip and knee kinematics.

METHODS

Equipment: Subjects were instructed to walk naturally across a vinyl tile walkway instrumented with two Bertec force plates (FP) so that each foot touched one plate. The left foot was the leading or stance leg. Ground reaction forces and whole body motion (8 VICON 612 motion cameras) were collected at 600 and 120 Hz., respectively.

Protocol: Five healthy subjects aged 35 or less (mean 24.8, SD 5.2), previously screened for neurological, vestibular, and orthopedic abnormalities, were informed that the first few trials would be dry to ensure natural walking (baseline condition). Next, one unexpected slippery trial, using glycerol, was collected. The subject was then alerted that the floor may be contaminated in the rest of the session (alert). Five dry, one slippery, and five additional dry trials were collected under the alert condition. Finally, one last known slippery trial was conducted (no-doubt condition). This study compared the dry baseline trials and the first five alert dry trials.

Data processing and analysis: To derive 3D kinematics of the knee and hip, a biomechanical rigid body model (left/right shank, left/right thigh and pelvis), Figure 1, was used. The flexion angle of the knee was found from rotation of the shank local frame with respect to the z-axis of the thigh's local system. The hip angle was found by using the rotation of the thigh's local frame with respect to the pelvis' local sagittal axis. The angles from a static anatomical position trial were subtracted from the measurements during gait trials. Within-subject repeated measures ANOVAs were performed on each gait variable of interest, evaluated at left heel contact time, determined by F.P. data, with the independent variable being the anticipation condition (baseline dry versus alert dry).

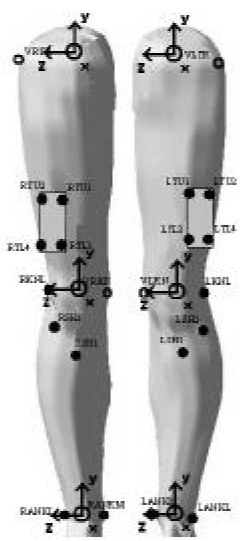

Figure 1: Biomechanical model, lower body used to derive kinematics of hip and knee. Local coordinate systems shown.

RESULTS

Knee Angle vs. % Time, Stance Leg

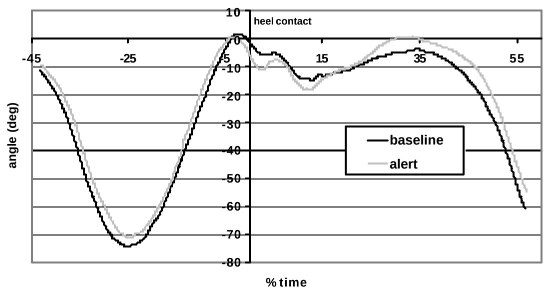

Hip Angle vs. % Time, Stance Leg

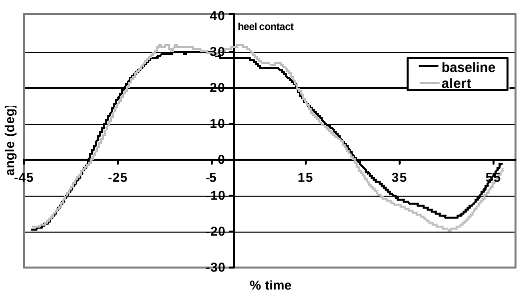

Figure 2: Angles for knee and hip, left leg, for one subject, one trial typical of all others. (+) indicates extension and (-), flexion. Time 0% corresponds to heel contact of stance leg.

Significant differences ($p < 0.001$) in the left knee and hip angles were found between the baseline dry and alert dry conditions. More specifically, increases in left hip angle (greater hip extension) and decreases in left knee angle (greater knee flexion) recorded during the alert dry conditions were compared to baseline trials. Figure 3 shows an average increase of 12.8% in left hip knee angle during alert compared to baseline

Hip Angle and Knee Angle of Stance Leg

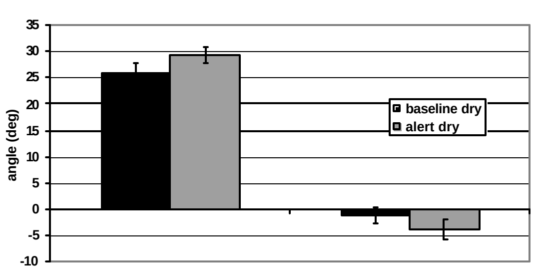

Figure 3: Average angle for knee and hip for left and leg [Error bars represent standard errors]

conditions. Knee angle increases from nearly fully extended in alert to 3.96° flexion. The differences in right hip and knee angles were not statistically significant ($p > 0.1$). The average difference in right hip and knee angles compared to baseline decreased by 2.24% and 9.28% respectively.

DISCUSSION AND CONCLUSIONS

The main finding of this study was that human adapt their gate to “potential” slippery surfaces (increased knee flexion and hip extension) for the stance leg. It is believed that subjects adopt proactive strategies to improve balance in case of a slip. Other gait adaptations include those observed at the feet (Margerum S., 2003). Overall, the gait adaptations adopted when the floor is suspected to be slippery proved effective at minimizing gait disturbances during slipping (Chambers A., 2003).

REFERENCES

Chambers A. et al. (2003) *submitted to American Society of Biomechanics*.

Courtney T.K. et al. (2001) *Ergonomics*, **44**, 1118-37.

Margerum S. et al. (2003) *submitted to American Society of Biomechanics*.

Redfern M.S. et al. (2001) *Ergonomics*, **44**,1138-66.

ACKNOWLEDGEMENTS

Funding provided by the National Institute of Occupational Safety and Health (NIOSH R03 OH007533). We would also like to thank Dr. J. Furman for conducting the neurological screening.

CAN WALKING AIDS IMPEDE COMPENSATORY STEPPING?

Hamid Bateni[1,2], Evelyn Heung[1], John L. Zettel[1], William E. McIlroy[1] and Brian E. Maki[1,2]

1. Sunnybrook and Women's College Health Sciences Centre, University of Toronto, Toronto, Canada
2. School of Rehabilitation Sciences, McGill University, Montreal, Canada
Email: hamid.bateni@swchsc.on.ca Web: http://www.sunnybrook.utoronto.ca/~csia/CSiAInfo/

Introduction:

Although assistive devices such as walkers and canes are often prescribed to aid in balance control, some studies have suggested that such devices may actually increase risk of falling[1, 2]. In this study, we investigated one possible mechanism: the potential for walkers or canes to interfere with, or constrain, lateral movement of the legs and thereby impede execution of compensatory stepping reactions during lateral loss of balance. Such compensatory stepping reactions are likely to be the only recourse in situations where the stabilizing force that can be generated by loading the device is insufficient to recover equilibrium.

Methods:

Compensatory stepping reactions were evoked, in ten healthy young adults (22-27 years), by sudden horizontal translation of a large (2mx2m) moveable platform. Perturbation direction (forward, backward, left, right) was varied unpredictably, and subjects were instructed to do whatever came naturally to prevent themselves from falling. Subjects used no assistive device, or held and loaded a walking frame or cane (instrumented to monitor loading) prior to perturbation. The cane and walker pre-perturbation loading levels were 10 and 20% of body weight, respectively. Reactions to m-l perturbation were analyzed, using video recordings to characterize the limb movements and to determine medio-lateral (m-l) and antero-posterior (a-p) step length. Analyses focussed on the most frequent types of steps: counterlateral, side-step sequence and crossover steps (as defined in previous studies[3]).

Results and discussion:

Collisions between the swing foot and device were very common during the walker task, occurring in over 60% (65/103) of stepping reactions. Such collisions also occurred in 14% (16/115) of stepping reactions when using the cane. For both cane and walker, collision led to a 50% reduction in absolute m-l step length, on average, when compared to no-collision trials ($p<0.05$). It appeared that subjects were able to avoid collision (and increase m-l step length) in no-collision trials by moving the swing foot forward or backward. This was most evident in walker trials: average absolute a-p step length in no-collision walker trials was larger by a factor of three in comparison to trials where collision occurred, and was twice as large as that occurring in no-device trials. It is also possible that collision was sometimes avoided by moving the cane laterally (15%, 18/120, of cane trials); however, attempts to lift and move the walker occurred in only three trials and all three attempts resulted in collision with the stance foot.

The observed collisions between the swing foot and mobility aid support the hypothesis

that walkers and canes can impede compensatory stepping. Subjects were sometimes able to avoid such collisions by increasing the a-p foot displacement or by lifting and moving the cane; however, swing-foot/device collisions were still remarkably frequent, particularly when using a walker.
Furthermore, such collisions appeared to alter the step characteristics, leading to a 50% reduction in m-l step length. The fact that compensatory stepping behavior was altered significantly in such a young and healthy cohort clearly demonstrates some of the limitations inherent to the design of these assistive devices. Ongoing studies with older adults are likely to yield even more compelling evidence that such devices, as currently designed, can actually jeopardize postural stabilization.

Summary:

Our study indicates that the use of an assistive device significantly alters compensatory stepping reactions among our healthy population. These findings clearly demonstrate some of the limitations inherent in the use and/or design of such assistive devices. It appears that these devices, as currently designed and utilized, may present a serious safety hazard to the user.

References:

1. Charron PM, Kirby RL, MacLeod DA. Amer J Phys Med Rehabil 1995;74:237-239.
2. Aminzadeh F, Edwards, N. “Use of Assistive Devices in Fall Prevention…”; University of Ottawa, Canada 1997.
3. Maki BE, Edmondstone MA, McIlroy WE. J Gerontol 2000;55:M270-M277.